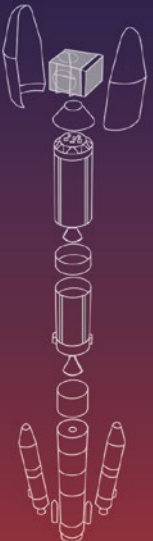


B.N. Suresh
K. Sivan

Integrated Design for Space Transportation System



Integrated Design for Space Transportation System

B.N. Suresh • K. Sivan

Integrated Design for Space Transportation System



Springer

B.N. Suresh
Indian Space Research Organisation
Bangalore, Karnataka, India

K. Sivan
Liquid Propulsion Systems Centre
Indian Space Research Organisation
Bangalore, Karnataka, India

ISBN 978-81-322-2531-7
DOI 10.1007/978-81-322-2532-4

ISBN 978-81-322-2532-4 (eBook)

Library of Congress Control Number: 2015946986

Springer New Delhi Heidelberg New York Dordrecht London
© Springer India 2015

This work is subject to copyright. All rights are reserved by the Publisher, whether the whole or part of the material is concerned, specifically the rights of translation, reprinting, reuse of illustrations, recitation, broadcasting, reproduction on microfilms or in any other physical way, and transmission or information storage and retrieval, electronic adaptation, computer software, or by similar or dissimilar methodology now known or hereafter developed.

The use of general descriptive names, registered names, trademarks, service marks, etc. in this publication does not imply, even in the absence of a specific statement, that such names are exempt from the relevant protective laws and regulations and therefore free for general use.

The publisher, the authors and the editors are safe to assume that the advice and information in this book are believed to be true and accurate at the date of publication. Neither the publisher nor the authors or the editors give a warranty, express or implied, with respect to the material contained herein or for any errors or omissions that may have been made.

Printed on acid-free paper

Springer (India) Pvt. Ltd. is part of Springer Science+Business Media (www.springer.com)

My wife Shobha Suresh, who is no more, was a great source of strength, support, and inspiration for me during my entire career at Vikram Sarabhai Space Centre and the Indian Institute of Space Science and Technology at Thiruvananthapuram including the period of the preparation of this book, till her last breath. She always took keen interest in all my tasks and extended full support, enduring the full responsibility on the domestic front, enabling me to concentrate on my tasks in the last 40 odd years. In the process she made significant sacrifices. Without her affection and continuous support, it would not have been possible to complete this book so elegantly and so soon. I have only words of gratitude to my late wife Shobha Suresh, and I dedicate this book to her for her unwavering and enthusiastic support not only during the preparation of this book but throughout my career at ISRO and IIST spanning more than four decades.

Without the unstinted support and care by my parents during my younger days and during

my education, it would not have been possible for me to reach where I am, and I am ever grateful to them.

B.N. Suresh
ISRO HQ

I dedicate this book to my parents who endured hard times in providing the right education for me to follow my ambitions throughout my childhood, my teachers who unveiled the beauty and mystique of aerospace engineering to me, and to my superiors at office who guided me on the intricate path of rocket science.

I am ever grateful to my wife Malathy for standing beside me while writing this book. She has been a source of immense inspiration and motivation for continuing to improve my knowledge. I also thank our wonderful children Sidharth and Sushanth for always making me smile and for understanding on those weekend mornings when I was writing this book instead of spending quality time with them. I hope that one day, they can read this book and understand why I spent so much time in writing it.

K. Sivan
ISRO

Foreword

Spectacular developments in space technology during the last six decades and their vast application for providing global communication, navigation, broadcasting, management of our natural resources, and timely monitoring of natural disasters have practically revolutionized the human way of living on our planet earth. The impact of rapid developments in space technology in exploring and mapping not only our own solar system but also the entire universe from its very beginning has surpassed all our expectations.

Many nations have employed extensive space-based services for establishing national/global communication systems, as well as for optimal usage of their natural resources and timely management of natural disasters. In spite of the heavy dependence of nations and institutions on space services, very few nations have developed their own capability to design, build, and operate highly reliable, incredibly complex, and expensive development of space rockets.

Indian Space Research Organisation (ISRO) initiated its space activities in a very modest way in 1960, with the establishment of Thumba Equatorial Rocket Launching Station (TERLS) at Thumba, near Thiruvananthapuram. This was soon followed by the establishment of the Space Science and Technology Centre (SSTC) which was subsequently renamed as Vikram Sarabhai Space Centre (VSSC). In the early 1970s, VSSC took up the challenge of building its first rocket SLV-3, capable of launching a 40 kg satellite into a near earth orbit. This was followed by the development of ASLV (augmented satellite launch vehicle) carrying a complete closed loop control and guidance system to place a 140 kg satellite into a 400 km low earth orbit, shaping the way for the development of operational PSLV (polar satellite launch vehicle) and GSLV (geostationary satellite launch vehicle) launch vehicles, which have been extensively used during the last two decades for launching a number of remote sensing as well as geostationary satellites. The versatile PSLV rocket has also been used by ISRO for successfully carrying out Chandrayaan-1 Moon mission in 2012 as well as the Mars Orbiter Mission (MOM) in 2014.

In spite of the tremendous popularity of space exploration, there is a dearth of material elaborating and discussing the scientific principles and technical

complexities of building reliable space transportation systems. Consequently, there is a great need to have a comprehensive textbook dealing with practical aspects of the design and development of space transportation systems for different applications. The book *Integrated Design for Space Transportation System* written by Dr. B.N. Suresh and Dr. K. Sivan, who have been intimately involved in the development of rockets at the Vikram Sarabhai Space Centre at Thiruvananthapuram, is an authoritative and extremely well-written textbook which has tried to fulfill this lacunae. It provides extensive details regarding the choice of materials; structural requirements; stage auxiliary systems; aerodynamics configuration; navigation, guidance, and control systems; and also design of the vehicle destruct system which has to be used in case of unforeseen circumstances. The book contains a large volume of data, facts, test and calibration methodology, and detailed account on how problems were solved in mastering rocket technology. Operational rockets in general are modularly designed to be able to change their overall configuration to suit the requirement of any particular satellite mission. The book provides a detailed description of each stage of the vehicle and the options available in mixing and matching the stages to achieve optimal performance for the desired launch. The last chapter of the book also deals with reentry dynamics including the special requirements that need to be considered to ensure safe reentry of payloads and systems. As the authors have stated, the book clearly highlights the complex design aspects including interdependencies and interface between various systems. In 15 very well-written chapters, the book has succeeded in elaborating the entire science of space rocketry in a comprehensive way.

I have no doubt that this book will become a very valuable textbook for those who wish to engage themselves in the field of space rocketry. I heartily congratulate both Dr. Suresh and Dr. Sivan for their painstaking effort involved in writing this elegant book which will be of immense value to all the engineers and scientists who wish to fully participate in the development of space technology.

Indian Space Research Organisation
Bangalore, India

U.R. Rao

Preface

Space transportation systems are important means of transportation to connect the Earth to outer space. Essentially it has to transport an identified spacecraft from Earth and deliver precisely into a specified orbit in space depending upon the mission requirements. In certain cases it has the task of bringing back the spacecraft safely from orbit to Earth. The satellites are designed and built to meet the specific demands of communication, remote sensing, navigation, meteorological applications, and science missions such as astronomical observations and planetary explorations. To derive the maximum benefits from these satellites, it is important that they are positioned into the right orbital slot by the space transportation system. Over a period, the technical advancements made in the space arena demand transportation of men and material too to space and bring them back safely.

The realization of such a transportation system is a very complex process as this involves multiple disciplines like propulsion, aerodynamics, structures, stage auxiliary systems, navigation, guidance and control systems, thermal protection systems, etc. Added to this, many of the technologies would not have attained the required maturity levels during the initial design phase. Hence, the design cycle invariably takes long periods, with very heavy investments. In addition to meeting the specified mission requirements, the design and development process should be aimed to achieve lower cost and higher reliability. It should also have the inbuilt mission flexibility with a capability to handle a wide range of missions.

Creation of optimum design of a highly complex, autonomous, and automatic space transportation system to operate in a severely disturbed environment is a challenging task. The design task is multidisciplinary in nature with high level of interactions. It demands a broader knowledge of a wide range of science and engineering disciplines which are closely interconnected. For a good design, it is also essential to have a clear understanding of the interactions, interdependencies, and interfaces between the disciplines. Although there are several books that address the design aspects of specialized areas, viz., structure, propulsion, aerodynamics, control, etc., which are essential for space transportation system design, there are hardly any books which focus on integrated design aspects of a space

transportation system, utilizing the systems engineering approach. This book attempts to fill this gap by addressing systems approach for space transportation systems design, highlighting the integrated design aspects, interactions between various subsystems, and interdependencies.

The design of each subsystem of a space transportation system demands in-depth knowledge and understanding of modern design and analysis tools in the specific area. The usage of state-of-the-art, cutting-edge technologies and tools is essential in the respective disciplines to arrive at an optimum design of each subsystem. This book is not the design tool for the detailed design process of subsystems. It is essential for the domain design experts to have full understanding of the overall integrated design aspects of space transportation systems, its subsystems, the interactions between different subsystems, and their impacts in order to carry out the subsystem design in an efficient manner.

This book is attempted based on the long experience of authors for more than three and a half decades in space vehicle design and development. This book is meant to assist all scientists and engineers involved in the complex multidisciplinary space vehicle design and aimed to provide broad-based design guidelines. Since this book covers end-to-end design aspects of space transportation system and all its subsystems, it will certainly be useful for the undergraduate- and postgraduate-level courses which deal with space vehicle design process.

The purpose of this book is only to describe the complex integrated design aspects including the interdependencies and interactions between various subsystems/systems, and hence it is not targeted as a design tool for any particular discipline or subsystem. Therefore, no attempt is made to derive some of the design-related equations or expressions from the first principle. However, the important analytical expressions, graphs, and sketches which are essential to provide in-depth understanding for the design process and to understand the interactions between different subsystems are appropriately included. The entire materials presented in the book are an outcome of the experience of authors in the development of a number of Indian launch vehicles, and only in very exceptional cases is the reference made to outside material. In all such cases wherever it is applicable, the corresponding references are suitably acknowledged.

Readers may find certain repetitions in different chapters, but it has been deliberately retained to avoid referring back and forth between chapters and to facilitate easier understanding of the concepts while reading each chapter.

To meet all these objectives, the book is organized in 15 chapters as per the details given below and addresses the integrated design processes encompassing various aspects of all subsystems of the space transportation system. The interactions, interdependencies, and interface aspects between various subsystems as applicable are included at appropriate places in these chapters.

Chapter 1 attempts to present in brief the salient aspects of planets, such as Earth, and the Sun. The satellite applications highlighting how the space activities assist to meet the application needs of a country and how it helps to improve the economic and social conditions of its people have been briefly given. The specific role of the space transportation system in meeting the national needs highlighting all essential

requirements is included. Typical system requirements and the issues and challenges involved in the design process are also brought out.

Chapter 2 presents in detail the overall integrated design aspects of space transportation system such as system approach for design, trade-off and options analysis, system life cycle considerations, important aspects in mission management, the risk assessment, etc. The interdependencies, interactions, and management of interfaces between various subsystems are also presented. Some of the integrated design processes are explained with typical examples.

The transportation of a satellite in space demands a clear understanding of the motion of an object in space, type of orbits, the orbital motion, orbital elements, etc. All these details are presented in Chap. 3 including the different coordinate frames relating to Earth and their relations. The orbital perturbations, orbital transfers, launch vehicle orbit requirements, inclination change of orbital plane, combined orbit size, and inclination correction are also discussed.

Chapter 4 gives the details of various aspects of satellite launching such as specific orbit requirements, achieving the same using a launch vehicle, ascent trajectory, optimum strategies to achieve the injection, and the importance of the launch site. The impact of dispersions of the vehicle state on the orbital elements, which need to be corrected by the spacecraft, is also highlighted.

The basic criterion for choosing a suitable launch vehicle configuration is a very important factor in space transportation system. This aspect is covered in detail in Chap. 5 which discusses the rocket equation, mass fractions, total velocity requirements, the velocity losses, and the benefits of multistaging.

The launch vehicle operating environment is another important consideration for the design of space transportation system, and it comprises of both external and internal operating environments. Different aspects of environment and various factors influencing the same have been brought out in Chap. 6.

The launch vehicle mission has to address various factors such as mission strategies, mission constraints, technically suitable mission profile, vehicle steering strategies, mission sequence design considerations, satellite orientation, passivation requirements, and many more. These aspects are discussed in detail in Chap. 7.

In the design process, trade-off studies with respect to vehicle configuration, payload capability, the trajectory design, and system performance analysis are essential. A comprehensive modeling and simulation tool such as integrated trajectory simulation tool is necessary to provide vital inputs to carry out the design for propulsion, aerodynamic configuration, mission sequencing, evaluation of vehicle loads, dynamic behavior of the vehicle, etc. under several parameter variations. They are generally dealt in flight mechanics. Chapter 8 addresses all these aspects in detail.

Propulsion systems are fundamental subsystems in a space transportation system. Chapter 9 addresses the basics of rocket propulsion, several propulsion options, and their relative merits and demerits. The staging aspects and criteria for selection of suitable propulsive modules are also highlighted. The design of a suitable propulsion system has to address all aspects of systems engineering since it

has a very large influence on several aspects of the vehicle. The qualification process for the propulsive stages is also explained in this chapter.

Since the vehicle has to pass through the atmosphere during the initial phase, aerodynamics plays a vital role in the design of space transportation system. Various factors which influence the design are aerodynamic configuration, understanding of aerodynamic forces and moments, unsteady flow, and pressure distribution across the vehicle. The aerodynamic characterization is carried out through experimentation using wind tunnel studies and also by theoretical evaluation using Computational Fluid Dynamics (CFD) tools. All important features of aerodynamics have been brought out in Chap. 10.

Chapter 11 deals with materials and structural design which are very vital for a space vehicle design. The structural design criteria, design loads, selection of a suitable type of structure, design tools, and all other related details have been discussed. The static and dynamic analysis and structural testing aspects have also been included.

The vehicle during its journey faces hostile thermal environment and needs appropriate thermal protection. It is therefore essential to have a sound thermal design, thermostructural analysis, and qualification tests on ground to ensure that the system withstands the severe temperature without any structural damage. All these aspects are discussed in Chap. 12.

Stage auxiliary systems play an important role in the ignition of propulsion modules and separation of various stages. Since most of the devices are single-shot operation and the hardware identified for flight are not fully testable for performance, the reliability of these systems should be very high. All essential features of these systems and various aspects of establishing the needed reliability are presented in Chap. 13.

The navigation, guidance, and control (NGC) system is a very mission-critical subsystem, and the accuracy with which the spacecraft has to be injected into orbit depends on the caliber of the NGC system. The selection of suitable sensors, their calibration, guidance algorithms, autopilot design, the design tools, control power plants, integrated validation of the NGC system, and all other associated factors have been detailed in Chap. 14.

In order to have a successful human space flight, it is imperative that reentry technologies are mastered. Various design features and complexities of a reentry vehicle have been brought out in Chap. 15.

Readers would also notice that the details on avionics subsystems like telemetry, tracking, and tele-command (TTC) and power are not included in the book. The integration and checkout aspects of the vehicle are also not discussed exclusively in this book. The vehicle avionics subsystems except the navigation, guidance, and control (NGC) subsystem do not contribute significantly to the integrated design of the vehicle. The NGC subsystem has very close interaction in the integrated vehicle design, and therefore the details of this subsystem are included in Chap. 14. With regard to TTC and power subsystems, one needs to consider the mass, volume, and power requirements of these packages during the design. The integration and checkout requirements for the vehicle entirely depend on the vehicle configuration,

launch philosophy adopted, etc. Therefore, the interactions of these subsystems are not very significant while discussing the integrated design of the space transportation system. Considering these aspects the authors have decided deliberately not to include these subsystems as part of the integrated design of space transportation system in the book.

Finally, regarding the usage of phrases, “space transportation system” or the short form of it, STS in this book, readers are advised not to be confused with the usage of these phrases to refer to the space shuttle in the literature. In this book, the phrase “space transportation system” or “STS” is used to refer to the general space vehicles, which are used to transport a payload from Earth to space or from space to Earth. Also, the phrase “launch vehicle” is used to refer to the ascent phase function (transport payload from Earth to space) of space transportation system, and “reentry vehicle” is used to refer to the descent phase function (transport payload from space to Earth) of space transportation system.

Karnataka, India
Karnataka, India

B.N. Suresh
K. Sivan

Acknowledgments

We gratefully acknowledge the intense interactions and discussions we had with a vast number of our colleagues at ISRO Centres during the design and development of Indian launch vehicles, in the last three and a half decades, from the very first Indian satellite launch vehicle-3 (SLV-3) to augmented satellite launch vehicle (ASLV), polar satellite launch vehicle (PSLV), geosynchronous launch vehicle (GSLV), space payload recovery experiment (SRE), and the next generation geo-synchronous launch vehicle-Mk3 (GSLV-Mk3) at the Indian Space Research Organisation (ISRO) which have helped immensely in generating the overall structure for this book and also the preparation of detailed contents and materials under various chapters. Our leaders and peers at ISRO gave us ample opportunities to work intensely in launch vehicle projects and also on various aspects of launch vehicle development, which over a long period helped us to understand may intricacies of systems engineering in such complex systems. We are very grateful to all our peers, Prof Satish Dhawan, Prof Brahm Prakash, Prof U.R. Rao, Dr. K. Kasturirangan, Dr. V.R. Gowarikar, Dr. S.C. Gupta, Dr. A.P.J. Abdul Kalam, the late Dr. S Srinivasan, Dr. G. Madhavan Nair, and many other eminent leaders, for their able guidance and directions on several aspects of design and development of the launch vehicles during the last three and a half decades in the country.

We profusely thank the Indian Space Research Organisation and particularly Dr. K. Radhakrishnan, who was chairman, ISRO, till December 2015, for his continuous support, assistance, and encouragement during the preparation of this book. He took considerable time to review the book in detail and has provided us very valuable review comments. In his remarks, he has kept his personal touch and concluded that this book is of immense value to all practicing space technologists and academicians in the field. His comments are included in the book. We also thank Shri A.S. Kiran Kumar, present chairman, Indian Space Research Organisation, for his continued support since he took over as chairman.

We requested Prof U.R. Rao, former chairman, ISRO, and Dr. S.C. Gupta, former director, Vikram Sarabhai Space Centre (VSSC), to review the entire manuscripts and give their valuable comments and offer their views about the

book. We express our deep appreciation and sincere thanks to Prof U.R. Rao for sparing his precious time to go through the book in detail and providing a Foreword, which nicely captures and summarizes the various aspects of the book. We also thank Dr. S.C. Gupta for his extra efforts in going through the entire manuscripts and offering his very valuable comments wherever essential, which are appropriately included in the book. He has also provided his review and views as “Nuances of Space Transportation Systems,” and it is included in the book.

Every chapter of the book has been reviewed thoroughly by a fairly good number of subject experts from ISRO Centres to ensure that the matter presented in the book is error-free. We requested many of our colleagues to review each chapter in detail and offer their suggestions and comments. We greatly appreciate and acknowledge their very valuable suggestions, which have been incorporated appropriately in the book.

We greatly appreciate and express our heartfelt thanks to Dr. K. Sudhakara Rao, former deputy director, System Reliability entity and a mission expert who was deeply involved in PSLV and GSLV missions, for taking great pains in reviewing a number of chapters and providing very valuable suggestions to improve these chapters.

We are indeed indebted to all our colleagues from ISRO, Dr. Ramanan, Mr Sowmyanarayanan, Mr C. Ravi Kumar, Mr D.S. Antuvan, Dr. U.P. Rajeev, Mr V. Balachandran, Dr. V. Narayanan, Dr. V. Ashok, Mr. S. Balakrishnan, Mr C.K. Krishnadasan Nair, Mr Deependran, Mr N.P. Giri, Mr Unnikrishnan Nair, Mr Suresh Babu, Dr. V. Lalithambika, Dr. P.P. Mohan Lal, Mr M. Selvaraji, Ms Geetha, Mr S. Pandian, Mr M.M. Patil, and Mr C. Geethakrishnan, who have put forth considerable efforts in reviewing the manuscripts meticulously and offered their valuable comments and suggestions for improvement wherever essential. Although the book has gone through very rigorous peer reviews by several experts, the authors own full responsibility for any unintentional errors which may still appear in the book.

We extend our sincere thanks to Mrs Lalitha Kashinath, personal assistant to the first author, ISRO HQ, for her patience in the preparation of the manuscripts, very meticulously without any errors. We sincerely thank the Imagic Creatives, Bangalore, particularly Mr Dileepan and Ms Leena, in the preparations of a number of drawings during the initial stage. The enthusiastic support extended by Mr M. Selvaraj, in the preparations of initial drawings, is gratefully acknowledged.

Mrs S. Savithriamma, GSLV Project, VSSC was a great source of strength in the preparation of the manuscripts for all chapters, entering the complex equations and laying out the chapters in a single format with detailed preparations of notations. Without her support it would not have been possible to complete this task in a time-bound manner. Mr Anurag Sinha, VSSC, has taken extra care in the final phases of the preparation of the book and put forth considerable efforts in finalizing the overall formatting of the chapters. His support in carrying out the mammoth task of preparing innumerable drawings with lots of care to ensure that they are error-free is commendable. Without the contributions and timely support of these two colleagues, it would not have been possible to bring out the final manuscripts so

elegantly and so soon without errors. We have no words to express our sincere thanks to both of them for their continuous support, involvement, and assistance.

Many of our colleagues and friends whose names may not appear here have extended their support and help in some form or another, directly or indirectly, during the preparation of the book, and we sincerely acknowledge all their contributions.

B.N. Suresh
K. Sivan

Contents

1	Space Transportation Systems: Introduction and Design Challenges	1
1.1	Introduction	1
1.2	Planets and Earth	2
1.2.1	The Planets	3
1.2.2	The Earth	4
1.3	Satellites and Space Applications	5
1.3.1	Telecommunications and Broadcasting	6
1.3.2	Remote Sensing and Earth Observations	6
1.3.3	Satellite Navigation	7
1.3.4	Weather Monitoring	8
1.3.5	Disaster Warning and Management	9
1.3.6	Scientific Satellites	9
1.4	Space Transportation System	10
1.4.1	Broad Systems Requirements	10
1.4.2	Operating Environments for STS	13
1.4.3	Cost Aspects of STS	13
1.4.4	Overall Design Guidelines	16
1.4.5	Design and Development Cycle for STS	17
1.4.6	Complexities and Design Challenges of STS	19
	Bibliography	22
2	Integrated Design Aspects of Space Transportation System	23
2.1	Introduction	24
2.2	Systems Engineering Approach for Design	25
2.3	System Life Cycle Considerations for Design and Development of STS	29
2.4	Overall Functional and Design Requirements	30
2.5	Overall System Requirements and Decomposition	34
2.6	Important System Engineering Aspects	38

2.6.1	The Trade-Off or Options Analysis	38
2.6.2	Interdependencies and Interactions	40
2.6.3	Risk Assessment and Management	42
2.7	Integrated Design Aspects for Launch	
	Vehicle Subsystems	43
2.7.1	Operating Environment to the Vehicle System	44
2.7.2	Propulsion Systems Selection and Vehicle Sizing Aspects	45
2.7.3	Structural Design Aspects	45
2.7.4	Vehicle Aerodynamics	46
2.7.5	Trajectory Design and Flight Sequence	47
2.7.6	Navigation, Guidance and Control Aspects	47
2.8	Modeling and Analysis of Integrated System	48
2.9	Subsystem and System Design and Performance Evaluation	49
	Bibliography	50
3	Astrodynamics	51
3.1	Introduction	52
3.2	Reference Frames	53
3.2.1	Celestial Sphere and Ecliptic	53
3.2.2	Heliocentric Inertial Reference Frame	54
3.2.3	Earth Centered/Geocentric Inertial (ECI) Reference Frame	55
3.2.4	Earth-Centered Rotating (ECR) Frame	56
3.3	Laws of Motion	56
3.3.1	Kepler's Laws	56
3.3.2	Newton's Laws of Motion	57
3.3.3	Newton's Law of Universal Gravitation	59
3.4	Two-Body Problem	59
3.4.1	Some Important Trajectory Parameters of Two-Body Problem	70
3.4.2	Circular Orbits	75
3.4.3	Elliptical Orbits	76
3.4.4	Parabolic Trajectories	79
3.4.5	Hyperbolic Trajectories	81
3.5	Satellite Orbit and Trajectory Requirements	83
3.5.1	Circular Orbits	83
3.5.2	Elliptic Orbits	84
3.5.3	Open Trajectories	84
3.6	A Note on Orbital Energy and Launching of Satellites into Orbit	84
3.7	Orbital Elements	86
3.8	Orbital Perturbations	88
3.8.1	Effects of Earth's Asphericity on Orbital Elements	89
3.8.2	Sun-Synchronous Orbits	92

3.8.3	Molniya Orbits	93
3.8.4	A Note on Osculating and Mean Orbital Elements	94
3.9	Restricted Three-Body Problem	94
3.10	Interplanetary Trajectories	96
3.10.1	Sphere of Influence	97
3.10.2	Patched Conic Trajectory	98
3.11	Orbital Transfers and Launch Vehicle Orbit Requirements	99
3.11.1	Coplanar Circular Orbit Transfer	100
3.11.2	Coplanar Elliptic Orbit Transfer	102
3.11.3	Coplanar Orbital Transfer from Ellipse to Circular Orbit	104
3.11.4	Inclination Change of Orbital Plane	105
3.11.5	Combined Orbit Size and Inclination Correction . .	107
3.11.6	Launch Vehicle GTO Requirements for Geostationary Satellite Missions	108
	Bibliography	109
4	Space Transportation Requirements and Launching of Satellites	111
4.1	Introduction	112
4.2	Space Transportation Functional Requirements	113
4.3	Vehicle Trajectory	116
4.4	Achieving Satellite Orbital Elements by STS	119
4.5	Selection of Launch Azimuth and Ascent Trajectories	122
4.6	Selection of Launch Site	125
4.7	Optimum Strategies to Achieve the Satellite Injection	126
4.7.1	Direct Ascent	127
4.7.2	Hohmann Transfer Ascent	130
4.8	Trade-Off Studies and Integrated Mission Aspects	132
4.9	Vehicle Subsystem and Design Requirement	132
4.10	Satellite Orbit Deviations Due to Space Transportation Systems Errors	134
4.11	Mission Definition for STS	136
	Bibliography	137
5	Space Transportation System Configuration, Staging and Performance	139
5.1	Introduction	140
5.2	STS Configuration Selection Requirements	141
5.3	STS Performance	145
5.3.1	Performance Parameters	146
5.3.2	Technology Limitations and Trade-Off Analysis	147
5.3.3	Single Stage STS Performance	149

5.4	Multistage STS Configurations	152
5.4.1	Multiple Stage Concept	153
5.4.2	Multistage Performance	153
5.4.3	Optimal Staging	156
5.4.4	Important Considerations for Configuring Multistage STS	158
5.4.5	Types of Multistage Configurations	160
5.5	Optimum Staging Aspects and Vehicle Performance	163
5.6	Design Sensitivities and Trade-Offs	166
5.7	Satellite Interfaces with STS and Payload Fairings	168
5.8	External Configurations of STS	169
5.9	Infrastructure for Ground Operations	171
	Bibliography	172
6	Operating Environment	173
6.1	Introduction	174
6.2	Broad Classification of Operating Environments	175
6.3	Earth Geometry and Gravity Environment	177
6.3.1	Earth Shape and Gravitational Potential	178
6.3.2	Gravitational Acceleration	181
6.3.3	Vehicle Position Definition	183
6.3.4	Effects of Earth Oblateness on STS Mission Target	184
6.4	Atmospheric Properties	186
6.5	Aerodynamic Environment	190
6.6	Atmospheric Winds	192
6.6.1	Wind Effects on Space Transportation Systems	193
6.6.2	Influence of Wind Characteristics	196
6.6.3	Wind Statistics	202
6.6.4	In-Fight Wind Data for Design Studies	206
6.7	Thermal Environment	208
6.7.1	Thermal Environment on Launch Pad	208
6.7.2	Thermal Environment During Atmospheric Flight Phase	209
6.7.3	Thermal Environment Caused by Propulsion Systems	209
6.8	Vehicle Internal Steady Loads and Disturbances	209
6.8.1	Thrust offset	210
6.8.2	Thrust Misalignment	210
6.8.3	Differential Thrust	212
6.8.4	Attachment Misalignment	215
6.9	Dynamic Environment	215
6.9.1	External Dynamic Environment	216
6.9.2	Vehicle Flexible Modes	217
6.9.3	Propellant slosh	218
6.9.4	POGO Oscillation	219

6.9.5	Thrust Oscillations	222
6.9.6	Other Dynamic Environments	224
6.10	Random Vibration Environment	224
6.10.1	Propulsion System Noise	225
6.10.2	Aerodynamic Noise	225
6.10.3	Impact of Noise on Vehicle System Design	226
6.10.4	Noise Reduction Strategies	226
6.11	Influence of Parameter Dispersions	227
6.11.1	Primary Critical Parameters	227
6.11.2	Secondary Critical Parameters	228
	Bibliography	229
7	Mission Design	231
7.1	Introduction	232
7.2	Mission Design Activities	233
7.3	Mission Design Strategy	234
7.4	Mission Specification Requirements and Constraints	236
7.4.1	Mission Specifications	237
7.4.2	Mission Requirements	239
7.4.3	Mission and Vehicle Constraints	240
7.4.4	Mission Studies	241
7.5	Trajectory Phases and Mission Design Tasks	241
7.6	Lift-Off Studies and Analysis	244
7.7	Vehicle Load Reduction Strategies	246
7.7.1	Thrust Profile Shaping	247
7.7.2	Load Relief Systems	248
7.8	Gravity Turn Trajectories and Wind Biasing	249
7.8.1	Gravity Turn Trajectories	249
7.8.2	Wind Biasing	251
7.8.3	Implementation Aspects of DOL Wind Biasing	255
7.9	Thermal Constraints	258
7.10	Mission Sequence Design	259
7.10.1	Mission Sequence Strategy	259
7.10.2	Typical Stage Transition Sequence	262
7.11	Propellant Loading Requirements	262
7.12	Velocity Reserve Requirements	265
7.13	Satellite Injection Requirements	267
7.14	Propulsion Stage Passivation Requirements	269
7.15	Vehicle Tracking Requirements	270
7.16	Range Safety Constraints	272
7.17	Integrated Trajectory Design	273
7.17.1	Trajectory Design Considerations	274
7.17.2	Trajectory Design Strategy	276
7.17.3	Integrated Trajectory Design Process	279
7.17.4	Optimum Mission Profile	280
	Bibliography	282

8 Flight Mechanics	285
8.1 Introduction	286
8.2 Role of Flight Mechanics in STS Design Process	287
8.3 Need for Integrated Design Approach with Flight Mechanics	288
8.4 Coordinate Systems	289
8.4.1 Reference Frames	290
8.4.2 Vehicle Attitude and Sign Convention	292
8.4.3 Coordinate Transformations	294
8.5 Environment Model	298
8.5.1 Earth Geometry	298
8.5.2 Earth Gravitational Model	300
8.5.3 Atmospheric Model	301
8.5.4 Wind Model	303
8.5.5 Vehicle Velocity	304
8.6 Vehicle Model	305
8.6.1 Propulsion Model	305
8.6.2 Aerodynamic Model	306
8.6.3 Jet Damping Model	308
8.6.4 Auxiliary Forces Model	308
8.6.5 Slosh Model	309
8.6.6 Mass Properties	310
8.7 Guidance and Control Model	311
8.7.1 Sensor Dynamics Model	312
8.7.2 Navigation Model	313
8.7.3 Guidance Model	313
8.7.4 Autopilot Model	313
8.7.5 Control Power Plant Model	314
8.8 Vehicle Dynamics	315
8.8.1 Equations of Motion	315
8.8.2 Initial Conditions for Equations of Motion	319
8.8.3 Solutions for the Equations of Motion	322
8.8.4 Equations of Motion During Lift-Off	323
8.8.5 Instantaneous Change in State Vector	324
8.8.6 Instantaneous Velocity Addition Due to Tail-Off	324
8.9 Flexible Vehicle Dynamics	325
8.10 Integrated Flight Mechanics Model	326
Bibliography	327
9 Propulsion Systems	329
9.1 Introduction	330
9.2 System Considerations in Propulsion System Selection and Design	331

9.3	Propulsion System Requirements, Selection and Design Guidelines	335
9.3.1	Propulsion System Requirements	335
9.3.2	Propulsion System Selection Criteria	335
9.3.3	Overall Design Guidelines	337
9.4	Propulsion Fundamentals	338
9.4.1	Thrust	340
9.4.2	Exhaust Velocity	342
9.4.3	Rocket Nozzle Configuration and Performance	345
9.4.4	Effect of Nozzle Geometry	350
9.4.5	Performance with Different Nozzle Expansions	352
9.4.6	Performance Parameters	355
9.5	Solid Propulsion Systems	363
9.6	Liquid Propulsion Systems	365
9.6.1	Propellant Feed System Classification	366
9.6.2	Feed System Cycles of Pump-Fed Engines	368
9.6.3	Cryogenic Propulsion Systems	370
9.6.4	Semi-Cryogenic Propulsion Systems	372
9.7	Critical Subsystems of Liquid Propulsion Systems	373
9.7.1	Propellant Tanks	373
9.7.2	Propellants Used in Liquid Propulsion Systems	375
9.7.3	Propellant Feed Systems	375
9.7.4	Injector	376
9.7.5	Thrust Chamber	377
9.7.6	Engine Cooling	377
9.7.7	Propulsion Control Systems	379
9.8	Hybrid Propulsion Systems	381
9.9	Air-Breathing Chemical Propulsion	381
9.9.1	Types of Air-Breathing Propulsion Systems	382
9.9.2	Typical Air-Breathing Propulsion Systems for STS Applications	384
9.10	Non-Chemical Propulsion Systems	385
9.11	Qualification of Propulsion Systems	386
9.11.1	Qualification Methodology for Solid Motors	386
9.11.2	Qualification Tests for Liquid Propulsion Systems	387
	Bibliography	390
10	Aerodynamics of Launch Vehicles	391
10.1	Introduction	392
10.2	Aerodynamic Flow Characteristics	392
10.2.1	Continuum, Transitional and Free Molecular Flow Regimes	393
10.2.2	Laminar and Turbulent Flows	393

10.2.3	Incompressible and Compressible Flows	395
10.2.4	Separated Flows	399
10.3	Overall Vehicle Aerodynamic Features	400
10.3.1	Representation of Aerodynamic Forces and Moments	402
10.3.2	Aerodynamic Force and Moment Model for a Generic Launch Vehicle	405
10.4	Aerodynamic Characteristics and Loads	410
10.4.1	Lift-Off Phase	411
10.4.2	High-Dynamic Pressure Flight Phase	414
10.4.3	Free Molecular Flow Regime	437
10.5	Aerodynamic Characterization	438
10.5.1	Aerodynamic Characterization Using Wind Tunnel Tests	441
10.5.2	Aerodynamic Characterization Using CFD	443
10.6	Launch Vehicle Aerodynamics Configuration Design	444
10.6.1	Aerodynamic Configuration Design of Payload Fairing (PLF)	444
10.6.2	Configuration Design of Strap-on Nose Cones	449
10.6.3	Fin Design	449
10.6.4	External Configuration Design of Protrusions	452
	Bibliography	453
11	Structures and Materials	455
11.1	Introduction	456
11.2	Structural Design Requirements	457
11.3	Structural Loads and Analysis	458
11.3.1	Axial Load	460
11.3.2	Shear Force	460
11.3.3	Bending Moment	461
11.4	Structural Design Aspects	462
11.4.1	Design Load Factors	463
11.4.2	Motor Case or Liquid Stage Tanks	464
11.4.3	Interstage Structure	466
11.4.4	Structural Joints	467
11.4.5	Other Key Design Characteristics	468
11.5	Shapes and Constructions for STS Structures	469
11.6	Materials for Structures	472
11.7	Structural Analysis	475
11.7.1	Analysis Tools	476
11.7.2	Static Analysis	477
11.8	Structural Dynamic Analysis and Testing	481
11.8.1	Dynamic Characterization of Structures	483
11.8.2	Ground Resonance Tests	484
11.9	Dynamic Response and Stability Analyses	485
11.10	Structural Static Testing	487

11.11	Environmental Testing for Space Structures	489
11.11.1	Qualification Tests	490
11.11.2	Acceptance Tests	490
11.12	Aeroelastic Analysis and Testing	491
11.12.1	Flutter Phenomenon	491
11.12.2	Divergence	492
11.12.3	Buffet Phenomenon	492
	Bibliography	493
12	Thermal Systems and Design	495
12.1	Introduction	496
12.2	Heating Problems in Launch Vehicles	497
12.2.1	Aerodynamic Heating Over a Flat Surface	497
12.2.2	Aerodynamic Heating Over Launch Vehicle Surface	499
12.2.3	Heating Due to Jet Exhaust	501
12.2.4	Impact of Thermal Environment on the Vehicle Systems	501
12.3	Thermal Design Requirements and Constraints in a Vehicle	503
12.3.1	Thermal Design Requirements	506
12.3.2	Design Constraints	507
12.4	Thermal Design Strategy and Guidelines	507
12.4.1	Approach for Thermal Design	507
12.4.2	Thermal Design Process Guidelines	508
12.4.3	Thermal Protection System Selection and Design Criteria	509
12.5	Thermal Environment and Design for Launch Vehicle Systems	511
12.5.1	Thermal Environment and Thermal Management of Avionics Bay of Vehicle	512
12.5.2	Thermal Protection System of Earth Storable Liquid Propellant Stages	514
12.5.3	Thermal Environment and Protection of Launch Pad Elements	514
12.5.4	Ascent Phase Thermal Environment	515
12.5.5	Aeroheating Environment, Thermal Design and Analysis	517
12.5.6	Base Heating Environment and Thermal Design	528
12.5.7	Thermal Protection for Destruct Systems	533
12.6	Thermal Protection Systems for Cryogenic Stage	533
12.7	Tests for Thermal Protection Systems and Qualification	535
	Bibliography	536

13 Stage Auxiliary Systems	539
13.1 Introduction	540
13.2 Functional Requirements of Stage Auxiliary Systems	541
13.3 System Requirements of SAS	543
13.4 Design Aspects of Separation Systems of Launch Vehicles	545
13.4.1 Operating Environment and Design Input	545
13.4.2 Integrated Design Aspects	546
13.5 Separation System Design Process	549
13.5.1 Lateral Separation of Strap-on Motors in Atmospheric Phase	550
13.5.2 Longitudinal Separation of Large Stages	552
13.5.3 Payload Fairing Separation	557
13.5.4 Upper-Stage Separation	558
13.5.5 Role of Separation Dynamics Studies in the Separation System Design	561
13.6 Explosive devices used in separation systems	562
13.6.1 Bolt Cutter	563
13.6.2 Explosive Bolts	563
13.6.3 Explosive Nuts	564
13.6.4 Flexible Linear Shaped Charge (FLSC)	565
13.6.5 Confined Detonating Cords	565
13.7 Separation and Jettisoning Mechanisms	566
13.7.1 FLSC-Based System Separation	566
13.7.2 Merman Clamp Band Separation System	567
13.7.3 Ball Lock Separation System	569
13.7.4 Collet Release Separation System for Upper Stages	570
13.7.5 Ball-and-Socket Joint-Based Lateral Separation System	572
13.7.6 Linear Bellow- Based Longitudinal Separation System	573
13.7.7 Expanding Tube Separation System	575
13.8 Testing Methodology for Fault-Free Performance	575
13.9 Vehicle Destruct Systems	577
13.10 Other Stage Auxiliary Systems	579
Bibliography	580
14 Navigation Guidance and Control System	581
14.1 Introduction	582
14.2 Requirements of NGC System	584
14.2.1 Functional Requirements	584
14.2.2 Systems Requirements	584
14.3 NGC System and Integrated Design Requirements	585
14.3.1 Functional Configuration of NGC	585
14.3.2 Integrated System Engineering Approach for Design	586

14.4	Navigation System	588
14.4.1	Navigation Sensors	591
14.4.2	Navigation Computations	595
14.4.3	Characterization of INS Errors and Performance Specifications	601
14.4.4	Redundancy Management	602
14.4.5	Aided Navigation	603
14.5	Guidance and Steering Law	604
14.5.1	Guidance System Objectives and Functional Requirements	605
14.5.2	Guidance Concepts	606
14.5.3	Closed Loop Guidance Schemes	608
14.5.4	Implicit Guidance Schemes	608
14.5.5	Explicit Guidance Schemes	614
14.5.6	Guidance Robustness and Velocity Reserves	621
14.5.7	Mission Salvage Aspects	622
14.5.8	Mission Accuracy Achievable by Guidance System	622
14.6	Autopilot and Control Law	623
14.6.1	Functional Requirements and Specifications of Autopilot	624
14.6.2	Design Criteria and Guidelines	626
14.6.3	Autopilot Design Methodology	627
14.6.4	Vehicle System Dynamics	632
14.6.5	Additional Design Considerations for Autopilot	642
14.6.6	Robustness Aspects and Design Validation	644
14.7	Control Power Plants and Actuation Systems	647
14.7.1	Functional Requirements	647
14.7.2	Types of Control Systems	647
14.7.3	Salient Design Aspects and Specifications for Actuation Systems	651
14.8	Integrated NGC System Validation	654
14.8.1	Requirements and Simulation Test Beds	654
14.8.2	Integrated Validation Strategy	657
14.8.3	Progressive Tests with NGC Hardware in the Loop	658
14.8.4	Criteria for Generation of Test Cases and Validate Results	659
	Bibliography	660
15	Re-entry Missions	663
15.1	Introduction	664
15.2	Operating Environment and Reentry System Design Guidelines	666
15.2.1	Reentry Flight Environment	668
15.2.2	Reentry System Design Process	672
15.2.3	Reentry System Mission Management	674

15.3	Reentry Dynamics and Reentry Vehicle Configurations	675
15.3.1	Reentry Dynamics	676
15.3.2	Ballistic Bodies Reentry	678
15.3.3	Influence of Reentry Flight Path Angle	680
15.3.4	Influence of Vehicle Lift on the Reentry System	682
15.3.5	Skipping Trajectory Reentry System	683
15.3.6	Range Capabilities and Reentry Foot-Print	686
15.3.7	Winged-Reentry Vehicles	688
15.4	Aero Thermodynamic Environment and Reentry Vehicle Design Aspects	690
15.4.1	Reentry Hypersonic Flow Environment	690
15.4.2	Hypersonic Flow Over a Typical Reentry Vehicle	692
15.4.3	Hypersonic Aerothermodynamics	693
15.4.4	Reentry Heating	697
15.5	Reentry Mission Management	703
15.5.1	System Requirement	703
15.5.2	Reentry Trajectory Guidance Strategy	704
15.5.3	Reentry Guidance system	710
15.5.4	Terminal Area Energy Management (TAEM) Phase	718
15.5.5	Approach and Landing Phase	719
	Bibliography	720
	Annexure A: Mathematical Modeling Aspects of Vehicle Dynamics	721
A.1	Propulsion Model	721
A.2	Aerodynamic Model	727
A.3	Jet Damping Model	730
A.4	Slosh Model	731
A.5	Mass Properties	734
A.6	Control Power Plant Model	740
	Annexure B: Inertial Sensors	745
B.1	Gyroscopes	745
B.2	Different Types of Gyros	746
B.3	Accelerometers	750
	Nomenclature	755

Book for Practicing Space Technologists and Academicians

Space is the last frontier of the human race. The rising quest of humans about the universe and solar system as well as the curiosity to understand planet Earth itself as a total system, has kept up space exploration as an exciting, enterprising, and exacting professional domain. Space-based systems for communication, broadcasting, navigation, and earth observation as well as their downstream value chains have been making profound impact in accelerating the socioeconomic development and improving the quality of life of humankind. Space has also emerged as an indispensable medium of strategic importance. Security of space assets, space commerce, space economics, space law, and space diplomacy emanate from this unique potential of outer space. The recent stride in planetary exploration, space manufacturing, space robotics, human-in-the-loop, space colonization, and space tourism has accelerated global and national synergies in exploration and utilization of outer space.

Central to this human endeavor is the development of capability in space transportation systems that are crucial for reaching out to the outer space defying Earth's gravity and atmosphere and ensuring a safe reentry to Earth when required. In this book, Dr. B.N. Suresh and Dr. K. Sivan have brought out the wealth of their knowledge gained in their long journey with decisive roles at the Vikram Sarabhai Space Centre (VSSC), Thiruvananthapuram, the lead center of ISRO for the development of space transportation systems.

Dr. Suresh started his illustrious career as a control engineer in 1969 when SLV-3 was in the conceptual phase, and he led the development of the fin tip control system for SLV-3. Later, in the 1980s he shouldered responsibility to develop the navigation, guidance, and control systems for Indian launchers (ASLV, PSLV, and GSLV). He steadily rose to become the director of VSSC (2003–2007), member of the Space Commission (2005–2009), and founder-director of the Indian Institute of Space Science and Technology (2007–2010). The successful space capsule recovery experiment of 2007 was largely executed under his direct technical guidance. Since 2011, Dr. Suresh has been diligently

chairing the pivotal Mission Readiness Review Committee that gives final technical clearance for ISRO's launch missions.

It is pertinent to state that Dr. Suresh has been my friend, philosopher, and guide since my entry into VSSC in 1971, and both of us cherish being groomed under the tutelage of Dr. Suresh Chandra Gupta (Director, VSSC during 1985–1994), who had truly been a stalwart in ISRO. Also, it was my special honor to succeed Dr. Suresh as director of VSSC in 2007, and he became a role model of an ideal predecessor, in my view. I gratefully acknowledge the yeomen support that I received from him since November 2009 in my stint leading the Indian Space Programme.

Dr. K. Sivan is a multifaceted launch vehicle expert with rich experience in control and guidance as well as mission design, simulation, and synthesis of PSLV and GSLV. He also spearheaded the Re-usable Launch Vehicle Technology Demonstrator Project, the Aeronautics Entity of VSSC. He took on the heavy mantle of the GSLV Project in its most crucial phase and led from the front toward its historic successful flight (GSLV-D5) with Indian Cryogenic Stage in January 2014. In July 2014, ISRO entrusted Dr. Sivan to lead its Liquid Propulsion Systems Centre. I cherish my intense professional association with Dr. Sivan in my capacities as director of VSSC and chairman of ISRO.

This book is a confluence of theory and hands-on experience of Dr. Suresh and Dr. Sivan, synthesized from (a) the 44 missions of Indian launchers so far, (b) the innovative mission design for the launch of Chandrayaan-1 and Mars Orbiter Spacecraft using PSLV, (c) the space capsule recovery experiment, (d) reusable launch vehicle technology, (e) development phase of India's next generation launcher LVM-3, and (f) the theoretical and experimental studies toward a possible Indian human spaceflight in near future.

One unique quality that both Dr. Suresh and Dr. Sivan symbolize is systems thinking insights into the complex interrelationships of large and multidimensional system such as the space transportation system. The book lucidly covers the integrated design aspects of space transportation systems for a given mission requirement and operating environment and the nuances of mission design; and it provides the basic understanding of astrodynamics; flight mechanics; aerodynamics; propulsion systems; aero-structures and materials; stage auxiliary systems; navigation, guidance, and control systems including inertial sensors; as well as reentry and aero-thermal aspects. The section on "Mathematical Modelling Aspects of Vehicle Dynamics" deserves a special mention.

This book will be of immense value to any practicing space technologist and academicians in the field. I whole-heartedly recommend this book for study by scientists and engineers aspiring a bright career in space science and technology.

Chairman, ISRO, Bangalore, India
December 20, 2014

Dr. K. Radhakrishnan

Nuances of Space Transportation Systems

The knowledge base of a space transportation system (STS) is vast and complex, spanning mathematical and physical sciences and an array of esoteric technologies. This book has covered the subject comprehensively. So, this note attempts only to highlight a few nuances, rather than for emphasis.

While disciplines encompassing propulsion, aerodynamics, structures, control, and guidance constitute the prominent areas of studies of an STS system, it is useful to master a few analytical tools. Modeling and simulation enable prediction of the performance and validation of the theoretical design and its embodiment. Significant deviations from prediction indicate a lot of possibilities, such as incomplete knowledge of the system, erroneous implementation of design, and deficiency in modeling and simulation. The search for remedies is self-evident. Finding of satisfactory remedies leads to virtual mastery of the design. The ultimate goal is the realization of optimum design with high reliability, thereby deriving attractive and creditworthy economic returns on investment in manpower and financial resources.

The job of STS is to lift the satellite from Earth to a required orbit. The defining output parameters of an orbit are apogee and perigee heights and the angle between the equatorial and the orbital planes. A host of parameters of STS, such as velocity addition capability defined by the mass of the propellant, its specific impulse, inert mass of combustion chambers, and other hardware, constitute some of the crucial input parameters. Some other parameters are the duration of combustion of propellant, vehicle attitude profile of the trajectory, duration of coast phase, and altitudes of staging. The study of relative sensitivities of the output parameters to the various input parameters helps to grade the weightages to be assigned during the optimization exercise. This procedure is known as sensitivity analysis. It is a cardinal systems theoretic procedure for the optimization of design.

The input parameters may have a range of values within upper and lower bounds. All subsystems of STS will have intended mean values of the input parameters and also a statistical distribution. It is beneficial to map the output parameters as function of the input parameters, in order to identify boundaries of

acceptable outputs. Acceptability may be in respect of limits of safe excursions. This procedure too comes under systems theoretic procedures and is referred to as the Monte Carlo Simulation.

STS also termed as a satellite launch vehicle (SLV) is a multistory towerlike structure, each story/stage housing its main propulsion elements, control actuating devices, and auxiliaries for staging, such as sensing instruments, data collection and processing elements, and stage sequencing and transmitting circuits. An SLV is erected on a launch pedestal, which is fitted with flame deflector; required passivation facilities; launch-hold-and-release mechanisms, if required; and a network of fluid fill-and-drain accessories and gas charging devices. Each stage has its own command destruction ordinances. In addition to stage-specific elements, there are equipments which serve the entire vehicle from liftoff to the end of the launch phase, requiring their housing on the last stage. A central inertial navigation system; onboard processors; telemetry, tracking, and tele-command units; onboard sources of electrical power supply; and conditioning units are some of them and are housed at the top stage of the vehicle. The satellite, referred as payload, is housed on the top stage of the SLV. It is protected against the aerodynamic and solar heating by a payload fairing during the atmospheric phase of the launch.

The totality of propulsive units located in various stages constitutes the entire lifting and velocity imparting capability of the STS. The stages operate in a sequence, taking the satellite from Earth to the point of injection of the desired orbit. Sizing the STS starts with sizing of propulsion units, basically to meet the ideal velocity requirement, which is an estimate of the total energy required to lift the STS mass from Earth to the orbital height and impart it to the orbital velocity to the satellite. Thus, it comprises potential and kinetic energies. Subtracting various losses, such as aerodynamic drag, gravitational pull during trajectory phase yields the net velocity addition capability. Propulsion units impart in sequence incremental velocities. Delta-v which is velocity addition is a function of the start mass, end mass, and specific impulse. Specific impulse is the figure of merit of the propellant. End mass, being inert from the propulsion point of view, comprises the combustion chamber, insulation, and nozzle hardware. Also, other inert portions of the stage belong to avionics, interstage hardware, and accessories. The overall weight is minimized by using structural materials with high strength to weight ratio. Minimization of electrical power consumption also offers optimization possibilities.

Jettisoning inert mass once its utility is over leads to higher payload performance. Corollary is to adopt as large a number of stages as practical. However it is not practical because each stage transition, known as staging, involves extinguishing the ongoing stage, transferring control thrusters located in the ongoing stage to those located in the next stage, separating the spent stage and ignition of the next stage. Each of these operations demands highly specialized devices with precise timing and enacting clean separation mechanism. As such, each staging is referred as the rebirth of the mission, which calls obviously for minimizing the number of staging. In this context, payload performance and reliability are mutually exclusive. So, selection of the number of stages depends on availability of infrastructure for developing large boosters.

While we are on the topic of propulsion, it is appropriate to discuss the potential benefits of air-breathing propulsion. Air-breathing propulsion involves drawing oxidizer from the ambient air enveloping the rocket motor, rather than carrying on board, which appears at first glance to be beneficial for payload performance. But a close look reveals serious counter-implications. The rocket has to fly at high speeds in order to take in air encountering aerodynamic drag, which is proportional to the square of the speed. Also, in this process the rocket experiences aerodynamic heating, which is proportional to the cube of its speed. Aerodynamic heating leads to thermal protection, which increases inert mass of the rocket. For these reasons, air breathing does not yield payload improvement to a satellite launch vehicle. Of course, when the mission of a rocket requires dwelling in air atmosphere, for reasons of stealth, air breathing is conducive to the mission performance.

Higher payload performance of STS requires lowest practical mass of the structural elements, as they do not contribute to propulsive action. Noting that mass of the structure is closely related to loads incident on it, the loads are minimized systematically. Scanning the sources of loads, we note that there are internal pressure loads in the combustion chamber as well as external loads. The latter are due to air flow past the STS, which increase with the angle of attack. Accordingly, the aim during design of nominal trajectory is to keep the effective angle of attack low. During the liftoff phase, once the vehicle clears the launch tower, the vehicle is made to roll to align the pitch plane with the desired launch azimuth. Then, a calculated pitch kick is imparted before commencing the pitch program. In order to keep the angle of attack low, the pitch program follows gravity turn. It is kept low by biasing the vehicle attitude program according to the predicted mean wind profile. To make the prediction as close to reality as possible, wind data is collected both for the season and the day of the launch.

The structure of STS is rigid only as a first approximation. Actually, it is a flexible body having bending mode shapes of fundamental and higher order. So, the delineation of the body axes is not straightforward. The propulsive thrust operates on this flexible body. The translational and angular movements have to be appropriately defined, sensed, and incorporated in mathematical computation of the trajectory. The facility to locate motion sensors is limited architecturally to interstages. As such, the angular rates of the flexible rocket body have to be derived mathematically from the measurements made with sensors constrained to be located in the interstages. This issue is handled satisfactorily and is evident from the innumerable successful launches into precise orbits and also operating autopilots without deleterious control-structure interaction. Yet another implication of flexibility is about 25 % higher consumption of control fuel.

Air flow past the rocket body assumes patterns depending on the surface geometry, speed of air flow, and viscosity and density of ambient air. So long as the flow is laminar, theoretical estimation of forces and moments incident on the rocket body is accurate and dependable. However, once the flow is separated, the boundary layer becomes turbulent, and the estimates are uncertain.

The role of control and guidance is to stabilize, steer, and guide the multistage STS from takeoff till injection of its payload into the planned orbit. Indeed, this role

is shared between the autopilot and the guidance system. Though the control, navigation, and guidance system relies on rigorous mathematics, it is simplified by approximations. The formulations take note of the fact that the mass, moment of inertia, center of gravity, center of aerodynamic pressure, and coefficients of various aerodynamic forces and moments vary continuously as the velocity increases and also the properties of enveloping air change. A simplifying premise is to assume that these parameters are constant during carefully delineated time slices. So, the duration of flight in lower atmosphere is divided in slices of time, such that the assumption of constancy during a time slice does not introduce a great deal of error in modeling. As instantaneous attitude errors in autopilot contribute to the buildup of the angle of attack, these errors have to be kept low by tuning up the autopilot.

Low cost access to space beckons all engaged in space transportation systems to contribute innovative ideas and realize them. Reusability like in the US Space Shuttle programme is one option. However, at present the prohibitively high cost of refurbishment has virtually doomed this approach. So cutting of cost of the current technologies in propulsion and structures appears as a fruitful approach. As the frequency of launches increases, pollution of the environment by propulsion elements will raise concern. So, the search for alternate fuels is bound to intensify.

This book covers architecture and design of space transportation system, the mission, and associated subsystems needed for the launch vehicles. It covers lucidly the various motivations for pursuing these areas for research and development. To comprehend any complexity, grasp of the underlying theory is indispensable. The book does justice to this requirement, such that both beginners and veterans will find it adequate. In this sense the book promises to be an adequate source of reference. It avoids unnecessary jargon and brings out the knowledge clearly and succinctly.

The authors have immense experience in design and development as well as in mentoring a large number of dedicated professionals. The content and presentation reflect these qualities.

Former Director, Vikram Sarabhai Space Centre
Thiruvananthapuram

SC Gupta

About the Authors

Dr. B.N. Suresh is Vikram Sarabhai Distinguished Professor at ISRO HQ. He is also president of the Indian National Academy of Engineering, Delhi; a member of the Board of Governors, IIT Madras; and chairman of the Research Board for Aeronautical Development Establishment, DRDO. After his degree in science and engineering from Mysore University, he took his postgraduate degree from IIT Madras. He got his doctorate under Commonwealth Scholarship in Control Systems from Salford University, UK. He joined Vikram Sarabhai Space Centre, Thiruvananthapuram, in 1969 and discharged several responsibilities before taking over as director of the Vikram Sarabhai Space Centre and served 4 and half years till the end of November 2007. He took over as founder-director for the newly established Indian Institute of Space Science and Technology (IIST) at Thiruvananthapuram in 2007 and served for 3 and a half years. He was a distinguished scientist and served as member of the Space Commission for 4 years. He was also distinguished professor at IIT, Bombay, and MIT, Manipal. His areas of specialization are design of launch vehicles; aerospace navigation, guidance, and control systems; actuation systems; modeling and simulation; and R&D management.

He is a fellow of several professional societies like the International Academy of Astronautics, Paris; Indian National Academy of Engineering; Astronautical Society of India; and Aeronautical Society of India. He was president of the System Society of India for 6 years. He was head of the Indian delegation in the United Nations Committee on Peaceful Uses of Outer Space (UNCOPOUS) at Vienna, Austria, for 4 years till 2007. He also actively participated in the International Academy of Astronautics (IAA) and International Astronautical Federation. He was the chairman of the selection board for 5 years of the S and T area for IAA. He was cochair of the program committee for the conduct of International Astronautical Congress (IAC) in 2007. He has won several awards and honors, and prominent among them are the “Dr. Biren Roy Space Science Design Award” from the Aeronautical Society of India; “Agni Award” from DRDO for achieving self-reliance; “ASI Award” for his contribution to space technologies, by the Astronautical Society of India; “Distinguished Alumni Award” from IIT Madras;

“Outstanding Achievement Award” by the Dept. of Space, Govt. of India; “Lifetime Contribution Award” in engineering by the Indian National Academy of Engineering (INAE) for his significant contributions for space technologies; “National Systems Gold Medal” for his lifetime contributions to large systems from the System Society of India; “Aryabhata Award” by the Astronautical Society for his invaluable contributions for aerospace developments; “Karnataka State Rajyotsava Award” for 2014 for science and technology, the top award from the Government of Karnataka; and “MR Kurup Endowment Award” by the Centre for Indian Consumers Research, Thiruvananthapuram, for his outstanding contributions in space education and research in 2015. In recognition of his meritorious contributions for science and technology, the Govt. of India conferred on him “Padmasree” during the year 2002 and “PadmaBhushan” during the year 2013.

Dr. K. Sivan is a graduate of Madras Institute of Technology and has done masters in aerospace at the Indian Institute of Science Bangalore. He got his doctorate from the Indian Institute of Technology, Bombay. He joined Vikram Sarabhai Space Centre, Thiruvananthapuram, in the year 1982 and has worked in the PSLV Project and Mission group of avionics dealing with various aspects of vehicle and mission design. Subsequent to the successful development of PSLV, he held various responsibilities such as group director of the Mission Synthesis and Simulation Group, project director of the Re-usable Launch Vehicle Technology Demonstrator Project; deputy director of Aeronautics and Structures entity dealing with various aspects of launch vehicle and mission design, testing, validation, and flight clearance. He was project director of the GSLV Project and presently the director of Liquid Propulsion Systems Centre. He is a distinguished scientist having expertise in the areas of project management, launch vehicle configuration, mission design, control and guidance design of launch vehicles, aerodynamics design, structural design, and mission simulation and testing. His contributions are well recognized by several awards and some of them are “Shri Hari Om Ashram Prerit, Dr. Vikram Sarabhai Research Award” for the year 1999; “ISRO Merit Award” for the year 2007; “Dr. Biren Roy Space Science Award” for the year 2011; “The Distinguished Alumnus Award for 2013” from MIT Alumni Association, Chennai; and “Doctor of Science (honoris causa)” conferred by Satyabama University, Chennai, for the year 2014. His technical and managerial leadership led to the historical achievement of most successful GSLV flights with indigenous cryogenic stage, making India proud.

He is a fellow of several professional bodies like the Indian National Academy of Engineering (INAE), Aeronautical Society of India (AeSI), Astronautical Society of India (ASI), and Systems Society of India (SSI). He held different positions such as chairman and vice chairman of local chapters of these professional bodies. His contribution to space science and technology plays a vital role in the successful launches of India’s launch vehicles.

Chapter 1

Space Transportation Systems: Introduction and Design Challenges

Abstract The satellite systems provide a number of services to mankind in the areas of societal applications. To derive maximum benefits from the satellites, they have to be positioned into the right orbital slot in space. Space transportation systems (STS) play a key role in transporting the satellites from Earth and placing in the specified orbits depending on the application requirements. With the limitations of the technologies available as on date, STS has to be configured with multi-stages and the vehicle subsystems have to be totally autonomous and automatic. To reduce the cost of launching satellites by a specified STS, the STS must deliver maximum payload mass into the specified orbit with very high accuracy. The vehicle must be highly robust and this poses conflicting requirements on the design of each of the subsystems. The robustness demand of STS increases many fold when the humans are onboard, and in such cases, the transportation systems have to meet the stringent requirements of human rating. Therefore, various aspects of the optimum and robust design of such STS satisfying all specified conditions are discussed in this chapter. The functional requirements of STS to transport these satellites to space or to bring back to the Earth, typical subsystems and operating environments are also included. Development cycles and cost aspects of STS are explained. The design challenges for the complex subsystems and the need for the integrated design using systems approach to arrive at an optimum, cost effective and robust design are also included. The development of advanced technologies involving design, characterization, testing, and qualification has a major implication on the cost and schedule for realization of the vehicle and their salient aspects are discussed.

Keywords Satellite • Space transportation system (STS) • Planet • Earth • Space application • Launch vehicle • Operating environment • Design cycle

1.1 Introduction

Space science and technology play a major role in the everyday life of mankind. Space-based satellite systems provide impeccable services to the common man in the areas of societal applications, quality and safety of daily life on the Earth. They act as platforms to carry out science experiments to discover various unknown

phenomenon of universe and solar system. In order to derive maximum benefits from the satellites, it is essential that they are positioned into the right orbital slot in space. Space transportation systems (STS) play a key role in harnessing space-based technology-enabled services by transporting these satellites from Earth and placing in the specified orbits depending on the application requirements.

To carry out these functions, the STS must be capable of lifting the satellite, fly successfully through the hostile environments and deliver the payload safely at the specified position with the required velocity. With the present day technologies, every satellite delivery requires a fresh vehicle thereby making the cost of launching prohibitively high. With the constraints of the technologies available as on date, STS has to be configured with multi-stages and the vehicle subsystems have to be totally autonomous and automatic. In order to reduce the cost, the STS must be able to deliver maximum payload into the specified orbit with very high accuracy. The vehicle must be highly robust and this poses conflicting requirements on the design of each of the subsystems. Therefore, the optimum and robust design of such complex STS satisfying all specified conditions is indeed a challenging task.

Over a period, technical advancements made in space arena demand transportation of human and materials to space and bring them back safely. The robustness demand of STS increases many fold when the humans are onboard, and in all such cases, the transportation systems have to meet the stringent requirements of human rating. In order to bring a payload from orbit to Earth, the STS subsystems must be capable of dissipating the energy acquired by the vehicle during its ascent mission. Very high thermal environment to the vehicle associated with energy dissipation process adds further complexity to the optimum and robust design of such STS.

Before looking into the various aspects of a STS, its design complexities and challenges, it is important to understand the end use of its payloads in terms of providing the essential data needed for the betterment of society and to explore the planets and Earth. Therefore some of the salient aspects of planets and Earth are presented here. The functional requirements of STS to transport these satellites to space or to bring back to the Earth, typical subsystems and operating environments are also included in brief. Development cycles and cost aspects of STS are explained next. Challenges involved in the design of the complex subsystems and the need for the integrated design using systems approach to arrive at an optimum, cost effective and robust design are given in the last section of this chapter.

1.2 Planets and Earth

It is believed that the universe took birth due to big-bang effect and consists of stars, planets, and their moons. It is estimated that the universe contains approximately 50 billion galaxies. Each galaxy is a large complex structure and has a distinct shape, consisting of billions of stars, dust, and gas. They are all held together by gravitational forces. The galaxies in certain part of space are grouped and known as

clusters. Group of clusters are known as super clusters. A star once born, starts to shine and changes too. The process of change depends on the nuclear energy produced in it and the mass of the star. Once the hydrogen supply of massive stars decreases, the center of the star begins to contract thereby raising the temperature. At the same time, the outer part of star expands and cools and this makes the star as a Red Giant. The increased temperature and expansion cause the explosion and results into the end of the star. The explosion also causes a temporary brightness of millions of suns, a phenomenon known as supernova. Gravity of such a massive star forces the core to shrink, and as core shrinks, the gravity increases. The core continues to collapse and finally ends up with a singularity called black hole, which is a point mass of infinite density and gravity. Objects orbiting around a star are called planets.

The distances in space are measured in astronomical units (AU) and light years (ly). One Au is the average distance of Earth to Sun which is about 149.6 million km. Similarly, one ly is the distance traveled by light in 1 year which is about 9.46 billion km. The light from Sun takes about 8.3 min to reach Earth. It is told that the universe is continuously expanding, and hence the distances between stars change. The concentration of stars seen in the night sky is part of the milky way galaxy and it is about 100,000 ly across with 100 billion stars. On an average, the stars are 4 ly apart and Sun is one of the stars of the milky way galaxy. Earth is one of the planets of the Sun and thus the Earth is considered to be a tiny object in the universe.

The Sun, the eight planets, and the moons that orbit around the planets are a solar system and it is 27,700 ly away from the center of the milky way galaxy. Sun's energy is considered central to the existence of all planets including Earth and comprises 99.86 % of all matters of solar system and is spinning about its axis. While equatorial region takes about 25 days to complete one rotation, polar region takes about 35 days. Sun is made up of hydrogen and some helium and it is 0.3 million times heavier compared to Earth. The burning of hydrogen is termed as nuclear reaction and releases large amounts of energy. The energy generated at core passes through radiation and convection to the surface of Sun (photosphere) then through the atmosphere of Sun (chromosphere) to the outer space. It takes millions of years for the energy released to reach the surface.

1.2.1 *The Planets*

According to ancient Greeks, the Earth was the center of the universe and Sun and other planets moved around the Earth. While Copernicus, Polish astronomer, stated that the Sun is the center of the Universe, today's astronomers explored and learnt much about the Universe through the advanced scientific and technological investigations. The International Astronomical Union (IAU), which is responsible to oversee the celestial objects, recently decided that to define a planet, it should meet three important characteristics. First, it should have an elliptical orbit with Sun as one of foci. Second, it must have enough mass to generate the gravity sufficient to

maintain the hydrostatic equilibrium. Third, it must also clear its neighborhoods so that it is capable of clearing the debris around it. As a result of IAU's guidelines in 2006, there exists eight planets namely, Mercury, Venus, Earth, Mars, Jupiter, Saturn, Uranus, and Neptune. The Earth and the other planets in the Solar System are formed from the solar nebula, a mass of dust and gas left over from the formation of the Sun. All the objects orbiting the Sun came from the same cloud of gas and dust. Mercury, Venus, Earth, and Mars are formed from the dust nearest to the Sun and are called inner or terrestrial planets. Snow, gas, and dust together formed Jupiter, Saturn, Uranus, and Neptune. They are called gas planets and are treated as the bigger planets of the solar system. The inner planets have rocky cores and are smaller compared to gas planets which have a dense atmosphere. All these planets have liquid and rocky cores.

Comets, asteroids, and planetary moons are smaller bodies in Solar System, which are formed from the left over materials not swept into planets. While comets are snow and dust balls asteroids are millions of rocky objects orbiting as a belt around the Sun and located between the orbits of Mars and Jupiter. The smallest is tiny particle whereas the biggest one is Ceres, with the size more than 900 km. The gravity of Jupiter prevents these objects to form a planet. About 90 % of the asteroids are part of the asteroid belt whereas the remaining 10 % formed into two groups and orbit the Sun along the orbit of Jupiter. They are called Trojan asteroids, one group in front and other in the back of Jupiter.

The pieces of rocks originated from planets, asteroids, and comets are termed as meteoroids and travel through space and sometimes reach the surface of Earth. Meteoroids of smaller size burns when they pass through Earth's atmosphere and produce streaks of light called meteors. Meteoroids of large size survive the atmospheric friction and impact on the surface of Earth called meteorites. The meteorite impact causes a large crater, and hence it is a potential danger to the livelihood on Earth as it enters the atmosphere with very high speed.

There is a renewed interest by all space faring countries to explore the outer planets. Already several missions have been executed to Moon and Mars and more are being planned. Travel to Jupiter, Venus, and other asteroids are also being pursued vigorously to have better understanding of the Universe. Protecting the Earth from the meteorite impact and strategy of diverting the meteors from impact is another major study being pursued worldwide.

1.2.2 *The Earth*

As per the estimates available, Earth was formed about 4.6 billion years ago. It was a cloud of gas and dust in the beginning and remained very hot for a long period. It gradually started cooling down to form a solid crust and the water vapor started accumulating due to storms from time to time.

Periodic eruptions which released the gases and water vapor from the surface of the Earth also happened and this release is said to have formed the atmosphere. The

water collected in pockets formed the oceans. The crusts split into blocks are the plates and they have been moving continuously causing the change of the surface by forming new landmasses and mountains. Plates continue to move even today causing earthquake time to time in different part of the globe. The Earth is having a major advantage in that it is just at the right distance (about 150 million km) from the Sun and it is neither hot nor cold. Two substances available on Earth i.e. water and oxygen facilitate the existence of life.

Earth is considered as a sphere with an average radius of about 6,370 km and mass of about 5.98×10^{24} kg with a mean density of about $5,520 \text{ kg/m}^3$. The mean density of materials near the surface of Earth is about $2,700 \text{ kg/m}^3$ and the density of inner core is much higher. The outer layer of the Earth is crust with a layer of rocks with varying thickness. Beneath the oceans, the depth is about 6–11 km whereas under mountains, the depth of crust extends up to 70 km. Below the crust, there is mantle which is a partially molten layer extends up to about 2,900 km. Below the mantle, there is outer core with the thickness of about 2,000 km, which is mainly molten iron and nickel. Beneath outer core, there exists the solid inner core, made of iron and nickel with the size comparable to the size of Moon. The Earth rotates about its spin axis with a rate of about $0.25'/\text{s}$. The inner solid core portion of the Earth spins faster than the outer liquid core. The rapid spin and molten nickel-iron core provides extensive magnetic field which shields us from all harmful radiation coming from Sun and other stars.

Oceans cover 70 % of the Earth's surface. The shape of the Earth is an oblate spheroid having a pear sphere with equatorial radius of 6,378.14 km and polar radius of 6,356.755 km. A better approximation to the Earth's shape is that its north polar radius is about 38 m longer than south polar radius and the equator is an ellipse with major axis of about 138 m longer than the minor axis (further aspects of Earth are detailed in Chap. 6). The planet Earth is not only a complex system but also a combination of several interconnected processes which generate conditions suitable for life. A change in one part has unpredictable impact on other parts. The Earth provides all the materials and resources needed for human life.

Earth observation satellite missions provide data to improve the quality of life on Earth in terms of surveying the natural resources and identifying the damage done to the resources by exploiting them thoughtlessly. These satellites also provide valuable data for the safety of life on the Earth through early warnings of natural disasters which are caused by the change of processes of the Earth systems.

1.3 Satellites and Space Applications

The space assets are essentially the effective satellites in orbit, with a variety of application provisions. These satellites are essential tools to maximize the social, environmental and economic benefits of any country including the needs of the national security. Therefore, more and more nations all over the globe are

establishing the space assets to meet their national needs. The various space applications can be broadly classified as:

1. Telecommunications and broadcasting
2. Remote sensing and Earth observations
3. Satellite navigation
4. Weather monitoring
5. Disaster warning
6. Scientific satellites

1.3.1 Telecommunications and Broadcasting

Communication satellites provide a variety of societal applications for the daily use of common man in a most efficient and cost effective way. Satellite telecommunication systems today offer a variety of services like fixed and mobile telephone, data services, radio and broadcast services, internet and other IP-based information services, etc. covering the entire globe including the territories which are difficult to access. These systems also provide communications to ships and offshore platforms and to flying aircraft. The services offered can be widely categorized as the fixed satellite services (FSS), the broadcast satellite services (BSS) and the mobile satellite services (MSS). The BSS satellites today with very high powered beams provide the radio or television services directly to end users. These services have become economical over a period by having smaller receiver terminals, and their installation and operation have become quite simple. The MSS have been offering excellent services to all users who are in motion in maritime, airborne and land-based systems. The MSS satellite is initially designed for the maritime service and later extended to support both airborne and land-based mobile services. The other communications satellites services are short messaging services and hybrid communications services, which are directly linked to space navigation services.

To achieve the effective and efficient usage of modern communication satellites, depending on the region, applications and requirements, these satellites are placed in geostationary orbits, Molniya orbits and low Earth orbits (LEO).

1.3.2 Remote Sensing and Earth Observations

Earth observation satellites provide information regarding the global environment and play a key role in the quality and safety of everyday life of humankind. Space remote sensing offers significant advantage in the survey of natural resources on Earth, weather prediction, environmental analysis and many other applications. The identification of natural disasters by Earth observation satellites provides vital information for the disaster management. It is also used for military reconnaissance

by more and more nations. The usage of Earth observation satellites for such applications provide a cost effective solution, whereas other data sources are very expensive or too much restricted in scope or in some cases, it is not feasible too.

Over a period, a wide range of sophisticated sensors are being utilized to capture the data across a broad spectrum, both above and below visible light, the analysis tools and skills have also improved. The introduction of modern electro-optical systems and advanced processing systems has facilitated the easier data acquisition, storage and analysis not only for Earth but for all the neighboring planets. With continuous improvement of spatial resolution from 80 to 1 m to under 0.2–0.5 m with the ultrahigh resolution systems, the monitoring quality has improved substantially. Further, the careful integration of different types of remote sensing data, with other types of information from various sources, has practically led to many new scientific investigations and practical applications. The Geographic Information Systems (GIS) facilitate the integration of remote sensing data with population, all other demographic data in situ, GPS positioning and other relevant data. It has now become a powerful tool and has a large segment of commercial market compared to remote sensing.

Sun synchronous polar orbit, between 500 and 1000 km, enables excellent coverage of the entire planet on a regular basis with reasonably good or moderate resolution and is used for Earth observation satellites. This orbit also helps for the satellite to pass over the same location at the same time of day with same solar illumination which is essential for these applications.

1.3.3 Satellite Navigation

Another important application is the satellite navigation. This ranging through the use of satellite positioning systems started basically for the scientific research. The initial use of these satellites was for position and location. In order to provide accurate position information within a specified region or for the global coverage uninterruptedly for 24 h basis, satellite navigation system consisting of multiple satellites in different orbits is required. These space-based navigational systems have the capability to provide the real-time information all over the world whether on land, seas or in the air. These space systems, with increasing accuracy, can inform the precise location of any object of interest which is needed for a variety of applications. With such data, one can track the goods anywhere in the global transportation network. Another highly sensitive application is to assist the aircraft in the takeoff and landing. When the navigation system is utilized for strategic purposes, the deactivation of the same at a crucial juncture is one of the major concerns. This has led to the development of independent satellite navigation systems by different countries which helps them to utilize their own system for strategic purposes rather than depending on some other nation for such services.

Satellite navigation and positioning systems have evolved over a period. The development of extremely precise atomic clocks which are precise within

picoseconds has immensely helped to identify the precise location and positioning. A multiple network of satellites in a carefully designed constellation helps the ground receivers to instantly calculate one's precise location on the Earth. With the tracking of four or more satellites at exactly the same time, the propagation time between various visible satellites can be precisely estimated. Nowadays, the navigation systems are widely used by car rental agencies, bus, rail systems and shipping lines. They are also used to precisely estimate the time and to synchronize computer networks or communications systems. There has been spectacular development of software needed for satellite positioning and navigation systems. This has helped to identify precisely the location of roads, highways, railroads, canals, rivers, bridges and the layout of towns, cities, colleges, industrial and governmental complexes and many more.

1.3.4 Weather Monitoring

The weather monitoring satellite enables a synoptic view of weather patterns, sea ice and all other relevant features needed for the forecast of weather. The advantage of weather satellite is the global coverage, especially remote areas and oceans wherein the conventional methods of observations are not possible. These satellites are important for every nation to have reliable weather forecasts, key storm warnings and to forecast potential disaster alerts in case of hurricanes, tornadoes, floods and many other hazardous meteorological events. Weather satellites in the geosynchronous orbits offer an advantage of continuously viewing a portion of the globe at a lower resolution. Presently a host of such satellites, operated by a number of nations all over the globe provide data on weather and broad climate conditions. This global view has helped to improve the understanding of global weather patterns and also the ability to accurately forecast the weather. The sophisticated instruments on board the meteorological satellites gather a wide variety of essential data for climate change studies. Satellites can detect not only atmospheric temperatures, cloud cover, oceanic current flows and pollution but also monitor the storm development and their energy levels. These satellites can provide imaging and soundings over a wide range of frequencies from microwave, infrared, multi-spectral imaging (in the optical range) up to the ultraviolet spectra.

The mission of meteorological satellites in the recent times has been extended from the short-term weather forecasts to medium- and long-term forecasts as well. There has been continuous effort to further expand from weather forecasting to environmental monitoring. This is essential to have a better understanding on the influence of atmospheric, oceanic and glacial pollution on environmental issues. With the combination of data from polar and geosynchronous meteorological satellites, the ability to predict weather accurately has improved considerably. Reliability has also increased substantially including the prediction for longer periods of time.

1.3.5 Disaster Warning and Management

Natural disasters of varying intensity can happen anywhere in the globe, ranging from less frequent like earthquake, volcanic eruption to more frequent like floods, drought, cyclones, landslides, etc. One of the key elements in disaster management is the right mitigation strategy. One good example is the use of satellite system with cyclone tracking for the early warning. In present times, this is effectively utilized to reduce the loss of human lives and livestock. Similarly using digital sound broadcast system, audio alarms can be sent out to selected areas as warning system. The MSS terminal can be used for sending the short messages directly through satellite. The satellite phones are also utilized for effective audio communication from remote areas. Such a system can send video pictures of the affected areas.

Remote sensing techniques are effectively utilized for an accurate assessment of the affected area/s during disasters. The optical remote sensing data has limited application in providing such an assessment due to cloud cover during the cyclones and subsequent flooding. In such circumstances, the data from microwave sensors like radars are very useful to overcome the problem of cloud cover. Effective integration of data from satellite communication and remote sensing not only plays a very major role in the disaster management system but it offers excellent services to save the lives of the people due to natural disasters. Some of the important tasks in disaster management are creating data base for flood and cyclone prone areas, ortho-photomaps of cities and towns located in high risk seismic zones, GIS-based decision support systems, etc. Application satellites play a major role in the world's search and rescue (SAR) infrastructure for the stranded passengers, crews of shipwrecked vessels or people affected due to natural disasters.

1.3.6 Scientific Satellites

Although considerable amount of research work has been carried out in space sciences, still there are many more mysteries on the structure and evolution of the universe, the processes of planet formation, the origin of life, etc. Satellites facilitate to conduct several space-based experiments to improve our understanding of science in several areas like aeronomy, astronomy, high-energy cosmic ray variability using neutron/meson, equatorial electro jet and spread-F ionization irregularities, ozone, aerosol and cloud phenomena, middle atmospheric radiation, dynamics and electrodynamics, solar physics, IR astronomy, neutron star and black hole astrophysics, planetary science, origin/evolution of life and so on. Other interesting areas in science are competence building in planetary science studies, development of sensors for planetary probes/missions to the moon or to asteroids or nearby planets and microgravity science/ exploration programme. The size of the satellite and the orbits are to be defined based on the specific scientific application. There are dedicated small satellites to undertake the specific

phenomenon of one or more areas listed above. Small satellites also provide opportunities, particularly for scientists from universities and academic institutions.

There are two types of scientific satellites viz., astronomy satellites and space exploration satellites. An astronomy satellite is basically a big telescope placed in orbit. Due to the absence of atmospheric effects, these satellites can see deep into space and are used for in-depth analysis of such science experiments. Generally these satellites are placed in low earth orbits. On the other hand, space exploration satellites are space probes (not orbiting about planet) sent deep into space to discover the new phenomenon which are not known to mankind and provide insight into the universe, understanding the origin and history of universe and solar system, etc.

1.4 Space Transportation System

Various satellites used for different applications are to be positioned in their predetermined orbits to carry out the intended function. In certain cases, it is essential to bring materials back from space to Earth. Space transportation systems are used to carry out the above functions precisely and safely. In order to meet the various applications, the functional requirements of STS can be categorized as given below:

1. Earth to orbit, to position the satellite
2. Earth to orbit and return, for the transport of humans
3. Earth to orbit and return for cargos
4. Orbit to orbit, for deep space voyages

Considering the system requirements, the STS can also be broadly categorized into

1. Launch vehicle (LV), to transport a payload from Earth to space
2. Reentry vehicle (RV), to transport a payload from space to Earth

Various features of STS, operating environments and design and development issues such as cost aspects, subsystems complexities and design challenges are explained in the following sections.

1.4.1 *Broad Systems Requirements*

1.4.1.1 **Systems Requirements for Ascent STS (Launch Vehicle)**

The primary function of the space transportation system (STS) is that it has to deliver the identified satellite into its specified orbit. The satellite orbits are generally Keplerian trajectories around Earth. For a satellite to remain in the specified

orbit for its entire service period, it must possess the specific energy (additive of potential and kinetic energies per unit mass), defined by the size of the orbit. As an example, the satellites placed in low earth orbit (LEO) have specific energy of about 33,000 kJ/kg and that in geo transfer orbit (GTO) has the value of about 54,000 kJ/kg and for the interplanetary missions, this value goes up further. Therefore, to position a satellite with a defined mass (m), in the specified orbit with the specific energy (ϵ), the STS must be capable of injecting the satellite with the required energy (ϵm). Energy requirements for orbital missions are large compared to that of conventional transport systems. The energy for injecting higher mass satellite or higher orbit is even more as the total energy is the product of specific energy, ϵ and mass, m of the satellite. Conventional transport systems cannot generate such huge energy and it is feasible only by rocket propulsion systems. STS uses rocket propulsion system's chemical energy to generate the kinetic and potential energies required for a satellite delivery. Therefore, size of the propulsion systems required to carry out the specific function depends on the available propulsion system's energy. With the available matured technologies as on date, STS has no option but to adopt multi-stages chemical propulsion systems to achieve the energy level as required.

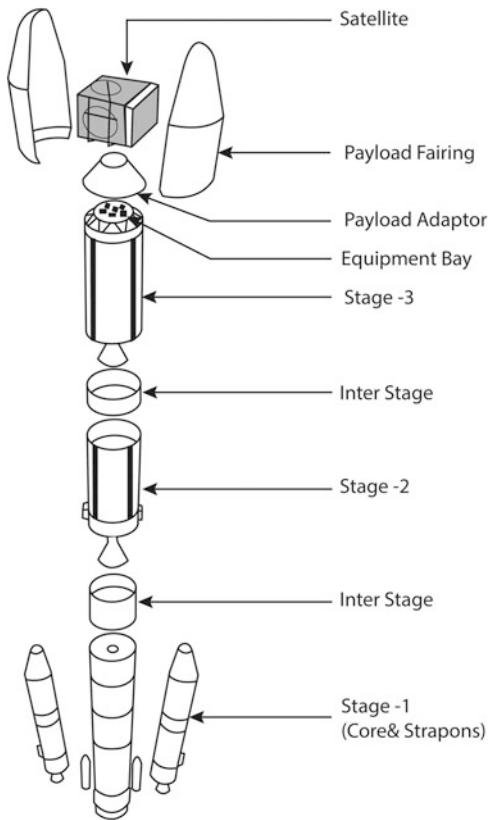
To meet the desired orbital conditions of satellites precisely, the propulsion energy of STS has to be directed in the optimum direction to achieve the required position and velocity accurately. To execute flawlessly these functions, the vehicle has to be stabilized against the disturbances encountered during its flight and has to be directed to follow the desired trajectory during its entire mission. These functions are achieved by navigation, guidance and control (NGC) systems of STS. These systems consist of linear acceleration and attitude rate sensors, navigation, guidance and control algorithms, its software, onboard computers and control power plants.

Vehicle structural systems are basically load carrying members of the vehicle, which comprises of structural elements of propulsion stages, inter-stage structures, payload fairings and interface elements. In addition to meeting their basic functional requirements, the structural systems provide the shape to the vehicle and houses avionics and all other associated elements. These systems are built with different types of materials having different strength-to-weight ratios and meeting the strength requirements while minimizing the mass.

Since the STS is generally configured with multi-staging concepts, various staging events like separation, ignition, etc. require ultrahigh reliable systems called stage auxiliary systems. These systems involve high energy materials. The electrical systems also play a major role in the STS design and integration of the entire vehicle.

During the atmospheric phase of flight, the vehicle encounters severe aerothermodynamic environment, which introduces high level of aerodynamic disturbances to the vehicle and harsh thermal environment to the vehicle systems. The aerodynamic shaping to reduce disturbance levels and selection of suitable thermal protection system are other major areas in the STS design process.

Fig. 1.1 Typical subsystems of STS (LV)



Various subsystems of a typical three stage launch vehicle are given in Fig. 1.1. The core and strap on motors form the stage-1 of propulsive elements, and stage-2 and stage-3 are other propulsion systems. Structural subsystems are the hardware of propulsive systems, inter-stages, payload fairing, payload adaptor and the structural element of equipment bay. Vehicle navigation, guidance and control systems and other avionics systems are accommodated in the equipment bay.

1.4.1.2 Systems Requirements for Descent STS (Reentry Vehicles)

The function of STS reentry vehicle is just opposite to the ascent phase of launch vehicle. To transport the satellite and materials from space to Earth, the energy imparted by the launch vehicle to place them in orbit has to be completely dissipated. This is done, utilizing the atmospheric drag during its atmospheric phase of flight. During this energy conversion process, the dissipated kinetic and potential energy are converted into thermal energy, which introduce severe thermal environment to the vehicle structure and to the contents housed inside the vehicle. To ensure safety of the vehicle, the vehicle subsystems have to be designed to

ensure “controlled dissipation” of the energy. Thermal protection system for such vehicles is a major design challenge. Functional requirements of other vehicle subsystems are similar to that of launch vehicle STS.

1.4.2 Operating Environments for STS

Vehicle subsystems have to be designed for their operating environments, which are originated by the external sources and within the vehicle itself. External operating flight environments are ranging from vacuum flight to highly complex and disturbed atmospheric flight. The atmospheric flight phase is mainly characterized by the larger aerodynamic disturbance forces and moments caused by large atmospheric winds. The atmospheric flight phase itself is highly varying due to wide regimes of flight Mach numbers ranging from 0 to 25 with the characteristics of large dispersions on atmospheric properties and wind variations. The problem is further aggravated with the dispersions on the aerodynamic characteristics with respect to the predicted ones.

Vehicle subsystems have to be designed for the static loads caused by the large thrust and high pressures. High thermal loads acting on structural elements of the vehicle propulsion systems and thermal stress induced loads caused by temperature gradients are other major operating environments. The loads caused by wind-induced aerodynamic loads, aerodynamic unsteady loads, control system response to aerodynamic disturbances, vehicle flexible dynamic loads, etc. are also important inputs for the design process. In addition, the design has to cater to the disturbances created within the vehicle due to fabrication imperfection and the dynamic coupling caused by the systems such as slosh and POGO due to their interactions with other subsystems. The design of subsystems should also ensure normal functions under the performance dispersions of various subsystems with respect to predictions due to various reasons.

1.4.3 Cost Aspects of STS

To achieve the required capabilities or to improve the system performance and reliability, often the advanced technologies have to be utilized. Development of advanced technologies involves design, characterization, testing and qualification. This has a major implication on the cost and schedule for realization of the vehicle.

Costs involved in the development and realization of advanced technologies and services of a STS are grouped into the following categories:

1. Design and development cost
2. Unit cost of a vehicle
3. Operating cost of a vehicle

1.4.3.1 Design and Development Cost

During design and development of a new vehicle, it is essential to develop a number of technologies which are suitable for the STS. Typical examples are development and characterization of new materials, advanced propulsion systems, avionics systems, etc.

Technology developments of an advanced propulsion system involve huge numbers of ground tests with sea level operating conditions as well as high altitude tests, simulating flight conditions to arrive at the optimum propulsion system for the STS. This demands establishment of test facilities, realization of development hardware, elaborate tests and analysis. Similarly to qualify the structural systems, it is essential to establish the elaborate test facilities, test fixtures and a number of qualification hardware.

To define a suitable external configuration, extensive wind tunnel tests and computational fluid dynamics simulations are essential. This involves fabrication of wind tunnel models, wind tunnel tests and high fidelity computer simulation facilities.

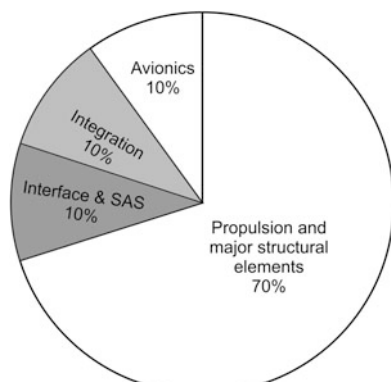
Regarding avionic systems, control power plants, engineering models have to be realized based on the proposed design and they are to be characterized extensively. These systems need to be validated at subsystem level as well as integrated system level. For this purpose, suitable simulation facilities and test laboratories have to be established and the systems have to be evaluated in the near real flight environment.

Design and development cost involves the design cost, costs required for the development towards the realization of development hardware, establishment of test facilities and operating costs for carrying out the tests. Thus this component of cost is a major cost towards STS design and development process.

1.4.3.2 Unit Cost of a Vehicle

Unit cost of a vehicle is the cost incurred for launching a satellite. Cost distributions for a typical STS system are given in Fig. 1.2. It is seen that out of the total vehicle

Fig. 1.2 Cost distribution of a typical STS system



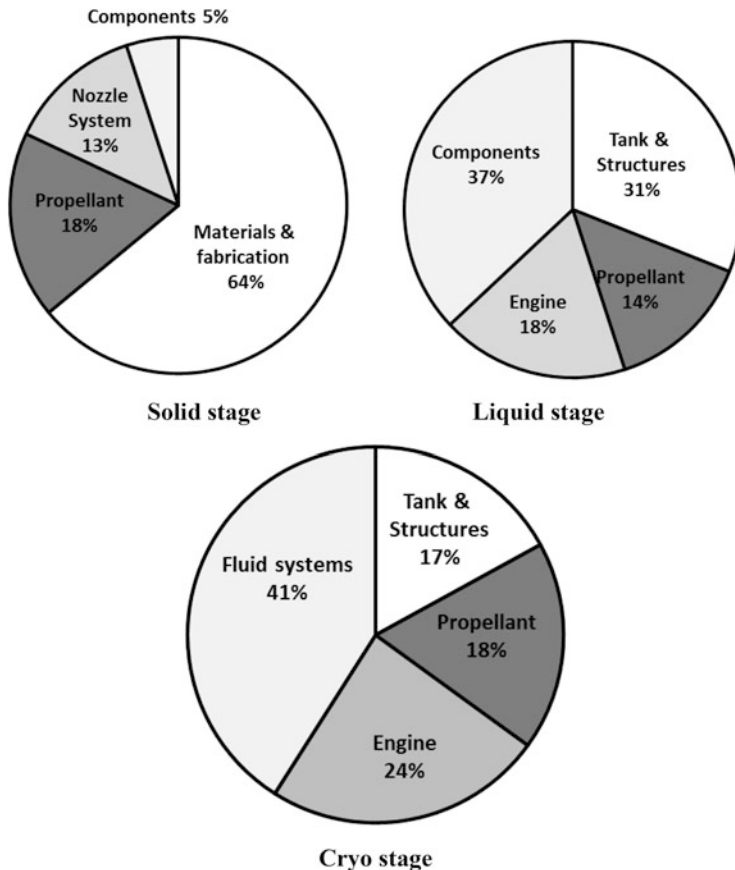


Fig. 1.3 Cost for different propulsion system

cost, propulsion systems along with the major structural elements cost about 70 %, avionics systems cost 10 %, interface systems along with stage auxiliary systems cost about 10 % and the total integration of the vehicle cost about 10 %. The propulsion and structural systems form the major part.

Typical cost break down of different propulsion systems including their structural elements of a STS is given in Fig. 1.3. It is seen that, out of total propulsion cost, about 14–18 % is the propellant cost and the remaining cost goes to structural elements and propulsion systems hardware. Therefore, the major part of vehicle cost goes to the material and manufacturing process. In order to reduce the vehicle cost, it is essential to minimize the material and fabrication cost. Even though a vehicle is efficient in payload carrying capabilities (i.e. vehicle with an optimum size having higher payload fraction), due to the use of advanced technologies, demanding expensive materials and fabrication make the cost of the vehicle quite

high. One of the strategies to reduce the cost is to reuse the vehicle propulsion and structural systems hardware after completing its defined function.

Although there has been a long debate over reusable launch vehicles (RLVs) vis-a-vis expendable launch vehicles (ELVs) to reduce the cost, so far the Space Shuttle is the only launch vehicle which has been used for multiple flights. But it was decommissioned recently due to several factors. Comparing the cost of reusable and expendable rockets is quite complex, and there is need to consider both recurring and nonrecurring costs while comparing. For each launch, the cost of a new expendable rocket is a recurring cost, and for reusable launchers, the construction cost is the upfront cost amortized over each launch. Because reusable launch vehicles have to fly many times, they have to be highly reliable and more robust. This results into higher initial costs and a possible reduction in the payload weight. Therefore, in order to design a feasible RLV capable of launching heavier payloads, advanced technology developments are essential in several disciplines especially in the areas of materials, propulsion systems and thermal protection system.

1.4.3.3 Operating Cost of a Vehicle

Each transport mission of STS needs preflight preparations and support during flight phase. This includes the checkout systems, ground servicing facilities for preparing the vehicle for a mission, range facilities for tracking the vehicle and acquiring the vehicle telemetry data during its flight. Cost involved in establishing these systems and their functions during preparation and flight phases of STS are termed operating costs.

1.4.4 Overall Design Guidelines

The primary function of a STS is the safe, precise and reliable delivery and injection of satellite/ human/materials to an orbit in space or back to Earth. With the expendable vehicle technologies, each mission requires a fresh vehicle, thus making the cost of space transportation to be prohibitively high. As the STS operations are totally autonomous and automatic, in order to achieve the successful mission, the designs have to be highly robust. While ensuring the reliable delivery through robust vehicle subsystems, cost effectiveness of the vehicle should also be a major driving factor for the STS design process. The economics of such a system has to include not only the vehicle costs and facilities but all the relevant operating costs. Considering the above factors, general guidelines for the design of a STS are as follows:

1. Trade-off between new technologies and existing ones with respect to meeting the payload capability requirements while reducing total cost (development, unit and operating costs) and schedule.

2. Trade-off between various options available for a particular system in the selected technology in terms of development costs and schedule as well as cost of material and manufacturing process.
3. For the selected option, optimum design of various subsystems to achieve maximum payload capability while meeting the specified robustness and reliability requirements.

In addition, during the design and development of a STS system, it is essential to ensure that the system caters to certain important requirements like (a) changes in payload specifications within a reasonable band, (b) varying mission requirements, (c) provision for the growth possibilities and (d) meet the projected schedules and cost within reasonable limits. Depending on the payload and the mission definition, the weight and volume requirements are to be worked out which are likely to be different. The STS system should have the capability to perform satisfactorily within the defined parametric variations. No doubt there has to be well-defined boundary limits for all the parameters, but aiming to design the subsystems to function even with wider range of dispersions beyond these bounds makes the system very robust.

The operational system should also possess the flexibility to position multiple payloads into a variety of orbits without having major changes in the configuration. It should possess the capability to return from the orbit under different conditions.

1.4.5 Design and Development Cycle for STS

The STS consists of multidisciplinary subsystems (Sect. 1.4.1), which are operating in severe environments (Sect. 1.4.2). Therefore, a clear understanding of the subsystem responses, their interactions and constraints etc. are essential to arrive at an optimum configuration, which makes the design and development cycle for a STS complex. It involves not only several interactive design procedures and iterations but also certain key design considerations as described in Fig. 1.4.

First and foremost, the mission definition has to be worked out based on the satellite mass and orbit requirements. The subsequent operation is to arrive at suitable vehicle configuration with well defined number of stages during the initial phase of vehicle definition. Similarly choosing the right propulsion systems to meet the specified objectives is another important design component. The selection of propulsion stages depends largely on the state-of-the-art technology available in propulsion systems. The main yard stick is to maximize the performance and minimize the overall weight of the vehicle. Continuous efforts are needed to decrease the structural weight and at the same time attempt to increase the propulsion performance without sacrificing the overall reliability of the vehicle.

The multidisciplinary analyses are inevitable to arrive at suitable configuration and also to derive the optimal performance of subsystems under various constraints. While making the performance analysis, it becomes essential to resort to several

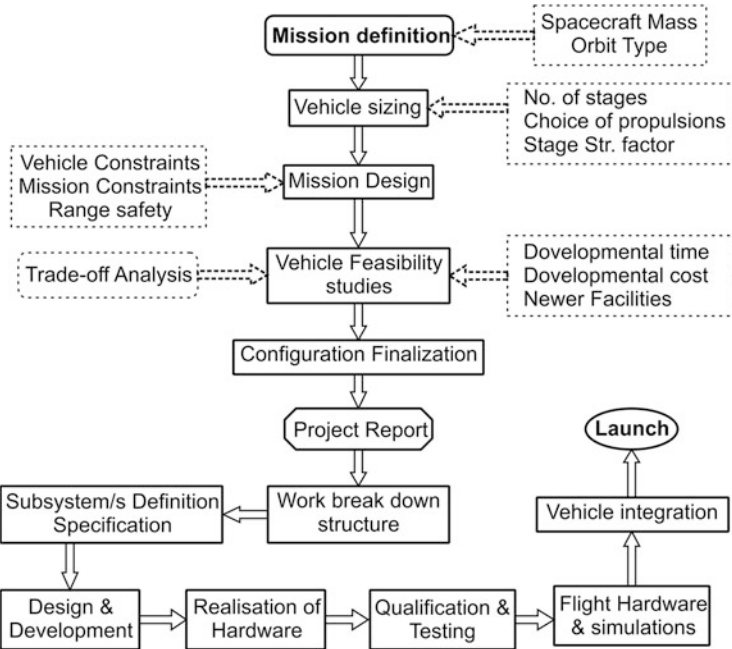


Fig. 1.4 Design and developmental cycle for STS

trade-off analyses to understand the conflicting requirements of various disciplines. It is equally important to maintain a balance between various competitive objectives to achieve the required performance without sacrificing safety, reliability and cost.

The newer facilities required for the realization of the subsystem or system, their testing and validation are also to be worked out. Once the overall configuration of the STS system has been arrived, it is important to generate a detailed Project Report giving all the necessary technical details. It should also contain the detailed work break down structure, facilities needed and the costing aspects.

Next logical step is to derive the subsystem definitions and specifications. The subsystems have to be designed for their operating flight environments. Once the design is completed, the development cycle includes the hardware realization, assembly and testing at different phases of operations. During the entire phase of design, development and testing of the subsystem/s or systems they have to be subjected to rigorous reviews at different levels. The specific phases of review milestones are conceptual design, preliminary design, detailed critical design, system readiness reviews, etc.

Uncertainties at the early phases of design and development in all these subsystems are quite high, due to the limited knowledge of their characteristics. The clarity on interactions between disciplines is also less. In addition, it is not possible to have the high fidelity simulations and detailed analyses due to the lack of

required data in the initial stages. Therefore, the system engineers have to spend considerable time to improve their understanding of the system characteristics, interdependencies and coupling between disciplines. They also have to carry out extensive trade-off studies to achieve (a) the optimum system performance, while meeting the reliability requirements (b) the minimization of the design cycle time, cost and risk and (c) the robustness of launch vehicle to meet uncertainties during the entire development phase.

1.4.6 Complexities and Design Challenges of STS

The complexities and design challenges of STS are mainly caused by the prevailing technology limitations to meet the various requirements as specified by the design guidelines and represented in Fig. 1.5.

While the conventional transportation system has a comfortable structural mass of about 55 % and fuel mass of about 23 %, which lead to the payload factor of about 22 % of total vehicle mass, the overall mass of the fuel is 86 % of STS mass. This huge amount is essential to achieve the specified energy as demanded by satellite orbits with the present day propulsion systems. After subtracting the propellant mass, the remaining 14 % only is available for structural components and for all other systems including payload.

The remaining 14 % for structural component is very small, specifically for the systems operating in the harsh environment. However, the structural components are to be further optimized to achieve 0.5–1 % fraction for payload. Configuring a vehicle to achieve these objectives and also to arrive at an optimum design to maximize the payload involves an elaborate task as highlighted in Fig. 1.6.

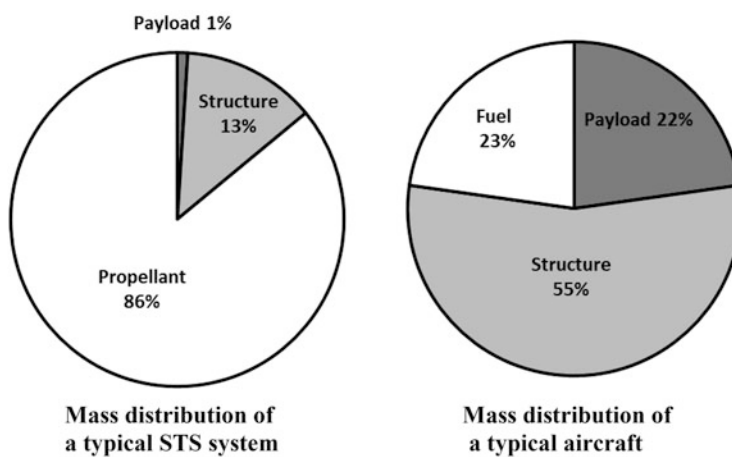


Fig. 1.5 Typical payload fractions

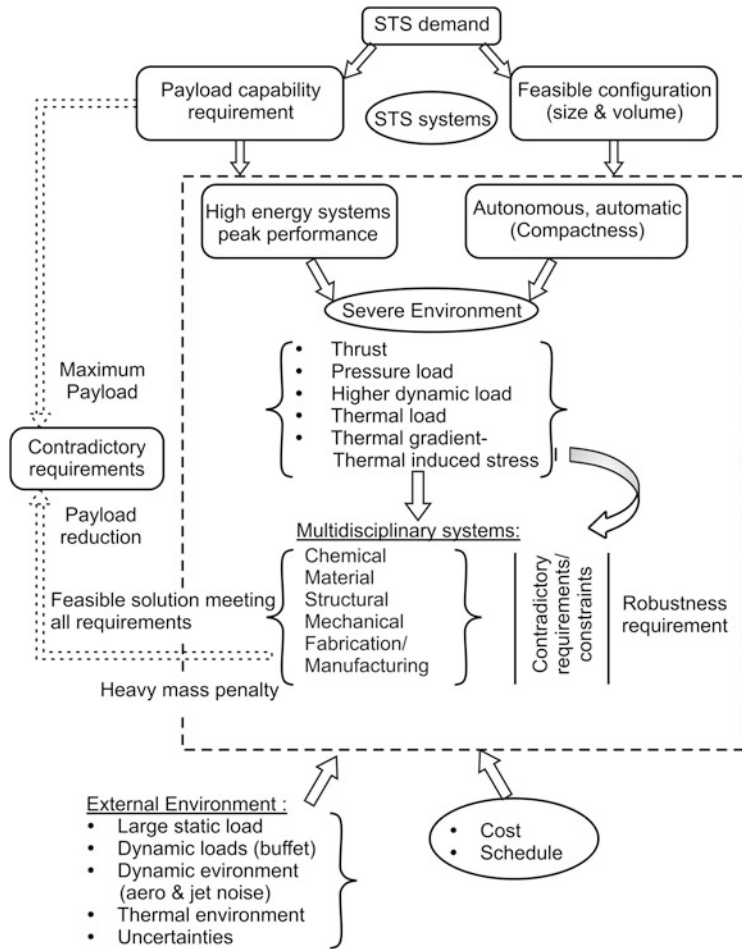


Fig. 1.6 Complexities of STS and design challenges

The various tasks of STS in flight have to be necessarily configured as autonomous. For example, both fuel and oxidizer necessary for the chemical propulsion from lift-off till end of its mission have to be carried by the vehicle, the electrical power for the operations of avionics systems has to be drawn from vehicle power system, the power required to drive the propulsion system turbines has to be drawn from that system itself and so on. Also, the present multi-staging concept demands that all the staging events to be automatic onboard, based on the real time decisions and the subsequent sequencing functions. The subsystems operations have to be automatically linked to the staging events.

Space transportation systems, especially the launch vehicles, are high energy systems, and in order to build a feasible autonomous and automatic system, these high energy systems are to be packed into a very small volume. Therefore, the

energy density for STS has to be very high. Also, these systems are required to operate at their peak performance levels with sufficient energy to deliver the specified payload in the specific orbit. Due to these features, the operating environment for the subsystems becomes very severe, in terms of very high static thrust load, pressure load, thermal load, higher dynamic load, thermal induced stress due to thermal gradient, etc. For avionics systems, which are high technology elements, packed in compact volumes have to operate at their peak performance and similar is the case for other subsystems too. These autonomous, automatic, high energy, high-end technology systems operating in severe environment add further complexities for the space transportation systems.

The subsystems operating under severe conditions need a robust design to ensure reliable operation. Various disciplines to be considered in the design process are chemical systems, material systems, structures, mechanical systems, manufacturing/fabrication processes, avionics systems, etc. Design robustness requirements for these disciplines are generally conflicting with each other. A design which meets the robustness requirement of all disciplines is extremely difficult and may not meet the objective of achieving maximum payload requirements. Therefore, optimum design of STS which gives maximum payload, satisfying robustness requirements and constraints of each discipline and each subsystem, requires several iterations. In order to arrive at such an optimum design, it is essential to understand the subsystems operating environments and the performance of the systems under these varying conditions.

In addition to the operating environment within the vehicle systems, external disturbances also severely influence the subsystems designs. The static aerodynamic loads, dynamic loads like buffet, dynamic environment such as jet and aero acoustic loads and thermal environment have major impact on the vehicle subsystems design. These additional flight environments along with their uncertainties further aggravate the design of the vehicle subsystems.

During the design process, previous experience on the design of similar systems has to be seriously considered. The uncertainties which cannot be predicted correctly by ground tests have to be properly accounted. To handle such situations, adequate design margins have to be provided. In addition, there may be a few uncertainties which are extremely difficult to assess. To account for such uncertainties, each and every subsystem has to be designed with adequate robustness. Generally, the first flight has to be used as a test bench to identify such issues and to incorporate the necessary corrections based on the flight performance, before attempting the subsequent flights.

In a launch vehicle flight, many of the subsystems have only one chance to operate and the operation has to be absolutely successful for the mission success. Propulsion modules and pyro elements are good examples of such subsystems. They are subjected to operation only in the flight after their manufacturing and assembly. Due to these factors, these systems have to be ultra reliable and extra efforts are essential in design, manufacture and integration of such systems. The overall quality management system for the realization of such systems has to be sound and elaborate to weed out the defects. Design of such complex space

transportation system has to meet all the specified requirements simultaneously and also has to satisfy the overall projected schedules and development cost. The design has to (a) accommodate the maximum payload, (b) minimize the overall cost and (c) ensure robustness and reliability requirements of subsystems. This demands an integrated multi-disciplinary design with systems approach. It is also essential that the interfaces between different subsystems, interdependencies of various disciplines, their impacts on constraints and performance of various subsystems and overall vehicle are to be considered in detail during the design phase itself. The essential features of the integrated design with systems approach are highlighted in the next chapter.

Bibliography

1. Hammond, W.E.: Design Methodologies for Space Transportation Systems (AIAA Education Series). American Institute of Aeronautics and Astronautics, Inc., Reston (2001)
2. Griffin M.D., French J.R.: Space Vehicle Design. AIAA education series (1991)
3. Gupta, S.C., Suresh, B.N., Sivan, K.: Evolution of Indian launch vehicle technologies. Spec. Ed. Curr. Sci. **93**(12), (2007)
4. Suresh, B.N.: Space transportation systems in India, present scenario and future perspectives. J. Aerosp. Sci. Technol. **61**(1), (2009)
5. Sankar, U.: The economics of India's Space Programme. Oxford University Press, YMCA, Library Building, New Delhi (2007)

Chapter 2

Integrated Design Aspects of Space Transportation System

Abstract The design of a launch vehicle demands close involvement of many disciplines like propulsion, vehicle structures, aerodynamics, flight mechanics, navigation, guidance and control (NGC) systems, vehicle avionics, stage auxiliary systems, thermal systems, etc. It is essential to integrate the requirements of these systems to obtain the best design for the specified mission, and the design iterations are inevitable to arrive at a good design. The interfaces among disciplines are not always well defined. Design of a launch vehicle is essentially making suitable compromises to achieve a good balance between many conflicting requirements and interactions. The design process also has to depend a great deal on analyses, experimentation and simulations. To arrive at an optimum launch vehicle design, it is essential to apply systems approach involving various steps like: (a) mission definition, (b) requirements analyses, (c) subsystems definition, (d) concept analyses and definition and (e) design. Design iterations are necessary to understand the interaction among subsystems, interfaces between various disciplines and relation between various design functions to meet the specified requirements. There are severe dynamic coupling between various systems which further aggravates the complexity of the design process. The clear understanding of the interfaces between various disciplines and their functional interdependencies with respect to various operating conditions is a vital factor. Therefore, it is essential to integrate various subsystems through a structured multidisciplinary process. The complex design problem of a launch vehicle can be handled only by understanding the roles of each of the vehicle subsystems and by utilizing the systems engineering approach right from the concept stage. As space missions are expensive, the quality, reliability and cost should get maximum attention all through the design and development phases. Various aspects of integrated design of STS using systems approach, which are essential to arrive at an optimum, robust and cost effective design of STS are explained in this chapter. An integrated approach for STS design evaluation using suitable vehicle system models to arrive at robust and optimum design is also discussed in brief.

Keywords System engineering • System life cycle • Requirements analysis • Trade-off analysis • Interdependencies • Interactions • Risk management • Propulsion • Structure • Aerodynamics • Vehicle sequence • Navigation • Guidance and control • Analysis of integrated system

2.1 Introduction

The objective of space transportation system (STS) is to transport a specified payload from Earth and deliver into the specified orbit in space depending upon the satellite mission requirements or to bring it back safely from orbit to Earth. Based on the present day technologies, nearly 85 % of the STS mass necessarily has to be propellant to provide energy to achieve the required orbital conditions, leaving only 15 % mass for the propulsion elements, structural systems and payload mass. The structural mass has to be optimized to carry the required payload to the specified orbit. Therefore, the payload carrying capability of the vehicle depends on the level of optimization in the vehicle system design. With highly optimized design, the payload can vary from 0.5 to 1.5 % of the vehicle mass, leaving the remaining 13.5–14.5 % to the vehicle structure which demands design of the STS to be highly optimum.

Each satellite mission demands a new vehicle, and for each mission, the vehicle cost has to account propellant, structural material, fabrication and operational cost as well as amortized developmental cost which in general is very high with the existing technologies. Therefore, the cost of launching a satellite is quite high and the economics of STS is generally expressed in terms of cost of launching per kilogram of satellite. There is a need to reduce this cost. Since the vehicle cost for a mission is fixed, maximizing the payload capability of the vehicle automatically brings down the cost per launch and hence the major functional requirement for STS design is to maximize the payload in a specified orbital mission.

Even though, the launch vehicle objective is to achieve the mission defined orbit, depending on the characteristics of the vehicle sub-systems, there would be deviations in orbital parameters achieved by the vehicle. The satellite, using on-board fuel, has to correct these deviations to bring the orbit to the target. To meet this requirement, satellite has to carry additional propellant which in turn reduces the mass of application payloads. If the STS can achieve the targeted orbit with high precision, then the satellite mass budget for on-board fuel can be reduced thereby increasing the application payload mass. This is a highly desirable feature from the customer/satellite user point of view. Therefore, the STS has to achieve the targeted orbital conditions with greater precision.

As of now, multi-stage STS is the only effective configuration for launching satellites into orbits around the Earth or for launching satellites into interplanetary trajectories. This necessitates smooth stage transitions for successful mission and many of the stage transition subsystems have only one chance to operate in flight after manufacturing. Such systems have to function without any failure to achieve mission success. Once the lowest stage is ignited through ground checkout system, the successive operations in flight are fully automated and autonomous. Therefore, to achieve successful mission, the STS subsystems have to be highly reliable.

In summary, the functional requirements of the space transportation system can be stated as to deliver maximum payload into the orbit with high accuracy and high order of reliability.

To maximize the payload, the propulsion systems have to operate at their peak performance limits and it results into severe operating environment for the vehicle systems in terms of high load, high temperature, high pressure, increased level of vibrations, etc. Also, operating environments for the structural systems are very severe in terms of high aerodynamic loads induced by external winds, aerodynamic un-steady loads along with extreme dynamic loads and coupled loads. Similarly, the vehicle control systems are subjected to high disturbances such as aerodynamic disturbance forces and dynamic disturbances such as propellant slosh, etc. To ensure normal functioning of the vehicle systems even under such hostile environments, the vehicle systems have to be designed with high level of robustness. Design with high robustness increases the structural mass of the systems thereby reducing the payload mass considerably. This poses contradictory requirements for maximizing the payload capability. The design driver for a vehicle has to be essentially an optimum design attempting to maximize the payload. Such a design in turn introduces severe interactions and interdependencies between various sub-systems of the vehicle and between vehicle sub-systems and environment. There are also severe dynamic coupling between various systems which further aggravates the complexity of the design process.

During the design, clear understanding of the interfaces between various disciplines and their functional interdependencies with respect to various operating conditions is a vital factor. Therefore, during the design process, it is essential to integrate various subsystems through a structured multidisciplinary process. The wide range of technical expertise encompassing several disciplines and the interactions and interdependencies with respect to severe constraints have also to be brought out at the early design stage. Such a complex design problem can be handled only by understanding the roles of each of the vehicle subsystems and by utilizing the systems engineering approach right from the concept stage.

As space missions are expensive, cost factor should also get priority during the design phase. Similarly, space systems do not tolerate even a minor quality lapse and hence the quality and reliability should get maximum attention all through the design and development phases.

Various aspects of integrated design of STS using systems approach, which are essential to arrive at an optimum, robust and cost effective design of STS are explained in this chapter.

2.2 Systems Engineering Approach for Design

Systems engineering approach explained in this section for the design of launch vehicle is valid for re-entry vehicles too.

The design of a launch vehicle demands close involvement of many disciplines, and the specialists from each of these disciplines have to carefully integrate their requirements in order to obtain the best design for the specified mission. Quite often the design process for a particular discipline is constrained by the requirements of

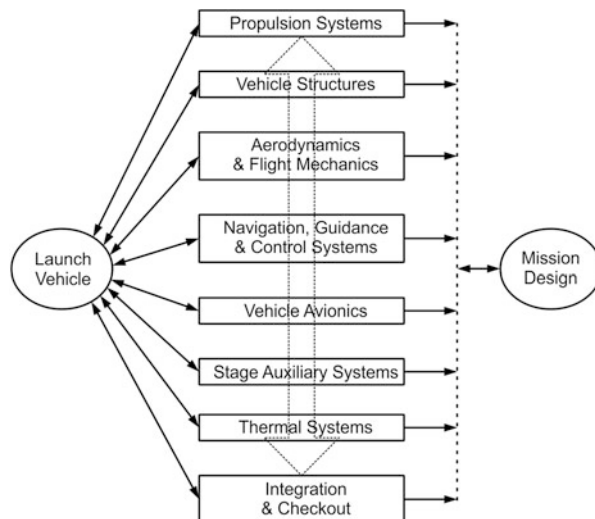
other disciplines and thereby causing conflicting situations. Therefore design iterations are inevitable to arrive at a good design. The interfaces among disciplines are not always well defined. In the absence of this, there occurs inaccurate and delayed data transfer, leading to non-optimal designs. Design of a launch vehicle is essentially making suitable compromises to achieve a good balance between many conflicting requirements and interactions. For example, the design process cannot be initiated till the system requirements are well understood. But it is difficult to firm up the system requirements till the design issues are resolved. The design process also has to depend a great deal on analyses, experimentation and simulations to arrive at a good design, and hence the design process is totally coupled.

To arrive at an optimum launch vehicle design, it is essential to apply systems approach involving various steps as: (a) mission definition, (b) requirements analyses, (c) subsystems definition, (d) concept analyses and definition and (e) design. Design iterations are necessary to understand the interaction among subsystems, interfaces between various disciplines and relation between various design functions to meet the specified requirements.

The major participating subsystems in a launch vehicle are propulsion, vehicle structures, aerodynamics, flight mechanics, navigation, guidance and control (NGC) systems, vehicle avionics, stage auxiliary systems, thermal systems and overall integration and checkout as shown in Fig. 2.1. These subsystems have strong interactions between them as explained later in this chapter. It is a difficult task to define the interfaces without any ambiguity between each one of these subsystems. All such issues are to be addressed in detail during the initial phase of vehicle and mission design.

The design process for the STS needs top down approach starting from overall mission requirements. Various subsystems needed to achieve the specified mission goals are to be carefully defined, and decomposition of the subsystem design tasks

Fig. 2.1 Major participating subsystems in a launch vehicle



is to be carried out by understanding the interactions between various disciplines and also the overall constraints of operations. The decomposition of the subsystems has to address the clear definition of each subsystem and their requirements. It is essential to carry out detailed trade-off studies while finalizing the selection of subsystems to meet the intended functional requirements as decided by decomposition process. The trade-off analysis has to be carried out with respect to performance requirements, reliability of the systems, schedule and cost. The requirements for achieving the specified performance using the existing flight proven systems vis-à-vis the new systems, demanding the advanced technologies have to be weighed against schedule and cost involved in the design and development. Additional ground tests to get the needed confidence on new technologies and the associated schedule requirements for these tests are also to be considered for the judicious selection of a suitable one. While considering the advanced technologies to improve the performance, it is essential to account for the material cost, manufacturing complexities and cost involved in the fabrication as it directly affects the unit cost of the vehicle. This is true for all vehicle systems viz., propulsion, structure, NGC systems, aerodynamic configuration, thermal systems, stage auxiliary systems, etc. Therefore each subsystem has to be carefully selected considering all these aspects for meeting the specified functional requirements. Once the subsystems are selected, the next important step to be considered is the clear definition of the operating environment for each subsystem which becomes the major input for the subsystem design process. The various aspects of operating environment are presented partly in Sect. 2.7 of this chapter and subsequently in detail in Chap. 6.

There are always dispersions on the predictions of environmental parameters. Therefore, uncertainty bounds on the predicted environmental parameters have to be specified and suitable margins have to be built into the design to take care of such uncertainties. Due to limitations of simulating exact flight conditions at ground and uncertainties in prediction strategies, it is difficult to characterize the dispersion bounds of certain parameters with required confidence level (say 3 sigma). Typical examples are structural dynamic characteristics of the vehicle, mode shape vibrations, comprehensive aerodynamic characteristics of the vehicle, wind characteristics variations, etc. with respect to the ones used for design. Similar is the case for onboard software design and testing. Under such cases, the parameter dispersion levels have to be suitably increased to build the design margins. While designing the systems under such extreme environments, there could be loss in performance in the expected nominal operating environment. Therefore design margins have to be judiciously decided to function even for the extreme environment with degraded performance while meeting the required performance under nominal and specified 3 sigma dispersions on the systems parameters. Generally, first flight of the vehicle always performs as a test bench to bring out such uncertainties, and correspondingly, the design modifications have to be incorporated wherever necessary for the subsequent flights.

For each subsystem, it is essential to quantify all the performance parameters and their uncertainties which influence the design process. The general practice is to

define the parameters dispersion based on earlier experience or on the engineering judgment. All parameters are defined with a nominal and range of uncertainties based on statistical measure say, 3 sigma levels relative to the nominal. The uncertainties levels are to be refined over a period based on the analysis, experimentation, specific ground tests and initial flight tests. It is also necessary to define the application needs of these uncertainties during the design phase. The sensitivity of each parameter on the system response should also to be verified and sensitivity matrix is to be generated. Design has to give special attention to such parameters which are highly sensitive. Very careful quantification of these parameters is needed either through detailed analysis or through experimentation wherever essential.

The next step is the design of the subsystems to meet the functional requirements considering the operating environment encountered by them. The design of each subsystem should consider the multidisciplinary requirements of other subsystems without any conflicts, while meeting the overall system requirements. It is also essential to ensure that all constraints of the system are met with.

Influences of typical interactions on the subsystems are explained later in this chapter. Discussions on detailed interactions and design of a particular subsystem in such an environment are detailed in the relevant chapters of this book. As the vehicle is optimally designed to achieve the intended function, the design margins are generally kept just sufficient to operate in the hostile flight environment. Some of the vehicle systems after assembly operate for the first time in flight as mentioned already. Therefore it becomes essential to carry out the detailed risk analysis for each of the subsystems. Depending on the criticalities of the parameters, design robustness or redundancy has to be built into the system. Typical examples are strict compliance of functionally critical dimensions (FCD) of the subsystem components, sensor redundancy in inertial systems, triple modular redundancy for mission critical avionics systems, etc.

The successful design process should ultimately lead to achieve the smooth technical integration of all subsystems of the launch vehicle so that they function in an efficient manner without any failures. The process should clearly define the analysis, simulation, ground and flight tests, tests set up needed during the development phase. Using the test beds and analysis tools, the designs are to be evaluated in a systematic manner to understand the influence of interactions of various subsystems and performance validation. The results of analysis and tests are to be carefully examined to identify the design flaw, design weakness and the influence of the parameters on the design margins. Based on the tests and analysis results, the design has to be tuned to meet the functional requirements wherever necessary.

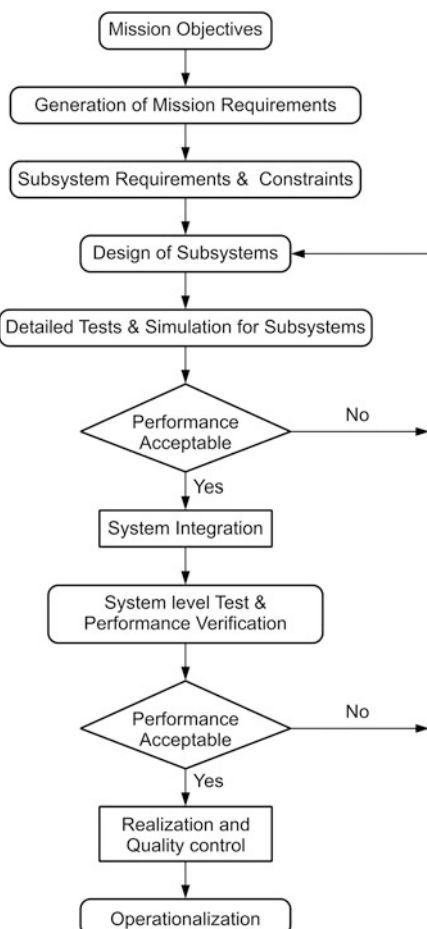
Various steps involved in the systems engineering approach for design process and overall integrated design aspects of a launch vehicle are explained in the subsequent sections of this chapter. The details of the design aspects of each of the subsystems of a launch vehicle are explained in the subsequent chapters of this book.

2.3 System Life Cycle Considerations for Design and Development of STS

The systematic procedure to be followed for the design, development and realization of multidisciplinary STS is given in Fig. 2.2. The broad guidelines to be followed during the design and development of STS system are as given below.

- Generation of overall functional requirements from the mission objectives.
- Generation of unambiguous vehicle system definition and overall system requirements.
- Carrying out trade-off analysis to select the systems and subsystems considering the performance requirements, schedule and cost.
- Decomposition of the overall vehicle system into various subsystems and components which are amenable for independent design and development.

Fig. 2.2 Systematic approach for design and development of STS system



- (e) Translate system requirements into subsystem requirements. Generation of specifications for all subsystems and components from the requirements.
- (f) Spelling out all vehicle constraints including the constraints imposed by the participating subsystems.
- (g) Defining the interdependency of subsystems and interactions between subsystems and components.
- (h) While working out the interfaces between subsystems, ensure minimum complexity, minimum interaction, minimum integration efforts, ease of realization and testability.
- (i) Assessing the risk involved by carrying out systematic failure analysis right in the design phase itself and deciding the subsystems/system configurations to achieve higher reliability, meeting the schedule and cost constraints.
- (j) Design the subsystems to meet the functional requirements while satisfying all the constraints imposed by other subsystems and overall vehicle and mission constraints.
- (k) Defining systematic test plans for components/subsystem/system to evaluate the performance including the simulations wherever necessary. The performance evaluation has to be carried out both at subsystem level and integrated system level. Progressive addition of hardware in simulation has to be attempted wherever possible to verify the interface, interdependency and interaction.
- (l) Based on the results and analysis, the design iterations are to be repeated to ensure the satisfactory performance of the system.
- (m) Strictly follow the configuration control to maintain the full traceability for materials, components and subsystems during the entire realization phase.

It is evident that the design and development activities consist of: (a) concept formation, (b) definition of system/subsystem requirements, (c) subsystem design with clear definition of constraints and interactions, (d) generation of test matrix to evaluate the subsystems and (e) verification and validation of performance of each of the subsystem and system at appropriate stage/s with respect to defined requirements/specifications. This systematic procedure helps to minimize the design iterations.

The following sections highlight each of these systems engineering aspects with specific examples wherever necessary.

2.4 Overall Functional and Design Requirements

The functional requirements for launch vehicle subsystems are derived from the mission requirements. The design requirements for each of the subsystems are decided by their functional requirements, satisfying the interfaces and constraints imposed by other subsystems of the vehicle and overall mission.

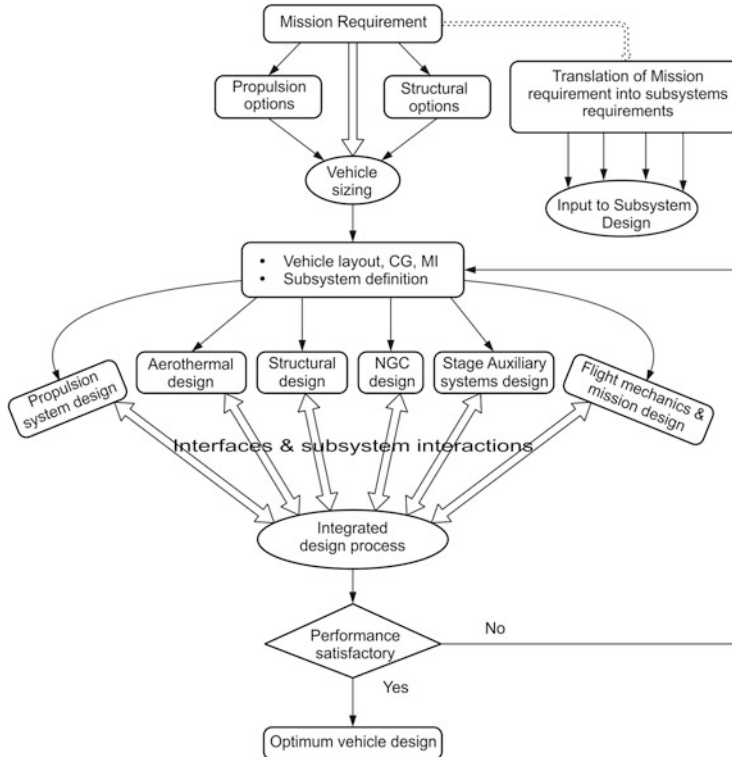


Fig. 2.3 Overall design process for space transportation system

The functional and design requirements of launch vehicle subsystems are analyzed through the overall design process given in Fig. 2.3. The basic input for the launch vehicle systems design is the clear definition of the mission requirements in terms of the payload mass and the orbital parameters. The specific energy required to achieve the specified orbital mission and the total mechanical energy required to inject the specified mass into desired orbit are derived from the mission requirements. The equivalent ideal velocity required to achieve the above energy considering various velocity losses caused by the aerodynamic drag, gravity, atmosphere and three-dimensional trajectory is worked out. Propulsive systems are required to generate the ideal velocity so worked out. The details of these aspects are discussed in detail in Chaps. 4 and 5. The vehicle size depends on the type of selected propulsion systems, structural options as well as number of stages and size of each stage. The selection of the propulsive stages largely depends on the state-of-the art technology available, advanced technology developments, cost, schedule and reliability considerations. The selection of structural material options depends on the performance requirements while meeting load carrying capabilities and cost aspects.

Once the vehicle sizing is finalized, first cut details of the vehicle like layout, surface geometry, stage mass, propellant mass and inertial properties are worked out. For this configuration, the aerodynamic characterization is needed through the detailed analysis and experimentation. Propulsion and structural designs and analysis considering various options are taken up in parallel. Suitable trajectory design is to be carried out considering the entire vehicle and mission related constraints. A set of trajectories are to be simulated and a suitable trajectory meeting the overall mission requirements while satisfying the vehicle systems requirements such as the dynamic pressure, the load on structure, the thermal load on vehicle systems and subsystems and mission related constraints like range safety is to be chosen. Thermal design of the vehicle has to be carried out using the results of trajectory. Similarly, NGC system design is to be carried out to meet the mission requirements for the finalized trajectory requirements. The design of stage auxiliary systems for ignition and the separation of the stages using high energy pyro systems are also carried out in parallel meeting the mission design requirements. The functional requirements for all the subsystems are derived from the overall mission requirements while satisfying various constraints of other subsystems of the vehicle and integrated mission.

All the design processes explained so far are highly interdependent. Therefore it demands a balanced multidisciplinary design process with several design iterations before arriving at a good design. This process should lead to the definition of a suitable vehicle configuration and design. The various requirements and design processes of STS can be summarized into the following major steps:

1. Define payload and mission requirements.
2. Select the propulsion options based on the available technology and technology developments required.
3. Select suitable structural options considering the optimization of mass and sufficient strength to withstand loads.
4. Size the suitable propulsion modules and correspondingly the structural mass to meet the specified requirements.
5. Carry out Optimal Vehicle Sizing (OVS)
6. Choose the suitable control systems to meet the overall mission requirements.
7. Select all other vehicle subsystems based on the technological choice, reliability and cost aspects.
8. Define various launch and mission constraints
9. Carry out trajectory design considering all constraints.
10. Carry out detailed design and evaluate subsystem and integrated system performance.
11. If the mission requirements are not met, repeat steps 4–10 to arrive at an optimum design.
12. Finalize the launch vehicle configuration and design.

While the basic design sequence listed above defines various major steps, the detailed procedure required to be followed during the design phase are given below:

- (a) The vehicle functional requirements are to be defined without any ambiguity considering the demands of mission, various subsystems including all possible constraints and subjecting the same for detailed review.
- (b) The vehicle sizing in terms of propulsion and structural system has to meet the final mission objectives. This process largely depends on the selection of propulsion and structural systems based on the available technology, new development needed, overall schedule, cost and the risks.
- (c) Once the selection process for propulsion modules is completed, it is necessary to estimate the performance parameters of all propulsion systems chosen.
- (d) The overall vehicle configuration is to be defined considering the finalized vehicle structures. The structural options have to be decided based on the important criteria of proper material selection, overall mass, sufficient strength to withstand the loads, meeting the defined envelope, ease of manufacture and fabrication.
- (e) The next important step is the aerodynamic characterization of the vehicle configuration using computational fluid dynamic (CFD) analysis tools and through experimentation (wind tunnel tests). The aerodynamic forces and moments are needed for mission design, whereas the force and moment distributions along the vehicle length are required for the vehicle structural and control systems design.
- (f) Subsequent to this, it is necessary to define a base line mission design. The vehicle subsystem related constraints and trajectory shaping constraints based on range safety considerations during the entire phase of flight path for safe impact of the spent stages during nominal and disturbed flights and also under abort and failure conditions are to be considered. From these, the reference trajectory parameters are to be generated, which form the basic input data for the control, structural and thermal design and analysis.
- (g) Structural design has to be carried out considering the maximum internal and external loads at different phases of flight.
- (h) Thermal design involving suitable thermal protection systems for the vehicle has to be based on the thermal environment generated by the reference trajectory.
- (i) Stage auxiliary systems such as vehicle separation systems, pyro systems and other mechanisms wherever needed are to be worked out considering all aspects including the loads and thermal environments.
- (j) Navigation, guidance and control schemes for each phase of flight are to be worked out. Analysis in terms of control logic, control authority and rigid body response against all disturbances is needed. Vehicle stability has to be assessed against structural deformations, liquid sloshing, POGO interactions and subsystems performance deviations.
- (k) Overall avionics configuration for the vehicle to cater to all electrical requirements of vehicle including telemetry, tracking and telecommand is to be finalized. This should consider the redundancy requirements for mission critical functions to enhance the overall reliability.

- (I) The design sequence should also include overall performance analysis to ensure that defined performance goals are met with.

From the overall functional and design requirements as defined above, the overall system and subsystem requirements are derived as discussed in the next section.

2.5 Overall System Requirements and Decomposition

The mission objective decides the overall primary and secondary functional requirements for the launch vehicle design. The overall vehicle systems requirements are generated from the functional requirements which are then decomposed into various subsystem requirements. The subsystem requirements are finally translated into subsystem specifications. The subsystems are designed to meet the specifications. The subsystems thus designed are integrated into vehicle to meet the functional requirements thereby meeting the mission objectives. Incorporating the specific requirements of several disciplines, one has to arrive at optimum design of vehicle systems to meet the mission objectives and to generate unambiguous system requirements. The system requirements and decomposition process to generate the subsystem specifications are explained with specific examples in this section.

In STS, it is extremely important to define the basic objective of the mission. This is closely linked to the function of the satellite defined by the user. The satellite functions are directly linked to the type of mission viz. remote sensing, communications, weather monitoring, scientific experiments, etc., and all such functions are to be clearly specified. Once these functions are defined by the user, the mission requirements in terms of orbital elements are determined. In addition, there are several system constraints in terms of mass, volume and environmental conditions depending on the instruments onboard the satellite. There are other requirements in terms of cost, schedule and reliability which have to meet the specified goals. Therefore the requirements have to be well defined to meet the user or customer needs in terms of critical functional and operational requirements.

It is always advantageous to generate initially the overall primary functional requirements of the vehicle and then derive the corresponding secondary functional requirements of the system and subsystems. The basic goals and constraints defined by the user generally dictate the primary requirements. For example a satellite mission could be for Earth observations, weather monitoring, communications or any other specific purpose. The payload size, mass and orbital elements for a specific mission would become the primary requirements. Secondary functional requirements are generated from these primary requirements in terms of number of stages, types of propulsion modules, velocity increments, visibility during entire mission, accuracy of injection, etc. But these functional requirements are closely linked to the available technological capabilities and other demands such as cost,

schedule and risk. Therefore critical assessment of several factors is to be carried out before the functional requirements are firmed up. It is also necessary to ensure that there are no unrealistic requirements which have a much greater influence on the cost, schedule and risk. While finalizing the overall requirements for STS design, it is essential to consider the vehicle environment. The STS has to ensure that the satellite is not subjected to any hostile environment during its journey and particularly protects it in the atmospheric phase of flight. These constraints have to be suitably factored during the initial phase. The requirement should also include the definition of a suitable launch base which meets the mission. The launch bases are generally located on east coast to take advantage of Earth's rotation to achieve the needed velocity. While deciding the vehicle trajectory, the range safety constraints such as avoiding the impact of the spent stages in the densely populated areas of land mass has to be seriously considered.

System requirements are generated from the primary and secondary functional requirements. The systems engineer has a major role in arriving at a realistic set of requirements and the interaction between disciplines and conflicting requirements are to be carefully analyzed. It is not possible to finalize all requirements right at the beginning since many of them depend on technology options. But it is feasible to firm up these requirements as the design process is continued. Therefore, it is important that all functional requirements are frozen at the early phase of the programme. Since the changes may have adverse impact and impose additional constraints on the vehicle systems, systems engineer has to continuously track and make sure that the changes are not allowed unless otherwise it is mandatory.

While finalizing the systems requirements, the performance capability of the launch vehicle has to be closely matched to meet the needs of satellite mission requirements and constraints. It is always beneficial to provide the performance margin in the launch vehicle to take care of the uncertainties in the realized satellite mass from the projected mass allocations. The interface requirements between spacecraft and the launch vehicle have to be strictly defined so as to make them compatible. Specific constraints of the satellite from the overall launch and mission point of view are to be clearly understood and communicated to the launch vehicle designers who in turn have to satisfy all such constraints. Absence of these aspects during the definition of system requirements lead to redesign which will have a great impact on the overall schedule and cost.

Once the overall system requirements are spelled out, the next logical step is to transform the same into various subsystems requirements, by considering the various constraints, interdependencies and interactions between them. This decomposition is necessary to facilitate clear definition of specifications for each subsystem so that its design is carried out independently. The methodology used for carrying out such an analysis is explained below by a simple example by choosing two subsystems of a launch vehicle namely (a) propulsion and (b) NGC subsystems. Figure 2.4 illustrates a typical propagation of system requirements to propulsion and NGC subsystem requirements.

The functional requirement of propulsion module is to provide necessary energy to inject the specified satellite into mission defined orbit. Once the clear cut

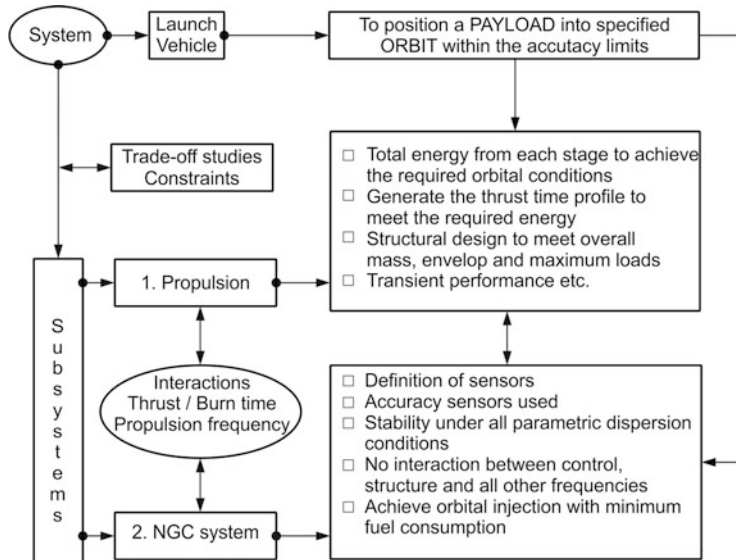


Fig. 2.4 Typical example for generation of subsystems requirements

missions requirements in terms of payload mass, payload volume, target orbital parameters, the allowable dispersions, various constraints of mission, range safety, etc. are determined, the selection of propulsion modules is to be based essentially on the terminal trajectory state vector (altitude, velocity, flight path angle, velocity azimuth, latitude and longitude) to be achieved by accounting all losses and also on the state-of-the-art technology available.

Next step is to define the propulsion system requirements for each stage such as: (a) total impulse for each stage; (b) thrust time profile meeting the system constraints such as lower dynamic pressure profile, lower acceleration profile; (c) structural design requirements to meet the overall mass, envelope and capability to withstand maximum loads; (d) transient performance at the ignition and shut-off.

The main function of NGC system in a launch vehicle is to direct the propulsion system energy, stabilize the vehicle against the disturbances and to ensure that the payload is injected into the required orbit within the specified orbital injection errors. To meet this demand the NGC system requirements are to be specified as: (a) type of sensors used such as gyros, accelerometers; (b) allowed errors on the selected sensors to meet the specified orbital injection accuracies; (c) control stiffness to reject the disturbances; (d) vehicle stability during the entire regime of flight; (e) avoidance of interaction with structure, slosh, POGO, etc.; (f) no large maneuvers in atmospheric phase of flight to avoid angle of attack build up intentionally; and (g) guidance to achieve the specified orbital injection with minimum fuel. There are several such requirements for each of the subsystems which are to be specified to the extent possible in the beginning phase itself.

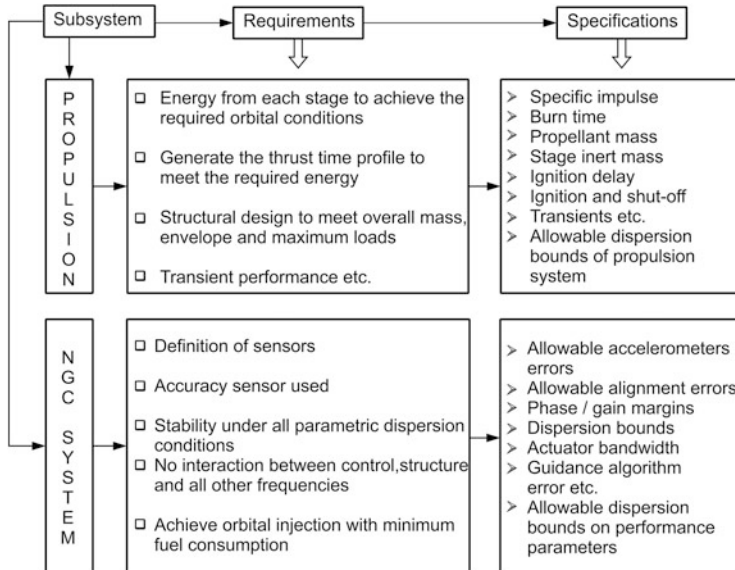


Fig. 2.5 Translation of requirements into specifications

The vehicle control is generally derived through thrust vector control by deflecting the main nozzle or engine of the propulsion systems and therefore the control systems have very close dependency on propulsion system parameters such as the deflection needed in propulsion system to generate the maximum control force, tail-off characteristics of engine, engine cut off, differential thrust if more engines are used. The steady state thrust level, burn time, propulsion system frequency, ignition and shut-off transients of propulsive stages, etc. have influence on the NGC system. Similarly, NGC system and propulsion system influence each other mutually through slosh, POGO interactions, etc. Therefore, while deriving the propulsion and NGC system requirements, it is essential to consider the interactions between these two systems.

Once the generation of subsystem requirements is complete, they are to be translated into clear cut specifications, and a typical example explaining this process for the propulsion and NGC systems is given in Fig. 2.5. In case of propulsion, the requirements specified in Fig. 2.4 get translated into specifications for each stage as: (a) specific impulse, (b) burn time, (c) propellant mass, (d) stage inert mass, (e) ignition delay, (f) differential thrust if more engines are used, (g) ignition and shut-off transients and (h) allowable performance parameters dispersion bounds, etc. Similarly NGC system requirements can be transformed into specifications as: (a) allowable sensor errors, (b) bounds for alignment errors, (c) phase and gain margins, (d) actuator bandwidth, (e) guidance law and its accuracy, (f) allowable performance dispersion bounds, etc.

The conceptual studies should lead to generation of system and subsystems requirements and also first cut specifications for all subsystems and components. This gets refined subsequently during the preliminary design, and both requirements and specifications are to be firmed up at the end of conceptual design phase.

Based on the specifications, the subsystems are designed to meet the overall functional requirements. The important aspects to be considered during finalization of system requirements, specification and design are explained in the next section. The integrated design and validation aspects of launch vehicle are explained in the subsequent sections.

2.6 Important System Engineering Aspects

While finalizing the systems requirements, system selection and specifications, the important system aspects to be considered are the trade-off analysis and interactions between the subsystems. Similarly, the risk analysis and management are essential part of the subsystem design process.

2.6.1 *The Trade-Off or Options Analysis*

The trade-off or options analysis is one of the important considerations of systems design. For each of the system or subsystem, several alternate concepts are feasible to achieve the specified functional requirements. All such concepts are to be listed and critically evaluated considering the performance requirements, technical feasibility, schedule and cost. The selection of the most suitable concept should be based on meeting the specified goals and satisfying the stipulated conditions and constraints.

To meet the widely varying requirements of several subsystems which are often conflicting brings in another dimension to trade-off analysis. To achieve the maximum performance for STS, sometimes it is necessary to introduce advanced technologies. It may demand high costs for manufacture, assembly, integration and tests. However, in STS design, minimization of the cost without sacrificing the overall performance is extremely important. Therefore, during the design phase much more rigorous attention is needed to deploy the cost effective designs including the costs towards manufacturing, fabrication and development costs.

In the options analysis, it is always a difficult decision to introduce a new technology. Good system engineering practice is to continue with the existing technology, if it meets the performance goals with sufficient margin, no constraints on availability of components and less expensive. The introduction of a new technology has its own risk and uncertainty. The change of technology in one subsystem may have inadvertent effect on other subsystems and hence detailed study of all such effects is needed before deciding the changes. However in case of

obsolescence of materials or components of a subsystem, insufficient design margin, higher performance requirements, it may become essential to opt for a new technology. Detailed analysis in terms of performance advantage, availability, schedule, manufacturing and fabrication cost, development cost and risk involved are needed before arriving at a decision. The importance of trade-off analysis is explained through the following typical examples.

Assuming flight proven solid and earth storable liquid propulsion systems are readily available, it may be possible to configure the STS with the above systems to meet the functional requirements in terms of injecting specified satellite into intended orbit. The same functional requirements can be achieved with a smaller vehicle configured with new advanced semi-cryogenic or cryogenic propulsion systems. But the new advanced system involves development, cost and schedule. Therefore, trade-off analysis has to be carried out to select the system which meets the functional requirements considering the cost and schedule aspects. However, if the functional requirements are not met with the existing system, then it becomes essential to adopt new advanced propulsion system and while doing so reduction in developmental cost and schedule to be considered while meeting the functional requirements.

In order to improve the payload carrying capability of the vehicle, it is always preferable to use high strength to weight ratio materials. Firstly, it may increase the material cost, additional cost for material development and increased manufacturing and fabrication cost too. The cost and schedule involved in such options have to be weighed against the cost of vehicle utilizing existing materials and meeting the functional criteria before a suitable choice is made. However, if it is mandatory to use the advanced materials, the suitable ones which reduce the total cost and schedule are to be adopted.

Proper selection of inertial sensors plays a major role in meeting the functional requirement of achieving the orbit within the specified dispersion bands. If the allowable orbital parameter dispersion is very small, then accuracy of the sensors has to be very high and new developments may be required. On the other hand, if the allowable orbital parameter dispersions are wide, then existing inertial sensors may itself be sufficient to meet the requirements. Therefore, the integrated mission analysis of launch vehicle orbital parameter dispersions along with the satellite fuel necessary for correcting such deviations is to be carried out before suitable sensors are selected. However, if the advanced systems are with considerable mass reduction, in addition to improvement in orbital parameter dispersions, then introduction of such systems provide the increase in the payload mass. Under such cases, the new system which is advantageous may be adopted.

Such trade-off analyses have to be carried out for all the subsystems while selecting the system, system requirements and specifications. These aspects are addressed in detail at appropriate sections in the forthcoming chapters of this book.

2.6.2 Interdependencies and Interactions

In space transportation systems, the interdisciplinary interactions are quite strong and the requirements of subsystems sometimes tend to be conflicting. It is therefore essential to understand the conflicts and arrive at judicious solutions which meet the overall functional requirements. This calls for detailed analysis to understand the mutual compatibility of subsystems. Appropriate design modifications are necessary to avoid the undesirable interactions and minimize the interdependence effects.

Integrated design approach plays a very vital role in complex systems by continuously monitoring the vehicle design and keeping track of interactions between several disciplines. Figure 2.6 illustrates the intricacies of integrated design approach with a typical example which considers four major segments of a launch vehicle viz., propulsion, structures, aerodynamics and NGC system. These subsystems are not only closely linked with the overall mission but they have interdependency and interactions between them.

Propulsion systems are chosen to provide the energy needed to achieve the required position and velocity vector to the specified payload. Selection of number of stages, types of propulsion and propellant loading required to achieve the specified mission depend largely on the state-of-the-art technology available and advanced technology development requirements. Once the number of stages is determined, judicious distribution of energy among various stages is needed. The propulsion module design is also influenced by the type of structure, aerodynamic loads, thermal environment and type of control system used.

Similarly the structural design has to address overall loads, proper material selection and type of structure to be used. This depends on the propulsion modules

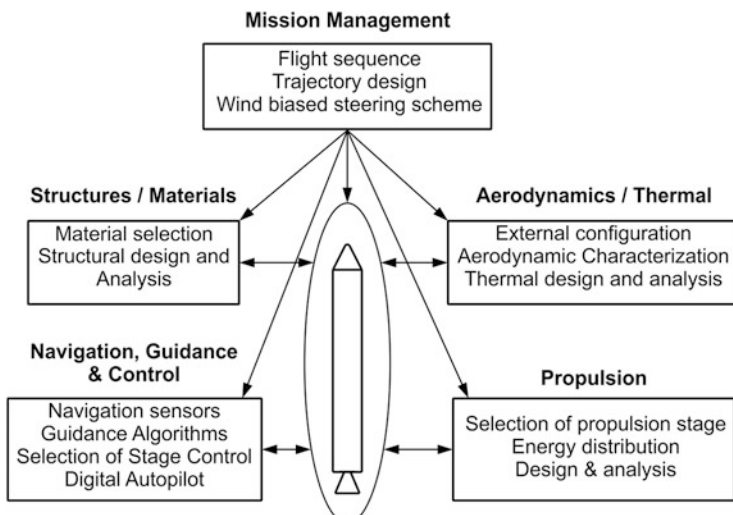


Fig. 2.6 Intricacies of integrated design

used and overall vehicle characteristics. Selection of suitable baffles in the propulsion module depends on the overall damping needed for control systems. The stiffness requirements for the actuator mounting has close link with actuator design used for stage control. Considering all these aspects the design and analysis are to be carried out.

The aerodynamics depends largely on the overall configuration, type of payload fairing used, the protrusions on the vehicle due to various requirements and also the vehicle flexible modes. Aerodynamic heating during ascend phase and venting requirements are also to be considered. The aerodynamic effects wherever essential are to be studied.

Generally vehicle control is derived by deflecting the engines or nozzles of the propulsion systems. Various studies needed are type of control, control loads on structure, actuator mounting stiffness and sensitivity analysis due to performance deviations.

Typical interactions influencing the above subsystems design are as given below. Type of propulsion system influences the vehicle structure and structural mass. While solid motor propulsion system increases the structural mass, the liquid propulsion system reduces the structural mass considerably. The static loads such as thrust, tank pressure and atmospheric drag influences the structural design and the vehicle overall mass in a major way. The structural mass and propulsion system thrust influences the payload carrying capability. The aerodynamic lateral force during atmospheric flight regime which is dependent on thrust, external wind and aerodynamic characteristics of the vehicle influences the structural design and drift in the trajectory to a large extent. The aerodynamic configuration has to be suitably designed to minimize the structural loads.

Due to aerodynamic unsteady loads such as aerodynamic buffeting, vehicle structural modes get excited. If the low frequency of this high pressure oscillating loads is closer to the structural modes, there could be severe coupling between the dynamics of the unsteady loads and structural dynamics. The severity of coupling can be more at the high dynamic pressure which in turn influences the thrust level. In order to avoid such scenarios, it is essential to design the vehicle with stable buffet configuration. The above examples amply illustrate the complexity of interactions between these four disciplines like aerodynamics, propulsion, structure and mission trajectory design.

Another interesting example is the coupling between propulsion and structural systems. Vehicle axial structural oscillations induce oscillations in the liquid propulsion system tank bottom and subsequently in the flexible fluid lines. The fluid line oscillations fluctuate the propellant flow to the engines thus generating thrust oscillations. The thrust oscillations excite the axial structural modes and therefore there is sever structure-propulsion system interactions. This phenomenon is called POGO in liquid propulsion system. In order to avoid such oscillations, suitable POGO correctors have to be implemented in the propulsion system depending on the structural axial and propulsion feed line frequencies.

The aerodynamic disturbance forces during the atmospheric flight regime de-stabilize the vehicle. The rotational motion of the vehicle is sensed by sensor

and fed into the control system to stabilize the vehicle. But, in addition to the rigid body motion of the vehicle, the sensor output contains vehicle flexible responses also. If it is not designed properly, the control system can further excite the flexible modes leading to structural failure. Therefore the control system is to be designed to stabilize the vehicle against the external aerodynamic disturbances while rejecting or attenuating the vehicle flexible modes. The control system response in turn changes the aerodynamic force through change in angle of attack further influencing the vehicle structural modes. Therefore there are severe aerodynamics – control system – structural interactions.

To handle such interactions on the subsystem design, data on each of these subsystems are to be generated and carefully used during the design. The important aspect is to ensure enough separation between various frequencies viz., control bandwidth, vehicle flexible modes, propellant sloshing and actuator bandwidth. Wherever the interaction is noticed, suitable design modifications are necessary to achieve the required performance.

The vehicle and mission designer has to address all these aspects carefully during the initial design phase of the vehicle and continuously track the subsystem performance throughout the development. The flight sequence and trajectory have influence on all the subsystems and they have to be carefully designed satisfying the overall performance requirements and the constraints imposed by various subsystems. If there are any changes in any of the subsystems it has to be tracked in real time and has to be communicated to all other subsystem designers to verify that the changes suggested have no implication on their subsystems. There are several such mission related aspects which are influenced by various subsystems and the details of such influence are covered at the appropriate chapters of this book.

2.6.3 Risk Assessment and Management

The risk assessment is an integral part of the design and has to be necessarily addressed in the early phase of the design. The risk analysis should be carried out in respect of each subsystem in terms of: (a) what can go wrong, (b) what is the likelihood of going wrong, and (c) what are the consequences. Well established procedures and analysis tools, like Fault Tree Analysis (FTA), Failure Mode and Effects Analysis (FMEA), Failure Mode Effects and Criticality Analysis (FMECA), etc., have to be used to analyze the risks involved and the consequences on the subsystem/system in the event of such failures. Further analysis is needed to classify them as unacceptable, undesirable and acceptable with reservations, depending on the severity of the consequences. Based on the analysis outcome, suitable design improvements have to be incorporated in the subsystem/components without violating other constraints and requirements. Some of the typical examples are as given below.

The liquid propulsion system contains several high speed rotating elements, valves operating in high pressure, high pressure gas bottles, propellant feed lines,

injectors and thrust chamber. Impact of failure or performance deviation in any of the elements can propagate downstream and may affect severely the functions of critical elements of the system or even lead to total mission failure. Therefore, detailed risk analysis have to be carried out with respect to the performance deviation/failure of each of the elements and suitable design modifications are to be implemented wherever essential to improve the robustness against such failures.

The vehicle mission critical functions like navigation, guidance and control depends on the navigational sensor outputs. Any failure in any of the sensors or the vehicle response beyond the sensor limits may lead to wrong input to the navigation, guidance and control system which ends up with wrong trajectory prediction. As a consequence the vehicle is directed along the undesirable direction. In addition, wrong sensor may destabilize the launch vehicle. Therefore, it becomes essential to provide sensor redundancy to avoid single point failure. To avoid wrong computation of trajectory under the environment of large vehicle rate, it is essential to widen the dynamic range of sensors. This provides reasonable data of the deviated path while providing accurate results for the nominal operating regime of flight.

The avionics systems comprises of several components, sensors, actuators, etc. operating in the hostile flight environments. The failure in any one of the critical components may lead to mission failure. Therefore, suitable redundancy is to be implemented in these elements too to avoid mission failure. At the same time, proper care has to be taken to avoid additional failure modes due to implementation of redundancy and it should meet the computational requirements with adequate margin.

The risk assessment and management has to be carried out for all the mission critical elements of the vehicle system and suitable design modification/redundancy are to be implemented to improve the robustness of the system. These details are discussed in the appropriate chapters of this book.

2.7 Integrated Design Aspects for Launch Vehicle Subsystems

As explained in the previous section, the overall system and subsystems requirements and specifications are generated based on the functional requirements and options analysis. Next step is to design each subsystem to meet the specifications under the specified operating environment, disturbances, etc. The design of each subsystem has close links with other design elements of vehicle systems. Therefore, integrated design of the vehicle systems has to be carried out considering the interdependency of various disciplines as well as other aspects such as material, manufacturing, quality, cost and schedule as given in Fig. 2.7. It should also consider several other aspects viz., influencing performance parameters, environment parameters, their dispersions as well as risk analysis and management.

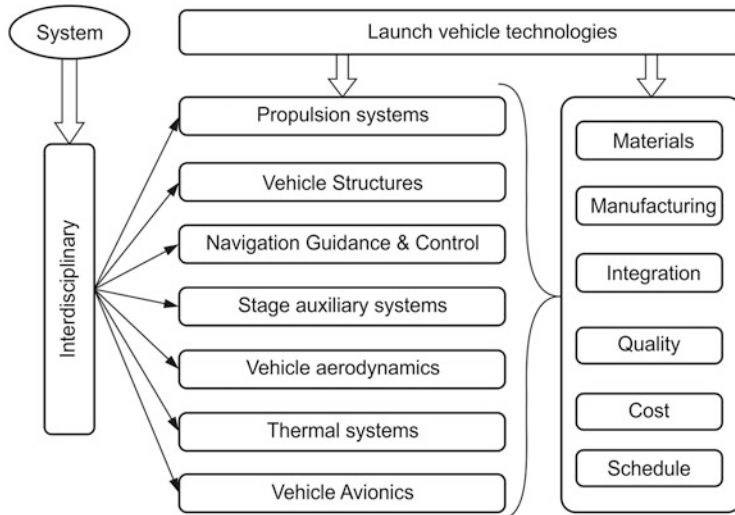


Fig. 2.7 Integrated design elements with processes

The various processes of the design are number of propulsion stages, sizing of propulsion modules, steady state thrust, transient behavior of stages during ignition and tail off, slosh damping in liquid stages, vehicle structural design, structural dynamic aspects to avoid interaction with control and propellant sloshing, selection of suitable control power plants, scheme for the real time identification of staging events, suitable separation sequence to ensure smooth separation of stages, control strategy in this regime, autopilot design to guarantee vehicle stability all through the flight and to ensure robust control against all disturbances, selection of suitable navigation sensors and guidance algorithms to provide accurate satellite injection, etc.

The design process cannot be carried out without understanding the influence of one over the other. It is the task of the systems engineer to address all these issues in an integrated manner. Some of the very salient aspects pertinent to the design of each of the subsystem which gets influenced by other subsystems have been highlighted below. However, various chapters organized in the book give specific attention to these issues and address them in greater detail at appropriate sections. These aspects are to be considered in a holistic manner during the initial design phase, to arrive at a robust design.

2.7.1 *Operating Environment to the Vehicle System*

The subsystems are designed to meet the specifications while functioning in the operating environment. The operating environment of the vehicle systems are

generated within the vehicle as well as caused by external sources. The salient operating environments are steady/quasi steady loads, dynamic loads and random vibration environment. Typical steady loads include gravity, thrust, tank pressure, thermal loads caused by aerodynamic heating, propulsion system, thermal gradient and other steady disturbances such as thrust misalignment, thrust offset with respect to center of gravity, differential thrust, etc. The dynamic loads are caused by propellant slosh, aerodynamic loads due to wind, control force reactions to aerodynamic disturbances, unsteady aerodynamic loads, vehicle flexible dynamic loads, POGO oscillations, thrust oscillations etc. The random vibration environment is caused by aerodynamic noise and propulsion noise of the vehicle system. In addition to above, the dynamic coupling due to interactions of various system dynamics causes severe environment to the vehicle systems. Further details of operating environment are given in Chap. 6.

2.7.2 Propulsion Systems Selection and Vehicle Sizing Aspects

The number of stages and sizing of propulsion systems are to be based on the total ideal velocity to be imparted to deliver and inject the defined payload into the specified orbit, state-of-the-art technologies, technology base available, development lead time and cost advantage. The specific impulse of propulsion systems plays a major role in the selection process. Various other propulsion system parameters which influence the mission are: (a) thrust time and propellant consumption history along with dispersions bounds, (b) ignition and shut-off transients with dispersion bounds, (c) influence on longitudinal acceleration, (d) depletion mode transients, (e) slosh and POGO phenomenon in liquid stages, (f) longitudinal excitations during liquid engine shut off and (g) estimation of liquid propellant loading to meet the mission requirements. The shocks generated during the ignition and shut off transients are to be properly assessed to study its influence on the payload and the avionics equipment. During the start of the liquid engines, positive acceleration of the vehicle is to be maintained to ensure smooth ignition process. The maximum deflection angle of the engine to generate the required control force is to be assessed considering the engine thrust and also the overall thrust loss.

2.7.3 Structural Design Aspects

The launch vehicle is an assemblage of a large number of propulsive stages and interstage structures with a number of interface joints. It is essential to ensure that structures are of light weight and withstand the maximum vehicle loads and environments encountered in flight. The vehicle dynamic characteristics is another

important aspect wherein the flexible mode frequencies have to be kept at least 3–5 times higher than the vehicle control loop frequency to avoid the control structure interaction. The influence of vehicle local structural modes on the output of the sensitive instruments, rate gyros and accelerometers are to be assessed carefully. Proper characterization of structural modes for the movable nozzles and engines needs serious consideration. Similarly aeroelastic behavior of the structure, wherein the aerodynamic forces interact with the elastic modes of the vehicle, has to be carefully studied. In such cases, the aerodynamic forces deform the vehicle structure and the deformation of the structure in turn modifies the aerodynamic forces. Under certain flight conditions, this force can cause severe instability leading to catastrophic failure of structure.

In liquid stages, the propellant slosh effects have to be suitably damped to avoid interaction with control. Damping improvement can be done by suitably designing the necessary baffles in liquid tanks. POGO is another phenomenon in liquid vehicles where longitudinal oscillations cause oscillations in the flexible propulsive system hardware elements which have the potential to introduce thrust oscillations. These oscillations in turn influence the longitudinal structural oscillations due to tight coupling between these systems. Therefore POGO characteristics have to be studied in detail and suitable POGO corrector has to be introduced to suppress these oscillations.

2.7.4 Vehicle Aerodynamics

External configuration of the vehicle decides the vehicle aerodynamic characteristics which along with external environment such as wind and flight parameters and critical flight regimes cause severe load and hostile environment to the vehicle structure and subsystems. Therefore, it has to be carefully designed to cause benign environment to the vehicle subsystems. It is preferred to avoid the external protrusions on the vehicle as far as possible. Aerodynamic forces along with the aerodynamic static stability characteristics of the vehicle form the major input for the design of vehicle structural and control systems. It is always advantageous to configure a neutrally stable vehicle but it is difficult to meet this criterion for the entire regime of atmospheric flight. However, depending on the design criticalities, the required aerodynamic stability features at the critical zones of the flight can be achieved by suitable design of fins and this has to be done during the initial design phase itself.

The load distribution along the vehicle length required for the vehicle structural and control systems design is generated from the pressure distribution measured over the entire vehicle surface using wind tunnel tests. These tests are to be carried out using scaled down models of the vehicle to generate the quasi steady aerodynamic parameters. The unsteady pressure measurements are also essential to estimate the effects of aerodynamic buffet on the vehicle dynamic loads. Generation of dispersion bounds for various aerodynamic parameters is a tricky task and it has to be properly assessed taking into account all the contributing factors.

2.7.5 *Trajectory Design and Flight Sequence*

The vehicle trajectory and flight sequence have close links with propulsion, aerodynamics, vehicle structure, mechanisms, navigation, guidance and control (NGC) and many other subsystems of the vehicle. The designed trajectory has to meet several vehicle and mission related constraints such as: (a) maintaining the maximum dynamic pressure within the specified value, (b) reducing the aerodynamic loads during atmospheric phase of flight, (c) ensuring the impact of spent stages in safe zones and (d) meeting the overall heat flux limits for the vehicle and payload. The net acceleration history during atmospheric flight has to be shaped to reduce the dynamic pressure at critical regimes of flight. This has a direct bearing on the specifications of thrust time history for boosters. In order to minimize the vehicle loads, the aerodynamic load indicator, ‘Q alpha’ (product of dynamic pressure and angle of attack) has to be reduced. One should carry out studies in detail during the initial design phase to examine the need of the passive load relief adapting the wind biasing technique or active load relief during flight using the lateral accelerometer feedback.

The identification of tail-off and ensuring benign environment during transition regimes between two stages is essential for the success of staging events. This is achieved by implementing robust real time decision (RTD) strategies in vehicle onboard and suitable sequencing based on the RTD to meet the various requirements. In order to ensure clean separation of a spent stage from ongoing vehicle, the thrust level has to be below certain specified value, whereas the vehicle control requires higher value of thrust thus posing contradictory requirements. To meet both the requirements, it is essential to locate the tail-off region of the propulsive stages and then identify the pre-specified value of acceleration. By measuring the longitudinal acceleration using the inertial navigation system, the tail-off region of the stage is identified in real time termed as RTD time and all further sequence is referenced to this new timing.

The time gap between the stage transition zones has to be large enough to ensure smooth separation of stages whereas the gap has to be small to reduce the no control zone. Judicious sequence selection is essential to meet both the requirements. Various subsystems participating in the transition phases have to be designed with adequate robustness to achieve the mission success of multi-stage STS.

2.7.6 *Navigation, Guidance and Control Aspects*

The navigation errors generally lead to orbital injection errors, and therefore high accuracy gyros and accelerometers are to be chosen to minimize the errors. The various errors of sensors due to drift, scale factor, gravity effects and temperature effects are to be characterized in detail at ground. Excepting the random component of errors, all other errors are compensated continuously in flight to obtain high

accuracies. The environment levels for the sensors have to be carefully addressed, and any deformations at the sensor mounting location lead to erroneous data and may even end up with mission failure if the deformations are large. Therefore, selection of sensor locations and mounting mechanisms are crucial for the successful missions.

The control system has to ensure vehicle stability all through the flight by avoiding interaction with vehicle flexible structural modes and propellant, slosh modes. In a vehicle with liquid strap-ons, if there are longitudinal oscillations due to POGO effect in propellant lines, there is a chance that the phase difference between two can cause control structure and POGO interaction. Similarly the sensor dynamics, actuator dynamics, disturbances caused by aerodynamics and separation play a dominant role on control. The interdependence and interaction of control between these disciplines are very strong, and to avoid interaction, design should ensure sufficient separation between the control systems bandwidth and frequencies of actuators, structures and liquid slosh subsystems.

The control and guidance system has to achieve the end condition of inserting the payload precisely into the mission defined orbit under all parametric dispersions of propulsion, aerodynamics, separation dynamics, actuators, sensors and therefore generation of dispersion bounds for all parameters are to be judiciously decided considering all possible flight scenarios.

Modeling and analysis of the subsystem play a major role in the subsystem design process. This aspect is discussed in the next section.

2.8 Modeling and Analysis of Integrated System

An integrated approach for STS design evaluation during the initial phase using suitable vehicle system models is required to arrive at robust and optimum design. Modeling and analysis of such a complex STS system involving several disciplines play an important role in validating the designs and understanding the interactions. Therefore detailed modeling of all subsystems is necessary and extensive studies using six degrees of freedom trajectory with full vehicle dynamics, propulsion, aerodynamics, sensors and actuators are needed. The modeling and analysis methods are explained in detail in Chap. 8. The vehicle structural flexibility effects and stability characteristics are to be evaluated, simulating all the flexible modes with perturbations to understand the interactions, and the salient aspects are detailed in Chap. 14. The system evaluation is not complete without detailed failure analysis studies. It has to be carried out at different phases by identifying the failure modes of various elements along with the assessment of probabilities of the failures. The usual practice is to generate a logic diagram of a system and to identify all elements which can have potential failures. The impact of failure on the overall system also needs to be assessed. If the consequence is very severe then

suitable robustness in terms of increasing design margins or redundancy may have to be introduced in the design. The finalized design of each system has to be evaluated under the flight simulated environment.

2.9 Subsystem and System Design and Performance Evaluation

Generation of suitable test plan for the evaluation of subsystem and system during design phase is a very essential component of STS design process. It also helps in planning suitable test facility which may require a long lead time. The test matrix so generated should be comprehensive to evaluate the performance of the system vis-à-vis specifications of components, subsystems and system. The operating environment of each of the subsystem has to be properly assessed and suitable tests and test levels are to be carefully designed (thermal, vibration, EMI, shock, acoustics) to evaluate the system in the near real environment. Depending on the subsystem, suitable tests are to be defined at component, subsystem and system levels. The tests enable the designers to evaluate the interfaces, system performance and also the design margins. Certain aspects of integrated system performance cannot be evaluated in a single test bed. In such cases, it is essential to design different simulation test beds with specified objectives of evaluating different aspects of the integrated system performance. It is also necessary to carry out simulations by integrating the flight hardware in a progressive manner to evaluate the performance of flight systems. The integrated simulation test bed also enables to carry out system robustness tests for all combinations of flight environment, parametric dispersions of subsystems and various failure modes.

An example for the generation of a test matrix for typical stage separation system of a launch vehicle is given in Fig. 2.8.

The figure depicts the type of tests needed for atypical separation system of a vehicle at component, subsystem and system levels. The validation procedure includes the analysis and simulation, progressive integration of some of the actual hardware during the simulation and six degrees of freedom (6D) integrated digital simulations. Based on this test matrix, suitable test facilities are to be planned for each of these tests. The test cases and number of tests are to be defined carefully to ensure that all aspects of the system are evaluated. Such an exhaustive test scheme should evaluate the trouble free separation of the system in flight. The simulation test bed should attempt to include all possible flight conditions, and the test cases are to be designed with great care to ensure that it encompasses all conditions that a separation system may face during the actual flight.

Test plan generation and performance evaluation of the designed system with respect to the specification under the simulated flight environment has to be carried out for all the vehicle systems. The system design is finalized only after achieving

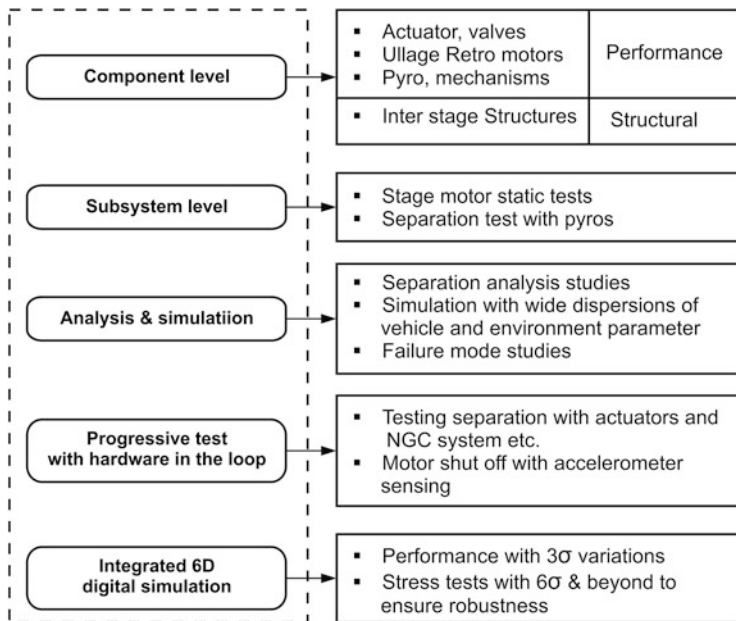


Fig. 2.8 Typical test matrix for a vehicle separation system

the satisfactory performance. The relevant test matrix for each of the system and the relevant performance evaluation strategies of the system are discussed in details in the corresponding chapters of this book.

Bibliography

1. Walter E. Hammond W.E.: Design Methodologies for Space Transportation Systems. AIAA Education Series
2. Hammond, W.E.: Space Transportation: A Systems Approach to Analysis and Design, vol. 1 AIAA Education Series
3. Gupta, S.C., Suresh, B.N., Sivan, K.: Evolution of Indian launch vehicle technologies. Special Edition of Curr. Sci. **93**(12), 1697–1714 (2007)
4. Suresh, BN.: Space transportation systems in India, present scenario and future perspectives. J. Aerosp. Sci. Technol. **61**(1) (2009)
5. Gupta, S.C., Suresh, B.N.: Development of navigation guidance and control technology for Indian Launch Vehicles. Sadhana. **12**(3), 235–249 (1988)

Chapter 3

Astro dynamics

Abstract To specify the functional requirements of STS, it is essential to understand the orbital motion of the injected satellites under the influence of a central gravitational force and other disturbing forces. This chapter deals with astrodynamics which explains the motion of celestial bodies as well as human-made satellites under the influence of gravitational force field of celestial bodies and other external forces. Orbital motions of Low Earth Orbit (LEO) satellites are the solutions of two-body problems i.e. the Earth and the satellite, in the specified reference frame, considering the Earth's gravitational force as the primary central body force field. The deviation of the gravity force away from the central force field and other disturbance forces affect the orbital motion of the satellites. In addition to the central force field, gravitational forces of other planets and Moon also influence the higher altitude orbital motions. Solutions for such motions are achieved by solving restricted three body problem, considering the Earth's gravity force as the central gravity field whereas the perturbing gravitational force is from the third body such as Moon. Depending on the type of trajectory, different reference frames are used and these aspects are explained first. Then, this chapter discusses the orbital mechanics of satellites and various aspects of orbital motions of two-body problems. The restricted three body problem and the resulting orbital motion are also briefly explained. Even though the launch vehicles are capable of injecting the satellites in the near Earth orbits, for certain scientific applications, these satellites have to reach and orbit around Moon or distant planets. The interplanetary trajectories of such satellites from the Earth bound orbits to the target planets are also included. In an integrated mission management, optimum strategies like transferring the satellite at suitable time from the initial orbit to the required one in an optimum fashion are required. Various optimum orbital transfer maneuver strategies are explained in this chapter.

Keywords Astrodynamics • Reference frame • Two-body problem • Orbits • Orbital elements • Three-body problem • Interplanetary trajectory and orbits transfer

3.1 Introduction

The functional requirement of a space transportation system (STS) is to lift a specified satellite with a defined mass and to inject it into the mission defined orbit (within allowable dispersion band) in space. To achieve the above requirements, the subsystems of the STS are designed to achieve the targeted state with the specified accuracy bands in space, which in turn lead to the specified orbit within the allowable error bounds. In order to specify the functional requirements in terms of the required final state of STS, it is essential to understand the orbital motion of the injected satellites under the influence of a central gravitational force and other disturbing forces which can alter the orbits achieved by the STS.

Astrodynamics deals with the motion of celestial bodies as well as human-made satellites under the influence of gravitational force field of celestial bodies and other external forces. While the motion of celestial bodies are referred as celestial mechanics, that of the human-made satellites are classified under orbital mechanics.

Generally, orbital motions of Low Earth Orbit (LEO) satellites are the solutions of two-body problems in the specified reference frame, considering the Earth's gravitational force as the primary central body force field. In these problems, the Earth and the satellite are the two bodies. The deviation of the gravity force away from the central force field changes the characteristics of Earth-bound satellite orbits. In certain cases, these particular orbital characteristics are favorably used to achieve the satellite-specific mission requirements. In addition, other disturbance forces also affect the orbital motion of the satellites.

In addition to the central force field, gravitational forces of other planets and Moon also influence the higher altitude orbital motions. Solutions for such motions are achieved by solving restricted three body problem, considering the Earth's gravity force as the central gravity field whereas the perturbing gravitational force is from the third body such as Moon. Depending on the type of trajectory, different reference frames are used and these aspects are explained first. Then, this chapter deals with the orbital mechanics of satellites and various aspects of orbital motions of two-body problems. The restricted three body problem and the resulting orbital motion are also briefly explained.

Even though the launch vehicles are capable of injecting the satellites in the near Earth orbits, for certain scientific applications, these satellites have to reach and orbit around Moon or distant planets. The interplanetary trajectories of such satellites from the Earth-bound orbits to the target planets are also included.

In the integrated satellite mission management, optimum strategies are being adopted considering: (i) launching satellites into a suitable Earth bound orbit and (ii) transfer the satellite at suitable time from the initial orbit to the finally required orbit in an optimum fashion. Various optimum orbital transfer maneuvers are also brought out in this chapter.

Considering the integrated mission requirements and the various factors as defined above, the mission target defined for the STS is also explained.

3.2 Reference Frames

Orbital mechanics deals with the trajectories of satellites around central bodies. The motion of a satellite is described in terms of its position and velocity vectors as functions of time. Therefore, a reference frame is required with respect to which the position and velocity vectors are defined. In order to define a coordinate reference frame, three fundamental elements are required:

1. Origin
2. A reference plane passing through the origin
3. A reference axis, lying in the reference plane, originating from the origin and pointing towards a well-defined reference point

The three dimensional coordinate system is defined by specifying one axis along the direction of reference axis, second axis normal to the reference plane and third axis in the reference plane, thus completing the right-handed orthogonal system.

Once the origin and reference plane are fixed in space and reference axis is pointed towards distant stars, then the reference frame is fixed in space. The reference frames, either fixed in space or moving with uniform velocity, without rotation with respect to distant stars are un-accelerated. Such frames are called inertial reference frames. If a reference frame is inertial, then every other reference frame which is in uniform motion relative to it is also an inertial reference frame.

Inertial reference frames are important as it is useful to define motion of an object as per the Newtonian mechanics. Alternatively, inertial reference frame is one in which Newton's laws of motion are valid.

In order to describe the motion of a satellite, the inertial reference frame makes use of celestial references. Therefore, the corresponding celestial references are explained first, followed by the reference frames being used in orbital mechanics to describe the motion of satellite orbits.

3.2.1 Celestial Sphere and Ecliptic

Celestial sphere is a fictitious sphere of infinitely large radius with the Earth at its center. All the celestial bodies appear to be on the surface of the sphere and move westward over the celestial sphere due to the rotation of the Earth about its spin axis. This is called diurnal motion. The extensions of the Earth's equator and the spin axis intersect with the celestial sphere and are called celestial equator and celestial poles respectively. For an observer on the Earth, in addition to its daily motion, there is a motion of the Sun towards eastwards over the celestial sphere at the rate of approximately $1^\circ/\text{day}$ and return to its initial position on the celestial sphere in one year. The path of this apparent motion of the Sun over the celestial sphere is called the ecliptic. With respect to the Sun, ecliptic is the Earth's orbit around the Sun. The ecliptic plane is inclined to the equatorial plane by an angle ϵ ,

which is called as the obliquity of the ecliptic. The present value of ϵ is about 23.5° . Axis of the ecliptic intersects the celestial sphere at the ecliptic poles. Therefore, obliquity of the ecliptic ϵ is the angle between celestial North Pole and ecliptic pole.

Sun in apparent motion along ecliptic crosses the celestial equator at two points, called equinoxes, and reaches highest point with respect to celestial equator, called solstices. During its motion from the southern hemisphere to northern hemisphere, the Sun crosses the celestial equator at Vernal equinox and reaches Summer solstice in northern hemisphere. Subsequently, the Sun crosses the celestial equator at Autumnal equinox during its motion from northern hemisphere to southern hemisphere and reaches the Winter solstice. Approximate dates of occurrence of these events over a year are:

Vernal equinox	: March 21st
Summer solstice	: June 21st
Autumnal equinox	: September 21st
Winter solstice	: December 21st

However, there could be a variation of ± 1 day due to the variation of prediction methodologies and perturbations of planetary orbital characteristics. In effect, the line joining the equinox points is the intersecting line of equatorial plane and ecliptic plane. Due to the Sun, planets and Moon gravitational effects on Earth's orbit and spin axis, the equinox line is not fixed in space as given below:

1. The obliquity angle oscillates between 22.1° and 24.5° with a period of about 41,000 years. Currently the angle is 23.44° and decreasing.
2. The effect of other planets on the plane of Earth orbit causes smaller motion of the ecliptic about $0.114''/\text{year}$. This is known as planetary precession.
3. Due to the gravitational effect of the Sun and Moon on the Earth's gravitational bulge, the Earth spin axis rotates about the poles of ecliptic with the period of approximately 26,000 years. This motion is called lunisolar precession.

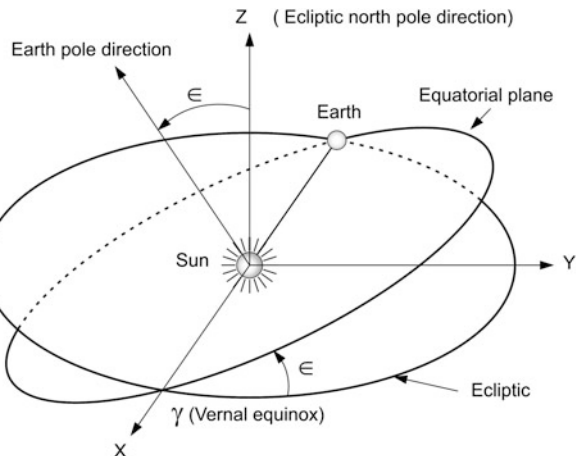
Orbital plane of the Moon is also precessing with the period of 18.6 years. This causes a nutation of smaller amplitude with a period of 18.6 years on the Earth spin axis.

However, as the period involved in the variation of equinox line is very large compared to the mission durations of STS and human-made satellites, the equinox line can be considered as fixed in space and this plays a fundamental role for the definition of inertial reference frames.

3.2.2 *Heliocentric Inertial Reference Frame*

Origin of the heliocentric reference frame is the Sun's mass center. The fundamental plane is the ecliptic, X-axis of this frame is passing through the Vernal equinox, Z-axis is along the ecliptic north pole direction and Y-axis lies in the ecliptic plane

Fig. 3.1 Heliocentric inertial frame



and completes the right-handed system as given in Fig. 3.1. Even though the Vernal equinox is not fixed in space, still the heliocentric reference frame is considered as an inertial frame for most of our missions since the time duration of most of the missions are much smaller than the period of variations of the reference X-axis (Vernal equinox).

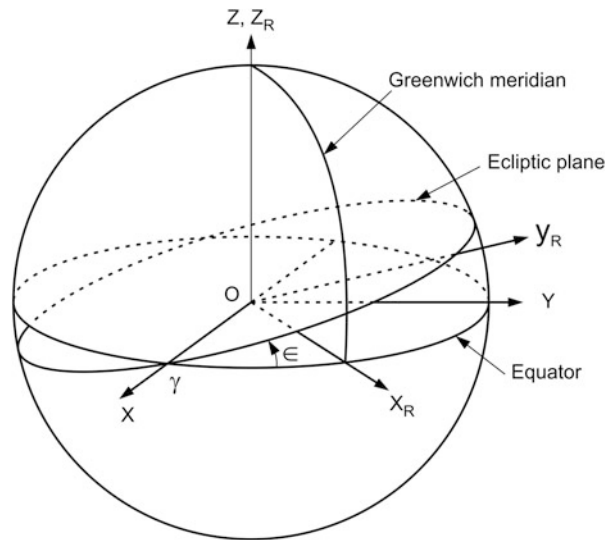
This frame is useful for describing planetary motions or motion of human-made satellites for the interplanetary missions.

3.2.3 *Earth Centered/Geocentric Inertial (ECI) Reference Frame*

Origin of ECI is the Earth's center. The fundamental plane is the equator, X-axis is the reference axis, passing through the Vernal equinox, Z-axis is along the Earth's North Pole direction and Y-axis lies in the equatorial plane and completes the right-handed system as shown in Fig. 3.2. It is pertinent to note that XYZ is not fixed with the Earth and that it is non-rotating with respect to the distant stars, whereas the Earth rotates.

As in the case of heliocentric reference frame, though the reference direction towards Vernal equinox is not truly inertial, for the purpose of missions carried out by the STS as well as for the orbital motions of satellites around the Earth, the ECI frame can be considered as inertial reference. Earth gravitational accelerations are calculated in this reference frame and the orbital elements of satellites are computed based on the state vector given with respect to this ECI reference frame.

Fig. 3.2 Earth centered inertial and Earth centered rotating frames



3.2.4 Earth-Centered Rotating (ECR) Frame

Origin of ECR is the Earth's center. The fundamental plane is the equatorial plane. The reference axis, X_R -axis is in the equatorial plane, passes through the Greenwich meridian and rotates along with it, Z_R -axis is along the Earth's north pole and Y_R lies in the equatorial plane, completes the right-handed system as given in Fig. 3.2. The ECR frame rotates about Z_R -axis at the spin rate of the Earth, i.e., $15.0411^\circ/h$ with respect to the ECI frame. This frame is also termed as World Geodetic System (WGS) and is mostly used in Satellite Navigation System.

3.3 Laws of Motion

3.3.1 Kepler's Laws

Many astronomers studied the motions of planetary bodies. Aristotle hypothesized that all planetary bodies move in circular paths. Danish astronomer Tycho Brahe (1546–1606) collected huge amount of accurate data on planetary motions for many years. Johannes Kepler (1571–1630) joined Tycho Brahe as his assistant in 1600 and studied the Tycho's data in detail during 1601–1606. Based on the extensive studies, he deduced three laws of planetary motions as given below:

1. The orbit of each planet lies in a fixed plane containing the Sun and is an ellipse with Sun at one focus.
2. The line joining a planet to the Sun sweeps equal areas in equal intervals of time.

3. The square of the period of revolution of a planet is proportional to the cube of the semi-major axis of its elliptical orbit.

While the Kepler's laws describe the motions of planets, orbital mechanics based on the applications of Sir Issac Newton's (1642–1727) law of universal gravitation and his three laws of motion provide more general explanations for the motions of the bodies. Kepler's laws can be proved through Newtonian mechanics. Since the velocities involved in the motion of the bodies are small compared to the velocity of light, classical or Newtonian mechanics is sufficient for describing the motion of satellites.

3.3.2 Newton's Laws of Motion

Newton's three laws of motion are given below:

1. A body continues its state of rest or of uniform motion in a straight line unless compelled by external force to change the state.
2. The rate of change of momentum of a body is directly proportional to the applied force and this change takes place in the direction of the applied force.
3. For every action there is always an equal and opposite reaction.

The first law is about the motion, which is relative. It is necessary to describe the motion with respect to a reference frame. Therefore, the first law can be interpreted as that there exists a reference frame with respect to which a body, free of all external forces, is in uniform motion. Such a reference frame is inertial reference frame. Therefore, Newton's laws of motion are valid in inertial frame only.

While the first law gives qualitative statement that a force is the cause of motion, the Newton's second law provides the quantitative definition of the force. The second law is valid only with respect to an inertial frame.

Consider a body of mass, m , moving with velocity \mathbf{V} , then the linear momentum of \mathbf{P} of the body is given by,

$$\mathbf{P} = m\mathbf{V} \quad (3.1)$$

As per the Newton second law,

$$\mathbf{F} \propto \frac{d\mathbf{p}}{dt} \quad (3.2)$$

Considering mass, m is constant, then the Eq. (3.2) can be written as

$$\mathbf{F} \propto m \frac{d\mathbf{V}}{dt} \quad (3.3)$$

Considering the rate of change of velocity as acceleration, \mathbf{a} , Eq. (3.3) can be written as

$$\mathbf{F} = k \mathbf{ma} \quad (3.4)$$

where a is the acceleration and k is the constant of proportionality, which depends on the units of the parameters used in the equation. Considering force in Newton (N), mass in kilogram (kg), acceleration in m/s^2 , for the case of $F = 1 \text{ N}$, $m = 1 \text{ kg}$, $a = 1 \text{ m/s}^2$ then $k = 1$. Therefore, Eq. (3.4) can be written as

$$\mathbf{F} = \mathbf{ma} \quad (3.5)$$

There are two types of masses viz., inertial mass and gravitational mass. The mass used in Eq. (3.5) is the inertial mass whereas the mass used in the Newton law of gravitation (as explained later) is gravitational mass. The inertial mass of a body depends on the motion and is given by

$$m = \frac{m_0}{\sqrt{1 - \frac{v^2}{c^2}}} \quad (3.6)$$

where m_0 is the mass at rest, C is speed of light and V is the speed of the body in motion. As the speed of the body considered is much less than the speed of light, in Newtonian mechanics, mass can be assumed as constant, which corresponds to the value at rest, m_0 .

Newton's third law of motion explained that mutual forces of two bodies acting upon each other are equal in magnitude and opposite in direction, and these actions and reactions are collinear. Consider body 2 exerts a force \mathbf{F}_{12} on body 1 as given in Fig. 3.3, then body 1 exerts an opposite force \mathbf{F}_{21} on body 2, so that

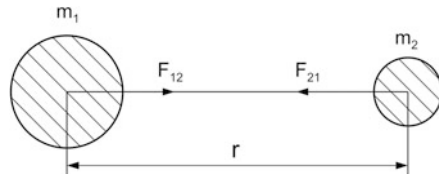
$$\mathbf{F}_{12} + \mathbf{F}_{21} = 0 \quad (3.7)$$

and

$$\mathbf{F}_{12} = -\mathbf{F}_{21} \quad (3.8)$$

In summary, Newton's first law of motion tells that the state of motion of a body can be changed only if there is a force acting on it. The second law tells how much change in the state of motion of the body, if there is a force and the third law tells how the forces are exerted.

Fig. 3.3 Two bodies separated by distance r



3.3.3 Newton's Law of Universal Gravitation

Newton's law of universal gravitation states that two bodies exert a force on each other along the line joining them and is directly proportional to the product of their masses and inversely proportional to the square of the distance between them. Consider two homogenous bodies with masses m_1 and m_2 as shown in Fig. 3.3. The two bodies are subject to mutual gravitational forces. The gravitational force acting on each body can be written as

$$F \propto \frac{m_1 m_2}{r^2} \quad (3.9)$$

i.e.,

$$F = \frac{G m_1 m_2}{r^2} \quad (3.10)$$

where the proportionality constant G is known as the Universal gravitational constant and the value is about $6.67 \times 10^{-11} \text{ Nm}^2/\text{kg}^2$.

Assuming F_{21} is the gravitational force exerted on body 2 by body 1 and is given as

$$F_{21} = \frac{G m_1 m_2}{r^2} \quad (3.11)$$

Similarly, the force on body 1 by body 2 is given by

$$F_{12} = \frac{G m_1 m_2}{r^2} \quad (3.12)$$

In vector notations, F_{21} and F_{12} are in the opposite direction.

3.4 Two-Body Problem

In universe, each and every body is attracted to each other. Since the distance between the bodies is large, the motion of two close bodies is influenced by their gravitational forces alone where the other body effects are negligible. Therefore, most of the orbital mechanics can be treated as the solution of a two-body problem. Two-body orbital mechanics is the determination of the motion of two point masses which are subjected only by their own mutual gravitational forces. This is the case when both the bodies are homogeneous spheres. The deviations in the solutions of two-body problems may arise when the bodies are not true point masses or some other forces are exerted on the bodies apart from the mutual gravitational forces. Such forces can be considered small compared to the gravitational forces and the effects can be treated as perturbations over the solutions of two-body problems.

In this section, general two-body problem is explained first, and then the special case of motion of a very small body compared to the primary central body (as in the case of satellite motion about the Earth) is described in detail. The perturbations due to non-central force field are explained in a later section of this chapter.

Consider two homogeneous spherical bodies in inertial frame as shown in Fig. 3.4. As per Newton's law of universal gravitation, F_{21} is the force exerted on body 2 by body 1 and is given as

$$F_{21} = \frac{G m_1 m_2}{r^2} \quad (3.13)$$

where r is the distance between the bodies. Let \mathbf{r} be the position vector of m_2 with respect to m_1 , and \mathbf{u}_r is the unit vector along the \mathbf{r} , then

$$\mathbf{u}_r = \frac{\mathbf{r}}{r} \quad (3.14)$$

In vector notation, Eq. (3.13) can be written as

$$\mathbf{F}_{21} = -\frac{G m_1 m_2}{r^2} \mathbf{u}_r \quad (3.15)$$

and the same can be expressed as

$$\mathbf{F}_{21} = -\frac{G m_1 m_2}{r^3} \mathbf{r} \quad (3.16)$$

Using Newton's second law of motion and referring Fig. 3.4a, the force, \mathbf{F}_{21} , can also be written as

$$\mathbf{F}_{21} = m_2 \ddot{\mathbf{R}}_2 \quad (3.17)$$

Using Eqs. (3.16) and (3.17),

$$m_2 \ddot{\mathbf{R}}_2 = -\frac{G m_1 m_2}{r^3} \mathbf{r} \quad (3.18)$$

Using Newton's third law, the force exerted on body 1 by body 2 can be written as

$$\mathbf{F}_{12} = -\mathbf{F}_{21} \quad (3.19)$$

As explained earlier,

$$m_1 \ddot{\mathbf{R}}_1 = \frac{G m_1 m_2}{r^3} \mathbf{r} \quad (3.20)$$

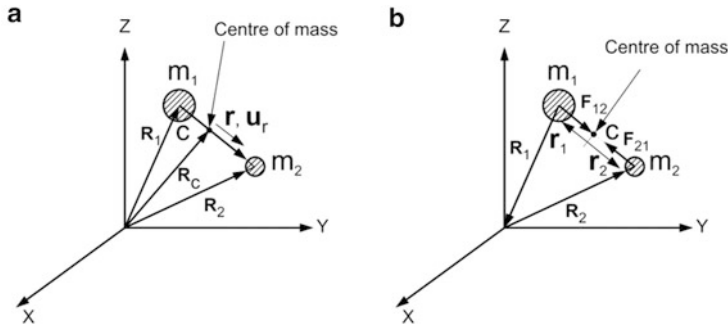


Fig. 3.4 Two-body system: (a) two bodies in inertial frame (b) free-body diagram

Let \mathbf{R}_c be the center of mass of the two body system. Then,

$$\mathbf{R}_c = \frac{m_1 \mathbf{R}_1 + m_2 \mathbf{R}_2}{m_1 + m_2} \quad (3.21)$$

and

$$\ddot{\mathbf{R}}_c = \frac{m_1 \ddot{\mathbf{R}}_1 + m_2 \ddot{\mathbf{R}}_2}{m_1 + m_2} \quad (3.22)$$

Adding Eqs. (3.18) and (3.20) yields

$$m_1 \ddot{\mathbf{R}}_1 + m_2 \ddot{\mathbf{R}}_2 = 0 \quad (3.23)$$

Applying Eq. (3.23) in Eq. (3.22) shows that the acceleration of the center of mass is zero. Therefore, center of mass of a two-body system can be considered for inertial frame.

Eqs. (3.18) and (3.20) can be written as

$$\ddot{\mathbf{R}}_2 = -\frac{G m_1}{r^3} \mathbf{r} \quad (3.24)$$

and

$$\ddot{\mathbf{R}}_1 = -\frac{G m_2}{r^3} \mathbf{r} \quad (3.25)$$

Subtracting Eq. (3.25) from Eq. (3.24),

$$\ddot{\mathbf{R}}_2 - \ddot{\mathbf{R}}_1 = -\frac{G(m_1 + m_2)}{r^3} \mathbf{r} \quad (3.26)$$

By the definition of position vectors,

$$\mathbf{r} = \mathbf{R}_2 - \mathbf{R}_1 \quad (3.27)$$

which gives

$$\ddot{\mathbf{r}} = \ddot{\mathbf{R}}_2 - \ddot{\mathbf{R}}_1 \quad (3.28)$$

Using Eq. (3.28), Eq. (3.26) can be written as

$$\ddot{\mathbf{r}} = -\frac{G(m_1 + m_2)}{r^3} \mathbf{r} \quad (3.29)$$

Equation (3.29) governs the motion of mass m_2 relative to mass m_1 . This can also be written as

$$\ddot{\mathbf{r}} = -\frac{\mu}{r^3} \mathbf{r} \quad (3.30)$$

where $\mu = G(m_1 + m_2)$ is the gravitational constant of the specified two-body system.

Since center of mass has zero acceleration, it can be considered as an inertial reference and motion of each body can be defined about the center of mass. Let \mathbf{r}_1 and \mathbf{r}_2 be the position vectors of masses m_1 and m_2 with respect to the center of mass. Then,

$$\mathbf{r} = \mathbf{r}_2 - \mathbf{r}_1 \quad (3.31)$$

Since the position vector of center of mass relative to itself is zero,

$$m_1 \mathbf{r}_1 + m_2 \mathbf{r}_2 = 0 \quad (3.32)$$

Therefore,

$$\mathbf{r}_1 = -\frac{m_2}{m_1} \mathbf{r}_2 \quad (3.33)$$

Using Eq. (3.33) in Eq. (3.31) yields

$$\mathbf{r} = \frac{m_1 + m_2}{m_1} \mathbf{r}_2 \quad (3.34)$$

The equations of motion of m_2 with respect to the center of mass is given by

$$m_2 \ddot{\mathbf{r}}_2 = -\frac{Gm_1 m_2}{r^3} \mathbf{r} \quad (3.35)$$

Using Eq. (3.34) in Eq. (3.35) yields

$$\ddot{\mathbf{r}}_2 = -\frac{Gm_1^3}{(m_1 + m_2)^2 r_2^3} \frac{\mathbf{r}_2}{r_2^3} \quad (3.36)$$

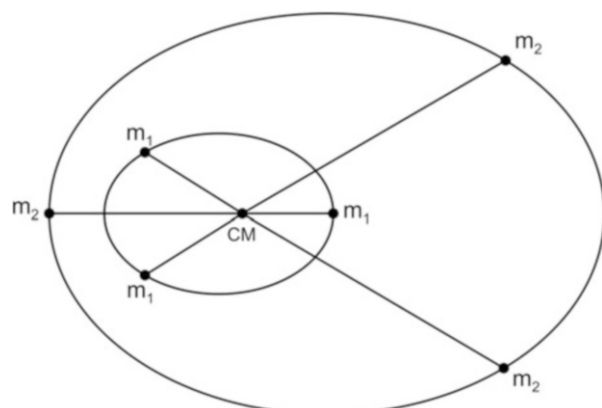
Equation (3.36) gives the motion of m_2 about center of mass. The path of m_2 relative to center of mass is a conic with C as a focus, which is explained later. If V_2 is the velocity and r_2 is the position of m_2 , with respect to C, then this conic can be

$$\left. \begin{array}{l} \text{Ellipse} \\ \text{Parabola} \\ \text{Hyperbola} \end{array} \right\} \text{ if } \left\{ \begin{array}{l} V_2^2 < 2Gm_1^3 / [(m_1 + m_2)^2 r_2] \\ V_2^2 = 2Gm_1^3 / [(m_1 + m_2)^2 r_2] \\ V_2^2 > 2Gm_1^3 / [(m_1 + m_2)^2 r_2] \end{array} \right.$$

Similarly, the expression for the path of m_1 about center of mass can be derived. Typical paths (ellipse) of the two bodies with respect to center of mass of two-body problem are represented in Fig. 3.5.

Consider the Sun-Earth system, the ratio of masses is $\cong 1/332900(m_2/m_1)$. The distance between the Sun and the Earth is of the order of 150 million kilometers (r), whereas the center of mass of the system is of the order of 455 km from the center of the Sun. The angular velocity of line joining the Sun and Earth, ω is given by

Fig. 3.5 Two-body motions



$$\omega = \frac{V_1}{r_1} = \frac{V_2}{r_2} \quad (3.37)$$

where V_1 and V_2 are velocity of Sun and Earth with respect to center of mass respectively, and r_1 and r_2 are distance of center of Sun and Earth with respect to the center of mass of the system.

Therefore, the velocity V_2 of the Earth (m_2) about center of mass is of the order of 30,000 m/s whereas that of the Sun (m_1) of the order of 0.1 m/s.

When $m_1 \gg m_2$, as in the case of Earth-satellite systems, then the center of the principal attracting body (in this case the larger body is Earth) can be taken as the center of mass and hence can be considered as the origin of the inertial system. The governing equations of such two-body system can be given using Eq. (3.29) as such.

$$\ddot{\mathbf{r}} = -\frac{Gm_1}{r^3} \mathbf{r} \quad (3.38)$$

and

$$\ddot{\mathbf{r}} = -\frac{\mu}{r^3} \mathbf{r} \quad (3.39)$$

where m_1 is the mass of the larger body (Earth). In this case, the gravitational constant, μ , is Gm_1 . The value of Earth's gravitational constant is $3.986013 \times 10^5 \text{ km}^3/\text{s}^2$. The Eq. (3.39) describes the motion of the restricted two-body system.

Cross product of Eq. (3.39) with \mathbf{r} leads to

$$\mathbf{r} \times \ddot{\mathbf{r}} = 0 \quad (3.40)$$

As

$$\frac{d}{dt}(\mathbf{r} \times \dot{\mathbf{r}}) = \dot{\mathbf{r}} \times \dot{\mathbf{r}} + \mathbf{r} \times \ddot{\mathbf{r}} \quad (3.41)$$

Using Eq. (3.40), the Eq. (3.41) leads to

$$\frac{d}{dt}(\mathbf{r} \times \dot{\mathbf{r}}) = 0 \quad (3.42)$$

Therefore, the angular momentum per unit mass \mathbf{H} , given by

$$\mathbf{H} = \mathbf{r} \times \dot{\mathbf{r}} = \text{constant} \quad (3.43)$$

As \mathbf{r} and $\dot{\mathbf{r}}$ are normal to the angular momentum, the orbital motion of the mass m_2 is in a plane normal to \mathbf{H} .

Let A be the area swept by the line joining the two bodies in a specified time. Then,

$$\frac{dA}{dt} = \frac{1}{2} |\mathbf{r} \times \dot{\mathbf{r}}| = \frac{1}{2} |\mathbf{H}| = \text{constant} \quad (3.44)$$

This proves Kepler's second law. Solution to Eq. (3.39) can be obtained by taking cross product of Eq. (3.39) with H.

$$\mathbf{H} \times \ddot{\mathbf{r}} = -\frac{\mu}{r^3} (\mathbf{H} \times \mathbf{r}) \quad (3.45)$$

$$\frac{d}{dt} (\mathbf{H} \times \dot{\mathbf{r}}) = \dot{\mathbf{H}} \times \dot{\mathbf{r}} + \mathbf{H} \times \ddot{\mathbf{r}} \quad (3.46)$$

Since the angular momentum is constant, $\dot{\mathbf{H}} = 0$. Therefore, Eq. (3.46) can be written as

$$\mathbf{H} \times \ddot{\mathbf{r}} = \frac{d}{dt} (\mathbf{H} \times \dot{\mathbf{r}}) \quad (3.47)$$

The right-hand side of Eq. (3.45) can be written as

$$\frac{1}{r^3} (\mathbf{H} \times \mathbf{r}) = \frac{1}{r^3} [(\mathbf{r} \times \dot{\mathbf{r}}) \times \mathbf{r}] \quad (3.48)$$

Using vector rule,

$$(\mathbf{r} \times \dot{\mathbf{r}}) \times \mathbf{r} = (\mathbf{r} \mathbf{r}) \dot{\mathbf{r}} - (\mathbf{r} \dot{\mathbf{r}}) \mathbf{r} \quad (3.49)$$

Using Eq. (3.49), Eq. (3.48) can be written as

$$\frac{\frac{1}{r^3} (\mathbf{H} \times \mathbf{r})}{r^2} = \mathbf{r} \dot{\mathbf{r}} - \dot{\mathbf{r}} \mathbf{r} \quad (3.50)$$

But,

$$\frac{d}{dt} \left(\frac{\mathbf{r}}{r} \right) = \frac{\mathbf{r} \dot{\mathbf{r}} - \dot{\mathbf{r}} \mathbf{r}}{r^2} \quad (3.51)$$

Therefore, using Eqs. (3.47) and (3.51), Eq. (3.45) can be written as

$$\frac{d}{dt} (\mathbf{H} \times \dot{\mathbf{r}}) = -\mu \frac{d}{dt} \left(\frac{\mathbf{r}}{r} \right) \quad (3.52)$$

Integrating the Eq. (3.52) gives

$$\mathbf{H} \times \dot{\mathbf{r}} = -\mu \left[\frac{\mathbf{r}}{r} + \mathbf{e} \right] \quad (3.53)$$

where \mathbf{e} is the dimensionless vector constant of integration called eccentricity.

Equation (3.53) can be written as

$$\frac{\mathbf{r}}{r} + \mathbf{e} = \frac{\dot{\mathbf{r}} \times \mathbf{H}}{\mu} \quad (3.54)$$

Taking dot product of Eq. (3.54) with \mathbf{H} gives

$$\frac{\mathbf{r}\mathbf{H}}{r} + \mathbf{e}\mathbf{H} = \frac{(\dot{\mathbf{r}} \times \mathbf{H})\mathbf{H}}{\mu} \quad (3.55)$$

\mathbf{H} is perpendicular to both \mathbf{r} and $\dot{\mathbf{r}}$. Therefore, $\mathbf{r} \cdot \mathbf{H} = 0$. Similarly, the vector $(\dot{\mathbf{r}} \times \mathbf{H})$ is perpendicular to both $\dot{\mathbf{r}}$ and \mathbf{H} . Therefore, $(\dot{\mathbf{r}} \times \mathbf{H}) \cdot \mathbf{H} = 0$. Considering the above aspects, Eq. (3.55) can be written as

$$\mathbf{e}\mathbf{H} = 0 \quad (3.56)$$

Equation (3.56) shows the eccentricity vector, \mathbf{e} is perpendicular to \mathbf{H} and therefore lies in the orbital plane formed by \mathbf{r} and $\dot{\mathbf{r}}$. \mathbf{e} vector lies along the line of apsides as explained below.

To express scalar equation of motion of two-body problem, take the dot product of Eq. (3.54) with \mathbf{r} as given below:

$$\frac{\mathbf{r}\mathbf{r}}{r} + \mathbf{r}\mathbf{e} = \mathbf{r} \frac{(\dot{\mathbf{r}} \times \mathbf{H})}{\mu} \quad (3.57)$$

Using the vector identity of interchange of dot and cross products, Eq. (3.57) can be written as

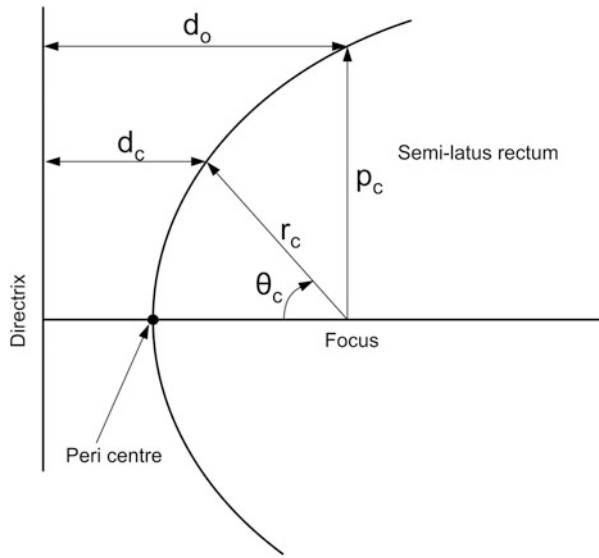
$$\frac{\mathbf{r}\mathbf{r}}{r} + \mathbf{r}\mathbf{e} = \frac{(\mathbf{r} \times \dot{\mathbf{r}})\mathbf{H}}{\mu} \quad (3.58)$$

Since $\mathbf{r} \cdot \mathbf{r} = r^2$, $\mathbf{r} \times \dot{\mathbf{r}} = \mathbf{H}$ and $\mathbf{H} \cdot \mathbf{H} = H^2$, Eq. (3.58) can be written as

$$\mathbf{r} + \mathbf{r}\mathbf{e} = \frac{\mathbf{H}^2}{\mu} \quad (3.59)$$

$\mathbf{r} \cdot \mathbf{e}$ can be expressed as

$$\mathbf{r} \cdot \mathbf{e} = r e \cos\theta \quad (3.60)$$

Fig. 3.6 Conic section

where e is the magnitude of eccentricity vector, θ is the angle between eccentricity vector (line of apses) and position vector \mathbf{r} . Then Eq. (3.59) is written as

$$\mathbf{r} = \frac{H^2/\mu}{1 + e \cos\theta} \quad (3.61)$$

In general, conic section is the locus of all points which follow the constant ratio for (r_c/d_c) as shown in Fig. 3.6, where r_c is the distance of a point from focus and d_c is the distance of the point from a given line called directrix. The constant ratio (r_c/d_c) is called the eccentricity, e_c of the conic section.

From Fig. 3.6,

$$d_0 = d_c + r_c \cos\theta_c \quad (3.62)$$

As per the definition of eccentricity,

$$\frac{p_c}{d_0} = \frac{r_c}{d_c} = e_c \quad (3.63)$$

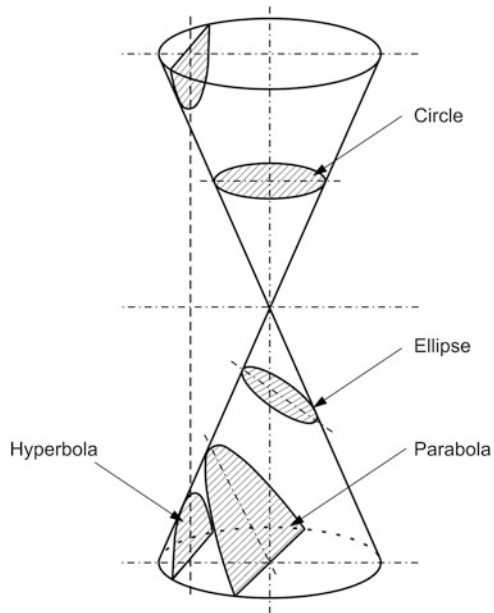
Using Eqs. (3.62) and (3.63), it can be shown that a conic equation is represented as

$$r_c = \frac{p_c}{1 + e_c \cos\theta_c} \quad (3.64)$$

The value of e_c decides the various conic sections as represented in Fig. 3.7.

$e_c = 0$, conic is circle

$0 < e_c < 1$, conic is ellipse

Fig. 3.7 Conic sections

$e_c = 1$, conic is parabola

$e_c > 1$, conic is hyperbola

Therefore, it can be concluded that the trajectory of a smaller body (in this case, satellite) with respect to the bigger body (in this case, Earth) in the central gravitational force field as represented in Eq. (3.61) is a conic as given below:

$$r = \frac{p}{1 + e \cos \theta} \quad (3.65)$$

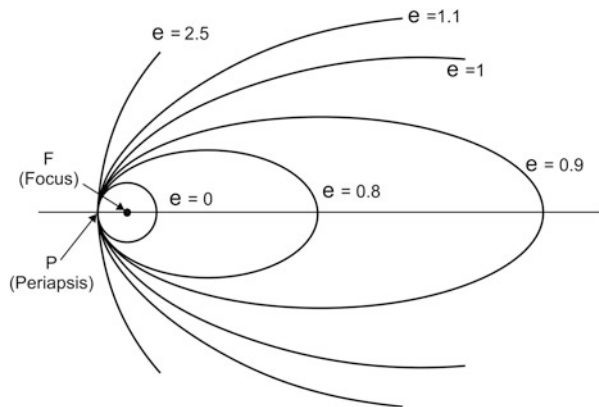
where the semi-latus rectum of the trajectory is given by

$$p = \frac{H^2}{\mu} \quad (3.66)$$

The eccentricity, e , of the Eq. (3.65) decides the shape and type of the trajectory of small body with respect to the bigger one as given below:

$e = 1$ represents a closed trajectory called circular orbit of smaller body around the central body, whereas $0 < e < 1$ also represents a closed trajectory, and in this case, the orbit is an ellipse. If $e = 1$, the trajectory of smaller body is an open trajectory with the shape of parabola and $e > 1$ represents the motion of smaller body as an open trajectory of hyperbola about the central body. This gives the mathematical statement of Kepler's first law. The orbit of a body under central force field is called Keplerian orbit. Typical orbits and trajectories for various

Fig. 3.8 Orbits with various eccentricities with the same focus and common periapsis



values of e which have the same focus and common periapsis are represented in Fig. 3.8.

As explained above, the cross product of Eq. (3.39) with specific relative angular momentum (angular momentum per unit mass), gives the equation for the motion of a smaller body in central force field. The dot product of Eq. (3.39) with specific relative linear momentum gives the energy at any point on the orbit as explained below:

The relative linear momentum of mass m_2 is given by

$$\mathbf{L} = m_2 \dot{\mathbf{r}} \quad (3.67)$$

Therefore, the specific linear momentum is $\dot{\mathbf{r}}$. Taking dot product of Eq. (3.39) with $\dot{\mathbf{r}}$ gives

$$\ddot{\mathbf{r}} \cdot \dot{\mathbf{r}} = -\mu \frac{\mathbf{r} \cdot \dot{\mathbf{r}}}{r^3} \quad (3.68)$$

It is to be noted that

$$\frac{1}{2} \frac{d}{dt} (\dot{\mathbf{r}} \cdot \dot{\mathbf{r}}) = \ddot{\mathbf{r}} \cdot \dot{\mathbf{r}} \quad (3.69)$$

Assuming $\mathbf{V} = \dot{\mathbf{r}}$,

$$\frac{1}{2} \frac{d}{dt} (\dot{\mathbf{r}} \cdot \dot{\mathbf{r}}) = \frac{1}{2} \frac{d}{dt} (\mathbf{V} \cdot \mathbf{V}) = \frac{1}{2} \frac{d}{dt} (V^2) \quad (3.70)$$

Therefore, Eq. (3.69) can be written as

$$\ddot{\mathbf{r}} \cdot \dot{\mathbf{r}} = \frac{d}{dt} \left(\frac{V^2}{2} \right) \quad (3.71)$$

The right-hand side of Eq. (3.68) can be written as

$$\mu \frac{\mathbf{r} \cdot \dot{\mathbf{r}}}{r^3} = \mu \frac{\dot{\mathbf{r}}}{r^2} = -\frac{d}{dt} \left(\frac{\mu}{r} \right) \quad (3.72)$$

Substituting Eqs. (3.71) and (3.72) in Eq. (3.68) gives

$$\frac{d}{dt} \left(\frac{V^2}{2} - \frac{\mu}{r} \right) = 0 \quad (3.73)$$

This gives

$$\frac{V^2}{2} - \frac{\mu}{r} = \epsilon \quad (3.74)$$

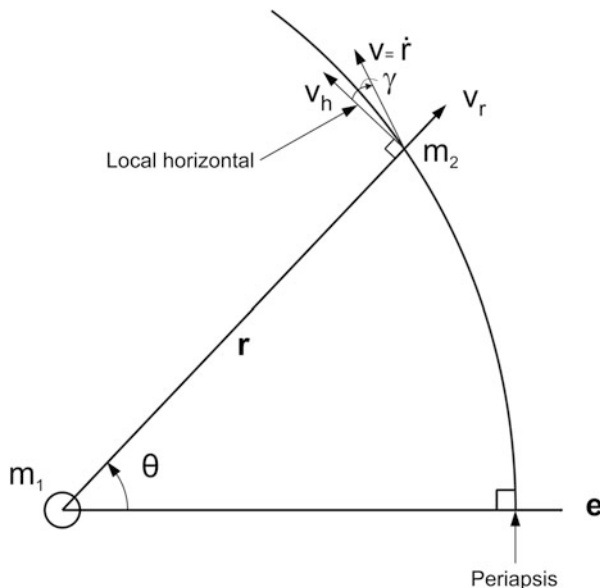
where ϵ is a constant called total energy. ($V^2/2$) is the specific relative kinetic energy (kinetic energy per unit mass) and (μ/r) is the specific potential energy (potential energy per unit mass) of the body m_2 in the gravity field of m_1 . The Eq. (3.74) gives the total mechanical energy per unit mass. Also the Eq. (3.74) gives the conservation of the specific mechanical energy for the defined trajectory, i.e., the total energy at any point of the trajectory is same and is given by the relation (3.74). Equation (3.74) is also called *vis-viva* (living force) integral.

3.4.1 Some Important Trajectory Parameters of Two-Body Problem

As explained above, motion of the smaller body with respect to the bigger one is a conic, which can be either a closed trajectory in terms of circular and elliptic orbits or an open trajectory defined by a parabola or hyperbola depending on the eccentricity value. Also, depending on the velocity magnitude at the instantaneous location, energy of the trajectory is defined.

In the trajectory, the closest point to the primary focus (central body) is called periapsis, and the farthest point is called apoapsis. The line joining the apses is called apse line. In the case of motion of a satellite about the Earth, the periapsis and

Fig. 3.9 Trajectory of orbiting body (m_2) with respect to the primary body (m_1)



apoapsis are referred to as perigee and apogee, respectively. For the case of motion about the Sun, the corresponding points are called perihelion and aphelion, respectively. Typical trajectory of a smaller body m_2 about the bigger body m_1 is represented in Fig. 3.9.

The eccentricity vector is always defined from the primary focus towards periapsis and this becomes the reference for the measure of true anomaly, θ , the location of the body with respect to the apse line. The flight path angle, γ , at any location on the trajectory is defined as the angle between the velocity vector and the local horizontal.

Angular velocity of the position vector \mathbf{r} is $\dot{\theta}$. Therefore, the horizontal velocity, V_h is given by

$$V_h = r\dot{\theta} \quad (3.75)$$

Magnitude of angular momentum is the product of r and horizontal velocity. Thus

$$H = r^2\dot{\theta} \quad (3.76)$$

Equation (3.76) along with Eq. (3.65) gives

$$V_h = \frac{\mu}{H}(1 + e \cos \theta) \quad (3.77)$$

The radial velocity, V_r is \dot{r} . Therefore,

$$V_r = \frac{dr}{dt} = \frac{H^3}{\mu r^2} \frac{e \sin \theta}{(1 + e \cos \theta)^2} \quad (3.78)$$

Using Eq. (3.66) gives

$$V_r = \frac{\mu}{H} e \sin \theta \quad (3.79)$$

From the Fig. 3.9,

$$\tan \gamma = \frac{V_r}{V_h} \quad (3.80)$$

Substituting Eq. (3.77), Eqs. (3.79) and (3.80) becomes

$$\tan \gamma = \frac{e \sin \theta}{1 + e \cos \theta} \quad (3.81)$$

The magnitude of angular momentum at any location r is also expressed as

$$H = r V \cos \gamma \quad (3.82)$$

where V is the velocity of the smaller body and γ is the flight path angle.

Assume r_p and r_a are the distances of periapsis and apoapsis respectively with respect to the primary focus and the corresponding velocities are V_p and V_a respectively. r_p is the location when $\theta = 0$ and r_a is the location of satellite when θ becomes 180° . Using Eqs. (3.65) and (3.66),

$$r_p = \frac{H^2}{\mu} \frac{1}{(1 + e)} \quad (3.83)$$

and

$$r_a = \frac{H^2}{\mu} \frac{1}{(1 - e)} \quad (3.84)$$

r_p and r_a are the minimum and maximum distances of the trajectory about the primary body. At the periapsis and apoapsis, the flight path angle is zero.

The semi-major axis, a is given by

$$a = \frac{r_p + r_a}{2} = \frac{H^2}{\mu} \frac{1}{(1 - e^2)} \quad (3.85)$$

Since the angular momentum is constant along the trajectory,

$$H = r_p V_p = r_a V_a \quad (3.86)$$

This gives

$$V_p = \frac{H}{r_p} \quad (3.87)$$

and

$$V_a = \frac{H}{r_a} \quad (3.88)$$

From the above, it can be seen that V_p and V_a are the maximum and minimum velocities along the trajectory.

Since the energy along the trajectory, ϵ is constant, at the periapsis,

$$\epsilon = \frac{V_p^2}{2} - \frac{\mu}{r_p} \quad (3.89)$$

Using Eq.(3.87) into (3.89) yields

$$\epsilon = \frac{1}{2} \frac{H^2}{r_p^2} - \frac{\mu}{r_p} \quad (3.90)$$

Using Eq. (3.83) in Eq. (3.90) gives

$$\epsilon = -\frac{1}{2} \frac{\mu^2}{H^2} (1 - e^2) \quad (3.91)$$

It can be seen from Eq. (3.91) that the energy is function of trajectory parameters. Also, it can be concluded that:

1. For elliptic orbit (including circular orbit), ϵ is negative value
2. For parabolic orbit, $\epsilon = 0$
3. For hyperbolic orbit, ϵ is positive value

Using Eq. (3.85) in Eq. (3.91) gives

$$\epsilon = -\frac{\mu}{2a} \quad (3.92)$$

Alternatively,

$$a = -\frac{\mu}{2\epsilon} \quad (3.93)$$

Thus, the semi-major axis is dependent only on the specific total energy. Using Eq. (3.93) in Eq. (3.74) yields

$$V^2 = \mu \left(\frac{2}{r} - \frac{1}{a} \right) \quad (3.94)$$

Using Eq. (3.93) in Eq. (3.94) with the initial conditions of velocity and distance as V_0 and r_0 respectively, the achieved trajectory characteristics can be identified as follows:

$$\left. \begin{array}{l} \text{Elliptic orbit} \\ \text{Parabolic trajectory} \\ \text{Hyperbolic trajectory} \end{array} \right\} \text{if} \left\{ \begin{array}{l} V_0 < \sqrt{\frac{2\mu}{r_0}} \\ V_0 = \sqrt{\frac{2\mu}{r_0}} \\ V_0 > \sqrt{\frac{2\mu}{r_0}} \end{array} \right.$$

Therefore, the following conclusions can be arrived at: At r_0 , for the lower velocity V_0 , the orbit is ellipse. As V_0 is increased the closed orbit gradually changes into open trajectory. The minimum velocity required to achieve open trajectory is called escape velocity and is given by

$$V_{\text{esc}} = \sqrt{\frac{2\mu}{r_0}} \quad (3.95)$$

At this velocity, the trajectory of the smaller body with respect to the bigger body is a parabola. Any increase in velocity leads to hyperbolic trajectory of the body with respect to the primary body.

In summary, the following conclusions are arrived at:

1. Eccentricity determines the shape and type of trajectory
2. Semi-major axis defines the size and energy of the trajectory

The relations between these parameters and the trajectory are summarized below in Table 3.1.

The following sections give the significance and specific features of each of the above orbits and open trajectories.

Table 3.1 Trajectories in two-body problem

Trajectory	Eccentricity, e	Semi-major axis, a	Specific energy
Circular orbit	0	$a = r$	Negative
Elliptic orbit	$0 < e < 1$	> 0	Negative
Parabola	1	∞	0
Hyperbola	> 1	< 0	Positive

3.4.2 Circular Orbits

Applying $e = 0$ in the Eq. (3.65) gives the radial distance of the circular orbit as

$$r = \frac{H^2}{\mu} \quad (3.96)$$

Also, for circular orbit, there is no radial velocity and the velocity, V , is always tangential. Therefore, angular momentum of circular orbit is

$$H = rV \quad (3.97)$$

and

$$V = \frac{H}{r} \quad (3.98)$$

Equations (3.96) and (3.98) show that the radial distance and velocity at any point on the orbit are constants. Using Eq. (3.97) into Eq. (3.96) yields

$$V_{\text{cir}} = \sqrt{\frac{\mu}{r}} \quad (3.99)$$

Equation (3.99) gives velocity of satellite along the circular orbit of distance of r .

Time required to travel along the orbit once is called the period of the orbit, T , and given by

$$T = \frac{\text{Circumference}}{\text{Speed}} \quad (3.100)$$

For the circular orbit of radius r , period is as given in Eqn. 3.100

For the circular orbit of radius r , period is given by

$$T_{\text{cir}} = \frac{2\pi r}{V_{\text{cir}}} = \frac{2\pi r}{\sqrt{(\mu/r)}} \quad (3.101)$$

The specific energy of a satellite at circular orbit is obtained by substituting $e = 0$ in Eq. (3.91) as

$$T_{\text{cir}} = 2\pi \sqrt{\frac{r^3}{\mu}} \quad (3.102)$$

Using Eq. (3.96) in Eq. (3.102) yields

$$\varepsilon = -1/2(\mu^2/H^2) \quad (3.103)$$

$$\varepsilon_{\text{cir}} = -\frac{\mu}{2r} \quad (3.104)$$

Equation (3.104) gives shows that the energy along a circular orbit is negative. As r increases, the energy becomes less negative, indicating higher specific energy for the higher circular orbits.

3.4.3 Elliptical Orbits

For the cases of $0 < e < 1$, the relative radial distance calculated by the Eq. (3.65) remains bounded for θ ranging from 0 to 2π and the orbit is elliptic one as shown in Fig. 3.10. The minimum distance r_p is from focus to the periapsis (P) and the maximum distance r_a is from F to apoapsis (A). r_a and r_p are values of r corresponding to $\theta = 0$ and $\theta = 180^\circ$ respectively as are explained in Sect. 3.4.1:

Some additional parameters are explained in this section. Using Eq. (3.85) in Eq. (3.65) an alternate form of orbit equation can be written as

$$r = \frac{a(1 - e^2)}{1 + e \cos \theta} \quad (3.105)$$

From the above equation, the r_p and r_a are expressed as

$$r_p = a(1 - e) \quad (3.106)$$

$$r_a = a(1 + e) \quad (3.107)$$

From Fig. 3.10, CF is expressed as

$$CF = ae \quad (3.108)$$

Also, from the Fig. 3.10,

$$CF = ae = r_B \cos(\pi - \beta) = -\left[\frac{a(1 - e^2)}{(1 + e \cos \beta)} \right] \cos \beta \quad (3.109)$$

From Eq. (3.109), e can be expressed as

$$e = -\cos \beta \quad (3.110)$$

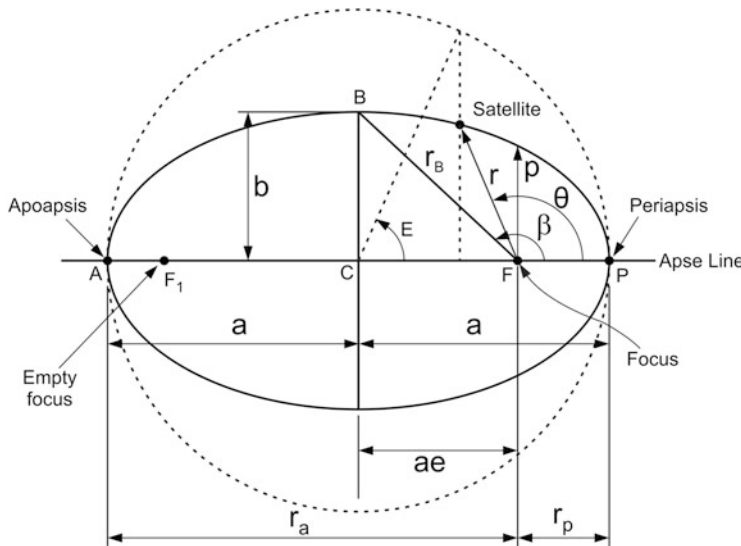


Fig. 3.10 Elliptic orbit parameters

Using this, the value of r_B can be given as

$$r_B = a \quad (3.111)$$

Therefore, the semi-minor axis, b is given by

$$b = a(\sqrt{1 - e^2}) \quad (3.112)$$

The area of ellipse is given by

$$A = \pi ab \quad (3.113)$$

As per Eq. (3.44),

$$\frac{dA}{dt} = \frac{H}{2} \quad (3.114)$$

which can be used to obtain

$$\Delta A = \left(\frac{H}{2}\right) \Delta t \quad (3.115)$$

For one complete revolution, ΔA is πab and Δt is the period, T . Therefore,

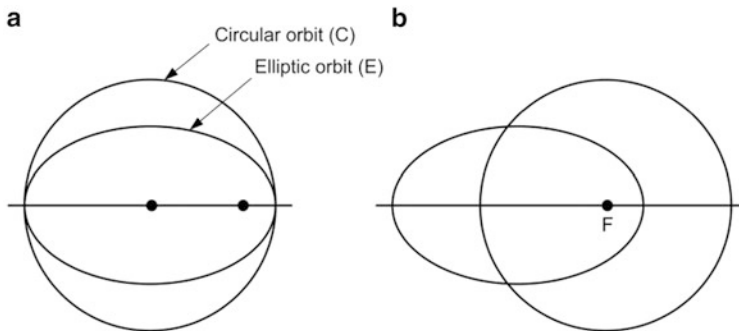


Fig. 3.11 Elliptic and circular orbits with same energy and period: (a) orbits comparison with center aligned (b) orbits about the focus

$$T = \left(\frac{2\pi ab}{H} \right) \quad (3.116)$$

Using Eq. (3.85) and (3.112) for a and b respectively yields

$$T = \frac{2\pi}{\mu^2} \left[\frac{H}{\sqrt{1 - e^2}} \right]^3 \quad (3.117)$$

Using Eq. (3.85) the period, T given as

$$T = 2\pi \sqrt{\frac{a^3}{\mu}} \quad (3.118)$$

which proves Kepler's third law.

This expression reveals that the period of elliptic orbit is independent of eccentricity and depends only on the semi-major axis. The two orbits having the same period are represented in Fig. 3.11.

The eccentricity of the elliptical orbit can also be represented using Eq.(3.83) and (3.84) as

$$\frac{r_p}{r_a} = \frac{1 - e}{1 + e} \quad (3.119)$$

which can be used to derive e as

$$e = \frac{r_a - r_p}{r_a + r_p} \quad (3.120)$$

The Eq. (3.120) shows that

$$e = \frac{\text{distance between the two focii}}{\text{distance between the apse points}}$$

It can be seen from the above that the size of the elliptic orbit is defined by ‘a’ whereas the shape is decided by ‘e’. Together ‘a’ and ‘e’ define the elliptical orbit characteristics.

Using the eccentric anomaly E, the position on an elliptic orbit is given by

$$r = a(1 - e \cos E) \quad (3.121)$$

Another important relation is Kepler’s equation defined by

$$M = E - e \sin E \quad (3.122)$$

where M is the Mean anomaly and

$$M = t_p \sqrt{\frac{\mu}{a^3}} \quad (3.123)$$

where

t_p = time elapsed since the previous passage of periapsis

3.4.4 Parabolic Trajectories

Consider the orbit equation

$$r = \left(\frac{H^2}{\mu} \right) \left(\frac{1}{1 + e \cos \theta} \right)$$

and the orbit energy equation

$$\epsilon = -\frac{1}{2} \frac{\mu^2}{H^2} (1 - e^2)$$

and

$$\epsilon = \frac{V^2}{2} - \frac{\mu}{r}$$

From the above equations, it can be observed that, for the case of $e = 1$, the specific energy ϵ is zero and as the true anomaly tends to 180° , the radial distance approaches infinity.

The velocity at $r = \infty$ is called residual velocity, V_∞ (sometimes referred as excess velocity). For the case of parabolic trajectory, V_∞ is 0, meaning that, once the body is placed in parabolic trajectory, it won't come back, thus referred to as open trajectory. Also, since the residual velocity V_∞ is zero, parabolic trajectory is the boundary between the closed elliptical orbit and open hyperbolic trajectory. Thus, the velocity on the parabolic trajectory is referred as escape velocity and is given by

$$V_{\text{esc}} = \sqrt{\frac{2\mu}{r}} \quad (3.124)$$

Considering the Eq. (3.99), it can be seen that

$$V_{\text{esc}} = \sqrt{2} V_{\text{cir}} \quad (3.125)$$

Thus at any distance, the required escape velocity is about 41.4 % more than the circular orbital velocity at that location. Typical values of escape velocities are given below:

11.12 km/s for escape from Earth from the Earth's surface

617 km/s for escape from Sun from the Sun's surface

42.1 km/s for escape from Sun from the Earth orbit

It is to be noted that if a body (satellite) is injected into a parabolic trajectory about the primary body (Earth) with the escape velocity, V_{esc} , the satellite does not go to infinity. As the distance increases, gravitational attraction of the Earth reduces, and the influence of the Sun becomes predominant. At one point of time, the satellite velocity with respect to Earth becomes zero; but the satellite velocity about the Sun is same as that of the Earth and therefore both the Earth and the satellite move about the Sun in the same orbit.

Typical parabolic trajectory is given in Fig. 3.12. Considering the Eq. (3.81), the flight path angle at any location of a parabolic trajectory is given by

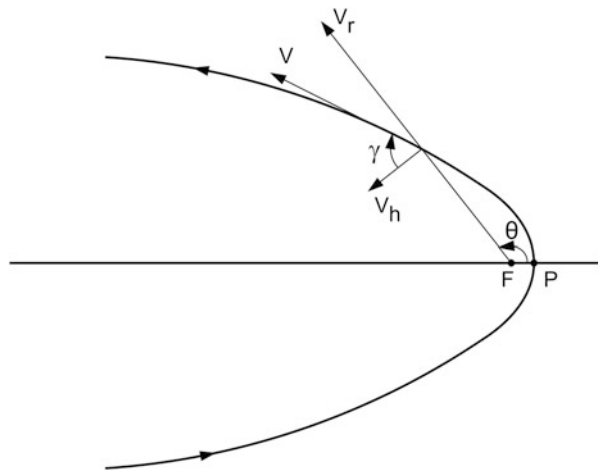
$$\tan \gamma = \frac{\sin \theta}{1 + \cos \theta} \quad (3.126)$$

On simplifying the Eq. (3.126), it can be seen that

$$\gamma = \frac{\theta}{2} \quad (3.127)$$

Thus, along parabolic trajectory, the flight path angle at any location is half of the true anomaly.

Fig. 3.12 Typical parabolic orbit



3.4.5 Hyperbolic Trajectories

Hyperbola is an open trajectory as represented in Fig. 3.13. Since the trajectory is open one, the distance r can increase without limit. When r approaches ∞ , the tip of the position vector meets the asymptote. The asymptotes intersect at the centre, O. The centre falls outside the trajectory.

The angle between the asymptote and major axis is θ_∞ . Since the trajectory meets the asymptote at infinity, θ_∞ , is the true anomaly at infinity. Using the equation,

$$r = \frac{H^2}{\mu} \frac{1}{1 + e \cos \theta}$$

at $r = \infty$, the term $1 + e \cos \theta = 0$. Therefore, θ_∞ can be expressed as

$$\theta_\infty = \cos^{-1} \left(-\frac{1}{e} \right) \quad (3.128)$$

The angle between the asymptotes is turning angle, δ . As the body travels from $-\infty$ to $+\infty$, δ is the angle through which the velocity along the hyperbolic trajectory turns. From Fig. 3.13, it can be seen that

$$\cos(\pi - \theta_\infty) = \cos \left(\frac{\pi}{2} - \frac{\delta}{2} \right) \quad (3.129)$$

Using Eq. (3.128), Eq. (3.129) gives

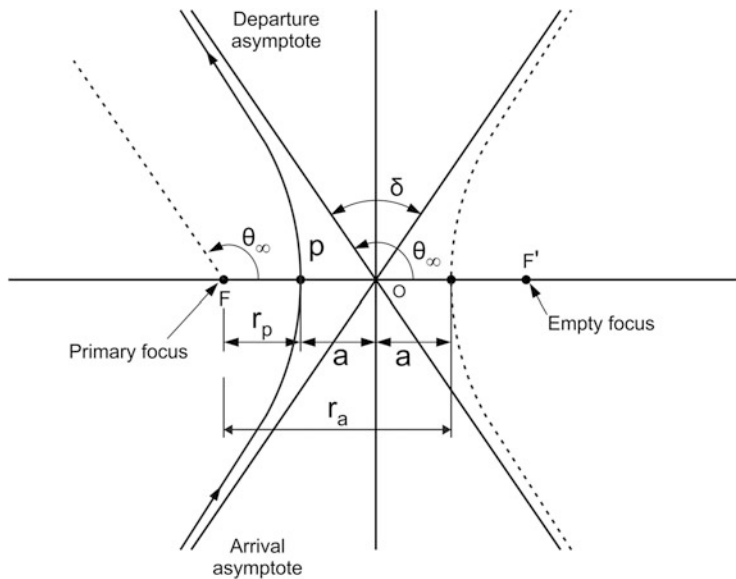


Fig. 3.13 Hyperbolic trajectory

$$\delta = 2\sin^{-1}\left(\frac{1}{e}\right) \quad (3.130)$$

For the case of parabola, $e = 1$ which gives θ_∞ as 180° . Therefore, for parabola, the asymptotes are parallel and do not intersect, and this is the limiting case between closed elliptical orbits and the open hyperbola trajectory.

Consider the energy equation,

$$\frac{V^2}{2} - \frac{\mu}{r} = \epsilon$$

As for hyperbolic trajectory, ϵ is a positive value; at $r = \infty$, the velocity is not zero and this is called residual velocity, V_∞ which is given by

$$V_\infty^2 = 2\epsilon \quad (3.131)$$

For the case of hyperbolic trajectory of a satellite from the Earth, at $r = \infty$, there is a positive residual velocity and therefore the satellite has its own orbit around Sun, which is different from that of the Earth.

At any point on the hyperbolic trajectory, the velocity is given by

$$V = \sqrt{2\left(\epsilon + \frac{\mu}{r}\right)} \quad (3.132)$$

This gives,

$$V = \sqrt{V_{esc}^2 + V_\infty^2} \quad (3.133)$$

3.5 Satellite Orbit and Trajectory Requirements

The previous section deals with two-body problem, which defines the motion of a smaller body with respect to a bigger body. From the human-made satellite requirements point of view, these solutions can be used to define the motion of satellites (small body) about the Earth (bigger body). The requirements of orbits can be classified into two categories: (i) closed orbits (circular and elliptic) and (ii) open trajectories.

Closed orbits are used for the near Earth space utilization. These types of orbits are used for the utilization of Earth for survey of natural resources, Earth observation and its surrounding environments, communication and navigational systems. In another important application, these orbits are used as parking orbits, from which the satellites are injected into interplanetary trajectories which are open trajectories. This section gives uses of various types of orbits/trajectories required for various applications.

3.5.1 Circular Orbits

Circular orbits of different altitudes are utilized for various applications. Circular orbits are generally classified as Low Earth Orbit (LEO), Medium Earth Orbit (MEO) and High Earth Orbit (HEO). There is a hazardous Van Allen radiation belt around Earth, which starts at about 2400 km. The Van Allen belt consists of an inner zone of high energy protons and an outer zone of high energy electrons. Generally, the circular orbits are planned below the high intensity inner zone peak (altitude ~ 3700 km) or above the high intensity outer zone peak (altitude $\sim 28,000$ km). Low Earth circular orbits limit between around 150 km (where the atmospheric drag effect on orbit is less) to 1000 km (which is well below the Van Allen belt). The HEO is above the Geosynchronous Earth Orbit (GEO). In between, orbits are referred as MEO.

A circular orbit which skim the surface of the Earth (assumes a spherical Earth with no atmosphere) is referred as Earth-surface circular orbit and is many times used as reference orbit. This orbit has the minimum energy, maximum circular orbit velocity and minimum period. The period of this orbit is 84.4 min. This period is called Schuler period and is used in inertial navigation.

Solar day (synodic day) is the time from noon to noon, which is the time taken by Earth to rotate one full rotation about its axis, which is 24 h. But Earth also moves

around the Sun. The siderial day is time taken by the Earth to complete one rotation relative to inertial space. Siderial day period is 23 h 56 min 4.091 s.

Orbit with the period equal to a siderial day is called Geosynchronous orbit. If such orbit is circular one and over equator and a satellite is placed on such orbit looks stationary with respect to a specified point on the Earth. Such orbit is called Geostationary Earth Orbit (GEO). The radial distance of GEO is 42,164 km and the altitude is 35,786 km. Such orbits are useful for communication satellites and weather satellites due to global coverage.

A satellite placed in GEO covers the latitudes range of $\pm 81.3^\circ$ and Earth surface area of 42.4 %. Therefore, 3 such satellites are required to cover the entire globe.

3.5.2 Elliptic Orbits

The elliptical orbits are used for reconnaissance satellites. The targets are near the perigee of such orbits whereas the apogee phase is utilized for transmitting the acquired information as well as to make the intercept problem more difficult. Also, elliptic orbits with high eccentricity are used for communications of high latitude regions as explained later.

Elliptic orbits are also used as the intermediate Geo Transfer Orbit (GTO) to place a satellite into GEO. In order to achieve the maximum performance, initially the launch vehicle places the satellite into an elliptic orbit of perigee altitude of about 200 km with apogee altitude of about 36,000 km. The satellite further uses its own propulsion system to transfer the satellite to GEO. This aspect is explained later.

3.5.3 Open Trajectories

The open trajectories, primarily hyperbolic trajectories, have been used for escaping Earth's gravitational force field and to place a satellite in interplanetary or lunar trajectories. Also, when the satellite enters or reenters the sphere of gravitational attraction of another planet, the satellite follows hyperbolic trajectory. These aspects are also covered in later part of this chapter.

3.6 A Note on Orbital Energy and Launching of Satellites into Orbit

The previous section defines specified orbits or trajectories for specified spacecraft depending upon application. This section gives the launch vehicle requirements to achieve the specified orbits for the specified satellite.

Specific energy of an elliptical orbit (circular orbit is a special case of elliptical orbit) is given by

$$\epsilon = \frac{V^2}{2} - \frac{\mu}{r} \quad (3.134)$$

where $V^2/2$ is the specific kinetic energy and $(-\mu/r)$ is the specific potential energy. Considering a satellite of mass, m in the specified orbit, then the mechanical energy of the satellite E is given by

$$E = m\epsilon \quad (3.135)$$

Therefore, even though specific energy of an orbit is a defined value, depending on the mass of the satellite, the mechanical energy of the satellite in that orbit would vary. Therefore, for a heavier satellite, the mechanical energy of the satellite is larger. Similarly, the mechanical energy of a satellite in a bigger orbit is higher than that of the lower orbit. For the specified satellite to be placed in the defined orbit, the satellite has to be injected into the orbit with the mechanical energy as given by Eq. (3.135).

The specific kinetic energy depends on the square of orbital velocity at the specified radial distance. As the velocity increases, the kinetic energy also increases. For the radial distance close to zero, the potential energy is near to negative infinity. At the surface of Earth, the specific potential energy is about -62.6 MJ/kg , i.e., the energy becomes less negative and thus the energy increases. Similarly, for the Earth bound orbit at the altitude of 360 km ($r = 6738 \text{ km}$), the specific potential energy is -59.2 MJ/kg . Thus at the altitude of 360 km above the surface of Earth, there is potential energy increase by 3.4 MJ/kg . From these it can be seen that as r increases, the negative value decreases, thus causing an increase in the potential energy compared to that at the surface of Earth.

Therefore, while defining the energy of satellite orbit, one should not confuse with its negative value. Even though the energy is negative, increase in the energy with respect to its value at the surface of Earth has to be considered for all the computations. From these explanations, it can be concluded

1. Energy increases for the orbits with larger r
2. Energy increases for the orbits with higher velocity

In order to launch a satellite of mass m from the surface of the Earth to the specified orbit, it is essential to impart the mechanical energy, $E = m\epsilon$, to the satellite, where ϵ is the specific energy as per the requirements of the specified orbit. The mechanical energy to the satellite is imparted by the launch vehicle. The following are the requirements of the launch vehicle:

1. For the specified satellite mass, a larger launch vehicle is required to position the satellite to a higher orbit than that required to launch the same satellite into a lower orbit.

2. A specified launch vehicle can launch higher mass satellite into a lower orbit or a lesser mass satellite into a higher orbit.

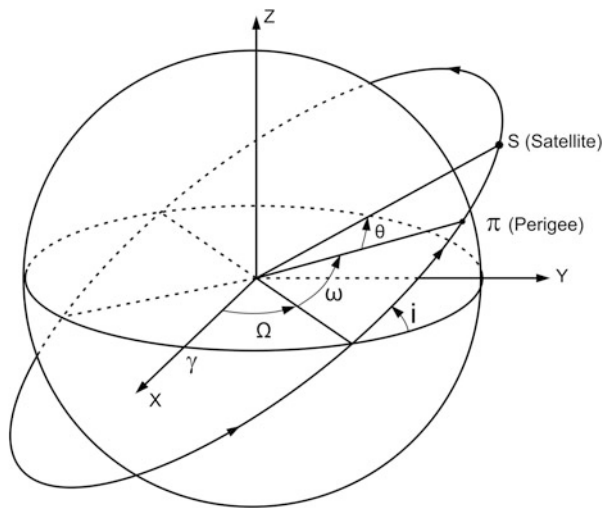
These discussions give the total energy required to be generated by a launch vehicle. In reality, the velocity addition and correspondingly the increase in r happens during the STS operation time. The pattern of increase of these parameters depends on the vehicle configuration, the type of propulsion system and the vehicle attitude history during thrusting phase and thrusting duration. In order to reach the required orbit with the specified energy, at satellite injection at the specified distance r , the velocity components and the flight parameters are to be achieved by the launch vehicle as specified in Eqs. (3.77), (3.79) and (3.81). These functions are carried out by the launch vehicle subsystems as per the details provided in the subsequent chapters of this book.

During the launch vehicle operation, while propulsion system is adding energy which in turn increases the velocity and altitude to the vehicle and satellite systems, the Earth gravity reduces the velocity. The velocity loss due to gravity depends on the vehicle attitude with respect to gravity acceleration direction during thrusting phase and thrusting duration. Therefore, the energy provided by the propulsion system has to be effectively utilized to impart the maximum mechanical energy to the satellite to achieve the maximum performance. Generally, maximum energy utilization of the launch vehicle and in turn the maximum performance can be achieved if the satellites are injected at a lower orbit. However, depending on the complexities of integrated launch vehicle – satellite mission, a trade-off between the altitude of injection and velocity losses, suitable mission strategies are to be defined.

3.7 Orbital Elements

The state of a satellite at any instant in inertial space is defined by its instantaneous position and velocity components along the three axis of a specified reference frame.

The solution of two-body problem as discussed earlier gives the motion of the satellite in a plane, and the motion is along a closed orbit (circular or elliptic) or open trajectory (parabola or hyperbolic). The two body solution thus defines only type, shape and size of the orbits through two constants namely, eccentricity (e) and semi-major axis (a). But these two constants are not sufficient to define completely the location and velocity of the satellite at any instant. The additional constants required are: (i) orientation of the orbit with respect to a reference frame (3 constants) and (ii) position of the satellite in the orbit at any instant (1 constant). Together, these six constants are called orbital elements. It is to be noted that the components of position and velocity vectors in the defined Cartesian reference frame is related to these orbital elements.

Fig. 3.14 Orbital elements

The six orbital elements corresponding to a geocentric orbit as defined in Fig. 3.14 are summarized below:

1. Orientation of orbital plane in inertial space is given by inclination (i) and right ascension of ascending node (Ω)
2. Location of perigee in the orbital plane is defined by the argument of perigee (ω)
3. Type, shape and size of the orbit is defined by eccentricity (e) and semi-major axis (a)
4. Location of the satellite in the orbit is defined by the true anomaly (θ). Other equivalent parameters viz., mean anomaly, time since elapse of perigee, etc. can also be defined as the sixth element.

The parameters ‘ a ’ and ‘ e ’ define size, shape and type of orbit. The orientation of the orbital plane is defined by ‘ Ω ’ and ‘ i ’ and the location of perigee in that plane is defined by ω . The position of satellite in the defined orbit as above is decided by ‘ θ ’. These six orbital elements are explained below:

1. Right Ascension of Ascending Node (Ω)

The satellite during its orbital motion from southern hemisphere to northern hemisphere crosses the equator at ascending node, while its motion from northern hemisphere to southern hemisphere crosses the equator at descending node. The line joining the nodes is called the line of nodes. The nodal line is the line of intersection of orbital plane with equatorial plane. The angle of nodal line at ascending node location measured eastward from the X-axis of ECI frame is called the right ascension of ascending node.

2. Orbital Inclination (i)

The angle between the equator and orbit at the location of ascending node, measured from equator along the counter clockwise direction is called the inclination of the orbit.

3. Argument of Perigee (ω)

The angle between the line of nodes at the ascending node to the apsis line at the perigee location is called argument of perigee. This angle is measured counter clockwise from the line of nodes to the apsis line along the orbital plane.

4. Eccentricity (e)

This constant defines the type and shape of the orbit as explained earlier.

(v) Semi-major axis (a)

This constant defines the size of the orbit as explained earlier.

5. True anomaly (θ)

This is the angle measured clockwise from the apsis line at perigee location to the position vector of the satellite. This is defined earlier as part of two-body motion.

3.8 Orbital Perturbations

Perturbations of geocentric orbital elements are explained in this section. The two-body problem as explained in the previous sections considered central gravitational force field. In reality, the actual force field is not central force field due to the asphericity of Earth and due to the presence of atmospheric drag, third body perturbations such as Moon, Sun and solar radiation pressure.

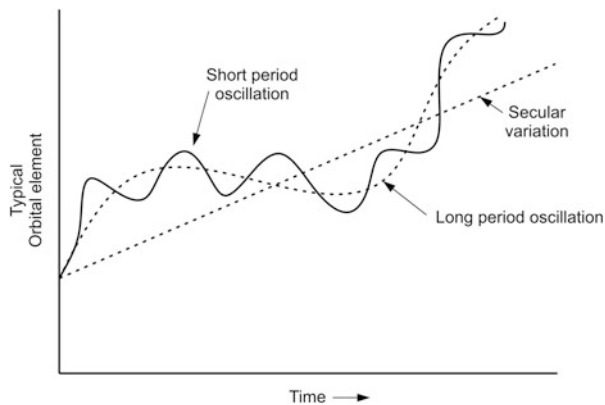
These perturbation forces can be added to the central force field and the equation of motion of the satellite can be written as

$$\ddot{\mathbf{r}} = -\frac{\mu}{r^3} \mathbf{r} + \mathbf{f} \quad (3.136)$$

The solution of Eq. (3.136) is not a Keplerian orbit as defined by the first part of right hand side (RHS) of Eq. (3.136). However, the major force is the gravity force (central force) due to spherical Earth which keeps the satellite in the Keplerian orbit whereas the perturbation forces cause the variations in the Keplerian orbital elements.

Variations in the orbital elements consist of the following components: (i) secular, (ii) short period variation and (iii) long-period term as shown in Fig. 3.15. Depending on the types of disturbing forces and orbital characteristics, each orbital element has the specific variations.

Fig. 3.15 Typical variation of an orbital element



For near Earth satellites orbits, Earth's asphericity causes major disturbing force compared to the other sources and its effects are explained in the following section.

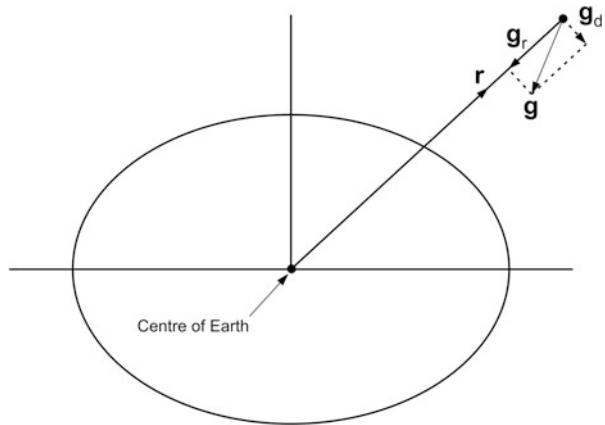
3.8.1 Effects of Earth's Asphericity on Orbital Elements

Earth is an irregular shaped body which causes the gravitational force not passing through its center and its gravitational potential is defined as

$$U = -\frac{\mu}{r} \left[1 - \sum_{n=2}^{\infty} J_n \left(\frac{R_e}{r} \right)^n P_n(\sin \lambda) - \sum_{n=2}^{\infty} \sum_{m=1}^n J_{n,m} \left(\frac{R_e}{r} \right)^n P_n^m(\sin \lambda) \cos m(\Phi - \Phi_{n,m}) \right] \quad (3.137)$$

where r, λ, ϕ are geocentric distance, latitude and longitude respectively. $P_n(\sin \lambda)$ is Legendre's polynomial of degree n in $\sin \lambda$, $P_n^m(\sin \lambda)$ is the associated Legendre function of degree n and order m . R_e is the equatorial radius of Earth. J_n , $J_{n,m}$ and $\Phi_{n,m}$ are numerical coefficients that describe the mass distribution. The terms having J_n are called zonal harmonics, which describe the deviation of gravity away from Newtonian in the north-south direction. The terms having $J_{n,m}$, $n \neq m$ are called tesseral harmonics and $J_{n,m}$, $n = m$ is known as sectorial harmonics, which represent the deviation of gravity acceleration in the east-west direction.

The term with $n = 1$ is absent due to the assumption that the origin of reference frame coincides with center of mass of the Earth. The term J_2 represents the oblateness of Earth, J_3 represents the Earth as pear shaped, $J_{2,2}$ represents ellipticity of the equator and so on. For an orbit inclined to the equator, the effects of tesseral and sectorial harmonics can be assumed to be averaged out over a long period of time. In this case, the Earth can be assumed to be an axi-symmetric body with zonal

Fig. 3.16 Oblate Earth

harmonics terms alone. However, for equatorial orbit, especially geostationary orbit, wherein the satellite is positioned at same location with respect to the Earth, tesseral and sectorial harmonics play a major role in the orbital elements variations. Considering only zonal harmonics terms, the value of J_2 is 1.0826×10^{-3} and other coefficients are of the order of 10^{-6} . Therefore, J_2 term is having the major impact on the orbital perturbations and is further analyzed as given below.

Considering only J_2 in Earth potential, define the Earth as oblate spheroid, and due to this feature, the gravity acceleration is away from the center of Earth as shown in Fig. 3.16, and the deviation is the function of latitude and radial distance.

The gravity component g_r towards center of the Earth defines Keplerian orbital elements whereas the disturbance component g_d causes perturbation to the Keplerian orbital elements. The disturbing potential considering only J_2 term is given as

$$\Delta U = -\frac{\mu}{r} (J_2) \left(\frac{R_e}{r} \right)^2 P_2(\sin \lambda) \quad (3.138)$$

In this case, the gravitational acceleration of oblate Earth as defined by Eq. (3.136) is

$$\ddot{\mathbf{r}} = -\frac{\mu}{r^3} \mathbf{r} + \mathbf{f}$$

where

$$\mathbf{f} = f_r \mathbf{u}_r + f_h \mathbf{u}_h + f_v \mathbf{u}_v \quad (3.139)$$

f_r , f_v and f_h are the radial, normal (to orbital plane) and perpendicular to \mathbf{r} and lying in the orbital plane components of \mathbf{f} and \mathbf{u}_r , \mathbf{u}_v and \mathbf{u}_h are the corresponding unit

vectors along these directions respectively. The disturbing force components corresponding to J_2 term, with respect to the orbital plane in terms of orbital elements, can be expressed as

$$f_r = -\frac{\mu}{r^2} \left(\frac{3}{2}\right) J_2 \left(\frac{R_e}{r}\right)^2 [1 - 3 \sin^2 i \sin^2(\omega + \theta)] \quad (3.140)$$

$$f_h = -\frac{\mu}{r^2} \left(\frac{3}{2}\right) J_2 \left(\frac{R_e}{r}\right)^2 \sin^2 i \sin[2(\omega + \theta)] \quad (3.141)$$

$$f_v = -\frac{\mu}{r^2} \left(\frac{3}{2}\right) J_2 \left(\frac{R_e}{r}\right)^2 \sin 2i \sin(\omega + \theta) \quad (3.142)$$

The disturbance forces as given in Eqs. (3.140), (3.141), and (3.142) induce rates of change of all the orbital elements. The rate of change of two orbital elements of interest is given below:

$$\dot{\Omega} = \frac{H}{\mu} \frac{\sin(\omega + \theta)}{\sin i(1 + e \cos \theta)} f_v \quad (3.143)$$

$$\dot{\omega} = -\frac{r \cos \theta}{e H} f_r + \frac{(2 + e \cos \theta) \sin \theta}{e H} f_h - \frac{r \sin(\omega + \theta)}{H \tan i} f_v \quad (3.144)$$

It can be seen that the rate of change of Ω is caused by disturbance normal to orbital plane whereas disturbances in all the directions caused $\dot{\omega}$. Integrating $\dot{\Omega}$ and $\dot{\omega}$ over one orbit gives the average rate of change and is given by

$$\dot{\Omega}_{av} = \frac{1}{T} \int_0^T \dot{\Omega} dt; \quad \dot{\omega}_{av} = \frac{1}{T} \int_0^T \dot{\omega} dt$$

where T is orbital period

After simplifications, the average rate of change of Ω is given by

$$\dot{\Omega}_{av} = - \left[\frac{3}{2} \frac{\sqrt{\mu} J_2 R_e^2}{(1 - e^2)^2 a^{7/2}} \right] \cos i \quad (3.145)$$

and the average rate of change of ω is given by

$$\dot{\omega}_{av} = - \left[\frac{3}{2} \frac{\sqrt{\mu} J_2 R_e^2}{(1 - e^2)^2 a^{7/2}} \right] \left[\frac{5}{2} \sin^2 i - 2 \right] \quad (3.146)$$

Equations (3.145) and (3.146) are the secular variations on Ω and ω respectively.

For the case of orbits with $0 \leq i < 90^\circ$, which are called posigrade orbits, the nodal line drifts westward and this phenomenon is called regression of the nodes. For the case of retrograde orbits, i.e., $90^\circ < i \leq 180^\circ$, the nodal line advances. Similarly for the orbits with $0 \leq i < 63.4^\circ$, or $116.6^\circ < i \leq 180^\circ$, the perigee advances in the direction of orbital motion. i.e., the whole orbit rotates in the orbital plane along the direction of satellite motion. If $63.4^\circ < i \leq 116.6^\circ$, the perigee regresses. For the case of $i = 63.4^\circ$, or $i = 116.6^\circ$, the apse line does not move. These inclinations are called critical inclinations.

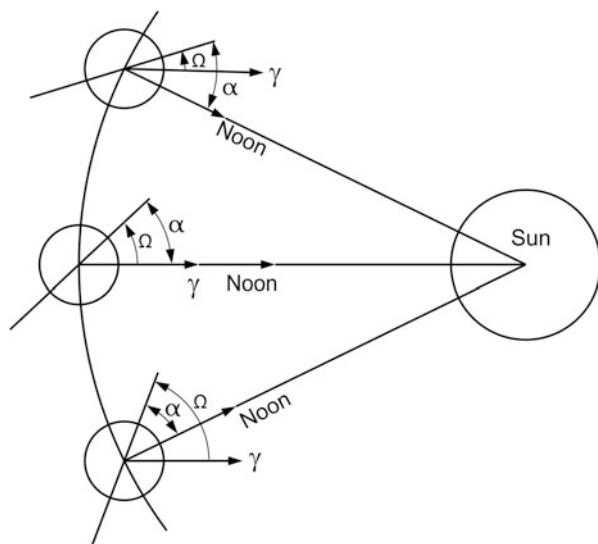
The phenomenon of nodal regression and perigee advancement due to Earth asphericity are effectively utilized for the two important applications of satellite orbits as explained below.

3.8.2 Sun-Synchronous Orbit

Sun-synchronous orbits are those orbits whose orbital plane makes constant angle with the Sun-Earth line, i.e. for the Sun-synchronous orbits the angle between the nodal line and the Sun-Earth line is always constant. For a defined orbit size (a) and shape (e), inclination i can be found such that $\dot{\Omega} = 0.9856^\circ/\text{day}$. This set of (a, e, i) defines a Sun-synchronous orbit. As the Earth moves around Sun with the angular rate of $0.9856^\circ/\text{day}$, and the nodal line also moves with the same rate, the nodal line always form a constant angle with Sun-Earth line, which is decided by the satellite applications. This is represented in Fig. 3.17.

Such satellites, for every swath, pass through same sunlight conditions or darkness. This is particularly advantageous for Earth observation satellites to

Fig. 3.17 Sun-synchronous orbit

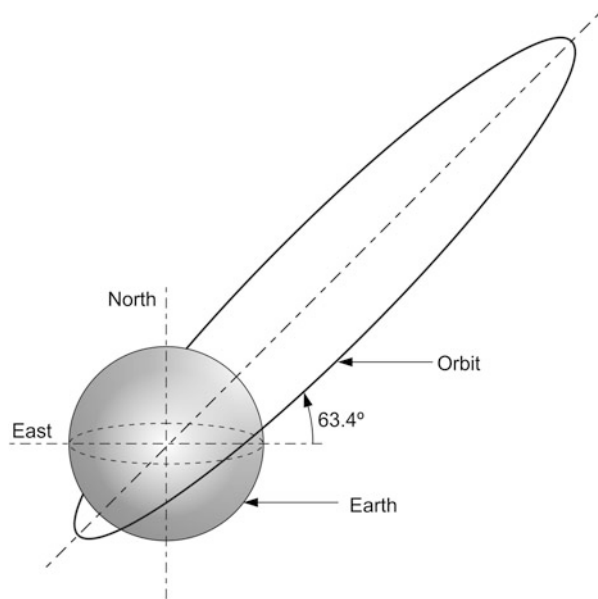


establish the correlations of various observations with respect to several phenomena such as crop growth, forest coverage, drought conditions, etc. Sun-synchronous orbits with nodal line perpendicular to the Sun-Earth line is also important. Since Sun's declination δ is within the range $-23.5^\circ < \delta < 23.5^\circ$, by carefully selecting launch date and orbital height, such orbit remains continuously in sunlight for more than 8 months. These orbits are useful for solar power generation satellites.

3.8.3 Molniya Orbits

From the Eq. (3.146), it can be seen that if $i = 63.4^\circ$, or $i = 116.6^\circ$, then $\dot{\omega} = 0$. i.e., for such orbit, the apse line remains stationary in space. This feature was used by erstwhile USSR for communication satellite, Molniya (lightning). The Russian launch sites are at high northern latitudes, the northern most is Plesetsk at 62.8°N . As can be seen later, the lowest inclination orbit achievable for the launch from this site is 62.8° . Therefore, from such launch sites, launching satellites into geostationary orbit is costly. Also, the geostationary satellites positioned over equator cannot effectively view the far northern latitude region of erstwhile USSR. Under such situations, Molniya satellites launched into high eccentric orbit with perigee of about 500 km altitude and apogee altitude of about 40,000 km with inclination of 63.4° . The period of this orbit is about 12 h. The apogees of such orbits are placed over northern latitude to ensure that the satellite is visible over USSR for most of its period. Molniya constellation consists of 8 satellites; each separated by 45° . Each satellite is above 45°N latitude for 8 h. Typical Molniya orbit is given in Fig. 3.18.

Fig. 3.18 Molniya orbit



3.8.4 A Note on Osculating and Mean Orbital Elements

Due to continuous variation of orbital elements of short period and long period, there are two terms used for defining orbital elements: (i) osculating elements and (ii) mean orbital elements. Osculating orbital elements are the instantaneous Keplerian orbital elements. If the perturbation forces at that instant vanishes, then the orbital elements for the remaining period of time is constant, which is corresponding to the osculating element at that instant. The mean orbital elements and osculating elements are related by

$$\xi_{\text{osculating}} = \xi_{\text{mean}} + \Delta\xi_{\text{perturbation}} \quad (3.147)$$

where ξ is an orbital element ($a, e, i, \Omega, \omega, \theta$). Due to the non-variation nature of mean orbital elements, satellite mission targets are on the mean orbital elements. Since the launch vehicle mission target is at a specified latitude, longitude and altitude, the launch vehicle achieved orbit is corresponding to the osculating orbital elements. Therefore, there should be suitable interface between the satellite requirements and launch vehicle mission target.

3.9 Restricted Three-Body Problem

For the satellite orbit trajectories beyond Earth such as lunar mission or interplanetary mission, the satellite motion is influenced by both Earth and moon or Sun and Earth. Under such cases, the two-body problem as described in previous section is not valid and one has to adopt three-body problem as explained in this section. Consider two massive bodies m_1 and m_2 ($m_1 > m_2$), which are under motion due to their mutual gravitational attractions about the center of mass. Now consider a small body m , which is very small compared to that of m_1 and m_2 as shown in Fig. 3.19. Motion of the third body m under the influence of the gravity attraction of bigger bodies m_1 and m_2 is called the restricted three-body problem. (Example: m_1 : Earth, m_2 : Moon and m : satellite or m_1 : Sun, m_2 : Earth and m : satellite). There is no closed form solution to this problem. Detailed discussion on such a problem is beyond the scope of this book. Certain important aspects relevant to space transportation system under such condition are briefly summarized.

There are five equilibrium locations in this system, where the mass m has zero velocity and acceleration with respect to m_1 and m_2 . These equilibrium locations are called libration or Lagrange points. The equilibrium points lie in the orbital plane of $m_1 - m_2$ system. Once a body m is placed at the libration point, the body stays there. However, for an inertial observer, a mass m placed at such locations move around m_1 and m_2 in circular orbit.

For the Earth-Moon system, the locations of Lagrange points are given in Fig. 3.20. L_1 point of Sun-Earth system is about 1.5 million km from Earth. The

Fig. 3.19 Restricted three-body problem

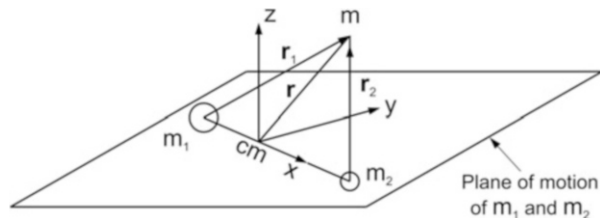
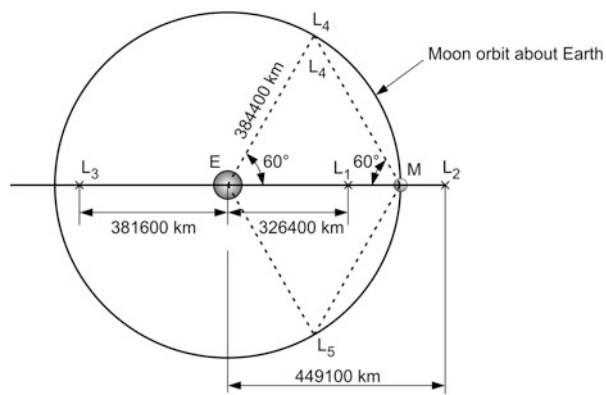


Fig. 3.20 Lagrange points of Earth-Moon system



L_1 , L_2 and L_3 are the saddle points i.e. unstable equilibrium points. The small body occupying these locations can stay there only if there is no disturbance. L_1 , L_2 and L_3 are the locations wherein the centrifugal force on the small mass m balances the combined collinear gravitational forces of Earth and Moon for three conditions. Due to unstable nature, any satellite placed in these points need fuel for keeping in that location.

The Langrange points L_4 and L_5 are the stable equilibrium points. At these locations, the gravitational forces from the massive bodies are in the ratio as that of the masses of the bodies so that the resultant force passes through the barry center. As the barry center is the center of mass of the system as well as center of rotation of the three body system, the resultant force is the one required to keep the smaller body at the Langrange point L_4 or L_5 . Any disturbance caused to the small body at this location results into stable oscillation about the equilibrium point, i.e. the small body m orbits about the equilibrium point. Thus a satellite placed in a small orbit about the stable equilibrium point stays there without any need for the fuel for station keeping. These orbits are called halo orbits. The stable equilibrium points are located at 60° with respect to the primary bodies. In nature, the Trojan asteroids occupy the stable equilibrium points L_4 and L_5 of Sun-Jupiter system.

Even though L_4 and L_5 are stable equilibrium locations, due to orbital perturbations caused by the other planetary bodies, some amount of fuel is required to keep and maintain halo orbits.

The satellites placed at the Liberation points (especially L_2 of Earth-Moon system) are useful as transit stations for interplanetary mission and for permanent space colonies (especially placed at L_4 or L_5). They also can be used as stations for permanent activities on Moon such as lunar mining etc.

3.10 Interplanetary Trajectories

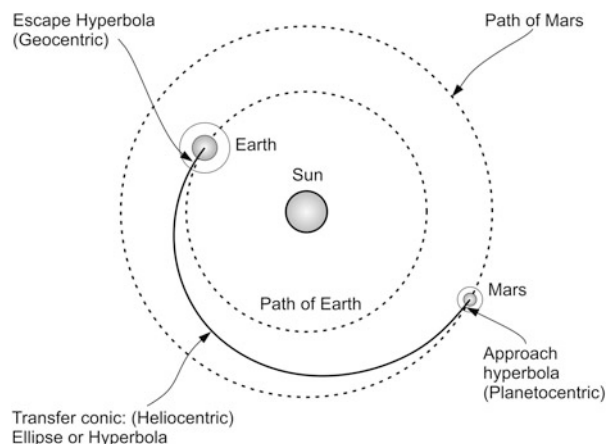
In order to achieve an interplanetary mission (travel from Earth to another planet), the satellite has to escape from the Earth's gravitational attraction. Even though the parabolic trajectory is an open trajectory which takes the satellite to infinity, if the satellite is launched with just escape velocity, at infinity, the residual velocity is zero and the satellite mission ends up with an orbit, same as that of Earth around Sun. In order to ensure that the satellite escapes from the Earth's gravitational attraction and to reach the target planet, there must be an excessive residual velocity at infinity, which is a characteristic of hyperbolic trajectory. Therefore, to achieve interplanetary mission from Earth, the satellite has to be launched in a hyperbolic trajectory. As the distance from the Earth increases, the Earth's gravitational attraction reduces and Sun's gravitational attraction increases and at one point of time, the satellite enters into a heliocentric trajectory with gravitational attraction of the Sun. This heliocentric trajectory depends on the residual velocity of the vehicle when it departs the Earth's gravitation. As the vehicle enters into the gravitational field of the target planet, the orbit becomes the planetocentric one.

The escape velocity at the time of Earth departure and trajectory during its entire journey are decided on the specific mission of the satellite. There are three types of interplanetary missions: (i) Fly-by mission, (ii) Orbiter mission and (iii) Lander mission.

In the fly-by mission, the satellite passes through the target planet at a short distance with respect to the planet and fly away further. In the orbiter mission, once the satellite is reached at a specified location and distance with respect to the target planet, propulsion system onboard the satellite is activated to reduce the velocity of the satellite to end up with an orbit around the target planet, as per the mission definition. In the case of lander mission, after reaching the orbit around the planet, the vehicle velocity is further reduced in a controlled fashion by the propulsion system. For the planets with atmosphere, the aerobreaking strategies are used to reduce the chemical propulsion requirements. Due to the high residual velocity requirements and the long distance travel, the interplanetary missions demand high energy requirements as well as longer travel time. In order to achieve the higher energy requirements and to reduce the travel time, advanced propulsion systems are required.

The main attracting bodies involved in an interplanetary trajectory are Earth, Sun and target planet. In addition, the gravitational attractions of Moon, other planets and radiation pressure act as disturbance forces to the satellite. Therefore, in reality, the interplanetary trajectories are many-body problems.

Fig. 3.21 Interplanetary trajectory conics to Mars



Consider an interplanetary mission from Earth to a target planet (say, Mars) as shown in Fig. 3.21. Initially, heliocentric conic section from Earth to target planet locations meeting the energy requirements and travel duration is finalized. After finalizing the requirements, the interplanetary trajectory is divided into three Keplerian conic sections as given below:

1. Geocentric hyperbolic trajectory
2. Heliocentric trajectory
3. Planetocentric hyperbolic trajectory

The velocity requirements at the interfaces and the trajectory in the three phases are decided to meet the integrated interplanetary mission requirements, i.e. the above three conic sections are patched together to arrive at the defined interplanetary trajectory. This approach is called patched conic method. After designing the trajectory with the above method, considering all the disturbance forces, their detailed trajectory analysis is carried out. While designing the interplanetary trajectory with patched conic approach, the spheres of influence plays a key role.

3.10.1 Sphere of Influence

In the patched conic approach, when a satellite follows Keplerian conic under the influence of one body (say, mass, m_2) the body is under the sphere of influence of m_2 whereas the second body (say, mass, m_1) gravitational attraction acts as disturbance to the satellite. Sphere of influence is a surface along which the influence of each body m_1 and m_2 are equal. Within the sphere of influence of m_2 , the trajectory of satellite is influenced by gravitational acceleration of m_2 whereas the gravitational acceleration of m_1 is acting as disturbance.

Fig. 3.22 Sphere of influence

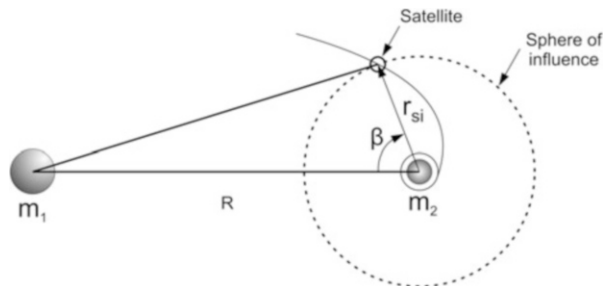
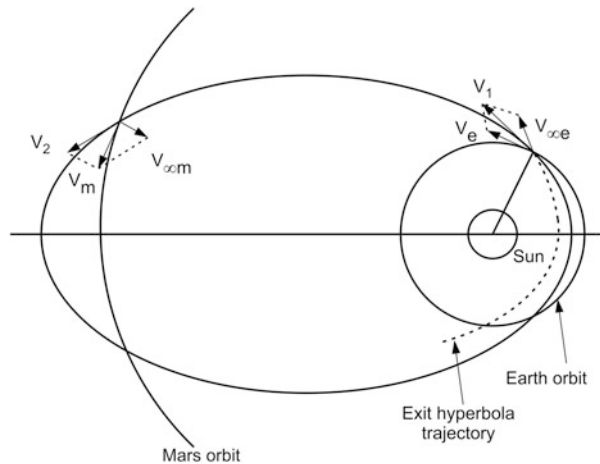


Fig. 3.23 Earth-Mars trajectory



Consider two bodies and satellite as shown in Fig. 3.22. The sphere of influence or activity sphere of m_2 is defined by

$$r_{si} = R \left(\frac{m_2}{m_1} \right)^{2/5} \frac{1}{(1 + 3 \cos^2 \beta)^{1/10}} \quad (3.148)$$

The surface is rotationally symmetric with respect to the line joining the bodies and the shape of the surface is slightly different from a sphere.

For the case of Sun-Earth system, the sphere of influence of Earth varies from 0.8×10^6 km to 0.925×10^6 km. For the case of Earth-Moon system, the sphere of influence of Moon varies between 58×10^3 km and 66×10^3 km.

3.10.2 Patched Conic Trajectory

As an example, the interplanetary trajectory from Earth to Mars is considered as shown in Fig. 3.23. The satellite velocity required at the sphere of influence of Earth to follow the heliocentric trajectory to reach Mars is $V_\infty e$.

$$\mathbf{V}_{\infty e} = \mathbf{V}_1 - \mathbf{V}_e \quad (3.149)$$

where \mathbf{V}_e is the Earth's orbital velocity and \mathbf{V}_1 is the velocity at the start of the heliocentric conic near to the Earth side. Generally, at the surface of sphere of influence, the velocity of the hyperbolic trajectory equals to the hyperbolic excess (residual) velocity \mathbf{V}_{∞} . In case additional velocity is required it can be imparted to \mathbf{V}_{∞} to get the required $\mathbf{V}_{\infty e}$. Once the satellite arrives at the Mars, the planetocentric excess velocity, $\mathbf{V}_{\infty m}$, is achieved by

$$\mathbf{V}_{\infty m} = \mathbf{V}_2 - \mathbf{V}_m \quad (3.150)$$

where \mathbf{V}_2 is the heliocentric conic velocity at the approach and \mathbf{V}_m is orbital velocity of Mars. If required, satellite velocity can be reduced to achieve the required $\mathbf{V}_{\infty m}$.

By this process, the interplanetary trajectory from Earth to Mars is achieved.

3.11 Orbital Transfers and Launch Vehicle Orbit Requirements

Although this section can be a part of chapter on Mission Design or Satellite Launching, it is included here due to its close links with this chapter. Orbital transfer is an integral part of satellite mission design. Requirements of a specific orbit for a satellite depend on the application for which the satellite is intended for; it needs to be placed in the specified orbit in terms of size, shape and orientation in inertial space. As an example, remote sensing satellites need to be placed in the circular orbits with the altitude ranging from 500 to 900 km along with the inclination varying between 97° and 99° , whereas communication satellites need to be placed in the circular orbit with an altitude of about 36,000 km above the Earth over the equator (inclination = 0). The satellite orbits used for communication in the high latitude region of Earth require high eccentric orbits with critical inclination ($i = 63.4^\circ$) with apogee over the specified region of Earth, whereas global navigational satellite systems need to be placed in orbits about 20,000 km with inclination about 50° .

In addition, the satellites for lunar and interplanetary missions need to depart from the Earth bound orbits at a specified time, day, month and year. Therefore, depending on the applications, it is essential to place the satellite in its specified orbit.

An efficient launch vehicle has to deliver the energy in the shortest possible time. Sometimes, although the velocity achieved by the vehicle is substantial, the altitude travelled by the vehicle may not meet the satellite requirements. Therefore, to achieve the high altitude requirement of satellite, ensuring the required velocity, the vehicle energy has to be appropriately utilized to increase the potential energy.

This in turn reduces the share of kinetic energy, resulting in the reduction of payload capability of the vehicle.

Thus, for a specified launch vehicle, there is trade-off between the orbital altitude and the payload mass which can be placed in the specified orbit. To enhance the payload capability, launch vehicle always prefers to place a satellite in an orbit with lower altitude. The best performance of a launch vehicle is achieved by planar trajectory missions. To obtain the required inclination, from the launch site, a suitable launch azimuth is to be defined. Due to range safety limitations, the required launch azimuth may not be feasible and hence it is difficult to achieve the required inclination from the specified launch site. In certain cases, although the best launch azimuth is feasible, the inclination of the orbit achieved is restricted by the geographical location of launch site. For example, to achieve zero orbital inclination, the launch site has to be located over equator with an azimuth of 90° . Any deviation from this, results into different orbital inclination and this needs to be corrected by the satellite.

Therefore, an integrated optimum strategy for achieving the maximum performance is to target the launch vehicle to inject the satellite into the ‘best possible’ orbit, which achieves maximum payload. Further the satellite has to carry out the needed orbital transfers from the orbit provided by the vehicle to the final specified orbit. This needs additional fuel in satellite onboard.

Thus, launch vehicle design and mission planning is a trade-off between vehicle capability vis-à-vis extra fuel required in satellite to carry out the needed orbital transfers. The quantity of fuel in satellite depends on the type of orbital transfer maneuver needed. This section briefly explains the orbital transfer maneuvers from the satellite. It is assumed that the propulsive system used for the orbital transfer is imparting the required velocity in impulsive fashion.

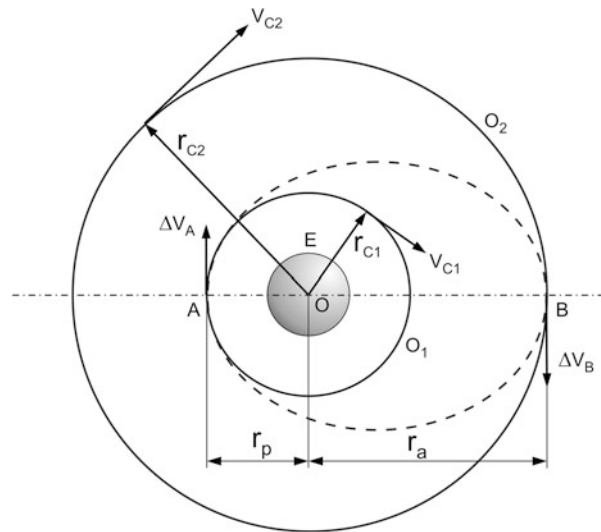
3.11.1 Coplanar Circular Orbits Transfer

Assume the launch vehicle achieved orbit, O_1 is a circular orbit with radius r_{c1} , and the satellite required orbit O_2 , is also circular orbit with radius r_{c2} , as shown in Fig. 3.24. Assuming O_1O_2 are coplanar (i.e., orbital inclinations are same), the minimum energy path from O_1 to O_2 is Hohmann transfer. This is a semi-elliptic trajectory with perigee tangential to the orbit altitude r_{c1} of O_1 and apogee tangential to the orbit altitude r_{c2} of O_2 as shown in figure.

Velocity of vehicle at A on the circular orbit O_1 is as derived in Eq. 3.99 is given by

$$\mathbf{V}_{c1} = \sqrt{\frac{\mu}{r_{c1}}} \quad (3.151)$$

Fig. 3.24 Coplanar circular orbits transfer



The parameters of Hohmann transfer ellipse as given in Fig. 3.24 are given below:

$$r_p = r_{c1} \quad (3.152)$$

$$r_a = r_{c2} \quad (3.153)$$

$$a = \frac{r_{c1} + r_{c2}}{2} \quad (3.154)$$

Velocity of vehicle in elliptic path is given by

$$\mathbf{V} = \sqrt{\mu \left(\frac{2}{r} - \frac{1}{a} \right)} \quad (3.155)$$

Velocity of the vehicle at A (perigee), if the vehicle needs to travel in Hohmann ellipse of Fig. 3.24 is given as

$$\mathbf{V}_A = \sqrt{\mu \left(\frac{2}{r_{c1}} - \frac{1}{a} \right)} \quad (3.156)$$

Therefore the velocity increment required to transfer the vehicle from the launch vehicle orbit O_1 to transfer ellipse is given as

$$\Delta \mathbf{V}_A = \mathbf{V}_A - \mathbf{V}_{c1} \quad (3.157)$$

Velocity of the vehicle at apogee of the transfer ellipse (B) is given by

$$\mathbf{V}_B = \sqrt{\mu \left(\frac{2}{r_{c2}} - \frac{1}{a} \right)} \quad (3.158)$$

and velocity, V_{c2} of the circular orbit altitude r_{c2} of O_2 is given by

$$V_{c2} = \sqrt{\frac{\mu}{r_{c2}}} \quad (3.159)$$

Therefore, the velocity increment required to transfer the vehicle from the transfer ellipse to the required satellite orbit O_2 is given by

$$\Delta V_B = V_{c2} - V_B \quad (3.160)$$

Thus applying the impulsive velocity increments ΔV_A in the plane of orbit when the vehicle reaches the location A, tangential to the orbit and subsequently ΔV_B in the plane of orbit when the vehicle reaches the location at B, tangential to the orbit, the satellite will reach the final orbit O_2 .

Therefore, total velocity imparted by the satellite to transfer from launch vehicle orbit to the satellite specified orbit is given by

$$\Delta V = \Delta V_A + \Delta V_B \quad (3.161)$$

Assuming the specific impulse, I_{sp} (in seconds) used by the satellite propulsion system, the propellant needs to be stored in the satellite, m_p , to achieve the final orbit is given by

$$m_p = m_i \left[1 - e^{-\left(\frac{\Delta V}{g I_{sp}}\right)} \right] \quad (3.162)$$

where m_i is the mass of satellite injected by launch vehicle into initial orbit which includes useful payload, propulsion system accessories and propellant.

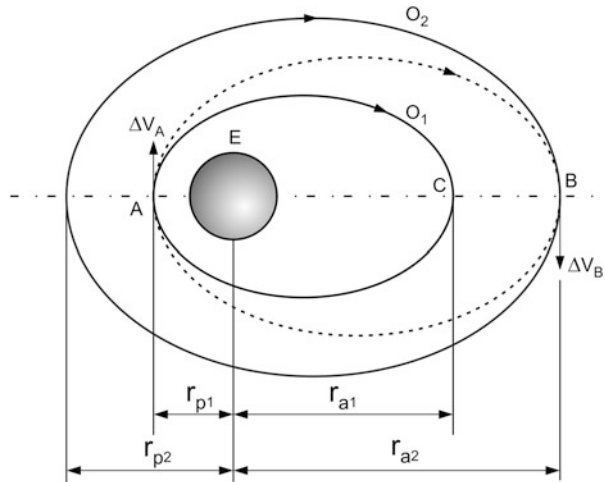
3.11.2 Coplanar Elliptic Orbits Transfer

In this case, the initial orbit O_1 and final orbit O_2 are ellipses with the same focus as given in Fig. 3.25. The coplanar Hohmann transfer ellipse and the locations and directions of velocity increment applications are computed as given below:

Launch vehicle achieved orbital characteristics are: perigee radius = r_{p1} , apogee radius = r_{a1} and $a_1 = (r_{p1} + r_{a1})/2$.

Satellite required orbital characteristics are perigee radius = r_{p2} , apogee radius = r_{a2} and $a_2 = (r_{p2} + r_{a2})/2$.

Fig. 3.25 Coplanar elliptic orbits transfer



Perigee velocity of O_1 at A is given by

$$\mathbf{V}_{p1} = \sqrt{\mu \left(\frac{2}{r_{p1}} - \frac{1}{a_1} \right)} \quad (3.163)$$

The transfer ellipse is with perigee radius of r_{p1} and apogee radius of r_{a2} . Therefore, the semi-major axis of transfer ellipse is

$$a_t = \frac{r_{p1} + r_{a2}}{2} \quad (3.164)$$

and the perigee velocity of transfer ellipse at A is given by:

$$\mathbf{V}_{pt} = \sqrt{\mu \left(\frac{2}{r_{p1}} - \frac{1}{a_t} \right)} \quad (3.165)$$

Therefore, the velocity increment, ΔV_A , required to be applied at A in the orbital plane along the direction of velocity to transfer the vehicle from initial orbit, O_1 , to transfer orbit is given by

$$\Delta V_A = \mathbf{V}_{pt} - \mathbf{V}_{p1} \quad (3.166)$$

Similarly, the apogee velocity of transfer ellipse at B is given by

$$\mathbf{V}_{at} = \sqrt{\mu \left(\frac{2}{r_{a2}} - \frac{1}{a_t} \right)} \quad (3.167)$$

and the apogee velocity of the required orbit O_2 , at B is given by

$$\mathbf{V}_{a2} = \sqrt{\mu \left(\frac{2}{r_{a2}} - \frac{1}{a_2} \right)} \quad (3.168)$$

and therefore, the velocity increment, $\Delta\mathbf{V}_B$, required to be applied at B in the orbital plane along the direction of velocity to transfer the vehicle from the transfer orbit to the final required orbit, O_2 , is given by

$$\Delta\mathbf{V}_B = \mathbf{V}_{a2} - \mathbf{V}_{at} \quad (3.169)$$

and the total velocity requirement is given by

$$\Delta\mathbf{V} = \Delta\mathbf{V}_A + \Delta\mathbf{V}_B \quad (3.170)$$

3.11.3 Coplanar Orbital Transfer from Ellipse to Circular Orbit

In this case, the launch vehicle is assumed to inject the satellite in an elliptic orbit O_1 with a suitable perigee and apogee altitude corresponding to the circular orbit height of the satellite. The satellite in turn circularizes the orbit to O_2 . Assuming these orbits are coplanar, the incremental velocity required to be imparted by satellite is computed as follows:

The launch vehicle orbit is an elliptic one with perigee radial distance of r_p and apogee radial distance of r_a . The satellite required orbit is a circular orbit with altitude of r_a . In this case, the velocity increment need to be applied at the apogee location, A, of launch vehicle orbit along the velocity direction.

The apogee velocity of launch vehicle orbit is given by

$$\mathbf{V}_a = \sqrt{\mu \left(\frac{2}{r_a} - \frac{1}{a} \right)}; \quad a = \frac{r_a + r_p}{2} \quad (3.171)$$

The circular velocity of required orbit is given by

$$\mathbf{V}_c = \sqrt{\frac{\mu}{r_a}} \quad (3.172)$$

and the required velocity increment $\Delta\mathbf{V}_A$ to be applied at A along the velocity direction is given by

$$\Delta\mathbf{V}_A = \mathbf{V}_c - \mathbf{V}_a \quad (3.173)$$

3.11.4 Inclination Change of Orbital Plane

Assume that the launch vehicle injects the satellite into a circular orbit O_1 with the altitude as specified by the satellite. But it could not achieve the required inclination, and in such case, the satellite needs to maneuver the orbital plane to reach the final one, O_2 , as given in Fig. 3.26.

The inclination of the orbit is measured at equator when the satellite crosses the line of nodes. Therefore, it is essential to apply the correction maneuver at the time of equatorial crossing of the satellite. In this case, it is important not to change the magnitude of the satellite velocity but to rotate the velocity vector, V_c , in a plane normal to the original orbital plane. The incremental velocity required to change the inclination has to be applied in the normal plane with magnitude and direction as detailed below.

For simplicity, the velocity diagram of initial orbit O_1 with inclination of i_1 and final orbit O_2 with inclination of i_2 of Fig. 3.26 is reproduced in Fig. 3.27.

From the figure, using trigonometrical relations, the velocity increment ΔV required to rotate the velocity vector V_c with inclination of i_1 to the velocity vector of V_c with inclination of i_2 can be computed as

$$\Delta V = \sqrt{2V_c^2[1 - \cos(i_1 - i_2)]} \quad (3.174)$$

This velocity increment needs to be applied when the satellite crosses the equator in the plane normal to orbital plane. This has to be along the direction ψ with respect to the initial velocity vector and given by

$$\psi = \frac{\pi}{2} + \frac{(i_1 - i_2)}{2} \quad (3.175)$$

Fig. 3.26 Inclination change of circular orbits

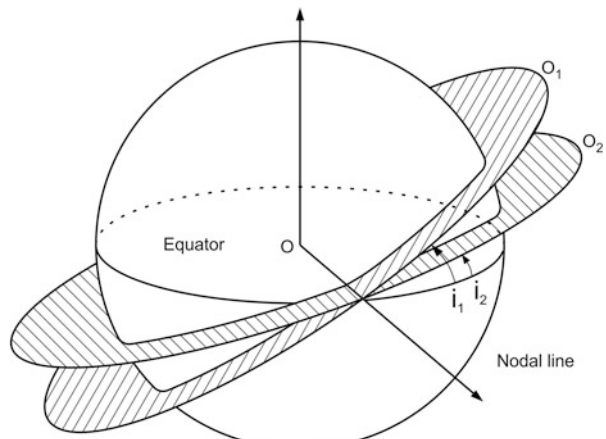


Fig. 3.27 Velocity diagram for change of inclination

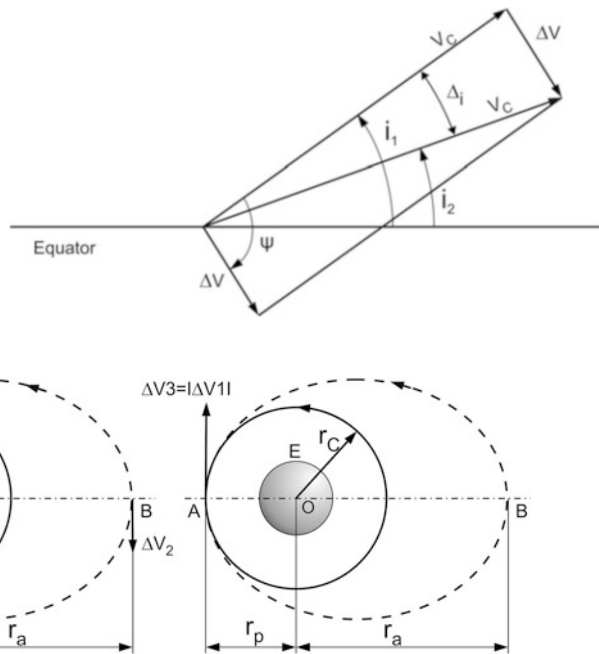


Fig. 3.28 Optimum inclination correction maneuvers

As per Eq. (3.174), the velocity increment required for inclination correction is proportional to the velocity of the vehicle. Due to this, at high velocities the correction velocity is rather high and the inclination correction maneuver is not beneficial. It is always advantageous to carry out the correction when the satellite is at lower velocity. Therefore, when there is large inclination correction, the preferred option is to increase the orbit size to elliptic and carry out the correction at apogee, where the velocity is less. Subsequently circularize the orbit to the required height as shown in Fig. 3.28.

The total velocity required is given below:

$$\Delta \mathbf{V}_1 = \sqrt{\mu \left(\frac{2}{r_c} - \frac{2}{r_c + r_a} \right)} - \sqrt{\frac{\mu}{r_c}} \quad (3.176)$$

$$\mathbf{V}_a = \sqrt{\mu \left(\frac{2}{r_a} - \frac{2}{r_c + r_a} \right)} \quad (3.177)$$

$$\Delta \mathbf{V}_2 = \sqrt{2 \mathbf{V}_a^2 (1 - \cos \Delta i)} \quad (3.178)$$

$$\Delta \mathbf{V}_3 = |\Delta \mathbf{V}_1| \quad (3.179)$$

and therefore,

$$\Delta \mathbf{V} = \Delta \mathbf{V}_1 + \Delta \mathbf{V}_2 + \Delta \mathbf{V}_3 \quad (3.180)$$

i.e.,

$$\begin{aligned} \Delta \mathbf{V} = & 2 \left[\sqrt{2\mu \left(\frac{1}{r_c} - \frac{1}{r_c + r_a} \right)} - \sqrt{\frac{\mu}{r_c}} \right] \\ & + \sqrt{4\mu \left(\frac{1}{r_a} - \frac{1}{r_c + r_a} \right) (1 - \cos \Delta i)} \end{aligned} \quad (3.181)$$

Equation (3.174) gives the incremental velocity required for correcting the inclination of the orbit directly whereas Eq. (3.181) gives the incremental velocity required for correcting the inclination through transfer ellipse. On analysis of Eqs. (3.174) and (3.181), it can be seen that for correcting inclination up to about 39° , direct correction requires less impulse whereas for correcting inclination beyond 39° , transfer ellipse method requires less incremental velocity than correcting directly. For each inclination, there will be an optimum apogee for inclination correction beyond 39° and beyond 60° , the apogee required for such maneuver is ∞ , which is the limit.

3.11.5 Combined Orbit Size and Inclination Correction

In certain cases, from the launch vehicle achieved orbit to the satellite specified orbit, both orbit size and inclination corrections have to be carried out.

This is the typical case of orbital transfer from launch vehicle achieved Geo Transfer Orbit (GTO) to the Geo Stationary Orbit (GEO). In order to carry out the orbital corrections, it is possible to use two strategies as given in Fig. 3.29.

As shown in the figure two strategies are: (i) First correct for the inclination and then increase the orbit size, or (ii) First increase the orbit size and then correct for the inclination. In both these strategies, the total velocity required will be large and therefore third strategy of carrying out these maneuvers together as given in Fig. 3.29d can be adopted which demands least velocity increment.

Assuming initial orbit velocity as \mathbf{V}_i with inclination of i_i and final orbit velocity as \mathbf{V}_f with inclination of i_f , the optimum incremental velocity magnitude is given by

$$\Delta \mathbf{V} = \sqrt{\mathbf{V}_i^2 + \mathbf{V}_f^2 - 2\mathbf{V}_i \mathbf{V}_f \cos \Delta i} \quad (3.182)$$

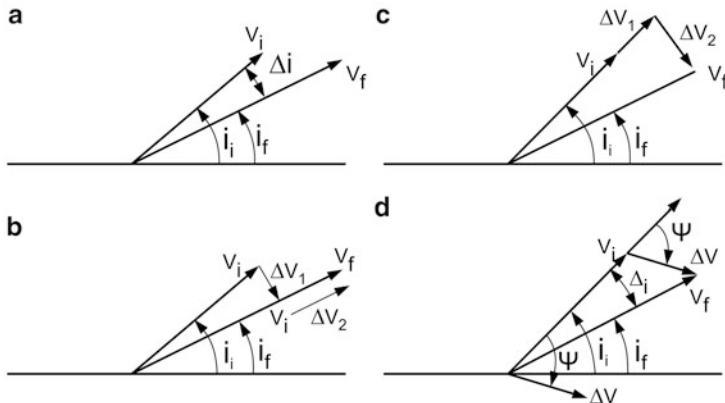


Fig. 3.29 Optimum correction for orbit size and inclination: (a) requirement (b) velocity change + Inclination change (c) inclination change + velocity change (d) inclination and orbits size change together

where

$$\Delta i = i_i - i_f \quad (3.183)$$

and this impulsive velocity is to be applied to the vehicle when it crosses the equator in a plane perpendicular to orbital plane. This has to be done at an orientation ψ with respect to the initial orbital velocity vector V_i and is given by

$$\psi = \pi - \cos^{-1} \left[\frac{V_i^2 + \Delta V^2 - V_f^2}{2V_i \Delta V} \right] \quad (3.184)$$

3.11.6 Launch Vehicle GTO Requirements for Geostationary Satellite Missions

The geostationary satellites need to be placed in the circular orbit with altitude of about 36,000 km and to be placed over equator, i.e. inclination of the orbit is zero. Generally, if the launch vehicle needs to inject these satellites directly into the geostationary orbit, there will be heavy loss. In addition, due to the limitations of launch site location and launch azimuth, the finally achieved orbit may not be over equator and it will have a certain inclination with respect to the equator.

The trade-off between the launch vehicle achieved orbit and the propellant required in satellites to correct the orbit is needed. Based on such analysis, the optimum strategy for launch vehicle orbit has to be decided.

1. Elliptic orbit with apogee equal to the orbital height required by the satellite (i.e. 36,000 km) whereas the perigee height can be decided based on the launch vehicle capability and other operational and satellite life time constraints.

2. Due east launch which provides the minimum orbital inclination from the specified launch site (equal to the latitude of the launch site)

The satellite carries out the orbit size maneuver at the apogee of the launch vehicle achieved orbit as explained earlier. At the same time, the inclination correction needs to be done. The inclination correction is optimum, if it is done at the lowest velocity point of the orbit, i.e. at the apogee of the launch vehicle achieved orbit. The efficient way of achieving both these corrections is to carry out these operations together, i.e. at the apogee. At the same time, the inclination correction needs to be carried out when the vehicle crosses the equator. Therefore considering all these aspects, the launch vehicle achieved GTO is planned such that the line of apsides is over the equator, i.e. argument of perigee of launch vehicle GTO is either 180° or 0° depending upon the launch site and launch azimuth.

From the launch vehicle achieved GTO as defined earlier, satellite has to carry out the maneuver as given in Eqs. (3.182), (3.183), and (3.184) to achieve the final required orbit. Due to operational reasons and other maneuver constraints, sometimes multiple maneuver are needed when the vehicle crosses the equator at the apogee location and it is continued till the satellite reaches the required orbital height with zero inclination.

Bibliography

1. Roy, A.E.: *The Foundations of Astrodynamics*. Macmillan, New York (1965)
2. Danby, J.M.A.: *Celestial Mechanics*. Macmillan, New York (1962)
3. Herick, S.: *Astrodynamics*, vol. 2. Van Nostrand Reinhold, London (1971)
4. Battin, R.H.: *An Introduction to the Mathematics and Methods of Astrodynamics*. American Institute of Aeronautics and Astronautics, AIAA Education Series, Reston (1987)
5. Vallado, D.A.: *Fundamentals of Astrodynamics and Applications*. McGraw Hill, New York (1997)
6. Geyling, F.T., Westerman, H.R.: *Introduction to Orbital Mechanics*. Addison Wesley, Reading (1971)
7. Hale, F.J.: *Introduction to Space Flight*. Prentice Hall, Englewood (1994)
8. Roy, A.E.: *Foundations of Astrodynamics*. Macmillan, New York (1961), Fairly Concise

Chapter 4

Space Transportation Requirements and Launching of Satellites

Abstract The function of space transportation system is not only to lift the specified satellite from Earth surface, travel through space and to inject it precisely into the defined orbit but also to achieve all specified orbital specifications simultaneously. To achieve these objectives, the STS has to provide the required mechanical energy to the satellite, defined by the orbit size and satellite mass. It is also necessary to have an optimum location of launch site on the surface of the Earth and launch direction (launch azimuth). Therefore, each orbital mission demands specified location of launch site and launch azimuth. But, due to geographical constraints, it is not possible to have an optimum launch site, and the allowable launch azimuth directions are also limited due to range safety related issues. In such cases, launch vehicle has to provide extra energy to reach the defined target. The influence of Earth's gravity field and aerodynamic drag during atmospheric flight phase causes the energy loss and to compensate these losses extra energy has to be provided. All these effects need to be considered for configuring STS to provide the necessary energy to the satellite. The satellites requirements are widely varying, ranging from low Earth orbits to high altitude orbits, depending on their applications. Therefore with the effective utilization of available energy in the STS, the maximum performance has to be achieved by adopting suitable strategies and the details of all these methods are explained in this chapter. The functional requirements for STS design have to start with the orbital mission requirements and the satellite mass to be placed in the specified orbit. The step by step procedure starting from mission design to STS design process, which satisfies the overall functional requirements, is also described. Various errors occurring during the operation of several subsystems of STS, their effects on overall mission and how to alleviate them are also explained here.

Keywords Functional requirement • Rocket equation • Vehicle trajectory • Launch site • Launch Azimuth • Direct ascent • Hohmann transfer • Mission definition and integrated mission

4.1 Introduction

To meet the specific applications, the satellite needs to be placed into the specified orbit, defined by six orbital elements viz., a , e , i , Ω , ω and θ . As explained in Chap. 3, a and e define the size and shape of the orbit, Ω and i define orientation of the orbital plane in an inertial system, ω specify the location of perigee in the orbital plane and θ refers the position of the satellite with respect to perigee in the orbit at the specified time. The function of space transportation system is to lift the specified satellite from Earth surface, travel through space and to inject it precisely into the defined orbit. The functional requirement of space transportation system (STS) is not only to meet the specified spacecraft in an orbit with the required size and shape; but to achieve all the six orbital elements simultaneously.

To achieve the above functional requirements, the STS must be capable of lifting the satellite to the specified orbit, i.e. the STS must provide the required mechanical energy to the satellite, defined by the orbit size and satellite mass. To achieve these requirements in an efficient way (maximum performance), for each satellite mission, there exists an optimum location of launch site on the surface of the Earth along with an optimum launch direction (launch azimuth). Therefore, each orbital mission demands specified location of launch site and launch azimuth. But, due to geographical constraints, launch sites are located at convenient places and for each launch site, the allowable launch azimuth directions are also limited due to range safety related issues. In such cases, launch vehicle may have to provide extra energy to reach the defined target. Also, it is to be noted that the STS imparts energy in a finite time and during this period, the vehicle is under the influence of Earth's gravity field and aerodynamic drag during atmospheric flight phase. Therefore, the STS needs to provide extra energy to work against the above environments. All these effects need to be considered for configuring STS to provide the necessary energy to the satellite.

The satellites requirements are widely varying, ranging from low Earth orbits to high altitude orbits, depending on their applications. With the effective utilization of available energy in the STS, to achieve the maximum performance, it is always preferable to inject the satellite at lower altitudes. These contradicting requirements of satellites and the payload capabilities of STS have to be resolved by adopting one of the following strategies: (1) STS to directly inject the satellite into the desired orbit and (2) STS to inject the satellite into an intermediate orbit and satellite in turn uses its own propulsion system to transfer the satellite to the desired orbit. A trade-off has to be carried out considering the integrated mission aspects of satellite requirements and STS capabilities.

Considering the above aspects, the STS mission target is to be specified and to achieve the target the subsystems of STS are to be defined. Thus, in summary, the satellite requirements are to be translated into STS functional requirements. In reality, the targets specified by satellites cannot be achieved exactly by the STS

due to the various errors of the subsystems, which in turn reflect as errors in the achieved orbit. This error has to be corrected by the propulsion system of the satellite, which demands extra fuel and extra mass to the satellite. Therefore, a trade-off has to be arrived at between the satellite requirements and STS subsystem capabilities, and an integrated mission specification has to be arrived at for the STS mission target with the allowable dispersions on it. This forms the specifications for STS subsystems design process. The vehicle subsystems have to be configured and designed to meet the above specifications.

The above aspects are explained in the following sections of this chapter, whereas the design and validation procedures for each of the subsystems are explained in the subsequent chapters.

4.2 Space Transportation Functional Requirements

In order to place a satellite of mass m_s in a specified orbit, the mechanical energy of $m_s \epsilon$ has to be imparted to the satellite, where ϵ is the specific mechanical energy of the orbit given by

$$\epsilon = -\frac{\mu}{2a} = \frac{V^2}{2} - \frac{\mu}{r} \quad (4.1)$$

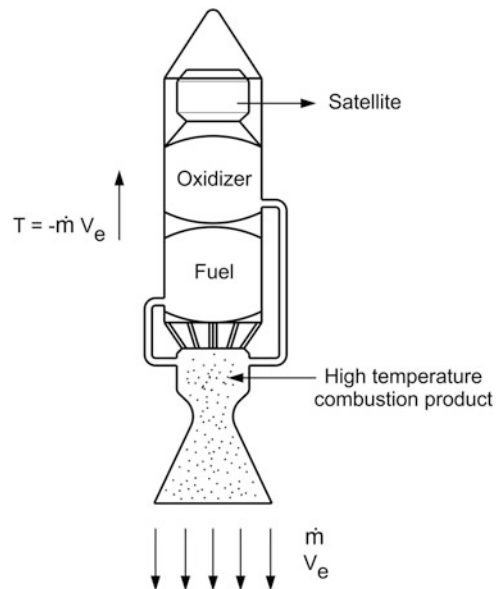
where a is semimajor axis of the orbit and r and V are radial distance and velocity respectively at a location of the orbit. The functional requirement of space transportation system is to provide the necessary energy $m_s \epsilon$ to the satellite. The mechanical energy dealing is very large. As an example, for a circular orbit of 540 km altitude, the specific energy is 33.7 MJ/kg, and for geostationary orbit, energy is 57.8 MJ/kg. To provide such high energy to reach a higher altitude orbit, with present day technologies, it is feasible only by the rockets with non-air breathing chemical propulsion system, wherein both oxidizer and fuel have to be carried along with the vehicle.

In rockets, chemical energy (of propellants) is converted initially into thermal energy (of combustion products), which further is converted into kinetic energy by the exhaust velocity of combustion products by expanding high temperature combustion products through nozzle. This provides the kinetic energy to the vehicle by the principles of Newton's third law. The complete process is shown in Fig. 4.1.

The kinetic energy of the vehicle finally reflected as velocity increase and with certain loss of kinetic energy, the altitude of the vehicle also increases.

As per the Newton's second law, the rate of change of momentum is the force. The rate of change of momentum of the exhaust gas is $\dot{m}V_e$, where \dot{m} is combustion product exhaust flow rate and V_e is exhaust velocity (constant). Therefore, the force

Fig. 4.1 Simple rocket engine



produced is $\dot{m}V_e$. As per Newton's third law, the thrust force acting on the vehicle is given by

$$T = -\dot{m}V_e \quad (4.2)$$

where the exhaust flow rate \dot{m} is same as the propellant consumption rate. The exhaust velocity is nothing but the specific impulse in the rocket terminology. It can be seen that, to get higher thrust, either mass flow rate has to be increased or specific impulse to be increased. V_e is the characteristics of the selected propulsion system and \dot{m} depends on the size of the selected propulsion system.

The acceleration imparted to the vehicle due to the thrust given by Eq. (4.2) is expressed as

$$\frac{dV}{dt} = a = \frac{T}{m} \quad (4.3)$$

where m is mass of the vehicle. Eq. (4.3) can be written as

$$\frac{dV}{dt} = -\frac{\dot{m}}{m}V_e \quad (4.4)$$

Expanding variables results in

$$dV = -\frac{dm}{m}V_e \quad (4.5)$$

Integrating Eq. (4.5) from t_0 (ignition time) to t_b (burnout time), the velocity imparted by the rocket from t_0 to t_b is

$$\Delta V = \int_{m_0}^{m_f} \left[-\frac{dm}{m} \right] V_e \quad (4.6)$$

i.e.,

$$\Delta V = -V_e [\ln(m)]_{m_0}^{m_f} \quad (4.7)$$

Assuming m_0 is the initial mass of the vehicle at the time of ignition (when propellants are full) and m_f is the final mass of the vehicle at burnout (i.e., when all the propellants are depleted), Eq. (4.7) can be written as

$$\Delta V = V_e \ln \left(\frac{m_0}{m_f} \right) \quad (4.8)$$

Equation (4.8) is called Tsiolkowski equation or rocket equation. The velocity given by Eq. (4.8) is called ideal velocity of a rocket engine. When the unit of specific impulse is specified in terms of seconds (s), then

$$V_e = g I_{sp} \quad (4.9)$$

where g is the acceleration due to gravity. Once the initial vehicle mass m_0 is specified to provide the required velocity, ΔV with the specified propulsion system, final achieved mass is given as

$$m_f = m_0 e^{-\frac{\Delta V}{V_e}} \quad (4.10)$$

or, the propellant mass required, m_p is given by

$$m_p = m_0 \left[1 - e^{-\frac{\Delta V}{V_e}} \right] \quad (4.11)$$

Further details on vehicle sizing are explained in Chap. 5. The STS energy requirement is explained in the following section.

In order to convert the orbital mission requirements into STS functional requirements, the energy required to achieve the specified orbit, given in Eq. (4.1) has to be translated into the required velocity ΔV to be achieved by the STS system. Once ΔV is estimated, specifying the selected propulsion system, the vehicle sizing in terms of required propellant loading is decided using Eq. (4.11). Therefore, it is essential to estimate the equivalent launch velocity to reach the specified orbit as given below:

Assuming the entire orbital energy is given by an equivalent velocity on the surface of the Earth, the energy equation can be written as

$$\varepsilon = -\frac{\mu}{2a} = \frac{V_{el}^2}{2} - \frac{\mu}{R_e} \quad (4.12)$$

where

a is the semi-major axis of the desired orbit

R_e is the radius of Earth

V_{el} is the equivalent velocity required to reach the orbit from the surface of Earth

Eq. (4.12) can be written as

$$V_{el} = \sqrt{\mu \left[\frac{2}{R_e} - \frac{1}{a} \right]} \quad (4.13)$$

Equation (4.13) gives the velocity required to be given by a STS to achieve an orbit specified by semi-major axis, a .

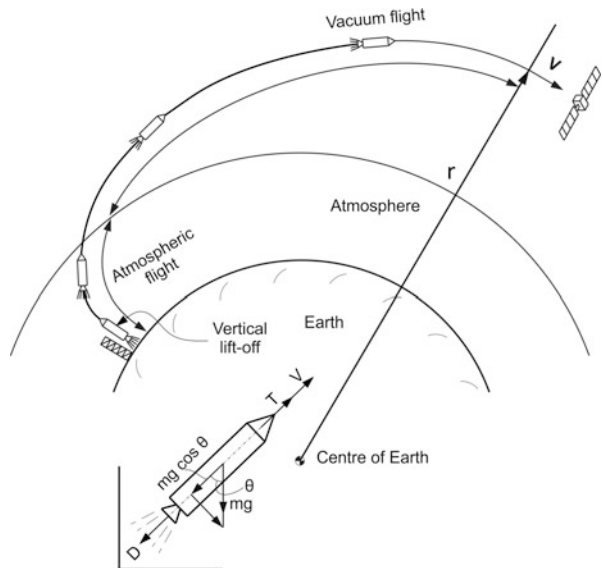
4.3 Vehicle Trajectory

The previous section explained the details on equivalent velocity required to launch a satellite into a specified orbit and the ideal velocity generated by a rocket engine, which is used for space transportation system. In reality, the space transportation has to follow a defined trajectory to carry out its task of injecting the satellite into the desired orbit. The implication of the trajectory on the space transportation system requirements is given below.

The operating environment of a space transportation system is severe. The vehicle has to work against the gravitational force throughout its mission. The gravity force causes performance (velocity) loss to the vehicle. In addition, initial phase of the vehicle travel is in the dense atmosphere. Generally, the atmosphere has effect upto 100–120 km depending on the vehicle configuration and velocity build up. In this phase, both drag and lateral forces act on the vehicle. The drag force causes performance loss to the vehicle. In addition, atmospheric flight phase is the most crucial phase for the space transportation system mission due to the large magnitude of disturbing lateral forces and moments which have destabilizing effect on the vehicle and causes heavy structural loads.

The flight environments clearly demand that the vehicle has to move out of the atmospheric flight (flight up to denser atmosphere) in shortest possible time with the maximum performance of the vehicle. To achieve these objectives in an efficient way, the ascent phase trajectory of space transportation system is normally planned as represented in Fig. 4.2.

Fig. 4.2 Typical trajectory of a space transportation system



The vehicle is assembled vertically, and after ignition, the vehicle lifts-off vertically. Once the vehicle clears the launch support structure on ground, the vehicle is tilted (pitch down) along the launch direction. Then vehicle flies along the path which minimizes the load on the vehicle (zero angle of attack trajectory) and extends till the vehicle crosses the atmosphere. Normally, the vehicle trajectory during atmospheric flight phase is steeper to cross the atmosphere quickly. The trajectory is designed as a compromise between performance loss and vehicle safety during this phase. After crossing the atmosphere, the vehicle is steered in optimum direction to get maximum performance, by changing the vehicle trajectory at the exit of atmosphere and continued till it achieves the required position and velocity vector at the end of its mission. Details on trajectory design aspects are given in Chap. 7 on launch vehicle mission design. In this section, the impact of vehicle trajectory on the velocity requirement of space transportation system is explained.

If the velocity vector is aligned with the thrust direction, then the acceleration of the vehicle as explained in Fig. 4.2 is given by

$$a = \frac{dV}{dt} = \frac{T - D - mg \cos \theta}{m} \quad (4.14)$$

Substituting Eq. (4.2) in Eq. (4.14) yields

$$m \frac{dV}{dt} = -V_e \frac{dm}{dt} - D - g \cos \theta \quad (4.15)$$

Separating variables in Eq. (4.15) gives

$$dV = -V_e \frac{dm}{m} - \frac{D}{m} dt - g \cos \theta dt \quad (4.16)$$

Integrating Eq. (4.16) gives,

$$\Delta V = V_e \ln \left(\frac{m_0}{m_f} \right) - \int_{t_0}^{t_b} \frac{D}{m} dt - \int_{t_0}^{t_b} g \cos \theta dt \quad (4.17)$$

i.e.,

$$\Delta V = \Delta V_{\text{ideal}} - \Delta V_{\text{drag}} - \Delta V_{\text{gravity}} \quad (4.18)$$

where

ΔV is the actual velocity gained by the vehicle

ΔV_{ideal} is the ideal velocity imparted by the vehicle

ΔV_{drag} is the loss in vehicle velocity due to atmospheric drag

$\Delta V_{\text{gravity}}$ is the loss in vehicle velocity due to gravity

In order to guarantee the required orbit, the equivalent velocity to be achieved by the vehicle is ΔV_{req} after compensating the drag and gravity losses, i.e. the vehicle has to be configured to provide the ideal velocity,

$$\Delta V_{\text{ideal}} = \Delta V_{\text{req}} + \Delta V_{\text{drag}} + \Delta V_{\text{gravity}} \quad (4.19)$$

Now, the velocity losses are

$$\Delta V_{\text{drag}} = \int_{t_0}^{t_b} \frac{D}{m} dt \quad (4.20)$$

$$\Delta V_{\text{drag}} = \frac{1}{2} \int_{t_0}^{t_b} \left(\frac{\rho V^2 S C_D}{m} \right) dt \quad (4.21)$$

where ρ is density of the atmosphere, V is the vehicle velocity, S is the reference area and C_D is drag coefficient. Assuming the dynamic pressure as $q = (\frac{1}{2})\rho V^2$, then Eq. (4.21) is written as

$$\Delta V_{\text{drag}} = \int_{t_0}^{t_b} \left(\frac{q S C_D}{m} \right) dt \quad (4.22)$$

From Eq. (4.22), it can be concluded that the drag loss is more when dynamic pressure is more, and drag coefficient is large. If the vehicle mass is less (high accelerating vehicle), drag loss is more. Similarly, if the vehicle stays in atmospheric flight for more time, then the drag loss is more. In summary, drag loss depends on the vehicle characteristics and trajectory parameters.

The velocity loss due to gravity is given as

$$\Delta V_{\text{gravity}} = \int_{t_0}^{t_b} g \cos \theta dt \quad (4.23)$$

For the vehicle flying vertically ($\theta = 0$), the gravity loss is maximum (this is always the case for initial trajectory up to crossing atmosphere). After crossing the atmosphere, the vehicle generally flies near horizontal to reduce gravity loss. Also, it can be seen that the gravity loss is function of time. Therefore, to reduce gravity loss, it is essential to reduce the flight duration and also to fly the vehicle near horizontal.

In summary, the gravity and drag losses depend on the vehicle characteristics, burn duration, trajectory parameters, trajectory shape and mode of achieving the launching mission. Generally, the gravity losses vary between 1200 and 2500 m/s whereas the drag losses vary between 100 and 700 m/s.

4.4 Achieving Satellite Orbital Elements by STS

The space transportation system carries a specified satellite and follows an optimum trajectory. Finally, the vehicle reaches the position and velocity vectors required to achieve the specified orbit in space, and the satellite is separated from the vehicle by a suitable separation mechanism as shown in Fig. 4.3. The position and velocity vectors at the time of satellite separation are referred as satellite injection parameters, and the time of separation is called injection epoch. The injection parameters along with injection epoch together decide the orbital elements.

The position and velocity vectors decide the orbital elements viz., a , e , i and ω , whereas the injection parameters along with the injection epoch decide the orbital elements Ω and θ . Therefore, considering the flight duration of space transportation system (with the expected dispersions on the flight time), the vehicle is launched from the identified launch site at a specified local time with the target of achieving the required position and velocity vectors as specified by injection parameters and injection epoch. Once the required parameters are achieved, the satellite is separated from the vehicle and positioned into the specified orbit.

The orbital elements of the satellite can be expressed in terms of position and velocity vectors at injection as given below:

Let the position and velocity vectors of injection conditions are specified in terms of r_0 , ϕ_0 , λ_0 , V_0 , γ_0 , ψ_0 as shown in Figs. 4.3 and 4.4, where

r_0 = Radial distance from the centre of the Earth

V_0 = Magnitude of velocity

γ_0 = Flight path angle measured from local horizontal

ϕ_0 = Longitude

λ_0 = Latitude

ψ_0 = Velocity azimuth measured from local north

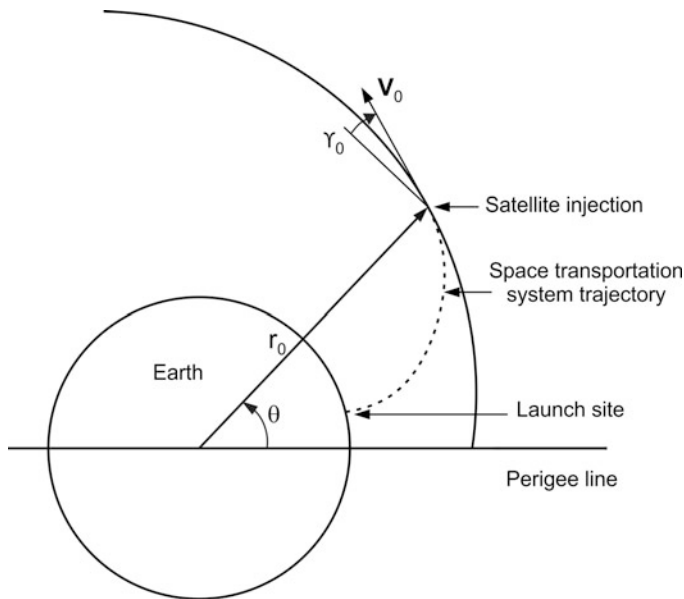
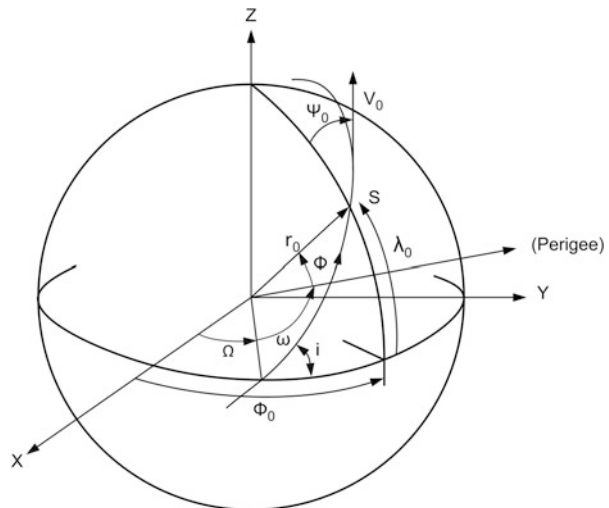


Fig. 4.3 Satellite injection conditions and orbit (r_0, V_0, γ_0)

Fig. 4.4 Satellite injection conditions and orbit (θ, ψ_0, ϕ_0)



Then the orbital elements are given as

$$a = \frac{\mu r_0}{2\mu - V_0^2 r_0} \quad (4.24)$$

$$e^2 = \left(\frac{r_0 V_0^2}{\mu} - 1 \right)^2 \cos^2 \gamma_0 + \sin^2 \gamma_0 \quad (4.25)$$

$$\tan \theta = \frac{(r_0 V_0^2 / \mu) \sin \gamma_0 \cos \gamma_0}{(r_0 V_0^2 / \mu) \cos^2 \gamma_0 - 1} \quad (4.26)$$

From the spherical triangles as given in Fig. 4.4, the remaining orbital parameters can be computed as given below:

$$i = \cos^{-1}(\cos \lambda_0 \sin \lambda_0) \quad (4.27)$$

$$\Omega = \phi_0 - \tan^{-1} \left[\frac{\tan \lambda_0 \cos i}{\cos \psi_0} \right] \quad (4.28)$$

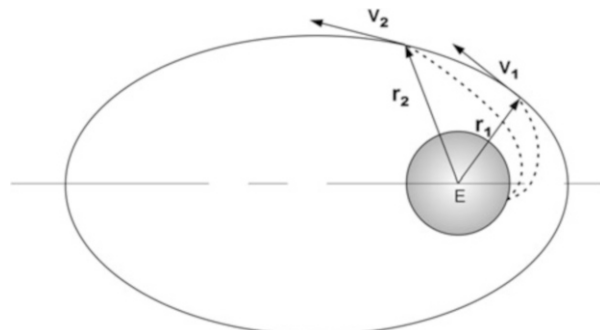
$$\omega = \tan^{-1} \left[\frac{\tan \lambda_0}{\cos \psi_0} \right] - \theta \quad (4.29)$$

Depending on the space transportation system capability and flight duration, the injection can be at any point on the orbital track as given in Fig. 4.5 to achieve the specified orbital conditions.

Assuming that from launch site, the vehicle travels in a planar trajectory defined by the launch azimuth (optimum energy utilization of the STS to achieve the specified orbit), the orbital elements are decided by: (1) energy provided by the vehicle; (2) how the energy is utilized to achieve the orbital elements, accounting for loss of energy due to various factors like gravity, drag etc.; (3) launch site location; (4) launch azimuth; (5) local time at launch site at the instant of launch and (6) flight duration. Time of launch is not a parameter for vehicle and subsystem design. Launch vehicle capability requirement to launch a specified satellite into the specified orbit is already discussed earlier.

The launch azimuth selection, launch site location and methods of utilizing energy have major impact on the vehicle sizing and STS configuration selection in terms of additional requirements on the vehicle energy.

Fig. 4.5 Same orbital elements with different injection conditions



4.5 Selection of Launch Azimuth and Ascent Trajectories

After vertical rise to clear the launch support structure, the vehicle tilts in an inertially fixed plane. The orientation of this plane with respect to local north at launch site is called launch azimuth. Optimum path to achieve the mission always lies on this plane till the satellite is injected, travelling through minimum energy trajectory. Once the vehicle is tilted after lift-off, the vehicle travels in the same azimuth plane till achieving the mission. The vehicle velocity and position vector at any point during its travel through the space always lies in this plane. This type of vehicle trajectory is called planar ascent.

In the planar ascent, the velocity vector always lies in the launch azimuth plane. Therefore, the velocity azimuth at the time of injection would be nearly equal to the launch azimuth except the contributions due to the vehicle's down range motion in the direction of the launch. The inclination of the orbit achieved by planar ascent is determined to a large extent by Eq. (4.27) by suitable substitution of launch point coordinates and launch azimuths as given below:

$$\cos i = \cos \lambda_L \sin A_{ZL} \quad (4.30)$$

where

i = Orbital inclination

λ_L = Geocentric latitude of launch site

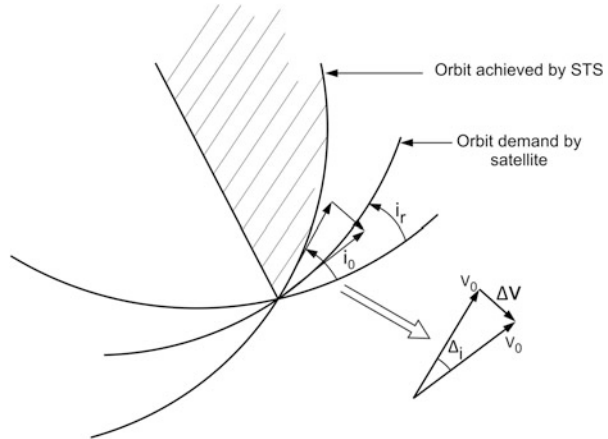
A_{ZL} = Launch azimuth

The important conclusion by using Eq. (4.30) is that in order to achieve minimum energy trajectory or to get the best performance of a STS from a specified launch site in terms of carrying maximum satellite mass, the optimum launch azimuth is

$$A_{ZL} = \sin^{-1} \left[\frac{\cos i}{\cos \lambda_L} \right] \quad (4.31)$$

During ascent phase, the spent parts of the vehicle are separated from the vehicle, which fall on to the ground along the ground track of the vehicle on the surface of Earth. For a typical launch vehicle mission, this ground track extends up to 8000 km whereas for the cases of separation at higher velocity, the impact point of the spent stage can be as large as 20,000 km with respect to the launch site along the direction of ground track. That means, once launch site is fixed, the launch azimuth should be selected such that along the track, there should not be any land mass which is populated. If there is any land mass, then planned impact point of the separated stage should be in the ocean as per the approved international range safety norms. Therefore, for a defined launch site, there is always a launch azimuth bound within which the launch ascent is allowed. In case the satellite orbital mission demands launch azimuth beyond the allowable bounds, the launch azimuth is generally fixed

Fig. 4.6 Orbital inclination correction maneuver by satellite



at the maximum allowable boundary and the mission is managed in the following ways.

The planar ascent trajectory mission of STS achieves the required orbital conditions except the inclination. The ascent mission ends up with the maximum (or minimum as per requirements) orbital inclination possible, which is decided by the allowable launch azimuth. The exact orbital inclination demand of the mission is achieved by the satellite propulsive system as given in Fig. 4.6. The inclination correction required by the satellite propulsion system demands extra fuel as given below:

$$\Delta V = \sqrt{2V_0^2(1 - \cos \Delta i)} \quad (4.32)$$

where

V_0 = Orbital velocity

$$\Delta i = i_r - i_0$$

i_0 = Orbital inclination as achieved by the launch vehicle

i_r = Orbital inclination as demanded by the satellite

The extra fuel required in the satellite to achieve the above ΔV is given by Eq. (4.11)

$$m_p = m_0 \left[1 - e^{-\frac{\Delta V}{V_e}} \right] \quad (4.33)$$

Therefore, this type of mission management is feasible only if the propulsion system requirement ΔV for correcting such inclination is minimal. That means Δi has to be minimum. Typically, for low Earth orbit missions around Earth, $V_0 \cong 7.4$ km/s and

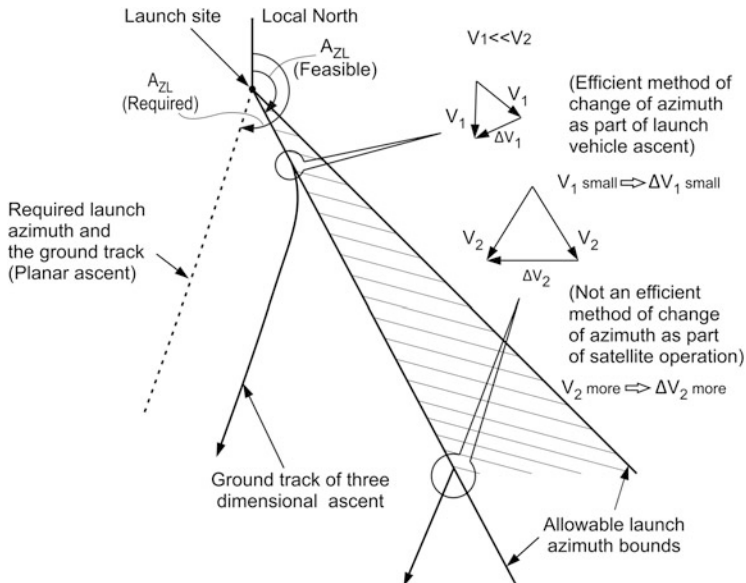


Fig. 4.7 Three dimensional ascent strategies

in order to correct the inclination by 10° , the required velocity, ΔV to be applied in suitable direction is computed as 1.3 km/s, which is a large value to be corrected by the satellite.

From Eq. (4.32), it can be seen that ΔV is less when V_0 is less. Thus, it is advisable to correct for the inclination when the vehicle velocity is less. This approach leads to the concept of three-dimensional trajectory ascent for the launch vehicle missions as explained below.

In the case of allowable launch azimuth severely restricting the required inclination as demanded by satellite orbit, the effective payload that can be launched by a specified STS into the orbit is less. In order to maximize the payload mass under such scenarios, the best strategy is to follow three-dimensional trajectory ascent. In such cases, unlike the mission management through planar ascent as given above, the ΔV required to correct velocity azimuth (which in turn change the inclination) can be given at an early phase of STS flight wherein the velocity is not picked up to the orbital value, thereby reducing the velocity loss. The vehicle can be maneuvered during its ascent trajectory (at suitable instant) as soon as the restriction on the range safety is over, which in turn introduces ΔV continuously which finally results into azimuth change as per the requirement of the satellite. In this case, the resulting trajectory becomes a three-dimensional one as shown in Fig. 4.7.

4.6 Selection of Launch Site

Selection of launch site is crucial for achieving best performance of a STS with reference to the constraints on the launch azimuth as explained earlier. As seen by Eq. (4.30), to achieve orbital mission with zero inclination in optimum fashion, the launch site has to be located over the equator (latitude, $\lambda_L = 0$) and launch azimuth, A_{ZL} has to be necessarily 90° . If the launch site is away from the equator, the minimum orbital inclination that can be achieved is equal to the latitude of the site even for the launch azimuth of 90° . For other launch azimuths, the orbital inclination further increases. Similarly, for polar missions or Sun synchronous orbital missions, which demand orbital inclination more than 90° , the launch azimuth has to be more than 180° . Any deviation with respect to the above conditions lead to the loss of performance from the vehicle as it demands three-dimensional trajectory to reach the mission defined orbital conditions.

The important factor for selecting the launch site is the utilization of the Earth rotation to the benefits of STS. Due to the rotations of Earth, linear velocity towards east at the launch site, as explained in Fig. 4.8, is given as

$$V_L = \omega_e r_{SL} \cos \lambda_L \quad (4.34)$$

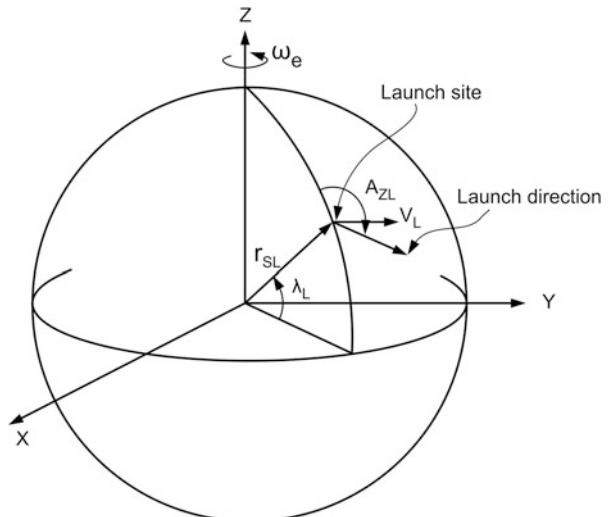
where

ω_e = Earth rotation rate about its axis

r_{SL} = Radius of Earth at launch site

λ_L = Geocentric latitude of launch site

Fig. 4.8 Velocity at launch site due to Earth rotation



This eastward velocity, V_L at the location of launch site has the component along the launch azimuth direction as given by

$$V_0 = \omega_e r_{SL} \cos \lambda_L \sin A_{zL} \quad (4.35)$$

V_0 is the initial velocity of the vehicle in the defined launch plane with respect to the inertial reference. The orbital plane and orbital parameters are referred with respect to the inertial reference frame, and therefore, to achieve the required orbital injection conditions, the space transportation system needs to impart the velocity less by V_0 . For the launch site located in the east coast on the equator and for the launch azimuth of 90° , vehicle has a fairly large initial velocity of 465 m/s. Therefore, to utilise this velocity, launch sites are to be located preferably in the east coast.

4.7 Optimum Strategies to Achieve the Satellite Injection

As explained in the previous sections, to carry a specified payload mass to the mission defined orbit, STS has to be designed to provide the ideal velocity defined by

$$\Delta V_{\text{vehicle}} = \Delta V_{\text{requirement}} + \Delta V_{\text{gravity}} + \Delta V_{\text{drag}} + \Delta V_{\text{yaw}} \pm \Delta V_{\text{Earth}} \quad (4.36)$$

where

$\Delta V_{\text{requirement}}$ = Equivalent velocity to achieve the defined orbital energy

$\Delta V_{\text{gravity}}$ = Velocity loss due to gravity during the trajectory of the vehicle. This depends on the vehicle attitude history and thrusting duration of the vehicle

ΔV_{drag} = Velocity loss due to drag. This depends on the dynamic pressure, aerodynamic characteristics of the vehicle and atmospheric flight duration

ΔV_{yaw} = Velocity loss due to the out of plane motion of the vehicle with respect to the launch plane (three dimensional trajectory)

ΔV_{Earth} = Velocity along launch direction due to Earth rotation. Velocity gain for the eastward launches (represented as $-$ sign in Eq. 4.36). Velocity loss for the westward launches (represented as $+$ sign in Eq. 4.36)

Consider the specific mechanical energy of the orbit defined by,

$$\xi = \frac{V^2}{2} - \frac{\mu}{r} \quad (4.37)$$

where $\left(\frac{v^2}{2}\right)$ is the specific kinetic energy and $(-\mu/r)$ is the specific potential energy. The total energy of the satellite in the specified orbit is

Table 4.1 Specific energies

Orbit	Specific energy (MJ/kg)		
	Kinetic energy	Potential energy	Total energy
500 km circular	28.97	-57.95	-28.98
36,000 km circular	4.70	-9.40	-4.7
Elliptic orbit	52.45	-60.60	-8.15
Perigee = 200 km			
Apogee = 36,000 km			

$$\epsilon = m_s \xi \quad (4.38)$$

where m_s is satellite mass. The following Table 4.1 gives the comparison of typical specific energies of three different orbits: For lower orbit, the specific orbital energy is less than that of higher orbit. Therefore, to launch a specified satellite mass into a lower orbit, a smaller vehicle is sufficient compared to the vehicle to launch the same mass in a higher orbit.

Once the vehicle is designed with a specified payload mass, then the achieved equivalent velocity of the vehicle is given by,

$$\Delta V_{\text{achieved}} = \Delta V_{\text{vehicle}} + \Delta V_{\text{Earth}} - \Delta V_{\text{gravity}} - \Delta V_{\text{drag}} - \Delta V_{\text{yaw}} \quad (4.39)$$

If the orbit size requirement is less than the one for which the vehicle is designed for, then the $\Delta V_{\text{achieved}}$ is more than the $\Delta V_{\text{required}}$. In this case, $\Delta V_{\text{vehicle}}$ can be decreased by increasing the satellite mass, thereby the $\Delta V_{\text{achieved}}$ is equivalent to $\Delta V_{\text{required}}$. Thus the satellite mass is increased. Similarly for the case of higher orbit compared to the designed orbit, the satellite mass has to be decreased.

4.7.1 Direct Ascent

The velocity loss term due to gravity given in Eq. (4.39) plays a major role in the direct ascent trajectories to orbit. In these cases, the types of ascent trajectories to improve the STS performance are to be selected judiciously.

Consider a vehicle used for two orbital missions as shown in Fig. 4.9. To achieve higher orbital mission, the trajectory has to be steep as shown in Fig. 4.9. The steeper trajectory demands the vehicle attitude more closer to vertical, which in turn increases the velocity loss due to gravity. Therefore, as per Eq. (4.39), $\Delta V_{\text{achieved}}$ is reduced. To compensate this loss, the satellite mass has to be reduced to increase the $\Delta V_{\text{vehicle}}$ thus meeting $\Delta V_{\text{required}}$. Thus the net loss in satellite mass is due to (a) steeper trajectory and (b) high energy requirement for higher orbit.

Even for the same orbit as shown in Fig. 4.10, the steeper trajectory results into the increase of velocity loss due to gravity thereby reducing the payload carrying capability. Therefore to overcome this problem in both elliptic orbit missions or

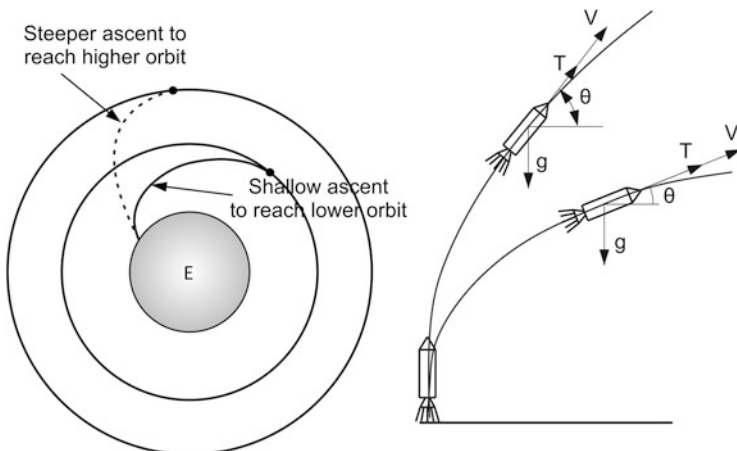
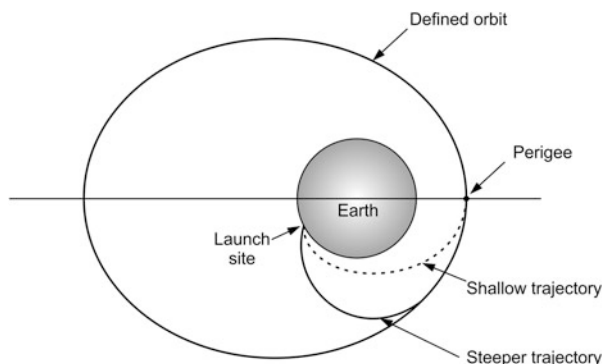


Fig. 4.9 Shallow and steeper ascent

Fig. 4.10 Steep and shallow trajectories for the same orbital mission

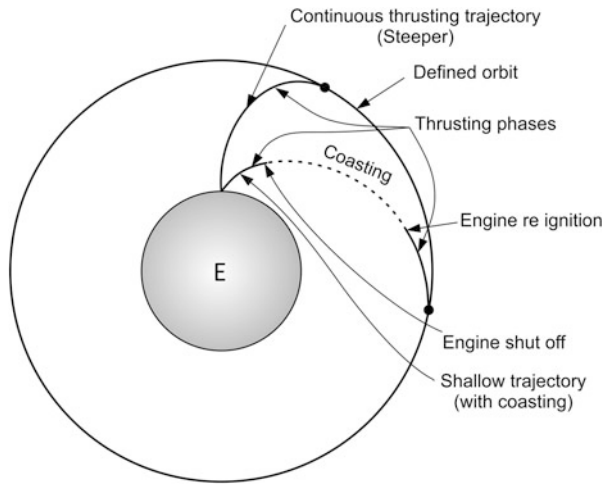


geo-transfer orbit (GTO) mission, the vehicle has to target the injection of the satellite at the perigee, which is the lowest point on the orbit. This ensures the maximum possible shallow trajectory for the mission, increasing the payload carrying capability of STS.

For a defined orbit, by minimizing the velocity loss due to gravity, the performance of STS can be improved. For direct ascent to relatively higher orbit, another strategy can be adopted to minimize the velocity loss.

Initially the vehicle follows relatively shallow trajectory to reduce the velocity loss. After certain time, the thrust of the engine is shut down thus making the vehicle to follow free fall trajectory (coasting). At the instant of shut down, vehicle has certain energy which consists of kinetic energy and potential energy. During coasting, only gravity field is acting on the vehicle and hence the kinetic energy is reduced. As the gravity force field is conservative, the energy during coasting is

Fig. 4.11 Direct ascent with coasting



constant, and therefore, the reduction in kinetic energy is reflected as increase in potential energy, which follows the relation

$$\frac{V^2}{2} - \frac{\mu}{r} = \frac{V_0^2}{2} - \frac{\mu}{r_0} \quad (4.40)$$

where V_0 , r_0 are velocity and radial distance of the vehicle at the start of the coasting respectively. V and r are the corresponding values at the end of coasting. $V < V_0$ and $r > r_0$. Once the required radial distance is reached during coasting, the rocket engine is reignited to follow another phase of very low velocity loss due to gravity trajectory segment to achieve the required orbital conditions as shown in Fig. 4.11. Even though there is loss of velocity during coasting phase, the velocity loss due to gravity during the entire mission is considerably lower, thus improving the vehicle performance.

The commencement of coasting time is very important for these types of direct ascent. Consider the specific energy at any point of the ascent trajectory,

$$\epsilon = \frac{V^2}{2} - \frac{\mu}{r} \quad (4.41)$$

Using Eq. (4.41), during coasting phase, the increase in radial distance is related to reduction in velocity as given below

$$\Delta r = -\left(\frac{r^2}{\mu}\right)V\Delta V \quad (4.42)$$

From the above equation, it can be seen that for higher initial velocity, although there is a velocity loss during coasting phase, the increase in radial distance is more.

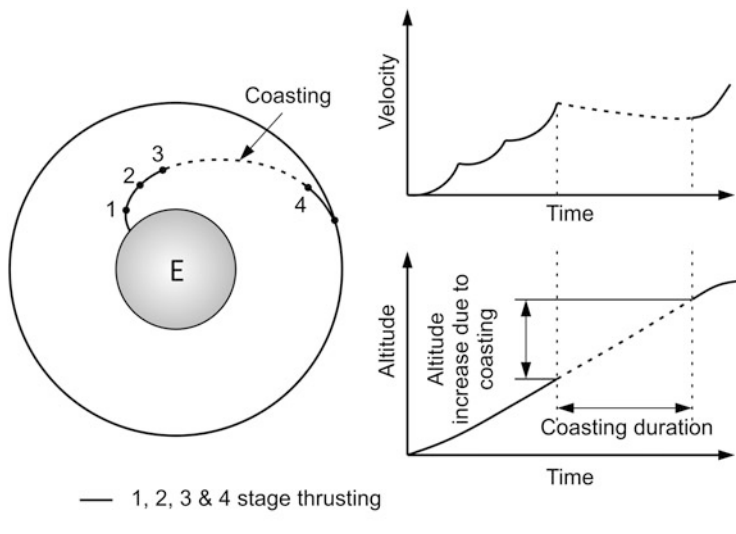


Fig. 4.12 Coasting to increase altitude during ascent

To obtain the same increase in radial distance at the lower velocity of the vehicle, the corresponding velocity loss is large, thus reducing the overall performance. Therefore, for a defined STS mission, the initiation of coasting time and coasting duration have to be judiciously selected.

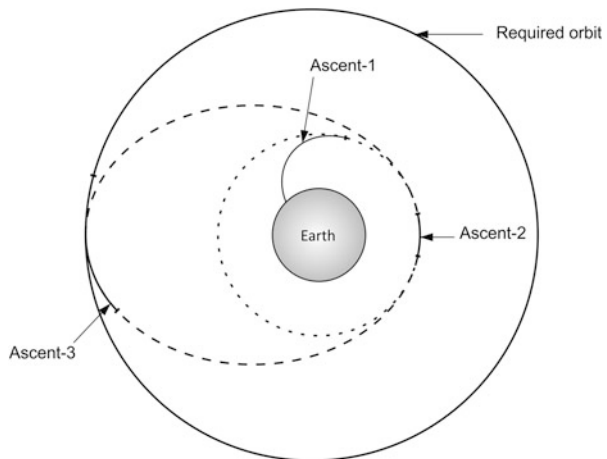
In missions with multiple stages, to meet the above requirement, the coasting is introduced between the final stage and penultimate stage as shown in Fig. 4.12.

4.7.2 Hohmann Transfer Ascent

In the direct ascent mode, there is always additional velocity loss due to gravity. For the case of direct ascent with coasting, the state at the beginning of coast phase generally results into suborbital conditions. In case the re-ignition does not happen as planned, the final mission ends up with suborbital flight. To avoid such problems and to minimize the velocity loss to the lowest extent, Hohmann transfer ascent trajectory is preferred.

In Hohmann transfer ascent, initially, the vehicle achieves a specified orbital condition below that of final orbit required by the satellite called parking orbit. Generally, parking orbital conditions are planned at a low altitude wherever atmospheric effects are less and orbit height is of the order of 180–200 km. Subsequently, propulsive impulses are given at appropriate locations as given in the Fig. 4.13 to achieve the required orbit.

Fig. 4.13 Hohmann transfer ascent



The main advantage of this mode of ascent is that the vehicle follows shallow trajectory segments for the entire mission duration, the loss is considerably less and this is a minimum energy ascent. Therefore the payload injected into the final orbit is maximum, and this is the most efficient way of launching satellites into any orbit. Since the initial portion of the ascent is very shallow to achieve specifically low altitude orbit, the velocity loss due to gravity is the minimum in the Hohmann transfer ascent whereas the propulsive stages operate horizontally in the subsequent phases as given in Fig. 4.13 causing zero gravity loss. Therefore, ultimately, this mode reduces the velocity loss to the barest minimum, resulting into high performance of the vehicle.

Even for the low orbit mission, considering the initial orbit at near zero altitude, theoretically providing all propulsive energy as impulse, can make the ascent an efficient one. However, due to the presence of atmosphere, a low safe parking orbit above the atmosphere is essential. The negative aspect is that it requires at least one more propulsive stage in the vehicle or a stage with multi-start capability which reduces the reliability of space transportation system. Also, long duration mission of this type introduces large errors due to navigation system which reflects as the errors on the achieved orbit. However, for very high altitude missions, the Hohmann transfer ascent mode is the only approach to achieve feasible mission and the propulsive system of the vehicle must have restart capability. Alternatively suitable propulsive system has to be made as part of satellite and after completion of launch vehicle mission with the parking orbit, the satellite propulsive system has to transfer the satellite from the parking orbit to the final required orbit. Under such cases, the STS subsystems have to be designed suitably to meet the requirements while maintain the required reliability.

4.8 Trade-Off Studies and Integrated Mission Aspects

For each orbital mission, an optimum STS configuration and design demand a specific launch site along with a specific launch azimuth. Once the desired launch site location and launch azimuth are available, optimum STS design can be achieved (minimum size vehicle) to launch the required satellite mass into the specified orbit. Generally, optimum launch site and launch azimuth are not feasible as launch site is decided by geographical constraints, and launch azimuth is decided by range safety constraints. These parameters are having impact on the STS size and configuration design. To meet the specific requirement of the optimum launch site and azimuth, the satellite mass of the vehicle already designed has to be reduced or to meet the satellite mass requirements, the size of STS has to be increased.

Similarly, the demands for STS are to launch satellites of different masses to various orbits ranging from low Earth orbit to higher altitude orbits and the requirements extend to interplanetary missions also. The performance of a designed STS for these orbits depends on the velocity loss due to gravity defined by the ascent trajectory requirements. The performance is maximum for shallow trajectories but for higher orbits, due to the steep nature of ascent trajectories, there is heavy loss in vehicle performance. That means the satellite mass to be launched is reduced considerably.

Once the satellite is separated from the STS, the satellite propulsion system can be effectively utilized to transfer the satellite from the intermediate orbit, achieved by the vehicle to the final required orbit. But this option needs extra propulsion system and propellant mass in the satellite. Therefore, to follow this strategy, effectively the mass to be lifted by STS to the intermediate orbit is increased and accordingly it has implication on the STS sizing and design.

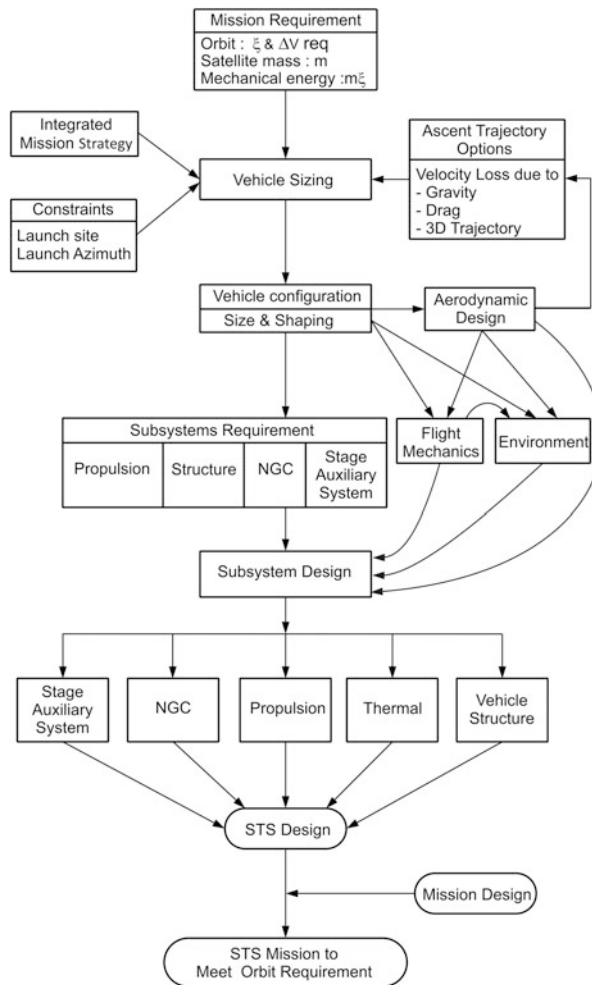
Therefore, it is essential to carry out the trade-off studies between the two strategies in the initial stage of the STS design process. The choice has to be between these options, and the option which gives higher effective satellite mass has to be selected for the STS configuration design.

4.9 Vehicle Subsystem and Design Requirement

The functional requirements for STS design have to start with the orbital mission requirements and the satellite mass to be placed in the specified orbit. The step by step procedure starting from mission design to STS design process, which satisfies the overall functional requirements, is summarized in Fig. 4.14.

Various inputs needed for sizing the vehicle, meeting the above requirements are: (1) launch site and launch azimuth constraints, (2) various trajectory options, (3) velocity losses due to various factors and (4) trade-off options between STS and satellite propulsion options. In addition, the aerodynamic shaping which generates

Fig. 4.14 Subsystems and STS design requirements



low disturbances and drag are also to be studied. This process finally leads with vehicle configuration.

The next step is to specify the vehicle subsystems requirements, which are (1) optimum propulsion parameters to achieve the required ΔV_{req} ; (2) optimum structural parameters and structural options to minimize the structural mass, ensuring the load carrying capability; (3) navigation, guidance and control (NGC) systems parameters which predict the vehicle state in real time and steer the vehicle to the target as defined by mission requirements; and (4) stage auxiliary systems to carry out the staging functions during flight.

The major inputs for the subsystem design process are derived from the operating environment as well as from the flight mechanics. Suitable thermal protection systems have to be designed to ensure normal thermal environment for the vehicle

subsystems. Subsequent step is the mission design which can achieve the satellite orbital requirements. This integrated design process has to ultimately lead to launch vehicle configuration and design which meet the overall functional requirements.

4.10 Satellite Orbit Deviations Due to Space Transportation Systems Errors

Achieving the exact satellite injection conditions from the space transportation system is quite difficult and has to account several sources of errors like navigational errors, errors due to the vehicle internal systems imperfections, performance deviations and external disturbances. The disturbance caused during atmospheric flight phase is the main source for external disturbances. The vehicle internal disturbances are caused by the fabrication imperfections of the launch vehicle, dynamics of vehicle subsystems and system performance deviations with respect to the predicted ones. The fabrication imperfections cause the deviation of the thrust away from the vehicle centre line as well as shifting the vehicle centre of gravity from the predicted location. In the process of stabilizing the vehicle against such disturbances, the vehicle thrust direction deviates from the launch azimuthal plane, thus causing the trajectory deviation from the predicted one. The performance deviation of propulsion system during flight with respect to the nominal mission is the main source of internal disturbance for the deviation of the planned trajectory. In addition, the dynamic disturbance created by propellant sloshing in the tanks is another source of disturbance. The cumulative disturbances of various subsystems thus contribute to the deviations in the ascent trajectory.

Normally, the navigation system predicts the deviated trajectory due to these disturbances and the guidance system corrects the trajectory in real time to follow the nominal defined trajectory. If the propulsive stages cumulatively fail to provide the needed impulse to the vehicle due to underperformance, the final injection end conditions are not achieved. To ensure this, the final propulsive stage of the vehicle is normally provided with extra propellant and is termed as guidance margin. The guidance system utilizes this extra fuel to achieve the final targeted injection parameters.

It may be seen that the error in predicting the trajectory by navigation system remains as the deviation from the nominally targeted one and that reflects as error in the final achieved satellite orbital parameters. The navigation computations are based on the accelerometers and rate gyros measurements and any errors in these sensors reflect in the launch vehicle injection parameters dispersions. Once the final stage is commanded to shut-off after reaching the targeted orbital parameters, the valves of the propulsive stage take additional time due to valve delays to close completely which introduces a tail-off thrust profile. Normally a nominal tail-off thrust profile is accounted for fixing the target for the guidance system and any deviation from the nominal profile causes dispersions in the injection parameters.

These injection errors are generally small but due to the high velocities, they can introduce large deviations in the final orbital parameters. Since the errors are small, the deviations in the injection parameters can be obtained by applying Taylor's series expansion, after neglecting higher order terms as given below:

$$\delta\Sigma = \frac{\partial\Sigma}{\partial r}\delta r + \frac{\partial\Sigma}{\partial V}\delta V + \frac{\partial\Sigma}{\partial \gamma}\delta\gamma + \frac{\partial\Sigma}{\partial\phi}\delta\phi + \frac{\partial\Sigma}{\partial\lambda}\delta\lambda + \frac{\partial\Sigma}{\partial\psi}\delta\psi \quad (4.43)$$

where

Σ : Particular orbital parameter

$\delta\Sigma$: Change in orbital parameter with respect to the target value

$r, V, \gamma, \phi, \lambda, \psi$: Nominal injection radial distance, velocity, flight path angle, longitude, latitude and velocity azimuth respectively

$\delta r, \delta V, \delta\gamma, \delta\phi, \delta\lambda, \delta\psi$: Changes in the injection conditions with respect to nominal values

Let $r_i, V_i, \gamma_i, \phi_i, \lambda_i, \psi_i$ are the nominal injection parameters and $\delta r, \delta V, \delta\gamma, \delta\phi, \delta\lambda, \delta\psi$ are the deviations in the injection parameters. Similarly, $a, e, i, \Omega, \omega, \theta$ are the nominal orbital parameters corresponding to nominal injection parameters. The deviations in the orbital parameters due to deviations in injection parameters are given by:

$$\delta a = \left(\frac{2a^2}{r_i^2} \right) \delta r + \left(\frac{2a^2 V_i}{\mu} \right) \delta V \quad (4.44)$$

$$\begin{aligned} \delta e = & \left[\frac{V_i^2 r_i \cos^2 \gamma_i}{\mu e a} (a - r_i) \right] \delta r + \left[\frac{2r_i V_i \cos^2 \gamma_i}{\mu e a} (a - r_i) \right] \delta V \\ & + \left[\frac{r_i^2 V_i^2 \sin 2\gamma_i}{2\mu e a} \right] \delta \gamma \end{aligned} \quad (4.45)$$

$$\delta i = \left(\frac{\sin \lambda_i \sin \psi_i}{\sin i} \right) \delta \lambda_i - \left(\frac{\cos \lambda_i \cos \psi_i}{\sin i} \right) \delta \psi_i \quad (4.46)$$

$$\delta \omega = \left[\frac{\frac{r_i V_i^2}{\mu}}{\left(\frac{r_i V_i^2}{\mu} - 1 \right)} \right] \delta \gamma_i + \left(\frac{\cos \psi_i}{\sin^2 i} \right) \delta \lambda_i + \left[\frac{\sin 2\lambda_i \sin \psi_i}{2 \sin^2 i} \right] \delta \psi_i \quad (4.47)$$

$$\delta \Omega = \delta \phi - \left(\frac{\cos \lambda_i \sin 2\psi_i}{2 \sin^2 i} \right) \delta \lambda_i - \left(\frac{\sin \lambda_i}{\sin^2 i} \right) \delta \psi_i \quad (4.48)$$

$$\begin{aligned} \delta \theta = & - \left[\frac{\sin \theta (1 + e \cos \theta)}{ae(1 - e^2)} \right] \delta r - \frac{2 \sin \theta}{e} \left[\frac{a(1 - e^2)}{\mu(1 + 2e \cos \theta + e^2)} \right]^{\frac{1}{2}} \delta V \\ & + \left[2 + \frac{(1 - e^2)}{e} \cdot \frac{\cos \theta}{1 + e \cos \theta} \right] \delta \gamma \end{aligned} \quad (4.49)$$

The above expressions are valid for the non-zero eccentric orbits.

4.11 Mission Definition for STS

The orbital errors as shown in Eqs. (4.44, 4.45, 4.46, 4.47, 4.48, and 4.49) caused by the STS subsystems have to be corrected by the satellite propulsion system. This essentially demands an apportionment of satellite fuel for correcting orbital deviations, which in turn reduces the life time of the satellite or the mass of the effective application payload. Alternatively, the accuracy of the vehicle orbit can be improved, if the performance requirements of the vehicle subsystems are made very stringent which results into expensive technology development and increased development time. Therefore, trade-off studies are required to decide on (a) the design and development strategy for vehicle subsystems, (b) the extra fuel required in the satellite and c) the allowable orbital errors. The orbital errors so decided are used as the specification for the design of vehicle subsystems.

Another important factor is specifying the right orbital elements for the STS subsystem design. The vehicle during its ascent mission achieves the specified position and velocity vectors. As explained in Chap. 3, the orbital elements computed by the position and velocity vectors at an instant are osculating orbital elements. Generally, the satellite mission specifies mean orbital elements due to its non-varying nature. The osculating elements depend on the location of injection, i.e., for the same position and velocity vectors, depending on the geographical location in terms of geodetic latitude and longitude, the osculating orbital elements vary. Therefore, once the trajectory of STS, the possible injection location and position and velocity vectors are decided, the required osculating orbital elements to achieve the specified mean orbital elements are utilized as the specification for STS mission. A typical mission specification for STS is given below:

Launch site: (ϕ_L, λ_L)

Launch azimuth: Az_L

Osculating orbital elements:

$$\left. \begin{array}{l} h_p : h_{pn} \pm \Delta h_p \\ h_a : h_{an} \pm \Delta h_a \\ i : i_n \pm \Delta i \\ \omega : \omega_n \pm \Delta \omega \end{array} \right\} \quad \text{or} \quad \left\{ \begin{array}{l} a = a_n \pm \Delta a \\ e = e_n \pm \Delta e \\ i = i_n \pm \Delta i \\ \omega = \omega_n \pm \Delta \omega \end{array} \right.$$

where

ϕ_L, λ_L : Geodetic latitude and longitude of launch site

Az_L : Launch azimuth

h_p, h_a : Perigee and apogee altitudes

i : Inclination

ω : Argument of perigee

a, e : Semi-major axis and eccentricity

$$\left. \begin{array}{l} h_p, h_a, i_n, \omega_n, a_n, e_n \\ \Delta h_{pn}, \Delta h_{an}, \Delta i_n, \Delta \omega_n, \Delta a_n, \Delta e_n \end{array} \right\} : \begin{array}{l} \text{Corresponding nominal values} \\ \text{Allowable } 3\sigma \text{ errors (in Normal distribution) in the nominal parameters} \end{array}$$

It is to be noted that generally Ω and θ are not specified. The required values for these parameters are achieved by selecting launch day and launch time. The launch time is corrected to the selected launch day, considering the required flight duration to injection of the satellite.

The above mission specifications are generally used as inputs for the subsystems design. The design process indicated in Sect. 4.9 and Fig. 4.14 are further explained in detail in the subsequent chapters of this book.

Bibliography

1. Bong vie: Space Vehicle Dynamics and Control. AIAA Education Series, Reston (2008)
2. Cornelisse, J.W., Schoy, H.F.R., Wakker, K.F.: Rocket Propulsion and Spaceflight Dynamics. Pitman Publishing Ltd, London (1979)
3. Curtis, H.D.: Orbital Mechanics for Engineering Students. Elsevier, Oxford (2005)
4. Brown, C.D.: Spacecraft Mission Design. AIAA Education Series. AIAA, Reston (1998)
5. Pocha, J.J.: An Introduction to Mission Design for Geostatinary Satellites. D. Ridel publishing Company, Boston (1987)
6. Thomson, W.T.: Introduction to Space Dynamics. Dover Publications, New York (1986)
7. Wiesel, W.E.: Spaceflight Dynamics. McGraw-Hill, New York (1989), Second edition 1997

Chapter 5

Space Transportation System Configuration, Staging and Performance

Abstract In all space missions, the main objective during the design phase is to define a suitable STS configuration which has the needed capability to inject the defined spacecraft into the specified orbit. To achieve these objectives, STS is configured with suitable propulsion systems to impart the required equivalent velocity to the satellite, after accounting for the various velocity losses the vehicle encounters during its mission. This chapter discusses the STS configuration, selection criteria to provide the required energy to inject the satellite into the orbit, while meeting the various other subsystems requirements. The optimum STS configuration has to provide the maximum performance with respect to the vehicle size, maximum reliability, reduced unit cost for the vehicle, minimum cost for design and development and a reasonable schedule for the realization of the vehicle. To arrive at an optimum vehicle sizing and configuration, exhaustive trade-off studies are required. The studies have to address existing technologies and advanced new technologies with respect to performance improvements, performance requirements, demonstrations, process technologies, advanced technology developments, overall vehicle reliability, unit cost of the vehicle, technology risks, increased development cost and schedule, limitations on the realization of the systems, etc. The selection methodology for STS configuration, design guidelines and the various processes involved in the design of an optimum configuration are discussed in this chapter. Design strategies for various vehicle subsystems which influence the vehicle performance and the vehicle configuration are highlighted. The constraints imposed by the existing technology limitations and the possible future technology improvements are explained. The requirements of multi-staging and their relative merits and demerits are highlighted. The optimum staging aspects, the design sensitivities and various factors which influence the vehicle performance are elaborated. Attention to ground and launch operations while finalising the configuration of the vehicle is of utmost importance because it has large influence on the technology options for the vehicle, schedule and cost. The infrastructure needed for ground operations like launch complex, launch tower, propellant servicing facilities, etc. has to be closely linked to the vehicle configuration. Therefore these aspects are addressed in brief at the end of the chapter.

Keywords Space transportation system configuration • Payload • Mass fraction • Single stage • Multistage • Partial staging • Parallel staging • Piggyback staging • Design trade-offs • Payload fairing and Ground operations

5.1 Introduction

The functional requirement of STS is to provide the necessary energy to the satellite to reach the specified orbital conditions. In order to achieve the above objectives, STS is configured with suitable propulsion systems to impart the required equivalent velocity to the satellite, after accounting for the various velocity losses the vehicle encounters during its mission. The propulsion systems decide the size of the vehicle depending on the type of the propulsion modules chosen and also on the energy required to be generated by the propulsion systems to accomplish the specified satellite mission. This chapter discusses the STS configuration, selection criteria to provide the required energy to inject the satellite into the orbit, while meeting the various other subsystems requirements. The optimum STS configuration is the one which provides the maximum performance with respect to the vehicle size (minimize the vehicle size and mass and maximum payload capability), a configuration which provides maximum reliability, reduced unit cost for the vehicle, minimum cost for design and development and a reasonable schedule for the realization of the vehicle.

To arrive at an optimum vehicle sizing and configuration, it is essential to carry out exhaustive trade-off studies between existing technologies and advanced new technologies with respect to performance improvements, performance requirements, demonstrations, process technologies, advanced technology developments, overall vehicle reliability, unit cost of the vehicle, technology risks, increased development cost and schedule, limitations on the realization of the systems, etc. Based on the trade-off studies, an optimum configuration has to be selected.

This chapter starts with the selection criteria for STS configuration, design guidelines and the various processes involved to arrive at an optimum configuration design. Design strategies for various vehicle subsystems which influence the vehicle performance and in turn decide the vehicle configuration are highlighted. The major parameters influencing the vehicle sizing and the configuration design are analyzed and the typical values of these parameters with the present day technologies are compared. The constraints imposed by the existing technology limitations and the possible future technology improvements are explained. The requirements of multi-staging and their relative merits and demerits are highlighted. The optimum staging aspects and various factors which influence the vehicle performance are elaborated. The design sensitivities, the trade-off needed during the configuration design and the optimum strategies to arrive at the vehicle configuration with the existing technologies are also included.

5.2 STS Configuration Selection Requirements

In all space missions, the main objective during the design phase is to define a suitable STS configuration which possesses the needed capability to inject a spacecraft into the specified orbit. The vehicle also has to meet the following requirements.

- (a) The payload has to be maximised.
- (b) The overall vehicle mass has to be minimised.
- (c) The vehicle should possess very high reliability.
- (d) Aerodynamic configuration of the vehicle has to ensure reduced drag forces as well as reduced vehicle loads.
- (e) The launch cost has to be reduced considerably to achieve the minimum cost per kilogram of payload.
- (f) Has to satisfy all defined constraints.
- (g) Should enable the future growth potential without effecting too many changes in the basic chosen configuration.

In addition, to reduce the overall cost, the following criteria are also to be satisfied:

- (a) Reduce development cost
- (b) Minimise the development schedule

The configuration selection demands detailed evaluation of several options available, the performance capability of each of these options, the available technical expertise, the cost, the overall reliability and the capacity of the chosen configuration to meet the defined goals. The infrastructure needed for ground operations, their complexity, cost and timely realisation of the same are other important considerations.

At the initial stage of configuration selection, it is preferred to study the existing space transportation systems of same class (across the globe), which have the capability for transporting the payloads under consideration and carry out a detailed technical assessment. These data are quite useful in selecting the baseline vehicle. The important metrics are number of stages, serial or parallel staging, gross lift-off mass of the vehicle, the overall height of the vehicle, stage diameters, length to diameter ratio, the booster thrust, the reliability, cost, future growth potential, the needed ground infrastructure and finally the compliance with the mission requirements.

The selection of a launch system demands very systematic procedure to arrive at a best suitable configuration for a given mission. The important steps to be followed in such a selection are as given below.

- (a) Work out the requirements and constraints in detail depending on the mission operations.
- (b) Carry out detailed survey of various vehicles of similar class, available elsewhere and study the merits and demerits of different configurations.

- (c) Conduct the detailed analysis of various possible options to arrive at a baseline configuration.
- (d) Study the spacecraft requirements in terms of mass, volume, mechanical and electrical interfaces, overall environment needed during the launch phase, etc.
- (e) Study the ground infrastructure and facilities needed for launch and assess the possibility of using the existing facilities and requirements for additional facilities.
- (f) Assess the performance capability of the vehicle to meet the mission objectives and also ensure that adequate performance margin is available.
- (g) Carry out iterations to arrive at an optimum configuration meeting the specified requirements in terms of performance, schedule and cost. The risk assessment has to be part of this exercise.

For a baseline vehicle, the configuration selected should be capable of delivering at least thrust to weight ratio of 1.2 at lift-off. The length to diameter (L/D) ratio is important, because the configuration so selected is a feasible vehicle from aerodynamic and structural integrity considerations. Higher the L/D ratio, greater the tendency of the vehicle becoming flexible and from structural and dynamic stability point of view, it can lead to inefficiency, whereas the lower ratio makes the vehicle aerodynamically inefficient. The vehicle configuration has to be carefully decided by proper selection of stages which facilitates the discarding of empty mass of the vehicle at regular intervals.

In all vehicles as the propellant is consumed during the flight, the stage motor or tanks become dead weight which also has to be accelerated. This dead weight demands larger energy to achieve the required velocity. Therefore, multistage rockets offer greater advantage in that stages can be designed to provide best performance in both atmospheric phase for lower stages and in vacuum phase for upper stages. The decision on number of stages, the magnitude of thrust for each stage and total impulse of stage depend largely on the mass of the payload and the mission to be accomplished. Smaller the payload, the vehicle can be configured with less number of stages. The number of stages increases for heavier payload thus making the vehicle heavier. The cost of the vehicle also increases. There are several factors which need to be considered while configuring the stages. For example, booster stage has to provide higher thrust with less importance to mass ratio and efficiency of the nozzle. On the other hand, upper stages are to be configured with smaller engine/s having higher payload mass ratio and increased nozzle efficiency.

The selection also depends on other important factors like technical maturity of propulsive stages, the performance margin, manufacturing capability, overall reliability, safety and cost. The lesser the number of stages, the vehicle attains higher reliability but the propulsive stages become large. The relative advantages and disadvantages of all possible options are to be assessed considering various factors, before arriving at a suitable configuration. The booster stage is generally the lowest stage which provides the needed thrust to lift the vehicle. The thrust values keep on decreasing with each subsequent stage but attempt is to be made to have propulsion systems with higher specific impulse in upper stages.

Based on the factors discussed so far, one has to narrow down to a few options which can satisfy the overall requirements of the baseline vehicle. The existing stages or engines are to be assessed for their suitability, and if they are infeasible, they are taken out of the design space. The performance has to be evaluated with respect to each metrics discussed earlier and the options have to be narrowed down by eliminating infeasible systems which do not meet the specified metrics. Therefore optimum configuration selection for a STS involves several iterations by carrying out detailed design exercises and simulations.

The baseline vehicle definition demands primarily the following:

- (a) Deciding the number of stages
- (b) Generation of geometric dimensions, mass and mass moment of inertia, etc.
- (c) Specifying the burn sequence for various stages to satisfy all defined requirements and constraints
- (d) Detailed studies for evaluating the vehicle performance
- (e) Generation of external vehicle environment and
- (f) Subsystems preliminary requirements.

One need to consider options available for various important subsystems, during the definition of basic configuration such as propulsion, structures, control and sequencing system, separation systems and control power plants for each stage control. It is essential to derive the subsystem requirements from the overall mission definition which defines the top level requirements of the vehicle. This process can be effectively carried out if there is a clear understanding of the subsystem requirements, constraints and interface between subsystems.

1. Propulsion Subsystem

It is the propulsion subsystems which provide the needed power to the vehicle to impart the required velocity to the spacecraft in orbit. Therefore, the state-of-the art technology for propulsion ultimately governs the launch vehicle design and also the overall vehicle configuration. The space vehicles today depend on chemical rockets and therefore the technological maturity of propulsion systems, their characteristics and the performance behaviour play a major role in deciding the launch vehicle configuration. The choice of sequential or parallel staging for the booster depends on the payload mass and selection criteria have to be based on requirements analysis, handling experience and overall risks. A particular stage may be configured with one or more engines but these engines have to be accommodated within the envelope available in the stage. Various aspects of propulsion systems to be considered in configuration selection are discussed in detail in Chap. 9.

2. Structural Subsystem

The mass ratio i.e. the ratio of payload mass and the gross lift-off mass of the vehicle has to be maximised and it is possible to achieve this objective by selecting suitable structural elements for propulsion stages, interstages, payload fairing, etc. The selection of suitable materials, shapes and construction methods plays a vital role during the definition of baseline configuration and hence these aspects are to be

carefully analysed for proper selection. The composite materials provide advantage in minimising the structural mass but the manufacturing process and the infrastructure for manufacturing them are quite complex. The overall shape, load path in the vehicle is other important considerations while defining the vehicle. Details of structures and materials are covered in detail Chap. 11.

3. Separation Subsystem

In multistage vehicles, the stage which has completed its functional requirement has to be separated from the ongoing vehicle to achieve the maximum performance. These separation systems are generally configured using high energy systems and the system has to have very high reliability. The failure of this system leads to total mission failure. There are several schemes for separation systems, and a suitable choice for each of the separation system in the vehicle has to be based on the extensive evaluation of the merits and demerits of all available systems. The use of high energy pyro systems causes severe environmental disturbance to the vehicle systems. All these aspects are to be analysed in detail, and this analysis should be the basis for the selection of a suitable separation system for each stage of the vehicle. The description of various types of separation mechanisms and their selection criteria are presented in detail in Chap. 13.

4. Control and Sequencing Subsystem

A suitable baseline control system configuration needs to be worked out in the initial stage of vehicle definition, since this system has close interaction with several disciplines of the vehicle. Structural dynamics, aerodynamics characteristics, loads on the vehicle, propulsion parameters have large influence on the control system design. Hence the iterations in control design are needed till it meets the requirements and constraints defined for the vehicle. It has additional requirements of meeting the safe lift-off criteria, ensuring the pogo stability, slosh stability and guarantee the clearances needed during the separation process. The vehicle sequencing is closely linked with several design functions of various subsystems. Even to study the basic performance of the vehicle under definition, the baseline sequencing is essential and it also undergoes several iterations to satisfy all the specified conditions for the vehicle. The details of functional requirements of these systems, interactions, constraints and the design philosophy are discussed in detail in Chap. 14.

5. Control Power Plants

The control power plants are essentially the control effectors and play a pivotal role in the success of launch vehicle missions. The sizing of the control effectors, type of the system to be used, the duty cycle and dynamic characteristics of the actuation systems are some of the essential design parameters which have to be decided during the vehicle definition phase. The effectiveness of control power plants has to be assessed carefully so as to overcome the maximum possible disturbances the vehicle encounters during the entire duration of the flight. The rate capability of the actuation system is another essential design function and it has to be decided

in the beginning phase. The interface issues, mass and volume of the system to be selected are to be examined in detail before a decision on a suitable system is arrived. The performance of the actuation system is mission critical and hence the introduction of suitable redundancy in these systems is to be studied in the initial design phase of the vehicle. The cost and complexity of the systems have also to be factored in the selection process. Details on each of these attributes for the control power plants are highlighted in Chap. 14.

5.3 STS Performance

Rocket propulsion systems are required in STS to provide the necessary energy to transport the satellite from the surface of the Earth to the specified orbit. This section gives the selection of necessary propulsion system performance parameters for configuring a STS.

As explained in Chap. 4, the ideal velocity ΔV , imparted by a rocket propulsion system is given by

$$\Delta V = V_e \ln \left(\frac{m_i}{m_f} \right) \quad (5.1)$$

where (m_i/m_f) is called the mass ratio, m_i is the initial mass of the vehicle and m_f is the mass of the vehicle after consuming the propellants. The vehicle sizing process involves the selection of V_e , the exit velocity (which is equal to specific impulse in seconds multiplied by acceleration due to gravity) and the mass ratio such that the ideal velocity, ΔV , given by the propulsion system is equal to the required equivalent velocity to achieve the specified orbit after compensating the various velocity losses during the STS flight phase.

It is to be noted that the STS as represented in Fig. 5.1 is divided into three major components: (1) satellite mass which is the payload of STS, represented as m_{PL} ; (2) propellant mass, m_p , the total usable propellant mass; and (3) structural mass, m_s . The propulsion system consumes the propellant during its operation to generate the necessary thrust, which in turn gives energy to the payload. The structural mass includes all other masses such as motor cases, propellant tanks, engines, nozzles, pumps, NGC systems, thermal protection systems, non-usable propellants trapped in the feed lines and gaseous part of propellant, etc. Therefore,

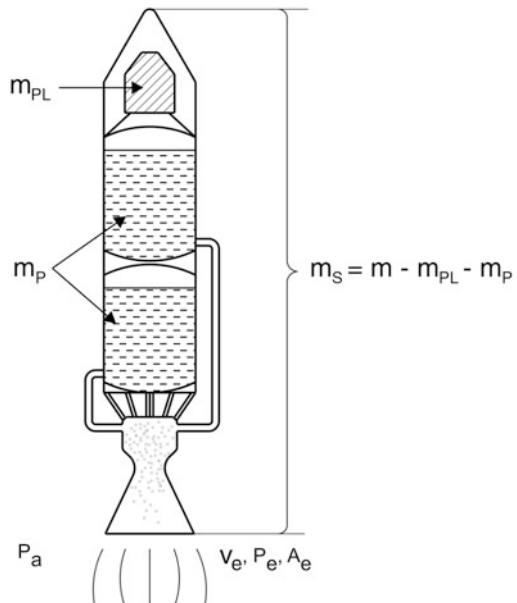
$$m_i = m_p + m_s + m_{PL} \quad (5.2)$$

and

$$m_f = m_s + m_{PL} \quad (5.3)$$

Thus, the STS sizing and configuration design involves the design of m_p , m_s and V_e to achieve the required ΔV for the satellite mass, m_{PL} . In order to decide the above

Fig. 5.1 Basic propulsion parameters



design parameters, it is essential to understand certain important design parameters as explained in the next section.

5.3.1 Performance Parameters

The following are the performance parameters:

1. Propellant mass fraction, $\zeta = \frac{m_p}{m_i}$
2. Payload mass fraction, $\mu = \frac{m_{PL}}{m_i}$
3. Structural mass fraction, $\epsilon = \frac{m_s}{m_i}$

From Eq. (5.2), it can be seen that

$$\frac{m_p}{m_i} + \frac{m_s}{m_i} + \frac{m_{PL}}{m_i} = 1 \quad (5.4)$$

i.e.,

$$\zeta + \epsilon + \mu = 1 \quad (5.5)$$

As the structural mass of the vehicle depends mainly on the type of propulsion system and the loaded propellant mass, it is more appropriate to use another parameter, called structural factor, λ defined as

$$\lambda = \frac{m_s}{m_p + m_s} \quad (5.6)$$

The structural mass factor is expressed in terms of payload mass fraction as given below:

$$\lambda = \frac{m_s}{m_i - m_{PL}} = \frac{(m_s/m_i)}{1 - (m_{PL}/m_i)} \quad (5.7)$$

The structural mass fraction can be derived from Eq. (5.4) as

$$\frac{m_s}{m_i} = 1 - \zeta - \frac{m_{PL}}{m_i} \quad (5.8)$$

Using Eq. (5.8) in Eq. (5.7) yields

$$\frac{m_{PL}}{m_i} = 1 - \frac{\zeta}{1 - \lambda} \quad (5.9)$$

The objective of STS configuration design is to achieve the maximum payload for the defined vehicle or for the defined payload, minimize the initial vehicle mass, i.e. (m_{PL}/m_i) to be maximum. In order to achieve the above objective, from the Eq. (5.9), it can be seen that the structural factor and in turn structural mass has to be low and propellant mass fraction also has to be reduced. In addition, to achieve the required ΔV with the minimum mass for the defined m_{PL} as per Eq. (5.1), V_e has to be increased and m_s has to be reduced. These parameters cannot be arbitrarily selected as they are linked with other subsystems requirements and propulsion system types. Also, the maximum and minimum possible values for these parameters are fixed due to the existing technology limitations. Therefore, trade-off analyses are required for selecting these parameter values as explained in the next sub-section:

5.3.2 Technology Limitations and Trade-Off Analysis

Even though the rocket equation given in Eq. (5.1) is derived based on momentum thrust, the actual thrust imparted by the rocket engine is given by

$$T = \dot{m} V_e + (P_e - P_a) A_e \quad (5.10)$$

where P_e is the exit pressure, P_a is atmospheric pressure and A_e is nozzle exit area as shown in Fig. 5.1.

The term in V_e is known as momentum thrust and the term $(P_e - P_a)A_e$ is known as pressure thrust. As the expansion ratio increases (i.e., A_e/A_t increases, where A_t is throat area of the nozzle), thrust and V_e increase. The maximum thrust occurs

when $P_e = P_a$. During vacuum flight, $P_a \cong 0$, therefore theoretically the nozzle area ratio can be increased to get P_e almost equal to zero, which gives the maximum thrust and V_e . But, the increased expansion ratio of the nozzle leads to increase in structural mass. Therefore, there exists an optimum value for nozzle expansion which gives maximum vehicle performance. Beyond this, the performance reduction due to increased structural mass overrides the benefit of higher V_e .

During atmospheric flight phase, due to the presence of atmospheric pressure, P_a , the nozzle expansion ratio is limited such that P_e almost becomes equal to P_a . Any further increase in expansion ratio leads to over expanded nozzle, wherein $P_e < P_a$, which makes the nozzle flow complicated and hence not used. Therefore, atmospheric flight phase nozzles are generally with lower expansion ratio, which ensures $P_e \geq P_a$. $P_e = P_a$ leads to the correct expansion which gives maximum thrust and $P_e > P_a$ gives under expansion. With the lower expansion ratio nozzles, the delivered V_e is less.

The major part of the structural mass includes the propellant tanks and engine masses. The propellant tanks are designed to withstand the expected flight loads caused by the tank internal pressure and external loads. Also, the engine structural elements have to withstand higher pressure and thermal loads. The structural mass can be reduced by the use of high strength-to-weight ratio materials and special materials. However, in order to ensure structural integrity with the reasonable margins of safety, minimum structural mass is essential.

For the case of solid propulsion systems, wherein the motor cases have to withstand high pressure loads, the motor case masses are higher. However, for the cases of liquid engines, as the propellants are stored in separate tanks with relatively lower pressure, the tank masses are lower. In such cases, the engine mass has to be appropriately designed to withstand higher pressure loads. There are differences between control systems of vehicle which uses solid motors and liquid engines. The solid motor either uses flexing the nozzle to generate the required control force or uses secondary injectant thrust vector control system, whereas the liquid engines use engine gimbal control system. These systems have different contributions to the vehicle structural mass. All these aspects lead to the higher structural mass factors for the solid motors than liquid engine propulsion system.

The engine structural systems have to be designed for higher operating environment. The mass can be reduced only by the use of high strength and high temperature materials with suitable thermal propulsion systems.

During vacuum flight, the structural system has to withstand only internal pressure loads and the vehicle thrust loads, whereas during atmospheric flight phase, the vehicle structure has to be designed for the external loads as well as internal loads. Therefore, structural mass factors of lower stages (operating in the atmosphere) are generally higher than that of upper stages (operating in vacuum).

It can be concluded that the structural mass of the vehicle depends on the type of propulsion systems used, size of the propulsion system, operating environment and the selection of structural materials with the specified strength-to-weight ratio, which need to function at the room temperature and elevated temperatures as per the application. Any advancements in this area lead to the high performance of STS.

Table 5.1 Performance parameters

Propulsion systems		Structural systems	
Propulsion system	Vacuum Isp ($= V_e/g_0$)(s)	Stage/propulsion system	Structural factor
Solid system	260–270	Solid	0.15–0.20
Storable liquid system	280–320	Liquid (lower stages) Liquid	0.10–0.12
Semi-cryo liquid system	330–350	(Upper stages)	0.05–0.08
Cryogenic system	430–460		

With the present day technologies, the vehicles are configured with chemical propulsion systems. At present, solid motors, liquid engines with storable liquid propellants, semi-cryogenic propellants and cryogenic propellants are being used. Typical performance parameters for these systems being used in space transportation systems globally are given in Table 5.1. It is to be noted that there is a maximum limit on the V_e , that can be achieved for their usage in STS design. Therefore, it is essential that, depending on the specific characteristics of these systems with respect to their relative merits and demerits, a suitable combination of the above systems have to be used to achieve the best possible STS design.

For the specified propulsion system, the higher values of specific impulse are due to higher nozzle expansion ratio, operating in vacuum flight. The lower structural factor is achieved through highly optimized design, which is designed for the exact operating environment. It is to be noted that the initial Atlas vehicle configurations were designed with structural factor as low as 0.036 to achieve the maximum performance of the vehicle. However, in such cases of lower structural factors with the existing material technologies, the handling process is very difficult and complex. It is also essential that such vehicles are launched in benign operating environment which reduces the launch probability considerably.

Therefore, after detailed trade-off analysis, one has to select the suitable values for the performance parameters for configuring STS.

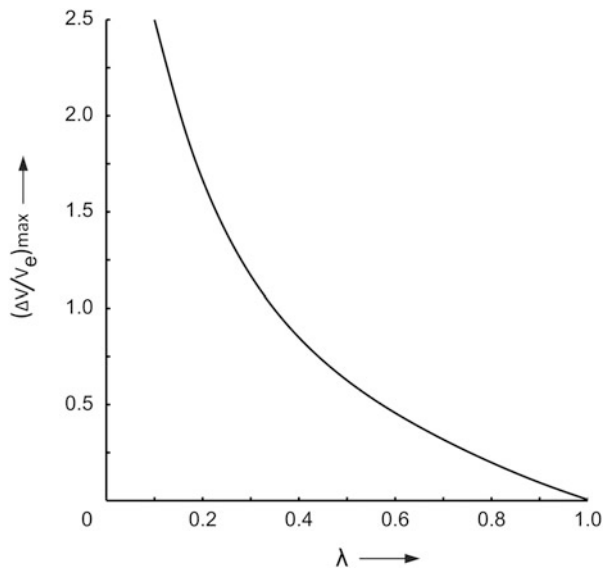
5.3.3 Single Stage STS Performance

In order to evaluate the single stage STS performance, the rocket equation is further analysed as given below:

Eq. (5.1) can be written as

$$\frac{\Delta V}{V_e} = \ln \left[\frac{1}{(m_s/m_i) + (m_{PL}/m_i)} \right] \quad (5.11)$$

Fig. 5.2 Limiting velocity of single stage STS for various structural factors



Using Eq. (5.8) in Eq. (5.11) yields

$$\frac{\Delta V}{V_e} = \ln \left[\frac{1}{1 - \zeta} \right] \quad (5.12)$$

Using Eq. (5.9) in Eq. (5.12) yields

$$\frac{\Delta V}{V_e} = \ln \left[\frac{1}{\lambda + (1 - \lambda)(m_{PL}/m_i)} \right] \quad (5.13)$$

The limiting velocity of the vehicle is achieved with zero payload. Using $m_{PL} = 0$ in Eq. (5.13) gives the limiting velocity (maximum velocity) of single stage STS and is given as

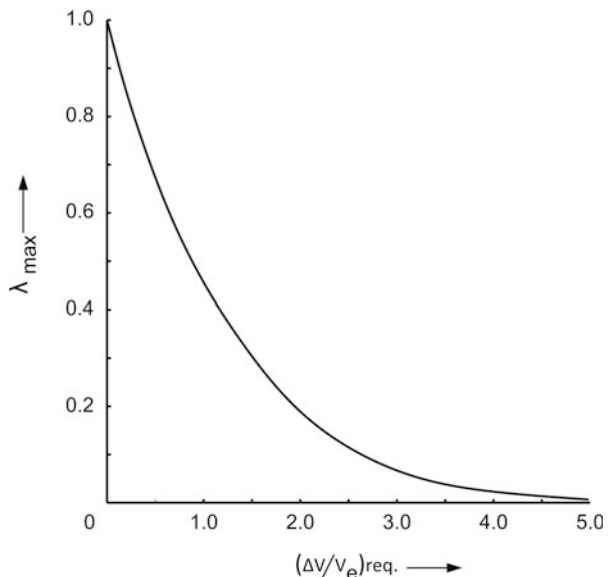
$$\left(\frac{\Delta V}{V_e} \right)_{max} = \ln \left[\frac{1}{\lambda} \right] \quad (5.14)$$

and represented in Fig. 5.2. The figure shows that even with very small structural factors, the limiting velocity of single stage STS is not very much. The maximum allowable structural ratio to achieve the required ΔV can be obtained from Eq. (5.14) as given below:

$$\lambda_{max} = e^{-(\Delta V / V_e)_{req}} \quad (5.15)$$

and represented in Fig. 5.3.

Fig. 5.3 Maximum possible structural factor for single stage STS



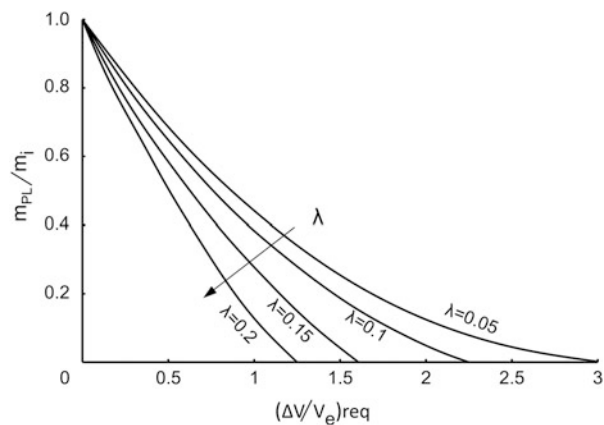
It is to be noted that in order to achieve orbital mission using STS even with highest performance propulsion system, the required non-dimensioned velocity is of the order of 2.5, and with the lower performance propulsion system, the non-dimensional velocity can go further higher. From Fig. 5.3, it can be seen that to achieve meaningful orbital mission using single stage STS, the allowable structural factor is very low and it is not possible to achieve with the present day material technologies. This can be further explained with the payload mass ratio. Using Eq. (5.13), the payload mass ratio obtained from a single stage STS, which gives the required velocity ΔV , as given below.

$$\frac{m_{PL}}{m_i} = \frac{e^{-(\Delta V / V_e)_{\text{req}}} - \lambda}{1 - \lambda} \quad (5.16)$$

The payload mass ratios for various structural factors with respect to the dimensionless velocity are given in Fig. 5.4. It can be observed that, for higher structural factors, at relatively low $(\Delta V / V_e)$ itself, the payload mass ratio shows zero, meaning it is infeasible to get the payload capability. At the same time, to get even a very small payload ratio with the required dimensionless velocities, the required structural factors are unrealistically small values. In this case, it is not possible to define a STS with such a small structural factor. These are further explained with two typical cases:

1. Requirement for orbital transfer vehicles
2. Requirement for ascent STS (launch vehicles)

Fig. 5.4 Payload mass ratio for single stage STS



For the case of orbital transfer from a GTO of (200 km \times 36,000 km, $i = 20^\circ$), to GEO mission (36,000 km circular, $i = 0$), ΔV required is about 1660 m/s. Assuming, $V_e = 3140$ m/s ($I_{sp} = 320$ s), $(\Delta V/V_e)_{req}$ is 0.5286. For this value, the maximum possible value of λ is 0.59. This value is much more than realizable one. Using the most feasible value of $\lambda = 0.1$ (corresponding to the liquid engines), the payload mass ratio, (m_{PL}/m_i) is 0.54. This is very much feasible option.

For the case of STS mission from Earth to orbit, even for the Low Earth Orbit, the required equivalent velocity ΔV to be provided by STS is about 11,000 m/s. Assuming the same specific impulse of 320 s (as used in the previous example), the λ_{max} possible without payload is 0.03, which is not feasible to achieve. Assuming the realistic value of λ as 0.1, the (m_{PL}/m_i) is negative, indicating ascent mission of STS is not feasible. Even with the V_e of 4500 m/s ($I_{sp} = 460$ s), (m_{PL}/m_i) is negative.

From the above analysis, the following conclusions can be arrived at:

1. For the cases of lower velocity requirements such as orbital transfer vehicles, single stage propulsion systems configured STS is feasible.
2. For the cases of ascent STS vehicles, which need to place a satellite into a specified orbit, it is not possible to have a realistic and robust single stage STS with the present day technology limitations

Therefore, it is essential to configure ascent STS (launch vehicle) with multiple propulsion stages as explained in the following sections.

5.4 Multistage STS Configurations

This section gives the concept of multistaging, multistage performance, optimal staging and trade-off analysis required in configuring the STS as well as types of staging.

5.4.1 Multiple Stage Concept

As explained in Sect. 5.3, a realistic and robust single stage STS cannot deliver the ΔV required for the satellite launch missions, whereas if the required velocities are reduced, then it is feasible to configure a stage to provide the necessary ΔV . Therefore, the required total ΔV as demanded by a satellite orbital mission is divided into smaller components, configure propulsion stages to provide these velocities and combine them into a STS which provides the net required velocity for achieving the mission. As an example, the mission required ΔV is divided into two smaller components ΔV_1 and ΔV_2 such that,

$$\Delta V_{\text{req}} = (\Delta V_{\text{req}})_1 + (\Delta V_{\text{req}})_2 \quad (5.17)$$

The first stage is designed to provide $(\Delta V_{\text{req}})_1$ and second stage is designed to provide $(\Delta V_{\text{req}})_2$. During mission, after delivering $(\Delta V_{\text{req}})_1$, the first stage is separated from the vehicle. Continuing the velocity addition process, the second stage provides the additional $(\Delta V_{\text{req}})_2$ so that at the end of second stage, the required velocity ΔV_{req} as demanded by the satellite mission is achieved.

For the first stage during its operation, the payload is the second stage and the satellite mounted on top of it. After first stage separation, second stage, with the payload function as conventional single stage STS as explained in Fig. 5.5. In this configuration, since lower stage carries upper stage and satellite as its payload, the lower stage is large compared to the upper stage.

5.4.2 Multistage Performance

Assume 'n' number of stages in the STS, then extending Eq. (5.17) to 'n' stages yields

$$\Delta V = V_{e_1} \ln\left(\frac{m_{i_1}}{m_{f_1}}\right) + V_{e_2} \ln\left(\frac{m_{i_2}}{m_{f_2}}\right) + \dots + V_{e_n} \ln\left(\frac{m_{i_n}}{m_{f_n}}\right) \quad (5.18)$$

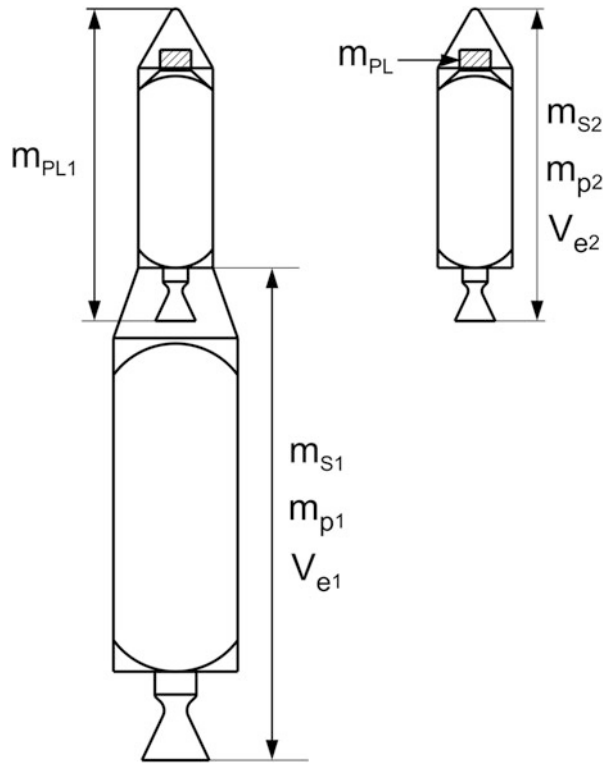
Consider the STS configuration with same propulsion system for all the stages, then $V_{e_1} = V_{e_2} = \dots = V_{e_n} = V_e$. Then, Eq. (5.18) becomes

$$\frac{\Delta V}{V_e} = \ln\left(\frac{m_{i_1}}{m_{f_1}} \times \frac{m_{i_2}}{m_{f_2}} \times \dots \times \frac{m_{i_n}}{m_{f_n}}\right) \quad (5.19)$$

Assume again that all the stages have the same mass ratios, then Eq. (5.19) yields

$$\frac{\Delta V}{V_e} = \ln\left(\frac{m_{i_j}}{m_{f_j}}\right)^n \quad (5.20)$$

where (m_{i_j}/m_{f_j}) is the mass ratio of jth stage, which is same for all the stages.

Fig. 5.5 Multi-staging

Since all stages have the same mass ratio and V_e , therefore, ΔV imparted by each stage is given by

$$\Delta V_j = \frac{\Delta V}{nV_e} \quad (5.21)$$

and the mass ratio of individual j th stage is given by

$$\left(\frac{m_{i_j}}{m_{f_j}} \right) = e^{-\left(\frac{\Delta V}{nV_e}\right)} \quad (5.22)$$

Using Eq. (5.16), the payload mass ratio of individual j th stage is given by

$$\left(\frac{m_{PL_j}}{m_{i_j}} \right) = \frac{e^{-\left(\frac{\Delta V}{nV_e}\right)} - \lambda_j}{1 - \lambda_j} \quad (5.23)$$

Assuming that the propellant mass fraction and structural factor for the individual stage are same, as per Eq. (5.9), the payload mass ratio, (m_{PL_j}/m_{i_j}) of individual stage is same. Therefore,

Table 5.2 Vehicle Sizing with same performance parameters ($I_{sp} = 310$ s)

Number of stages (n)	m_{PL}/m_0	Vehicle mass at lift-off	Percentage change in lift-off mass compared to previous configuration
		m_0 (kg)	
1	-0.053	Not possible	-
2	0.020	250,000	-
3	0.027	180,000	-28
4	0.031	162,300	-10
5	0.032	154,496	-4
6	0.033	150,060	-3.2

Table 5.3 Vehicle sizing with same performance parameters ($I_{sp} = 350$ s)

Number of stages	m_{PL}/m_i	Vehicle mass at lift-off m_0 (kg)	Percentage change in lift-off mass
1	-0.030	Not possible	-
2	0.035	140,970	-
3	0.044	114,180	-19.0
4	0.047	106,300	-6.9
5	0.048	102,554	-3.5
6	0.049	100,369	-2.1

$$\left(\frac{m_{PL}}{m_0}\right) = \left(\frac{m_{PLj}}{m_{ij}}\right)^n \quad (5.24)$$

where m_{PL} is the actual payload mass and m_0 is the vehicle mass at lift-off. Using Eq. (5.23) in Eq. (5.24) yields

$$\left(\frac{m_{PL}}{m_0}\right) = \left[\frac{e^{-(\Delta V/nV_e)} - \lambda}{1 - \lambda} \right]^n \quad (5.25)$$

In order to understand the effectiveness of staging on STS sizing, consider the following example.

ΔV required to achieve a specified orbit = 9000 m/s

Specific impulse for the stages = 310 s

Therefore, $V_e = g_0 * I_{sp} = 3040$ m/s

Structural factor, $\lambda = 0.1$

Mass of the satellite to be injected into the specified orbit = 5000 kg

Using the Eq. (5.25), the STS vehicle's sizing with different numbers of stages are worked out and given in Table 5.2. For the same case with specific impulse of 350 s, the results are given in Table 5.3.

From the above examples, the following conclusions can be arrived at:

1. Minimum two stages are required for STS to achieve the orbital missions.
2. As the specific impulse increases, the vehicle mass reduces
3. As the number of stages increases, the vehicle mass reduces. Performance point of view, configuring a vehicle with more number of stages is preferable; but adding more number of stages, the vehicle reliability reduces considerably.

For the case of reduced V_e , there may not be any benefit to go for a configuration beyond four stages. For the cases of higher specific impulse, the required performance can be achieved in three stages. In order to understand the real benefits of configuring STS with large number of stages, the limit case of infinite stage configuration is analysed. Applying the limit of $n \rightarrow \infty$ in Eq. (5.25),

$$\left(\frac{m_{PL}}{m_0}\right)_{n \rightarrow \infty} = \left(\frac{m_{PL}}{m_0}\right)_{\max} = e^{\frac{-\Delta V/V_e}{(1-\lambda)}} \quad (5.26)$$

Considering the first example (specific impulse of 310 s), using Eq. (5.26), the minimum lift-off mass is worked out to be 134,140 kg which is merely about 10 % reduction with respect to that of STS configuration with six number of stages. Considering the efforts involved and poor reliability of the vehicle and the performance, it is preferable to configure STS with minimum number of stages which meets the satellite mission requirements.

The cases discussed above are ideal vehicle configurations with same mass ratio, propulsion systems with identical V_e , same propellant mass fractions and structural factors to show the effects of multistaging on the STS performances. In reality, depending on the functional requirements (as explained later), feasibility of configuring STS with multiple stages along with the suitable technologies for each stage and trade-off analyses have to be carried out involving several iterations. Based on the analysis, suitable multistage STS configuration has to be arrived at.

5.4.3 Optimal Staging

This section gives the optimal staging aspects of multistage STS configuration. Once the satellite mass, the orbit and the number of stages and the type of propulsion systems are defined, it is essential to compute the minimal propellant loading required in each stage to inject the specified payload mass into the defined orbit. The methodology of computations is called optimal staging as explained below:

Consider the multistage STS configuration with ‘n’ propulsion stages, which provide the required ΔV as given below,

$$\Delta V_{req} = \sum_{i=1}^n V_{e_i} \ln \mu_i \quad (5.27)$$

where the mass ratio of i th stage, μ_i is defined as

$$\mu_i = \frac{m_{0i}}{m_{0i} - m_{pi}} \quad (5.28)$$

The structural factor of i th stage is defined as

$$\lambda_i = \frac{m_{si}}{m_{pi} + m_{si}} \quad (5.29)$$

The ratio of initial mass to the payload mass of i th stage is given as

$$\frac{m_{0i}}{m_{PLi}} = \frac{m_{0i}}{m_{0i} - m_{pi} - m_{si}} \quad (5.30)$$

Using Eq. (5.28) and Eq. (5.29) in Eq. (5.30) yields

$$\frac{m_{0i}}{m_{PLi}} = \frac{\mu_i(1 - \lambda_i)}{1 - \mu_i \lambda_i} \quad (5.31)$$

The payload mass of i th stage is the initial mass of $(i+1)^{th}$ stage. Therefore, the ratio of lift-off mass to the payload (satellite) mass can be defined as

$$\frac{m_{01}}{m_{PL}} = \frac{m_{01}}{m_{PL1}} \frac{m_{02}}{m_{PL2}} \dots \frac{m_{0n}}{m_{PLn}} \quad (5.32)$$

Using Eq. (5.31) in Eq. (5.32) and taking natural logarithm gives

$$\ln\left(\frac{m_{01}}{m_{PL}}\right) = \sum_{i=1}^n \ln\left[\frac{\mu_i(1 - \lambda_i)}{1 - \mu_i \lambda_i}\right] \quad (5.33)$$

Equation (5.33) can be further expanded as

$$\ln\left(\frac{m_{01}}{m_{PL}}\right) = \sum_{i=1}^n [\ln\mu_i + \ln(1 - \lambda_i) - \ln(1 - \mu_i \lambda_i)] \quad (5.34)$$

The objective of optimum multistage STS sizing and configuration design is to minimize the initial mass of the vehicle for the defined payload mass, which satisfies the Eq. (5.27). For this purpose, Lagrange multiplier technique is applied in Eqs. (5.34) and (5.27) as follows:

$$\ln\left(\frac{m_0}{m_{PL}}\right) = \sum_{i=1}^n [\ln\mu_i + \ln(1 - \lambda_i) - \ln(1 - \mu_i \lambda_i) + \delta \{V_{ei} \ln\mu_i - \Delta V_{req}\}] \quad (5.35)$$

where δ is the Lagrange multiplier.

To minimize m_0/m_{pl} Differentiate Eq. (5.35) with respect to μ_i and equate to zero which yields ‘n’ equations as given below:

$$\frac{1}{\mu_i} + \frac{\lambda_i}{1 - \mu_i \lambda_i} + \delta \frac{V_{e_i}}{\mu_i} = 0 \quad (5.36)$$

Equation (5.36) gives the optimum value of μ_i as

$$\mu_i = \left[\frac{1 + \delta V_{e_i}}{\delta V_{e_i} \lambda_i} \right] \quad (5.37)$$

Using Eq. (5.37) into Eq. (5.27) gives

$$\sum_{i=1}^n V_{e_i} \ln \left[\frac{1 + \delta V_{e_i}}{\delta V_{e_i} \lambda_i} \right] = \Delta V_{req} \quad (5.38)$$

ΔV_{req} is known. Once the number of stages and propulsion systems for each stage are defined for a vehicle, V_{e_i} is known. By selecting the suitable structural material for each stage, λ_i is known. Using these parameters in Eq. (5.38) gives the value of δ . Substituting this value in Eq. (5.37), the optimum mass ratio of each stage is obtained. Further using these parameters, the propellant mass distribution and structural mass details are worked out, which gives the optimum multistage STS to inject the specified satellite mass into the defined orbit.

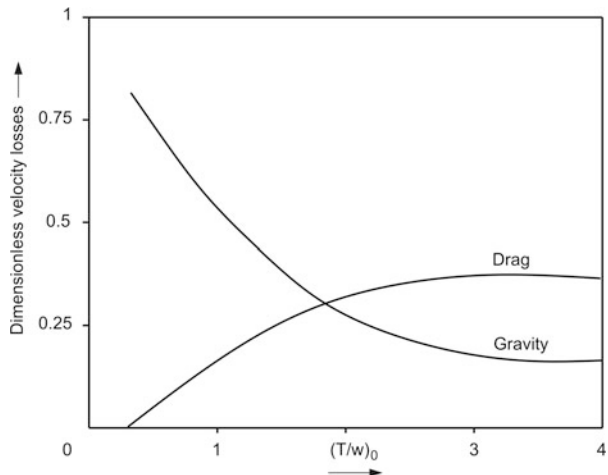
The above analysis gives the overall aspects of multistage STS configuration. However, the realistic vehicle configuration can be arrived at after trade-off studies to meet the various other requirements.

5.4.4 Important Considerations for Configuring Multistage STS

The previous section explained the optimum propellant loading for each stage; but not about the size and thrust level requirements of the stage.

One important parameter to be considered for the STS configuration is the thrust-to-weight ratio. First of all, the lower stage propulsion system has to produce thrust level more than the vehicle weight (mass \times acceleration due to gravity) to lift the vehicle from the ground. For the case of higher thrust level, after vertical rise, the vehicle can be aligned more towards horizontal, which reduces the velocity loss due to gravity considerably while exiting the atmosphere quickly. In addition, the higher thrust propulsion systems add velocity to the vehicle at a faster rate. Therefore, higher thrust vehicle during atmospheric flight phase increases the vehicle velocity at lower altitudes, thus increasing the dynamic pressure, which in

Fig. 5.6 Effect of lift-off (T/W) on velocity losses



turn increases the drag loss. However, as the velocity loss due to gravity is for the entire duration of flight whereas the drag loss is only during the atmospheric flight phase, the total velocity loss during the entire mission for higher (T/W) vehicle is generally less, which in turn reduces the vehicle size. Typical dimensionless velocity losses due to gravity and drag of a typical vehicle for various levels of initial thrust-to-weight ratio (T/W) are given in Fig. 5.6.

It is seen that the total velocity loss is reduced as $(T/W)_0$ increases. Therefore, generally vehicle with higher $(T/W)_0$ is preferable. But it is to be noted that, higher thrust level of the vehicle demands higher structural mass, which has impact on the vehicle performance. Therefore, trade-off study is essential to finalise the $(T/W)_0$ ratio at different phases of flight. This has implication on the selection of propulsion systems and the associated structural mass factors.

Regarding the size of a stage, the functional requirements can either be achieved by a single large propulsion stage or partitioned into smaller systems and clustering to provide the same effect. The selected option has impact on vehicle sizing and configuration design. There can be limitations on realizing the bigger single stage and the associated complexities regarding handling and realization; but smaller stages have the advantages of less developmental efforts and easily realizable. But adding more number of stages has serious impact on the overall reliability of the vehicle which demands trade-off studies required to arrive at a suitable configuration.

In order to overcome such problems, various types of multistage configurations of STS can be considered.

5.4.5 Types of Multistage Configurations

In the multistage STS, the propulsive stages can be configured in different ways. While generally the stages are arranged in sequence (tandem) configuration, depending on the functional requirements and technology limitations, it is also possible to configure the vehicle with

1. Partial staging
2. Parallel staging
3. Piggyback staging

In the tandem staging, the propulsion stages are assembled one over the other as represented in Fig. 5.7. The two stages are integrated through suitable interface structural elements with the required stiffness called interstages. After functioning of lower stage, the empty stage is jettisoned and the next stage is operated sequentially. This process continues till the satellite is injected into the required orbit. In order to improve the performance of the vehicle, while separating the lower stage, the associated interstage structure is also separated along with it. In this case, to get the required (T/W) ratio, either single stage large engine (Fig. 5.7a) or

Fig. 5.7 Sequential (Tandem) staging (a) Single Engine (b) Multi Engine

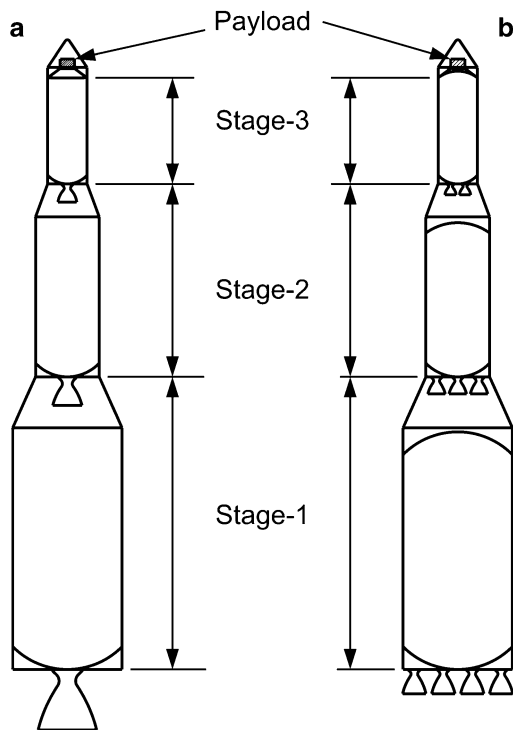
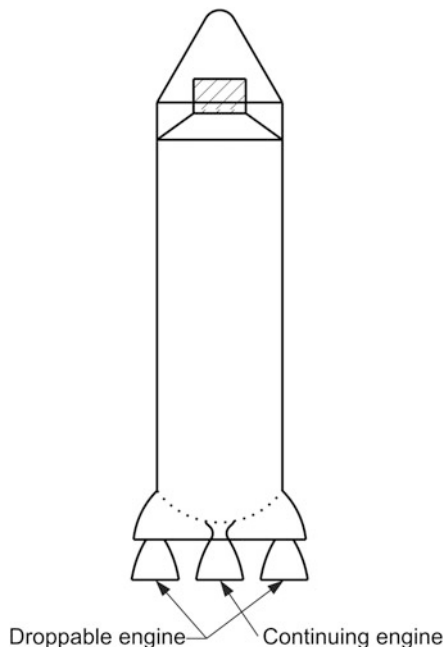


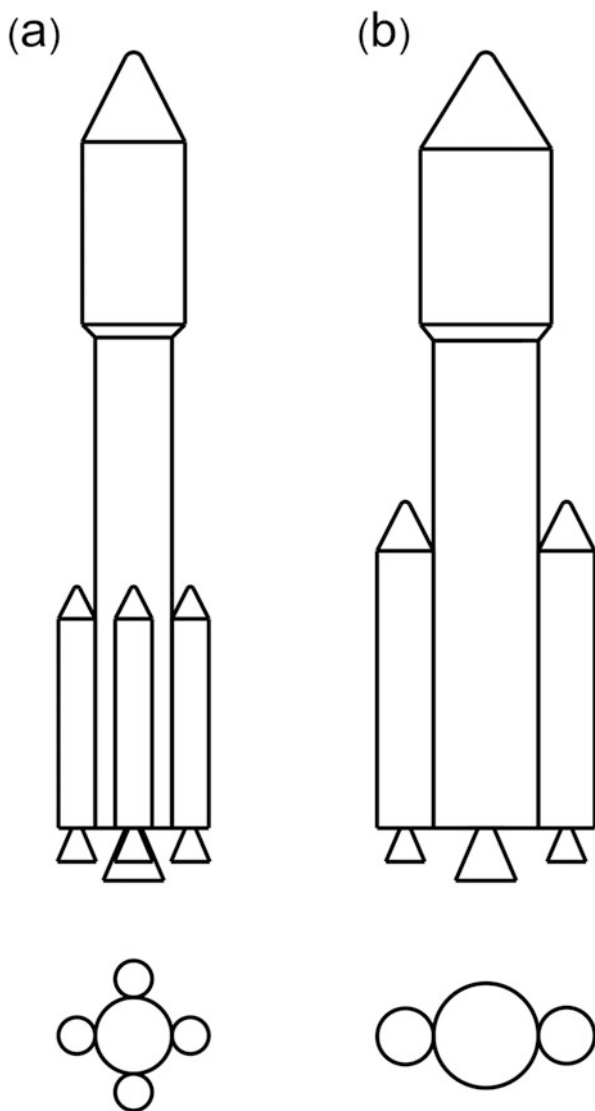
Fig. 5.8 Partial staging configuration



multiple small engines (Fig. 5.7b) are used. However, in both the cases, to contain large amounts of propellants, vehicle has to be configured with large tanks wherein the length and diameter of the tanks are limited by the fabrication facilities and infrastructure available. To overcome these difficulties, the staging options as explained below are to be adopted.

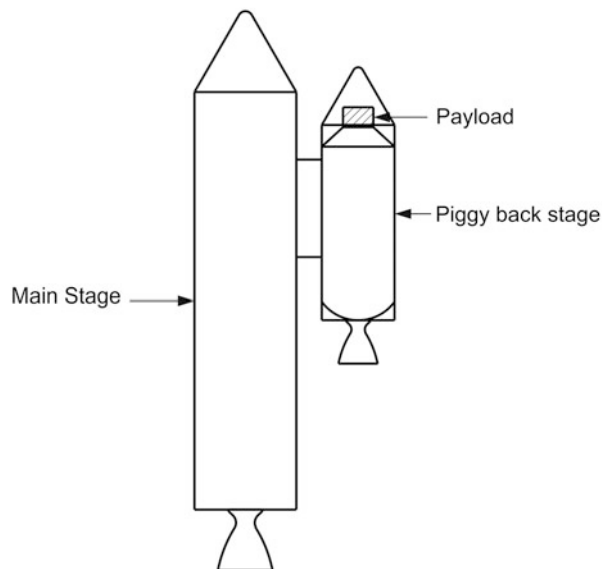
In the cases of partial staging, once the functional requirements are met, some of the structural elements are jettisoned on the way to improve the vehicle performance. A typical example is initial configurations of Atlas vehicle. Initially, three engines are in operation to generate the required thrust to meet the (T/W) ratio. Once the higher thrust requirement is over, two of the engines are disconnected from the main propulsion system and jettisoned to gain the additional performance to the continuing vehicle. The third engine continues till the required velocity conditions are achieved. Typical such configuration is represented in Fig. 5.8.

In the parallel staging, more numbers of propulsive stages are clustered to the core vehicle as shown in Fig. 5.9. The clustered stages are called strapon stages. These configurations are generally adopted when there is thrust augmentation required in the lower stages to achieve the required (T/W) ratio. Along with the core vehicle propulsion system, the strapon propulsion systems are also in operation at the appropriate time to provide the necessary energy to the vehicle (Fig. 5.9a). If the strapon stages are powerful enough, core booster stage is brought into operation during flight at suitable predefined sequence to increase the performance (Fig. 5.9b). Once their functions are over, generally the empty strapon stages are jettisoned from the main vehicle to gain the vehicle performance.

Fig. 5.9 Parallel staging

The reasons behind these types of configurations are to meet the requirements with smaller propulsion stages (which are easy to design, develop and realize) than one very big stage/engine to generate the required (T/W) ratio. In certain configurations, to avoid one more separation event, the empty strapon stages are separated along with the core vehicle stage if their operation durations are very closer to the core stage. After separation of strapon stages, the main vehicle continues to be in operation till meeting the mission requirements.

Fig. 5.10 Piggyback staging



There are several vehicles globally which have parallel staging concepts to meet the requirements considering the new technology developments and realization difficulties.

Figure 5.10 illustrates the piggyback staging. In these configurations, the second stage is attached to the first stage as a piggyback. Either the piggyback stage operates after the first stage operation or both can operate together, wherein the first stage can be separated after completing its functional requirements. The Space Shuttle is one typical example of using parallel staging and piggyback staging concepts together. These configurations also provide the necessary thrust to the vehicle. The second stage (piggyback stage) continues further to achieve the required orbital conditions.

5.5 Optimum Staging Aspects and Vehicle Performance

In multistage vehicles, the number of stages, the mass ratios, the specific impulse of the propellant used, thrust levels, propellant burn duration, the separation sequence, etc. are to be optimized to derive the maximum benefit of achieving the highest payload for the given lift-off-mass of the vehicle. Similarly one has to optimize the flight vehicle performance during the initial design phase. Some of the important parameters which need serious consideration while defining each of the stages are as given below:

- (a) Effective exhaust velocity, V_e
- (b) Nozzle area ratio

- (c) Specific impulse of propellant
- (d) Stage mass ratio
- (e) Burn duration of stages
- (f) Minimisation of velocity losses due to drag and gravity
- (g) Maximum propulsion efficiency
- (h) Optimum vehicle sequencing

The higher value of effective exhaust velocity always provides higher velocity to the vehicle. Selection of a suitable propellant and a suitable nozzle configuration are important to achieve higher exhaust velocity. Nozzle area ratio has to be judiciously selected depending upon the operation of the stages either at sea level or at higher altitudes. The specific impulse is closely linked to effective exhaust velocity and it largely depends on the propellant used and the nozzle configuration. It has direct influence on the vehicle performance.

The mass ratio has to be kept minimal to achieve optimum performance from the vehicle. This can be achieved by reducing the inert mass of the structures, avionics and all other associated elements. The design also has to ensure that the unused propellant is kept minimum. All these aspects need greater emphasis while finalizing the vehicle configuration. In order to minimize the velocity loss due to gravity it is always advantageous to reduce the burn time of stages by protecting the overall impulse needed for the vehicle. The vehicle drag is another important factor which causes severe velocity loss during the atmosphere phase of flight. The aerodynamic shaping, smooth external surfaces, and minimization of local projections are some of the areas which need greater attention to reduce the vehicle drag while finalising of the vehicle configuration.

During the initial definition phase of the vehicle, not only proper selection of propulsion systems for each of the vehicle stages is important but careful definition of propulsion parameters are needed to improve the overall propulsion efficiency and the vehicle performance. The vehicle sequencing is closely linked with the trajectory and has to consider several constraints which are specified. In order to reduce the no control region between two stages, real time decision to define a new time line with respect to the burn out of the lower stage is required. Various events during these operations are to be properly sequenced to obtain the optimum performance from the vehicle.

In solid propulsion systems, the structural mass factor is more and exit velocity and specific impulse are less. Therefore, the energy imparted by this system to the vehicle is less and the vehicle performance with solid motor staging is limited. But the thrust levels of solid motors are generally higher with very short duration flight time. The higher (T/W) ratio along with reduced operation time reduces the velocity loss due to gravity considerably. Therefore, even though the ideal velocity imparted by solid motors is less, the net effective velocity is more. This feature is especially useful for the vehicle during lift-off, wherein vehicle mass is more along with almost vertical flight of the vehicle. During lower stage flights, vehicle attitude is generally towards vertical. With higher (T/W), the vehicle can fly more towards horizontal. Due to the higher thrust, the burn time is less which results into reduced

velocity loss due to gravity to vehicle. This gain supersedes the performance loss due to increased structural mass and less energy propulsion system.

During upper stage flights, due to the almost horizontal flight of the vehicle, already the velocity loss due to gravity is less. Therefore, the advantage of solid motors with respect to the velocity loss is minimum, and in such cases, the less energy content of this propulsion system along with higher structural mass makes this system less attractive for upper stages. However, the solid motor system is much simpler, compared to the complex liquid engine propulsion system.

For the liquid engines, especially cryogenic engines, thrust levels are less; but they burn for very long duration to provide the higher energy with the stored propellants. The low thrust along with the long duration have the following implications: (1) (T/W) ratio is less than unity especially at the time of ignition and (2) Long duration thrusting increases the velocity loss due to gravity considerably. If these propulsion systems are used for lower stages, there is very high velocity loss due to gravity. Therefore, in spite of imparting high energy, the net effective velocity achieved is not high for lower stage operations.

During upper stage operations, the vehicle attitude is almost horizontal, and therefore, the velocity loss due to gravity is minimum in spite of long duration flight. Under such cases, thrust level is not the major criteria, but total impulse is important so that almost full energy of high efficient liquid propulsion performance is effectively utilized for the vehicle performance. Another important feature is that the structural factors of liquid engines are generally lower. These two features make the liquid engines more attractive for the upper stages. Additional advantage of liquid engines for upper stages is that, when the required orbital conditions are achieved, the engine can be shut down which ensures precise injection of the satellite into the defined orbit. However, the liquid engines are more complex due to the more numbers of rotating elements, high pressure systems and valves with leak tight requirements to ensure the vehicle safety. The contamination control is also of paramount importance for the liquid engines.

Due to vacuum flight operations, the nozzle expansion ratio can be more to get more specific impulse. The increase in structural mass due to the extended nozzle reduces payload carrying capacity. Therefore, these aspects are to be considered while arriving at a suitable configuration.

To effectively utilize the high energy of liquid engine propulsion systems, these systems can also be used in the lower stages along with the augmented thrust of solid motors. Also, more number of liquid engines is used in the lower stages to get the required (T/W) ratio.

Considering the above aspects, the more preferable options for the STS configuration are given below:

1. Lower Stages

- (a) Solid motors for the main propulsion system
- (b) Solid motors augmented by solid strapon motors
- (c) Multiple liquid engines

- (d) Liquid engines (Earth storable or cryo engines) with augmentation by solid motors
- (e) Liquid engines augmented by liquid engine strapon stages
- (f) Structures to withstand internal and external loads

2. Upper Stages

- (a) Liquid engines (Earth storable or cryo engines)
- (b) Multiple liquid engines
- (c) Engines with maximum possible area ratio
- (d) Highly optimized structures (only internal loads)

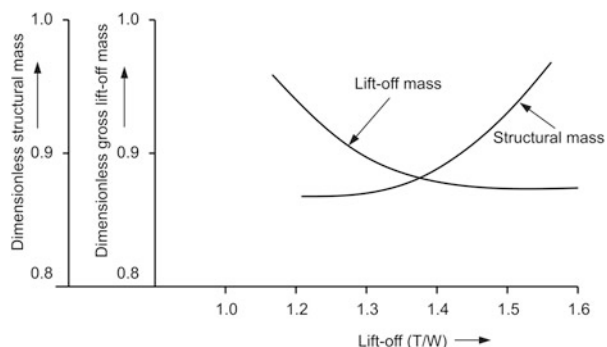
The above strategies have been used globally in all the STS configurations.

5.6 Design Sensitivities and Trade-Offs

During the initial definition phase of the vehicle, it is essential to carry out detailed design synthesis involving the identification of design options, their trade-offs which have to be based on the sensitivity and selection of a suitable technology. These trade-offs are quite useful to assess the parameter sensitivity, its influence on system effectiveness and to arrive at an optimum configuration meeting the overall mission objectives. The trade-off process has to consider the technology availability, the schedule and cost constraints. This process is quite complex and needs several iterations. Some of the major factors which need to be considered during the design phase are discussed below.

The lift off (T/W) ratio is one of the important factors which need to be studied in detail to arrive at an optimal value. It largely depends on vehicle parameters. For example, for a typical vehicle, dimensionless lift-off mass and structural mass as function of (T/W) ratio are given in Fig. 5.11. It can be observed from Fig. 5.11 for higher (T/W) ratio, the structural mass increases in order to have larger thrust and this causes increase in the propulsion system mass. At the same time, due to reduced

Fig. 5.11 Parameter trade in two stage vehicle



velocity loss, the lift-off mass of the vehicle decreases. A value of (T/W) ratio between 1.35 and 1.4 provides an optimum configuration.

Trade-offs for the selection of propulsion systems depend on several factors such as complexity, reliability, overall cost, ease of operation, maximum propellant utilization with a small amount of left out propellant, capability to adjust ΔV and many more. The number of stages also depends on the technology maturity of booster and upper stage propulsion systems. There is also a trade-off possible between number of engines and the overall thrust of engines. Lower thrust engines are useful in reducing the operating design parameters for the engine. This helps in enhancing the reliability of engines. At the same time, increasing the number of engines has limitations in size, weight, interaction between flumes and overall integration aspects.

Another important trade-off is the development of advanced technologies to meet the functional requirements against the usage of available technologies. No doubt, that advanced technologies (such as propulsion systems and structural materials) improve the performance, but associated issues are the increased cost for design and development, the risks involved, schedule and development cost. In addition, high-end technologies require precision manufacturing processes along with the costly materials. Therefore, even though there is considerable performance improvement (maximum payload mass fraction) with the advanced technologies, the design and development cost and the unit cost of the vehicle increase, which makes the vehicle economically expensive. Sometimes, it is possible to upgrade the available technologies to meet the functional requirements without impacting the schedule and the cost.

However, if there is a demand for quantum jump in the performance requirements, which may not be feasible with available technologies, then there is no other option but to develop the advanced technologies. Even in such cases, there can be an optimum route of developing smaller engines and design them to achieve the required performance. The associated mass increase and its impact on the performance have to be considered in the trade-off studies.

With respect to the vehicle structure, there are several tradeoffs. The overall weight of the vehicle needs to be minimised meeting the strength and stiffness requirements. External shape of the structure has to be carefully arrived at to avoid undesired aerodynamic effects. There are many choices for shapes and construction methods for structures, and suitable selection depends on the type of applications in the vehicle.

The overall shape, size and external protrusions have larger influence on aerodynamics effects and load on the vehicle. The detailed trade-off studies are needed for all other subsystems like sensors, control, vehicle avionics, separation, etc. considering various available options. Choosing a suitable one has to meet all specified requirements.

The general approach in all such trade-offs is to carry out detailed analysis and sensitivity studies with respect to the overall performance of the vehicle. The performance evaluation has to be carried out not only under the perturbation conditions of parameters within 3-sigma values but also under all adverse operating

conditions of the vehicle. Therefore, the final selection is to be based on the detailed simulations, tests and past experience. The chosen configuration has to provide the optimum performance meeting the schedule and cost criteria.

5.7 Satellite Interfaces with STS and Payload Fairings

To carry the satellite and deliver safely to the defined orbit, suitable mechanical and electrical interfaces of the STS with spacecraft are essential. One should also have full understanding of the constraints imposed by the vehicle like payload envelope and vehicle flight dynamic environment.

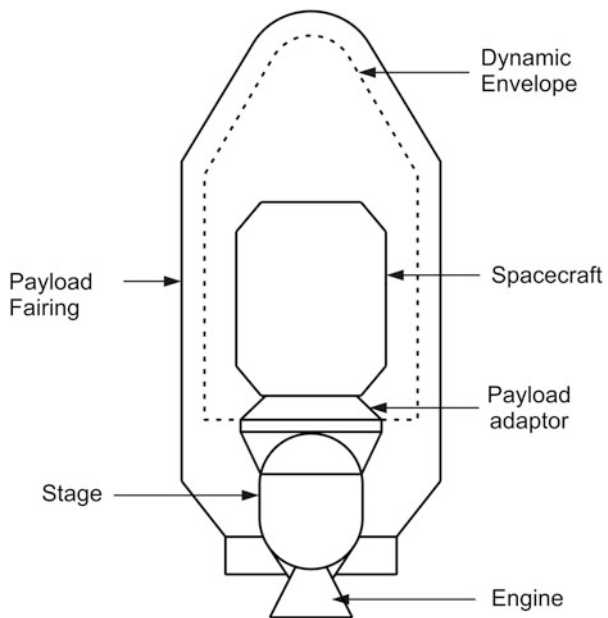
The spacecraft is generally mounted on the payload adaptor through proper mounting mechanism with a suitable separation system. It is essential that the joints are suitably designed to provide the specified joint characteristics. The separation system is mostly configured by a system which has a number of helical compression springs. They are released by a pair of bolt cutters used in redundant mode as release devices. The maximum separation velocity for the spacecraft has to be specified and the launch vehicle has to ensure that the separation velocity is within the specified value. A restricted centre of gravity offset is allowed for spacecraft and hence it has to be maintained within this value. Similarly the disturbance due to separation has to be minimum, generally less than one degree per second. The interface between spacecraft and launch systems has to be designed to keep the interface requirements as minimum as possible. Functional and physical interfaces have to be well-defined and dependence of one on the other has to be maximally avoided.

The satellite during the integration with the vehicle has to be maintained in a clean environment and the assemble bay has to be with 10,000 class cleanliness with appropriate facilities. The outgassing properties of the launcher material have also to be assessed and the molecules arising out of this are to be controlled.

The payload fairing should have provision for spacecraft telemetry transmission through its body smoothly. Therefore radio frequency (RF) transparent panels are needed in the cylindrical section of payload fairing. The spacecraft designer has to provide the initial data on (a) operating frequency range, (b) antenna pattern, (c) power of the transmitter and (d) power attenuation. The electromagnetic compatibility analysis is necessary to ensure the interference free electromagnetic environment. In payload fairing, generally provision is made to have detachable doors to have easy access to the spacecraft after the installation of the payload fairing.

The payload envelope is another important criterion to be considered between STS and satellite. This envelope represents the maximum allowable satellite external configuration. This includes all manufacturing tolerances, static and dynamic deflections during assembly of payload fairing and in flight. In order to protect the satellite against the acoustic load encountered during atmospheric flight, acoustic blanket with suitable thickness provided. These thicknesses are also to be accounted

Fig. 5.12 Typical payload envelope



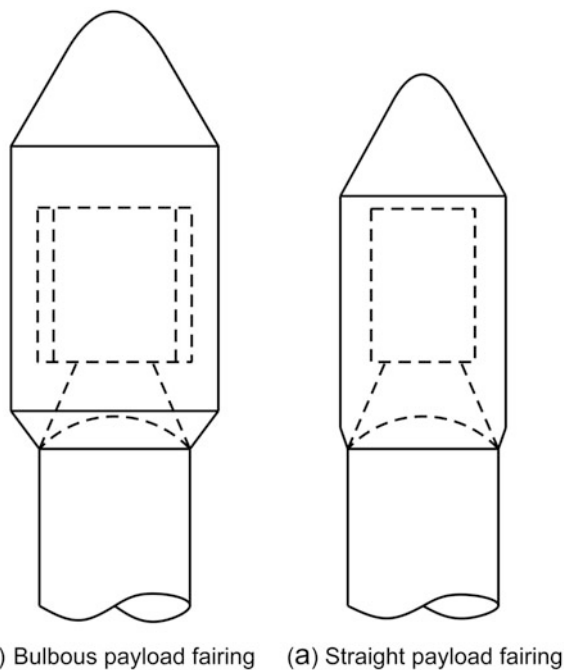
for deciding the dynamic envelope requirements. Dynamic envelope clearance has to be determined based on the detailed analysis. A typical payload envelope is as shown in Fig. 5.12.

While mass of the satellite decides the propulsion systems sizing and configuration, size, shape and volume of satellite along with the dynamic envelope explained above decides the payload fairing size. Depending on the satellite requirements, there are demands for bulbous payload fairing and straight payload fairing as shown in Fig. 5.13.

The fairing size has major impact on the aerodynamic characteristics of the vehicle. As this forms front portion of the vehicle, faces the air flow directly, the entire aerodynamic characteristics of the vehicle in terms of drag, lateral disturbance forces and moments depend on the shape of the payload fairing. Therefore, optimum design has to be carried out to arrive at a suitable aerodynamic shaping of the payload fairing. These aspects are explained in detail in Chap. 10 on aerodynamic design.

5.8 External Configurations of STS

Till now, the vehicle sizing in terms of propulsion systems requirements to achieve the required ΔV and payload fairing sizing requirements with respect to the satellite mass and size are discussed without any emphasis on the external shaping of the

Fig. 5.13 Payload fairings

vehicle. Once the sizes of the required propulsion stages are finalized, the next task is to provide the aerodynamic shaping to the vehicle.

The aerodynamic drag force acting on the vehicle during atmospheric flight phase has major impact on the vehicle performance in terms of velocity loss. Similarly, the aerodynamic lateral forces and moments acting on the vehicle during atmospheric flight phase form the major design input for vehicle structural, control and other subsystems designs. In addition, the functional protrusions introduced in the vehicle external configuration such as propellant servicing system at the ground etc. generate highly localized load.

The abrupt change at the aft end of the vehicle can introduce aerodynamic load on the propulsion system nozzle which may have major impact on the structural design aspects of nozzles as well as control systems of propulsion stages. Therefore, suitable aerodynamic shaping has to be provided to the vehicle and subsystems to reduce all the above-mentioned aerothermal environments. More details on external aerodynamic aspects are explained in Chap. 10 on aerodynamic design.

5.9 Infrastructure for Ground Operations

Attention to ground and launch operations while finalising the configuration of the vehicle is of utmost importance because it has large influence on the technology options for the vehicle, schedule and cost. The infrastructure needed for ground operations like launch complex, launch tower, propellant servicing facilities etc., has to be closely linked to the vehicle configuration. They should not only meet the requirements of launch support for the chosen vehicle configuration but also has to cater for the possible growth potential of the vehicle in the immediate future. The launch operations involve various important steps like assembly, integration and testing of vehicle subsystems and the integrated vehicle. This demands a number of facilities for mechanical, electrical and fluid systems depending on the requirement of each stage and the vehicle. Provision has to be made for the final testing of the payloads and all associated facilities are to be planned. The launch management calls for launch tower and all other associated service facilities. The launch phase electrical checkout is a complex system.

If the launch facilities are already established and existing, the suitability of the same has to be critically examined. Maximum usage of such facilities for the vehicle being configured should be one of the important considerations. The physical integration of the vehicle can be done either vertical or horizontal mode. The vertical integration restricts the access to subsystems and brings in a lot of safety related concerns while the horizontal integration has the advantage in both these specific areas. However the most common practice is to have vertical integration since it facilitates easier assembly of the vehicles.

The liquid stages demand suitable propellant storage and service facilities at the launch base. Proper facilities are to be established for loading the propellants into the vehicle. Depending on the stages used in the vehicle the propellant to be serviced can be either Earth storable propellants or cryogenic propellants. The facility has to satisfy the propellant storage and transfer requirements like the quantity of fluid to be stored, remote transfer of fluids, thermal conditioning of the fluids, various essential measurements of fluid parameters and rapid draining of propellants in the event of the call-off of launch. The system has to be configured with a lot of safety features to avoid any accident as these fluids are highly toxic. In order to achieve very high reliability, these systems have to be configured as simple as possible. Redundancy in very critical functions is necessary and has to be carefully decided.

Cryogenic fluids like liquid oxygen and liquid hydrogen have to be stored at low temperatures to avoid the increase in vapour pressures at ambient temperatures. Provision has to be made for proper venting to escape the excess pressure build up in fluid systems. Insulation of all fluid storage and transfer systems has to be provided to avoid the heat loss. These facilities requirements are to be assessed with respect to the configuration definition of the vehicle and appropriate facilities development are to be planned to meet the overall realisation plan meeting the schedule and cost constraints.

Bibliography

1. Thomson, W.T.: Introduction to Space Dynamics. Dover Publications, New York (1986)
2. Turner, M.J.L.: Rocket and Spacecraft Propulsion: Principles, Practice and New Developments. Springer Edition, Springer, Heidelberg/New York (2001)
3. Cornelisse, J.W., Schoyer, H.F.R., Wakker, K.F.: Rocket propulsion and spaceflight dynamics. Pitman Publishing Limited, London (1979)
4. Wiesel, W.E.: Spaceflight Dynamics. McGraw-Hill, New York (1989), Second edition (1997)
5. Ball, K.J., Osborne, G.F.: Space flight dynamics. Oxford University Press, Oxford (1967)
6. Rosenberg, R.M.: On optimum rocket trajectories and calculus of variations. *Aerosp. Eng.* **19**, 20–21 (1960)
7. Dommasch, D.O., Barron, R.L.: Optimum rocket trajectories, Part 1. *Aerosp. Eng.* **19**, 46–50 (1960)
8. Hall, H.H., Zambelli, E.D.: On the optimization of multi-stage rockets. *Jet propul.* **28**, 463–465 (1958)
9. Ragsac, R.V., Patterson, P.L.: Multistage rocket optimization. *J. Am. Rocket Soc.* **31**, 342–344 (1961)
10. Teren, F., Spurlock, O.F.: Payload optimization of multi-stage launch vehicles. NASA. TN D-3191 (1966)
11. Hiller, H.: Optimum arrangements of boost moors in multistage vehicles, for vertical flight in vacuum. R.A.E. TN-GW 519 (1959)
12. Cobb, E.R.: Optimum staging techniques to maximize payload total energy. *ARS J.* **31**, 342–344 (1961)
13. Cooper, R.S.: Performance of optimized multistage rockets. *J. Aerosp. Sci.* **29**, 1339–1343 (1962)
14. Leitmann, G.: Optimization techniques, pp. 1–31. Academic, New York (1962)

Chapter 6

Operating Environment

Abstract The space transportation systems and their subsystems have to perform normally under all kinds of adverse environments during their operation in flight. The vehicle experiences very severe external environments during atmospheric regime of flight and subsequent to that faces steady and dynamic loads during the remaining phases of flight till injection of satellite. The vehicle structure has to withstand all these extreme flight environments to achieve the mission successfully. To counteract the disturbance and to achieve the intended function, the various subsystems have to stretch their functional limits. The additional response caused by such efforts influences the performance of other related subsystems. Similarly, performance dispersions of a particular system have functional impact on other subsystems. Therefore, there is a strong coupling between environment and performance of subsystems in the vehicle. The disturbances are originated either from the external source to the vehicle or from a specific system within the vehicle which acts on the vehicle. The vehicle and subsystems have to be designed to operate against the expected environment disturbances. Typical external operating environments are gravity, atmosphere and aerothermodynamics. Atmospheric wind has specific characteristics and has major influence on the performance vehicle systems. The full understanding of the thermal environment which can cause severe effect on the performance of the subsystems is essential. Dynamic environments experienced by the vehicle systems, by both external and vehicle internal sources have the potential to induce the coupling between subsystems which can cause severe degradation in performance and at times failure too. This chapter describes in detail all such external, internal and dynamic operating environments experienced by the vehicle subsystems. How to deal with all such hostile environments during the design phase and how to enhance the robustness of the systems to work in such environments are discussed. Methodologies for understanding the vehicle operating environments thoroughly, predicting them accurately and utilizing those values in the design and qualification process are explained. The various parameter dispersions to be considered for the vehicle design and overall mission are also discussed.

Keywords Operating environment • Gravity • Atmosphere • Aerothermodynamics • Winds • Wind shear • Wind gust • Thermal environment • Thrust offset • Thrust misalignment • Differential thrust • Aeroacoustics • Slosh and POGO

6.1 Introduction

To inject maximum satellite mass into the mission-defined orbit, with the present-day technologies, the STS subsystems have to operate at their peak performance and the structural design of the vehicle has to be highly optimum. Peak performance of the subsystems demands higher operating conditions such as high pressure, high temperature, high thrust, etc. and the subsystems have to perform normally under such adverse environments to meet the specified functional requirements. The vehicle also experiences very severe external environments during atmospheric regime of flight along with various steady and dynamic loads during various phases of flight till injection of satellite and the vehicle structure should withstand the extreme flight environments to achieve the mission successfully. Therefore, to ensure the robustness of the systems to work in hostile environments, it is essential to understand the vehicle operating environments thoroughly, predict them accurately and use those values in the design and qualification process.

There are two broad categories of operating environments which need to be considered in the STS design process:

1. Disturbances which tend to deviate the vehicle systems away from the nominal intended function
2. Dispersions in the subsystem performance and environment parameters, which bring in additional demand on the vehicle systems, to meet the intended function

To counteract the disturbance and still achieve the intended function, a subsystem may have to stretch its functional limits. The additional response caused by such efforts certainly influences the performance of other related subsystems. Similarly, performance dispersions of a particular system have functional impact on other subsystems. Therefore, there is a strong coupling between environment and performance of subsystems in the vehicle. During design process, it is essential to understand and define the coupling between (a) the environment and specified subsystems and (b) the responses of the subsystems, to arrive at the robust design.

The disturbances are originated from both external to the vehicle and from a specific system within the vehicle which acts on the vehicle or other subsystems. In both cases the affected vehicle subsystems do not have any control on the disturbances. Therefore, the vehicle and subsystems have to be designed to operate in the expected disturbed environment. While the disturbances are the characteristics of the originating systems, the performance dispersions of a subsystem are generally caused by the (a) design insufficiency, (b) non-robust design, (c) prediction errors or (d) manufacturing and fabrication deviations.

The dispersions are also categorized into two types:

1. Dispersions on the operating environment with respect to the prediction
2. Dispersions on the vehicle system's performance parameters

To take care of the first category, the environment input has to be augmented accordingly to design for the extreme case of disturbances including the prediction

error. The dispersion levels of performance parameters can be reduced by adopting suitable robust, accurate design strategies as well as by reducing uncertainty levels in fabrication. If there are still some errors, those effects can be handled by providing extra margin in the design.

This chapter explains the overall external and internal operating environments to the vehicle subsystems. The various parameter dispersions to be considered for the vehicle design and overall mission are also discussed. It is to be noted that, for certain systems, the operating environment generated by the system itself is the design guidelines such as propulsion system, etc. Such environments are discussed along with the design aspects in the respective chapters of the book.

6.2 Broad Classification of Operating Environments

During its entire mission from lift-off till satellite injection, the vehicle and subsystems undergo several kinds of external disturbances. These vary from vacuum flight phase to severe atmospheric flight regimes ranging from subsonic to hypersonic flight phases with various levels of complexities specific to a particular regime of flight. Typical external operating environments are gravity, atmosphere and aerothermodynamics as shown in Fig. 6.1. Depending on the vehicle external shape, trajectory and attitude dynamics, these environments cause various types and levels of severity to the vehicle systems. By suitably designing these parameters, the impact of these environments on the vehicle systems can be reduced.

The acceleration due to gravity has major influence on the trajectory of STS. Generally a vehicle travels along a large ground range to inject the payload into the designated orbit. As a typical STS mission covers ground range as high as 8000 km, it is essential to consider the effect of gravity due to Earth asphericity on the vehicle trajectory dynamics. The random phenomenon of in-flight atmospheric wind generates angle of attack to the vehicle with respect to the velocity vector. The angle of attack and the dynamic pressure, which are functions of wind atmospheric properties such as density and vehicle trajectory combined with the external aerodynamic characteristics, induce severe aerothermal loads on the vehicle structure and destabilize the vehicle during atmospheric flight phase. In order to alleviate this severity, it is essential to design optimum aerodynamic configuration of the vehicle along with trajectory shaping and wind biasing to reduce the vehicle aerothermal loads. The aerodynamic noise at various locations of the vehicle caused by the vehicle external shape combined with the critical regimes of flight can induce severe environments to the vehicle systems. These noise levels can be reduced by proper shaping of the STS trajectory and by suitably designing external aerodynamic shape. However, the vehicle subsystems have to be designed and validated for this operating environment.

The important vehicle internal loads are thrust, pressure and thermal loads. In addition, there are several internal sources of disturbances caused by the vehicle systems. These disturbances have to be considered for designing the vehicle

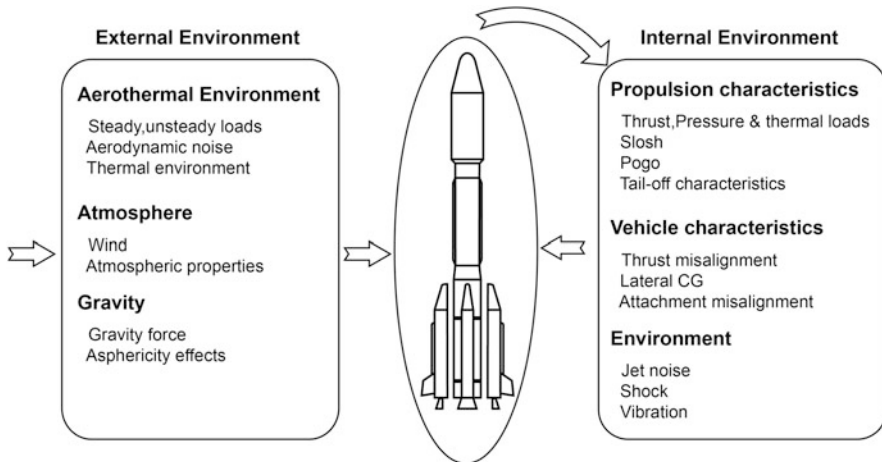


Fig. 6.1 Typical operating environments

systems. Typical examples as explained in Fig. 6.1 are (1) vehicle characteristics in terms of thrust misalignment and lateral centre of gravity (CG), vehicle subsystems attachment misalignment, (2) propulsion system characteristics such as propellant slosh, pogo and tail-off characteristics and (3) environments such as jet noise, shock and vibration.

With suitable design of the vehicle systems, the severity of the internal disturbances on the vehicle systems can be reduced. The thrust misalignment can be reduced by suitable design of nozzle throat and thrust frame. The CG offset can be reduced by proper vehicle layout design. Attachment misalignments can be reduced by adopting best strategies for vehicle assembly. In order to reduce propellant sloshing effects, depending on the criticalities, slosh baffles have to be provided at the suitable location. Pogo effects can be minimized by the design of structural elements of the propulsion system and with the pogo corrector. The acceptable tail-off characteristic has to be achieved by suitable propellant loading and propulsion subsystems such as valves. Additionally, vehicle subsystems designed to meet the specific functional requirements generate environments such as jet noise, shock and vibration. Therefore the vehicle subsystems have to be designed and validated to operate under such environments.

In addition, the performance dispersions of each of the subsystems and environments also have major impact on other vehicle systems and therefore, these aspects have to be considered in the vehicle design. The dispersions are caused by three factors: (a) error in predicted performance parameters/environments used in the design, (b) improper design, wherein the actual system performance can be different from the expected one, as per design, and (c) random process. The dispersion levels can be reduced by robust design of vehicle subsystems and with the improved prediction strategy. However, the random dispersions and the probable deviated performance of each of the vehicle subsystems have to be suitably considered in the design of vehicle subsystems and mission.

The sources of operating environments which generate various kinds of loads on the vehicle systems under different categories are as given below:

1. *Steady/quasi-steady loads*

- Gravity and thrust
- Propellant tank pressures (pressure loads)
- Thermal loads caused by
 - Propulsion system
 - Cryogenic propellants
 - Aerodynamic heating
- Thrust misalignment, cg offset, thrust offset and differential thrust

2. *Dynamic loads*

- Aerodynamic control forces (due to wind)
- Vehicle flexible structural modes
- Propellant slosh
- POGO oscillations
- Thrust oscillations
- Turbo machinery
- Mechanical shocks

3. *Random vibration environment*

This environment is generated by noises due to

- Jet noise
- Aerodynamic noise

The details of the operating environment, their characteristics and their influences on the vehicle systems design are discussed in the following sections.

6.3 Earth Geometry and Gravity Environment

Space transportation vehicle, during its entire mission from lift-off till satellite injection, is under the influence of Earth gravitational pull. Therefore, the gravitational acceleration has a major impact on the vehicle trajectory parameters. Since the mission design depends on the predicted trajectory of the vehicle, the trajectory thus designed is used as reference and input for vehicle subsystems design. It is therefore essential to consider precise Earth gravitational model in the STS design.

Even though different aspects of Earth's gravity are discussed in different sections of this book, the integrated aspects on Earth model, gravity, shape, etc., which are essential for STS design process, are consolidated in this section. Although it appears like a repetition, it has been presented deliberately here to bring full clarity on the influence of gravity on vehicle design process.

Earth, having mass of about 5.98×10^{24} kg with mean mass density of about 5520 kg/m^3 and rotating about its axis of rotation with the rate of about $0.25^\circ/\text{min}$, may be approximated as a sphere with the radius of about 6367 km. The gravity force acting on the vehicle under the influence of Earth's gravity field is due to the resultant of gravitational force and centrifugal force caused by the Earth's rotation. The gravity force acting on the vehicle is derived from the geopotential, which depends on vehicle position with respect to the Earth in terms of latitude, longitude and altitude. Typically, the gravity force per unit mass of the vehicle (gravitational acceleration) on the surface of the Earth varies from 9.78 m/s^2 at equator to 9.83 m/s^2 at poles.

6.3.1 Earth Shape and Gravitational Potential

In reality, Earth has an irregular shape with 30 % of its surface area covered with rocky material of different size and shape and 70 % with oceans. In addition, Earth is bulged at equator while flattened at poles. The largest local deviations at the rocky area are the Mount Everest (8848 m above local sea level) and the Mariana Trench (10,911 m below local sea level). The maximum distances from the centre of Earth to the surface are at the summits of Mount Chimborazo in Ecuador and Huascaran in Peru. Due to such irregularities, the geopotential is not strictly constant over the surface of Earth. However, for the Earth's shape, a fictitious equipotential surface with mean sea level, which is assumed to be extended into the continents, can be well approximated and the corresponding equipotential is called geophysical geoid. Even though this geoid is smoother than the actual surface, its mathematical form of representation is quite complex. The Earth's potential thus approximated can be expressed in terms of spherical harmonics as given below:

$$U = -\frac{\mu}{r} \left[1 - \sum_{n=2}^{\infty} J_n \left(\frac{R_e}{r} \right)^n P_n(\sin \phi) - \sum_{n=2}^{\infty} \times \sum_{m=1}^n J_{n,m} \left(\frac{R_e}{r} \right)^n P_n^m(\sin \phi) \cos m(\lambda - \lambda_{n,m}) \right] \quad (6.1)$$

where

μ = Earth's gravitational constant, $3.9860253 \times 10^{14} \text{ m}^3/\text{s}^2$

r = Geocentric radius at vehicle location

ϕ = Geocentric latitude

λ = Geographic longitude

R_e = Mean equatorial radius of Earth

$P_n(\sin \phi)$ is Legendre's polynomial of degree n in $\sin \phi$

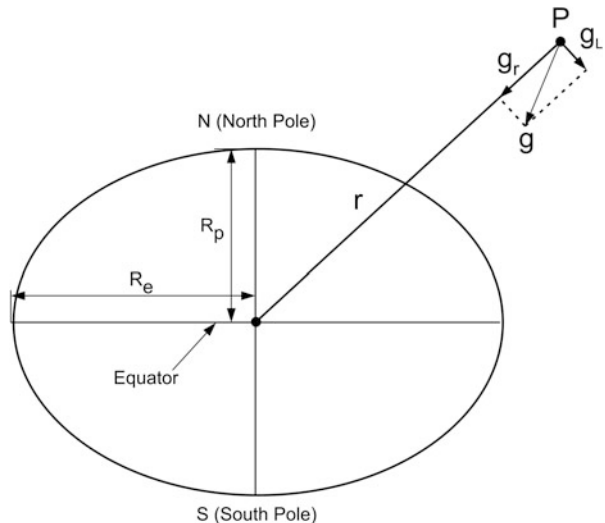
$P_n^m(\sin \phi)$ is associated Legendre function of degree n and order m

J_n , $J_{n,m}$ and $\lambda_{n,m}$ are numerical coefficients, represent mass distributions

The term $-\mu/r$ is the maximum contributing factor in Eq. (6.1), which represents the gravitational potential corresponding to spherical Earth and referred to as Newtonian gravitational potential, whereas other terms are out of deviations of Earth shape from sphere. It is to be noted that with the assumption that the origin of reference frame considered for the analysis coincides with the Earth's centre, the terms with $n = 1$ are absent. The terms in Legendre's polynomial J_n are called zonal harmonics whereas the terms in the associated Legendre function $J_{n,m}$, $n \neq m$ are called tesseral harmonics and terms with $J_{n,m}$, $n = m$ are referred as sectorial harmonics. The zonal harmonics represent the deviation of gravitational potential along the latitude direction (north–south) with respect to the Newtonian one, whereas the tesseral and sectorial harmonics represent the corresponding deviation along the longitudinal direction (east–west). The term containing J_2 represents the oblateness of Earth and the term J_3 describes the Earth as pear shaped one, whereas $J_{2,2}$ describes the ellipticity of equator. The value of J_2 is close to 1.0826269×10^{-3} whereas the remaining J_n and $J_{n,m}$ values are of the order of 10^{-6} or less.

The Earth makes one revolution in a day about its axis of rotation whereas the satellite orbits are inertially fixed; the effects due to tesseral and sectorial harmonics on satellite orbits are assumed to be averaged out except for the geostationary orbit. Since the satellite always keeps fixed position with respect to the Earth, the orbit is sensitive to the longitudinal variation of gravity. Therefore, the zonal harmonics has the major impact on satellite orbits. For the space transportation system applications too, neglecting the tesseral harmonics term due to their small values, the Earth shape can be approximated to the oblate spheroid as shown in Fig. 6.2. The gravity force at a typical position of the vehicle is also shown in Fig. 6.2, wherein the resultant gravity acceleration \mathbf{g} does not pass through centre of the Earth and has a radial component \mathbf{g}_R and a lateral contribution \mathbf{g}_L . For the same radial distance r from the centre of Earth, \mathbf{g}_R and \mathbf{g}_L vary across the latitude ranging from 0 to $\pm 90^\circ$.

Fig. 6.2 Earth shape and gravity



For the very short-duration flight, these variations do not have much effect on the trajectory. However, for the orbital mission trajectory extending beyond 5000 km down range, the gravity variation due to Earth asphericity has significant influence on the trajectory parameters and therefore need to be considered.

Considering small values of J_n ($n > 3$) and $J_{n,m}$, for general applications, the geoid can be approximated to an oblate spheroid or ellipsoid, which is obtained by rotating an ellipse about minor axis. The axes of the ellipse are selected such that the deviations of the geoid with respect to the ellipsoid are minimized. The reference ellipsoid thus obtained with semi-major axis of 6378.137 km (corresponding to equatorial radius of Earth) and semi-minor axis of 6356.755 km (corresponding to polar radius of Earth) is being used in Astrodynamics and space transportation vehicle applications.

Generally, this ellipsoid is represented by the equatorial radius (R_e) and one of the three parameters viz., (1) the reciprocal of the flattening, (2) polar radius (R_p) and (3) eccentricity. These parameters are related as given below:

$$f = \frac{R_e - R_p}{R_e} \quad (6.2)$$

$$e^2 = 2f - f^2 \quad (6.3)$$

$$R_p = R_e(1 - f) = a\sqrt{1 - e^2} \quad (6.4)$$

where

R_e = Equatorial radius of Earth (6378.137 km)

R_p = Polar radius of Earth (6356.755 km)

and

$$(1/f) = 298.257223563$$

These values are defined for the WGS84 ellipsoid, used by the GPS devices.

The major deviation of the geoid with respect to the reference ellipsoid is obtained by the satellite orbit perturbations caused by the actual gravitational deviations with respect to the one used for the system design. The variations of orbital parameters show that the geoid radius at North Pole is longer than South Pole radius by 38 m. The northern middle latitude is flattened whereas the southern middle latitude is bulged out, thus describing the pear shape of Earth. Similarly, the geoid's equator is having small deviations from a circle and obtained by the orbital perturbations of geostationary orbit. This orbit is sensitive to longitudinal variations of gravitational acceleration with respect to Earth. The major axis of the equatorial ellipse of the geoid intersects the circle of reference spheroid at the longitudes of about 18°W and 162°E and the major axis is longer by about 138 m with respect to the minor axis. Therefore, the better application of the geoid is an ellipsoid with corrections superimposed over that.

6.3.2 Gravitational Acceleration

Assuming negligible effects of tesseral harmonics, sectorial harmonics and higher-order zonal harmonics, the gravitational potential at a radial distance r of a launch vehicle from the centre of Earth can be approximated very close to the geoid as given below:

$$U = -\frac{\mu}{r} \left[1 - \sum_{n=2}^4 J_n \left(\frac{R_e}{r} \right)^n P_n(\sin \theta) \right] \quad (6.5)$$

where

$$\mu = 3.9860253 \times 10^{14} \text{ m}^3/\text{s}^2$$

$$R_e = 6,378,140 \text{ m}$$

$$J_2 = 1.0826269 \times 10^{-3}$$

$$J_3 = -0.00254 \times 10^{-3}$$

$$J_4 = -0.00161 \times 10^{-3}$$

Legendre's polynomials of degrees 2, 3, 4 in "θ" are expressed as

$$P_2(\theta) = \frac{3}{2}\theta^2 - \frac{1}{2} \quad (6.6)$$

$$P_3(\theta) = \frac{5}{2}\theta^3 - \frac{3}{2} \quad (6.7)$$

$$P_4(\theta) = \frac{1}{8}(35\theta^4 - 30\theta^2 + 3) \quad (6.8)$$

Assuming the vehicle's position is represented with respect to the Earth-centred Cartesian reference frame with X and Y axes lying in equatorial plane and Z axis along North Pole as given in Fig. 6.3, then

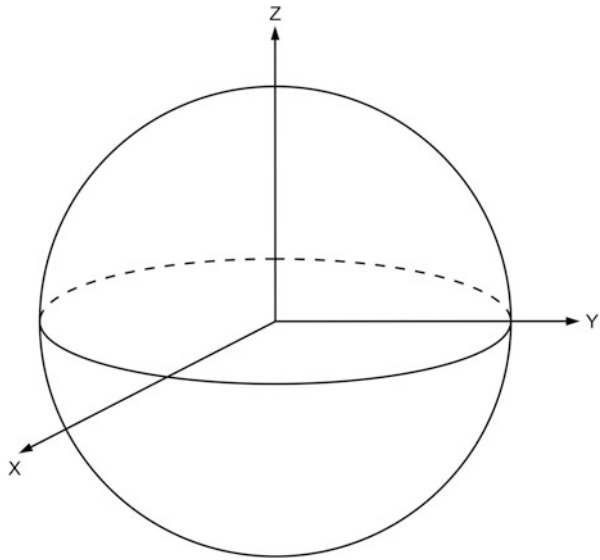
$$\sin \theta = \frac{z}{r} \quad (6.9)$$

and therefore, the gravitational potential represented in Eq. (6.5) can be written as

$$U = -\mu \left[\frac{1}{r} - \frac{J_2}{2} R_e^2 \left(3 \frac{z^2}{r^5} - \frac{1}{r^3} \right) - \frac{J_3}{2} R_e^3 \left(5 \frac{z^3}{r^7} - 3 \frac{z}{r^5} \right) - \frac{J_4}{8} R_e^4 \left(35 \frac{z^4}{r^9} - 30 \frac{z^2}{r^7} + \frac{3}{r^5} \right) \right] \quad (6.10)$$

and the gravitational acceleration on the vehicle along the reference frame can be computed using

Fig. 6.3 Typical earth centered coordinate system



$$g_x = -\frac{\partial U}{\partial x} \quad (6.11)$$

$$g_y = -\frac{\partial U}{\partial y} \quad (6.12)$$

$$g_z = -\frac{\partial U}{\partial z} \quad (6.13)$$

$$g_x = -\frac{\mu x}{r^3} \left[1 + \frac{3J_2}{2} \left(\frac{R_e}{r} \right)^2 \left\{ 1 - 5 \left(\frac{z}{r} \right)^2 \right\} + \frac{5J_3}{2} \left(\frac{R_e}{r} \right)^3 \left\{ 3 \left(\frac{z}{r} \right) - 7 \left(\frac{z}{r} \right)^3 \right\} - \frac{15J_4}{8} \left(\frac{R_e}{r} \right)^4 \left\{ 1 - 14 \left(\frac{z}{r} \right)^2 + 21 \left(\frac{z}{r} \right)^4 \right\} \right] \quad (6.14)$$

$$g_y = -\frac{\mu y}{r^3} \left[1 + \frac{3J_2}{2} \left(\frac{R_e}{r} \right)^2 \left\{ 1 - 5 \left(\frac{z}{r} \right)^2 \right\} + \frac{5J_3}{2} \left(\frac{R_e}{r} \right)^3 \left\{ 3 \left(\frac{z}{r} \right) - 7 \left(\frac{z}{r} \right)^3 \right\} - \frac{15J_4}{8} \left(\frac{R_e}{r} \right)^4 \left\{ 1 - 14 \left(\frac{z}{r} \right)^2 + 21 \left(\frac{z}{r} \right)^4 \right\} \right] \quad (6.15)$$

$$g_z = -\frac{\mu z}{r^3} \left[1 + \frac{3J_2}{2} \left(\frac{R_e}{r} \right)^2 \left\{ 3 - 5 \left(\frac{z}{r} \right)^2 \right\} + \frac{5J_3}{2} \left(\frac{R_e}{r} \right)^3 \left\{ \frac{-3}{5} \left(\frac{r}{z} \right) + 6 \left(\frac{z}{r} \right) - 7 \left(\frac{z}{r} \right)^3 \right\} - \frac{15J_4}{8} \left(\frac{R_e}{r} \right)^4 \left\{ 5 - \frac{70}{3} \left(\frac{z}{r} \right)^2 + 21 \left(\frac{z}{r} \right)^4 \right\} \right] \quad (6.16)$$

6.3.3 Vehicle Position Definition

The position of a vehicle at any instant of flight over Earth is generally represented in terms of altitude, latitude and longitude. The ellipsoid shape of Earth makes two definitions for the latitude. The geocentric latitude ϕ_{GC} is the angle between the vehicle position vector and equatorial plane as given in Fig. 6.4. The vehicle altitude h is measured along the vertical distance from the vehicle to the surface of Earth, which makes 90° with respect to the local horizontal and does not pass through the centre of the Earth. It meets the equatorial plane at an angle called geodetic latitude ϕ_{GD} as represented in Fig. 6.4. The maximum difference between ϕ_{GD} and ϕ_{GC} is about $11.5'$ at the geodetic latitude of $45^\circ 5'$. In order to make the computations easier without losing accuracy for a typical STS mission, a better approximation can be made as given in Fig. 6.5. Using the above approximation, the trajectory parameters can be computed as given below:

$$\phi_{GC} = \sin^{-1}(z/r) \quad (6.17)$$

$$\phi_{GD} = \tan^{-1}\{k \tan \phi_{GC}\} \quad (6.18)$$

where

$$k = (R_e/R_p)^2 \quad (6.19)$$

Fig. 6.4 Definition of vehicle location

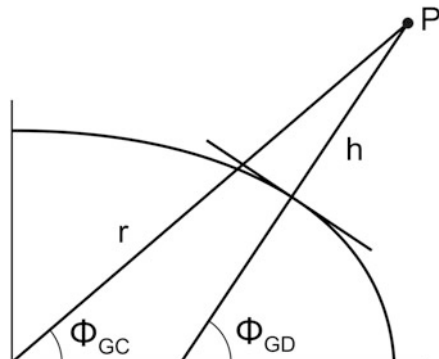
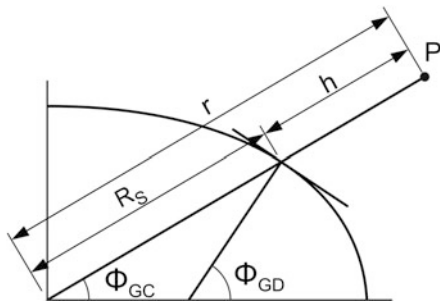


Fig. 6.5 Approximations on the location parameters



$$r = (x^2 + y^2 + z^2)^{1/2} \quad (6.20)$$

The radius of Earth corresponding to ϕ_{GC} is given by

$$R_s = R_e [1 + (k - 1) \sin^2 \phi_{GC}]^{1/2} \quad (6.21)$$

and the altitude is given by

$$h = r - R_s \quad (6.22)$$

If the X -axis of the reference frame coincides with the Greenwich meridian, then longitude of the vehicle is given by

$$\lambda = \tan^{-1}(y/x) \quad (6.23)$$

It is to be noted that the maximum errors in altitude and radius of Earth computations using the above expressions are of the order of 100 m, which is sufficient for the STS vehicle applications.

6.3.4 Effects of Earth Oblateness on STS Mission Target

Oblateness of Earth brings two important aspects related to mission design process: (1) orbit specification for the mission target, (2) orbital altitude definition. Satellite orbital elements of an STS mission can be uniquely defined with position vector \mathbf{r} and velocity vector \mathbf{V} achieved at the time of satellite injection with respect to a Cartesian coordinate system, beyond which the STS does not have any control over satellite orbit. These orbital elements remain constant provided the gravitational field is corresponding to the Newtonian gravitational potential as defined by $-\mu/r$. However, due to the ellipsoid shape of the Earth, in addition to the Newtonian gravitational potential, variations in gravity accelerations act on the satellite at further instants as given in Fig. 6.2 and Eqs. (6.14, 6.15, and 6.16). These gravity

variations change the orbital parameters continuously as explained in Chap. 3. The orbital parameters computed at any instant where the gravity perturbations suddenly disappear are treated as osculating orbital elements. Therefore, osculating orbital parameters are continuously varying and these elements are tangential to the actual orbital elements at that instant. Thus in general terms, the osculating orbital elements are defined as

$$\zeta_{\text{osc}} = \zeta_{\text{mean}} + \Delta\zeta_{\text{pert}} \quad (6.24)$$

where

ζ_{osc} = Osculating orbital element, which is computed using instantaneous \mathbf{r} , \mathbf{V} (varying along the trajectory)

ζ_{mean} = Mean orbital elements, which remain to be constant

$\Delta\zeta_{\text{pert}}$ = Mean perturbations caused by the Earth's asphericity

The real orbital elements ζ_{osc} at any instant of flight are varying depending on the satellite location with respect to Earth. Imaginary orbital elements ζ_{mean} remain constant. Therefore, once the expected longitude, latitude and altitude of satellite injection for a launch vehicle are given, satellite team can define the osculating orbital elements which meet the mean orbital elements of the satellite. These osculating orbital parameters become targets for launch vehicle mission.

As can be seen from Figs. 6.4 and 6.5, the local radius of Earth is a function of geodetic latitude. Therefore, the launch vehicle altitude at any instant of its flight depends on the latitude. Satellite orbital altitude also depends on the radius of Earth used for the altitude computations. Generally, the radius location of satellite injection can vary during flight and apogee and perigee need not correspond to the injection latitude. In order to get a unified definition for satellite orbital heights, one of the following approaches is needed:

1. Using satellite injection state vector \mathbf{r} , \mathbf{V} , compute the exact location of perigee/apogee; compute the Earth radial distance at these locations and compute orbital altitudes as given in Eq. (6.22).
2. For the near-circular orbits, a small variation in injection parameters can cause the deviation of the apogee/perigee locations to a large extent. Since the maximum variation of Earth radius is up to 21 km, orbital altitude by such definition introduces variation by 21 km which may lead to wrong information. Therefore, under these circumstances, it is advisable to use a fixed value of radius of Earth R_e .

Alternatively, in order to avoid such ambiguities, it is better to use the apogee/perigee radial distance or semi-major axis for defining the orbital parameters.

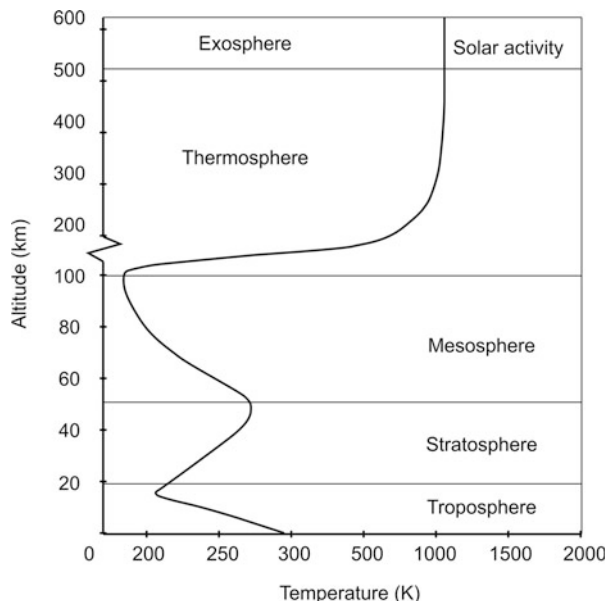
6.4 Atmospheric Properties

Atmosphere plays a significant role in the launch vehicle design. The aerodynamic flow characteristics and flight environment are decided by the external shape of the vehicle. This, coupled with atmospheric properties and flight trajectory parameters during the crucial atmospheric flight phase, causes steady and unsteady aerodynamic forces on the vehicle, which form major input for the STS subsystems and mission trajectory design.

Atmosphere is highly dynamic and its properties viz., temperature, pressure, density and molecular weight vary with altitude, latitude (geographical variation), time of day (diurnal variation), day of the year (seasonal variation), solar and geomagnetic activities. The atmosphere gets thinner as altitude increases and there is no clear boundary between atmosphere and outer space. Depending on the applications, the extent of atmosphere which has significant influence on the vehicle design has to be used. Atmospheric pressure and density reduce as altitude increases whereas temperature profile has a unique pattern with altitude. Based on the temperature variations, the atmosphere is divided into five different layers as represented in Fig. 6.6 and explained below:

Troposphere: This is the lowest layer of Earth atmosphere. In this layer, the temperature decreases with altitude and this layer extends from sea level to about 8–9 km over the poles and 17–18 km over the equator. This is the region of atmospheric turbulence and contains about 80 % of the total mass of the atmosphere, which is about 5×10^{18} kg. At the end of troposphere, the

Fig. 6.6 Temperature variation with altitude



atmospheric pressure is about 24 % and density is about 32 % of their respective values at sea level.

Stratosphere: This is the second layer of Earth atmosphere, which starts at about 8–18 km and extends up to 50 km, wherein temperature increases. At the end of stratosphere, both density and pressure are about 0.08 % of their sea-level values.

Mesosphere: The next level of atmosphere is mesosphere which starts at 50 km and extends up to 85–90 km, wherein the temperature decreases with altitude.

Thermosphere: This is the fourth layer of atmosphere, which starts from 85 to 90 km and extends up to about 500 km. Temperature increases rapidly with respect to altitude in the lower portion of thermosphere till it reaches the exospheric temperature (T_{∞}) and beyond which, the temperature remains constant. The atmospheric properties in thermosphere are influenced significantly by solar activity. Therefore, the height of this atmosphere layer generally varies between 350 and 800 km depending on the solar activity.

Exosphere: The atmosphere beyond thermosphere is called exosphere.

The region between two layers is called pauses of lower layer, i.e. tropopause is the one where troposphere ends at 8–18 km. Similarly, stratopause, mesopause, etc. can be defined accordingly.

Apart from the above atmospheric layers, several other layers are defined by their properties within these five principal layers. Typical ones are

1. Ozone layer: Atmosphere layer wherein ozone concentration is higher. Ozone layer is within 15–35 km, which is within the stratospheric layer.
2. Ionosphere: This is part of the atmosphere that is ionized by solar radiation. This layer is defined from 50 to 1000 km.

Generally, atmosphere up to 90 km is called lower atmosphere, wherein molecular weight is almost constant and atmospheric properties' dispersions are also less. The atmosphere above 90 km is called upper atmosphere which is highly dynamic and atmospheric properties in these regions vary significantly with respect to time, location as well as solar activities as given in Figs. 6.7 and 6.8.

Since the atmosphere is highly dynamic and atmospheric properties vary with respect to geographical locations and solar activities, for an STS vehicle mission from a specified launch site, mean atmosphere of that region is generally used. The standard atmosphere is generated using measured data on atmospheric properties over the years as well as data generated using suitable models assuming mean input parameters for solar and geomagnetic activities for the specified location, day, time, etc. These atmospheric properties along with the corresponding parameter dispersions are used for the STS vehicle design process.

A typical standard atmospheric model used for launch vehicle design is given in Fig. 6.9. The parameters represented in Fig. 6.9 are mean values and there are

Fig. 6.7 Temperature dispersions

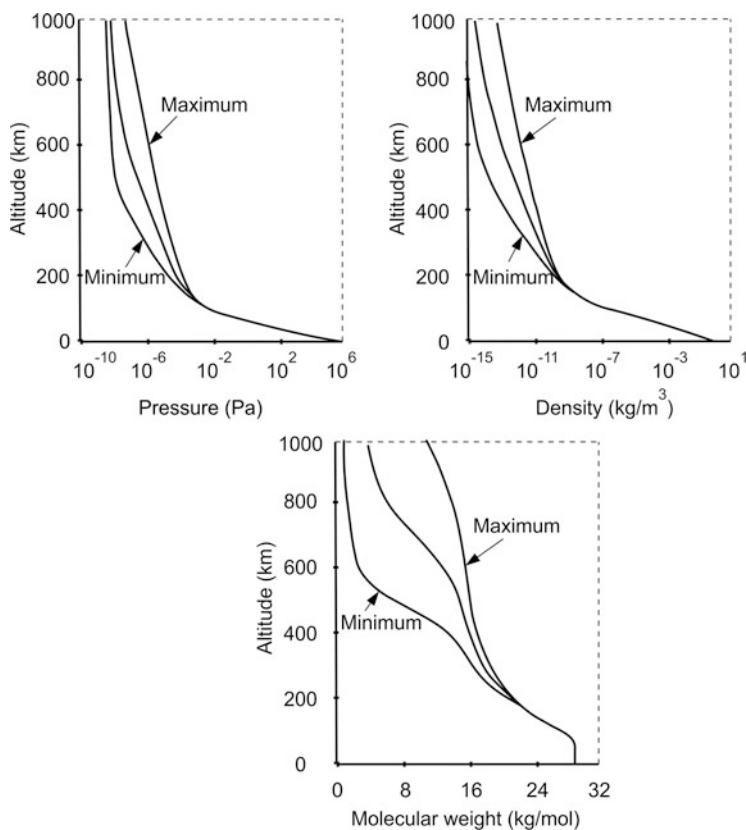
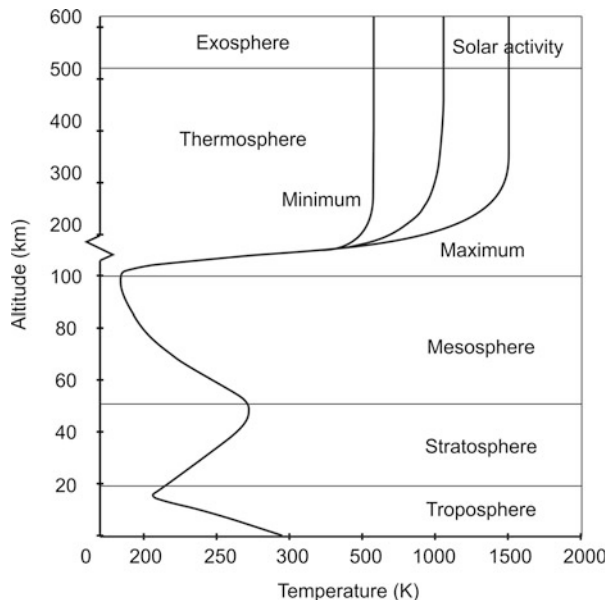
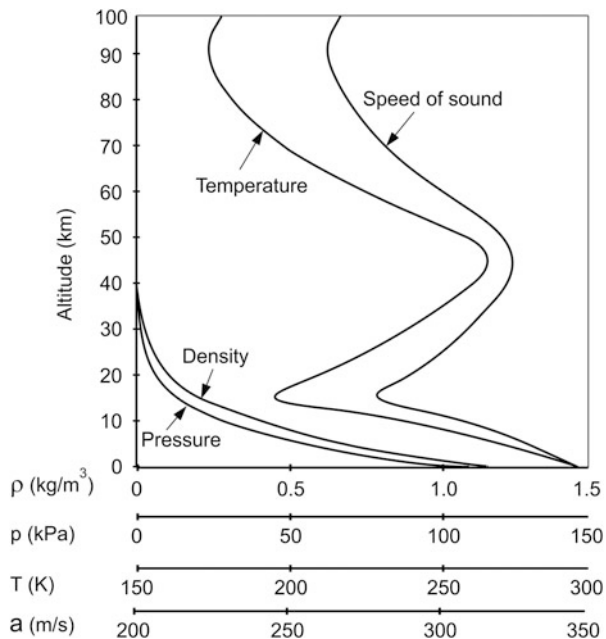


Fig. 6.8 Atmospheric properties dispersions

Fig. 6.9 Typical standard atmosphere properties



dispersions on these parameters. As the mean standard atmosphere is derived from the basic measurement of temperature, any dispersion on the temperature measurement leads to dispersions on pressure and density. Therefore, dispersions on the atmospheric properties are specified in terms of variations in temperature. Typical values are: up to 35 km, temperature dispersion can be 9 K whereas beyond 35 km, temperature dispersion can go as high as 20 K. However, beyond 120 km, since the atmospheric properties' variations are larger, it is advisable to use the lower and upper bounds of the atmosphere for the STS vehicle subsystem design. Generally, for space transportation vehicles, atmosphere has measurable effects up to about 100 km, whereas upper atmosphere data is required for the satellite system design.

Some of the relations between atmospheric properties, useful for the launch vehicle design applications, are given below:

The density ρ is given by

$$\rho = \frac{P}{RT} \quad (6.25)$$

where

P = Pressure (P_a)

T = Temperature (K)

R = Gas constant = $287.05 \text{ m}^2/\text{s}^2(\text{°K})$

$$R = \frac{\mathfrak{R}}{M} \quad (6.26)$$

\mathfrak{R} = Universal Gas Constant = 8314.32 $\frac{J}{(^\circ K \text{-mole})}$

M = Molecular weight

Speed of sound at any altitude is given by

$$a = \sqrt{\gamma RT} \quad (6.27)$$

where

γ = Ratio of specific heats = 1.4

6.5 Aerodynamic Environment

Whether the vehicle is on the launch pad or having atmospheric phase of flight the aerodynamic forces acting on a space transportation system are the major factors to be considered for the vehicle systems and mission design process. The aerodynamic environment of the vehicle during atmospheric flight phase can be classified into (1) steady loads, (2) unsteady loads and (3) aeroacoustic environment to the vehicle systems. These loads depend mainly on the vehicle external aerodynamic characteristics, trajectory parameters, atmospheric properties and environment parameters such as angle of attack. Different flight regimes such as subsonic, transonic, supersonic and hypersonic phases greatly influence the type of aerodynamic loading as well as its magnitude.

Aerodynamic environment to the vehicle is caused by (1) aerodynamic characteristics of the vehicle and (2) external influences. The external sources such as wind-induced angle of attack, along with the aerodynamic characteristics of the vehicle, produce aerodynamic drag and lateral disturbance forces viz., normal and side forces. Depending on the aerodynamic characteristics of the vehicle, drag force and aerodynamic environments such as unsteady buffet loads and aerodynamic noise can occur on the vehicle systems during various regimes of flight even without external influences. However, the level of severity of such environments increases with the influence of external sources such as wind. The steady aerodynamic forces acting on the vehicle during entire regime of atmospheric flight phase is given as

$$F_{AD} = qSC_D(M, \alpha, \beta, R_e) \quad (6.28)$$

$$F_{AN} = qSC_N(M, \alpha, \beta, R_e) \quad (6.29)$$

$$F_{AS} = qSC_S(M, \alpha, \beta, R_e) \quad (6.30)$$

where q is dynamic pressure, S is reference area, C_D , C_N , C_M are aerodynamic drag, normal and side force coefficients which are functions of Mach number, M , angle of attack in pitch plane, α , angle of attack in yaw plane, β , and Reynolds number R_e .

In order to reduce the vehicle loads, generally the vehicle is flown with small angles of attack. For such small values, the aerodynamic coefficients C_D , C_N , C_S given in Eq. (6.28) to Eq. (6.30) can be linearized as given by

$$F_{AD} = qS[C_{D_0} + C_{D_\alpha}\alpha] \quad (6.31)$$

$$F_{AN} = qS[C_{N_0} + C_{N_\alpha}\alpha] \quad (6.32)$$

$$F_{AS} = qS[C_{S_0} + C_{S_\beta}\beta] \quad (6.33)$$

The dynamic pressure q in the above equations are given as

$$q = \frac{1}{2}\rho V_R^2 \quad (6.34)$$

where ρ is atmospheric density and V_R is relative velocity of the vehicle with respect to the atmosphere including wind. The coefficients C_{D_0} , C_{N_0} , C_{S_0} are the aerodynamic drag, normal and side force coefficients at zero angles of attack whereas C_{D_α} , C_{N_α} , C_{S_β} are slopes of the corresponding coefficients with respect to angle of attack in the specified plane, α is the angle of attack of the vehicle in pitch plane and β is the angle of attack of the vehicle in yaw plane. The aerodynamic coefficients C_{D_0} , C_{D_α} , C_{N_0} , C_{N_α} , C_{S_0} , C_{S_β} are functions of Mach number, Reynold's number and vehicle external shape and configuration. Generally these aerodynamic coefficients are generated through wind tunnel tests using scaled-down models or through computational fluid dynamics (CFD) computations.

For the axi-symmetric bodies such as general vehicle configuration, C_{N_0} and C_{S_0} are negligible and $C_{D_0} \neq 0$. Therefore, it can be seen that there is always drag force acting on the vehicle which has influence on the vehicle performance as it is just opposite to the vehicle thrust force direction. On the other hand, the aerodynamic normal and side forces caused by the angles of attack combined with the vehicle aerodynamic characteristics are the main disturbance forces. They destabilize the vehicle during atmospheric flight phase greatly and influence the design of the vehicle structural and control systems. Additionally, the drag force also influences the structural design.

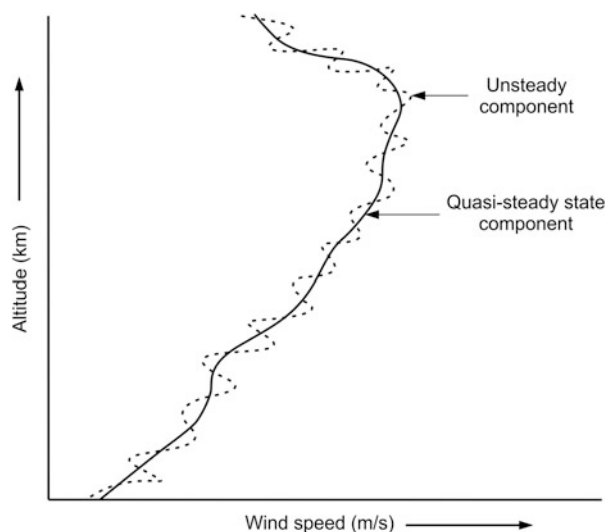
In addition to the steady forces as explained above, the unsteady loads such as aerodynamic buffet loads influence the structural design. The aerodynamic noise imparts severe environments to the vehicle subsystems such as sensitive avionics and satellite systems. Therefore, suitable systems have to be designed to protect the sensitive elements against such environments. Once the systems are designed, it is essential to validate the systems in the expected hostile flight environment. These aspects are discussed in later part of this chapter. The total aerodynamic aspects are discussed in Chap. 10 on vehicle aerodynamic design.

6.6 Atmospheric Winds

Atmospheric winds are caused by the three-dimensional motion of air, which consists of large- to small-scale spatial and temporal variations. The wind variations are caused by the revolution of Earth, motion of Earth around the Sun, geographical characteristics and the available solar energy. This energy drives large-scale circulation of air due to the imbalances between the atmospheric regimes, creating winds. Due to the motion of the Earth around the Sun, seasonal wind variations occur which can be seen in the synoptic weather changes of all locations. The dominating factors which cause drastic wind variations are solar activity at a specified location, land-sea influence, geographical locations, terrain type, water and vegetation. Due to the above factors, each geographical location on the Earth has a specific pattern of wind for each season of the year. There are spatial and temporal variations of the wind over the specific pattern. Therefore, the wind over a specified geographical location can be expressed as function of altitude. At each altitude there are temporal variations of wind speed. The entire wind profile over a specified geographical location can be divided into quasi-steady-state wind (defined as a time average over 2 minutes) and unsteady components as represented in Fig. 6.10.

At a given altitude, wind velocity is in random direction with major components in the horizontal plane along with a smaller vertical component. Therefore, the horizontal velocity can be considered to be consisting of quasi-steady-state as well as unsteady components whereas the vertical component has only unsteady components such as turbulence. Where the vehicle flight is almost vertical, considering the frequency content, the vertical component can be neglected. Therefore the horizontal component plays a major role in the vehicle dynamics during atmospheric flight. The horizontal component of wind velocity can be represented in two

Fig. 6.10 Typical wind profile



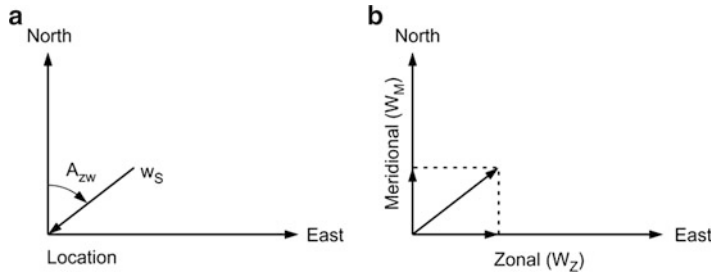


Fig. 6.11 Wind representations (a) Speed and azimuth (b) Zonal – meridional component

forms as shown in Fig. 6.11: (1) at a specified location, wind speed and direction with respect to the local north and (2) wind velocity along the east–west direction (zonal component) with wind along eastward direction as positive, and north–south direction (Meridional component) with wind along northward direction as positive.

Wind plays a major role in the vehicle systems design process as it influences the vehicle trajectory, structural and control system design during atmospheric flight phase. Therefore, it is essential that the vehicle response to the winds must be carefully evaluated to arrive at a robust STS design to meet the specified functional requirements. This section discusses the wind effects on the vehicle, important wind characteristics, wind statistics and the possible design winds.

6.6.1 Wind Effects on Space Transportation Systems

When the vehicle is on the launch pad, generally the vehicle is exposed to wind for a specified duration before lift-off. Wind velocity profile along the vehicle length as shown in Fig. 6.12a causes the dynamic pressure variations at various locations of the vehicle. This dynamic profile along with the external shape of the vehicle defines the local normal force which causes a disturbance profile along the vehicle length as given by

$$F_{AN}(l) = \frac{1}{2} \rho_{SL} V_w^2(l) S(l) C_N(l) \quad (6.35)$$

where ρ_{SL} is the density of air at sea level, $V_w(l)$ is the wind velocity at location “l” on the vehicle, $C_N(l)$ is the sectional aerodynamic normal force coefficient and $S(l)$ is the sectional area at the specified location. The sectional forces result in the integrated load and moment about the vehicle anchoring point at base shroud and this load has the tendency to destabilize the vehicle on the launch pad. Therefore, it is essential that the vehicle anchoring mechanism as well as the vehicle base shroud is designed for such loads in addition to the other loads. The net wind load acting on

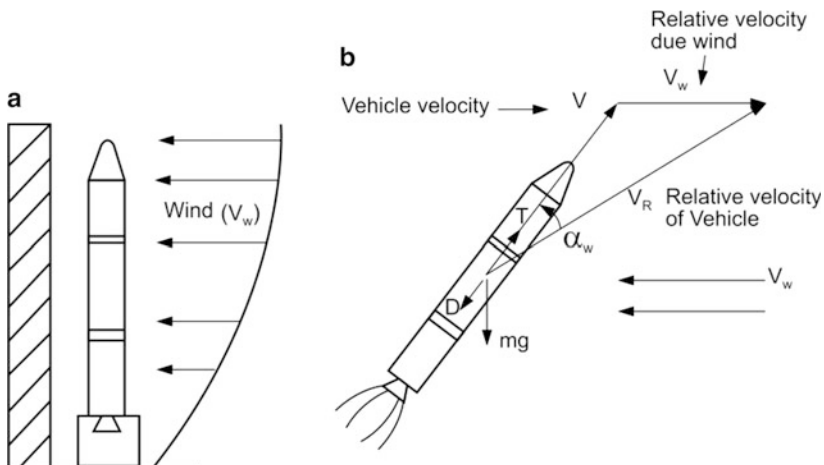


Fig. 6.12 Impact of wind on vehicle (a) Wind on vehicle at launch pad (b) Inflight wind on vehicle

the vehicle has two components: (1) steady load due to the quasi-steady-state wind and (2) unsteady load caused by the unsteady component of the ground wind. In addition to the above, due to the bluff body nature of the vehicle, the wake caused by the wind behind the vehicle generates unsteady load. The wind can be from any random direction and in case the wind is blowing from launch tower towards the vehicle, the wake caused by the tower impinges on the vehicle, which in turn imparts unsteady loads. These additional loads also need to be considered for the vehicle systems design, which are discussed in the chapters on aerodynamic design and structural systems design.

The in-flight winds cause angle of attack on the vehicle as shown in Fig. 6.12b. Assume vehicle velocity V achieved by the propulsion system is along the longitudinal axis of the vehicle as shown in the above figure. When there is wind, represented by wind velocity (V_w), with respect to the atmosphere, the relative velocity of the vehicle is shifted away from the longitudinal axis as shown in Fig. 6.12b. The angle between the relative velocity vector and the vehicle longitudinal axis is called angle of attack.

For axi-symmetric vehicle, when there is no angle of attack, only aerodynamic drag force is acting on the vehicle. When there is angle of attack, additionally aerodynamic lateral forces are also acting on the vehicle as given by Eqs. (6.31, 6.32, and 6.33) which tend to destabilize the vehicle during flight. This aerodynamic disturbing force has major influence on the structural and control systems designs as explained in appropriate chapters.

Assuming the vehicle and trajectory parameters are in frozen conditions (for the specified location on the trajectory and for the specified aerodynamic, structural and

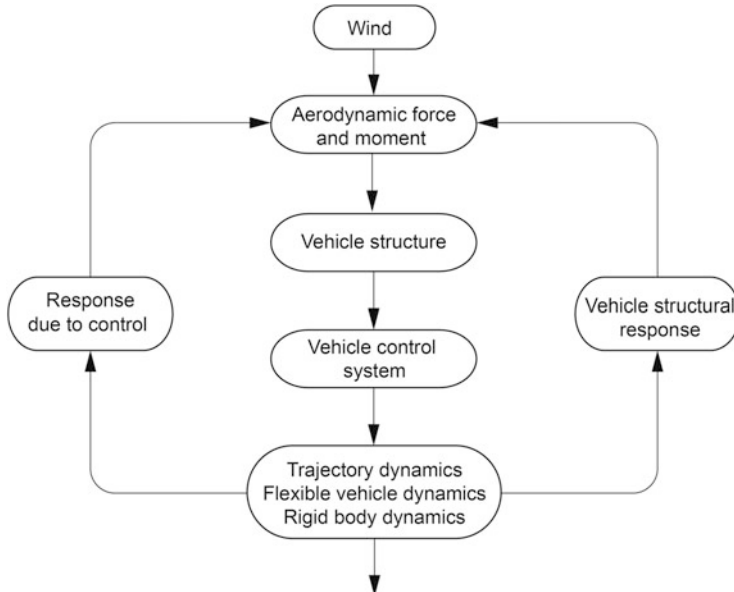


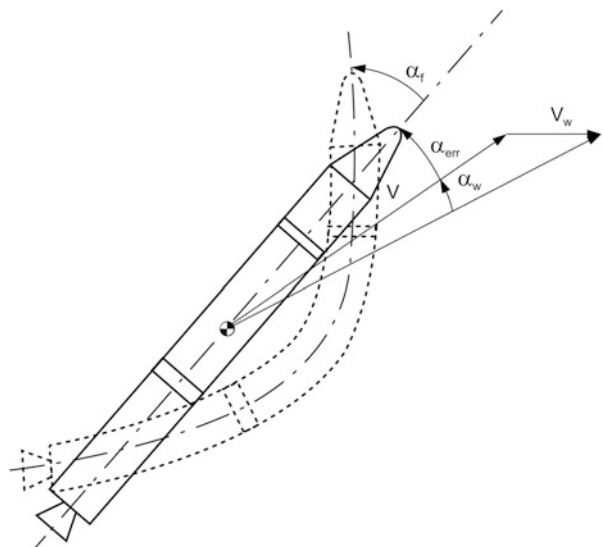
Fig. 6.13 Effects of winds

mass characteristics of the vehicle), the in-flight loads are generated in two ways: (1) externally imparted loads, generated by wind, and (2) loads generated by the vehicle response. The vehicle response generated load in turn has two components as explained in Fig. 6.13. When the control system is attempting to stabilize the vehicle, the required orientation cannot be achieved instantaneously. Low-frequency (rigid body) response of the vehicle under such environments generates the attitude error, which reflects as angle of attack, α_{err} . Additionally, once the control forces and aerodynamic forces are acting on the vehicle structure, the elastic modes of the vehicle get excited which in turn produce local angle of attack, α_f . Therefore, the externally induced aerodynamic force is due to wind angle of attack α_w , whereas the aerodynamic force due to vehicle response is through angle of attack α_{err} and α_f as represented in Fig. 6.14. The total angle of attack α is given by

$$\alpha = \alpha_w + \alpha_{\text{err}} + \alpha_f \quad (6.36)$$

The vehicle flexibility effects sensed by the sensors alter the control command and hence the vehicle structural and control systems are coupled. This interaction is further coupled with outer loop trajectory dynamics. The aerodynamic disturbance and control forces affect subsequently the trajectory dynamics and take the vehicle to another state, represented in terms of new altitude and velocity. These changed states along with the updated vehicle characteristics in terms of aerodynamic coefficients and mass properties cause changes into externally induced disturbances

Fig. 6.14 Components of angle of attack



and also the vehicle dynamics. Therefore, it can be seen that, with the presence of atmospheric wind, the entire vehicle systems, trajectory and environment are totally coupled.

Atmospheric wind has specific characteristics which has different impact on the vehicle systems. Therefore, it is necessary to understand the wind characteristics which influence the vehicle systems and carry out the vehicle systems design to achieve the robust design.

6.6.2 Influence of Wind Characteristics

The wind characteristics which influence the STS design are

1. Magnitude of quasi-steady-state wind speed
2. Wind shear in the quasi-steady-state wind speed
3. Unsteady wind components including wind gust and turbulence

Wind shear is the rate of change of wind speed with respect to altitude. As wind is a vector quantity, the wind shear includes changes of wind direction with respect to altitude also. Therefore, the wind shear is the vector difference of wind velocities between two altitudes divided by the height interval.

Wind gust is a finite increase or decrease in the wind speed relative to the quasi-steady-state value over a very short interval of time or height. It is basically a sudden change in the wind speed and/or direction, which may be filtered out during the process of generating the quasi-steady-state wind. Therefore, the measured quasi-steady-state wind may or may not consist of the wind gust. As per literature, the maximum wind gust measured is about 9 m/s. It is to be noted that change in the

wind speed or direction induces angle of attack, α_w which in turn induces large aerodynamic disturbance loads on the vehicle. Therefore, it is essential to consider the gust factor also in the vehicle systems design process.

Generally, the peak wind speed occurs at the altitude regime of 10–15 km, and in most of the cases around the same period, the dynamic pressure of STS also peaks. Wind shears are generally associated with peaking of wind and therefore wind shears are also maximum in the altitude range of 10–15 km. Therefore, high wind speed along with high wind shear has to be considered for the estimation of vehicle loads due to in-flight wind. However, it is not possible to measure the wind gust in quasi-steady-state measurement strategies, it is important to note that gust can occur at all altitudes and this aspect has to be considered at all regimes of flight, depending on the functional criticality of the vehicle systems.

Different wind characteristics and their impact on the vehicle systems design are explained below:

(a) *Influence of Quasi-Steady-State Wind Speed*

Two typical examples of quasi-steady-state wind velocities measured at a typical launch site location in different seasons, climates and weather conditions are given in Fig. 6.15. It can be seen that the wind velocity profile can slowly increase until reaching a peak value and then reduces back (Fig. 6.15a). Wind velocity can have a lower magnitude in yet another day (Fig. 6.15b). In Fig. 6.15a, even though the peak wind velocity is reaching up to 62 m/s, it is to be noted that the wind variation with respect to altitude is rather small. These types of winds can be considered as low-shear, high-magnitude winds.

Wind magnitude causes angle of attack and aerodynamic force, F_A . In order to avoid destabilization of the vehicle due to F_A , the vehicle control systems produce control force F_C as shown in Fig. 6.16. The lateral forces F_A and F_C cause lateral velocity, called vehicle drift, which acts normal to the vehicle longitudinal axis as represented in Fig. 6.16. As the vehicle velocity is slowly building up, the lateral velocity increases and drift magnitude also increases when the slowly building velocity is more. Therefore, for the case of the high-magnitude persisting wind (typical of wind with low wind shear), the drift velocity produces an angle of attack α_d as represented in Fig. 6.16. Under such conditions, the net angle of attack is given by

$$\alpha = (\alpha_w - \alpha_d) + \alpha_{err} + \alpha_f \quad (6.37)$$

where

$$\alpha_d = \frac{V_d}{V_R} \quad (6.38)$$

Therefore, if the wind is persisting, even if the wind velocity is large, the net angle of attack due to combined effect of drift and wind is less than that produced by wind alone, whereas the other effects α_{err} and α_f remain unchanged. This condition repeats for the case of slow-varying, lesser-magnitude wind also.

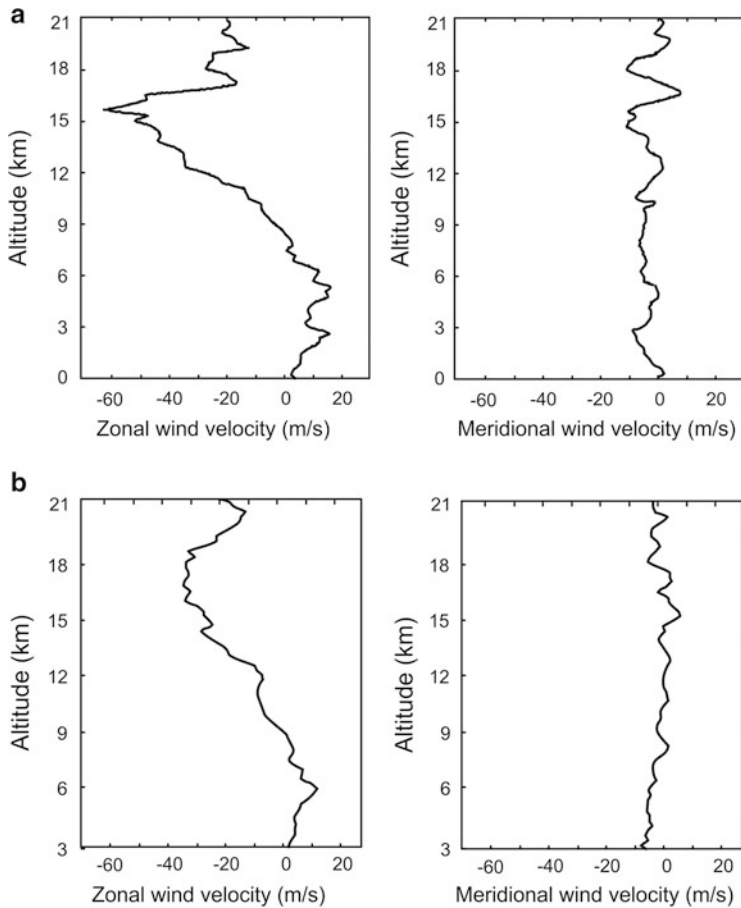
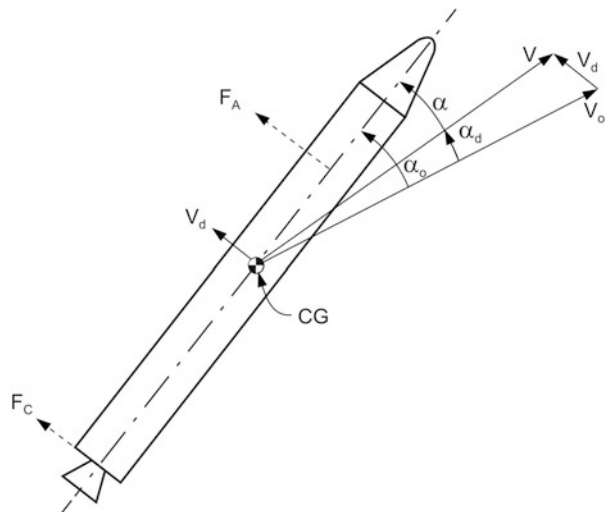


Fig. 6.15 Typical examples of quasi-steady state wind profile **(a)** Higher magnitude wind speed **(b)** Lower magnitude wind speed

(b) Effects of Wind Shear

Large wind shear is one of the characteristics of wind and is represented in a typical measured wind as given in Fig. 6.17a. The wind shear can also happen due to wind direction change as represented in Fig. 6.17b.

It is to be noted that in the case of high wind shear, the rate of change of wind speed and/or wind direction is such that this rate is faster than the integrated vehicle response which is caused by vehicle inertia, control band width limitation and rigid body band width. Therefore, the drift as explained above is very small. As the wind shear is large, the reduction in angle of attack due to drift velocity is minimum, and therefore, the angle of attack α is close to the wind angle of attack α_w and other

Fig. 6.16 Effect of drift

effects α_{err} and α_f . Therefore, the presence of shear in the wind profile introduces higher angle of attack α and in turn higher aerodynamic load. Even if the absolute wind speed is less, the presence of wind shear causes larger angle of attack. As the wind shear increases, the load induced by α_w also increases and finally ends up with gust response.

(c) Effects of Wind Gust

Gust characteristics in a typical measured wind profile are shown in Fig. 6.18. The gust is a sudden phenomenon, and therefore, the entire change in velocity is reflected as α_w without any vehicle response effects. This condition increases the aerodynamic load to maximum.

Taking into account the above characteristics, it is important that both wind shear and gust have to be considered for the design. As the measured wind may not contain the gust, the wind profile used for design necessarily has to have the gust characteristics and appropriate response studies and loads have to be evaluated before finalizing the design. Generally, there are two categories of studies carried out for the gust response studies: (1) gust immersion and (2) gust penetration. In the gust immersion studies, the vehicle length is assumed to be very small compared to the gust wavelength (i.e., vertical length of gust). Under such cases, a vehicle can be assumed to be a point mass, and the aerodynamic loads are computed as this point travels through the gust wavelength. The gust penetration analysis is also called as quasi-steady gust penetration. In this analysis, aerodynamic inertia effects are neglected and steady aerodynamic characteristic is used for the analysis. As the vehicle enters into the gust, the aerodynamic steady load on the vehicle up to penetrated part of vehicle is faced by gusty wind whereas the remaining portion of the vehicle is affected by the wind prevailing at that altitude. The gust penetrated

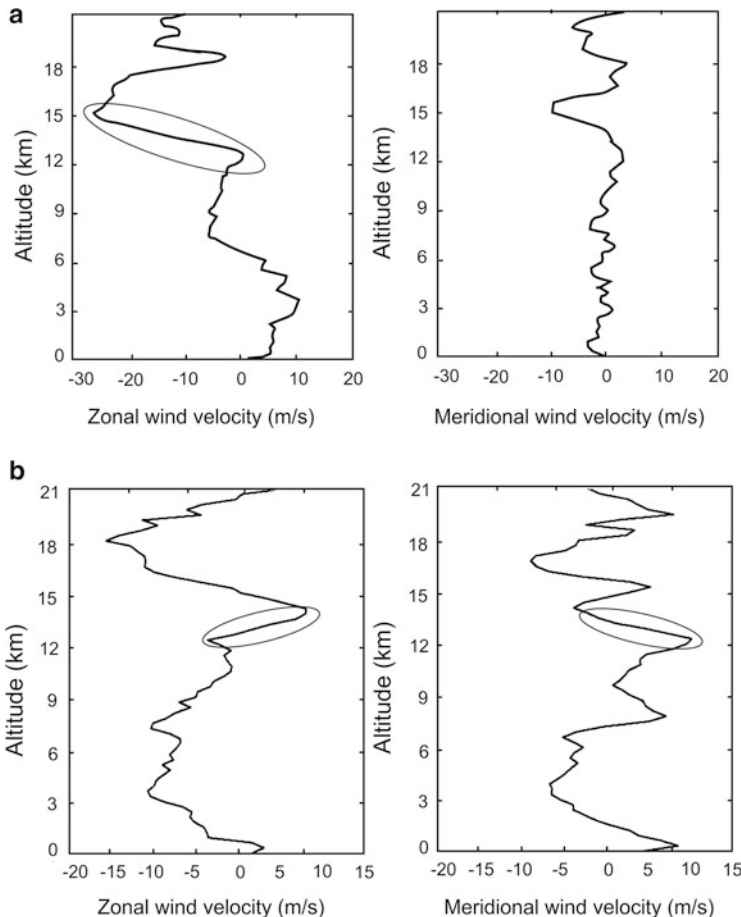


Fig. 6.17 Wind shear in typical measured wind profiles **(a)** Shear in magnitude **(b)** Directional shear

part of the vehicle increases as the vehicle moves. The response under such environments is evaluated till the vehicle moves out of the gust.

As it is known that the quasi-steady-state wind may not realistically represent the actual gust encountered by the vehicle, it is essential to model the gust on the measured wind profile. Depending on the functional criticalities of the vehicle systems, there are two approaches for modelling gust: (1) discrete gust and (2) continuous gust, which also can be called as turbulence.

The gust induces the dynamic response of the vehicle. The frequency of the response is a function of the gust wavelength and vehicle velocity and represented as

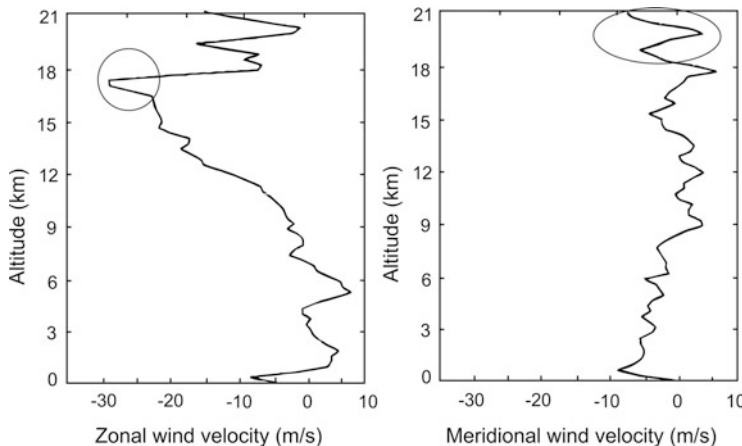
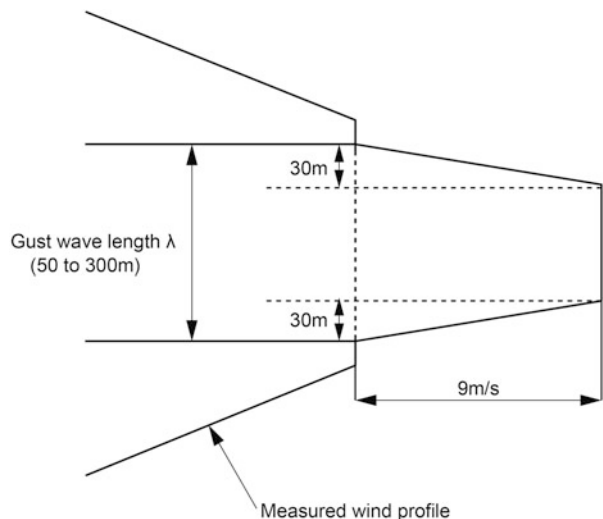


Fig. 6.18 Wind gust characteristics in a typical measured wind

Fig. 6.19 Discrete gust on a typical measured wind profile



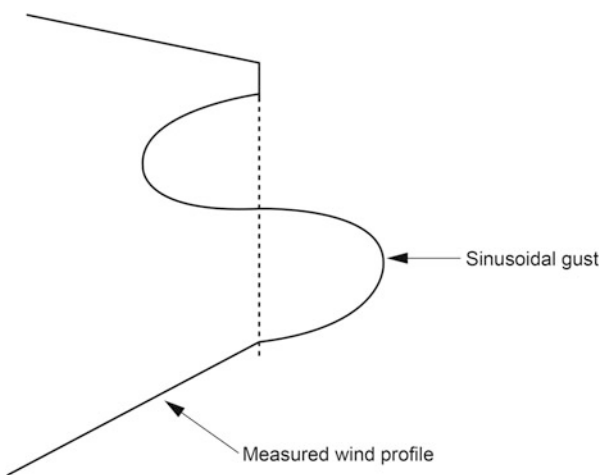
$$T = \frac{\lambda}{V} \quad (6.39)$$

where T is period of crossing the gust, λ is wavelength of the gust and V is vehicle velocity. The frequency is given by

$$f = \frac{1}{T} = \frac{V}{\lambda} \quad (6.40)$$

Simplest gust representation is to model it as a simple strong gust (discrete gust) as given in Fig. 6.19. Assuming vehicle velocity at different regimes of flight,

Fig. 6.20 Typical representation of Sinusoidal Gust



depending on the criticalities and response characteristics of the vehicle, the frequency of the excitation by the wind can be finalized and accordingly the gust wavelength can be tuned. Generally, gust wavelength is 50–300 m and height interval to reach the peak gust magnitude from the quasi-steady-state value is about 30 m.

In the second approach, continuous stream of random gusts are added to the prevailing wind profile as represented in Fig. 6.20. Several models are available to superimpose such spectral gusts of turbulence. The main characteristics of such gusts are (1) zero mean velocity, (2) amplitude of variation, called the strength of the turbulence and its wind speed and (3) frequency of occurrence of the peaks. As the details on the turbulence modelling is beyond the scope of this book, the relevant details may be obtained from the references given in this book.

6.6.3 Wind Statistics

Wind, a random phenomenon which has different characteristics, acts as disturbance to the vehicle systems during flight. In order to arrive at a robust design the following three approaches are considered:

1. The characteristics of the wind which affect the vehicle design have to be estimated a priori and design the system for the predicted characteristics.
2. Measure the wind on the launch day close to the launch time and estimate the vehicle load, check whether the loads are within the allowable band and give clearance for the launch.
3. In order to ensure near-total launch availability on any day, Day-Of-Launch wind biasing (as explained in the later part of the book) also may be adopted.

Since the wind is random in nature, the predominant wind characteristics which affect the vehicle systems during flight may not be measured by a single wind profile. Also, it is to be noted that wind is grossly dependent on season, weather, climate, time of the day in the year, launch site location, etc. The winds measured at the launch site, launch time, day of the year over a long period of time may have the specified characteristics. Therefore, it is essential to look into the statistics of winds measured at the specified launch site over a long period of time.

Both ground winds and in-flight winds affect the STS design process. Therefore, wind statistics has to be evaluated for both ground winds and in-flight winds. Salient features of these aspects are explained below.

(a) Surface Wind Measurements

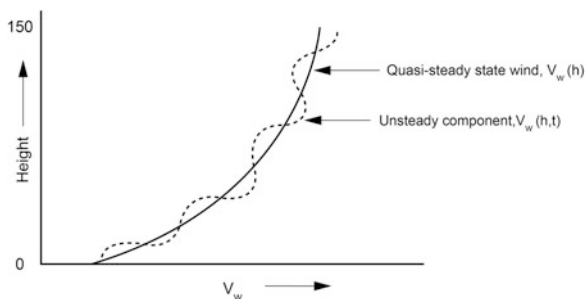
Wind below 150 m height in the specified launch site is referred as surface wind and the wind above 150 m is referred as in-flight wind.

Surface winds are generally measured by anemometers using propeller or cups for measuring the speed and vanes for measuring the wind direction. Anemometers generally measure quasi-steady-state wind speeds. Due to the slow response, they are not suited for measuring unsteady wind with frequency more than one cycle per second. High-frequency gusts are generally measured using high-response anemometers which consist of hot wires, drag spheres, etc. The anemometers are fixed at different heights near the launch pad. Each anemometer measures the wind velocity at that height as functions of time. Using the measurements at different heights, the ground wind profiles as function of height and time are generated. These profiles are further analyzed for the quasi-steady-state wind profiles and unsteady components as function of time as shown in Fig. 6.21.

Due to the friction effects of Earth's surface on the lower atmosphere, the lower-height wind speed is generally less as represented in Fig. 6.21 and increases logarithmically as function of height. The empirical formula (power law) used for the ground wind is given by

$$V_w = V_{w_0} \left(\frac{h}{h_0} \right)^p \quad (6.41)$$

Fig. 6.21 Typical ground wind



where V_{W_0} is wind speed at h_0 , near to the ground, V_w is the wind speed at height above h_0 and p is an exponent. p depends on the local terrain conditions, season of the year and time of the day. Generally, p is of the order of 0.14–0.2.

With the advancements of measurements and data processing, it is possible to incorporate all the features quantitatively viz., quasi-steady-state wind, wind shear, unsteady wind and gust.

(b) *In-Flight Winds*

In-flight winds are measured using (1) Balloon sensors, (2) Smoke trail technique and (3) Ground-based radars. Among them, the techniques adopting balloons are widely used to generate the wind data for the STS design. The surface area of the balloon is very high and the inertia is very low. Therefore, the acceleration of the balloon due to the wind speed is so high and measures almost the instantaneous wind. Different types of balloon techniques for measuring wind are explained below:

1. Radiosonde: Balloon that carries the tethered payload for measurement of temperature, humidity and dew point
2. Rawinsonde: This is same as radiosonde balloon along with a corner reflector. The motion of the reflector is tracked by a ground-based radar. Based on the radar output, the wind velocity profile as function of altitude is generated. Rawinsonde balloons expand as they rise and burst at a particular altitude. Most of the balloons can rise up to 18 km and high-altitude balloons can rise as high as 35 km. As the critical region of STS flight in terms of dynamic pressure is within this altitude, the wind predicted using balloon is sufficient for the STS applications.
3. Rawin: This is a balloon which carries only reflector.
4. Jimsphere: This is a 2 m diameter aluminized Mylar super pressure spherical balloon having conical reflectors to increase the surface roughness. As this feature reduces self-induced oscillations of the balloon, the accuracy of the wind measurements using Jimsphere is quite high and it can capture unsteady nature of wind characteristics also.
5. Rawin+GPS: This is same as Rawin balloon and the payload contains the GPS receivers. Based on the continuous measurement of position by the GPS receivers, they are transmitted to ground and the wind speed is derived. Of all the balloon-assisted wind measurement methods, this is independent of radar.

Using the tracked or transmitted data of the balloon, suitable data processing techniques are adopted to remove the wild points and smoothen the noise. The process has to be carefully done so that the real unsteady nature of the wind is retained as explained in Fig. 6.22.

Typical winds measured at a launch site over a period of time in a specified season are given in Fig. 6.23. As the wind measurement has a pattern for the specified season, the statistics of these winds can be represented as mean wind, and dispersion levels within $\pm 2\sigma$ and $\pm 3\sigma$ and so on. The mean wind and variations

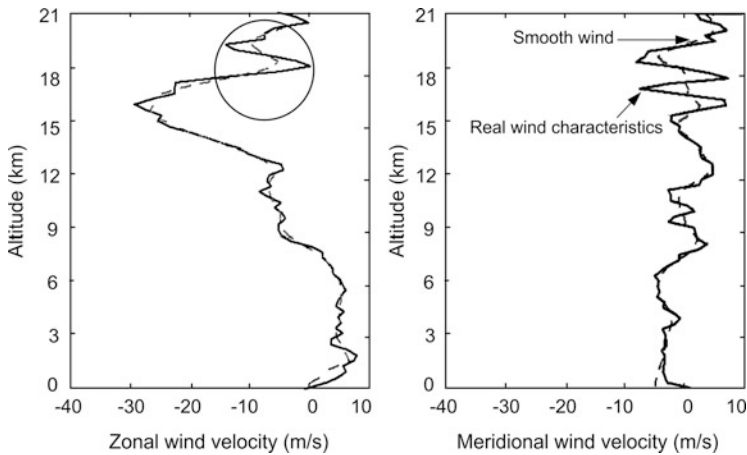


Fig. 6.22 Typical example of smoothing

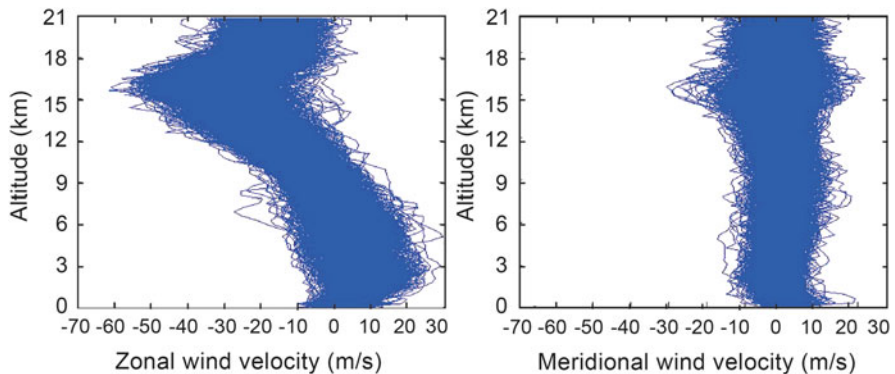


Fig. 6.23 Ensemble of measured winds over a typical launch site in a typical season

of the measured winds of Fig. 6.23 are represented in Fig. 6.24. From the above statistics, the following conclusions may be arrived at:

1. From a defined launch site, during specified seasons, at 95 percentile probability, the wind can be within the bands given by Mean $\pm 2\sigma$.
2. If the vehicle systems are designed with the characteristics of winds in terms of quasi-steady-state wind velocity, wind shear and gust within, mean $+ 2\sigma$, then the success probability of STS mission from these launch sites during the specified season is 95 %.

Wind has different patterns during different seasons. This can be represented as different mean winds during different seasons as given in Fig. 6.25. Thus, in order to ensure that all-weather launch of the vehicle (in all the days of a year), the vehicle systems have to be designed to cater for the winds of all the seasons.

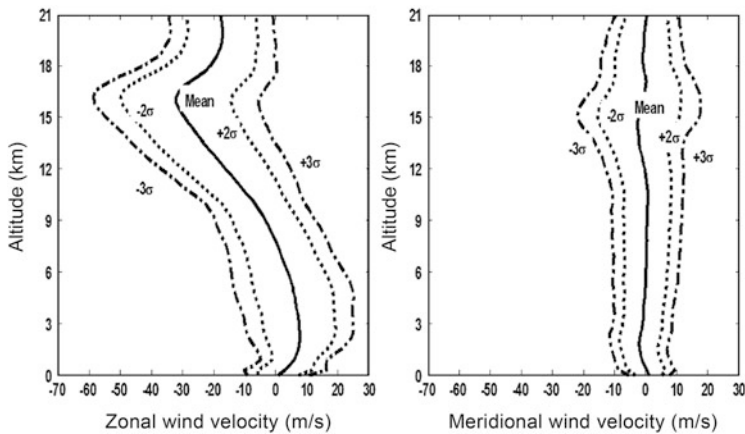


Fig. 6.24 Mean wind and dispersion band of typical season

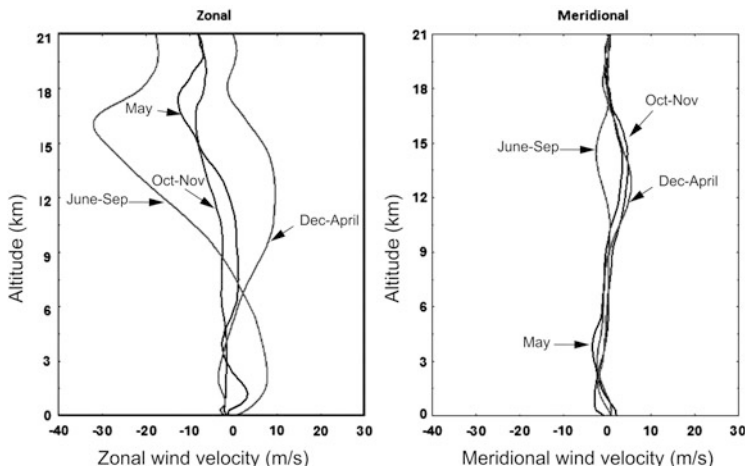


Fig. 6.25 Mean wind at a typical launch site

To ensure that the vehicle systems are robust to fly in all weather conditions, it is generally designed for ‘synthetic design winds’. Synthetic profile is not the realistic wind profiles, but synthesized one which has all the characteristics of winds in the additive fashion. This is required for ground wind and in-flight winds.

6.6.4 In-Flight Wind Data for Design Studies

In-flight wind data are required for the vehicle structural systems, control systems, trajectory design, integrated vehicle systems and mission design validations. Three

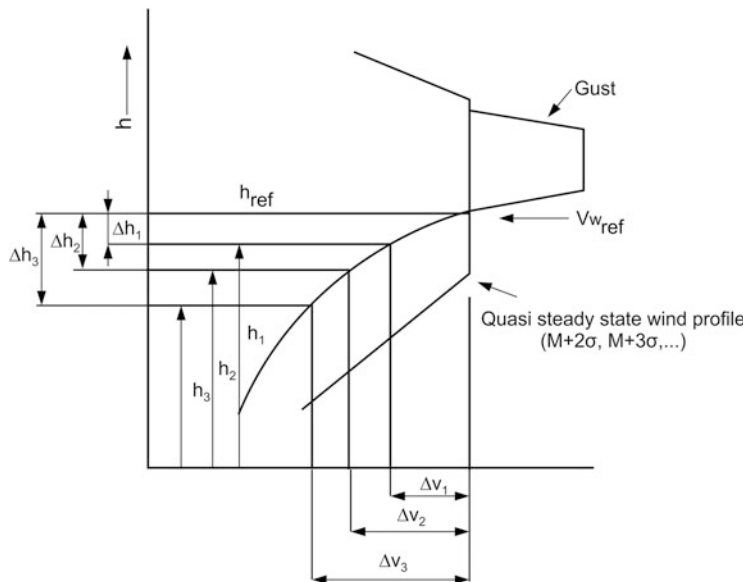


Fig. 6.26 Synthetic wind profile construction

categories of winds are used for these purposes: (1) synthetic winds, (2) measured wind profiles and (3) random wind profiles.

Synthetic wind profile approach produces robust vehicle systems design, especially during the early design phase. The synthetic wind profile includes all the features of wind characteristics viz., maximum quasi-state-wind speed magnitude, wind shear and gust in additive combination to establish the vehicle structural and control systems design. The synthetic wind profile is constructed using the maximum wind speed, conditional maximum wind shear and gust measured with respect to the given wind speed. Therefore, the use of synthetic wind profile assures specified success probability which is generally assumed with the design wind speed, shear and gust. For each season, at each altitude, there is a synthetic wind. Construction of synthetic wind profile at a specified altitude for a specified season is given in Fig. 6.26 and explained below:

From the measured wind profile statistics, generate the maximum wind speed ($V_{W_{ref}}$) measured at the specified altitude (h_{ref}) with specified percentile. Similarly generate the maximum wind shear measured from the low altitudes to the reference altitude. $\Delta h_1, \Delta h_2, \Delta h_3$ are the altitude intervals to the lower altitudes with respect to the reference altitude. $\Delta V_1, \Delta V_2, \Delta V_3$, etc. are the maximum shear measured during the altitude intervals $\Delta h_1, \Delta h_2, \Delta h_3$, etc. respectively, i.e. ΔV_1 is the maximum wind shear measured from h_1 to h_{ref} , ΔV_2 is the maximum wind shear measured from h_2 to h_{ref} and so on. Therefore, the wind speed at h_1 is computed as $(V_{W_{ref}} - \Delta V_1)$ and the wind velocity at h_2 is computed as $(V_{W_{ref}} - \Delta V_2)$ and so on. Joining the profile from the lower altitudes to the wind velocity $V_{W_{ref}}$ at reference altitude h_{ref} as

represented in Fig. 6.26 is the maximum shear build-up profile at the reference altitude. Over the shear build-up profile, wind gust as explained earlier is implemented. Therefore, this synthetic profile is having the characteristics of (1) maximum wind speed with the specified percentile, (2) maximum shear build-up and (3) wind gust. Such synthetic wind profiles are generated for different reference altitudes for defined season and used for the vehicle system design.

In addition to the above, measured winds are used in trajectory design and mission design validation. Random wind profiles are generated using the wind statistics obtained from the measured wind and used in the integrated mission design validation as well as in Monte Carlo analysis.

6.7 Thermal Environment

Mechanical properties of conventional structural materials reduce at elevated temperature. At very low temperature, many materials become brittle thus reducing their load-carrying capability. The internal stresses caused by differential temperature act on the structural elements which cause additional loads. To ensure normal functioning of sensitive electronic components, it is essential to maintain the specified thermal environment. In addition, the temperature of the propellants has to be maintained within the specified limit to ensure normal functioning of propulsion systems. Therefore, thermal environment is one of the major factors to be considered for the vehicle systems design.

Thermal environments for the vehicle and satellite systems are caused by (1) solar heat load, (2) Earth albedo, (3) aerodynamic heating, (4) propellant temperature especially cryogenic systems and (5) propulsion systems. Therefore, vehicle and satellite systems have to be protected against such adverse thermal environments during (1) vehicle on the launch pad, (2) atmospheric flight phase and (3) entire flight duration including vacuum flight.

6.7.1 *Thermal Environment on Launch Pad*

Generally, the integrated vehicle with satellite at launch pad is exposed to the ambient for a definite duration, depending on the functional requirements of a launch. During this period, thermal environment to the vehicle and satellite is caused by solar heat load, Earth albedo and heat generated by the vehicle onboard electronic systems. Under such environments, it is essential to protect the sensitive elements in the vehicle, satellite and the stored propellants in tanks through suitable thermal protection and cooling mechanisms. The details on the environment and protection schemes are explained in the chapter on thermal design.

6.7.2 Thermal Environment During Atmospheric Flight Phase

Aerodynamic heating caused by the aerodynamic flow over the external surface of the vehicle and protruding elements during different flight regimes is the major source of external thermal environments over the entire vehicle systems. Solar heat load also acts on the vehicle systems during the flight. The vehicle external surface, functional critical systems and satellite have to be protected against these adverse thermal environments. The vehicle sensitive systems such as control systems are further subjected to the convective and radiative heat transfer from the propulsion system. Therefore, suitable thermal protection systems for all the vehicle systems have to be adopted, depending on the type of heat transfer mechanisms and their functional requirements. Details on the thermal environment and protective mechanisms are given in the chapter on thermal design.

6.7.3 Thermal Environment Caused by Propulsion Systems

During chemical reaction process of combustion, hot gas with temperature level as high as 3500 K is generated in the combustion chamber and these combustion products are expanded through nozzle to generate the required thrust level. The thermal environments caused to the other functional critical systems through radiation from hot nozzle and through convection have to be addressed suitably in the vehicle systems design. To handle high-temperature combustion products, suitable high-temperature materials have to be used for the propulsion system elements. In addition, suitable cooling mechanisms have to be implemented for the combustion chamber, throat and nozzle.

Further details on these environments and the protective mechanisms are discussed in chapters on thermal design and propulsion systems.

6.8 Vehicle Internal Steady Loads and Disturbances

The important internal steady loads acting on the vehicle systems are (1) thrust loads, (2) pressure loads and (3) thermal loads. The thrust force is the functional requirement of STS and the high pressures are needed in certain vehicle subsystems to achieve the required thrust force. The thermal load is the by-product of these two requirements. To achieve the required thrust level, high-pressure, high-temperature combustion products are generated during combustion process in the solid motors and combustion chambers in liquid engines. In the case of solid motors the high pressure of combustion products directly acts on the motor cases. In liquid engines, the various components of pumps and feed lines experience high pressures to

achieve the required performance. For pressure-fed propulsion systems, the gases stored at high-pressure tanks are used to pressurize the propellant tanks. In addition, the high-pressure gases are used for control thrusters and for propulsion command systems. All these requirements bring in high-pressure environment to the vehicle systems. In addition, propulsion systems and other vehicle components experience high temperature. Therefore, it is essential that the vehicle systems are designed for pressure, thrust and thermal loads or combination of the above loads as per the operating environment. Details of these environments and the suitable design strategies are discussed in the chapters on propulsion and structural systems design.

In addition, there are several other steady disturbances due to the characteristics of the vehicle systems. Some of them are (1) thrust offset with respect to the vehicle centre of gravity, (2) thrust misalignment, (3) differential thrust and (4) attachment misalignment.

6.8.1 Thrust offset

Thrust offset with respect to centre of gravity produces a disturbance moment about vehicle centre of gravity (CG) as given by

$$M_{T0} = T\Delta x \quad (6.42)$$

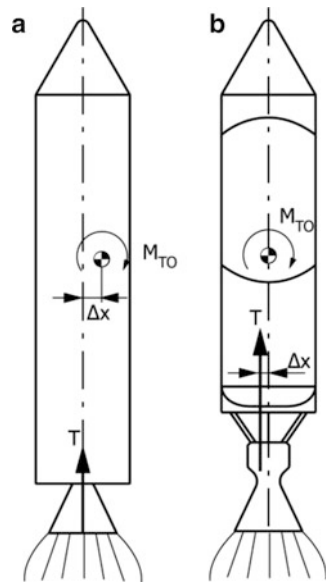
where T is the thrust generated by the rocket motor and Δx is the thrust offset. There are two sources of thrust offset as given in Fig. 6.27: (1) thrust along the longitudinal axis of the vehicle and CG of the vehicle is away from the central line as shown in Fig. 6.27a and (2) vehicle CG along the vehicle centre line and thrust is offset from the vehicle centre line as shown in Fig. 6.27b.

During the vehicle engineering design, depending on the functional requirements or due to space constraints, certain heavy components have to be necessarily placed laterally away from the vehicle centre line, which can cause CG offset. Therefore it is essential to carry out the vehicle layout, engineering design during the initial phase itself to ensure near zero CG offset. The layout has to be such that the components are placed at suitable locations which ensures balancing, resulting in zero CG offset. To minimize the assembly error, suitable precision assembly strategy has to be adopted during the vehicle integration.

6.8.2 Thrust Misalignment

Thrust misalignment is the angle between the thrust direction and longitudinal axis of the vehicle and this causes a lateral force at thrust acting location resulting in a steady disturbance moment about CG of the vehicle, as given below.

Fig. 6.27 Thrust Offset (a)
CG Offset (b) Thrust offset
from central line from
central line



$$M_{TM} = (T \sin \xi) l_t \quad (6.43)$$

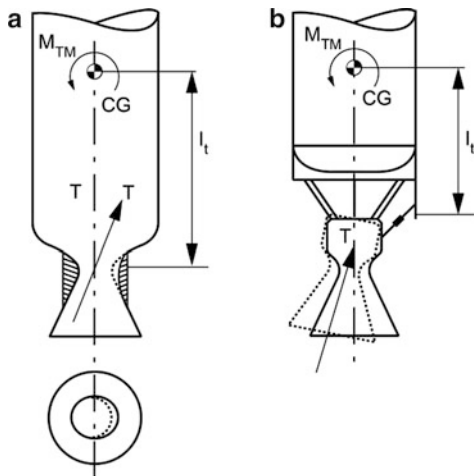
where ξ is the thrust misalignment angle, l_t is the distance between thrust acting location and CG. There are two sources of thrust misalignment as represented in Fig. 6.28: (1) uneven nozzle throat erosion, (2) thrust frame deflection.

When high-temperature combustion products pass through throat at sonic velocity, nozzle throat gets eroded to a certain extent. The thrust erosion rate depends on throat material, material properties at operating environment such as pressure, temperature, velocity, flow characteristics and constituents of combustion products. During the process of throat erosion, there can be uneven erosion along the circumferences, which finally ends up with throat centre line shift as represented in Fig. 6.28a. Due to the nature of the propellant formation, throat erosion is predominant in solid propulsion systems.

Any deviation of thrust or nozzle exit away from the vehicle axis produces thrust misalignment. During nozzle assembly, the misalignment due to deviation of line joining throat centre to exit centre away from the vehicle centre line also produces thrust misalignment.

In liquid propulsion systems, thrust misalignment generally occurs due to another phenomenon. The engine of liquid stage is attached to the stage through thrust frame as represented in Fig. 6.28b. Generally, engine gimbal control systems are used during thrusting phase of liquid engines. When thrust is increasing, the thrust frame gets deformed due to the compressive loads caused by the thrust. Due

Fig. 6.28 Thrust misalignment (a) Throat erosion (b) Thrust frame deflection



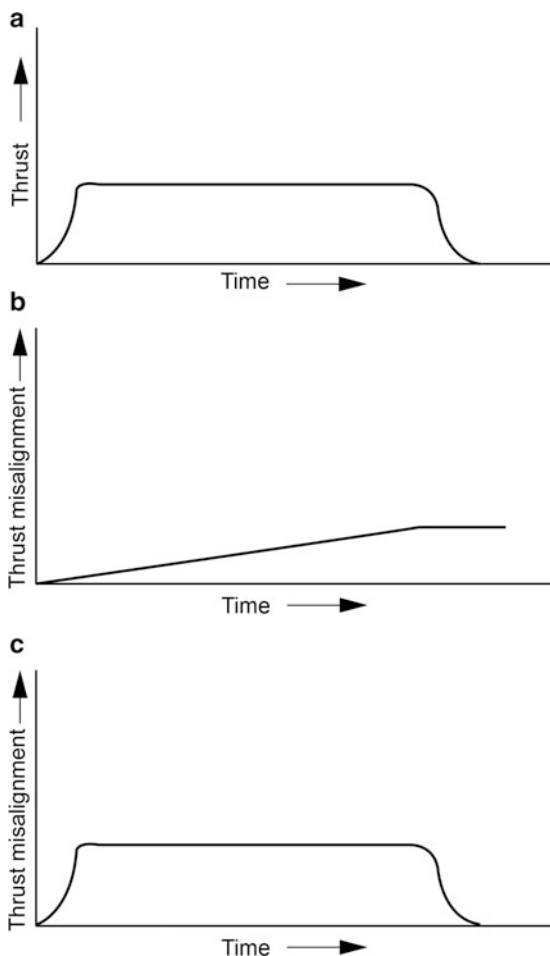
to the attachment of actuator mechanism at one side of the engine, the thrust frame deformation is non-uniform which tilts the engine at one side, as represented in Fig. 6.28b. As the thrust is along the axis of the deflected engine, this tilt causes the disturbance moment.

The thrust misalignment due to throat erosion is a function of action time of the motors and usually monotonic as given in Fig. 6.29b. Thrust misalignment due to thrust frame deformation is a function of engine thrust level. The misalignment becomes maximum when thrust is maximum and it follows the thrust shape as represented in Fig. 6.29c. This feature has predominant effect on the vehicle control system design, especially during cut-off phase of the engine. This aspect is further discussed in detail in the chapter on NGC systems design.

6.8.3 Differential Thrust

For the vehicle with strap-on motors or stages with multi-engines, the differential thrust is a major disturbance source, particularly during the burnout phase. A typical strap-on configuration with straight nozzle is represented in Fig. 6.30a. Normally, the design is such that both the strap-on motors are expected to have the same thrust value at any instant. But in reality there is always a small difference in the propulsion characteristics between the strap-on motors, causing a small differential thrust, which produces disturbance moment, given as

Fig. 6.29 Thrust misalignment variation
 (a) Thrust (b) Thrust misalignment due to throat erosion (c) Thrust misalignment due to thrust deflection

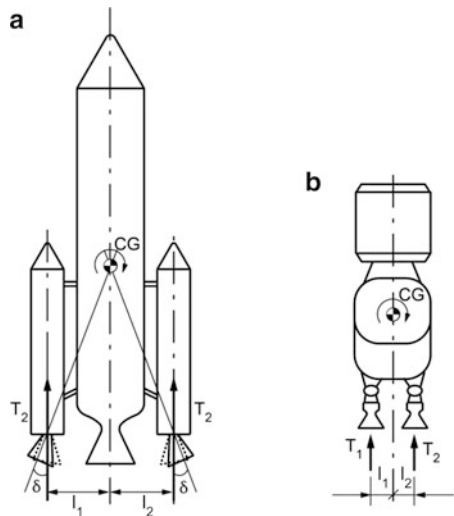


$$M_{TD} = T_1 l_1 - T_2 l_2 \quad (6.44)$$

where T_1, T_2 are thrust values and l_1, l_2 are the thrust locations with respect to the vehicle centre line where the CG lies. Generally, $l_1 = l_2$ except for the dispersions on the location of CG. Therefore, different values of T_1 and T_2 produce disturbance moment as represented in Eq. (6.44).

During burnout, there can be an extreme situation that one motor is still burning with full thrust whereas another is either burnt out or the thrust is near zero. Under such environments, the disturbance moment can be more than available control moment. This is usually the case in solid strap-on motors.

Fig. 6.30 Configurations with multiple propulsion systems (a) Strap-on configuration (b) Multiengine configuration



The disturbance moment due to differential thrust is minimized by utilizing the two strategies: (1) The vehicle CG is estimated at different flight instants. The nozzles of the motors are canted such that at the critical flight regime, the thrust passes through CG so that there is no disturbance moment even though there is a lateral unbalanced force. (2) Reduce the differential thrust level by adopting the pair-casting of the strap-on motors.

For the configuration with canting, longitudinal thrust is given by

$$T = T_1 \cos \delta + T_2 \cos \delta \quad (6.45)$$

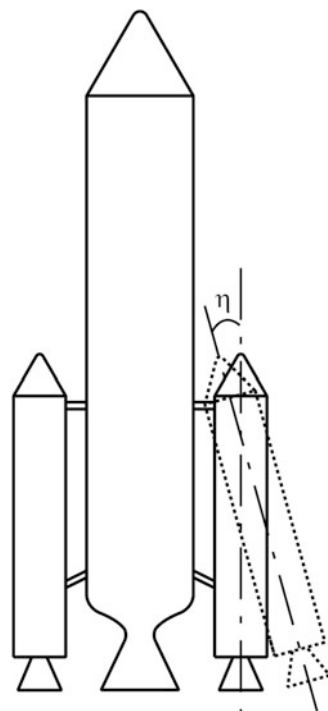
and the lateral force is given by

$$T_L = T_1 \sin \delta - T_2 \sin \delta \quad (6.46)$$

where δ is the cant angle. From Eqs. (6.45) and (6.46), it can be seen that, for the same thrust levels, the lateral force is balanced. However, the longitudinal thrust is reduced. For $\delta = 10^\circ$, the longitudinal thrust level is reduced by about 1.5 %. For vehicle with CG at much lower level, the cant angle required is large, which in turn reduces the longitudinal thrust component to a large extent. Under such conditions, to avoid performance loss, canting is not provided. But to take care of vehicle controllability problems, the method of pair-casting in solid motors with suitable control strategies is adopted.

The differential thrust effect is same for the cases, with multiple engines as explained in Fig. 6.30b. In both, strap-on motors or multiple engine configurations even for the same thrust level, there can be disturbance moment if the CG is not exactly at the mid way between the thrust locations. Therefore, it is essential to control this effect during the layout phase.

Fig. 6.31 Typical attachment misalignment



6.8.4 Attachment Misalignment

In a typical vehicle with strap-on motors, the angular misalignment can happen in the attachments as shown in Fig. 6.31. As the nozzle is attached with respect to the strap-on motors, the attachment misalignment can also cause the disturbance moment. The effect is similar to that of thrust misalignment. Therefore, it is essential to ensure suitable assembly procedure to minimize the attachment errors.

6.9 Dynamic Environment

Dynamic environments to the vehicle systems are caused by both external and vehicle internal sources. The main external sources of dynamic environments are (1) aerodynamic characteristics of the vehicle combined with atmospheric winds, (2) unsteady aerodynamic loads termed buffet loads and (3) aeroacoustic environments. The vehicle internal systems which cause dynamic environments are (1) vehicle structural bending and torsion, (2) propellant sloshing, (3) POGO

oscillations, (4) thrust oscillations, (5) rotor dynamics of turbo pump systems and (6) jet acoustics environments. Dynamic environments always induce a coupling between different systems and hence the design has to consider this coupling. Typical dynamic coupling environments during STS system operations are

1. Interactions between control systems and vehicle flexible dynamics
2. Dynamic loads induced by the interaction between quasi-steady and unsteady aerodynamic loads with the structural dynamics response. Typical examples are gust-induced responses of lower-frequency modes of vehicle and buffet load-induced responses of higher-frequency vehicle flexible modes
3. POGO instability interaction between vehicle propulsion systems and vehicle axial structural modes causing severe dynamic environments to the vehicle structural systems
4. Slosh dynamic interactions with vehicle control and structural systems
5. Thrust oscillation-induced interactions with vehicle structural systems leading to large coupled loads at the satellite interface with STS
6. Dynamic loads to the vehicle systems caused by the vehicle vibration and acoustic environment generated by the aerodynamic and jet noises

Causes and effects of typical dynamic environments are briefly explained in this section. The suitable design practices for the vehicle systems under such adverse dynamic environments are discussed in detail in the appropriate chapters of this book.

6.9.1 External Dynamic Environment

The sources of external dynamic environments are the atmospheric winds and vehicle aerodynamic characteristics.

As explained earlier, atmospheric wind plays a major role for inducing aerodynamic disturbance forces and moments. The wind contains different characteristics such as shear, gust and unsteady components. These wind characteristics combined with vehicle external aerodynamic characteristics cause oscillatory disturbances to the vehicle which in turn interact with vehicle systems to cause dynamic environments to the vehicle.

The aerodynamic flow over the vehicle during atmospheric flight phase causes aerodynamic steady and unsteady loads on the vehicle structure. The unsteady component has different frequencies of pressure fluctuation. The low-frequency pressure fluctuations cause fluctuating aerodynamic forces, which interact with vehicle structural modes, inducing dynamic loads on the vehicle structure. This phenomenon is called aerodynamic buffet.

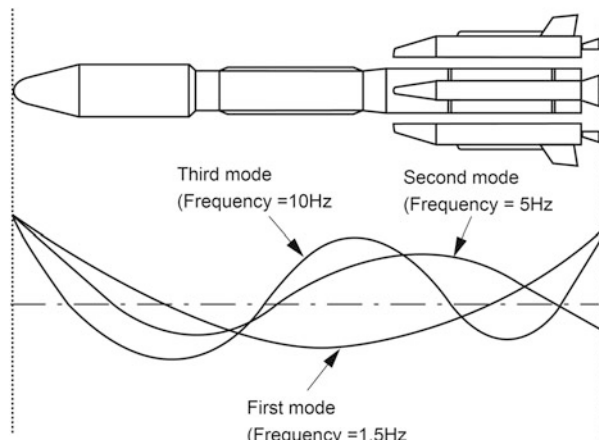
6.9.2 Vehicle Flexible Modes

Generally, STS is a structure with large length-to-diameter ratio. Therefore, in addition to the rigid body (infinitely rigid vehicle) motion, the vehicle is also flexing out of shape in response to the various forces acting on it. The flexible shape of the vehicle depends on the mass distributions along the vehicle length, diameter and joint stiffness between different structures, etc. The general flexing is characterized in terms of slopes and displacements with respect to the six degrees of freedom of the undeflected rigid vehicle. These vehicle elastic modes are classified in terms of its shape and energy content. Each mode shape is time dependent and vehicle acquires a particular mode shape at a set frequency. Realistically, a vehicle's elastic mode shape at any instant is a combination of several independent structural mode shapes and each mode vibrates at a certain frequency. Depending on the vehicle characteristics, the first bending frequency (vehicle shape in pitch or yaw plane) can be as low as 1.0 Hz and the higher mode shapes frequency can be successively higher. Theoretically the number of mode shapes and the corresponding frequencies can be infinite. Such mode shapes exist in all six directions (three rotations and three displacements). Typical first three lateral bending modes of a typical vehicle at a typical flight instant are represented in Fig. 6.32.

Depending on the forcing function magnitude and frequency a specific flexible mode of the vehicle gets excited and induces dynamic loads to the vehicle systems. If the vehicle systems are not designed properly, resonance can occur, which finally leads to vehicle and mission failure. Therefore, it is essential to understand the interfaces and coupling. The vehicle systems are to be designed to avoid such resonances.

Vehicle flexible modes interact with aerodynamic forces, unsteady aerodynamic buffet, propellant slosh, POGO and vehicle control systems, thus causing severe dynamic environments to the vehicle systems and structure. Therefore, vehicle

Fig. 6.32 Typical bending modes



flexible modes play a major role in the dynamic environment to the vehicle systems as well as vehicle systems design. Details are given in chapters on vehicle structural systems and NGC systems design.

6.9.3 Propellant slosh

Propellant sloshing is a major dynamic, interactive disturbance source in the STS employing liquid propulsion systems.

To have a certain amount of ullage volume at the ignition phase of the liquid engines, generally propellants are not filled to the full tank capacity. Similarly, during stage operation, the propellants are consumed continuously causing the gradual depletion of the tanks. Under both the conditions, sufficient amounts of propellants are available with free surface. Therefore certain quantity of propellants is free to oscillate under the influence of lateral disturbances, whereas remaining part of propellants towards tank bottom is rigid and not taking part in the motion. The propellant sloshing is the lateral dynamic force resulting from the lateral motion of liquids in the propellant tanks, which is induced by lateral acceleration caused by lateral forces (due to lateral disturbances, control forces and slosh force itself) as well as rotational acceleration.

The lateral dynamic oscillations of the propellants can be represented by the lateral motions of equivalent mechanical systems either as pendulum mass model or spring mass model as given in Fig. 6.33. In Fig. 6.33, the total mass of propellant

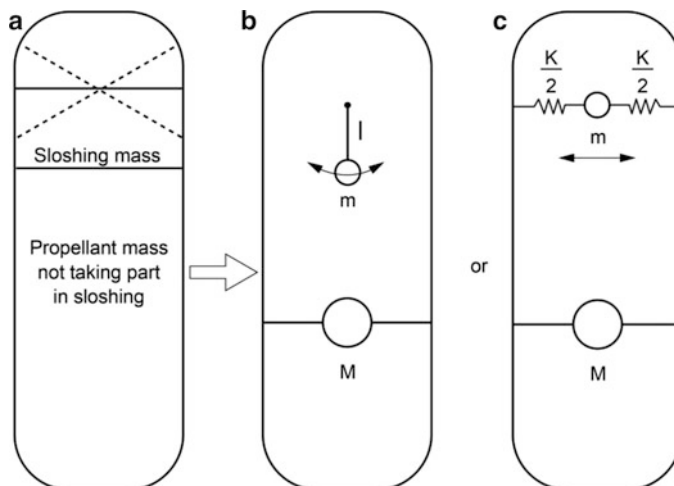


Fig. 6.33 Propellant sloshing phenomena (a) Propellant in tank (b) Pendulum mass model (c) Spring mass model

remaining in the tank is $(M + m)$, where m is the mass of propellant taking part in sloshing motion and M represents the non-sloshing mass. The frequency of oscillations of the sloshing liquid mass m is given by

$$f = \sqrt{\left(\frac{a}{l}\right)} \quad (6.47)$$

where l is the pendulum length, a is longitudinal acceleration of the vehicle. The frequency of propellant sloshing varies with vehicle acceleration and the length of the pendulum, which depends on the tank configuration, free surface area, etc. In the spring mass model, the spring constant K has to be changed to take care of the acceleration variations.

The slosh force acting on the vehicle structure causes it to respond. The response is fed into the control system and the control force acts on the vehicle structure, which in turn induces slosh oscillations. Slosh force itself acts as part of forcing function for the slosh oscillations. Thus, it can be seen that there is strong coupling between slosh-structure-control. If the frequency of dominant slosh mode (which gives maximum disturbance, caused by large slosh mass and location away from the vehicle CG) is close to the control system frequency (control bandwidth), it can cause instability to vehicle. Similarly, vehicle's higher-energy elastic body mode frequency closer to the control frequency may result into large-amplitude vehicle dynamic response. Such resonances may finally result into the disturbances exceeding the control system's capabilities to counteract or structural systems to withstand it and finally leading to vehicle break-up. Therefore, it is essential that the control system bandwidth, vehicle flexible mode frequency and dominant propellant slosh frequencies are having wide separations.

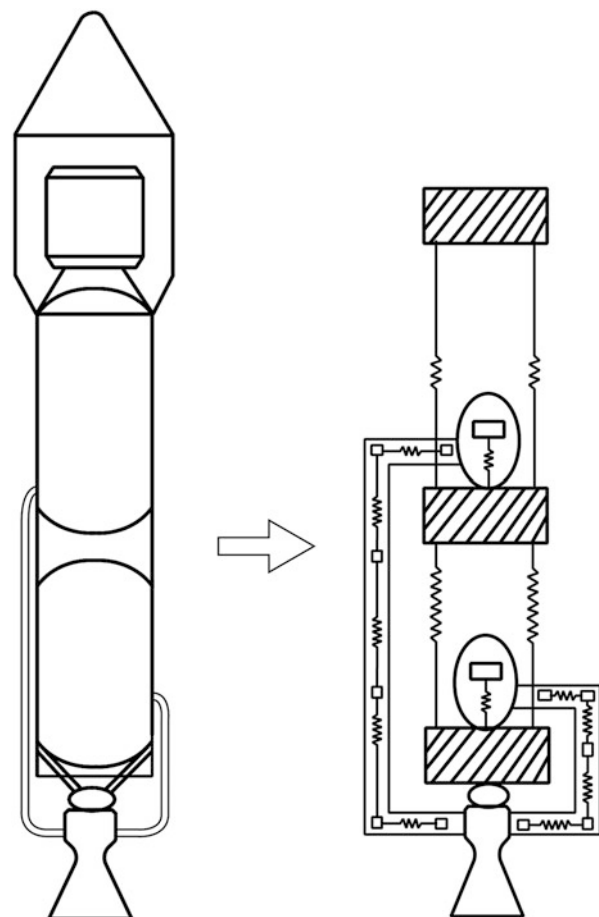
Generally, for a larger vehicle, employing liquid propulsion systems, the dominant slosh modes, dominant vehicle flexible modes and control frequencies are always closer. Under such conditions, it is essential to carefully consider the propellant tank configuration and its location with respect to the vehicle CG to reduce the slosh effects. In addition, depending on the criticalities due to slosh mass effects, suitable baffles have to be implemented at the appropriate locations of the tank and control systems have to be suitably designed to increase the damping of slosh dynamics.

The details on slosh dynamics model and vehicle system details are described in the subsequent chapters of this book.

6.9.4 POGO Oscillation

POGO phenomenon is the interaction between vehicle axial structural dynamics and propulsion system dynamics. Like vehicle structures, the propellant feed systems are also flexible. This feature along with the longitudinal structural

Fig. 6.34 Idealization for POGO analysis



dynamics leads to POGO oscillations. In order to understand the POGO phenomenon, the POGO dynamics of the propulsion system is idealized as represented in Fig. 6.34.

The axial dynamics of structures can induce oscillations at the tank bottom. These oscillations interact with the flexible dynamics of feed lines, which causes oscillations in propellant supplied to the engine system. The propellant oscillations in turn cause oscillations in combustion chamber pressure, which correspondingly induces thrust oscillations. The thrust oscillations further induce the vehicle axial structural mode and the interaction continues as given in Fig. 6.35. POGO instability occurs when the axial structural frequency of the vehicle is closer or crosses the propellant feed line frequency as represented in Fig. 6.36. Under such cases, resonance occurs on the vehicle thrust and acceleration as shown in Fig. 6.37.

In order to overcome this effect, the propulsion system frequency and vehicle axial frequency have to be separated. It is very difficult to alter the vehicle structural

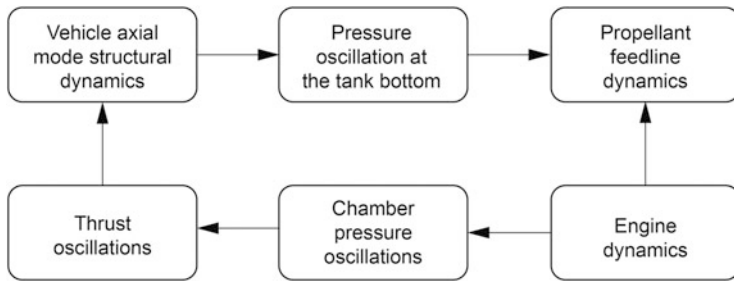


Fig. 6.35 Vehicle systems interactions in POGO phenomenon

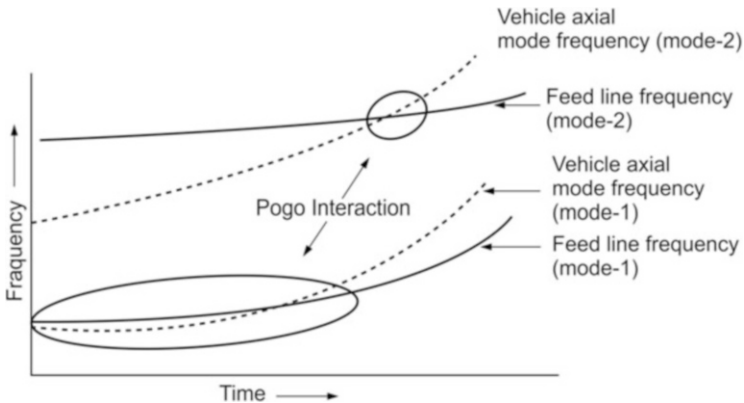


Fig. 6.36 POGO instability region

Fig. 6.37 Typical POGO instability problem

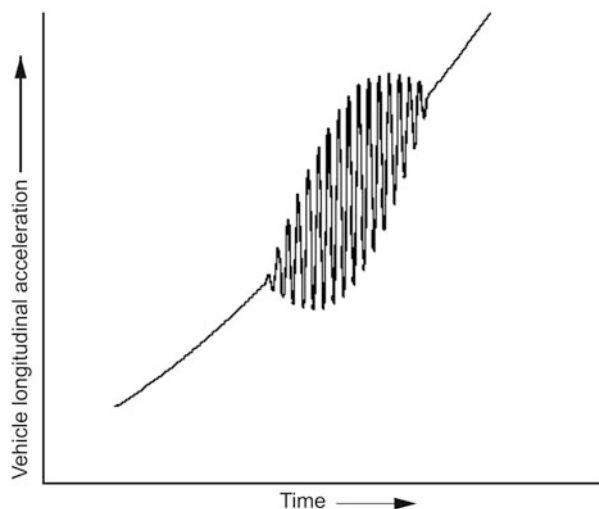
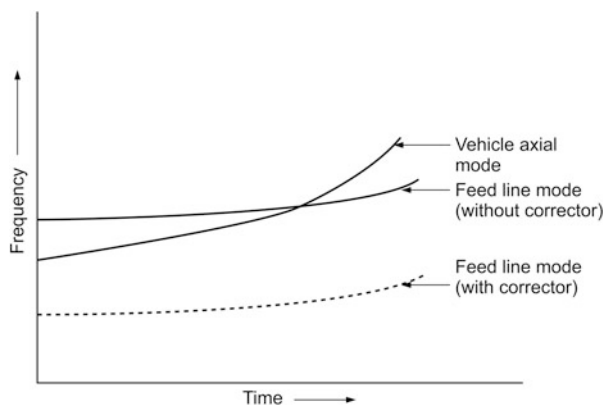


Fig. 6.38 Effect of POGO corrector



frequency. However, the propulsion system frequency can be altered by adding gas-filled cavities to the feed lines.

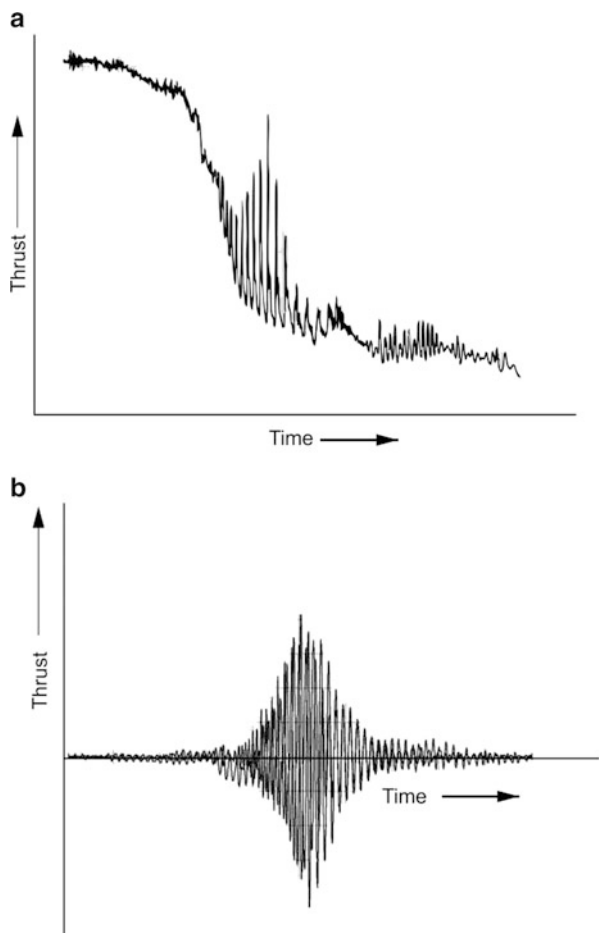
Generally, nitrogen gas is injected upstream of pump, which can reduce the propulsion frequency considerably, thus avoiding interaction with the vehicle structural frequency as represented in Fig. 6.38. This system is called POGO corrector, which can be initiated and stopped as per the requirements.

6.9.5 Thrust Oscillations

Thrust oscillations occur during various phases of solid motor and liquid engine operations. These dynamic environments have to be properly considered for vehicle systems design. Total analysis on these aspects is beyond the scope of this book. However, a typical example, explaining the effects of thrust transients on the vehicle system dynamic loads is explained below.

Thrust transients generated by liquid engines during engine shut-off phase induce significant dynamic loads on the vehicle and satellite systems. Liquid engines have different modes of shut-off. Generally the engines are commanded to shut off once the specific mission requirements are achieved. In certain cases, depending on mixture ratio variations, one of the propellants gets depleted earlier followed by the other one. Under such conditions, the thrust starts falling and once the thrust level is below the specified level, the engine is commanded to shut off. Depending on the type of depletion, combustion chamber is fed with varying flow rates of two propellants. This results in a mixture ratio which is away from the normal value thus generating thrust oscillations. The magnitude and frequency of the oscillations represented in Fig. 6.39a depend on the type of depletion (oxidizer or fuel) and the propulsion system characteristics. Generally, the magnitude of oscillation is high to excite the vehicle axial mode and frequency of oscillation can be close to the vehicle. Such thrust transients may adversely influence the dynamic

Fig. 6.39 Effects of thrust oscillations (a) Thrust transients (b) Response at satellite base



response of the vehicle due to resonance. A typical thrust transient and the corresponding dynamic loads at the satellite/space transportation system interface are represented in Fig. 6.39.

To assess the impact of such dynamic environments, the dynamic models of the satellite and the vehicle are to be integrated and the coupled load analysis has to be carried out for the expected thrust transient environment. Suitable modifications have to be incorporated in the vehicle systems if required. Also, suitable mechanisms have to be introduced in the propulsion system such as restriction check valve, which ensures the desirable thrust transient by ensuring the required oxidizer and fuel flow rates under all the environments of commanded shut-off and depletion cut-off. Once the vehicle systems are designed, the dynamic environment at the vehicle/satellite interface can be defined, which forms an input to the satellite systems design.

6.9.6 Other Dynamic Environments

Detailed description of dynamic environments is beyond the scope of this book and readers may refer to the references given at the end of this chapter to understand the full dynamic environment. However, some of the important ones are explained here.

(a) *Mechanical Shocks*

Vehicle systems experience mechanical shock during stage separation events caused by high-energy pyro systems. Mechanical shocks are non-periodic in nature and the time of action is extremely small. As the action time of the mechanical shock is so small, it excites all the modes of vehicle structure. The resultant acceleration load due to shock is of millions of gs. Even though the levels of these loads are very high, this does not affect the vehicle structure because the structure cannot respond to such short-duration pulses. But the sensitive electronic elements near such shock regions may be affected and therefore, suitable protective mechanisms have to be incorporated.

(b) *Rotor Dynamics*

Pump-fed liquid propulsion systems have many rotating components which are operating at very high rotational speed (as high as 40,000 rpm). Due to high speed, these systems, even with a small level of dynamic imbalance, can generate high level of dynamic loads to the propulsion subsystems. Therefore, these elements have to be fully balanced based on the results of suitable test strategies to ensure normal function of the systems.

6.10 Random Vibration Environment

The random vibration environment to the vehicle and its subsystem is caused by the noise generated during vehicle lift-off and flight. Any pressure fluctuation travelling at the speed of sound is called noise and the sources of noise environment to the STS are (1) jet noise (acoustic noise) and (2) aerodynamic noise. The acoustic environment is measured in terms of Sound Pressure Level, which is the magnitude of the pressure fluctuations relative to a reference pressure. Due to the extremely wide range, over which the human ear is sensitive, the Sound Pressure Level (SPL) in deciBel (dB) is expressed as a logarithmic function of pressure fluctuations as defined below:

$$\text{SPL} = 20 \log_{10} \left(\frac{P'}{P_{\text{ref}}} \right) \quad (6.48)$$

where P' is root mean square (rms) of fluctuating pressure, P_{ref} is reference pressure which human ear can hear and $P_{\text{ref}} = 2 \times 10^{-5} \text{ N/m}^2$.

6.10.1 Propulsion System Noise

During lift-off, noise environment caused by the propulsion system is predominant. Propulsion system noise can be divided into (1) noise due to exhaust jet shearing action (jet noise) and (2) noise due to unsteady burning of propellants. Jet noise has three components, namely, screen tones, turbulent mixing noise and shock-associated noise. Turbulent mixing and shock-associated noise in rocket exhaust of launch vehicle generate sound levels of about 165 dB. Generally, high-frequency noise excitation is generated near to the nozzle whereas low-frequency noise is generated at the faraway point on the jet exhaust. As the vehicle velocity increases, the effect of propulsion system noise on the vehicle system reduces as the vehicle moves faster than the speed of sound and noise cannot reach the vehicle structure. When the vehicle reaches high subsonic, transonic and supersonic speeds, the aerodynamic noise becomes predominant.

6.10.2 Aerodynamic Noise

The sources of aerodynamic noise are the disturbances caused by the flow instabilities. These disturbances result into fluctuations in fluid pressure that propagates with the speed of sound from the source. This disturbance propagation results into noise, called aerodynamic noise. There are four major sources of aerodynamic noise as represented in Fig. 6.40 and are (1) Shock wave – Boundary Layer interaction, (2) Separated flow, (3) Noise from wake of protuberances and (4) Boundary layer noise. Even with the exponential growth in the computational capability and advancement in numerical schemes, it is not possible to characterize the acoustic loading of space vehicle from first principle. Hence, one needs to resort to semi-analytical or empirical method to determine the acoustic loadings and use them for the initial design. Subsequently after finalization of configuration, accurate acoustic levels are determined through scaled model testing in wind tunnel.

In general shock wave oscillation/shock boundary layer interaction can generate levels as high as 172 dB. Separated flow in boat tail region of bulbous payload fairing experience nearly 140–150 dB. The above values change with respect to

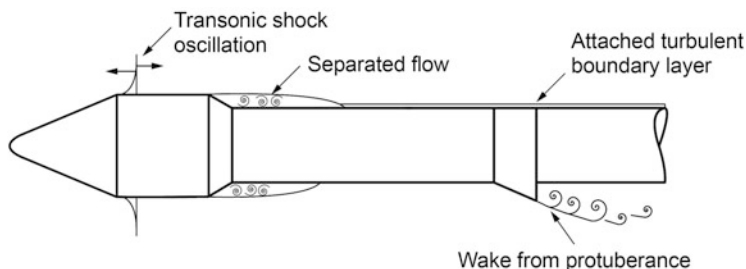


Fig. 6.40 Typical aerodynamic noise sources

dynamic pressure of the flight. The shock oscillation noise has highest level in low frequencies, typically up to 100Hz, and then comes down. The separated flow has more fluctuation level up to a typical frequency of 400–500 Hz, and then reduces. The turbulent boundary layer has white noise in which fluctuation level is nearly same up to few KHz. In general, the fluid flow-associated spectrum doesn't have any discrete spike at any specific frequency.

The nature of flow field viz., separated flow/reattachment region, shock location, attached flow regimes, is obtained through the oil flow visualization technique in wind tunnel test. Accordingly, the unsteady pressure sensors are mounted on the wind tunnel model and measurements are carried out. For each type flow the SPL spectrums are generated for various Mach numbers and angles of attack. It is not possible to carry out the acoustic tests for all spectrums. So a practical and conservative approach may be followed to arrive at a spectrum. Different types of flow prevailing on various areas are identified. In a given type of flow region, $(P'_{rms})^2$ value at each frequency band (of different locations) is obtained in area-weighted averaged method. This spectrum is used as an input in the acoustic testing.

6.10.3 Impact of Noise on Vehicle System Design

For space vehicle components, acoustic levels higher than 150 dB can lead to (1) fatigue failure of light weight structural components, electronic circuit boards and electrical connections, (2) wear and deformation of bearings and (3) malfunction of electronic components. Damage potential of the aero-acoustic levels depends on the spectral content. High SPL in low frequencies have more potential for damage/failure than that in high frequencies.

STS structures are subjected to acoustic excitations during launch and atmospheric regime of flight. At lift-off and during low subsonic portions of flight, these excitations result from the propulsion system-generated noise field surrounding the vehicle. In transonic and supersonic flight regimes, aerodynamically generated acoustic fields excite the structures. These excitations induce random vibration response in the vehicle structure and partially transmit to internal elements like spacecraft and other sensitive packages. Random vibration response and internal acoustic field can be determined accurately through acoustic tests. Acoustic test results are also useful in generating random vibration test specification for components/sub-assemblies. Based on acoustic test results, package mounting schemes, locations etc. are to be finalized accordingly.

6.10.4 Noise Reduction Strategies

If the random vibration levels caused by acoustic environments are beyond the allowable limit of the vehicle systems, then suitable strategies are to be adopted to reduce the noise levels.

(a) *In-light Noise Reduction*

By appropriate aerodynamic shaping of the vehicle configuration, the in-flight aero acoustic levels can be reduced. Ogive payload fairing almost eliminates the transonic terminal shock formation. This can bring down aero acoustic levels even up to 10–15 dB. Any local protuberances produce shock/separated flow and induce high acoustic levels. Hence, minimizing the number of protuberances and shaping them reduce the in-flight noise level. By reducing the dynamic pressure of the space vehicle (by suitable selection of rocket motors and trajectory optimization) in-flight acoustic loading can be brought down.

(b) *Lift-Off Noise Suppression*

Lift-off jet noise level is about 10–20 dB higher than undeflected free jet noise level. This increased noise level during lift-off can be reduced (1) by covering the jet deflector exit duct and (2) by massive injection of water into the deflected jet. Water injection reduces momentum of the exhaust jet and temperature of the jet. This in turn reduces the acoustic power generated. Massive water injection about 2–4 times the mass flow rate of jet exhaust into jet suppresses the acoustic levels by 5–10 dB.

6.11 Influence of Parameter Dispersions

The vehicle systems have to be designed to achieve the specified functional requirements under all operating environments explained hitherto. Therefore, it is essential to predict the operating environments through suitable models and elaborate ground tests. It is to be noted that the specified parameters cannot be predicted accurately *a priori* and the predictions are always within the specified error bands. The dispersion band depends on the accuracy of the model, measurement errors, deviations due to limitations of simulating the flight environment in the ground systems and variations caused by environments, etc. Similarly, predictions on the performance parameters of vehicle subsystems also have specified dispersion bands.

Vehicle systems have to be designed to cater to the dispersions in the predicted operating environments as well as vehicle system performance parameter dispersions. Based on the influence of these parameters on the functional performance of the vehicle subsystems and on integrated mission, they can be classified into primary and secondary critical parameters.

6.11.1 Primary Critical Parameters

Typical primary critical parameters which influence the vehicle and mission are from (1) propulsion systems, (2) aerodynamics and (3) atmosphere. Table 6.1 gives

Table 6.1 Typical primary critical parameters

Systems	SI No.	Parameters
Solid Propulsion System	1	Structural mass
	2	Propellant mass
	3	Specific impulse
	4	Action time
	5	Ignition delay
	6	Differential thrust for strapon motors
	7	Differential tail-off for strapon motors
Liquid Propulsion System	8	Structural mass
	9	Propellant loading: Fuel&Oxidizer
	10	Ignition delay
	11	Specific impulse
	12	Chamber pressure
	13	Mixture ratio
	14	Cut-off delay
	15	Tail-off characteristics
	16	Differential thrust
	17	Differential tail-off thrust for multi engine combination
Aerodynamic characteristics	18	Normal force coefficient
	19	Side force coefficient
	20	Axial force coefficient
	21	Centre of pressure in pitch plane
	22	Centre of pressure in yaw plane
Atmosphere	23	Atmospheric temperature
	24	Wind variations

typical primary critical parameters and their dispersions which cause direct influence on vehicle systems design. For each parameter mentioned in Table 6.1, depending on the nature of dispersions, the type of parameter variations and the dispersion levels are specified. For example, if the variations are defined in terms of normal distribution, the mean value (nominal) and 3σ dispersions (variations with respect to the mean) are to be defined. For uniform distributions, always the specified magnitude on the dispersion level with uniform probability of occurrence of such dispersions is used.

6.11.2 Secondary Critical Parameters

The system parameters which are not influencing the mission directly but influence the function through their performance deviations are called secondary critical parameters. Typical secondary critical parameters are given in Table 6.2. For

Table 6.2 Typical secondary critical parameters

Systems	SI No.	Parameters
Navigation System		<i>Gyro systems</i>
	1	Gyro fixed drift rate (short term)
	2	Gyro fixed drift rate (day to day)
	3	Mass unbalance
	4	g^2 sensitive
	5	Scale factor error
	6	Input axes misalignment
		<i>Accelerometer</i>
	7	Bias error
	8	Scale factor error
	9	Nonlinearity
	10	Input axis misalignment
		<i>Alignment</i>
	11	Level alignment
Thrust misalignment & CG offset	12	Azimuth alignment
		<i>Location error</i>
	13	Gyro location error
	14	Accelerometer location error
Control system response	15	Thrust misalignment angle and azimuth
	16	CG offset error and azimuth
Vehicle Flexible Mode	17	Natural frequency
	18	Damping ratio
	19	Frequency
	20	Damping ratio
	21	Generalised mass
Slosh Parameters	22	Mode shape
	23	Mode slope
	24	Slosh mass
	25	Slosh mass location
	26	Slosh mass hinge location
	27	Slosh frequency
	28	Slosh damping

secondary critical parameters also, the types of dispersions are to be specified for usage in the vehicle system design process.

Bibliography

1. Griffin, M.D., French, J.R.: Space Vehicle Design. AIAA Education Series. AIAA, Reston (1991)
2. Cornelisse, J.W., Schoyer, J.W., Hakk K.F er.: Rocket Propulsion and Space flight Dynamics. Pitman Publishing Ltd, London (1979)

3. Arthur L Greensite.: Control theory: Vol.II; Analysis and Design of Space Vehicle Flight Control Systems, Spartan Books, Geissler. E.D (1970)
4. Geissler E.D.: Wind Effects on Launch Vehicles. AGARDograph Number – 115, Paris (1970)
5. Adelfang, S.I., Evans, B.A.: Vector Wind Profile Gust Model – NAS8-33433, Huntsville, AL (1980)
6. Smith, O.E., Adelfang, S.I., Batts, G.W., Hill, C.K.: Wind Models for the NSTS Accent Trajectory Biasing for Wind Load Alleviation, NASA TM – 100375, NASA MSFC, Huntsville (1989)
7. “Effects of Structural Flexibility on Launch Vehicle Control System”, NASA SP – 8036, NASA, Huntsville (1970)
8. Ananthasayanam, M.R., Narasimha, R.: A proposed international tropical reference atmosphere upto to 1000 km. Adv. Space Res. 7(10), 117–131 (1987)
9. Rees. D. (ed.): COSPAR International Reference Atmosphere: 1986, Part I – Thermosphere models. Pergamon Press, Oxford (1989)
10. Abramson, N.H. (ed): The Dynamic Behavior of Liquids in Moving Containers, with Applications to Space Vehicle Technology. NASA SP-106, NASA, Washington, DC (1966)
11. Bender, R.L., Reardon, J.E.: Preliminary Base Heating Environments for a Generalised ALS LO2/LH₂ Launch Vehicle. Remtech Technical Note, RTN218-01 (1989)
12. Anderson, J.D.: Hypersonic and High Temperature Gas Dynamics. McGraw-Hill Book Company (1989)
13. Fletcher, D.G.: Fundamentals of Hypersonic Flow-Aerothermodynamics”, RTO-EN-AVT-116, Belgium (2004)
14. Hirschel, E.H.: Basics of Aerothermodynamics, vol. 206, Progress in astronautics and aeronautics, Ed.in Chief Zarchan P., Springer, Germany (2005)
15. NASA space vehicle design criteria (structures), Compartment venting, NASA SP-8060, NASA, Washington DC (1970)
16. NASA space vehicle design criteria (structures), Buffeting during atmospheric ascent, NASA SP-8001, NASA, Washington DC (1964)
17. NASA space vehicle design criteria (structures), Acoustic loads generated by the propulsion system, NASA SP-8072, NASA, Washington DC (1971)
18. Sissenwine, N.: Winds for aerospace vehicle design. National symposium proceedings. AF. CRL-62-273”, Parts I and II, Office of Aerospace Research, USAF (1962)

Chapter 7

Mission Design

Abstract During the entire phase of space transportation system mission, from lift-off till satellite injection, various constraints and requirements applicable not only to the mission but also to vehicle systems, ground systems, range safety and tracking systems are to be satisfied. Considering these constraints and requirements, an optimum feasible trajectory has to be designed to meet the mission requirements. The mission design process involves the utilization of the available energy for realizing the defined orbital mission by devising suitable strategies of directing the energy along the suitable path and sequencing the energy addition process. Optimum mission design strategies have to be arrived at to achieve the maximum performance, ensuring the defined mission under nominal and off-nominal flight environments and system parameter dispersions. The trajectory shaping satisfying vehicle loads and radio visibility for continuous tracking coverage during ascent phase are other essential parts of mission design. There are number of constraints like thermal loads on the spacecraft, the vehicle subsystems during ascent phase and jet plumes of reaction control system thrusters interacting with the spacecraft. The passivation requirements of the final stage after spacecraft separation are to be carefully worked out. Another important aspect of mission design is to finalize the flight events/sequences which generate various commands to separate the stages and to initiate the subsequent flight events. In such complex systems close interactions among various disciplines exist, and the mission design requires several iterations. In this chapter all these aspects of mission design are discussed in detail and various activities involved in mission design process explained. The mission design strategies and importance of the same for the vehicle design process are included. Mission requirements, constraints, design and analysis aspects and trajectory design constraints during various phases of trajectory are presented. Mission sequence design considerations and all other mission-related studies like satellite orientation requirements for multiple satellite launch and passivation requirements to ensure the safety of the spent stage are also highlighted.

Keywords Mission design • Mission specifications • Trajectory design • Lift-off studies • Load relief • Gravity turn trajectory • Wind biasing • Thermal design • Mission sequence • Stage passivation • Vehicle tracking and range safety

7.1 Introduction

Once a space transportation system and the associated vehicle subsystems are designed to provide the necessary energy to position the satellite into its specified orbit, it is essential to carry out a detailed integrated mission design to ensure that all the constraints and requirements of the mission, vehicle, range and tracking systems are satisfied. Mission design is the process of utilizing the available energy for realizing the defined orbital mission by devising suitable strategies of (1) directing the energy along the suitable path, (2) sequencing the energy addition process and (3) way of utilizing the energy by shaping the energy addition process. Optimum mission design strategies have to be arrived at to achieve the maximum performance, ensuring the defined mission under nominal and off-nominal flight environments and system parameter dispersions. While achieving the above performance requirement, the design has to satisfy the constraints and capabilities of the systems such as (1) vehicle systems (structural loads), (2) vehicle subsystems (control power plant, navigation, guidance and autopilot and thermal) and (3) mission constraints arising from lift-off, range safety and tracking.

The mission design comprises of studying the requirements and associated constraints in totality and carrying out detailed analysis and studies, to ensure that the mission objectives are completely fulfilled. The mission constraints vis-à-vis the objectives specified, launch vehicle capabilities and range safety-related aspects during the ascent phase are to be studied. The trajectory shaping/design satisfying vehicle loads, other constraints and radio visibility for continuous tracking coverage during ascent phase are other aspects which need consideration. There are also constraints like thermal loads on the spacecraft and the vehicle subsystems during ascent phase and jet plumes of reaction control system (RCS) thrusters of upper-stage control system interacting with the spacecraft. The passivation requirements of the final stage after spacecraft separation are to be carefully examined. Important element of mission design is the requirement for finalizing the flight events/sequences which generate various commands including the real-time decision for commands using on-board computer (OBC) to separate the stages and to initiate the subsequent flight events.

In such a complex system like STS close interactions among various disciplines exist, and the mission design requires several iterations. Therefore the design not only needs a systems approach for meeting all the defined objectives but also demands clear domain knowledge of all involved disciplines.

In this chapter all aspects of mission design are discussed in detail. Initially various activities involved in mission design process are explained. The mission design strategies and importance of the same for the vehicle design process are included. Mission requirements, constraints, design and analysis aspects and trajectory design constraints during various phases of trajectory are presented. Mission sequence design considerations and all other mission-related studies like satellite orientation requirements for multiple satellite launch and passivation requirements to ensure the safety of the spent stage are also highlighted.

7.2 Mission Design Activities

During different phases of STS mission, from lift-off till satellite injection and further passivation of the vehicle, various constraints and requirements applicable not only to the mission but also to vehicle systems, ground systems, range safety and tracking systems are to be satisfied. Considering these constraints and requirements, an optimum feasible trajectory has to be designed to meet the mission requirements. The total process comprising of the above activities is called mission design. The major tasks involved in the mission design process are given in Fig. 7.1.

The criticalities of each activity, the requirements and constraints imposed by these activities, which impact on the mission performance are summarized below and further explained in detail in the subsequent sections.

- (i) The lift-off sequence and vertical rise time have to be designed to ensure clear lift-off while maximizing the performance.
- (ii) During the crucial atmospheric flight phase, the primary criterion is to reduce the load on the vehicle while minimizing the trajectory deviation, which has impact on the mission performance.
- (iii) Stage transition is another major critical event wherein different conflicting requirements such as clean separation, controllability of the vehicle, smooth control transition, propulsion systems transition and performance impact are to be analysed. Based on the analysis optimum sequencing events are to be arrived at.
- (iv) While separating the spent stage, it is essential to ensure that the stage impact is in the safe zone.
- (v) Propellant management in liquid stages has to ensure engine safety while maximizing the mission performance.

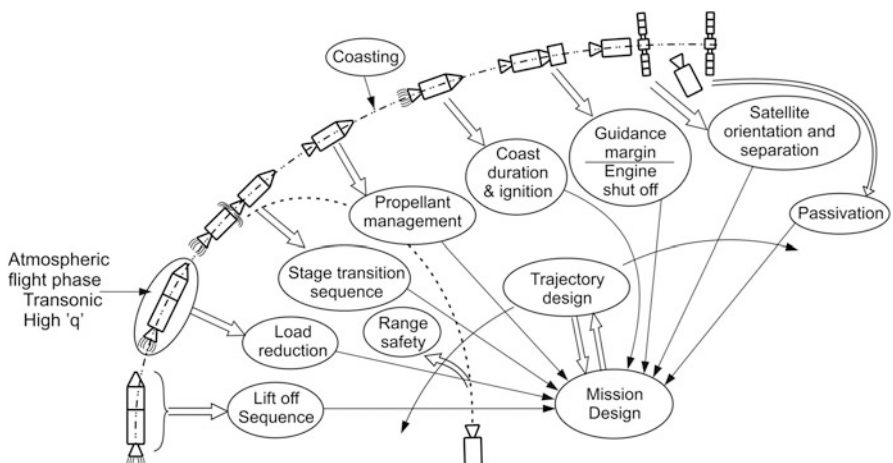


Fig. 7.1 Mission design process

- (vi) Coast duration (for the cases of mission with long coast between two propulsive stages) having a major impact on the vehicle performance has to be carefully designed to meet the requirements.
- (vii) It is essential to ensure sufficient velocity reserve (guidance margin) in the command cut off stages while minimizing the performance loss.
- (viii) Optimum mission design has to ensure minimum propellant consumption.
- (ix) The mission has to meet the satellite requirement of injecting into orbit with desirable orientation. Mission sequencing has to ensure sufficient separation between the satellite and spent stages and among satellites for the cases of multiple satellite missions.
- (x) Once the satellite is injected, it is essential to passivate the spent stage propulsion system to avoid collision with satellites in case of inadvertent re-ignition.
- (xi) During the entire mission, it has to be ensured that the thermal environment to the vehicle sensitive systems and satellite be within the allowable limits.
- (xii) It has to be ensured that commanded vehicle rates are within the allowable capabilities of control systems and the realized rates are within the vehicle structural limits.
- (xiii) During the entire mission, the radio visibility of the vehicle from the appropriate ground stations is important to ensure (a) acquiring the telemetry data and (b) sending telecommand to the vehicle to destruct in case of malfunction.

All the above requirements have to be considered in the vehicle trajectory design and optimum trajectory has to be determined to maximize the performance while satisfying the constraints and requirements in (i) to (xiii).

7.3 Mission Design Strategy

The interactions among the various disciplines of STS and their interfaces with mission design process are broadly represented in Fig. 7.2.

The mission requirements and mission constraints are the major functional requirements for the mission design. The mission requirements are to be reflected as the STS performance requirements for the mission design. The performance requirement in turn decides the propulsion system design and propellant loadings. The performance reserve to be built into the system has also to be decided, and all these parameters are determined through the process of the mission design and analysis.

Similarly, the vehicle load acting on the vehicle depends on the flight environment, vehicle aerodynamic characteristics, the thrust-time curve shapes and the vehicle trajectory parameters. Trajectory analysis and thrust-time curve shaping are essential to contain the vehicle loads within the specified limits. This in turn affects the vehicle performance and has major impact on the vehicle propulsion system

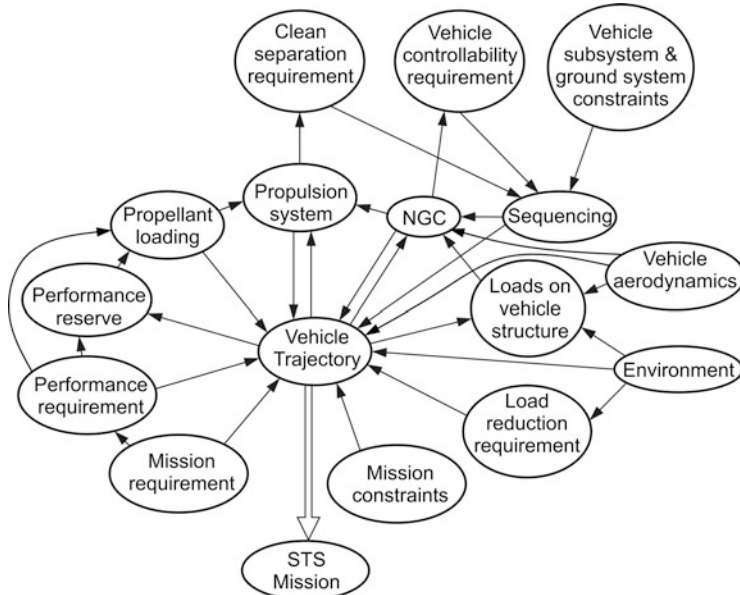


Fig. 7.2 Interactions among vehicle subsystems and mission design

parameter definition. Thus there is strong coupling between vehicle loads, propulsion system, vehicle trajectory and mission performance.

Another typical area of interaction during mission design is on the vehicle sequencing during stage transition. In this phase, almost all the systems requirements are conflicting in nature, and one has to arrive at an optimum sequence which meets all the requirements to ensure mission success. The stage transition has to be planned at low or near-zero thrust for clean separation, but it is not advantageous to meet the expected mission performance and vehicle controllability. If the additional systems are introduced to meet the requirements of separation and controllability, the vehicle becomes complex and reliability reduces. In addition, there is heavy performance loss with such additional systems. To achieve optimum sequencing, it is essential to decide event sequencing during the flight, based on real-time performance of the vehicle systems as per the specified performance criteria. This has to be implemented in navigation, guidance and control (NGC) system, and hence it brings in a strong coupling between NGC, propulsion and mission design.

During mission design, it is essential to ensure that the vehicle command rates are within the capability of control power plants and the realized vehicle rates are limited within the maximum allowable vehicle loads. To reduce the vehicle loads as per design, the real execution of the load reduction during the flight is implemented by the vehicle autopilot. This process causes a strong interaction between vehicle autopilot, control power plant, vehicle structure and mission design.

The optimum trajectory generated through the mission design is used as reference and the trajectory parameters so derived as the major inputs for the navigation, guidance and control system design. The finalized design is tuned to meet various vehicle and subsystem requirements and has impact on the vehicle performance. While designing the vehicle trajectory, it is essential to ensure that the specified range safety constraints are met. The range safety constraints during a specified stage separation also adversely affect the vehicle performance.

Thus it can be seen that the mission design has a strong coupling with almost all the disciplines of the vehicle systems and demands integrated systems design approach. To achieve the optimum design of the vehicle, the mission design has to start right at the beginning from configuration definition phase and undergo several iterations till the STS mission is firmed up.

Initially, the vehicle is configured with propulsion systems to achieve a specified equivalent velocity. Once the external vehicle configuration is finalized, with preliminary aerodynamic data, it is essential to carry out the preliminary mission design to determine the vehicle performance considering the velocity losses due to gravity and drag, pertaining to the specified mission, satisfying the entire vehicle and mission-related constraints. If the required performance is not achieved, the propellant loading or vehicle-related constraints and subsystem specification may have to be revised to meet the requirements. In this process, the requirements of performance parameters and subsystem limits are finalized.

With the finalized system parameters first-level design of subsystems is carried out along with the aerodynamic characterization of the vehicle through detailed wind tunnel tests. This process has to be repeated at various levels of development, incorporating more and more refined design parameters which are derived either through detailed analysis or experimentation. The final mission design is to be verified using all the pre-flight vehicle data.

7.4 Mission Specification Requirements and Constraints

The STS mission design has to start with a clear definition of mission objectives defining the broad goals, the mission has to accomplish. The design also has to cater for different types of spacecraft injection requirements which in turn depend on satellite applications such as remote sensing, communications, scientific investigations, interplanetary exploration, navigation, etc. When a single orbital mission is configured to cater to different satellites, it becomes necessary to define multiple objectives. Similarly if multiple satellites are to be injected in different orbits in a single STS mission then it is required to define the multiple objectives. The baseline objective in all such missions is to inject a satellite of a specified mass into a specified orbit defined in terms of orbital elements.

7.4.1 *Mission Specifications*

STS mission specifications are derived from two sources: (1) satellite requirements and (2) specified launch site and the associated constraints.

The satellite requirements are specified in terms of payload mass, payload envelope, orbital requirements and injection accuracy, satellite attitude requirements and the limits on attitude rates at the time of injection. The specified envelope of the satellite is the requirement for deciding the payload fairing (PLF) configuration acceptability or for the reconfiguration of PLF if the need arises. This forms part of the vehicle configuration.

It is to be noted that even though a nominal satellite mass is defined, in reality the specified mass cannot be realized exactly. Therefore the possible dispersion on the realized satellite mass has to be specified to meet the defined orbital requirements.

As per the satellite application requirements, nominal values of orbital elements are specified which need to be achieved by the STS. But in reality, the exact values of injection orbital elements are not possible due to the presence of dispersions of the engine shut-off characteristics, errors of navigation sensors and the errors caused by the guidance and control algorithms in the real operating environment. The propulsion system of the satellite has to correct the orbital errors caused by the STS mission. Depending on the capability of satellites to correct such errors, allowable dispersions of the orbital elements have to be specified. The STS systems have to be designed to meet the mission requirements as defined, within the specified dispersion band. During initial phase of vehicle design process, a trade-off study has to be carried out between the satellite capability and the STS system requirements. An optimum set of dispersions agreeable to both the systems have to be arrived at based on the preliminary mission design, and the corresponding specifications for the STS mission are to be generated.

The satellite demand is to achieve all the six orbital parameters simultaneously. Generally, two of the orbital parameters, viz. the longitude of ascending node (Ω) and true anomaly (θ), can be achieved by suitably selecting the day and time of launch from the specified launch site, considering the trajectory duration from lift-off to satellite injection.

Also, it is to be noted that generally the satellite orbital requirements are in terms of mean orbital elements, whereas in reality the STS mission achieves the osculating orbital elements corresponding to the locations of satellite injection. Therefore, considering the satellite requirements, STS trajectory and injection location, the osculating elements at the injection of satellite are to be worked out and defined as the specifications for the STS mission.

The specifications for STS mission defined by launch site are decided based on the suitability of identified launch site and limits on the allowable launch azimuth. The launch site location is defined in terms of longitude and geodetic latitude. From the specified launch site, based on the allowable launch azimuth corridor, the most suitable planar trajectory providing maximum performance has to be specified. If the optimum azimuth is beyond the allowable corridor, then the required orbital

inclination is not feasible to achieve. In such cases, there are two ways of managing the mission: (1) Maximum possible launch azimuth which provides orbital inclination close to the satellite requirement is specified. The exact inclination requirement of the orbit can be further achieved by the satellite systems. For such cases, the maximum possible launch azimuth and the corresponding orbital inclinations are the specifications for STS mission. (2) Initial flight of STS is along the launch plane specified by the maximum possible launch azimuth. Once the specified range safety boundaries are crossed, the vehicle has to follow three-dimensional trajectory motions, to achieve the required inclination. To achieve the maximum performance in three-dimensional trajectory, the yaw manoeuvre has to be initiated at the early part of the trajectory. But it has to be initiated only after meeting (a) the range safety constraints and (b) load constraints of the vehicle. In all such cases, the maximum possible launch azimuth, the required orbital inclination and the time of initiation of yaw manoeuvre are the specifications for the STS mission.

The launch tower at a given launch site is invariably configured in the specified direction as per the requirements of ground systems and ease of vehicle integration. In such cases the vehicle can be assembled at the launch tower only in a specified orientation depending on the various fluid lines, umbilical interfaces between the ground systems and vehicle. The vehicle pitch plane at launch pad may not align with the launch plane defined by launch azimuth. Under such conditions, the navigation system in the vehicle at the time of lift-off senses the difference in the vehicle roll orientation with respect to the launch azimuth plane. This difference is equal to the bias of launch tower orientation with respect to the launch direction. To correct this difference the vehicle is commanded to roll once the vehicle crosses the launch tower vertically. The roll angle is decided such that the vehicle pitch plane is aligned with the launch plane (defined by launch azimuth direction). The roll angle, time of initiation of roll manoeuvre and commanded roll rate also become the mission specification for STS.

Considering the above aspects, typical STS mission specifications are summarized as given below:

- (a) Satellite mass: $m_{\text{nominal}} \pm \Delta m$
- (b) Osculating orbital elements at injection:

1. In the case of circular orbit,

Orbital altitude: $h_c \pm \Delta h_c$

2. In the case of elliptical orbit,

Perigee altitude: $h_p \pm \Delta h_p$

Apogee altitude: $h_a \pm \Delta h_a$

(or)

Semimajor axis: $a \pm \Delta a$

Eccentricity: $e \pm \Delta e$

3. Orbital inclination: $i \pm \Delta i$

4. Argument of perigee: $\omega \pm \Delta \omega$

(c) Satellite orientation at the time of injection:

Local pitch angle: $\theta_L \pm \Delta\theta$

Local yaw angle: $(\psi_L \pm \Delta\psi)$

Local roll angle: $\phi_L \pm \Delta\phi$

(d) Attitude rate at the time of satellite injection:

Pitch rate: $\leq q_i$

Yaw rate: $\leq r_i$

Roll rate: $\leq p_i$

(e) Launch station coordinates:

Geodetic latitude: \varnothing_{GDL}

Longitude: λ_L

(f) Launch azimuth: A_{ZL}

(g) Time of launch: H hrs : M min : S seconds

The launch time can be specified in terms of universal time or can be converted into local time at the time of lift-off.

(h) Time of initiation of yaw manoeuvre: t_Y

(i) Roll manoeuvre during lift-off:

Time of initiation of roll manoeuvre: t_i

Time of stopping roll manoeuvre: t_e

Command roll rate of vehicle: p_{cl}

The STS mission design has to be carried out with the above specification. The system requirements and constraints to achieve the above mission by STS are explained in the following sections.

7.4.2 Mission Requirements

Once the broad mission specifications are defined, the next logical step is to specify the requirements and constraints and carry out requirements analysis. This analysis has to lead to matching the satellite and launch vehicle capability with the defined mission goal. The vehicle should be able to deliver the required velocity to the satellite, taking into account all losses during the flight and various constraints to guarantee the desired orbit. Important requirements are as given below:

- Defining a suitable vehicle configuration capable of meeting the mission goal.
- Identifying the suitable vehicle subsystems to meet the defined mission within the specified dispersion band.
- Generating an optimum suitable vehicle trajectory meeting all defined constraints.

- (d) Ensuring the vehicle visibility throughout the entire phase of flight and clearly defining the visibility constraints if any.
- (e) Specifying the maximum dynamic pressure and loads on the vehicle to ensure that the vehicle structure experiences the loads which are well within the maximum specified loads with adequate margin.
- (f) Shaping thrust profile to reduce the dynamic pressure while meeting the required mission performance. The finalized thrust profile is the requirement for the propulsion system.
- (g) Minimizing the loads if necessary by selecting a suitable strategy for load relief.
- (h) Defining range safety requirements to ensure safe impact of the spent stages.
- (i) Finalizing the propellant loading considering the mixture ratio dispersions to ensure maximum performance while ensuring safety of propulsion system and other subsystems.
- (j) Generating the ‘guidance margin’ to guarantee that the spacecraft is injected into the specified ‘injection pillbox’, even when the propulsion systems under perform within permissible limits.
- (k) Meeting all defined thermal constraints throughout the entire regime of vehicle flight.

These form major design guidelines/considerations/constraints in trajectory design and other mission studies. If the vehicle for a given mission is finalized, major changes in vehicle configuration may not be possible at this stage. However, a few changes like propellant loading in the propulsion stages, etc. meeting the overall constraints may be attempted.

7.4.3 *Mission and Vehicle Constraints*

While defining the mission, a clear understanding of all constraints stemming from the vehicle environment, vehicle safety and all other associated areas is needed. Some of the important constraints are

- (a) Axial acceleration limits on lift-off and stage separation, the acceleration levels are to be maintained within the maximum level with respect to structural loads as well as on humans in case of human space missions, etc.
- (b) Flight safety considerations to ensure that the impacts of spent stages are only in international water
- (c) Identifying the non-visibility zones for appropriate action
- (d) Vehicle loads during the atmospheric region, considering vehicle environmental factors
- (e) Maximum vehicle attitude rates and angular acceleration as specified by vehicle subsystems
- (f) Critical thermal constraints on vehicle and spacecraft systems

These have to be considered while carrying out detailed mission studies.

7.4.4 *Mission Studies*

The various studies needed for the launch vehicle mission encompass several areas. The following studies which are highly interactive form the basis to firm up the overall mission:

- (a) Configuration finalization to meet the spacecraft requirement
- (b) Aerodynamics design and analysis
- (c) Adequacy of propulsion
- (d) Design of a suitable optimum trajectory
- (e) Control and guidance design
- (f) Mission sequencing
- (g) Evaluation and definition of flight environment
- (h) Performance analysis considering dispersions to assess the effect of variation of different system parameters on mission

All these studies demand accurate generation of vehicle data, which includes data in terms of mass details, mass properties like centre of gravity, mass moment of inertia, aero-propulsion, actuators, sensors, flexible characteristics, slosh, etc. The vehicle sign convention has to be clearly spelled out.

The overall activities required for realizing a successful mission are detailed in Fig. 7.3. These activities play a vital role in a launch vehicle mission, right from the conceptual design. Various studies needed in respect of (a) configuration finalization, (b) aerodynamics design and analysis, (c) adequacy of propulsion, (d) aero-thermal design and analysis, (e) control and guidance design and (f) definition of flight environment have been described in detail in appropriate chapters of this book.

7.5 Trajectory Phases and Mission Design Tasks

Broad trajectory phases of a typical STS mission are represented in Fig. 7.4. The vehicle trajectory during ascent phase can be divided into two distinct phases, the atmospheric phase and the exo-atmospheric phase. The initial portion of ascent trajectory where the vehicle negotiates through the dense regions of the atmosphere is a critical phase of flight with the wind playing a significant role on the launch vehicle design process. In the exo-atmospheric phase generally the stage impact, separation of stages and payload fairings and visibility from tracking stations are of importance.

The atmospheric phase of flight can be further divided into three segments as shown in Fig. 7.4. Initial vertical flight of the vehicle is known as lift-off phase, when the vehicle moves vertically to several tens of meters to clear the launch pad. This is essential to avoid the collision of vehicle to the launch tower against various disturbances acting on the vehicle. The next segment refers to the initial pitch-down

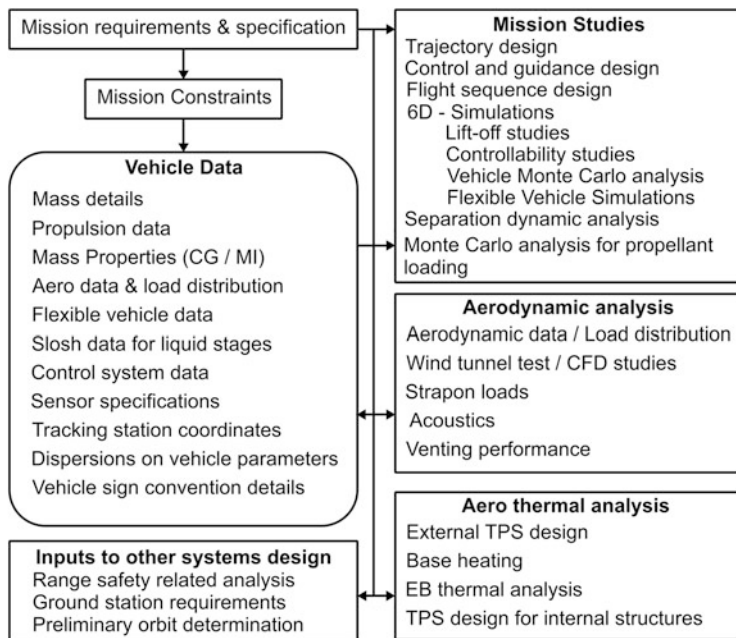


Fig. 7.3 Overall mission activities

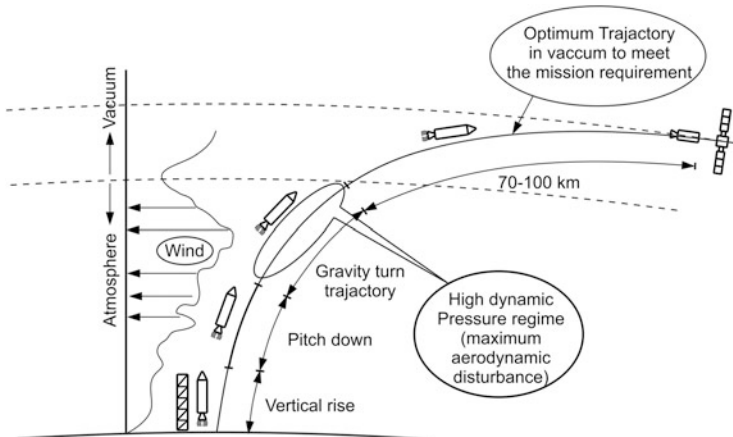


Fig. 7.4 Typical trajectory phases of an STS mission

phase after the vertical flight where it is possible to introduce larger manoeuvres since the dynamic pressure is low due to lower vehicle velocity. The higher angle of attack caused by large manoeuvre at this phase does not cause large loads on structures.

Third phase of atmospheric flight extends up to an altitude of about 40–70 km where atmospheric wind effects are significant. Generally the vehicle is steered along gravity turn trajectory in this segment to keep the angle of attack to a very low value and thus achieving minimum structural load on the vehicle. Zero angle of attack during this phase means minimum thrust vectoring of engines to keep the vehicle along gravity turn trajectory, and this leads to utilizing the maximum thrust of the motor for vehicle acceleration. The control in this regime is active and keeps the vehicle stabilized against disturbances. However spending more time in gravity turn trajectory during atmospheric flight region is an undesirable feature. In most of the vehicles, till the vehicle attains an altitude of about 70 km, open-loop steering programme is used for guiding the vehicle.

The exo-atmospheric phase as shown in Fig. 7.4 is beyond 70–100 km depending on vehicle characteristics and mission constraints till satellite injection. This phase allows controlled manoeuvre, and higher attitude rate commands from guidance do not cause any structural problem to the vehicle. Therefore closed-loop guidance algorithms are used in this phase, but the angular rate and acceleration of the vehicle are limited to the acceptable values from overall mission considerations. Higher angular rate to vehicle is affected using the higher thrust vectoring of the vehicle. Since this type of manoeuvre causes higher steering loss in the total vehicle velocity, it is advantageous to have higher manoeuvre (especially yaw manoeuvres) as far as possible during the earlier phases of vehicle where the velocity is lower.

Mission design tasks to be carried out during various phases of STS mission can be broadly categorized as given below:

- (a) Lift-off studies
- (b) Load relief methodologies
- (c) Thermal loads on the vehicle
- (d) Mission sequence design
- (e) Propellant loading requirements
- (f) Velocity reserve requirements
- (g) Satellite injection orientation
- (h) Propulsion stage passivation requirements
- (i) Tracking and visibility requirements
- (j) Range safety issues

Considering the various requirements and constraints of the above mission activities, an integrated trajectory design and analysis has to be carried out to maximize the vehicle performance to the specified satellite mission.

The details of these tasks and their design considerations are explained in the following sections.

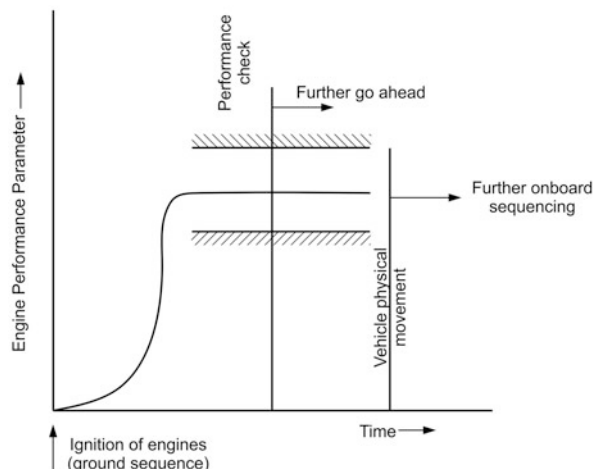
7.6 Lift-Off Studies and Analysis

Lift-off phase is one of the crucial phases of a STS mission. Generally, the first stage ignition for the vehicle is commanded by the ground checkout computer system. All the further sequencing commands are issued by vehicle on-board computers. Therefore, to ensure safety of the mission, vehicle, ground systems and facilities, it is essential to confirm that the first stage performance is as per the expectations. This can be achieved through two-tier logic as represented in Fig. 7.5. At a specified time from the ground ignition command, performance of the engine is checked by verifying the suitable engine performance parameters. Once the performance is within the specified bounds, further activities are allowed to proceed. In case the engine performance is outside the specified bounds, then shut-off command is issued and mission is called off. If the performance check is passed, then the physical lift-off of the vehicle is checked. This is done through confirming the connector demating status of last-minute plug or vehicle sit-on umbilical connector. If the vehicle physical lift-off is confirmed, then only vehicle on-board sequencing is commenced. All the further on-board sequencing is referred with respect to the physical lift-off time. Otherwise mission abort sequence is activated for saving the vehicle and calling off the launch.

The main design parameters during lift-off phase of STS mission are

1. On-board lift-off sequence (ignition time, control initiation time, etc.)
2. Vertical flight time, after which the pitch-down manoeuvre starts
3. Performance parameters, nominal values, their bounds and time of initiation for performance confirmation
4. Physical movement criteria and the corresponding values
5. Time of initiation and end of intentional roll manoeuvre

Fig. 7.5 Lift-off clearance strategy



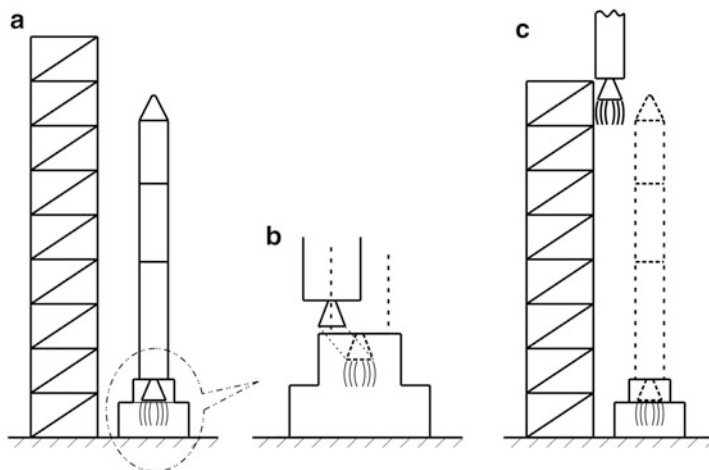


Fig. 7.6 Lateral movement during lift-off phase (a) Vehicle on pad (b) Lift-off (c) Clearing tower

The above design parameters have to be arrived at to meet the following requirements:

1. Clean lift-off of the vehicle with respect to the launch pedestal
2. Minimize the lateral drift of the vehicle towards launch tower
3. Reduce the thermal loads on the launch pad and launch tower
4. Minimize the stay-off of the vehicle over launch pad to reduce the jet acoustic loads and thermal loads
5. Vertical rise time has to be optimized to achieve maximum performance of the vehicle.

The various disturbances which affect the lift-off clearance are thrust misalignments of booster motors, differential thrust for strap-on motors (if any), lateral thrust offset, navigation system pointing error, pull-out forces of the umbilical cord, aerodynamic disturbances and surface winds. Since the direction of surface winds keeps on changing, appropriate direction which can cause the movement of vehicle towards tower is to be considered. These disturbances make the vehicle move laterally as shown in Fig. 7.6. Any collision during lift-off phase leads to the mission catastrophe. By suitably selecting the physical lift-off criteria, along with control design and control initiation time, the lateral displacements due to disturbances can be reduced to a greater extent. Therefore, suitable design of these parameters has to be carried out to ensure the safe clearance of the vehicle from umbilical tower even under worst-case disturbances. The safe clearance needed is to be checked not only with the launch tower but between the nozzles and launch pedestal, as shown in Fig. 7.6, and interference of the vehicle fin (if provided with) with any projection of launch tower during the ascent phase.

The vertical rise time along with the (T/W) ratio severely affects the mission performance of the vehicle. This time decides the vehicle stay time over the launch pad, which has major impact on jet acoustic loads on the vehicle as well as thermal loads on the launch pedestal. Initiation of pitch-down along with the vehicle lateral drift has an impact on thermal environment to the launch tower due to the interaction of jet exhaust of the engine with the tower. Therefore, the height of the vertical rise has to be judiciously selected considering all the above aspects.

7.7 Vehicle Load Reduction Strategies

The atmospheric phase flight of the vehicle after the initial pitch-down is quite complex. In this phase, as the dynamic pressure keeps increasing, the aerodynamic forces become significant. Therefore, the velocity loss due to aerodynamic drag increase is significant, and the increased lateral aerodynamic force associated with the increased control demand has the tendency to increase the loads beyond acceptable limit and break the vehicle. Not only the various losses due to drag, gravity and steering are to be minimized during the ascent phase but also the structural loads, to avoid the collapse of structure due to excessive loads beyond the design limits. The maximum load on the structure during the atmospheric stage is due to aerodynamic load which is characterized by the product of dynamic pressure Q and angle of attack α , that is, $Q \alpha$, as explained in the different chapters of this book.

The important parameters and features of atmospheric flight phase are represented in Fig. 7.7. As the vehicle rises through the atmosphere, the velocity and altitude of the vehicle increase continuously, whereas the density of the

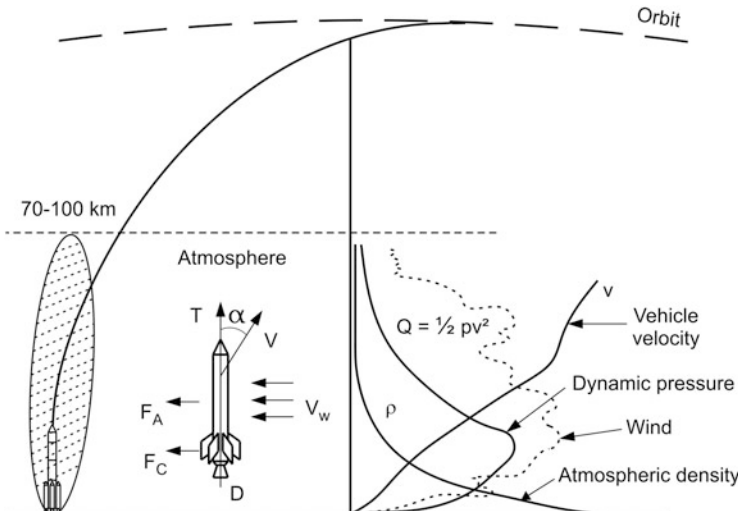


Fig. 7.7 Criticalities of atmospheric flight phase

atmosphere which is a function of altitude decreases. As the vehicle velocity increases, the dynamic pressure, $Q = (\frac{1}{2})\rho V^2$, also increases and the peak value of Q occurs when the vehicle reaches somewhat higher velocity where the density is still significant. Generally, the peak dynamic pressure occurs during the altitude range of 7 to 15 km. Atmospheric wind also generally peaks during this altitude regime. Wind velocities are the major contributing factor for inducing angle of attack α to the vehicle. Since the aerodynamic disturbance forces and vehicle loads are functions of $Q\alpha$, the combination of higher dynamic pressure and higher wind velocity occurs almost simultaneously creating a complex and high disturbing environment to the vehicle systems.

During the atmospheric phase of flight, the wind too plays a major role on dynamics of the launch vehicle. These factors induce aerodynamic force and moments as well as aerodynamic load on the vehicle. Therefore a proper strategy which minimizes the aerodynamic loads on the vehicle is required. The aerodynamic load in this region has to be minimized either by reducing Q or by restricting the maximum α or both.

7.7.1 *Thrust Profile Shaping*

The dynamic pressure profile depends on the velocity build-up with respect to the vehicle altitude. The velocity profile depends on thrust profile of the booster motors. Therefore, the dynamic pressure profile during atmospheric flight phase is essentially decided by the shape of the thrust profile of the propulsion system. To reduce the dynamic pressure, the thrust profile of the vehicle has to be such that the vehicle rises quickly to the higher altitude when the vehicle velocity is lower and the major velocity build-up happens at higher altitude. This demands higher thrust initially, and the thrust values have to be lower during the critical regime of flight, till the vehicle reaches sufficient altitude. Subsequently, the thrust has to be increased to build the velocity as per the mission requirement.

For liquid engines, the thrust value is generally constant. By throttling the engines, the required thrust profile as represented in Fig. 7.8a can be generated to achieve the reduced dynamic profile. In solid motors, generally, progressive thrust-time profiles are used. To meet the requirements of reducing dynamic pressure, the propellant grains of different segments of the motors can be suitably designed to generate the required profile as represented in Fig. 7.8b.

The thrust shape of booster motors in lower stages has impact on the vehicle and propulsion system performance. Therefore, while shaping the thrust profile to reduce the dynamic pressure, it is essential to ensure that the profile achieves the required performance and the shape of the profile is within the capability and constraints of the selected propulsion system. The derived thrust profile forms a major input for the propulsion system design.

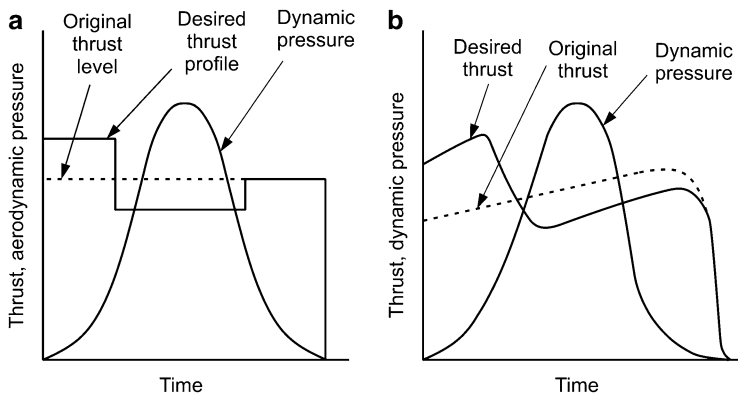


Fig. 7.8 Booster phase thrust shaping (a) Liquid engines (b) Solid motors

The aerodynamic load on the vehicle with the maximum possible reduced dynamic pressure is still beyond the vehicle capability; further strategies are to be considered in design to reduce the angle of attack.

7.7.2 Load Relief Systems

The major contributing factor for creating angle of attack is atmospheric winds. Hence it is necessary that efforts are to be made to reduce wind-induced angle of attack, α , during the atmospheric phase of flight. Such methods are called load relief systems. Basically the load relief system steers the vehicle into the wind, thus reducing the angle of attack. Load relief has to be attempted mainly during the high-dynamic pressure region of the flight, and duration of the load relief is to be critically analyzed based on the vehicle and trajectory. It may be noted that if the load relief trajectory is not attempted, launch availability in certain seasons gets reduced due to increase in the angle of attack beyond the allowable values.

The load relief can be done either by (a) using lateral accelerometer feedback (active load relief) or (b) designing the wind bias steering (passive load relief system). In active load relief it is possible to use angle of attack sensor, but proper implementation of this scheme is quite complex. The lateral acceleration signal represents the angle of attack. As this system is more robust, generally, lateral acceleration signals are used for active load relief system.

In active load relief system, the lateral accelerometer package with two accelerometers, one along pitch and another along yaw axis, placed at a convenient location from the centre of gravity of the vehicle is recommended to provide load relief. This sensor provides one more parameter (in addition to attitude and body rate) in the feedback signals for attitude control. The output of lateral accelerometer

has an analogy for angle of attack sensor, and the effect of adding this signal into control command is to tilt the vehicle into wind. This helps in reducing the vehicle angle of attack and also the corresponding engine gimbal angle. The resulting effect is the reduction of bending moment on the vehicle. In such active load relief control, it is possible to select suitable gains in the feedback signals to achieve the drift minimum or load minimum control depending on the requirements.

In drift minimum system the aerodynamic and control forces are fully balanced, and hence the drift of the vehicle is minimized. But it provides load relief only to some extent. Alternatively if the weightage to the attitude feedback is reduced the focus would be on minimizing the angle of attack which in turn causes considerable reduction of loads on the vehicle. However this causes the vehicle to drift away from the desired trajectory, which has to be corrected by the guidance system subsequently. Therefore it is essential to have a design which offers the best combination of load minimum and drift minimum. One of the solutions is to apply the load relief only for shorter durations in regimes where the dynamic pressure is high, and the time period has to be chosen such that it results in the reduction of high aerodynamic loading. Details of active load relief system are described in Chap. 14.

Another commonly used load relief system is following gravity turn trajectory with wind biasing, which is a passive system. In this system, the steering programme is designed in such a way that it compensates for the prevailing wind conditions during launch.

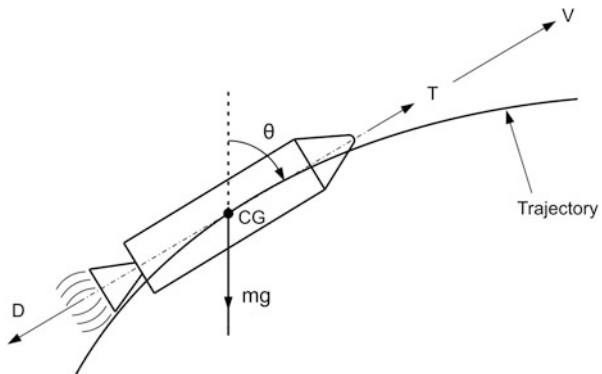
7.8 Gravity Turn Trajectories and Wind Biasing

The requirement of reducing angle of attack is achieved by following the gravity turn trajectory. This manoeuvre is an important feature of atmospheric phase trajectory, where the vehicle axis is aligned with velocity vector profile continuously. Such manueuvre ensures zero angle of attack thereby reducing the vehicle load to the barest minimum.

7.8.1 *Gravity Turn Trajectories*

In gravity turn trajectory manoeuvre, the vehicle axis (thrust direction) is aligned with the velocity vector. Consider STS as an axi-symmetric body and thrust direction along the longitudinal axis of the vehicle. Vehicle orientation and gravity turn trajectory of such a vehicle is represented in Fig. 7.9. For the gravity turn trajectories of axi-symmetric vehicles, the aerodynamic drag force acts on the vehicle whereas the lateral force is zero due to zero angle of attack.

Fig. 7.9 Gravity turn trajectory



Thus, the equations of motion of the vehicle following gravity turn trajectory represented along the vehicle longitudinal axis and normal to the vehicle axis are given as

$$m \frac{dV}{dt} = T - D - mg \cos \theta \quad (7.1)$$

$$mV \frac{d\theta}{dt} = mg \sin \theta \quad (7.2)$$

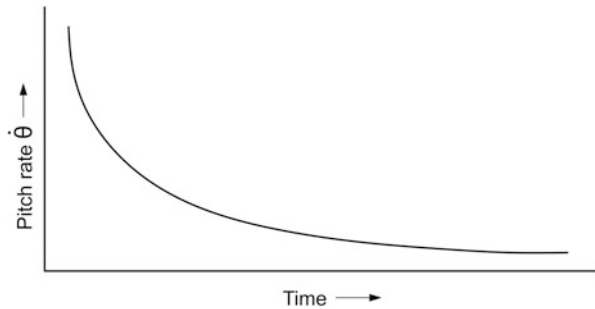
where m is the vehicle mass, V is the vehicle velocity, T is the thrust force, D is the aerodynamic drag force, g is the acceleration due to gravity at the flight instant and θ is the vehicle attitude with respect to the local vertical. From Eq. (7.2),

$$\dot{\theta} = \frac{d\theta}{dt} = \frac{g \sin \theta}{V} \quad (7.3)$$

The vehicle attitude rate to follow the gravity turn trajectory is given by Eq. (7.3). It can be seen from Eq. (7.3) that if there is no gravity, the vehicle trajectory is a straight line with constant vehicle attitude. The presence of gravity makes the trajectory to have a shape of curvature, and hence this trajectory is known as gravity turn trajectory.

It is to be noted that the vehicle attitude rate depends on vehicle instantaneous attitude, velocity and gravity to follow the gravity turn trajectory as given in Eq. (7.3). The following are the important aspects of gravity turn trajectories:

1. To have a meaningful gravity turn trajectory, vehicle has to achieve a certain velocity. Otherwise the required vehicle rates are very high.
2. At the end of vertical rise, the vehicle attitude with respect to vertical is zero. Therefore, the gravity turn trajectory initiation at the end of vertical rise is not possible.

Fig. 7.10 Gravity turn rate

3. Combining these two features, to achieve a realistic gravity turn trajectory, the gravity turn has to be initiated after intentional pitch-down manoeuvre of the vehicle.

Since the vehicle velocity is lower, the gravity turn rate can be relatively higher at the initial phase and subsequently can be reduced depending on the velocity build-up and instantaneous attitude of the vehicle as shown in Fig. 7.10.

It is to be noted that if the gravity turn is initiated at much early stage when the vehicle attitude is near vertical then the gravity turn rate is small and leads to steeper vehicle trajectory in atmospheric flight phase, ending up with more velocity loss due to gravity. Thus the mission performance of the vehicle drastically reduces. For the cases with larger θ , early initiation of gravity turn demands higher vehicle rates for the vehicle. These aspects demand that the gravity turn be initiated as late as possible. But to reduce the vehicle load, the gravity turn has to be initiated as early as possible. Also, at the initiation of gravity turn, there may be discontinuity between actual vehicle rate and the gravity turn rate demand at that instant.

Therefore, vertical lift-off time, pitch-down manoeuvre duration and transition phase as represented in Fig. 7.11 are decided judiciously to meet all the requirements. The intentional pitch-down manoeuvre rate after vertical rise is decided to meet the performance requirements at the end and to have smooth transition to gravity turn manoeuvre. The timings for these events are designed to meet the performance and load requirements simultaneously.

7.8.2 Wind Biasing

During the STS flight with gravity turn trajectory, if there is no wind, velocity vector is always aligned to the longitudinal axis of the vehicle as represented in '1' of Fig. 7.12. But the prevailing wind V_w at higher altitude makes the relative velocity of the vehicle away from the longitudinal axis, as represented by V_R in the figure. Thus, the vehicle flight direction is along V_R , which makes the angle of attack α to the vehicle axis as shown in Fig. 7.12

Fig. 7.11 Gravity turn trajectory transition

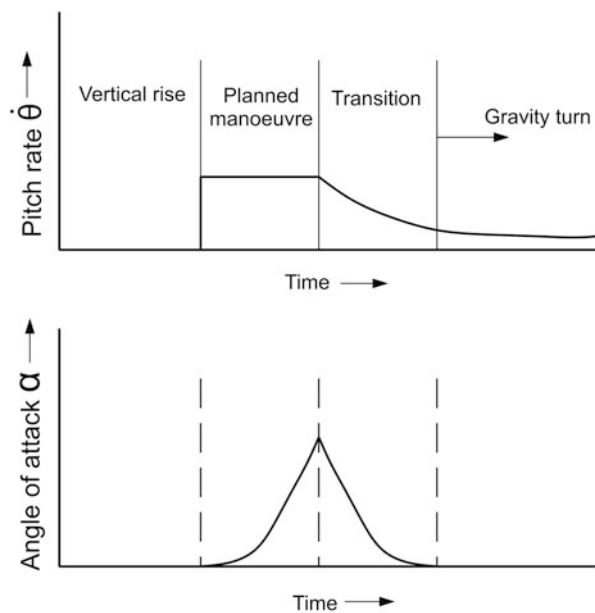
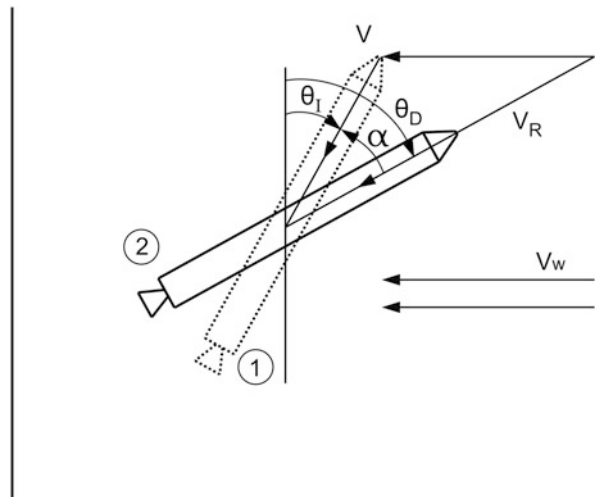


Fig. 7.12 Angle of attack and wind biasing



The angle of attack induces disturbing aerodynamic normal force on the vehicle. This force tends to rotate the vehicle about the centre of gravity, and the control system of the vehicle generates the necessary control force to stabilize the vehicle against the disturbances. The combined aerodynamic normal force and the balancing control force in turn introduce load on the vehicle structure. The aerodynamic load indicator 'Q α ' of a typical STS during its mission through a typical

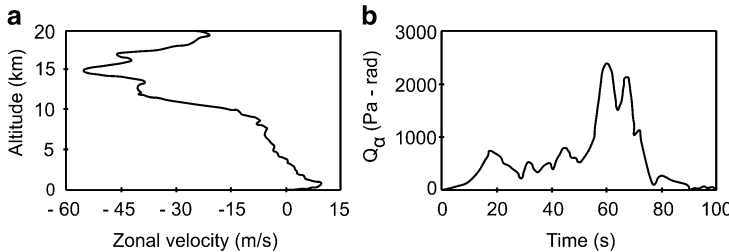


Fig. 7.13 Impact of wind on aero load indicator (a) Zonal wind velocity (b) Aero load indicator

measured wind profile is given in Fig. 7.13. It is seen that even though the trajectory is designed with zero angle of attack with no wind conditions, the in-flight wind induces considerable value of ' $Q\alpha$ '. To reduce $Q\alpha$, it is essential to reduce the angle of attack α .

The most efficient way of reducing angle of attack is to fly the vehicle such that longitudinal axis of the vehicle is aligned with V_R , which is caused by wind velocity as shown in '2' of Fig. 7.12. This feature is called 'wind biasing'.

Thus, in wind biasing trajectory, vehicle steering programme is designed such that at any instant, the vehicle attitude is always aligned with relative velocity vector. The important aspects to be considered during wind-biased trajectory are as follows:

Even though the angle of attack is represented in simple form in Fig. 7.12, the realistic contributions are represented in Fig. 7.14:

$$\alpha = (\theta_c - \theta) + \frac{V_d}{V} + \alpha_w \quad (7.4)$$

where $(\theta_c - \theta)$ is the difference between the desired attitude of the vehicle and the actual realized vehicle attitude, V_d is the lateral drift of the vehicle normal to the vehicle axis, which is caused by the control force and residual normal aerodynamic force and α_w is the angle of attack caused by the wind velocity, V_w .

Therefore, even though α is reduced to zero with wind velocity, V_w , there can be non-zero values for $(\theta_c - \theta)$ and V_d . These factors introduce lateral trajectory drift and affect the vehicle trajectory in subsequent phases, which in turn affect the vehicle performance. It is essential to design the integrated trajectory with wind biasing to achieve the required performance. Therefore, wind biased trajectory has to be attempted only when required. The initial conditions at the time of CLG initiation achieved by such design have to be considered for CLG design. The integrated steering programmes for both atmospheric flight and the CLG phases have to be validated through extensive simulations. Real on-board systems are also to be used in simulations to verify the on-board implemented logics before they are cleared for flight.

Fig. 7.14 Angle of attack components

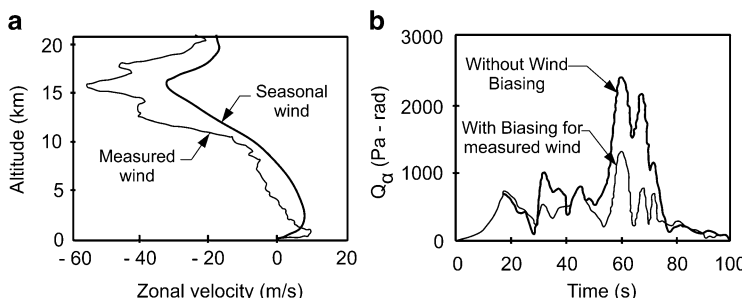
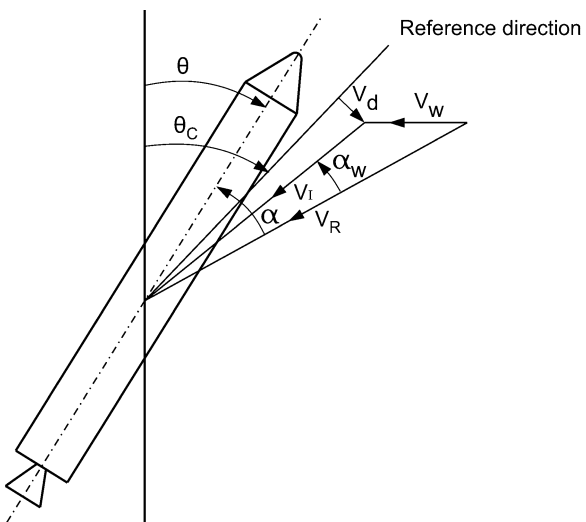


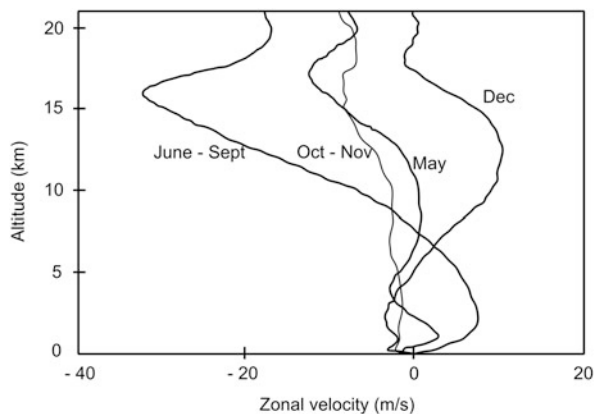
Fig. 7.15 Impact of seasonal wind biasing (a) Wind (b) Aero load indicator

To design wind-biased trajectory on ground, the in-flight wind profile is required. But it is to be noted that, due to the highly random nature of the wind profiles, the in-flight wind is not known a priori.

One possibility is to design the trajectory biased to the mean wind profile of the season of the launch. Due to this ‘biasing’, the vehicle is commanded into the mean wind at that altitude. Thus the wind-induced angle of attack is only due to difference of the actual wind prevailing at that altitude and the mean wind that is used in biasing as shown in Fig. 7.15a. Under such cases, there is considerable reduction in Q_α as shown in Fig. 7.15b. This strategy helps in increasing the launch probability of that season.

It can be seen from Fig. 7.16 that there are large deviations in mean wind between seasons. Therefore, this design has the disadvantage if the launch is postponed to different season due to unforeseen problems. In such cases it becomes

Fig. 7.16 Seasonal mean winds



necessary to redesign the steering programme with the changed seasonal winds, which is a cumbersome process.

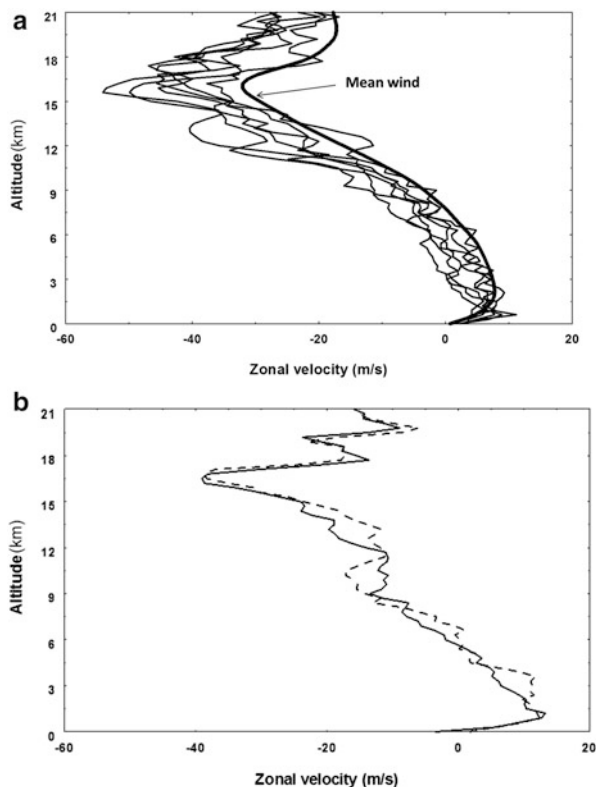
It is to be noted that there can be large variation in day-to-day winds measured during the launch campaign phase. Typical shape of profiles is as given in Fig. 7.17a. Therefore, the seasonal mean wind biasing still does not cater to the large variations between the seasonal mean wind and the prevailing wind during the day of launch. But the wind variations during a short period of time (within about 1 h) are very small as shown in Fig. 7.17b.

Therefore, the above drawback can be overcome by biasing the trajectory to wind that is prevailing on the day of launch. This is termed as Day-of-Launch (DOL) wind biasing. DOL wind biasing is based on the wind measurements which is as close to the launch as possible on the launch day and then generating the steering programme for this wind just before launch. The DOL wind biasing needs a reference trajectory which is capable of meeting the defined payload requirements. It is also necessary to define the target conditions at the end of open-loop trajectory phase, so that closed-loop guidance design remains unaffected. The powerful computing facilities, which are available presently, enable the process of generation of wind-biased steering programme within a short duration and its use for trajectory designs and its validation.

7.8.3 Implementation Aspects of DOL Wind Biasing

The major challenge in implementation of DOL wind biasing is to minimize the overall time needed to complete the entire process after the wind measurements are carried out very close to launch. This involves processing of measured wind data, generation of open-loop wind-biased steering programme and validation of the design in simulations. To utilize the latest wind data as close as possible to the flight time, on the launch date, the entire process of generation of trajectory has to be

Fig. 7.17 Wind characteristics: (a) day-to-day variation with respect to mean wind (b) wind variations within 1 h 20 min



completed within the stipulated period, validated and loaded in the on-board computer during the countdown sequence. This demands automation of all processes.

The approach needed is that a reference open-loop trajectory for a mission and a closed-loop guidance (CLG) suitably designed are available and validated through extensive evaluation through several phases of simulations. Entire CLG programme and data are to be coded and stored in flight computer. It is important to define the initial conditions for a pillbox at the end of open-loop trajectory and to ensure that the vehicle parameters meet these target conditions within allowable dispersions. Therefore the generation of DOL open-loop steering programme has to ensure that the specified end conditions are always met so that CLG design remains insensitive to wind variations and functions smoothly. This helps to avoid the revalidation of CLG algorithm which has been already designed and tested extensively.

Once the DOL wind-biased steering programme is generated, it is to be integrated with the total vehicle trajectory including the closed-loop guidance and validated using all digital simulation test beds and also in integrated on-board

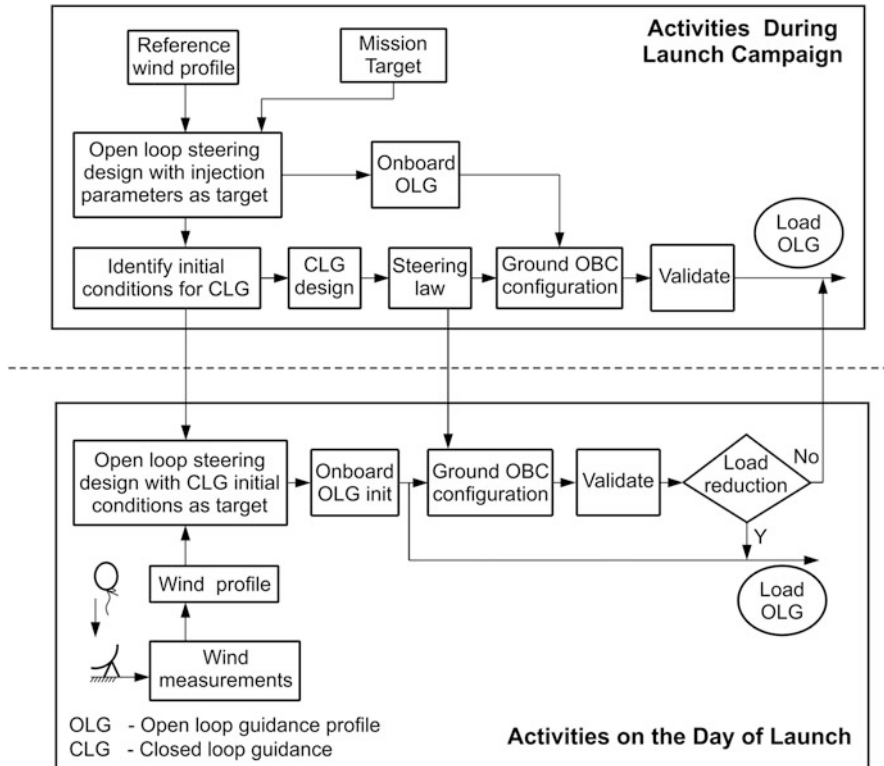


Fig. 7.18 Day-of-Launch wind biasing design and implementation strategy

equivalent systems. The major implementation issue is the seamless integration of all functionalities and their extensive validation to ensure that the entire scheme is without any flaw.

A typical block diagram of the total methodology for the design and validation of DOL wind biasing scheme is illustrated in Fig. 7.18.

The extensive measurements of winds over a period on the launch base are needed, and using this data the nominal and 3σ variation of the wind for each month is to be generated. The wind variation from the wind measured before launch and the wind prevailing at launch time is also to be assessed by measuring the winds for a few days prior to the launch date as well as just a few hours before flight. Generally this variation is not significant, and thus DOL wind biasing trajectory allows all weather launches and totally eliminates the risk of launch postponement.

Figure 7.19 shows a typical plot of $Q\alpha$ vs time during the atmospheric phase of a flight: (a) without wind biasing, (b) seasonal mean wind biasing and c) DOL wind biasing trajectory. The advantage of using DOL wind biasing is quite evident and ensures benign load conditions to the vehicle during the flight.

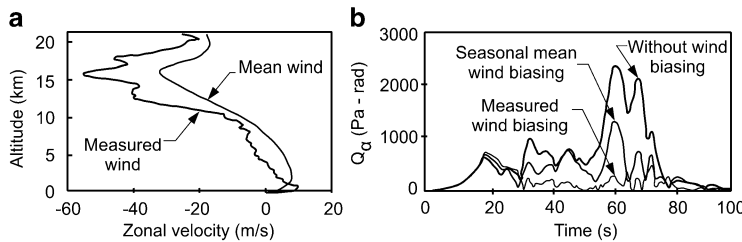


Fig. 7.19 Effect of Day-of-Launch wind biasing (a) Wind (b) Aero load indicator

7.9 Thermal Constraints

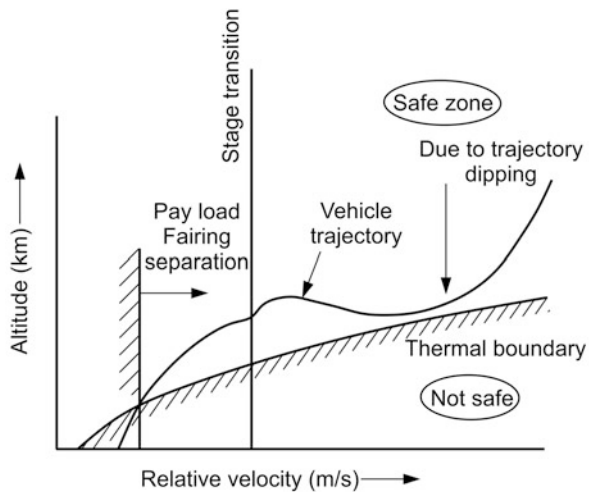
Another important mission requirement is to ensure that sensitive subsystems of vehicle and payload do not experience excessive thermal loads during the flight. The separation altitude of the payload fairing is to be carefully decided during trajectory design, and the basic guideline used is that the heat flux experienced by the payload has to be less than 1135 W/m^2 (1 sun heat), which is considered to be safe. Since the flow regime in this transition changes from continuum to free molecular the estimation of heat flux has to be carried out in detail and the separation altitude to be confirmed as safe.

For upper stages with low thrust-to-mass ratio and with a flight path angle very close to the local horizontal direction at stage ignition, the trajectory altitude may decrease or dip during certain segment of the flight before the vehicle gains enough acceleration. In such cases trajectory needs to be designed with restriction on the extent of dipping of altitude to ensure that the vehicle does not experience unsafe thermal loads.

These types of constraints are highly non-linear and very sensitive to changes in the variables in the initial and middle portions of the trajectory. The thermal boundary poses a critical constraint for the vehicle, and in this region it is better to use a flat trajectory with a limit on flight path angle. As the thermal environment is function of atmospheric density (altitude) and relative velocity, the allowable thermal boundary can be defined in terms of altitude-relative velocity space. During flight with sensitive systems exposed to ambient, the vehicle trajectory has to be in the safe zone. A typical profile of vehicle velocity and altitude indicating the safe thermal boundary is given in Fig. 7.20.

It is essential to define the minimum dip altitude based on thermal considerations and use it as a constraint during the trajectory design. The flight path of the upper stage is to be shaped such that the altitude does not dip beyond specified limits. Although the trajectory dip may help in maximizing the payload, the STS mission trajectory has to be designed such that the constraint on heat flux has to be strictly followed to protect the payload from the thermal considerations.

Fig. 7.20 Thermal boundary profile



7.10 Mission Sequence Design

Mission sequence design involves defining optimum sequence of launch events for the STS mission starting from T_0 , first-stage ignition time, till the satellite injection into orbit, satisfying all mission constraints. Mission sequence plays a vital role in achieving the required mission performance of STS while satisfying the vehicle, ground systems and subsystem requirements during its mission. Suitable mission sequence is essential for the smooth functioning of the vehicle systems and to achieve the defined mission successfully. To ensure this all the flight events in terms of engine ignition, vertical rise, pitch/yaw manoeuvre, engine shut-off, stage separation, payload fairing separation, coast phase, terminal stage engine shut-off and satellite separation, etc. take place as planned for the nominal as well as off-nominal flight environments. The optimum sequence of events valid for one flight environment may not be safe for another environment. Therefore, to meet all the system requirements, it is essential to define the event sequence in real time by vehicle on-board systems, depending on the flight environment. The optimum strategy is to detect the critical events in vehicle on-board, i.e. real-time decision (RTD) and further events sequencing are referenced with respect to the RTD till the next critical event is identified. This process starts from the first-stage ignition and continues till satellite injection.

7.10.1 Mission Sequence Strategy

Mission sequence strategy for a typical three-stage STS system is given in Fig. 7.21. First-stage ignition command is issued by ground checkout system. The entire

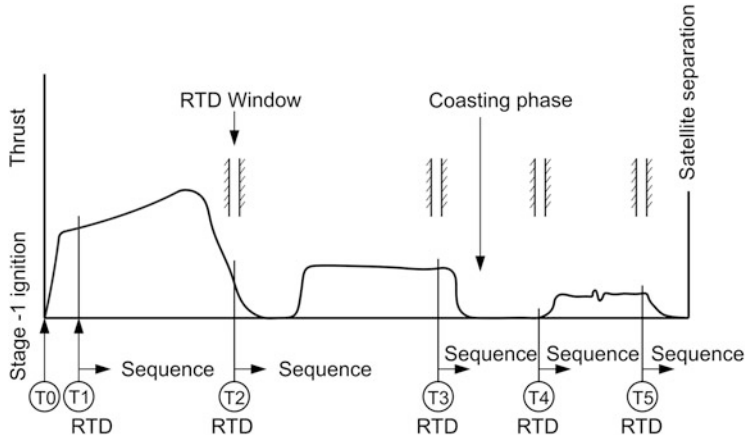


Fig. 7.21 Typical mission sequencing

vehicle sequencing is activated only after confirming the positive vehicle lift-off from launch pad which is linked to unambiguous connection de-mating between ground and vehicle and termed as last-minute plug (LMP) pullout. This RTD is identified as T1 in Fig. 7.21, and all subsequent events are linked to T1. It is possible to detect this event either by a sit-on-connector or by monitoring the chamber pressure of the booster motor. Appropriate values are to be fixed for these parameters considering all possible scenarios for absolute detection of T1.

Regarding the real-time decision between stage transitions, the longitudinal acceleration of the vehicle available in the inertial navigation system is generally used to detect the burnout of the stages. Once the propulsion stage thrust starts falling during the end of its burn (tail-off region), the acceleration starts dropping. Suitable value/threshold for acceleration sensing in each stage can be decided for detecting the tail-off based on clean separation requirement. This raises a flag in the on-board computer, which, in turn, initiates the RTD events for stage separation. This RTD is represented as T2 in Fig. 7.21. The value of the threshold for RTD sensing can be set considering various factors like the burn-time dispersions for the motor, tail-off dispersions, subsequent events during the tail-off region, etc. The detection of RTD has to be highly reliable and should not give false detection during any phase of flight. Therefore the redundant values of the longitudinal accelerations available in inertial navigation system are used for RTD with proper selection logic. Once the detection of real-time decision is available on board, all subsequent events of sequencing are linked to the new RTD timing till the next RTD detection.

In certain cases, once the instantaneous impact point of the vehicle reaches the allowable range safety boundary, it is essential to shut off the stage and separate it,

Table 7.1 Typical Event Sequencing

Event no.	RTD	Criteria for RTD	Time	Event
1	—	—	T0	Stage-1 ignition
2	T1	LMP pull out	T1 + 0	LMP pull out
3			T1 + x1	Stage-1 control on
4	T2	Acceleration $\leq a$	T2 + 0	RTD sensing
5			T2 + x2	Stage-1 control off
6			T2 + x3	Stage-1 separation
7			T2 + x4	Stage-2 ignition
8			T2 + x5	Stage-2 control on
9			T2 + x6	PLF separation
10	T3	Instantaneous	T3 + 0	Stage-2 shut-off
11		Impact point $>$ limit	T3 + x7	Stage-2 control off
12			T3 + x8	Stage-2 separation
13			T3 + x9	Coast control on
14	T4	Desirable position, velocity	T4 + 0	Stage-3 ignition
15			T4 + x10	Coast control-off/ Stage-3 control on
16	T5	Target orbit	T5 + 0	Stage-3 shut-off
17			T5 + x11	Stage-3 control off
18			T5 + x12	Stage-3 coast control on
19			T5 + x13	Stage-3 coast control off
20			T5 + x14	Satellite separation

to meet the mission safety requirements. This point is decided based on the vehicle reaching specified position and velocity vector. This RTD is marked as T3 in Fig. 7.21. All further sequencing is based on T3.

If the vehicle mission has the feature of coasting between two stages as shown in Fig. 7.21, it is essential to determine optimum time for igniting the next stage, represented as RTD T4. Further sequencing in this stage is referenced with respect to T4.

Once the mission target conditions are achieved, it is essential to shut off the final-stage engine. This is decided in the vehicle on-board by the closed-loop guidance algorithm and is represented as RTD T5 in Fig. 7.21. Vehicle sequencing beyond engine shut-off till satellite separation are linked with T5.

The sequencing events which are linked with RTD should not be triggered inadvertently (false alarm) at any other time than intended. This is taken care by defining appropriate time window for each RTD, by taking into account all possible dispersion scenarios of propulsion systems. In case of the failure in RTD identification, due to malfunctioning of any of the elements in the chain, the window-out is taken as default time, and rest of the sequencing events are linked with this time. Typical event sequencing based on RTD is given in Table 7.1.

7.10.2 Typical Stage Transition Sequence

Stage transition is a crucial event for STS mission. A typical event sequencing design strategy is explained below. There are three major conflicting requirements during stage transition: (1) performance, (2) clean separation and (3) vehicle controllability.

For a clean separation, the thrust of the spent stage has to be as low as possible. For the case of solid motors, this event can occur much later than motor burnout time. Also, for both the cases of solid motors and liquid engines, there can be large dispersions in the action time. Therefore, if the sequencing has to be based on time, to ensure minimum thrust for both the cases of shortest and longest burn time, one has to wait for long time for separating the spent stage even after motor burnout. Only after the separation of the spent stage the next stage can be ignited. The long gap between lower-stage burnout and upper-stage ignition has severe impact on the performance.

Regarding the vehicle controllability, it is essential to switch off the control in the spent stages when the thrust level is sufficiently high to avoid the control-induced disturbances. After control switch-off there is a time gap for stage separation, next stage ignition and control on from the next stage. This introduces a large no-control zone between the stage transitions. This can cause the increased rate and error, and in certain cases, the upper stage may not be able to capture the vehicle with such large error, finally ending up with mission failure. Therefore, to avoid such scenario, it is essential to reduce the no-control zone. For the cases of fixed time-based sequencing, the minimum thrust requirement for control jeopardizes the mission if there is large dispersion in the spent stage motor performance.

Because of these conflicting requirements, it is not possible to fix the time-based sequencing a priori for such crucial events. Thus it becomes absolutely essential to determine the burnout of each propulsive stage in real time on-board by utilizing proper sensors like pressure sensors measuring the motor chamber pressure or longitudinal acceleration using accelerometers in the navigation system. Based on the output of these sensors, RTD can be made by the on-board computer to find the time at which the stage has burned out, thrust requirement for control off and the thrust sufficiently small for safe stage separation. This is done in real time by the on-board computer. All further sequencing is fixed based on the RTD event as in Fig. 7.22. Suitable window-in and window-out times are fixed for the RTD as explained earlier. A typical event sequencing after the RTD considering the expected dispersions on the upper stage is explained in Fig. 7.22.

7.11 Propellant Loading Requirements

The propellant mass required in each stage to achieve the specified mission is decided during configuration design phase. This is one of the major requirements for the design of the propulsion systems along with performance parameters. One of

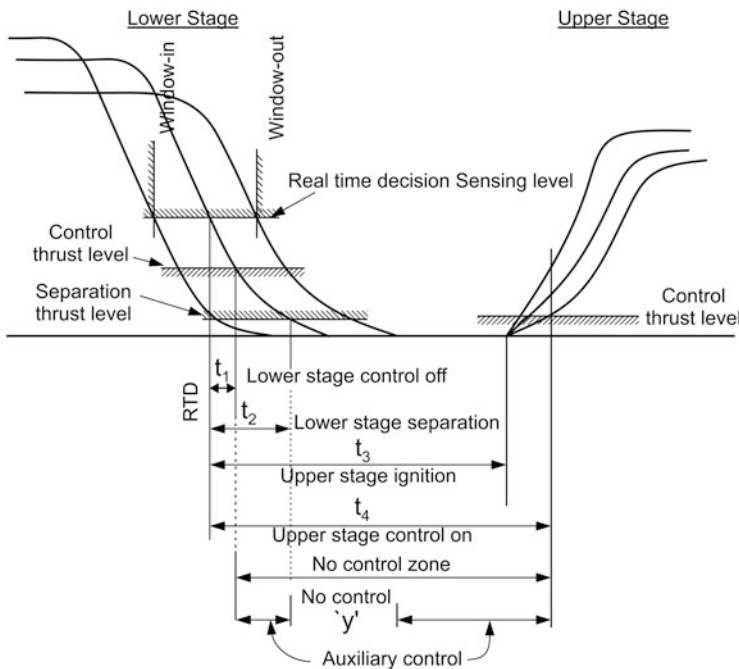


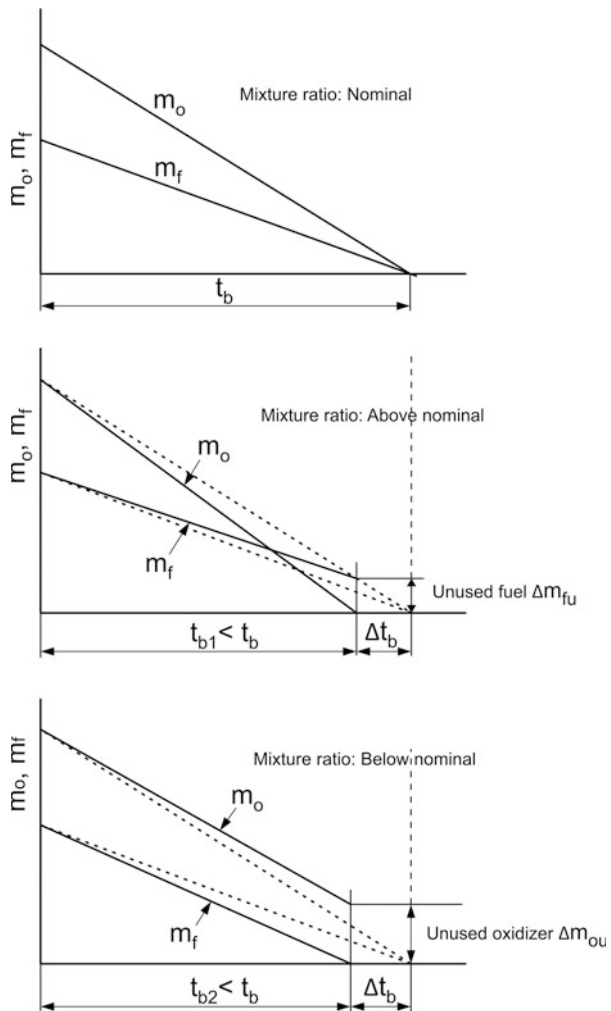
Fig. 7.22 Typical stage transition sequencing

the important performance parameters for the liquid propulsion system is the mixture ratio. Maximum performance in terms of specific impulse is achieved at an optimum mixture ratio, depending on the type of propulsion system and design specification. The propellant tanks are designed to accommodate the propellants which need to be consumed at the specified mixture ratio. Sometimes the optimum mixture ratio demands large tank size for one of the propellants, which in turn has the impact on the mission performance. Therefore, trade-off studies considering the improvement in specific impulse and reduction in structural mass have to be carried out to arrive at a suitable mixture ratio which gives the maximum performance. The details are explained in Chap. 9.

During flight, depending on the flight environment, there can be deviation in achieved mixture ratio. If it is more than the specified value, the oxidizer is consumed at a faster rate. Once the oxidizer depletes, the engine thrust comes down and the burnout of the stage happens. Under such conditions, to ensure the safety of the engine, it is essential to shut off the engine. Therefore, the effective functional duration of the stage becomes less than expected, and the total impulse imparted by the stage is also less. At the time of burnout, unused fuel Δm_{fu} remains in the tank as shown in Fig. 7.23.

In order to avoid such scenarios, generally either active or passive mixture ratio control systems are introduced in liquid propulsion systems, which ensure that the mixture ratio is close to the nominal even in the dispersed flight environments.

Fig. 7.23 Propellant consumption history pattern for different mixture ratios



However, due to the errors in sensors used for the mixture ratio control as well as due to the deviations in the subsystems used with respect to the predicted values, there can be small dispersions in the realized mixture ratio. The deviated mixture ratio and the propellant depletion before the expected time have the following implications: (1) reduction in the active functional duration of the stage, (2) tail-off characteristics.

The reduction in the burn duration has a significant impact on the mission performance. The different tail-off characteristics due to the different types of depletion cause severe environment to the vehicle subsystems and satellites. The tail-off characteristics and frequency contents of pressure and thrust fluctuations are different for the various types of depletion, viz. (1) simultaneous depletion,

(2) oxidizer depletion, (3) fuel depletion, (4) oxidizer followed by fuel depletion and (5) fuel followed by oxidizer depletion. Depending on the vehicle system characteristics and tail-off characteristics, the impact of the tail-off characteristics on the health of the subsystems are analyzed, and based on the results, the specified depletion characteristics are chosen. This is achieved by (1) tuning the valve parameters to ensure the specified depletion characteristics occur in flight and (2) loading the propellants (oxidizer and fuel) such that the specified depletion occurs. This is termed as propellant loading analysis in mission design process.

To achieve the specified depletion under all the possible environments of parameter dispersions including mixture ratio, the required loading can be ‘skew-loading’, i.e. one of the propellants has to be loaded much beyond that corresponding to the nominal mixture ratio. This extra loading has severe performance impact. Therefore, to get more favourable performance, the loading is finalized based on Monte Carlo (MC) analysis. In the propellant loading MC analysis, a detailed propulsion system model is used considering all performance parameters and other vehicle systems and the interfaces among them. Using this model, for different propellant loading combinations, MC analysis is carried out, perturbing various performance parameters including mixture ratio which gives the probability of each type of depletion and the vehicle performance. Using these results, the propellant loading combination within the capacity of propellant tanks is to be selected. This has to meet the ullage volume requirement which gives the desired depletion while meeting the required performance. This propellant loading has to be used in the mission design process and implemented in flight.

7.12 Velocity Reserve Requirements

The propellant loading requirement computed as part of configuration design is mainly to meet the equivalent velocity as demanded by a specific mission and skewed loading to meet the required depletion characteristics. In reality, during flight, the vehicle performance can have dispersions with respect to the predicted parameter values. In addition, due to the in-flight disturbances caused by the external and vehicle internal sources, there can be tracking error in the vehicle attitude with respect to the desired attitude as computed by the vehicle closed-loop guidance system. Under such environments, the energy provided by the propulsion system designed for the nominal vehicle performance may not be sufficient to achieve the mission target. Therefore, it is essential to provide extra energy in the vehicle propulsion system to take care of such in-flight uncertainties. The extra energy to be provided in the vehicle on-board is called ‘velocity reserve’ or ‘guidance margin’.

If the mission is planned to take care of all the possible disturbances in the additive sense, then margin required can be very large. If such huge margin is to be built into the system, then the available energy for nominal performance is restricted, which has direct impact on the vehicle performance. It is to be noted

Table 7.2 Equivalent velocity reserve required

SI No.	Parameter uncertainty	Incremental equivalent velocity required to achieve the target
<i>Stage-1 (solid)</i>		
1	I_{sp}	ΔV_1
2	Action time	ΔV_2
3	Propellant mass	ΔV_3
4	Structural mass	ΔV_4
<i>Stage-2 (Liquid)</i>		
5	I_{sp}	ΔV_5
6	Mixture ratio	ΔV_6
7	Oxidizer loading	ΔV_7
8	Fuel loading	ΔV_8
9	Chamber pressure	ΔV_9
10	Structural mass	ΔV_{10}
<i>Stage-3 (Liquid)</i>		
11	I_{sp}	ΔV_{11}
12	Mixture ratio	ΔV_{12}
13	Oxidizer loading	ΔV_{13}
14	Fuel loading	ΔV_{14}
15	Chamber pressure	ΔV_{15}
16	Structural mass	ΔV_{16}
17	PLF mass	ΔV_{17}
18	Satellite mass	Satellite mass

that the chances of all the performance parameters deviating simultaneously to create worst-case environment is very remote. Therefore, the guidance margin requirement is arrived at based on probability analysis. This is done in two ways: (1) Root Sum Square (RSS) method and (2) Monte Carlo Analysis method.

In RSS method, after the initial mission design for nominal vehicle parameters, each parameter is perturbed to its specified 3σ dispersion level. The impact of this dispersion is analyzed and extra equivalent velocity required to achieve the mission target under this dispersed environment estimated. The study is repeated for all the parameter dispersions, considering one at a time.

As an example, consider a three-stage vehicle with solid first stage, liquid second and third stages and assuming third stage is commanded to cut-off, the typical dispersion parameters are about 18. Their details and equivalent velocity variation due to each of these parameters are given in Table 7.2.

From data given in Table 7.2, the RSS of incremental equivalent velocity ΔV_m is computed as

$$\Delta V_m = \sqrt{\sum_{i=1}^{18} \Delta V_i^2} \quad (7.5)$$

The ΔV_m given in Eq. (7.5) is the velocity reserve required in the vehicle. Assuming ΔV_m has to be provided by third stage, considering the propulsion parameters of that stage, the extra propellant Δm required to provide ΔV_m is loaded additionally or kept as reserve, and this margin is called guidance margin.

In the MC analysis method, after the initial mission design with the nominal vehicle parameters, integrated mission simulation with detailed model as explained in Chap. 8 is carried out in MC mode. For all the specified dispersion parameters, type of dispersions, their specified distribution, etc. are analyzed. Each time, a set of parameters is selected assuming random variation on each of the parameters with the specified dispersions, and with the selected set, simulation is carried out. Such simulations are repeated with huge numbers of runs simulating that many sets of random values for the selected parameters. From each run, the incremental equivalent velocity required is computed. The total number of simulations n (say) depends on the convergence of the results. The n numbers of ΔV s are statistically analyzed to get the mean and 3σ of required ΔV . Then, depending on the defined success criteria, the required ΔV is finalized. This value can then be used to compute the required Δm as explained earlier. Once the Δm is loaded to the vehicle additionally or kept as a margin, then during STS flight, the probability of achieving the nominal targeted mission is same as the one used for designing Δm .

7.13 Satellite Injection Requirements

The satellites are required to be injected into the defined orbit with the following additional conditions: (1) rates at separation to be limited to the capabilities of the satellite control system, (2) sufficient distance between the separated stage and satellite is ensured and (3) attitude is achieved as desired by the functional requirements of satellites.

To meet the above requirements after the final stage cut-off, sufficient time is given before satellite separation to ensure that the residual thrust of the vehicle propulsion stage is zero. The satellite separation system is designed to provide the necessary differential velocity so that the distance between the satellite and separated stage is progressively increasing. The control system of the vehicle is designed such that, during the combined flight phase after cut-off, the vehicle is controlled to achieve the attitude as defined by the satellite requirements and the vehicle rate less than the specified limits. After achieving the required injection conditions, the satellite is injected into the orbit as represented in Fig. 7.24. To meet the specified distance between satellite and separated stage, satellite injection can be done along the orbital plane or in the out-of-plane direction. To avoid collision in

Fig. 7.24 Satellite orientation requirements

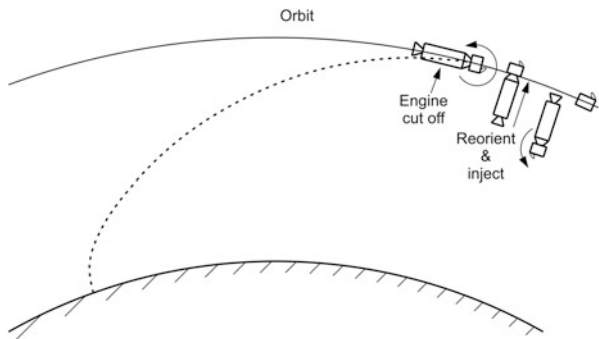
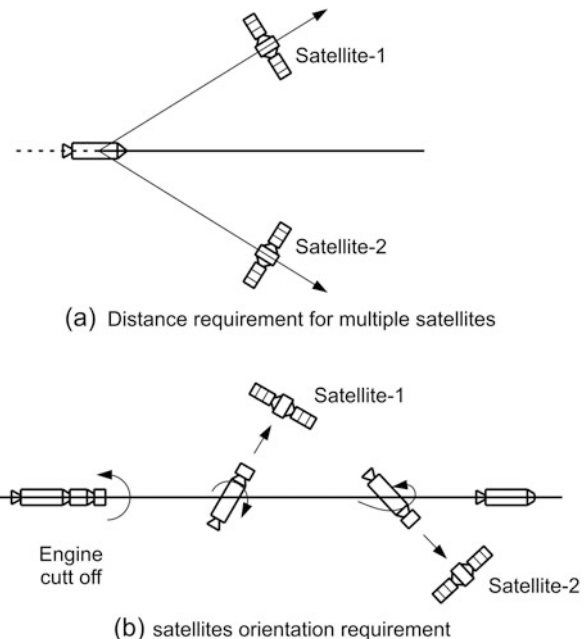


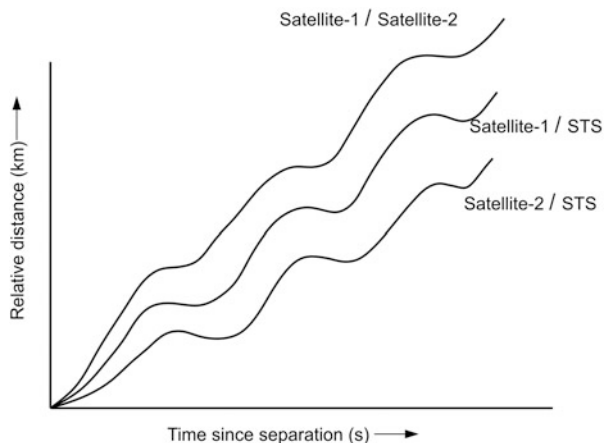
Fig. 7.25 Multiple satellite injection requirements



the case of inadvertent re-ignition of the separated stage, generally, the separated stage is oriented in a direction away from the satellite motion.

In certain missions there are requirements for the launch of multiple satellites. In such cases it is essential to ensure that these satellites after separation continue to move in defined orbits without having any collision between any of the satellites during the entire period of their life as represented in Fig. 7.25a. This is achieved by defining proper sequence of satellite separation timings and reorientation requirements as given in Fig. 7.25b. The selection of separation velocities and flight sequence for the spacecraft are chosen such that they move in different but close orbits. It is also necessary to carry out long-term relative orbital motions for these

Fig. 7.26 Relative motion of bodies after separation



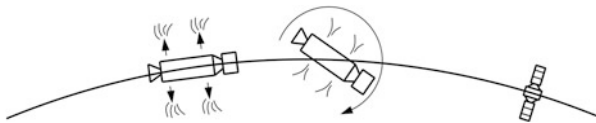
spacecraft. The possibility of plume interaction during the operation of reaction control thrusters and also during the passivation of terminal stage are to be analyzed in detail to avoid the potential damage to any of the spacecraft.

The collision possibility of any of the spacecraft or the final vehicle stage has to be studied considering the nominal and off-nominal performance of the final stage. The possible dispersions on separation system parameters are also to be considered. The orbital elements of the final stage and all spacecraft at respective separated conditions are to be estimated and relative distance movements of the objects at different time instances after separation analyzed. A typical analysis showing a typical relative motion between two spacecraft missions is shown in Fig. 7.26. From Fig. 7.26, it can be seen that the relative distances with respect to time are monotonically growing.

The relative minimum distance between various bodies has also to be assessed using Monte Carlo studies taking into account various dispersions like the left-out propellant in the final stage, separation velocity, the reaction control thruster variations, etc.

7.14 Propulsion Stage Passivation Requirements

The final stage of all launch vehicles enter the orbit, and as per the international guidelines on space debris it is mandatory to deplete all left-out propellants in a planned manner and the stage is put in a passive mode. This operation is termed as passivation of the stage. The quantity of left-out propellant in the stage depends on the propulsion performance of earlier stages. The requirement for passivation of the terminal stage is to initiate this action immediately after the satellite separation. But this can lead to contamination of the spacecraft. Therefore sufficient time gap has to

Fig. 7.27 Stage passivation

be provided between the separation of satellite and the initiation of the passivation as shown in Fig. 7.27.

The effective method for passivation is to introduce suitable vent nozzles. In order to avoid the reaction on the vehicle doublet-type nozzle configuration is generally chosen. There are several schemes for venting the trapped propellants, and their details are available in the references quoted. The vent circuits are prone to ice formation due to freezing, and this can lead to blockage or sometimes explosions. These issues are to be tackled during the design phase to confirm the smooth operation of venting as planned. Additionally one has to verify the lowest temperature attained and also the ice formation during the process to avoid failure of the system. To ensure high reliability, experimental evaluation of the thrusters in a high-altitude test facility using an identical scheme on ground has to be carried out.

7.15 Vehicle Tracking Requirements

Radio visibility of the vehicle during its entire mission duration from ground station tracking network is required for real-time monitoring of the flight to obtain the telemetry data from the flight for post-flight analysis. There is also requirement for issuing the tele-command from the ground whenever it is essential. The important parameters needed for vehicle tracking during the flight from a defined ground station are given in Fig. 7.28.

During trajectory design all the visibility parameters from a tracking station, namely, elevation, slant range, aspect angle, antenna azimuth, range rate and aspect angle, have to be estimated. Range information is needed to decide about the signal strength. Aspect angle is used to determine the loss in signal due to rocket exhaust coming in the path of the signal. During acquisition of signal (AOS) at least 5° elevation and during loss of signal (LOS) 2° elevation angle are desirable. However, a minimum of 2° elevation angle from AOS to LOS generally gives satisfactory visibility. For a better visibility, aspect angle has to be more than plume angle.

Therefore, even though there is good visibility in terms of elevation, when there is plume angle more than aspect angle as shown in Fig. 7.29, it is essential to plan an alternate ground station to acquire the telemetry data. If a taller or wider structure is present in front of the tracking station then for some combinations of elevation and antenna azimuth, the structure may block the passage of signal. In such cases, visibility has to be improved by positioning a mobile terminal at a vantage location or by redesigning the trajectory with implication on the payload and performance.

Fig. 7.28 Tracking parameters

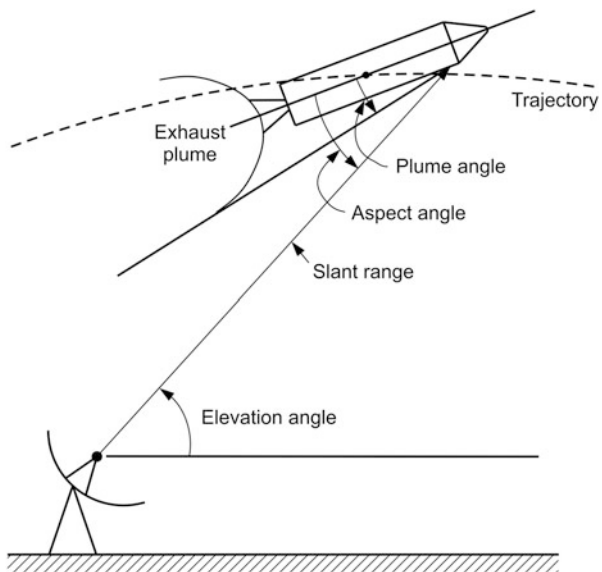
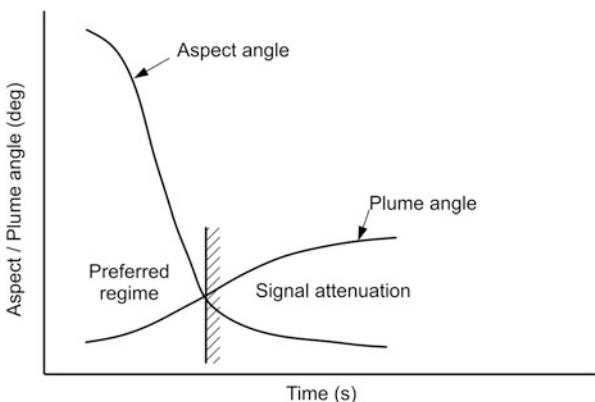


Fig. 7.29 Aspect and plume angles



Further, the visibility coverage is needed for a certain length of time after the final stage separation and spacecraft injection for monitoring the passivation and re-orientation manoeuvres of the separated final stage. For preliminary orbit determination (POD) of the spacecraft, range, range rate, elevation and aspect angle information are required.

The tracking station locations are to be planned, depending on the mission, in such a way that all critical events like stage ignition, stage burnout, stage separation, strap-on separation, payload fairing separation and spacecraft injection are visible at least from one of the tracking stations. Continuous coverage is essential except for long coasting phase where some gap in visibility may be acceptable. Hence tracking stations are to be planned such that adequate overlap of coverage

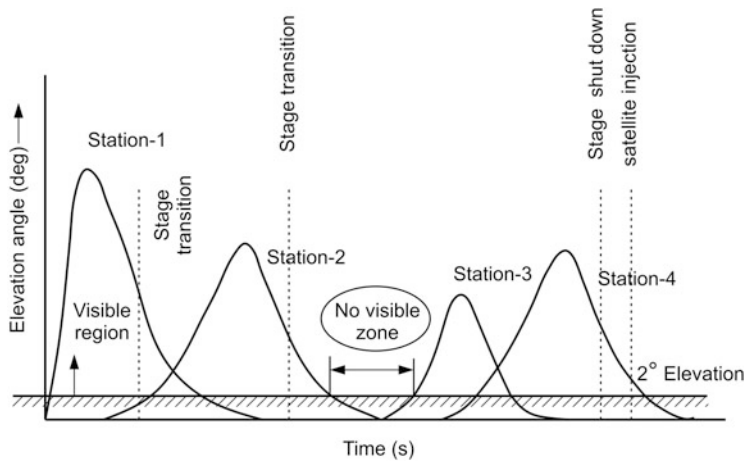


Fig. 7.30 Elevation angles of typical STS mission

from successive stations exists. Elevation angles from four ground stations of a typical STS mission with three stages are represented in Fig. 7.30. In case there is no visibility from any of the specified ground stations as shown in Fig. 7.30, the trajectory should be designed such that there are no critical events during that segment. This might have some implication on the payload that can be carried. For such regions where visibility does not exist and no critical events occur, data storage and delayed transmission has to be planned. In case of trajectories wherein critical events occur during the flight and the visibility from ground-based tracking stations is not available one has to necessarily plan the ship-based tracking during these periods.

7.16 Range Safety Constraints

The spent stages of launch vehicle are to be impacted either in safe land zones belonging to the country from which launch is originated or in safe international waters limited by specified boundaries. The mission design has to observe these conditions very strictly. Selection of a suitable launch azimuth depends not only on the final mission considerations but also on the safety aspects of the launch even if it has a penalty on the payload mass. At low altitudes the ground and instantaneous impact point (IIP) traces of the launch cannot violate the defined international boundaries.

The IIP trace of the vehicle is decided by the instantaneous position and velocity vectors as represented in Fig. 7.31. IIP is the point of impact of the vehicle on the Earth's surface in case the vehicle power goes off instantaneously. The separated stage impact point is the IIP corresponding to separation instant. Therefore, during

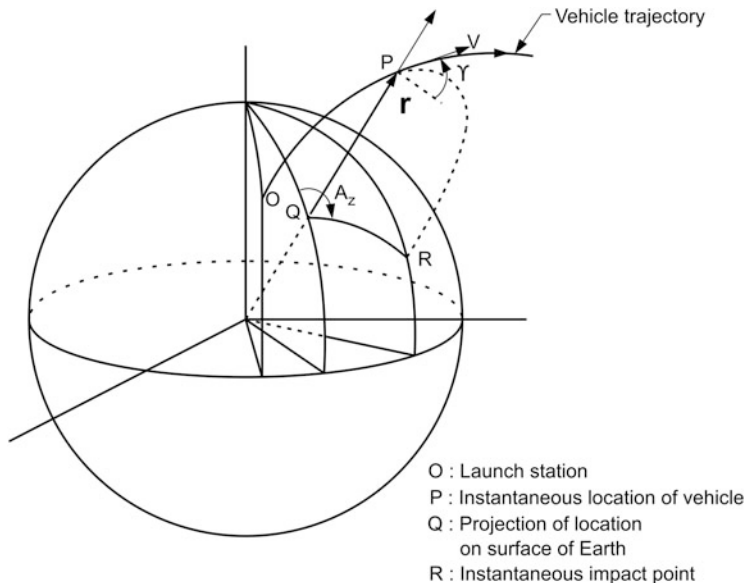


Fig. 7.31 Instantaneous impact point (stage impact)

mission design process, the position and velocity vector profiles have to be suitably designed to ensure that the range safety constraints are not violated.

During the mission design, another important study is the assessment of the hazards and risk levels to life and property in case of malfunction/failure of the vehicle during the ascent phase of the trajectory. The risk has to be assessed both during the lift-off phase involving the launch base facilities and during the subsequent phase of the flight involving the down range land masses. Therefore detailed studies are needed on vehicle failure modes, its impact on the trajectory and the land impact probability. The damage potential also depends on the type of failure and time at which failure occurs during flight. All these aspects have to be studied in detail during the initial mission studies. These data have to be appropriately utilized during launch to decide on the destruction of stages from range safety considerations.

7.17 Integrated Trajectory Design

Once the vehicle configuration is defined and mission specifications and constraints are identified, the integrated trajectory of the vehicle during ascent phase has to be suitably designed to meet the final satellite injection conditions in an optimum manner, while satisfying all the specified requirements and constraints. The trajectory design process involves generation of optimum trajectory profile, i.e. position and velocity histories from lift-off till satellite injection such that the end conditions

meet the required orbit. The selected trajectory has to inject maximum payload for the defined propulsion stages or maximize the reserve fuel (guidance margin) for the defined payload.

The vehicle trajectory in simple terms can be specified thus: the vehicle rises vertically at launch pad and then is made to orient its path smoothly on a continuous basis to achieve the required flight path angle at the specified altitude and velocity conditions for insertion of payload into the orbit. The vehicle has conflicting requirements like, on the one hand, moving vertically as far as possible to get out of the atmosphere very quickly and, on the other hand, to turn the vehicle as early as possible to attain the required flight path angle at relatively lower velocity regimes to avoid the steering losses in vehicle velocity. A trade-off study has to be made during trajectory design to ensure minimum losses due to drag and due to steering and to meet other constraints of thermal vehicle loads and range safety and tracking.

7.17.1 Trajectory Design Considerations

The main objective of trajectory design is to maximize the vehicle performance. During the integrated trajectory design process, various mission and vehicle subsystem requirements and constraints have to be carefully considered. The requirements are summarized as given below:

1. Launch azimuth has to be selected depending on the requirement on orbital inclination. For low inclination orbits, eastward launches are preferred whereas for high inclination orbits such as Sun-synchronous polar orbits, southward launch is desirable. But designer has to select only those launch azimuths which are declared safe throughout the flight path of the vehicle. The range of allowable azimuth is termed as the safe launch corridor.
2. Unlike a sounding rocket that is launched from a launch lug at an elevation, the launch vehicle which is resting on the launch pad is to be launched vertically. It ascends vertically for a given time to avoid the collision of the vehicle with the launch tower even under all combinations of disturbances. During the ascent, it is necessary to minimize the jet plumes from the vehicle impinging on the umbilical tower to avoid the damage to the tower. The impact of vertical rise time on payload is also to be considered.
3. The vehicle roll is facilitated to coincide with the pitch plane with the launch azimuth immediately after the initial lift-off and before any other manoeuvres are carried. This becomes essential in vehicles where the pitch axis of the vehicle is not aligned with the launch azimuth due to constraints of launch tower.
4. Subsequent to this the vehicle starts pitching down optimally. The upper limit on the pitch rate is dictated by the control system, vehicle inertia and tracking error. The lower limit is driven by the need to move away from the launch pad

- as soon as possible to ensure safety of the range in the vicinity of the launch pad.
- 5. Once this phase is over, the gravity turn to the vehicle is initiated. This causes a transition in pitch and yaw rates from optimal values to the values which are needed to minimize the angle to attack to near zero.
 - 6. Gravity turn is initiated based on altitude, transonic Mach number, aerodynamic load indicator values and payload obtainable. The trajectory is initially designed for seasonal mean wind profiles and follows gravity turn during the atmospheric portion till the closed-loop guidance is initiated.
 - 7. For the vehicles with strap-on motors, their ignition and separation sequences have to be decided based on the optimum payload capability, peak dynamic pressure and acceleration at peak dynamic pressure for nominal and off-nominal trajectories. The dynamic pressure, angle of attack and body rates have to be kept small at strap-on separation.
 - 8. Peak dynamic pressure is an important parameter from aerodynamic and structural considerations. If the peak dynamic pressure exceeds the prescribed limit, the trajectory has to be reshaped to obtain the specified values. It may be noted that large reduction is possible only by suitable design of thrust profile of the booster motor.
 - 9. At burnout of stages, the dynamic pressure, angle of attack, bounds on attitude and attitude rates and also suitable design for the tail-off of the motors are to be ensured to meet the specified conditions. At the time of separation of each stage, unused propellant like injectant fluid used in secondary injection thrust vector control (SITVC) in the stage is jettisoned along with the inert mass, wherever possible.
 - 10. Yaw manoeuvre, if necessary, is initiated after the atmospheric flight to avoid high angle to attack during the high dynamic and complex atmospheric flight regime. It is carried out generally from second stage burn phase in order to achieve the required inclination. Plane change is achieved during the ascent phase satisfying the constraints on instantaneous impact and planned stage impact points.
 - 11. All the stage impacts have to be in safe zone, and instantaneous impact requirements with respect to flight over the land mass are also to be considered. Impact of spent stages is one of the difficult constraints which are encountered in trajectory design. Management of the impact of the spent upper stage in the safe zones is even harder since usually at that point the flight velocity is closer to orbital velocity. Hence for such cases, suitable orbit size has to be selected, and the trajectory has to meet the impact constraints even under off-nominal conditions.
 - 12. An optimum unpowered duration of flight known as coasting can be employed to achieve the desired range, altitude and orientation whenever necessary and feasible. Thus the desired end conditions can be achieved without any expenditure on fuel. This segment can be between the powered flight portions of the same stage or two different stages.

13. The end constraints such as altitude and inclination have to be satisfied for circular orbits whereas for elliptical orbits perigee altitude, apogee altitude, arguments of perigee and inclination constraints have to be satisfied.
14. Suitable ‘guidance margin’ fuel has to be reserved as explained earlier.
15. ‘No-control zones’ between stage transitions are to be minimized during the steering design.
16. The $\pm 3\sigma$ variations of the critical parameters of the subsystems of the vehicle like propulsion systems, aerodynamics and navigation system are to be specified. Trajectory designer has to simulate these variations (like the off-nominal performance of motors, aerodynamic drag, etc.) and verify the performance. Designer has to ensure that the constraints are met to the extent possible under these variations.

7.17.2 Trajectory Design Strategy

It is to be noted that all the requirements and constraints explained above depend on trajectory (position and velocity vectors) profile. Therefore, in order to achieve the specified requirements, it is essential to modulate the trajectory profile as per the requirements of various phases of mission, and there must be suitable control variables required to modulate the trajectory. This is achieved as explained below:

Consider three-dimensional trajectory dynamics of the vehicle as explained in Chap. 8:

$$\dot{r} = V \quad (7.6)$$

$$\dot{V} = \frac{1}{m} [BI] [F_T + F_A] + G_I \quad (7.7)$$

where

r, V = Position and velocity vectors of vehicle with respect to ECI frame

m = Vehicle mass

$[BI]$ = Body-to-ECI frame transformation matrix, function of vehicle attitude θ, ψ, ϕ .

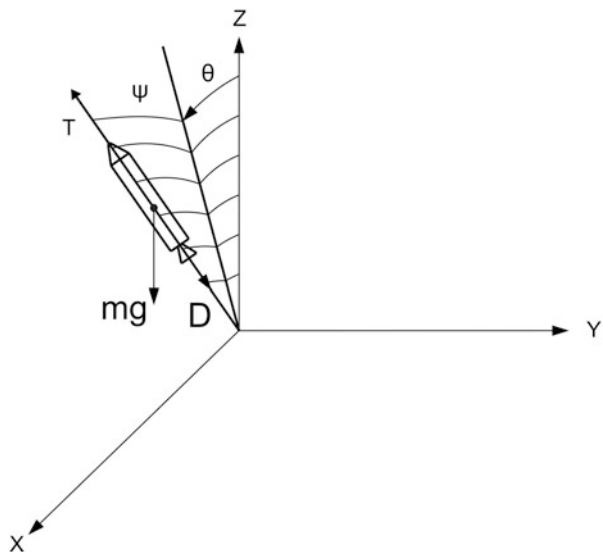
G_I = Gravity acceleration vector

F_T = Thrust vector of the vehicle

F_A = Aerodynamic force vector of the vehicle

The thrust vector F_T depends on the propulsion performance and atmospheric density. The atmospheric density is function of altitude, which in turn depends on r . Mass m is function of propellant depletion history, decided by the propulsion system used. The aerodynamic force vector F_A depends on the aerodynamic characteristics of the vehicle (C_N, C_S, C_A), dynamic pressure and angles of attack. Therefore, F_A can be assumed as function of vehicle shape and r and V . The gravity vector G_I is function of r . The body-to-inertial transformation matrix depends only

Fig. 7.32 Vehicle trajectory dynamics



on vehicle attitude profile. Therefore, it can be concluded that for a defined vehicle, the trajectory dynamics is function of vehicle attitude.

For a simplified version as shown in Fig. 7.32, where thrust and velocity vectors along vehicle longitudinal axis (normal and side forces) are zero, the translational dynamics is given by

$$\ddot{X} = \left[\frac{T(T_V, x, y, z) - D(C_D, x, y, z, u, v, w)}{m} \right] \cos \Psi \sin \theta + g_x(x, y, z) \quad (7.8)$$

$$\ddot{Y} = \left[\frac{T(T_V - x, y, z) - D(C_D, x, y, z, u, v, w)}{m} \right] \sin \Psi + g_y(x, y, z) \quad (7.9)$$

$$\ddot{Z} = \left[\frac{T(T_V - x, y, z) - D(C_D, x, y, z, u, v, w)}{m} \right] \cos \Psi \cos \theta + g_z(x, y, z) \quad (7.10)$$

The vehicle position and velocity are given by

$$x = \int u \quad (7.11)$$

$$y = \int v \quad (7.12)$$

$$z = \int w \quad (7.13)$$

$$u = \int \ddot{X} \quad (7.14)$$

$$v = \int \ddot{Y} \quad (7.15)$$

$$w = \int \ddot{Z} \quad (7.16)$$

From the above discussions, it can be concluded that for a given vehicle configuration with the specified propulsion stages, the trajectory is a function of vehicle attitude θ, Ψ and ϕ . By modulating θ, Ψ, ϕ the required trajectory can be achieved.

Therefore, the trajectory design process can be stated as the estimation of optimum attitude profile (steering profile) which generates the desired trajectory which maximizes the vehicle performance while satisfying various requirements and constraints.

The above problem can be stated mathematically thus:

Select control variable vector $c(t)$ such that

$$\text{minimize} \quad J = \phi(X(t_f), t_f) \quad (\text{performance index}) \quad (7.17)$$

subject to

$$dX/dt = f(X(t), c(t), t) \quad (X(t) : \text{state variable vector}) \quad (7.18)$$

$$\psi(X(t_f), c(t_f), t_f) = 0 \quad (\text{boundary condition}) \quad (7.19)$$

$$g_l \leq g(X(t, c(t), t)) \leq g_u \quad (\text{path constraints}) \quad (7.20)$$

In the trajectory optimization process

$$c = \{\theta, \Psi\}$$

$$X = \{x, y, z, u, v, w\}^T$$

$$\Psi = \{\text{orbital parameters at injection}\}$$

$$g = \text{Inequality constraints such as range safety, tracking, heat flux, etc.}$$

$$g_l, g_u = \text{Limits of the constraints}$$

Therefore, it can be concluded that the trajectory design process is an optimal control problem. By suitable parameterization process, the trajectory design can also be considered as constraint non-linear optimization problem.

Typical equivalent parameters are given below:

1. Control variables:

- (a) θ and $\dot{\Psi}$ profile
- (b) $\dot{\theta}$ and $\dot{\Psi}$ history
- (c) Staging duration
- (d) Coasting duration
- (e) Stage ignition in case of multi-stages

2. *Optimization variables:*

- (a) Maximization of payload
- (b) Minimization of burn time
- (c) Maximization or minimization of one of the orbital parameters

The optimization parameter depends on the specific mission requirements:

3. *Boundary conditions:*

- (a) Required orbital conditions at injection

4. *Path constraints:*

- (a) Range safety constraints
- (b) Dynamic pressure constraints
- (c) Tracking parameter constraints
- (d) Thermal constraints

7.17.3 *Integrated Trajectory Design Process*

The integrated trajectory design is an iterative procedure. The central core of the process consists of vehicle flight mechanics and an optimizer. The input to the flight mechanics process is the vehicle data, vehicle sequencing and environment such as gravity, atmospheric properties and wind conditions. The input conditions for the optimizer are the mission requirements and vehicle constraints. The flight mechanics and optimizer interact iteratively, and the converged optimum trajectory is the output of the design process as explained in Fig. 7.33.

Using vehicle data, wind data and with initial estimates for the attitude programme and staging events such as coasting time, stage ignition and cut-off times, the flight mechanics model propagates the trajectory from lift-off till the initially defined cut-off time. During the trajectory propagation process, various events as defined such as vertical rise, gravity turn initiation, wind biasing with the defined wind profile, initiation of steering after gravity turn from the specified time, stage events, etc. are used. The propagated trajectory parameters are given as input to the optimizer. Using the trajectory parameters, mission-defined requirements and constraints, optimizer updates the steering angles, the coasting time, cut-off time and other design parameters to optimize the objective function while satisfying the constraints. These updated steering and control parameters are used in the flight mechanics to re-propagate the trajectory from the lift-off till the refined cut-off time and the trajectory outputs passed to the optimizer. This process repeats till the solution converges.

The converged solution gives the optimum steering programme and trajectory profile which achieves the optimum performance of the vehicle while meeting all the requirements and constraints including the wind biasing requirements.

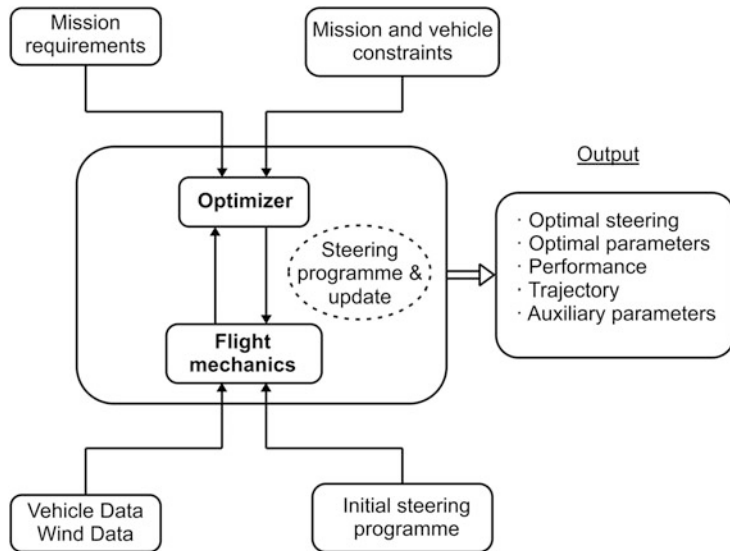
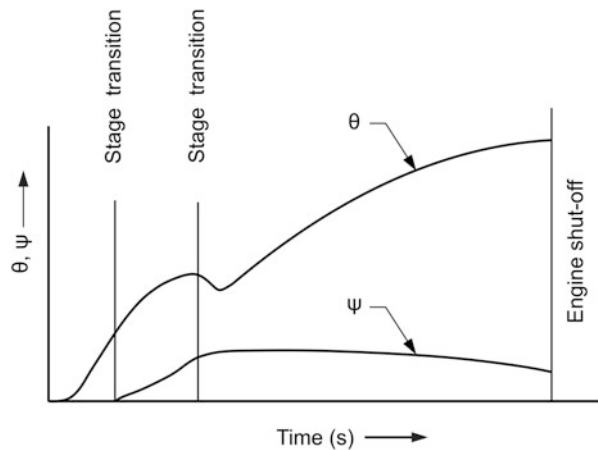


Fig. 7.33 Integrated trajectory design

Fig. 7.34 Steering profile



7.17.4 Optimum Mission Profile

The optimum steering program of a typical three-stage STS mission is given in Fig. 7.34. The altitude and inertial velocity profiles are given in Fig. 7.35. The flight parameters during atmospheric flight phase are represented in Fig. 7.36. A typical mission profile is given in Fig. 7.37.

Three-dimensional point-mass trajectory dynamics as defined above has to be expanded to include the rotational motions of the vehicle about the centre of gravity

Fig. 7.35 Trajectory profiles

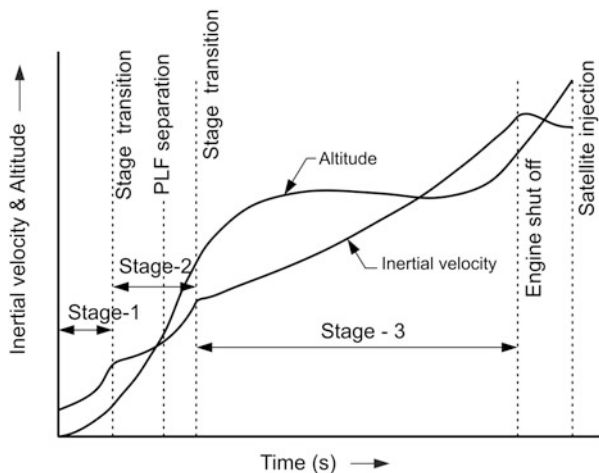
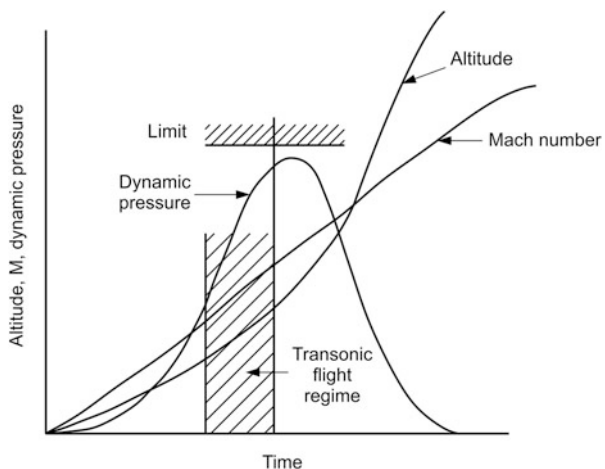


Fig. 7.36 Flight parameters during atmospheric flight phase



to suitable six-degrees-of-freedom trajectory dynamics. Once the basic trajectory meeting the overall (6-DOF) requirement is generated, the navigation, guidance and control (NGC) functions are progressively integrated into this 6-DOF trajectory dynamics to evaluate the detailed performance of the vehicle, subsystems and mission. Details of dynamics, their formulations, performance evaluation, etc. are given in Chap. 14.

The mission thus designed forms as reference input for all further subsystem design studies. These design aspects of subsystems are discussed in detail in the subsequent chapters of the book.

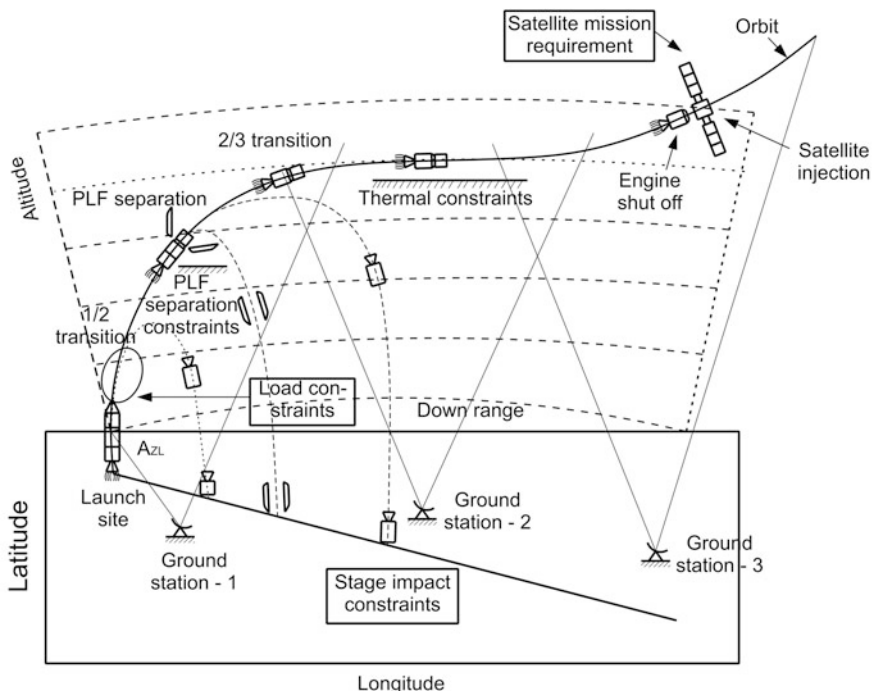


Fig. 7.37 Typical STS mission profile

Bibliography

1. Wiesel, W.E.: Spaceflight Dynamics. McGraw-Hill, New York (1997)
2. Hammond, W.E.: Design Methodologies for Space Transportation Systems, AIAA Education Series, Reston (2001)
3. Wertz, J.R., Larson, W.J. (eds.): Space Mission Analysis and Design. Microcosm, Torrance (1999)
4. Adimurthy, V.: Launch vehicle trajectory optimization including rotational dynamics". Journal of Spacecraft and Rockets **13**, 59–61 (1976)
5. Adimurthy, V.: Launch vehicle trajectory optimization". Acta Astronautica **15**, 845–850 (1987)
6. Adimurthy, V.: Trajectory and mission design of launch vehicles". In: Ramakrishnan, C.V. (ed.) Current trends in Engineering practice. Lectures under the Distinguished Visiting Professorship Scheme of Indian National Academy of Engineering, pp. 417–436. Narosa Publishing House, New Delhi (2006). ISBN 81-7319-689-3
7. Thomson, W.T.: Introduction to Space Dynamics. Dover Publications, New York (1986)
8. Isakowitz, S.J.: AIAA International Reference Guide to Space Launch Systems, 2nd edn. American Institute of Aeronautics and Astronautics, Washington, DC (1995)
9. Vinti, J.P., Der, G.J., Bonavito, N.L. (eds.): Orbital and Celestial Mechanics. Progress in Astronautics and Aeronautics". AIAA, Reston, VA (1998)
10. Turner, M.J.L.: Rocket and Spacecraft Propulsion: Principles, Practice and New Developments. Springer, Heidelberg/New York (2006)

11. Leitmann, G.: Optimization Techniques, pp. 1–31. Academic, New York (1962)
12. Ehricke, E.A.: Space flight, Vol.-II, Dynamics. Van Nostrand, New York (1962)
13. Brown, C.D.: Spacecraft Mission Design. AIAA, Reston (1992)
14. Cornelisse, J.J., Schoyer, H.F.R., Wakker, K.F.: Rocket Propulsion and Spaceflight Dynamics. Pitman Publishing Ltd, San Francisco (1979)
15. Pocha, J.J.: An introduction to Mission Design for Geostationary Satellites. D.Riedel Publishing Company, Boston (1987)
16. Rheinfurth, M.H.: The Alleviation of Aerodynamic Loads on Rigid Space Vehicles. NASA TM X-53397, Mrshall Space Flight Centre, Huntsville (1966)
17. Ernsberger, G.: Wind Biasing Techniques for use in obtaining Load Relief. NASA TMX-64604 (1971)
18. Sinclair, A.J., Flowers, G.T.: Coupled Flight-Dynamic and Low-Order Aero-elastic Model for a Slender Launch Vehicle
19. Wertz, J.R., Larson, W.L. (eds.): Space Mission Analysis and Design, 3rd edn. Microcosm and Kluwer, El Segundo (1999)

Chapter 8

Flight Mechanics

Abstract The flight mechanics is an important ingredient in vehicle and subsystem design, its performance evaluation and its validation. It deals with forces and moments acting on bodies and the response of the bodies to the applied forces and moments. Typical applications are trajectory design, optimum payload estimation, navigation, guidance and control (NGC) system algorithm design, estimation of loads on vehicle and various subsystems, mission design, vehicle sequencing, performance evaluations of subsystems, validation of NGC systems and evaluation of mission performance. Flight mechanics consists of two processes, namely, modelling and solution where the modelling represents subsystems, vehicle, forces and moments acting on it, their operating environment and the dynamics of vehicle and subsystem. The solution involves obtaining the solutions to the mathematical models, which truly represent the response of the vehicle and subsystems. To achieve the error-free design, the various models used for the vehicle, subsystems, environment, forces and moments generated by the respective systems as well as the dynamics of the systems under the influence of the forces and moments have to represent very close to the physical system and process. The systems models vary from simple three-dimensional model for the translational motion of the vehicle centre of gravity to the detailed six-degrees-of-freedom model along with the flexible vehicle structural dynamics. In addition, to evaluate the integrated system performance, the modelling of the vehicle onboard system elements such as sensors, navigation, guidance and control systems, the corresponding algorithms and signal flows simulating the delays in data transmission among various systems are required. In this chapter, the role of flight mechanics in the STS design process and the need for the integrated design approach are explained. The different coordinate systems used to represent the mathematical models, vehicle attitude sign conventions and the coordinate transformation to transfer the data between the reference frames are described. Subsequently, various models necessary for representing vehicle, subsystem and environment and the methodology for evaluating the system response are included. The usage of the flight mechanics models in the design process is also highlighted.

Keywords Flight mechanics • Coordinate systems • Vehicle attitude • Environment model • Gravitational model • Atmospheric model • Wind model • Vehicle model • Jet damping • Slosh • Guidance and control • Navigation and flexible dynamics

8.1 Introduction

Flight mechanics deals with forces and moments acting on bodies and the response of the bodies to the applied forces and moments. Orbital motions of satellites as explained in Chap. 3 deal with the flight mechanics of satellites under the influence of central gravitational force of Earth as well as disturbance forces due to the asphericity of Earth and perturbations caused by third bodies such as planets, moon, Sun and aerodynamic drag forces, solar radiation pressure, etc. Flight mechanics of Space Transportation Systems (STS) plays an important role during various phases of its design and development. Typical application includes (1) trajectory design and optimum payload estimation, (2) Navigation, Guidance and Control (NGC) system algorithm design, (3) determining the loads on vehicles and subsystems of various disciplines, (4) mission design including vehicle sequencing, (5) design input to the vehicle subsystems, viz. thermal, NGC systems, etc., (6) performance evaluations of subsystems designs, (7) validation of NGC systems, (8) mission performance evaluation, (9) mission performance prediction for a defined vehicle system and (10) vehicle systems flight performance evaluation through post-flight analysis. Flight mechanics is not a vehicle subsystem but used as an important tool to design the subsystems as well as to provide input to the design process.

Flight mechanics consists of two components: (1) modelling process and (2) solution process. The modelling process represents the physical subsystems, vehicle, forces and moments acting on it, environment in which the vehicle and subsystems operate and vehicle and subsystem dynamics through suitable mathematical expressions in terms of either algebraic or differential equations. The solution process involves obtaining the solutions to the mathematical models, which truly represent the response of the vehicle and subsystems.

The flight mechanics is an important ingredient in vehicle and subsystem design, its performance evaluation and its validation. To achieve the error-free design, it is essential that the various models used for the vehicle, subsystems, environment, forces and moments generated by the respective systems as well as the dynamics of the systems under the influence of the forces and moments have to represent very close to the physical system and process. To meet the specific needs, based on the functional requirements, various levels of complexities are to be incorporated in the systems models. This varies from simple three-dimensional model for the translational motion of the vehicle centre of gravity to the detailed six-degrees-of-freedom model for the vehicle along with the flexible vehicle structural dynamics. In addition, to evaluate the integrated system performance, it is essential to model the vehicle onboard system elements such as sensors, navigation, guidance and control systems, guidance and control laws, the corresponding algorithms, onboard computers and signal flows simulating the delays in data transmission among various systems.

In this chapter, the role of flight mechanics in the STS design process and the need for the integrated design approach are explained. The different coordinate systems used to represent the mathematical models, vehicle attitude sign

conventions and the coordinate transformation to transfer the data between the reference frames are explained. Subsequently, various models necessary for representing vehicle, subsystem and environment and the methodology for evaluating the system response are included. The actual usage of the flight mechanics models in the design process are highlighted in the respective chapters.

8.2 Role of Flight Mechanics in STS Design Process

Flight mechanics plays a very crucial role during the various phases of design, development and validation of an STS. The application starts along with the initial configuration finalization phase and extends up to the integrated vehicle on the launch pad and also to evaluate the subsystem performance in flight as illustrated in Fig. 8.1.

The contribution of flight mechanics is vital in the STS configuration design. Initially, the vehicle is configured with the suitable propulsion systems and the aerodynamic data is generated for the proposed external configuration. Even though the configuration is defined to carry the identified satellite mass to the specified orbit, in the realistic flight mechanics sense, the required payload mass may not be achieved. Therefore, it is essential to design an optimum trajectory for the defined configuration to achieve the maximum payload capability. For this purpose, flight mechanics models are used. If the required payload is not achieved, alternate propulsion systems are selected or the propulsion performance parameters and

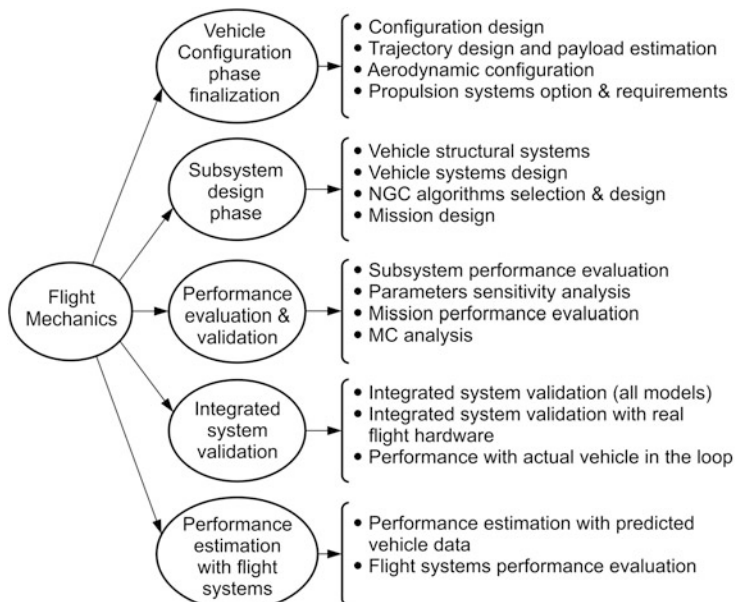


Fig. 8.1 Role of flight mechanics in STS design

aerodynamic configurations are redefined to meet the vehicle and mission requirements. This is an iterative process to finalize the configuration for STS.

Once the vehicle configuration is finalized, next step is to define the vehicle subsystems and to carry out the design process. One such activity is to identify suitable navigation, guidance and control laws and algorithms to meet the mission requirements. Performances of various algorithms are studied using detailed flight mechanics models and the one which meets the requirements of vehicle subsystems and mission is selected. For the finalized vehicle and subsystems configuration, it is essential to carry out the detailed design process as well as mission design for the intended mission. The various inputs required for the vehicle subsystems design are arrived at through flight mechanics. Typical inputs include (1) loads on vehicle subsystems, (2) flight parameters for NGC systems and (3) mission sequencing, etc.

Once the design is completed, it is essential to ensure that the subsystems have performed as per the expectations. Flight mechanics models are used to evaluate the performance of (1) the subsystems, (2) integrated mission performance, (3) sensitivity analysis and (4) mission performance through Monte Carlo analysis. In case the required performance is not achieved, suitable design modifications of subsystems are necessary to achieve the target and in such case, the design cycle is repeated.

After arriving at the final design, the subsystems are realized and integrated into systems. Through suitable simulation strategies using flight mechanics models and realized flight systems, integrated flight simulations are carried out to evaluate the system performance in near real flight environment. This includes (1) simulation with all models, (2) simulation with flight systems and (3) flight simulation with real vehicle subsystems in the loop.

On satisfactory performance of the vehicle systems at various levels of simulation, the flight is cleared. Before flight, using the predicted performance parameters of the flight systems, integrated system performance and mission performance are evaluated through flight mechanics. During flight, the necessary flight parameters are acquired through telemetry system. After flight, using the above flight parameters, subsystem performance in real flight is evaluated through suitable estimation algorithms using flight mechanics models.

Subsystem performance parameters during flight thus evaluated are used to improve the corresponding subsystem design in the subsequent flight. Thus, it can be seen that the flight mechanics plays a very crucial role in all phases of STS design process.

8.3 Need for Integrated Design Approach with Flight Mechanics

As already explained, during various phases of STS design and development, flight mechanics is closely linked with almost all the vehicle subsystem design process. Flight mechanics provides the necessary input to the subsystem design as well as serves as design, performance and validation tool as explained in Fig. 8.2.

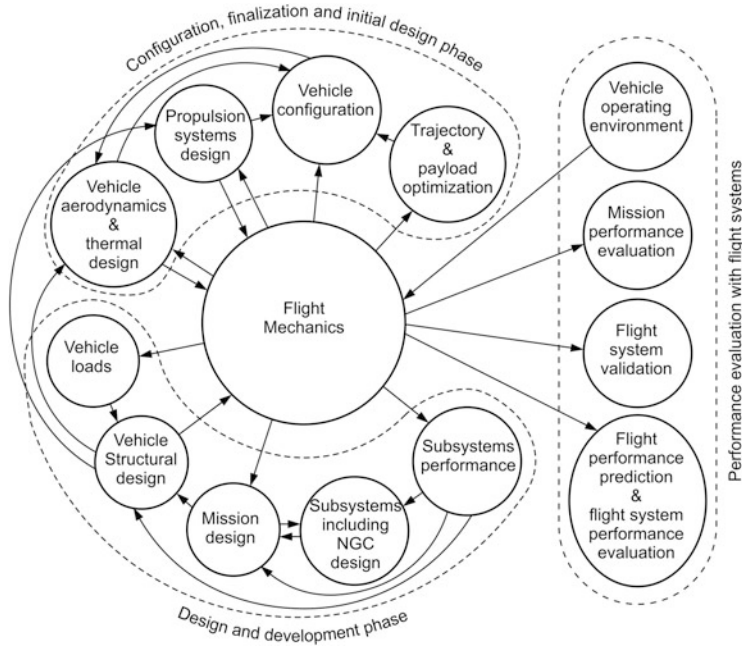


Fig. 8.2 Interactions of flight mechanics with vehicle subsystems

Any insufficiency in the initial design phase can lead to unsatisfactory system performance during final design evaluation and validation process. This can lead to repeating the design, which in turn leads to schedule slippage along with increase in development cost. Therefore, it is essential that all the interfaces of subsystems with flight mechanics have to be identified during the initial conceptual phase itself. Also, in order to avoid costly errors, the various models of vehicle systems and environment used in flight mechanics have to be very close to the reality with respect to the functions for which it is used. Finally, an integrated design approach with realistic flight mechanics models with all the interfaces of subsystems have to be followed to arrive at an optimum design in the early phase itself.

Different aspects of flight mechanics are explained in the following sections.

8.4 Coordinate Systems

As the flight mechanics deals with the motion of bodies, reference frames are to be defined and with respect to these both translational and attitude motions of STS are to be described. In addition, the reference frames are necessary to represent the input data and to define the forces and moments generated by subsystems and environments. The reference frames are selected such that the models of various

subsystems, environments and dynamics of vehicle and subsystems can be represented easily. The parameters defined in one frame can be represented in another frame through suitable coordinate transformations. This section gives the major reference frames, vehicle attitude definition and coordinate transformation matrices. The coordinate reference frames applicable for specific models are defined along with the description of such models.

8.4.1 Reference Frames

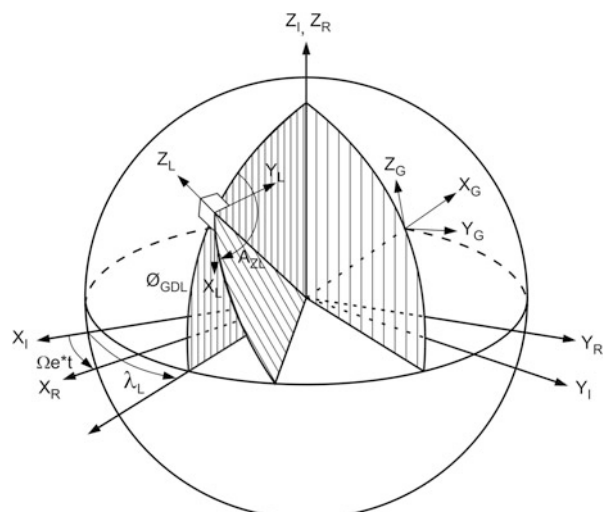
8.4.1.1 Earth-Centred Inertial (ECI) Frame (X_I, Y_I, Z_I)

This system is an Earth-centred Cartesian system with Z_I passing through the North Pole, X_I coincident with the Greenwich Meridian at time = 0 and in the equatorial plane and Y_I completing the right-handed system as shown in Fig. 8.3. Translational equations of motion are expressed in this frame. Gravitational accelerations and the orbital elements are also computed based on the state vector given with respect to this frame.

8.4.1.2 Earth-Centred Rotating Frame (ECR) (X_R, Y_R, Z_R)

This system is similar to the ECI frame except that this frame rotates with Earth. X_R is in equatorial plane coincident with prime meridian and rotates at the spin rate of the Earth, i.e. $15.0411^\circ/h$ with respect to ECI frame, Y_R is at 90° from X_R in the equatorial plane and Z_R coincides with Z_I as shown in Fig. 8.3. This frame is also

Fig. 8.3 Coordinate reference frames



termed as World Geodetic System (WGS) and is mostly used in GPS navigation. All the computations with respect to the rotating Earth are carried out in this frame.

8.4.1.3 Geographic (G) Frame (X_G, Y_G, Z_G)

This system is at the surface of the Earth located at the vehicle's current geocentric latitude and longitude. The X_G is in the local horizontal plane and points North, the Y_G axis is in the local horizontal plane and points East and X_G completes the right-handed system as shown in Fig. 8.3. This system is useful to calculate the parameters associated with azimuth and elevation angles, viz. tracking parameters, wind data and impact points, etc.

8.4.1.4 Launch Point Inertial Frame (LPI)

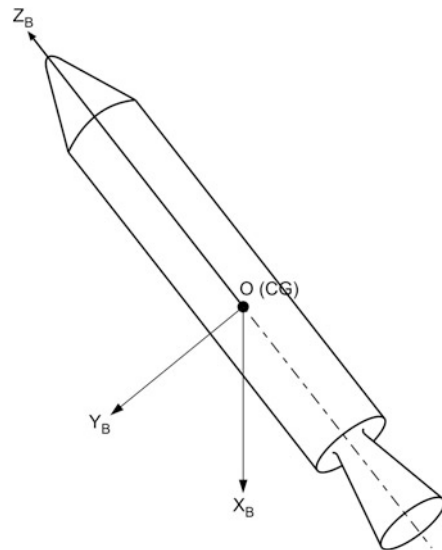
This frame is an inertial reference frame, with respect to which the inertial attitude angles of the vehicle are measured. The launch point inertial frame is located on the surface of the Earth at the defined geodetic latitude and longitude of the launch base of the vehicle. The local horizontal plane is the fundamental plane of this reference frame and the origin is the launch point of the vehicle. Z_L axis is along the local vertical. X_L and Y_L axes are in the local horizontal plane where X_L is along with launch azimuth direction. Launch azimuth A_{ZL} is defined as the angle measured clockwise from local north to the plane of vehicle launch. Y_L completes the right-handed system. This frame is given in Fig. 8.3. LPI goes inertial at T_0 when the vehicle lifts off. Otherwise the launch point coordinate system co-rotates with Earth till the vehicle lifts off from launch pad.

Vehicle attitude in terms of inertial Euler angles θ, Ψ, Φ (as explained later) is defined with respect to this reference frame. Normally navigation computations are carried out in this frame of reference.

8.4.1.5 Body Frame for the Vehicle (X_B, Y_B, Z_B)

This system is centred at the vehicle's instantaneous centre of gravity and fixed with the vehicle. Z_B axis of this orthogonal system points towards vehicle nose along the longitudinal axis of the vehicle, Y_B axis points towards left when looking from nozzle end and Z_B axis completes the right-handed system as shown in Fig. 8.4. This system coincides with the LPI reference frame at the time of lift-off, i.e. Z_B axis coincides with the local vertical, Z_L , and X_B coincides with the launch azimuth direction, X_L . After lift-off, the body axes move as it is fixed with respect to the body whereas LPI frame is inertially frozen at T_0 . The rotational equations of motion are expressed in this frame. Also forces and moments due to thrust, aerodynamics, control, etc. are computed in this frame.

Fig. 8.4 Body frame for the vehicle



8.4.2 Vehicle Attitude and Sign Convention

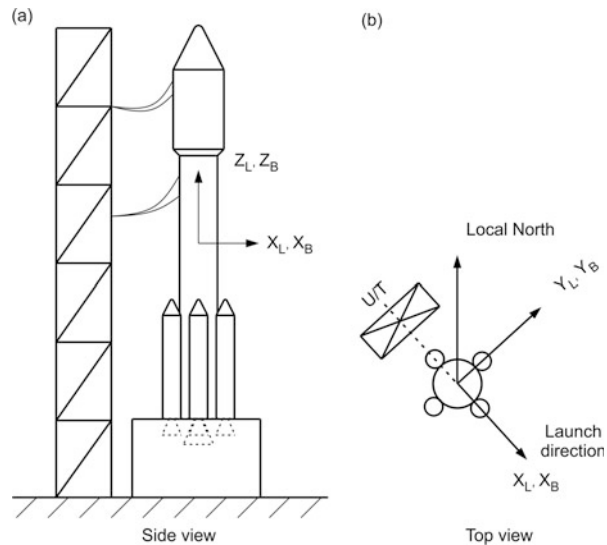
As explained above, the LPI and body reference frames are represented in Fig. 8.5. At the time of lift-off, Z_LX_L plane and the Z_BX_B plane coincide and X_L and X_B axes are along the launch direction. In this configuration, Z_LX_L plane is the launch plane, i.e. after vertical lift-off, the vehicle pitches down in the launch plane. Therefore, the pitching-down motion of the vehicle is achieved by rotating the vehicle in the Z_BX_B plane about Y_B axis. In a planar trajectory motion, the intentional motion of the vehicle is in the launch plane, which coincides with the desired orbital plane.

To represent the three-dimensional motion, Z_BY_B plane is called the pitch plane of the vehicle, Y_BZ_B plane is referred as yaw plane whereas X_BY_B plane is defined as the roll plane of the vehicle. Vehicle angular motion in Z_BX_B plane can be represented as a rotation of the vehicle about Y_B axis, similarly to the attitude motions about the other axes. Therefore, rotation about Y_B axis is referred to as pitch attitude motion of the vehicle, rotation about X_B axis is called yaw attitude motion and rotation about the Z_B axis is defined as roll attitude motion.

As the vehicle lifts off and executes attitude motion to reach the final targeted designation, the rotational motion can be represented in two forms: (1) vehicle attitude at any instant can be defined with respect to LPI frame and (2) vehicle attitude rate in the body frame.

Vehicle attitude with respect to LPI frame can be represented through three Euler angles: pitch (θ), yaw (Ψ) and roll (ϕ). These angles define body frame at any instant of flight with respect to LPI frame. For the planar motion cases, only one angle is defined whereas other two angles have zero values. The definitions of these angles are (1) θ (pitch): angle between Z_L axis and projection of Z_B axis on the

Fig. 8.5 Vehicle and reference frames at launch pad

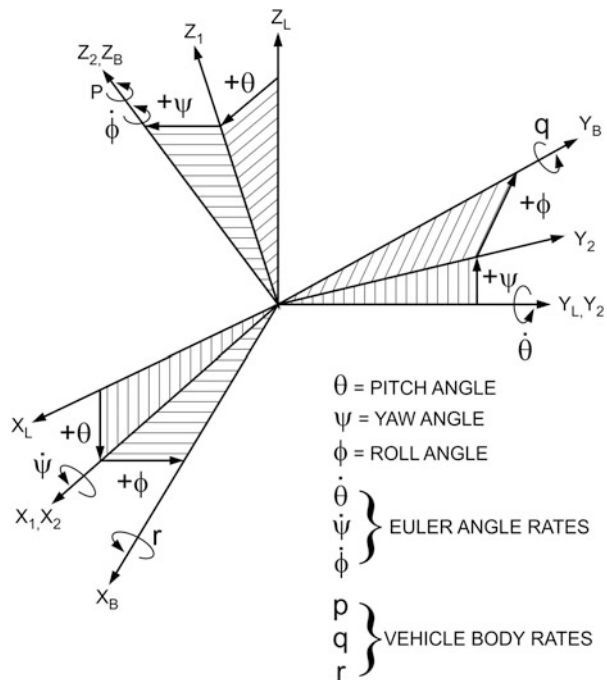


$Z_L X_L$ plane, (2) Ψ (yaw): angle between the projection of Z_B axis on the $Z_L Y_L$ plane and Z_B axis and (3) ϕ (roll): angle between the $Z_L X_L$ plane and X_B axis. This is the same as angle between $Y_L Z_L$ plane and Y_B axis. When the vehicle attitude is not lying in any single plane, there exists coupling and therefore, under such general cases, the Euler angle representation of vehicle attitude with respect to LPI frame is defined as sequence of rotations. The order of sequence is important in the Euler angular representation. The sequence pitch (θ), yaw (Ψ), roll (ϕ) is followed for the flight mechanics models given in this book. Under the above sequence, the Euler angle attitudes are defined as follows: LPI coordinates $X_L Y_L Z_L$ are rotated by an angle θ about Y_L axis to get a new frame $X_1 Y_1 Z_1$. $X_2 Y_2 Z_2$ frame is obtained by moving $X_1 Y_1 Z_1$ through ψ about X_1 axis. $X_B Y_B Z_B$, the body axes, are achieved by rotating $X_2 Y_2 Z_2$ axis about Z_2 axis by an angle ϕ . The sequence of Euler angle rotations and the angular representation are given in Fig. 8.6. The anticlockwise motion about the above axes is considered as positive rotations.

It is to be noted that, to define the Euler angles, Euler angular rates are carried out about axes of different orthogonal systems as shown in Fig. 8.6.

Vehicle attitude motion is also represented in terms of vehicle rates about the body axes as follows: vehicle pitch rate, q (vehicle angular rate about Y_B -axis), vehicle yaw rate, r (vehicle angular rate about X_B - axis), and vehicle roll rate, p (vehicle angular rate about Z_B - axis). Positive angular rates are the anticlockwise rotation about these axes. Vehicle rates about body frame axes and the Euler angular rates are related as shown in Fig. 8.6.

Fig. 8.6 Euler angles and body rates



8.4.3 Coordinate Transformations

The coordinate transformations are needed to transform the data between the coordinate systems described above. The coordinate transformation essentially changes the vector's basis, retaining the vector's length and direction even after the transformation. As discussed the coordinate transformation is done through a series of single axis rotations.

8.4.3.1 Transformation Matrix from ECI Frame to Body Frame

The most important coordinate transformation is the ECI-to-body transformation matrix [IB]. This transformation is achieved by transforming a vector from ECI to LPI frame, i.e. [IL], and then transforming from LPI frame to body frame, i.e. [IB]. The transformation matrix from ECI frame to body frame is given by $[IB] = [LB][IL]$. The inverse of this matrix (transpose) is used to transform accelerations in the body frame to ECI frame. The sequence of Euler angle rotations plays an important role in the generation of transformation matrices. Typical sequence of rotation from LPI frame to body is explained in Fig. 8.7.

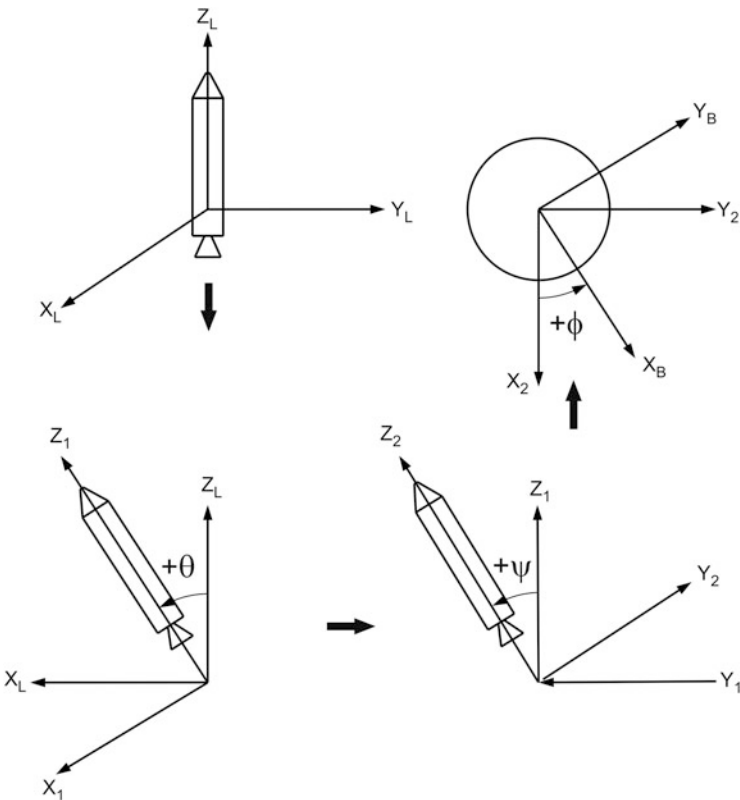


Fig. 8.7 Transformations from ECI Frame to body frame

The sequence of rotation needed for transformation from ECI frame to LPI frame is given below:

Coordinate	Rotation Axis	Angle	New Co-ordinate
$X_I Y_I Z_I$	Z_I	$λ_L$	$X_1 Y_1 Z_1$
$X_1 Y_1 Z_1$	Y_1	$ϕ_{GDL}$	$X_2 Y_2 Z_2$
$X_2 Y_2 Z_2$	Z_2	A_{ZL}	$X_L Y_L Z_L$

where

$λ_L$ = Launch point longitude

$ϕ_{GDL}$ = Launch point geodetic latitude

A_{ZL} = Launch azimuth

The transformation matrix $[IL]$, i.e. from ECI to LPI, is as given below. The symbols S and C denote Sin and Cos respectively.

$$[IL] = \begin{bmatrix} -C_{AZL}S_{\Phi_{GD_L}}C_{\lambda_L} - S_{AZL}S_{\lambda_L} & -C_{AZL}S_{\Phi_{GD_L}}S_{\lambda_L} + S_{AZL}C_{\lambda_L} & C_{AZL}C_{\Phi_{GD_L}} \\ -S_{AZL}S_{\Phi_{GD_L}}C_{\lambda_L} + C_{AZL}S_{\lambda_L} & -S_{AZL}S_{\Phi_{GD_L}}S_{\lambda_L} - C_{AZL}C_{\lambda_L} & S_{AZL}C_{\Phi_{GD_L}} \\ C_{\Phi_{GD_L}}C_{\lambda_L} & C_{\Phi_{GD_L}}S_{\lambda_L} & S_{\Phi_{GD_L}} \end{bmatrix} \quad (8.1)$$

Similarly transformation from LPI frame to body frame is computed by the following sequence of rotation:

Coordinate	Rotation Axis	Angle	New Coordinate
$X_L Y_L Z_L$	Y_L	θ	$X_1 Y_1 Z_1$
$X_1 Y_1 Z_1$	X_1	ψ	$X_2 Y_2 Z_2$
$X_2 Y_2 Z_2$	Z_2	ϕ	$X_B Y_B Z_B$

where θ = Pitch angle

ψ = Yaw angle

ϕ = Roll angle

Transformation matrix from LPI to body frame is

$$[LB] = \begin{bmatrix} C_\phi C_\theta + S_\phi S_\psi S_\theta & S_\phi C_\psi & -C_\phi S_\theta + S_\phi S_\psi C_\theta \\ -S_\phi C_\theta + C_\phi S_\psi S_\theta & C_\phi C_\psi & S_\phi S_\theta + C_\phi S_\psi C_\theta \\ C_\psi S_\theta & -S_\psi & C_\psi C_\theta \end{bmatrix} \quad (8.2)$$

If the quaternion parameters are used for the kinematic relations, then the transformation matrix is given by

$$[LB] = \begin{bmatrix} (e_0^2 + e_1^2 - e_2^2 - e_3^2) & 2(e_1 e_2 + e_0 e_3) & 2(e_1 e_3 - e_0 e_2) \\ 2(e_1 e_2 - e_0 e_3) & (e_0^2 - e_1^2 + e_2^2 - e_3^2) & 2(e_0 e_1 + e_2 e_3) \\ 2(e_1 e_3 + e_0 e_2) & 2(e_2 e_3 - e_0 e_1) & (e_0^2 - e_1^2 - e_2^2 + e_3^2) \end{bmatrix} \quad (8.3)$$

where e_0, e_1, e_2, e_3 are the quaternion parameters.

8.4.3.2 Transformation Matrix from ECI Frame to ECR Frame

$$[IR] = \begin{bmatrix} C_v & S_v & 0 \\ -S_v & C_v & 0 \\ 0 & 0 & 1 \end{bmatrix} \quad (8.4)$$

where

$$\nu = \Omega_e t$$

8.4.3.3 Transformation Matrix from ECI Frame to G Frame at the Time of Lift-Off

The sequence of rotation is

Coordinate	Rotation Axis	Angle	New Coordinate
$X_I Y_I Z_I$	X_I	λ_I	$X_I Y_I Z_I$
$X_I Y_I Z_I$	Y_I	$-\phi_{GC}$	$X_G Y_G Z_G$

where λ_I = Longitude with respect to ECI frame

ϕ_{GC} = Geocentric latitude

The transformation matrix is

$$[IG] = \begin{bmatrix} C_{\phi_{GC}} C_{\lambda_I} & C_{\phi_{GC}} S_{\lambda_I} & S_{\phi_{GC}} \\ -S_{\lambda_I} & C_{\lambda_I} & 0 \\ -S_{\phi_{GC}} C_{\lambda_I} & -S_{\phi_{GC}} S_{\lambda_I} & C_{\phi_{GC}} \end{bmatrix} \quad (8.5)$$

8.4.3.4 Transformation Matrix from G Frame to LPI Frame at the Time of Lift-Off

The sequence of rotation is

Coordinate	Rotation Axis	Angle	New Coordinate
$X_G Y_G Z_G$	Y_G	A_{ZL}	$X_I Y_I Z_I$
$X_I Y_I Z_I$	Z_I	π	$X_2 Y_2 Z_2$
$X_2 Y_2 Z_2$	Y_2	$-\frac{\pi}{2}$	$X_L Y_L Z_L$

The transformation matrix is

$$[GL]_L = \begin{bmatrix} 0 & S_{A_{ZL}} & C_{A_{ZL}} \\ 0 & -C_{A_{ZL}} & S_{A_{ZL}} \\ 1 & 0 & 0 \end{bmatrix} \quad (8.6)$$

The transformations between other coordinate systems can be computed by the product of two or more of the above transformation matrices. Typical transformation matrix from ECI frame to body frame is given by

$$[IB] = [LB] [IL] \quad (8.7)$$

Having explained the coordinate system, the next step is to represent the vehicle system and environment models with respect to these reference frames. Various models of representing vehicle subsystems and environment are explained in the following section.

8.5 Environment Model

Environment model consists of the following:

1. Earth geometry and constants
2. Gravitation model that computes gravity acceleration
3. Atmosphere model that computes the atmospheric pressure, density, temperature and speed of sound
4. Wind model

8.5.1 Earth Geometry

For the flight mechanics of STS, non-spherical Earth gravitational potential with zonal harmonic terms is sufficient. Such model of Earth is defined by the equatorial radius R_e , the polar radius R_p , the Earth rotation rate Ω_e , the gravitational constant μ and second, third and fourth gravitational harmonics J_2, J_3, J_4 , respectively.

Typical values for these constants are given below:

$$R_e = 6378165.8 \text{ m}$$

$$R_p = 6356783.8 \text{ m}$$

$$\Omega_e = 7.29211 \times 10^{-5} \text{ rad/s}$$

$$\mu = 3.986013 \times 10^{14} \text{ m}^3/\text{s}^2$$

$$J_2 = 1.0826268 \times 10^{-3}$$

$$J_3 = 0.00254 \times 10^{-3}$$

$$J_4 = 0.00161 \times 10^{-3}$$

Vehicle position vector with respect to ECI frame is given by

$$\mathbf{r}_I = \begin{bmatrix} X_I \\ Y_I \\ Z_I \end{bmatrix} \quad (8.8)$$

Then, the radial distance of the vehicle from Earth centre is given by

$$r_I = (\mathbf{r}_I \cdot \mathbf{r}_I)^{\frac{1}{2}} \quad (8.9)$$

The geocentric latitude of the vehicle position is

$$\phi_{GC} = \sin^{-1} \left(\frac{Z_I}{r_I} \right) \quad (8.10)$$

The geocentric radial distance, r_I , the geocentric latitude, (ϕ_{GC}) and altitude and geodetic latitude of the vehicle at any instant (position P) are represented in Fig. 8.8. To make easier computations of these parameters, closer approximation for the STS trajectories considering the Earth's parameters as represented in Fig. 8.9 may be used.

Fig. 8.8 Position and coordinates with respect to Oblate Earth

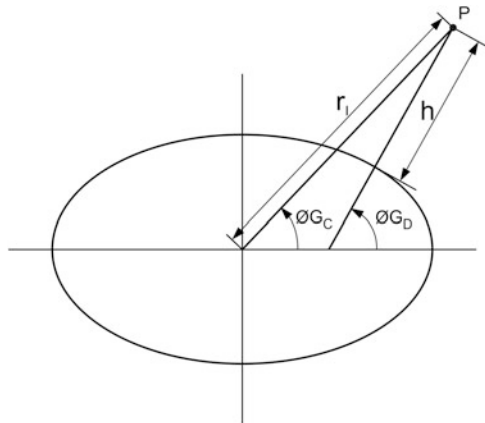
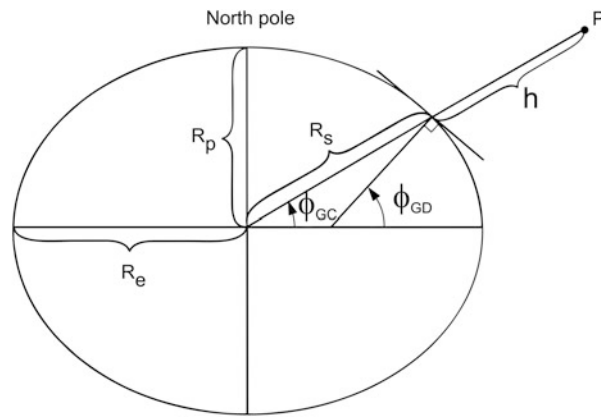


Fig. 8.9 Oblate earth geometry



For such model, the geodetic latitude of the vehicle position is computed as

$$\phi_{GD} = \tan^{-1} \left(k \tan (\phi_{GC}) \right) \quad (8.11)$$

where

$$k = \left[\frac{R_e}{R_p} \right]^2 \quad (8.12)$$

The radius of the Earth corresponding to ϕ_{GC} is given by

$$R_s = \frac{R_e}{\left[1 + (k - 1) S_{\phi_{GC}}^2 \right]^{\frac{1}{2}}} \quad (8.13)$$

and the altitude of the vehicle is computed as

$$h = r_I - R_S \quad (8.14)$$

The inertial longitude of the vehicle position is

$$\lambda_I = \tan^{-1}(Y_I/X_I) \quad (8.15)$$

The relative longitude of the vehicle is given by

$$\lambda = \lambda_I - \Omega_e t \quad (8.16)$$

where t = trajectory time

8.5.2 Earth Gravitational Model

Even though second harmonic term is the major contributing factor for the deviation of Earth gravity field away from the central force field, more accurate model may be used considering up to the fourth harmonic terms. The general gravitational potential of the Earth under such assumption may be written at the vehicle's current position in terms of position vector with respect to ECI frame as follows:

$$U = -\mu \left[\frac{1}{r_I} - \frac{J_2 R_e^2}{2} \left(3 \frac{Z_I^2}{r_I^5} - \frac{1}{r_I^3} \right) - \frac{J_3 R_e^3}{2} \left(5 \frac{Z_I^3}{r_I^7} - 3 \frac{Z_I}{r_I^5} \right) - \frac{J_4 R_e^4}{8} \left(35 \frac{Z_I^4}{r_I^9} - 30 \frac{Z_I^2}{r_I^7} + \frac{3}{r_I^5} \right) \right] \quad (8.17)$$

Using this potential, gravitational acceleration along the ECI frame is computed as

$$G_{XI} = -\frac{\partial U}{\partial X_I} \quad (8.18)$$

$$G_{YI} = -\frac{\partial U}{\partial Y_I} \quad (8.19)$$

$$G_{ZI} = -\frac{\partial U}{\partial Z_I} \quad (8.20)$$

Thus,

$$G_{XI} = -\frac{\mu X_I}{r_I^3} [1 + JR^2(1 - 5z^2) + HR^3(3z - 7z^3) - DR^4(1 - 14z^2 + 21z^4)] \quad (8.21)$$

$$G_{YI} = -\frac{\mu Y_I}{r_I^3} [1 + JR^2(1 - 5z^2) + HR^3(3z - 7z^3) - DR^4(1 - 14z^2 + 21z^4)] \quad (8.22)$$

$$G_{ZI} = -\frac{\mu Z_I}{r_I^3} \left[1 + JR^2(3 - 5z^2) + HR^3\left(-\frac{3}{5z} + 6z - 7z^3\right) - DR^4\left(5 - \frac{70}{3}z^2 + 21z^4\right) \right] \quad (8.23)$$

where

$$J = \frac{3J_2}{2}; \quad H = \frac{5J_3}{2}; \quad D = \frac{15J_4}{8}; \quad R = \frac{R_e}{r_I}; \quad z = \frac{Z_I}{r_I} \quad (8.24)$$

Equations (8.22), (8.23), and (8.24) give the acceleration due to Earth gravity at the instantaneous position of the vehicle, defined by the position vector given in Eq. (8.9).

8.5.3 Atmospheric Model

The parameters required to define the atmospheric model for the STS flight mechanics are atmospheric pressure (P_a), atmospheric density (ρ), speed of sound (C_s) and temperature (T). These parameters are functions of the oblate earth altitude, h . The atmospheric model can be formulated using table lookup or from the temperature information as given below.

8.5.3.1 Table Lookup (Standard Atmosphere)

In this case, the atmospheric properties of standard atmosphere can be defined entirely by tables of temperature, pressure, speed of sound and density as functions of altitude. The speed of sound and density tables can be defined if desired. In this case, the speed of sound and density at any altitude are computed as follows:

$$C_s = \sqrt{k_1 T} \quad (8.25)$$

$$\rho = \frac{k_2 p_a}{T} \quad (8.26)$$

where

$$k_1 = \frac{\gamma^{\mathfrak{R}}}{M_0} \quad (8.27)$$

$$k = \frac{M_0}{\mathfrak{R}} \quad (8.28)$$

γ = Ratio of specific heats = 1.4

\mathfrak{R} = Universal gas constant = 8314.32 $\frac{\text{J}}{(\text{K})(\text{kg-mol})}$

M_0 = Molecular weight = 28.9644

Using the above constants, the speed of sound and density can be expressed as

$$C_s = 20.046803 \times \sqrt{T} \quad (8.29)$$

$$\rho = 3.48367 \times 10^{-3} \frac{P_a}{T} \quad (8.30)$$

8.5.3.2 Atmospheric Properties from Temperature Information Alone

In this case, the input to the model is temperature table as function of oblate Earth altitude, pressure, density, speed of sound and temperature at sea level. At any instant, temperature is computed by interpolating the input table. Other atmospheric properties, viz. pressure, density, speed of sound, are computed from temperature as follows:

The state equation relation for the atmosphere is

$$\frac{dp_a}{dh} = -\rho g \quad (8.31)$$

and the ideal gas relation is

$$P_a = R\rho T \quad (8.32)$$

where

P_a = Atmospheric pressure (N/m^2)

ρ = Atmospheric density (kg/m^3)

T = Atmospheric temperature ($^\circ\text{K}$)

h = Oblate earth altitude (m)

R = Gas constant = $\mathfrak{R}/M_0 = 287.05 \text{ m}^2/\text{s}^2 (\text{K})$

g = Acceleration due to gravity at the altitude h (m/s^2)

From (8.31) and (8.32), the pressure and density at the altitude h_2 in terms of that at h_1 can be derived as

$$p_{a_2} = p_{a_1} e^{\ln\left(\frac{T_2}{T_1}\right) \frac{g}{R\alpha}} \quad (8.33)$$

$$\rho_2 = \rho_1 e^{\ln\left(\frac{T_2}{T_1}\right) \left(\frac{g}{R\alpha} - 1\right)} \quad (8.34)$$

where

ρ_2, p_{a_2}, T_2 are density, pressure and temperature at altitude h_2 .

ρ_1, p_{a_1}, T_2 are density, pressure and temperature at altitude h_1 .

α = Lapse rate of temperature

$$\alpha = \frac{T_1 - T_2}{h_2 - h_1} \quad (8.35)$$

Thus, density and pressure at any instant are computed using the Eqs. (8.33) and (8.34). The speed of sound is computed using the Eq. (8.29).

8.5.4 Wind Model

Generally measured wind profiles are used for the vehicle and subsystems' performance evaluation. During design phase, synthetic wind profiles are used. For the mission performance evaluation, random winds are generally used. These wind profiles are available as functions of altitude. In the flight mechanics, the atmospheric winds are modelled either as zonal and meridional components or as wind velocity and azimuth. If the wind is not modelled, then the atmosphere is assumed to rotate along with the Earth. Sign convention for the wind input data is given in Fig. 8.10.

In the case of meteorological notations, the inputs for the wind model are

Wind speed in horizontal plane (V_{WH})

Wind azimuth (A_{ZW})

Wind azimuth bias (A_{ZWB}) (normally 180°)

Vertical wind (U_w)

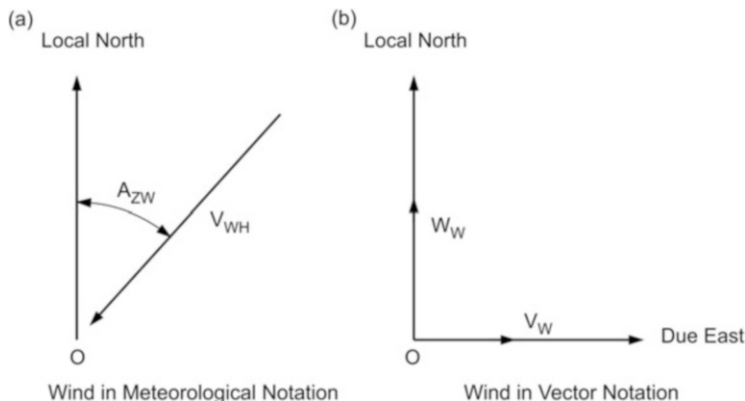


Fig. 8.10 Sign conventions for winds. (a) Wind in meteorological notation. (b) Wind in vector notation

The resulting wind velocity components in the geographic frame is computed as

$$\mathbf{V}_{WG} = \begin{bmatrix} U_W \\ V_W \\ W_W \end{bmatrix} = \begin{bmatrix} U_W \\ V_{WH}S_{(A_{ZW}+A_{ZWE})} \\ V_{WH}C_{(A_{ZW}+A_{ZWE})} \end{bmatrix} \quad (8.36)$$

The wind velocity in ECI frame is given as

$$\mathbf{V}_{WI} = [IG]^{-1} \mathbf{V}_{WG} \quad (8.37)$$

If the wind input data at launch point (instead of local wind) is used, then

$$\mathbf{V}_{WI} = [IL]^{-1} [GL]_L \mathbf{V}_{WG} \quad (8.38)$$

In the case of vector notation, the wind velocity components are given directly in geographic frame by defining

- | | |
|--------------------------|-------------------|
| Vertical wind | (U _W) |
| Wind in zonal plane | (V _W) |
| Wind in meridional plane | (W _W) |

Further usage of wind is the same as explained above.

8.5.5 Vehicle Velocity

Atmospheric wind plays a major role in the relative velocity vector of the vehicle with respect to the atmosphere which has the following components: (1) inertial velocity of the vehicle (assuming non-rotating Earth), (2) velocity components with respect to the rotating Earth and (3) velocity components with respect to the atmosphere (wind velocity). The relative velocity vector is defined as follows:

The vehicle inertial velocity with respect to ECI frame is defined as

$$\mathbf{V}_I = \begin{bmatrix} u_I \\ v_I \\ w_I \end{bmatrix} \quad (8.39)$$

where u_I, v_I, w_I are vehicle velocity components in ECI frame.

The magnitude of inertial velocity is

$$V_I = (\mathbf{V}_I \cdot \mathbf{V}_I)^{1/2} \quad (8.40)$$

The atmospheric relative velocity vector in the ECI frame is

$$\mathbf{V}_{AI} = \mathbf{V}_I - \Omega_e \times \mathbf{r}_I - \mathbf{V}_{WI} \quad (8.41)$$

and its magnitude is given by

$$V_A = (\mathbf{V}_{AI} \cdot \mathbf{V}_{AI})^{1/2} \quad (8.42)$$

where

Ω_e = Earth's rotational velocity, expressed in ECI frame.

The Mach number is given by

$$M = \frac{V_A}{C_S} \quad (8.43)$$

8.6 Vehicle Model

The vehicle model consists of the following:

1. Propulsion model
2. Aerodynamic model
3. Jet damping model
4. Auxiliary forces model
5. Slosh model
6. Mass properties model

The propulsion model comprises of thrust, moment due to thrust, flow rate and remaining propellant mass for as many separate motors as the vehicle has at one instant. It also has the thrust and moment due to thrust of ullage rocket system if any at that instant. The aerodynamic model gives the aerodynamic forces and moments. The jet damping force and moment are represented by the jet damping model. The auxiliary force model is needed to simulate the forces and moments due to the sources other than propulsion and aerodynamics. The slosh model represents the forces and moments due to liquid sloshing in the fuel tanks. The mass properties model gives the vehicle mass, centre of gravity location, moments and products of inertia at any instant.

8.6.1 Propulsion Model

Generally vehicle contains clustered propulsion system with different characteristics for each engine. The propulsion model needs to simulate the realistic propulsion configuration. The atmospheric thrust of i^{th} engine in a clustered configuration of a rocket is given by

$$T_i = T_{v_i} + (p_{e_i} - p_a)A_{e_i} \quad (8.44)$$

where

T_i = Atmospheric thrust of i^{th} motor

T_{v_i} = Vacuum thrust of i^{th} motor

p_a = Atmospheric pressure

p_{e_i} = Exit pressure of ith motor

A_{e_i} = Nozzle exit area of ith motor

The direction of thrust given by Eq. (8.45) is arbitrary with respect to body frame because of the following reasons:

1. Orientation of the motors with respect to body frame
2. Attachment misalignments of the motors with respect to the core vehicle
3. Canting of the rocket motor nozzles
4. Thrust misalignment angles with respect to nozzle axis

Once the orientations of the rocket motor with respect to body frame, cant angle, attachment misalignment and thrust misalignment angles are specified, the thrust vector with respect to body frame can be defined. The entire propulsion modelling related to ith motor is explained in Annexure A.

Using the expression given in Annexure A, the total thrust force (due to all motors of a stage) at any instant along the body axes is given as

$$\mathbf{F}_{TB} = \begin{bmatrix} F_{TX} \\ F_{TY} \\ F_{TZ} \end{bmatrix} = \sum_{i=1}^{n_m} \mathbf{F}_{TB_i} \quad (8.45)$$

and the total moment about body axes is given by

$$\mathbf{M}_{TB} = \begin{bmatrix} M_{TX} \\ M_{TY} \\ M_{TZ} \end{bmatrix} = \sum_{i=1}^{n_m} \mathbf{M}_{TB_i} \quad (8.46)$$

where

n_m = number of motors of the stage

\mathbf{F}_{TB_i} = thrust force vector of ith motor in body frame

\mathbf{M}_{TB_i} = moment vector about body axes due to ith motor thrust

8.6.2 Aerodynamic Model

Aerodynamics plays a major role in the flight mechanics of STS during atmospheric phase of flight. The angles of attack during this flight phase is caused by

1. Vehicle drift due to the lateral forces such as aerodynamic force, control force, propellant sloshing forces and thrust misalignments, etc.
2. Error during tracking of desired attitude profile (normally these attitude profiles are designed to follow zero angles of attack)

3. Wind velocities (in case the attitude profile is biased for a defined wind profile, then the wind velocity variations with respect to the biased wind profile causes the angles of attack)

The above parameters shift the velocity vector of the vehicle away from the longitudinal axis of the vehicle, thus introducing angle of attack. The atmospheric relative velocity of the vehicle is expressed in body reference frame and using the components along the axes, pitch angle of attack (angle of attack in pitch plane of the vehicle) and yaw angle of attack (angle of attack in yaw plane of the vehicle) are computed.

Combination of angle of attack, vehicle trajectory and aerodynamic parameters such as dynamic pressure, Mach number, Reynolds number and altitude as well as aerodynamic characteristics of the vehicle induce aerodynamic forces along the vehicle axes and moments about the vehicle axes.

These aerodynamic forces and moments are the major disturbance sources during atmospheric phase of flight. Therefore, to stabilize the vehicle against these disturbance forces, vehicle control system generates necessary control forces. The combination of aerodynamic forces and control forces in turn induce loads on the vehicle. These loads form major inputs for the vehicle and subsystems structural design. Both aerodynamic load distributions as well as rigid body forces are used for control systems and structural systems design. Therefore, it is essential that the aerodynamic modelling has to be accurate and very close to the real flight environment.

More details about the vehicle aerodynamics are explained in Chap. 10. A general rigid body vehicle aerodynamics model is explained in Annexure A. Using this model, the rigid body aerodynamic force and moment vectors are given as

$$\mathbf{F}_{AB} = \begin{bmatrix} F_{AX} \\ F_{AY} \\ F_{AZ} \end{bmatrix} = QS \begin{bmatrix} C_X \\ C_Y \\ C_Z \end{bmatrix} \quad (8.47)$$

$$\mathbf{M}_{AB} = \begin{bmatrix} M_{AX} \\ M_{AY} \\ M_{AZ} \end{bmatrix} = QSD \begin{bmatrix} C_n \\ C_m \\ C_l \end{bmatrix} \quad (8.48)$$

where C_X , C_Y , C_Z and C_n , C_m , C_l are the aerodynamic force and moment coefficients which are functions of angles of attack, Mach number and aerodynamic characteristics of the vehicle and are measured in wind tunnels and stored as tables. Using these data, depending on the vehicle and trajectory parameters, aerodynamic characteristics are computed in the flight mechanics model. Using other trajectory parameters such as angle of attack as explained in Chap. 10, the aerodynamic coefficients are computed. Other parameters used in Eqs. (8.47) and (8.48) are explained below:

Q is the dynamic pressure, given by

$$Q = \frac{1}{2} \rho V_A^2 \quad (8.49)$$

where ρ is the atmospheric density and V_A is the magnitude of relative velocity vector.

S is the reference area and d is the reference diameter which are used to derive the aerodynamic characteristics using wind tunnel model.

8.6.3 Jet Damping Model

The modelling aspects of jet damping forces and moments are given in Annexure A. Based on this model, the total jet damping force and moment are given as

$$\mathbf{F}_{JB} = \begin{bmatrix} F_{JX} \\ F_{JY} \\ F_{JZ} \end{bmatrix} = \sum_{i=1}^{n_m} \mathbf{F}_{JB_i} \quad (8.50)$$

and

$$\mathbf{M}_{JB} = \begin{bmatrix} M_{JX} \\ M_{JY} \\ M_{JZ} \end{bmatrix} = \sum_{i=1}^{n_m} \mathbf{M}_{JB_i} \quad (8.51)$$

where

F_{JB_i} = jet damping force vector of i th motor in body frame

M_{JB_i} = moment vector about body axes due to i th motor jet damping force

n_m = number of motors

8.6.4 Auxiliary Forces Model

These are needed to simulate the effects of separation devices such as retro rockets, springs and others or moments imparted by spin motors or any other external forces and moments.

The forces along the body axes is given as

$$\mathbf{F}_{AUB} = \begin{bmatrix} F_{AUX} \\ F_{AUY} \\ F_{AUZ} \end{bmatrix} \quad (8.52)$$

The moment about the body axes is given as

$$\mathbf{M}_{\text{AUB}} = \begin{bmatrix} M_{\text{AUX}} \\ M_{\text{AUY}} \\ M_{\text{AUZ}} \end{bmatrix} \quad (8.53)$$

8.6.5 Slosh Model

Most of the vehicles use liquid propulsion system which involves storage of liquids in tanks. Generally, to ensure the requirement of minimum ullage volume, for achieving specific initial conditions for the engines, the propellants are not filled to the full tank. Also, during engine operations, the propellants get depleted continuously, which causes free surface for the propellants in the tanks. The lateral acceleration acting on the vehicle, induced by lateral disturbances during flight, control forces needed to stabilize the vehicle and the lateral acceleration due to rotational velocity and acceleration, cause pressure gradient across and along the length of liquid propellant column. This pressure gradient finally reflects as forces and moments about vehicle centre of gravity. Because of the exciting lateral accelerations, slosh forces and moments become oscillatory in nature and in turn introduce further oscillations. Due to the oscillatory nature of the fluid column and the possible coupling of these oscillations with vehicle autopilot, the propellant sloshing is having a major impact on the vehicle design. To reduce severity of this problem, generally damping is provided through suitable baffles. Locations of the baffles are to be decided based on the vehicle and subsystems functional criticalities. To represent realistically the impact of slosh on the vehicle systems, it is essential to model the sloshing phenomena. For simplification, the total slosh phenomenon which depends on the shape of the propellant tank, free surface, density and longitudinal accelerations is to be modelled as equivalent simple harmonic oscillation with a specified mass, frequency, damping and forcing function of lateral acceleration. These equivalent parameters are evaluated through experimental setups and used for flight mechanics models. The modelling details of one slosh mass (ith mass) as shown in Fig. 8.11 are explained in Annexure A.

In this model, the spring mass analogy is used for computing forces and moments due to liquid propellant sloshing in the tanks. For each slosh mass of each tank, separate dynamics is simulated in pitch and yaw directions as shown in Fig. 8.11. The forcing functions model for the slosh oscillations includes vehicle translational lateral acceleration and lateral acceleration due to vehicle rotation rate and rotational acceleration. The effects of slosh forces on the moment components (pitch, yaw and roll) are also included in the model which makes the system totally coupled.

The parameters of Fig. 8.11 are explained as

1. m_{S_i} , K_{S_i} , Z_{IS_i} are the ith slosh mass, equivalent spring constant and its location from centre of gravity respectively.
2. X_{SP_i} , X_{SY_i} are the displacement of the ith slosh mass in the spring-mass analogy.

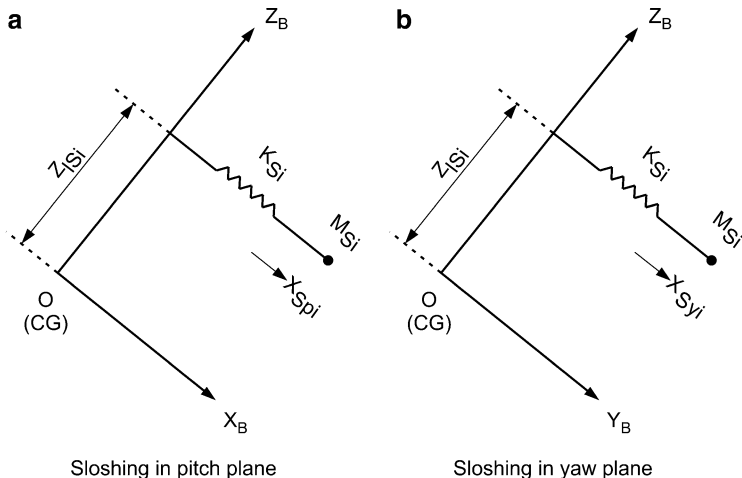


Fig. 8.11 Spring mass analogy of liquid sloshing. **(a)** Sloshing in pitch plane. **(b)** Sloshing in yaw plane

The forces along body axes and moments about body axes for the i th slosh mass as explained in Annexure A are given as

$$\mathbf{F}_{\text{SB}_i} = \begin{bmatrix} F_{X\text{S}_i} \\ F_{Y\text{S}_i} \\ F_{Z\text{S}_i} \end{bmatrix} \quad (8.54)$$

$$\mathbf{M}_{\text{SB}_i} = \begin{bmatrix} M_{X\text{S}_i} \\ M_{Y\text{S}_i} \\ M_{Z\text{S}_i} \end{bmatrix} \quad (8.55)$$

The total forces and moments are given as

$$\mathbf{F}_{\text{SB}} = \sum_{i=1}^{n_s} \mathbf{F}_{\text{SB}_i} \quad (8.56)$$

$$\mathbf{M}_{\text{SB}} = \sum_{i=1}^{n_s} \mathbf{M}_{\text{SB}_i} \quad (8.57)$$

where n_s is number of slosh masses.

8.6.6 Mass Properties

Mass properties model represents the instantaneous vehicle mass, centre of gravity, moments and products of inertia and their rates at any instant.

During operation of rocket engines, combustion products and some of the non-propulsive mass are continuously expelled and the vehicle mass gets reduced as the flight proceeds. This in turn changes the centre of gravity as well as the moments and products of inertia of the vehicle. In addition, during staging events, the empty stages and the payload fairings used for protecting the payload are jettisoned at the appropriate time to improve the vehicle performance. This change would introduce discontinuities to the vehicle mass properties. In order to evaluate the vehicle performance and to simulate realistically the response of the vehicle, the mass properties are to be modelled as close to the actual vehicle properties. The details are given in Annexure A. The output of this is at any instant of flight given below:

m = Vehicle mass

\dot{m} = Rate of change of vehicle mass

$$\mathbf{r}_{cg} = \begin{bmatrix} X_{cg} \\ Y_{cg} \\ Z_{cg} \end{bmatrix} = \text{Centre of gravity location with respect to the body reference frame}$$

$[I]$ = Inertia matrix

$\dot{[I]}$ = Rate of change of inertia matrix

$[I]^{-1}$ = Inverse of inertia matrix

8.7 Guidance and Control Model

To stabilize the vehicle along the desired trajectory and to follow a desired trajectory to achieve the defined orbit, navigation, guidance and control systems are used. This is given schematically in Fig. 8.12 and explained in detail in Chap. 14.

The input for this system is output of the vehicle attitude, rate and acceleration sensors mounted on the vehicle and the system finally activates suitable control systems to generate the required control forces and moments to stabilize the vehicle against the disturbances and to control the vehicle along the desired trajectory. The forces and moments generated by these control systems are with respect to body frame.

The various features needed to be simulated in NGC system model are

1. Sensor dynamics, which includes the effects of associated onboard sensor electronics, sensor hardware response and the delay introduced from the data acquisition to transmission to the functional system
2. Navigation algorithm as implemented onboard including the onboard limitations
3. Guidance algorithm and guidance law as implemented in the vehicle onboard
4. Autopilot algorithm and control law as implemented onboard
5. Control power plant dynamics

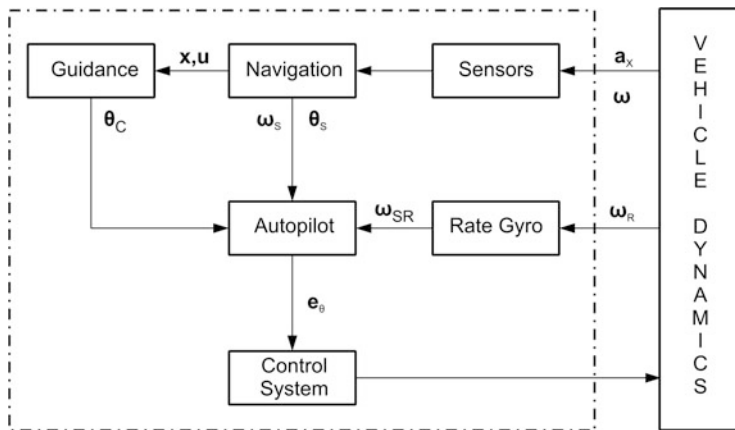


Fig. 8.12 Guidance and control system model

6. Simulation of onboard computers and the associated delay in data transmission between various subsystems
7. Simulation of sensor errors and noises in the signals as in the case of realistic flight environment

8.7.1 Sensor Dynamics Model

Inertial sensors (gyros for vehicle angular rates and accelerometers for linear acceleration of the vehicle) used in the onboard inertial navigation system have drifts which are in nature of fixed drift, g-sensitive, g^2 -sensitive and scale factor errors for gyros, bias stability errors and scale factor errors for servo accelerometers and other associated errors. The sensor responses due to the electronics, hardware and transmission delay are represented by suitable dynamics. Typically, a second-order dynamics for representing sensor response is given below:

$$\frac{\xi_0}{\xi_i} = \frac{\omega_\xi^2}{s^2 + 2\omega_\xi\zeta_\xi + \omega_\xi^2} \quad (8.58)$$

where

ξ_i = Input to the sensor ξ (vehicle rate or acceleration)

ω_ξ = Undamped natural frequency of the sensor ξ

ζ_ξ = Damping ratio of the sensor ξ

ξ_0 = Sensor output (vehicle rate or acceleration as sensed by the sensors)

ξ = Rates (p, q, r) and acceleration (a_x, a_y, a_z)

In addition to the above, measured noises are also to be introduced into the output and therefore, sensor output to a functional system is given as

$$\xi_s = \xi_0 + \delta\xi_e + \delta\xi_n \quad (8.59)$$

where $\delta\xi_e$ is sensor errors and $\delta\xi_n$ is noise. More details on sensors are given in Chap. 14.

8.7.2 Navigation Model

Using the sensor output as given by Eq. (8.59), navigation computations have to be modelled as implemented in vehicle onboard. The limitations of onboard computer are also to be implemented in this model. More details are given in Chap. 14.

8.7.3 Guidance Model

The guidance system computes the desired attitude from two strategies:

1. Attitude command computed from the predetermined steering histories. At any instant, the required attitude of the vehicle is computed from the pre-stored input tables. This is generally known as open-loop guidance (OLG).
2. Attitude command computed using suitable guidance algorithm. The guidance algorithm takes the vehicle's instantaneous state vectors as computed by navigation system and computes the optimum attitude through suitable guidance law and cut-off command for the final stage to meet the target (injection) state vector. This is essentially a closed-loop guidance (CLG).

The entire algorithm and guidance law as implemented in vehicle onboard has to be modelled in the NGC system model.

8.7.4 Autopilot Model

The main features of this model are

1. Gain scheduling
2. Computation of error function
3. Filters/compensators
4. Control commands for the respective power plant

The control commands are generated based on the attitude control law taking into account desired attitude (as computed by guidance system), measured attitude (sensor output) and measured body rates (sensor output). The control commands generated by autopilot model are used to command the control power plant to

generate the required control forces and moments. The data acquisition delay as well as the delay in posting control command to the control power plant as in flight also essentially are simulated in this model.

8.7.5 Control Power Plant Model

Based on the control commands generated by the autopilot, the control system hardware generates the required control forces. This is a hardware system, having a finite response to the control commands. The response of control power plant has to be simulated through suitable dynamics, which are generally derived through ground testing. For a system with second-order dynamics, the control power plant response is given by

$$\frac{\delta}{\delta_c} = \frac{\omega^2}{s^2 + 2\zeta\omega s + \omega^2} \quad (8.60)$$

where

δ_c = Control command issued to the power plant (generated by autopilot)

δ = Response of the power plant

ω = Undamped natural frequency of the power plant

ζ = Damping ratio

Based on the value of δ , the control forces and moments are generated. In addition to the control forces and moments, in the cases of engine gimbal control system, there are additional forces and moments due to engine inertia. The model details of two typical control power plants are explained in Annexure A. The net control forces and moments are given below:

$$\mathbf{F}_{CB} = \begin{bmatrix} F_{CX} \\ F_{CY} \\ F_{CZ} \end{bmatrix} \quad (8.61)$$

$$\mathbf{M}_{CB} = \begin{bmatrix} M_{CX} \\ M_{CY} \\ M_{CZ} \end{bmatrix} \quad (8.62)$$

and inertia forces and moments are given by

$$\mathbf{F}_{EB} = \begin{bmatrix} F_{EX} \\ F_{EY} \\ F_{EZ} \end{bmatrix} \quad (8.63)$$

$$\mathbf{M}_{\mathbf{EB}} = \begin{bmatrix} M_{EX} \\ M_{EY} \\ M_{EZ} \end{bmatrix} \quad (8.64)$$

8.8 Vehicle Dynamics

Having explained the various models and forces and moments acting on the vehicle, the dynamics of vehicle and trajectory as functions of time need to be simulated. This can be achieved by solving equations of motion and the aspects covered are

1. Equations of motion
2. Initial conditions for the equations of motion
3. Solutions for the equations of motion

8.8.1 Equations of Motion

The dynamics of the vehicle is expressed through the equations of motion of the vehicle in three-dimensional space. The complete dynamics is described by the motion of the centre of gravity of the vehicle (translational equations of motion) in 3D space, the motion of the vehicle about its centre of gravity (rotational equations of motion) and the instantaneous orientation of the vehicle with respect to a reference frame.

8.8.1.1 Translational Equations of Motion

Translational equations of motion describe the motion of the centre of gravity of the vehicle with respect to some reference frame. The translational equations of motion are generally solved in ECI frame. In this case, the forces like thrust force, aerodynamic force, jet damping force and control force, etc. are computed first in body frame and then transferred to ECI frame. The gravitational accelerations are computed in ECI frame directly. Then the equations of motion are solved. The equations of motion are described as follows:

$$\dot{\mathbf{r}}_I = \mathbf{V}_I \quad (8.65)$$

$$\dot{\mathbf{V}}_I = \frac{1}{m} [\mathbf{IB}]^{-1} \mathbf{F}_B + \mathbf{G}_I \quad (8.66)$$

where

\mathbf{r}_I = Vehicle position vector with respect to ECI frame,

$$\mathbf{r}_I = \begin{bmatrix} X_I \\ Y_I \\ Z_I \end{bmatrix} \quad (8.67)$$

V_I = Vehicle inertial velocity vector with respect to ECI frame,

$$\mathbf{V}_I = \begin{bmatrix} u_I \\ v_I \\ w_I \end{bmatrix} \quad (8.68)$$

m = Instantaneous mass of the vehicle

[IB] = Transformation matrix from ECI frame to body frame

G_I = Acceleration due to gravity in ECI frame,

$$\mathbf{G}_I = \begin{bmatrix} G_{XI} \\ G_{YI} \\ G_{ZI} \end{bmatrix} \quad (8.69)$$

F_B = Total force expressed in body frame

$$\mathbf{F}_B = \mathbf{F}_{TB} + \mathbf{F}_{AB} + \mathbf{F}_{JB} + \mathbf{F}_{AUB} + \mathbf{F}_{SB} + \mathbf{F}_{CB} + \mathbf{F}_{EB} \quad (8.70)$$

The right-hand sides of Eqs. (8.69) and (8.70) are explained in the previous sections.

Translational equations of motion are solved in body frame also. In this case, gravitational acceleration computed in ECI frame is transferred to body frame. Also, to obtain the position of the vehicle centre of gravity, the velocity in body frame is transferred to ECI frame and then the equations of motion are solved. The equations of motion are described as follows:

$$\dot{\mathbf{r}}_I = [\text{IB}]^{-1} \mathbf{V}_B \quad (8.71)$$

$$\dot{\mathbf{V}}_B = \frac{1}{m} \mathbf{F}_B + [\text{IB}] \mathbf{G}_I - \omega \times \mathbf{V}_B \quad (8.72)$$

where

V_B = Vehicle inertial velocity expressed in body frame

$$\mathbf{V}_B = \begin{bmatrix} u_{B1} \\ v_{B1} \\ w_{B1} \end{bmatrix} \quad (8.73)$$

ω = Rotational velocity of the vehicle expressed in body frame

8.8.1.2 Rotational Equations of Motion

Rotational equations of motion describe the motion of the vehicle about its centre of gravity. Rotational equations of motion are solved with respect to body frame, which are described as follows:

$$\dot{\boldsymbol{\omega}} = [\mathbf{I}]^{-1} \{ \mathbf{M}_B - [\dot{\mathbf{I}}] \boldsymbol{\omega} - \boldsymbol{\omega} \times [\mathbf{I}] \boldsymbol{\omega} \} \quad (8.74)$$

where

$\boldsymbol{\omega}$ = Rotational velocity vector of the vehicle expressed in body frame

$$\boldsymbol{\omega} = \begin{bmatrix} r \\ q \\ p \end{bmatrix} \quad (8.75)$$

r = Yaw rate (about X_B axis)

q = Pitch rate (about Y_B axis)

p = Roll rate (about Z_B axis)

$[\mathbf{I}]$ = Inertia matrix

$$[\mathbf{I}] = \begin{bmatrix} I_{XX} & -I_{XY} & -I_{ZX} \\ -I_{XY} & I_{YY} & -I_{YZ} \\ -I_{ZX} & -I_{YZ} & I_{ZZ} \end{bmatrix}$$

$[\dot{\mathbf{I}}]$ = Rate of change of inertia matrix

$$[\dot{\mathbf{I}}] = \begin{bmatrix} \dot{I}_{XX} & -\dot{I}_{XY} & -\dot{I}_{ZX} \\ -\dot{I}_{XY} & \dot{I}_{YY} & -\dot{I}_{YZ} \\ -\dot{I}_{ZX} & -\dot{I}_{YZ} & \dot{I}_{ZZ} \end{bmatrix}$$

$[\mathbf{I}]^{-1}$ = Inverse of inertia matrix

\mathbf{M}_B = Total moment about body axes

$$\mathbf{M}_B = \mathbf{M}_{TB} + \mathbf{M}_{AB} + \mathbf{M}_{JB} + \mathbf{M}_{AUB} + \mathbf{M}_{SB} + \mathbf{M}_{CB} + \mathbf{M}_{EB} \quad (8.76)$$

The terms in the right-hand side of Eq. (8.76) are explained in the previous section.

8.8.1.3 Kinematic Relations

Kinematic relations describe the instantaneous vehicle attitude with respect to LPI frame. Kinematic relations can be described in two forms as given below:

1. Using Euler angles
2. Using quaternion parameters

Kinematic Relations Using Euler Angle Rates

The Euler angle rates are expressed in terms of the body rates as follows:

$$\dot{\theta} = \frac{1}{C_\Psi}(rS_\phi + qC_\phi) \quad (8.77)$$

$$\dot{\Psi} = rC_\phi - qS_\phi \quad (8.78)$$

$$\dot{\phi} = p + \frac{S_\Psi}{C_\Psi}(rS_\phi + qC_\phi) \quad (8.79)$$

where

θ, Ψ, ϕ are the vehicle pitch, yaw and roll angles with respect to LPI frame.

Kinematic Relations Using Quaternion Parameters

For the cases of vehicle rotating through large yaw angle (ψ), when it turns to 90° , the attitude dynamics given in Eqs. (8.77) and (8.79) poses mathematical singularity. In order to avoid this phenomenon, the kinematic relations are represented in terms of quaternions.

The quaternion parameter rates are related to body rates as follows:

$$\dot{\mathbf{e}} = \frac{1}{2}[\mathbf{E}]\boldsymbol{\omega} \quad (8.80)$$

where

\mathbf{e} = Vector of quaternion parameters

$$\mathbf{e} = \begin{bmatrix} e_0 \\ e_1 \\ e_2 \\ e_3 \end{bmatrix} \quad (8.81)$$

$[\mathbf{E}]$ = Quaternion matrix

$$[\mathbf{E}] = \begin{bmatrix} -e_1 & -e_2 & -e_3 \\ e_0 & -e_3 & e_2 \\ e_3 & e_0 & -e_1 \\ -e_2 & e_1 & e_0 \end{bmatrix} \quad (8.82)$$

However, when this option is used, the attitude of the vehicle with respect to LPI frame is computed from the elements of $[\mathbf{LB}]$ matrix. The details are given in Chap. 14.

8.8.2 Initial Conditions for Equations of Motion

8.8.2.1 Initial conditions for Translational Equations of Motion

Three options may be used to define the initial conditions for the position vector with respect to ECI frame:

1. Input is the vehicle position with respect to ECI frame (X_{I_0} , Y_{I_0} , Z_{I_0}) at time = t_0 , the initial time as given below:

$$\mathbf{r}_{I_0} = \begin{bmatrix} X_{I_0} \\ Y_{I_0} \\ Z_{I_0} \end{bmatrix} \quad (8.83)$$

2. Input is the geocentric radial distance (r_{I_0}), geodetic latitude (ϕ_{GD_0}) and longitude (λ_0) at the initial time = t_0 . Then the position vector is computed as follows:

Let

$$\phi_{GC} = \tan^{-1} \left[\frac{\tan \phi_{GD_0}}{k} \right] \quad (8.84)$$

$$\lambda_{I_0} = \lambda_0 + \Omega_e t_0 \quad (8.85)$$

Then,

$$\mathbf{r}_{I_0} = r_{I_0} \begin{bmatrix} C_{\phi_{GD_0}} * C_{\lambda_{I_0}} \\ C_{\phi_{GD_0}} * S_{\lambda_{I_0}} \\ S_{\phi_{GD_0}} \end{bmatrix} \quad (8.86)$$

3. If the initial time t_0 is the same as the launch time t_L , then the initial position vector in ECI frame is computed as follows:

Let

h_0 = Vehicle centre of gravity height above the oblate Earth

ϕ_{GD_L} = Geodetic latitude of launch point

λ_L = Longitude of launch point

t_L = Launch time

then,

$$\mathbf{r}_{I_0} = \begin{bmatrix} (R_{SL}C_{\phi_{GC_L}} + h_0C_{\phi_{GD_L}}) * C_{\lambda_{I_0}} \\ (R_{SL}C_{\phi_{GC_L}} + h_0C_{\phi_{GD_L}}) * S_{\lambda_{I_0}} \\ (R_{SL}S_{\phi_{GC_L}} + h_0S_{\phi_{GD_L}}) \end{bmatrix} \quad (8.87)$$

where

$$\lambda_{I_0} = \lambda_L + \Omega_e * t_0 \quad (8.88)$$

$$\phi_{GC_L} = \tan^{-1} \left[\frac{\tan \phi_{GD_L}}{k} \right] \quad (8.89)$$

$$R_{SL} = \frac{R_e}{[1 + (k - 1)S_{\phi_{GC_L}}^2]^{1/2}} \quad (8.90)$$

The initial conditions for the velocity vector in ECI frame also can be defined from three methods:

(i) Input is initial velocity vector with respect to ECI frame ($u_{I_0}, v_{I_0}, w_{I_0}$) at time t_0 . Then,

$$\mathbf{V}_{I_0} = \begin{bmatrix} u_{I_0} \\ v_{I_0} \\ w_{I_0} \end{bmatrix} \quad (8.91)$$

1. Input is the vehicle initial velocity magnitude (V_{I_0}), azimuth (A_{ZI_0}) and flight path angle (γ_{I_0}) at time t_0 .
2. In this case, from the initial vehicle position, the geocentric latitude (ϕ_{GC}) and longitude (λ_I) with respect to ECI frame are computed. Using the values, the [IG] matrix is generated. Then the vehicle velocity is computed as follows:

$$\mathbf{V}_T = V_{I_0} \begin{bmatrix} S_{\gamma_{I_0}} & S_{A_{ZI_0}} \\ C_{\gamma_{I_0}} & S_{A_{ZI_0}} \\ C_{\gamma_{I_0}} & C_{A_{ZI_0}} \end{bmatrix} \quad (8.92)$$

$$\mathbf{V}_{I_0} = [IG]^{-1} \mathbf{V}_T \quad (8.93)$$

3. If the initial time t_0 is the launch time t_L , then the initial velocity vector in ECI frame is computed as follows:

$$\mathbf{V}_{I_0} = \Omega_e \times \mathbf{r}_{I_0} \quad (8.94)$$

where

Ω_e = Earth rotational velocity vector, expressed in ECI frame

\mathbf{r}_{I_0} = Initial position vector of the vehicle, expressed in ECI frame

In the case of equations of motion in body frame, the position vector initializations are the same as that given above. Two options can be used for the velocity vector initialization as follows:

1. Input is the vehicle inertial velocity vector in body frame ($\mathbf{u}_{IB_0}, \mathbf{v}_{IB_0}, \mathbf{w}_{IB_0}$) at the initial time t_0 .

$$\mathbf{V}_{B_0} = \begin{bmatrix} u_{IB_0} \\ v_{IB_0} \\ w_{IB_0} \end{bmatrix} \quad (8.95)$$

2. Input is the vehicle inertial velocity magnitude (V_{I_0}), azimuth (A_{Zl_0}) and flight path angle (γ_{I_0}) at the initial time t_0 .

In this case, the vehicle inertial velocity in ECI frame is computed as per Equation (8.93). Then the velocity is transferred to the body frame as

$$\mathbf{V}_{B_0} = [IB] \mathbf{V}_{I_0} \quad (8.96)$$

8.8.2.2 Initial Conditions for Rotational Equations of Motion

Two options are used to define the initial conditions for the rotational equations of motion:

1. Input is the initial rotational velocity of the vehicle in body frame (r_0, q_0, p_0) at the initial time t_0 . Then,

$$\boldsymbol{\omega}_0 = \begin{bmatrix} r_0 \\ q_0 \\ p_0 \end{bmatrix} \quad (8.97)$$

2. If the initial time is the launch time t_L , then the body rates are the Earth rotational rate expressed in body frame. Thus,

$$\boldsymbol{\omega}_0 = [IL]\boldsymbol{\Omega}_e \quad (8.98)$$

8.8.2.3 Kinematic Relations Initialization

Euler Angles Initialization

The initial conditions for the vehicle pitch, yaw and roll angle are the input values, viz. θ_0, ψ_0, ϕ_0 .

Quaternion Parameters Initialization

From the initial Euler angles, θ_0, ψ_0, ϕ_0 , the quaternion parameters can be computed as

$$\mathbf{e}_0 = \mathbf{e}(\theta_0) * \mathbf{e}(\Psi_0) * \mathbf{e}(\phi_0) \quad (8.99)$$

where

$$\begin{aligned}\mathbf{e}(\theta_0) &= C_{(\theta_0/2)} + S_{(\theta_0/2)}\mathbf{j} \\ \mathbf{e}(\Psi_0) &= C_{(\Psi_0/2)} + S_{(\Psi_0/2)}\mathbf{i} \\ \mathbf{e}(\phi_0) &= C_{(\phi_0/2)} + S_{(\phi_0/2)}\mathbf{k}\end{aligned}\quad (8.100)$$

* Denotes quaternion multiplication as explained in Chap. 14.

The initial conditions for the quaternion parameters can also be taken from the input values, viz. $e_{0_0}, e_{1_0}, e_{2_0}, e_{3_0}$. Thus,

$$\mathbf{e}_0 = \begin{bmatrix} e_{0_0} \\ e_{1_0} \\ e_{2_0} \\ e_{3_0} \end{bmatrix} \quad (8.101)$$

8.8.3 Solutions for the Equations of Motion

The equations of motion described in Eqs. (8.65), (8.66), (8.71), (8.72), (8.74), (8.77), (8.78), (8.79), (8.80) are solved simultaneously with the appropriate initial conditions using numerical integration methods. Fourth-order Runge–Kutta method is the recommended method for solving the equations of motion. This method is described as follows:

Let 'm' simultaneous first-order equations be given as

$$\dot{\mathbf{X}} = \mathbf{f}(t, \mathbf{X}) \quad (8.102)$$

where

$$\mathbf{X} = \begin{bmatrix} X_1 \\ X_2 \\ \vdots \\ X_m \end{bmatrix} \quad (8.103)$$

$$\mathbf{f} = \begin{bmatrix} f_1 \\ f_2 \\ \vdots \\ f_m \end{bmatrix} \quad (8.104)$$

t = time

Let, at time t_n , the state be given as \mathbf{X}_n . Then the state at time t_{n+1} is computed as follows:

Let.,

$$\mathbf{k}_1 = \mathbf{f}(t_n, \mathbf{X}_n) \Delta t \quad (8.105)$$

$$\mathbf{k}_2 = \mathbf{f}\left(t_n + \frac{\Delta t}{2}, \mathbf{X}_n + \frac{\mathbf{k}_1}{2}\right) \Delta t \quad (8.106)$$

$$\mathbf{k}_3 = \mathbf{f}\left(t_n + \frac{\Delta t}{2}, \mathbf{X}_n + \frac{\mathbf{k}_2}{2}\right) \Delta t \quad (8.107)$$

$$\mathbf{k}_4 = \mathbf{f}(t_n + \Delta t, \mathbf{X}_n + \mathbf{k}_3) \Delta t \quad (8.108)$$

The increment in the state \mathbf{X} is given as

$$\Delta \mathbf{X} = \frac{1}{6}(\mathbf{k}_1 + 2\mathbf{k}_2 + 2\mathbf{k}_3 + \mathbf{k}_4) \Delta t \quad (8.109)$$

Then, the state at t_{n+1} is given as

$$\mathbf{X}_{n+1} = \mathbf{X}_n + \Delta \mathbf{X} \quad (8.110)$$

$$t_{n+1} = t_n + \Delta t \quad (8.111)$$

where

Δt = Integration time

8.8.4 Equations of Motion During Lift-Off

During initial lift-off phase, if the thrust is less than the weight of the vehicle, or if there is any physical constraint that holds the vehicle on the launch pad until it is released, there is no relative movement of the vehicle with respect to the launch pad. In this case, the relative position and velocity remain constant while the inertial position changes by the Earth rotation. The inertial velocity magnitude remains constant while its direction changes. The equations used to describe these motions are given as

$$\dot{\mathbf{r}}_I = \mathbf{V}_I \quad (8.112)$$

$$\dot{\mathbf{V}}_I = \boldsymbol{\Omega}_e \times \mathbf{V}_I \quad (8.113)$$

8.8.5 Instantaneous Change in State Vector

In order to simulate the disturbances due to stage separation and payload fairing separation, instantaneous increments need to be added to the state vector.

8.8.5.1 Instantaneous Change in the State Variables

The instantaneous change in the state vector \mathbf{X} is modified as follows:

$$\mathbf{X} = \mathbf{X} + \Delta\mathbf{X} \quad (8.114)$$

where

$$\mathbf{X}^T = [X_I, Y_I, Z_I, u_I, v_I, w_I, r, q, p, \theta, \psi, \phi] \quad (8.115)$$

$$\Delta\mathbf{X}^T = [\Delta X_I, \Delta Y_I, \Delta Z_I, \Delta u_I, \Delta v_I, \Delta w_I, \Delta r, \Delta q, \Delta p, \Delta \theta, \Delta \psi, \Delta \phi] \quad (8.116)$$

\mathbf{X} is the disturbance vector of the state variables.

8.8.5.2 Inertial Velocity Changes

In this case, the inertial velocity changes are expressed in body frame. The instantaneous velocity vector is modified as follows:

$$\mathbf{V}_I = \mathbf{V}_I + [\mathbf{IB}]^{-1} \Delta\mathbf{Y} \quad (8.117)$$

where

$\Delta\mathbf{Y}$ = change in velocity given in body frame
i.e.

$$\Delta\mathbf{Y}^T = [\Delta u_B, \Delta v_B, \Delta w_B]$$

The velocity changes in body frame $\Delta\mathbf{Y}$ are to be used only when the translational equations of motion are solved in ECI frame.

8.8.6 Instantaneous Velocity Addition Due to Tail-Off

In the case of liquid engines with guidance cut-off, the thrust cut-off command is issued by the guidance system during operation of a stage. To simulate the tail-off

characteristics after cut-off, the incremental velocity due to tail-off is added instantaneously to the vehicle velocity as follows:

Let $\Delta \mathbf{V}$ be the velocity increment due to tail-off (input)

$$\Delta \mathbf{V} = \begin{bmatrix} 0 \\ 0 \\ \Delta V \end{bmatrix} \quad (8.118)$$

$$\mathbf{V}_I = \mathbf{V}_I + [\mathbf{IB}]^{-1} \Delta \mathbf{V} \quad (8.119)$$

If the body frame is used for the translational equations of motion, then

$$\mathbf{V}_I = \mathbf{V}_I + \Delta \mathbf{V} \quad (8.120)$$

8.9 Flexible Vehicle Dynamics

The flight mechanics model explained above assumes that the vehicle is infinitely rigid. In reality, the launch vehicles are flexible bodies, wherein the vehicle structure is vibrating with fundamental structural modes with relatively low frequency. Output of the sensors mounted on the flexible vehicle measures these structural deflections in addition to the rigid-body motion. As these sensor signals are used in the autopilot command generation, without proper autopilot design, there can be coupling between autopilot and vehicle structural systems which may end up with vehicle structure failure. To avoid such scenarios, vehicle autopilot is designed suitably. In order to ensure that the autopilot designs are robust under the realistic environment of vehicle flexibility, it is essential to model the flexible vehicle dynamics in the flight mechanics model.

The satisfactory performance of a flexible launch vehicle crucially depends on accurate representation of the elastic motion of the vehicle under prescribed forces. As the vehicle moves, it experiences disturbing forces and moments such as aerodynamics, propellant sloshing, engine inertia, thrust misalignments, attachment misalignments, centre of gravity offsets, nozzle canting, etc. in addition to the controlling forces and moments to counteract these disturbances. Under this environment, in addition to the rigid-body response, the flexible modes are also excited and cause adverse effects on vehicle stability due to coupling of these modes with the vehicle control system.

The various types of elastic modes in the launch vehicle are

1. Lateral
2. Torsional
3. Longitudinal

Axial loads acting on the vehicle during flight induce the longitudinal oscillations. The effect is a slight decrease in the lateral bending mode frequencies. This effect is generally small and can be neglected.

The torsional vibrations are due to elastic angular displacement about the longitudinal axis. The mathematical development of torsional mode is analogous to that of lateral vibrations. In large vehicles with strap-on motors the torsional modes are also important. The lateral vibration modes are of primary importance, since these motions are sensed by the sensors and fed back to the autopilot for control command generation. The sensors measure local elastic distortions along with the rigid-body motion. Under unfavourable phase relationship the rocket engines will deflect in such a way to reinforce the elastic vibrations.

For launch vehicles with high degree of axial symmetry there is negligible coupling between pitch and yaw lateral and longitudinal modes or torsional modes. Under this condition only planar modelling and studies are sufficient. However the situation changes for the case of clustered booster vehicles, where the coupling between lateral and torsional modes is significant. To analyze the flexible vehicle response and bending loads acting on the vehicle and to evaluate the autopilot performance under flexible vehicle environment, it becomes necessary to simulate the vehicle motion very close to the flight environment.

The necessary equations for the simulation of the elastic motion of the vehicle, sensor output and the flexibility contribution to rigid-body and slosh dynamics are explained in Chap. 14.

8.10 Integrated Flight Mechanics Model

The integrated flight mechanics model with the interfaces between vehicle and subsystems and environmental models are given in Fig. 8.13. The above figure shows a simplified model representing the entire STS. This integrated model can be used to generate necessary input for designing the subsystems and to validate the subsystem designs as well as to evaluate the subsystems and integrated mission performance.

Once the systems are realized, in the above integrated model, the corresponding model is replaced with the real system. In such cases, suitable interfaces have to be implemented between the real systems and flight mechanics model. Under this configuration, again validation of the real systems is carried out. The details are explained in Chap. 14.

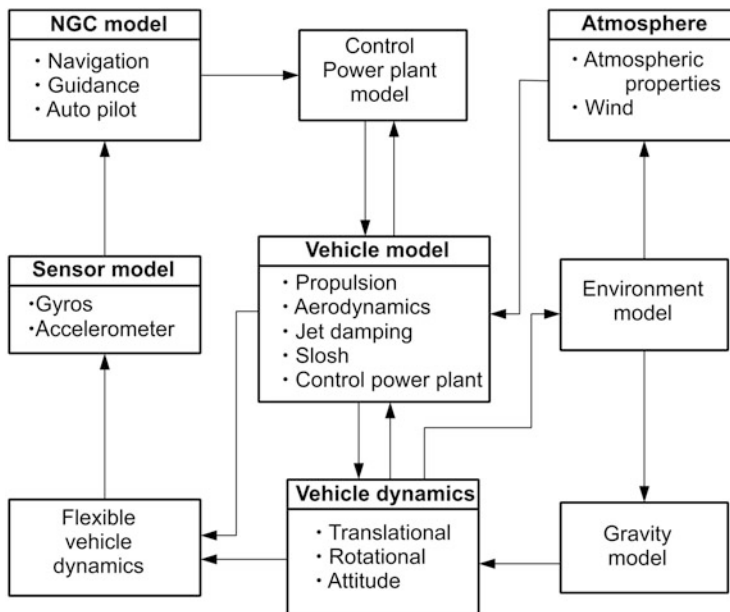


Fig. 8.13 Integrated flight mechanics model

Bibliography

1. Zipfel, P.H.: Modeling and simulation of aerospace vehicle dynamics. AIAA Education Series, Reston (2007).
2. Etkin, B., Reid, L.D.: Dynamics of flight: stability and control. Wiley, New York (1995)
3. Blakelock, J.H.: Automatic control of aircraft and missiles. Wiley-Interscience, New York (1991)
4. Brauer, G.L., Cornick, D.E., Habeger, A.R., Petersen, F.M., Stenvenson, R.: Program to optimize simulated trajectories (POST) Vol-1: formulation manual, NASA CR – 132689, Martin Marietta Corporation; April 1975.
5. Suddath JH. Use of an inertia sphere to damp the angular motions of spinning space vehicles. NASA. TR R-110 (1961)
6. Fogarty, L.E., Howe, R.M.: Computer mechanization of six degrees of freedom flight equations. NASA CR-1344, Washington, DC (1969)
7. Drisol, T.R., Eckenroth, H.F.: Hybrid simulation – key to successful flight test packages. Simulation **26**(1), 17–27 (1976)
8. Greensite, A.L.: Analysis and design of space vehicle flight control systems. Vol.II – Trajectory Equations. NASA CR-821, Washington, DC (1967)
9. James, R.L.: A three dimensional trajectory simulation using six degrees of freedom with arbitrary wind. NASA TND – 641, Washington, DC (1961)
10. Wagner, W.E., Serold, A.C.: Formulation on statistical trajectory estimation programmes. NASA CR – 1482, Washington, DC (January 1970)
11. Greensite, A.L.: Analysis and design of space vehicle flight control systems, control theory : Vol. II. Spartan Books, New York (1970)

12. Etkin, B.: Dynamics of atmospheric flight. Wiley, New York (1972)
13. Robinson, A.C.: On the use of quaternions in simulation of rigid bodies. WADC Techinal Report **58-17** (1958)
14. Schletz, B.: Use of quaternion in shuttle guidance, navigation and control. AIAA Paper No. 82-1557. AIAA Guidance and Control Conference, San Diego (1982)
15. Ickes, B.P.: A new method for performing digital control system attitude computations using quaternions. Paper No. 68-825. AIAA Guidance, Control and Flight Dynamics Conference, Pasadena, California, 12-14 August 1968
16. Anon.: Propellant slosh loads, NASA Space Vehicle design criteria monograph (Structures), NASA SP-8009, (August 1968)
17. Wiesel, W.E.: Spacecraft dynamics, 2nd edn. McGraw-Hill Book Company, New York (1996)
18. Miele, A.: Flight mechanics. Addison-Wesley, Reading (1962)
19. Etkin, B., Reid, L.D.: Dynamics of flight: stability and control. Wiley, New York (1995)
20. Harris, R.J.: Trajectory simulation applicable to stability and control studies of large multi-engine vehicles. NASA TN D-1838, (August 1963)
21. Sivan, K., Ashok Joshi, Suresh, B.N.: Reentry trajectory modeling and simulation: application to reusable launch vehicle mission. Paper No-53, Proceedings of the International Conference on Modeling, Simulation, Optimising for Design of Multi Disciplinary Engineering Systems (MSO-DMES), Goa, India, 24-26 (September 2003)
22. Ashok Joshi, Sivan, K.: Modeling of open loop simulation of reentry trajectory of RLV application. Proceedings of the 4th international symposium on atmospheric reusable vehicle and systems, Arcachon, France, 21-23 (March 2005)

Chapter 9

Propulsion Systems

Abstract Propulsion systems in space transportation systems have to impart the necessary energy to the vehicle to achieve the desired orbital conditions for the specified satellite. Different categories of propulsion systems such as chemical propulsion, electric propulsion, nuclear propulsion, solar sail, etc. are being used in various applications of space missions, depending on the requirements. For the boost phase with the present day technologies, chemical propulsion systems are generally being used and the energy source is the chemical reaction. There are two types of chemical propulsion systems like air breathing propulsion and non-air breathing propulsion. In air breathing propulsion, the oxygen available in the atmosphere and the fuel stored vehicle onboard are used for the combustion process, whereas in the case of non-air breathing propulsion system, both oxidizer and fuel stored vehicle onboard are used for generating the necessary thrust. Depending on the type of propellants used, the chemical rocket propulsion systems are classified into solid motors rockets, liquid engines and hybrid propellant rockets. In solid propellant rocket motor, the propellant is stored in combustion chamber and propellant burns from the surface. The liquid propellants are categorized into bipropellant and monopropellant. Depending on the propellants used, the bipropellant systems are further classified into Earth storable systems, cryogenic systems and semi-cryogenic systems. In the hybrid rocket propulsion system, generally the fuel is solid and the oxidizer is liquid. The payload capability of a multi-stage vehicle has to be maximized and in achieving this objective the propulsion module for each stage has to be carefully selected. The selection of the number of stages and type of propulsion system depend on the mission objectives, state-of-the-art technologies in propulsion, technology base available, development lead time, and cost and reliability requirements. The selection and design of a suitable propulsion system has to be carried out by considering various factors and also its close interactions with several other major subsystems of the vehicle. This chapter addresses important system engineering aspects of propulsion systems like the selection and design of propulsion modules for a STS, the basics of rocket propulsion, several propulsion options and their relative merits and demerits. The staging aspects and criteria for selection of suitable propulsive modules are highlighted. The qualification process for the propulsive stages is also included. A brief discussion on air breathing propulsion system also outlined.

Keywords Propulsion • Trajectory • Exhaust velocity • Specific impulse • Nozzle configuration • Solid motors • Liquid engines • Cryogenics • Semicryogenics • Hybrid motors • Airbreathing • Ramjet • Scramjet

9.1 Introduction

The fundamental requirement of propulsion systems in space transportation systems is to impart the necessary energy to the vehicle to achieve the desired orbital conditions for the specified satellite. To achieve the above objective, the propulsion systems have to convert the available energy either stored onboard the vehicle or derived from elsewhere into kinetic energy to the vehicle. Based on the usage of the energy source and the process of converting it into useful kinetic energy, different categories of propulsion systems such as chemical propulsion, electric propulsion, nuclear propulsion, solar sail, etc. are being used in various applications of space missions, depending on the requirements. Especially for the boost phase with the present-day technologies, chemical propulsion systems are generally being used.

In chemical propulsion, the energy source is the chemical reaction. The propellants (atmospheric oxygen or stored oxidizer and stored fuel) are reactants used for the chemical reaction process, which in turn produces high-temperature and high-pressure combustion products. The thermal energy thus generated by the chemical reaction process is converted into kinetic energy by expanding the hot compressed gases through suitable thrust-producing device. The kinetic energy of the expelled combustion products in turn generates thrust to the vehicle, which is converted into kinetic and potential energies necessary to transport and position the satellite into the desired orbit.

There are two types of chemical propulsion systems: (1) air-breathing propulsion and (2) non-air-breathing propulsion. In air-breathing propulsion, the oxygen available in the atmosphere and the fuel stored vehicle onboard are used for the combustion process, whereas in the case of non-air-breathing propulsion system, both oxidizer and fuel stored vehicle onboard are used for generating the necessary thrust.

During the boost phase, the vehicle has to operate from sea level to very high altitude, typically up to 1000 km. For such a mission, atmospheric operation of the vehicle is very short compared to the entire duration. Most of the time, the vehicle operates in vacuum and therefore it is essential to use non-air-breathing propulsion systems. This propulsion system is called rocket propulsion. Nowadays worldwide research activities are being pursued on the feasibility of using air-breathing propulsion systems for STS to improve the vehicle performance. This book deals mainly with the rocket propulsion aspects with brief mentioning on the feasibility of air-breathing propulsion systems.

The energy provided by the propulsion system is oriented towards optimum direction in space by navigation, guidance and control system of the vehicle to achieve the desired orbital conditions precisely. Vehicle structure is either holding the propulsion system or sometimes the propulsion system itself is part of the vehicle structure. As thrust produced by the propulsion system is the primary force acting on the vehicle, the complete vehicle systems are interacting with the propulsion system, through various types and levels of couplings, as explained later

in the chapter. With the existing technologies, to achieve the maximum performance of the vehicle, the propulsion subsystems have to operate in its peak performance whereas the vehicle structural design (some part of the propulsion systems) has to be highly optimum. The design challenges of such systems are further aggravated due to the hostile operating environment for the propulsion and structural subsystems. Therefore, optimal design of propulsion systems under such conditions demands integrated design approach.

The payload capability of a multi-stage vehicle as a percentage of its total lift-off mass has to be maximized and therefore the selection of a suitable propulsion module for each stage plays a major role in achieving this objective. Generally the propellant mass in almost all vehicles forms 82 to 89 % of its total mass while the rest is from all other non-propulsive systems termed as inert mass. The selection of the number of stages and type of propulsion system largely depends on the mission objectives, state-of-the-art technologies in propulsion, technology base available, development lead time, cost and reliability requirements. The mission objectives are essentially the payload size, payload mass and its orbital requirements. In addition the trajectory options and range safety constraints defined by the launch scenario are other important inputs. Once the vehicle and mission requirements are clearly spelled out and practical considerations like the technology base, development lead time, cost, etc. are assessed it is possible to derive the propulsion module requirements for a vehicle. It is equally important to achieve the highest payload mass fraction for the vehicle right at the beginning of the project definition. The overall vehicle size, its performance, the integration aspects, the reliability and many such critical requirements are closely related to the type of propulsion systems. Therefore the selection and design of a suitable propulsion system have to be carried out by considering not only various factors listed above but also its close interactions with several other major subsystems of the vehicle. This demands detailed system engineering studies to understand the interactions and their influence on propulsion system design. Therefore the selection process for suitable propulsion systems for a vehicle has to undergo several iterations. This iterative process has to consider the number of possible candidates, based on the existing modules, with or without modifications or include a new module which can be realized within the overall constraints of time, reliability and cost.

This chapter addresses important system engineering aspects to be considered during the selection and design of propulsion modules for an STS, the basics of rocket propulsion, several propulsion options and their relative merits and demerits. The staging aspects and criteria for selection of suitable propulsive modules are highlighted. The qualification process for the propulsive stages is also included. A brief discussion of air-breathing propulsion systems is also outlined at the end of this chapter.

9.2 System Considerations in Propulsion System Selection and Design

Propulsion system is a major STS system which provides the principal force to the vehicle by consuming the stored chemical propellants. The vehicle Navigation, Guidance and Control (NGC) systems orient the thrust along the suitable directions

and shut off the engine at the appropriate time to meet the specified requirements and to achieve the desired mission precisely. In most of the cases, the main propulsive thrust chambers are suitably deflected to generate the required control forces necessary to stabilize the vehicle during the entire mission. In the multi-stage vehicle, it is essential to separate the lower stage once its function is over. During this process, the functionally completed stage causes disturbed environment to the vehicle. To ensure normal functioning of the sensitive and highly optimized propulsion system elements, it is essential to protect them against the hostile external environment such as mechanical and thermal loads. Similarly, the propulsion systems during its operation cause severe structural and thermal environments to the vehicle's other sensitive systems. Therefore, the propulsion system is very strongly coupled to almost all the subsystems of the vehicle. This necessitates that detailed system engineering studies are essential during the design phase to have a clear understanding of these interactions and their influences on propulsion system design. Some of the important interactions and interdependencies of major subsystems like (a) structures, (b) mechanisms, (c) trajectory, (d) control and guidance and (e) thermal design with the propulsion systems are given in Fig. 9.1 and are explained below:

(a) *Structure:*

Generally the propulsive stages like rocket motors in case of solid motors and propellant tanks in case of liquid motors form the main structural members of the vehicle. The various loads on vehicle due to aerodynamics, gravity, acceleration, vibrations, thrust, sloshing, dynamic interactions, etc. are to be factored during the design of these stages. During the atmospheric phase of flight the vehicle velocity increases during the dense atmospheric phase. Accordingly the dynamic pressure also increases on the vehicle. It is therefore essential to minimize the maximum dynamic pressure to avoid the higher aerodynamic forces on the vehicle structure. The thrust time profile of the propulsion system has to be accordingly shaped to ensure that the maximum load on the vehicle structure during the atmospheric phase of flight is well within the allowable limits. There is also a requirement to limit the 'g' load on the vehicle particularly if the vehicle carries humans onboard. The acceleration of the vehicle depends on the motor thrust and mass of the vehicle which reduces continuously due to consumption of propellant. Therefore the thrust time curve has to be suitably designed to limit the required acceleration levels. The start and shut-off transients of the propulsion system cause severe shock on the structure on which very sensitive components like avionics, control components, etc. are mounted. The propellant depletion sometimes causes severe oscillations in thrust generated by the propulsion system which in turn introduces higher load on vehicle structures and satellites. These aspects are to be suitably factored during design to minimize their effects.

(b) *Mechanisms:*

Various separation systems which are detailed in Chap. 13 are utilized to separate the spent stages once their functions are completed. The residual thrust of the spent stage is one of the prominent loads to be considered for the separation system design. The separation system demands lowest thrust during separation process

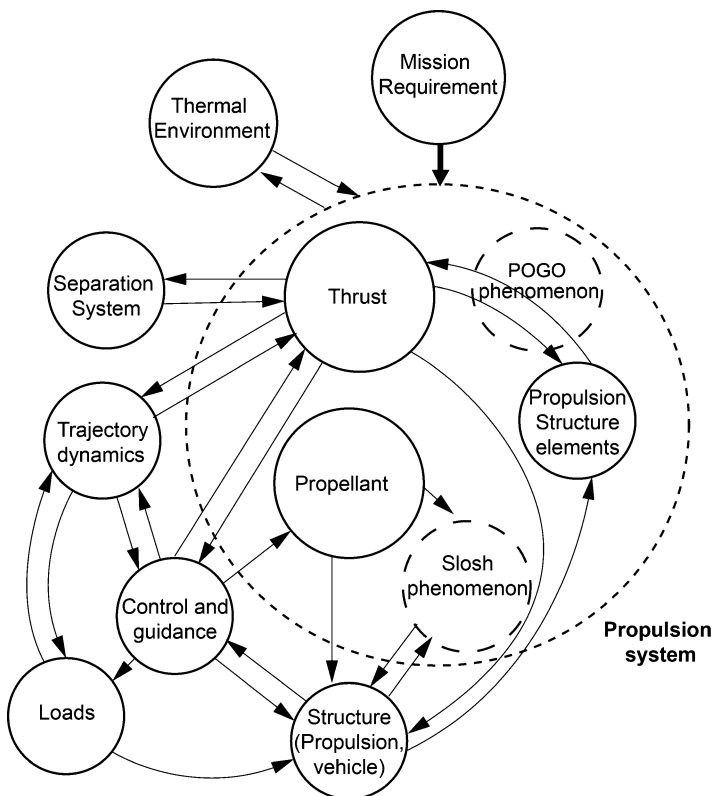


Fig. 9.1 Propulsion systems interfaces with vehicle subsystems

whereas the performance and vehicle controllability demand the transition process to happen at a higher thrust level. Thrust level at the time of separation has to be judiciously decided and all the vehicle systems have to be designed for this optimum level. In case of strap-on motors, the entire thrust load is transferred to the main motor through the separation mechanism used. Hence this thrust load has to be considered in addition to other loads in the design of mechanisms.

(c) *Trajectory:*

The trajectory is strongly coupled to the propulsion systems. Depending on the launch azimuth decided by the mission and other land mass constraints, the stages are to be terminated to ensure that the range safety requirements are met with. The propulsive stage sizing should be accounted for this requirement to avoid carrying extra propellant as this acts as inert mass onboard which has an impact on the payload. To obtain the optimum performance from the vehicle, it may be necessary to throttle down or augment the thrust of the engine depending on the requirement during certain phases of trajectory. This requirement has to be accounted during the design phase of propulsion systems.

(d) *Control and Guidance:*

In most of the vehicles the attitude control is achieved by deflecting the nozzle or engine of the propulsive stages. The maximum angle of deflection of the nozzle or engine depends on the control requirement of the vehicle based on various disturbances encountered during the flight. Therefore the propulsion stages are to be suitably configured to meet the control requirements. In some of the solid booster stages secondary injection control systems are used for control. The nozzle design has to factor all the requirements of secondary injection systems such as number of valves, their location, the flow rate, nozzle erosion and the related flow analysis to estimate the required control force.

In case of liquid propulsion systems the lateral oscillations of the liquid propellants in tanks known as fluid sloshing can interact with control and structure. Suitable fluid damping in the tanks corresponding to critical events of flight is to be ensured. The damping is generally improved by providing the slosh baffles in the propellant tanks. The longitudinal oscillations of liquid columns in the liquid stages termed as POGO can cause control and structure interaction particularly when the liquid strap-ons are used. The phase difference in the longitudinal frequencies of POGO in liquid stages of strap-ons can influence the lateral motions of the vehicle and hence can cause the interaction with control and structure. This aspect needs to be studied during the initial design and suitable POGO suppression system has to be introduced to alleviate such problems.

The propellant loading in each stage, particularly in liquid stages, has to be based on the mission requirements and certain quantity of propellants are to be reserved as guidance margin to cater to the underperformance of the vehicle during the flight. The tail-off thrust of liquid engines after the guidance command cut-off would add certain additional velocity to the vehicle. It is always advantageous to have a sharp tail-off in liquid engines and it has to be taken into account during the design phase.

(e) *Thermal aspects:*

The thermal environment of the vehicle is greatly influenced by the propulsion systems. The various thermal aspects which are to be considered for the propulsion systems design are

1. Heating from the rocket exhaust gas
2. Interaction of plumes in case of multiple engines
3. Hot walls of propulsion system elements, particularly nozzle
4. Interfaces between the cryogenic tanks and the vehicle structures
5. Insulation for cryogenic tank
6. Insulation requirements for the Earth storable liquid stages during the launch phase
7. Cooling requirements for the nozzles
8. Transfer of heat from propulsion subsystem to vehicle structure and other subsystems

The effect of each one of these thermal aspects is discussed in detail in Chap. 12 of this book.

9.3 Propulsion System Requirements, Selection and Design Guidelines

9.3.1 Propulsion System Requirements

The total ideal velocity needed for a given mission to position the specified spacecraft into the desired orbit considering all losses due to drag, gravity and other causes is the fundamental driving factor for the selection of propulsion systems. The primary requirement of the propulsion systems is to achieve maximum performance and to reduce the cost of launching the spacecraft into the desired orbit. This requirement is reflected as (a) to minimize the vehicle mass for a given payload or (b) to maximize payload for a given vehicle. To achieve these objectives, it is essential that the propulsive systems provide the maximum propulsion performance in terms of thrust levels, maximum specific impulse, maximum total impulse for the given propellant loading and reduce the velocity losses while minimizing the structural mass of the propulsion systems.

In addition, the selected propulsion systems must have the following attributes: (1) reliability, (2) safety, (3) operational ease and (4) reduced overall cost of the vehicle. To achieve the reduced cost, important aspects in the propulsion system are reduced development schedule, development cost, product cost and operational cost.

9.3.2 Propulsion System Selection Criteria

Proper selection of propulsion systems is one of the key factors in deciding the effective STS design. The aim is to achieve high performance with low cost and high reliability. Figure 9.2 defines a typical selection methodology for a propulsion system of STS.

The requirements of propulsive stages are to be generated from the overall system requirements which are defined in terms of payload mass, number of stages, overall mass fraction, flight trajectory, launch base, range safety constraints, control system definition and gross lift-off weight (GLOW). The propulsion system has to meet the overall requirements of propellant mass fraction, thrust time profile, specific impulse, total impulse, allowable envelope, temperature constraints, schedule and cost requirements, etc.

As discussed in Chap. 5, the decision on number of stages to meet the ΔV requirement of a mission largely depends on the technical maturity of the

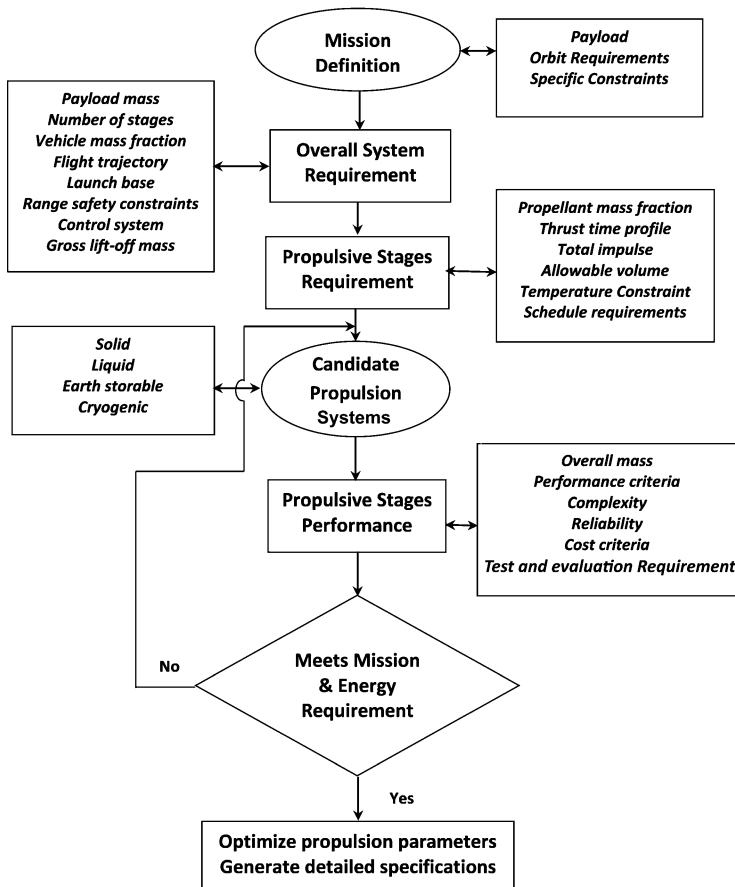


Fig. 9.2 Typical selection methodology for a propulsion system

propulsive stages, the performance margins, reliability, safety and cost. Once the decision is made on number of stages, the thrust and total impulse requirements for each stage depends on the payload mass, the mission to be accomplished and the range safety constraints. Subsequently the choice of a suitable propulsion system for each stage of the vehicle is the priority. The candidate propulsive systems generally considered for a STS are (a) solid or (b) liquid, earth storable or semi-cryogenics or cryogenics. Each system has specific advantages and disadvantages. Selection has to be based on the performance requirements, mission operational needs, overall mass, available technology, new technology developments, complexity, reliability, ease of manufacture, cost, test and evaluation requirements, development cost and schedule.

The mission operational needs include the requirements of thrust cut-off, restart capability, range safety constraints, desired thrust time profile to satisfy the constraints and meeting the specified mass fraction. The minimization of GLOW, dry

mass, product cost and operational cost are also driving factors. The design requirements for attitude controls which are derived by thrust vector control of the engines or nozzles are also to be accounted during the selection process.

The performance requirement and technology maturity are major factors for deciding the propulsion systems. In order to reduce the risk and increase reliability, it is always advantageous to use the already developed and available technology. But to meet the performance requirements, certain augmentations and improvements may be required which may increase the vehicle cost and complexity. In certain cases, to meet the performance requirements, it is essential to adopt advanced technologies which may end up with new development cost, schedule, risk and reliability. Additionally, the advanced system may demand advanced materials development and fabrication process, which may have implications on unit cost of the vehicle and overall schedule. Therefore, trade-off studies have to be carried out for the judicious selection of the propulsive systems. The overall safety of subsystems during the vehicle preparation, integration and launch is an important factor. The selected vehicle configuration has to satisfy the overall launch constraints like range safety. The entire process is iterative before arriving at a suitable optimum configuration.

The selection process ends up with the specifications and the requirements for the detailed system design.

9.3.3 Overall Design Guidelines

The propulsion system is the important subsystem of the vehicle and any malfunction of the propulsion system elements leads to the vehicle and mission failure. Therefore, it is essential that the propulsion subsystems have to be designed to ensure safe and normal operations of the systems under nominal and dispersed environments. Design has to ensure that there is no combustion instability. While designing the propulsion subsystems to achieve the specified thrust profile and specific impulse, it is essential to ensure that the systems are safe, less complex, reliable and minimize the structural mass of the systems. Therefore, trade-off studies and optimization are needed in terms of number of engines/motors, chamber pressure, optimum operating mixture ratio, nozzle area ratio and overall vehicle performance. All the interface requirements between the propulsion systems and other systems of the vehicle are to be suitably addressed. In addition, to reduce the overall stage structural mass, suitable materials have to be selected for motor cases and propellant tanks.

Even though there is an optimum mixture ratio for the best performance of the propulsion system, normally, there is a range of mixture ratio, within which the system performs normally with marginal reduction in the performance. Such a deviated mixture ratio with respect to the optimum, results into major reduction in the propellant tank volume requirement, which in turn helps in saving in the structural mass of the tank. Therefore, trade-off studies have to be carried out and

the suitable mixture ratio which meets the requirements of a propulsion system at both its nominal and maximum performance has to be selected.

To reduce the propellant slosh effects on the vehicle systems, the propellant tanks are to be suitably designed to ensure the slosh mass to be near to the vehicle centre of gravity during critical operational phase. In case such design is not possible, to avoid propellant slosh-structure-control interaction, the required damping has to be provided by implementing the baffles at suitable locations as per the criticalities. In order to avoid the POGO interactions, studies have to be carried out at the early stage itself and propellant feed lines have to be suitably modified and POGO correcting systems have to be implemented in the propulsion system.

To achieve the maximum performance, the propulsion has to provide the specified thrust level. In order to achieve this requirement under varying operating environment, suitable thrust regulation system has to be implemented in the propulsion system. This can be achieved by either passive or active regulation system. In the case of the liquid propulsion system, operating mixture ratio deviated away from the nominal can cause the depletion of one of the propellants before the other and finally ends up with early shutdown of the engine. To ensure maximum utilization of the propellants in the tanks, either active or passive mixture ratio control has to be implemented.

Tail-off thrust oscillation caused by the depletion characteristics of the propulsion system has major impact on vehicle subsystems and satellite interface loads. To reduce or avoid such thrust oscillations, it is necessary to design the shut-off valve with specific characteristics.

Finally, to ensure normal functioning of propulsion subsystems, the thermal environment has to be maintained within the allowable limits. This is achieved by implementing suitable cooling mechanisms to the engine systems.

9.4 Propulsion Fundamentals

The fundamental requirement of a propulsion system is to produce thrust force. To meet this requirement, propulsion system consists of (1) energy source, (2) reacting medium to generate the energy, (3) systems needed to aid the energy conversion process and (4) thrust producing device. Many types of propulsion systems are available which can be used based on the specific requirements. For the boost phase of STS, the requirement is to generate large thrust force in short duration. Considering the technology developments till date, the above requirement can be achieved only by chemical propulsion. Two major classes of chemical propulsion systems as already highlighted are air-breathing and non-air-breathing propulsion systems.

Since the air-breathing propulsion system has to carry only fuel, this is much efficient system which is being developed throughout space faring nations as an advanced technology to improve the vehicle performance and as on now is not matured enough to use in STS applications. But, even though less efficient, non-air-

breathing propulsion systems of various types are being used in STS. These propulsion systems are called as rocket propulsion. In this chapter, the discussions are mainly on the chemical rocket propulsion.

In the chemical rockets, the energy source is the chemical reaction, which is called combustion process. The reacting medium necessary for the combustion process is the propellant, which consists of oxidizer and fuel. Different subsystems are used for combustion process, which happens at the combustion chamber. The thrust-producing device is the convergent-divergent nozzle, which makes use of the original energy into useful form.

In the combustion chamber, the chemical reaction (combustion) takes place between fuel and oxidizer. The chemical energy released due to the chemical reaction heats the gaseous combustion products. This combustion process happens in small volume of combustion chamber. Therefore, thermal expansion of gases results into a very high pressure within the combustion chamber. The high-temperature, high-pressure gases are expanded through the convergent-divergent nozzle, which accelerate the combustion products and result into ejecting the gases at very high velocity. The momentum created by the ejection of the combustion products resulting into reaction force on the vehicle is called thrust. In summary, in chemical rockets, the chemical energy is converted into thermal energy which is then converted into kinetic energy. The kinetic energy of the gaseous products gives necessary thrust to the vehicle, which finally results into the total kinetic and potential energy to be achieved by the vehicle to carry out its tasks.

The essential components of chemical rockets are propellants (both oxidizer and fuel), required to produce high-temperature combustion products due to chemical reaction, combustion chamber, mechanism to inject the propellant with required ignition conditions into the combustion chamber, system to initiate the chemical reaction process and thrust producing device such as convergent-divergent nozzle. In the process of converting chemical energy into thermal energy, the temperature of the combustion chamber can go as high as 2000–3500 K. Therefore, it is essential to implement suitable cooling, insulation, heat sink mechanisms as well as the use of high-temperature materials such as graphite to ensure normal functioning of critical components at such high thermal environments.

Depending on the type of propellants used, the chemical rocket propulsion systems are classified into (1) solid motor rockets, (2) liquid engine rockets and (3) hybrid propellant rockets.

In solid propellant rocket motor, the propellant is stored in combustion chamber and propellant burns from the surface. The solid propellants are classified into double and composite propellants. In double-base propellant, both oxidizer and fuel are combined into one molecule whereas composite propellant is the mixture of oxidizer and fuel.

The liquid propellants are categorized into bipropellant and monopropellant. In monopropellant system, propellants such as hydrogen peroxide or hydrazine are stored in tanks. When these propellants are passed through catalyst, they break into high-temperature gases. In bipropellant system, both oxidizer and fuel are stored in separate tanks. Through pump-fed or pressure-fed systems, these propellants are injected into combustion chamber for chemical reaction. Depending on the

propellants used, the bipropellant systems are further classified into Earth storable systems, cryogenic systems and semi-cryogenic systems.

In the hybrid rocket propulsion system, one of the propellants is solid and the other is liquid. In such rockets, generally, the fuel is solid whereas the oxidizer is liquid propellant. Through pressure-fed system, liquid oxidizer stored in separate tank is injected into the combustion chamber where the solid fuel is placed. At the fuel surface, chemical reaction takes place with the oxidizer, thus providing hot gases.

In all chemical rocket propulsion systems, the hot gas produced in the combustion chamber is expanded through convergent-divergent nozzle to achieve high exit velocity to generate the necessary thrust. Each of the above propulsion systems has specific characteristics and has advantages and disadvantages. Depending on the requirements of STS, suitable systems can be selected for the application of each stage of a multistage vehicle.

In all chemical rockets, the working principle is same. The major performance parameters of chemical rockets and their functional relationships are useful for the design of propulsion systems. The details on each of the systems are explained in the subsequent sections.

9.4.1 Thrust

The primary requirement of propulsion system is to generate the thrust as specified by the requirement. The thrust producing mechanism by a chemical rocket is explained as follows:

An idealized rocket motor with combustion chamber and a convergent-divergent nozzle is represented in Fig. 9.3. The following assumptions are made for the ideal rocket:

1. Neglect the motion of rocket motor and no other external forces on the body.
2. Steady combustion and flow of combustion products.
3. Combustion is assumed to take place in shorter time in a small region called combustion zone and the details of combustion process is neglected.
4. At the start of the nozzle, uniform chamber conditions for temperature, pressure and velocity assumed.
5. At the start of the nozzle, the velocity of the combustion products is assumed to be negligible
6. The combustion products are assumed to be ideal gas, which obeys the perfect gas law, $P = \rho RT$, and has constant specific heats, where P is pressure, ρ is density, R is gas constant and T is temperature.
7. The flow of combustion product is assumed to be isentropic (reversible and adiabatic) expansion, i.e. there is no viscous and friction losses or external heat transfers across the flow.
8. The flow is assumed to be frozen, equilibrium one (i.e. there is no dissociation)

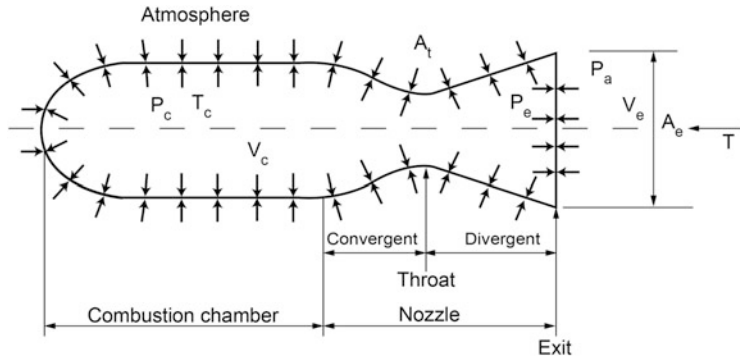


Fig. 9.3 Schematic of a rocket motor

The parameters represented in the Fig. 9.3 are explained as given below:

$T_c \left. \begin{array}{l} \\ \end{array} \right\}$ $P_c \left. \begin{array}{l} \\ \end{array} \right\}$ = Temperature, pressure and velocity of combustion products inside the combustion chamber. Generally, P_c , T_c are maximum and V_c is negligible.
 $V_c \left. \begin{array}{l} \\ \end{array} \right\}$

$P_e \left. \begin{array}{l} \\ \end{array} \right\}$ $V_e \left. \begin{array}{l} \\ \end{array} \right\}$ = Pressure and velocity of combustion products at the nozzle exit

m_e = Expelled mass at the nozzle exit

A_e = Nozzle exit area

A_t = Nozzle throat area

P_a = Ambient pressure, constant around the rocket motor

The pressure distribution within the rocket motor is asymmetric. In the chamber pressure the distribution remains the same but in the nozzle it decreases. The relative magnitude of the pressures is indicated through arrows. The integration of the pressure over the surface of the motor gives a force which is due to difference between the internal and external pressures. This resultant force is termed as thrust which is opposite to the direction of exhaust gases and it causes the acceleration of the rocket in forward direction.

Alternately, thrust is generated due to the change of momentum of expelled gas as well as pressure differentials between internal and external to the motor.

The momentum of combustion product at the nozzle exit is the product of the exit velocity and mass of expelled mass m_e as given by

$$p = m_e V_e \quad (9.1)$$

As per Newton's second law of motion, the rate of change of momentum is the force

$$F = \dot{m}_e V_e + m_e \dot{V}_e \quad (9.2)$$

Assume the exit velocity is constant; the force is given by

$$F = \dot{m}_e V_e \quad (9.3)$$

This force F is along the direction of V_e . As per Newton's third law, the reaction to this is the thrust force, T , acting on the motor in the opposite direction of V_e as represented in Fig. 9.3. Therefore,

$$T = -\dot{m}_e V_e \quad (9.4)$$

When there is no loss, combustion process time is very short along with high velocities and it can be assumed that the mass flow rate of propellant exhaust gas is same as the consumption rate of propellant \dot{m} . As the propellant consumption continues, the vehicle mass reduces continuously (\dot{m} is negative); therefore, the thrust can be written as

$$T = \dot{m} V_e \quad (9.5)$$

There is an additional pressure force due to surrounding atmosphere and this force is equal to the product of exit area of the nozzle A_e and the differential pressure between the exit pressure at the nozzle end P_e and the atmospheric pressure P_a . Thus the overall thrust of the rocket motor is given as

$$T = \dot{m} V_e + (P_e - P_a)A_e \quad (9.6)$$

The term $\dot{m} V_e$ is called momentum thrust and the term $(P_e - P_a)A_e$ is called pressure thrust. It can be seen that, to increase the thrust level, for a given flow rate, it is essential to increase the exit velocity. The factors contributing for the thrust, V_e , and mass flow through nozzle are discussed in the subsequent sections.

9.4.2 Exhaust Velocity

The exhaust velocity expressions can be derived with the assumption of ideal nozzle, ideal gas and isentropic flow.

As per the continuity (mass balance) equation, \dot{m} is constant and is given by

$$\dot{m} = \rho_e A_e V_e = \text{constant} \quad (9.7)$$

where ρ_e is density of gases at exit. As per the energy equation (first law of thermodynamics), the energy in terms of specific enthalpy and kinetic energy is constant. This is given as

$$h_c + \frac{V_c^2}{2} = h_e + \frac{V_e^2}{2} \quad (9.8)$$

where h is specific enthalpy given by

$$h = C_p T \quad (9.9)$$

where C_p is specific heat at constant pressure and T is temperature. h_c , h_e are the specific enthalpy at combustion chamber and exit location respectively. As $V_c \ll V_e$, V_c can be assumed as zero. Using the above assumption, Eq. (9.8) can be solved to get the exit velocity as

$$V_e = \sqrt{2C_p T_c \left(1 - \frac{T_e}{T_c}\right)} \quad (9.10)$$

The gas constant R is given as

$$R = \frac{\mathfrak{R}}{\mathcal{M}} = C_p - C_v \quad (9.11)$$

where \mathfrak{R} is universal gas constant (8.314 kJ/mol-K), \mathcal{M} is molecular weight of exhaust gas, C_v and C_p are specific heat at constant volume and pressure respectively. The ratio of specific heat γ is given as

$$\gamma = \frac{C_p}{C_v} \quad (9.12)$$

Using Eq. (9.11), the difference between the specific heats is given as

$$C_p - C_v = C_p \left(\frac{\gamma - 1}{\gamma} \right) \quad (9.13)$$

Using Eq. (9.12) in Eq. (9.10) yields

$$C_p = \frac{\mathfrak{R}}{\mathcal{M}} \left(\frac{\gamma}{\gamma - 1} \right) \quad (9.14)$$

Using Eq. (9.13) in Eq. (9.9) gives the velocity at exit, V_e as

$$V_e = \sqrt{\frac{2\gamma}{\gamma - 1} \frac{\mathfrak{R}}{\mathcal{M}} T_c \left(1 - \frac{T_e}{T_c}\right)} \quad (9.15)$$

Poisson relations for isentropic expansion of perfect gas are given by

$$T = k_1 P^{\left(\frac{\gamma-1}{\gamma}\right)} \quad (9.16)$$

$$P = k_2 \rho^\gamma \quad (9.17)$$

and

$$T = k_3 \rho^{(\gamma-1)} \quad (9.18)$$

where k_1 , k_2 and k_3 are constants.

Using Eq. (9.15), (T_e/T_c) can be written as

$$\frac{T_e}{T_c} = \left(\frac{P_e}{P_c} \right)^{\left(\frac{\gamma-1}{\gamma}\right)} \quad (9.19)$$

Using Eq. (9.17) in Eq. (9.14) yields the expression for exhaust velocity, V_e as

$$V_e = \sqrt{\frac{2\gamma}{\gamma-1} \frac{\mathcal{R}}{\mathcal{M}} T_c \left[1 - \left(\frac{P_e}{P_c} \right)^{\left(\frac{\gamma-1}{\gamma}\right)} \right]} \quad (9.20)$$

The term (P_c/P_e) is called pressure ratio. The limiting value of V_e for a given propellant combination and nozzle configuration is achieved by expanding the hot gases to vacuum ($P_e = 0$) and the corresponding value is given by

$$V_{e_{max}} = \sqrt{\frac{2\gamma}{\gamma-1} \frac{\mathcal{R}}{\mathcal{M}} T_c} \quad (9.21)$$

From Eq. (9.19), it can be seen that the maximum value is still a finite one. However, this value cannot be achieved realistically. As the exhaust gas cools down rapidly under such expansion process, the temperature may become less than liquefaction or freezing temperature of the gases.

To increase thrust for a given mass flow rate, V_e has to be increased. The increase in V_e is achieved by

1. Increasing the pressure ratio (P_c/P_e) . This can be done in two ways: either increase P_c or decrease P_e . The exit pressure depends on the nozzle geometry.
2. Increasing the combustion chamber temperature T_c
3. Reducing the molecular weight of the combustion product

From Eq. (9.18), it can be seen that the lower molecular mass of propellant and combustion products results into relatively large exhaust velocity. This feature is used in liquid propulsion systems, especially in cryogenic systems. The low molecular mass of hydrogen is utilized to improve the performance of LOX/LH₂ system.

The effect of nozzle geometry on P_e and propulsion system performance are explained in the next section.

9.4.3 Rocket Nozzle Configuration and Performance

In all propulsion systems, it is the nozzle which translates the high-pressure, high-temperature gas available in the combustion chamber into high-velocity gases. The thermodynamic expansion in a nozzle converts the thermal energy generated by chemical, electrical or nuclear energy sources into kinetic energy. The configurations, size and shape of the nozzle largely influence exhaust velocity (V_e) and exit pressure (P_e).

The combustion chamber is designed to withstand the high pressure (P_c) generated by the combustion process and the high temperature (T_c) resulting from it. Inside the combustion chamber, kinetic energy is negligible compared to the enthalpy and therefore the total temperature is almost equal to the combustion chamber temperature (T_c). The pressure-and-temperature ratios during the expansion process are given as

$$\frac{P_c}{P} = \left(1 + \frac{\gamma - 1}{2} M^2\right)^{\gamma/(\gamma-1)} \quad (9.22)$$

$$\frac{T_c}{T} = \left(1 + \frac{\gamma - 1}{2} M^2\right) \quad (9.23)$$

where P_c and T_c are pressure and temperature in combustion chamber, P and T are pressure and temperature at expansion location, γ is ratio of specific heats of combustion product and M is the Mach number of flow during expansion process. A typical nozzle cross section along with the combustion chamber used for thermal expansion process is given in Fig. 9.4. The nozzle represented in Fig. 9.4 is *De Laval* nozzle, which has the following geometry. Starting from the combustion chamber, the nozzle converges and later portion diverges. The convergent and divergent portions are connected by narrow portion, called throat. Generally, the

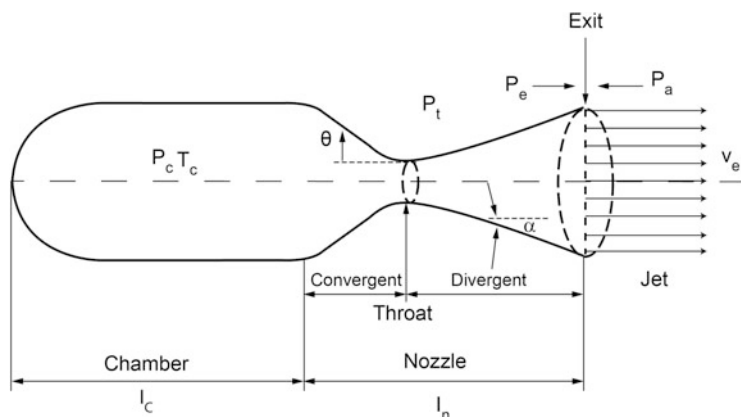


Fig. 9.4 A typical nozzle cross section

throat section is a toroid with radius of curvature about 2–3 times the radius of throat.

The need for the convergent-divergent sections for the expansion process is explained as given below:

Consider the continuity equation,

$$\rho V A = \text{constant} \quad (9.24)$$

Taking logarithmic differential of Eq. (9.23) yields

$$\frac{dp}{\rho} + \frac{dV}{V} + \frac{dA}{A} = 0 \quad (9.25)$$

Using Poisson relation (9.16) and speed of sound in exhaust gases given by

$$a = \sqrt{\left(\frac{dp}{d\rho}\right)} \quad (9.26)$$

and the definition of Mach number,

$$M = \frac{V}{a} \quad (9.27)$$

and using the energy equation,

$$\frac{\gamma}{\gamma - 1} \frac{P}{\rho} + \frac{V^2}{2} = \text{constant} \quad (9.28)$$

finally, the Eq. (9.22) simplifies into

$$(1 - M^2) \frac{dV}{V} = - \frac{dA}{A} \quad (9.29)$$

Nozzle is configured to increase the velocity of combustion product from the combustion chamber value V_c (near to zero) to the required exit velocity V_e and exit pressure P_e . At the entry to the nozzle, the velocity of combustion product is very small and the pressure is maximum, which is the chamber pressure P_c . During initial portion of the nozzle, $M < 1$ and in this region, to increase the velocity, as shown in Eq. (9.25), the area has to be reduced, i.e. convergent portion of the nozzle. This configuration is required till reaching $M = 1$. For the sonic flow, wherein $M = 1$, dA has to be zero to ensure a positive dV . This is the throat portion of the nozzle. Subsequent to that, when $M > 1$, to increase the velocity, the area has to be more, i.e. divergent portion of the nozzle. Therefore, to accelerate the flow from combustion chamber velocity V_c , to very high exit velocity, V_e , the nozzle has to have convergent-divergent geometry, wherein, in the convergent section, the

velocity increases and reaches sonic velocity at throat and in the divergent section, the velocity of the gases is supersonic.

It is to be noted that, in supersonic flow, the downstream disturbances cannot propagate to the upstream. Therefore, the nozzle exit condition including atmospheric effects does not influence the chamber conditions.

The nozzle is normally configured such that the high pressure of combustion chamber is reduced to atmospheric pressure at the nozzle exit plane. The design of the exhaust nozzle has to be optimized to obtain the maximum exhaust velocity and in turn maximum thrust from the motor. This demands suitable expansion of pressure on the nozzle to ensure that the exit pressure P_e is equal to the ambient pressure P_a . The contour of the convergent nozzle is critical and apex cone angle θ can be higher. The inlet area A_c is decided based on combustion chamber design in the Fig. 9.4. Various parameters are

A_c = Chamber area at inlet to nozzle

A_t = Throat area

A_e = Exit area of nozzle

P_c = Chamber pressure

T_c = Temperature in combustion chamber

θ = Half cone angle for convergent section

α = Half cone angle for divergent section

P_e = Exit pressure at nozzle end

P_a = Atmospheric pressure

P_t = Pressure at throat

l_c = Length of the chamber

l_n = Length of the nozzle

From Eq (9.20) and Eq. (9.21), it can be seen that the pressure ratio and temperature ratio increase with Mach number. The pressure ratio corresponding to $M = 1$ is called critical pressure ratio and is given by

$$\frac{P_c}{P} = \left(\frac{\gamma + 1}{2} \right)^{\gamma / (\gamma - 1)} \quad (9.30)$$

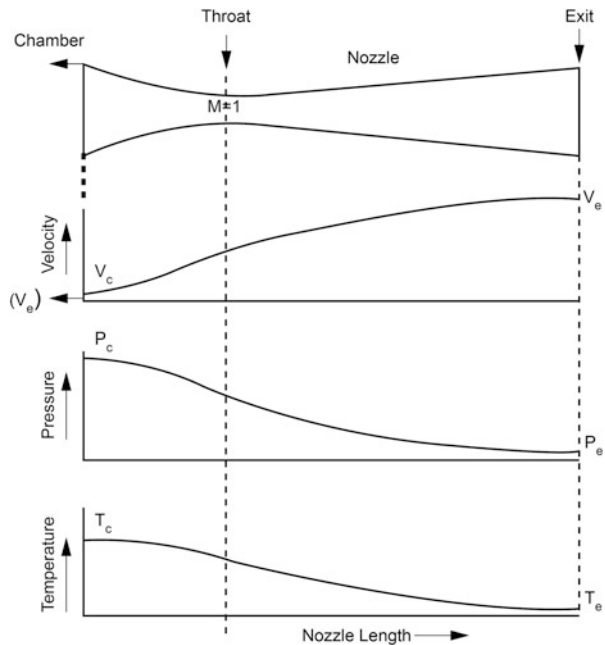
In general, through the nozzle, the velocity increases whereas pressure, temperature, density and local speed of sound decrease. Typical flow parameters are represented in Fig. 9.5.

In order to explain the effect of nozzle geometry on the exit pressure, consider the expansion ratio of the nozzle, given by

$$\epsilon = \frac{A_e}{A_t} \quad (9.31)$$

The expansion ratio of the nozzle related to the pressure ratio is given by [2]

Fig. 9.5 Typical flow characteristics



$$\frac{A_e}{A_t} = \frac{\sqrt{\gamma} [2/(\gamma + 1)]^{(\gamma+1)/(2(\gamma-1))}}{\sqrt{\frac{2\gamma}{\gamma-1} \left(\frac{P_e}{P_c}\right)^{(2/\gamma)} \left[1 - \left(\frac{P_e}{P_c}\right)^{(\gamma-1)/\gamma}\right]}} \quad (9.32)$$

Equation (9.28) shows the pressure ratio and exit pressure P_e are functions of nozzle expansion ratio (A_e/A_t). The throat size decides the mass flow rate as given by [2]

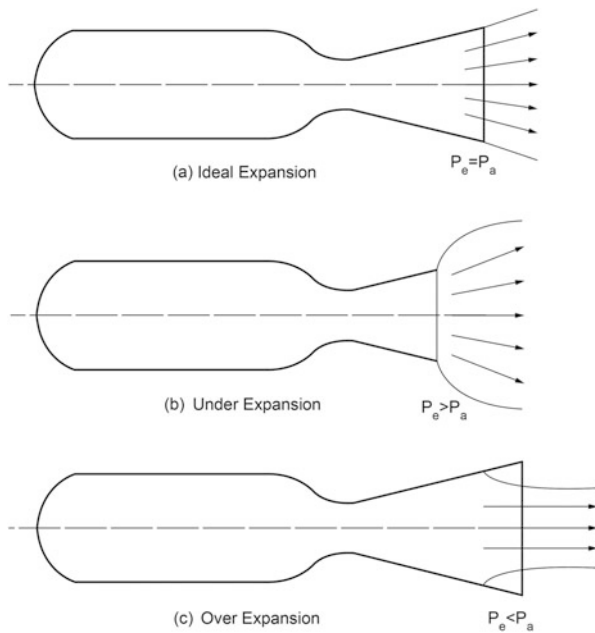
$$\dot{m} = \frac{P_c}{\sqrt{\frac{\gamma}{M}} T_c} A_t \left[\sqrt{\gamma} \left(\frac{2}{\gamma + 1} \right)^{(\gamma+1)/(2(\gamma-1))} \right] \quad (9.33)$$

The amount of thrust depends mainly on the exit velocity, pressure and mass flow rate as given in Eq. (9.6) and repeated below as

$$T = \dot{m} V_e + (P_e - P_a) A_e \quad (9.34)$$

From the above equation and using Eq. (9.18), it can be observed that both momentum thrust and pressure thrust components depend on P_e . Even though pressure thrust value is positive for $P_e > P_a$, under such P_e , V_e is low and hence momentum thrust value is less and therefore the total thrust is less. By increasing the expansion, P_e comes down and correspondingly V_e increases. Therefore both the momentum thrust and the total thrust increase. In the case of $P_e < P_a$, the

Fig. 9.6 Three cases of nozzle expansion



pressure thrust becomes negative. Therefore, even though there is increase in momentum thrust, the net thrust reduces. Maximum thrust occurs when there is no pressure thrust, i.e. when $P_e = P_a$. In an ideal nozzle the pressure of the exhaust gas at nozzle exit should be equal to atmospheric pressure, i.e. $P_e = P_a$. In such cases the nozzle expansion is to the ambient.

When the nozzle exit pressure is greater than the atmospheric pressure, i.e. $P_e > P_a$, the gases cannot expand fully and the nozzle is termed as underexpanded. The enthalpy is not converted into full velocity and generally this happens when the vehicle is operating into vacuum. During the vehicle lift-off region, P_e is less than P_a , since the atmospheric pressure is more than exit pressure. This is called overexpansion. Under such cases, the high pressure generally causes the shock wave at the nozzle exit which in turn causes the kinetic energy to dissipate as heat and pressure. This results into lowering the exhaust velocity thereby decreasing the overall thrust of the motor. All three cases of nozzle expansions are represented in Fig. 9.6.

When the vehicle moves from launch pad in the atmospheric phase, the increase in altitude causes the decrease in the ambient pressure. Therefore if the nozzle is designed to have the ideal conditions at certain altitude where $P_e = P_a$, the nozzle performs in the underexpansion mode above this altitude and in the overexpanded mode below this altitude.

The ambient pressure for the first stage of a vehicle which flies through the dense atmosphere varies during its flight regime. It is therefore essential to compute the

optimum exit pressure through trajectory studies and decide on the optimum length of the nozzle which gives maximum performance.

During vacuum flight, as $P_a = 0$, it is always advantageous to have a large nozzle expansion ratio to reduce P_e to a smaller value, which in turn increases V_e and thrust. However various constraints like (a) the exit diameter of nozzle has to be less than the outer diameter of the preceding stage, (b) the extra weight due to increased length should not offset the performance, etc. are to be accounted properly in design.

In nozzles the contour of the diverging section has larger influence on the flow velocities involved. The important design considerations for an optimum nozzle therefore are to be based on (a) uniform axial gas flow at exit, (b) length of the nozzle to minimize the mass, overall space and envelope, (c) low turbulence losses inside the nozzle and (d) minimum complexity in realization. These aspects are discussed in next section.

9.4.4 Effect of Nozzle Geometry

From Eq. (9.18), it can be seen that the exit velocity depends on exit pressure ratio. The exit pressure ratio depends on nozzle expansion ratio as per Eq. (9.28). Therefore, the exhaust velocity V_e and exit pressure are functions of nozzle expansion ratio A_e/A_t . Therefore thrust depends on the nozzle geometry. For deriving the thrust expression,

$$T = \dot{m} V_e + (P_e - P_a) A_e$$

it is assumed that the exit surface with constant properties are planar and normal to the axis of the nozzle. The flow considered is one dimensional and along the axis of the nozzle. But nozzle configuration needs to be with convergent-divergent sections. For the conical nozzles as represented in previous figures, the assumption that the exit flow is parallel to the nozzle axis is not true.

For such conical nozzle, the exhaust flow is assumed to be originated from the apex point A of the divergent conical section. The surface of constant properties is

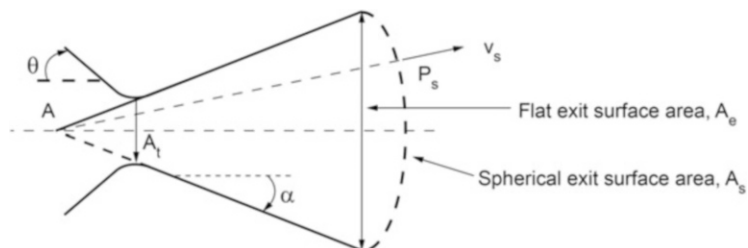


Fig. 9.7 Conical nozzle configuration

assumed to be part of the sphere whose centre is at the apex point. Therefore, at exit, the surface of constant properties is represented in Fig. 9.7 and velocities of constant magnitude V_s are normal to this surface as given in Fig. 9.7. Under such configuration, the thrust generated by the conical nozzle is given in Eq. (9.31) as

$$T = \dot{m} V_s \left(\frac{1 + \cos \theta}{2} \right) + (P_s - P_a) A_s \quad (9.35)$$

The non-axial component of the exhaust gas in a divergent section of the conical nozzle always results into a performance loss, which is also termed as divergent loss. This performance loss occurs on the momentum thrust part, which is represented by the factor λ , which is given as

$$\lambda = \frac{1 + \cos \alpha}{2} \quad (9.36)$$

where α is the half cone angle of the nozzle divergent. This term is sometimes referred as thrust efficiency, which is the ratio of exit gas momentum of nozzle with half cone angle α to an ideal nozzle with parallel and axial gas flow. Therefore, Eq. (9.31) can be written as

$$T = \lambda \dot{m} V_s + (P_s - P_a) A_s \quad (9.37)$$

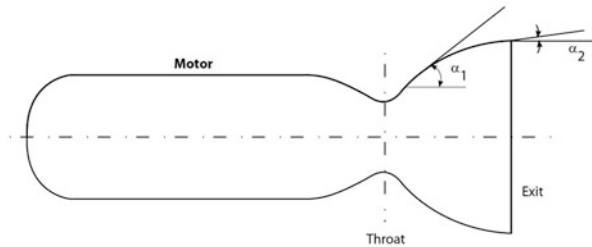
The velocity V_s and pressure P_s on the spherical exit surface A_s are very close to V_e , P_e of flat exit surface A_e , and the thrust equation of Eq. (9.33) can be written as

$$T = \lambda \dot{m} V_e + (P_e - P_a) A_e \quad (9.38)$$

The conical nozzle is always easy to realize and hence it is used in several applications. The half cone angle of convergent section ranges from 20° to 45° and that of divergent varies between 12° and 18° . Standard practices are to have divergent half angle of 15° which generally provides the advantage in performance, overall length and mass. Under such nozzles, the performance loss is about 1.7 %. One can observe that smaller the divergence half angle, better is the performance since the momentum is mostly axial. But it results into larger nozzle with a penalty in overall length and mass. On the contrary if the angle is larger the overall length and mass reduce considerably but the performance suffers. Therefore design has to address all these factors and arrive at a suitable configuration without compromising the overall rocket performance, mass and length.

The performance loss can be reduced by contoured or bell-shaped nozzles. The bell-shaped nozzle is advantageous to achieve higher performance with shorter length and is the most commonly used nozzle in rocket applications. A typical cross section of a bell-shaped nozzle is given in Fig. 9.8. In this nozzle, immediately after the throat rapid expansion is allowed with having half cone divergence angle of 20° to 50° . The nozzle contour is changed gradually to have half cone angle of about

Fig. 9.8 A typical motor with bell nozzle



10° at nozzle exit to have uniform axial flow. For such nozzle configuration, the performance loss can be very low. Hence supersonic bell nozzle ensures better efficiency compared to straight nozzle. However, the wall contour has to be designed carefully to avoid the losses. Changing of wall contour gradually prevents the presence of oblique shocks within nozzles which have adverse impact such as flow separation and vibration.

There are several other variations of nozzles like extendable nozzles, plug nozzle, dual bell nozzle, etc. which can be used to obtain better performance and detailed descriptions of these nozzles are beyond the scope of the book and they are available in the references listed.

9.4.5 Performance with Different Nozzle Expansions

As discussed earlier, the thrust is maximum when exit pressure $P_e = P_a$, where P_a is ambient pressure. This is called ideal expansion.

In the case of $P_e > P_a$, there is underexpansion and still expansion is feasible. Even after the flow leaves the nozzle exit, the expansion process continues by a series of expansion and compression waves occur at the jet boundary as shown in Fig. 9.9. This phenomenon reduces the momentum thrust, which otherwise has no other adverse implications. This is normally the case when the rocket motors operate in high altitude or vacuum.

On the other hand, $P_e < P_a$ leads to overexpansion. Unlike underexpansion, overexpansion has severe implications which need to be addressed. If the overexpansion is too much, then normal shock occurs in the flow path inside the nozzle, across which there is discontinuity in the flow properties and sudden increase in temperature, pressure and density of the flow.

Different scenarios of overexpansions with specified P_e and different values of P_a (viz., P_{a1} , P_{a2} , P_{a3} , P_{a4}) are given in Fig. 9.10. When ambient pressure is P_{a1} , the entire flow through nozzle is subsonic and the pressure variation is as shown in curve (a). When ambient pressure is P_{a2} , where, $P_{a2} < P_{a1}$, the flow in throat is sonic, but still the flow through divergent section is subsonic and the pressure variation is represented in curve (b) of Fig. 9.10. If the ambient pressure is $P_{a3} < P_{a2}$, there is

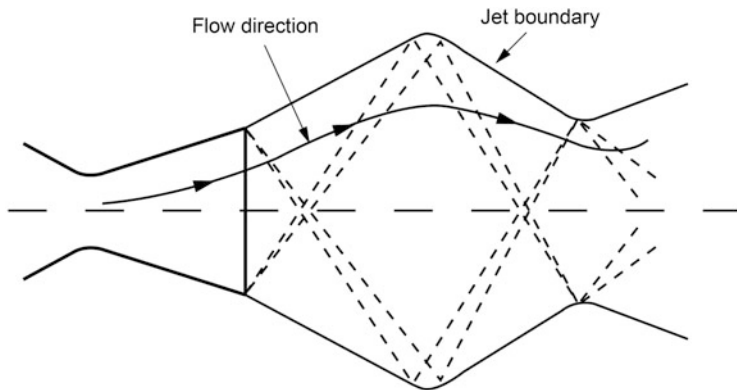
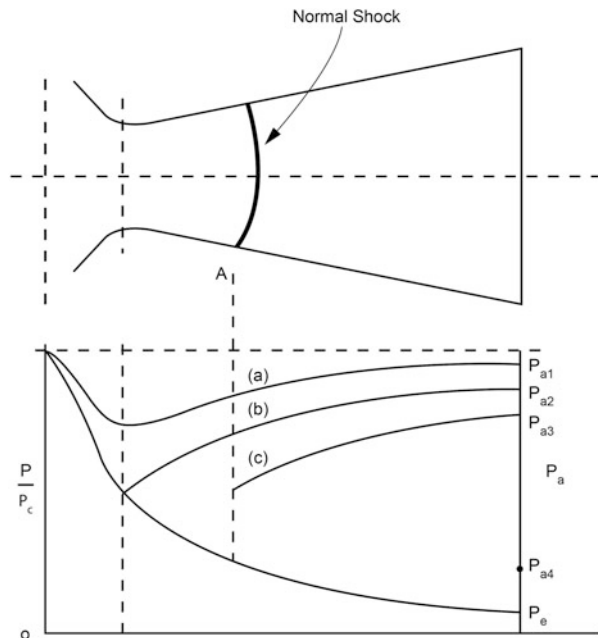


Fig. 9.9 Under expansion flow pattern

Fig. 9.10 Various scenarios in over expansion



expansion up to point A in the divergent section of the nozzle. A normal shock at point A causes discontinuities in flow parameters, sudden increase in pressure at A and subsequently pressure increases as shown in curve (c) of Fig. 9.10. After the shock, the flow in the nozzle is subsonic. When the ambient pressure is $P_{a4} < P_{a3}$, the normal shock formed at the nozzle exit and the flow expansion is normal within the nozzle. It is to be noted that at this condition also, the ambient pressure is more than P_e . Therefore, the exhaust flow is compressed by an oblique shock which is

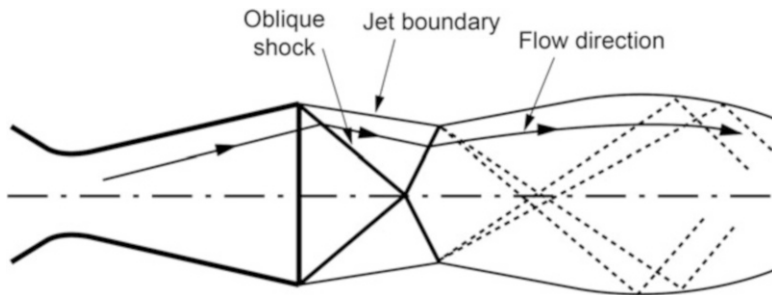
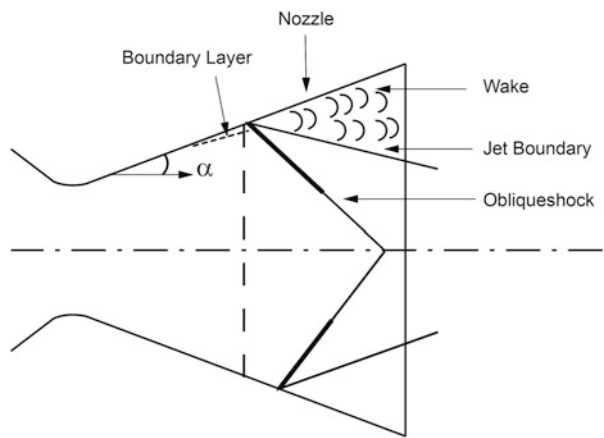


Fig. 9.11 Over expansion flow pattern

Fig. 9.12 Flow separation in over-expanded nozzle



originated at the nozzle exit. This compression is followed by expansion and subsequently compression waves and so on as shown in Fig. 9.11.

The above patterns are explained only for the ideal non-viscous gases for the combustion products. In reality, due to the viscous effects of combustion gases, there is boundary layer build-up within the nozzle which depends on the nozzle geometry and length. Since the flow within the boundary layer is subsonic, the external conditions can affect the upstream flow through the boundary layer. In the case of overexpansion, due to the effect of ambient pressure, the adverse pressure gradient can make the flow to separate locally from the nozzle and oblique shock formed as shown in Fig. 9.12. The flow separation across the nozzle cross section may not be symmetric and the flow fluctuates. The oblique shock in turn contracts the jet and wake is formed. This again makes the environment more complex and the nozzle performs as if with lower expansion ratio. The location of oblique shock moves upstream with reduced P_e/P_a .

As per thumb rule, the flow separates when

$$\frac{P_e}{P_c} \leq \delta \left(\frac{P_a}{P_c} \right) \quad (9.39)$$

where δ depends on nozzle wall roughness, nozzle expansion ratio, composition of combustion products and adverse pressure gradient. Depending on the above parameters, the value of δ is between 0.25 and 0.35. Eq. (9.35) is called Summerfield criterion. For the conical nozzle with $\alpha = 15^\circ$, the flow separation occurs for the value about 0.35.

9.4.6 Performance Parameters

This section describes important characteristic coefficients and performance parameters of a rocket motor.

(a) Total and Specific Impulse

Total impulse delivered by a rocket motor operating for the duration of t_b is defined as

$$I = \int_0^{t_b} T(t) dt \quad (9.40)$$

If thrust is constant, then total impulse is given by

$$I = T t_b \quad (9.41)$$

During the period from 0 to t_b , the rocket consumes the propellant mass of m_p . The specific impulse is defined as the total impulse delivered by consuming unit weight of the propellant. Therefore, specific impulse is given by

$$I_{sp} = \frac{\int_0^{t_b} T(t) dt}{m_p g_0} \quad (9.42)$$

where g_0 is acceleration due to gravity at the surface of the Earth. Extending this definition, the specific impulse can also be defined as the ratio of total impulse and propellant weight consumption in the infinitesimal interval, δt , given as

$$I_{sp} = \frac{T\delta t}{\dot{m}} g_0 \delta t \quad (9.43)$$

where \dot{m} is the mass flow rate of the propellant. Eq. (9.39) can also be written as

$$I_{sp} = \frac{T}{\dot{m}} g_0 \quad (9.44)$$

Sometimes the I_{sp} referred in Eq. (9.40) can also be called as specific thrust, which is thrust per unit weight flow rate. The definitions of specific impulse given in Eq. (9.40) and Eq. (9.38) are more or less same and are identical if the thrust and mass flow rates are constant.

The specific impulse can also be interpreted as the time of consuming the propellant if the motor thrust is equal to the initial weight of the propellant.

The specific impulse gives the impulse delivered by consuming unit weight of the propellant. For rocket motors, it is always advantageous to achieve maximum impulse for a given propellant loading. It is obvious that higher specific impulse of a rocket motor is always desirable. Therefore, specific impulse is the most important measure of efficiency of a motor performance.

The thrust of a rocket motor is given as

$$T = \lambda \dot{m} V_e + (P_e - P_a) A_e \quad (9.45)$$

λ depends on nozzle configuration. The exit velocity V_e , mass flow rate \dot{m} , exit pressure P_e depend on chamber pressure, temperature, propellant combination and expansion ratio of the nozzle. Therefore, specific impulse depends on propellant combination, chamber pressure, temperature and nozzle geometry.

For the ideal expansion ($P_e = P_a$) and with $\lambda = 1$, using Eq. (9.40) and Eq. (9.41), the specific impulse can be given as

$$I_{sp} = \frac{V_e}{g_0} \quad (9.46)$$

Thus, the specific impulse is the ratio of exit velocity to the acceleration due to gravity at the Earth's surface. Therefore, the maximum specific impulse can be achieved when $V_e = V_{e_{max}}$ and is given by

$$I_{sp_{max}} = \frac{V_{e_{max}}}{g_0} \quad (9.47)$$

where $V_{e_{max}}$ is defined in Eq. (9.19), given by

$$V_{e_{\max}} = \sqrt{\frac{2\gamma}{\gamma - 1} \frac{\mathfrak{R}}{M} T_c}$$

As $V_{e_{\max}}$ depends only on propellant combination and not on combustion chamber pressure, pressure ratio or expansion ratio, $I_{sp_{\max}}$ is purely characteristic of propellant combination.

Generally, for solid propellant motors, I_{sp} varies between 260 and 300 s, Earth storable liquid engines, the values vary between 270 and 310 s. For semi-cryogenic engines, the specific impulse varies between 320 and 350 s whereas for cryogenic engines, the value lies between 440 and 460 s. The values of I_{sp} for hybrid rocket motors are generally between that of solid motors and liquid engines.

Another performance parameter called volumetric specific impulse, defined as

$$I_\delta = \rho_p I_{sp} \quad (9.48)$$

is also used in rocket propulsion. Here, ρ_p given in Eq. (9.44) is the density of the propellant. I_δ is the measure for the influence of different propellants. Generally, for small rockets, where propellant mass (m_p), is very small compared to the empty mass of the stage (m_e), the volumetric specific impulse plays major role. Under such vehicles, higher-density propellant gives higher performance. However, for larger rockets such as STS, wherein $m_p \gg m_e$, this parameter is not sensitive and the specific impulse plays a major role.

(b) Propellant Combustion Process and Nozzle Efficiency Factors

The previous section discussed that the specific impulse is the measure of performance efficiency of a rocket motor. This section gives the propellant and combustion process efficiency and nozzle efficiency factors and how they are related to the integrated performance defined in terms of specific impulse.

The actual thrust of rocket motor represented in Eq. (9.34) is given as

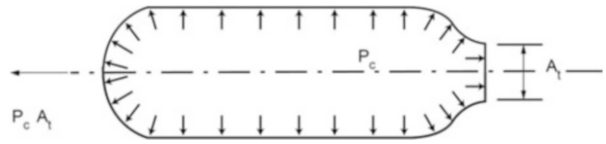
$$T = \lambda \dot{m} V_e + (P_e - P_a) A_e$$

Assuming that there is no nozzle divergence loss, $\lambda = 1$ and the thrust equation is given by

$$T = \dot{m} V_e + (P_e - P_a) A_e \quad (9.49)$$

Eq. (9.45) gives the thrust produced by integrated rocket motor system which comprises of propellant combination, combustion process in combustion chamber, expansion of gases due to convergent-divergent nozzle with required expansion ratio, A_e/A_t , pressure ratio and ambient pressure P_a . If the nozzle of the motor is only up to throat as represented in Fig. 9.13, then the thrust is given by

Fig. 9.13 Combustion chamber without nozzle divergent



$$T_0 = P_e A_t \quad (9.50)$$

Thrust coefficient C_F is defined as the ratio between T and T_0 as given by

$$C_F = \frac{T}{T_0} = \frac{T}{P_c A_t} \quad (9.51)$$

Then thrust T is given by

$$T = C_F P_c A_t \quad (9.52)$$

Therefore, the thrust coefficient C_F given in Eq. (9.47) is considered to be nozzle efficiency, which can be computed by applying experimental results to Eq. (9.48). The thrust coefficient C_F in turn can be used to define thrust of the rocket motor. The thrust coefficient C_F can be computed theoretically as explained below:

As per Eq. (9.29), mass flow rate is given as

$$\dot{m} = \Gamma \frac{P_c}{\sqrt{\frac{\gamma}{M} T_c}} A_t \quad (9.53)$$

where

$$\Gamma = \sqrt{\gamma} \left(\frac{2}{\gamma + 1} \right)^{(\gamma+1)/(2(\gamma-1))} \quad (9.54)$$

As per Eq. (9.18), the exit velocity is defined as

$$V_e = \sqrt{\frac{2\gamma}{\gamma - 1} \frac{\mathcal{R}}{M} T_c \left[1 - \left(\frac{P_e}{P_c} \right)^{\frac{(\gamma-1)}{\gamma}} \right]} \quad (9.55)$$

Using Eq. (9.49) and Eq. (9.51) in Eq. (9.45) and using Eq. (9.47) gives

$$C_F = \Gamma \sqrt{\frac{2\gamma}{\gamma - 1} \left[1 - \left(\frac{P_e}{P_c} \right)^{\frac{(\gamma-1)}{\gamma}} \right] + \left[\left(\frac{P_e}{P_c} \right) - \left(\frac{P_a}{P_c} \right) \right] \frac{A_e}{A_t}} \quad (9.56)$$

It is to be noted that the pressure ratio (P_c/P_e) and expansion ratio (A_e/A_t) are related. Therefore, it can be concluded that the thrust coefficient depends on expansion ratio γ , P_c and ambient pressure P_a .

The characteristic thrust coefficient C_F^o is the maximum value of C_F , which occurs for the ideal expansion, $P_e = P_a$, and is given by

$$C_F^o = \Gamma \sqrt{\frac{2\gamma}{\gamma - 1} \left[1 - \left(\frac{P_e}{P_c} \right)^{\frac{(\gamma-1)}{\gamma}} \right]} \quad (9.57)$$

The maximum value of C_F^o is the one when the flow is expanded to vacuum, i.e. $P_e = 0$, and this given by

$$C_F^o \text{max} = \Gamma \sqrt{\frac{2\gamma}{\gamma - 1}} \quad (9.58)$$

The characteristic velocity is the exhaust velocity of the motor as represented in Fig. 9.13 (i.e. without divergent section of the nozzle). The characteristic velocity C^* can be obtained as follows:

$$T_0 = P_c A_t = \dot{m} V_e = \dot{m} C^* \quad (9.59)$$

From Eq. (9.55), C^* can be given as

$$\frac{C^*}{\dot{m}} = \frac{P_c A_t}{\dot{m}} \quad (9.60)$$

Using Eq. (9.49) in Eq. (9.56) yields

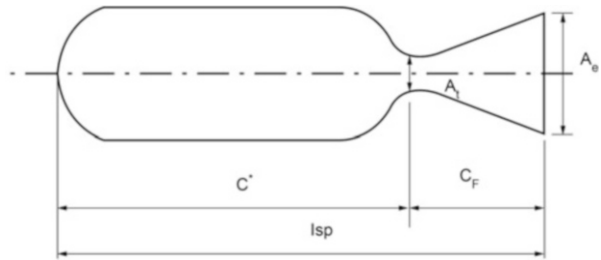
$$C^* = \frac{1}{\Gamma} \sqrt{\frac{\mathcal{R}}{\mathcal{M}} T_c} \quad (9.61)$$

From the above equation, it can be concluded that as nozzle is not involved, C^* can be considered as propellant (due to \mathcal{M}) and combustion process (due to T_c) efficiency.

Considering the propellant and combustion process efficiency factor C^* and the nozzle efficiency factor C_F , thrust can be written in terms of C^* and C_F as given below. Use of Eq. (9.56) into Eq. (9.48) yields

$$T = C_F C^* \dot{m} \quad (9.62)$$

Fig. 9.14 Performance parameters of a typical rocket motor



The mass flow factor C_D is related to characteristic velocity as given below:

$$\frac{C_D}{P_c A_t} = \frac{\dot{m}}{C^*} \quad (9.63)$$

The effective exhaust velocity C is defined as

$$C = \frac{T}{\dot{m}} \quad (9.64)$$

Using Eq. (9.58) in Eq. (9.60), C can also be written as

$$C = C_F C^* \quad (9.65)$$

Using Eq. (9.40), the specific impulse is given by

$$I_{sp} = \frac{T}{\dot{m}} g_0 = \frac{C}{g_0} \quad (9.66)$$

From Eq. (9.62), it can be concluded that the specific impulse I_{sp} is the performance measure of integrated propellant, combustion process and nozzle efficiencies. This aspect is explained in Fig. 9.14.

(c) Mixture Ratio

The previous sections discussed about total mass flow rate \dot{m} of the propellants which contain both oxidizer and fuel as given below:

$$\dot{m} = \dot{m}_{ox} + \dot{m}_f \quad (9.67)$$

where \dot{m}_{ox} and \dot{m}_f are mass flow rates of oxidizer and fuel respectively. From Eq. (9.63), it is to be noted that with different combinations of \dot{m}_{ox} and \dot{m}_f , still the total required mass flow rate \dot{m} can be achieved. But in addition to the total required mass flow rate, the ratio between the oxidizer and fuel flow rates, which is called mixture ratio, r which is defined below

$$r = \frac{\dot{m}_{ox}}{\dot{m}_f} \quad (9.68)$$

also plays a major role in the combustion process, especially in the liquid engines.

While the total flow rate \dot{m} decides T_c , the parameters T_c and \mathcal{M} greatly depend on the mixture ratio r . Therefore, in addition to the other performance parameters, mixture ratio is also another major parameter to be considered for the design of liquid engine propulsion system.

Once the required total flow rate \dot{m} and the mixture ratio r are specified for an engine, the individual flow rate of oxidizer and fuel are computed as follows:

$$\dot{m}_{ox} = \left(\frac{r}{1+r} \right) \dot{m} \quad (9.69)$$

$$\dot{m}_f = \left(\frac{1}{1+r} \right) \dot{m} \quad (9.70)$$

The initial ignition process of non-hyperbolic propellant engines such as cryogenic engines strongly depends on the specific mixture ratio for successful ignition and this mixture ratio may be different from the one which provides maximum performance during steady-state operation. Therefore, suitable mechanisms have to be implemented in the propulsion systems to vary the mixture ratio as per the requirements.

Detailed discussion on combustion process involves the thermo-chemistry of chemical reactions of propellants, which is beyond the scope of this book. However, dependence of mixture ratio on the combustion process and the performance parameter I_{sp} are very briefly discussed below.

During combustion process, chemical reaction between oxidizer and fuel (reactants) leads to high-temperature combustion product. The content of the combustion product, which in turn decides the molecular mass \mathcal{M} of combustion gases and flame temperature (thermal energy released during chemical reaction), which is same as T_c , depends on the ratio with which the oxidizer and fuel takes place in the combustion process. Stoichiometric mixture ratio is the mixture ratio which ensures the complete chemical reaction process of the propellants. With the stoichiometric mixture ratio, all the reactants are consumed, with no deficiency of reactant or no excess reactant in the combustion product. The stoichiometric mixture ratio gives the maximum flame temperature. As an example, for the case of LOX/LH₂ propellant combination, the stoichiometric mixture ratio is 8 which gives the chemical balance equation as



This process produces T_c of about 3500 K whereas the combustion product is water. Various combinations of mixture ratios generate different values of T_c and molecular mass \mathcal{M} . As per Eq.(9.42), and Eq.(9.18), the specific impulse depends on T_c ,

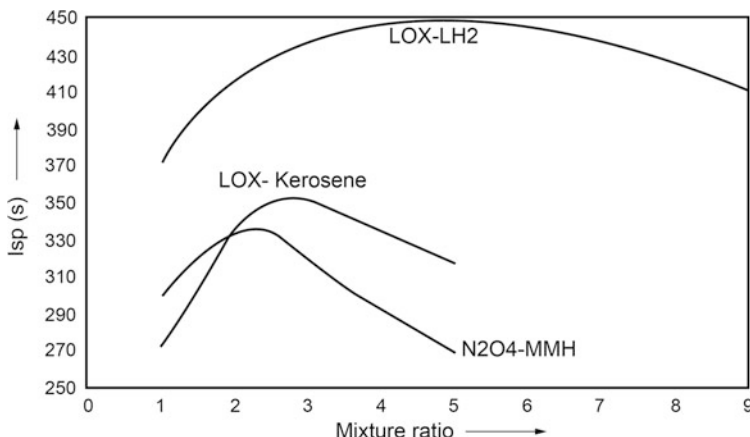


Fig. 9.15 Dependence of Isp on mixture ratio for different propellant combinations

\mathcal{M} and pressure ratio. For the specified chamber pressure P_c and nozzle expansion ratio, the specific impulse depends on the ratio (T_c/\mathcal{M}) . Specific impulse for different propellant combinations for a typical P_c and (A_e/A_t) with respect to various mixture ratios is represented in Fig. 9.15. It can be seen that for LOX/LH₂ propellant combination, even though the T_c is maximum for stoichiometric mixture ratio of 8, for the fuel rich mixture ratio of about 4.8, which adds more unburned hydrogen, reduces the value of \mathcal{M} . This results into maximum specific impulse. Therefore, generally for rocket engines, fuel-rich mixture ratio is adopted.

For selecting the mixture ratio for propulsion system design, another important factor is to design propellant tanks to carry the required quantities of oxidizer and fuel as per the specified mixture ratio. The propellant tank mass adds to the structural mass of the vehicle which has direct impact on the performance of the rocket. It can be seen from Fig. 9.15, for the case of LOX/LH₂ propellant combination for a mixture ratio of about 5.5, the tank size required to carry liquid hydrogen is smaller than that of 4.8. This reduction in tank structural mass has direct impact on the performance, whereas it can be seen from Fig. 9.15, for the increased mixture ratio, the reduction in specific impulse is not significant. Therefore, one has to carry out integrated performance analysis to arrive at a suitable mixture ratio and specific impulse, which provides maximum performance to the vehicle. Once these parameters are decided they are considered as the specification for the propulsion system design.

Various types of propulsion systems being used in STS applications are explained in the subsequent sections.

9.5 Solid Propulsion Systems

In chemical rocket propulsion the simplest type is the solid propulsion. A solid rocket propellant contains the fuel, oxidizer and a binder. They are blended together in proper proportion and solidified to form the propellant. Generally the blended compound is moulded in a core which is removed later to generate a cavity core. The most commonly used fuel is the powdered aluminium and oxidizer is ammonium perchlorate. The binder is generally a rubber-like material such as polyurethane or poly butadiene. The hydroxyl terminated poly butadiene is widely used as a binder material and it also burns as fuel. The performance of the motor is dictated by the chemicals used, the shape of the grain and the nozzle design adopted.

The configuration of a typical solid motor is given in Fig. 9.16. It consists of a motor case, the thermal insulation to protect the case from the hot combustion gases, a liner to assist the bonding of propellant to the liner and propellant cast into the motor.

An igniter invariably integrated at the head end provides the required energy to ignite the propellants. A convergent-divergent nozzle attached at the aft end of the motor ensures the expansion of exhaust gases to provide the supersonic flow to generate the thrust.

The motor case can be high-strength light-weight metal or composite material and typically cylindrical with dome on one end and nozzle assembly on the other. The igniter is assembled on the dome end as shown in Fig. 9.16. The motor case has the insulation layer and liner materials appropriately designed to provide the protection to the motor case and bonding to propellant. In case of bigger motor, the case is built as a number of segments and joined appropriately to provide the leaktight joints and to withstand the internal pressures. Once the motor case is insulated and lined, the propellant after suitable mixing is cast into the case using a suitable mandrel to provide the required grain shapes. The propellant is cured using elevated temperatures.

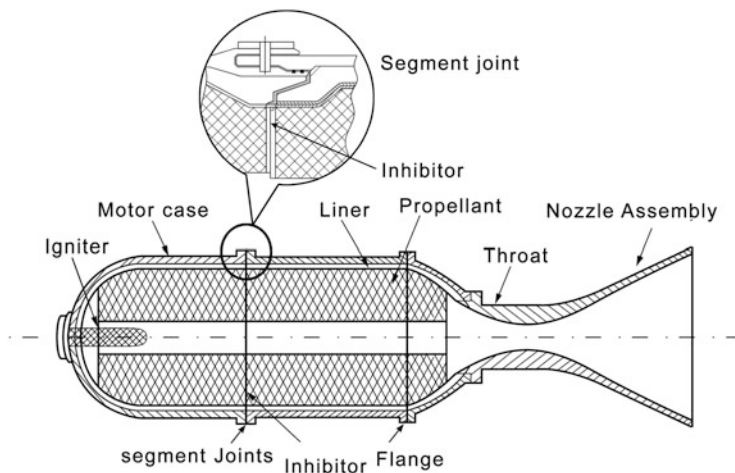


Fig. 9.16 A typical solid motor

In a solid rocket motor, the combustion product mass flow depends on the burn rate of the propellant and the burning surface area of the grain. These two parameters also decide on the performance characteristics of motor such as motor pressure and thrust. While the burn rate depends on the parameters like fuel, oxidizer, binding material and their combination ratio, burning area solely depends on the geometrical shape of the internal grain of the propellant. The grain design is suitably chosen for a given flight mission and the thrust time curve of the motor can be shaped accordingly. During casting of the propellant, the required grain shape can be achieved by using suitably shaped mandrel.

Depending on the mission requirement the vehicle designer has to specify the performance characteristics of the motor in terms of initial thrust, peak thrust and the thrust at the end of the motor burning, etc. There are several factors like vehicle acceleration, maximum dynamic pressure, aerodynamic load, vibration, etc. which dictate the thrust time curve of the solid motor to be realized. Figure 9.17 gives some of the typical grain configurations and the corresponding shape of the thrust time curves.

Depending on the requirement it is possible to have a grain design to generate the progressive, neutral, regressive or a combination of thrust time curves. Figure 9.17e shows the combination of tube at head end and deep slot shape at nozzle end to generate large thrust during the boost period to provide higher initial acceleration and lower thrust during the later stage to limit the maximum acceleration and also to reduce the velocity loss due to drag.

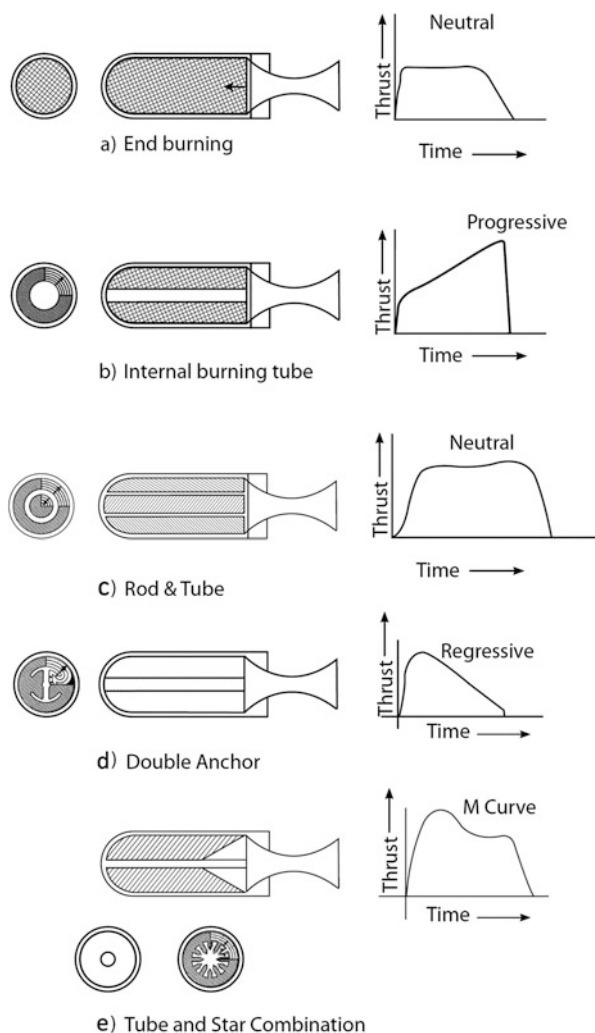
Since the exposed surface area decides the vehicle thrust, it is essential to ensure that the grains should not have any cracks and also should not develop cracks due to aging effects. The crack surface acts as additional burning surface area and correspondingly the pressure increases, which can lead to motor failure. The solid propellant motors are simple, reliable and provide cost-effective performance. There is no requirement for propellant management and also cooling of combustion chambers. The drawback is it offers lower specific impulse of around 250–280 s. And once ignited it is difficult to terminate the motor.

The ignition of solid motor is achieved by using an igniter which upon initiation produces hot gases around the propellant surface thereby raising the temperature to the auto-ignition level. The igniters are classified based on the energy release in terms of heat flux and pressure needed for the propellant combustion. Generally two types of igniters such as pyrotechnic or pyrogenic are used. The pyrotechnic igniter is used in small motors whereas pyrogenic igniters are used in large boosters and also in motors which operate at high altitudes.

In pyrotechnic igniter the charge is in the form of pellets which are produced by the combination of fuel and oxidizer with the addition of binder to form pellets. They are contained in a perforated tube and the ignition is initiated through electrical means. The pellets have the advantage of having longer and controllable burn time. The propellant characteristics, ignition transient requirements and the operating environment dictate the selection of igniter material.

The pyrogen igniter is having a fast burning propellant grain as compared to the main charge and is in fact a small rocket motor. Igniter grain consists of fuel,

Fig. 9.17 Typical grain configurations for solid motors



oxidizer, binder, a curing agent and number of additives. It is also having high percentage of fine oxidizer particles and generally burn rates are higher. Igniter for large motors is a small igniter housed inside the main igniter and the igniter initiation is by electrical means.

9.6 Liquid Propulsion Systems

The liquid propulsion system offers several advantages such as (a) higher specific impulse, (b) termination of thrust when desired, (c) thrust and mixture ratio controlled through proper control system and (d) restart capability. Therefore, these subsystems are widely used in STS. However the systems are far more

complex since they contain many elements. The combustion product temperature is much higher, needing suitable thermal control systems. The general liquid propulsion systems and the specific features of cryogenic systems are discussed in the subsequent sections.

Liquid propulsion systems are fairly complex involving several subsystems like propellant tanks, propellant management system to control the flow of fluids, gas bottles for storage of high-pressure gases, controlled gas flows using precision valves, feed mechanisms using pumps, turbines, pressurization devices and a combustion chamber.

The fuel and oxidizer are stored separately in two tanks. These propellants are fed to the combustion chamber through appropriate feed systems to supply the same at required pressures and flow conditions. The injection of the propellant into the combustion chamber is done through an injector to ensure the flow of propellants in right proportions and right atomization conditions to yield a stable combustion. The combustion products are expanded through nozzles to generate the required thrust. The injector is located in the combustion chamber and the combination of injector, combustion chamber and nozzle is termed as thrust chamber.

9.6.1 Propellant Feed System Classification

(a) Pressure-Fed Liquid Engines

Based on the propellant feed systems the engines are classified as pressure-fed or pump-fed engines. In pressure-fed engines the propellants are pressurized by a pressurant gas stored at very high pressure in separate gas bottles and fed to tank at regulated pressures using pressure regulation system. Since the tanks are pressurized, the tank walls are to be made thicker to withstand higher pressures, resulting in increase in structural mass. Therefore generally pressure-fed systems are used for low-thrust engines. A typical pressure-fed rocket engine is shown in Fig. 9.18.

(b) Pump-Fed Liquid Engines

In pump-fed systems, the propellants are fed into the combustion chamber by pumps and the power requirement to drive the pumps is quite large. It can be managed by having turbines driven by hot gases at high speeds. The turbine coupled to pumps drives these pumps. The pump-fed systems are generally used in high-thrust engines and allows high propellant flow rates. The advantage is tank pressure in such systems can be at low pressures just to meet the pump requirements. Figure 9.19 gives a typical schematic diagram of pump-fed engine.

Fig. 9.18 A typical pressure fed rocket engine

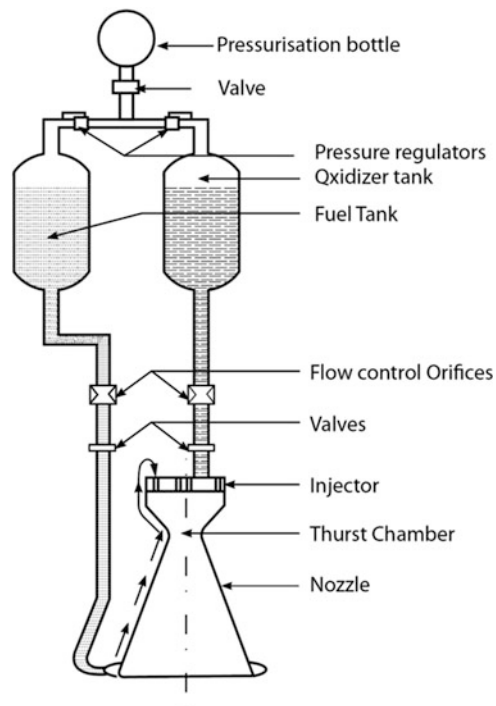
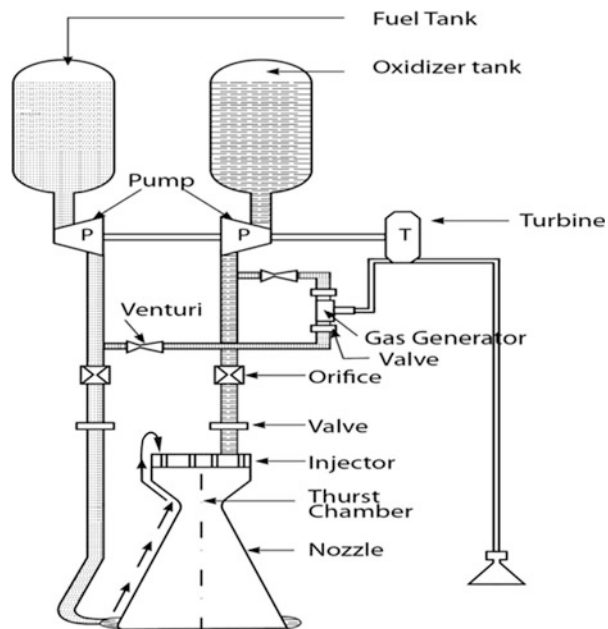


Fig. 9.19 A typical diagram for the pump fed engine



9.6.2 Feed System Cycles of Pump-Fed Engines

The pump-fed rocket engine cycles can be classified into two categories, namely, open-cycle and closed-cycle engines. Basically these power cycles define how the power is derived to feed propellants to the combustion chamber.

In an open-cycle engine the fluid exhausting from turbine is discharged overboard after expanding the same in a separate nozzle or discharged through the nozzle of the main engine at appropriate section of the divergent portion. The open-cycle engines can be further classified into three types as gas generator (GG) cycle, combustion tap-off cycle and coolant bleed cycle.

The closed-cycle engine enables the injection of partially burnt turbine gas into the combustion chamber through the injector thus enhancing the engine performance. Although it is very effective due to the maximum energy conversion it also increases the complexity of the system. The closed-engine cycles can be categorized as two types, namely, (a) expander cycle (EC) and (b) staged combustion cycle (SCC) and, both of them offer higher performance compared to GG cycle. This in turn helps to provide higher mission performance.

(a) Gas generator (GG) cycle

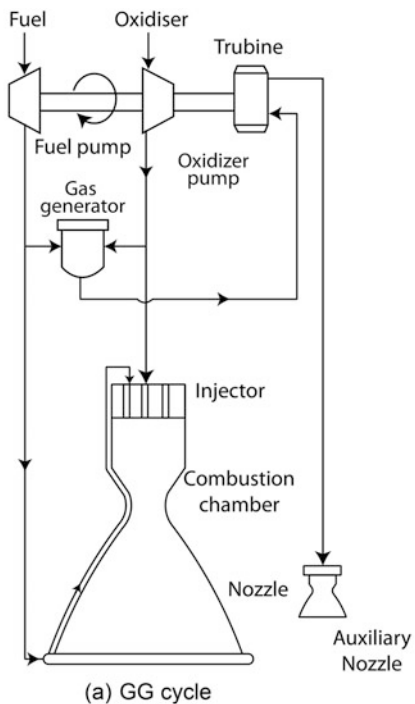
In GG cycle the gas generator produces the hot gases by tapping the small quantities of oxidizer and fuel to the gas generator from main lines and igniting it. This hot gas is utilized to drive the turbine and the exhaust gases are discharged through small nozzles or within the thrust chamber. The turbines cannot operate at high temperatures due to limitations in the material of the turbine and therefore suitable mixture ratio of propellants are to be chosen or sometimes the water is additionally used to cool the turbines. The engines working on GG cycle give lower I_{sp} at higher chamber pressures. These engines are simpler; the pump speeds are lower and have lower pump delivery pressures. This facilitates the independent testing and qualification of subsystems. A typical gas generator cycle is given in Fig. 9.20a.

(b) Combustion tap-off cycle

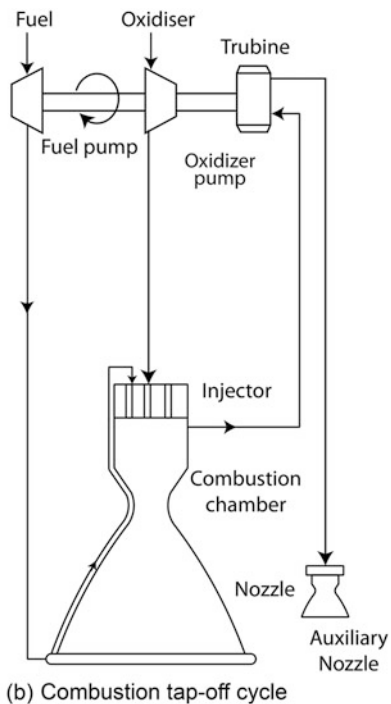
A typical combustion tap-off cycle is given in Fig. 9.20b. A similar process like GG cycle is used in the combustion tap-off cycle without gas generator. In this case a small portion of hot gas tapped from the main combustion chamber is used to drive the turbine.

Generally hot gases are tapped very near to the injection zone to utilize the fuel-rich mixture ratio. This also ensures the low temperature needed for the operation of turbine. The drive exhaust of the turbine is either discharged through a separate nozzle or fed into the nozzle divergent section. This has a limitation in that the reproducible property for the fuel-rich hot gases cannot be guaranteed.

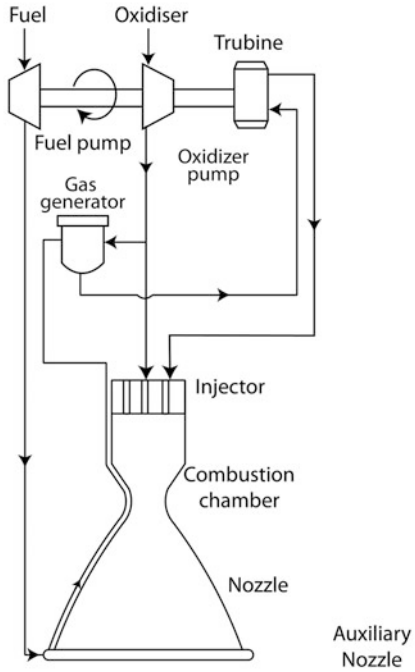
Coolant bleed cycle is another open-cycle feed system and it also does not need the gas generator. A small quantity of vaporized coolant hydrogen is tapped from the coolant jacket of the main chamber in the supersonic region of the nozzle and



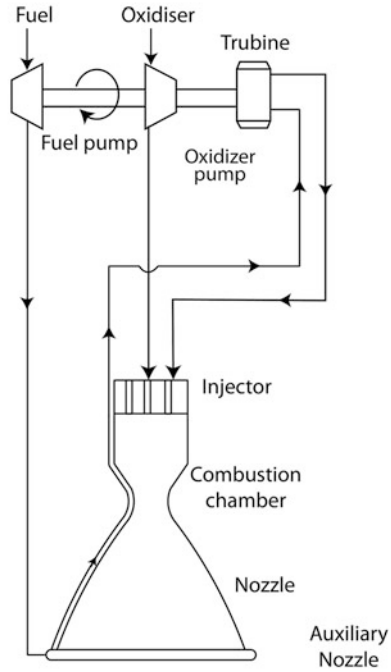
(a) GG cycle



(b) Combustion tap-off cycle



(c) Staged combustion cycle



(d) Expander cycle

Fig. 9.20 Typical feed system cycles used in turbopumps

used to drive the turbine. In this case too the gas from turbine is exhausted similar to the combustion tap-off cycle.

(c) *Staged combustion cycle (SCC)*

A typical staged combustion cycle is given in Fig. 9.20c. The staged combustion cycle is different from the GG cycle in that major portion of fuel passing through the coolant jacket of the thrust chamber is utilized to burn in a pre-combustion chamber along with oxidizer at a highly fuel-rich mixture ratio. This hot gas so produced is used to drive the turbines and then enters the main combustion chamber where it burns with the oxidizer injected into the chamber. This cycle provides high chamber pressure and also high specific impulse compared to other cycles. There is additional pressure drop in pre-combustion chamber and the turbine. This demands higher discharge pressure and pump speed for both the pumps.

(d) *Expander cycle*

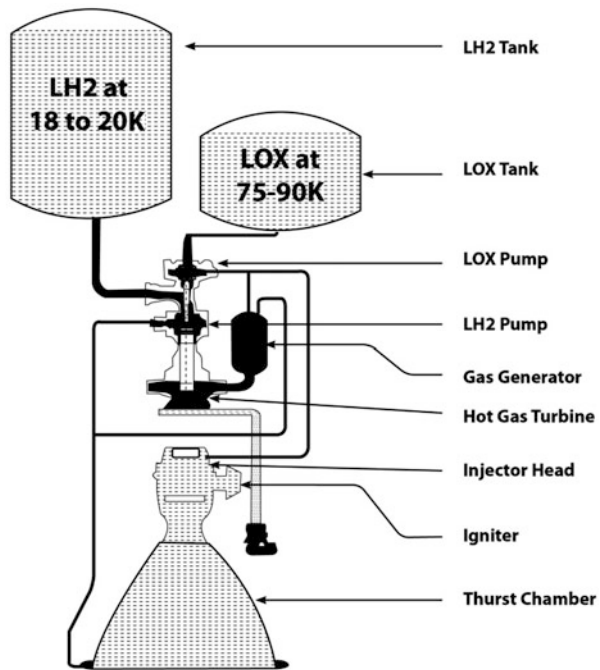
In expander mode the thrust chamber coolant is allowed to evaporate into hot gas. This is used to drive the low-pressure ratio turbines and the turbine exhaust is admitted into combustion chamber to burn with oxidizer. Due to limitation of vaporizing the large quantity of propellant using the hot chamber wall, this cycle can be used only in low-thrust liquid rockets. The major advantages of expander cycle are simplicity, higher specific impulse and relatively lower weight. A typical expander cycle is given in Fig. 9.20d.

9.6.3 Cryogenic Propulsion Systems

Cryogenic rocket engines use propellants which are stored at low temperatures, below 123 K. The combination of liquid oxygen (boiling point 90 K) and liquid hydrogen (boiling point 20 K) provides a specific impulse of 440–460 s. This is quite high compared with 260–300 s of solid propellants, 270–310 s of earth storable propellants and 320–350 s of semi-cryogenic propellants. This high performance is the driving factor to use cryogenic engines in terminal or even in booster stages of STS. A simplified schematic diagram of a cryogenic system working on gas generator (GG) cycle is given in Fig. 9.21.

Propellant tanks with insulation to maintain the low temperature of propellants is needed for storing the cryogenic fluids. Another important subsystem is thrust chamber assembly comprising of an injector, combustion chamber and a nozzle. Injectors play a significant role in injecting the propellants at the required atomized condition into the combustion chamber. The hot gas generated in the combustion chamber is expanded in the nozzle to produce the thrust. Since both liquid oxygen (LOX) and liquid hydrogen (LH_2) are non hypergolic, suitable igniters are needed for initiating the ignition. In these systems the temperature of the hot gas can be around 3500 K and hence there is a need to cool the chamber. It is done by regenerative cooling of the nozzle and engine using LH_2 . Pumps are needed to

Fig. 9.21 Schematic diagram of a cryogenic system



drive the propellants from tank to the thrust chamber at the rated pressure and flow rate. The pumps are driven using the hot gases generated by the gas generator or pre-burner. In GG cycle the gas generator produces the hot gas by burning the small quantity of LOX and LH₂ bled from outlet of respective pumps. In SCC, hot gas is generated by burning the full hydrogen after regenerative cooling of thrust chamber and small quantity of LOX bled from pump outlet.

For effective and efficient functioning of cryogenic engine and stage, the following aspects are to be seriously considered:

- Suitable selection of a cycle, its analysis to finalize the engine power cycle, operating parameters of various subsystems, functional fluid circuits and the system configuration.
- The very high heat flux experienced in the thrust chamber has to be managed by introducing appropriate cooling system. Since liquid hydrogen is an efficient coolant it is used as a regenerative coolant before injecting into the thrust chamber. The regenerative coolant passage has to ensure safe operating temperature at critical throat section with minimum pressure drop.
- Liquid hydrogen, being a low-density fluid, demands high-speed multi-stage pumps to develop the required delivery pressures. Cavitating inducers are needed in the upstream of main pumps to develop the needed net positive suction head (NPSH).

- (d) Gas generators have to operate at low mixture ratio and hence the ignition at this mixture ratio is a critical activity.
- (e) Suitable igniter has to be chosen carefully from pyrogen, pyrotechnique or electrical to initiate the positive ignition and the selection depends on the performance requirements.
- (f) The engine has to be operated at the specified thrust and mixture ratio to ensure the safe engine operation and to achieve the needed vehicle performance and minimum propellant outage. These conditions can be achieved only if the thrust and mixture ratio are controlled within the specified limits.
- (g) Proper selection of start and cut-off sequence controls are needed to ensure that engine systems smoothly transit from start signal to nominal operation to rapid and safe engine shutdown.
- (h) The propellant tanks are to be insulated properly to maintain the tank pressure and bulk temperature of the propellant within the required limits at launch pad as well as in flight.
- (i) The heat in leak through the wall of the propellant tank from ambient, in spite of the insulation causes formation of stratified layer along the wall and free surface of the tank. It is important to prevent the growth of this stratified layer in order to avoid the entry of this vapour into the pump and resulting in cavitation due to high vapour pressure. Figure 9.22 shows a typical stratified layer phenomenon inside a propellant tank. Necessary remedial measures are needed to avoid the growth of stratified layer in tanks.

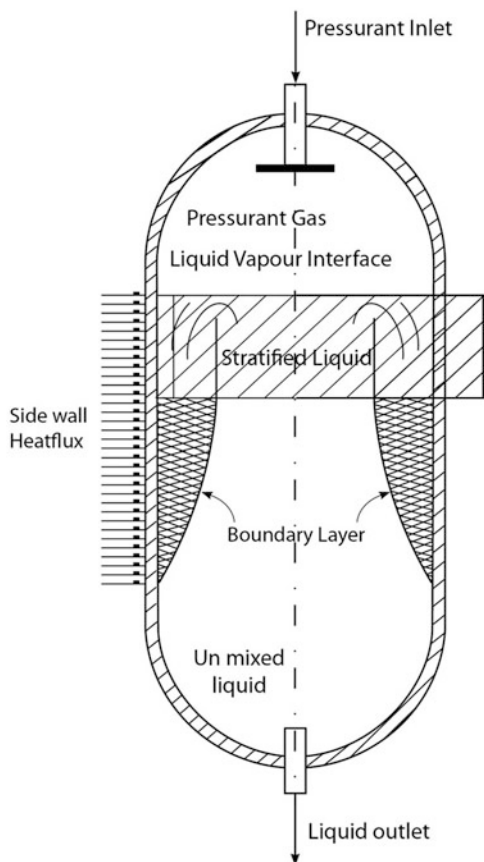
9.6.4 Semi-Cryogenic Propulsion Systems

The semi-cryogenic propulsion uses liquid oxygen as oxidizer and liquid hydrocarbon like alcohol, kerosene, methanol, ethanol, propane, etc. as fuel. In this case the deliverable specific impulse is lower than cryogenic propulsion system, whereas the density impulse is higher than the cryogenic system. However it has higher deliverable specific impulse of around 320–350 s as compared to the earth storable or solid propulsion systems. Utilizing the semi-cryogenic propulsion in the booster stage offers the following advantages.

1. Cleaner, non-toxic and non-corrosive exhaust during the atmospheric phase
2. Provision for engine throttling from 50 to 110 % during the booster operation phase
3. High density impulse
4. Low unit cost compared to other fuels used
5. Ease of handling the propellant

The commonly used fuel is kerosene, gasoline or RP1. While this propulsion offers several advantages for the booster stage it has certain technical limitations like (a) coking and (b) soot formation. Hydrocarbons tend to decompose at a fluid-specific temperature threshold and form a soot of carbon layer at the coolant

Fig. 9.22 Typical stratified layer phenomenon in a tank



channel walls. There is a tendency to increase the coke layer in the channels which in turn increases the resistance to heat flow which causes increase in temperature leading to the failure of coolant channels. Similarly in LOX/hydrocarbon engines the possibility of soot deposition is more, particularly when the combustion is not perfect. The soot layer on the chamber wall has a tendency to reduce the resistance to heat flow. This phenomenon depends on the engines' operational conditions like combustion chamber pressure, mixture ratio, coolant pressure and temperature.

9.7 Critical Subsystems of Liquid Propulsion Systems

9.7.1 Propellant Tanks

Depending on the available space, mass reduction and manufacturing limitations, different tank configurations are being adopted for liquid propulsion systems of

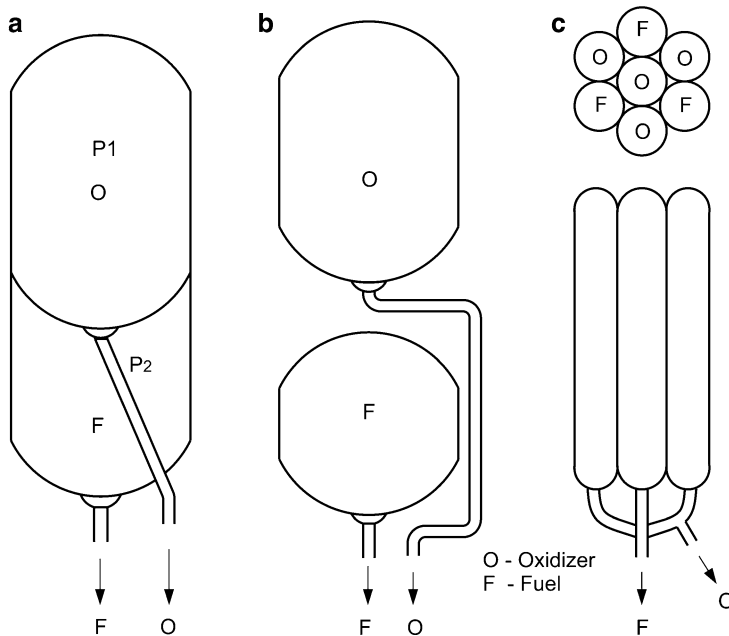


Fig. 9.23 Typical propellant tank configuration (a) Common bulkhead (b) Separate tanks (c) Multiple tanks

STS. Typical ones are given in Fig. 9.23. Figure 9.23a shows a single tank with a common bulk head for storing both oxidizer and fuel. Under such configuration, to ensure structural integrity of the common bulk head, it is essential to ensure that the upper compartment pressure (P_1) is more than bottom compartment pressure (P_2). The common bulk head tank configuration is the minimum mass tank configuration. In the second configuration as represented in Fig. 9.23b, separate tanks are used for storing oxidizer and fuel. Even though this configuration is more massive than common bulk head tanks, this is very simple and easy to manufacture and more reliable. Due to the limitation of space, in many cases, multiple tanks are used for storing fuel and oxidizer as represented in Fig. 9.23c. Under such cases, the propellant outlets are interconnected to draw the propellants uniformly from each tank.

In bigger stages, the propellant tanks act as vehicle structure, and therefore they have to be designed for the expected flight loads. The baffle requirements to provide damping for propellant sloshing also have to be implemented in the tanks.

9.7.2 Propellants Used in Liquid Propulsion Systems

The liquid propellants used in liquid engines are classified as monopropellants, bipropellants and cryogenic propellants. The monopropellants are a mixture of oxidizer and combustible matter and can be easily decomposed. It produces decomposed gases when pressurized, heated or fed through a catalyst. Hydrazine produced from ammonia is commonly used and the catalyst for combustion is alumina granules coated with iridium. Similarly hydrogen peroxide (H_2O_2) generally known as high test peroxide (HTP) produces hot gases when it is passed through a catalyst made of a platinum and silver mesh. Majority of the liquid propellant engines utilize the bipropellants using two fluids, one as a fuel and another as an oxidizer. The bipropellant combination can be (a) hypergolic combination where they ignite spontaneously on mixing and (b) non-hypergolic combination where separate igniters are needed.

Commonly used oxidizers are nitrogen tetroxide (N_2O_4), liquid oxygen (LOX), and nitric acid and the fuels are unsymmetrical dimethyl hydrazine (UDMH), mono methyl hydrazine (MMH), liquid hydrogen (LH_2), and hydrocarbons like RP-1 and kerosene. Liquid oxygen boils at 90 K at atmospheric pressure and has a specific gravity of 1.14 whereas liquid hydrogen boils at 20 K with a specific gravity of 0.07. In all liquid propulsion systems for effective and efficient combustion, the oxidizer and fuel have to mix in the specified mixture ratio. The hypergolic propellant combinations are $N_2O_4/UDMH$, N_2O_4/MMH . Typical propellant combinations which need ignition system to start the combustion process are LOX/ LH_2 , LOX-RP-1. The choice of propellant combination depends on the performance requirement, availability, material compatibility and qualities of handling, storage and environment friendliness.

9.7.3 Propellant Feed Systems

The propellant feed systems' functions are to ensure that the propellants from the tanks are injected into the combustion chamber with the required initial conditions. The system consists of pump, turbine, injector and feed lines.

(a) Propellant Feed Lines

The feed lines transport the propellants from the tanks to the pumps and to the combustion chamber. These feed lines have to be structurally stable under all flight environments. Normally, for Earth storable systems, metallic feed lines with bellows are used. For the case of cryogenic propulsion system, wherein there is large differential thermal expansion due to the fact that one end of the feed line is at elevated temperature whereas other end is at cryogenic temperature, the specifically fabricated polyimide pipelines are needed. This gives high level of flexibility, minimum mass and meets high pressure requirements at different temperature

ranges. In fact the polyimide pipeline performance is better in cryogenic temperature where the metallic pipeline is not suitable.

The interaction between these feed lines and thrust of the engine can lead to POGO oscillation, and therefore, care has to be taken during the design of the feed lines to provide adequate stiffness or to implement POGO correctors in the propellant feed lines to avoid such phenomena.

(b) *Turbo Pumps*

The pumps are used to feed the propellants into the combustion chamber with the required initial conditions. The pumps are located near to the combustion chamber and the propellant pressure at the pump inlet has to be sufficient to avoid cavitations. The pump speed requirements come from the propellant mass flow rate requirements. As an example, to inject low-density propellant such as liquid hydrogen, the required pump speed has to be more than 40000 rpm (revolutions per minute). Generally the pumps adopted for liquid propulsion system rockets are of centrifugal type due to its characteristics of high performance, small volume and less mass. The power required to drive the pump is provided by turbines. The pump and turbine are generally arranged in common shaft and such configurations with both units together are called turbo pump assembly.

(c) *Gas Generator (GG)*

Gas generators produce hot gases required to drive turbines. Small amounts of propellants drawn from both outlets of oxidizer and fuel pumps are burned in combustion chamber to produce the necessary hot gas for driving the turbine. In the case of GG cycle, combustion products are with high fuel-rich mixture ratio (e.g., as in the case of staged combustion cycle of cryogenic propulsion) and the temperature has to be within the limits. In case temperature limit exceeds, mixture ratio of propellants to GG has to be suitably designed such that the required temperature is maintained. If the combustion of propellants in GG produces high-temperature gases which are beyond the allowable limits of turbine materials, it is necessary to use water to reduce the temperature of gas mixture in GG.

9.7.4 *Injector*

Injector in liquid propulsion system is a major subsystem that plays a crucial role of ensuring stable combustion process. The pumps inject the propellant to the combustion chamber through injectors, which is a plate having orifices. To ensure smooth and stable combustion, specific functions of the injectors are (1) atomizing the propellants and (2) proper mixing and distribution. Generally mixing is done by impinging the propellants on each other. But other methods are also being used. Typical injector configurations are given in Fig. 9.24.

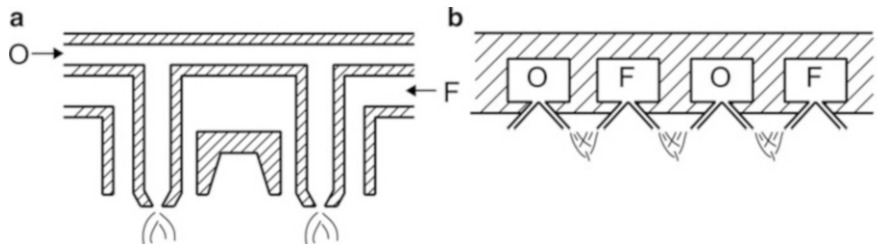


Fig. 9.24 Types of injectors (a) Co-axial (b) Doublet

The injector design parameters such as spacing, pattern, size and shape of orifices depend on many factors: (1) heat transfer characteristics, (2) heat energy release and (3) combustion characteristics.

9.7.5 *Thrust Chamber*

After the propellants enter into combustion chamber, the vaporization, mixing and reactions take place. Depending on the combustion cycle, part of the combustion takes place at GG pre-burner level. In certain cases, only the combustion products are injected in gaseous form. Under such conditions, the time taken to complete the combustion process in thrust chamber is very short. This has two advantages: (1) combustion process efficiency is high and (2) the combustion chamber length is shorter.

The high-temperature combustion product produced in combustion chamber is expanded through nozzle to develop necessary thrust. Major components of thrust chamber are

- Propellant manifolds and injector, which admits the required quantity of propellants for burning
- Combustion chamber where propellants burn

Nozzle assembly is where the hot gases are expanded to attain the required exhaust velocity. To withstand high heat flux at the throat, generally throat insert which is made out of silica-phenolic material is used. This material acts as insulation cooling at throat location.

9.7.6 *Engine Cooling*

In liquid engines the thrust chambers are subjected to severe thermal environments and demands efficient cooling system to ensure the safe and normal functioning of the engines. The main aim of a cooling system is to limit the wall temperature

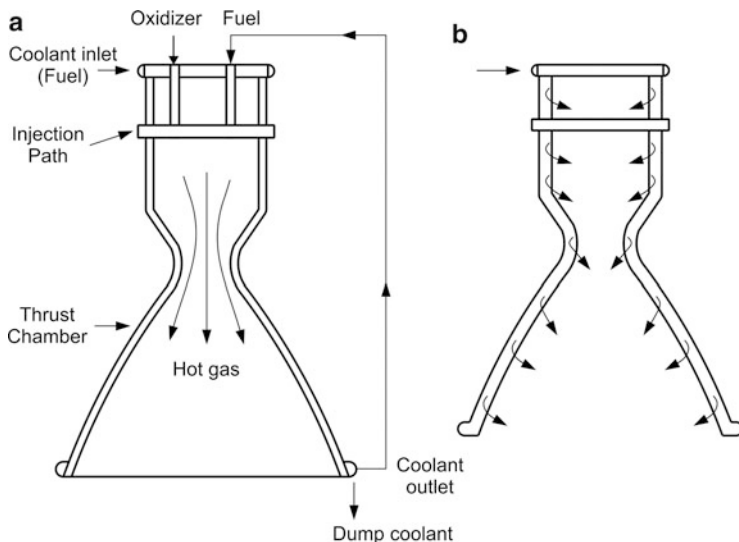


Fig. 9.25 A typical active cooling (a) Regenerative cooling (b) Film cooling

within the safe operating limit of the material used for the thrust chamber and nozzle.

Generally, active cooling methods like regenerative cooling, film cooling, dump cooling, etc. are adopted in liquid engines to achieve the efficient cooling. The passive cooling scheme used in rockets includes insulation, heat sink, ablation and radiation cooling.

Thermal management of nozzle divergent regions are generally achieved through radiative cooling. Heat felt by the nozzle is radiated away from the outer wall of the chamber to the external surroundings. In case of engine nozzles, where high heat flux is felt, suitable high-temperature materials are chosen for the nozzle. In engines which operate at high pressure and long durations the cooling is carried out using regenerative cooling. The schematic of a typical regenerative cooling is given in Fig. 9.25a.

The thrust chamber wall and nozzle wall contain passages as shown in Fig. 9.25a. The passage may be constructed through double wall construction, having coolant tube around the chamber. Coolant is passing through these coolant passages and convecting the heat which reduces the temperature of chamber and nozzle. Generally for rocket engines, fuel is used as coolant and injected into a toroid at the injector location thrust coolant inlet. After cooling, the temperature of the fuel is increased and this fuel is injected into the combustion chamber as represented in Fig. 9.25a. In cryogenic engines hydrogen is used as the regenerative coolant. The quantity of coolant through the engine has to be carefully computed considering the cooling needed, thrust and mixture ratio requirements. After

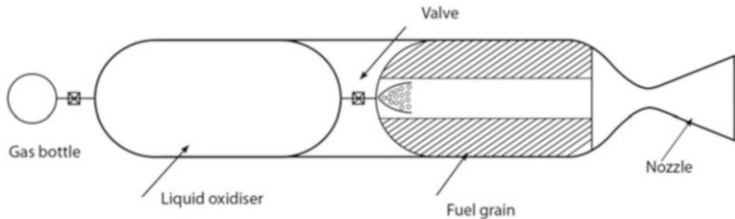


Fig. 9.26 Typical hybrid motor

cooling, if the fuel is dumped out of rocket engine as shown in Fig. 9.25, then this scheme is called dump cooling.

The inner wall surface of the thrust chamber is protected from excessive heating by injecting a thin film of coolant at the outer periphery of the injector head as shown in Fig. 9.26b. This is termed as film cooling. The film layer adjacent to the wall reduces the heating of the divergent position of the nozzle. Both liquid and gaseous cooling are used depending on the overall cooling requirements. The combination of cooling is also used in engines where the heat flux levels are high, like cryogenic engines.

Insulation cooling is the use of extremely low—thermal conductivity material, which reduces the heat flux to wall. Typical material is pyrolytic graphite. This material has conductivity of the order of 2×10^3 W/(mK) in a direction parallel to the layer planes whereas along the normal to the plane, the value is merely 5.75 W/(mK). Therefore, it is preferred to conduct the heat in one direction whereas avoiding heating of mission critical elements. The heat sink cooling, ablation cooling strategies are similar to the one used for re-entry missions.

9.7.7 Propulsion Control Systems

As discussed earlier, in order to ensure maximum performance of the vehicle, the following are the additional requirements on propulsion system:

1. Defined thrust profile for each stage has to be ensured within the allowable dispersion band.
2. Both stored propellants have to be consumed maximally. This is achieved by suitable propellant management by ensuring the specified mixture ratio within the allowable band.

Normally the propulsion systems contain many complex components along with a wider dispersion on operating environment viz., pressure and temperatures. All these aspects can contribute to the large variations on the realized thrust and mixture ratio. Therefore, closed-loop control system is required in the propulsion system to regulate and control these parameters to the required level. Either the

system can be autonomous mechanical system as part of engine design or an external driven system based on the vehicle and propulsion system measurements by computers external to the engine system.

1. Mechanical System

The mechanical system-based thrust and mixture ratio control system works based on balanced piston principle. No electrical or electronic systems are involved.

(a) *Thrust Control System*

The thrust of a rocket engine is directly proportional to the mass flow rate through the thrust chamber. For a given thrust chamber and nozzle, the mass flow rate remains linear to chamber pressure. Hence the thrust can be maintained constant by controlling the chamber pressure. Thrust regulation is achieved by regulating the output of the gas generator used for driving the turbine. The thrust regulation system employed in the engine receives chamber pressure as the feedback. The thrust regulation system compares chamber pressure feedback with a constant (reference) pilot pressure and regulates the flow rate to the gas generator so that the chamber pressure is maintained at a predefined value.

(b) *Mixture Ratio Control System*

Mixture ratio controller known as equilibrium regulator ensures constant mixture ratio in the thrust chamber. The main injector is calibrated in such a way that the required mixture ratio is obtained, if the injection pressures of fuel and oxidizer are the same. This calibration method simplifies the function of the mixture ratio controller. Hence the mixture ratio of the main chamber is controlled by equalizing the injection pressures of both fuel and oxidizer through a mixture ratio controller. By design, the oxidizer pump outlet pressure is generally kept higher than the fuel pump outlet pressure for the pump inlet pressure conditions. The mixture ratio controller is positioned at the oxidizer pump outlet. It monitors the fuel injection pressure and introduces pressure loss in the oxidizer line so that the injection pressure of oxidizer is equal to that of the fuel.

2. External Driven System

In the external systems, the required sensors measure the thrust of the engine or chamber pressure along with other required parameters. Using these sensor outputs and a defined algorithm, the onboard computer generates the flow command to the GG. Based on the input flow to GG, the hot gas generation is modulated, which in turn alters the turbine input. Correspondingly the pump output regulates both oxidizer and fuel flow to the engine in the same proportion as the required mixture ratio which controls the chamber pressure and thrust.

In the case of mixture ratio control system, using the measured and required flow rates, based on the defined algorithm, the computer generates the command which regulates one of the flow rates to injectors (generally oxidizer flow rates, which directly injected into the combustion chamber), thus maintaining the required mixture ratio.

9.8 Hybrid Propulsion Systems

The hybrid rocket propulsion, as the name suggests, uses two different states of matter with oxidizer in liquid form and fuel as solid. The general configuration of a typical hybrid motor is as shown in Fig. 9.26.

The oxidizer stored in a separate tank and pressurized by the gas is injected into the thrust chamber consisting of moulded fuel grain. The hybrid thrust chamber is similar to the solid motor discussed earlier with a motor case, insulation and propellant grain depending on the propellant combinations. The ignition of the motor is achieved either by separate igniter or through hypergolic action. The hot gases produced through combustion are expanded through a nozzle. A valve at the outlet of the oxidizer tank regulates the flow of oxidizer to the thrust chamber. Hybrid motors are generally low-thrust systems and hence pressure-fed systems are used.

The typical propellants used in hybrid rockets are hydroxyl-terminated polybutadiene (HTPB) or polyethylene (PE) as fuel and liquid oxygen (LOX) or nitrous oxide (N_2O) or high test hydrogen peroxide (H_2O_2) as oxidizer. When the liquid propellant enters into the combustion chamber it vaporizes and reacts with the solid propellant. In solid motor the burning always takes place close to the grain surface whereas in hybrid motors the combustion takes place over the solid fuel surface. This happens since the fuel and oxidizer vapours mix in stoichiometric ratio in the boundary layer zone above the fuel grain. The hybrid rockets are relatively simple since it requires only single liquid propellant demanding less number of valves, plumbing and other associated operations. It offers higher Isp compared to bipropellant fluids. The denser fuel has high density and hence reduces the overall system volume. The fuel grain facilitates the addition of reactive metals such as aluminium, lithium, beryllium, etc. and thereby the corresponding increase in Isp. With the control of oxidizer flow it is possible to achieve the start, stop and throttling unlike solid motors.

Similar to liquid engines, here too the oxidizer has to be atomized and vaporized by using suitable injector. The combustion instability in this engine is one of the important issues and it is generally avoided by having high pressure drop across the injector. But it limits the thrust chamber pressure and also the engine thrust.

9.9 Air-Breathing Chemical Propulsion

The present-day STS uses rocket chemical propulsion and this configuration makes the vehicle more heavy and inefficient with respect to vehicle performance point of view. The performance deficiency further aggravates by the limit on the specific impulse achievable by the chemical propulsion technologies.

Depending on the propellant combinations used in the existing rocket propulsion systems, the propellant mixture ratio varies between 2 and 6. This demands about

55 % of rocket mass as oxidizer which has to be carried by the vehicle. Out of this, about 75 % of the total oxidizer is being consumed during atmospheric flight phase of the vehicle up to 50 km. This mass works out to be about 40 % of the total vehicle mass. If the oxygen from atmosphere is used during this phase, vehicle mass can be reduced to the extent of 40 %. The mass reduction along with the increased specific impulse can make a quantum leap in vehicle performance. Therefore, all space-faring nations are seriously investigating the use of air-breathing propulsion systems for STS vehicle. But it demands advanced technologies which are to be developed and qualified before applying for STS.

Air-breathing propulsion deals with the usage of air from atmosphere for chemical reactions. Unlike aircraft, the STS vehicles pass through dense atmosphere quickly with very high velocity. Even though density of air falls rapidly with altitude, air availability for combustion is related to product of density and velocity. Therefore, higher velocities of STS in principle can facilitate high-altitude operations.

9.9.1 *Types of Air-Breathing Propulsion Systems*

Turbo jets, turbo jet with after burning and turbo fan engines are basic air-breathing engines being used in aircraft and their operations are limited to Mach number up to about 2 whereas STS vehicle operations are at very high Mach numbers.

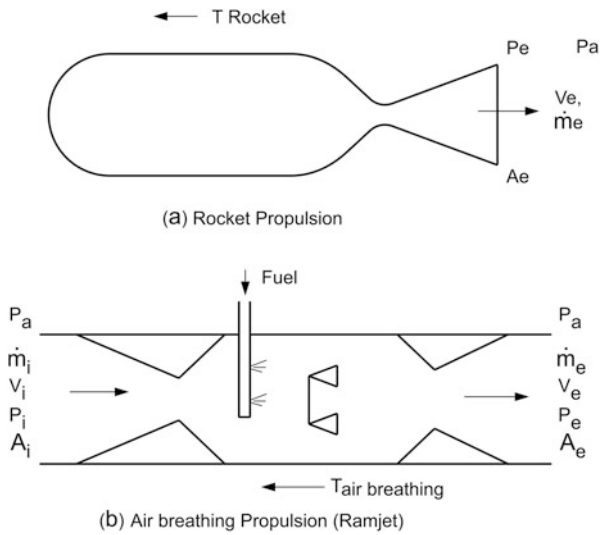
(a) Ramjet

As the flight speed increases, the total pressure of free stream increases compared to free stream static pressure. Their ratio crosses 2 at $M = 1.1$, and at $M = 2$, the ratio increases to 8, and at $M = 3$, the pressure ratio is about 40. Therefore, ram effect of flight velocity is used to compress the air, recovering the free stream total pressure before it is fed into the combustion chamber. At the combustion chamber, fuel is injected along with ignition system to produce combustion product due to chemical reactions. The combustion product is expanded through nozzle. Typical ramjet is represented in Fig. 9.27b. The advantage of ramjet is that there is no rotating component and the system is simple. But the main disadvantage is that, to have the compression of air by ram effect, the propulsion system has to reach a specified minimum velocity. Generally other propulsion systems have to be used to reach $M > 2$ before starting the ramjet.

In rocket chemical propulsion, high-pressure, high-temperature combustion products are expanded through nozzle to get high exit velocity as shown in Fig. 9.27a. But in air-breathing propulsion system, there is both inlet jet and exit jet as represented in Fig. 9.27b. The net thrust of air-breathing engine is the difference between exit jet and inlet jet.

The thrust produced by rocket propulsion system is given by

Fig. 9.27 Comparison between rocket and air breathing propulsion



$$T_{\text{rocket}} = \dot{m} V_e + (P_e - P_a) A_e \quad (9.72)$$

whereas for the air-breathing propulsion system as explained in Fig. 9.28b, the net thrust produced in the forward direction is given by

$$T_{\text{air breathing}} = [\dot{m}_e V_e + (P_e - P_a) A_e] - [\dot{m}_i V_i + (P_i - P_a) A_i] \quad (9.73)$$

where, \dot{m}_i , V_i , P_i are mass flow rate, velocity, pressure of inlet air and A_i is the inlet area.

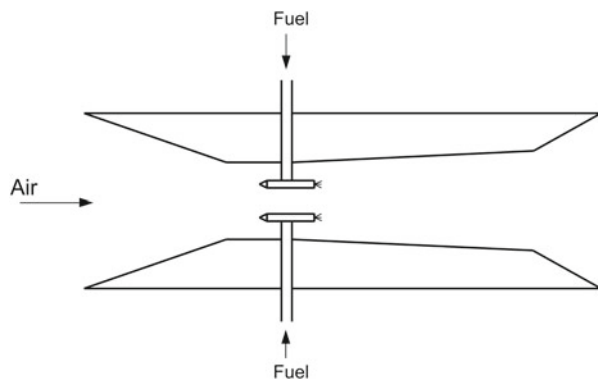
A system of intricate shocks generated internally due to air intake configuration is carrying out the task of compressing the air. Therefore, the shape and geometry of ‘air intake’ has to be carefully designed considering all the aspects.

(b) Scramjet

At hypersonic speeds beyond $M > 5$, decelerating of the air to lower subsonic speeds at the entry point of combustion chamber becomes inefficient. The temperature of air reaching combustion chamber is very high (at $M = 7$, the temperature is about 2300 K), which is comparable to stoichiometric air-fuel combustion temperature. Therefore, the extra thermal energy added due to combustion process is being used for dissociation process. This clearly indicates that for efficient generation of thrust at hypersonic speeds, free stream air cannot be decelerated to subsonic speeds at entry into the combustion chamber. Under such conditions, scramjet engines are useful.

In the scramjet (supersonic ramjet) engine, the hypersonic free stream air, decelerated to a lower Mach number at combustion entry, is still at supersonic velocity. Generally the intake design of scramjet engine is to achieve about one-third of free stream Mach number at the combustor.

Fig. 9.28 Typical scramjet configuration



$M = 0 - 3$: Rocket, Turbojet, Air augmented rocket

$M = 3 - 6$: Ramjet

$M = 6 - 15$: Scramjet

$M > 15$: Rocket

Alternately

$M = 3 - 15$: Dual Mode Ram Jet

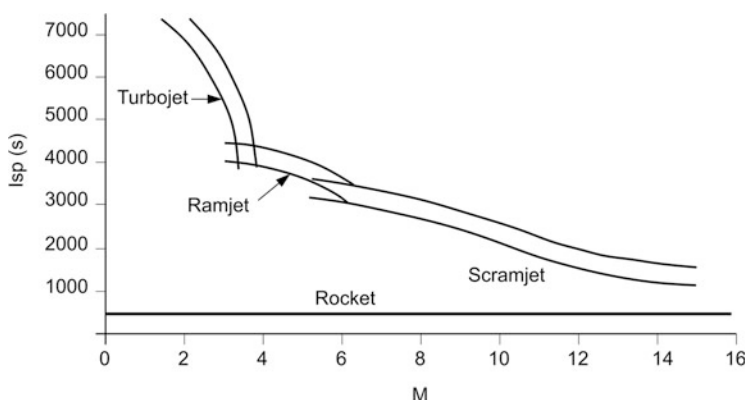


Fig. 9.29 Operating regimes of Air breathing propulsion system

Combustor design and operation are very complex for scramjet. The air and fuel have to be mixed, ignited and burned within short residence time available as air enters combustion chamber at very high speed. Typically for flight $M = 7$, the speed of air at combustion location is about 1500 m/s. Typical scramjet representation is given in Fig. 9.28. The dual-mode ramjet (DMRJ) being designed combines the operation of ramjet and scramjet in one system (Fig. 9.29).

9.9.2 Typical Air-Breathing Propulsion Systems for STS Applications

Typical specific impulse for different propulsion systems with hydrogen as fuel is given in Fig. 9.30. It can be seen that the ramjet is effective from $M = 3-6$. Scramjet

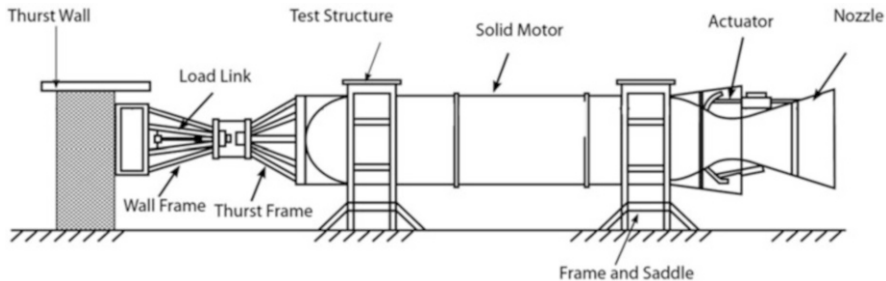


Fig. 9.30 A typical test facility for testing a solid motor

gives the better performance from $M = 6\text{--}15$ whereas beyond $M = 15$, essentially rocket propulsion system is essential. Therefore, a typical STS configuration adopting air-breathing propulsion system can be configured with the following propulsion combinations.

9.10 Non-Chemical Propulsion Systems

In chemical propulsion systems, there is limitation in obtaining high jet exhaust velocities. They are generally limited to a maximum of 5000 m/s. The high combustion temperature and low molecular mass of the exhaust gases pose a severe limitation in chemical rockets to achieve higher exhaust velocities. But it is possible to achieve higher velocities using electrical energy. Electric propulsion, for example, depends on electrons or magnetic fields to accelerate the charged particles to high velocities thus giving very high Isp. The electrostatic thrusters make use of electric field to accelerate the ionized particles. Typical propellants used are xenon, cesium, etc. These thrusters are also known as ion thrusters and provide very high specific impulse. The plasma thrusters utilize the electric and magnetic fields jointly to accelerate the positive ions within plasma. Although all these propulsion systems are able to offer high specific impulse, the thrust levels achieved are generally smaller. Therefore these systems find wide applications in spacecraft control, interplanetary travel, etc.

The idea of using nuclear energy for rocket propulsion was initiated almost with the development of chemical propulsion. In such systems the propellant enters into the reaction chamber to absorb the heat generated by the nuclear reaction. The hot gas so produced undergoes thermodynamic expansion through a nozzle. These systems are capable of producing high thrust and high specific impulse. This system virtually can use any propellant but a typical propellant like liquid hydrogen provides high Isp. The development and use of nuclear propulsion is highly constrained due to problems associated with radiation and the shielding requirements. Serious discussions are on to generate international treaties to avoid the use of nuclear rockets in the Earth's atmosphere.

9.11 Qualification of Propulsion Systems

In order to ensure reliable performance of propulsion systems, all their subsystems have to undergo elaborate tests and qualification at different levels. The tests are to be planned at components/subsystems level and then at the integrated systems level. Propulsion module development is generally initiated with an engineering model and tested under the atmospheric conditions. These tests are to be extended to encompass the higher altitude or vacuum to qualify them for flight conditions. System reliability has to be established by carrying out a series of ground tests to measure the performance over the entire range of operating conditions and sometimes even beyond to establish the margins. All these tests demand extensive test facilities built for the purpose of meeting various test conditions and ensuring the highest level of safe and reliable operation.

The wide range of tests needed is to be categorized as given below. These tests are to be carried out in sequence.

- (a) Tests at components or subsystem level like igniters, valves, actuators, nozzles, motor case, controls, structures, etc.
- (b) Static tests for propulsion modules where the tests are carried out under a wide range of operating conditions which includes parameters even beyond three sigma conditions
- (c) Propulsion system tests with progressive integration of other vehicle subsystems like interstage, structures, flight avionics, control systems, etc.
- (d) Space environment testing like thermal, vacuum, etc. to the extent possible

9.11.1 Qualification Methodology for Solid Motors

All subsystems of solid motor like motor case, nozzle, igniter, etc. undergo detailed subsystem-level tests to ensure that they meet the specified performance and can withstand the severe temperature conditions. All these tests are to be planned by giving utmost importance to safety issues. The subsystems are to be integrated carefully using special tools, equipments and facilities to ensure the safe and reliable performance. These components are also to be subjected to several other tests like thermal, vibration and acceleration tests. The number of units to be tested depends on the severity of the function. For example, the igniters are evaluated using a large number of units to ensure their reliable operation since these components are highly mission critical. In all these tests extensive instrumentation is necessary to measure the strain, pressure, temperature, etc. depending on the requirements.

Once all components and subsystems are certified for their performance the propulsion module involving the motor case, igniter, nozzle, control system and all other associated elements are integrated. Then this propulsion module has to be subjected to static tests in a test stand specially prepared for the purpose to evaluate

its ballistic performance. The number of tests should encompass the entire range of operating conditions, simulated environment and even off-design conditions. The number of qualification tests needed is to be decided judiciously without sacrificing the overall reliability requirements. It is also necessary to build a mathematical model of the system incorporating all essential design features and to carry out detailed simulation studies with dispersions to establish the margins. The result from experimental test has to be utilized to validate the mathematical model. A typical test facility for evaluating the performance of a solid rocket motor is given in Fig. 9.30.

The test bay consists of main structure to house the motor case horizontally, an axial thrust measurement system on the head end consisting of a rigid thrust wall, a thrust frame, a load link capable of measuring the required thrust and necessary fixtures for fixing the motor on the structure. Entire test setup is housed inside a strong block house protected using strong concrete structure to withstand the explosion if any due to any unforeseen reason. The motor is adequately instrumented to measure the ballistic performance, temperature across the motor case and nozzles, strain measurement and vibrations. The control system performance also needs to be evaluated in one of the tests by integrating the actuators and all other associated control elements with the motor. Detailed measurements in terms of nozzle deflections are needed and the performance is to be evaluated for different input conditions. The instrumentation and control room is to be generally located at a safe distance from the test bay to protect them against any mishaps during the test. All elements used in the test bay are to be protected by making them explosion proof as far as possible and to minimize the damage in the event of any mishap. The number of static tests needed to qualify a solid motor has to be judiciously estimated based on the performance, schedule, cost and other programmatic considerations.

9.11.2 Qualification Tests for Liquid Propulsion Systems

The liquid propulsion systems consist of several components and subsystems unlike solid motors. They are engine, stage, control components, igniters whenever needed, actuation systems, etc. Extensive tests at different levels are needed to qualify the liquid propulsion systems as given below:

- (a) Cold flow tests for characterization of injector, turbo pump, control components, etc.
- (b) Engine qualification tests
- (c) Engine and stage hot tests
- (d) High-altitude tests for engine wherever applicable

Apart from these, detailed structural tests are needed for tankages and structures. All these tests are to be carried out using specially prepared test facilities under closely controlled conditions to ensure the safety. For engine and stage tests in

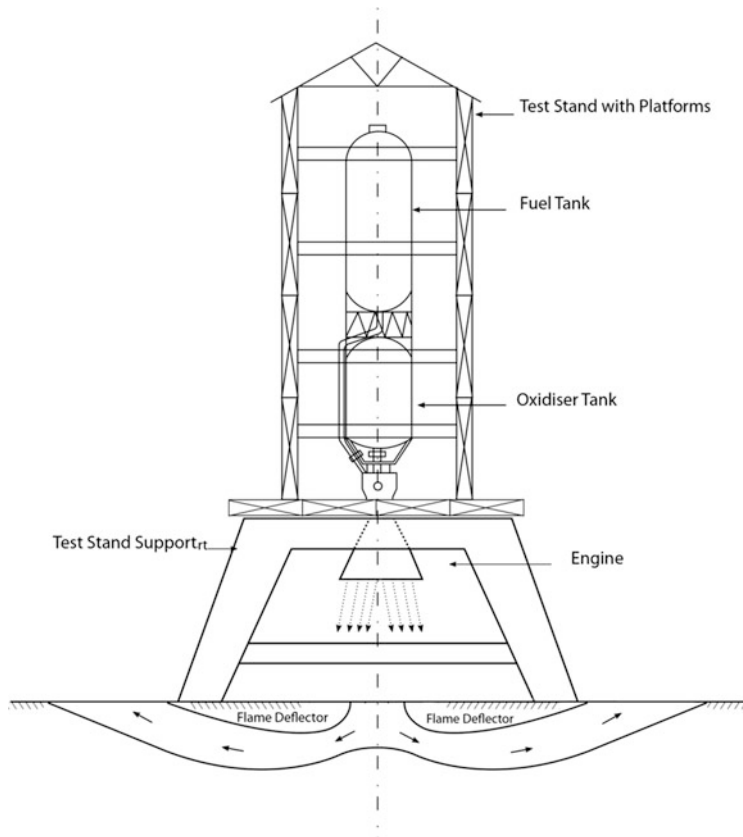


Fig. 9.31 A typical liquid stage test set up

liquid propulsion systems, elaborate ground facilities like propellant storage tanks, safety features to detect/manage propellant leakages, pressurization systems, extensive plumbing systems with automated valves, propellant disposal yard, instrumentation and data acquisition systems are needed. In all these systems safety practices are to be meticulously followed to protect the installations and personnel in the event of any unforeseen accident. Necessary pollution control for both atmosphere and ground water has to be put in place.

In liquid systems it is possible to abort the test in the event of any of the parameters exceeding the set values by automatically shutting off the fuel and oxidizer valves. Therefore suitable abort logic has to be worked out and implemented in tests to avoid damage due to any mishaps. A typical engine and stage static test setup is shown in Fig. 9.31.

The main objectives of the static test for the liquid engine and stage are

- (a) To evaluate the performance of the integrated stage with all subsystems as close to flight as possible
- (b) To verify the loading of propellants and other fluids including the functioning of sensors in the stage
- (c) To assess the control system performance by subjecting the same to the maximum duty cycle
- (d) To measure the thermal conditions of the engine and stage by suitable instrumentation
- (e) To estimate the left-out propellant after the engine firing for the specified flight duration
- (f) To verify the start and shut-off transients
- (g) To assess the vibration and acoustic levels at critical points
- (h) To study the dynamic behaviour of the entire fluid system

Therefore the test articles of the engine stage and all other subsystems have to be similar to flight systems excepting the tank which is generally built rugged so that number of static tests can be conducted using the same hardware. The liquid stage tests are generally done in vertical configuration and the test stand is built to accommodate the engine and stage as shown in Fig. 9.31. The structure is to be built to withstand all loads including the main engine thrust. It contains a few platforms to assist the integration of stage. All necessary handling fixtures to erect the liquid stage on the test stand are needed and appropriate deflector pit to direct the exhaust gas of the engine is to be incorporated. For flame cooling appropriate water cooling system is needed. Elaborate instrumentation is required to measure all essential parameters of the engine and stage like strains, temperatures, heat fluxes at all identified locations, vibration, acoustic and control system parameters. The instrumentation bay is to be located far from the test stand from safety considerations. The engine and stage tests are carried out in phases, initially for a very short duration to verify that all test subsystems function properly. Then test duration is extended to an intermediate value before the total flight duration tests are carried out. The number of tests to be carried out using the facility depends on several factors and to be judiciously decided to establish the reliability of the liquid stage.

Location of test facilities is to be decided considering the safety aspects, impact on the environment and ecology. It is essential to have provisions for pollution control for both atmosphere as well as ground water. Whenever large engines are tested acoustic levels are to be assessed and it can be as high as 160 dB which certainly affects the surrounding life. The test scheme has to choose suitable test profiles to account for the real operating conditions of the engine in flight. Therefore test plan is to be designed not only to validate the performance of the propulsion system under its operating conditions but also to demonstrate the margins under extreme conditions.

Wherever the engines are used for igniting and operating at higher altitudes, the tests at high-altitude conditions (HAT) are necessary to qualify the engine and thrust chamber under vacuum conditions. Main objectives in such tests are to

demonstrate the vacuum ignition, the vacuum thrust and to study the engine performance during start and tail-off transients. In cryogenic engines the vacuum ignition and qualification of suitable engine start sequence are important. The test facility for such tests should have provision to accommodate the engine and thrust chamber, a vacuum system to simulate the high-altitude vacuum conditions, a suitable thrust measurement system to measure the vacuum thrust and a diffuser system to eject the engine exhaust from low pressure (vacuum) to high pressure (ambient condition). During the starting phase the recovered pressure downstream has to be less than the ambient pressure and therefore diffuser alone cannot expel the exhaust gas. In such cases an ejector system which is essentially a fluid dynamic pump is needed. This system utilizes the high-velocity fluid to expel the exhaust gases from low pressure to high pressure. For short-duration tests ejectors have to be continuously used, whereas in long-duration tests they are needed only during the start and shut-off transients.

Bibliography

1. Sutton, G.P., Biblarz, O.: Rocket Propulsion Elements, 7th edn. Wiley-Interscience, New York (2001)
2. Cornelisse, J.W., Schoyer, H.F.R., Wakker, K.F.: Rocket Propulsion and Spaceflight Dynamics. Pitman Publishing, London (1979)
3. Davenas, A.: Solid Rocket Propulsion Technology. Pergamon, Oxford (1993)
4. Brown, C.D.: Spacecraft Propulsion, Education Series. AIAA, Reston (1996)
5. Shepherd, D.G.: Aerospace propulsion. American Elsevier publishing Co., Inc., New York (1972)
6. Cochran, C.D., Gorman, D.M., Dumoulin, J.D. (eds.): AU-18 Space handbook, Air Command & Staff college, Air University Press, Maxwell AFB, AL (1985)
7. Huzel, D.K., Huang, D.H.: Design of Liquid Rocket Propellant Rocket Engines. AIAA, Washington, DC (1992)
8. Timnat, Y.M.: Advanced Chemical Rocket Propulsion. Academic Press, London (1987)
9. Hill, P.G., Peterson, C.R.: Mechanics and Thermodynamics of Propulsion. Addison-Wesley, Reading (1964)
10. Turner, M.J.L.: Rocket and Spacecraft Propulsion: Principles, Practice and New Developments. Third Edition Springer, Praxis Publishing, Chichester (2009)
11. Shu, Q.-S. (ed.): Advances in Cryogenics Engineering, vol. 45, Materials for cryogenic engineering, Plenum Press, New York (1999)

Chapter 10

Aerodynamics of Launch Vehicles

Abstract Aerodynamics plays a vital role in STS design process. The steady and unsteady aerodynamic loads generated due to the relative motion between vehicle body and surrounding air during the atmospheric flight phase of the vehicle, its aerodynamic characteristics, external environment and flow characteristics are the major inputs for the vehicle systems design. The aerodynamic axial force is used for the mission design and vehicle performance evaluation. The steady aerodynamic disturbance moments and loads acting on the vehicle are required for vehicle control and structural systems design. Further the aerodynamics-related issues become complex since the maximum dynamic pressure, maximum aerodynamic force and moment coefficients, unsteady loads, maximum wind velocity, large wind shear and measured uncertainties of wind occur almost simultaneously. The vehicle sizing with clustered propulsion systems complicates the aerodynamic flows with unfavourable additional aerodynamic loads. The unsteady pressure fluctuations are due to shock oscillations during the transonic regime and local aeroacoustic loads due to flow separation because of protrusions form a major input for the qualification of structural and other sensitive systems. This chapter presents the aerodynamic characteristics of a launch vehicle during various phases of its atmospheric flight, different types of aerodynamic loads acting on the overall vehicle/its subsystems and their importance for the launch vehicle systems design. Methods of estimating these loads under different conditions are also outlined. Subsequently, aerodynamic force and moment on overall vehicle, its impact on the vehicle systems design and the methods of aerodynamic characterization using the computational fluid dynamics and wind tunnel studies are briefly covered. The salient features of aerodynamic configuration design of a launch vehicle are also included.

Keywords Aerodynamics • Flow characteristics • Forces • Moments • Steady and unsteady loads • Buffet • Aeroacoustics • Aeroelasticity • Vent holes • Computational fluid dynamics • Wind tunnel tests • Payload fairing and Fin

10.1 Introduction

Aerodynamics plays a vital role in STS design process. The steady and unsteady aerodynamic loads are generated due to the relative motion between vehicle body and surrounding air during the atmospheric flight phase of the vehicle along with its aerodynamic characteristics, external environment and flow characteristics form the major input for the vehicle systems design. While the aerodynamic axial force is used for the mission design and vehicle performance evaluation, the steady aerodynamic disturbance moments and loads acting on the vehicle have major roles in the vehicle control and structural systems design. In addition, the structural design loads need to be augmented for the unsteady flow phenomena to ensure sufficient structural design margin during the crucial atmospheric flight phase of the vehicle. The aerodynamics-related issues get further aggravated since the maximum dynamic pressure, maximum aerodynamic force and moment coefficients, unsteady loads, maximum wind velocity, large wind shear and measured uncertainties of wind occur almost simultaneously. The optimum vehicle sizing with clustered propulsion systems further complicates the aerodynamic flows with unfavourable additional aerodynamic loads on the vehicle. The functional protrusions provided on the vehicle external surface produce localized steady and unsteady loads which need to be considered for the design of the corresponding protrusions and vehicle structural systems.

The unsteady pressure fluctuations caused due to shock oscillations during the transonic regime and local aeroacoustic loads caused by protrusions due to flow separation form a major input for the qualification of structural elements as well as sensitive avionics and spacecraft systems. This chapter initially provides a brief account on the typical aerodynamic flow characteristics on ascent phase of STS (launch vehicles). Subsequently, aerodynamic force and moment on overall vehicle, aerodynamic characteristics, its impact on the vehicle systems design and the methods of aerodynamic characterization are explained. The salient features of aerodynamic configuration design of a launch vehicle are also included at the end of this chapter. The aerodynamic aspects of reentry vehicle STS is explained in Chap. 15.

10.2 Aerodynamic Flow Characteristics

Aerodynamic loads act on a launch vehicle throughout its mission duration, starting from vehicle on launch pad, flight through dense atmosphere and even during flight in the rarefied atmosphere. The aerodynamic flows featuring specific characteristics at different regimes of flight generate aerodynamic loads of different natures with different magnitudes. Based on various physical phenomena and its relative importance to the vehicle design process, the aerodynamic flows can be classified into the following categories:

1. Continuum, transitional and free molecular
2. Laminar and turbulent
3. Incompressible and compressible
4. Subsonic, transonic, supersonic and hypersonic
5. Inviscid and viscous
6. Separated

10.2.1 Continuum, Transitional and Free Molecular Flow Regimes

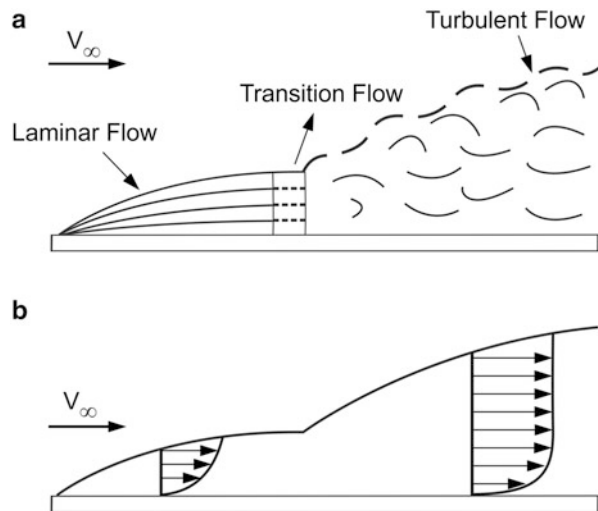
Atmospheric phase of launch vehicle mission can be classified into flight through continuum, transitional and free molecular flow regimes. Knudsen number (Kn), which is the ratio of mean free path of air particles to the characteristic length of the vehicle (reference diameter, for the launch vehicle case) is used to distinguish these flow regimes. The continuum flow regime, wherein $\text{Kn} < 0.001$, is more critical for launch vehicle design as the vehicle encounters high dynamic pressure during this flight phase. However, the vehicle flight at higher altitudes (generally altitude more than 120 km) encounters very low-density free molecular flows, wherein the characteristic length of the vehicle is much smaller than mean free path of the air molecules and $\text{Kn} > 10$. Flow regimes which have Kn between 0.001 and 10 are called as transitional flows.

10.2.2 Laminar and Turbulent Flows

Boundary layers play an important role in aerodynamic characteristics of a launch vehicle. Boundary layer is a very thin layer of aerodynamic flow close to the vehicle surface, across which the velocity rises rapidly from zero at the vehicle wall to about 99 % of free stream velocity at the outer edge of the layer. The pressure within the attached boundary layer remains constant, which is the same as the pressure on the surface. However, when the flow is separated or when the flow is hypersonic with strong viscous inviscid interaction, the pressure within the boundary layer is not constant. Boundary layer is part of aerodynamic flow in the vicinity of launch vehicle, and the viscous flows within the boundary layer distort the non-viscous flows outside its boundary. Thus, the aerodynamic flow around the launch vehicle during its atmospheric flight phase can be divided into two parts:

1. Flow inside the boundary layer, wherein viscous and skin friction effects as well as heat transfer between environment and vehicle are dominant
2. Flow outside the boundary layer called as inviscid flow, wherein the viscosity effects can be neglected

Fig. 10.1 Laminar and turbulent boundary layers.
(a) Flows. **(b)** Velocity Profiles



Boundary layer characteristics depend on vehicle size, viscosity and density of flow medium and flow speed. Therefore, in order to take care of variations in the operating environment of the vehicle as well as to take care of the vehicle size, these flows are characterized with respect to the non-dimensionalized parameter, Reynolds's number, R_e , which is the ratio of inertial force to viscous forces in a flow as defined below:

$$R_e = \frac{\rho_\infty V_\infty D_{ref}}{\mu_\infty} \quad (10.1)$$

where ρ_∞ , μ_∞ , V_∞ and D_{ref} are the free stream density, viscosity, velocity and reference diameter of the vehicle respectively.

To start with, the flow is laminar over a vehicle and the boundary layer is thin. As the flow progresses, the ratio of destabilizing inertial force to the stabilizing viscous force increases. At a critical Reynolds number of about 0.5 million, the flow undergoes transition from laminar to turbulent flow. Inside the turbulent boundary layer, the flow is unsteady and is characterized with eddies of various sizes. Also the boundary layer thickness is more as compared to the laminar flow. The laminar and turbulent boundary layers are explained in Fig. 10.1

Typical features of boundary layers and its effects on aerodynamic characteristics of launch vehicle are given below:

1. Laminar flow generates lower skin friction drag as compared to the turbulent flow.
2. For the attached flows, the effective body size is proportional to the boundary layer thickness. Therefore, for a thicker boundary layer, the form drag is more.

3. Very smooth body generates very thin laminar boundary layer for the initial portion of the vehicle which produces lower drag. However, a very thin laminar boundary layer subsequently gets severely affected by the adverse pressure gradient which makes the flow separate. The separated flow causes large increase in the pressure drag.
4. Rough surface tends to make the boundary layer turbulent, and a turbulent boundary layer can withstand larger adverse pressure gradient as compared to the laminar boundary layer without undergoing flow separation. Thus, although the skin friction drag is more for the turbulent boundary layer, this would delay the flow separation as compared to the laminar boundary layer and the associated large increase in pressure drag.
5. Shock and boundary layer interaction makes the flow separate. Along with increase in the pressure drag, the flow separation process introduces flow unsteadiness and in turn unsteady loads.

10.2.3 Incompressible and Compressible Flows

Incompressible flow is the one in which the density of the air remains constant during flow over the launch vehicle surface. Alternatively, for the incompressible flows, the density changes and the change has a negligible impact on the output of interest. As a rule of thumb, if the airflow density change is less than 5% of stagnation point density, then it is called incompressible flow. The airflows are generally incompressible if the flow speeds are much less than the speed of sound, i.e. when Mach number $M < 0.3$. This is the characteristic of airflow due to wind over a vehicle on the launch pad as well as during initial phase of vehicle flight. Subsequent to that, till the end of the atmospheric flight phase, higher vehicle speeds cause the airflow to get compressed as it contacts with the vehicle surface. The flow phenomenon during high-speed flight is explained below.

As the vehicle moves, the air particles brought to rest relative to the vehicle in front of the vehicle create a stagnation pressure built up at that location. This pressure build-up acts as a disturbance in the flow field and the difference in pressure present in the flow is propagated in all directions of the fluid medium with the speed of sound. When the vehicle speed is very low, this pressure disturbance can propagate upstream of the flow with the speed of sound and change the flow pattern ahead of the vehicle. This causes a smooth flow over the vehicle, giving the impression as if the flow ‘knows’ in advance the presence of the vehicle and negotiates the flow over the body. This phenomenon is represented in Fig. 10.2a. As the speed builds up, the pressure difference in the forward direction is not able to propagate to a longer distance with respect to the vehicle as the vehicle also moves at a speed comparable to the speed of sound as represented in Fig. 10.2b.

When the vehicle moves with the speed of sound, the pressure difference travelling against the flow direction cannot propagate further with respect to the vehicle. This happens as both pressure difference and vehicle moving with the same

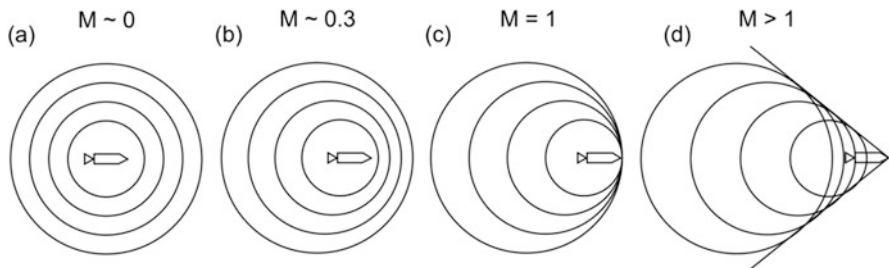


Fig. 10.2 Flow phenomena at various speeds

speed and pressure difference in front of the vehicle progressively builds up and a high-pressure shock wave forms in front of the vehicle as represented in Fig. 10.2c. In this case the pressure difference cannot be communicated to the upstream, when the airflow strikes the vehicle and it is forced to change its properties abruptly. Thus, across the shock, the flow properties, i.e. temperature and pressure, change almost instantaneously, density increases and speed decreases. The shock wave thickness is approximately of the order of microns in the dense regions of flight. In fact the thickness of the shock depends on the Reynolds number. For rarefied flows, i.e. at altitudes more than 80 km, the shock wave thickness is of the order of centimeters. For a very small region, the shock wave is normal to the flow direction (normal shock) and due to accumulation of all pressure differences, shock strength is also high in that regime. As the vehicle speed further increases beyond the speed of sound, the shock wave becomes oblique to the vehicle and flow direction (oblique shock) as shown in Fig. 10.2d.

High-speed flows over the launch vehicle produce shock waves in the flow field. All the flow variables are discontinuous across the shocks which in turn create steady and unsteady loads on the launch vehicle. For very high speeds, in addition to the loads, aerodynamic heat transfer also occurs from flow to the vehicle. The compressible flow regime can be classified into subsonic, transonic, supersonic and hypersonic depending on the non-dimensional parameter, free stream Mach number, which is the ratio of free stream velocity to free stream speed of sound as defined below:

$$M = \frac{V_\infty}{a_\infty} \quad (10.2)$$

10.2.3.1 Subsonic Flows

If all regions of flow over the launch vehicle have local Mach number less than 1, then the flow is subsonic, which is normally the case for free stream Mach numbers less than 0.8. For free stream Mach numbers between 0.8 and 1.2 the flow over the vehicle is having regions of subsonic and supersonic flow and is termed as transonic flow. For free steam Mach number between 1.2 and 5.0 the flow is termed

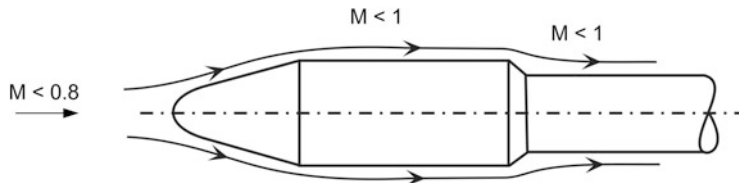


Fig. 10.3 Subsonic flows

as supersonic and Mach numbers larger than 5 is termed hypersonic where the viscous inviscid interaction of the shock layer is dominant.

Subsonic flows are characterized by smooth streamlines without any discontinuity. This generally exists up to a free stream Mach number of about 0.8, wherein the flow speed over the vehicle surface is always less than the local speed of sound as shown in Fig. 10.3.

10.2.3.2 Transonic Flows

When the free stream Mach number reaches about 0.8, the subsonic free stream flow expands and the speed increases locally to the sonic speed ($M = 1$) as shown in Fig. 10.4a.

The free stream Mach number at which the flow reaches sonic speed locally is called critical Mach number. This Mach number is the start of the transonic flow regime. As the free stream Mach number increases further, still less than sonic speed, the flow locally expands to a supersonic pocket terminated with shock, beyond which the flow speed is subsonic as shown in Fig. 10.4b. Shock thus generated interacts with the boundary layer and makes the flow separate. Further increase in free stream Mach number leads to further expansion leading to the formation of supersonic pocket after the cone–cylinder junction which is a region of strong expansion. When the free stream Mach number reaches about 1.2, there will be clear expansion fans at the shoulders and oblique shock in front of the vehicle. Depending on the boat-tail angle the flow would sometimes separate and reattach as shown in Fig. 10.4d. At this free stream Mach number, the flow Mach number over the entire vehicle surface reaches above the sonic speed. The flight with free stream $M = 0.8\text{--}1.2$ is referred as transonic regime of flight wherein the flow over the vehicle surface is a combination of subsonic and supersonic pockets.

The transonic regime of the flight is crucial for a launch vehicle mission as this phase induces additional loads on the vehicle. The formation of shocks over the vehicle increases the pressure drag. The shock formation at the different axial locations between the windward and leeward sides causes large differential pressure which increases lateral load on the vehicle. Also during this regime, the shocks formed on the surface oscillate and move back and forth due to shock wave–boundary layer interaction. The position change of the shocks with time causes pressure fluctuations and unsteady loads. In addition, the shock interacts with the

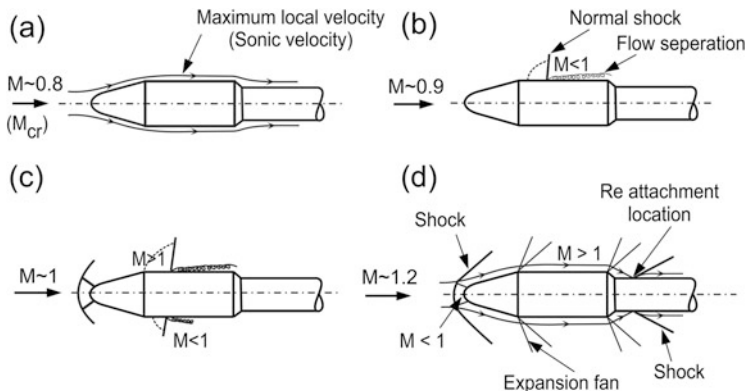


Fig. 10.4 Transonic flows

boundary layer and flow separates from the vehicle causing unsteady flow and hence unsteady loads. These issues aggravate further due to the fact that the high dynamic pressure regime is very close to this phase of flight. Thus, the launch vehicles are generally designed for the transonic flight regime loads.

10.2.3.3 Supersonic Flows

The flow beyond the Mach number 1.2 is referred to as supersonic flow, wherein the flow speed over the entire body is more than sonic speed except for a small region near the forward portion of the vehicle as shown in Fig. 10.4d. In supersonic flow regime, shocks and expansion fans are fully developed. Supersonic flow is characterized by shock and expansion waves depending on the flow turning angle and the flow over the vehicle is generally smooth. As the Mach number increases in the supersonic flows, the pressure differential between the windward and leeward sides caused by the flow incidence angle reduces. Therefore the aerodynamic force level decreases with Mach number in this flow regime. Supersonic flows are dominated by the viscous effects, which in turn heat the vehicle surface due to viscous dissipation in the boundary layer. Generally supersonic flow regime starts at the free stream Mach number of about 1.2 and extends up to the Mach number of about 5.

10.2.3.4 Hypersonic Flows

As the free stream Mach number increases beyond supersonic flows, the flow speed over the vehicle increases further. The free stream kinetic energy of the flow would become larger than the static enthalpy of the flow and the shock angle reduces so

much that the shock wave moves very close to the body, which in turn interacts with the boundary layer. At higher Mach number, temperature of the gases downstream of the strong normal shock increases to a very large value. These hot gases bathe the vehicle surface and heat is transferred to the vehicle surface through convective and radiative heat transfer mechanisms. In addition, the high temperature causes chemical decomposition of the air and the real gas effects are predominant, which alters the aerodynamic characteristics of the vehicle. Therefore, high thermal environment to the vehicle along with the real gas effects caused by chemically reacting flows are the characteristics of hypersonic flow regimes. For very high Mach numbers, beyond 10, the shocks are very close to the vehicle surface and the aerodynamic force and moment coefficients are almost independent of the Mach number.

10.2.4 Separated Flows

The flow separation on the wall occurs due to adverse pressure gradient, i.e. with increase in pressure along the flow direction. Under the pressure gradient, the particles of the fluid in the relatively slowly moving region near the surface of the body is retarded by the pressure and also there would be loss of kinetic energy for fluid particles near the wall due to viscous dissipation. If the pressure gradient is strong enough, the speed near the surface falls to zero and subsequently reverses the direction. If this occurs, large eddies are formed and smooth flow stream lines are lifted away from the surface, creating a large region of slowly moving, eddying flow which is known as flow separation.

Flow separation is caused by (1) geometric change in the vehicle shape, (2) shock boundary layer interaction and (3) wake behind the body. Flow separation caused due to typical geometry changes are represented in Fig. 10.5. These flow separations cause reverse flow.

Wakes are the separated flows from the vehicle geometry, generally behind the body. These types of flows occur over the bluff bodies and at the boundary of a body geometry as represented in Fig. 10.6.

In wake flow, the flow rotations take place and are called vortices. It depends on the vehicle shape and flow speed, and contains vortex of various strengths, which can strike the vehicle systems as represented in Fig. 10.6.

Thus, the main characteristics of a separated flow are reverse flow with associated vortices. In addition, due to the unsteady nature of separated flows, large unsteady loads are also imparted on the vehicle in these flow regimes. Flow separation can occur at all the flow regimes as explained in the previous sections.

Fig. 10.5 Separated flow due to geometric change.
(a) Flow over Boat Trail.
(b) Flow over a protrusion

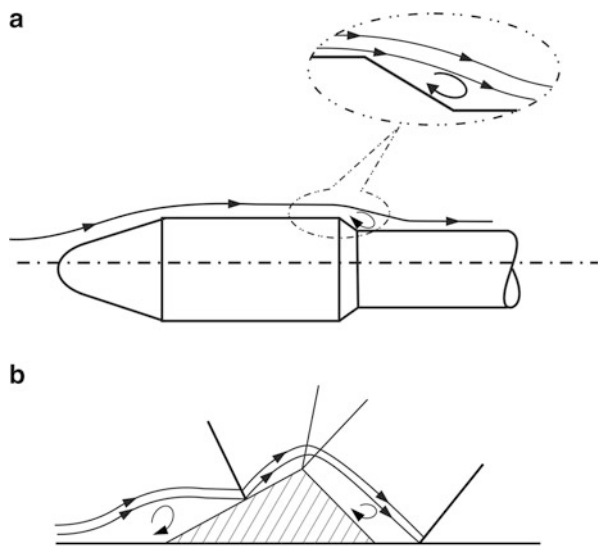
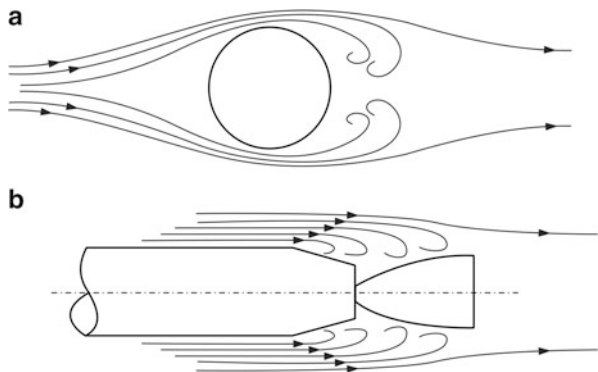


Fig. 10.6 Flow separation in the wake. **(a)** Vortex on the vehicle. **(b)** Vortex on the nozzle



10.3 Overall Vehicle Aerodynamic Features

The various flow phenomena form the aerodynamic features for a launch vehicle during the different regimes of atmospheric flight and are shown in Fig. 10.7. Due to the ground winds, vehicle on the launch pad faces aerodynamic flow at almost normal to the vehicle surface. As the wind speed at ground is much lower than the speed of sound at sea level, the flow is incompressible. But due to the bluff body effects, the flow separates from the leeward side of the vehicle. As the vehicle lifts

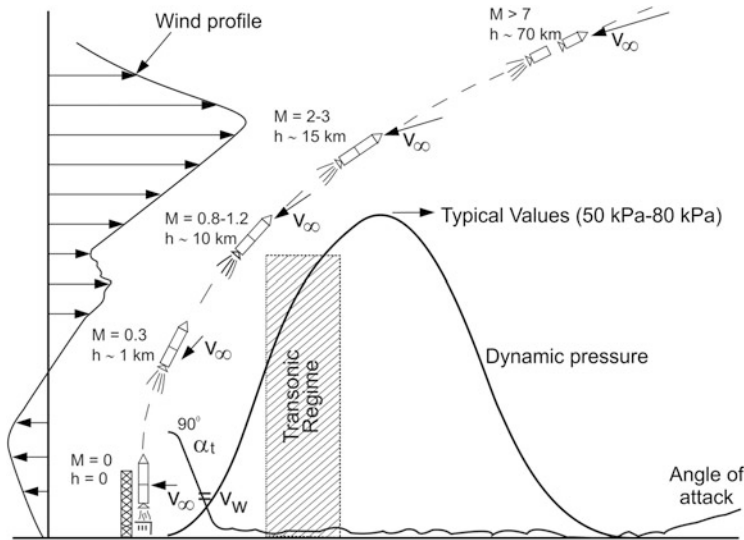


Fig. 10.7 Flight environment during atmospheric phase of a launch vehicle

off, the vehicle velocity builds up which in turn reduces the flow incidence angle and vehicle follows subsonic flight. As the vehicle velocity increases further, the compressibility effects become predominant and the vehicle passes through subsonic, transonic and supersonic flow regimes. Along with this, the dynamic pressure on the vehicle builds up.

Generally, for a launch vehicle ascent mission, the increase in atmospheric wind velocity almost coincides with this region, which causes a highly disturbed environment during this regime. Therefore, to reduce the disturbance levels, the vehicle is steered to follow zero incidence with respect to the expected airflow direction estimated with the winds measured close to the launch. However, in flight wind velocity variations and large wind shear (which are the characteristics of winds in these regions) cause a flow incidence of the order of 1° to 2° which in turn induces loads on the vehicle subsystems. Approximately, at the altitude of about 40 km, the vehicle enters into hypersonic flight and due to the high altitude, the dynamic pressure reduces to a smaller value. Generally the stage separation occurs at the hypersonic regime with the dynamic pressure of the order of 100–200 Pa. Subsequent flight phase follows transitional and finally free molecular flight regime.

During the atmospheric flight phase, laminar, turbulent, separated flows, steady flows and unsteady flows occur on the vehicle. The various aerodynamic flow features as explained above along with the free stream characteristics, flight environment, size and shape of the vehicle and protrusions cause steady and unsteady loads on the overall vehicle structure and vehicle subsystems. These loads are essentially due to skin friction, pressure variations, shock waves, their interactions, separated flows, vortex-induced and interference effects. The skin friction effects

are generated due to viscosity of fluid whereas non-uniform pressure distribution caused by the vehicle geometry at a particular attitude produces pressure force. The shock wave causes additional steady loads and also unsteady loads if associated with flow separation. In addition to this, there can be a load induced by vortices of wake flow. The interference between the bodies of considerable size such as core and strap-on motors in the clustered launch vehicle configuration causes interference loads.

Total aerodynamic loads on launch vehicle systems are categorized into

1. Overall force and moment on the vehicle
2. Launch vehicle surface steady pressure distribution
3. Distributed steady aerodynamic loads along the vehicle structure
4. Low-frequency unsteady loads on the vehicle structure
5. Unsteady pressure fluctuations greater than 20Hz frequency causing aeroacoustic loads
6. Steady and unsteady pressure loads at the protrusion locations

The steady loads are generally represented as integrated forces and moments on the vehicle as well as sectional forces and in certain cases in terms of pressure loads. Unsteady loads are generally represented in terms of pressure fluctuations. The magnitude of various loads acting on a launch vehicle during atmospheric flight regime is higher than the other flight regimes and the vehicle systems are designed for such loads. Therefore, the atmospheric regime of flight is the most crucial one for a launch vehicle ascent mission. The overall vehicle aerodynamic force and moment and the aerodynamic characteristics with steady and unsteady loads on various subsystems during atmospheric flight regime are explained in the following sections.

10.3.1 Representation of Aerodynamic Forces and Moments

Airflow over the vehicle causes shear force due to skin friction between air particles and vehicle body which is primarily a function of wetted surface area, Reynolds number, Mach number and surface roughness of the vehicle. In addition, due to airflow, changes in local velocity and pressure are created by the vehicle geometry. They are also influenced by the flow incidence angle to the body, shock waves and effects of induced flow and interference of multiple bodies. Pressure is a measure of momentum of air particles; change in pressures results into the change of momentum of air particles and the change in momentum produces force, called pressure force. Therefore, pressure distribution and its variation around the vehicle surface generates a net force acting on the vehicle and a net moment about its centre of gravity. The force and moment thus generated are due to incremental pressure forces, which are normal to the vehicle body. The shear force is along the body and these forces are caused by the airflow over the launch vehicle body due to relative motion of vehicle with respect to air. The shear and pressure force acting on the

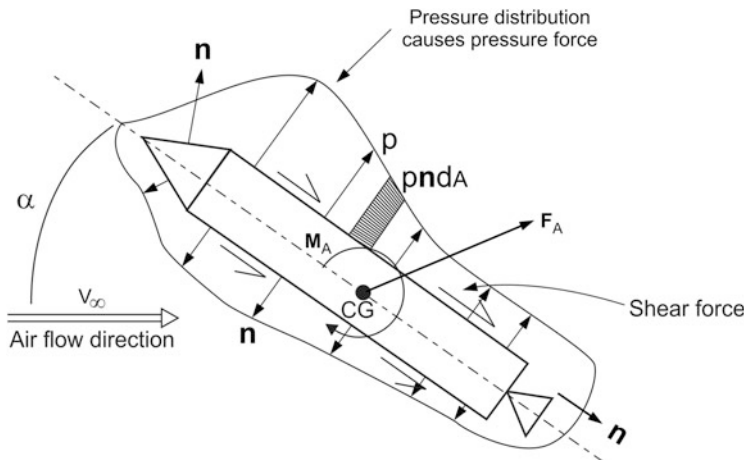


Fig. 10.8 Aerodynamic force and moment generation phenomenon

vehicle and moment due to them about centre of gravity of the vehicle are represented in Fig. 10.8.

The pressure forces acting normal to the vehicle are computed as the vector sum of the product of pressure and area around the entire vehicle body as given below:

$$\mathbf{F}_p = \oint p \mathbf{n} dA \quad (10.3)$$

where

p = Pressure at the specified location

\mathbf{n} = Normal vector at the specified location

dA = Infinitesimal area considered at the specified location

This, along with the shear force \mathbf{F}_S , forms the vector aerodynamic force as given below:

$$\mathbf{F}_A = \mathbf{F}_S + \mathbf{F}_p \quad (10.4)$$

Similarly, the vector aerodynamic moment about centre of gravity \bar{M}_A is expressed as

$$\mathbf{M}_A = \mathbf{M}_S + \mathbf{M}_p \quad (10.5)$$

where

\mathbf{M}_S = Aerodynamic moment contribution due to shear force

\mathbf{M}_p = Aerodynamic moment contribution due to pressure force

For the given shape of a vehicle, the aerodynamic force and moment depend on the following parameters:

1. Relative orientation of the vehicle with respect to airflow (α). This is defined as the angle between vehicle longitudinal axis and relative free stream velocity vector
2. Free stream speed (V_∞), i.e. the magnitude of relative velocity of air with respect to the vehicle
3. Free stream density (ρ_∞), i.e. local density of air at the vehicle operating altitude
4. Viscosity of air (μ_∞) (the shear force due to this contributes to the aerodynamic force and moment)
5. Size of the body: represented by the reference length D_{ref}
6. Compressibility of the air: It is related to the variation of density throughout the flow field around the body and certainly the aerodynamic forces and moments are sensitive to any such variation. In turn, compressibility of air is related to the speed of sound (a_∞) in air at the vehicle operating altitude

Therefore, the magnitude of aerodynamic force on a launch vehicle and moment about its centre of gravity with a given shape may be expressed as

$$F_A = f_1(\alpha, V_\infty, \rho_\infty, \mu_\infty, D_{ref}, a_\infty) \quad (10.6)$$

$$M_A = g_1(\alpha, V_\infty, \rho_\infty, \mu_\infty, D_{ref}, a_\infty) \quad (10.7)$$

The aerodynamic forces and moments are generally represented in their non-dimensional coefficient form through similarity parameters because of the ease in generation and application. The force coefficient C_F is given by

$$C_F = \frac{F_A}{q_\infty S_{ref}} \quad (10.8)$$

where q_∞ is the free stream dynamic pressure and S_{ref} is the reference area. Similarly, the moment coefficient C_M is given by

$$C_M = \frac{M_A}{q_\infty S_{ref} D_{ref}} \quad (10.9)$$

where D_{ref} is the reference length (for launch vehicle, diameter is used as reference length).

Thus, the force and moment coefficients which define the aerodynamic characteristics of a launch vehicle are expressed as

$$C_F = f_2(\alpha, V_\infty, \rho_\infty, \mu_\infty, D_{ref}, a_\infty) \quad (10.10)$$

$$C_M = g_2(\alpha, V_\infty, \rho_\infty, \mu_\infty, D_{ref}, a_\infty) \quad (10.11)$$

During atmospheric flight phase, the vehicle velocity continuously increases, and correspondingly, vehicle altitude also increases. Therefore, the density of air at the operating environment reduces continuously along with the corresponding changes in air viscosity. In order to take care of the variations in the operating environment of the vehicle and also the vehicle size, the Reynolds and Mach numbers are used.

Considering these, the aerodynamic coefficients are considered as functions of the non-dimensionalized parameters as given below:

$$C_F = f_3(\alpha, R_e, M) \quad (10.12)$$

$$C_M = g_3(\alpha, R_e, M) \quad (10.13)$$

For a complex external configuration of a vehicle, these coefficients are generated in wind tunnel tests using scaled-down model simulating all the required external features of the vehicle and the required α , R_e and M as in flight conditions. Using the wind tunnel evaluated aerodynamic coefficients, for the actual flight configuration with real flight environments, the aerodynamic forces and moments are computed as given below:

$$F_A = C_F q_\infty S_{ref} \quad (10.14)$$

$$M_A = C_M q_\infty S_{ref} D_{ref} \quad (10.15)$$

where q_∞ is the dynamic pressure during flight and is given by

$$q_\infty = \frac{1}{2} \rho_\infty V_\infty^2 \quad (10.16)$$

ρ_∞ = Instantaneous density of air at the vehicle operating altitude

V_∞ = Relative velocity of vehicle with respect to the atmosphere

S_{ref} = Reference area of actual vehicle, corresponding to the one used in the model for generating the coefficient

D_{ref} = Reference length of actual vehicle, corresponding to the one used in the model for generating the coefficient

10.3.2 Aerodynamic Force and Moment Model for a Generic Launch Vehicle

During a launch vehicle flight, the magnitude and direction of aerodynamic force and moment about its centre of gravity are dependent on (1) the vehicle configuration, (2) vehicle operating environment parameters and (3) vehicle attitude with respect to the free stream velocity. The vehicle attitude in turn depends on the rotational and linear motions of the vehicle and the wind magnitude and direction, which is a function of altitude and highly random. Therefore, the magnitude and

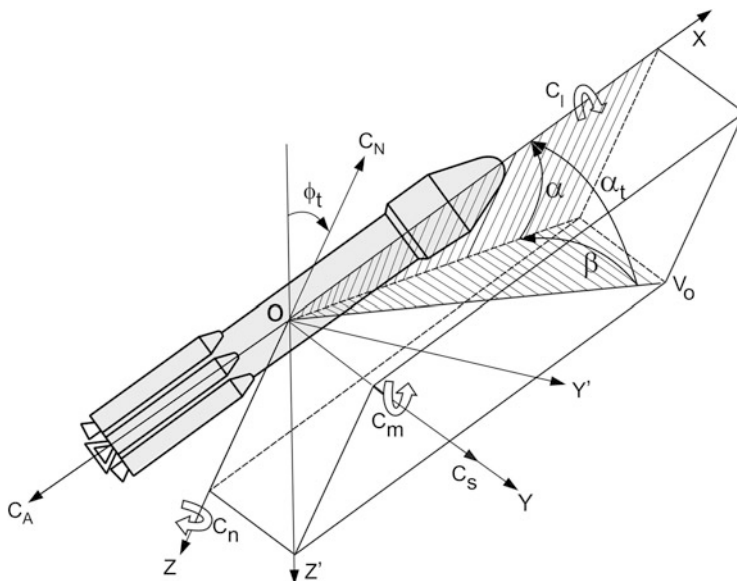


Fig. 10.9 Overall aerodynamic forces and moments on a typical launch vehicle

direction of vehicle attitude with respect to the airflow as well as the aerodynamic force and moment vectors are highly random during flight. To understand and analyze the flow direction, aerodynamic force and moment vectors, these parameters are resolved conveniently in a reference frame fixed to the vehicle. Generally, launch vehicle aerodynamicists follow the body axes frame as referred in Fig. 10.9. The aerodynamic coefficients measured in the wind tunnel are referred in the above frame. It is to be noted that this reference frame is different from the one used in Chap. 8. Suitable coordinate transformation can be applied for transforming the data represented in the reference frame of Fig. 10.9 to the one given in Chap. 8. The reference frame represented in Fig. 10.9 is explained below:

O = Centre of gravity of the vehicle

X = Along the longitudinal axis of the vehicle, pointing towards nose

Z = Along the lateral direction, aligned with launch plane and pointing towards launch direction at the time of lift-off

Y = Along another lateral direction, completes the right-handed triad

ZX plane is referred as the pitch plane and YZ plane is referred as the yaw plane. X axis is called the roll axis of the vehicle, Y axis is referred as the pitch axis and Z axis is referred as the yaw axis of the vehicle.

The airflow direction is defined with respect to the vehicle axis frame through a cone angle (α_t) and a clock angle (ϕ_t) as given below:

α_t = Angle between free stream relative velocity vector and vehicle longitudinal axis (X-axis)

ϕ_t = Angle between projection of relative velocity vector on YZ plane and Z-axis

Usually, α_t is referred as the total angle of attack and ϕ_t is referred as the aerodynamic flow roll angle. The airflow direction can also be defined with respect to the pitch and yaw planes of the vehicle as given in Fig. 10.9.

α = Angle of attack, angle between longitudinal axis (X-axis) and projection of relative velocity vector in the pitch plane (ZX-plane). This angle defines the airflow in the pitch plane.

β = Yaw angle of attack (side slip angle in aircraft notation), angle between the relative velocity vector and its projection in the pitch plane. This angle defines airflow in the yaw plane.

Aerodynamicists usually resolve aerodynamic forces and moments in stability axis frame. According to this notation, the force along the relative velocity direction (opposite to free stream velocity direction) is referred as drag whereas force normal to the velocity direction is referred as lift. For launch vehicle applications, the aerodynamic force and moment vectors are resolved along the vehicle body axes as given below:

C_A : Axial force coefficient, acts along X-axis of the vehicle

C_N : Normal force coefficient, acts along Z-axis of the vehicle

C_S : Side force coefficient, acts along Y-axis of the vehicle

C_l : Rolling moment coefficient, which produces aerodynamic moment about longitudinal axis (X-axis) of the vehicle

C_m : Pitching moment coefficient, which produces aerodynamic moment about pitch axis (Y-axis) of the vehicle

C_n : Yawing moment coefficient, which produces aerodynamic moment about yaw axis (Z-axis) of the vehicle

Generally C_A and C_N are defined positive along the direction opposite to X and Z axes of the vehicle respectively while C_S is defined positive along the positive direction of Y. The sign convention of C_l , C_m and C_n is positive for positive rotation about roll, pitch and yaw axes respectively. For small angles of attack, as in the general case of launch vehicle flights, axial force is very close to drag and normal force is very close to lift.

The aerodynamic force components along the vehicle axes are given by

$$F_{AX} = C_A q_\infty S_{ref} \quad (10.17)$$

$$F_{AY} = C_S q_\infty S_{ref} \quad (10.18)$$

$$F_{AZ} = C_N q_\infty S_{ref} \quad (10.19)$$

and the moment components about the vehicle axis are

$$M_{AX} = C_l q_\infty S_{ref} D_{ref} \quad (10.20)$$

$$M_{AY} = C_m q_\infty S_{ref} D_{ref} \quad (10.21)$$

$$M_{AZ} = C_n q_\infty S_{ref} D_{ref} \quad (10.22)$$

Each of the coefficients of Eqs. (10.17), (10.18), (10.19), (10.20), (10.21), and (10.22) is a function of the variables α , β , $\dot{\alpha}$, $\dot{\beta}$, p , q , r and can be expanded in Taylor series form about some operating conditions (normally zero angle of attack). The general expression for any C_θ , where θ stands for A, S, N, l, m, n, of the Eqs. (10.17), (10.18), (10.19), (10.20), (10.21), and (10.22) is given below:

$$\begin{aligned} C_\theta = & C_{\theta 0} + C_{\theta \alpha} \alpha + C_{\theta \beta} \beta C_{\theta \alpha \beta} \alpha \beta + \frac{D_{ref}}{2V_\infty} C_{\theta \dot{\alpha}} \dot{\alpha} + \frac{D_{ref}}{2V_\infty} C_{\theta \dot{\beta}} \dot{\beta} \\ & + \frac{D_{ref}}{2V_\infty} C_{\theta p} p + \frac{D_{ref}}{2V_\infty} C_{\theta q} q + \frac{D_{ref}}{2V_\infty} C_{\theta r} r + \dots \text{higher order terms} \end{aligned} \quad (10.23)$$

where

$C_{\theta 0}$ = Aerodynamic coefficient for zero angle of attack

$C_{\theta \alpha}$ = $\frac{\partial C_\theta}{\partial \alpha}$ etc.

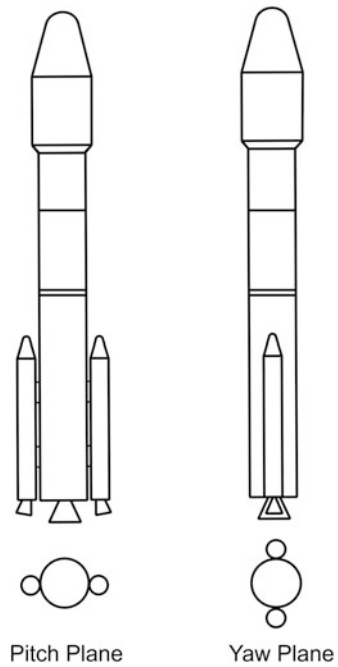
D_{ref} = Reference length

and the quantity ($D_{ref}/(2V_\infty)$) is used to ensure the corresponding coefficients are dimensionless. The coefficients $C_{\theta \alpha}$, $C_{\theta \beta}$, etc. are the stability derivatives and normally independent of the variables α , β , $\dot{\alpha}$, $\dot{\beta}$, p , q and r .

For a near axi-symmetric body like launch vehicle, flying at small angles of attack, the flow angle α can be assumed to generate normal force coefficient C_N and pitching moment coefficient C_m and correspondingly F_{AZ} and M_{AY} . Similarly the flow angle β can be assumed as the cause for the side force coefficient C_S and yawing moment coefficient C_n and correspondingly F_{AY} and M_{AZ} . But the rolling moment coefficient C_l and M_{AX} is the combined effect of α and β and vehicle asymmetry. The axial force coefficient C_A and F_{AX} is due to the combined effect of α and β as well as shear force. Aerodynamic forces and moments for a typical launch vehicle flying at small angles of attack are explained below. Even though the launch vehicles are generally axi-symmetric, due to functional requirements, the configuration of the vehicle in pitch and yaw planes can be different as given in Fig. 10.10.

Due to the pressure distribution around the vehicle, there is a net aerodynamic force acting on the vehicle and aerodynamic moment acting about its centre of gravity. These effects can be modelled as the aerodynamic force acting at a location called aerodynamic centre of pressure and the moment caused by this aerodynamic force about the centre of gravity of the vehicle is equivalent to the moment due to the distributed aerodynamic force over the vehicle. Generally, for these configurations, the normal or side forces at zero angles of attack are negligible and the axial force coefficient variation due to angle of attack is very small compared to that of zero angle of attack values. In addition, due to functional requirements, protrusions on the vehicle may affect the symmetry of the vehicle, and this introduces rolling

Fig. 10.10 Typical launch vehicle configuration



moment even for zero angles of attack and gets further aggravated by the combined effects of angles of attack. Also, for the configuration with multiple strap-on motors, the errors caused during the assembly of the motors with core vehicle introduce aerodynamic rolling moment.

Thus, the aerodynamic force and moment model with respect to the vehicle axes (as defined in Fig. 10.9) for a typical launch vehicle configuration (as given in Fig. 10.10) with near zero angle of attack is represented in Fig. 10.11. The governing equations are as given below:

$$F_{AX} = -C_{A_0} q_\infty S_{ref} \quad (10.24)$$

$$F_{AY} = C_{S\beta} \beta q_\infty S_{ref} \quad (10.25)$$

$$F_{AZ} = -C_{N_\alpha} \alpha q_\infty S_{ref} \quad (10.26)$$

$$M_{AX} = (C_{l_0} + C_{l_{\alpha\beta}} \alpha \beta + C_{l_\delta} \delta) q_\infty S_{ref} D_{ref} \quad (10.27)$$

$$M_{AY} = C_{N_\alpha} \alpha q_\infty S_{ref} (X_{cg} - X_{cp}) \quad (10.28)$$

$$M_{AZ} = C_S \beta q_\infty S_{ref} (X_{cg} - X_{cy}) \quad (10.29)$$

where the coefficient values are assumed to be positive for positive angles of attack.

The parameters given in Eqs. (10.24), (10.25), (10.26), (10.27), (10.28) and (10.29) are

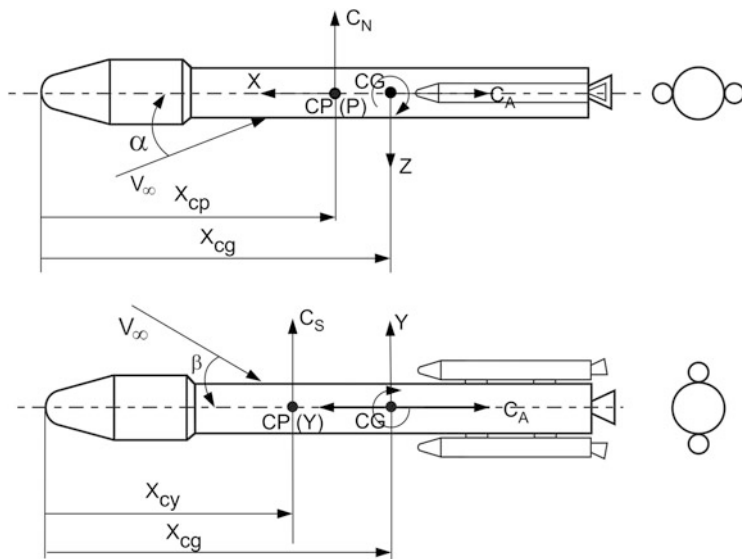


Fig. 10.11 Aerodynamic force and moment of a launch vehicle

C_{A_0} = Axial force coefficient for zero angle of attack. The variation of axial force coefficient for non-zero angle of attack is assumed to be very small.

C_{S_β} = Side force slope. The side force is assumed to be linear with respect to yaw angle of attack for small angles.

C_{N_α} = Normal force slope. The normal force is assumed to be linear with respect to pitch angle of attack for small angles.

C_{l_0} = Rolling moment coefficient for zero angle of attack.

$C_{l_{\alpha\beta}}$ = Rolling moment coefficient slope for the combined α and β .

C_{l_s} = Rolling moment coefficient slope due to the misalignment of strap-on motors and fin attachments, etc.

X_{cg} = Centre of gravity of the vehicle, measured from nose tip

X_{cp} = Aerodynamic centre of pressure in pitch plane, measured from nose tip

X_{cy} = Aerodynamic centre of pressure in yaw plane, measured from nose tip

10.4 Aerodynamic Characteristics and Loads

Aerodynamic characteristics of a launch vehicle during various phases of its atmospheric flight, different types of aerodynamic loads acting on the overall vehicle/its subsystems and their importance for the launch vehicle systems design are explained in this section. Methods of characterizing these loads are also outlined.

10.4.1 Lift-Off Phase

Ground winds play a major role in the vehicle aerodynamic characteristics, the vehicle response during its stay at launch pad and lift-off. During this phase, the ground winds flow over the vehicle almost normal to the vehicle longitudinal axis. Since the vehicle velocity is negligibly small compared to the wind speed (zero at launch pad), the vehicle attitude with respect to the free stream velocity is close to 90° . As the vehicle velocity builds up, the angle of attack reduces to a smaller value as shown in Fig. 10.12.

Also, magnitude of the relative velocity of the vehicle is small in this phase. Therefore, the aerodynamic characteristics of the vehicle on the launch pad and during lift-off phase are corresponding to the incompressible flows with large angles of attack. The flow is dominantly viscous and the aerodynamic load acting on the vehicle is mainly due to wind.

In addition to the steady loads, due to bluff body nature of the vehicle at these large angles of attack, the flow is separated from the body in the leeward side as shown in Fig. 10.13 (for the case of wind blowing from the vehicle to the umbilical tower). The separated flow generates vortex-induced unsteady loads on the vehicle.

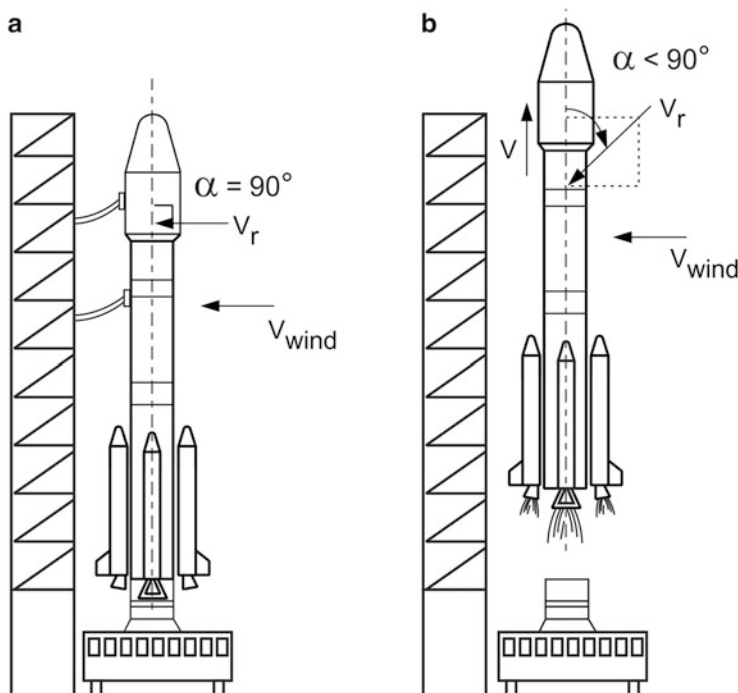


Fig. 10.12 Angle of attack during lift off phase (a) Vehicle on the Pad (b) Lift-off Phase

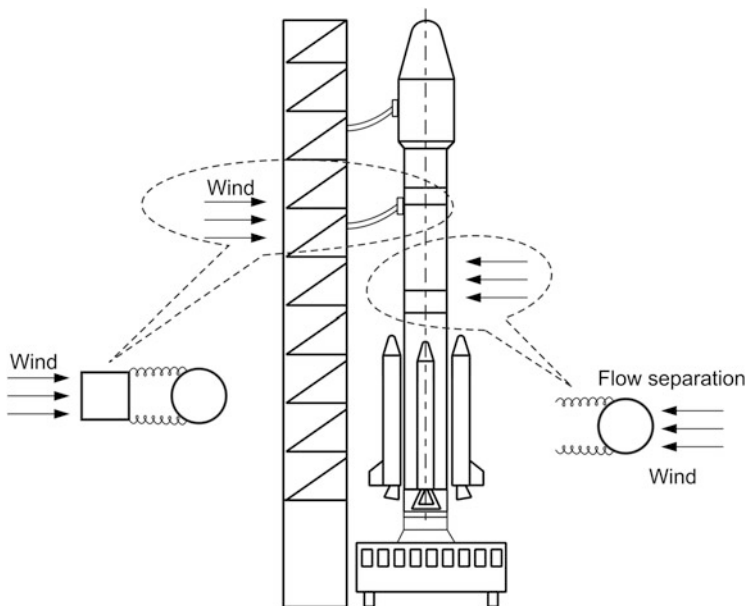


Fig. 10.13 Aerodynamic flow at launch pad

The unsteady loads act on the vehicle due to wake generated by umbilical tower as indicated in Fig. 10.13 (for the wind blowing from umbilical tower direction towards the vehicle). The above unsteady low-frequency load along with the flexible nature of the vehicle can cause serious concern for the structural design. These effects are generally characterized through the experiments with rigid and aeroelastic models of the vehicle and engineering methods based on the cross flow theory. In effect, total aerodynamic forces acting on the vehicle are summarized as

- Load due to steady wind
- Load due to wind gust
- Unsteady low-frequency loads
- Umbilical tower-generated unsteady loads

The effect of steady wind during this phase is very crucial for the safety of the ascent phase mission. The load distribution at 90° angle of attack for a typical launch vehicle is shown in Fig. 10.14.

The integrated value of force coefficient for the case of constant lateral velocity throughout the vehicle length assuming rigid vehicle is given by

$$C_N = \frac{1}{S_{ref}} \int_0^1 \frac{S(x) dC_N}{xdx} dx \quad (10.30)$$

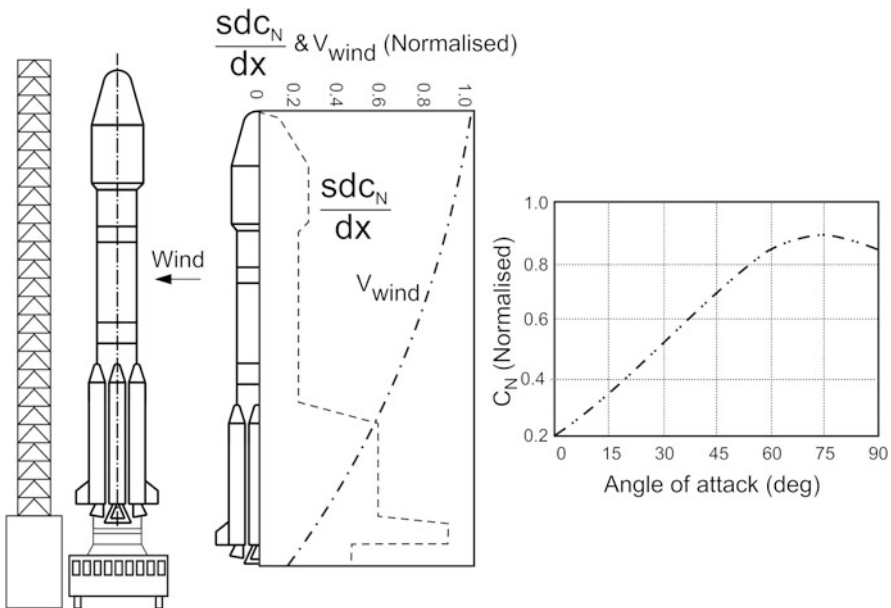


Fig. 10.14 Vehicle on launch pad and aerodynamic characteristics

The aerodynamic force coefficient as function of angle of attack is also given in Fig. 10.14. Therefore, aerodynamic force and moment about centre of gravity are given by

$$F_A = C_N q S_{ref} \quad (10.31)$$

$$M_A = F_A (X_{cp} - X_{cg}) \quad (10.32)$$

where S_{ref} = reference area

$$q = \frac{1}{2} \rho_0 V_r^2$$

ρ_0 = sea-level density

V_r = wind velocity when vehicle is on the launch pad = V_w

= resultant of V_w and vehicle velocity V during lift-off

X_{cp} = centre of pressure location from nose tip

X_{cg} = centre of gravity location from nose tip

Depending on the wind direction, the aerodynamic force causes the drift of the vehicle and the aerodynamic moment rotates the vehicle towards or away from the umbilical tower. Therefore, in order to ensure the safe lift-off, it is essential to launch the vehicle when the ground winds are less than the allowable limiting wind speed, which is a function of the aerodynamic characteristics and inertial properties of the vehicle.

Generally, the vehicle length will be of the order of 40–50 m, and due to the ground effects, the wind velocity near to the ground varies along the vehicle length as given in Fig. 10.14. In this case, the aerodynamic force on the vehicle is given as

$$F_A = \int_0^L S(x) \frac{dC_N}{dx} q(x) dx \quad (10.33)$$

where

$$q(x) = \frac{1}{2} \rho_0 V^2(x) \quad (10.34)$$

$V(x)$ = wind velocity at the station location x

The aerodynamic force computed by Eq. (10.33) is different from that computed by Eq. (10.31). In addition, the variation of wind velocity with respect to the vehicle length shifts the centre of pressure as compared to that used in Eq. (10.32). The combination of these effects has different impacts on the lift-off dynamics of the vehicle. Therefore, for launch clearance, the realistic wind profile as well as constant wind profile are to be considered and the one which drifts the vehicle more towards the umbilical tower has to be considered for the launch clearance.

In addition, it is necessary to analyze the response of the vehicle to unsteady loads due to gusts and turbulent wake from the umbilical tower. These parameters are generated using wind tunnel test on aeroelastic model to find out the high-amplitude self-excited oscillations.

Not only the vehicle is analyzed for the safe launch clearance but the launch hold mechanism is also to be introduced to avoid toppling of the vehicle due to the wind. The vehicle structural designs should ensure sufficient design margins under these loads. In addition, dampers are to be provided between umbilical tower and vehicle to damp out the oscillations.

10.4.2 High-Dynamic Pressure Flight Phase

Once the vehicle reaches the Mach number 0.3, the compressibility effects become predominant and the remaining part of launch vehicle flight is in the compressible flow regime. The compressibility effects bring new dimension, i.e. the formation of shocks over the vehicle. The shocks introduce discontinuity in the flow characteristics and all the flow parameters, namely, pressure, temperature and density, change almost instantaneously across the shock which increases the steady and unsteady aerodynamic loads on the vehicle.

Compressible flow regime in the high-dynamic pressure flight phase can be classified into subsonic, transonic, supersonic and hypersonic flight regimes.

During subsonic flight regime, the flow over the body does not have shock waves and hence is relatively smooth. During the transonic flow regime, shock starts forming over the body. These shocks may be strong or weak, normal or oblique depending on the free stream Mach number. The shock formation in the leeward and windward side causes large differential pressure which increases the load on the vehicle, both along lateral and axial directions, during this flight regime. The shock position changes with time, thus causing pressure fluctuation. In addition, the shocks interact with the boundary layer and flow separates from the body which causes unsteady loads.

In the supersonic flow regime, there is an attached shock in front of the body and the flow is relatively smooth as compared to the transonic flight regime. Due to reduced pressure differential between the windward and leeward side of the vehicle in this flow regime, the aerodynamic loads decrease with Mach number. For the hypersonic flow regime, the temperature effects influence the flow characteristics, and for $M > 10$, the aerodynamic loads are almost independent of Mach number.

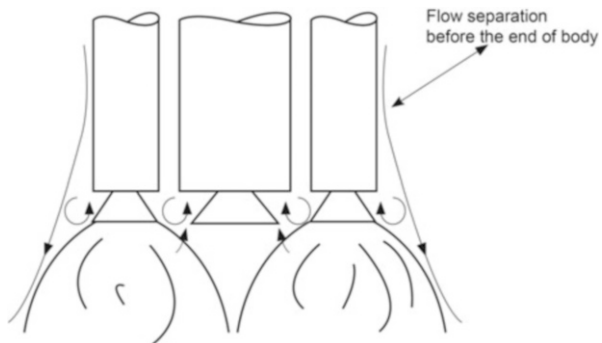
As the vehicle velocity increases, even though density decreases, due to the product of ρ and V^2 , the dynamic pressure also builds up. Dynamic pressure is significantly higher when the vehicle passes through the most complex transonic flight regime. The in-flight wind speeds are also peaking along with high wind shear during the high-dynamic pressure flight phase which again is close to the transonic flight regime. To reduce the aerodynamic loads in this region, the launch vehicle trajectories are designed to fly near zero angle of attack utilizing the winds measured closer to the launch time. But the actual in-flight wind variations along with the unexpected wind shear over the expected ones induce angles of attack which in turn cause aerodynamic loads on the vehicle.

The following steady and unsteady loads acting on the vehicle during this crucial and complex atmospheric flight regime are the major inputs for the vehicle structural, control and other subsystems design:

1. Steady aerodynamic forces and moments
2. Steady pressure and load distributions
3. Unsteady loads
4. Additional loads due to aeroelastic effects
5. Loads on protrusions
6. Loads pertaining to special aerodynamic problems
7. Steady Aerodynamic Forces and Moments

The overall aerodynamic characteristics of the vehicle are represented in their coefficient form because of the ease in generation and application. These coefficients are generated for the operating flight regime of high dynamic pressure (typically Mach number range is 0.3–4) and wide angle of attack (typically from -6° to $+6^\circ$) using wind tunnel tests and through Computational Fluid Dynamics (CFD) simulations. The basic data is generated through wind tunnel tests with the scaled-down rigid model, simulating all the external features of the vehicle. Since the operating environments for the launch vehicle are near zero angle of attack, it is

Fig. 10.15 Jet and base pressure effects



advantageous to use the data in derivative form; therefore the aerodynamic force coefficient slope with respect to angles of attack is derived for the entire Mach number range and these data are used in different subsystems design process.

Due to the scaled-down model, some of the detailed protrusions and external features may not be possible to be captured in the wind tunnel models. Similarly, in order to withstand the extra loads due to the wind tunnel start-up and shut-down, the scaled-down models are designed with extra attachments which may not represent the true configuration of the vehicle. Such effects are evaluated through detailed CFD simulations and are incorporated.

Initially, the above data are generated using the wind tunnel models without jet. During flight, the free stream flow over the launch vehicle body interacts with the jet exhaust of the engine. As the altitude increases, the jet expands more due to lower atmospheric pressure. This jet acts like a bluff body and therefore, the free stream flow over the vehicle may separate on the aft body as shown in Fig. 10.15 and also there would be multiple jet interactions leading to reverse flow of the hot gases. This leads to loss of normal force on the aft portion of the vehicle and therefore the aerodynamic centre of pressure moves forward. The reverse flow in the vehicle base region causes the local pressure to be more than the ambient pressure which gives rise to base thrust; i.e. the net drag acting on the vehicle reduces. These effects are evaluated through CFD and added to the aerodynamic characteristics obtained using wind tunnel test results. Since this is an important phenomenon, which otherwise could be obtained only from the flight data, the jet effects are also being evaluated in wind tunnel tests using special purpose test rigs.

The measurement inaccuracies in the wind tunnel testing process, wind tunnel inaccuracies, scale effect and data normalization through derivatives, etc. introduce error in the aerodynamic coefficients prediction. Therefore, a dispersion band on the predicted aerodynamic data is generated to account for these inaccuracies and the actual aerodynamics during flight is expected to be within the specified dispersion band. Even though the vehicle subsystems are designed for the predicted

Fig. 10.16 Axial force coefficient

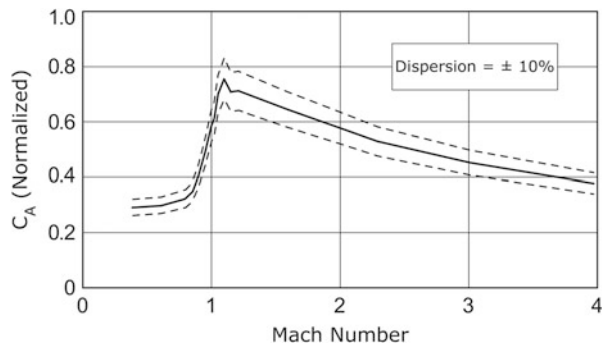


Fig. 10.17 Normal force coefficient

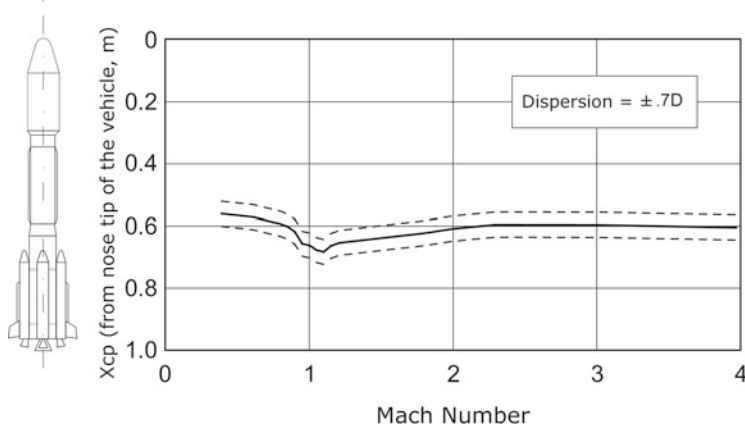
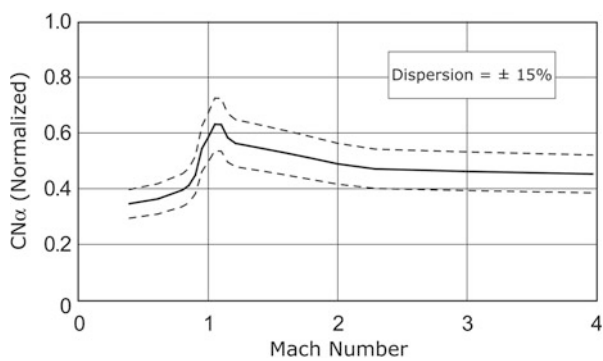


Fig. 10.18 Centre of pressure locations

aerodynamic data, the design has to ensure sufficient margins for these dispersions also.

The aerodynamic force coefficients along with the dispersion bounds for a typical launch vehicle are given in Figs. 10.16, 10.17, 10.18, 10.19 and 10.20.

Fig. 10.19 Rolling moment coefficient for zero angle of attack

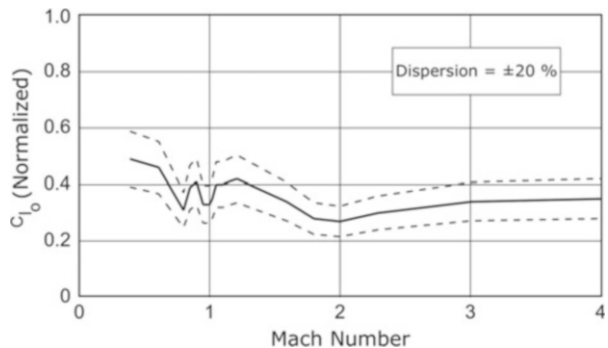
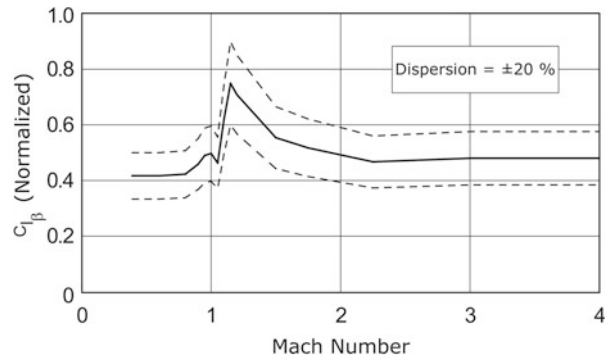


Fig. 10.20 Rolling moment coefficient due to strap-on attachment



10.4.2.1 Steady Pressure and Load Distribution

The pressure at any location around the vehicle surface caused by the aerodynamic flow is represented in terms of the non-dimensionalized parameter coefficient of pressure c_p as given below:

$$c_p = \frac{p - p_\infty}{q_\infty} \quad (10.35)$$

where

p = local pressure at the surface

p_∞ = free stream pressure

q_∞ = free stream dynamic pressure

It is to be noted that, for the area wherein local suction takes place, the local surface pressure is less than atmospheric pressure and c_p is negative.

For the location where pressure build-up occurs, the local pressure is more than ambient pressure which makes c_p positive. The c_p distribution along a typical generator in the windward and leeward direction of a typical launch vehicle is

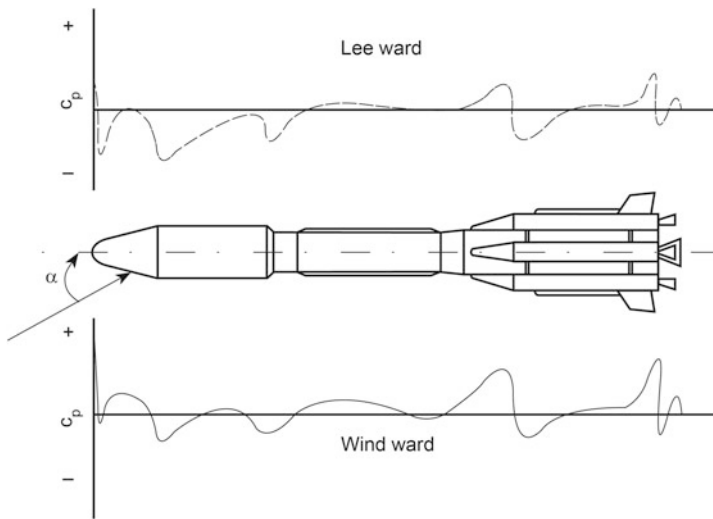


Fig. 10.21 Windward and leeward C_p distribution along vehicle length

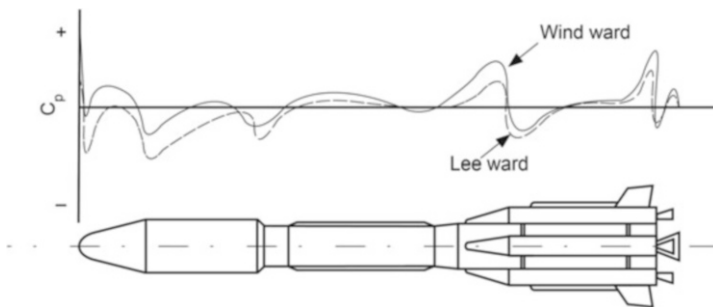


Fig. 10.22 Comparison of windward and leeward C_p distributions

represented in Fig. 10.21. The differential pressure between the windward and the leeward pressure distributions as represented in Fig. 10.22 causes aerodynamic force. The magnitude and direction of the force depend on the magnitude and sign of the localized c_p .

The pressure distributions as shown in Figs. 10.21 and 10.22 are the locus of distributions along two generators (leeward and windward side) of circumferential pressure distributions across each section from the vehicle nose tip.

The pressure distribution around the vehicle circumference at a typical location is given in Fig. 10.23.

The circumferential pressure distribution across each section as a function of aerodynamic roll angle ϕ is integrated to obtain the sectional loads along the normal and axial directions of the vehicle.

The infinitesimal element considered around a typical vehicle surface and the infinitesimal aerodynamic force due to pressure distribution are given in Fig. 10.24.

Fig. 10.23 C_p distribution around circumference at a typical location at a typical angle of attack, α

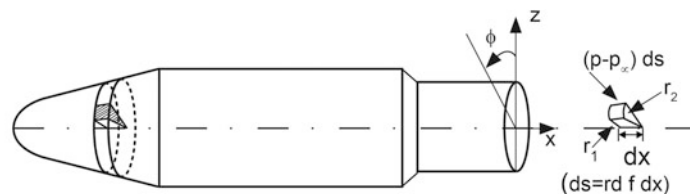
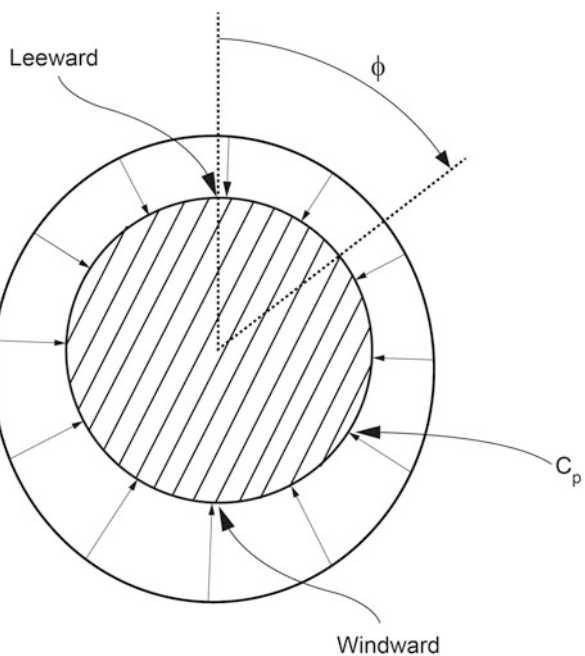


Fig. 10.24 Infinitesimal element and aerodynamic force due to pressure distribution

From the above figure, the infinitesimal normal force along Z-direction is given by

$$\Delta N = (p - p_{\infty}) ds \cos \phi \quad (10.36)$$

With substitution of relevant parameters as explained in Fig. 10.24, Eq. (10.36) can be written as

$$\Delta N = (p - p_{\infty}) r d\phi dx \cos \phi \quad (10.37)$$

where r is the average radius at the element location. Similarly, the infinitesimal axial force due to pressure distribution along X-direction is given by

$$\Delta A = (p - p_{\infty}) ds \frac{(r_2 - r_1)}{r} \quad (10.38)$$

where r_2 and r_1 are the radii within which the infinitesimal element is considered. With substitution of the relevant parameters, Eq. (10.38) can be written as

$$\Delta A = (p - p_\infty) d\phi dx \Delta r \quad (10.39)$$

where

$$\Delta r = r_2 - r_1 \quad (10.40)$$

Using the above equations, the sectional loads along the normal and axial directions due to pressure distributions around circumference are given as

$$S \frac{dC_{N\alpha}}{dx} = \frac{1}{\alpha} \int_0^{2\pi} c_p r \cos \phi d\phi \quad (10.41)$$

$$S \frac{dC_A}{dx} = \int_0^{2\pi} c_p \Delta r d\phi \quad (10.42)$$

The sectional normal load distribution thus obtained for a typical launch vehicle configuration is represented in Fig. 10.25.

The overall normal force and axial force coefficients are then obtained by integrating the sectional load distributions along the vehicle length as

$$C_{N\alpha} = \frac{1}{S_{ref}} \int_0^l \frac{S dC_{N\alpha}}{dx} dx \quad (10.43)$$

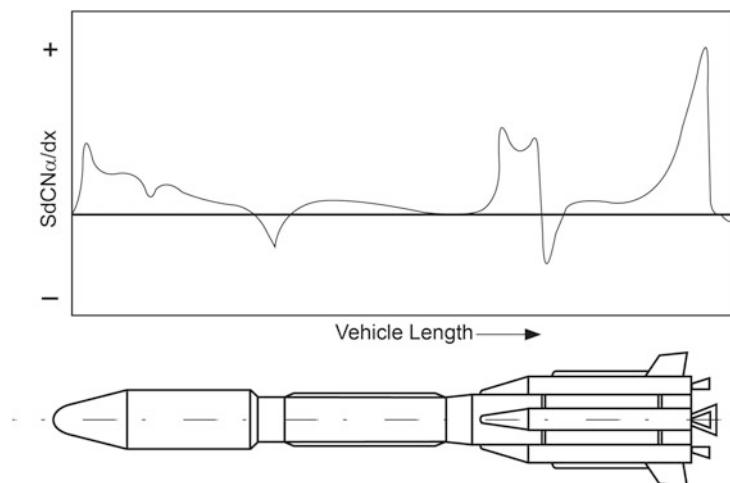


Fig. 10.25 Vehicle sectional load distributions

$$C_A = \frac{1}{S_{ref}} \int_0^1 \frac{S dC_A}{dx} dx \quad (10.44)$$

The overall aerodynamic force and moment are used for the mission design, performance evaluation, control designs and also for the vehicle load computations. The load distributions are used for computing sectional bending moments, shear force and equivalent axial force, thereby forming major inputs for the vehicle structural design. The load distributions are also essential for analyzing the vehicle structural response as well as to evaluate the control system performance of a flexible vehicle as part of aeroelastic phenomenon. The pressure distributions over the external functional protrusions are the major inputs for the structural designs of these subsystems. In addition, the surface pressure distributions are used for the vent hole and thermal protection systems design.

10.4.2.2 Unsteady Loads

In addition to the steady loads, the unsteady loads caused by various flow phenomena during atmospheric flight phase form an important input for the vehicle structural systems design. Specific feature of unsteady flows is the one in which all the flow quantities are fluctuating with respect to time. The main flow variable for the vehicle design is the pressure, wherein the fluctuations in it cause the time-varying unsteady loads on the vehicle. The primary source of unsteadiness is turbulence in the flow, wakes from the protrusions, shock movements over the surface of the vehicle during transonic regime of flight, flow separation caused by the shock-boundary layer interactions, geometrical flow separation and reattachment as represented in Fig. 10.26.

The unsteady loads contain pressure fluctuations with different frequency contents, varying from low to very high frequencies. While low-frequency contents are called buffet loads, the high-frequency part is referred as aeroacoustic loads. The low-frequency buffet loads excite the vehicle lateral flexible modes, thus introducing additional structural loads on the vehicle. Therefore, it is essential to consider the buffet load during overall structural design of the vehicle. High-frequency unsteady loads act as acoustic noise for the local structural elements wherein appropriate design improvements have to be incorporated to ensure structural integrity of the sensitive components during flight.

The unsteady loads on the vehicle are characterized through unsteady pressure measurements at specified locations on rigid models in wind tunnel tests.

Buffet

Buffet is the unsteady aerodynamic load on the vehicle structure caused by the unsteady pressure fluctuations. Buffet is classified as transonic buffet, wake buffet and shock-boundary layer separation buffet. Transonic buffet is caused by the

shock movements during low transonic to higher transonic regime of flight ($M = 0.8\text{--}1.2$). The wake buffet is due to the flow unsteadiness caused by wakes generated from the functional protrusions on the vehicle surface. Buffet load is also generated due to the flow separation at shock location as well as at the flow reattachment location due to shock-boundary layer interaction.

In addition to the buffet characterization through rigid model unsteady pressure measurements, the dynamic components of loads caused by the interactions of aerodynamic buffet and flexible vehicle modes are characterized through the wind tunnel aeroelastic model tests, simulating all the external features and dominant lateral structural modes of the vehicle.

It is always preferable to avoid buffet loads on a launch vehicle by suitable aerodynamic configuration design. Generally, forebody configuration of a launch vehicle influences the aerodynamic flow behaviour during its atmospheric flight phase and dominates the buffet contributions. Therefore, the payload fairing configuration plays a major role in generating buffet loads. NASA has generated a general guideline [3] for the buffet free configuration, which was arrived at based on extensive wind tunnel testing. The above guidelines for the buffet free configuration as per the forebody geometry given in Fig. 10.27 are outlined below:

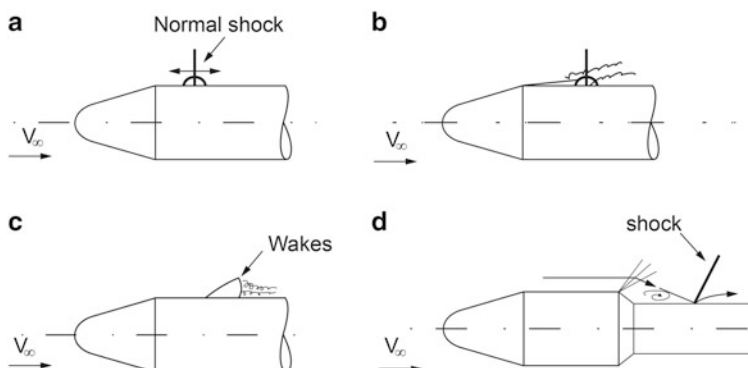


Fig. 10.26 Causes of unsteady loads. (a) Movement of shock wave during transonic regime. (b) shock boundary layer interaction cause flow separation. (c) Pressure oscillation due to wake. (d) Flow separation due to geometric shape and reattachment

	Criteria		
Geometrical parameters of launch vehicle forebody (payload fairing)	Buffet free	Buffet prone & stable (stable buffet)	Unstable buffet
l_1/D	≥ 0.8		
l_2/D	> 1.5		
δ_1	$\leq 15^\circ$		
D/d	< 1.1	< 1.6	> 1.6
δ_2	Not critical		

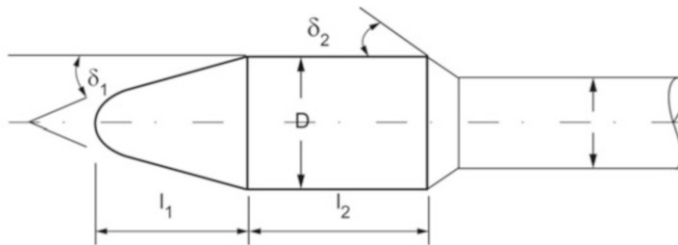


Fig. 10.27 Geometrical parameters of forebody for deciding buffet force configuration

If the guidelines are strictly followed, sometimes the payload may not be possible to be accommodated within the available payload envelope inside the payload fairing. Therefore, generally the launch vehicle configurations are designed with stable buffet configuration. For such vehicle configuration, the dynamic bending moments caused by the buffet loads are evaluated using wind tunnel tests. Vehicle structural design loads are suitably augmented for these additional contributions of the stable buffet loads.

The dynamic bending moment contribution due to buffet is measured using aeroelastic wind tunnel scaled-down model, simulating the fundamental flexible modes of the vehicle. The wind tunnel aeroelastic model is simulated with the flexible mode frequency as given below:

$$f_{\text{model}} = \frac{f_{\text{vehicle}}}{L} \quad (10.45)$$

where L is the model scaled-down factor.

Based on the dynamic bending moments measured on the model in the wind tunnel tests, dynamic bending moment at a specific location for the vehicle is computed as given below:

$$BM_{\text{vehicle}} = \left(\frac{BM_{\text{model}}}{Q_R L^2 x_{\text{model}}} \right) \times x_{\text{vehicle}} \quad (10.46)$$

where

Q_R = Ratio of wind tunnel dynamic pressure and flight dynamic pressure

x_{model} = location of the specific point on the model

x_{vehicle} = location of the same point on the vehicle

Typical dynamic bending moment measured in wind tunnel for a typical launch vehicle model is given in Fig. 10.28. The vehicle structural design loads are augmented with this load to ensure that vehicle structure is capable of handling the additional loads due to buffet.

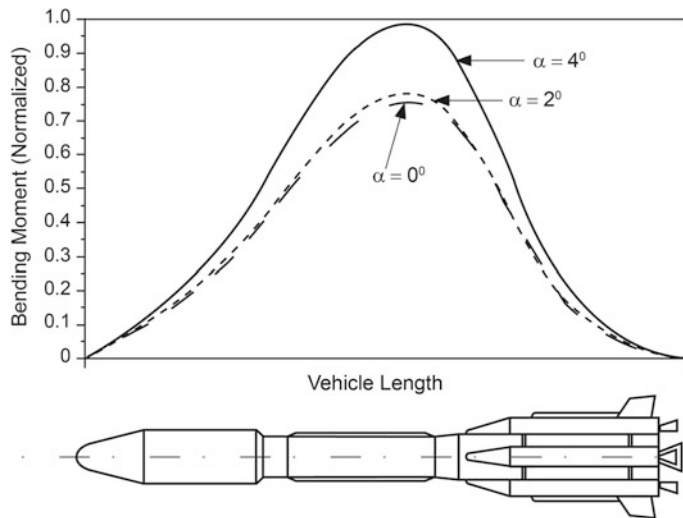


Fig. 10.28 Measured dynamic bending moment on a typical launch vehicle model

Aeroacoustics

Noise generated by pressure fluctuations from aerodynamic flow is called aeroacoustics. This phenomenon is dominant during transonic shock oscillations, separated flow and reattachment caused due to geometrical change such as payload fairing boat-tail and protrusions. While the buffet has the impact on the integrated vehicle structural design, the dynamic load generated by aeroacoustics has the effect on the local structural system design such as protrusions as well as on the vehicle subsystems mounted near to the specific location. Therefore, the sensitive subsystems, viz. avionic packages, sensors and control system actuators mounted near to the critical locations such as flow reattachment point are to be tested to the environmental levels generated by the aerodynamic noise. If the test results indicate high levels for such components, suitable design modifications are needed and necessary protective measures have to be taken.

The aeroacoustic levels at various locations on a vehicle during different regimes of flight are generated through unsteady pressure measurements in the wind tunnel model. Based on the test results, the acoustic levels are generated as given below.

The unsteady pressure is the time-dependent pressure fluctuations and therefore the wind tunnel-measured pressures have both steady (constant with time) and unsteady components.

$$P_{\text{total}} = P_{\text{steady}} + P' \quad (10.47)$$

where P' is the unsteady component.

The unsteady component P' is derived from the total pressure as

$$P' = P_{\text{total}} - P_{\text{steady}} \quad (10.48)$$

The average or root mean square (rms) of unsteady pressure at a specified location is given as

$$P'_{\text{rms}} = \sqrt{\frac{\sum_{i=1}^N (P_{\text{total}} - \bar{P})^2}{N}} \quad (10.49)$$

where

N = Total number of samples considered at the specified location for a particular flight condition (such as M , α , etc.)

\bar{P} = Mean steady value of pressure at the specified location for the specified flight condition

Coefficient of unsteady pressure is given as

$$C'_{P_{\text{rms}}} = \frac{P'_{\text{rms}}}{q_\infty} \quad (10.50)$$

where q_∞ is the free stream dynamic pressure.

The Overall Sound Pressure Level (OASPL) of the flow at the specified location for the given flight environment is then computed as

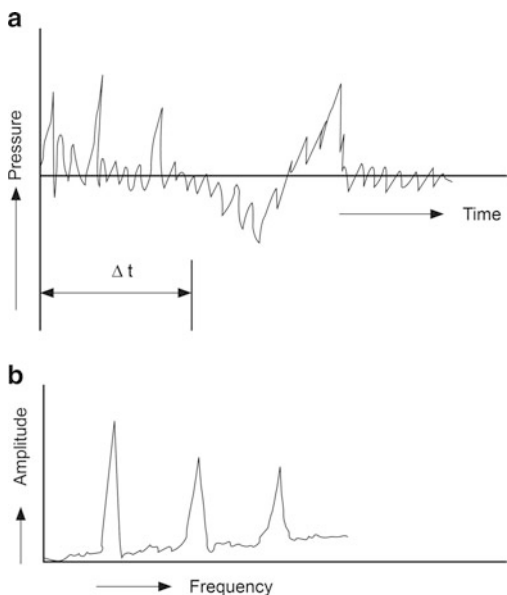
$$\text{OASPL} = 20 \log_{10} \left(\frac{C'_{P_{\text{rms}}} \times q_\infty}{P_{\text{ref}}} \right) \quad (10.51)$$

where P_{ref} is the reference pressure of sound, which human ear can hear and the value is given as

$$P_{\text{ref}} = 2 \times 10^{-5} P_a \quad (10.52)$$

The unsteady pressure measured above is time varying with different frequency content. It is important to analyze the frequency domain data rather than huge time domain data. These data can be analyzed for a particular time interval and fast Fourier transform (FFT) is generated, which gives the peak amplitudes at various frequencies as shown in Fig. 10.29 and based on the above, the spectrum is generated.

Fig. 10.29 Unsteady data processing. (a) Pressure variation at a specific location for a defined environment. (b) FFT of data during time interval ‘ Δt ’



The energy content of the pressure variation at the specified frequency is calculated from power spectral density (PSD), defined as

$$\text{PSD} = \frac{P'^2}{\Delta f} \quad (10.53)$$

where Δf is the frequency of interest (called resolution) and P' is the amplitude derived from FFT.

The unsteady pressure data can be analyzed for each frequency. But it is time consuming to analyze the signal for each frequency. To make the analysis easier, a set of frequencies are selected for analysis. If a set consisting of eight frequencies is considered for the analysis, it is called octave band analysis or 1 octave spectrum. Since octave spectrum is coarse, a finer band is defined using one third of octave band.

The Sound Pressure Level (SPL) spectrum is estimated from the PSD values as given below:

$$\text{SPL} = 10 \log_{10} \left[\frac{\text{PSD}_{\text{integrated}} \times \Delta f}{P_{\text{ref}}^2} \right] \quad (10.54)$$

As an example, let f_1, f_2, \dots be the frequencies and PSD_1, PSD_2, \dots the PSDs corresponding to the above frequencies, in order to get the SPL for the five-frequency interval, i.e. $f_1 - f_5$, and $f_6 - f_{10}$, etc.:

$$SPL = 10 \log_{10} \left[\frac{\left(\sum_{i=1}^5 PSD_i \right) \times 5}{P_{ref}^2} \right] \quad (10.55)$$

Generally, for the attached flow, OASPL is of the order of 148 dB to 150 dB for the dynamic pressure of about 40–50 kPa. For a typical launch vehicle during transonic flight regime, the OASPL measured at the flow reattachment location (caused by the geometry change) is about 160 dB for the dynamic pressure of about 40–50 kPa.

As the transonic Mach number increases, the transonic shock location changes, the flow impingement location varies and correspondingly the maximum OASPL location also changes. At a specified location for an identified Mach number, when the flow reattachment happens, the OASPL peaks and as the Mach number increases, the reattachment location is shifted. Therefore, in that specified location, the measured OASPL is less as indicated in Fig. 10.30a. For the case of unsteady loads due to protrusions, the OASPL measured is almost the same as given in Fig. 10.30b.

10.4.2.3 Aeroelastic Phenomenon

For a rigid vehicle, the flow incidence angle with respect to the external surface is the same at all locations. For the case of flexible vehicle, in addition to the rigid body incidence angle, the rotation of local surface with respect to the rigid vehicle introduces additional flow incidence angle to the local surface. Due to this varying angle of attack along the vehicle surface, the load distribution along the flexible vehicle length is different from that of rigid vehicle and hence the integrated overall aerodynamic force and moment are different. The aeroelastic phenomenon occurs in launch vehicles when vehicle structural deformation changes local angle of attack and thereby induces changes in the aerodynamic force. The additional aerodynamic force in turn increases the structural deformation which may lead to further increase in the aerodynamic forces. The interactions continue till achieving an equilibrium state for a structurally stable vehicle whereas for an unstable system, the interaction may lead to divergence, ending with vehicle failure. There are two categories of aeroelastic phenomenon in launch vehicles: (1) static aeroelasticity and (2) dynamic aeroelasticity.

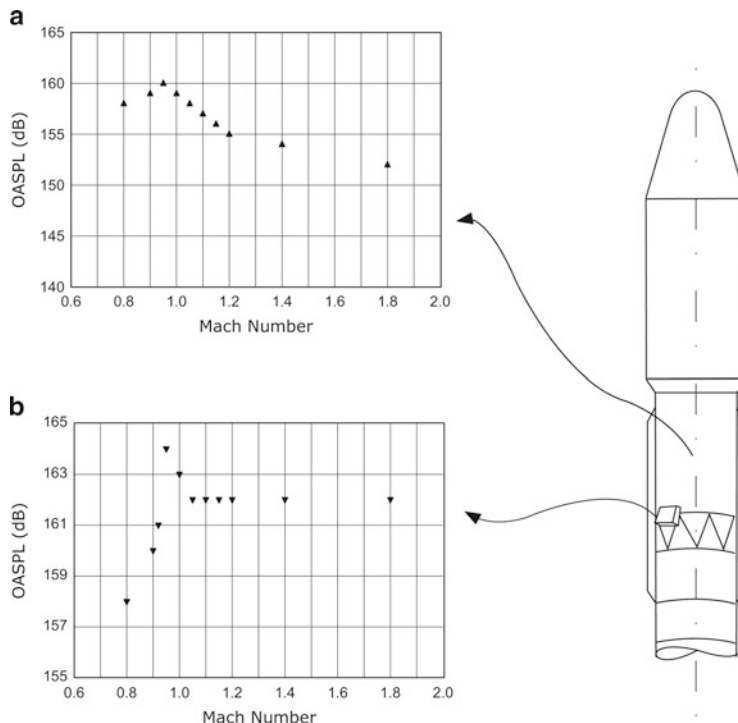


Fig. 10.30 Unsteady pressure measurement model & OASPL. (a) OASPL at a specified location (flow reattachment effect). (b) OASPL at specified locations (Protrusion effect)

Static Aeroelasticity Phenomenon

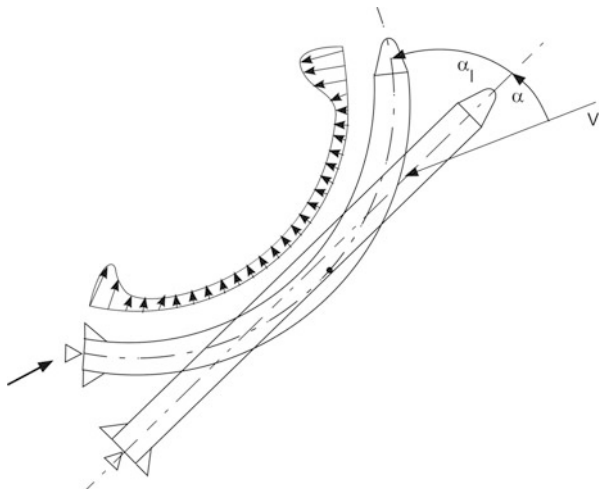
This is an interaction between aerodynamics and elastic structure of the vehicle. The integral value of aero load distribution over the vehicle gives the overall aerodynamic normal force coefficient as given in Eq. (10.43) and correspondingly the aerodynamic force as given in Eq. (10.26). But, realistically, the load distribution acts on the flexible vehicle as given in Fig. 10.31. Therefore, the net aerodynamic force is given by

$$F_N = \alpha q \int_0^1 S \frac{dC_{N\alpha}}{dx} dx + q \int_0^1 S \frac{dC_{N\alpha}}{dx} \alpha_l dx \quad (10.56)$$

where α is the rigid body angle of attack and α_l is the local angle of attack due to the elastic deformation of the vehicle.

Vehicle flexible modes have the following effects on the vehicle aerodynamics:

Fig. 10.31 Load distribution on flexible vehicle



1. Due to the vehicle deformation, the overall aerodynamic force and moment are different from the ones measured through rigid model.
2. Since the local angles of attack at different locations vary, the actual load distribution is different from that of rigid values which may further change the aerodynamic force and moment.

Therefore, it can be seen that, due to deformation of the vehicle, the aerodynamic force, moment and their distributions get altered, which in turn, along with control force activation, alters the structural deformation and the interaction continues.

It is therefore essential that the vehicle control system is designed to reduce the magnitude of interactions and the structural design loads are augmented considering the increased interactive loads.

Dynamic Aeroelastic Phenomenon

Dynamic aeroelastic phenomenon is due to the interaction between aerodynamic, elastic and inertial forces. Typical examples are flutter, gust response and buffet.

Flutter is a dynamic instability and is a self-induced vibration phenomenon wherein the aerodynamic forces on a component interact with its structural natural vibration mode to generate rapid increase in structural response. The vibration of the component increases local aerodynamic load acting on the component which in turn drives the component to vibrate further. If the aerodynamic excitation input energy in a cycle is more than the energy dissipation capability of the structure through its damping characteristics, the amplitude of structural response further increases resulting into self-excited oscillations. Due to atmospheric gust, aerodynamic flow changes. This introduces structural oscillations which further changes the aerodynamic flow resulting into forced dynamic response.

Buffet is another dynamic aeroelastic phenomenon which has been already discussed.

10.4.2.4 Effects of Protrusions

Launch vehicles are designed with suitable external aerodynamic configuration, to reduce the issues related to aerodynamic flow. However, to meet the functional requirements of mission, propulsion and avionic systems, there exists fairly good numbers of external protrusions which invariably do not possess a proper aerodynamic shape. Typical ones are the retro and ullage rocket motors, electrical cables, propellant feed lines, fuel supply and drain system and vehicle destruction system. Due to the aerodynamic loads acting on these protrusions, they have to be designed to withstand these loads. Also many of these protrusions are provided with suitable covering to protect against aerothermal loads. It is to be noted that these protrusions or protection systems are not the active load-carrying structures for the vehicle but are passive in nature.

These protrusions are generally blunt bodies in nature and affect the local steady aerodynamic flow over the vehicle, which introduces local steady aero load as well as unsteady loads. Depending on the size and shape of the protrusions, these local effects may have impact on the overall aerodynamic characteristics of the vehicle; nevertheless these localized loads have a major impact on the structural design of the protrusions, the attachments as well as their shapes. In addition, the local unsteady loads generated by these protrusions cause severe environments on the nearby sensitive elements, which need suitable protective systems. Even though they are passive systems, since they are attached to active structures, the main structure at these locations also needs to be strengthened; otherwise these local loads may cause failure of the vehicle structural system. Impacts of two typical protrusions on the aerodynamic characteristics are given below.

Wire Tunnel Ducts

On the propulsive stages, generally electrical cables are routed through external surface. Wire tunnel ducts used to carry the electrical cables are mounted on the vehicle surface as given in Fig. 10.32. Depending on the functional requirements, there are changes in the wire tunnel shapes and this forms a non-aerodynamic shape and causes local flow disturbances. The local flow acceleration and deceleration generate expansions and shocks leading to steady and unsteady loads. The effect of flow expansion introduces local suction pressure on the parent structure as shown in Fig. 10.32. If these local loads are not accounted in the design, it can lead to the failure of parent structure. In addition, it is essential to characterize the structure for the low-frequency unsteady load caused by such protrusions.

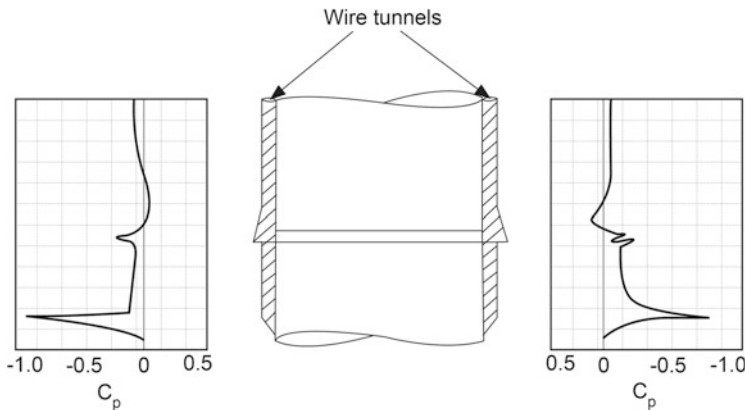


Fig. 10.32 Loads of typical wire tunnel ducts

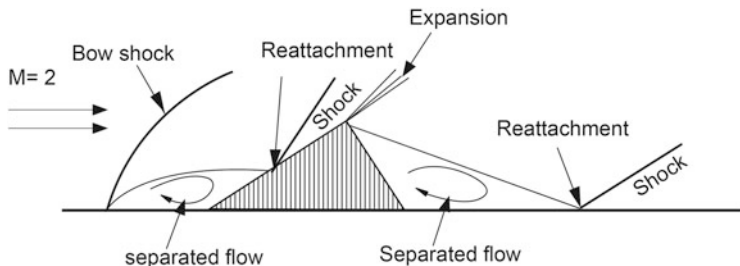


Fig. 10.33 Loads on umbilical covers

Umbilical Covers

Protective covers are implemented on the launch vehicle surface for safeguarding the protruded fuel supply and drain system in flight as given in Fig. 10.33. Shape of these protective covers greatly influences the local flow field. Due to large angles, the flows ahead of these covers are separated and reattached on it as shown in Fig. 10.33. The resultant shock introduces a higher unsteady pressure load on the system. Therefore, it is essential that the protective cover, nearby systems and the vehicle structure are characterized for the vibration environment generated by unsteady load due to the protrusion and suitable strengthening has to be incorporated in the launch vehicle system design process.

Therefore, to alleviate the loads due to these protrusions, wherever possible, suitable aerodynamic shaping has to be implemented. In addition, aerodynamic characterization has to be carried out with these protrusions and vehicle structure at these locations as well as protrusions are to be designed for the estimated steady and unsteady loads.

10.4.2.5 Specific Aerodynamic Problems

In addition to the effects of external aerodynamic flow explained so far the internal aerodynamic airflow also has an impact on certain systems of launch vehicle. Typical ones are (1) vent hole aerodynamics, (2) flow over open structures and (3) separations in aerodynamic flows. These issues are addressed as specific aerodynamic problems.

Vent Hole Aerodynamics

There are launch vehicle systems with certain amount of empty space after meeting the functional requirements. Typical examples are interstages, base shroud and payload fairing. These enclosures have the air or purged gas at local atmospheric pressure at the time of vehicle lift-off. As the vehicle ascends, the external ambient (atmospheric) pressure falls rapidly, whereas the pressures in these enclosures are nearly 1 atm of sea level (100 kPa) if not vented out. Thus the pressure differential across these enclosures increases from zero at lift-off to as high as 100kPa when the vehicle reaches higher altitude which has a major impact on these structures' design. In order to achieve minimum mass design for these structures, the differential pressure ($P_{\text{compartment}} - P_{\infty}$) has to be maintained at a smaller value, generally 0.1 atm. This is achieved by venting the trapped air or gas through suitable venting scheme.

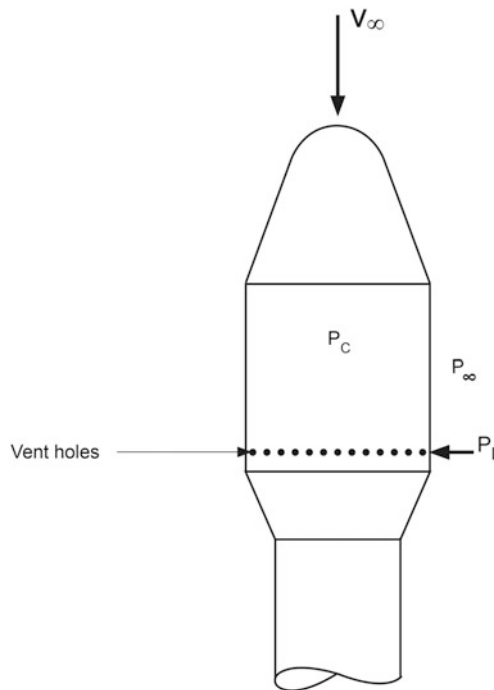
During the launch vehicle flight, due to external aerodynamic flow, all along the vehicle surface, there is local surface pressure build-up or suction compared to the atmospheric pressure. Since inside pressure (P_c) is greater than atmospheric pressure (P_{∞}), in order to allow the inside air to flow out, the local aerodynamic surface pressure at the vent hole location (P_l) has to be equal to the atmospheric pressure (P_{∞}) at the flight altitude.

Pressure distribution on the surface of the launch vehicle is given by

$$C_p = \frac{P_l - P_{\infty}}{q_{\infty}} \quad (10.57)$$

Therefore, the ideal location for the vent holes is where $C_p = 0$. But due to the continuous change of flight environment in terms of Mach number increase as well as variations in angles of attack, $C_p = 0$ at a specified location cannot be ideally achieved always. If C_p is large positive value, then the hot external gas enters into the compartment. If the C_p is large negative, then the compartment air is sucked out fast and both are not acceptable from the structural design point of view. The criteria for locating the vent holes are where the C_p value is close to zero, preferably having the negative value. The above criterion is generally met at locations close to the aft end of payload fairings for a typical vehicle as given in Fig. 10.34 except at transonic Mach numbers. The locations and vent hole area are designed for the

Fig. 10.34 Vent hole locations



specified compartment mass flow rate and pressure fall rate as acceptable to the structure. The mass flow rate and pressure fall rates are given by

$$\frac{dm}{dt} = -C_D A \sqrt{\frac{2\gamma}{\gamma-1} P_c \rho_c \left[1 - \left(\frac{P_l}{P_c} \right)^{\frac{\gamma-1}{\gamma}} \right] \left(\frac{P_l}{P_c} \right)^{\frac{2}{\gamma}}} \quad (10.58)$$

and

$$\frac{dP_c}{dt} = -C_D n \frac{P_l A}{V} \sqrt{\frac{2\gamma}{\gamma-1} \frac{P_c}{\rho_c} \left[1 - \left(\frac{P_l}{P_c} \right)^{\frac{\gamma-1}{\gamma}} \right] \left(\frac{P_l}{P_c} \right)^{\frac{2}{\gamma}}} \quad (10.59)$$

where

C_D = discharge coefficient of the vent holes

m = mass of the air inside the compartment

A = sectional area of the vent hole

P_c = inside compartment pressure

P_l = outside compartment pressure

ρ_c = inside compartment air density

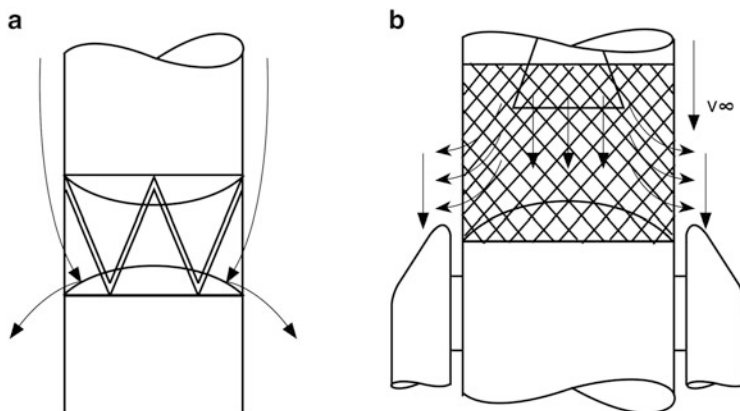


Fig. 10.35 Flowover open structures. (a) Open interstage. (b) Vented interstage

n = polytropic index

V = compartment volume

γ = ratio of specific heat of air = 1.4

The discharge coefficient is evaluated experimentally, simulating external flow, mass flow rate and P_c . Generally multiple holes are provided for better efficiency, to reduce the C_p variations caused by the local flow difference and also from the structural point of view to have minimum reduction in strength due to the vent holes. The launch vehicle integration process necessitates functional gaps, which also function as vent holes. Therefore, during vent hole design process, these functional gaps also have to be considered.

Flow Over Open Structure

In multistage launch vehicles, two adjacent stages can thermally contract and expand differentially due to the difference in thermal conditioning of each stage. Conventional design of load-carrying interstage elements for such environment leads to complex structural system. Under such conditions, open interstage made of intertank load-carrying truss members allowing rotation and linear movements at one end and fixed at the other end is an optimum structural system design. Typical schematic for such system is represented in Fig. 10.35a. Aerodynamic flow passes through such open interstages as shown in Fig. 10.35a and creates local loads on the components which are sometimes same order as overall loads.

To achieve successful stage transition in a multistage launch vehicle mission, three major requirements have to be met, i.e. (1) ensure positive acceleration during stage transition to aid successful ignition of upper stage, (2) have a suitable system to separate the lower stage from the ongoing vehicle and (3) maintain vehicle

attitude control during stage transition. Generally, autonomous complex ullage rocket systems, separation rocket system and control systems are employed to meet the above requirements. Alternatively, to avoid the complexity, the above requirements can be achieved by a simple scheme of igniting the upper stage during tail-off phase of lower stage. The exhaust of upper stage is used to assist the separation process of the lower stage and then vented out through vented interstage (VIS) as shown in Fig. 10.35b. This poses two problems: (1) the exhaust gas passes through the gaps provided in the VIS which in turn interacts with the external flow, and (2) the exhaust gas imparts the required force on the dome of the lower stage to aid the separation process and subsequent to that, reverse flow is generated in the cavity between the nozzle and interstage. The flow is highly complex due to very high jet expansion ratio (P_i/P_∞) and high plume angle of the order of 75° . The complex flow patterns of such systems produce loads and disturbance to the vehicle systems and the subsystems have to be designed suitably.

Aerodynamic characteristics of the flows over open structures are carried out using experiments and CFD process to generate flow features as well as aerodynamic loads on the associated structures.

Stage Separations in Complex Aerodynamic Flows

To improve the performance capability, structural systems are separated from the vehicle after meeting the functional requirements. Even though these separations are planned at the benign environment, separation process of certain systems in the aerodynamic flow environment is inevitable. Two such processes are explained.

Parts of interstages are being separated during thrusting phase of the vehicle. Dynamically, this is analogous to barrel separation through high-speed jet of thrusting stage as shown in Fig. 10.36a. The jet imparts forces and moments and rotates the uncontrolled separated component. The flow is highly complex due to protrusions caused by the electronic packages attached to the barrel. The aerodynamic characteristics of such complex flow phenomenon are generated using experimental and CFD means and using these data, suitable systems are designed to ensure safe separation.

After burnout, the strap-on motors are generally separated to gain payload advantage. The separated strap-on motor encounters complex aerodynamics in the vicinity of the ongoing stage as shown in Fig. 10.36b. The reflected shock from the core body and the jet impingement forces on the body are characterized through wind tunnel tests to generate aerodynamic forces and moments. These data are used for separation system design to ensure collision-free separation of the strap-on motors from the ongoing stage. Once the system design is completed, the same is validated through strap-on separation time-march wind tunnel tests (these aspects are covered in Chap. 13).

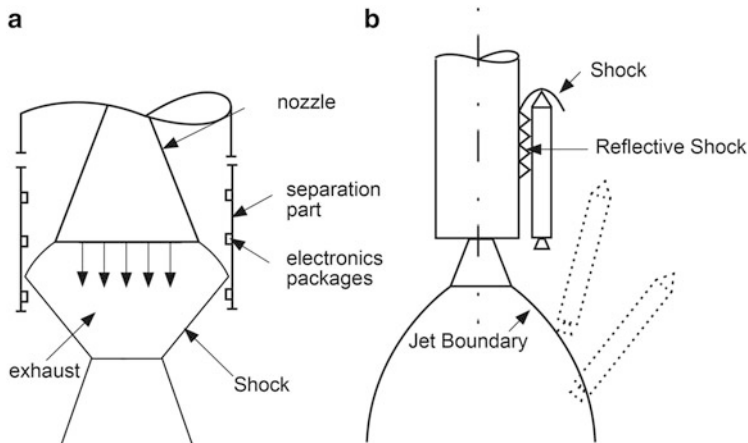


Fig. 10.36 Separation process. (a) Barrel separation. (b) Strap-on Separation

10.4.3 Free Molecular Flow Regime

Once the vehicle crosses the dense atmosphere, the external aerodynamic flows over the vehicle are mainly free molecular flows, which generally occur in the upper stages of flight phases. After the vehicle clears sensible atmosphere, in order to achieve the target conditions, the guidance system provided in the vehicle steers the vehicle in the optimum direction, which in turn generally introduces high angle of attack to the vehicle. During this flight phase, although the atmospheric density is very low, due to very high velocity of the vehicle and also large angle of attack, the aerothermal environment on the vehicle systems is higher. Therefore suitable thermal protection systems need to be designed. In addition, the control system's capability of the upper stages is generally lower as the aerodynamic forces and moments of free molecular flight regimes need to be considered for the corresponding stage control systems design.

In the free molecular flight regime, the aerodynamic characteristics of the vehicle are generated as functions of vehicle operating altitudes along with high angles of attack, on actual flight configuration (Fig. 10.37) using closed-form solution.

Correspondingly, the aerodynamic forces and moments are computed as given below:

Axial aerodynamic force is given by

$$F_A = C_A(h, \alpha) q_\infty S_{ref} \quad (10.60)$$

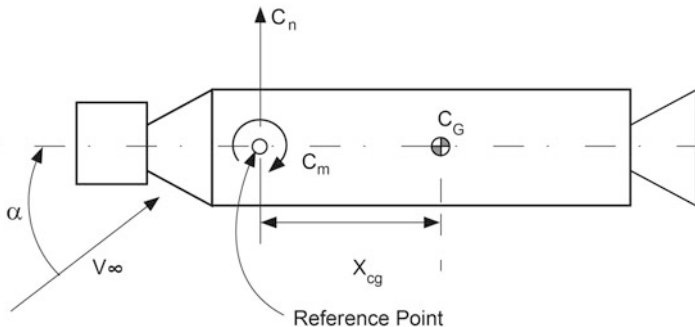


Fig. 10.37 Free molecular flight regime aerodynamic configuration

Lateral aerodynamic force is given by

$$F_N = C_N(h, \alpha) q_\infty S_{ref} \quad (10.61)$$

And the moment about centre of gravity is given by

$$M_N = C_m(h, \alpha) q_\infty S_{ref} L_{ref} + F_N X_{cg} \quad (10.62)$$

where C_m , C_N and C_A are referred with respect to a point away from centre of gravity by X_{cg} .

10.5 Aerodynamic Characterization

The previous sections explained the different aerodynamic phenomena during atmospheric flight phase of launch vehicle and their impacts on the vehicle and subsystems. Therefore, it is essential to evaluate the various aerodynamic characteristics of the vehicle with different configurations to arrive at an optimum aerodynamic configuration, which minimizes the loads while meeting all the functional requirements.

The aerodynamic characterization of launch vehicle with complex flow patterns in severe environments ranging from subsonic to hypersonic flight regimes is a challenging task and is beyond the scope of this book. However, summary of aerodynamic characterization strategies being adopted for a typical launch vehicle design is given below.

The aerodynamic characteristics are generated through empirical and semi-empirical methods, detailed wind tunnel tests and Computational Fluid Dynamics (CFD) analysis and ultimately through flight measurements. While the empirical or semi-empirical methods are used to generate the aerodynamic data quickly for usage in the preliminary launch vehicle configuration evolution studies, the total aerodynamic characteristics are evaluated through detailed wind tunnel tests and CFD analysis. Considering the functional requirements, correctness and limitations,

the aerodynamic characteristics generated through wind tunnel tests and CFD analysis have their own merits and demerits. The characteristics evaluated through both the methods are complementary in nature and the results are to be judiciously combined to obtain the total characteristics of the vehicle.

In the wind tunnel testing, scaled-down model of the vehicle incorporating all the external features of the vehicle is used. The vehicle model is mounted on the suitable test rigs in the wind tunnel which simulates all the flight environments in terms of Mach numbers ranging from low subsonic to hypersonic flows, angles of attack, etc. The required measurements are made on the model under flight simulated environments. The measured data is analyzed to evaluate the required aerodynamic characteristics. This data is further scaled up in the real vehicle and flight environments and used in the vehicle design. Depending on the required characteristics, suitable models are used to simulate the external features and dynamic characteristics of the vehicle. Similarly, as per the test requirements, different test rigs and measurement systems are adopted to evaluate the specified aerodynamic characteristics of the model which can be scaled up to real vehicle accordingly.

The advantage of the wind tunnel testing is that the characterization is more correct as it simulates the actual vehicle features as well as real flight environments. Certain important aerodynamic parameters peak during critical flight phases such as transonic and high dynamic regimes of flight and at specified orientation of the vehicle with respect to the flow. The exact Mach number and orientation for occurrences of such peaks as well as peak magnitude depends on the vehicle configuration. Due to discrete simulation of flight environments such as Mach number and vehicle orientation, normal wind tunnel tests may sometimes miss to capture such events and peaks. In order to ensure complete aerodynamic characteristics, Mach sweep, angle of attack sweep and roll sweep tests are to be devised in wind tunnel test programs. Also, it is to be seen that while the wind tunnel tests provide the correct aerodynamic characteristics of the overall vehicle, due to finite and discrete measurement locations on the model, the flow features at critical locations may be missed. For such cases, the critical locations have to be judiciously identified and suitably instrumented to evaluate the characteristics at the specified location.

The inaccuracies of the aerodynamic characterization through wind tunnel tests arise from the limitations of the models and wind tunnels. To ensure that the model is the true representation of the vehicle with all the features, the scale of the model has to be large. While it is feasible for simulation of low subsonic flows in large wind tunnels, the wind tunnel system required to simulate the flight environment corresponding to transonic flows and beyond is very complex, costly and in certain cases not feasible. Therefore, there is limitation in size of the test section of transonic, supersonic or hypersonic wind tunnels. To avoid tunnel blockage effects, the tunnel test section limitation decides the size of the model, in which case, it may not be possible to represent the model as the true replica of the vehicle. To withstand the start/stop loads of the wind tunnel, certain joints in the wind tunnel models have to be modified which may be different from that of the vehicle in terms of size and shape. These configuration changes may induce different flow

characteristics compared to that of the true vehicle. In addition, the mounting mechanism as well as local deviations of the vehicle model with respect to real vehicle to accommodate such mechanisms also may have influence on the flow patterns over the vehicle which is different from the true vehicle environment. Therefore, considering the above aspects, the mounting mechanism and other associated elements have to be suitably designed to minimize such effects.

In order to evaluate the overall measurement uncertainties in the aerodynamic characteristics, repeat tests are to be carried out at critical environments such as transonic, maximum dynamic pressure conditions, etc. In general, the flow inclination in the wind tunnel, strain gauge balance and sting deflection corrections are applied to correct the systematic errors in the measurements. The above repeatability test represents the random error in that particular wind tunnel measurement scheme. Even though appropriate model scale is chosen to meet the particular wind tunnel blockage, depending upon the wind tunnel configuration like slotted wall, perforated wall, etc., the type of sting, strain gauge balancing rating, the aerodynamic characteristics may be different to a small extent. Therefore, it is a general practice to carry out wind tunnel tests in different wind tunnels with different model scales and arrive at tunnel-to-tunnel repeatability and model-to-model (instrumentation) repeatability and use them judiciously in defining error bounds in the generated aerodynamic characteristics.

On the other hand, Computational Fluid Dynamics (CFD) analysis involves the mathematical modelling of the fluid flow, defining the vehicle external features through suitable boundary conditions and numerical solution of the models to generate the flow patterns and required aerodynamic characteristics. Due to the feasibility of simulating the full vehicle and all the flight environments, CFD analysis gives the details of realistic flow patterns with complete details which otherwise are impossible to generate through wind tunnels. But the accuracy of the CFD analysis is decided by the limitations of the model and computer system used for the analysis. Due to these limitations with the present-day systems, it is not possible to simulate exactly the real flow patterns accurately.

The present trend of CFD analysis is that for single-body configuration where there is no large-scale flow separation, CFD is able to predict the aerodynamic characteristics within 10–12% of the true values. Depending upon the type of code, type of grids, number of grids and turbulence model, code-to-code variations are prevailing and the accuracy of the generated characteristics rely on the nature of configuration, Mach number regime, etc. For multi-body configuration, the CFD prediction characteristics and the wind tunnel test data may vary to an extent of 20–25 % especially in the transonic regime.

Therefore, considering the merits and demerits of CFD and wind tunnel test results, one has to judiciously combine the wind tunnel and CFD results to arrive at the integrated aerodynamic characteristics of the vehicle. Typical aerodynamic characterizations for typical launch vehicle through wind tunnel and CFD analysis strategies are given below.

10.5.1 Aerodynamic Characterization Using Wind Tunnel Tests

10.5.1.1 Vehicle on the Launch Pad and Lift-Off Phase

Suitable scaled-down model of the launch vehicle and launch tower are realized and tested in wind tunnel for measuring the force and moment acting on the vehicle due to ground wind. During this phase, as the vehicle faces low subsonic flows ($M < 0.2$), it is feasible to simulate large models in larger wind tunnels simulating flight parameters such as Reynolds number and Mach number. The tests are carried out for the flow incidence angle of 90° , considering various relative positions of launch vehicle and tower, simulating the wind and vehicle on the launch pad and initial lift-off phase. Along with that, wind tunnel tests for the launch vehicle alone are also carried out for large angle of attack simulating the flight environment during initial flight phase of the vehicle. For this phase of flight, aeroelastic models of the vehicle and tower are also made and wind tunnel tests carried out to evaluate the augmentation of the overall loads and moments and to assess the frequency of vortex shedding if any. The above data sets are used to design and validate the vehicle systems on the launch pad and for the lift-off phase.

10.5.1.2 Overall Force and Moment During Atmospheric Flight Phase

To evaluate the overall aerodynamic forces and moments during high-dynamic pressure flight regimes, rigid scaled models are realized, simulation of the flight environment in the wind tunnel is done with the model and measurements are made through suitable mechanisms. The models are designed to meet the requirements of maximally simulating the vehicle features considering the limitations of the wind tunnel. The measurements are made in all the simulated flight regimes ranging from subsonic to hypersonic Mach numbers (typically $M = 0.2\text{--}5$). For each Mach number, simulations are carried out at all the expected flight environments of angles of attack ($\alpha = -6^\circ$ to 6°) and flow roll angles ($\varphi = 0$ to 360°). Wherever necessary, M-sweep, α -sweep and φ -sweep tests are carried out to identify and capture the peak aerodynamic parameters. In case of deviations in the model due to wind tunnel limitations, the same effects can be evaluated through CFD analysis after suitable matching process and added to the basic wind tunnel test data. After removing the systematic errors, considering the uncertainty due to measurement inaccuracies, model-to-model and tunnel-to-tunnel variations, the nominal aerodynamic characteristics along with the possible dispersion bounds are generated. This forms the basic data for launch vehicle performance evaluation and vehicle systems design.

10.5.1.3 Load Distribution

To evaluate the local sectional load and its distribution along the vehicle length, suitable steady rigid body pressure model with large numbers of steady pressure ports distributed circumferentially and longitudinally is realized. Using suitable electromechanical/electronic multiplexing, the steady pressures are measured. These pressures are integrated and load distributions are obtained for various flight regimes (Mach numbers) and flight environments (angle of attack). In general, the above integrated loads and overall force measured load match within 10 % level due to finite number of pressure ports. Wherever missing, pressure distributions are judiciously augmented with CFD results after suitable matching process. By this method, the load distribution over the entire vehicle including the functional protrusions is generated. The distribution thus generated is used for vehicle structural control system as well as propulsion design.

10.5.1.4 Unsteady Pressures and Aeroacoustics

In order to qualify the vehicle structures for the acoustic levels prevailing due to aerodynamic flow separation, shock oscillation, etc., high-response transducers are used in scaled rigid body model and unsteady pressures are measured in wind tunnel at appropriate locations on the model. This data is converted into flight environment using a suitable scale factor and an envelope is generated to carry out the required tests in acoustic test facility.

10.5.1.5 Aeroelastic Model Testing

In order to characterize the launch vehicle for buffet loads, aeroelastic model of the vehicle simulating the fundamental mode shapes and frequencies is realized and wind tunnel tests are carried out for the critical flight regimes and environments. The measurements lead to the evaluation of augmentation of structural loads due to buffet. Generally, the rigid body forces and moments are augmented by 6–10 % due to buffet depending on the configuration. The augmented factor is considered for the vehicle system design.

10.5.1.6 Separation System Aerodynamic Characterization

Depending on the mission requirements, the spent stages (sequential and parallel) may have to be separated under aerodynamic environments. For the collision-free separation of such stages, suitable separation systems like spring or jettisoning rocket have to be used based on the aerodynamic behaviour of the separating bodies. In order to evaluate the aerodynamic forces acting on separated and ongoing bodies under severe separating environment, suitably designed stage

separation rigs are realized and wind tunnel tests are carried out for various degrees of freedom possible for the separating stages. The wind tunnel test data thus generated with appropriate error band is used for the separation system design and dynamic analysis of separated stages.

10.5.1.7 Aerodynamic Characteristics with Presence of Jet (Jet-on Effect)

During the evaluation of aerodynamic characteristics in the wind tunnel, the vehicle model alone is used. But in actual flight environment, there exists rocket exhaust jet during atmospheric flight regime. Presence of jet depending on the pressure ratio (nozzle exit pressure to free stream pressure) influences the aerodynamic base pressure, base heating and the overall forces and moments on the vehicle. With high-capacity computational facility, these effects are captured to a certain extent by CFD. However, to get the final data, wind tunnel tests are carried out by simulating jets and free stream. This data is used for correcting the overall aerodynamic data.

10.5.2 Aerodynamic Characterization Using CFD

All the aerodynamic characterization obtained through wind tunnel tests can be generated by CFD analysis also. The greatest advantage of CFD is that there is no limitation on the simulations as in the case with wind tunnel tests imposed by model and tunnel limitations. Since CFD deals with the actual vehicle configuration with real flight environment, the data can be used as it is without any scaling-up factors and corrections required for the actual environment. As the CFD analysis considers the total system without any loss of information, this analysis provides flow features and patterns with intrinsic details, but off course within the limited accuracy. Therefore, CFD analysis is considered to provide the total qualitative details of flow features on the vehicle and protrusions with minute details. Due to these features, the result of the CFD analysis is used extensively in the launch vehicle aerodynamic characterization process.

1. To visualize qualitatively the flow patterns and aerodynamic features and their impact on the vehicle system.
2. To identify the critical zones in the vehicle system such as flow attachment locations, etc., which need in-depth characterization through wind tunnel tests.
3. To fill in the gaps of the wind tunnel generated data caused by the limitations of the wind tunnel model by using the CFD data can be used after suitable validation.
4. To correct wind tunnel test results to account for the deviations in the wind tunnel models with respect to the actual vehicle configuration.

5. To use this data for design of vehicle systems where it is not possible to generate wind tunnel data. Typical examples are loads on protrusions, wire tunnel ducts, vented interstages, etc. In all such cases data has to be used judiciously with higher uncertainty bands.

10.6 Launch Vehicle Aerodynamics Configuration Design

This section gives the strategies to achieve the optimum aerodynamic configuration design using various characteristics explained so far. The vehicle size in terms of length and diameter including clustered configuration is designed to achieve the specified mission objectives. Therefore, the aerodynamic configuration design of the vehicle has to address the shaping of the forward part of the vehicle, viz. payload fairing (PLF) and strap-on nose cones which dictate the aerodynamic flow characteristics of the remaining parts of the body and correspondingly the aerodynamic features of the vehicle. In addition, the vehicle stability issues, local steady and unsteady loads and shaping of external protrusions are also to be addressed in the vehicle aerodynamic design. Another essential part of aerodynamic design process is to accurately characterize the steady and unsteady aerodynamic loads on each of the external features of the vehicle and use them as input for the vehicle subsystem design.

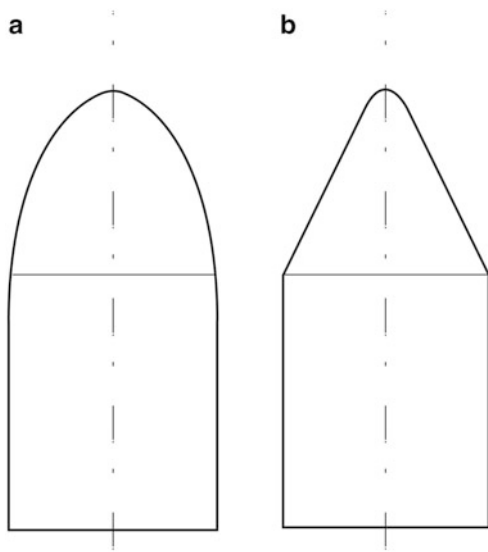
The general guidelines for the aerodynamic design are to reduce the overall drag, normal and side forces, moments, steady and unsteady aerodynamic loads and aero loads on the external protrusions as well as to reduce aerothermal environment to the vehicle systems. To achieve the above characteristics of the launch vehicle, the aerodynamic configuration design is carried out in shaping payload fairing (PLF), strap-on nose cones, fins and external protrusions.

10.6.1 Aerodynamic Configuration Design of Payload Fairing (PLF)

The fundamental requirement of PLF is to accommodate the satellite and protect it against the harsh aerothermal environment during atmospheric flight. PLF is the most forward part of the vehicle and therefore plays a major role in the aerodynamic characteristics of the vehicle. While length and diameter of PLF is dictated by the payload size and volume, the shape is designed to reduce the aerothermal environment on the vehicle and subsystems. The configuration design has to address reducing the vehicle drag, stagnation point heat flux, low-frequency loads for the vehicle structural design and high-frequency aeroacoustics for the vehicle and satellite systems.

Fig. 10.38 Types of PLFs.

(a) Ogive shape. (b) Conical shape

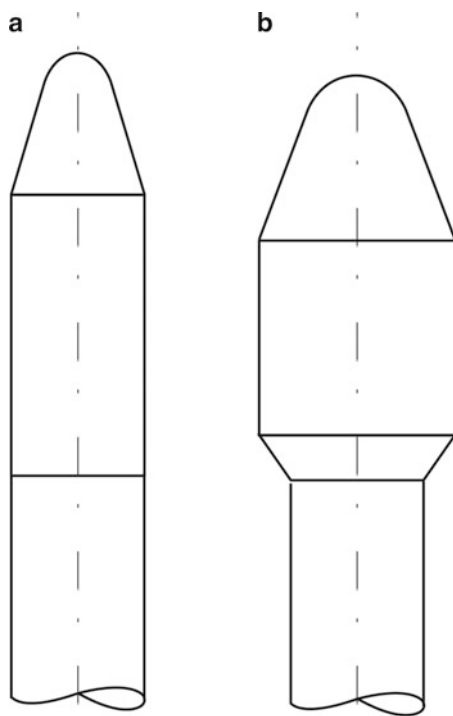


The shape of PLF can be either ogive or conical as shown in Fig. 10.38. The ogive shape provides higher volume for a given base to accommodate bigger payloads, better aerodynamic characteristics in terms of reduced drag, with minimum unsteady loads for the vehicle and the satellite. The negative feature of ogive shape is the difficulty involved in its manufacturing to the required precision level. Any deviation results into higher unsteady loads. In case of conical-shape PLF, although the drag is more, the manufacturing process is simple. The conical shape gives higher unsteady loads but the variations on the unsteady loads due to changes in geometry resulting from the manufacturing process are very low. The actual height and mass of ogive or conical PLF depends on the satellite volume requirements and actual aerodynamic loading conditions.

While the vehicle diameter is decided by the propulsion unit size, the diameter of PLF is decided based on the satellite requirements. If the payload dimensions are less than the diameter of the propulsion stages, in such cases, PLF diameter is kept same as that of the vehicle diameter known as straight PLF. Advanced and heavier satellites generally require a larger diameter which necessitates the PLF diameter to be more than that of vehicle diameter. In such a situation, after meeting the satellite requirements, the cylindrical portion of the PLF is joined to the vehicle through a defined boat tail and this type is called bulbous PLF. Typical configurations of straight and bulbous conical PLFs are given in Fig. 10.39. With respect to unsteady loads point of view, straight PLF is preferable to the bulbous one.

The main design parameters for a conical bulbous PLF as represented in Fig. 10.40 are (a) nose bluntness (R), (b) nose cone angle (δ_1), (c) nose cone

Fig. 10.39 Types of conical PLFs. (a) Straight PLF. (b) Bulbous cone PLF

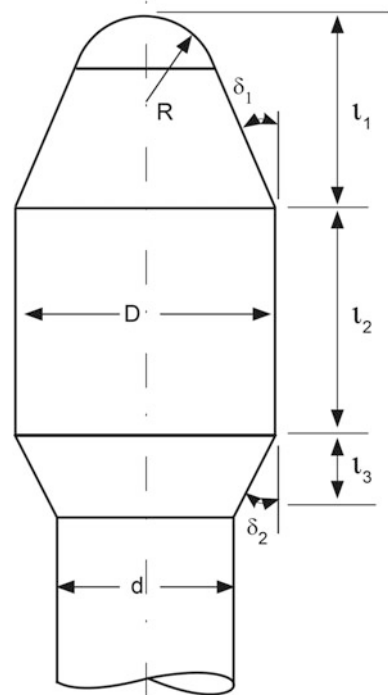


length (l_1), (d) cylindrical length (l_2), (e) boat tail angle (δ_2) and (f) boat tail length (l_3). The design guidelines of each of these parameters are

10.6.1.1 Nose Cone Bluntness

The design of nose cone bluntness is based on the trade-off between drag, structural mass and stagnation point heat flux limits. If the bluntness radius is too small, the vehicle drag is less but there is sharp increase in the stagnation heat transfer rates causing the nose cone to melt. Too large bluntness radius makes the nose cone look like a real blunt body and in such case, heat transfer rates are less whereas the drag increase leads to performance loss. At the same time, the nose cone length created by the small radius leads to unutilized volume inside PLF, which in turn leads to structural mass increase. Hence, nose radius is designed with the criteria of minimizing drag, heat transfer rate and structural mass in an integrated fashion.

Fig. 10.40 PLF design parameters



10.6.1.2 Nose Cone Angle

Nose cone angle is generally designed less than 15° . For the nose cone angle beyond 20° , when the flow expands over the shoulder, the strong transonic shock creates separated flow regimes on the cylindrical portion of PLF, which increases the unsteady loads. For the cone angle less than 15° , expansion of the flow from the cone cylinder junction is lesser as compared to the 20° and the weaker transonic shock would be in the cylindrical portion which moves downstream as the free stream Mach number increases. Since the shock is weaker, the unsteady loads are less as compared to 20° nose cone. In general, drag force also reduces for PLF with less angle and increased length for nose cones.

10.6.1.3 Nose Cone Length

If the nose length is too short, for small angles of attack, the flow is non-uniform even at the end of the cone, leading to more unsteady loads on the PLF. On the other hand, for the longer nose cones, the flow develops from stagnation flow into uniform conical flow before the end of cone itself, which reduces the unsteady

loads. To achieve this, the nose cone length has to be more than 0.8 D. Another advantage of increased length reduces the nose cone bluntness, which in turn reduces the drag. However, the increased length increases the structural mass. Trade-off between structural mass increase and aerodynamic load reduction needs to be carried out to arrive at an optimum nose cone length.

10.6.1.4 Cylindrical Length

The cylindrical length is mostly decided by the payload dimension. From the aerodynamics point of view, the cylindrical portion of conical PLF has to be sufficiently longer to keep the two separated flow regimes, one on the boat tail and the other near the shoulder, to remain distinct and not merging with each other. If the cylindrical length is too short, then these two flow regimes interact, which creates large unsteady, low-frequency loads. The cylindrical length has an influence on the boat tail flow and therefore, as per the design guidelines, this length has to be more than 1.5D, but generally any length beyond 1D may be acceptable but the design has to be validated with the wind tunnel characterized buffet loads.

10.6.1.5 Boat Tail Angle

Usually a PLF without boat tail (straight PLF) is preferable as it avoids the unsteady aero loads caused by the separated flow due to geometry change. But the boat tail is unavoidable for the cases of bulbous PLF. Boat tail geometry is decided by the change in the PLF diameter to the propulsion unit diameter and the necessary structural design requirements. Due to geometry change, transonic shock forms over the boat tail. For the lower boat tail angles, below 5°, the transonic shock formed over the boat tail is weak and therefore the separated flow formed over the boat tail is also weak. It is confined to a smaller zone and correspondingly the unsteady loads are lower. For boat tail angle beyond 30°, wake like separated flow exists over a longer zone, extending to longer lengths beyond the base of the PLF, which generally occurs over propulsion units. Generally, in such cases the propulsion unit is designed for higher loads and the unsteady loads may not cause any problem. However, for the boat tail angles between 5° and 30°, the shock incidence on the boat tail is very strong, which can lead to higher acoustic loading to PLF base regime.

10.6.1.6 Boat Tail Length

Boat tail length fixed once, D, δ and δ_2 are known.

10.6.2 Configuration Design of Strap-on Nose Cones

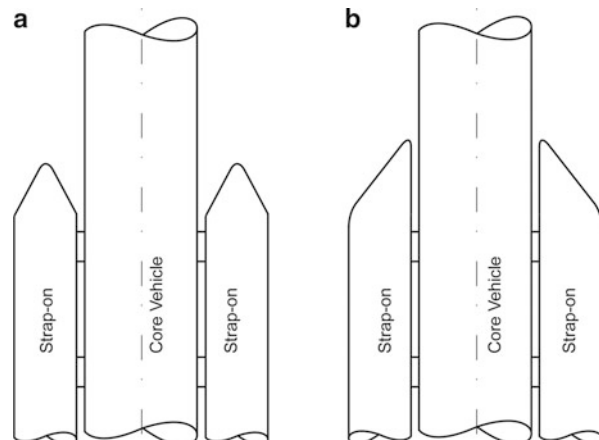
The design criteria outlined for PLF is applicable to strap-on nose cone also. To take care of interactions of core airflow with that of strap-on, additional points need to be considered. Depending upon applications, strap-on nose cones can either be straight or slanted as given in Fig. 10.41.

Due to the interference between the strap-on and core vehicle, the shape of nose cone plays a vital role in determining the aerodynamic drag and normal force on the vehicle. The straight nose cones are simpler to manufacture. Due to the nose-opening effects caused by flow interaction between core and strap-on, which aids the separation process, the straight nose cone configuration is preferable for the vehicle with strap-on separation during core thrusting phase. For the vehicle without strap-on separation, slanted nose cone is preferable as it shifts the centre of pressure towards aft of the vehicle, which improves the static stability. In order to reduce the moments and local loads due to jet impingement over strap-on, slanted nose cones are preferred for vehicle with vented interstage. In this configuration there is a possibility of jet impingement on strap-on nose cone, along with gap flow between strap-on and core. The strap-on attachments with the core vehicle can introduce unsteady loads and local heating of the vehicle and therefore this area also needs special attention during vehicle design.

10.6.3 Fin Design

The aerodynamic normal force on a launch vehicle is caused mainly by the geometry of PLF, and therefore, the centre of pressure is towards the forward part of the body. Due to heavy first stage, the centre of gravity of the vehicle is generally

Fig. 10.41 Strap-on nose cone configurations. (a) Straight nose cone. (b) Slanted nose cone



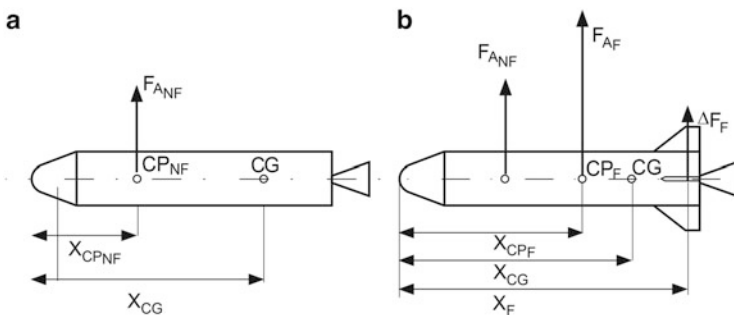


Fig. 10.42 Vehicle configuration with and without fins. (a) Vehicle without fins. (b) vehicles with fins

towards aft of the vehicle and this combination makes the vehicle statically unstable configuration. The strap-on motors in the clustered vehicle configuration cause additional aerodynamic force towards aft portion of the vehicle, which in turn shifts the centre of pressure towards base. Due to the mass of strap-on motors, the centre of gravity also moves backwards. Thus, in general, launch vehicles are aerodynamically unstable configuration.

During high-dynamic pressure regime of flight, although the launch vehicle's attitude profiles are designed to follow zero angle of attack, the variation in wind velocities and large wind shear introduce 1° to 2° angle of attack, which in turn generate large aerodynamic force and moment on the vehicle. Therefore, to stabilize the unstable launch vehicle in high-dynamic pressure regime of flight, the autopilot system demands large control force. This has two implications: namely, (1) the steady aerodynamic disturbance moment demands a large portion of the vehicle control capability, leaving very low margin to stabilize the vehicle under transient disturbances such as wind gust, which is not desirable during this critical phase of flight; (2) large aerodynamic force towards the fore end together with large control force at the aft end of the vehicle generates large bending moment, which increases the vehicle structural load beyond the design limit.

To reduce the control demand and the structural load, the aerodynamic disturbance moment has to be reduced. The aerodynamic force level is fixed for the given external configuration of the vehicle; therefore, the aerodynamic disturbance moment is reduced by improving the vehicle stability characteristics. Fins are one such option to improve the aerodynamic stability margins of launch vehicles. Fins are usually fixed at the aft portion of the vehicle so that the normal force generated by the fin moves the centre of pressure backwards as represented in Fig. 10.42.

Assume for a vehicle without fin, F_{ANF} and X_{CPNF} are the aerodynamic normal force and centre of pressure respectively and X_{CG} is the centre of gravity of the vehicle. Then, $(X_{CPNF} - X_{CG})$ is the static margin of the vehicle without fin. With the introduction of fin at the aft portion of the vehicle, the aerodynamic incremental force ΔF_F is generated at the location X_F from the nose tip. Therefore, the net

aerodynamic force F_{A_F} and location of centre of pressure X_{CP_F} of vehicle with fin are given below:

$$\{F_A\}_F = F_{AN_F} + \Delta F_F \quad (10.63)$$

$$\{X_{CP}\}_F = \frac{\{F_A\}_{NF} \{X_{CP}\}_{NF} + \Delta F_F X_F}{\{F_A\}_F} \quad (10.64)$$

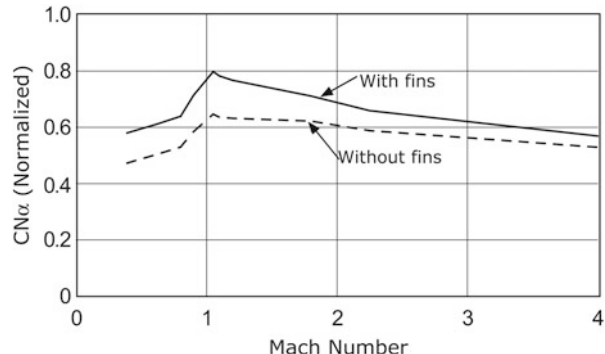
From the above, it can be seen that X_{CP_F} moves backwards compared to $X_{CP_{NF}}$, and therefore, the static stability margin is improved for the vehicle.

It is to be noted that since the fins produce additional normal force, in addition to the shift in the centre of pressure towards base, the normal force magnitude also increases. Therefore, design of fins is to be carefully carried out to reduce the net aerodynamic disturbance moment.

Fins are usually flat plate-like surfaces and are fixed configuration in general, whereas in launch vehicles which use aerodynamic surfaces for vehicle control, the fins are made with fixed and movable parts. The best design option for fins is the one which ensures zero static margin for the entire Mach numbers regime of flight, which is not feasible. Usually, the fins are designed for the critical flight environment of the vehicle. Generally, at transonic Mach numbers, the aerodynamic force increases and the dynamic pressure at this regime of flight is considerably larger as the peak dynamic pressure occurs close to this regime of flight. Therefore, the fins are designed for transonic and supersonic Mach numbers and for these Mach numbers, fins are more effective and meet the vehicle design requirements. However, the effectiveness of the designed fins is assessed at other flight conditions. The fins are mounted on the base shroud of vehicle to improve its effectiveness. The interference between the body and fin improves fin effectiveness. The fin effectiveness is maximum when the flow is two dimensional (2D), and therefore, the fins are designed such that the flow component normal to the leading edge of the fin be supersonic. The fin effectiveness can also be improved by using end plates that prevent the tip vortices due to 3D flow.

Aerodynamic characteristics of a typical launch vehicle with and without fin are given in Figs. 10.43 and 10.44. It is to be noted that the static instability margin at

Fig. 10.43 Effect of fins on normal force coefficient



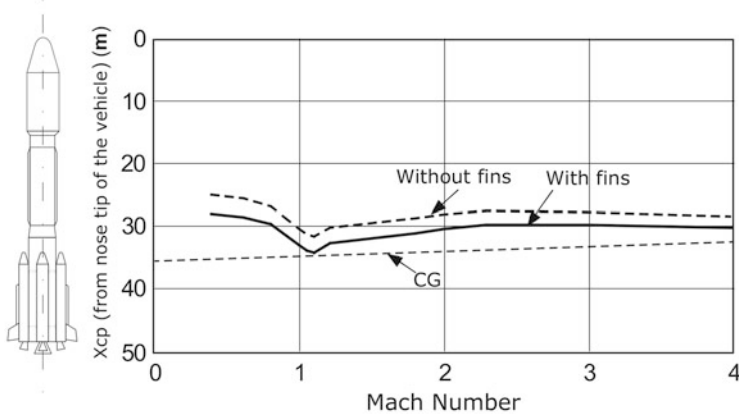


Fig. 10.44 Effectiveness of fins on centre of pressure

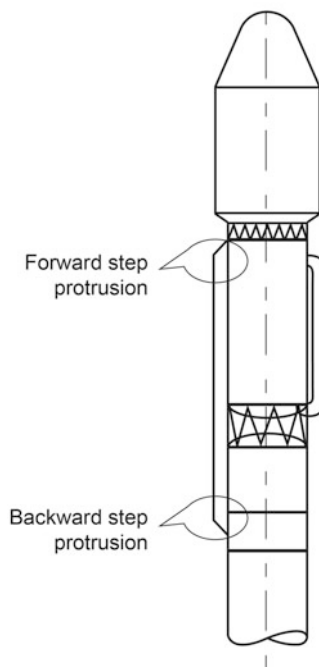
transonic Mach number is reduced nearly to zero by adding fins. Even though the normal force is increased the net aerodynamic moment about the centre of gravity of the vehicle at the critical Mach number is near zero. However, the fins have effects during subsonic and high supersonic Mach numbers regimes also.

10.6.4 External Configuration Design of Protrusions

The functional protrusions attached to the external surfaces of a vehicle play a significant role on the launch vehicle aerodynamic design. Apart from the overall vehicle aerodynamic characteristics decided by PLF, strap-ons and fins, the local aerodynamics of a launch vehicle is mainly influenced by the presence of protrusions. Protrusions, which are irregular surfaces on the surface of the vehicle, can cause high local loads on the protrusions and in turn on the active vehicle structure. Depending on the functional requirements, these protrusions can be classified into two categories: (1) Forward facing step protrusions, (2) Backward facing step protrusions as given in Fig. 10.45.

Generally, the forward facing protrusion produces a high local pressure distribution and higher drag while backward step protrusion generates a local separated flow leading to unsteady loads. Depending on size and shape, both categories of protrusions can generate steady and unsteady loads. Therefore, given the shape and size of a protrusion, it is essential to characterize both steady and unsteady loads at these locations and use the data for structural design. Depending on the criticalities, aerodynamic shaping and in certain cases relocation of protrusions are to be carried out as part of aerodynamic design processes.

Fig. 10.45 Types of protrusions



Bibliography

1. Krasnov, N.F., Koshevoy,V.N., Danilov A.N., Zakharchenko,V.F.: Rocket aerodynamics. NASA TT F-601
2. NASA space vehicle design criteria (structures), Compartment venting. NASA SP-8060
3. NASA space vehicle design criteria (structures), Buffeting during atmospheric ascent. NASA SP-8001
4. Turner, M.J.L.: Rocket and spacecraft propulsion: principles, practice and new developments. Springer edition
5. NASA space vehicle design criteria (structures), Acoustic loads generated by the propulsion system. NASA SP-8072
6. Nielsen, J.N.: Missile aerodynamics. McGraw Hill Book Co. (1960)
7. Krasnov, N.F.: Aerodynamics, Vol. 1&2. MIR Publisher, Moscow
8. Robert E., Wilson, Maurer, F.: Turbulent boundary layer separation at low supersonic mach numbers. AIAA J., pp 189–191 (Jan 1971)
9. Sigal, A.: Aerodynamic effects of body roughness. J. Spacecr. Rockets **30**(3) (May–June 1993)
10. Coe, C.F., Nute, J.B.: Steady and fluctuating pressures at transonic speed on hammerhead launch vehicles. NASA-TMX-778.
11. Coe, C.F., Chyu, W.J., Dods, J.B. (Jr): Pressure fluctuations underlying attached and separated supersonic turbulent boundary layers and shock waves. AIAA paper 73-996
12. Walters, W.P., W.F., et al.: Experimental determination of generalized venting characteristics. NASA-CR-61241.

13. Tam, C.K.W.: Computational aeroacoustics: issues & methods. *AIAA J.* **33**, 1788–1796 (1995)
14. Etkin, B.: Dynamics of atmospheric flight. Wiley, New York (1972)
15. Anon: Panel flutter. NASA space vehicle design criteria monograph (Structures). NASA SP-8004 (May 1965)
16. Schlichting, H.: Boundary layer theory. McGraw-Hill, New York (1962)
17. Anderson, J.D.: Fundamentals of aerodynamics. McGraw-Hill, New York (1991)

Chapter 11

Structures and Materials

Abstract The structure of the space transportation system is the physical body of the vehicle which houses all major or minor subsystems. It consists of propellant tanks, motor cases, payload fairing and interstage structures. The entire structure of the vehicle has to support all associated secondary elements like mechanisms, pyros, avionics, actuators, etc. Structures are classified as primary and secondary structures. Load-bearing structures like the solid stage motors, liquid stage tanks, interstage structures, payload fairing and interface joints are all primary structures. Gas bottles, fuel tanks for control systems, brackets, avionics packages, etc. which do not experience direct loads are known as secondary structures. The design of structural elements has to ensure the structural integrity of the vehicle during its various phases of flight starting from lift-off till satellite injection. Loads, materials, their characteristics, structural construction, manufacturing processes, structural dynamic response, stability characteristics, development schedule, cost, etc. strongly influence the structural designs. During the structural design process the mass of the structure has to be kept minimum to maximize the vehicle performance while ensuring adequate design margin. This makes the launch vehicles very flexible and hence the detailed structural dynamic studies are essential. Therefore, selection of suitable materials for structures and their shape and construction methods are important. To ensure that the designed product meets the specified requirements, the compliance has to be checked through detailed analysis and testing. Structures designed and analyzed for various load cases are to be qualified through a series of structural static and dynamic tests. This chapter discusses in detail the STS structural design requirements, load analysis and different configurations to meet different requirements. The materials' selection for structures, their shape and construction methods are included. Static and dynamic analyses are described and some insight on design tools is presented. The various static, environmental and dynamic tests needed for the qualification of the structures are highlighted.

Keywords Structures • Loads • Bending moment • Design load • Motor case • Liquid tank • Interstage • Construction methods • Metallic and composite materials • Static analysis • Environmental analysis • Ground resonance test • Dynamic response test • Aeroelastic • Divergence • Flutter and buffet

11.1 Introduction

The structure for the space transportation system is the physical body of the vehicle which has to house all the major or minor subsystems and holds all these elements together. It consists of propellant tanks, motor cases, payload fairing and a number of intermediate structures which link the propulsion modules, known as interstage structures. The important intermediate structures are base shroud, open interstage, intertank structure, payload adaptor, nose cone, etc. suitably chosen based on the functional requirements. The propulsion modules can either be solid motors or liquid stages. The payload fairing on top of the vehicle protects the spacecraft from the aerothermal load during the atmospheric phase of flight. The entire structure of the vehicle has to support all associated secondary elements like mechanisms, pyros, avionics, actuators, etc. used in the vehicle. Various structures used in a typical STS are shown in Fig. 11.1.

The design of various structural elements of the vehicle has to ensure the structural integrity of the vehicle throughout the mission during its various phases of flight starting from lift-off till satellite injection. In addition, the structural design also has to deal with stringent constraints such as the minimum mass, hostile operating conditions, prospect of modular manufacturing, cost-effectiveness, etc.

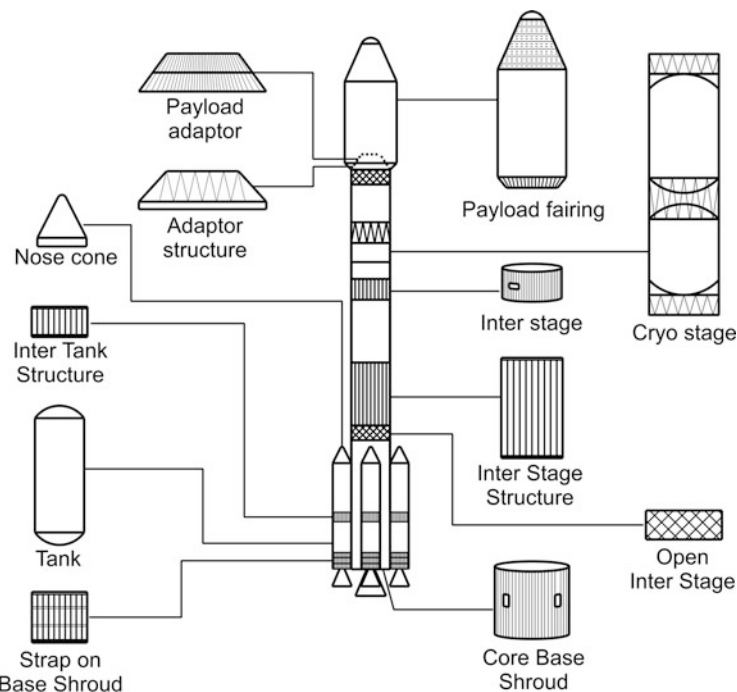


Fig. 11.1 Structures used in a typical STS

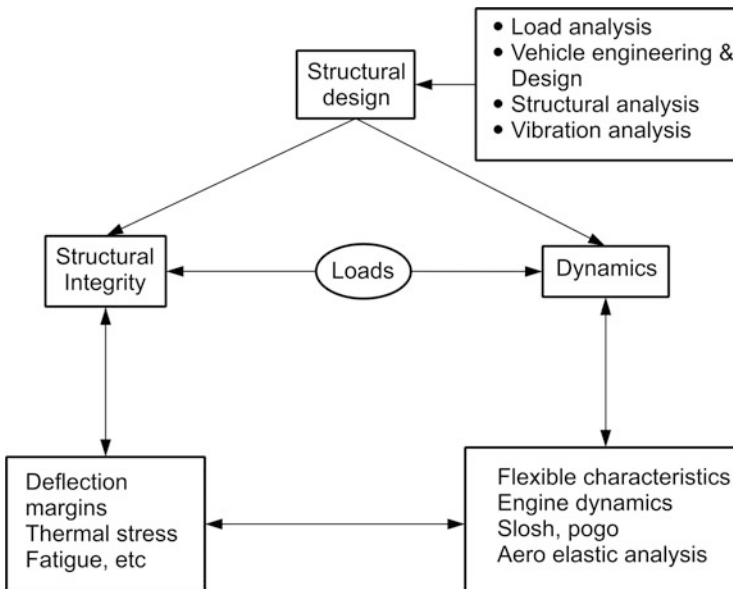


Fig. 11.2 Structural design, integrity and dynamics aspects

Several factors, such as loads (mechanical, aerodynamic, thermal, control, separation, acoustic), materials, their characteristics, structural construction, manufacturing processes, structural dynamic response, stability characteristics, development schedule, cost, etc. strongly influence the structural design process. Hence, the structural design is an integrated multidisciplinary task, closely linked with several disciplines. The interaction of the structure with external disturbances along with aerodynamic characteristics and mechanical forces from major vehicle functional systems like propulsion, control, liquid mass movements etc. causes interactive dynamics. POGO, slosh, buffeting, servo-structure feedbacks, etc. are typical examples. The close interlinking of the structural design, structural integrity and the dynamics are shown in Fig. 11.2. It is required to ensure that such interactions are studied in detail and ensured that they are controlled so that they never diverge. Therefore, the design of STS structures is complex and highly iterative from preliminary design onwards till the structure is qualified and cleared for the mission.

This chapter discusses in detail the STS structural design requirements, load analysis, types of constructions to meet different requirements, materials for structures, static and dynamic analysis and some insight on design tools and testing aspects.

11.2 Structural Design Requirements

While the major requirement of the STS structures is to withstand all the loads and the flight environment, it is essential to ensure that the mass of the structure has to be minimum to maximize the vehicle performance. Therefore, suitable material has

to be selected for each structure depending on the functional requirements and optimum design has to be carried out with the selected material to minimize the mass while meeting the load-carrying capabilities under the expected flight environment.

Structures of space transportation systems are classified as (a) primary structures and (b) secondary structures. Load-bearing structures which provide the needed strength and stiffness to withstand all loads during the flight are known as primary structures. The solid stage motors, liquid stage tanks, interstage structures, payload fairing and interface joints are all primary structures. In a vehicle several other structures like gas bottles, fuel tanks for control systems, brackets, avionics packages, etc. which do not experience direct loads are known as secondary structures.

The important requirements in vehicle engineering and structural design are as given below:

- (a) Estimation of various loads on the vehicle systems caused by the various sources
- (b) A comprehensive analysis of loads during different phases of flight
- (c) Selection of suitable materials, their characterization and failure behaviour
- (d) Using high-strength material and suitable approach for design
- (e) Carrying out optimum design without affecting the structural integrity, guaranteeing adequate margin against all loading conditions and environment
- (f) Adapting modular concepts in design for ease of manufacture
- (g) Considering various constructional plans in the early phase of design and selection of suitable processes to account for the ease of fabrication and the cost
- (h) Providing the needed tolerances and identifying carefully all stress concentration regions
- (i) Identifying the local stiffening at cut-outs and joining regions
- (j) Evolving proper assembly, inspection and installation aspects

In structural design there has to be a set of criteria like strength, fatigue, fracture, load analysis and vibro-acoustics analysis. The validation and verification requirements such as qualification and acceptance criteria in static and dynamic tests are to be appropriately planned. During the detailed design phase, derived requirements such as (a) reducing loads due to active load relief or day of launch wind biasing, (b) providing damping for the propellant sloshing by using baffles and (c) ensuring the launch constraints due to increased ground winds, etc. are also to be considered.

11.3 Structural Loads and Analysis

Loads acting on an STS during flight can be broadly divided into steady loads, transient or dynamic loads and thermal loads. Bending moment, shear forces and axial forces on complete vehicle are steady loads. Thrust transients, control forces and acoustics are typical examples of dynamic loads. Aerodynamic heating and heat generated during combustion process are typical examples of thermal loads. In the initial development phase, the structural load estimation is done in quasi-static

manner and suitable factors are assumed for unknowns over the estimation. In the detailed design phase, complete model of the structural elements along with the realistic flight environments are used for the static and dynamic analysis and suitably modify the designs, if required to meet the requirements.

During the ascent phase flight, the vehicle has to travel through dense volatile atmosphere and follow the preplanned trajectory. Even though the trajectory planning is based on minimum load constraint, the planned environment may not be achievable due to the existence of wind. Since wind is a random phenomenon, taking into uncertainties, aerodynamic load becomes the most severe for the structures during atmospheric flight phase. The atmospheric phase varies from subsonic to hypersonic flight regimes in a single mission. Both scale model wind tunnel tests and computational fluid dynamics (CFD) are to be employed to fully characterize both steady and unsteady aerodynamics characteristics. The vehicle stability is achieved by applying the balancing control moment through control systems. The aerodynamic steady and unsteady forces, control forces and the propulsion system forces form the major input data for load analysis during atmospheric flight phase. Subsequent to atmospheric phase, the structures are subjected to loads due to ignition and shut-off transients at various stages, stage separation, control actuation loads, etc. along with the propulsive forces.

Considering the above aspects, a comprehensive load analysis is required at different phases of flight taking into account all loads due to several events. Since the aerospace structures are very delicate due to optimum design, the handling and transportation loads on ground are also to be considered in the design. Figure 11.3 shows the load analysis methods in a simplified manner.

Structural load analysis needs comprehensive data on (a) vehicle configuration, (b) aerodynamic characteristics, (c) flight environment, (d) materials, (e) trajectory parameters, (f) thermal loads, (g) control and (h) propulsion. Since the STS development is a continuously evolving process, loads have to be updated often. In order to achieve the acceptable loads, the structural load analysis needs close interaction with other disciplines to understand the resolution of aerodynamic coefficients at several critical events, spatial resolution of pressure distribution, trajectory reshaping wherever possible within the constraints, control logic used, the dynamic responses, etc. It is possible to find solutions to alleviate the excess loads by marginal adjustments of some of the parameters listed above.

Structural design, based on the loads, can be classified broadly into the following categories;

- I. Design based on internal pressure
- II. Design based on aerodynamic pressure distribution
- III. Design based on axial force, bending moment and shear force, etc.

Solid motors, liquid stage tanks, gas bottles, thrust chambers, etc. are all designed based on the operating pressure. Payload fairing is designed based on aerodynamic pressure distribution (both internal and external pressure is considered). Interstages, base shrouds, stage end rings, etc. are designed based on equivalent axial loads.

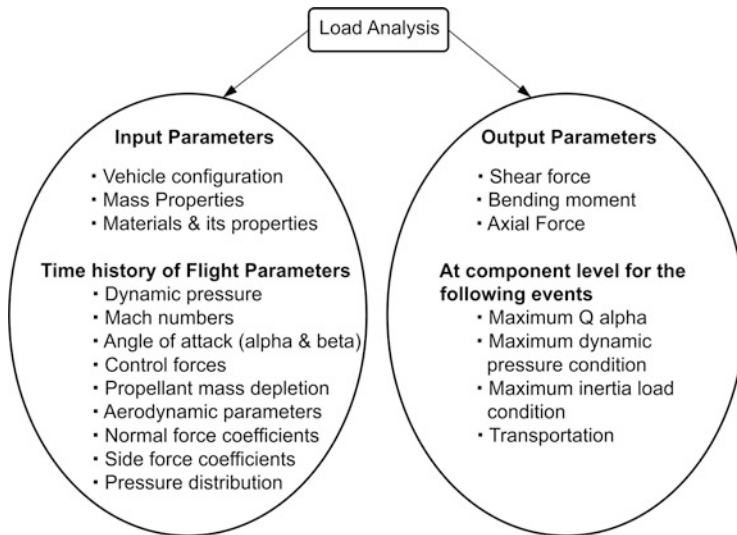


Fig. 11.3 Load analysis

11.3.1 Axial Load

Axial loads are due to thrust, drag and longitudinal inertial force acting at given station, computed as

$$F_x = qSC_D + m\ddot{x} \quad (11.1)$$

where

C_D = Drag coefficient

q = Dynamic pressure

S = Surface area

m = Mass up to that section

\ddot{x} = Axial acceleration of the vehicle

11.3.2 Shear Force

Shear loads are due to lateral aerodynamic and control forces and inertia given by

$$F_z = qSC_N + m\ddot{z} + C_{FP} \quad (11.2)$$

$$F_y = qSC_S + m\ddot{y} + C_{FY} \quad (11.3)$$

where

F_z and F_y are pitch and yaw plane shear forces respectively.

C_N = Lateral aerodynamic coefficient along the pitch plane for the defined α and β

C_S = Lateral aerodynamic coefficient along the yaw plane for the defined α and β

\ddot{z} = Lateral acceleration in the pitch plane

\ddot{y} = Lateral acceleration in the yaw plane

C_{FP} = Pitch control force

C_{FY} = Yaw control force

11.3.3 Bending Moment

The total bending moment consists of bending moment due to aerodynamics, control forces and buffet phenomenon estimated all along the vehicle length. Since the vehicle is in free-free condition, inertia relief technique is to be used for load estimation. The equivalent axial load F_{xb} due to total bending moment is calculated as

$$F_{xb} = \frac{2 \times \text{Total bending moment}}{\text{Radius of the structure}} \quad (11.4)$$

and the total equivalent axial load (EAL) F_{xe} is given by

$$F_{xe} = F_x + F_{xb} \quad (11.5)$$

Generally, in the initial phase of development, quasi-static loads at particular flight instances are computed and the structural design process is initiated. In order to consider the uncertainty in understanding the aerodynamic/structure interaction, it is a common practice to provide a margin of 15–20 % as dispersion based on the loads so worked out. On bending moment, the dispersion considered may vary from 40 to 60 %, depending on the location, aerodynamic coefficient uncertainties, buffet, dynamic load factors, etc.

Vehicle structural components are subjected to dynamic loads during ground transportation and also in flight till satellite injection. During the road transportation, the rough roads cause dynamic loads on the components. While standing on the launch pad, the vehicle structure is subjected to ground winds. During ignition, the main motor ignition causes high acoustic loads impinging on the vehicle. During flight, the jet noise reduces, but acoustics due to aerodynamics increases. Aerodynamic noise reaches the maximum in the transonic regime and then reduces. Since the vehicle is a flexible body, all components of the launch vehicle are subjected to vibratory loads. Engine ignition, shut-off transients and combustion instability as and when it happens cause very high dynamic loads on components.

Apart from random dynamic loads, heat transfer variation during the flight also causes thermal loads. When the liquid stages are in operation, the liquid columns experience longitudinal oscillations known as POGO and lateral oscillations called Slosh. Pogo and Slosh load oscillations are to be damped out properly to avoid serious structural problems. But it is difficult to estimate precisely these loads, which are due to random environment. Proper characterization of the vehicle

environment and past experience derived from earlier flights of different vehicles are some of the guiding factors in generating this data.

Interstages and payload fairings are generally subjected to acoustic loads and they have to be designed with good acoustic attenuator characteristics. With the increase in size of propulsion stages the acoustic noise increases particularly in low-frequency range. However its effect on STS structure is limited to the modules which are mounted near to the acoustics environment. But it severely affects the spacecraft elements.

The wind characteristics at the launch base have a major bearing on vehicle loads. The wind measurements are needed for both ground and upper atmospheric winds. Generally limits on wind speed are imposed for ground winds to decide on the go or no-go for launch. The upper atmospheric winds are a major contributing factor for vehicle loads during atmospheric flight phase. The alleviation of load through load relief or generation of wind-biased trajectory is resorted wherever the loads are to be minimized in flight and the details are discussed elsewhere in the book.

11.4 Structural Design Aspects

Broad methodology for structural design process of an STS is illustrated in Fig. 11.4. The basic inputs for the design are derived from the vehicle and mission requirements. Before initiating the design, the vehicle level requirements are to be translated to specific requirements of the structure and all the constraints are to be specified. This leads to proper definition of a suitable configuration of the structure and the first cut interfaces. The structural loads are to be estimated considering all factors including the thermal loads and the uncertainties are to be worked out. Using all these inputs the structural design is carried out. The design has to be verified under dynamic conditions like vehicle flexibility and it has to be ensured that specified margin of safety is guaranteed. Similarly the design has to be checked for stability margins under various interactions like POGO, slosh and aero-servo-elasticity. It is also necessary to verify the dynamic envelope and the dynamic response for the spacecraft. All these processes undergo several iterations and final design is arrived at. The proto-hardware is realized with the finalized design and subjected to the specified qualification tests. Any indication of loss of margin or failure during the phase of qualification tests would cause further redesign and tests. This process is repeated till the structural hardware meets all the defined requirements.

The design of the specific structure has to be approached considering the type of structures. The material choice and construction type depend largely on the category of structure to be designed. The design has to cater to all defined constraints, interface requirements, maximum loads and thermal environment while minimizing the mass. During the design, the sizing of each of the structural members in terms of thickness of the shell in case of motor cases or propellant tank, the cross section and number of stiffeners, bulkheads and the cross section of end ring interface joints in case of interstage structures has to be carried out to meet the

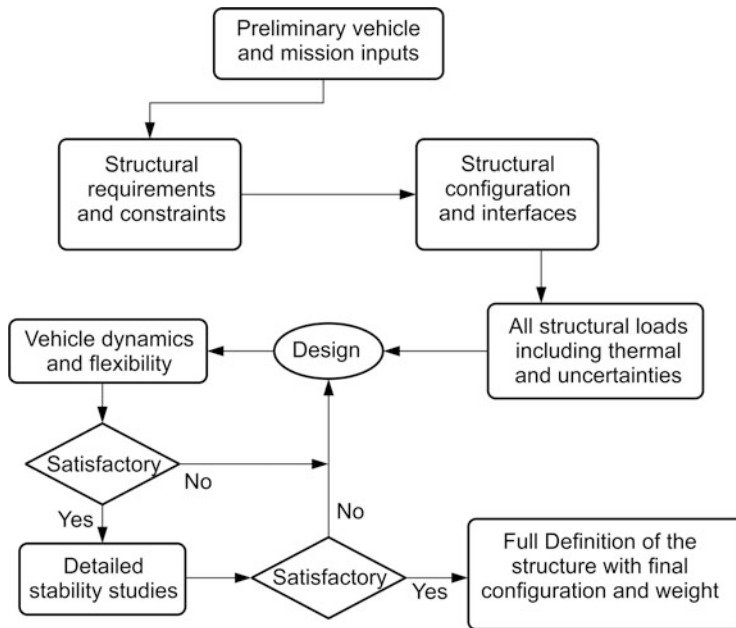


Fig. 11.4 Structures design methodology

specified design loads with a positive margin of safety. Simple mechanics theory, strength of materials theory, empirical or special formulas are to be utilized depending on the application.

11.4.1 Design Load Factors

The structural design for STS is largely influenced by the requirements of strength, mass and cost. The choice of an appropriate factor of safety is a major decision the designer has to make. Factor of safety or safety factor describes the structural capacity of a system beyond the actual or expected loads. Factor of safety is defined as

$$FS = \frac{\text{Allowable Load}}{\text{Design Load}} \quad (11.6)$$

The allowable stress can be yield strength or ultimate strength or buckling strength.

Factor of safety indicates the additional strength for the system compared to the strength needed for handling the actual load. The margin of safety MS is defined as

$$MS = FS - 1 \quad (11.7)$$

To minimize the structural mass, generally margin of safety of structures is designed to be slightly greater than zero. The maximum expected load on structures

has to be carefully worked out as described in earlier sections and it is termed as limit load. The load factor is the multiplication factor applied on limit load. They are usually different for different applications to meet the specified reliability goals. Proof load is that load which does not cause any global yielding whereas the ultimate load does not cause any failure. For unmanned flights the proof load is generally 1.1–1.15 times the limit load and ultimate load is 1.25–1.5 times the limit load. For manned flights where higher reliability goals are set, the values for proof load is 1.2–1.5 times limit load and for ultimate load it is 1.4–2.0 times limit load.

Selection of suitable design factors has to be based on several aspects such as accuracy of estimated load, environmental effects on the material used in structure, fatigue, etc. Therefore margin of safety has to ensure that it caters to all unknown factors and guarantees positive margin.

The vehicle structure can be categorized into three major groups, namely, motor cases or propellant tanks, interstage structures and interface joints. The motor cases or propellant tanks are used for different propulsive stages of the vehicle. Interstage structures facilitate the interconnection between the propulsive stages and houses many of the vehicle subsystems corresponding to avionics, control systems, pyros, mechanisms, etc. Different structures are connected through interface joints. Although this book is not intended to describe the structural design in detail, basic design approach to these three categories of structures which form the STS is briefly given below.

11.4.2 Motor Case or Liquid Stage Tanks

The basic inputs for the design of these structures are maximum operating pressure, overall diameter and volume. They are generally designed as monocoque structures with end domes. The cylindrical shell and domes are attached through the machined rings. The loads felt by these structures are internal pressure and external loads like axial, bending and shear loads. The basic design features for propellant tanks are as given below:

- (a) Ultimate strength-based design
- (b) Material to be compatible with the propellant used
- (c) Material to withstand the temperature without degrading even when they are subjected marginally beyond limits
- (d) Compatible with adjacent structures
- (e) Zero leak rates across the welds

If the length of the motor case is longer than segmented construction, then suitable intersegment connection is resorted. On either end of motors, flanged joints

are used as interface between motor to igniter and nozzle. The shell thickness is one of the important parameters and it is decided as given below:

$$t_s = \frac{Pd}{2\sigma} (1 + MS) \quad (11.8)$$

P = (Maximum Expected Operating Pressure) $\times 1.25$

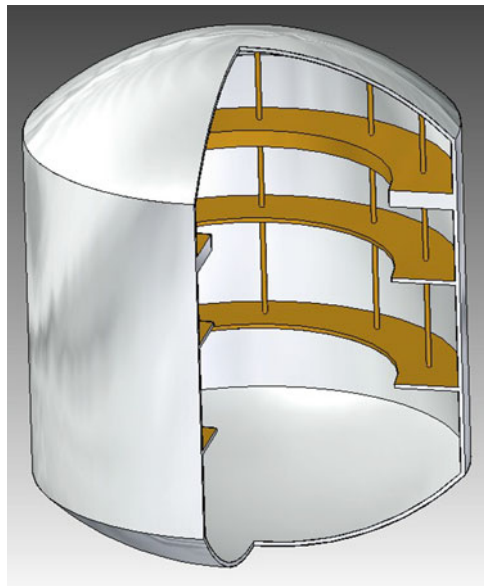
d = Mean diameter

σ = Ultimate strength

MS = Margin of safety

Theoretically, any margin beyond zero is sufficient. But considering the minimum mass requirement and to account for the uncertainties due to constraints in fabrication, assembly, etc. certain margin of safety is essential and hence it has to be at least 0.1. The motor cases are constructed generally using ferrous alloys and are strength-based designs. For liquid propellant tanks aluminium alloy or composite cases are generally used. In liquid tanks there are additional requirements to provide longitudinal or ring baffles inside the tank at identified locations to meet the slosh damping requirements as shown in Fig. 11.5. It is also a common practice to provide local reinforcements in tanks at the location of concentrated loads to minimize all the overloads. Chemical milling as explained in Sect. 11.6 is generally adopted for aluminium shells to minimize the mass and to meet the functional requirements of higher thickness near weld.

Fig. 11.5 Baffles used in liquid tanks



11.4.3 Interstage Structure

The commonly used interstage structures in an STS are structures between propulsive stages, base shrouds for core and strap-on stages, nose cones, payload fairing, payload adaptor, avionics bay shrouds, etc. Interstage structures are constructed either by using light alloys or by composite materials. These structures are having the necessary cut-outs in hardware to facilitate the access to various avionics packages after the vehicle integration. If the structure is metallic, it can be monocoque, semi-monocoque or closely stiffened shell constructions. If it is composite material, several construction options described in the later section can be considered. Just to understand the design approach for interstage structure, the widely used structure like a closely stiffened shell construction is taken as an example. This structure is having a shell formed by sheet metal skin, stiffened with sufficient number of stringers. In order to accommodate the cut-outs skin panels are to be reinforced using doubler plates. The structure has to have two end rings. To improve the buckling strength, sufficient number of bulk heads is to be introduced between two end rings appropriately arranged without interference of cut-outs. The basic inputs for design are generally the overall diameter of structure, height, the axial load (compression) and bending moment. Failure mode for this structure is essentially from buckling. Design has to decide on thickness of the shell, cross sections and number of stringers, cross section of end rings and also the cross section and number of bulk heads to enhance the stiffness. The average stress in the structure can be deduced as follows:

Total compression load in terms of EAL is generated using the expression

$$F_{xe} = F_x + \frac{4M}{d} \quad (11.9)$$

where

F_x = Axial load

M = Bending moment

d = Diameter of the shell

F_x and M are the ultimate values and generally taken as 1.25 times the limit load. Once EAL is worked out, the average stress μ on the structure is given by

$$\mu = \frac{F_{xe}}{A} \quad (11.10)$$

where

A = Total area of cross section

In addition to flight loads, some structures have to be designed for local loads, induced due to auxiliary rockets like retro and ullage rockets.

The design has to be iterative and demands suitable design computer code. Initially several configurations are to be considered and based on the analysis of strength, margin of safety and overall mass, a suitable configuration is to be selected. The structure has to be robust to withstand all possible failure modes, which are due to local buckling, yielding, global buckling, etc. Lower mass, fabrication constraints, cost and damage tolerance during use are also to be considered during the design phase. The various joints used in structure are to be checked for possible failures. In some of the structures, cut-outs are necessary to access the critical packages or components and accordingly necessary arrangements are to be made. It is important to detail the number and overall size of the cut-outs, the corner radius needed, etc. The skin panels are to be reinforced appropriately using doubler plate and the stringers adjacent to cut-outs are to be strengthened by using C stiffeners.

11.4.4 Structural Joints

Different structures of a launch vehicle are to be integrated through structural joints which have to withstand the loads. Joints have to offer minimum rotation. In a larger-diameter vehicle, these joints experience higher bending moments. In such cases, flanged bolted joints are used. The end ring flange of interstages on either end has to interface with the appropriate structure by utilizing number of bolts of suitable sizes as shown in Fig. 11.6. The design of such joints has to be carried out to withstand the maximum tension load experienced by the joint with sufficient margin. Maximum bolt load can be estimated by

$$L_{\max} = \frac{4M}{dn} \quad (11.11)$$

where

M = Ultimate bending moment

d = Bolt pitch circle diameter

n = Number of bolts

Once the maximum tension load is determined, the bolt size has to be decided to provide sufficient margin on yield strength. Generally bolts are preloaded 60–65 % of the yield strength to prevent the joint separation.

Different types of joints are utilized in STS such as riveted joints, bolted joints, ball-and-socket joints, merman band joint, tongue-and-groove joint, etc., as shown in Fig. 11.6.

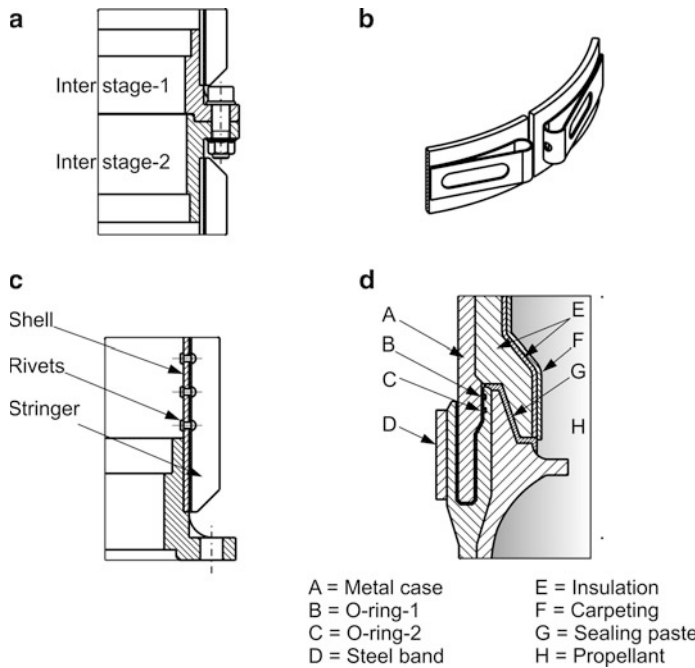


Fig. 11.6 Different types of structural joints. (a) Flanged joint (b) Merman Band joint (c) Riveted joint (d) Tongue and groove joint

11.4.5 Other Key Design Characteristics

Apart from strength and stiffness there are several other key design characteristics for an STS structure. The structure has to be designed to have a natural frequency above a certain defined value and within a certain range. This is essential to avoid the interference with any other dynamic systems in the vehicle including the control systems or to avoid excessive structural loading. Depending on the loading spectrum on the structure and also the maximum predicted loading cycles the structural life is decided. This factor has to be appropriately accounted in design to avoid the failure of the structure.

The ‘dynamic envelope’ is another important consideration during the design of payload fairing and the payload interface. The payload should not foul with the payload fairing even under all dynamic conditions of flight. It is essential to estimate the relative deflections of the structure and payload during design and coupled load analysis of the structural assembly and payload is carried out to ensure that sufficient dynamic envelope is available.

In an STS structure the stability is another important factor. Instability in structure leads to (a) overall structure buckling as a column or (b) buckling of any member of the structures resulting in the collapse of the structure. Therefore

during the design phase it is essential to ensure that structural member selected is having the needed cross-sectional area and moment of inertia so as to guarantee the stability.

Additionally standard design practices like avoiding the stress concentration regions, rounding of sharp corners, stiffening the cut-outs and carrying out detailed engineering incorporating fabrication, assembly and inspection requirements are to be meticulously adopted to arrive at a good design.

11.5 Shapes and Constructions for STS Structures

The optimum design of STS structure depends not only on the proper selection of material but also on suitable choice of shapes and constructions for tanks and interstage structures. Appropriate selection of manufacturing process for any structure such as welding metals, joining through bolts, rivets or adhesives is also important. The shapes and construction methods are different for each of the structures listed below, namely,

- (a) Motor cases for solid stages
- (b) Tanks for liquid propellants
- (c) Base shroud
- (d) Interstage structures which also includes vented interstage
- (e) Payload fairing
- (f) Structure for avionics bay
- (g) Nose cone
- (h) Payload interface adaptor
- (i) Thrust transfer joints for strap-on motors, etc.

The important considerations for realization of these structures are that each one of them has to meet the specified strength and stiffness requirements. The overall mass of each of the structures has to be minimized but without sacrificing the ease of fabrication, assembly and overall cost. The fixtures used for the assembly of various structures are to be suitably designed to reduce the overall cost.

The commonly used construction techniques for these structures are truss/framed, monocoque, semi-monocoque or skin stringer, closely stiffened shell, isogrid or waffle.

Truss or framed construction consists of members connected by joints. The members used are generally subjected to torsion or compression. This type of construction is generally used for internal structures which are housed within payload fairing or interstages. They are also used as open type of structure. A typical configuration of truss/framed construction is shown in Fig. 11.7.

In monocoque structures, the external skin of the object takes the load. This structure is having an unstiffened shell with practically no or very few stiffening rings. These structures are generally used for solid motor cases, for liquid stage

Fig. 11.7 Truss/framed construction



Fig. 11.8 Monocoque structure

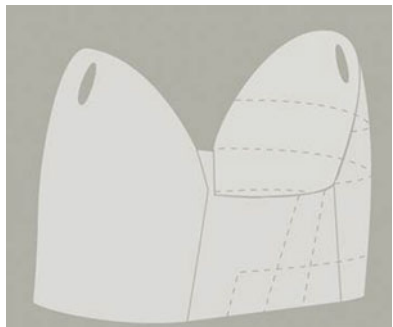
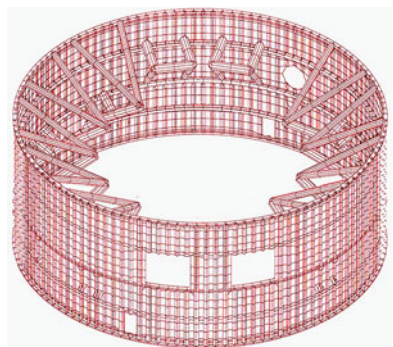


Fig. 11.9 Closely stiffened structures



propellant tanks and for interstage structures with a small diameter up to 0.5 m. A typical monocoque construction is shown in Fig. 11.8.

A semi-monocoque structure consists of a shell stiffened by the longerons and stringers. Even ring bulk heads are used sometimes. These structures are used generally up to diameter of 4 m. If the diameter is larger closely stiffened shell is used. The construction is to stiffen the thin shell by bulk heads in transverse direction and by closely shaped stringers formed out of metal sheets in longitudinal direction. A typical closely stiffened structure is shown in Fig. 11.9.

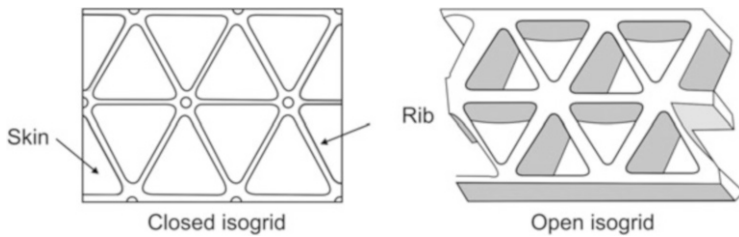


Fig. 11.10 Isogrid constructions

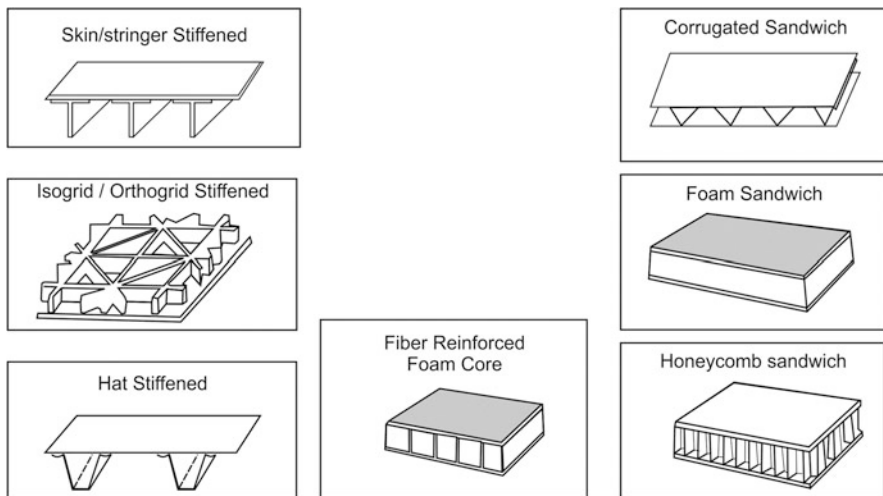


Fig. 11.11 Composite structural compositions

An isogrid structure is having integral grid stiffness and grids form equilateral triangle pattern. The isogrid structure acts like an isotropic material with uniform properties in all directions. Such structures demonstrate very good strength-to-weight and stiffness-to-weight characteristics. Isogrids are used for structures which are subjected to internal or external pressures along with longitudinal loads. The waffle pattern structures are having rectangular pockets. They are used when compressive stress field is not uniform on the shell. Isogrid shell can take uniform compressive field on the shell, like externally pressurized shells. Isogrid structures are realized using aluminium alloys such as AA2024, AA2219, AA6061 and AA7075, titanium alloy Ti-6 Al 4V and graphite epoxy composites. The metallic isogrid panels are easily machined from solid plates by controlled milling. Proper lay-ups and curing are used to achieve the required grid pattern in graphite/epoxy material. Typical isogrid panels are shown in Fig. 11.10.

With the advancement of technologies, composite interstage structures are being increasingly used in STS with the main aim of reducing the structural mass, while maintaining the same structural performance as metallic designs.

Several design concepts have been evolved and the various compositions of composite structures are as shown in Fig. 11.11. They can be broadly classified as

stiffened or sandwiched. The options available in stiffened structures are skin/stringer stiffened, hot stiffened or isogrid/orthogrid stiffened. The possible sandwich constructions are foam core sandwich, corrugated sandwich, fiber reinforced foam core sandwich and honey comb sandwich. The figures of merit to be considered in the selection of a suitable composite structural configuration are the basic mass, ease of fabrication, damage tolerance, repairability, ability to inspect components, sensitivity to hygroscopic absorption and ability to handle high temperature. The composites chosen for a structure should have flexibility to incorporate the changes with requirements at a later stage.

11.6 Materials for Structures

The key characteristics such as high strength-to-weight ratio, capability to operate in hostile environment and ease of manufacturability dictate the selection of materials. The method of construction also strongly influences the selection of materials. Mechanical properties such as strength, stiffness, density, ductility, weldability, corrosion resistance, propellant compatibility, thermal conductivity, malleability, magnetic properties, fracture characteristics, availability and cost restricts the selection of raw material. In certain applications wear resistance, conductivity and insulation properties are also important. Depending on the application, appropriate materials need to be selected. The material properties of high specific strength and high specific stiffness are important considerations in selection.

Commonly used metallic materials in aerospace structure are (a) alloy steels (15CDV6, maraging steel, stainless steel, etc.), (b) aluminium alloys (AA 2014, AA 2219, AA 2024, AA 6061, AA 7010, etc.) and (c) titanium alloys (Ti6 Al 4V).

Alloy steels used in structures like solid motor cases, rocket engine parts, brackets and fasteners have to have high strength. Typical mechanical properties of alloy steels are given in Table 11.1. Maraging steel is a low-carbon iron-nickel steel and with appropriate heat treatment, this material has very high strength, good dimensional stability, excellent toughness and ease of fabrication. Based on the yield strength of maraging steels, expressed in ‘kilopounds per square inch’, they are classified as 200, 250 or 300 grade. Generally 250 grade maraging steel is used in solid motor cases. The maraging steel gains its high strength through precipitation hardening which is an ageing process of martensite matrix. Hence it is named as maraging steel. Heat treatment of maraging steel is relatively simpler. Due to very low carbon, maraging steel has excellent welding capability. 15CDV6 alloy steel is a low-carbon steel with reasonably good yield strength. It also has very good weldability and toughness properties. This material is used in smaller solid motor cases.

In an STS most of the interstage structures, liquid propellant tanks, liquid engine components, payload fairing and many other structural elements deploy aluminium

Table 11.1 Mechanical properties of alloy steels

Material	Ultimate tensile strength (MPa)	Yield strength (MPa)	Elongation (%)	Fracture toughness (MPa)
15CDV6	1000	835	12	
Maraging steel M 200	1480–1520	1400–1450	12	155–200
M 250	1750–1800	1700–1725	8	>90
M 300	1900–1930	1880–1900	6	80
M 350	2480–2520	2400–2460	6	54

alloy materials. The advantage of this material is high specific strength and high specific modulus even under different temperature ranges. In addition aluminium alloys facilitate easy fabrication and have high corrosion resistance. Commonly used aluminium alloys are AA 2014, AA 2024, AA 2219, AA 6061 and AA 7075. All these materials are heat treatable with precipitation hardening. Solution treatment and ageing is the process used for heat treatment and it is possible to treat them to obtain different levels of strength. The nomenclatures generally adopted for various heat treatment processes are explained below:

1. T4: Solution heat-treated and naturally aged
2. T6: Solution heat-treated and artificially aged
3. T62: Solution heat-treated from ‘O’ or ‘F’ temper and artificially aged (O – Annealed, F – As fabricated)
4. T651: Solution heat-treated, stress-relieved by stretching and artificially aged
5. T87: Solution heat-treated, cold worked to approximately 7 % and then artificially aged (applies to AA 2219 and AA 2195 sheets and plates)

Table 11.2 gives the typical mechanical properties of aluminium alloys along with the heat treatment nomenclature.

Special materials like Al-lithium, Boron-Al, etc. are also used in certain designs to reduce the mass while meeting the required strength characteristics. Aluminium-lithium alloys have 10 % lower density and 11 % higher modulus than the conventional aluminium alloys. AA 8090 exhibits superior mechanical properties at cryogenic temperature. Typical mechanical properties of such materials are given in Table 11.2.

The titanium alloys play a major role in the realization of space structures since they have excellent properties like high specific strength, compatible with liquid propellants and high fracture toughness. They are widely used in propellant tanks, gas bottles and as structural elements in cryo applications to reduce the mass. Mechanical properties of commonly used titanium alloy Ti6Al4V is given in Table 11.3. In order to gain the weight advantage titanium linings are used in composite gas bottles.

Fibre-reinforced composite materials are finding more and more applications in structures like motor cases, payload adapter, payload fairing, vehicle instrument bay, etc. Glass fibre, Kevlar fibre and carbon reinforced plastic composites, honey

Table 11.2 Mechanical properties of aluminium alloys

Material	Ultimate tensile strength (MPa)	Yield strength (MPa)	Elongation (%)	Fatigue strength (MPa)
AA 2014 (T6)	483	414	13	125
AA 2024 (T4)	470	325	20	140
AA 2219 (T-62)	414	290	10	103
AA 6061 (T6)	310	275	17	97
AA 7075 T6	570	505	11	160
Al-lithium alloy	550	530	8	44
AA 2195 (T87)				

Table 11.3 Mechanical properties of typical titanium alloy

Material	Ultimate tensile strength (MPa)	Yield strength (MPa)	Elongation (%)	Fracture toughness (MPa)
Ti6Al4V	910	840	10	75

comb core sandwich structures are some of the composites widely used in aerospace structures. They have high specific strength and high specific stiffness. They also have very good fatigue strength and excellent resistance to crack propagation. The fibres act as arresters of cracks. It is possible to get the desired properties by proper selection of fibres and also careful lay-up of sequence for fibres. It is advantageous to realize the complex shape of structures in composites with proper selection of moulding and curing process. The composites used in structural applications are manufactured by laying up unidirectional or woven pre-peggs on a suitable moulding surface. The number of layers used and the orientation of lay-ups are decided based on design for a particular application. The product is subjected to specified temperature and pressure based on the resin used in a hot press or an autoclave. The orientation of lay-up adopted for a product depends on the load conditions on that product and are generally at $0^\circ \pm 45^\circ$ and 90° as shown in Fig. 11.12. The product with 0° lay-up is efficient to handle the load in principal axis whereas lay-ups at $\pm 45^\circ$ and 90° are good to handle the torsional and transverse loads respectively. Table 11.4 gives the salient properties of the fibres used in aerospace applications.

Fig. 11.12 Typical lay up of composite structures

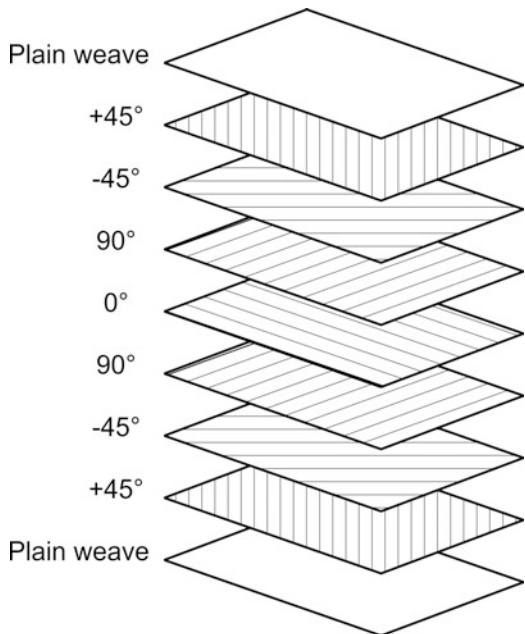


Table 11.4 Salient properties of the fibers

Material	Ultimate tensile strength (MPa)	Ultimate strain (%)	Modulus of elasticity (GPa)	Specific gravity (gm/cc)	Specific strength (MPa/(gm/cc))	Specific stiffness (GPa/(gm/cc))
Aramid	1100	2	70	1.2	917	58
Carbon Epoxy (High strength)	2000	1.2	150	1.7	1176	88
Carbon Epoxy (High modulus)	1000	1.3	320	1.7	588	188
S2- Glass fiber	1800	5.4	5.1	2.5	720	20
M250 (for reference)	1750	8	190	7.8	231	24

11.7 Structural Analysis

In the beginning of the aerospace structural design era, strength-based design approach was followed. So, basic structural design was carried out using strength of material (SOM) approach. Since the SOM approach is macroscopic approach, it

is difficult to estimate the stresses and strains in the critical areas, like cut-outs, in a complex geometry. In addition, this approach always results in non-optimized structures, which are always heavier than required. Therefore, it is essential to follow the stiffness-based approach, based on theory of elasticity which is a microscopic method. Whatever may be the maturity of the design methodology, a detailed analysis with theory of elasticity approach is required for establishing stresses, strains and margin of safety, which leads to highly optimized structures. But structural stability becomes an issue with highly optimized structures. Hence it is essential to consider strength, stiffness and stability during the initial phase. A trade-off is required between them for arriving at highly optimized structures.

Once engineering design is completed, detailed structural analyses are carried out to finalize the configuration. Subsequent to this engineering detailing, test requirement generation and finally qualification of the structures are needed before they are cleared for final mission. Structural analyses can be categorized into static and dynamic analyses and both of them influence the design requirements.

To ensure that the designed product meets the specified requirements, the compliance has to be checked through detailed analysis and testing. Rigorous analyses provide the insight into the structural behaviour in terms of its suitability and the margin available. If any deficiency in design is noticed in any of the elements, they are to be redesigned to meet the requirements.

The nature of complex loading, boundary conditions, interactions between several structural elements, interfaces with the adjoining structures, complicated geometries and varying material properties makes the analysis very complex. All these factors need to be accounted suitably in modelling. When it is an assembly of several structures, the analytical solution is not easily feasible. However if the components of the vehicle are suitably modelled the numerical techniques can be used for analysis. During the analysis, displacements, strains and stresses, frequencies and mode shapes for critical loads and various conditions are evaluated in detail.

11.7.1 Analysis Tools

With the advancement of powerful computers, faster numerical methods using numerous general-purpose software have been developed for structural design and analysis. One of the methodologies is finite element method (FEM). FEM can be defined as a numerical technique to solve a continuum problem, in which the continuum is divided into number of elements. These elements are connected to points, which are known as nodes. In a broad sense, FEM is a curve-fitting technique. FEM can also be divided into three categories: (a) displacement formulation, (b) stress formulation and (c) hybrid technique, which couples both the approaches listed earlier. The displacement formulation is very versatile and widely used. It is applicable for linear and non-linear problem solutions.

The general procedure in finite element analysis consists of preprocessing, analysis and postprocessing the results. The preprocessing involves (1) generation of geometry, (2) dividing the geometry into assembly of finite elements, (3) applying appropriate boundary conditions, (4) allocating material and geometrical properties and (5) specifying the forces acting on the structure. The analysis involves (1) static analysis to estimate the stresses and strain, (2) structural dynamic analysis which consists of frequency, mode shape and dynamic response evaluation and (3) stability analysis such as buckling analysis and interdisciplinary coupled analysis such as aeroelasticity, thermo-structural analysis, etc. Post-processing and the results' analysis are basically interpreting and assessing the results, which is the most complex job and requires efficient tools. Many efficient graphical postprocessors are available with various analysis tools, to plot or animate the deformed shape, contour plots of stress and strains, mode shapes, extracting the maximum displacement and calculation of various types of stresses and strains in required coordinate system.

The desirable features of a general-purpose code are (1) large number of finite elements to handle linear and non-linear analyses and (2) good material handling capability, like isotropic, orthotropic, anisotropic, viscoelastic and temperature-dependent material properties.

There are several general-purpose computer codes, which are readily available to analyze the structure using FEM. Most of the packages provide the capability for optimization and can be used during the initial phase of design for reducing the mass of the structure. All these packages have very efficient pre- and postprocessors for modelling and processing the results. Proper tool selection has to be based on the nature of the analysis needed and the specific features available in each of these software. These tools facilitate proper modelling of the structure to represent its actual behaviour through a combination of several finite elements.

11.7.2 Static Analysis

Static analysis, which is also known as stress analysis, for estimating the deflections, deformations, stresses and strains for known applied loads, may be linear or non-linear analysis depending on the requirement. The fundamental equation solved in FEM for static analysis is

$$\{F\} = [K]\{\delta\} \quad (11.12)$$

where

$\{F\}$ = Applied force matrix (Unit: N)

$[K]$ = Global stiffness matrix (Unit: N/m)

$\{\delta\}$ = Unknown displacement (Unit: m)

Different types of polynomials of different order are assumed for the displacements for different types of elements to derive the element stiffness matrices using principle of minimum potential energy. Details of deriving the stiffness matrix are out of the scope of the book and are available in standard textbooks. The above equation is solved for displacement, using various numerical techniques like the Gauss elimination technique, Gauss-Seidal method, etc.

Once the displacement is estimated, the strain and stress components are derived using the following equations:

$$\{\epsilon\} = [B]\{\delta\} \quad (11.13)$$

$$\{\sigma\} = [D]\{\epsilon\} \quad (11.14)$$

where

$\{\sigma\}$ = Stress component matrix

$\{\epsilon\}$ = Strain matrix

$[B]$ = Differential matrix, depends on the formulation

$\{\delta\}$ = Displacement matrix

$[D]$ = Material constituent matrix, depends on the problem, like plane stress, plane strain, bending, composite construction, etc.

Finite element models for stress analysis should have very large degrees of freedom to accurately predict the stresses and strains, especially in the critical regions such as cut-outs, sharp edges, near joints, etc. Near these critical regions, the mesh should be finer, in order to capture the stress concentration. But for buckling and dynamic analyses moderately coarse mesh is enough.

An engineering problem can be modelled in many ways depending on the application. Using mathematical concepts, complex finite element models can be simplified. Use of symmetry reduces largely the computational time and cost. If both structure and loads are symmetric with respect to an axis, an axi-symmetric model is enough with appropriate boundary conditions. Figure 11.13 shows a typical model

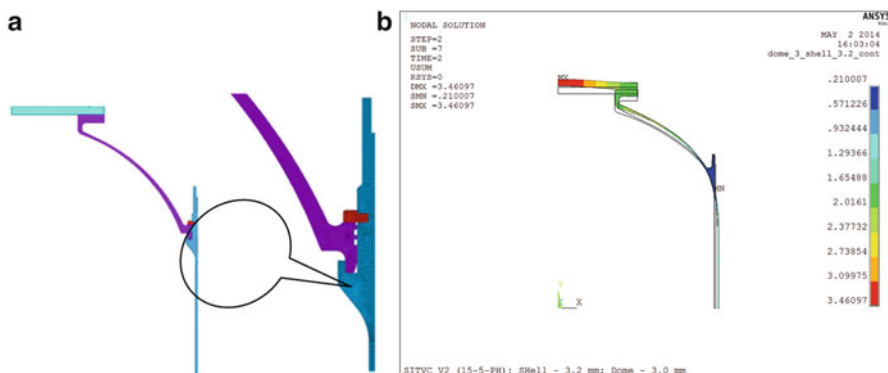
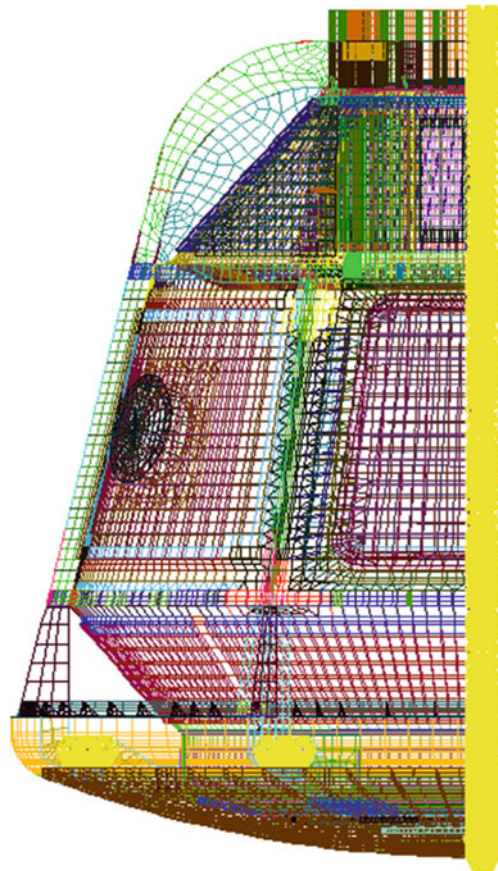


Fig. 11.13 FEM model and displacement contour of a typical pressure vessel **(a)** FEM model **(b)** Displacement

Fig. 11.14 Typical half model



of a pressure vessel made of axi-symmetric concept and displacement contour plot. The colour code in the contour plot represents the magnitude of the displacement.

If the structure and loads are symmetric with respect to one or two planes, half or quarter models are enough with appropriate symmetric and anti-symmetric boundary conditions for evaluating the structural characteristics. Figure 11.14 shows a typical half model. If it is a stiffened shell, a 3D model with stiffeners modelled using beam or shell elements is essential. Finite element 3D model of a typical structural shell with stringers is shown in Fig. 11.15.

The isogrid construction is mostly idealized using equivalent shell properties or completely modelling the packets using shell elements. Truss constructions are modelled using rod elements and any rod element should not be divided. Extra care has to be taken in analyzing the dome/cylinder junction, tongue/groove joints and core-strap-on links.

Solid propellant motors should be analyzed for stress, fracture and visco-elastic propellant structural integrity. Stresses on the propellant grains, at the interface of propellant, loose flaps and motor cases have to be estimated and positive margin

Fig. 11.15 Typical 3D – FEM model

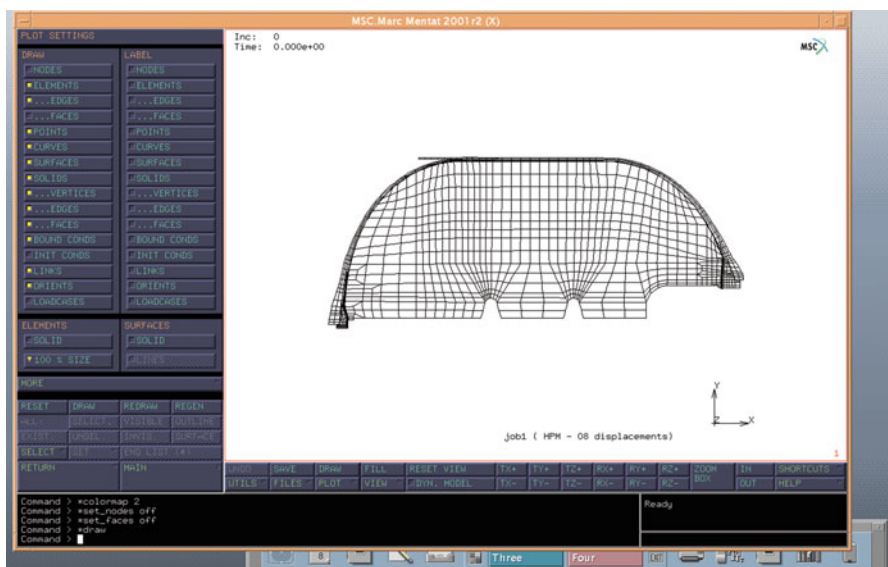
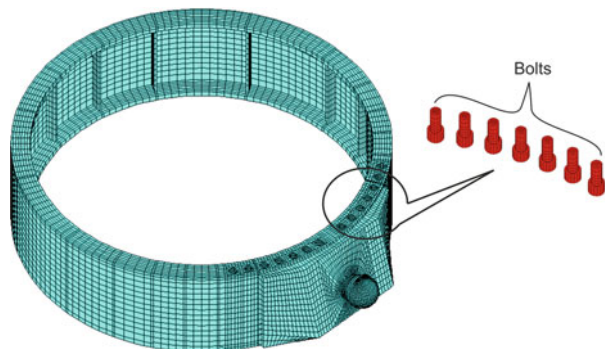


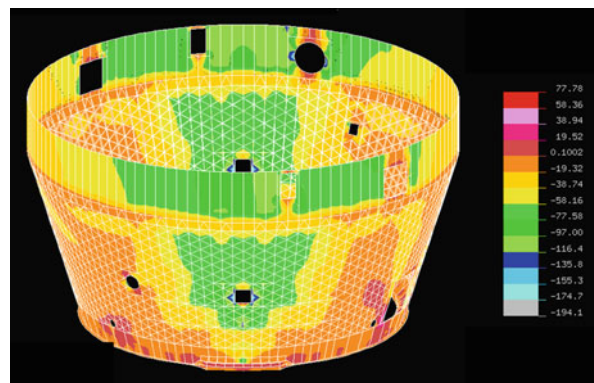
Fig. 11.16 FEM model for solid propellants

should be established. Since the propellant has Poisson's ratio near 0.5, special hybrid elements have to be used. A typical finite element model of solid propellant motor is shown in Fig. 11.16.

Thermo-structural analyses are to be carried out to study the dimensional stability of structures, which undergo very high temperatures. Usually, non-linear analysis is carried out by combining both thermal and structural loads in iterative manner.

A typical stress contour on the surface of a typical aerospace structure is given Fig. 11.17. From this figure, it is evident that the stress concentration, near the cut-out, is large compared to other regions. By observing these stress patterns, the low stressed area can be identified and structural optimization can be carried out. Similarly, stiffener around the cut-out can be properly modified in such a way that the stresses around are reduced to acceptable limit.

Fig. 11.17 Stress contour of a typical structure



Once a structural configuration is finalized, static stability studies are to be carried out, by performing buckling analysis. Buckling is not a structural failure mode, it is a stability problem. Various types of buckling modes are (1) skin buckling, (2) crippling, (3) column buckling and (4) overall buckling of total structure. Through buckling analysis, eigen values can be obtained and the margin can be estimated after multiplying with knock-down factor, which is due to imperfection in the construction. Buckled mode shape of a typical structure is shown in Fig. 11.18.

11.8 Structural Dynamic Analysis and Testing

The STS structure is an assemblage of a large number of stage motors, interstage structures and a number of structural elements with different sizes and shapes. The length-to-diameter ratio in most of the vehicles is large and it also has varying stiffness and mass all along the length. This makes the launch vehicles very flexible and hence the detailed structural dynamic studies are essential. They can be classified into four major categories:

- Dynamic characterization: Evaluation of free vibration characteristics such as frequencies, mode shapes, generalized mass
- Evaluation of dynamic excitations
- Dynamic response and stability studies: Involves coupled load analysis, pogo stability analysis, control structure interaction studies, aeroelastic studies, dynamic stability studies, etc.
- Vibration and acoustic testing: Involves generation of environmental test level specification for component level and subassembly level for both qualification level tests and flight acceptance tests

The comprehensive structural dynamic activities needed for an ascent phase STS vehicle are illustrated in Fig. 11.19.

Fig. 11.18 Buckled mode of a typical structure

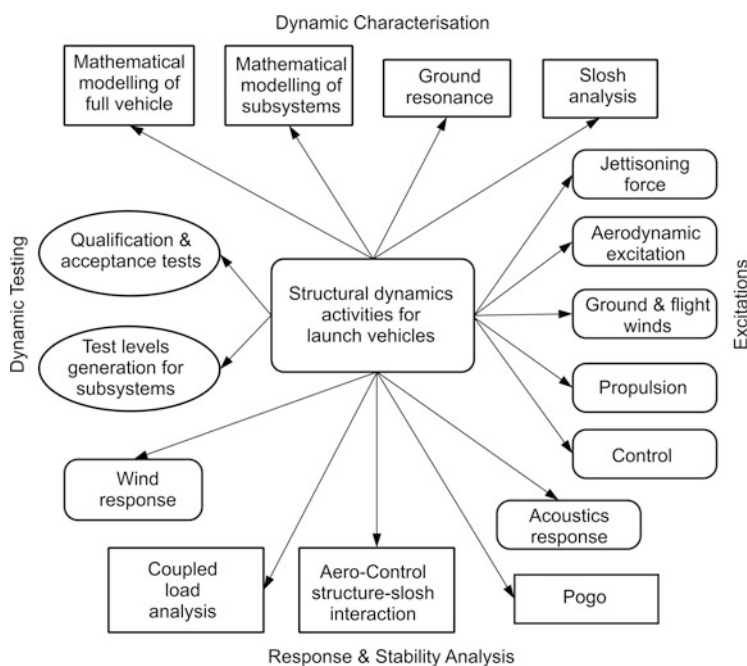
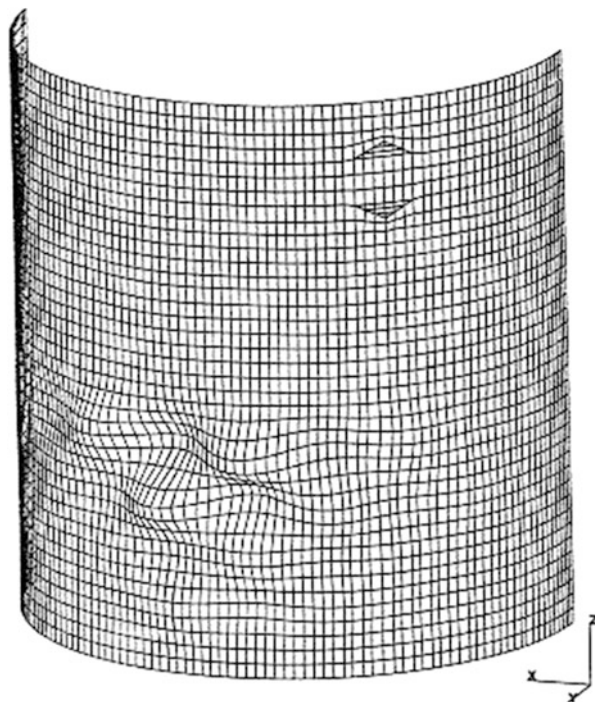


Fig. 11.19 Various steps in structural dynamic characterization

11.8.1 Dynamic Characterization of Structures

Frequencies and mode shapes are the fundamental requirements for digital autopilot design and analysis, Pogo system design and analysis, structural dynamic response estimation, etc., and these parameters are independent of external excitation. Proximity between structural frequencies and control, propulsion, excitation frequencies may cause resonance and hence for the launch vehicles, it should be ensured that there is adequate separation between them. These parameters are obtained by solving the free vibration equations of motion

$$[M]\{\ddot{x}\} + [K]\{x\} = \{0\} \quad (11.15)$$

where

$[M]$ = Mass matrix

$[K]$ = Stiffness matrix

$\{x\}$ = Displacement

Generally in a launch vehicle system finite element method is used to find the frequencies and mode shapes. Different finite element models are generated for a particular purpose. There is no unified model possible for all the STS vehicles.

Since the accuracy of response and dynamic stability analyses completely depend on the natural frequencies and modes, the evaluations of these parameters are to be done meticulously. The major steps involved in dynamic finite element model generation are

1. Preliminary finite element models: This model is generated based on geometrical drawing and estimated mass properties.
2. Ground resonance tests (GRT): Ground resonance test configuration is decided based on the preliminary finite element models and practical restrictions.
3. GRT test-validated finite element models: Updatement of the models based on the GRT results.
4. Generation of flight-updated finite element models.

Depending on the applications, vehicle models are generated with predominantly beam model or a complex three-dimensional shell model. Depending on the requirements and accuracy, either total beam model or combination of beam and shell models is used. Various idealizations of a typical vehicle are given in Fig. 11.20. Since the stiffness contributions of solid propellant do not have significant effect on the vehicle modes and frequencies, it is generally neglected. But in the literature, it can be seen that the solid propellants are also modelled using viscoelastic solid elements.

Slosh dynamic characteristics are generated separately, by idealizing the liquid propellants contained in a rigid container. Slosh frequencies, slosh masses and their positions are obtained using either finite or boundary element methods. But in the launch vehicle lateral dynamic models, slosh dynamics is represented by a set of equivalent spring mass systems. Generally, first two fundamental slosh modes are

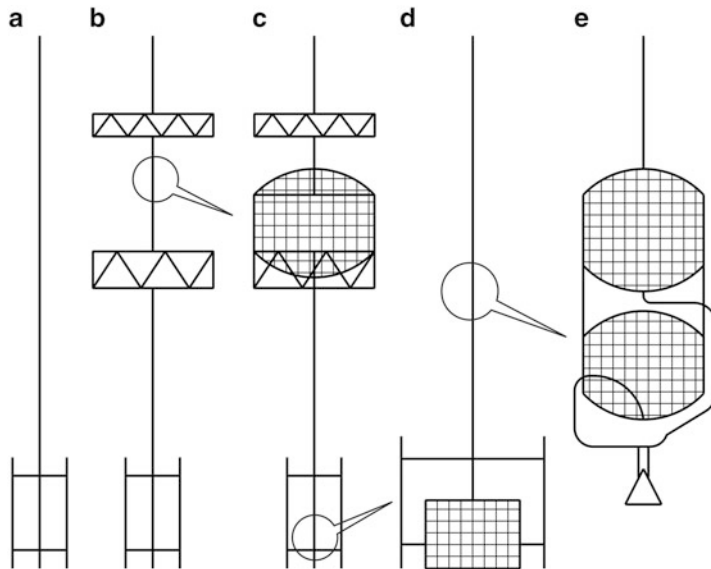


Fig. 11.20 Typical FEM models for dynamic analysis. (a) Total beam model (b) Beam interstage model (c) Beam + interstage propellant tank shell model (d) Beam + detailed model for base shroud (e) Propulsion stage model

considered. The non-sloshing fluid in the tank is lumped as rigid mass and mass moment of inertia.

For Pogo (an instability phenomenon, when liquid stages are in operation) stability analysis, propellant feed line mode shapes and tank bottom modal pressures are essential. Hence, in Pogo models, the fluid is represented by virtual mass technique.

As far as vehicle joints are concerned, generally, they are assumed as excellent category and provision has to be made to introduce joint rotation constants in the model. The engines used in the stages are treated as a vehicle branch and the lateral dynamics is estimated by lumping the mass and mass moment of inertia at engine centre of gravity.

Mode shape of a typical vehicle evaluated using dynamic analysis is given in Fig. 11.21. The frequency range corresponding to mode shape is also given in the same figure.

11.8.2 Ground Resonance Tests

The finite element model used for dynamic characterization of the vehicle has to be validated by subjecting a suitable proto-hardware of the vehicle by dynamic testing

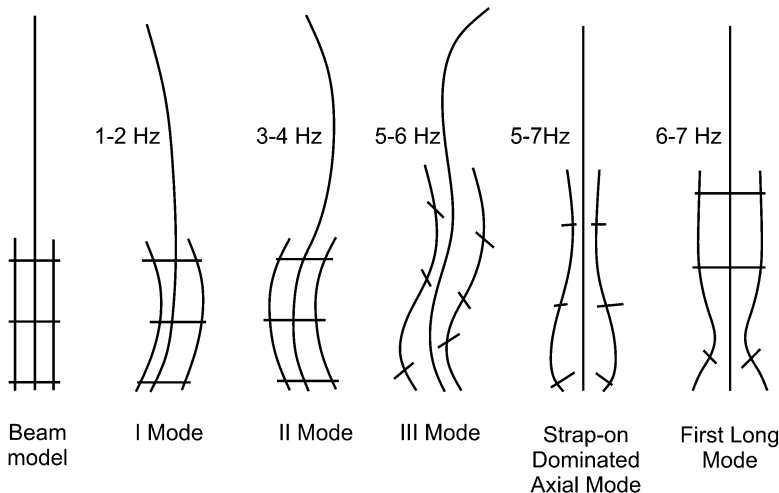


Fig. 11.21 Mode shapes of a typical vehicle

known as ground resonance testing (GRT). This test simulates the free flight conditions to obtain the natural modes of the full vehicle. If the dynamic models are not validated through ground tests the uncertainties are too large and designs have to cater with higher safety margin leading to larger mass. It is also essential to have realistic values of vehicle modes for control system designers in order to avoid instability during flight.

In ground resonance tests generally full-scale hardware with mass, stiffness and interfaces are simulated equivalent to flight hardware. Various other subsystems like avionics, actuators, engines, gas bottles, etc. are mass simulated. The test article is suspended on a suitable suspension system which provides near free-free condition to the test article. The suspension system should be capable of supporting the total loads with sufficient margin and the rigid body frequency of the entire assembly with suspension system should be at least five times lower than the frequency of the simulated vehicle. The test article is excited simultaneously by multiple shakers at identified locations to extract all axial, lateral, torsion and coupled modes. The responses at different identified locations are measured using accelerometers. Using this data the modal characteristics, damping for various modes, transfer functions at excitation sources, etc. are evaluated. Since it is not possible to test the flight hardware, such as solid propellant motors and also time variation of propellants, GRT models are to be updated for flight conditions.

11.9 Dynamic Response and Stability Analyses

Once a reliable finite element model is generated, a series of response and stability analyses are to be carried out. Modal superposition technique is generally used to solve the structural dynamic equation

$$[M]\{\ddot{x}\} + [C]\{\dot{x}\} + [K]\{x\} = \{F\} \quad (11.16)$$

where

- [M] = Mass matrix
- [K] = Stiffness matrix
- {x} = Displacement
- [C] = Damping matrix
- {F} = Excitation force

The response analyses are carried out in time domain and the stability analyses are carried out in s-domain. For linear system, the total dynamic response can be represented as a summation of responses due to various numbers of modes, which is represented by the following equation:

$$\{x\} = \sum_{i=1}^n \phi_i q_i \quad (11.17)$$

where

n = Number of modes

ϕ_i = Normalized mode shape of ith mode

q_i = Generalized coordinate of ith mode

By substituting Eq. (11.17), Eq. (11.16) becomes

$$\{\ddot{q}\} + [2][\zeta][\omega]\{\dot{q}\} + [\omega^2]\{q\} = \frac{\{\phi\}^T\{F\}}{\{\phi\}^T[M]\{\phi\}} \quad (11.18)$$

where

$[\zeta]$ = Mode damping ratio matrix

$[\omega]$ = Mode shape frequency matrix

Equations (11.18) and (11.17) are solved for displacement, velocity and acceleration in time domain using numerical techniques like Runge-Kutta technique, Newmark-Beta technique, etc. For stability analysis the above equations are converted into s-domain using Laplace transformation and solved for complex eigen values.

Coupled load analysis, basically the transient response analysis, is carried out, for evaluating the loads on the satellite components for various engine burnout transients for low frequency range (1–100 Hz). Usually it is not carried out for ignition transients, because of the high energy levels of the systems. For carrying out the coupled load analysis, satellite models are needed in the form of reduced stiffness and mass matrices. This analysis is also useful for generating the sine test level specification for the spacecraft.

Flexible vehicle response analysis is to be carried out for assessing the aeroshock-control-structure interaction. This analysis has to be carried out along with the

six degrees-of-freedom rigid body simulation. In this simulation, incremental force and moments, incremental control forces, incremental rates at rate gyro location and inertial system unit are to be estimated. Bending moment and equivalent axial force at various locations are also to be calculated. These values are to be used for launch clearance purposes.

Pogo is a stability problem which occurs due to the interaction of propulsion system dynamics and structural dynamics. Like structural frequencies, the propellant feed lines have their own natural frequencies. When the axial structural frequency coincides with the propulsion frequency, resonance occurs, which results in large oscillations in the thrust. This thrust oscillation pressure wave travels back through the flow and reaches the tank bottom and increases the pressure on the domes. Therefore, pogo is a closed loop stability problem, occurring only when liquid engines are in operation. Pump-driven liquid stages are more susceptible for pogo. Even pressure feed system also undergoes different types of pogo, which is due to ullage pressure oscillation.

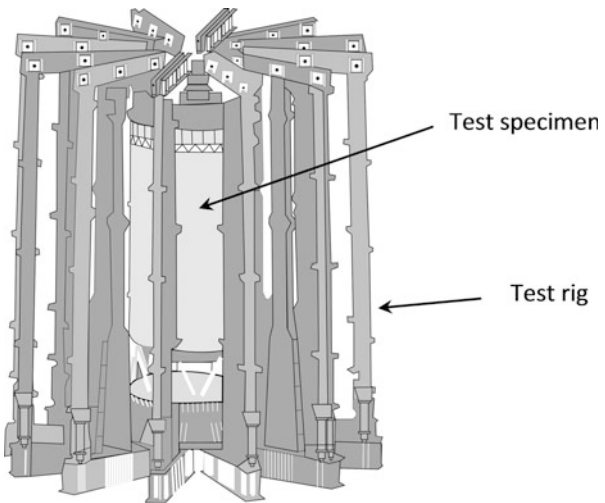
Theoretical approach similar to autopilot analysis is carried out in s-domain using discrete time instances. To start with, estimation of longitudinal modal parameters, axial frequencies, mode shape of feed line, modal pressure at the tank bottom are to be carried out. Parallelly, propulsion system modelling using finite element approach is to be developed involving various propulsion elements like tank outlet, compressible and incompressible ducts, pogo corrector pump, bellows, junctions, accumulator, thrust chamber, etc. Propulsion system equations are to be coupled with structural motion and solved simultaneously for complex eigen values, from which the system damping is calculated.

11.10 Structural Static Testing

Structures designed and analyzed for various load cases are to be qualified for their flightworthiness, through a series of structural static tests. Static tests are the main means of understanding adequacy of structural design and manufacturing. Although these structures are subjected to detailed analysis to evaluate the design margins, it is extremely difficult to predict the exact behaviour of joints, to quantify the locked-up stresses during realization and other imperfections leading to high stress regions. Proper static tests reveal the actual stress state of the structure and useful for correction of mathematical models, the estimation of structural margin, reliability of manufacturing process, etc. Extreme care should be exercised in test planning, since improper loading may lead to structural premature failures and may lead to wrong conclusions.

The structural test planned has to cater to the loads experienced during flight due to thrust, inertia, control, aerodynamics, separation, etc. Depending on the component, these loads are simulated in the tests by combining tensile load, compressive load, bending moment, shear force, internal or external pressure, etc.

Fig. 11.22 Typical structural testing



Unique test setups, which include test stand design and development, conceptualizing and development of loading facilities, instrumentation, data acquisition and analysis, are, to be established for different tests. Often component level testing may not be sufficient, because load path deviation makes it vital to have integrated structural tests. One of such typical integrated tests for a structure is shown in Fig. 11.22.

The test specimen is kept vertically as shown in Fig. 11.22. The loads are to be applied either as a point load or uniformly distributed load through appropriately designed adaptors. Figure 11.22 shows the uniformly distributed load by suitable selection of fixtures. Multi-channel feedback control systems are used for proper load application and aborting the tests. The simulated loads are applied through a number of hydraulic jacks. The actuator sizing and the working hydraulic pressures are estimated on the overall maximum load to be applied on the specimen. Pretest predictions are used to identify the measurement locations, such as maximum stress locations, joints, cut-outs, etc. The test specimen is instrumented with a large number of strain and displacement measurements, throughout component at the critical locations. Nowadays, acoustic emission techniques are also used to identify the faults during the test.

For structures, such as payload fairing and nose cones, external pressure loads are predominant. In such cases, the structure is enclosed using a bladder to create the pressure chamber. Variable pressures along the length of the structures are created by using multiple pressure chambers and applying different pressures.

Similarly various tanks, which are subjected to internal pressure, are tested by filling them with appropriate fluid medium and pressurization. As the temperature affects the mechanical properties of materials, the fluid medium has also to be properly chosen. For example, cryo tankages, which are subjected to low temperatures, have to be tested using liquid nitrogen as the medium.

Liquid stages are to be tested for combined pressure and axial loads. Due to test facility constraints, sometimes the hardware may have to be tested for equivalent

Table 11.5 Acceptable test factors for structures

Structure type	Qualification test (or) ultimate load test	Flight acceptance tests (or) proof pressure test
Low pressure vessel & other structures	1.25	1.1 for metallic 1.05 for composites
Very high pressure vessels	2.0	1.5

axial load. When structure is subjected to ultimate load test (qualification test), which is 125 % of limit load, no global yielding is accepted. Local yielding is allowed. Whenever cut-outs are provided in the structure, they are not used during the tests since they are not expected to transfer any load during the flight. Table 11.5 gives the details of acceptable test factors.

Further, during qualification time, some of the structural elements are destructed to evaluate the exact margin in the design. It is mandatory in the case of pressure vessels; they are tested for burst and the margin availability is established. For interstage type of structures, only qualification or ultimate load tests are carried out. But all the pressure vessels are subjected to flight acceptance or proof pressure test before the flight and no yielding is accepted.

11.11 Environmental Testing for Space Structures

Every structural element on the STS is subjected to vibration, acoustics and shock loadings by carrying out environmental tests in order to qualify them for flight applications. Environmental tests can be categorized into mechanical, thermal and electromagnetic interference (EMI) tests. The main purposes of these tests are for assessing the components for their in-service performance, for qualifying them for flight environment and also to detect any workmanship error.

The mechanical tests are sine vibration tests, random vibration tests and acoustic tests. Different tests are required to ensure reliability of the product before the flight. Sine vibration test is carried out for frequency range up to 100 Hz, with the excitation of one mode at particular time. Random vibration test is carried out for frequency range up to 2000 Hz, in which all the modes are excited simultaneously. But in random vibration tests, spring mass types of modes are excited well. Both sine and random vibration tests are performed in all three axes using appropriate shaker systems. Further acoustic tests are carried out in the acoustic chamber, in which acoustic levels are generated using horns. In this test, flat surface modes are effectively excited and the component is excited across the surface.

All the structural elements undergo two levels of testing, namely, (a) qualification or prototype level tests and (b) flight acceptance tests.

Table 11.6 Typical sine vibration specifications for qualification tests

Sine vibration: Qualification test level				
	Frequency (Hz)	Longitudinal axis	Lateral axes	Sweep rate
Component level	10–16	20 mm DA ^a	12 mm DA ^a	2 Oct/s
	16–100	10 g	6 g	
Sub assembly level	5–10	7.5 mm DA	3.75 mm DA*	
	10–50	1.5 g	0.75 g	
	50–100	0.75 g	0.375 g	

^aDA displacement amplitude

11.11.1 Qualification Tests

The main purpose of qualification tests is essentially to assess the design sufficiency of the structure and also to establish the structural margin. The basic requirement of the hardware for qualification tests has to be that it has to be identical to flight hardware in all respects. In qualification test, the hardware is subjected to higher environmental levels and the practice is to test the components to 1.5 times of the test level predicted for random vibration tests and +3 dB in acoustic levels. Additionally, the testing duration is also doubled in random vibration tests.

The test levels to be used have to be derived depending on the vehicle, the atmospheric disturbances and the propulsion system used. To illustrate the test levels for a typical vehicle the sine vibration specifications can be as given in Table 11.6.

11.11.2 Acceptance Tests

The main purpose for flight acceptance tests is to carry out the performance check of various modules with flight expected levels and flight duration to identify any workmanship-related issues, to assess the flightworthiness and integrity of the structural elements. Usually flight acceptance tests for structures are carried out at subassembly level with all important components. Acoustic and random vibration tests are to be carried out at acceptance test level. Test levels vary for components and it depends on its spatial location and the flight environment. For example, the components near nozzle are to be tested for higher values. Typical sine vibration specifications for flight acceptance test can be as given in Table 11.7.

Table 11.7 Typical sine vibration specifications for flight acceptance tests

Sine vibration: Flight acceptance test level				
	Frequency (Hz)	Longitudinal axis	Lateral axes	Sweep rate
Component level	5–10	5 mm DA	2.5 mm DA	4 Oct/s
	10–50	1.0 g	0.5 g	
	50–100	0.5 g	0.25 g	
Subassembly level	5–10	7.5 mm DA	3.75 mm DA	
	10–50	1.5 g	0.75 g	
	50–100	0.75 g	0.375 g	

11.12 Aeroelastic Analysis and Testing

The optimized design processes used for structures results into low mass thus making the aerospace structure into highly flexible configuration. Elastic deformations in a structure play a dominant role in defining the external aerodynamic loads. In aeroelasticity the aerodynamic forces interact with elastic forces of the vehicle structure. The loads and deformations not only interact but under certain conditions of structural configuration, dynamic pressure and Mach number, the interaction between them can turn unstable. The structural vibration generates elastic and inertial forces which in turn interact with aerodynamic forces to cause aeroelastic problem. These three forces form three vertices of a triangle and the classification of aeroelastic problem depends on the interaction of these forces.

The unstable interaction of these forces causes failure to the structure. Therefore the design has to address the instability and ensure that the operating conditions are always within the stable region. The huge developmental or operational cost necessitates the inclusion of aeroelastic studies in the design stage itself.

Typical aeroelastic problems in structures of STS are (a) flutter, (b) aeroelastic divergence and (c) transonic buffeting. Further, controlling the unstable system is a difficult task.

11.12.1 Flutter Phenomenon

Flutter is a dynamic aeroelastic phenomenon which occurs due to interaction of aerodynamic, inertial and elastic forces. It is a self-induced oscillatory phenomenon and there is no need of any external disturbance. Flutter is generally associated with skin panels, fins of rockets, control surface with hydraulic actuators and blades of turbines. For example, in a wing when the airflow increases, it causes the increase in bending frequency and reduction in torsional frequency. At critical flutter speed, these two frequencies coincide causing instability in oscillations leading to structural failure. The overall damping at this point becomes zero.

There are different types of flutter as detailed below:

- (a) Classical flutter, which occurs with lifting surfaces (like wings, fins, etc.), is due to the coalescence of two different structural modes. In stable conditions, the energy caused by the interaction of elastic, aerodynamic and inertial forces is dissipated to the environment from structure through damping. At particular vehicle velocity, which is known as flutter velocity, the system starts acquiring energy from the aerodynamic flow, which results in often destructive oscillations. At flutter velocity, the system damping becomes zero. The physical mechanism is that as the vehicle velocity changes, the virtual mass acting on the lifting surfaces changes the fundamental frequencies. When two frequencies coincide, resonance occurs. Classical flutter is a dynamic stability problem. Fins of the rockets are to be studied for classical flutter; it is always better to ensure a flutter margin of 1.0 due to the uncertainty in aerodynamic theories.
- (b) Unlike classical flutter, panel flutter occurs only in supersonic conditions and leads to a structural failure. In STS, all the structures are to be checked for panel flutter condition.

11.12.2 Divergence

Another type of aeroelastic static instability is divergence. Divergence speed for lifting surfaces and for a full rocket has two different meanings. For lifting surfaces, like wing and fins, it is based on the static torsion stiffness of the surface. For rockets, the static stability is based on the centre of pressure (CP) and centre of gravity (CG) locations. For a rocket to be statically stable, the CP should be behind CG. At some critical dynamic pressure the CP and CG coincide, which is known as divergence dynamic pressure and the corresponding velocity is known as divergence speed. Flexibility of the vehicle also has its influence on static instability. Generally, the sounding rockets do not have control. During design phase itself, divergence speed of uncontrolled rockets should be determined to ensure static stability. Divergence margin, the distance between CP and CG location, is usually defined in terms of diameter of the rocket. It should be ensured that the divergence margin is two times the diameter of the vehicle.

11.12.3 Buffet Phenomenon

Buffet is defined as the structural response for unsteady aerodynamic loads. Mostly it happens in transonic regime, where the aerodynamic flow is unsteady and unpredictable.

The larger payloads necessitate the introduction of bulbous payload fairings in STS. The larger diameter of the payload fairing is connected to the core body through a boat tail (conical position), which in turn causes the separation of airflow

at boat tail and reattachment later at cylindrical core body. When the vehicle is traversing from subsonic to supersonic, shock is formed. During transonic regime, these shocks oscillate over the payload fairing and generate additional dynamic oscillations, which cause additional bending moment on the structure. Usually, additional factors from 20 to 60 % are considered on design bending moment for buffet. The factor varies for various structures all along the length. Simulating this phenomenon theoretically is not amenable, which requires a strongly coupled aerodynamics and structure software. Hence experimental studies are to be carried out for estimating the buffet bending moment. Aeroelastic scale models, which represent the first two global bending modes, are to be realized and instrumented with strain gauges. These models are subjected to various flow conditions in the wind tunnel, and from the strain measurements, the buffet bending moment is estimated.

Bibliography

1. Bruhn, E.F.: Analysis and Design of Flight Vehicle Structures. Tri-state offset company, Ohio (1965)
2. NASA space vehicle design monograph: Structural design criteria applicable to a space shuttle (January 1971)
3. Wiesel, W.E.: Spaceflight Dynamics. McGraw Hill, New York (1989)
4. Young, W.C.: Roark's Formulas for Stress and Strain. McGraw Hill Book Company, New York (2007)
5. Timoshenko, S.P., Goodier, J.N.: Theory of Elasticity. McGraw-Hill Book International Book Company, New York (1984)
6. Shigley, J.E.: Mechanical Engineering Design. Eighth edition, McGraw-Hill Book International Book Company, New York (2008)
7. Bruhn, E.F.: Analysis and Design of Missile Structures. Tri-state offset company, Ohio (1967)
8. Bathe, K.J.: Finite Element Procedures. Prentice-Hall of India Pvt. Ltd., New Delhi (1996)
9. NASA space vehicle design monograph. Flight loads measurements during launch and exit. (December, 1964)
10. Thornton, E.A.: Thermal Structures for Aerospace Applications. AIAA Education Series. AIAA, Reston (1996)
11. US Air Force Materials Laboratory: MIL-HDBK-5E, metallic materials and elements for aerospace vehicle structures. Air Force Materials Laboratory, Wright-Patterson AFB (1987)
12. Hammond, W.E.: Design Methodologies for Space Transportation Systems, AIAA education series, AIAA, Reston, VA (2001)
13. Hammond, W.E.: Space Transportation: A Systems Approach to Analysis and Design, vol. 1, AIAA education series, AIAA, Reston (1999)
14. Griffin, M.D., French, J.R.: Space Vehicle Design. AIAA Education Series. American Institute of Aeronautics and Astronautics, Washington, DC (1991)

Chapter 12

Thermal Systems and Design

Abstract The STS during its entire flight regime is exposed to different thermal environments, causing severe thermal loads to the vehicle, structural elements and several other sensitive elements. All thermal effects such as local heating rate and total heat load are to be analyzed in detail to understand the thermal loads during flight. Thermal environment of the vehicle and subsystems caused by aerodynamic heating depends mainly on their external configuration, vehicle surface material characteristics, flow field characteristics and vehicle trajectory. The thermal load caused by propulsion system depends on the type of propulsion system, vehicle operating altitude, nozzle expansion ratio and the vicinity of the subsystem elements with respect to the propulsion elements. Thermal protection materials and thickness in turn decide the thermal protection system mass depending on thermal environment, type of thermal load, materials used in the system and temperature constraints specified for the various subsystems. Thermal protection systems (TPS) are passive, semi-passive and active depending on the application. While appropriate TPS is used to ensure the normal function of the subsystem to meet the specified functions, the mass of the integrated vehicle has to be minimized. During the initial development phase, an integrated system design approach is required to arrive at optimum structural and thermal designs for the vehicle subsystems. Once the suitable thermal protection materials are chosen based on the detailed analyses, it is essential to carry out thermophysical and mechanical property tests for these materials within the temperature range they are expected to experience in flight. This chapter presents the thermal design aspects of vehicle and subsystems for a launch vehicle. The impact of the thermal environments, on vehicle and subsystems, the need for the integrated design strategy, the requirements of various subsystems which need thermal protection, design constraints and approach for optimum thermal design for each of the subsystems are highlighted. The various aspects of the heating environment due to jet exhaust are described. Thermal response analysis and the methodology for the analysis are covered. Tests for thermal protection systems and their qualification methods are also included.

Keywords Thermal system • Aerodynamic heating • Stagnation point heating • Base jet interaction • Vent hole • Thermal protection system • Heat flux • Thermal response analysis and Thermal tests

12.1 Introduction

The STS during its entire flight regime is exposed to different thermal environments, causing severe thermal loads to the vehicle, structural elements and several sensitive elements. During the pre-launch phase, the important sources of thermal loads are due to (1) direct solar radiation, (2) Earth reflected (Albedo) radiation, (3) Earth emitted radiation and (4) internal power dissipation of avionics elements. In addition to the above sources, the thermal loads during flight are (1) aerodynamic heating and (2) jet plumes and jet interactions and the thermal loads that affect the subsystems are local heating rate and total heat load. The heating rate induces thermal gradients across the thickness and along the surface of the structures resulting in a non-uniform temperature distribution whereas the total heat load increases the temperature of the elements.

The heat thus generated by the external thermal environments through the heat transfer mechanisms of conduction, convection and radiation either impairs sensitive elements or severely affects their performance. The non-uniform temperature distribution causes local distortions which in turn induces thermal stresses to the vehicle structural elements. For the structures with different materials which have different thermal expansion coefficients, even the uniform temperature distributions induce thermal stress. The non-uniform temperature causes additional stresses acting on the vehicle structural elements over and above the mechanical stresses due to steady and dynamic structural loads. Also, for many of the conventional structural materials used for the vehicle structures, the strength reduces drastically at elevated temperatures. Therefore, to ensure the integrity of the vehicle and subsystem structural elements and to ensure normal functions of the sensitive systems during flight, it is essential to restrict the temperatures within the allowable levels using suitable thermal protection systems (TPS).

Thermal environment of the vehicle and subsystems caused by aerodynamic heating depends mainly on their external configuration, vehicle surface material characteristics, flow field characteristics and vehicle trajectory. The thermal load caused by propulsion system depends on the type of propulsion system, vehicle operating altitude, nozzle expansion ratio and the vicinity of the subsystem elements with respect to the propulsion elements. Thermal protection materials and thickness in turn decide the TPS mass depending on (1) thermal environment and type of thermal load, (2) materials used in the system and (3) temperature constraints specified for the various subsystems. While appropriate TPS is used to ensure the normal function of the subsystem to meet the specified functions, in order to achieve the optimum performance of the vehicle, the mass of the integrated vehicle has to be minimized. Therefore, during initial development phase, an integrated system design approach is required to arrive at optimum structural and thermal designs for the vehicle subsystems.

Thermal design aspects of vehicle and subsystems of launch vehicle are given in this chapter, whereas the same for re-entry vehicles is included in Chap. 15 on Re-entry Missions.

In addition to launch vehicle thermal environments, their impact on vehicle and subsystems and the need for the integrated design strategy, the requirements of various subsystems which need thermal protection, design constraints and approach for optimum thermal design for each of the above subsystems are given in this chapter.

12.2 Heating Problems in Launch Vehicles

Before explaining the heating problems and the related issues, some important definitions are described:

1. *Heat* is defined as the energy transferred from a high-temperature object to a lower-temperature object. It is a vector quantity, in the direction of decreasing temperature. Unit is Joule (J).
2. *Heating rate* is defined as the rate at which a body is heated. Unit is J/s (W).
3. *Heat flux* is the heating rate per unit area. This is a vector quantity represented generally as \dot{q} . Unit is W/m².
4. *Heat load* is the heating rate per unit area, integrated over a period of time. This is generally represented as Q and the unit is J/m².
5. *Thermal load* is defined as the load on a structure induced by change in temperature.

Heating due to solar radiation, Earth reflected radiation, Earth emitted radiation and internal power dissipation is of general nature. The aerodynamic heating and jet plume effects are the major sources for thermal environment for the vehicle and its flight environment.

12.2.1 Aerodynamic Heating Over a Flat Surface

When there is a flow of air over a body, the air particles in contact with the surface of the body are brought to rest due to the viscosity of the air and the surface roughness. In this process of slowing down, the kinetic energy of the air particles is converted into thermal energy, which raises the temperature of the air at the surface. The high temperature air that surrounds the vehicle structure induces transfer of heat to the surface with which it is in contact and this process is termed aerodynamic heating. The total temperature rise occurs within the boundary layer and the temperature increase also depends on the type of boundary layer. If the flow velocity is more, the temperature rise is also more.

The velocity profile within the boundary layer caused by viscosity on a typical flat surface is given in Fig. 12.1. The flow within the boundary layer is viscous whereas the flow outside the boundary layer is considered as non-viscous

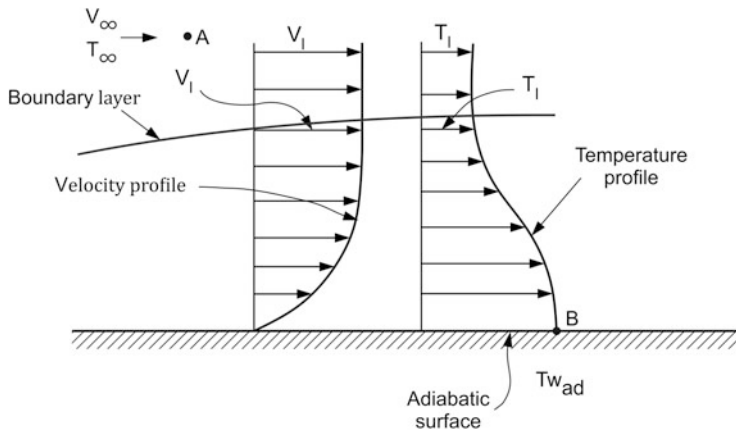


Fig. 12.1 Velocity and temperature profile within the boundary layer

(or inviscid). The flow velocity is zero at the surface (called no slip condition) and reaches the free stream velocity at the edge of boundary layer. The corresponding temperature profile within the boundary layer is also given in Fig. 12.1 and the entire temperature increase of air particles is within the boundary layer itself.

Consider the surface is adiabatic, i.e. there is no heat transfer to and from the surface. Consider A is the point in the free stream and B is at the surface and assume the flow from left to right is adiabatic. Since the flow velocity at B is zero, the adiabatic temperature at B on the surface $T_{w_{ad}}$ is given by

$$\frac{T_{w_{ad}}}{T_{\infty}} = \frac{T_0}{T_{\infty}} = 1 + \frac{\gamma - 1}{2} M_{\infty}^2 \quad (12.1)$$

where T_0 is stagnation point temperature and γ is ratio of specific heats. But, in reality, the process is not fully adiabatic. As the temperature profile increases towards the surface, there is heat transfer within the boundary layer towards the colder section of the gas towards upper portion of the boundary layer. Therefore, the temperature rise at the surface is less than the stagnation point temperature. For this, the recovery factor r is defined as

$$r = \frac{T_r - T_{\infty}}{T_0 - T_{\infty}} \quad (12.2)$$

where T_r is the recovery temperature. ‘ r ’ is the measure of the ratio of actual temperature rise across the boundary layer to the maximum possible temperature.

Using Eqs. 12.1 and 12.2, it can be seen that

$$\frac{T_r}{T_\infty} = 1 + r \left[\frac{\gamma - 1}{2} \right] M_\infty^2 \quad (12.3)$$

The high temperature of gas at the surface T_r causes increase in the surface temperature through convective heat transfer mechanism. As the speed of the flow increases, the stagnation and recovery temperature also increases causing a correspondingly higher thermal loading on the surface. For very high flow speeds, in addition to the convective heat transfer process, the radiative heat transfer from the hot air to the surface also happens.

The heat transferred to the surface is conducted through the material, causing temperature increase of the structural elements and to the components housed inside the structure. In addition, the high temperature of the material also radiates the heat to the sensitive elements.

The convective heat flux to the surface is given by

$$\dot{q} = h(T_r - T_w) \quad (12.4)$$

where T_r is the recovery temperature, T_w is the wall temperature and h is the heat transfer coefficient.

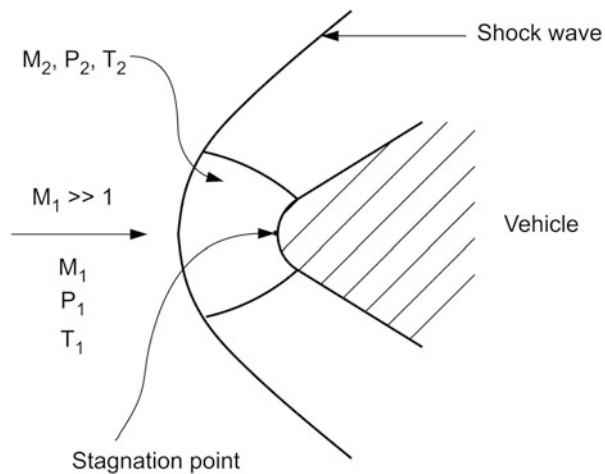
The heat transfer coefficient ‘ h ’ depends on the local flow characteristics, surface shape and surface characteristics. Also h depends on the flow conditions within the boundary layer. Compared to the laminar boundary layer, the convective heating within the turbulent boundary layer is more intensive due to the turbulent velocity features. The recovery temperature depends on the flow characteristics and the free stream temperature and therefore depends on the geometrical shape, vehicle trajectory and atmospheric parameters. The wall temperature depends on the surface material characteristics. Therefore, it can be concluded that the aerodynamic convective heat transfer over a launch vehicle depends on vehicle geometrical shape, material characteristics, flow characteristics, vehicle trajectory and atmospheric parameters.

12.2.2 Aerodynamic Heating Over Launch Vehicle Surface

The aerodynamic convective heating over a flat surface is explained earlier. But, in reality, launch vehicles have complex shapes with various external protrusions depending on the functional requirements. The atmospheric flight of a launch vehicle passes through different flight regimes, viz. subsonic, transonic, supersonic and hypersonic flight phases. Therefore, all the external parts of the vehicle are exposed to aerodynamic flows of various types. The flow characteristics along with the corresponding shapes induce different thermal environments.

From high subsonic flight phase onwards, shock waves get formed along the various regions of the vehicle and external protrusions. These shock waves initially

Fig. 12.2 Flow field in the stagnation region



decelerate the flow and increase the flow temperature to a larger extent. Decelerating the flow further to zero velocity at the surface of the vehicle is caused by the viscosity and surface friction. Therefore, in the launch vehicles, in most of the regimes of the flight, the aerodynamic heating is caused by viscosity and compression process by shock waves.

The maximum heating on a launch vehicle occurs at the stagnation point. At supersonic speed, the shock wave formed in front of the body as in Fig. 12.2 compresses the air. Flow through the shock wave is adiabatic and also the flow downstream of a normal shock is subsonic. The temperature outside the boundary layer near to the stagnation point region is almost the same as that at the stagnation point. The temperature increase across the boundary layer due to viscous dissipation is very small. Therefore, the recovery factor is almost equal to 1. By using Eq. (12.1), the temperature of air at the stagnation point is given by

$$T_0 = T_\infty + \frac{V^2}{2C_p} \quad (12.5)$$

where

T_∞ = Static temperature of impacting air

V = Velocity

$C_p = \frac{\gamma}{\gamma-1} R$, specific heat of air at constant pressure

γ = Ratio of specific heats

R = Gas constant

The convective heat flux at stagnation point region is given by

$$\dot{q} = h(T_0 - T_w) \quad (12.6)$$

The flow reattachment, wake and flow interactions caused by the geometry change away from the flow directions, effects of protrusions and multi-body interactions also introduce severe aerodynamic heating to the components.

The details of aeroheating environments and the corresponding thermal design aspects are discussed later in this chapter.

12.2.3 Heating Due to Jet Exhaust

Another major source of heating during the vehicle flight is the rocket engines. The thrust chambers of rocket engines are subjected to severe thermal environments, which demands efficient cooling system to ensure the safe and normal functioning of the engines. These aspects are covered in detail in Chap. 9, which deals with propulsion systems.

Radiatively cooled thrust chambers and the hot jet exhausts of the rocket engines are the sources causing thermal environment to vehicle subsystems. They are (1) convective heating due to jet impingement on the vehicle subsystems, (2) convective heating resulting from the jet interactions where multiple rocket engines are used and (3) radiative heating from the jet exhaust and due to the hot thrust chambers of radiatively cooled engines.

The heating environment due to jet exhaust is influenced by (1) type of propulsion system, (2) contents of exhaust, (3) operating altitude and (4) aerodynamic flow field over the base region.

12.2.4 Impact of Thermal Environment on the Vehicle Systems

(a) Thermal effects on the vehicle structural systems

To reduce the mass of the launch vehicles, generally, aluminium alloy or composite materials are used for the vehicle structures. Strength of these materials drastically reduces at the elevated temperature. Typically, strength of aluminium alloy reduces at the temperature beyond 393 K. In the case of composite materials, the resins used for winding the fibres decide the temperature limit, which is usually of the order of 393 K, beyond which the resin degrades, resulting in the loss of strength of the structure. Therefore, load-carrying capability of the cold structural elements reduces at elevated temperature.

In addition to the strength reduction at the elevated temperature, the non-uniform and uniform temperature distribution over the surface causes structural distortions

which in turn introduce thermal strain and thermal stress as follows. The thermal strain is defined as

$$\Delta l = \alpha l \Delta T \quad (12.7)$$

$$\epsilon = \frac{\Delta l}{l} \quad (12.8)$$

where

α = coefficient of thermal expansion

ΔT = temperature change

l = original length

Δl = expansion due to temperature change

ϵ = thermal strain

Restricting thermal strain causes thermal stress σ as given below:

$$\sigma = E\epsilon = E\alpha\Delta T \quad (12.9)$$

where E is the elastic modulus (Young's modulus)

Even for uniform temperature distribution, different materials have different thermal expansion coefficients causing thermal strain and in turn thermal stress.

Thermal gradient across the thickness of the material due to the heat rate also causes thermal stress. Thermal stress increases at the elevated temperatures and this stress occurs on the vehicle structural elements and it is in addition to the mechanical stress due to steady and unsteady structural loads.

In summary, it is observed that at elevated temperature, the load-carrying capability of the structural elements decreases whereas due to thermal induced stress, the structure experiences more load than flight loads. Therefore, in order to ensure integrity of vehicle structural elements during flight, it is essential to restrict the temperature on the structures through suitable TPS.

(b) Thermal effects on the vehicle sensitive elements

Mission-critical elements are housed inside the structures. This includes sensitive avionics packages, computers, sensors, control systems and very crucial propulsion elements. The heat from the external thermal environments is transferred to these elements through convective, radiative and conduction heat transfer mechanisms. In addition, internal temperature also increases due to power dissipations of electronic components and radiative heat transfer from the propulsion systems. All these sensitive elements need benign thermal environments for their safe functioning and normal performance. Therefore, these systems also require suitable TPS.

In addition to the above elements, the thermal load acts on the vehicle structure and the convective aerodynamic heating during flight is transferred through the tanks to the propellants. To ensure normal functioning of the propulsion systems, it is essential to maintain the temperature of the liquid propellants within the

allowable limits during the prelaunch and flight phases through suitable thermal protection mechanisms.

12.3 Thermal Design Requirements and Constraints in a Vehicle

The various thermal issues to be addressed in a typical launch vehicle are highlighted in Fig. 12.3 and they are described below:

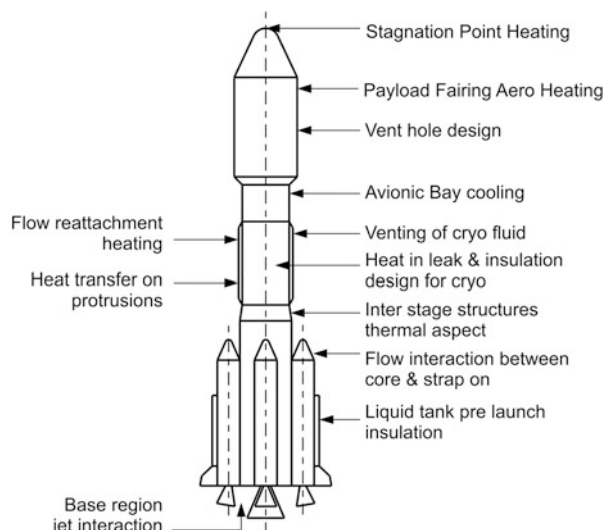
1. Stagnation point heating

In the nose cone region of the vehicle, heating happens due to air stagnation. Proper heat flux estimation of this zone in the payload fairing is very essential. The bluntness radius of the nose cone plays an important role in deciding the stagnation point heat transfer rates. More the bluntness, lesser the heating but leads to increased drag and flow instabilities in the aft region of the heat shield. Therefore the limit for stagnation heat flux has to be carefully decided to meet the overall requirements.

2. Aerodynamic heating

Estimation of aerodynamic heating loads, on various components of the vehicle such as payload fairing, interstage structure, nose cone of strap-on stages, protrusions, attachment links between strap-on motors and main vehicle, etc., requires detailed design and analysis. The maximum thermal load locations such as flow reattachment point, etc. have to be identified correctly using wind tunnel and CFD

Fig. 12.3 Typical thermal issues in a launch vehicle



analysis and suitable protective measures are to be implemented. It has to be ensured that the maximum temperature experienced by these components is well within the allowable temperature limits.

3. Interstage structures' thermal aspects

The interstage structures mainly built from aluminium alloy or CFRP material are subjected to aerodynamic heating during the ascent phase and also to exhaust-plume heating depending on where they are used in the vehicle assembly. The exhaust plume heating is due to main engines of the stages, control, retro and ullage motors. The heating is transmitted to the structure depending on the type of usage due to radiation and particle impingement. Detailed analysis is needed to decide on a suitable thermal protection system for these structures.

4. Flow interaction between core and strap-on stages

In vehicles with strap-on motors, there is always interaction of core air flow with strap-on motors. The interference flow between them depends on the type of nose cone used in the strap-on motors. The slanted nose cones generally reduce the moments and local loads due to jet impingement. The gap flow between the strap-on and core stages induce flow interactions, causing local heating to the forward end of the strap-ons. This area needs detailed analysis and suitable thermal design.

5. Base region jet interaction

Major mode of heating in the base region of a vehicle is due to exhaust plumes and radiation from nozzle divergents. At higher altitudes the nozzle exhaust plumes expand and its interaction becomes severe. The problem becomes complex in case of multiple engines like core and strap-on motors where there exists the possibility of reverse flow of hot gases to the base region of launch vehicle. The thermal design and required protection system are to be carried out from lift-off phase onwards. The thermal loads in the base region can also be significant due to reflected radiation and reverse flow of exhaust plumes during its impingement at the launch pad on jet deflector.

6. Vent hole design

During ascent phase of the vehicle flight, the ambient pressure falls rapidly and the pressure differential across the payload fairing builds up rapidly. Suitable venting holes are needed to be designed. The expansion of the air contained inside the fairing during the venting process is assumed to happen *isothermally*. The size, number and location of holes are to be decided carefully during the design phase.

7. Venting of cryo-fluids

During flight, the pressure inside the cryogenic propellant tank builds up due to vaporization. Therefore proper venting scheme for cryo-fluid is necessary to maintain the internal pressure within the specified limits. The venting rate has to be appropriately fixed to avoid the ignition of hydrogen by coming into contact with

the hot boundary layer or any hot surfaces. Venting also can cause significant changes in the local field and subsequent local heating.

8. Heat-in-leak and insulation design for cryo-propellant tanks

In cryogenic stages, the heat-in-leak into liquid oxygen (LOX) and liquid hydrogen (LH₂) tanks is to be computed considering all thermal loads due to convection and radiation to ensure that they are within the specified values. The aerodynamic heating rates on tankages, protuberances and plumbings during the ascent phase is to be properly assessed. Heat-in-leak studies on propellant tankage during the pre-launch phase are also to be carried out. Thermal insulation systems for the tanks have to be suitably designed considering all thermal loads starting from pre-launch, ascent phase till satellite separation.

9. Insulation requirements for liquid tanks

Generally Earth storable propellants used in liquid stages are nitrogen tetroxide (N₂O₄) as oxidizer and unsymmetrical dimethyl hydrazine (UDMH) as fuel. They are filled at low temperature of 15–18 °C and the vehicle is exposed to ambient wherein the liquid tanks are subjected to heating due to convection of ambient air, solar radiation, Earth albedo and moisture condensation on tank surface. For the successful engine operation, there is always a temperature constraint for the liquid propellants. To maintain the temperature within the allowable limits, the different heat sources are to be accounted and thermal analysis has to be carried out taking into account the maximum duration of exposure for the tanks to these heat sources. The extended duration owing to possible launch hold is also to be accounted. The common methodology used for thermal protection system is to provide insulating foam pads around the tanks which are jettisoned during the vehicle lift-off by using suitable wrap release mechanisms for these pads. In some cases chilled air circulation is also provided between insulation pads and the liquid tank.

10. Avionics bay cooling

The avionics packages which are used for the vehicle navigation guidance and control, telemetry and tracking are generally mounted on a separate bay termed as the avionics bay and this is located at the forward end of the vehicle on top of the terminal stage. It is essential to ensure that temperatures of all avionics packages are well within the prescribed limits during their operation in the ground and the entire flight phase. The specified temperature in this bay is achieved during the pre-launch phase by introducing suitable cooling systems at launch pad. The temperature of the avionics packages at lift-off is decided such that increase in their temperature during in-flight operation is maintained within the allowable limit.

12.3.1 *Thermal Design Requirements*

For a suitable thermal design for a launch vehicle, several requirements as given below have to be considered:

- (a) Thermal loads on each subsystem of the vehicle from nose cone to the vehicle base are to be estimated considering the various sources of heating.
- (b) Aerodynamic heating rates and the total thermal load are to be estimated using the worst-case vehicle trajectory considering the expected dispersions in vehicle performance and atmospheric parameters.
- (c) The thermal loads due to aerodynamics are to be computed by assuming fully turbulent flow to overcome the uncertainties in the modelling of boundary layer transition.
- (d) Convective heating due to jet interaction, jet impingement, radiative heating from jet exhaust and radiative heating from hot nozzle divergent are to be properly estimated for the base region.
- (e) Heating loads due to solar radiation and Earth albedo are to be properly assessed.
- (f) At the time of lift-off, the effect of reflected radiation and recirculating flow after jet impingement on flame deflector are to be appropriately estimated.
- (g) In the vicinity of protuberances, the augmentation of heating rates is to be computed (a) by using the experimental data available in literature for similar protuberances or (b) by generating appropriate heat transfer coefficient.
- (h) 15 % margin on thermal protection system thickness is to be provided to account for uncertainties in properties of insulation material.
- (i) The ambient temperature of spacecraft and vehicle avionics systems inside the payload fairing is to be maintained well within allowable limit by proper cooling during the pre-launch phase.
- (j) The heat-in leak into cryogenics tankages during flight has to be maintained well within the allowable limit.
- (k) Dispersions in the atmospheric data like pressure, temperature and air density are to be considered.
- (l) Venting of propellants or ullage gases into the boundary layer influences the heat transfer due to change in the flow characteristics or due to local combustion and hence this phenomenon is to be accounted.
- (m) During the launch phase, the temperatures of various avionics packages distributed at different interstage compartments are to be ensured within the specified limits.
- (n) The temperature of the liquid propellants should not exceed the set limits at the time of lift-off.
- (o) During the lift-off phase, it is essential to establish the adequacy of flame deflector and thermal protection system for the launch pedestal. Thermal design for umbilical tower during vehicle lift-off has to protect the same from serious damages.

Table 12.1 Temperature Limits on Launch Vehicle Subsystems

Sl No.	Details	Temperature limit (° C)
1.	Components employing aluminium alloy material	120
2.	Components with 15CDV6 or maraging steel	300
3.	Explosive Charge	70
4.	Avionics Packages	60
5.	CPRP sandwich panel	120
6.	Hypergolic propellants at lift off	<25

- (p) Overall mass of the thermal protection system for the vehicle has to be minimized without sacrificing the thermal constraints specified for various elements.

12.3.2 Design Constraints

The various constraints to be considered during the thermal design are as given below:

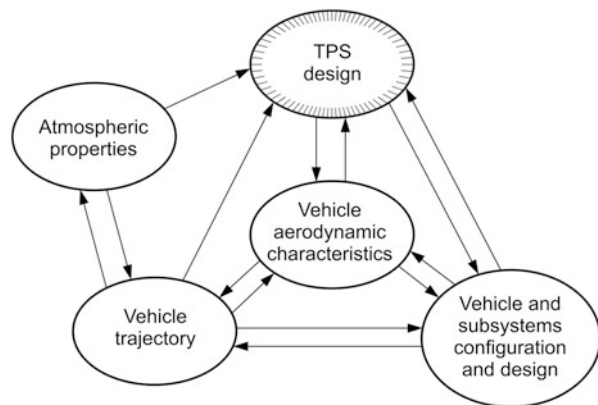
- (a) The skin temperature of various subsystems of the vehicle, payload fairing, stage motors, interstage structures, nose cones, etc. should not exceed the set limits.
- (b) The heat flux emitted by the inner surface of payload fairing should not be more than the specified limit.
- (c) The payload fairing is to be jettisoned at an altitude where the aerothermal heat flux on payload is less than 1135 W/m^2 .
- (d) The temperatures of the liquid propellants should not exceed the set limits at the time of launch.
- (e) The temperature on the explosive charge used for the vehicle destruct system should be strictly within safe limits.
- (f) Various typical temperature limits of subsystems used in a launch vehicle thermal design are given in Table 12.1.

12.4 Thermal Design Strategy and Guidelines

12.4.1 Approach for Thermal Design

From the thermal environments explained in the earlier sections, it is seen that the temperature of the vehicle subsystems due to aerodynamic heating depends on the aerodynamic flow properties, flow characteristics, geometrical shape of the vehicle including protrusions and surface material properties. Flow field and flow characteristics on the vehicle are dependent on the external geometric shape of the vehicle

Fig. 12.4 Interactions of TPS with vehicle subsystems



and the selection of vehicle trajectory to meet the mission goals. Other important parameters that influence the aerothermal environments are the atmospheric properties such as temperature, pressure and density. The heating rates further depend on the type of the boundary layers and the transition zone.

The heating due to the rocket exhaust depends on the type of propulsion systems, their operating characteristics, protection system used, trajectory and aerodynamic flow characteristics. The thermal load generated by the above heating process forms input to the TPS design process. TPS selection and design have influence on the selection of the vehicle subsystems and their designs. The total system is tightly coupled as shown in Fig. 12.4. While protecting the subsystems with suitable TPS for the normal functions, it is essential to achieve the maximum performance of the vehicle by reducing the mass of the integrated vehicle. Therefore, to achieve the above objectives, integrated design of TPS using systems approach is required.

12.4.2 Thermal Design Process Guidelines

Thermal design is generally carried out by utilizing either (a) hot structure approach or (b) cold structure approach depending on the type of structure used in the vehicle.

In hot structure approach, high-temperature materials are used, which act as load-carrying structure while withstanding high temperatures. Such materials are carbon-carbon composite, Inconel, etc. Thermo-structural design is carried out considering both structural and thermal loads during entire flight regimes using structural and thermal properties at elevated temperatures. Material thermal limit, deformation, thermal stress and structural margins are kept within the specified limits. It results into an optimum design. This approach is used generally for re-entry vehicles. In the cold structure approach, thermal protection system design is carried out to limit the temperature of the vehicle's primary load-carrying structure (such as aluminium alloy) such that there is no significant strength

reduction up to that temperature. In this case, the structural design and thermal design are carried out independently. Thermal design is conservative and this method is usually adopted in launch vehicle thermal design.

Thus thermal design of launch vehicle involves detailed estimation of all thermal loads on various structural and sensitive elements of the vehicle through various convective and radiative heat transfer modes and thermal response analysis of the structures to these thermal loads during the flight. Further, various thermal protection choices, detailed response analysis of the systems, accounting for multi-layer structure, spatial and temperature dependence of thermo-physical properties of various materials and other mission constraints are also to be considered. Aerodynamic thermal loads are functions of altitude, relative velocity, angle of attack and duration of flight for a given vehicle configuration. Jet plume thermal loads are functions of trajectory, propulsion and aerodynamic flow characteristics in the base region. Thermal design is carried out for the extreme flight environment which results into higher heat load and heat flux. For the selected flight environment, temperature on the structural elements are to be estimated and if the temperature and the thermal gradients exceed the corresponding allowable limits, suitable thermal protection system is to be designed to ensure that these parameters are within the specified limits. If the structure houses electronic components or pyro-elements or propellants, then the temperature limit is decided by the electronic components/pyro-elements and at the interface of the propellant.

12.4.3 Thermal Protection System Selection and Design Criteria

(a) *Types of TPS*

Thermal protection systems are classified as passive, semi-passive and active as shown in Fig. 12.5. In the heat-sink structure, the thick material absorbs the heat and it is not transmitted to the structural component. The hot structure functions as load-carrying structure at elevated temperature. For the insulated structure, the insulation acts as poor conductor and transmits only a low amount of heat to the base structure. The function of passive TPS for the structures used in heat sink and hot structure is achieved by increasing the mass of TPS and surface radiation.

In the case of semi-passive TPS like heat pipe, the heat is removed by working fluid and surface radiation. In ablation TPS, the heat is removed by surface ablation and injection of cold pyrolysis gases into the airflow thereby reducing the convective heating. Ablatives such as carbon phenolic and silica phenolic are efficiently used for heating levels of more than 300 W/cm^2 , which is prevailing in solid motor exhaust and re-entry missions.

Active TPS include transpiration cooling, film cooling and coolant flow within channels to restrict the temperature within limits.

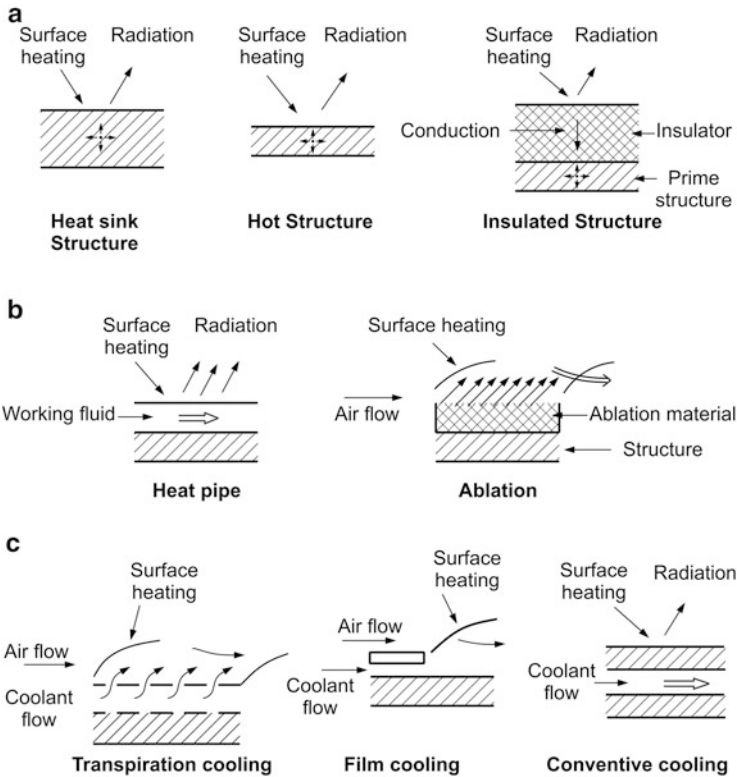


Fig. 12.5 Types of TPS (a) Passive TPS, (b) Semi-Passive TPS, (c) Active TPS

Depending on the application, the TPS scheme selected has to be simple, less in mass, cost effective and reliable.

(b) Selection of TPS material and TPS design criteria

Function of TPS is to restrict the temperature of structural and sensitive elements within the specified limits. While meeting the functional requirements, TPS should withstand high temperature, temperature gradients, higher elongation than the protecting element, aerodynamic shear and should be intact with the backup structure during the flight regime.

Choice of a suitable TPS material is based on the peak heat flux experienced on a specific component of the vehicle so that the selected TPS withstands the heat flux without degradation. The thickness of the selected TPS material depends on the total heating load over the entire flight trajectory duration to restrict the temperature within the specified limit.

In order to reduce the TPS mass, the selected TPS should have the following characteristics. The numbers indicated within the brackets are only typical values.

1. Lower thermal conductivity (0.1 W/mK)
2. Higher specific heat (2 kJ/kgK)
3. Lower density (340 kg/m^3)
4. High emissivity (>0.8)
5. Low solar absorptivity (<0.4)

The selected TPS should have compatibility with the primary structure and withstand aerodynamic shear under room temperature and at elevated temperature.

Normally, for the large structure of launch vehicles, high-temperature thermal paints are widely used as TPS material. These paints are subliming ablatives. The thickness of the paint is decided based on the thermal input and the specified temperature limit of the primary structure. The criteria for selection of thermal paint TPS are

1. Should be brushable or sprayable on the base material.
2. Should have good adhesive properties with the substrate
3. Should be able to cure at room temperature
4. Should have a shelf life of at least 1 year

There are several high temperature resistance coatings. Selection of a suitable coating depends on the mechanical and thermal properties. Therefore there is a need to evaluate the mechanical and thermal characteristics of the insulation material by carrying out detailed tests. These characteristic tests are carried out using aerodynamic heating simulation facility and heat transfer tunnel, simulating the combined thermal and shear environments. Certain specific components are not amenable for either brush or spray coatings. In such cases protection is achieved by wrapping such components by fibre glass or silica cloth.

For small cylindrical structures, layers of silica cloth are used. Similar scheme is used for wiring harness inside the vehicle structure. For irregular shapes of the components like control systems, valves, multi-layer blankets with fibrous insulation are used and stitched according to the shape of the body. Thickness of the insulation is decided by the heat load.

12.5 Thermal Environment and Design for Launch Vehicle Systems

TPS design for various components of launch vehicle systems are required to protect the systems against the thermal environment caused during pre-launch, lift-off and ascent flight phases as given below:

1. *Pre-launch phase:*

During pre-launch phase, the main thermal design requirements for spacecraft and various electronics packages housed in different interstage compartments

for temperature of storable liquid propellant and cryo-propellants have to be as explained in Sect. 12.3.1.

2. *Lift-off phase:*

During lift-off phase, thermal design and analysis requirements are

- (a) Adequacy of flame deflector and launch pad TPS on different systems due to jet impinging loads
- (b) Thermal environments for umbilical tower during vehicle vertical rise and vehicle pitching and the suitable thermal protection system
- (c) Effect of convective and reflected radiation from hot gas jets on base thermal environments and adequacy of TPS

3. *Ascent flight phase:*

During vehicle ascent phase, the thermal loads on the vehicle are essentially due to aerodynamic heating during vehicle ascending through the denser atmosphere and heating due to jet exhausts. Suitable thermal protections are essential to restrict the temperatures of the components under the above thermal environments.

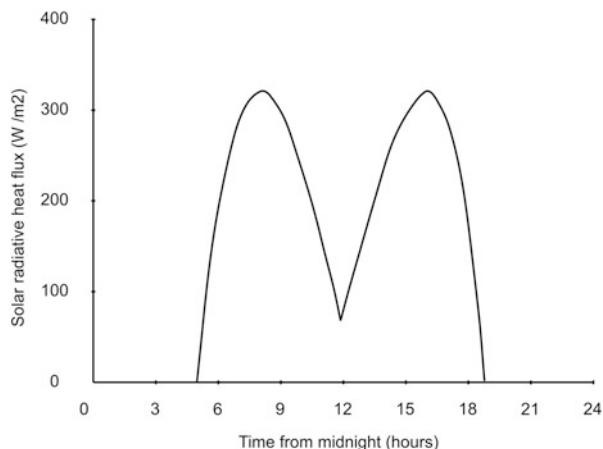
This section gives thermal environments during the different phases of the flight for several subsystems of the vehicle and their thermal design aspects.

12.5.1 Thermal Environment and Thermal Management of Avionics Bay of Vehicle

Most of the avionics packages used for vehicle navigation, guidance control, tracking, telemetry, power, etc. are housed in a single avionics bay generally termed as equipment bay (EB) or avionics bay and mounted on the forward end of the final stage of the vehicle. The spacecraft is mated with the vehicle through an appropriate payload adaptor on top of the final stage. Both avionics bay and the spacecraft are housed inside the payload fairing of the vehicle which protects them from direct solar heating during the pre-launch and flight phases and also from direct aerodynamic heating during the flight. During the pre-launch phase the vehicle avionics bay and some equipment of spacecraft are to be switched on. These packages dissipate considerable amount of heat thereby increasing the ambient temperature inside the payload fairing. Solar heating of the payload fairing during the pre-launch phase further increases the temperature inside. To ensure the health of the avionics packages prior to lift-off, it is essential to maintain temperature of each element within the allowable operating limits. The avionics packages inside the avionics bay experience the following thermal loads on ground:

1. Solar radiation, Earth albedo
2. Convection heating due to wind
3. Radiation exchange with nearby structures

Fig. 12.6 Solar radiative heat flux on cylinder of a typical launch vehicle at a typical launch site and launch pad



4. Radiation exchange between the adjacent packages and inside structures
5. Power dissipation profile of the electronic packages

In addition, during flight, aerodynamic heating on external structure and the back wall radiation to the packages are also to be considered.

Solar radiation and Earth albedo are estimated considering the launch site location, season, day and time of launch. Typical heat flux due to solar radiation on the cylindrical portion of a typical vehicle on a typical launch day is represented in Fig. 12.6 for a launch site close to the equator.

Convective heating due to wind is estimated based on the measured ambient temperature and wind velocities at different heights of the launch vehicle. Radiation exchange with nearby structure and packages are calculated using view factors and their emissivity. Power dissipation of the packages is usually a measured quantity. The thermal loads for these packages are based on the number of packages in the equipment bay, power dissipation, heat sink provisions and powering sequence of packages particularly during the pre-launch phase.

Generally for almost all the spacecraft, the temperature around it should be below 25 °C during the pre-launch phase. Similarly it has to be ensured that temperatures of various avionics packages on the equipment bay are restricted within the allowable limit. Under the above thermal environments, the temperature limits are achieved by circulating cooled air at low temperature through the vehicle umbilical. The total coolant flow rate inside the payload fairing area has to be carefully computed to achieve the specified cooling requirements for the avionics packages. Depending on the high power dissipation of the packages in the equipment bay, localized cooling for such packages has to be planned by providing forced convective cooling. The cooling air is generally allowed inside the payload fairing through the umbilical connection and let out through properly designed vent holes provided in the heat shield in the boat tail region.

During the ascent phase, the cool air supply is cut off and the temperature inside the payload fairing increases due to aerodynamic heating. Therefore, considering the temperature increase during the atmospheric phase, the temperature limit at lift-off is decided so as to ensure that the net increase in temperature remains within the allowable specified temperature limit of the subsystems.

12.5.2 Thermal Protection System of Earth Storable Liquid Propellant Stages

During pre-launch phase, the thermal environments for Earth storable liquid propellant tanks are

1. Direct solar radiation
2. Convective heat transfer with ambient atmosphere
3. Conduction from the adjacent structures
4. Deflected radiation and differential radiation from the surroundings

In addition, heat transfer to the propellant tanks due to moisture condensation is another source of heat.

Thermal problem in the case of Earth storable propellants is mainly because of longer duration (of the order of 30 h) exposure to the above thermal environments. Due to the high thermal environment, vapour formed inside the propellant tank can cause two-phase flow, which in turn can cavitate the turbo pump during the stage ignition. To avoid such situation, it is essential to restrict the temperature of the propellant less than the specified limit.

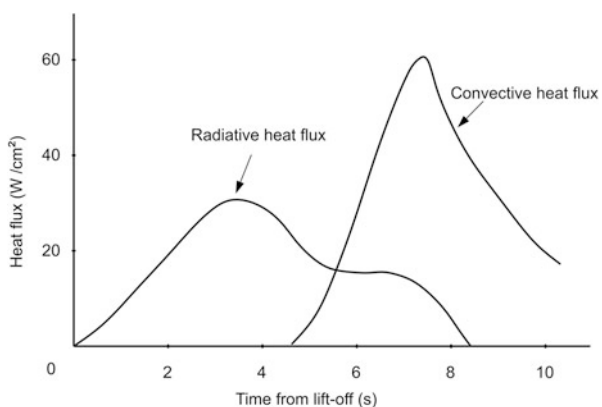
To restrict the temperature of propellant tanks, generally, polyurethane foam pads ($k = 0.036 \text{ W/mK}$) of density of the order of 40 kg/m^3 are used. In addition to this, circulating air at lower temperature of the order of 15°C between the foam pads and tank are also provided to avoid moisture condensation. The foam pads are jettisoned during lift-off through suitable mechanism. No protection is required for the atmospheric flight phase as this is very small and the temperature rise in the propellant tank is less than 1°C due to the large thermal capacity.

12.5.3 Thermal Environment and Protection of Launch Pad Elements

During the lift-off, the umbilical tower which supports the vehicle during its stay at launch pad is exposed to radiation from the high-temperature Al_2O_3 particles in the exhaust of solid boosters and convective heating from jet exhausts.

The duration of exposure to these environments is short, of the order of 5–8 s. The radiation levels for a typical launch vehicle at lift-off are of the order of

Fig. 12.7 Heat flux levels on umbilical tower for a typical launch mission



20–50 W/cm² depending on the distance between the vehicle and umbilical tower as shown in Fig. 12.7. Similarly, the convective heating range from 50 to 150 W/cm² and the value for a typical vehicle lift-off are shown in the above figure. It is essential to quantify the heating levels during this phase and suitable thermal protection is provided on the flame deflector, umbilical tower and other supporting elements to restrict the temperature levels to the specified values (typically 573 K).

12.5.4 Ascent Phase Thermal Environment

Ascent phase thermal environment to the vehicle system is caused by (a) aerodynamic heating and (b) heating due to jet exhaust and jet interactions. The aerodynamic heating depends on the aerodynamic flow field, vehicle configuration, material characteristics, trajectory parameters and atmospheric parameters. The flow field in turn is a function of vehicle system configuration and flight regimes. The heating due to jet exhaust depends on the type of propulsion systems adopted for the vehicle, propulsion system characteristics, propulsion system configurations and the aerodynamic flow field in the base region of the vehicle.

To meet the various functional requirements, the launch vehicles are generally configured with complex external shape. Typical vehicle configuration and the flow fields over the vehicle during a typical flight regime are represented in Fig. 12.8.

The need to accommodate larger spacecraft demands larger volume within the payload fairing. This requirement leads to the choice of bulbous configuration for the fore body. The common configuration selected in such vehicles is a spherically blunted cone cylinder and boat tail, merging with the aft body. Such configuration is prone for buffeting and hence it is important to follow the general guidelines which are generated after detailed studies in fixing the geometry of bulbous fore body. The details on this aspect are discussed in Chap. 10. Generally blunt noses are preferred to reduce higher thermal loads but it has a penalty in higher drag. Therefore suitable

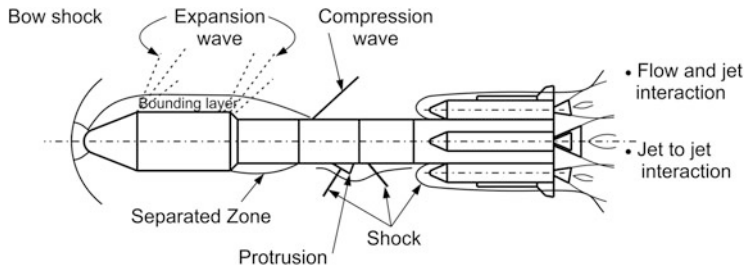


Fig. 12.8 Flow field over a vehicle

geometry for nose cone has to be finalized considering the thermal load and drag on the vehicle. Proper estimation of heat flux at different locations of payload fairing is essential to decide about thermal protection system.

In a launch vehicle it is impossible to eliminate the protuberances since they are needed to accommodate the smaller retro- and ullage rockets, wire tunnels, destruction system covers, propellant feed lines, etc. These protrusions cause geometric and thermal discontinuities in the vehicle and thus cause larger local heat transfer. Generation of wake due to protrusions, flow separation caused by shock boundary layer interaction near them and reattachment following flow separation are to be studied in detail to understand the intensity of heating in these regions.

In the configuration with the strap-on motors, the shock produced by the strap-on nose cones and the associated flow characteristics cause severe thermal loads, which need to be considered.

Towards the base region, the thermal environment generated by the jet exhausts and jet-to-jet interactions generate the thermal environment.

The flow features on the launch vehicle for a typical supersonic flight regime are

1. Bow shock forms in front of the vehicle.
2. Stagnation point region is at the tip of the payload fairing.
3. Flow expands at the cone-cylinder junction.
4. Further expansions of flow happens at the cylinder-boat tail junction.
5. Due to geometry change, the flow separates and reattaches at the cylindrical portion aft of boat tail. At the flow reattachment location, shock wave is formed.
6. Shock formed in front of the protrusion.
7. Flow reattaches after separation due to protrusion and at reattachment location, there is a shock.
8. Shock forms in front of strap-on nose cone and there is flow interaction.
9. In base region, jet interacts with adjacent jets and external flow.

From the flow pattern, the flow feature in the payload fairing region is

1. At the stagnation point region, the flow is a laminar.
2. At the cap portion, the flow becomes turbulent and subsequent portion of the boundary layer is a turbulent one.

3. The boundary layer is thin at the cap region, and subsequently it increases continually.

Because of the above flow pattern, the heat flux at stagnation point region is more. In the cone region, the boundary layer thickens and therefore the heat flux reduces. The heat flux further reduces in the cylindrical region due to rapid expansion and pressure is fully recovered in the cylindrical region. Heating in the cylindrical region is typical of heating in the aft body. Subsequently due to rapid change of geometry away from the flow direction, there is the possibility of flow separation. This happens due to increase in pressure causing an adverse pressure gradient. The flow separation occurs at the region of boat tail in payload fairing. The separated flow would reattach to the core body after an oblique shock causing an increased heating on the body.

Flow separation occurs near protrusions due to shock boundary layer interactions causing an adverse pressure gradient. Flow separation also causes the generation of unsteady pressure and also unsteady loads at these locations. Following flow separation, the reattachment happens in the proximity of the protrusions downstream and it causes higher rate of heating.

In the base region, the thermal environments are primarily due to radiation from hot nozzle divergent, radiation heating from the jet exhausts and convection heating due to jet and external flow interactions.

12.5.5 Aeroheating Environment, Thermal Design and Analysis

At supersonic and low hypersonic speeds aerodynamic heating becomes predominant and also causes higher structural temperatures. There are many parameters affecting aeroheating environment during atmospheric flight phase. The prominent among them are

1. Atmospheric parameter variations, viz. pressure, temperature and density
2. The overall vehicle geometry
3. Trajectory parameters, viz. altitude, velocity and angle of attack
4. Flow field which depends on local geometry and flight regimes

The vehicle trajectory parameters are closely linked with atmospheric data, which largely depends on the season of flight and the geographic location of the launch base. Appropriate variations in atmospheric data in terms of pressure, temperature and density are to be used to generate the maximum heating trajectory.

The geometric shape of the vehicle plays a major role and from the perspective of aero-thermodynamic design, the shape of the payload fairing, the nose cone of strap-on stages, control surfaces, base region geometry and all protuberances in the vehicle influence the flow field considerably.

When the vehicle passes through a dense atmosphere, aerodynamic heating of the body happens within a boundary layer which is essentially a thin fluid layer attached to the vehicle body. The boundary layer remains laminar at the leading edge of a vehicle body. As it moves away from the edge, the boundary layer transits to turbulent due to faster growth and nature of random motion. The region between laminar and turbulent is termed as transition boundary layer. The heat transfer rates are totally different in all these three regions. The estimation of heating in the transition region is quite complex since this region is influenced by several factors like Reynolds number, pressure distribution, Mach number, shock layer thickness, etc.

Aero thermal design for various vehicle elements demands clear understanding of flow fields at various Mach number regimes of flight. Well-established analytical methods are available to determine the flow fields for both laminar and turbulent flow. Most of the aerodynamic heating in a launch vehicle happens during the ascent phase at low altitudes and high Reynolds numbers. The basic input data needed for the aerodynamic heating analysis and design of thermal protection systems are

1. Vehicle external configuration with protuberances
2. Vehicle trajectory data for both nominal and off-nominal conditions
3. Details of structures used
4. Flow field data over the vehicle at different Mach numbers and flight angles of attack
5. Temperature constraints on various materials used in structures
6. Temperature limits for various sensitive components housed inside the structure
7. Choice of insulation materials

Aerodynamic characterization in terms of flow field data at critical Mach numbers and flight angles of attack for the vehicle can be obtained through Computational Fluid Dynamics (CFD) simulations and detailed wind tunnel tests. The Navier-Stokes (N-S) equations using conservation laws of mass, momentum and energy can be utilized to describe the flow field over a body. These equations can be used to generate the aerodynamic convective heat transfer rates. But this method is highly computational intensive. For estimating the heat transfer (which is important for thermal protection design) one can use simple and accurate engineering methods that are validated against the CFD and wind tunnel data.

For aerodynamic heating analysis one should use a maximum heating trajectory where various parameters are perturbed to give the maximum rate of heat input. To evaluate the effects of trajectory parameters on heating, the commonly used method is to compare the altitude versus velocity history. Since aerodynamic heating is directly proportional to the factor ' ρV^3 ', a more conservative method would be to choose that trajectory that gives the maximum value of ' ρV^3 ' and has the longest flight duration. The variations of atmospheric parameters and angles of attack are not generally accounted in this simple method.

Various design methods for the estimation of heating rates have been developed over the years and are being utilized. A detailed discussion of these methods is

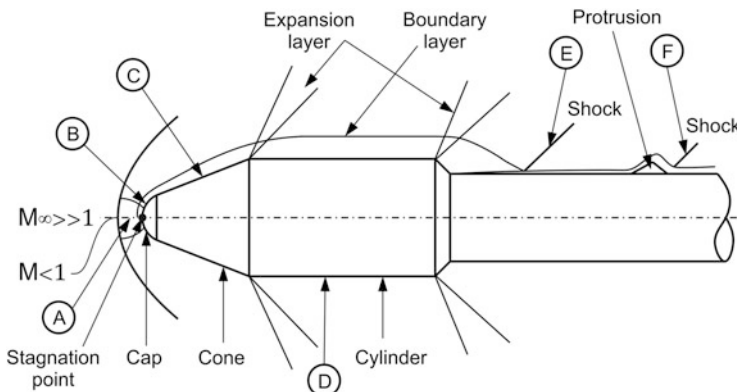


Fig. 12.9 Typical points on the payload fairing

beyond the scope of this book, but the general methods used in the design and analysis of heating rates are briefly described here. Several analytical methods for estimation of aerodynamic heating at supersonic and low hypersonic speeds are available and they are discussed in detail in the references given in the end.

For aerothermal design it is essential to estimate the aerodynamic heating loads for the maximum heating flight trajectory and to analyze the thermal response of various structures to the maximum heating loads encountered during flight. The heat flux and wall temperatures during the vehicle flight are generally coupled and hence aerodynamic heating can be obtained by solving simultaneously boundary layer equation and heat conduction equations. For design purposes, a safe approach would be to estimate the aerodynamic heating assuming the wall temperature as isothermal or cold wall, which would result in the estimation of a higher heat level leading to a conservative thermal design.

Generally, to reduce thermal environment, the payload fairings of launch vehicles are configured as blunt bodies as shown in Fig. 12.9. The thermal environments of typical supersonic flight regime of the above configuration are indicated in Fig. 12.9. Analysis and thermal design are discussed at following typical locations: (1) stagnation point (point-A), (2) nose cap region (point-B), (3) nose cone region (point-C), (4) cylindrical region (point-D), (5) flow reattachment location and protrusions (points-E and F).

(a) *Stagnation point heat flux (Point-A)*

The flow stagnates on the forward portion of the body. For the thermal analysis and design, it is required to estimate the heating on the stagnation region. The flow parameters after the shock are required to calculate the heating rate. Consider a sphere of radius R_N and it is required to estimate the heating at a particular instant of flight (specified trajectory point). From the trajectory, the altitude and relative velocity are obtained. This defines the free stream conditions, viz. P_∞ , T_∞ , M_∞ .

Using conservation equations for one-dimensional flow, the post-shock values ρ_s , P_s , V_s , T_s , h_s are given as

Mass conservation:

$$\rho_s V_s = \rho_\infty V_\infty \quad (12.10)$$

Momentum conservation:

$$\rho_s + \rho_s V_s^2 = \rho_\infty + \rho_\infty V_\infty^2 \quad (12.11)$$

Energy conservation:

$$h_s + \frac{V_s^2}{2} = h_\infty + \frac{V_\infty^2}{2} \quad (12.12)$$

Enthalpy:

$$H_s = f(P_s, T_s) \quad (12.13)$$

Equation of state:

$$\rho_s = g(P_s, T_s) \quad (12.14)$$

h_s and ρ_s of Eqs. (12.13) and (12.14) can be obtained from Air tables. Using these, and Eqs. (12.10, 12.11, and 12.12), the post-shock parameters are obtained. Post-shock stagnation conditions can be obtained using the isentropic relations

$$P_0 = P_s \left[1 + \frac{\gamma - 1}{2} M_s^2 \right]^{\frac{\gamma}{\gamma-1}} \quad (12.15)$$

$$T_0 = T_s \left[1 + \frac{\gamma - 1}{2} M_s^2 \right] \quad (12.16)$$

where γ is evaluated at (P_s, T_s) from Air tables. The local flow conditions P_e , T_e are evaluated by the relations

$$P_0 = P_e \left[1 + \frac{\gamma - 1}{2} M_e^2 \right]^{\frac{\gamma}{\gamma-1}} \quad (12.17)$$

$$T_0 = T_e \left[1 + \frac{\gamma - 1}{2} M_e^2 \right] \quad (12.18)$$

where M_e is the edge Mach number, i.e. at the end of boundary layer, and is given by

$$M_e^2 = \left[\left(\frac{P_0}{P_e} \right)^{\frac{\gamma-1}{\gamma}} - 1 \right] \frac{2}{\gamma - 1} \quad (12.19)$$

The stagnation point heat flux can be computed using well-known Fay and Riddel formula, [1]

$$\dot{q} = k (P_r)^{-0.6} (\rho_w \mu_w)^{0.1} (\rho_0 \mu_0)^{0.4} (H_0 - H_w) \sqrt{\left. \frac{du}{ds} \right|_{s=0}} \quad (12.20)$$

Equation (12.20) corresponds to the conditions without considering real gas effects and is applicable for launch vehicle missions. The parameters given in Eq. (12.20) are explained below:

$$k = \begin{cases} 0.763 & \text{for axi-symmetric flow (like sphere)} \\ 0.57 & \text{for two-dimensional flow (like cylinder)} \end{cases}$$

P_r = Prandtl number

ρ_w, μ_w = Density and viscosity evaluated at wall temperature

ρ_0, μ_0 = Density and viscosity evaluated at stagnation conditions

H_0 = Total enthalpy

H_w = Enthalpy at wall temperature T_w

$\left. \frac{du}{ds} \right|_{s=0}$ = Velocity gradient at stagnation point and is given by

$$\left. \frac{du}{ds} \right|_{s=0} = \frac{1}{R_N} \sqrt{\frac{2(P_0 - P_\infty)}{\rho_\infty}} \quad (12.21)$$

R_N = Radius

From the above Eq. (12.20), it is seen that the stagnation point heat flux is given by

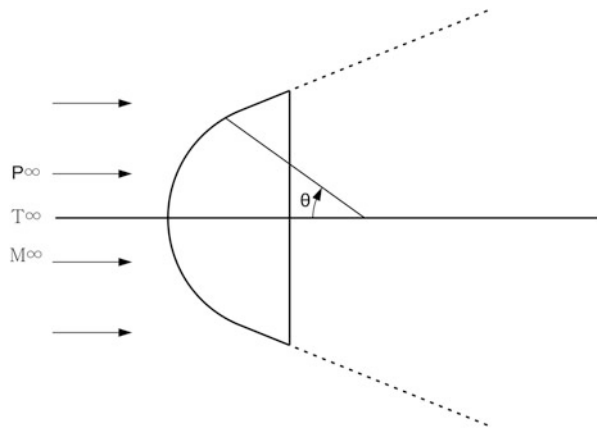
$$\dot{q} \propto \frac{1}{\sqrt{R_N}} \quad (12.22)$$

Therefore, for blunt bodies, the stagnation point heat flux reduces.

(b) Heat transfer over blunt bodies (Point-B)

Blunt body approximation is valid for the nose cap region as shown in Fig. 12.10. For estimation of laminar heat transfer distribution on the spherical cap region, methodology by Lee [2] can be adopted as given by

Fig. 12.10 Blunt body of nose cap



$$\frac{\dot{q}}{q_0} = \frac{2\theta \sin \theta \left\{ \left[1 - \frac{1}{\gamma M_\infty^2} \right] \cos^2 \theta + \frac{1}{\gamma M_\infty^2} \right\}}{[D(\theta)]^{1/2}} \quad (12.23)$$

where $D(\theta)$ is a function of γ , M_∞ and θ , given by

$$\begin{aligned} D(\theta) = & \left[1 - \frac{1}{\gamma M_\infty^2} \right] \left[\theta^2 - \frac{\theta \sin 4\theta}{2} + \frac{1 - \cos 4\theta}{8} \right] \\ & + \left[\frac{4}{\gamma M_\infty^2} \right] \left[\theta^2 - \theta \sin 2\theta + \frac{1 - \cos 2\theta}{8} \right] \end{aligned} \quad (12.24)$$

where \dot{q}_0 is stagnation point heat flux.

(c) Heat transfer at cone (Point-C) and cylinder (Point-D)

For the cone and cylinder region of the vehicle, the heat flux is estimated using the van Driest formula [3]. This is based on boundary layer flow over a flat plate and applicable for both laminar and turbulent flow with local Reynold's number corrections. The angle of attack has influence on the heating rate and it is accounted by considering the change in flow parameters at the edge of boundary layer for angles of attack less than 5° . For higher angles of attack, heat transfer rates are generated using yawed cylinder approach.

Heat flux over a flat plate is given by

$$\dot{q} = C_h \rho_e V_e (H_r - H_w) \quad (12.25)$$

i.e.

$$\dot{q} = C_h C_p \rho_e V_e (T_r - T_w) \quad (12.26)$$

This can be expressed as

$$\dot{q} = h(T_r - T_w) \quad (12.27)$$

where

$$h = C_h C_p \rho_e V_e \quad (12.28)$$

The parameters are expressed as

C_h = Stanton number

C_p = Specific heat at constant pressure

ρ_e = Density at local flow conditions

V_e = Velocity of local flow

T_r = Recovery temperature

T_w = Wall temperature

The recovery factor r is given as

$$r = \frac{T_r - T_\infty}{T_0 - T_\infty} \quad (12.29)$$

$$r = (P_r)^{1/2} \quad \text{for laminar flow}$$

$$r = (P_r)^{1/3} \quad \text{for turbulent flow}$$

From Eq. (12.3),

$$T_r = T_\infty \left[1 + r \left(\frac{\gamma - 1}{2} \right) M_\infty^2 \right] \quad (12.30)$$

From Reynold's number analogy,

$$C_h = \frac{C_f}{2} (P_r)^{-2/3} \quad (12.31)$$

$$C_f = 0.664 (R_e)^{0.5} \quad \text{for laminar flow}$$

$$C_f = 0.023 (R_e)^{0.139} \quad \text{for turbulent flow}$$

Once C_f is computed, C_h can be computed using Eq.(12.31) and hence the heat transfer coefficient h is computed using Eq.(12.28) to estimate the heat flux ' \dot{q} ' using Eq.(12.27).

In order to take care of axi-symmetric flow over cone (Point-C), the flat plate relations are used with a correction factor on the Reynold's number as follows:

$$R_{eC} = \frac{R_e}{3} \quad \text{for laminar flow}$$

$$R_{eC} = \frac{R_e}{2} \quad \text{for turbulent flow}$$

For the case of cylindrical portions (Point-D), the flat plate relations can be used without any corrections.

(d) *Heat rate at flow reattachment point (Point-E) and at protrusions (Point-F)*

Protrusions can be treated as a separate body and engineering methods can be applied to estimate the heating on the protrusions. Effect of protrusions on a launch vehicle is to increase the heating locally in the vicinity of the protrusions and the heat transfer coefficient is augmented locally. The augmentation in local heating rates at protuberances is generated by using the correlation derived from experiments on similar protrusions or by carrying out fresh experiments. Specific tests are to be devised for the evaluation of heating rates at (a) areas adjacent to protuberances, (b) wake areas downstream of protrusions, (c) separated flow and reattachment region and (d) shock impingement regions.

The augmentation is following the pressure distribution profile as given below:

$$\frac{h}{h_0} = \left(\frac{P}{P_0} \right)^n \quad (12.32)$$

where

$$n = \begin{cases} 0.5 & \text{for laminar flow} \\ 0.8 & \text{for turbulent flow} \end{cases}$$

(P/P_0) = pressure ratio across normal shock

h_0 = heat transfer coefficient in undisturbed stream

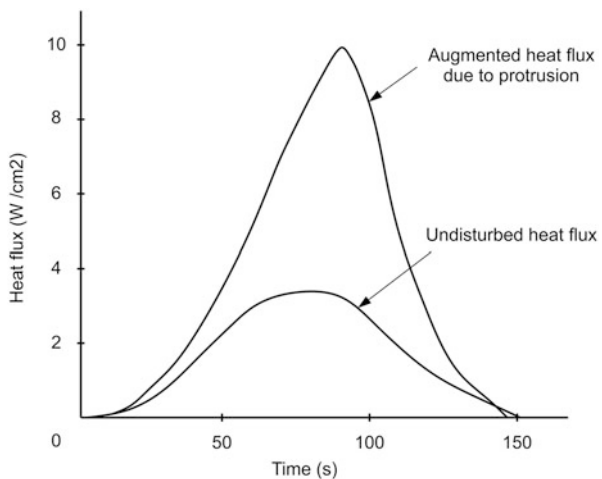
h = augmented heat transfer coefficient

Augmented heat flux at typical protrusion of a typical launch vehicle is given in Fig. 12.11.

(e) *Thermal response analysis and design*

Once the heat flux values are computed, it is essential to estimate the temperature on the structure. Based on the predicted incident transient heating, the temperature of the material has to be estimated. To determine the temperature field, $T(x, y, z, t)$, in a body, the boundary conditions, initial condition, shape, material thermo-physical properties such as conductivity, specific heat capacity and density and optical properties of the surface such as absorptivity and emissivity are required as inputs. The multi-dimensional transient heat transfer equation can be written as

Fig. 12.11 Heat flux due to protrusions



$$\rho C_p \frac{\partial T}{\partial t} = k \left(\frac{\partial^2 T}{\partial x^2} + \frac{\partial^2 T}{\partial y^2} + \frac{\partial^2 T}{\partial z^2} \right) + S \quad (12.33)$$

where S is the internal volumetric heat generation. For the launch vehicles, generally, $S = 0$. Therefore, Eq. (12.33) can be written as

$$\frac{\partial T}{\partial t} = \alpha \nabla^2 T \quad (12.34)$$

where

$\alpha = k/\rho C_p$ is the thermal diffusivity of the material

k = thermal conductivity of the structural material

ρ = density of the material

C_p = specific heat capacity of the material

This indicates that for substance with high thermal diffusivity, heat moves rapidly through because the substance conducts heat quickly relative to its volumetric heat capacity or ‘thermal mass’.

The Eq. (12.34) governs the temperature distribution for a three-dimensional unsteady heat transfer problem involving heat generation in Cartesian coordinate system. For steady-state conditions, $\frac{\partial T}{\partial t} = 0$. To solve the above set of equations and obtain the temperature field, computer-based numerical methods using finite difference or finite element schemes are generally put to practice.

(f) *Methodology for thermal response analysis*

A simple methodology using finite difference scheme is presented for evaluating the thermal response of simple shapes. For solving temperature field of complex shapes, more elaborate finite element schemes are recommended.

To determine the temperature field in a body, the first step is to ascertain the initial conditions, boundary conditions, material properties (k , ρ , C_p), surface properties (ϵ , α) and geometry of the body. Material properties (k , C_p) and surface properties (ϵ , α) vary with temperature and this variation has to be accounted for in the material data used for thermal analysis, particularly at elevated temperatures. The next step is to discretize the domain into finite number of nodes. The nodal distance has to be sufficiently small so as to minimize the discretization errors. The governing equations (Eq. 12.33) can be expressed in finite difference form and apply to all the nodes in the domain with appropriate boundary conditions. This results in a set of algebraic equations that can be solved using various explicit or implicit schemes to obtain the transient temperature distribution of the body.

The temperature of the material can be obtained for different thermal environments by specifying suitable boundary conditions:

1. For the case of specified temperature,

$$T = \text{constant}$$

2. For the case of specified heat flux (in one dimension),

$$-k \frac{\partial T}{\partial x} = \dot{q} \quad (12.35)$$

3. For the case of combined convective and radiative heat transfer,

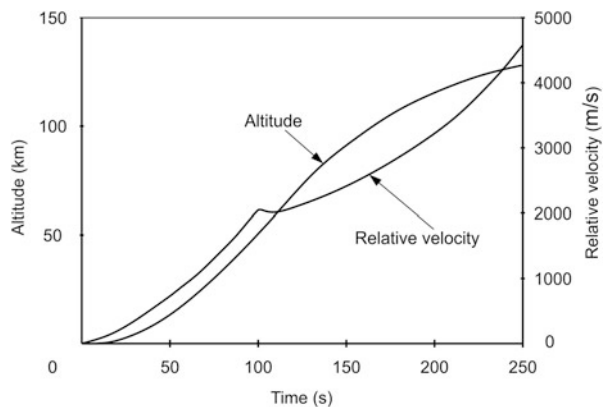
$$-k \frac{\partial T}{\partial x} = h(T_r - T_w) + \epsilon \sigma (T_a^4 - T_w^4) \quad (12.36)$$

where ϵ is emissivity, σ is Stefan-Boltzmann constant, T_a is ambient temperature.

(g) *TPS design for a typical vehicle*

The trajectory which induces maximum thermal environment for a typical vehicle configuration (refer Fig. 12.9) is given in Fig. 12.12. The heat flux profiles along the length of the payload fairing for a free stream Mach number of 5 is given in Fig. 12.13. When the flow is laminar over the heat shield, the stagnation point would experience the maximum heat flux. The flow accelerates and expands downstream and the heat flux progressively decreases away from the stagnation region to the cone and cylindrical region. As the Reynolds number increases, the flow in the cap region immediately aft of the stagnation point becomes turbulent. Also the accelerating flow aft of the stagnation region reduces the thickness of the boundary layer. As a result, the heat flux immediately aft of the stagnation region becomes higher than the stagnation heat flux. Subsequently, the boundary layer thickens. Due to this the heat flux reduces in the cone region. Beyond nose cone,

Fig. 12.12 Ascent phase trajectory parameters for a typical launch vehicle



before the cylindrical region, the flow expands. Under this condition, along with thick boundary layer, the heat flux is still lesser as shown in Fig. 12.13. A typical plot of the transient heat flux on the payload fairing for the entire flight duration is given in Fig. 12.14. Notice that the heat flux during the initial phase of flight is higher at point-B when compared to the stagnation region (point-A). This is because the launch vehicle experiences higher Reynolds number during the initial phase of flight due to the relatively higher atmospheric densities. As the vehicle ascends to higher altitudes, even though the Mach number is higher the free stream density reduces substantially, which reduces the Reynolds number resulting in a laminar over the payload fairing. During this high Mach number regime at higher altitudes where the flow is laminar, the stagnation heat flux is maximum.

Considering the payload fairing is constructed with aluminium alloy material with different thickness at different zones to withstand the structural loads, without any thermal protection the temperature history at the critical locations can be evaluated and typical values are as represented in Fig. 12.15. In the above figure, it can be seen that even though the heat flux at cap region is more than that at cone, the thermal response on the cone is higher compared to the nose cap. The reason for this is essentially due to the design of the structure with nose cap thickness more than nose cone material thickness to withstand the aerodynamic load.

From Fig. 12.15, it can be seen that a typical temperature profile at all the critical locations exceeds the allowable temperature of 120°C corresponding to aluminium alloy material. Therefore, suitable thermal design is to be carried out considering thermal paint as thermal protection system. Depending on the heat flux histories, material thickness and using thermo-physical characteristics of base aluminium alloy material and thermal protection material (thermal paint), thickness of TPS at each location is to be appropriately designed to limit the temperature of the base material corresponding to the limit of 120°C . With the optimum design of TPS thickness, temperature profiles of base material at all critical locations are limited to 120°C . Also, the TPS design is such that the temperature histories at base structure at all locations closely follow the same pattern.

Fig. 12.13 Heat flux distribution

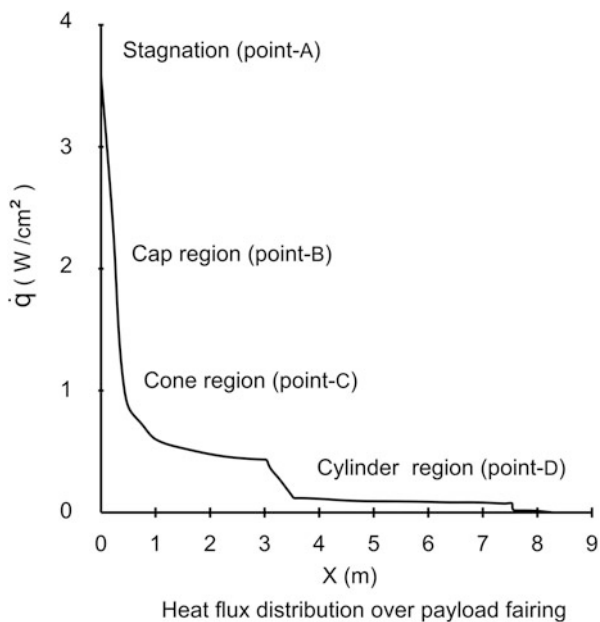
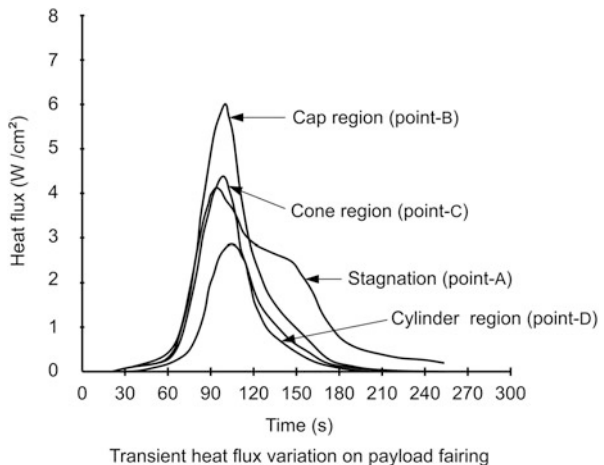


Fig. 12.14 Transient heat flux distribution

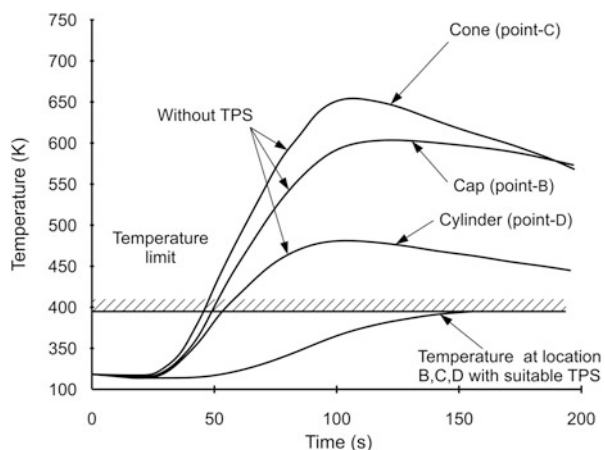


12.5.6 Base Heating Environment and Thermal Design

(a) Thermal Environment

In a launch vehicle, the propulsion exhaust plumes cause the base heating of the vehicle. The major thermal loads at the base region are

Fig. 12.15 Temperature profiles on the payload fairing



- (a) Convective heating due to jet interactions of multiple motors
- (b) Convective heating due to direct jet impingement on the nearby structure
- (c) Convective heating due to jet interactions with external flow field
- (d) Radiation heat from the hot solid particles of jet exhaust of solid motors and from the hot gases
- (e) Radiation from the hot nozzle divergents of radiatively cooled engines

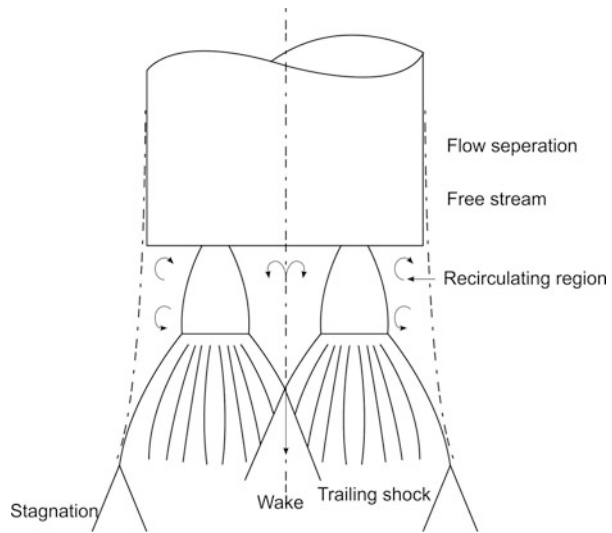
The thermal environment depends on the characteristics of plume, the type of propulsion system used in the vehicle, combustion product of exhaust jets and the external aerodynamic flow pattern in the base region. The vehicle altitude also influences the exhaust plume shape which in turn affects the thermal environment.

The base heating rates due to radiation depend very much on altitude, geometry and operating characteristics of the motors while the convective heating due to reverse flow depends primarily on the altitude and the proximity of adjacent jets and their jet pressure ratios. At high altitudes, jets expand and in the process interact. Figure 12.16 explains the base flow field at high altitudes. As the altitude of the vehicle increases, the rocket engine plume expands and is a function of P_j/P_∞ , where P_j is the nozzle exit pressure and P_∞ is the free stream pressure. As the plume expands, plume-to-plume and plume-to-free stream interactions take place and the effects are as given below.

When two jets interact, it forms the trailing shock at the intersection causing circulatory reverse flow of hot gases in the base region which generates convective heating on various base structures. When the free stream of air hits the plume boundary it results in turbulent mixing and a free shear layer is developed. A position of the shear layer is unable to move with the high-pressure region and results in reverse flow towards the base region. This circulatory reverse flow in the base region causes the convective heating.

Radiation heating comprises of radiation from the combustion exhaust products of solid motors. Al_2O_3 particles in the exhaust plumes of solid motors are the dominant radiating heat source in the base region. The radiation from the

Fig. 12.16 Base flow fields at high altitudes



radiatively cooled liquid engine nozzle divergent radiates heat to various structures in the base region.

Base heating at launch pad is influenced by geometry of flame deflector and the type of cooling provided at launch pad.

Generally base region of the vehicle accommodates several sensitive elements like liquid-stage control components, vehicle control actuation systems, gas bottles, etc. and all of them are to be protected for their satisfactory performance by restricting the temperature within 60 ° C. This calls for a suitable thermal protection system for this region and commonly used system is an aft end cover with layers of thermal protection appropriately designed to meet the thermal requirements. However whenever movable nozzles are used, rigid covers cannot be used and call for design of flexible thermal shield which can withstand all flight loads and offers least loads on the actuation systems.

(b) Thermal Design and TPS for base region

For ensuring the allowable thermal environment and the heating rate at the base region, the thermal design has to address all the following contributing factors:

- (a) Jet interaction and the corresponding convective heating
- (b) Direct jet impingement and its heating due to convection
- (c) Jet exhaust of solid motors if any and the radiative heating
- (d) Radiative heating from the liquid engine nozzle extensions
- (e) Aerodynamic heating contribution in the base region

The jet flow field data can be generated using computational fluid dynamics (CFD) by solving Navier–Stokes (N-S) equations. Once the flow field data is generated, the engineering methods like Fay and Riddell [1], van Driest and

Beckwith [3] and Gallagher methods [4] can be used to compute the heat flux. Inherent assumption used in this analysis is that the body is facing an infinite and uniform stream. The contribution of particle impingement becomes significant when the amount of particles in the plume is quite high. For estimating the heat transfer in the base region due to jet impingement one should consider the local radius and jet properties. There too Beckwith and Gallagher method can be used for calculating the heat flux. It is better to assume conservative incidence angles to estimate the heat flux for design.

The radiative heating in the base region is essentially due to exhaust of solid motors and the heat radiated from exterior of liquid engine nozzles. Solid motors where aluminized composite propellants are used cause very high thermal radiation due to the presence of aluminium oxide particles. These particles coupled with gaseous species like CO, H₂O, CO₂, etc. in the exhaust plume radiate heat to base region. During launch, the interaction of plume with launch pad also causes significant amount of convective and radiative heat transfer. In general the emissivity of combustion gases is lower when compared to that of aluminium solid particles in the exhaust plume. Gases emit thermal radiation in discrete bandwidths while solid particles do so in all wavelengths. Further, as the jet expands, jet pressure comes down and the gas emissivity values are reduced. This results in a negligible amount of gaseous radiation when compared to the radiant energy emitted by the particles. Thus the total plume thermal radiation is approximated as that due to the cloud of metallic oxide particles. Radiative heating due to solid particles in the exhaust plume of solid rockets is modelled using the engineering method adopted by Fontenot.[5]

The radiative heating emanating from the liquid engine nozzles is calculated using the maximum temperature measured on the engine divergent during ground tests. The emitted radiant load is estimated using a suitable emissivity value, as given by

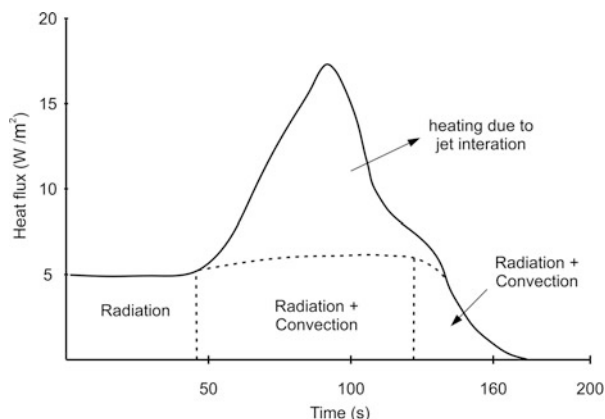
$$\dot{q} = \sigma \epsilon F_{1-2} T^4 \quad (12.37)$$

where ‘ σ ’ is the Stefan-Boltzmann constant, ‘ ϵ ’ is the emissivity of nozzle divergent at the functional temperature, F_{1-2} is the view factor of nozzle divergent to the surface receiving radiation and ‘ T ’ is the surface temperature of the nozzle divergent. The view factor is defined as the fraction of energy emitted from surface 1, which directly strikes surface 2.

There are several uncertainties in the computation of radiative heat flux like variation of emissivity of aluminium particles in the exhaust plume, variation in the shape of the plume at different altitudes, emissivity variation for the divergent nozzle with temperature and surface temperature variation along the divergent body. In order to account for such uncertainties, 20 % additional heat flux is used to provide the design margin for the thermal protection system.

The heat flux of a base region of a typical launch vehicle as function of flight time is given in Fig. 12.17.

Fig. 12.17 Typical heat flux at base region



Generally, in a launch vehicle, there are annular gaps between the nozzle and the structural shroud. This region also houses several sensitive elements and components which are to be protected from the radiative and convective heating of the base region. In most of the stages, the vehicle control is achieved by flexible nozzles or engine gimbaling and hence the thermal protection system has to be flexible to allow the engine deflection. This flexible thermal protection system is often termed as thermal boot which is connected between the movable nozzle of the stage and the external structural shroud. A typical thermal boot used to protect the base region of the vehicle is shown in Fig. 12.18. This flexible boot enables the gimbaling of the nozzle within specified gimbal angles. The configuration is essentially a multilayered flexible insulation and it comprises of different layers of glass cloth, silica cloth, aluminium-impregnated silica cloth and rubber layer. The functional lay-up and number of layers to be used has to be based on the maximum heat flux encountered in the base region during the flight regime. The specific layer configuration chosen has to provide at least a margin of 10°C at the back wall of the thermal boot. The final configuration has to be selected based on the full-scale test simulating all conditions of heat flux, differential pressure and also the gimbal cycle needed.

If the vehicle has multiple engines and also solid motor at the base, the engine nozzles are exposed to radiative heating from solid motor exhaust and convective heating due to reverse flow of jets. The reverse flow of jets at times may disturb the orifices near the fore end of nozzle divergent and also the thermal coating inside the nozzle. It is therefore essential to analyze the thermal effect on the nozzle and ascertain whether a thermal protection system (TPS) is needed for the nozzle. If needed a suitable multilayered TPS with a configuration similar to thermal boot has to be introduced.

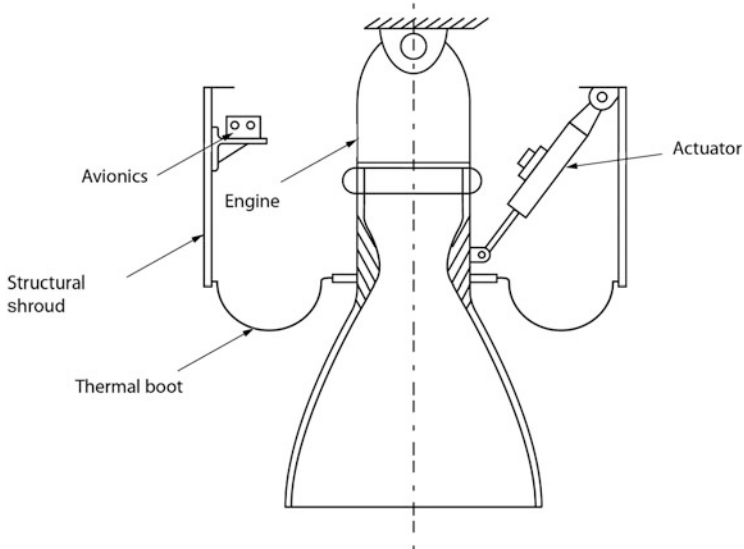


Fig. 12.18 A Typical Thermal boot used in deflectable engine

12.5.7 Thermal Protection for Destruct Systems

Destruction systems used in the vehicle have an environmental cover generally made of aluminium alloy with a gap of a few millimetres. Various elements of destruction system like flexible linear-shaped charge (FLSC), rigid linear-shaped charge (RLSC), explosive transfer assembly (ETA) and detonating transfer joint (DTJ) are having a temperature constraint of 70°C to ensure that explosive charges are safe. The free convection and radiation are the modes of heat transfer from the outside cover to these assemblies. Therefore the heat transfer has to be analyzed for trajectories which produces severe thermal environments and the requirement of TPS is to be worked out accordingly.

12.6 Thermal Protection Systems for Cryogenic Stage

In cryogenic stage, one of the essential requirements is to keep the temperature of cryogenic fluids (LOX and LH₂) always within allowable limits. The boil-off losses are also to be minimized, which happens mainly due to heat-in-leak to the cryogenic fluids stored inside the tank from the external environment through the composite insulation. It is important to ensure the heat-in-leak is within limits during the pre-launch and flight phase till satellite injection. Therefore appropriate thermal protection system for the entire structure, fluid lines, component modules

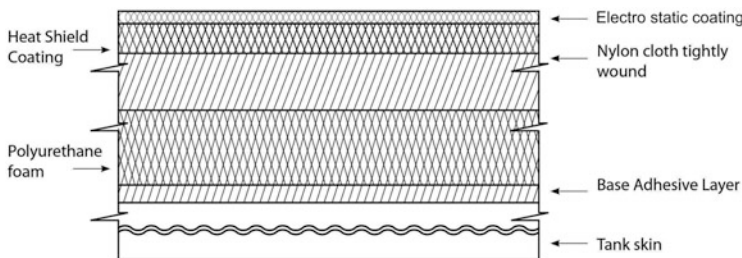


Fig. 12.19 Typical insulation system for cryo-system

and various valves is needed to insulate them against all thermal loads and reduce the heat-in-leak to the fluids.

During the pre-launch phase the important thermal loads are due to (a) direct solar radiation, (b) Earth reflected (Albedo) radiation and (c) Earth emitted radiation. During the flight additional thermal environment is due to aerodynamic heating at atmosphere region and plume base heating during the engine operation region. While designing a suitable thermal protection system for cryogenic stage, two important requirements needed to be considered are boil-off losses due to heat-in-leak and minimum weight due to insulation. Therefore selection of the material has to be based on low-density insulator. Generally low-density rigid foam is used as the main thermal insulator. The various essential requirements for the insulation are as given below:

- (a) To ensure proper surface adherence to the base material
- (b) To act as a thermal barrier so as to maintain the temperature within limit
- (c) To possess sufficient mechanical stiffness to withstand flight loads
- (d) To thermally protect from the aerothermodynamic load
- (e) To prevent static electricity build-up

To meet these requirements a composite thermal protection system involving several layers of coating is needed. There are several ways of realizing the same which satisfy the conditions listed above. One of the commonly used systems is the polyurethane foam which can be sprayed as the basic thermal insulator. To provide the mechanical stiffness a suitable cloth is wound tightly over the foam and applied with vapour barrier coating. Low-density thermal insulation paint is usually applied as the shield coating to protect the foam insulation from aerodynamic heating. It is also essential to avoid the electrostatic discharge from the outer surface and it is achieved generally by applying an antistatic enamel paint. Figure 12.19 gives a typical composite insulation used in cryo-system.

It is necessary to evaluate the heat-in-leak for a chosen composite insulation scheme by carrying out experiments using a subscale tank and liquid nitrogen (LN₂) as the test fluid to simulate the cryo-fluid conditions. The tank has to be subjected to the simulated convective environment and solar radiation. The tanks need instrumentation to measure temperatures at skin and at different depths of the insulation to generate the thermal gradient across the thickness of the insulation to

simulate the flight conditions. To simulate the aeroheating as per the extreme trajectory, specially contoured heaters have to be used. The heat-in-leak is to be estimated using the temperature gradients established from the tests. The configuration of the thermal protection system in terms of thickness for the foam material is to be finalized to ensure that the heat-in-leak values are well within the allowable limits.

12.7 Tests for Thermal Protection Systems and Qualification

Once the suitable thermal protection materials are chosen based on the detailed analyses, it is essential to carry out thermophysical and mechanical property tests for these materials within the temperature range they are expected to experience in flight. The various material characterization tests for these materials are the measurements of thermal conductivity, specific heat, lap shear strength, tensile strength, peel strength, elongation and coefficient of linear expansion at different temperatures, likely to be experienced during flight. The thermal coating systems in flight are exposed to (a) thermal environment due to aerodynamic heating and (b) aerodynamic shear loads. Therefore the qualification of the high-temperature coating system has to be carried out in two distinct phases. Suitable test panels of reasonable size (generally 150×150 mm panel) are to be coated with the designed thickness of the chosen insulation on the base material and are to be exposed to expected thermal environment in aerodynamic heating simulation facility. In this facility the expected convective heating is simulated on the test specimen using a radiative heat source. The heating cycle used in simulation has to be based on the maximum heating trajectory. The test panel has to be instrumented with thermocouple and heat flux gauges to measure the back wall temperature and incident heat flux. The combined effect of heating load and aerodynamic shear is tested in heat transfer tunnel by properly simulating close to flight conditions. Another important test is to study the ageing effect. The procedure is to prepare a number of specimens with coated panels and subject them for tests at different intervals for the specified duration (say 18 or 24 months) after the test specimen preparation.

The thermal boot which is provided in the base region connecting between the movable nozzle and the external structural shroud needs to be qualified through a series of experimental tests. The performance of the boot has to be verified against the following essential functional requirements:

1. Back wall temperature has to be maintained within the specified temperature limit with sufficient margin.
2. The back flow of hot gas to the subsystems compartment has to be totally arrested.
3. The differential pressure across the thermal boot has to be maintained within 0.1 bar. This specification is essential during the atmosphere ascent phase.

4. The system has to endure specified number of cycling due to engine gimbaling and also has to withstand the inertial loads due to engine gimbal dynamics.

Detailed qualification tests are needed at specimen panels to study the thermal response, effect of differential pressure and effect of convective heating due to plume impingement. To study the thermal response, the panels are subjected to the overall heat flux history experienced by the material during the flight. The structural integrity and back wall temperatures are to be verified. To study the plume impingement on the specimen convective heat simulation is needed. One of the possible methods is to use LPG-fired burner in which the flame impinges on the test specimen simulating the convective heat flux. Simultaneous simulation of convection and radiation is also needed where radiation heating is simulated using the heater module in parallel. Here too the structural integrity and back wall temperature of the specimen are to be verified. In order to ensure full qualification of the system it is necessary to carry out full-scale tests on the actual thermal boot by subjecting the same to total flight heat flux, differential pressure and the gimbal cycles. Based on these exhaustive tests the configuration of the thermal boot with sufficient number of layers which provide at least 10 °C margin on the back wall of the boot has to be finalized.

Bibliography

1. Fay, F.A., Riddell, F.R.: Theory of stagnation point heat transfer in dissociated air. *J. Aeronaut. Sci.* **25**, 73–85 (1958)
2. Lees, L.: Laminar heat transfer over blunt nosed bodies at hypersonic flight speeds. *Jet Propul.* **26**, 259–269 (1956)
3. Van Driest, E.R.: Investigation of Laminar Boundary Layer in Compressible Fluids Using the Cross Method. NACA TR, NACA TN 2597 (1952)
4. Beckwith, C.E., Gallagher J.J.: Local Heat Transfer and recovery temperature on a Yawed Cylinder at a Mach number of 4.15 and at High Reynolds Number. NASA TR, Issue, NASA-TR- R-104 (1961)
5. Fontenot Jr., J.E.: Thermal radiation from solid rocket at high altitude. *AIAA J* **3**(5), 970–972 (1965)
6. “Aerodynamic and Rocket Exhaust Heating during Launch and Ascent”, NASA Space Vehicle Design Criteria, NASA SP-8029, NASA, Washington DC (1969)
7. White, F.M.: Viscous Flow. McGraw Hill, New York (1974)
8. Rohsenow, W.M., Hartnett, J.P.: Handbook of Heat Transfer. McGraw Hill, New York (1973)
9. Irwin, T.F., Hartnett, J.P.: Advances in Heat Transfer, vol. II. Academic, New York (1965)
10. Bender, R.L., Reardon, J.E.: Preliminary Base Heating Environments for a Generalised ALS LO₂/LH₂ Launch Vehicle. Remtech Technical Note, Huntsville, Al, RTN218-01 (1989)
11. Anderson, J.D.: Hypersonic and High Temperature Gas Dynamics. McGraw-Hill Book Company, New York (1989)
12. Fletcher, D.G.: Fundamentals of Hypersonic Flow-Aerothermodynamics. RTO-EN-AVT-116, Von Karman Institute, Belgium (2004)
13. Miller, C.G.: Aerothermodynamic simulation capabilities for aerospace vehicles. 20th AIAA advanced measurements and ground testing technology conference, AIAA, 98–2600 (1998)
14. Hirschel, E.H.: Basics of Aerothermodynamics, vol. 206. Progress in astronautics and aeronautics, Ed. in Chief Zarchan P. Springer, Germany (2005)

15. Hosizaki, H., Chou, Y.S., Kulgei, N.G., Meyer, J.W.: Critical Review of Stagnation Point Heat Transfer Theory. Technical Report, AFFDL-TR-75-85 (1975)
16. Hamilton, H.H.: Approximate Method of Calculating Heating Rates at General Three Dimensional Stagnation Points During Atmospheric Entry. NASA TR, NASA-TM-84S80, Hampton, VA (1983)
17. Eckerts, E.R.G.: Engineering relations for heat transfer and friction in high velocity laminar and turbulent boundary layer flow over surface with constant pressure and temperature. *J. Aerosp. Sci.* 22, 585 (1955)
18. Chen, K.K., Thyson, A.: Extension of emmons spot theory to flows on blunt bodies. *AIAA J* Vol 9, no 5, 821–825 (1971)
19. Reeves, B.L.: Aerodynamic Heating in the Slip, Intermediate and Free molecular Flow Regimes. Report No: 6859. McDonnel Dondles Aircraft Corporation (1959)
20. Detra, R.W., Hidalgo, H.: Generalized heat transfer formulas and graphs for nose cone re-entry into the atmosphere. *ARS J* 31, 318–321 (1961)
21. Higgins K.: Comparison of Engineering Correlations for Predicting Heat Transfer in Zero-pressure-gradient Compressible Boundary Layers with CFD and Experimental Data. Defence Science and Technology Organisation DSTO-TR-2159 (2008)
22. Hansen, C.F.: Thermodynamic and Transport Properties of High Temperature Air. NASA TR-R -50. Advisory Group for Aeronautical Research and Development, Paris (1959)
23. "Liquid Rocket Engine Self-Cooled Combustion Chambers" NASA SP-8124, NASA, Washington DC (1977)
24. Cunningham, G.R., Funai, A.I., McNab, T.K.: Radiative Properties of Advanced Spacecraft Heat Shield Materials. NASA Contractor Report 3740 (1983)
25. Scala, S.M., Sampson, D.H.: Heat Transfer in Hypersonic Flow with Radiation and Chemical Reaction. Space Sciences Laboratory, Defense Document Centre, Scientific and Technical Formation, AD 410408 (1980)
26. Howell, J.R., Siegal, R.: Thermal Radiation Heat Transfer. McGraw Hill, New York (1972)
27. Dawbarn, R.: Analysis of the Measured Effects of the Principal Exhaust Effluents from Solid Rocket Motors. NASA TR, NASA CR 3136 (1980)
28. Simons, F.S.: Rocket Exhaust Plume Phenomenology. Aerospace Press and AIAA, The Aerospace Corporation, El Segundo (2000)
29. Morizumi, S.J., Carpenter, H.O., Thermal radiation from the exhaust plume of an aluminized composite propellant rocket. *AIAA, J Spacecraft Rockets*, **1**(5), 501–507 (1964)
30. Dobbins, R.A.: Measurement of mean particle size in a gas-particle flow. *AIAA J* **1**, 1940–1942 (1963)
31. Adelman, H.M.: Computational Aspects of Heat transfer in Structures. NASA TR, Issue, NASA CP-2216, Hampton (1982)
32. Swan, R.T., Pittman, C.M., Smith, J.C.: One dimensional Numerical Analysis of the Transient Response of Thermal Protection Systems. NASA TN D 2976. NASA TR, Issue, Washington, DC (1965)
33. Quinn, R.D.: A Method for Calculating Transient Surface Temperatures and Surface Heating Rates for High-Speed Aircraft. NASA/TP-2000-209034. NASA, CASI, Hanover, MD, (2000)
34. Myers, D.E., Martin C.J., and Blosser, M.L.: Parametric Weight Comparison of Advanced Metallic, Ceramic Tile, and Ceramic Blanket Thermal Protection Systems. NASA/TM-2000-210289. NASA, Hampton/Langley (2000)
35. Patankar, S.V.: A numerical method for conduction in composite materials flow in irregular geometries and conjugate heat transfer. In Proceedings of 6th international heat transfer conference, vol. 3, p 297, Toronto (1978)
36. Patankar, S.V., Balinga, B.R.: A New Finite Difference Scheme for Parabolic Differential Equations. *J Numer Heat Transf* **I**, 27–37 (1978)
37. Stone, H.L.: Iterative Solution of Implicit Approximations of Multidimensional Partial Differential Equations. *SIAM J Numer Anal* **5**(3), 530–558 (1968)
38. Burmester, L.C.: Convective Heat Transfer. Wiley, New York (1983)

Chapter 13

Stage Auxiliary Systems

Abstract The launch vehicles are generally configured with multiple stages to achieve the required orbital velocity. To achieve the required orbital conditions, the burnt-out stages are to be separated from the vehicle immediately after meeting their intended functional requirements. These separation processes are mission-critical functions as the inadvertent collision during separation can lead to vehicle failure. All these systems are generally termed as stage auxiliary systems (SAS) and carry out the mission critical separation processes in the vehicle as per the specified requirements, thus ensuring the vehicle safety and successful mission. The stage auxiliary systems are configured with high-energy systems and they are built with pyro-elements, which, once assembled in the flight systems, are not amenable for ground tests. Thus, the stage auxiliary systems have only one chance to operate, that too directly in the flight after its manufacturing and these systems have to operate successfully in the first attempt itself. Therefore, these systems have to be highly reliable. They have to be necessarily robust with suitable built-in redundancy to achieve the safer and successful mission. The design of SAS is closely linked with all other subsystems of the vehicle. The high-energy pyro-systems during their operation induce severe environment to the vehicle systems. Design of the SAS is based on the vehicle systems inertial properties, vehicle subsystems, performance parameters and the vehicle operating environment. Therefore, integrated design approach is essential to achieve the robust and highly reliable designs for the complex, high-energy stage auxiliary systems. During the vehicle flight from lift-off till satellite injection, the vehicle can deviate from its nominal path due to abnormal behaviour or due to failure of any of the subsystems onboard. In such cases where the deviation is beyond the safe allowable corridor, the flight has to be terminated using vehicle destruct system. Additional care should be taken to avoid the inadvertent activation of the vehicle destruct system during normal flight. The stage auxiliary systems' requirements of a launch vehicle, their functional aspects, integrated design aspects of SAS and the various elements involved in the SAS design process are explained in this chapter. The details of the actuators used in these systems based on pyro-mechanical devices, the jettisoning and destruct systems, their performance in a typical vehicle and the validation strategy of these important subsystems are also presented. Detailed analysis of the separated body dynamics with respect to the ongoing vehicle is very vital in the separation system design. The various aspects of system analysis are included.

Keywords Stage auxiliary system • Separating system • Jettisoning system • Longitudinal separation • Payload fairing • Vented interstage • Separation dynamics • Explosive devices • Jettisoning mechanism • Vehicle destruct system and safe arming device

13.1 Introduction

Most of the present-day launch vehicles are configured with multiple stages to achieve the required orbital velocity. Depending on the available technologies and feasibility of manufacturing process, both parallel and tandem staging concepts are adapted for design, development and realization of vehicles to meet the specific functional requirements. In addition, several structural elements are used to protect the vehicle subsystems against hostile flight environments and to transfer the thrust from the propulsive stages to the vehicle main structure. To achieve the required orbital conditions, it is essential to separate the above structural elements and the propulsive system structures from the ongoing active vehicle, immediately after meeting their intended functional requirements. Finally, once the specified injection conditions are achieved, the satellite has to be separated from the final stage of the vehicle. These separation processes are mission critical functions as the inadvertent collision during separation can lead to vehicle failure. Similarly, higher body rates induced by the separation system can make the ongoing vehicle uncontrollable, which can lead to the loss of mission. All these systems are generally termed as stage auxiliary systems (SAS) and carry out the mission critical separation processes in the vehicle as per the specified requirements, thus ensuring the vehicle safety and successful mission.

The major functional requirements of stage auxiliary systems are to quickly and smoothly separate the spent stages and systems from the ongoing vehicle and move them far away as fast as possible, without interfering with the functioning stages or vehicle systems, thus ensuring safety of the vehicle and mission. To carry out the above functions, invariably the stage auxiliary systems are configured with high-energy systems. Due to the requirements of quick actions, these high-energy stage auxiliary systems are built with pyro-elements, which, once assembled in the flight systems, are not amenable for ground tests. Thus, the stage auxiliary systems have only one chance to operate, that too directly in the flight after its manufacturing, and these systems have to operate successfully in the first attempt itself. Therefore, these systems have to be highly reliable. They have to be necessarily robust with suitable built-in redundancy to achieve the safer and successful mission.

Another important aspect is that SAS is not a stand-alone system in the vehicle. The design of SAS is closely linked with all other subsystems of the vehicle. While the high-energy pyro-systems of SAS during its operation induce severe environment to the vehicle systems, design of the SAS is based on the vehicle systems' inertial properties, vehicle subsystems' performance parameters and the vehicle operating environment. Therefore, integrated design approach is essential to

achieve the robust and highly reliable designs for the complex, high-energy stage auxiliary systems.

During the vehicle flight from lift-off till satellite injection, the vehicle can deviate from its nominal path due to abnormal behaviour or due to failure of any of the subsystems onboard. In such cases where the deviation is beyond the safe allowable corridor, the flight has to be terminated using vehicle destruct system. Generally, the manual destruction causes the delay in operation, therefore the vehicle has to be automatically destructed by the onboard systems. However, if there is sufficient time gap available from the initiation of vehicle deviation to the time of potential hazard, manual destruction of the vehicle from the ground can also be planned through suitable tele-command system. For both the cases, it is essential to provide suitable destruct systems onboard. Additional care should be taken to avoid the inadvertent activation of the vehicle destruct system during normal flight. Therefore, design of destruct system has to be robust and highly reliable with all suitable built-in redundancies. Even though the functional requirements of these systems are different from that of the separation systems of the vehicle, the system requirements of destruct systems are the same as that of the separation systems. Therefore, the destruct systems are also considered as part of the vehicle stage auxiliary systems.

The stage auxiliary systems' requirements of a launch vehicle, their functional aspects, integrated design aspects of SAS and the various elements involved in the SAS design process are explained in this chapter. The SAS used in launch vehicles, their performance in a typical vehicle and the validation strategy of these important subsystems are also explained in this chapter.

13.2 Functional Requirements of Stage Auxiliary Systems

In a multistage launch vehicle, the separation systems perform mission critical functions of separating the spent stages and structural elements from the normal functioning vehicle and the destruct system performs the function of destructing the vehicle when there is malfunction of vehicle and subsystems. These systems are activated by the vehicle onboard sequencing system as per the specified sequence, meeting the overall requirements. Stage auxiliary systems of a typical launch vehicle are given in Fig. 13.1. Depending on the vehicle configuration, the various staging events that occur in a typical launch mission are separation of spent strap-on motors and stages, payload fairing, ullage rockets, interstages and finally the satellite. To meet the mission requirements as well as considering vehicle safety, the flawless stage transition process has to be executed almost instantaneously without inducing additional disturbances and severe environments to the vehicle systems. Therefore, many systems have to operate simultaneously to transfer the vehicle functions safely and smoothly from spent stage to the active upper stages. The stage transition process consists of a series of events such as (a) detection of the suitable condition for separation either by sensing the stage burnout or by sensing

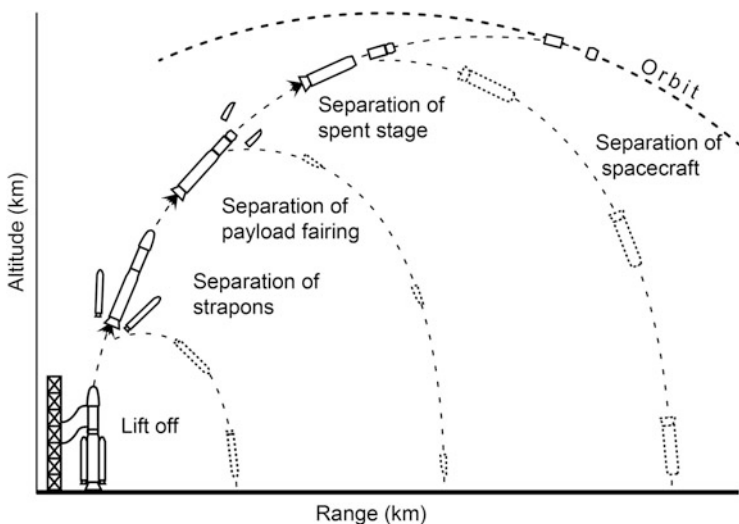


Fig. 13.1 Typical stage auxiliary systems

the specified vehicle acceleration, (b) shut-off of the engine and adaptation of suitable strategy for vehicle control, (c) separation of the spent stage and structural elements and (d) ignition of the next stage and transfer of the vehicle control to the next stage. To execute the stage transition process effectively, the separation systems have to execute their task within a short period of time. Similarly, to reduce the potential hazard due to the failed vehicle systems, the destruct system has to function as fast as possible.

The important functional requirements of a separation system to provide smooth and collision-free separation are given below:

- To provide structural rigidity in the attachment of the systems and also in the joints used to meet the functional requirements during their operational phase
- To ensure safe separation between the spent stage and active vehicle systems
- To impart sufficient separation velocity to the spent stage for its rapid movement away from the continuing stage, guaranteeing the needed clearances during separation of the spent stage
- To ensure that the tip-off rates to the ongoing stage are maintained within the specified level
- To avoid flying debris while the separation system is functioning
- To guarantee minimum shock transmission to the spacecraft and also to the functional critical elements of the ongoing stages
- To provide suitable means to sever the structural connection smoothly and in minimum time so that 'no control duration' of flight is kept minimum
- To accommodate the differential thermal expansion wherever cryogenic stages are used

- (i) To survive the flight and environmental loads due to vehicle acceleration, winds, aerodynamics, acoustics and vibration including thermal effects
- (j) To ensure adequate water proofing for a reliable operation in all weather conditions

The functional requirements of vehicle destruct system are given below:

- (a) To destruct the vehicle system at the earliest as per the onboard or ground command
- (b) To burn the propellants of the propulsive stages in the atmosphere itself before reaching the ground
- (c) To destruct the vehicle systems into pieces so that no major vehicle subsystem impacts on the ground to avoid potential hazard
- (d) To ensure the destructed debris fall within the safe corridor

To achieve the above functional requirements, the suitable stage auxiliary systems are designed and implemented in the vehicle. The system requirements and design aspects of SAS are given in the following sections.

13.3 System Requirements of SAS

The major functional requirement of SAS is to separate the spent stages and systems almost instantly or to destruct the vehicle systems immediately after receiving the necessary command. As discussed earlier, to carry out the above function, high-energy SAS systems are essential. But these high-energy systems can induce severe environment to the vehicle systems. Therefore, considering the functional requirements and the safety of the vehicle systems, the separation systems are configured with basic elements as given in Fig. 13.2. The major sub-systems are (a) separating systems, comprising of a severance system to rip open the integrated structure and an actuator to initiate the event, which in combination make physical separation between the spent system and the active functioning vehicle and (b) jettisoning systems, which provide necessary energy for imparting the needed relative velocity to the spent system to move away from the ongoing vehicle.

Generally, in the multiple-stage launch vehicles, two separate subsystem structures are integrated together by mechanical joints or by fasteners. For the case of mechanical joints, merman clamp band or ball lock systems are used for joining mechanically two systems to provide the necessary structural rigidity and joint rotation during the system operation, which would be released during separation process. The activation of the release mechanism is carried out by the explosive devices such as bolt cutter, pin pusher, explosive bolt or frangible nut. Spring energy by the release of a set of preloaded compression springs, provides the required relative velocity between the spent system and ongoing vehicle. To provide the required structural rigidity under the environment of large flight

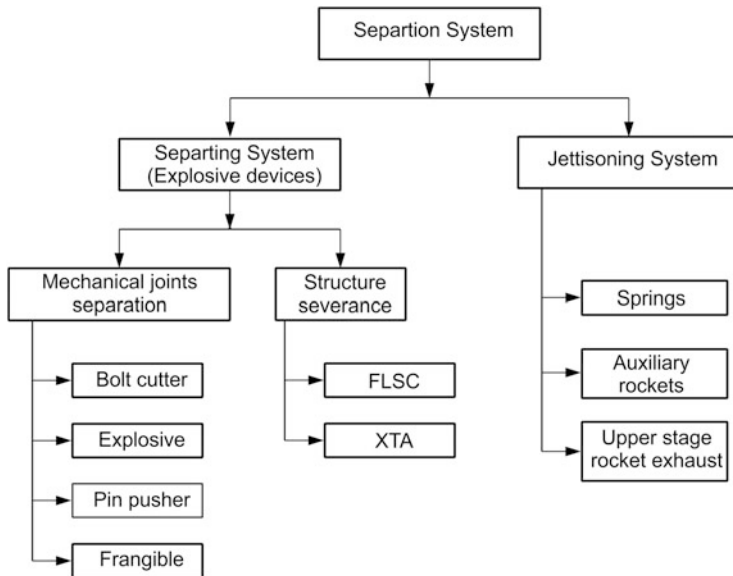


Fig. 13.2 Basic elements of a separation system

loads, the lower stage structures are normally joined through fasteners, making an integral structure. Explosive systems such as flexible linear shaped charge (FLSC) and expanding tube separation (XTA) systems are used to sever such integral structures, thus making physical separation between the spent system and ongoing vehicle. For imparting the required velocity to the spent system, preloaded compression springs or auxiliary rockets are used. For the case of hot separation system (as explained later), the jet impingement force due to the exhaust gas of upper stage engines are used to move the spent system away from the active vehicle system.

To achieve the specified mission requirements, depending on the vehicle inertial properties and flight environment, suitable separation system has to be selected for each separation process. The selected system has to meet the following requirements:

- Withstand the extreme loads in flight with adequate margins
- Should have compatibility with structures chosen
- Should satisfy the overall weight and volume constraints
- Compatibility with the surrounding environment and temperature gradients
- Ease of integration and handling
- Minimize the overall power requirement
- Have high reliability
- Minimization of overall shock loads
- Less severance or action time
- Less components and simple design
- Should be safe to handle

- (l) Shall not inadvertently activate
- (m) Proper debris management
- (n) Watch on allowable joint rotation constant at joints

The explosive devices chosen have to ensure the positive severance of the identified elements. Redundancy has to be considered for explosive devices and their electrical initiation elements to improve the reliability. Most of the shock in a separation system is generated by pyro-functioning and therefore it should not generate higher shock levels to the modules located in the vicinity of the severance zone.

The system requirements of destruct system are a subset of the separation system requirements and therefore not explicitly covered in this section.

13.4 Design Aspects of Separation Systems of Launch Vehicles

Even though the separation systems are not contributing for the performance aspects such as velocity addition, vehicle control and guidance, etc., they carry out mission critical functions. Failure in any one of the subsystems of any of the separation systems of a multistage launch vehicle during its flight leads to the overall mission failure. Therefore, a robust design approach by carefully integrating the information and data from various disciplines is essential for the successful development of such a mission critical system. The operating environment, design input, robust design approach and design guidelines of typical separation systems of a launch vehicle are explained in this section.

13.4.1 *Operating Environment and Design Input*

Separation process occurs during various phases of a multiple stage launch vehicle mission. Generally, strap-on motors are separated during the most disturbed atmospheric flight phase, the first stage is separated in the upper atmospheric flight phase whereas upper stages, payload fairings and satellite are separated in vacuum flight.

The predominant aerodynamic disturbance caused by the dynamic pressure at the time of separation is the major influencing factor for achieving the clean separation process of the spent strap-on motors. During these events, the continuing vehicle is with active control whereas the strap-on stages are uncontrolled and tumbled due to the presence of disturbing aerodynamic forces and moments. The separation process is further complicated by the residual tail-off thrust of the separated strap-on motors. The aerodynamic forces and moments along with the residual thrust of spent stages are the major environment input to the design of strap-on motors separation system.

Even though the first-stage separation occurs at upper atmosphere, due to the high velocity of the vehicle, the aerodynamic disturbances cannot be neglected. The specific feature of this separation process is that during this phase, both continuing and spent stages are uncontrolled. The residual tail-off thrust of the spent stage accelerates the separated body towards the continuing stage, which is not yet ignited and waiting for the completion of separation process. The aerodynamic forces and moments on the spent stage can laterally move the separated body with respect to the ongoing vehicle. Due to the fact that the upper stage is uncontrolled, the aerodynamic forces and moments along with the disturbance caused by the separation process can introduce rates to the ongoing vehicle. The separation process is further complicated with the requirement that the spent stage has to be pulled out of the ongoing vehicle for a longer length without collision. The environments described above are the major input data for the design of first-stage separation system.

Generally, payload fairing separation process occurs during the vehicle accelerating phase wherein the vehicle is actively controlled. In this event, the separation system has to impart sufficient velocity to the payload fairings to push them away at the earliest from the ongoing vehicle. Specific feature of this separation process is that, due to the large structure, the structural flexibility of payload fairings has to be considered as a major input for the separation system design.

For the cases of upper stages and satellite separation processes, tail-off thrust of the spent stage is the major input for the design. For all the cases, influences of the jet plumes of the continuing body on the spent stage dynamics have to be carefully ascertained and incorporated in the separation system design process.

Whenever twin engine stages are used in the vehicles, the differential thrust caused by the engines of spent stage is one of the key sources of disturbances. The difference between thrust of the engines generally becomes maximum during the tail-off region, at which the separation system is called upon to act. Therefore this problem is handled by canting the nozzles of the engines to pass through the centre of gravity of the vehicle as far as possible. This minimizes the disturbance due to differential thrust because the thrust almost passes near the centre of gravity of the vehicle, thus reducing disturbance moment. However, differential thrust is one of the major input data for separation system design of spent stages with twin engines.

The inertial properties, viz. mass, centre of gravity and mass moment of inertia of spent and ongoing vehicle along with the environments and disturbances as described above are the major input data for the design of individual separation system. In addition, the vibration and acoustic environment of the vehicle and dynamic input such as slosh disturbances are also used for the separation system design.

13.4.2 Integrated Design Aspects

Separation system design is essentially multidisciplinary in nature and closely linked with almost all the subsystems of the vehicle and operating environment

as explained in Fig. 13.3. The separation system design depends on the characteristics of interstage structure, spent-stage tail-off thrust, spent-stage inertial properties and external aerodynamic and vehicle environments. The external aerodynamic environment depends on vehicle system characteristics such as thrust and inertial properties. The vehicle structural systems design and vehicle dynamic environment depend on the external aerodynamic environment. The separation system during its operation creates severe environment to the vehicle systems of the ongoing vehicle. The shock induced by the separation system's activation, affects the performance of the vehicle active systems, whereas the rate induced during the separation process severely affects the controllability of the continuing vehicle.

In addition, there are several other factors which need to be considered during the design of separation systems. During stage transition phase, the tail-off requirements for clean separation, requirements of vehicle performance and vehicle control are conflicting. For clean separation, it is more favourable to separate the stage when there is no thrust. But in reality, there is always some residual thrust and therefore, it is preferable to separate a stage at the lowest possible thrust. But separation at a lowest thrust poses the following problems: (1) vehicle performance loss and (2) vehicle controllability issues.

For the case of strap-on motors, to achieve lower thrust of spent stages, even after burnout, the spent stage has to be carried along with the ongoing vehicle for longer time, which in turn leads to performance loss. For the case of sequential stage separation process, it is essential to ensure lower thrust for the spent stage after burnout. The very low thrust of the spent stage acting on the overall vehicle is almost equivalent to coasting of the vehicle before igniting the upper stage. The upper stage is ignited only after the separation of lower stage. Vehicle coasting leads to velocity loss, which in turn leads to mission performance reduction. Such losses are significant especially in the lower stages. Therefore, from performance point of view, it is essential to separate a spent stage as soon as its burnout but it is not favourable from separation point of view.

Separation system has a major interaction with vehicle control aspects. In most of the vehicles, control is achieved through the main propulsion stage by secondary injection thrust vector control (SITVC) or flex nozzle control (FNC) in solid motors and engine gimbal control (EGC) in liquid engines. During tail-off, the control effectiveness reduces and at certain thrust level, control effectiveness would be nil and below that thrust level, the control systems would create disturbances to the vehicle. Therefore to achieve the vehicle control till separation, the tail-off thrust level has to be above certain level, which may not be preferable from separation point of view. This problem can be resolved by adopting the following techniques:

1. Separate at higher level of the thrust to ensure vehicle performance as well as vehicle controllability. To achieve clean separation at high residual thrust, use auxiliary rockets, thereby meeting both requirements.
2. If control effectiveness is insufficient at a thrust level which cannot be handled by auxiliary rockets, coast the vehicle till meeting the requirements of auxiliary rockets and during this phase, use additional control systems.

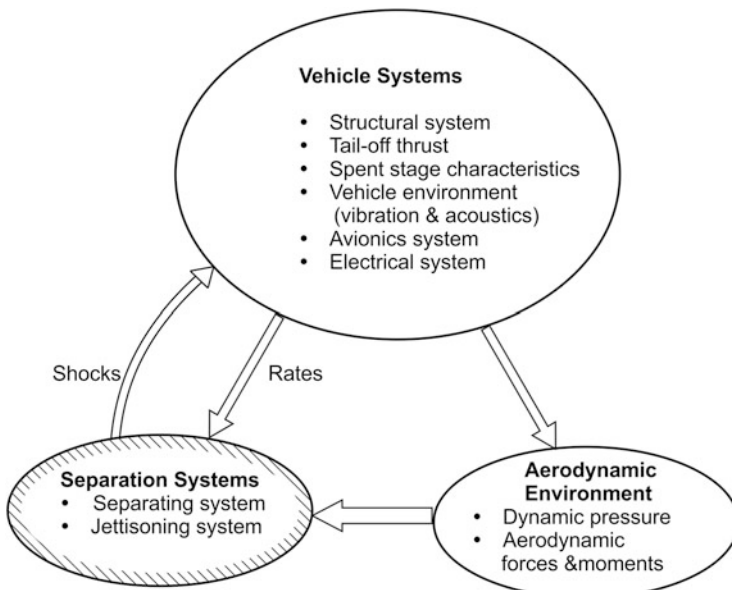


Fig. 13.3 Interaction between separation and vehicle/environment

3. In the above case the thrust value sometimes may approach near zero. In such cases it is important to ensure the positive acceleration for liquid upper stages to have a smooth ignition and it becomes essential to use auxiliary rockets.
4. To avoid all these complexities, alternate option is to adopt hot separation process requirements.

All these techniques need careful analysis and suitable onboard vehicle sequencing needs to be selected by avionics systems to meet the defined requirements.

One can observe that there is strong interaction among vehicle systems, environment and separation systems needing integrated design approach for the separation system. The entire stage separation system design, analysis and validation are multidisciplinary in nature as shown in Fig. 13.4. The selection of a suitable stage separation system in a launch vehicle needs careful consideration of the following factors:

- (a) The interstage structures which accommodate the stage separation system have significant influence on the design of separation systems and hence the requirements of separation systems have to be carefully analyzed and incorporated during the design of these structures.
- (b) The selection of pyro-systems for release or severance of systems has to be decided based on the type of mechanism chosen for jettisoning stage.
- (c) Several factors like overall mass, shock level, pullout length of the spent stage, overall diameter, lateral, circumferential or axial separation, the detachment

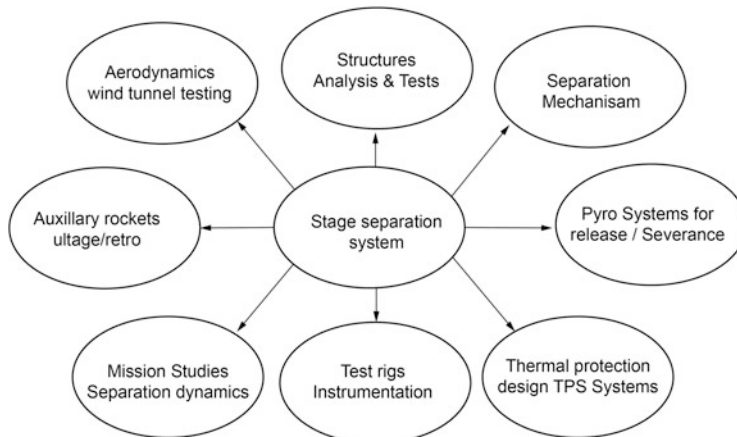


Fig. 13.4 Multidisciplinary aspects of separation systems

forces of electrical connectors at separation plane, vehicle aerodynamics, etc. have large influence on the selection of suitable mechanism.

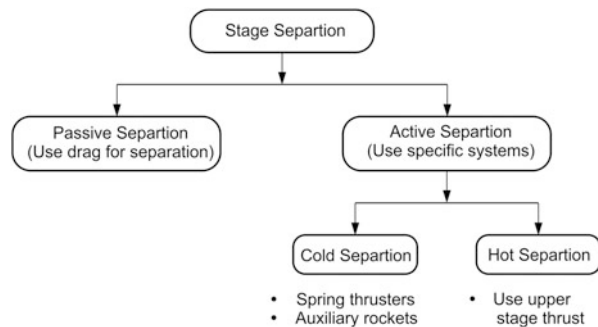
- (d) Separation in the aerodynamic region needs detailed aerodynamic characterization and hence elaborate wind tunnel tests are needed for the design and validation of separation systems.
- (e) Overall mission and separation dynamics studies are needed considering the start and tail-off transient characteristics of motors, control force available, no control region during stage transition, relative acceleration between spent stage and ongoing vehicle, proper sequencing of events, time delays, etc.
- (f) Design of a suitable thermal protection system wherever demanded and its implementation aspects are to be carefully addressed.
- (g) Design of test rigs to evaluate the system on ground and the instrumentation needed for defect-free performance are to be worked out in detail during initial stages of system developments.
- (h) Reliability, redundancy management, suitable cowling to give proper aerodynamic shape for the small motors used in the system, single or multipoint release system are some of the important considerations while selecting a suitable separation system.

13.5 Separation System Design Process

The separation processes of launch vehicle systems are categorized as given in Fig. 13.5.

In the passive separation process, no additional system is used for separation process. Instead the aerodynamic drag caused by the flare in the spent stage is used as the separation force. Generally, these types of separation systems are being

Fig. 13.5 Classification of separation process



employed for separating small bodies such as spent systems of sounding rockets. As the launch vehicle spent systems are bigger in size and mass, it is essential to employ active separation systems. Specific systems are chosen for generating the required separation force considering the surrounding environment and spent stage characteristics. There are two types of active separation processes. In the cold separation systems, the upper-stage engines are ignited only after the clear separation of the spent stages. In these cases, separation forces are generated by spring thrusters and auxiliary rockets. For the case of hot separation, the upper-stage engines are ignited before the separation of the spent stage and the force caused by the upper-stage jet impingement on the lower stage is used for the separation process. Typical active separation systems used in launch vehicles are given below:

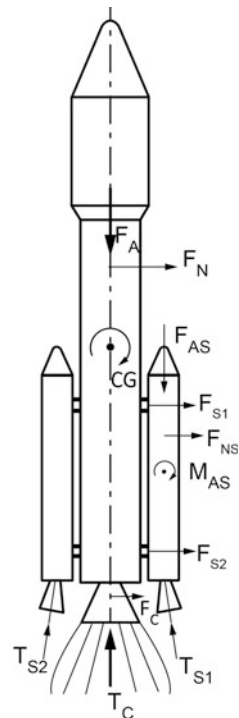
1. Spring-assisted lateral separation of strap-on motors in atmospheric phase (small motors)
2. Rocket-assisted lateral separation of strap-on motors in atmospheric phase (large motors)
3. Rocket-assisted longitudinal cold separation of large first-stage motors
4. Longitudinal hot separation process of large first-stage motors
5. Spring-assisted separation of spent upper stages and satellites
6. Separation process of large payload fairings

Design guidelines and design process of these separation systems are explained below.

13.5.1 *Lateral Separation of Strap-on Motors in Atmospheric Phase*

In the multistage launch vehicles with strap-on motors, the spent motors are separated during the core vehicle thrusting phase. Generally, this event occurs in the atmospheric flight phase. The forces and moments on spent motors and the ongoing vehicle are represented in Fig. 13.6.

Fig. 13.6 Forces and moments on the separated strap-on motors and ongoing vehicle



The main influence parameters that affect the separation process are (1) aerodynamic force and moment acting on the separated motors, (2) residual thrust of strap-on motors at the time of separation, (3) jet impingement effect on strap-on motors when it enters into the jet stream of core motor exhaust, (4) continuing vehicle dynamics during separation process, due to the aerodynamics, thrust, control, etc., (5) separated strap-on uncontrollability and (6) inertial properties of the spent motors.

It is always preferable to separate the strap-on motors when residual thrust is near to zero. But due to the performance loss with respect to the mission requirements, it is essential to separate the motors immediately after burnout. Considering these two requirements, an optimum time of separation needs to be arrived at. The incremental aerodynamic forces and moments on the separated strap-on motor are dependent on its relative orientation (three angles) and position (three linear displacements) with respect to the core vehicle. These forces are evaluated through detailed wind tunnel testing called grid tests, simulating all the possible combinations of positions and attitudes of strap-on motors. These data are used for the separation system design process.

The separation force, usually achieved by releasing compressed springs at the forward and aft joint locations F_{S1} and F_{S2} are designed such that the separated strap-ons are not collided with any part of the ongoing vehicle. In the design

process, the time of separation can be tuned, if required. With the final design, the clean separation process is validated through ‘time-march’ wind tunnel tests. The model settings at the wind tunnel tests are based on the states generated by the separation dynamics whereas the aerodynamic data for the set states is used to generate the new state and this interactive simulation between wind tunnel tests and separation dynamics is extended up to clean separation.

When the strap-on motor mass and size is more, auxiliary rockets are used to generate the necessary separating force. The results of a typical strap-on separation process are given in Fig. 13.7.

13.5.2 Longitudinal Separation of Large Stages

Generally in multistage launch vehicles, first stage is very heavy. To carry the large flight loads of atmospheric flight phase, closed and stiffened interstage structures are used for connecting the first stage to the upper stages as shown in Fig. 13.8a. After the first-stage burnout, during separation process, the spent first stage along with the interstage is separated from the ongoing vehicle as shown in Fig. 13.8b. Generally, the first-stage separation occurs in the upper atmosphere, wherein the aerodynamic effects cannot be neglected. Also, in order to reduce the performance loss, the first stage has to be separated as soon as its burnout.

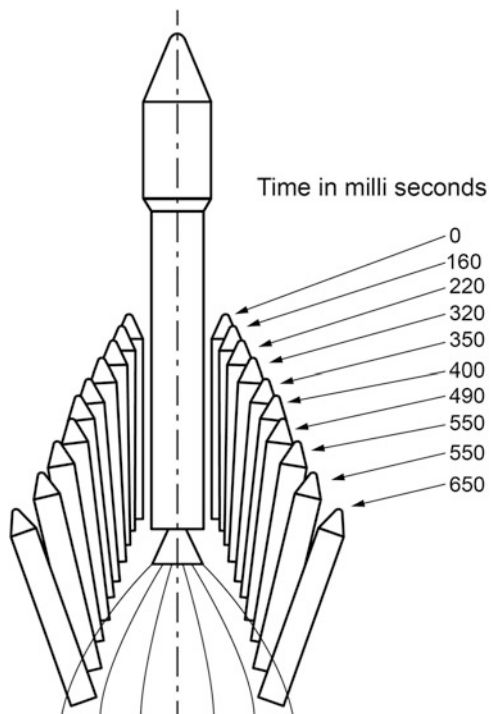
Therefore, the following parameters influence the separation process: (1) aerodynamic forces and moments on the separated stage and ongoing vehicle, (2) residual thrust of separated stage, (3) vehicle dynamics at the time of separation, (4) ongoing vehicle and spent-stage dynamics during separation process and (5) inertial properties of separating body and ongoing vehicle.

Another important feature to be considered in this type of cold separation is that both separated stage and continuing vehicle are uncontrolled during this phase, which further complicates the separation process.

Since there is residual thrust in the spent stage whereas the upper stage is not ignited till the completion of separation process, to achieve positive clearance between the bodies, auxiliary rocket (retrorocket) motors are used to impart separation force. In order to achieve the separation process quickly, these rocket motors have to impart higher thrust, more than residual tail-off thrust at the time of separation in short time (~ 1 s). For this purpose, special-purpose solid motors with high burn rate and high pressure are used. There should be more than one retrorocket motor and they are mounted symmetrically opposite in the spent stage to avoid angular tilt of the spent stage.

There are two more issues in this kind of separation process. They are (a) a definite no-control regime between the stages and (b) in case of liquid engines for the upper stages, possibility of movement of propellant from tank bottom due to negative acceleration, which can lead to non-ignition of upper stage. The no-control regime has two components: (i) duration between separation and control effectiveness from the upper stage and (ii) control effectiveness loss in the spent-stage tail-

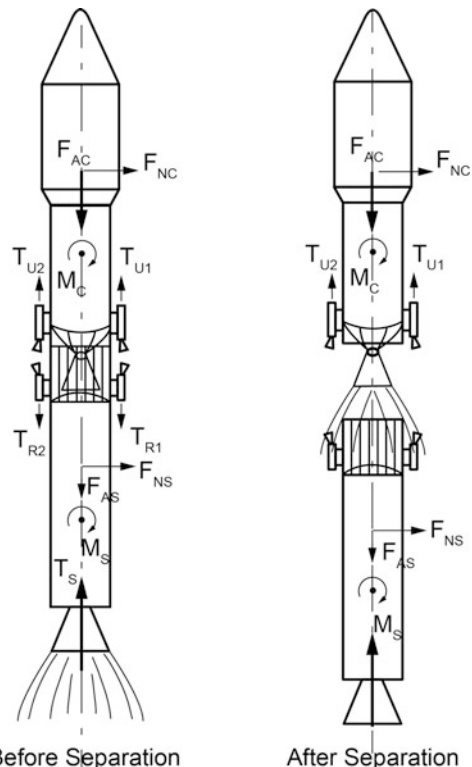
Fig. 13.7 Typical strapon separation process



off phase till separation event. Contribution from (i) cannot be avoided whereas contribution from (ii) can be overcome by the addition of auxiliary, autonomous control system to operate in this phase. For the successful ignition of upper stage, it is essential to ensure that the propellant of the stage is always available at the tank bottom. This can be guaranteed by having positive acceleration of the ongoing vehicle and this can be achieved by a set of auxiliary rockets, called ullage rockets. This motor again is a special-purpose solid motor. As the ongoing vehicle is also uncontrolled during the stage transition phase, to avoid tilting of the vehicle, it is important to have more than one ullage motor and they have to be mounted diametrically opposite. The thrust level and burn duration of these motors have to be decided to meet the required positive acceleration level for the specified duration. To improve the performance, these motors are to be jettisoned away by simple mechanisms once their function is completed. The retro and ullage motor thrusts act in opposite direction and functionally they are positioned closely. Therefore, to avoid plume interactions of retro and ullage motors, they have to be positioned at different circumferential locations.

An optimum sequencing timing for all the events during this phase has to be finalized and linked with real-time decision onboard to achieve a robust separation process. A typical sequencing of events is given in Fig. 13.9.

Fig. 13.8 Longitudinal separation process of a large stage



For this separation process, the aerodynamics on the separated stage is to be evaluated through wind tunnel testing and used as function of orientation and displacement with respect to the continuing stage.

It is to be noted that the avionics systems used for the first-stage flight are mounted inside the interstage whereas critical avionics systems corresponding to upper stages are mounted in the engine bay of the upper stage. Therefore, the main design criterion for separation system design is to ensure collision-free separation which means pull out very fast with least lateral movement. In addition, to ensure controllability of upper stage, the rate induced on the upper stage during separation process has to be minimum. The safer residual tail-off thrust level, optimum separation sequence and retro rocket thrust levels are the main design parameters to achieve the clean separation process.

Typical trajectory of spent stage during separation process with respect to the ongoing vehicle is given in Fig. 13.10.

It can be seen that the cold separation process of large stage as described above involves many systems such as multiple retro rockets, ullage motors, autonomous control systems, etc., which introduce higher chances of failure modes. Failure of any one system leads to mission failure, thereby causing the reduction of system

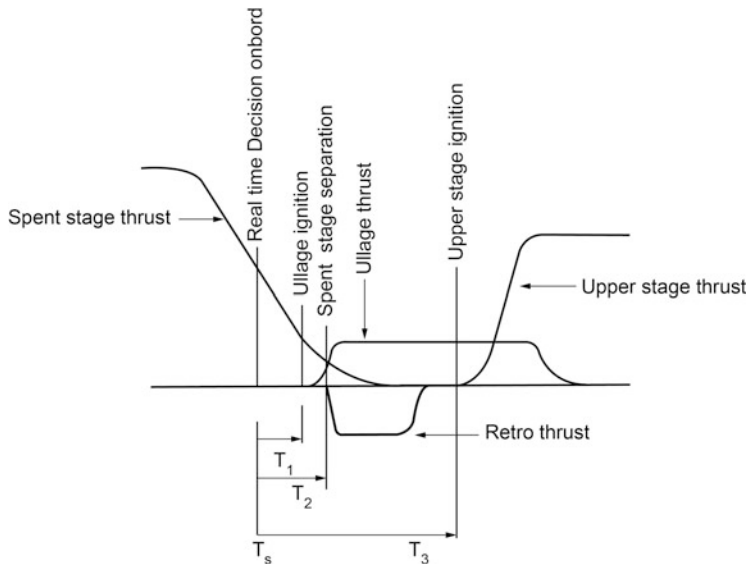


Fig. 13.9 Stage transition sequence for cold longitudinal separation process

reliability. However, the major advantage of this system is that the separation process is controlled, the entire process is very smooth and introduces very less disturbances to the ongoing vehicle, thus the separation-induced rates are kept minimal. To improve the reliability of the separation process of large lower stages, hot separation as explained below is also being used.

In hot separation, the upper stage is ignited even before the separation command is issued. The hot exhaust gases are vented through the interstage which has a lattice structure with a number of openings as shown in Fig. 13.11. Therefore, this separation process is also called as vented interstage separation. The interstage has to be designed to withstand high heat loads with proper insulation scheme on structural members. This scheme has several advantages like less no-control region, propellants settling at the bottom at the time of ignition, no requirement for retro rockets and ullage motors. The exhaust gas provides the required jet impingement force to push the spent stage immediately after separation. This enhances the overall reliability of the system. However, due to the possible asymmetrical flow of exhaust gases through the vented interstage, the disturbance induced by this separation process is large compared to that of the cold separation.

The separation dynamics of hot separation is also similar to that of the cold separation. The separation force due to jet impingement is evaluated through analysis using computational fluid dynamics and wind tunnel tests, simulating all the details of internal geometry of the interstage. These forces are generated as function of attitudes and displacements of spent stage with respect to the ongoing vehicle and used in the separation dynamics to design the separation system.

Fig. 13.10 Typical longitudinal separation process. (a) Before separation. (b) After separation

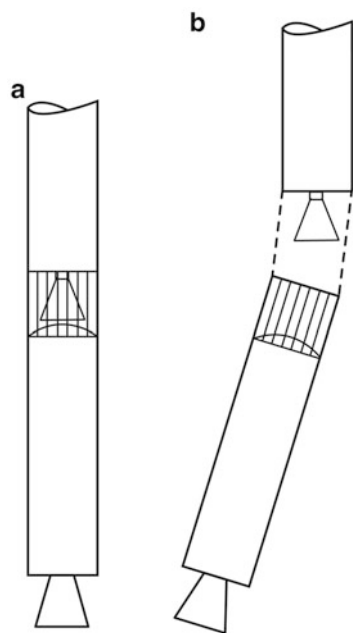
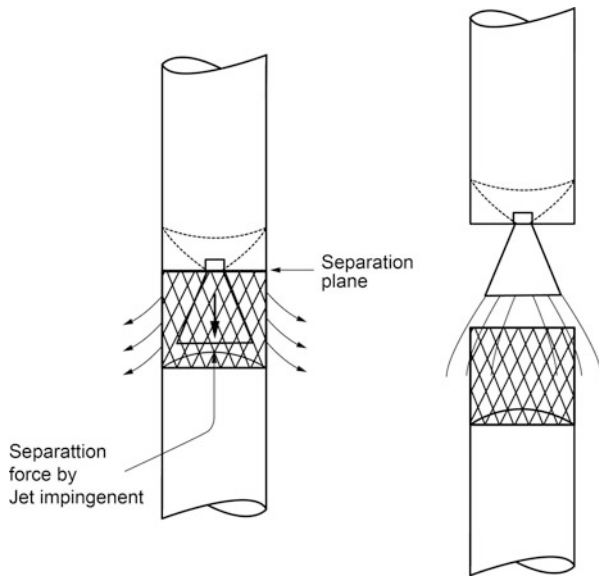
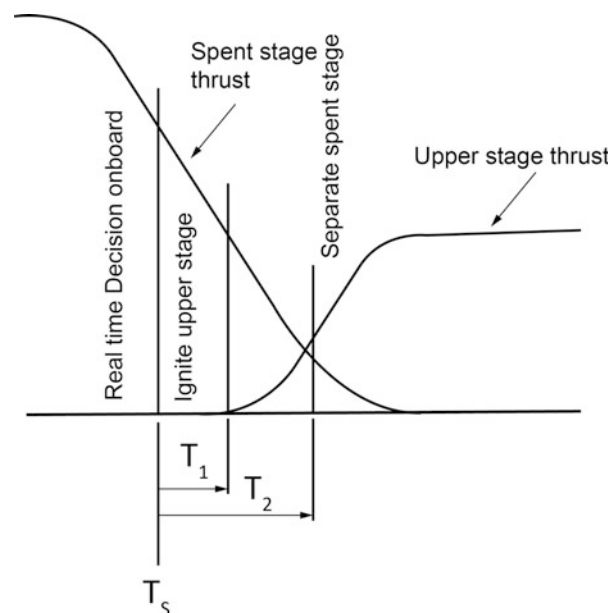


Fig. 13.11 Hot separation process



Considering the separation force generated by the upper-stage jet impingement and the inertial properties of the spent stages, a typical separation sequence is given in Fig. 13.12. It is important that all the events are to be carefully designed for the optimum and clean separation under all cases of disturbances.

Fig. 13.12 Stage transition sequence of hot longitudinal separation process



13.5.3 Payload Fairing Separation

In all launch vehicles the payload fairings (PLF) are used to protect the satellite and the vehicle sensitive systems against the aerodynamic, thermal and acoustic loads during the atmospheric ascent phase. Once the vehicle crosses the dense atmospheric region, the adverse loads on the payload become insignificant and the fairing is jettisoned. The PLF is assembled to the vehicle as two halves. The fairing has two separation systems: one for detaching PLF from the vehicle and the other for laterally separating the PLF into two halves as given in Fig. 13.13.

The lateral separation velocity is achieved by the zip-cord energy provided by the linear bellow system. As the PLF separation at the earliest improves the mission performance, normally, the separation process is initiated once the allowable level of heat flux on the satellite is achieved. Therefore, the PLF separation process occurs during vehicle thrusting phase and the optimum separation time has to be suitably decided onboard and executed by the vehicle sequencing system. In addition to this, the vehicle commanded attitude rate during PLF separation phase is also kept constant to avoid disturbances during separation process.

Once separated, the two halves of PLF become two large flexible bodies. Therefore, during separation dynamics process, in addition to the rigid body attitude and linear motions with respect to the ongoing vehicle, the separated PLF halves have flexible breathing modes also. This demands the PLF separation dynamics analysis to include flexibility effects of separated PLF halves.

The main criteria for the PLF separation process is that the separated system should not interfere with the satellite and upper stage housed inside the PLF.

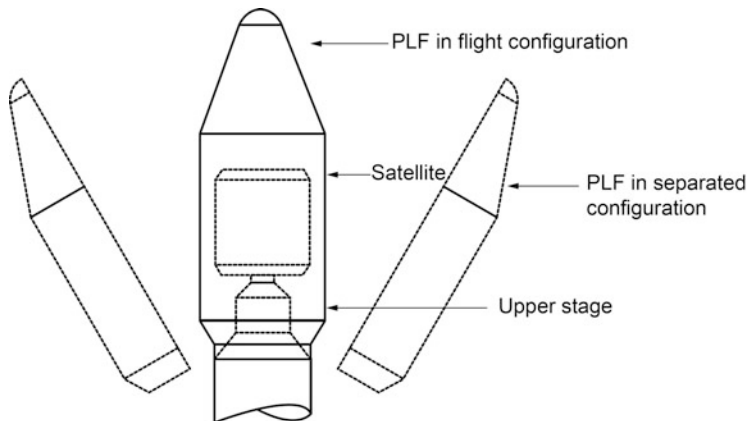


Fig. 13.13 PLF in assembled and separated configurations

Typical trajectory of aft end of two separated PLF halves is given in Fig. 13.14. Considering the inertial properties and flexible characteristics of PLF, the zip-cord energy is designed to ensure clean separation process under all possible combinations of disturbances.

13.5.4 Upper-Stage Separation

Spring-assisted longitudinal separation is generally employed for the separation of smaller upper stages and satellites. Satellite separation process of a typical launch vehicle is given in Fig. 13.15.

Merman clamp band or ball lock release mechanisms are used for releasing the spent stages. The spring energy due to the release of compressed springs provides the necessary relative separation velocity between the bodies as given below:

Let mass of satellite and spent stage be represented as m_s and m_u respectively as shown in Fig. 13.16.

The velocities imparted to the above bodies due to the spring energy are represented as V_s and V_u respectively. Then, using the conservation of linear momentum and energy relations,

$$m_s V_s + m_u V_u = 0 \quad (13.1)$$

$$\frac{1}{2} m_s V_s^2 + \frac{1}{2} m_u V_u^2 = E \quad (13.2)$$

Assuming k is the spring stiffness, δ is the stroke length, then the spring energy E can be expressed as

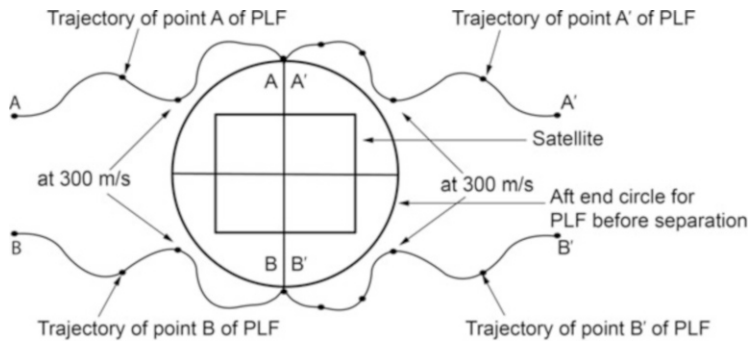
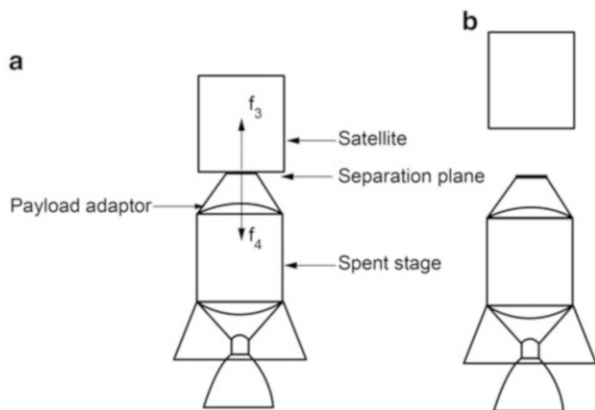


Fig. 13.14 Typical trajectory of aft end of PLF during separation process

Fig. 13.15 Typical satellite separation process.

- (a) Before separation.
- (b) After separation



$$E = \frac{1}{2}k\delta^2 \quad (13.3)$$

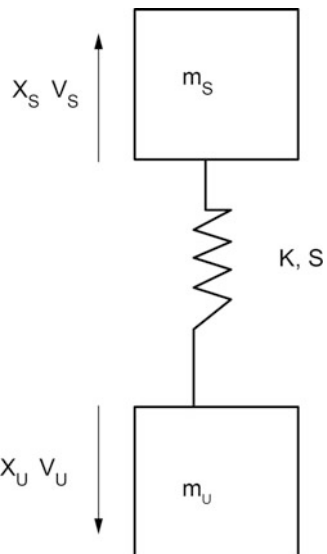
Substituting Eq. (13.3) in Eq. (13.2) gives

$$\frac{1}{2}m_s V_s^2 + \frac{1}{2}m_u V_u^2 = \frac{1}{2}k\delta^2 \quad (13.4)$$

Equation (13.1) can be expressed in the following forms:

$$V_s = -\frac{m_u V_u}{m_s} \quad (13.5)$$

Fig. 13.16 Spring assisted separation dynamics



$$V_u = -\frac{m_s V_s}{m_u} \quad (13.6)$$

Substituting Eq. (13.5) and Eq. (13.6) in Eq. (13.4), the velocities can be expressed as follows:

$$V_s^2 = \frac{m_u k \delta^2}{m_s(m_u + m_s)} \quad (13.7)$$

and

$$V_u^2 = \frac{m_s k \delta^2}{m_u(m_u + m_s)} \quad (13.8)$$

The relative velocity between the bodies can be given as

$$\Delta V = V_s + V_u \quad (13.9)$$

Squaring,

$$\Delta V^2 = V_s^2 + V_u^2 - 2V_s V_u \quad (13.10)$$

Substituting Eq. (13.7) and Eq.(13.8) in Eq. (13.10) gives

$$\Delta V = \sqrt{\frac{k \delta^2 (m_s + m_u)}{m_s m_u}} \quad (13.11)$$

Depending upon the mass and inertia properties of the spent bodies, number of springs is employed to achieve the required separation velocity. If n is the number of springs, having the same stiffness and stroke length, then ΔV is given as

$$\Delta V = \sqrt{\frac{n k \delta^2 (m_s + m_u)}{m_s m_u}} \quad (13.12)$$

The individual velocities imparted to the bodies are given as

$$V_u = \Delta V \left[\frac{m_s}{(m_s + m_u)} \right] \quad (13.13)$$

$$V_s = \Delta V \left[\frac{m_u}{(m_s + m_u)} \right] \quad (13.14)$$

The main requirements for the upper stages and satellite separation process are to ensure clean separation with minimum tip-off rate to the upper stages (and satellites). Use of multiple springs for separation with the centre of gravity offset for separating bodies can induce attitude rate disturbances. Therefore, considering the mass, inertia and centres of gravity offset of the separated and ongoing bodies, the preloads of springs at each location can be judiciously decided to minimize the tip-off rates.

13.5.5 Role of Separation Dynamics Studies in the Separation System Design

Analysis of the separated body dynamics with respect to the ongoing vehicle is an important factor in the separation system design. The studies involve the generation of the relative states of the six-degrees-of-freedom motion, viz. three attitude angles and position of the separated body along three axes with respect to the ongoing vehicle. Considering the external and internal disturbances, type of separation system, separation force history, vehicle and separated stage inertial properties and initial conditions of vehicle state at the time of separation, it is essential to generate the time history of the above relative state to understand the response of the system. The separation dynamic analysis provides the crucial information regarding the sensitivity of various design parameters on the dynamics of the separating body and the ongoing vehicle and these data are effectively utilized to design a robust separation system.

The various inputs needed for the separation dynamic studies are mass, mass moment of inertia, centre of mass locations of the separating bodies, geometry of separation, tail-off thrust details, jet impingement forces, spring tolerances, slosh effects and aerodynamic data of the separating bodies in the atmospheric phase. To generate the relative motion of the separating bodies with respect to the ongoing vehicle, the above data corresponding to the ongoing vehicle form as input to the separation dynamics analysis. Generally the separating bodies are assumed to be rigid and without any dynamic imbalance. However for bodies like PLF, both rigid and flexible contributions have to be considered for predicting the realistic dynamics during jettisoning. The mass properties are considered as time invariant as the separation process is for very short duration. The various dispersions to be considered for the extreme environments are centre of gravity offset, moments of inertia variation, dynamic imbalance, the thrust offset, thrust misalignment, differential thrust if multi-engines are involved and errors due to aerodynamics like variation of normal force coefficient, drag coefficient and centre of pressure. Sensitivity studies for the variation of each error source listed above are needed to assess the impact of these dispersions on clean separation process.

During the dynamic analysis, the clearances between the separating bodies are estimated by identifying the critical points in two bodies. For identification of collision hazard during the separation process, it is essential to estimate the relative distance between the critical points, relative velocity, body angular velocity and body orientation angles. During the analysis, the graphical simulation of separating bodies is necessary to identify any possible occurrence of collision.

The stage separation process generally involves pulling out of the nozzle of the ongoing vehicle from the spent stage of a multi-stage rocket under the influence of tail-off thrusts, retro and ullage motor thrusts and aerodynamic forces. Since ground testing, simulating all these conditions is nearly impossible or prohibitively expensive, the analysis has to guarantee sufficient lateral gap between two separating bodies during the pullout even under the worst combination of design variables. If the analysis indicates collision possibility, then necessary corrective steps are to be introduced to avoid the contact between them.

Separation dynamics analysis followed by Monte Carlo simulation studies involving large number of cases are to be carried out to estimate the probability of collision and to predict the least possible tolerance available. The separation mechanisms are modelled using dynamic simulation software to study clearances at micro level. Since most separations occur in vacuum, the results of ground tests have to be extrapolated suitably and used in the separation dynamics analysis to predict separation scenario in vacuum conditions.

13.6 Explosive devices used in separation systems

The actuators based on pyro-mechanical devices are used extensively in stage separation system, payload fairing jettisoning and destruct systems in launch vehicles. These actuators are basically single-shot devices and make use of piston

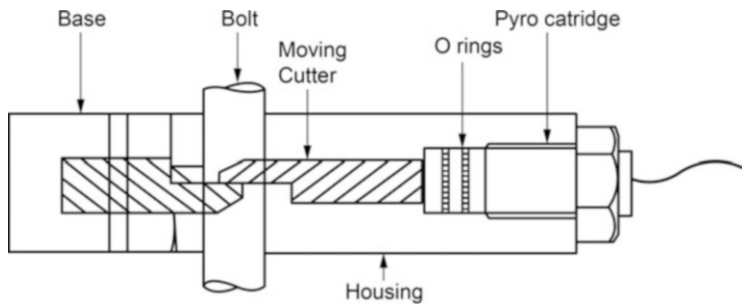


Fig. 13.17 A typical bolt cutter in action

cylinder assembly to transfer chemical energy of explosives into mechanical energy. Typical explosive devices used in the separation system mechanisms are briefly explained in this section.

13.6.1 Bolt Cutter

As the name suggests, this device is used for cutting bolts or cables and makes use of piston cylinder assembly. They are designed to cut the bolts carrying tension loads. A typical bolt cutter in action is shown in Fig. 13.17. The bolt or cable is in between the two cutters. After the pyro-cartridge is fired, the cutter cuts the bolt under the pressure created by explosion. Due to high-speed impact of the cutter blade on the bolt, shock is generated and the shock intensity depends on the size and stiffness of the bolt used. The bolt cutters are used in Merman band separation mechanism used in launch vehicle.

13.6.2 Explosive Bolts

These bolts use high explosive devices and when detonated, the shock generated by the device causes the severance of the identified material. Figure 13.18 shows the schematic of an explosive bolt. The threaded bolt is having an external notch, where it is intended to sever. Inside the cavity close to the notch, high explosive charge is embedded and when it is detonated the shock wave generated causes the stress at the notch plane beyond the ultimate strength of the material. This causes the severance of the bolt into two pieces. These bolts are reliable and hence they are used in separation systems. Since they impart high shock due to the use of high explosive device, they cannot be used where sensitive instruments are mounted in its proximity.

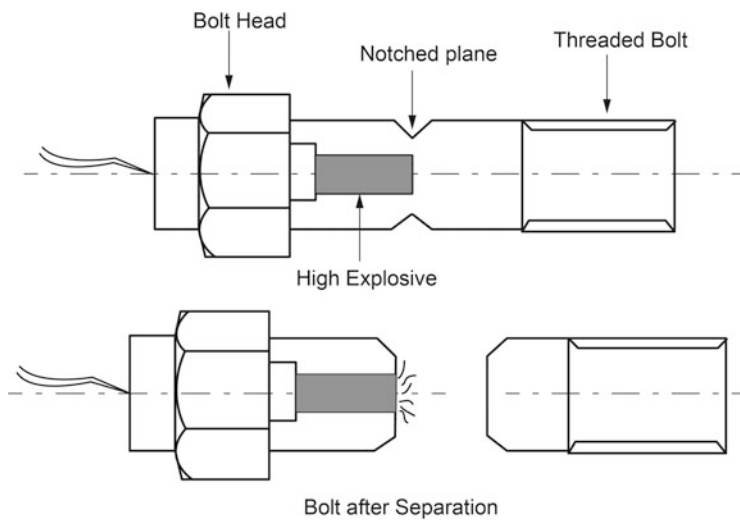


Fig. 13.18 Schematic of an explosive bolt

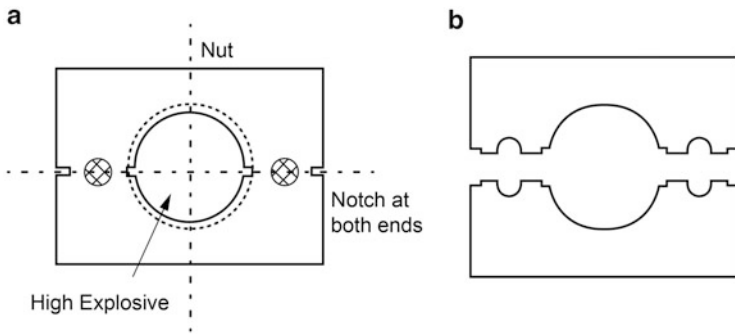


Fig. 13.19 Schematic of an explosive nut. (a) Before separation. (b) After separation

13.6.3 Explosive Nuts

These nuts are designed to carry tension loads of bolted joints and plates. In explosive nuts, the threads pass through the nut as shown in Fig. 13.19. These nuts have comparatively high load-carrying capability and are more reliable. The explosive nuts are designed with webs also known as stress concentrators. The high explosives are held near to the webs as shown in Fig. 13.19.

The nut generally holds the assembly and when the nut is detonated the shock wave produces very high stress levels beyond the ultimate strength of the material. This causes the nut to split into two pieces. It is also possible to control the number

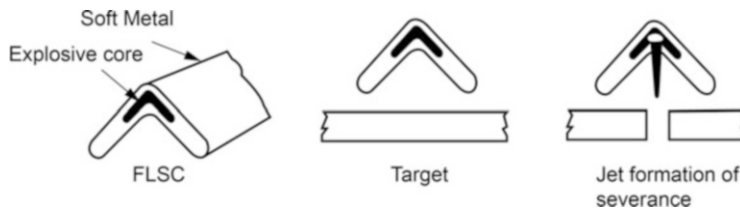


Fig. 13.20 Functioning of V shaped charge

of splits based on the web design. A suitable mechanism has to be designed to contain the debris within the systems. These nuts are used generally in strap-on separation systems.

13.6.4 *Flexible Linear Shaped Charge (FLSC)*

FLSC is extensively used for the separation of large lower stages. FLSC severs the integral rings, used in lower stages for high joint rigidity. This explosive system is not recommended for use in upper-stage separation as the shock and debris produced by the activation of FLSC have adverse effect on avionics bay of the vehicle and spacecraft. The shaped charges are generally rolled into inverted V shape and lined by soft metal like lead or silver. This works on the ‘Munroe effect’ principle, where the high-velocity metal jet penetrates into target material and cuts the thick metal structure. The high-velocity jet is formed when shaped charge is detonated. The shock level generated depends on the metallic thickness used and is very high reaching nearly 0.2 million g in the vicinity. The functioning of V-shaped charge is illustrated in Fig. 13.20. Generally the penetration of the jet due to high velocity is around 50 % of the material thickness and the balance is cut by shock-induced fracture.

In separation systems the shaped charge is used circumferentially along the separation ring and when commanded it cuts the separation ring along the separation plane thus severing the spent stage from the continuing stage.

13.6.5 *Confined Detonating Cords*

The higher shock and contamination are two major problems wherever the unconfined detonating cords are used. To overcome this problem, a new concept of embedding the explosive cord has been introduced by using a flattened tube or an expanding bellow system. In flattened tube the detonator cord is confined in an elastomer container. Generally it is a rubber matrix inside the metallic tube. This new concept reduces the shock levels considerably and the contamination is zero.

The flattened tube is assembled through two plates which have notches. The detonation of explosive causes the flattened tube to expand. This in turn results into severance of the flat plates at the notch plane due to deflection of the plates caused by expansion of the tube.

Similarly, the expanding bellow system too offers complete confinement of contamination generated by explosive action and considerably low shock during operation. The system is having a linear cylinder piston mechanism and a rubber bellow runs all through the mechanism. An explosive cord is running through the bellow. This bellow system is widely used for the separation of payload fairing, where the longitudinal separation of two halves of the fairing is needed.

13.7 Separation and Jettisoning Mechanisms

There are wide varieties of separation mechanisms and a suitable choice for a particular application has to be based on the extensive evaluation of the merits and demerits of candidate systems available. The highest reliability, ease of testing, ease of realization and ease of integration should be the major considerations. Detailed description of all available separation systems is beyond the scope of this book. Some major separation and jettisoning mechanisms which are widely used in most of the launch vehicles are given below:

- (a) FLSC-based separation system
- (b) Merman band separation system
- (c) Ball lock separation system
- (d) Collet release separation system for upper stages
- (e) Ball-and-socket joint-based lateral separation system
- (f) Linear bellow-based longitudinal separation system
- (g) Expanding tube separation system.

The first four systems listed above are used for separation of tandem stages. Merman band and Ball lock separation system are widely used for satellite separation due to their low shock. Ball-and-socket joint-based system indicated above is used generally for the separation of strap-on motors. The last two separation systems are used in payload fairing to provide the parallel longitudinal separation and the circumferential separation is carried out using the Merman band system.

13.7.1 *FLSC-Based System Separation*

The FLSC-based systems are generally employed in lower stages where the stage joint has to have high stiffness with low joint rotation. Suitable care is needed to avoid the sensitive component in the proximity of high-shock region and such systems are usually placed far away from lower portion of a vehicle. The shock

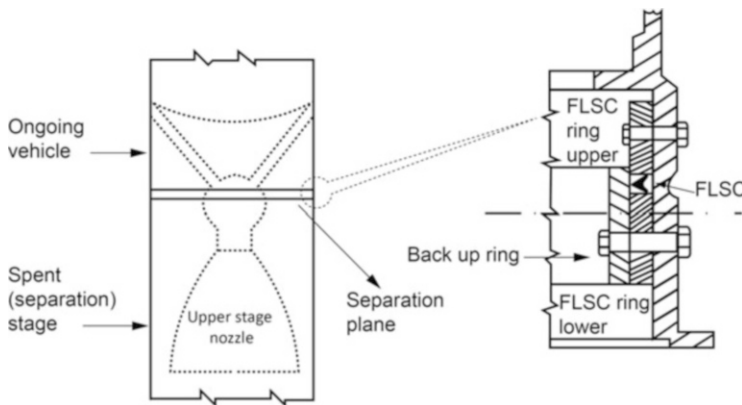


Fig. 13.21 A typical FLSC based separation system

transmitted to the payload or the vehicle avionics would be considerably less as these systems are located far away from this zone. FLSC consists of high explosive core accommodated in V-shaped lead sheath along the circumference of the separation plane.

The FLSC system is always located at the aft end ring of the interstage structure which connects the two stages. The cord is generally placed inside a groove provided in the end ring made in two halves. This will be backed up by another ring termed as backup ring made by a number of segments. A typical FLSC system used in stage separation is given in Fig. 13.21.

The thickness of the structural member in the separation plane facing the shaped charge is appropriately designed. When the shaped charge is fired through separation command the high-velocity jet is produced and this jet cuts the structural member along the separation plane severing the upper stage from the lower stage circumferentially. The spent stage which is below the separation plane separates and moves away from the ongoing vehicle.

13.7.2 Merman Clamp Band Separation System

The Merman band separation systems are generally used in upper stages of launch vehicles, where higher shock levels are not permitted due to proximity to satellite and sensitive avionics systems. It is also used to separate the payload from the vehicle and for circumferential separation of the payload fairing. A schematic of Merman band separation system is shown in Fig. 13.22.

The system consists of a fore ring attached to the upper stage and an aft ring connected to the lower stage. Both these rings are clamped together by floating wedge blocks as shown in the figure and they are held together at the flanges by two pre-loaded semi-circular bands which are generally called as Merman bands. The

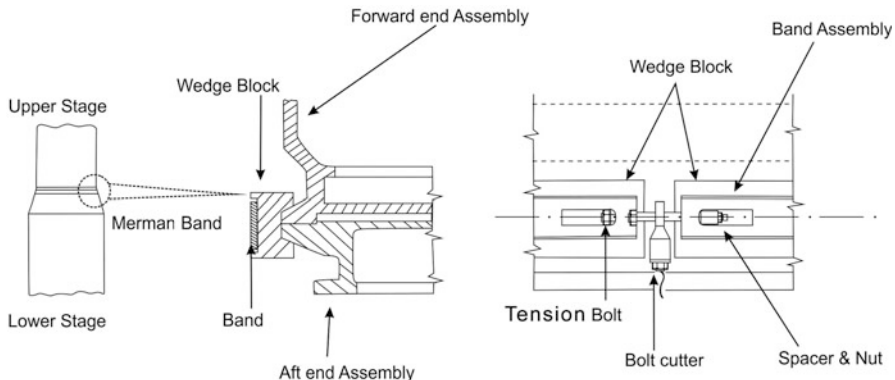


Fig. 13.22 Schematic of merman band separation system

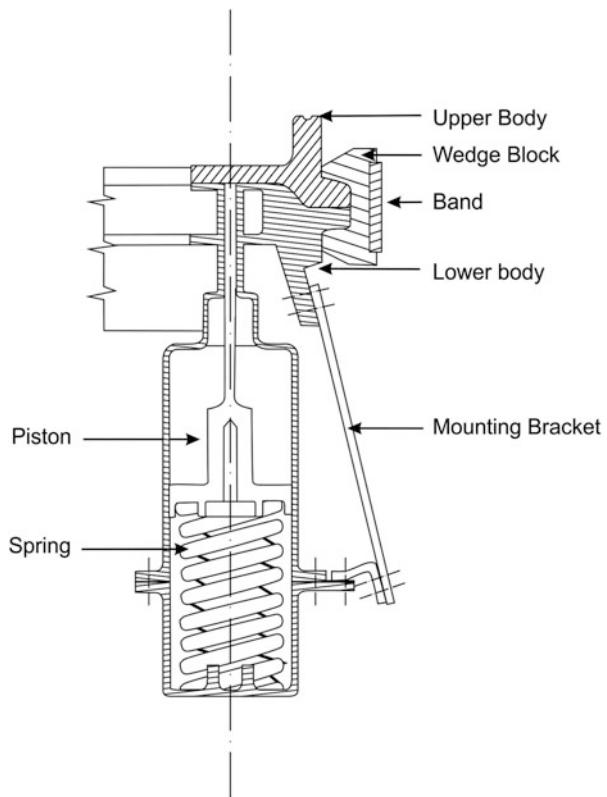
band segments are connected at diametrically opposite locations by tension bolt assemblies through which the mechanism is pre-loaded. To avoid bending on bolts and to ensure force alignment of bolts during tensioning, the band ends are connected by bolts through rollers which have spherical washers and spherical bearing on rollers. Lubrication is provided on the band wedge block interface to reduce the friction. It also helps to minimize the tension variation along the circumference.

The separation of the system is carried out through cutting the tension bolts by two pyro bolt cutters. Functioning of one bolt cutter ensures the separation. However two bolts are generally provided for redundancy, thereby improving the reliability. The jettisoning velocity to the ongoing body can be provided either by auxiliary rockets or spring thrusters depending on the mass of the ongoing stage. For spacecraft separation spring thrusters are mounted circumferentially to minimize the shock levels and the tip-off rates to the separating body.

For spacecraft separation, equi-spaced spring thrusters are mounted circumferentially and they are always guided in the spring thrusters. A typical spring thruster assembly used in merman band system is shown in Fig. 13.23. The spring thruster consists of a piston moving inside the housing through a guide as shown in the figure. The helical compression spring is positioned in the piston assembly. The number of spring thrusters used in the system depends on the overall requirements of jettisoning force, tip-off rate for payload, etc. To reduce the tip-off rate, the springs on diametrically opposite locations are having identical stiffness. It is also essential to ensure that the separation is made debris free. Debris containment along with prevention of recontact of clamps and band is achieved by suitably employing the band assembly retractors and band catchers at appropriate locations.

If the masses of the separating stages are larger, the relative jettisoning velocity is generally imparted by using retro rockets mounted on the lower-stage interstages. The retro motors are to be designed to provide the needed retardation to spent stage

Fig. 13.23 Typical spring thruster assembly in a German band system



thereby achieving required relative jettisoning velocity. Generally the command to the separation mechanism and retro rocket ignition is issued simultaneously.

13.7.3 Ball Lock Separation System

This system is simple and ideal for smaller-diameter bodies and mostly used for small payload separation system. However in certain cases it has been used with higher diameters too. This system always generates low shocks to the payloads. In this system, the upper and lower stages' adapter rings are held together by a number of balls which are kept in position by a retainer ring. The holes provided in the retainer ring have the provision for the balls to escape when the retainer ring is aligned. They are located in the assembly with an offset, keeping two separating parts in a locked condition. The retainer ring also has a provision for rotation. When it is rotated by a known angle, which nullifies the offset through the initiation of pyro-thrusters, the balls move into the escape holes of the retainer ring thus releasing the two assemblies. All the balls are collected in the cavity of the adapter

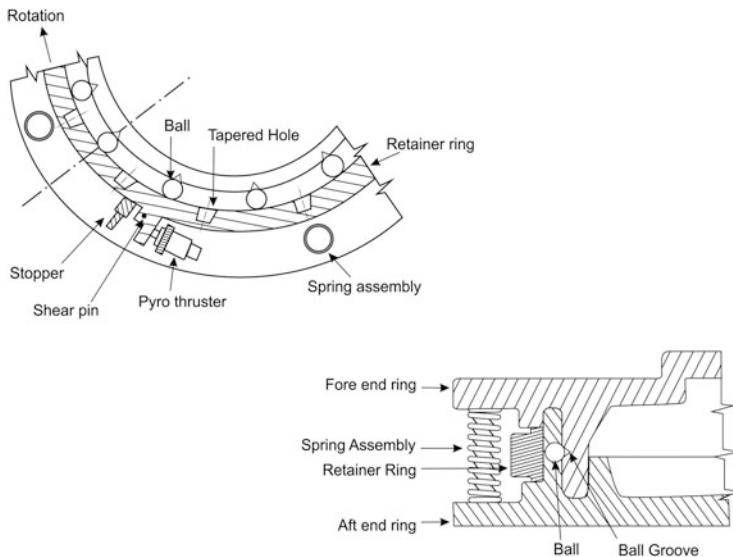


Fig. 13.24 A typical ball lock separation mechanism

ring, thereby eliminating any debris during functioning. The rotation of the retainer ring is limited by a stopper located in the assembly. The required separation velocity is provided by a number of spring thrusters positioned between the flanges. A typical ball lock separation mechanism is shown in Fig. 13.24.

Generally the outer ring is always located in the lower stage and provided with through holes for the balls, whereas the inner ring located in the upper stage will have conical ball seats. The radial component of the spring force generated by the spring thrusters causes the balls to move outward.

To avoid the accidental operation of the mechanism due to shock, vibration or any other loads, shear screws are provided between the retainer ring and main ring to prevent relative rotation. In addition, the pyro-thrusters also have shear screws as shown in Fig. 13.25.

The pressure developed by the cartridges inside the cylinder causes the shear pins in thrusters and retainer ring to shear and generates the necessary force to rotate the retainer ring. Once the holes in the retainer ring are aligned to the balls, the system is unlocked with the balls moving into the holes, thereby causing the separation of two rings.

13.7.4 Collet Release Separation System for Upper Stages

When there is differential expansion and contraction between the stages due to the differential thermal environments, collet-based separation system is widely used. In

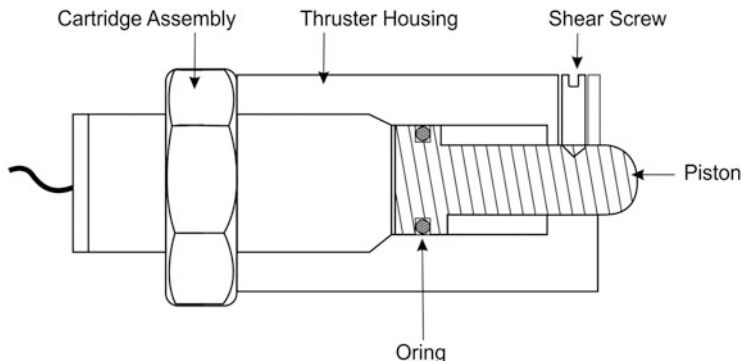


Fig. 13.25 Pyro thruster with shear screws

such system, the mechanism has to function with larger thermal gradients, say cryo-temperature at fore end and ambient temperature at the aft end of the separating body. The system also has to accommodate the shrinkage of the cryogenic tank without causing additional load on interface members. In such situations, collet-based separation mechanisms are ideal. A schematic of collet-based separation mechanism is shown in Fig. 13.26. Basically it is a multipoint separation system with a number of collet mechanisms and the number of collets is to be decided based on the level of loads on the system. Independent pyro-pullers are located in each collet mechanism to facilitate release of the mechanism whenever they are actuated. Generally cryogenic tank of the upper cryo-stage is interfaced with the ambient temperature lower stage structure with a number of truss members as shown in figure. Each pair of truss members consists of one separation unit. The aft ends of the truss members are connected to the bottom ring of interstage structure. The truss members on either end have ball joints which provide the necessary rotational freedom during the differential thermal cycling during servicing of the cryo-stage at ground as well as flight phases of lower stages.

The separation plane is located on the fore end of the truss members as shown in Fig. 13.26. In these mechanisms, retro rockets attached to lower stage impart the needed relative velocity for collision-free separation. The number of retro rockets, its location and orientation are to be decided based on the mass of the spent stage and the distance it has to travel before it clears the nozzle of the upper stage. In order to avoid collision of the lower stage with nozzle of the ongoing vehicle, guide system is used. This system starts functioning once the collets are detached from the supports.

The collet-based mechanism works on the principle of collet fingers which are held in position by a retainer piston. A typical assembly is shown in Fig. 13.27.

The fingers of the collapsible collet are held in position using a retainer piston. Pyro-pin puller has a piston, pyro-cartridge and also a damper. Lower end of the retainer piston is connected to the pyro puller piston as shown in the figure. There is a stopper nut attached to the bottom of the collet which prevents the inadvertent operation of the mechanism. When the pyro-cartridge is actuated, the pyro-piston and retainer piston move downwards causing the collapse of collet leaves and the

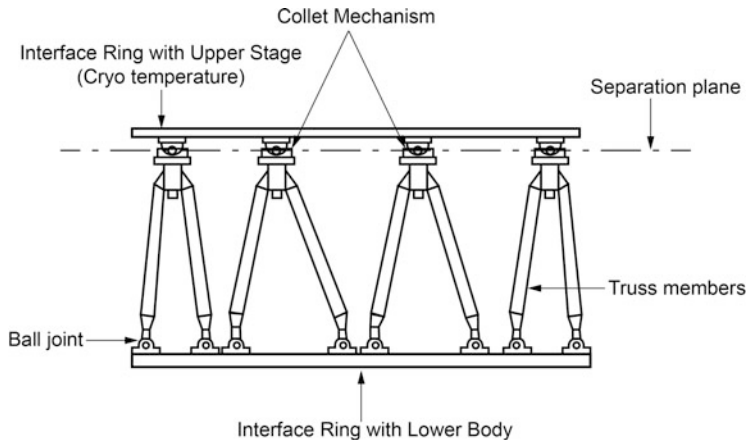
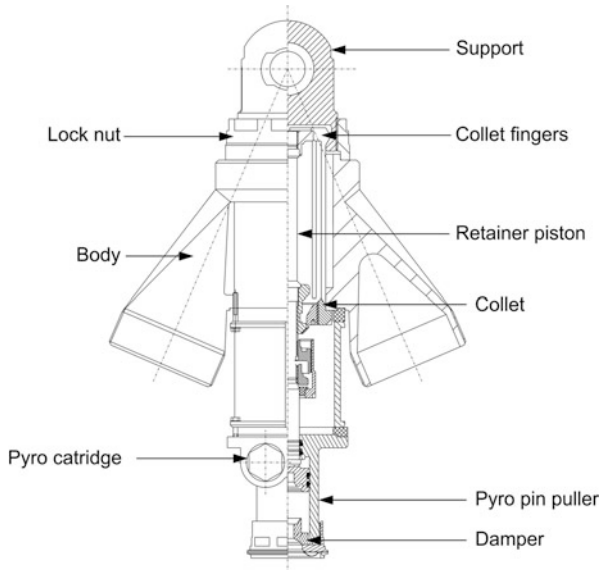


Fig. 13.26 Typical collet based separation mechanism

Fig. 13.27 Typical assembly with collet fingers

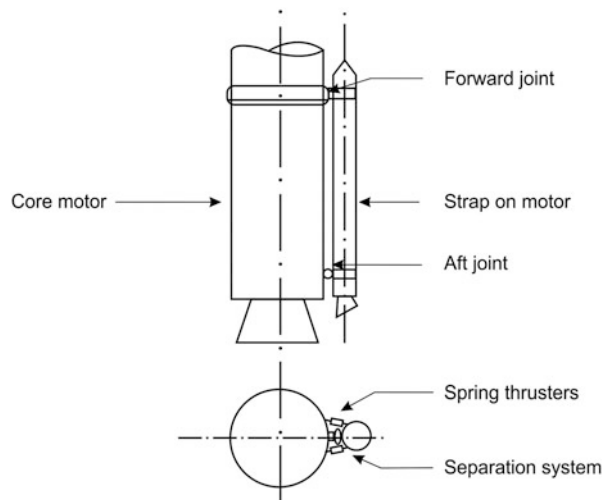


collet separates physically from the support at the separation plane. The damper at the bottom of the assembly prevents rebound of the piston during operation. The pyro-assembly is also sealed against the leakages of gas. Reliability of the system is enhanced through redundancy in pyro-cartridges.

13.7.5 Ball-and-Socket Joint-Based Lateral Separation System

Ball-and-socket joint with band clamp assembly-based separation systems are generally used for strap-on motor separation. The strap-on motors are attached to

Fig. 13.28 Typical strapon separation mechanism



the core motor through two separation joints, one at aft end and another at forward end as shown in Fig. 13.28.

These joints not only provide the needed support to attach strap-on motor to the core vehicle but also have to transfer the thrust and inertial loads of strap-on motors to the core vehicle during the powered flight phase. The jettisoning velocity to the separating body is provided by the set of spring thrusters mounted on either side of the separation mechanisms. Since the energy required is high, stacked belleville springs are used for imparting jettisoning energy. The spring thruster struts are capable of transferring all strap-on loads to the core. The separation system used in both forward and aft ends are ball-and-socket mechanisms as shown in Fig. 13.29 and are held together by U clamp assembly. Pyro-based frangible nuts connected to the band clamp assembly hold the two separating bodies together and when the pyro is commanded, the frangible nut releases the U clamp, thereby causing the separation. The forward joint assembly should have provision to allow for growth of the strap-on motors when fired.

13.7.6 Linear Bellow- Based Longitudinal Separation System

The payload fairing is assembled as two halves and the separation of the same from the vehicle requires both horizontal and vertical plane separation mechanisms. While the horizontal separation is achieved by the band joint system using V-shaped wedge blocks, tension band system, preload release device and pyro-bolt cutter, the vertical separation of the fairing is effected by using linear bellow-based longitudinal separation system. The vertical joint of the fairing halves is

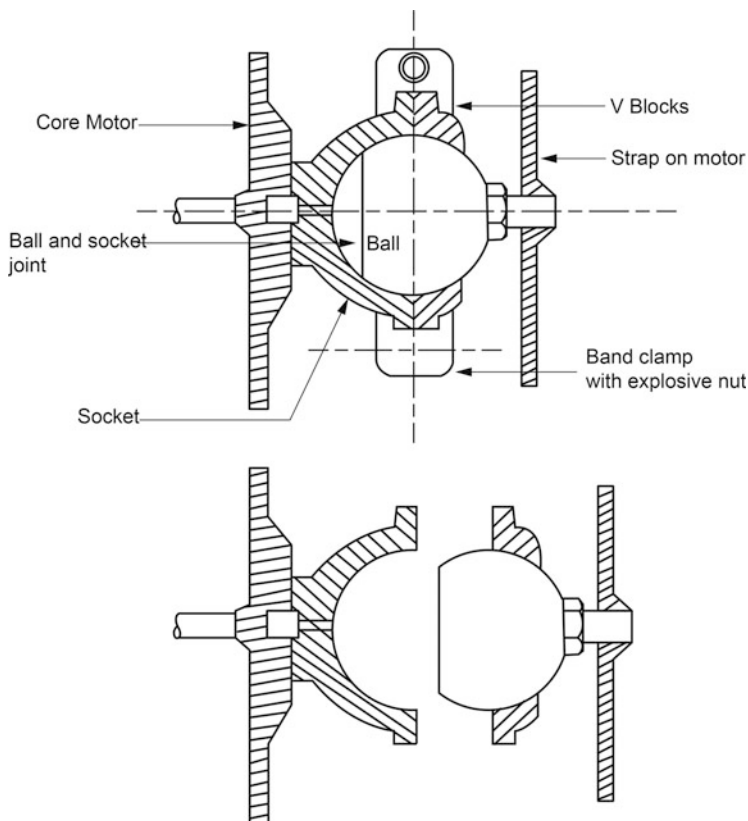
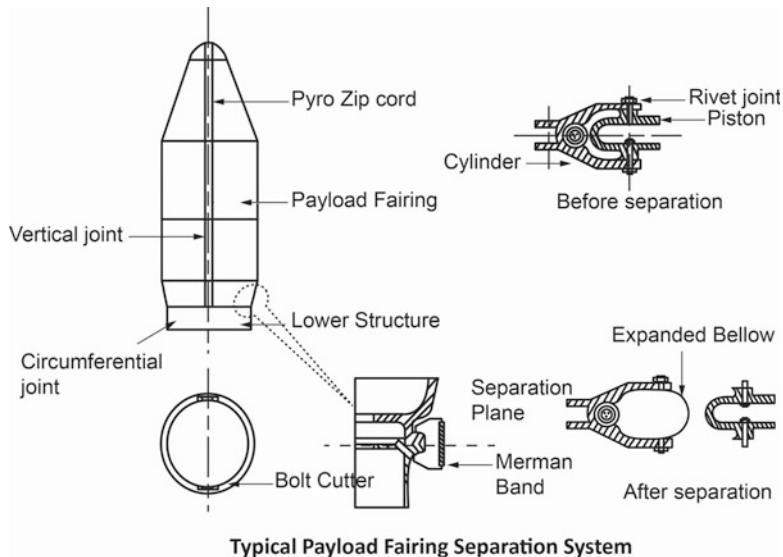


Fig. 13.29 Typical ball &socket joint

formed by a piston cylinder assembly held together by riveted joint as shown in Fig. 13.30. A reinforced rubber bellow in folded condition is running for the entire length through the cylinder and piston assembly. A mild detonating cord positioned in an attenuator tube runs all through the bellow. When the explosive cord is electrically commanded, it releases the instantaneous explosive energy through attenuator tube and the bellows are pressurized. It leads to shearing of the rivets thus causing separation of two halves. Further, the expansion of bellows imparts the required jettisoning velocity to the two separated halves. The separation sequencing commands for both vertical and circumferential joints are given simultaneously to effect the collision-free separation of the fairing. The number of rivets, the rivet material, pitch to be used, etc. for the vertical joint are to be considered carefully along with the dynamic properties of separated halves for a smooth and positive separation.



Typical Payload Fairing Separation System

Fig. 13.30 A typical payload fairing separation system

13.7.7 Expanding Tube Separation System

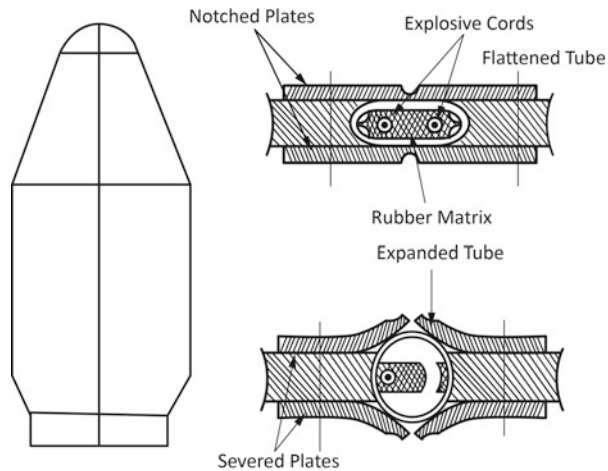
The expanding tube separation system (XTA) utilizes a flattened tube and single detonating cord embedded in silicone rubber extension runs through it. A typical cross section of this separation system is shown in Fig. 13.31.

Two plates with a V notch in the middle are held together by fasteners as shown in the figure. Each plate is fastened to structures on either ends. When the explosive charge embedded in the assembly is actuated, the flattened tube expands into a cylindrical shape resulting in the severance of the plates at the notch planes. The upper plate is connected to the upper stage, lower plate to the lower stage and with the severance of the plate joint at separation plane, the separation of the stages is effected. The jettisoning velocity is to be imparted to the structures using springs. Expanding tube-based system offers high joint stiffness with low joint rotation constant and the contamination is totally avoided. However XTA-based systems produce more shock compared to linear bellow-based or Merman band systems.

13.8 Testing Methodology for Fault-Free Performance

The design robustness and reliability of the realized separation systems have to be demonstrated in the flight configuration under the simulated flight environment through a series of tests at the ground. The test methodologies include the elaborate tests at unit level, subsystem level and integrated system level. The system has to be subjected to a series of structural, functional and environmental qualification tests.

Fig. 13.31 Expanding tube separation system



If the system is linked with cryogenic stage, tests are to be carried at low temperatures using liquid nitrogen (LN₂) to simulate the very low interface temperature. The main objective of structural tests is to qualify the separation units for the flight loads. The tests are carried out on the separation unit along with all the associated structural elements at appropriate loads using suitable test fixtures. In case of cryo-stage separation system, the associated forward and aft end joints are subjected to loads after simulating the low temperature using liquid nitrogen at the fore end joint.

After the structural test, the mechanism is to be subjected to functional tests to verify its performance at the expected service environment. The time of the separation of the unit with respect to the separation process initiation is measured at unit level tests. Subsystem level tests are needed in certain cases like strap-on separation system where the forward and aft joints are to be characterized and their functional performance is to be verified through appropriate tests.

The integrated system level tests are essential to qualify the system under its service conditions. This system level functional test is to be carried out with all simulated interfacing elements to demonstrate the collision-free separation. The major objectives for these tests are

- (a) To validate the system performance under simulated service condition with sequencing scheme similar to the one recommended for flight
- (b) To verify the time of separation of the various units with respect to the separation process initiation
- (c) To measure the shock levels on upper body and other critical elements located in the vicinity of separation plane
- (d) To estimate the tip-off rates of the ongoing and separated bodies
- (e) To measure the lateral clearance between separating bodies to assess the performance of the separation system

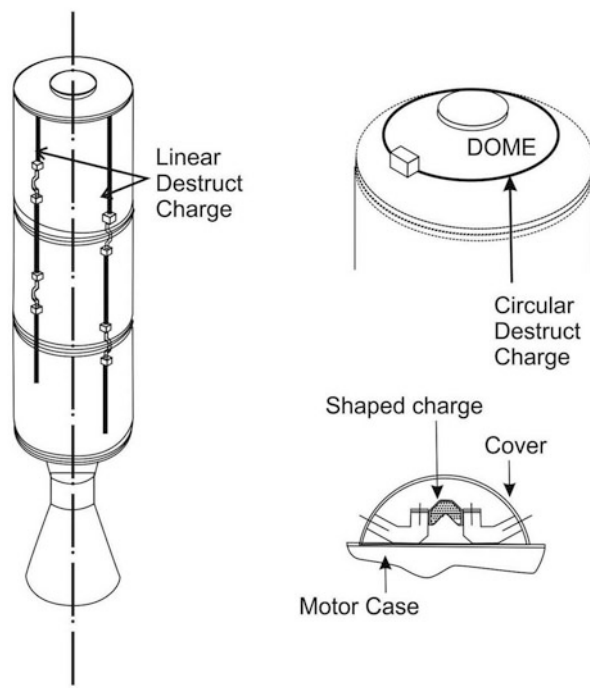
The separation system at unit level needs to be subjected to the qualification levels of vibration, both in longitudinal and lateral directions. The levels of vibration should be as per the environment test levels defined for the vehicle to be flown. Subsequent to vibration tests, the functional test has also to be carried out to verify the performance. Rain proofing tests as per stipulated standards are also required to ensure that even in rainy condition the performance of the system is unaffected.

Further, tests need to be carried out, simulating the vehicle acceleration condition at the time of separation. For satellite separation, the bodies fall under gravity and simulation of such a condition on ground is difficult. In such cases, suitable test setup has to be built to compensate for gravity. Certain events like PLF separation take place after crossing the atmosphere. Hence such large structures need to be tested on ground in large vacuum chambers to capture the performance of separated bodies. In cases when vacuum chambers are not available, ground testing combined with software modelling has to be used to evaluate the performance in flight conditions. Since pyro-nits are not retestable, after batch processing of units, large number of tests are carried out which involve margin demonstration tests, environmental tests, functional tests, etc., for batch acceptance.

13.9 Vehicle Destruct Systems

Launch vehicle trajectory is always designed to have a well-defined nominal ground trace of instantaneous impact point to meet the overall range safety considerations. Dispersions in vehicle parameters cause variations in the ground traces from the predicted nominal one. Therefore, to ensure the range safety, a safe corridor is defined during the entire duration of flight. Vehicle trajectory variation within this safety corridor is permitted whereas the vehicle flight beyond this corridor is not allowed. Due to any anomaly in any of the subsystems during the flight, the vehicle may depart grossly from its defined trajectory. If the malfunction of any subsystem causes the deviation of the vehicle beyond the defined safe corridor, it becomes necessary to destroy the vehicle to avoid any damages to properties and life. This is achieved using destruction systems of the vehicle. The vehicle is always equipped with a telecommand system on board and the range safety officer who is entrusted with the task of monitoring the vehicle flight in safe corridors is empowered to issue the destruction command whenever the officer is certain that the vehicle has deviated beyond the safe corridor. The long-range radars provided along the flight trajectory carry out the continuous tracking and transfer the essential vehicle parameters to the range safety officer. Additionally rate and attitude data obtained from inertial navigation system of the vehicle through telemetry are also used for knowing the vehicle behaviour during flight. The instantaneous impact point (IIP) trace of the vehicle is determined using the radar data in real time and this information is also used in the decision-making process.

Fig. 13.32 A typical vehicle destruct system



The destruction of the solid motor or liquid tanks of liquid stages is effected by longitudinally cutting the motor case or tanks at diametrically opposite locations using linear shaped cords. A typical destruct system is illustrated in Fig. 13.32.

Whenever the range safety officer sends the command to destruct the vehicle, the shaped charges mounted on the motor case or the liquid tanks over the length as shown in the figure is fired, the motors are cut linearly, thereby releasing the motor or tank pressure and resulting in termination of thrust. In case of motor dome, the circular form of the shaped charge rips open the dome, causing sudden depressurization and quenching of thrust. As shown in Fig. 13.32 the explosive cords are fixed on the pads which are mounted on the tanks using adhesives. A cover on the entire assembly protects the system from environment during flight.

Extreme care has to be taken to ensure that the destruct systems are not activated inadvertently at any phase of flight. Adequate safety features are to be incorporated into the pyro-chain to take care of this. Usually all pyro-systems are operated through a safe/arm device which guards against any electrical or mechanical inadvertent firing of pyro-systems.

13.10 Other Stage Auxiliary Systems

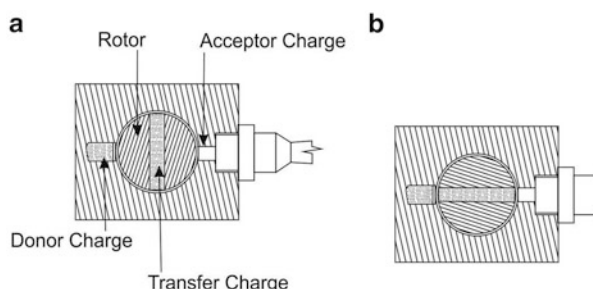
In addition to stage separation and destruction systems in a launch vehicle, the igniters used for stage motor ignition are based on space ordinance system or pyrotechnique. The basic function of an igniter is to generate the needed chemical and thermal state at the surface of the propellant so that sustained combustion is created. The time specification is also another important factor for smooth ignition. Launch vehicle stage motors use both pyrotechnique and pyrogen motors. The usage depends on the size of the motors. While pyrotechnique igniters are used in smaller motors, pyrogen igniters are used in relatively larger motors or at high-altitude ignition. More details of igniters are discussed in Chap. 9, dealing with propulsion systems.

Apart from the high reliability requirements of all explosive systems used in launch vehicles, safety is of utmost importance to avoid any inadvertent firing. Any such occurrence is disastrous for the entire mission. The inadvertent firing can be caused due to several reasons like static discharge, lightning or even stray current. It is therefore important to introduce enough safeguards into the system. In all launch vehicles, the safety is achieved by introducing safe and arming (SAFE/ARM) systems in the explosive circuits. A typical safe/arm device is shown in Fig. 13.33.

In this system there are two positions termed as safe and arm. The transfer charge shown in the centre is held in a rotor. The explosive train consists of donor charge, transfer charge and acceptor charge. When the rotor is positioned such that transfer charge is misaligned as shown in Fig. 13.33a, this inhibits the transfer of charge from donor to acceptor and thus avoids the premature firing.

But when the rotor is turned such that the donor and acceptor charges are aligned with transfer charge as in Fig. 13.33b the firing is made possible to actuate the pyro. The device can be designed to have both manual and remote operation depending on the requirements. Generally the command system to pyro detonator has an interface through a number of intercepts per chain and one of them is kept as manually operated and it is closed as late as possible during the vehicle preparation for launch.

Fig. 13.33 A typical safe arming device. (a) Safe condition. (b) Armed condition



Bibliography

1. Barbour, R.T.: Pyrotechnics in Industry. McGraw-Hill Book Co., New York (1981)
2. Conley, P.L.: Space Vehicle Mechanisms. Wiley, New York (1998)
3. Pollard, F.B., Arnold, J.H. Jr.: Aerospace Ordnance Handbook. Prentice Hall Inc., Englewood Cliffs
4. Brauer, K.O.: Handbook of Pyrotechnics. Chemical publishing Co. Inc., New York (1974)
5. NASA Space Vehicle design criteria: Flight separation mechanisms. NASA SP 8056, October 1970
6. Walkers, W.P., Zukas J.A.: Fundamentals of Shaped Charges. Wiley Inter-science (1989)
7. Sutton, G.P.: Rocket Propulsion Elements. Wiley, New York (1963)
8. Bement, L.J., Schimmel, M.L.: A manual for pyrotechnic design, development and qualification. NASA-TM-110172, NASA Langley Research Center, Hampton, Virginia 23681-0001, June 1993
9. "Solid Rocket Motor Igniters", NASA-SP-8051, National Technical Information Service, Springfield, March 1971
10. Smith, F.Z.: Pyrotechnic Shaped Charge Separation Systems for Aerospace Vehicles. NASA TM X-1607 (1968)
11. Aichroth, W.W.: Test report – Spacecraft/Interstage/Spacecraft separation test. Report 2401-6033-TU-000, TRW Systems (June 1963)
12. Hines, D.E.: Generation and propagation of stage separation shocks in missiles and space vehicles. Paper no. 1815, Douglas Aircraft Co., April 1964
13. Wasko, R.A.: Experimental investigation of stage separation aerodynamics, NASA TN D-868, 196
14. Thomson, W.T.: Introduction to Space Dynamics. Wiley, New York (1986), 1961

Chapter 14

Navigation Guidance and Control System

Abstract The navigation, guidance and control (NGC) system, the brain of the vehicle, is responsible for directing the propulsive forces and stabilizing the vehicle along the desired path to achieve the orbit with the specified accuracy. The NGC system has to define the optimum trajectory in real time to reach the specified target and steer the vehicle along the desired path and inject the spacecraft into the mission targeted orbit within the specified dispersions. The navigation system measures the instantaneous state of the vehicle, and using this information, the guidance system generates the optimum trajectory to achieve the target and desired vehicle steering command to realize the optimum trajectory in real time. The vehicle control system, comprising of autopilot and control power plants, receives the steering commands from the guidance system and steers the vehicle to follow the desired attitude in the presence of all disturbances. The guidance system charts out the remaining path continuously, recalculating the desired attitude of the vehicle to achieve the mission target. Final mission objectives and allowable orbital dispersions dictate the choice of a suitable guidance system. The vehicle autopilot has three major functions namely, to ensure that the vehicle loads are always well within the specified limits, to stabilize the vehicle all through the flight and to steer the vehicle to follow the desired attitude as decided by the guidance system. The autopilot generates the control commands as per the defined control law which is used to drive the actuation systems to generate the necessary control forces. Proper choice of inertial sensors, inertial systems, guidance schemes, control actuation systems and control laws depend on the mission objectives and requirements. This chapter starts with the functional requirements and systems requirements of NGC system of a launch vehicle. The need for the integrated design of NGC system using systems engineering approach is explained next. Various elements involved in NGC system like navigation, guidance and control, the selection of a suitable scheme and their design aspects are also explained. The performance evaluation of the integrated design of NGC system carried out using different test beds is described.

Keywords Navigation • Guidance and control • Navigation sensors • Redundancy management • Aided navigation • Explicit guidance • Implicit guidance • Mission salvage • Autopilot • Control law • Vehicle dynamics • Control power plants • Simulation and system validation

14.1 Introduction

The primary demands of a satellite launch vehicle are to achieve larger payload capability and inject the payload into the targeted orbit within the specified dispersion band. While the propulsion system provides the required energy to lift the payload to the orbit, it is the navigation, guidance and control (NGC) system, which is the brain of the vehicle, is responsible for directing the propulsive forces and stabilizing the vehicle along the desired path to achieve the orbit with the specified accuracy. The dispersions in realized propulsion parameters with respect to expected values, variations of the estimated aerodynamic characteristics during the atmospheric flight phase, the fluctuating winds both at ground and upper atmosphere and a variety of internal and external disturbances during the flight can increase the loads on the vehicle beyond the permissible limit and also cause deviations in the vehicle trajectory from its intended path. Under such environment, NGC system has to define the optimum trajectory in real time to reach the specified target and steer the vehicle along the desired path and inject the spacecraft into the mission targeted orbit within the specified dispersions while ensuring the vehicle loads remain within limits. Therefore, NGC system is among the most crucial and challenging field in launch vehicle design.

The navigation system measures the instantaneous state of the vehicle, and using this information, the guidance system generates the optimum trajectory to achieve the target and desired vehicle attitude steering command to realize the optimum trajectory in real time. The vehicle control system, comprising of autopilot and control power plants, receives the steering commands from the guidance system and steers the vehicle to follow the desired attitude in the presence of all disturbances listed earlier. A typical configuration of a NGC system is shown in Fig. 14.1.

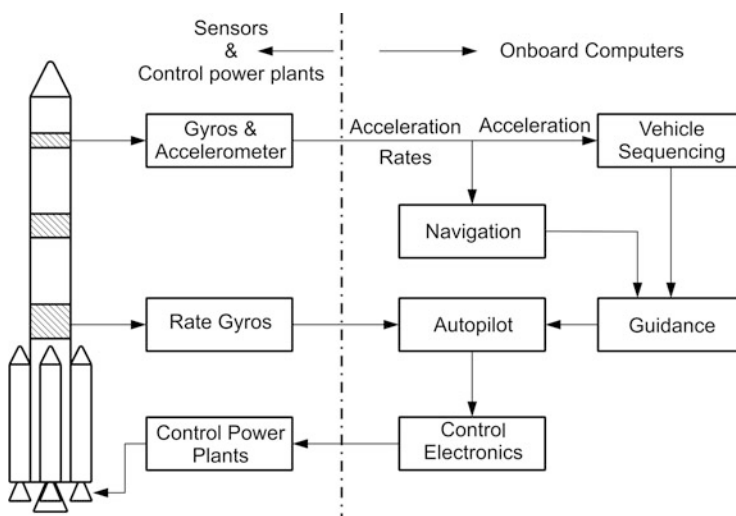


Fig. 14.1 Typical configuration of a NGC system

The navigation system is generally based on the high precision measurements of vehicle accelerations and vehicle attitude rates in all its three axes using accelerometers, gyros and high speed, high accuracy computations. The guidance system utilizes the navigation information of the instantaneous velocity and position of the vehicle and charts out the remaining path continuously, recalculating the desired attitude of the vehicle and remaining burn duration of the propulsion stage to achieve the mission target. Final mission objectives and allowable orbital dispersions dictate the choice of a suitable guidance system. The accuracy of orbital injection depends largely on the navigation sensor errors and effectiveness of guidance scheme. The vehicle autopilot has three major functions namely: (a) to ensure that the vehicle loads are always well within the specified limits, (b) to stabilize the vehicle all through the flight by avoiding the interactions between the rigid body, flexible structural modes, slosh modes, engine dynamics etc. and (c) to steer the vehicle to follow the desired attitude as decided by the guidance system. Utilizing the sensors data and desired attitude, the autopilot generates the control commands as per the defined control law which is used to drive the actuation systems to generate the necessary control forces to stabilize the vehicle and to steer it to follow the desired attitude.

To carry out the above functions, NGC system utilizes the following subsystems: (1) sensors; (2) navigation, guidance and control algorithms; (3) onboard computers hardware along with system software; (4) application software; (5) guidance; (6) autopilot; (7) servo electronics; and (8) control power plant hardware. NGC is a mission critical system since the effect of failure in any of the above elements of the chain propagates to the downstream which may finally lead to mission and vehicle failure. Therefore, generally redundancy is built into the hardware and software at different levels of NGC chain to achieve very high reliability.

Proper choice of inertial sensors, inertial systems, guidance schemes, control actuation systems and control laws depend on the mission objectives and requirements. If large orbital dispersions are acceptable, then a simple attitude reference system (ARS) using gyros is sufficient. Otherwise the vehicle needs closed loop guidance and in such cases a full-fledged inertial navigation system is needed. Similarly, depending on the requirement for reduction in the structural loads or reduction in trajectory dispersions, a suitable control scheme in terms of bandwidth, gain, dead zone, etc. need to be selected. Therefore, it is essential to carry out detailed system engineering studies right at the beginning phase of design to finalize suitable schemes considering the various aspects of mission, technology constraints and cost.

This chapter starts with the functional requirements and systems requirements of NGC system of a launch vehicle. The need for the integrated design of NGC system using systems engineering approach is explained next. Various elements involved in NGC system and design aspects of these subsystems are also explained in this chapter.

14.2 Requirements of NGC System

14.2.1 Functional Requirements

The main objectives of NGC system are to ensure integrity of the vehicle during flight and to direct the vehicle to achieve the intended target under all possible environments, viz., nominal, dispersed and disturbed flights as well as deviated flight due to partial failures of any of the subsystems. To achieve the above objectives, following are the functional requirements of NGC system.

1. To predict the instantaneous rotational and translational response (rates and acceleration with respect to body frame) of the vehicle during flight through suitable sensors
2. To predict the instantaneous state (position and velocity) of the vehicle with respect to a defined reference frame
3. To define the optimum trajectory to reach the target
4. To generate the necessary desired attitude and duration of propulsive stages to achieve the set target
5. To stabilize the vehicle against the disturbances, satisfying the vehicle load carrying capabilities
6. To steer the vehicle along the predicted trajectory by following the desired attitude history
7. As the vehicle response and vehicle states are varying continuously, these parameters to be updated at very short interval of time as per the systems and mission requirements
8. To provide suitable redundancy management

14.2.2 Systems Requirements

In order to carry out the above functions, the following are the systems requirements:

1. Suitable sensors required for predicting the in-flight response of the vehicle. Generally accelerations and rates sensors are used for this purpose.
2. As the entire NGC functions depend on the sensors, built-in sensor redundancy is essential.
3. Suitable inertial navigation system, either stabilized platform system or strap-down system as per the vehicle and mission requirements to be configured.
4. To reduce the errors in the mission target and to stabilize the vehicle, the sensor errors have to be minimum. Alternatively, suitable mechanisms have to be implemented to compensate the sensor errors.
5. Suitable data acquisition system to meet the functional requirements of navigation and autopilot subsystems.

6. Analog to digital and digital to analog converters.
7. Sensors scale factors and operating range to be selected to cater to the wide varying flight environment while meeting the autopilot and mission requirements.
8. Suitable location of sensors for meeting the navigation and autopilot requirements.
9. Algorithm for the selection of best sensor output and to filter the noise and retaining the required signal
10. Algorithm for navigation computations to provide the required accuracy in vehicle state prediction for the wider flight environment.
11. Robust guidance algorithm capable of generating optimum trajectory and desired attitude for the vehicle under wider flight environment.
12. Suitable guidance margin as velocity reserve.
13. Autopilot design to meet the requirements under nominal and off-nominal flight environment, dispersions and disturbances.
14. Autopilot control algorithm to meet wider flight requirements.
15. Servo system hardware for control systems and servo loop design to meet the specified requirements of autopilot.
16. Sensor bandwidth to meet the autopilot requirements.
17. Control power plant capability to be more than the disturbances during flight.
18. Efficient onboard computers to meet NGC computational requirements.
19. Distributed onboard computers and the associated interfaces to meet all the mission requirements simultaneously in real time.
20. Periodicity of computations of navigation, guidance and autopilot to be decided so as to meet the vehicle stabilization and mission accuracy requirements.
21. Sufficient margins in the computations to take care of unknown computational loads in the flight.
22. Redundancy in the onboard computers (mission computers) with space diversity in software.
23. Suitable switching algorithm for selecting the healthy subsystem in case of failure.

14.3 NGC System and Integrated Design Requirements

14.3.1 Functional Configuration of NGC

The functional configuration of a NGC system with closed loop guidance for a vehicle showing various signal flows is given in Fig. 14.2. The inertial navigation system at the avionics bay of the vehicle with gyros and accelerometers as inertial sensors measure vehicle attitude rates and linear accelerations. Using these sensors data, navigation algorithm computes vehicle attitude (θ, Ψ, ϕ), velocity (V_x, V_y, V_z) and position (X, Y, Z) with respect to a specified reference frame.

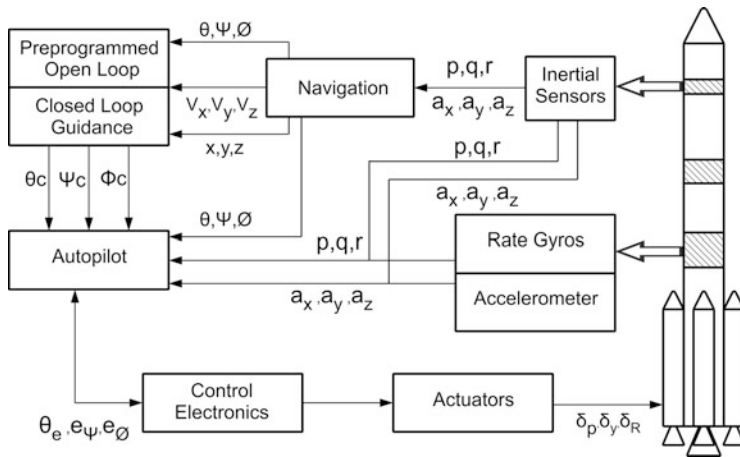


Fig. 14.2 Functional configuration of NGC system

The guidance system generates the steering commands θ_c, Ψ_c using pre-programmed steering, stored as tables during the open loop guidance regime. Roll maneuver is carried out after the initial vertical rise, to align the vehicle to the launch azimuth can be implemented as ϕ_c . During the closed loop guidance phase, the attitude commands (θ_c, Ψ_c, ϕ_c) are generated in real time by making use of the information from navigation.

The autopilot receives θ_c, Ψ_c, ϕ_c from guidance, vehicle attitudes (θ, Ψ, ϕ) from navigation, body rates (p, q, r) from rate gyro and lateral accelerations (a_x, a_y) from lateral accelerometer package. Using these information, the autopilot computes attitude error functions (e_θ, e_Ψ, e_ϕ) as per the control law. During the lower stage flights, the rates measured by the rate gyro package positioned at antinode points are used. If required, the lateral accelerations measured at the lower stage are used for vehicle stabilization during the first stage operations. The error function commands as computed by autopilot are issued to the actuators of control power plants to gimbal the engine (gimbalable liquid engine) or nozzle (for solid motors with flexible joint nozzle) or to actuate the valves of SITVC system of fixed nozzle solid motors. The engine deflection or the valve opening produces lateral forces to generate the necessary control moment about the centre of gravity of vehicle to stabilize and steer the vehicle. All these operations are carried out in real time using on board computers.

14.3.2 Integrated System Engineering Approach for Design

From the functional configuration as explained above, it can be seen that the NGC system and its robust design process involve several subsystems of multiple

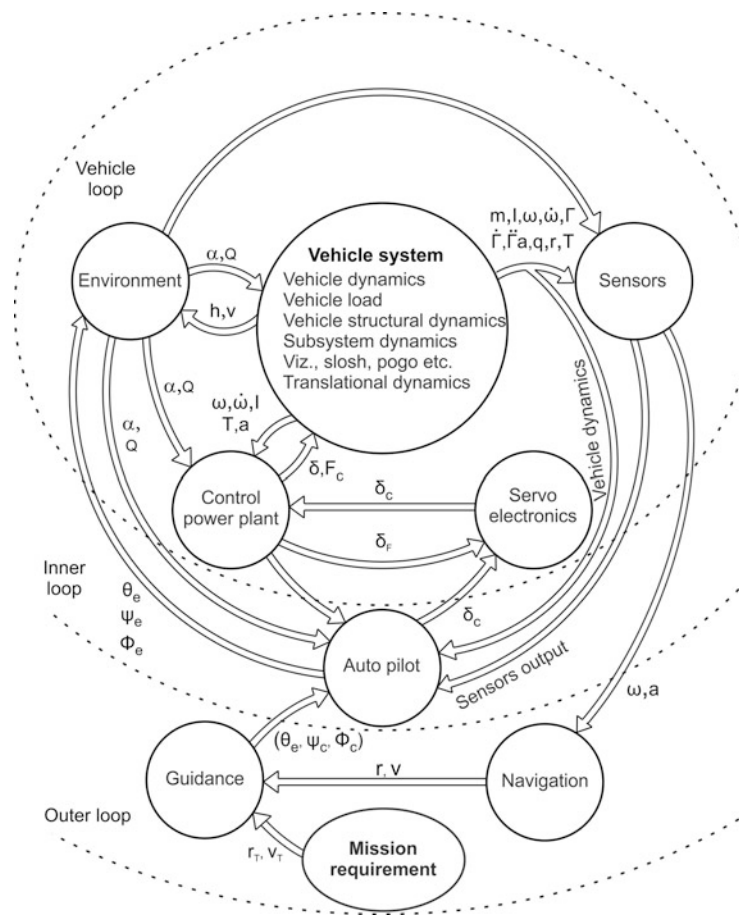


Fig. 14.3 Interactions between NGC and vehicle systems

disciplines such as sensors, hardware, onboard computers, mission critical software and control and guidance algorithm.

The integrated NGC system can be divided into three loops: (1) inner most loop with high bandwidth, involved in the control power plant responses; (2) inner loop with fast response, involved in the autopilot; and (3) the outer loop with rather slow response, involved in navigation and guidance. There is high level of interactions within the NGC subsystems and with the vehicle systems and environment as highlighted in Fig. 14.3. There is interaction between vehicle and environment through angle of attack (α), dynamic pressure (Q), altitude (h) and velocity (V). The sensor output depends on vehicle characteristics, vehicle response, structural dynamics, slosh dynamics as well as the environment. On ground, the vehicle and subsystem characteristics and disturbances are used for autopilot design. During flight, the sensors data is used for navigation computations. Vehicle autopilot uses

these sensors data during flight along with guidance and navigation output. The command generated by autopilot is used in servo electronics which in turn drives the actuator through command and feedback loops. During flight, control power plant response is affected by the vehicle characteristics and environment. Therefore, it can be seen that the total system is tightly coupled.

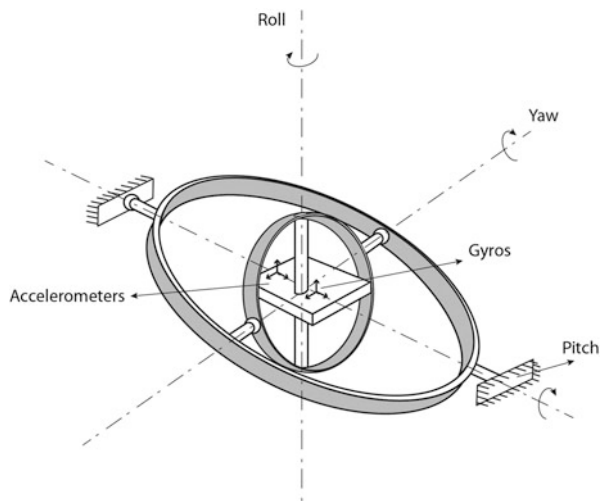
Due to very high level of interactions of NGC subsystems with vehicle and its environment, it is essential to follow an integrated NGC system design strategy using system engineering approach to achieve a robust design. Also, since the vehicle systems and mission performance are closely linked with the NGC system, it is necessary that the integrated NGC system design is addressed right at the beginning of vehicle design phase.

14.4 Navigation System

Navigation is essentially the process of determining the position and velocity of a moving body with respect to a defined reference coordinated frame. During the early days, the Sun at day time and stars at night were used as navigational aids. Subsequently magnetic compass, sextant and radio navigational aids were evolved. Development of inertial grade sensors viz. gyros and accelerometers revolutionized the autonomous inertial navigation systems which were used increasingly for military, ships and civil aviation. The inertial navigation system (INS) is a self-contained system and it does not rely on any signals from the ground. It is non-jammable, and with proper selection of inertial sensors, INS provides sufficiently accurate information. Therefore, the usage of INS is further extended to missiles, launch vehicles and spacecraft. The principles of inertial navigation system are based on Newton's laws of motion. The navigation is carried out with respect to a space fixed inertial frame, a frame which is non-rotating and non-accelerating with respect to stars and considered inertial.

Three gyros measure the angular rates of the vehicle, and three accelerometers measure the specific forces along the body axes. The vehicle attitude with respect to the defined navigational frame is computed using the measured angular rate. The specific force defines the acceleration of the body due to inertial forces as per Newton's law. The accelerometers cannot measure the gravitational acceleration, and therefore, it has to be appropriately accounted in calculations. The reason why accelerometers cannot measure the gravitational acceleration is due to the fact that the accelerometer as the observer is in accelerated frame of reference and the gravitational field is a conservative field. Therefore, the gravitational acceleration is computed using the position vector computed by the navigation system. The net acceleration in a navigation frame has to be computed using both measured specific force and the computed gravity accelerations and represented in the desired frame of reference by suitable transformations which is generated using the computed attitude of the vehicle. First integration of this net acceleration after resolving in the desired navigation frame provides the velocity and further integration of the

Fig. 14.4 Gimbaled inertial platform



velocity gives the position of the body. Thus measurements from both the gyros and accelerometer sensors are combined with the gravity model to generate the instantaneous velocity, position and attitude of the vehicle.

The navigation system based on inertial principles can be realized either as a platform system or a strap down system. The platform system consists of a gimbaled configuration and it is mechanized to have two important functions, namely: (a) providing an ideal platform which is mainly non-rotating and supports accelerometers and gyros and (b) measuring accurately the acceleration along this non-rotating frame. The vehicle is having angular motions about its three principal axes known as pitch, yaw and roll. It is essential that these motions are isolated to realize a non-rotating platform. It can be realized by using a simple three gimbaled inertial platform as shown in Fig. 14.4. The platform cluster houses three accelerometers and three gyros which are mounted orthogonally.

The three gimbal system is having a kinematic limitation. It cannot provide complete isolation to the base motion under all attitude condition. When the vehicle rotational motion is about the middle gimbal axis by 90° , the outer gimbal axis and innermost gimbal axis align. Under this condition, the isolation about the original outer and inner axis is lost. This phenomenon is generally termed as gimbal lock. To overcome this problem, a fourth gimbal is added and four gimbal systems have innermost, intermediate, middle and outer gimbals. This mechanization helps to maintain the orthogonality of inner three gimbals by slaving the intermediate gimbal to outer gimbal. This configuration provides all attitude inertial navigation capability. In the case of the gimbaled platform system, the dynamic range and bandwidth requirements of the gyroscopes is relatively low, since the residual angular rates after the isolation by the gimbals are only to be measured by the gyros.

In a strap down system, the sensors are directly mounted to vehicle body and measure the vehicle body rates and specific force in body frame. The specific force vector sensed in body frame is converted into inertial frame by appropriate

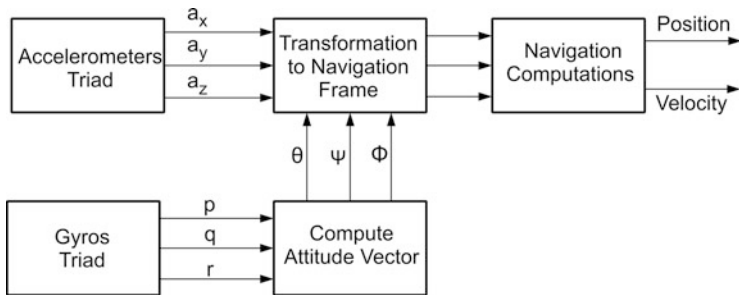


Fig. 14.5 Schematic of a strap-down navigation system

coordinate transformation using the vehicle attitude which in turn is computed using the measured angular rates of the vehicle. Therefore, this system is identified as analytical platform system. In all such transformations, translations and rotations are involved to transfer the vector from one coordinate system to other. Most commonly used schemes are direction cosines, quaternion, or Euler angle transformations. Once the transformation is carried out, the navigation computation remains similar to that used in gimbaled system. The schematic of a strap down navigation system is given in Fig. 14.5. In this case, the dynamic range and bandwidth for gyros are high compared to platform system.

The navigation output is used for the guidance computations. In addition, the navigation sensor output is used for the autopilot command generations. Therefore, the accuracy of sensor output and the navigation output decide the effectiveness of vehicle stabilization and the precision with which the satellites are injected into the specified orbit. Also, since these outputs provide vital data for the mission critical functions, sensor redundancy and suitable redundancy management are essential to achieve the reliable mission. In order to achieve the above objectives, the navigation system comprises of the following elements and functions:

1. Suitable sensor hardware with redundancy
2. Sensor electronics which includes the data acquisition, necessary analog to digital conversion, appropriate filters to achieve the desired band width of the sensor output
3. Suitable filtering mechanism to remove the sensor noises and select the best sensor data
4. Sensor redundancy management
5. Suitable Failure Detection and Isolation (FDI) system
6. Data sampling and periodicity of navigation computations to meet the specified requirements
7. Suitable navigation algorithm to compute navigational parameters from the selected sensor data

14.4.1 Navigation Sensors

Inertial sensors comprise of gyroscopes and accelerometers. While accelerometer measures the specific force, a gyroscope measures angular rate and both the measurements are components of the physical inertial force vector and component of the physical inertial angular rate vector along the input axis of the sensors. The measurement channels for rate gyros and accelerometers are given in Fig. 14.6. The gyros and servo accelerometers are closed loop sensors, which sense the vehicle attitude rates and linear accelerations. The basic output of sensor is in terms of voltage. Since the bandwidth of the sensor is high, the output contains measurement noises. These are filtered out by suitable filters (F1 and F3). The filtered signals are digitized through a suitable “Voltage to Frequency Converters (VFC)” followed by accumulators. The VFC output is pulse trains with suitable scale factors (for ex: 1 V = 2400 pulses). Integration of pulses is done by accumulators. The pulse accumulator is sampled at the specified interval. The pulse increment of accumulator output with respect to the previous cycle value is the measure of angular increment (in the case of gyro outputs) or velocity increment (in the case of accelerometers). These incremental values are used for navigation computations. Autopilot computation requires the analog attitude rates and the analog acceleration data is used for various onboard system functions, especially real time decisions (RTD). The analog data required for the above functions are passed through analog filters (F2 or F4) to meet the specified gain–phase requirements of specific application and the filtered signals are passed through a suitable analog to digital converter (ADC) and used in the applications of autopilot or RTD.

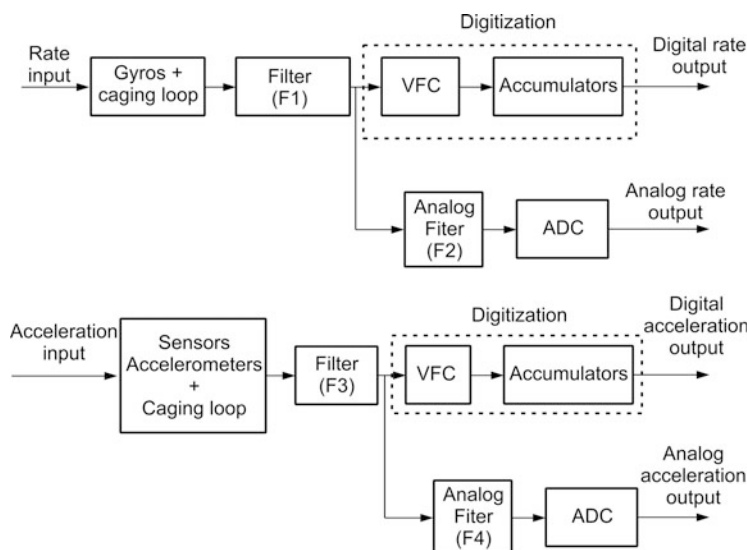


Fig. 14.6 Measurement channel of acceleration and attitude rates

The details of various types of sensors used for inertial navigation system are given in Annexure-B. Specific features of sensors characteristics which have the performance impact on mission and other NGC subsystem elements are briefly explained below:

(a) *Sensor Output Range and Resolution*

Each sensor and the associated closed loop system (caging loop) limits the maximum possible range of attitude rate (or acceleration) measurable by the sensors. As an example, maximum rate measured by typical sensor loop is $60^{\circ}/\text{s}$. Similarly, there is range limit for voltage frequency conversion (VFC) or analogue to digital conversion (ADC). As an example, this range may be represented as 10 V. This gives the equivalence of maximum range of digitization process and maximum range limit of the sensors, i.e., $10 \text{ V} = 60^{\circ}/\text{s}$. However, the read out sensor resistance can be adjusted to measure the smaller range of rates with full range of digitization process. As an example, $10 \text{ V} = 30^{\circ}/\text{s}$ (instead of $60^{\circ}/\text{s} = 10 \text{ V}$). Smaller measurement range for full scale leads to better resolution and correspondingly improved accuracy of navigation parameters. However, in this case, for the actual response of the vehicle beyond the range limit, the digital output would clamp to the maximum value, and therefore, navigation output computed using the above-clamped sensor output on vehicle state would be different from that of the real vehicle response. Under such conditions, it is essential to use wider range for the full scale. Therefore, the range of measurements and resolution requirements has to be judiciously decided to cater to the application requirements viz., autopilot and navigation computation.

(b) *Sensor Output Bandwidth*

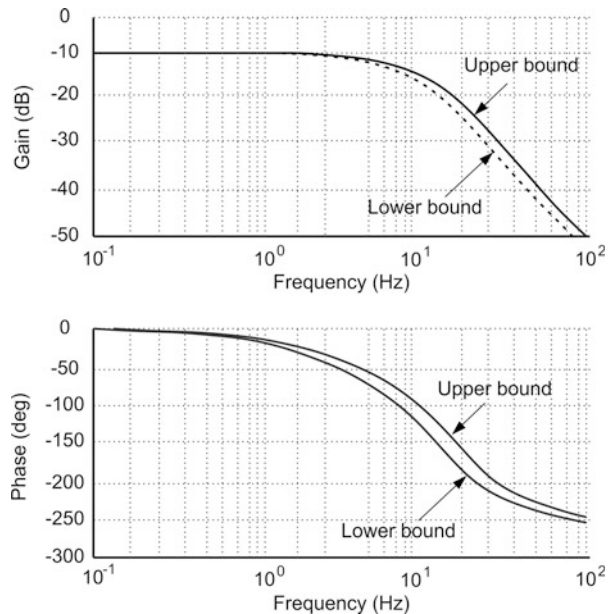
The rate gyros outputs to autopilot may not exactly represent the true response of the vehicle due to the sensor and the associated data acquisition systems characteristics, noises and the delay introduced by data sampling. The end-to-end features of measurement system can be represented by suitable dynamics. Therefore, to take care of this aspect in the autopilot system, it is essential to supply the sensor data to autopilot with the required gain-phase characteristics. In order to meet the above functions, depending on the realized sensors hardware along with the associated electronics, suitable filters (F2) are to be implemented to achieve the required characteristics.

The upper and lower bound characteristics are generated considering the dynamics of the vehicle and have been used in the design phase making use of the attenuation coming from these characteristics. Hence after realizing the sensor, the characteristics are tested against the bounds used in the design. Typical upper bound and lower bound characteristics of sensor dynamics are shown in Fig. 14.7. The characteristics are decided based on the following requirements:

1. Should have noise attenuation beyond 20Hz.
2. Should not give any gain till the cut off frequency
3. Should give less lag at rigid body and slosh frequencies.

(c) *Sensor Errors*

Fig. 14.7 Typical upper and lower bound characteristics of rate sensors



Typical mounting arrangement for the gyros and accelerometer sensors on the vehicle are given in Fig. 14.8. To measure the vehicle response with respect to the body axes, it is essential to mount the sensor clusters such that the cluster axes (X_C, Y_C, Z_C) are parallel to the defined body axes (X_B, Y_B, Z_B). But in reality, due to various reasons, the cluster axes may not be exactly aligned with the body axes as shown in Fig. 14.8.

The outputs of the sensors are different from the vehicle actual attitude rates and accelerations due to various sensor errors. The sensor errors are due to fixed or bias error, imperfections in the sensor elements coupled with the flight environment and the errors in the output caused by its improper mounting on the vehicle. Typical error sources in a gyro used in INS can be listed as,

1. Fixed or acceleration insensitive drift rate
2. Mass unbalance or g sensitive drift rate
3. Anisoelasticity or g^2 sensitive drift rate
4. Scale factor error
5. Scale factor non linearity/asymmetry
6. Input axis misalignment

Typical output of attitude rate sensor, which measures the rate about Z_B – axis, ω_{z_s} is given as

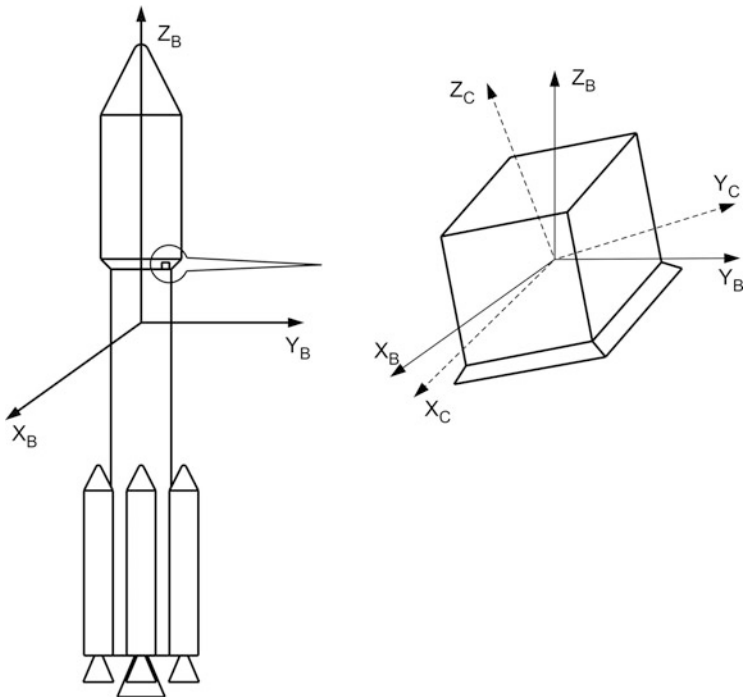


Fig. 14.8 Typical mounting configuration of sensors

$$\begin{aligned} \omega_s = & (1 + \delta_{\omega_z}) \left\{ \omega_{0z} + k_1 \omega_z + k_1' |\omega_z| + k_2 \omega_z^2 + k_2' \omega_z |\omega_z| + (\alpha_{zx} \omega_x + \alpha_{zy} \omega_y) \right. \\ & \left. + (p_1 a_x + p_2 a_y + p_3 a_z) + c a_z a_{sp} \right\} \end{aligned} \quad (14.1)$$

where

$\omega_x, \omega_y, \omega_z$ are the vehicle attitude rates

δ_{ω_z} = scale factor error

ω_{0z} = fixed bias drift

k_1 = scale factor

k_1' = scale factor asymmetry

k_2 = scale factor nonlinearity

k_2' = scale factor nonlinearity asymmetry

α_{zx}, α_{zy} = misalignment of x and y axes of sensors with respect to the vehicle z-axis

p_1, p_2, p_3 = mass unbalance drift (or g-sensitive) coefficients

c = anisoelasticity (or g^2 -sensitive) drift rate coefficients

a_x, a_y, a_z = specific forces along the vehicle x, y and z axes, respectively

a_{sp} = specific forces along spin axis of z-gyro

For the case of laser gyros, there are no mass unbalance or anisoelastic drift. Similarly the scale factor and input axis (IA) misalignment errors are applicable only in strap down systems.

Typical sources of errors in accelerometers are as follows:

1. Bias
2. Scale factor error
3. Scale factor non linearity
4. Input axis misalignment

Typical output of acceleration sensor which measures specific force along Z_B -axis, a_{z_s} is given as

$$a_{z_s} = (1 + \delta_{a_z}) \{ a_{0_z} + l_{1_z}a_z + l_{2_z}a_z^2 + (\alpha_{zx}a_x + \alpha_{zy}a_y) \} \quad (14.2)$$

where

a_x, a_y, a_z are the specific forces along the X_B, Y_B and Z_B axes, respectively

δ_{a_z} = scale factor error

a_{0_z} = bias

l_{1_z} = scale factor

l_{2_z} = scale factor nonlinearity

α_{zx}, α_{zy} = misalignment of x and y axes of sensors with respect to vehicle z-axis

All the error sources have two components: (1) systematic errors and (2) random errors. The systematic part of the errors are estimated by devising suitable test strategies and the same can be compensated at the sensor output whereas the random errors caused by the in-flight environment and end-to-end sensor systems result into error in the navigation parameters.

(d) *Sensor Data Selection*

In order to cater to the redundancy, multiple sensors are used. Due to the individual characteristics of the sensor hardware, each sensor of redundant configuration can measure different outputs within the specified band. Therefore, suitable strategy has to be implemented to select the sensor data to be used into the navigational computations. Also, appropriate strategy has to be implemented in the vehicle onboard to isolate the faulty sensor output from the computational loop.

14.4.2 Navigation Computations

Vehicle position, velocity, attitude and attitude rates at any instant of flight with respect to a specified reference frame define the navigational parameters. These parameters are computed onboard using the vehicle in-flight measurements of attitude rates and accelerations by the respective sensors with respect to the body

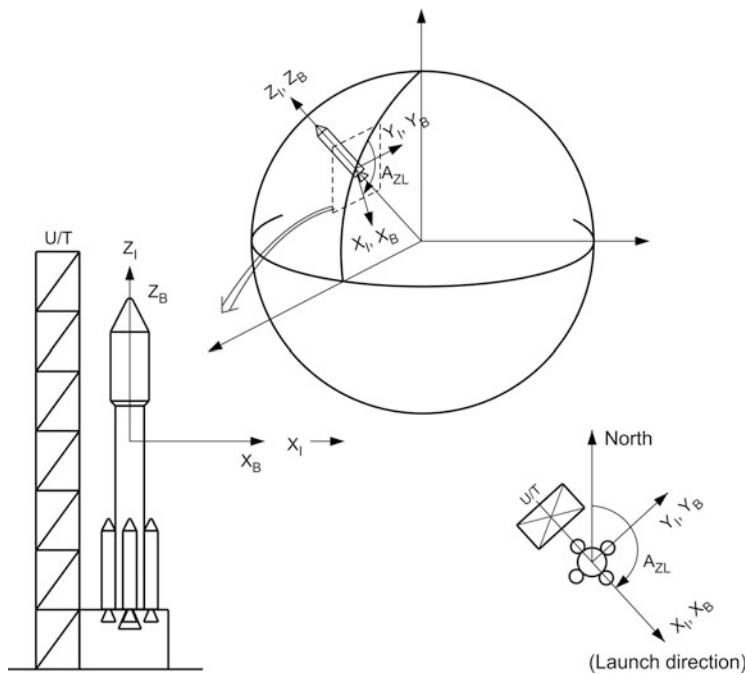


Fig. 14.9 LPI and body frame at time = 0

frame. Detailed formulations regarding the navigational parameters computations using the sensors output are beyond the scope of this book. However, a brief summary of methodology of computations is given in this section.

Generally, launch point inertial (LPI) frame is used to define the navigation parameters. Typical LPI frame, which is frozen at time = 0, is given in Fig. 14.9 and defined as given below:

O_I : Origin, at the launch point, coincides with vehicle CG

Z_I : Along the local vertical

X_I : Along the launch azimuth

Y_I : Completes the right handed system

When the vehicle is on the launch pad, the body axes coincide with the LPI frame axes as given below:

O_B : Vehicle centre of gravity, aligned with O_I

Z_B : Longitudinal (roll) axis of the vehicle, aligned with Z_I axis

X_B : Yaw axis of the vehicle, aligned with X_I axis

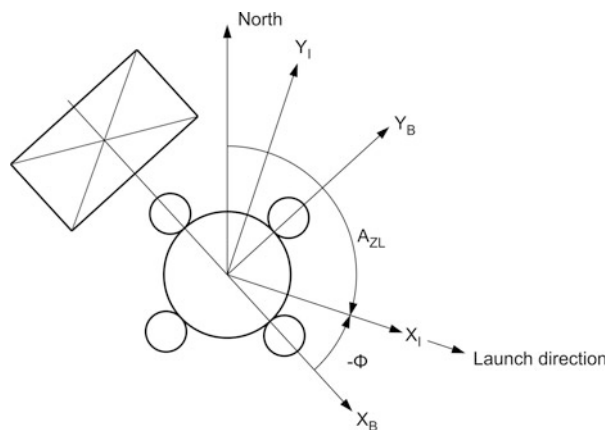
Y_B : Pitch axis of the vehicle, aligned with Y_I axis

$Z_B X_B$ plane is termed pitch plane of the vehicle.

$Y_B Z_B$ plane is termed yaw plane of the vehicle.

$X_B Y_B$ plane is termed roll plane of the vehicle.

Fig. 14.10 LPI and body frame at time = 0



After lift-off, the LPI frame is frozen corresponding to time = 0 whereas the body frame is always attached to the vehicle. Vehicle attitude motion about the pitch, yaw and roll axes are called the pitch, yaw and roll attitude motions, respectively.

Vehicle attitude at any instant of flight can be defined with respect to LPI frame through three Euler angles viz., θ (pitch), Ψ (yaw) and ϕ (roll). A specified sequence of rotation involving the above angles is required to rotate the LPI frame to align with body frame. Typical sequence is: Rotate X_I , Y_I , Z_I about Y_I axis through an angle θ (pitch) leads to a new frame X_1 , Y_1 , Z_1 . Rotating this frame about X_1 axis through an angle Ψ (yaw) leads to another frame X_2 , Y_2 , Z_2 . Now rotate this new frame about Z_2 axis through an angle ϕ (roll) to reach the body axes X_B , Y_B , Z_B . Generally, anticlockwise motion about these axes is considered to be positive motion.

Due to operational reasons, it may not be possible to align the body axes with LPI frame at launch pad. For a typical case, where Z_B coincides with Z_I and X_B , Y_B axes are rotated with respect to X_I , Y_I axes as shown in Fig. 14.10, the inertial system measures the misalignment as the vehicle roll angle ϕ , which can be corrected after vehicle lift-off, i.e., after lift-off, the vehicle control system rotates the vehicle about Z_B axis (roll attitude motion) so that X_B axis aligns with X_I axis before executing any intentional manoeuvre.

At any instant of flight, the navigation parameters are:

\mathbf{r} = position vector of the vehicle centre of gravity (CG) with respect to LPI frame

\mathbf{V} = Velocity (inertial) vector of the vehicle CG with respect to LPI frame

$\{\theta, \Psi, \phi\}$ = Euler angles (pitch, yaw and roll) define the vehicle attitude with respect to LPI frame

$\{\dot{\theta}, \dot{\Psi}, \dot{\phi}\}$ = Euler angle rates

$\{\omega_x, \omega_y, \omega_z\}$ = vehicle body rates with respect to body frame

$\{a_x, a_y, a_z\}$ = vehicle body accelerations with respect to body frame

In the above set $\{\omega_x, \omega_y, \omega_z\}$ and $\{a_x, a_y, a_z\}$ are the measured parameters where the remaining parameters are computed using the above parameters.

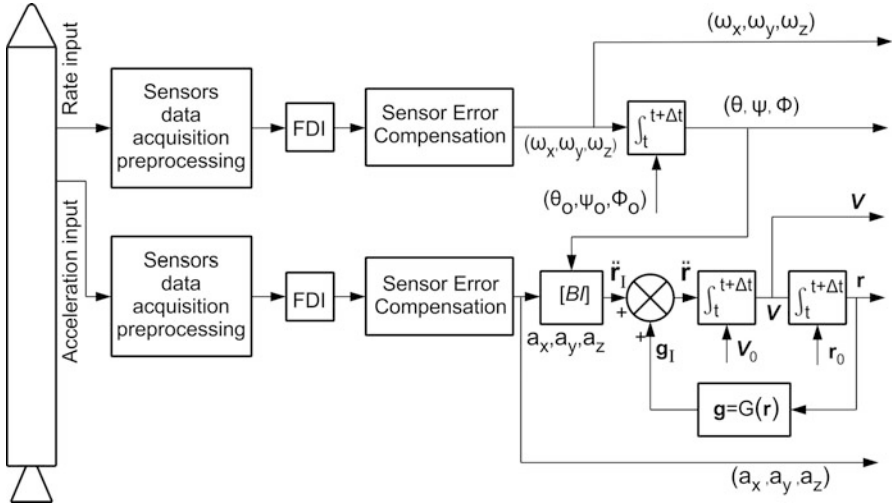


Fig. 14.11 Navigation computations

The accelerometers mounted on the vehicle measures the inertial accelerations (specific forces, i.e., force per unit mass of vehicle) without the gravitational accelerations. Therefore, the above-measured accelerations have to be transformed to LPI frame and total acceleration including gravity have to be numerically integrated to get \mathbf{V} and further integration leads to \mathbf{r} . The integrated navigation computations are explained in Fig. 14.11.

Assuming the matrix $[BI]$ is transforming a vector from body frame to LPI frame, the acceleration vector $\{a_x, a_y, a_z\}^T$ measured in body frame is expressed in LPI frame as given below:

$$\ddot{\mathbf{r}}_I = [BI] \begin{Bmatrix} a_x \\ a_y \\ a_z \end{Bmatrix} \quad (14.3)$$

The total acceleration in LPI frame is given by

$$\ddot{\mathbf{r}} = \ddot{\mathbf{r}}_I + \mathbf{g}_I(\mathbf{r}) \quad (14.4)$$

where $\mathbf{g}_I(\mathbf{r})$ is the gravitational acceleration as function of \mathbf{r} expressed in LPI frame. The velocity and position is then computed as given below:

$$\mathbf{V} = \mathbf{V}_0 + \int_t^{t+\Delta t} \ddot{\mathbf{r}} dt \quad (14.5)$$

$$\mathbf{r} = \mathbf{r}_0 + \int_t^{t+\Delta t} \mathbf{V} dt \quad (14.6)$$

where \mathbf{V}_0 and \mathbf{r}_0 are the initial velocity and position vectors at time t , Δt is the time interval corresponding to the navigation computation cycle.

The transformation matrix $[\text{BI}]$ given in Eq. 14.3 is basically the direction cosines matrix of body frame with respect to the LPI frame as given below:

$$[\text{BI}] = \begin{bmatrix} C_{11} & C_{12} & C_{13} \\ C_{21} & C_{22} & C_{23} \\ C_{31} & C_{32} & C_{33} \end{bmatrix} \quad (14.7)$$

where c_{ij} is the direction cosine of j th axis of body frame with respect to the i th axis of LPI frame. The direction cosines matrix $[\text{BI}]$ can be computed from the measured vehicle attitude rates as given below:

From the measured values of attitude rates $\boldsymbol{\omega} = \{\omega_x, \omega_y, \omega_z\}^T$, the Euler angular rates can be computed as

$$\dot{\theta} = \frac{1}{C_\Psi}(\omega_x S_\phi + \omega_y C_\phi) \quad (14.8)$$

$$\dot{\Psi} = (\omega_x C_\phi - \omega_y S_\phi) \quad (14.9)$$

$$\dot{\phi} = \omega_z + \frac{S_\Psi}{C_\Psi}(\omega_x S_\phi + \omega_y C_\phi) \quad (14.10)$$

From the above equations, Euler angles are propagated as

$$\theta = \theta_0 + \int_t^{t+\Delta t} \dot{\theta} dt \quad (14.11)$$

$$\Psi = \Psi_0 + \int_t^{t+\Delta t} \dot{\Psi} dt \quad (14.12)$$

$$\phi = \phi_0 + \int_t^{t+\Delta t} \dot{\phi} dt \quad (14.13)$$

The direction cosines matrix is then computed as

$$[\text{BI}] = \begin{bmatrix} C_\phi C_\theta + S_\phi S_\Psi S_\theta & -S_\phi C_\theta + C_\phi S_\Psi S_\theta & C_\Psi S_\theta \\ S_\phi C_\Psi & C_\phi C_\Psi & -S_\Psi \\ -C_\phi S_\theta + S_\phi S_\Psi C_\theta & S_\phi S_\theta + C_\phi S_\Psi C_\theta & C_\Psi C_\theta \end{bmatrix} \quad (14.14)$$

In the above equations, the notations, S_θ , C_θ , S_Ψ , C_Ψ , S_ϕ and C_ϕ refer to $\sin \theta$, $\cos \theta$, $\sin \Psi$, $\cos \Psi$, $\sin \phi$, and $\cos \phi$, respectively.

In the above method of attitude computation, when the vehicle yaw attitude, Ψ becomes 90° , there is singularity in the computations of $\dot{\theta}$ and $\dot{\phi}$ and $[BI]$ is undefined. Therefore, to overcome the above problem, generally, quaternion approach is followed for the computation of $[BI]$ matrix which is described briefly below:

Coordinate transformation using quaternion approach is based on Euler's theorem, which states that orientation of a body with respect to a reference frame can be achieved through a single rotation about a single axis. The axis of rotation is called Euler axis and angle of rotation is called Euler rotation. The above principle is used to define vehicle attitude with respect to LPI frame through quaternion parameters. Quaternion is a four parameter quantity represented as

$$\mathbf{e} = e_0 + i\mathbf{e}_1 + j\mathbf{e}_2 + k\mathbf{e}_3 \quad (14.15)$$

where, $\mathbf{i}, \mathbf{j}, \mathbf{k}$ follow the rules $\mathbf{ij} = -\mathbf{k}, \mathbf{jk} = -\mathbf{i}, \mathbf{ki} = -\mathbf{j}$ and $\mathbf{ijk} = -1$.

e_0 is the scalar part of quaternion called scalar and $\{i\mathbf{e}_1 + j\mathbf{e}_2 + k\mathbf{e}_3\}$ is the vector part of quaternion, called vector

Applying the quaternion for Euler theorem, the rotational quaternion can be defined as

$$\mathbf{e} = \begin{Bmatrix} \cos(\phi/2) \\ i \sin(\phi/2) \\ j \sin(\phi/2) \\ k \sin(\phi/2) \end{Bmatrix} \quad (14.16)$$

where $\{\mathbf{i}, \mathbf{j}, \mathbf{k}\}^T$ is the unit vector of Euler axis with respect to LPI frame and ϕ is the Euler rotation angle. Using the above rotational quaternion, the quaternion parameters rates are related to the body rates $\boldsymbol{\omega} = (\omega_x, \omega_y, \omega_z)^T$ as

$$\dot{\mathbf{e}} = \frac{1}{2}[\mathbf{E}]\boldsymbol{\omega} \quad (14.17)$$

where \mathbf{e} is defined as

$$\mathbf{e} = \{e_0, e_1, e_2, e_3\}^T \quad (14.18)$$

and the quaternion matrix $[\mathbf{E}]$ is defined as

$$[\mathbf{E}] = \begin{bmatrix} -e_1 & -e_2 & -e_3 \\ e_0 & -e_3 & e_2 \\ e_3 & e_0 & -e_1 \\ -e_2 & e_1 & e_0 \end{bmatrix} \quad (14.19)$$

With the initial conditions at lift-off, as explained in Chap. 8 (Eqs. 8.99 and 8.100), the quaternion parameters can be propagated using Eq. 14.17 as done for the Euler attitude angles. Using the instantaneous quaternion parameters, the [BI] matrix is computed as

$$[\text{BI}] = \begin{bmatrix} (\mathbf{e}_0^2 + \mathbf{e}_1^2 - \mathbf{e}_2^2 - \mathbf{e}_3^2) & 2(\mathbf{e}_1\mathbf{e}_2 - \mathbf{e}_0\mathbf{e}_3) & 2(\mathbf{e}_1\mathbf{e}_3 + \mathbf{e}_0\mathbf{e}_2) \\ 2(\mathbf{e}_1\mathbf{e}_2 + \mathbf{e}_0\mathbf{e}_3) & (\mathbf{e}_0^2 - \mathbf{e}_1^2 + \mathbf{e}_2^2 - \mathbf{e}_3^2) & 2(\mathbf{e}_2\mathbf{e}_3 - \mathbf{e}_0\mathbf{e}_1) \\ 2(\mathbf{e}_1\mathbf{e}_3 - \mathbf{e}_0\mathbf{e}_2) & 2(\mathbf{e}_0\mathbf{e}_1 + \mathbf{e}_2\mathbf{e}_3) & (\mathbf{e}_0^2 - \mathbf{e}_1^2 - \mathbf{e}_2^2 + \mathbf{e}_3^2) \end{bmatrix} \quad (14.20)$$

14.4.3 Characterization of INS Errors and Performance Specifications

The navigation performance plays a dominant role in deciding the accuracy of the achieved orbit. The errors that contribute to INS performance in any mission are due to:

- (a) Accelerometers errors in measuring the acceleration
- (b) Gyros errors in measuring the angular rates
- (c) Initial alignment error and
- (d) Navigational computational error

The above errors in a launch mission reflect as position, velocity vector and attitude errors with respect to the true values. Since the downstream guidance and control system uses the navigation computed parameters for generating the desired attitude and control command, the errors in navigational parameters reflect as errors in satellite injection parameters. These errors cause deviated satellite orbit with respect to the specified one. It is therefore necessary to carry out the performance analysis to decide on the design specification of INS for a given mission and to confirm the adequacy of the specifications to meet the final defined mission accuracies. All types of accelerometers and gyros used in the navigation system exhibit the errors such as bias, scale factor, cross coupling error, and random noise. In addition higher order errors are to be accounted depending on the type of sensor used. These errors have a systematic part and a random part. Each systematic error has components like a fixed contribution and a temperature dependent variation. The systematic part is generally determined experimentally and compensated in the onboard navigation computer. The repeatability variation on the errors is different each time the sensor is used but remains constant within single use. The in-run variation results in error changing slowly during the course of operation. It is difficult to correct such changes except the correction through other navigational aids. Additionally, the random part of the error also cannot be compensated.

All the systematic errors are appropriately modeled in the navigation computer and compensated based on the extensive calibration data. Once the navigation system is realized, the performance is evaluated to confirm that it meets the mission specifications. The performance evaluation is carried out under two accurate

inputs, namely: (a) acceleration due to gravity, and (b) the spin rate of the Earth. However, this evaluation is not adequate to validate the system under its full range of operation. Therefore, precision rate table, mobile test van, aircraft, etc. are used to evaluate the performance for its full range.

14.4.4 Redundancy Management

As the mission critical functions of, guidance and control are based on the navigational parameters and hence the INS should have very high reliability for mission success. Therefore, systems are to be built with high level of redundancy both at functional and component level. Triple modular redundancy (TMR) and quadruple modular redundancy (QMR) are some of the techniques generally employed in such systems. Suitable schemes for failure detection, isolation and reconfiguration (FDIR) are also necessary to achieve high reliability of the systems. FDIR algorithms are to be designed carefully to identify the failure, to isolate automatically the failed chain and to reconfigure the system to provide the continuity of operations. A typical diagram showing the triple modular redundancy for INS with three chains is given in Fig. 14.12.

In this TMR system, each chain is independent and the failure of each chain can be detected and isolated by comparing the outputs of chains through appropriate logic. The overall reliability of the system can be further improved by adopting an advanced fault tolerant architecture as given in Fig. 14.13.

In this system, the sensor and sensor electronics are considered as one module and the processor as other module. The sensor modules are cross strapped with processor module. This helps in enhancing the system reliability but considerable care is needed in generating the redundancy logics which is quite complex. The system can be further improved by increasing the number of modules in sensors,

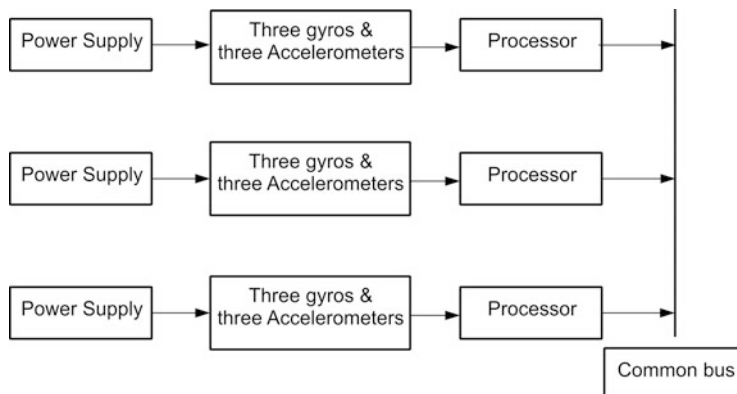


Fig. 14.12 Triple modular redundancy INS

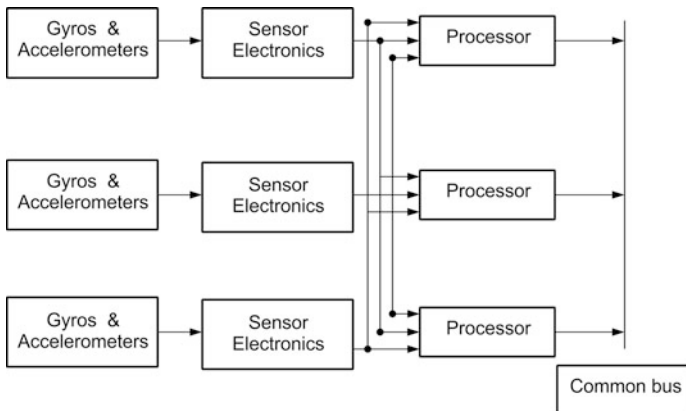


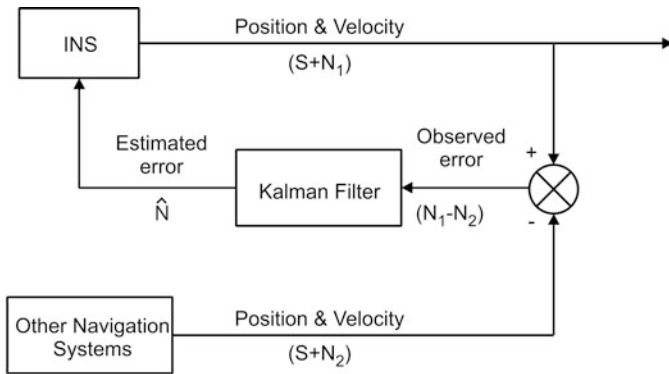
Fig. 14.13 Advanced fault tolerant architecture

sensor electronics and by introducing the cross strapping between these modules. However, the redundancy logics becomes much more complex and very detailed evaluation of the system is needed before implementing in the vehicle system.

14.4.5 Aided Navigation

In a navigation system the vehicle states, namely velocity, position and orientation at any given time instant are estimated by a relative increment from the previous known state using the information provided by the inertial sensors. The sensor output errors accumulate at each step and there is a growth of continuous unbounded error during the entire regime of flight. It is possible to minimize these errors with external aiding or with another navigational aid. Stellar inertial system using precision stellar sensors is another option, very useful in long duration missions including interplanetary missions and space platforms particularly for attitude aiding. Such systems are termed as aided inertial navigation systems. The error growth in the navigation system is corrected with assistance of an external measurement. A typical aided inertial navigation system is shown in Fig. 14.14.

The external measurement in this case has to duplicate the navigation parameters like velocity, position and orientation. The measurements from both INS and external sources are compared and the observed error is passed through a filter to estimate the errors of velocity and position and fed to INS to minimize the error growth. Generally, Kalman Filter is used which is essentially a recursive algorithm for the estimation of states in a system. It needs measurements from all essential sensors and also a comprehensive mathematical model of the system which describe the dependency of different states and dependency of measurements in the states.



S = True state

(N_1-N_2) = Observed error input to the estimate

N_1 = INS error

\hat{N} = Estimated INS error

N_2 = External navigation error

Fig. 14.14 Typical aided INS

Usually the Kalman Filter has an initial estimate at time t_0 . It predicts a new estimate at t_1 based on the mathematical model used. The initial uncertainty and the accuracy of the model contribute to the uncertainty in the predicted estimate. Utilizing the measurements available at t_1 and predicted estimate, the algorithm is able to generate an updated estimate at t_1 . The process is repeated at defined periodical intervals and is able to predict the optimal estimates.

The stellar navigation system utilizes the measurements of star sensors. Making use of the stellar observations, sensor error model using the available error statistics, and the real time vehicle motion, Kalman Filter updates and calibrates the integrated system. Thus the aided system offers self contained operation and improved performance.

14.5 Guidance and Steering Law

Optimum trajectory of a launch vehicle, which provides the maximum payload into the specified orbit, satisfying all the vehicle and mission related constraints is designed on ground with sophisticated software tools. Thrust is the main force acting along the longitudinal axis of the vehicle. Other disturbance forces can also be expressed in vehicle frame of axes. The optimum trajectory design involves the determination of a vehicle attitude (steering) program which directs the given thrust or acceleration history including the specified disturbances in the optimum direction with respect to a reference frame. Generally, the vehicle parameters, environment parameters and the known disturbance profiles as predicted on ground are used for the design of the optimum steering program.

However, during its flight, the vehicle experiences severe disturbances and also uncertainty on vehicle parameters such as thrust-time history, propellant consumption, specific impulse etc., with respect to the predicted values. The ground computed steering program is designed using the predicted propulsion parameters. The parametric uncertainties in flight cause the deviation of the trajectory from the desired one. This results into a different orbit from the mission targeted orbit. Therefore, to achieve high injection accuracy for the satellite under such environment, onboard closed loop guidance system is essential. The instantaneous position and velocity of the vehicle measured by the navigation act as inputs to guidance system. The major function of guidance system is to generate steering commands to the vehicle from lift off to satellite injection and also during the post-injection maneuvers. This has to be accomplished with the minimum expenditure of energy and minimum injection errors. While steering, the vehicle guidance system has to satisfy various constraints of trajectory such as limiting the vehicle turning rates within safe specified levels, impacting the spent stages within the safe zones and ensuring smooth transition from one phase of operation to another. Finally, the guidance system has to generate the necessary commands to shut-off the engine once the target conditions are satisfied.

14.5.1 Guidance System Objectives and Functional Requirements

Objective of the launch vehicle guidance system is to steer the vehicle from the instantaneous state to the desired destination optimally, satisfying the constraints imposed by various sub-systems and environment. Typical mission objectives have to satisfy the injection of the satellite: (a) into a maximum possible orbit, within the launch vehicle capability which is mission specified; and (b) into the specified orbit with minimum inclination

Typical constraints are:

- The range safety requirements which limits the instantaneous impact point of the vehicle during flight and the impact point of the spent stages
- The capacity limitations of the propulsion systems
- Vehicle structural load limitations
- Thermal loads on the vehicle
- Limitations imposed by the actuators and the control systems

To meet the above mission objectives, the general functional requirements of a guidance scheme are as given below:

1. Guidance function starts at lift-off and continues till the final target conditions of the vehicle are met.
2. Provision has to be there to account for variable launch azimuth to accommodate different missions.

3. During the atmospheric phase generally, ground-computed steering program stored onboard ensures the minimum load on the vehicle (altitude-based wind-biased steering program minimizes the vehicle loads considerably). As the steering program is not computed onboard using the vehicle instantaneous state, the guidance strategy in this phase is called open loop guidance.
4. Closed loop guidance is initiated once the vehicle clears the atmospheric phase.
5. The lower stages shut-off commands have to ensure safe impact of the spent stage.
6. Steering attitudes are generally held constant during the stage transition periods.
7. If there are coasting regimes in a mission, the steering attitude generated has to be such that at the initiation of the next stage the attitude steering is smooth.
8. If there is a need to dip altitude in a trajectory the thermal constraints of the vehicle are to be met with.
9. The attitude steering computation periodicity has to be decided based on the mission and overall NGC requirements.
10. The final stage shut-off command has to ensure the final mission specifications.
11. The commanded attitude rates throughout the guidance phase have to be within specified values.
12. The attitude steering rate has to be held constant during the ejection regime for the payload fairing.
13. The steering profile generated by guidance law has to meet the target conditions optimally with minimum expense of fuel for the conditions of trajectory deviations.
14. The guidance law has to be robust to cater to larger deviations of vehicle trajectory.
15. The guidance law has to have provision for fault detection and isolation.

14.5.2 *Guidance Concepts*

As part of mission design, optimum trajectory is to be designed to maximize a defined performance index. The payload is always optimized for the given vehicle data, satisfying all the vehicle and mission related constraints, and the design is carried out on ground for the integrated trajectory from lift-off till satellite injection using sophisticated trajectory optimization tools considering detailed models for vehicle and environment. The output of the trajectory design process is the vehicle attitude history (steering program) from lift-off till satellite injection. One primary criterion for steering program design during atmospheric flight phase is to reduce the vehicle load. This is achieved by designing the vehicle attitude history to follow zero angle of attack for the specified wind condition (gravity turn trajectory). Once the vehicle crosses the dense atmosphere, steering program is designed to maximize the payload while satisfying the path constraints such as heat flux, stage impact

points, instantaneous impact point and terminal constraints such as defined orbital conditions.

During flight, guidance functions are achieved through two approaches: (a) open loop guidance and (b) closed loop guidance. In the open loop guidance, the steering program designed on ground is stored onboard as look up table or segments of functions. The look up table is either stored as function of time or function of certain vehicle performance parameters such as altitude, inertial velocity, or relative velocity. During flight, depending on time or vehicle performance parameters from the navigation data, the instantaneous desired attitude (steering command) is generated from the look up table. This scheme is very simple to mechanize in the vehicle onboard and is having the following features:

1. If the vehicle and environment parameters during flight are exactly following the ones used for design on ground, then orbit achieved can be very close to the expected one.
2. In case, if there is deviation in vehicle performance (thrust, Isp etc.) and environmental parameters during flight, then the stored profile corresponding to the nominal performance can end up with larger orbital dispersions.
3. If the steering program is implemented as function of vehicle performance parameters, then the trajectory dispersions are less. Especially this strategy helps to a great extent during atmospheric flight phase wherein the additional angle of attack build up due to performance dispersion can be minimized. But the trajectory deviation still exists.

The closed loop guidance concepts make use of onboard navigation data as starting point, optimize the remaining trajectory, generate the desired attitude steering and decide the engine ignition and shut-off time in real time to achieve the defined target precisely. Due to these features, the closed loop guidance strategy has the ability to account for wider dispersions in the vehicle performance parameters and trajectory deviations with respect to the nominally predicted ones and improve the satellite injection accuracy considerably.

However, due to the complexity and limitations of existing systems to implement closed loop guidance during atmospheric phase which satisfies both vehicle load and mission constraints simultaneously and to get the feasible solution within the available computational time, normally, almost all launch vehicles follow open loop guidance concept till it crosses sensible atmosphere. Therefore, the closed loop guidance is initiated invariably in exo-atmosphere phase and trajectory deviations arising out of open loop guidance at the end of atmosphere phase are corrected by closed loop guidance system in the subsequent stages of flight. A large number of closed loop guidance algorithms are available for use in launch vehicles but the choice depends on (1) accuracy of injection, (2) pre-computation needed, (3) optimality of the solutions and (4) computational load on board.

14.5.3 Closed Loop Guidance Schemes

One primary function of closed loop guidance is to generate the desired vehicle attitude to optimize the trajectory in real time to ensure maximum payload or minimum consumption of propellant. The computation of optimum attitude demands online solution of an optimal control problem with the navigation measured states as the initial conditions and the targeted mission requirements as the final conditions. To increase the optimality of the computed desired attitude and in turn to improve the accuracy of the achieved orbit, the guidance computations are repeated at fixed intervals based on the updated navigation measurements. This calls for getting guidance solution within the allotted time in the vehicle onboard computers. Approaches based on nonlinear optimization and numerical solutions of optimal control which demand heavy computational load are not preferred. Due to the numerical iterations, requirements of such schemes reduce the reliability of the system due to the possibility of non-convergence. Therefore, guidance schemes which provide robust analytical solution onboard are preferable.

To derive closed form solutions for reliable on-board implementation, approximating assumptions are imposed on the optimal control formulation and simplified algorithms are derived. Large numbers of guidance laws are available in literature because each approximation leads to a different law which is suitable for the vehicle and mission satisfying those assumptions. Once the closed form solution is available, correction factors and compensation techniques are used on the solution to account for the errors introduced due to the approximations.

Guidance strategies can be broadly classified into two groups (a) explicit guidance schemes and (b) implicit guidance schemes. In explicit scheme, analytical solution of the equations of motion are used to compute the optimal trajectories in real time based on an optimum or near optimum steering law. In this scheme, minimum information from the nominal trajectory is used. Implicit algorithms, on the other hand, are based on a precomputed trajectory or trajectories. The nominal optimal trajectory is predetermined before the flight, and on board attitude steering computation is about correcting the errors from this optimal trajectory through appropriate guidance laws.

Advantages of implicit and explicit guidance strategies are exploited in dual mode guidance where computationally intense explicit guidance is used at larger interval to compute the attitude steering and trajectory. Implicit guidance is used to track the trajectory computed by explicit guidance during shorter intervals.

14.5.4 Implicit Guidance Schemes

Implicit closed loop guidance schemes are invariably used where the mission is fully defined. The nominal trajectory, which is defined before the flight, is used as a reference for onboard guidance computations. The onboard system measures the

trajectory deviations from the prestored one and generates optimum steering commands to drive the vehicle to follow the predefined trajectory. The various implicit schemes which are generally used for launch vehicle guidance are: (1) Delta-guidance, (2) Q-guidance and (3) Linearized perturbation guidance.

14.5.4.1 Schemes Based on Required Velocity

The Delta-guidance and Q-guidance schemes are based on the concept of required velocity. The required velocity vector is defined as the velocity vector that is needed at any instant of flight to achieve the desired terminal conditions under free flight trajectory. At each space-time point, the required velocity vector is computed satisfying the general guidance constraints. The attitude steering laws are designed such that the vehicle reaches the required velocity at the thrust cut-off. This objective is implemented through achieving velocity-to-be (V_g) gained to zero at burn out as follows: Guidance law steers the vehicle such that the vehicle thrust direction align with the V_g direction. If the vehicle has the capability of impulsive velocity addition, then the velocity-to-be gained can be instantaneously brought to zero, thus meeting the mission objectives. Since there is finite time for propulsive stage thrusting and also there is limit on the rotational velocity of the vehicle, steering laws are developed to drive all components of the velocity V_g to zero simultaneously at the stage burnout.

The delta-guidance computes the required velocity vector through Taylor series approach about a nominal value and achieves this at burnout through optimization. The Q-guidance computes the V_g and drives this quantity to zero at burnout. The required velocity is computed in these two schemes by different strategies. The target point definitions for these two methodologies are different. The target point of delta-guidance is the predefined optimum nominal point which is computed on ground by detailed methods, whereas target point in Q-guidance is the one in which V_g becomes zero.

Delta-Guidance

Delta-guidance scheme expands the required velocity in Taylor series about nominal target point. A good approximation for the required velocity at a location other than the nominal burnout point can be estimated by substituting the position vector into the Taylor series. The required velocity along the X-axis of reference frame is given as

$$V_{rx} = V_{rx0} + k_{xx}\Delta x + k_{xy}\Delta y + k_{xz}\Delta z + k_{xt}\Delta t + k_{xxx}\Delta x^2 + k_{xxy}\Delta x\Delta y + k_{xyy}\Delta y^2 + \dots \quad (14.21)$$

where (x_0, y_0, z_0, t_0) is the nominal target point, V_{rx0} is the nominal velocity at

target along x direction, $\Delta x = (x - x_0)$, $\Delta y = (y - y_0)$ etc., the delta quantities, giving the scheme the name. k_{xx} , k_{xy} , ... etc. are the partial derivatives as per Taylor series expansion. Similar is the case for V_{ry} and V_{rz} .

The number of terms to be selected depends on the accuracies required at burnout. The partial derivatives of Eq. (14.21) are computed as follows:

1. The required velocity vector (V_{rx} , V_{ry} , V_{yz}) corresponding to each set of (x , y , z , t) are computed using perturbations through iterative procedures with the help of detailed model for vehicle and environment.
2. The empirically generated (V_{rx} , V_{ry} , V_{rz}) and the corresponding perturbations are used to generate the partial derivatives by minimizing the error in least square sense as given below:

Let ϵ_k be the difference between the required velocity using Taylor's series and the required velocity as computed by detailed model as given by

$$\epsilon_k = V_{rx}(\Delta x_k, \Delta y_k, \Delta z_k, \Delta t_k) - V_{rx0} - \sum_{j=1}^n k_{xj} \Delta \xi_j (\Delta x_k, \Delta y_k, \Delta z_k, \Delta t_k) \quad (14.22)$$

where $V_{rx}(\Delta x_k, \Delta y_k, \Delta z_k, \Delta t_k)$ is the required velocity as computed in the simulations at the point $(x_0 - x_k), (y_0 - y_k)$ etc., and $\Delta \xi_j$ are the perturbation quantities Δx , Δy , Δz etc., n is the number of terms in Eq. (14.21). The mean square value of the error ϵ_k is found by evaluating the above error in m number of points evaluated during simulation as given by

$$\epsilon^2 = \sum_{k=1}^m \epsilon_k^2 \quad (14.23)$$

The partial derivatives are estimated by minimizing ϵ^2 as follows. Differentiating Eq. (14.23) with respect to each of k_{xj} where x is assigned 1 to m and equating to zero give n simultaneous linear algebraic equations, which can be solved for getting each of the k_{xj} .

Once the required velocity components are estimated, then the steering aspect of delta-guidance is similar to the Q-guidance as explained below.

Q-Guidance

This scheme also uses the required velocity concept to compute the desired attitude of the vehicle to the target point. This scheme makes use of the velocity-to-be gained (V_g) to achieve the required velocity at the specified target point. Instead of updating V_r as in the case of delta-guidance, in Q-guidance, V_g is updated through first order differential equations as given below:

Neglecting atmosphere and external disturbances,

$$\frac{d\mathbf{r}}{dt} = \mathbf{V} \quad (14.24)$$

$$\frac{d\mathbf{V}}{dt} = \mathbf{g} + \mathbf{a}_T \quad (14.25)$$

where \mathbf{r} is the position vector, \mathbf{V} is the velocity vector, \mathbf{g} is the gravitational acceleration vector and \mathbf{a}_T is the vehicle acceleration due to thrust. Assuming \mathbf{V}_r is the instantaneous required velocity vector, then the velocity-to-be gained vector is given by

$$\mathbf{V}_g = \mathbf{V}_r - \mathbf{V} \quad (14.26)$$

and the derivatives of \mathbf{V}_g is

$$\dot{\mathbf{V}}_g = \dot{\mathbf{V}}_r - \dot{\mathbf{V}} \quad (14.27)$$

$\dot{\mathbf{V}}_r$ can be given by

$$\dot{\mathbf{V}}_r = \left(\frac{\partial \mathbf{V}_r}{\partial \mathbf{r}} \right) \left(\frac{d\mathbf{r}}{dt} \right) + \frac{\partial \mathbf{V}_r}{\partial t} \quad (14.28)$$

Using Eq. (14.26) and Eq. (14.24), Eq. (14.28) can be written as

$$\dot{\mathbf{V}}_r = \left(\frac{\partial \mathbf{V}_r}{\partial \mathbf{r}} \right) (\mathbf{V}_r - \mathbf{V}_g) + \frac{\partial \mathbf{V}_r}{\partial t} \quad (14.29)$$

Using Eq. (14.29) and Eq. (14.25), Eq. (14.27) can be written as

$$\dot{\mathbf{V}}_g = \left(\frac{\partial \mathbf{V}_r}{\partial \mathbf{r}} \right) (\mathbf{V}_r - \mathbf{V}_g) + \frac{\partial \mathbf{V}_r}{\partial t} - (\mathbf{g} + \mathbf{a}_T) \quad (14.30)$$

For free fall trajectory,

$$\frac{d\mathbf{r}}{dt} = \mathbf{V}_r \quad (14.31)$$

And using Eq. (14.28)

$$\frac{d\mathbf{V}_r}{dt} = \mathbf{g} = \left(\frac{\partial \mathbf{V}_r}{\partial \mathbf{r}} \right) \mathbf{V}_r + \frac{\partial \mathbf{V}_r}{\partial t} \quad (14.32)$$

Using Eq. (14.32) in Eq. (14.30) lead to

$$\dot{\mathbf{V}}_g = - \left(\frac{\partial \mathbf{V}_r}{\partial \mathbf{r}} \right) \mathbf{V}_g - \mathbf{a}_T \quad (14.33)$$

which can be given as

$$\dot{\mathbf{V}}_g = \mathbf{Q}\mathbf{V}_g - \mathbf{a}_T \quad (14.34)$$

where,

$$\mathbf{Q} = -\left(\frac{\partial \mathbf{V}_r}{\partial \mathbf{r}}\right) \quad (14.35)$$

The matrix Q relates the differential change in the required velocity with respect to the differential change in position with time held constant. The Q-matrix can be precomputed as done for the delta guidance. In Q-guidance, the steering is designed to drive the \mathbf{V}_g to zero at target.

Steering Law

In both “delta” and “Q” guidance schemes, the steering law is designed to drive the components of \mathbf{V}_g to zero simultaneously. Two methods are explained below:

Method-1

The steering law is such that the vehicle attitude (thrust direction) is aligned with \mathbf{V}_g as shown in Fig. 14.15. This is achieved by rotating the vehicle longitudinal axis about an axis which is normal to \mathbf{a}_T and \mathbf{V}_g . Therefore, assuming ω_c is the steering rate of the vehicle with respect to the body axes, then

$$\omega_c \propto \mathbf{a}_T \times \mathbf{V}_g \quad (14.36)$$

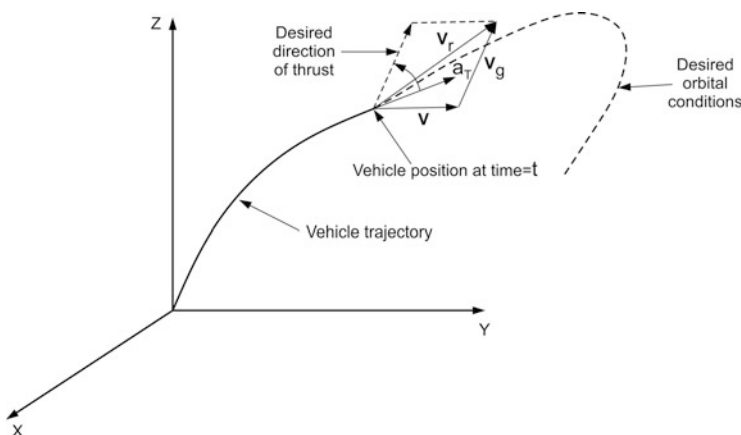


Fig. 14.15 \mathbf{V}_g – Guidance steering

Where, \mathbf{a}_T and \mathbf{V}_g are also expressed in vehicle body frame. Therefore,

$$\boldsymbol{\omega}_c = k \mathbf{a}_T \times \mathbf{V}_g \quad (14.37)$$

where the proportionality constant, k is called the gain. In order to take care of both pitch and yaw steering, different values of gain factors can be used for pitch and yaw. The gain values are designed such that the attitude steering ensures components of \mathbf{V}_g to zero simultaneously.

Method-2

Unit vector along \mathbf{V}_g is given by

$$\mathbf{u}_g = \frac{\mathbf{V}_g}{V_g} \quad (14.38)$$

and therefore,

$$\dot{\mathbf{u}}_g = \frac{V_g \dot{\mathbf{V}}_g - \dot{V}_g \mathbf{V}_g}{V_g^2} \quad (14.39)$$

The rotational rate of \mathbf{V}_g is given by

$$\boldsymbol{\omega} = \mathbf{u}_g \times \dot{\mathbf{u}}_g \quad (14.40)$$

After simplification,

$$\boldsymbol{\omega} = \frac{\mathbf{V}_g \times \dot{\mathbf{V}}_g}{V_g^2} \quad (14.41)$$

As V_g decreases, $\boldsymbol{\omega}$ increases rapidly. Therefore, in reality, the attitude steering law is given by

$$\boldsymbol{\omega}_c = k(\mathbf{V}_g \times \dot{\mathbf{V}}_g) \quad (14.42)$$

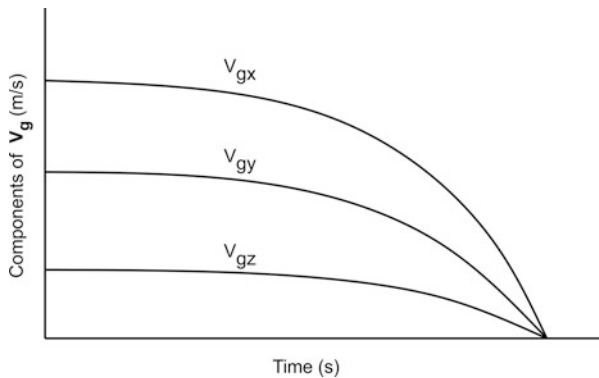
The cross product steering law makes the vehicle fly at near constant attitude. At the initiation of the scheme, the guidance law demands larger turning rate and once stabilized, the steering is almost constant ($\omega_c \approx 0$) and makes only changes thereafter. The system functions such that, even though some component of \mathbf{V}_g is small, it ensures that all the components become zero simultaneously as given in Fig. 14.16.

Once the steering command is computed, the vehicle attitude command in different frames can be computed as per the requirements of vehicle autopilot.

14.5.4.2 Explicit Form of Required Velocity-Based Guidance Scheme

In case the desired orbital conditions of Fig. 14.15 are expressed in terms of angular momentum (\mathbf{H}_d) and apogee radial distance (r_d), then the required velocity vector at

Fig. 14.16 Components of \mathbf{V}_g



any instant of flight can be analytically computed. The vehicle desired attitude steering can be designed using the cross product steering law as explained above.

14.5.4.3 Linearized Perturbation Guidance Scheme

In linearized perturbation guidance, it is assumed that the deviations between the nominal and actual trajectories are small since reference trajectory and control are well-defined for a flight. The nonlinear equations can be approximated to linear differential equations and thus linear theory can be applied to generate the optimum steering law. During the actual flight, there are errors in the system and it is necessary to correct these errors. The nonlinear equations of motion of the vehicle are having both state and control vectors and it is possible to linearize the same using appropriate technique. A suitable controller can be designed to adjust the associated control vector to eliminate the errors. The detailed derivation of the equations is beyond the scope of this book and can be seen in reference listed in the end.

14.5.5 Explicit Guidance Schemes

The implicit guidance schemes are very simple and depend largely on the precomputations on ground. Since these schemes are based on the predefined nominal, the optimality of the solution suffers for wider trajectory deviation. Therefore, operating regimes of these schemes are limited. However, these schemes are best suited for the solid propulsive stages. On the other hand, the explicit schemes generate the optimal steering in real time based on the actual performance of the vehicle without the necessity of ground-based computations and the solutions result into more accurate and optimal results. Due to the adaptive nature of this scheme, it can handle wider dispersions on the flight trajectory deviations and hence

this scheme is more attractive. Also, these schemes are best suited for propulsive stages with liquid engines as the constant thrust with constant mass flow rates of these engines are beneficial to achieve the closed form solutions. Along with this feature, the precise shut-off of the liquid engines based on “Time-to-go” as computed by this scheme ensures very accurate satellite injection. However, the onboard computations involved are large.

In the explicit guidance scheme, the optimal desired attitude is obtained by solving the equations of motion repeatedly during the flight. In these schemes, the aim is to find the vehicle attitude angle such that certain performance index and flight duration are minimized, satisfying the equations of motion and initial and target conditions. Applications of calculus of variation yield the optimal solution to the problem. But generally this requires numerical integration which is not suited for onboard applications. Analytical solutions are always preferred in the guidance mechanization and to achieve this, certain simplifications are essential. This in turn affects the optimality of the solution. However, suitable corrections can be implemented to retain the optimality of the solution.

In explicit guidance schemes, the guidance law is derived in a parameterized form either by empirical methods or by calculus of variations based optimal control approach. Once the guidance law, the boundary conditions defined by the mission requirements and the navigation measured states are available, the state equations are explicitly solved to compute the unknown parameters of the attitude steering law. The explicit guidance schemes are basically path adaptive and commonly used methods are: (a) Explicit path adaptive or explicit E guidance, (b) flat earth guidance (FE) and (c) empirical path adaptive guidance.

14.5.5.1 FE Guidance Scheme

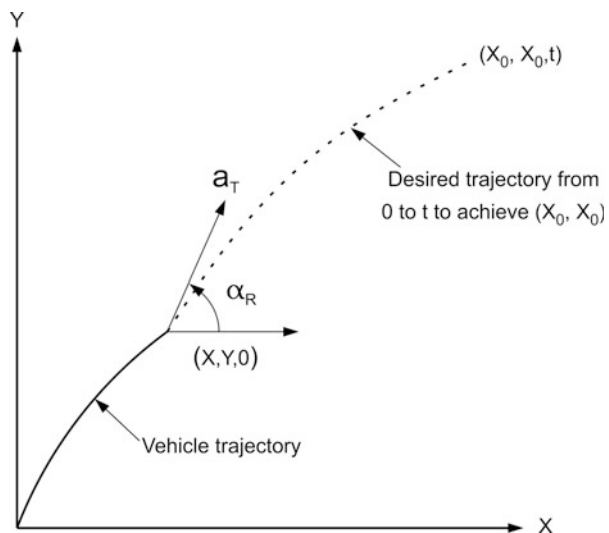
Based on the calculus of variations approach, optimum analytical solution for attitude steering law can be achieved for finite thrust-time curve with the following assumptions:

1. Flat Earth with constant gravitational field
2. No aerodynamic forces
3. Propulsive stages with constant thrust and constant mass flow rate (characteristics of liquid engines)

Under such conditions, for the case of planar motion as given in Fig. 14.17, to achieve the target position (X_0, Y_0) and velocity (\dot{X}_0, \dot{Y}_0) from an initial condition, the optimum thrust direction, α_R , is given by [16]

$$\tan \alpha_R = \frac{C_1 + C_2 t}{C_3 + C_4 t} \quad (14.43)$$

Fig. 14.17 Vehicle attitude and planar motion



where C_1, C_2, C_3, C_4 are constants and time t is measured from instantaneous point to the target. For the case of down range, distance is a free variable, i.e., the target X_0 is not constrained, then $C_4 = 0$. In this case, the optimum steering as given in Eq. (14.43) can be written as

$$\tan \alpha_R = \left(\frac{C_1}{C_3} \right) + \left(\frac{C_2}{C_3} \right) t = A + Bt \quad (14.44)$$

For the case where only target velocities are constrained, the optimum attitude is a constant angle given by

$$\tan \alpha_R = \left(\frac{C_1}{C_3} \right) \quad (14.45)$$

Generally, the launch vehicle guidance law has to take care of three-dimensional motion. This is the case either for three dimensional trajectory or for correcting the out-of-plane trajectory deviations. In order to solve this problem, a guidance frame as defined in Fig. 14.18 is used. This reference frame is explained below:

O: Origin, at the center of Earth

w: Along the line joining the centre of Earth and vehicle position, positive outward

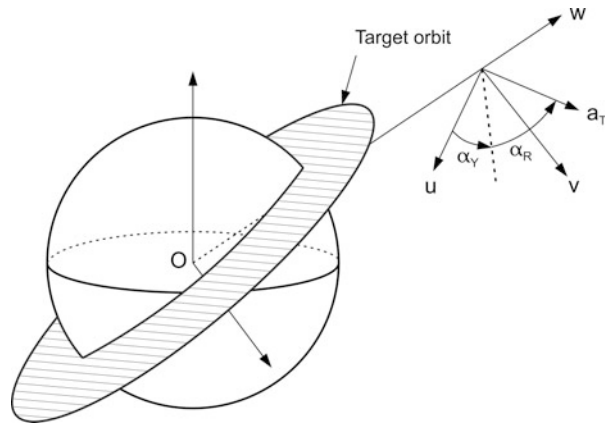
u: Parallel to the target orbital plane, positive along the orbital motion of satellite

v: Completes the right handed triad

The vehicle thrust direction is defined with respect to the guidance reference frame as given below:

α_R : Angle between thrust direction and projection of thrust in uv-plane

α_Y : Angle between u-axis and the projection of thrust in uv-plane

Fig. 14.18 Guidance frame

Using the assumptions of flat Earth, vacuum flight and liquid engines, the optimum steering angles for three-dimensional trajectory are given as [17]

$$\sec \alpha_Y \tan \alpha_R = A + Bt \quad (14.46)$$

$$\tan \alpha_Y = C + Dt \quad (14.47)$$

To compute the desired attitude angles of vehicle thrusting direction with respect to the guidance reference frame α_R and α_Y , it is necessary to compute the coefficients A, B, C, D and to shut-off the engine once the required orbital conditions are achieved, the time-to-go, T_{go} is also required. These five parameters are determined to meet the set target conditions, satisfying the trajectory dynamics.

The equations of motion with respect to the guidance frame over flat Earth are given below:

$$\dot{u} = a_T \cos \alpha_R \cos \alpha_Y \quad (14.48)$$

$$\dot{v} = a_T \cos \alpha_R \sin \alpha_Y \quad (14.49)$$

$$\dot{w} = a_T \sin \alpha_R - g \quad (14.50)$$

$$\dot{X} = u \quad (14.51)$$

$$\dot{Y} = v \quad (14.52)$$

$$\dot{Z} = w \quad (14.53)$$

where a_T is the specific acceleration and g is constant gravitational acceleration.

To ensure the solution α_R and α_Y be corresponding to the realistic one, two corrections terms are introduced. One correction term for α_R is \bar{g} and for α_Y is \bar{e} and the equations of motion is rewritten as

$$\dot{u} = a_T \cos \alpha_R \cos \alpha_Y \quad (14.54)$$

$$\dot{v} = a_T \cos \alpha_R \sin \alpha_Y \quad (14.55)$$

$$\dot{w} = a_T \sin \alpha_R - \bar{g} \quad (14.56)$$

$$\dot{X} = u/\bar{e} \quad (14.57)$$

$$\dot{Y} = v/\bar{e} \quad (14.58)$$

$$\dot{Z} = w \quad (14.59)$$

In order to integrate analytically the Eqs. (14.54), (14.55), (14.56), (14.57), (14.58), and (14.59), assuming small angle approximations and constant thrust, the trigonometric functions in the above equations are converted into algebraic equations and the modified equations are given below:

$$\dot{u} = \left(\frac{V_e}{\tau - t} \right) \quad (14.60)$$

$$\dot{v} = \left(\frac{V_e}{\tau - t} \right) (C + Dt) \quad (14.61)$$

$$\dot{w} = \left(\frac{V_e}{\tau - t} \right) (A + Bt)\bar{g} \quad (14.62)$$

$$\dot{X} = u/\bar{e} \quad (14.63)$$

$$\dot{Y} = v/\bar{e} \quad (14.64)$$

$$\dot{Z} = w \quad (14.65)$$

where V_e is exhaust velocity (specific impulse), $\tau = m_0/\dot{m}$.

Assuming X is free, the target conditions are:

$$u(T_{go}) - u_D = 0 \quad (14.66)$$

$$v(T_{go}) - v_D = 0 \quad (14.67)$$

$$w(T_{go}) - w_D = 0 \quad (14.68)$$

$$Y(T_{go}) - Y_D = 0 \quad (14.69)$$

$$Z(T_{go}) - Z_D = 0 \quad (14.70)$$

where T_{go} (time-to-go) is the remaining time required to shut off the engine and u_D , v_D , w_D , Y_D , Z_D are the required values of vehicle state at engine shut-off.

The explicit guidance scheme tackles three separate problems such as: (a) radial co-ordinate control; (b) horizontal speed control; and (c) plane control. Desired terminal radial distance and velocity are ensured by the radial coordinate control. This is achieved by Eqs. (14.68) and (14.70). The desired horizontal velocity is guaranteed through horizontal speed control. This is achieved by Eq. (14.66). Plane

control ensures the required orbital plane. This is achieved by Eqs. (14.67) and (14.69). Single thrust acceleration vector available on board, the vehicle has to be allocated along three controlled axes like radial, horizontal and perpendicular directions of guidance reference frame, the solutions to the problem along all three axes are to be obtained simultaneously. The quantity, T_{go} , appearing in the guidance equations provides the remaining time of functioning of propulsive stage in order to satisfy the specified end conditions. This parameter is the synchronizing variable which ensures the simultaneous solutions to all three separate problems.

T_{go} is computed to meet the horizontal velocity. Integrating the Eq. (14.60), upto T_{go} and equating the resulting horizontal velocity to the required velocity yields

$$u_D - u_0 = V_e \int_{t_0}^T \frac{dt}{\tau - t} \quad (14.71)$$

After different steps and assuming $T_{go} = T - t_0$,

$$u_D - u_0 = -V_e \ln \left[1 - \frac{T_{go}}{\tau - t_0} \right] \quad (14.72)$$

From Eq. (14.72), the T_{go} can be computed as

$$T_{go} = (\tau - t_0) \left[1 - e^{-\left(\frac{u_D - u_0}{V_e}\right)} \right] \quad (14.73)$$

where t_0 is the starting time and u_0 is the velocity at t_0 .

Similarly, integrating Eqs. (14.61), (14.62), (14.64), (14.65), and equating the corresponding values at T to the targeted one as given in Eqs. (14.67, 14.68, 14.69, and 14.70) yield

$$[M] \begin{Bmatrix} A \\ B \end{Bmatrix} = \{ \Delta \dot{r} \Delta r \} \quad (14.74)$$

$$[M] \begin{Bmatrix} C \\ D \end{Bmatrix} = \{ \Delta \dot{Y} \Delta Y \} \quad (14.75)$$

where the matrix $[M]$, given by

$$[M] = \begin{bmatrix} m_{11} & m_{12} \\ m_{21} & m_{22} \end{bmatrix} \quad (14.76)$$

and $\Delta \dot{r}, \Delta \dot{Y}$ are predicted radial and out of plane velocity errors and $\Delta r, \Delta Y$ are the corresponding displacement errors with respect to the targeted values. The elements of $[M]$ matrix are computed by the integrals, which are the analytical expressions.

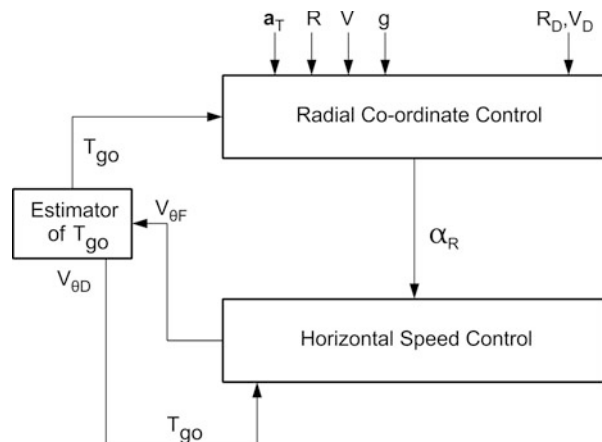
The values of A, B, C, D given by Eqs. (14.74) and (14.75) and T_{go} as given by Eq. (14.73) give the complete solution to the guidance problem: (1) to compute the desired attitude angles and (2) time to shut-off of the engine to achieve the specified target conditions.

Once the solution is obtained in the guidance frame, as per the requirements, the desired attitude can be computed at the specified frame by autopilot through suitable coordinate transformations.

14.5.5.2 E-Guidance Scheme

E-guidance scheme assumes spherical Earth and the optimal guidance solutions are achieved through iterations. Since the model is very close to reality and the solution procedure is rigorous till getting optimal solution, this guidance solution is more fuel optimal and more accurate. In this scheme, the radial control and the horizontal velocity control problems are split into two sub-problems. The solution of the two sub-problems are synchronized by (T_{go}) which is the time required to reach the target. The remaining burning time of the stage is taken as the first estimate of the T_{go} and this is used in the radial coordinate control block. The radial coordinate control block computes the desired attitude in plane (α_R) as a function of time for the remaining part of mission so that the radial distance and radial velocity are equal to the desired values after T_{go} . The horizontal velocity control block computes the expected horizontal velocity at the end of mission based on α_R computed by the radial coordinate control. If the horizontal velocity predicted is equal to the required value, the iteration is stopped. If they are different, the time to go value is adjusted and radial coordinate control and horizontal velocity control computations are repeated. A typical block diagram of E guidance scheme is given in Fig. 14.19.

Fig. 14.19 Block diagram of E guidance



14.5.5.3 Explicit Guidance at Terminal Phase

Explicit guidance schemes always tries to achieve the cut-off conditions accurately and in this process attempts to eliminate even smaller errors at injection. As the vehicle reaches the target conditions, the position errors become very small. Under this condition, to meet the velocity requirement without violating the position error, the desired attitude becomes oscillatory and can result into violent steering maneuvers. To overcome this problem, as the vehicle reaches closer to the target, the injection altitude constraint is relaxed and guidance equations use only velocity to find ∞_R and α_y . These conditions are imposed based on the time-to-go and once this value is less than certain predetermined value the guidance laws are modified and termed as injection guidance laws.

14.5.6 Guidance Robustness and Velocity Reserves

Performance of the guidance scheme chosen for a given mission has to be evaluated in detail under environments of trajectory deviation, vehicle and environment parameters dispersions to ensure the robustness of the guidance laws in meeting the final injection conditions, while satisfying various constraints such as loads on the vehicle, maximum heat flux felt by the vehicle and safe impact of spent stages. This is carried out using integrated trajectory simulation tools, simulating the various vehicle characteristics and environment models close to the reality. Using the simulation test beds, huge numbers of simulations are carried out by simulating all the feasible combinations of dispersions, and the guidance performance is evaluated under the simulated environments. Initially one can assume ideal navigation and control to evaluate the guidance system performance. Subsequently, the guidance system performance is evaluated under the realistic environment with the presence of navigation and control system. The various perturbations to be used in studies are propulsion parameters such as specific impulse, action time, propellant mass and thrust offset of the motor or engine. In liquid engines, the mixture ratio variation is essential. Other parameter variations pertaining to propellant slosh, aerodynamics, inert mass, vehicle CG offset and separation and wind disturbances. If more than one engine is used, the differential thrust also needs to be considered.

To compensate the performance loss in terms of cumulative velocity loss caused by dispersions and disturbances, extra energy is required to be provided by the propulsion system. For this purpose, over and above the propellant required to achieve the target orbit with nominal parameters, extra propellant is needed in the final propulsion stage. This is generally termed as guidance margin (or velocity reserve) and the quantity of extra propellant to be accommodated in the stage is decided through detailed simulations. For the case of final stage, as the spent stage also orbits the Earth, in order to avoid collision with the satellite in case of inadvertent re-ignition of the separated stage, the left out unutilized propellants

are needed to be vented out. For this purpose, the remaining propellant has to be minimum. Therefore, general practice for providing guidance margin is to generate the required extra propellant loading for three sigma performance dispersion of each of the sensitive parameters and consider the root sum square (RSS) of these values.

Two types of guidance scheme validation analyses are carried out: (1) The guidance performance analysis in Monte-Carlo sense, using the environment of dispersions within 3σ in random manner, the required guidance performance in terms of orbital accuracy within the specified dispersion band to be achieved; (2) In case of severe performance deviation, the guidance has to be robust to handle such large deviation and the system should not fail.

More details of validation of guidance system are given in the later section which discusses various aspects of integrated navigation guidance and control system validation.

14.5.7 Mission Salvage Aspects

As explained earlier, the guidance system functions are designed to provide the required performance within the specified dispersions band and the velocity reserve provided in the vehicle. In case there is gross performance deviation or a failure in any of the subsystems, the vehicle may deviate much away from the intended path and under such conditions, if the vehicle is still trying to achieve the original targeted mission, due to heavy performance loss, the final mission may end up with suborbital missions. Under such environment, depending on the remaining capability of the vehicle, still a lower orbital mission is possible. Subsequent to the launch vehicle mission, the satellite fuel can be utilized to go to the original defined mission, of course with certain amount of compromise in the satellite life. To achieve such a mission which performs gross under performance, guidance must be capable of quantifying the performance loss, assessing the remaining capability of the vehicle and based on these information, retarget to a suitable alternate mission, feasible for the satellite to correct it and direct the vehicle to the retargeted orbit. This scheme is called mission salvage options in guidance schemes.

14.5.8 Mission Accuracy Achievable by Guidance System

Once the engine shut-off command is raised by guidance system, still tail-off thrust generated by the propulsion system caused by the valves delays and valve response would add velocity to the vehicle. Therefore, normally, the target conditions for the guidance system are fixed, biasing the predicted tail-off thrust. If the in-flight tail-off thrust profile is same as the predicted one, then the final orbit achieved would be same as that targeted for. In case there is deviation in the tail-off thrust, resulting

orbit would be deviated from the nominal predicted one, depending on the extra velocity added or velocity deficiency during tail-off.

In addition, towards the end of the mission, to avoid violent maneuver, injection guidance with velocity control alone is to be implemented which can cause certain amount of dispersions on position at engine shut-off. Depending on the type of trajectory and performance deviations, there are errors in the final achieved orbit.

Another aspect is that, the vehicle attitude or rate is kept constant for 5–10s before the expected shut-off, the stage till the end of tail-off to meet the requirement of vehicle controllability. This results into commanded attitude being different from the optimum one, thereby introducing the error in the final achieved orbit.

Normally all these effects are nullified by suitably biasing the target considering these impacts. However, in flight, due to the deviations of flight trajectory away from the nominal, there would be error in the biasing and finally leading to the guidance error.

14.6 Autopilot and Control Law

The objectives of a launch vehicle autopilot are: (1) to stabilize the vehicle during its flight against various disturbance forces and moments due to aerodynamics, thrust misalignment, separation, liquid slosh, etc.; (2) to track the desired attitude of the vehicle as computed by guidance system so as to follow the desired trajectory with the specified accuracy to meet the final mission objectives; and (3) to reduce the in-flight loads on the vehicle structure by reducing the tracking error and attitude rates under dispersed environment.

Navigation, guidance and control of launch vehicles contain three loops. Autopilot is the inner loop as shown in Fig. 14.20. It receives data from sensors and desired attitude from the outermost navigation and guidance loop and generates the control commands. Using the control commands generated by the autopilot system, the innermost actuation system loop generates the necessary forces and moments to control and stabilize the vehicle as per the requirements.

Typical autopilot loop of a launch vehicle is given in Fig. 14.21. The position and rate gyros sense the vehicle attitude and attitude rate θ_s and $\dot{\theta}_s$, respectively. The sensor outputs are filtered with suitable feedback path filters to meet the specific requirements. The commanded attitude θ_c computed by the guidance and the filtered signals of sensor feedback with the suitable mixing with feedback gains K_r are used to generate the error functions. The error functions along with forward gain K_a and suitable compensators are used to generate autopilot commands. In certain cases, to reduce the steady state errors, integrators are also used in the forward path during generation of the control commands. The autopilot command signals are sent to control electronics to drive the actuators of the vehicle control systems. The system gain history, K_a and K_r , in forward and rate loops respectively and integrator gain K_i are to be appropriately worked out to stabilize the vehicle against all disturbances. Suitable compensators are to be designed to stabilize the vehicle structural

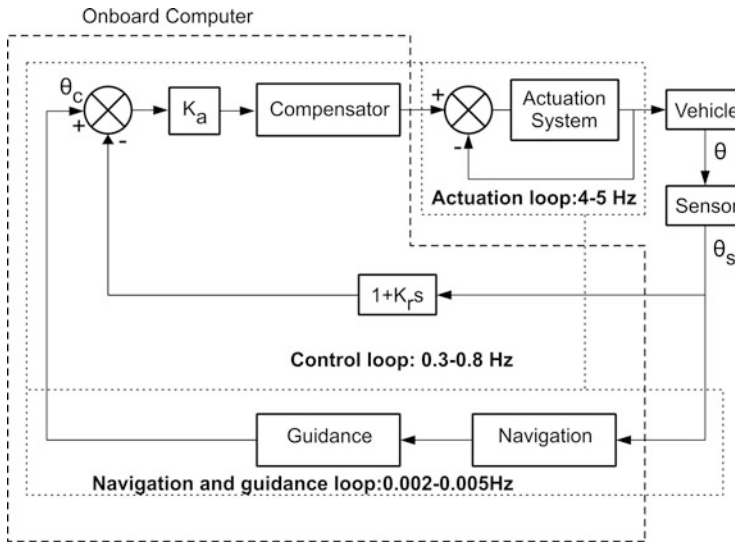


Fig. 14.20 Navigation, guidance and control loop for a launch vehicle

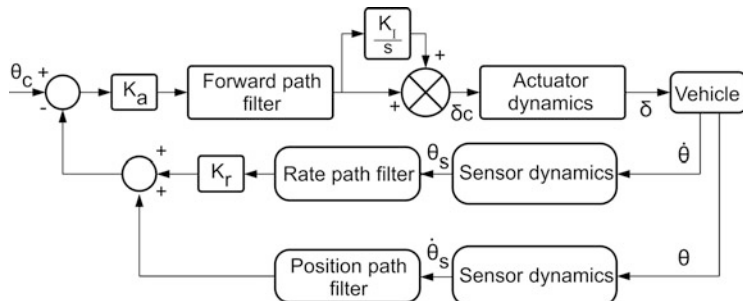


Fig. 14.21 A Typical autopilot loop

flexible modes. The overall design details of vehicle autopilot, highlighting functional requirements, specifications, design criteria and design methodology are described below.

14.6.1 Functional Requirements and Specifications of Autopilot

The essential functional requirements of an autopilot are:

- To achieve the mission objectives with required accuracy while reducing the load on the vehicle, the error in tracking the desired attitude has to be minimum. To minimize the error, generally, proportional control systems

are used during thrusting phases. Since the tracking error during the thrusting phase is having major impact on the parameters which decide the satellite injection accuracy and in-flight vehicle loads, the autopilot system generally has to achieve pitch and yaw attitudes within the error of 1° with respect to the desired attitude. As the roll error is not directly controlling the vehicle load and the trajectory dispersions, higher tracking error in roll, generally upto 5° can be allowed.

- (b) During the coast phase operation wherein the tracking errors are not having much impact on the trajectory dispersions, generally, simple nonlinear reaction control systems (RCS) are used. For these systems, tracking errors can be generally relaxed, typically upto 3° .
- (c) The demand on control force and impulse even under adverse disturbance conditions should be restricted within the limiting capability of control power plants.
- (d) During atmospheric flight phase, controllability has to be ensured even in the presence of high aerodynamic disturbances and winds.
- (e) The vehicle lateral drift and tracking errors are such that the structural loads in terms of axial and bending loads should not exceed the design limits of the structures.
- (f) During the exo-atmospheric and stage transition phases, the tracking errors can be relaxed to the values which are acceptable to the mission.
- (g) Robustness requirements are to be strictly adhered to ensure vehicle stability even under a wide range of parameter perturbations. To achieve these requirements, specifications generally aimed are as given below:

(a) *In frequency domain*

- 1. Rigid body margins:

Gain margin $> 6 \text{ dB}$

Phase margin $> 30^\circ$

Aero margin* $> 6 \text{ dB}$

(*low frequency gain margin)

- 2. Phase stabilized structural flexible modes: Phase margin $> 40 \text{ dB}$
- 3. Gain stabilized structural flexible modes: Attenuation margin $> 6 \text{ dB}$
- 4. Slosh modes: Phase margin $> 30^\circ$

(b) *In time domain*

- 5. Peak overshoot for step command $< 30 \%$

- (h) Vehicle should remain stable even under the combination of additive disturbances due to propulsion, aerodynamics, slosh, vehicle flexible modes, actuator /nozzle dynamics, centre of gravity (CG), moment of inertia (MI) properties of the vehicle, separation disturbances, sensor dynamics and time delays due to implementation of control laws in on board computers.

- (i) The attitude rate at the satellite injection generally has to be minimized, typically less than $0.2^{\circ}/\text{s}$
- (j) The vehicle flexible modes and liquid sloshing have to show damping behavior in response to disturbances due to winds, thrust misalignment, etc. These modes should have enough separation from rigid body dynamics.
- (k) The vehicle lateral drift and drift rates at the end of the first stage have to be maintained within the specified limits.
- (l) The peak to peak oscillations in the vehicle attitude rates due to slosh forces should be less than the allowable limits.

14.6.2 Design Criteria and Guidelines

During various phases of flight, a launch vehicle encounters complex flight environments as explained earlier. These severe disturbance forces and moments originated within the vehicle systems and also due to external sources such as wind can destabilize the vehicle during flight. The autopilot system generates the control commands and in turn the necessary control forces and moments to stabilize the vehicle against these disturbances. The task of stabilization of the vehicle further gets aggravated due to the following specific characteristics of launch the vehicle:

1. The vehicles are generally flexible structures and the sensor data contains the rigid vehicle and flexible mode responses.
2. Due to continuous depletion of propellants in a vehicle, the mass and inertial properties of the vehicle are rapidly changing.
3. Whenever liquid stages are used, sloshing of liquids introduces additional dynamics to the system.

The important design criteria in controlling such a flexible vehicle with multiple system dynamics under the extreme flight environment are as given below.

- (a) The control force available for each stage should be such that the control moment generated by the control power plant is more than the disturbance moment experienced by the vehicle due to all disturbances acting on the vehicle.
- (b) The design must ensure good stability margins as per specifications listed above during the entire duration of flight.
- (c) Drift of the vehicle from the reference trajectory has to be minimized. While the wind is the major disturbance causing the vehicle drift, the thrust misalignment, centre of gravity variation and sensor drift have secondary effect on the vehicle drift.
- (d) The system should provide fast response to achieve desired attitude generated by the guidance system. This is necessary to minimize the tracking errors.
- (e) The structural loads on the vehicle have to be maintained within the allowable limits even under the additive disturbances. If the loads are exceeding the set

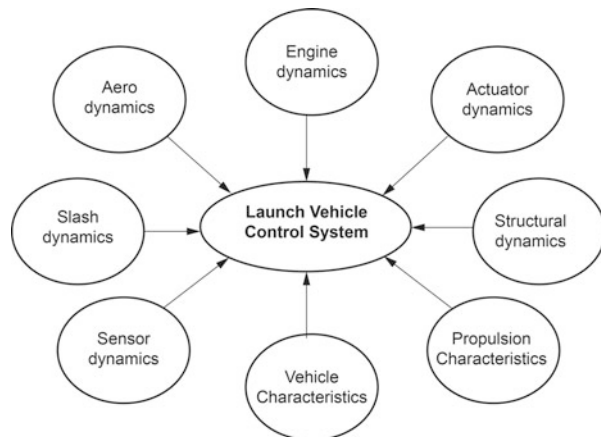
limits, it is essential to include the load relief control in the system. This is achieved either through active load relief using the lateral accelerometer or angle of attack sensors or by passive load relief using wind biased attitude steering programs. The details of these schemes are discussed elsewhere in the book.

- (f) The interaction between vehicle elastic and liquid oscillations with vehicle control system must be totally eliminated. This also demands selection of suitable location for sensors to minimize the control structure interaction. The noisy environment and dynamically active locations have to be avoided for sensors. Similarly the dominant mode of the gimballed engines or swivellable nozzles can cause the interaction with control. These aspects need serious attention during the design phase.
- (g) In addition to maintaining the stability and control of the vehicle, the control system has to ensure the desired transient and steady state response to disturbances.
- (h) The on-off controls are generally used in vehicle stages operating outside the atmosphere and during the coasting period of the vehicle. It is essential to guarantee the needed margin in the total control impulse provided in the system.
- (i) The choice of a suitable control frequency has to be based on the following considerations. Generally the control frequency has to be one fifth or less of the first bending mode frequency of the vehicle to keep the rigid and elastic modes separated. Lower bound on the control frequency has to be based on the operating frequency of guidance system and the sensitivity considerations. Higher frequency causes the control system to respond fast to wind disturbance causing larger gimbal deflection angles whereas lower frequency causes sluggish gimbal response which in turn results into larger angle of attack and load on the vehicle. Therefore best control frequency has to be such that the relative contribution of aerodynamic and thrust forces to vehicle bending moment is minimized.

14.6.3 Autopilot Design Methodology

As the launch vehicle control systems interact with several disciplines and dynamics as shown in Fig. 14.22, the autopilot design process is quite complex. The prerequisites for the autopilot design of a launch vehicle are the vehicle characteristics, various subsystems dynamics, flight environment, disturbance originated within the vehicle and external to the vehicle, mission profile and a reference trajectory. Therefore, it is evident that the control system designer has to have full understanding of not only vehicle characteristics but other dynamic characteristics of various subsystems such as propulsion, structure, actuator, sensors, aerodynamics, liquid slosh and also the engines or nozzles used for control.

Fig. 14.22 Interaction of vehicle control with other subsystems



14.6.3.1 Vehicle Data for Control Design

The essential vehicle data needed for control design are to be generated sufficiently accurately and to the extent possible, these data are to be validated from experimental methods. The required vehicle data are:

- (a) Reference trajectory defining altitude, Mach number, forward acceleration and dynamic pressure profiles.
- (b) The varying vehicle mass, centre of gravity and moment of inertia for the entire flight regime.
- (c) Structural data defining the vehicle flexible frequencies, mode shape and the corresponding generalized masses for all important flexible modes.
- (d) Slosh data with frequency and slosh mass variation for essential slosh modes for oxidizer and fuel tanks in the vehicle.
- (e) Sensor dynamics for all sensors used in control loop.
- (f) The characteristics and their nonlinear dynamics of control actuators used for generating the control force.
- (g) Aerodynamic data in terms of varying centre of pressure locations and force coefficients along with their permissible dispersion bands.
- (h) Sectional aerodynamic load distributions.
- (i) The entire flight sequence including the real time decision (RTD) details.
- (j) Thrust misalignment of motors, centre of gravity offset and gimbable engine inertial properties.
- (k) Wind characteristics such as wind speed, direction, wind shear and gust. Entire measured wind profile at the specified launch site collected over a period of years and wind statistics form important input for autopilot design and validation.
- (l) The total time delay in the loop during the implementation of control law in the on board computers.
- (m) For all the parameters given in (a) to (l), nominal profile and the possible dispersion bands are required.

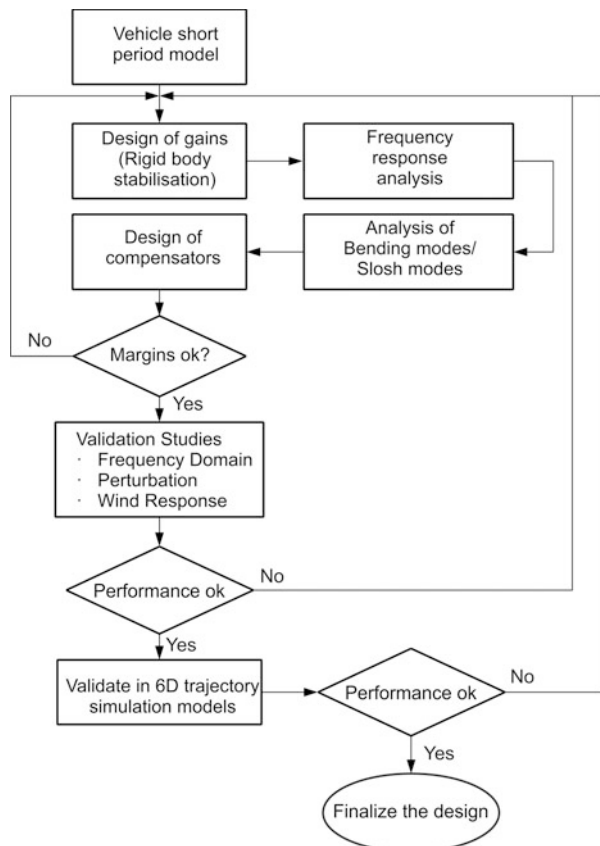
14.6.3.2 Design Procedure

The design of vehicle autopilot is carried out in several phases. The overall flow chart for autopilot design is shown in Fig. 14.23.

During the vehicle configuration evolution phase, a preliminary autopilot system is required to configure the vehicle systems. For this purpose, vehicle is considered as rigid body. With this design, the analysis is carried out with 3σ variations of vehicle parameters which help in determining the basic response characteristics and to decide the design input for the vehicle structures and approximate sizing of the control power plants. Generally the rigid body model is developed as a planar one. This assumption is made based on the fact that the vehicle is strongly stabilized in other planes.

Once the vehicle systems are configured and the requirements and specification of control systems are derived, the autopilot and control laws are designed to achieve the specified functional requirements, meeting the specification. The vehicle with nonlinear dynamics coupled with time varying parameters make the design of control system quite complex. Therefore the system is studied by simplifying the

Fig. 14.23 Autopilot design flow



analytical problem in two steps. The first step is to achieve the adequate short period stability by studying the short period dynamics using time slice approach. This approach facilitates to freeze the varying mass and inertial properties over a short period of time and helps to use the techniques of linear analysis thereby reducing the analytical difficulties. Experience has demonstrated that design using time slice approach has proved to be satisfactory. This has to be followed up by carrying further checks by utilizing the long period dynamics. This refers to the vehicle trajectory with respect to the specified inertial frame of reference. The long period simulation incorporates all time varying properties of the vehicle and helps to determine the vehicle stability and performance characteristics in response to various disturbances.

In short period dynamics, the selection of interval between two flight instants for studies depends on the rate of change of vehicle dynamics. Typically time interval of about 5–10s between two flight instants is considered as adequate. In the first design phase, the basic control gains are estimated for the entire duration of flight. While generating the gain values, the primary requirement is to ensure that the desired transient and steady state response for given disturbance are satisfied, in addition to maintaining the stability. Therefore the natural frequency of the control system ω_n and damping ratio ξ for the rigid body transient should be based on peak overshoot and settling time requirements. If the system responds very fast, it results in higher overshoot and hence introduces excessive loads on the vehicle structures. Similarly, the sluggish response leads to accumulation of errors in vehicle attitude, angle of attack and engine deflection, which again increase the load on the vehicle. Therefore, the design has to be carried out judiciously.

Once the control system configuration is worked out using the rigid body vehicle dynamics and the corresponding gain schedule is generated, next step is to introduce the higher order vehicle dynamics into the model. The various dynamics to be included in the control system design process are vehicle flexibility, liquid sloshing, engine inertia and sensor and actuator dynamics.

The sensors mounted on the vehicle to detect the vehicle motions sense both rigid body motion and elastic deformations at the points where the sensors are located. Hence flexibility effects are felt by control system through the sensor signals. The elastic deformations so sensed affect the control signals and in turn the control forces acting on the vehicle. This results into feeding the energy into the vehicle structure at various frequencies. It is also possible to excite the structures with resonant frequencies. Generally structural damping is small and the control system may add energy to the structure faster than its dissipation. This often results into larger structural deflections leading to structural failure.

Therefore, in the next phase, the design of control system has to address the choice of suitable compensators, to stabilize the vehicle flexible modes without appreciably changing the rigid body response. The main aim of the compensator design is to process the control signal such that there is net flow of energy out of the structure. Since the vehicle is a continuous body, the elastic modes of a vehicle consist of infinite number of degrees of freedom. Based on the modal gains of the dynamic modes, the significant bending modes to be considered for the design have

to be decided. Generally first 3–4 bending modes having high energy are considered for the autopilot design studies. However, it is essential to confirm that contribution of higher modes is negligible. For stabilization of the resonant structural modes, there are two approaches. In the first approach, the control system filters the sensor signals at resonant structural frequencies, thus preventing the system supplying the energy at these frequencies. Basically the filters are designed to attenuate the higher order bending modes having low energy. This method is termed as ‘gain stabilization’ and is used to avoid excessive response in higher frequency modes. The second approach is through ‘phase stabilization’, where the phase of the control signal at bending mode frequency is altered to have a phase opposite to that of vehicle vibration mode. This helps the control to actively damp out the bending mode oscillations. This technique is generally used for low frequency modes having higher energies. However for effective implementation of the stabilization, it demands accurate information of phase of the sensed signal and accurate estimation of mode shapes, slopes and frequency of the bending modes. The control system design for a launch vehicle generally employs both the approaches, i.e. phase stabilization of low frequency modes and gains stabilization of higher frequency modes.

The choice of a control frequency is decided by several considerations. One of the important considerations is that control frequency should be one fifth or less of the first bending mode frequency to keep enough separation between the rigid and elastic modes of the vehicle.

In most of the present day launch vehicles, liquid propellant stages are used. In such stages, almost 90 % of the total mass of the stage is liquid. External and internal lateral disturbances and lateral acceleration induced by the control forces as per the demand of autopilot to stabilize the vehicle causes the propellant to oscillate within the stage tanks. The propellant oscillations generate periodic lateral disturbances to the vehicle with frequency equal to the slosh frequency. This is called propellant sloshing phenomenon. The slosh frequency, amount of propellant mass taking part in the sloshing phenomenon depend on the propellant tank internal configuration, liquid levels in the tank and longitudinal acceleration of the vehicle. The disturbance levels caused by the propellant sloshing depend on the above parameters and the lateral acceleration levels which trigger the sloshing phenomenon. The addition of sectoring and providing baffles in the tanks helps in improving the damping of fluid motion. The forces and moments generated by the propellant slosh can be modeled by equivalent pendulum-mass analogy. In this analogy, the pendulum mass, pendulum length, pendulum hinge point and pendulum frequency are fixed such that the vehicle propellant slosh forces and moments are equivalent to that generated by the pendulum as described above.

The introduction of propellant slosh dynamics into the control system design brings restriction on the choice of control frequency since there should be enough separation between the control and the high frequency slosh modes to avoid resonance. Considering all inputs the control system design has to introduce appropriate filter to avoid unstable slosh oscillation. It is also important to carry out simulation for the entire duration of flight time since slosh parameters such as

hinge point, pendulum mass and length, etc., are continuously varying with the varying liquid propellant levels.

The control system design has to be carried out by progressively adding the dynamics due to engine inertia, sensors and higher order actuators in the system model. During the initial design phase, if the control structure interaction cannot be avoided by suitable control design it becomes necessary to stiffen vehicle structure wherever necessary. To the extent possible stiffening of structures has to be avoided since this causes the overall mass penalty. However if it is inevitable, the modifications are to be carefully introduced. The required stiffness for some of the essential elements in the control system hardware such as the linkages between the actuator connecting the vehicle and engine, mounting brackets for sensors and joints are to be ensured without causing the mass penalty.

Once the control system design is completed in all aspects, it is essential to validate the same in the realistic flight environment. This involves creating realistic detailed models simulating vehicle subsystems including all nonlinearities, inter axes coupling, interfaces, threshold levels for sensors, aerodynamic characteristics, all possible external and internal disturbances and dispersions on the vehicle and environment parameters. The vehicle translational, rotational and flexible modes dynamics are simulated using the above models and time varying six degrees-of-freedom motion of vehicle and trajectory from lift-off till satellite injection are evaluated. The control system performance is evaluated under various feasible flight environments through simulations using the above simulation models.

14.6.4 Vehicle System Dynamics

Vehicle and subsystem dynamics involved for the autopilot system design are: (1) rigid body translational dynamics, (2) rigid body rotational dynamics, (3) dynamics of vehicle flexible modes, (4) propellant slosh dynamics, (5) engine dynamics, (6) sensor dynamics and (7) control power plant dynamics. All the internal and external forces and moments, environments, disturbances and vehicle characteristics affecting the above dynamics are also to be considered for the control system design process.

In order to carry out the design and analysis, it is suggested to model the vehicle dynamics as perturbation model, frozen at an instant which is valid for a short period of time. This is often referred as linearized short period model.

During the entire regime of flight, the short period models are used as continuous small range segments for design and analysis. This also includes the critical events of the flight such as transonic regime, high dynamic pressure regime, peak disturbance and separation events, etc.

The equations describing the short period dynamics of the vehicle considering pitch, yaw, and roll attitude motions are given in the form of state space equations,

$$\dot{\mathbf{X}} = [\mathbf{A}]\mathbf{X} + [\mathbf{B}]\mathbf{U} \quad (14.77)$$

$$\mathbf{Y} = [\mathbf{C}]\mathbf{X} + [\mathbf{D}]\mathbf{U} \quad (14.78)$$

where \mathbf{X} and \mathbf{U} are state and control vectors respectively and \mathbf{Y} is the output vector.

$$\mathbf{X}^T = \left\{ \begin{array}{lllll} \text{Rigid} & \text{Bending} & \text{Slosh} & \text{Sensor} & \text{Actuator} \\ \text{body} & \text{modes} & \text{modes} & \text{dynamics} & \text{dynamics} \end{array} \right\} \quad (14.79)$$

The various states are given below:

$$\text{Rigid body} = \left\{ \theta, \dot{\theta}, \frac{\dot{z}}{V}, \Psi, \dot{\Psi}, \frac{\dot{y}}{V}, \phi, \dot{\phi} \right\}$$

$$\text{Bending} = \{q_1, \dot{q}_1, q_2, \dot{q}_2, \dots, q_n, \dot{q}_n\}$$

$$\text{Slosh} = \{\Gamma_{z1}, \dot{\Gamma}_{z1}, \Gamma_{y1}, \dot{\Gamma}_{y1}, \Gamma_{z2}, \dot{\Gamma}_{z2}, \Gamma_{y2}, \dot{\Gamma}_{y2}, \dots, \Gamma_{zk}, \dot{\Gamma}_{zk}, \Gamma_{yk}, \dot{\Gamma}_{yk}\}$$

$$\text{Sensor} = \{\theta_s, \dot{\theta}_s, \Psi_s, \dot{\Psi}_s, \phi_s, \dot{\phi}_s\}$$

$$\text{Actuator} = \{\delta_p, \dot{\delta}_p, \delta_y, \dot{\delta}_y, \delta_r, \dot{\delta}_r\}$$

The control vector \mathbf{U} is given by

$$\mathbf{U} = \{\delta_p, \delta_y, \delta_r\}^T$$

and the output vector, \mathbf{Y} is given by

$$\mathbf{Y} = \{\theta_s, \dot{\theta}_s, \Psi_s, \dot{\Psi}_s, \phi_s, \dot{\phi}_s\}^T$$

14.6.4.1 Dynamics of a Flexible Vehicle

Dynamic model for a plane (pitch plane) is given in this section. Typical configuration of an elastic vehicle in pitch plane along with the major forces is given in Fig. 14.24. The rigid body along with flexible mode is considered, and it is assumed that the main engine is deflected to get the required control force. The various dynamics are explained in the following sections:

Rigid Body Translational Dynamics

The rigid body lateral dynamics equation is given as

$$m_0(\dot{w} - V\dot{\theta}) = F_z \quad (14.80)$$

where

m_0 is mass of the vehicle

w perturbation velocity along lateral Z-direction

θ perturbation pitch attitude and $\dot{\theta}$ is its derivative

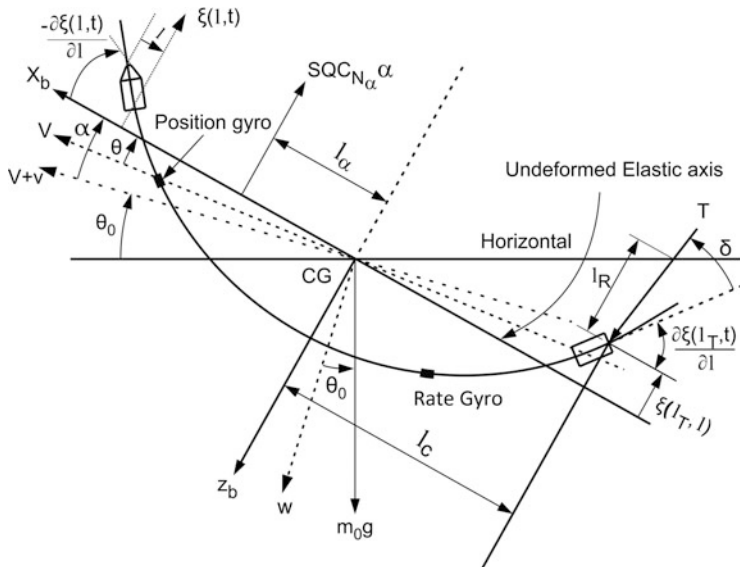


Fig. 14.24 Configuration of an elastic launch vehicle

V is velocity of the vehicle

F_z is the total perturbation force along Z-direction

The perturbation force is due to gravity, aerodynamics, control and thrust as given below:

$$F_z = F_g + F_c + F_T + F_A \quad (14.81)$$

The perturbation gravity force is given by

$$F_g = m_0 g \cos \theta_0 \quad (14.82)$$

where

g = acceleration due to gravity

θ_0 = steady state pitch angle

The perturbation control force is given by

$$F_c = T \delta \quad (14.83)$$

where

T = engine thrust

δ = engine deflection angle

Due to the vehicle bending shapes, the thrust gets deflected and the contribution of this is given as

$$F_T = -T \sum_{i=1}^n \frac{\partial \xi_i(l_T, t)}{\partial l} \quad (14.84)$$

where

$\xi_i(l_T, t)$ is the ith mode shape at thrust location

$\frac{\partial \xi_i(l_T, t)}{\partial l}$ is the slope of ith mode at thrust location

The aerodynamic model for rigid vehicle is assumed as

$$F_A = -\left(\frac{1}{2}\rho V^2\right) S C_{N_\alpha} \alpha \quad (14.85)$$

where

ρ is air density

S is reference area

C_{N_α} is coefficient of normal force slope with respect to angle of attack

α is the perturbation angle of attack

For the flexible vehicle as shown in Fig. 14.24, the angle of attack varies along the vehicle length and is given as

$$\alpha(l) = \alpha_w + \frac{w}{V} - (l_{cg} - l) \frac{\dot{\theta}}{V} - \sum_{i=1}^n \frac{\partial \xi_i(l, t)}{\partial l} - \sum_{i=1}^n \frac{\partial \dot{\xi}_i(l, t)}{V} \quad (14.86)$$

where

$\alpha(l)$ = angle of attack at location 'l'

α_w = wind angle of attack

l = the typical location

l_{cg} = the distance of centre of gravity from nose tip

$\xi_i(l, t)$ = the shape of ith mode at location l from nose tip

$\dot{\xi}_i(l, t)$ = velocity of mode shape

The mode shape along with varying angle of attack and distributed aerodynamic load defines the total aerodynamic normal force on the vehicle, as given below:

$$F_A = \left(-\frac{1}{2}\rho V^2\right) \int_0^L S \frac{\partial C_{N_\alpha}(l)}{\partial l} \alpha(l) dl \quad (14.87)$$

where

$S \frac{\partial C_{N_\alpha}(l)}{\partial l}$ is local aerodynamic load distribution parameter

L is total length of the vehicle

Rigid Body Rotational Dynamics

Rigid body rotational dynamics is given as

$$I_{YY}\ddot{\theta} = M_Y \quad (14.88)$$

where

$\ddot{\theta}$ is perturbation rotational acceleration

I_{YY} is pitch moment of inertia

M_Y is total perturbation moment about pitch axis of vehicle

Similar to the force, the perturbation moment is due to control, thrust and aerodynamics as given below:

$$M_Y = M_c + M_T + M_A \quad (14.89)$$

Referring to the Fig. 14.24, M_Y is expressed as

$$\begin{aligned} M_Y &= T\delta l_c - Tl_c \sum_{i=1}^n \frac{\partial \xi_i(l_T, t)}{\partial l} - T \sum_{i=1}^n \xi_i(l_T, t) \\ &\quad + \left(\frac{1}{2} \rho V^2 \right) \int_0^L S \frac{\partial C_{N_a}(l)}{\partial l} \alpha(l)(l_{cg} - l) \end{aligned} \quad (14.90)$$

Vehicle Flexibility Dynamics

The vehicle shape is defined as

$$\xi_i(l, t) = q_i(t)\phi_i(l) \quad (14.91)$$

where $\phi_i(l)$ is the normalized mode shape function for the i th flexible mode, q_i is generalized coordinate for the i th flexible mode given by

$$\ddot{q}_i + 2\zeta_i \omega_i \dot{q}_i + \omega_i^2 q_i = -\frac{Q_i}{M_i} \quad (14.92)$$

where ω_i and ζ_i are the frequency and damping ratio of the i th flexible mode.

The generalized force (Q_i) and generalized mass (M_i) of i th flexible mode are given by

$$Q_i = \int_0^L F_Z(l)\phi_i(l)dl \quad (14.93)$$

$$M_i = \int_0^L m(l) [\phi_i(l)]^2 dl \quad (14.94)$$

where $m(l)$ = Mass per unit length along l and

$$m_0 = \int_0^L m(l) dl \quad (14.95)$$

The relations between the mode shape and normalized mode shape are

$$\frac{\partial \xi_i(l, t)}{\partial l} = q_i(t) \frac{\partial \phi_i(l)}{\partial l} \quad (14.96)$$

$$\dot{\xi}_i(l, t) = \dot{q}_i(t) \phi_i(l) \quad (14.97)$$

Actuator Dynamics

The input to the actuator is the autopilot command,

$$\delta_c = K_a [(\theta_c - \theta_s) - K_r \dot{\theta}_s] \quad (14.98)$$

Assuming first order dynamics for the actuator, the dynamic equation is given by

$$\frac{\delta}{\delta_c} = \frac{K_c}{s + K_c} \quad (14.99)$$

Substituting the expression for δ_c , the actuator dynamics can be written as

$$\dot{\delta} = -K_c \delta + K_c K_a (\theta_c - \theta_s - K_r \dot{\theta}_s) \quad (14.100)$$

where

δ Actuator output

θ_c Desired attitude

θ_s Sensed attitude

$\dot{\theta}_s$ Rate sensor output

K_c Actuator gain

K_r Rate gain

K_a Forward gain of control loop

14.6.4.2 Sensor Dynamics

The sensors measure both rigid body and flexible body attitude and attitude rates. Therefore, input to the position gyro and rate gyro dynamics are given by

$$\theta_{si} = \theta + \sum_{i=1}^n \sigma_i(PG) q_i(t) \quad (14.101)$$

$$\dot{\theta}_{si} = \dot{\theta} + \sum_{i=1}^n \sigma_i(RG) \dot{q}_i(t) \quad (14.102)$$

where $\sigma_i(PG)$, $\sigma_i(RG)$ are the normalized mode slopes at position and rate gyro locations respectively, and they are given as

$$\sigma_i(l) = -\frac{\partial \phi_i(l)}{\partial l} \quad (14.103)$$

Assuming second order dynamics, the sensor output follows the dynamics as given below:

$$\ddot{\theta}_{PS} + 2\zeta_P \omega_P \dot{\theta}_{PS} + \omega_P^2 \theta_{PS} = \omega_P^2 \theta_{si} \quad (14.104)$$

and

$$\ddot{\theta}_{RS} + 2\zeta_R \omega_R \dot{\theta}_{RS} + \omega_R^2 \theta_{RS} = \omega_R^2 \dot{\theta}_{si} \quad (14.105)$$

where ω_P , ω_R , and ζ_P , ζ_R are the undamped natural frequencies and damping ratios of position and rate gyros. The output of the dynamics given by Eq. (14.104) to Eq. (14.105) give the sensor measured values of attitude and rate as given below:

$$\theta_s = \theta_{PS} \quad (14.106)$$

$$\dot{\theta}_s = \dot{\theta}_{RS} \quad (14.107)$$

The set of Eqs. (14.80, 14.81, 14.82, 14.83, 14.84, 14.85, 14.86, 14.87, 14.88, 14.89, 14.90, 14.91, 14.92, 14.93, 14.94, 14.95, 14.96, 14.97, 14.98, 14.99, 14.100, 14.101, 14.102, 14.103, 14.104, 14.105, 14.106, 14.107) describe the pitch plane short period dynamics of the flexible vehicle without engine and slosh dynamics used for the autopilot design and analysis.

The block diagram explaining the total flexible vehicle is given in Fig. 14.25.

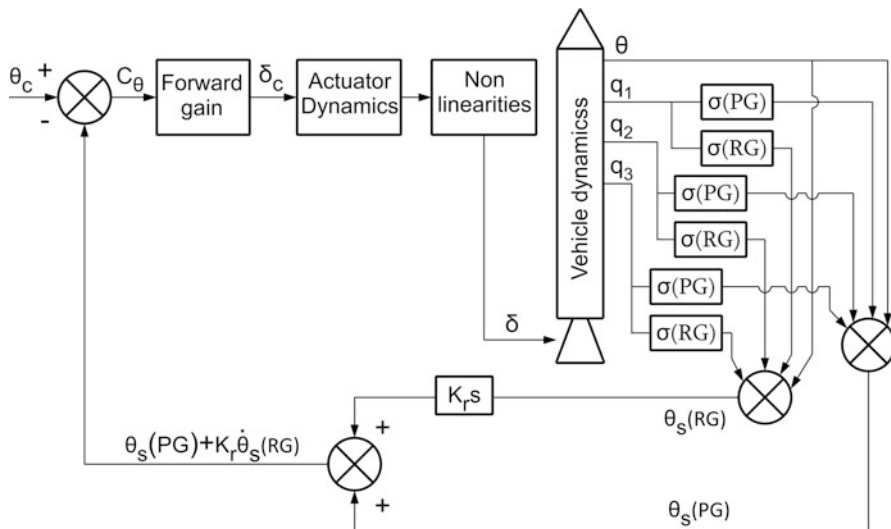


Fig. 14.25 Block Diagram for flexible vehicle system

14.6.4.3 Engine and Slopsh Dynamics

Engine Dynamics

Dynamics of gimbaled engine and actuator play a dominant role and have to be considered in autopilot design and analysis. Engine is hinged at gimbal point and act as a compound pendulum. The actuator motion can be simplified by a simple second order equation as:

$$\ddot{\delta} + 2\xi_n \omega_n \dot{\delta} + \omega_n^2 \delta = \omega_n^2 \delta_c \quad (14.108)$$

where

δ = engine deflection angle

ω_n = actuator natural frequency

ζ_n = damping ratio for actuator

δ_c = command signal to actuator

Referring to Fig. 14.24, due to engine dynamics, the lateral force acting on the vehicle is given as

$$F_{ze} = m_R \{ l_R \ddot{\delta} - (l_c + l_R) \ddot{\theta} - \dot{w} + \dot{V} \theta \} - \sum_{i=1}^n [\phi_i(l_T) - l_R \sigma_i(l_T)] \ddot{q}_i(l_T) \quad (14.109)$$

and the total torque applied to the vehicle is given by

$$\begin{aligned}
 M_{ye} = & (I_R + m_R l_R l_c) \ddot{\delta} + m_R l_R V \dot{\delta} \\
 & - [I_0 + m_R (l_c + l_R)^2] \ddot{\theta} - m_R (l_R + l_c) \dot{w} \\
 & + m_R l_c \dot{V} \theta - m_R l_R \dot{V} \sum_{i=1}^n \sigma_i(l_T) q_i(t) \\
 & - \sum_{i=1}^n [m_R (l_R + l_c) \phi_i(l_T) + (I_R + m_R l_R l_c) \sigma_i(l_T)] \ddot{q}_i(t)
 \end{aligned} \tag{14.110}$$

The load torque applied to the actuator is given by

$$\begin{aligned}
 T_L = & - [I_0 + m_R (l_c + l_R)^2] \ddot{\theta} - m_R (l_R + l_c) \dot{w} + m_R l_c \dot{V} \theta \\
 & - \sum_{i=1}^n [m_R (l_R + l_c) \phi_i(l_T) + (I_R + m_R l_R l_c) \sigma_i(l_T)] \ddot{q}_i(t) \\
 & - m_R l_R \dot{V} \sum_{i=1}^n \sigma_i(l_T) q_i(t)
 \end{aligned} \tag{14.111}$$

where

\dot{V} = vehicle forward acceleration

m_R = mass of engine

l_R = distance between gimbal point to engine centre of gravity

l_c = distance between vehicle CG and engine gimbal point

I_0 = moment of inertia of engine about its CG

I_R = moment of inertia of engine about gimbal point

$$= I_0 + m_R l_R^2$$

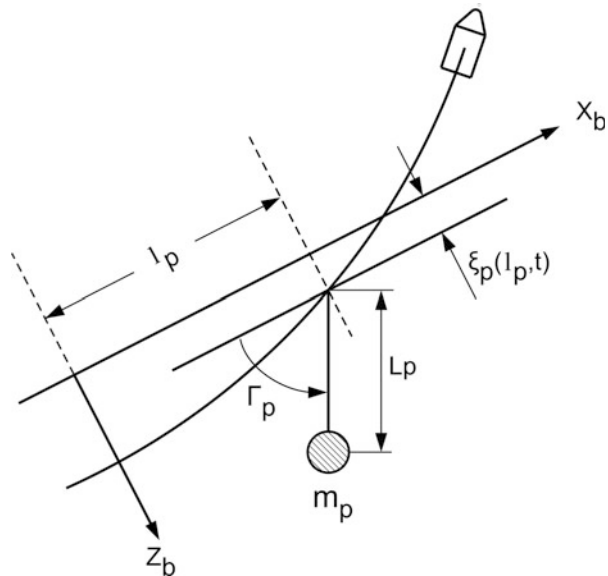
$\phi_i(l_T)$ = normalized mode shape at gimbal location

$\sigma_i(l_T)$ = normalized mode slope at gimbal point

Slosh Dynamics

Wherever large liquid stages are used, dynamics of sloshing liquid has to be considered in autopilot design and analysis. The liquid slosh can be modeled as an equivalent simple pendulum as shown in Fig. 14.26. The important pendulum parameters are mass, length and hinge point location. Each slosh mode in a propellant tank can be assumed as a pendulum. Similarly, each propellant tank has multiple pendulums. Generally, first slosh modes have predominant effect on the vehicle dynamics. The dynamics of i th pendulum in pitch plane as shown in Fig. 14.26 is given as

Fig. 14.26 Schematic of a pendulum in a liquid stage, pitch plane



$$\ddot{\Gamma}_{P_i} + 2\zeta_{P_i}\omega_{P_i}\dot{\Gamma}_{P_i} + \omega_{P_i}^2\Gamma_{P_i} = \frac{1}{L_{P_i}} \left[V\dot{\theta} - \dot{w} + \ddot{\theta}(l_{P_i} - L_{P_i}) + \sum_j \ddot{q}_j(t)\phi_j(l_{P_i}) \right] \quad (14.112)$$

The force and moment on the vehicle due to slosh are given below:

$$F_{zs} = \sum_i m_{P_i} \dot{V} \Gamma_{P_i} \quad (14.113)$$

$$M_{YS} = - \sum_i m_{P_i} l_{P_i} \dot{V} \Gamma_{P_i} \quad (14.114a)$$

where

Γ_{P_i} = ith slosh pendulum angle

ω_{P_i} = ith slosh frequency

ζ_{P_i} = ith slosh damping

L_{P_i} = ith slosh pendulum length

l_{P_i} = ith slosh pendulum hinge point location

$\phi_j(l_{P_i})$ = flexible mode shape at the ith slosh location

The damping of slosh can be achieved by the viscous effects as well as by baffles. The location and sizing of the baffles can be decided by the required response.

14.6.5 Additional Design Considerations for Autopilot

The autopilot designer has to have good understanding of several aspects in addition to various factors discussed so far. The following sections highlight the significance of such aspects and their consideration during the autopilot design and validation.

(a) Sensor location

It is important to identify a suitable location for vehicle sensor mounting to minimize the control structure interaction. Figure 14.27 illustrates a vehicle deflected in its fundamental mode showing the node and antinode points. A typical location of sensor in the vehicle which measures the pitch attitude is also shown in Fig. 14.27. The sensor not only measures the rigid body attitude but also the structural deflection. If it is not properly accounted in design and analysis it may lead to undesirable control interaction. Generally sensors are mounted on the nose side and never on the base shroud of the vehicle since the noisy environment due to main thrust can lead to saturation of the sensor. There are instances where two sensors are used with one located on the nose side as indicated in Fig. 14.27 and another on the antinode of first bending mode. It is possible to mix the signals of these sensors suitably to minimize or eliminate the effect of first bending mode.

(b) Local deformation effects

The local deformation at the sensor location either due to structure or the mounting bracket responding to local vibrations influences the control structure interaction. Sometimes the local bending mode slope has opposite sign to the body deflection slope at sensor mounting point. This causes severe instability in the system. Therefore all such locations are to be appropriately characterized and necessary stiffening has to be done to avoid such problems. The sensor mounting arrangement also has to be decided carefully.

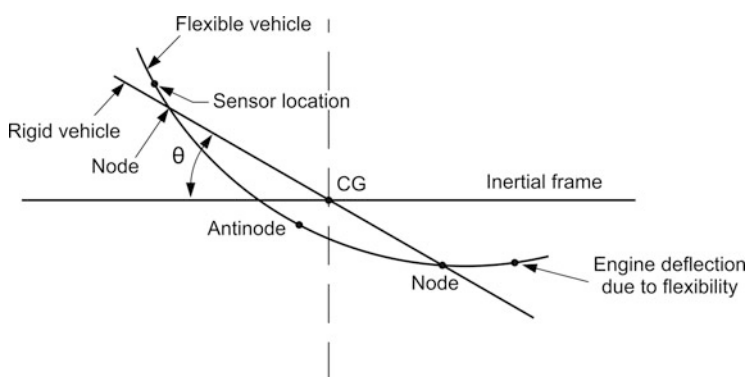


Fig. 14.27 Vehicle deflected in fundamental mode

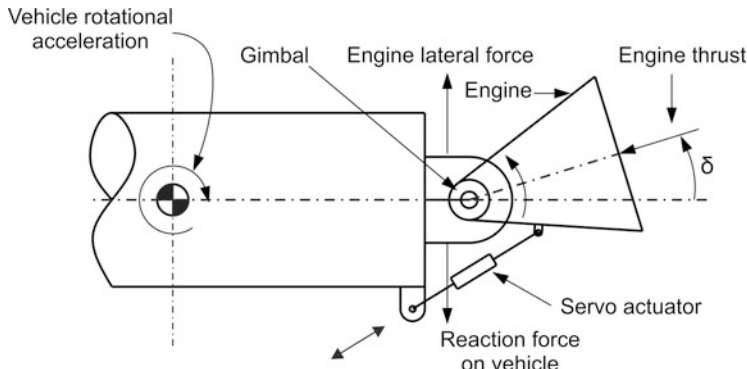


Fig. 14.28 Forces during engine gimbaling

(c) Engine inertia and dynamic instability

Generally, during thrusting phase, control forces are generated by gimbaling the engine as shown in Fig. 14.28. Motion of engines due to gimbaling introduces inertia forces on the vehicle. This engine inertia reaction force at certain excitation frequency becomes equal and opposite to the control force generated by thrust. This frequency is known as ‘tail-wag-dog’ (TWD) frequency. Above this TWD frequency, the engine inertia force produces the lateral force which is in phase with engine acceleration. Therefore under this condition the control system may be driven to divergent oscillation under the influence of one of the higher frequency vibration modes. It is therefore essential to adjust the control system gain during the tail off region and also to stop the control at appropriate flight time to avoid the phase reversal of the control force.

(d) Aeroelastic effects

In certain vehicles, the aerodynamic forces may couple with both rigid and flexible body dynamics. This aeroelastic coupling has a destabilizing effect on the vehicle by lowering the first bending mode frequency closer to control frequency. The aerodynamic centre of pressure can also move towards nose causing higher instability to vehicle. In such cases, control system designer has to carefully resort to phase stabilization instead of gain stabilization of lower vibration modes. If it is difficult suitable modifications have to be incorporated in the vehicle configuration.

(e) Response to winds

Vehicle response to winds is one of the important factors in control system design. While low frequency inputs manifest as ‘wind shear’, high frequency inputs are treated as ‘gusts’. Wind shear and gusts cause the increase of angle of attack on the vehicle and correspondingly the structural load. Therefore wind shear effect has to be considered in rigid body design. Depending on the response of the vehicle due to wind, it may be necessary to design the control loop with load relief to improve the rigid body performance. In addition, the flexible structure gets excited by gust and

hence the transient response of the vehicle due to gust can cause structural feedback. Therefore, the design of control system has to be carried out using the gust analysis to study the structural response for the recommended wind profiles.

(f) *Effect due to POGO*

In vehicles with liquid stages, there is a possibility of having sustained oscillations due to coupling of vehicle longitudinal structural oscillation and the propulsion systems. This is generally referred as POGO. Although this oscillation is essentially in longitudinal mode, there is a possibility of having coupling between longitudinal and lateral modes due to stiffness variations of structural elements. This causes the phase difference in the longitudinal modes which in turn causes certain lateral modes. Whenever such coupling occurs, it influences the vehicle sensor signals and may even lead to saturation under certain vibration levels. This would result into undesirable response of the vehicle and necessary corrective action has to be taken during the design phase.

14.6.6 Robustness Aspects and Design Validation

Vehicle and environment parameters and disturbances used for the autopilot design are predicted on ground, based on detailed tests and analysis. Errors in prediction strategies lead to dispersions on these parameters. Also, due to the insufficiency of prediction models and limitations in simulating real flight environment in ground test facilities, the in-flight parameters can be different from the predicted ones. Therefore, for all the parameters, there is a nominal predicted value and the flight realized value lying within a specified dispersion bound. In reality, the design can be done for a specified set of parameters only. For the cases of parameter deviations beyond the specified ones, the vehicle stability characteristics get affected. Generally, the autopilot is designed for the nominal parameters with built-in robustness margins to take care of the dispersions in the parameters. The design is such that the margins provided in the autopilot are sufficient to ensure that the vehicle is stable even in the dispersed flight environment. Once the design is finalized, it is essential to evaluate the performance and demonstrate the robustness of the autopilot design, under the parameter variations and ensure that the vehicle is stable even under the dispersed flight environment. Typical parameter variations and the impact of them on vehicle stability characteristics are given in Table 14.1.

The various steps involved in design validation and performance evaluation are given below:

1. Short period analysis:

(a) Frequency domain

- (i) Open loop for robustness and margins
- (ii) Closed loop to verify the bandwidth, disturbance rejection, etc.

Table 14.1 Parameter uncertainties

Sl No	Parameter	Perturbation level	Effect of perturbation on performance
1.	Forward gain K_a	$\pm 10\%$	Gain margin changes
2.	Feedback gain K_r	$\pm 10\%$	Phase lag changes
3.	First bending mode	Up to $\pm 10\%$	Rigid body performance is affected
4.	Second bending mode	$\pm 15\%$	Phase margin reduces
5.	Higher bending modes	$\pm 20\%$	Attenuation gets affected
6.	Actuator dynamics		
	Frequency	$\pm 10\%$	Phase lag due to actuator dynamics changes
	Damping ratio	± 0.2	
7.	Aerodynamic coefficients		Variation in aero loads and vehicle stability changes
	C_N, C_Y	$\pm 15\%$	
	X_{cp}, X_{cy}	$\pm 0.7 D$ (D is vehicle diameter)	
	Sensor dynamics		Phase lag gets affected
8.	Frequency	$\pm 2 \text{ Hz}$	
	Damping ratio	$\pm 0.2\%$	

(b) Time domain

- (i) With attitude command in step or ramp
- (ii) With wind disturbance

2. Long period simulations

- (a) Planar simulation
- (b) Six degrees-of-freedom simulation of rigid body with detailed models including engine inertia and slosh
- (c) Six degrees-of-freedom simulation with flexible vehicle dynamics including engine inertia and slosh

In short period model, the launch vehicle dynamics is frozen for a shorter period. The plant model is generated through perturbation equations of motion considered for that short period of time. The margins are verified by using the open loop transfer function of the compensated system as shown in Fig. 14.29.

The margins are to be verified under parameter perturbations on aerodynamic data, propulsion, actuator data, sensors data, slosh data and flexibility parameters in terms of frequency and mode shapes etc. These parameters are perturbed individually or in combination to establish the robustness of the system. If the margins are found to be inadequate to handle parameters dispersions, the autopilot design has to be tuned to obtain the required performance. The control bandwidth and disturbance rejection properties are to be evaluated using closed loop frequency response with respect to command and disturbance inputs such as wind, thrust misalignment, etc.

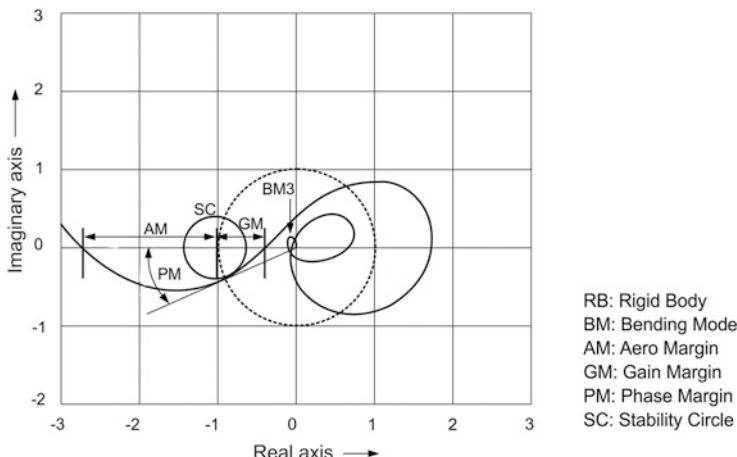


Fig. 14.29 Validation of autopilot in frequency domain

Time domain validation enables to evaluate the system response such as overshoot, rise time, settling time and also control demand. It is possible to include all non linearities, sensor accuracy, noise and all other aspects during the system modeling. The system response with slosh and flexibility is to be evaluated. One has to examine whether there are any substantial oscillations and whether it can be accepted. Similarly the system response to various disturbances like wind, thrust misalignment, differential thrust, etc. has to be studied to assess the disturbance rejection criteria. One needs to carry out these studies at different phases of flight particularly at critical time instants like high dynamic pressure, transonic regime, high upper atmosphere winds, etc. to assess the short-term stability of the system. Once these detailed studies are carried out incorporating detailed nonlinear models, the autopilot is integrated in long period simulation models for further analysis.

Long period six degrees-of-freedom simulation, incorporating the time varying models for propulsion, aerodynamic, mass, centre of gravity, moment of inertia, internal and external disturbances and navigation, guidance and control and vehicle and subsystem dynamics are needed to assess the performance of all subsystems and interactions. Initially low frequency dynamics such as rigid body, engine and slosh are included. Under the entire range of defined perturbation parameters for all subsystems, the simulations are carried out to evaluate the system stability, robustness and margins. Particularly the parameters viz. peak control demand, adequacy of stored control fuel, loads on the vehicle and maximum attitude errors and attitude rates in the controlled zones are evaluated. In the second phase, in order to study control structure interaction, the simulation is carried out with the additional degrees of freedom in the form of vehicle flexible modes. This is termed as flexible vehicle trajectory simulation and studies with perturbed parameters of the vehicle structural modes indicate the interactions if any between structure and control. Validation using other simulation test beds is explained in Sect. 14.8 under integrated NGC validation.

14.7 Control Power Plants and Actuation Systems

14.7.1 Functional Requirements

In a NGC system, vehicle autopilot subsystem generates the control command as per the control law and commands the control power plant to deflect the thrust vector with respect to vehicle axis to produce the necessary control force and moments. The main function of the actuation system is to realize thrust vectoring of the engines to achieve the control forces and moments as per the requirements of the autopilot. The thrust vector control (TVC) is achieved either by secondary injection (SITVC) of the fluid into the nozzle or by deflecting the engine/nozzle by means of closed loop actuation system. In systems where single engine is used, pitch and yaw controls are achieved by using two actuation systems mounted 90° apart. In stages where twin engines are used, pitch yaw and roll control is achieved by actuating each engine in two planes.

The actuation systems used generally in aerospace applications are either electro hydraulic, electro pneumatic, or electro mechanical system. Depending on the type of applications, one of the above actuation systems is used. Figure 14.30 shows a typical block diagram of an actuation system.

It is basically a position control system used to deflect the engine precisely to the commanded position as per the autopilot requirement. The position error is generated by computing the difference between sensed and commanded positions, and the same is appropriately processed through the control algorithm implemented in servo electronics to drive the actuator to correct the position error to zero.

14.7.2 Types of Control Systems

The various types of control power plants used in a launch vehicle can be classified as

- (a) Fin tip (and Jet vane) surface control system
- (b) Secondary injection thrust vector control system

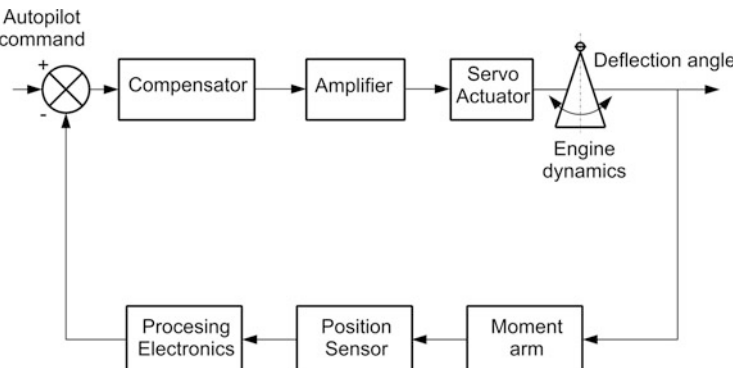


Fig. 14.30 Typical block diagram of an actuation system

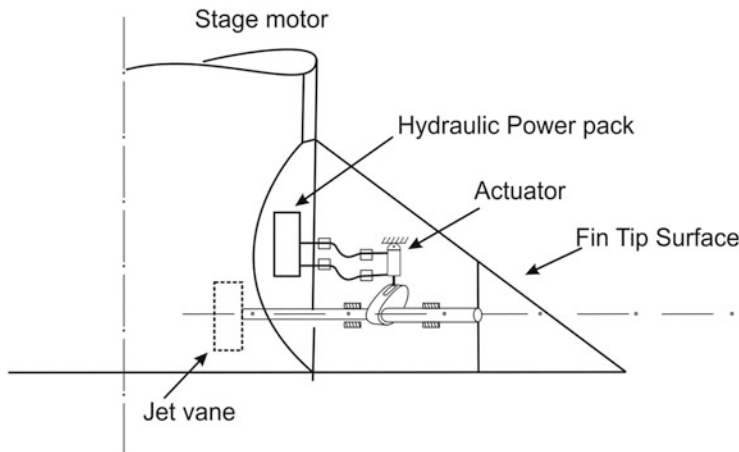


Fig. 14.31 Typical aerodynamic surface control system

- (c) Engine gimbal control system
- (d) Flex nozzle control system
- (e) Mono propellant or Bi propellant reaction control system

The selection of a suitable actuation scheme depends on several factors such as flight phase, type of stage used (solid or liquid), minimum performance loss, overall weight, ruggedness, overall reliability, ease of integration, cost and other relevant factors.

(a) Aerodynamic fin tip (and Jet vane) surface control

During the atmospheric phase of flight, the aerodynamic control system can be effectively used. A typical aerodynamic surface control is shown in Fig. 14.31.

A certain portion of the fin surface is deflected with respect to fixed fin using a shaft and an actuator. Figure 14.31 shows electro hydraulic system. It is possible to introduce jet vane on one other end of the shaft into the nozzle, made out of high temperature material which can withstand the high thermal loads and jet loads on the surface. Whenever the control surface is deflected the fin tip generates a side force due to the aerodynamic flow and the load acts at the centre of pressure of the surface exposed. Depending on the rotation of the shaft, the jet vane introduced into the nozzle deflects the combustion product and jet exhaust, thus generating a side force to control the vehicle. The side force generation with respect to angle of deflection has to be characterized in wind tunnel tests.

(b) Secondary injection thrust vector control system (SITVC)

In this system, a secondary fluid such as freon, nitrogen tetroxide (N_2O_4), or strontium perchlorate is injected under pressure into the rocket exhaust nozzle. The block diagram of a typical SITVC system is shown in Fig. 14.32.

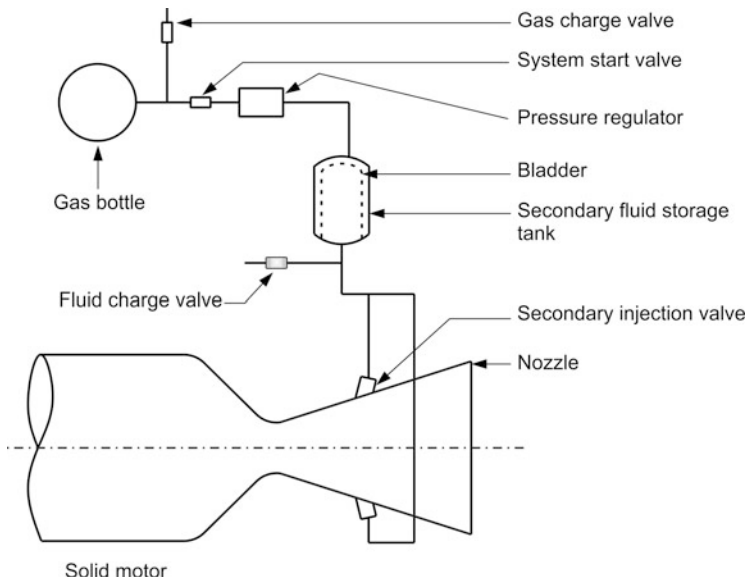


Fig. 14.32 Block diagram of a typical SITVC system

This secondary stream in the nozzle creates a shock wave which in turn causes an effective deflection of the thrust vector, causing a side force on the vehicle. The essential component in this system is the proportional injection valve which is operated using an electro hydraulic or electro mechanical system. The shape of pintle of the valve has to be designed such that fluid injection into the nozzle is proportional to the input signal.

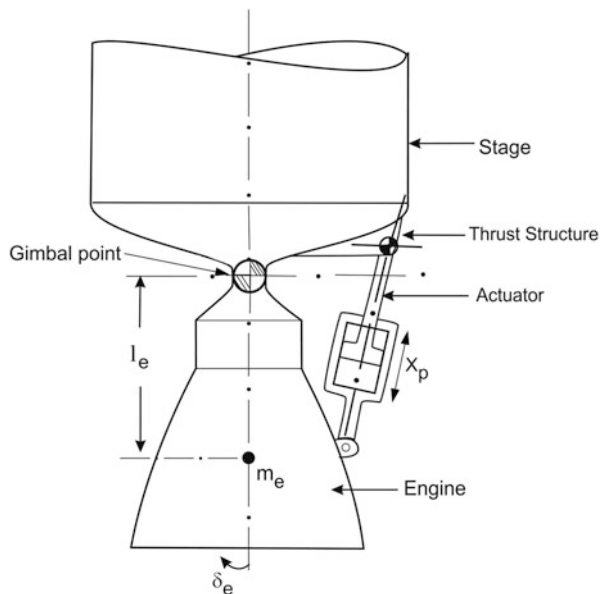
The secondary fluid and pressurized gas requirements have to be worked out considering the stage operation time, the quantity of fluid to be injected into the nozzle and also the duty cycle. It has to be ensured that sufficient quantity of secondary fluid is available to meet the overall control impulse requirements.

(c) Engine Gimbal control System

In this system, the main engine of the vehicle is mounted to stage through a gimbal bearing which is designed to have the engine thrust pass through the centre of the bearing and to facilitate the two axis movement of the engine. The main thrust of the engine is deflected to produce the lateral control force on the vehicle. The maximum deflection of the engine to be decided based on the maximum force needed to control the stage. A typical engine gimbal control system is shown in Fig. 14.33.

The servo actuator used in the system can be electro mechanical or electro hydraulic actuation system. One end of the servo actuator is mounted on to the fixed structure of the vehicle whereas other end is attached to the engine. The stiffness of the structural elements connected on either end of actuator has to meet the specified values to ensure the required response from the actuator.

Fig. 14.33 Typical engine gimbal control system



(d) Flex Nozzle Control System

In solid motors, the pitch and yaw control can be achieved using flexible nozzle control (FNC) system. A schematic diagram of a FNC system is given in Fig. 14.34. Nozzle of the stage is connected to the main solid motor through a flexible bearing as shown in the figure. The bearing is made up of alternate layers of metallic shims and elastomeric rings. The nozzle is submerged into the main motor and the flex seal is connected between the motor and nozzle. The characteristic of the flex seal varies with the nozzle deflection and motor chamber pressure.

The actuator is mounted between the motor case and movable nozzle in both pitch and yaw axes. The actuators can be either electro mechanical or electro hydraulic. In flex seal systems, when the seal is subjected to motor pressure at the time of motor ignition, the seal tends to move axially. But the actuator connected in one of the planes does not allow the movement of flex seal since it is commanded at null. This causes the instantaneous tilt of the nozzle towards the actuator and this is not allowed as it produces the undesirable side force on the vehicle. To overcome this situation, two position sensors are used with one mounted on the actuator and the other mounted at 180° to the actuator called mirror image sensor. The differential average of these two diametrically opposite sensors provides the angular tilt of the nozzle and the servo system brings back the nozzle to the null condition to avoid the angular deflection of nozzle. Since the flex seal is submerged into the nozzle it has to be protected against high temperature by providing a thermal boot.

(e) Monopropellant or Bipropellant reaction control systems

Reaction control systems are basically on-off control systems and mostly preferred during the coast phase although it has been used in some vehicle during the powered

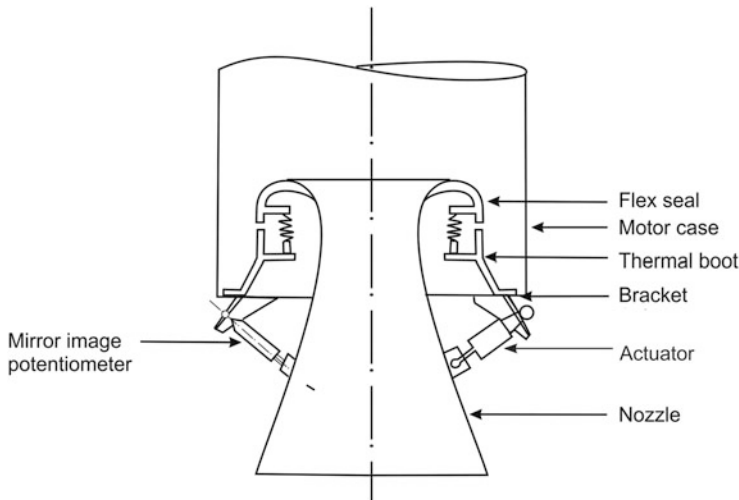


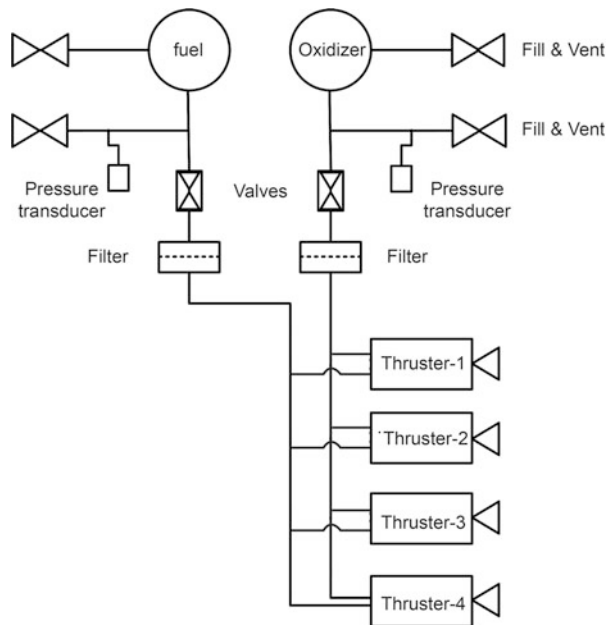
Fig. 14.34 Typical flex nozzle control system

phase also. These systems can be realized by using either cold gas where the control force and impulse requirements are low or by employing reactive fluids. Commonly used mono propellant system is hydrazine with a suitable catalytic reaction. When the thrust and impulse requirements are high, bipropellant systems such as N₂O₄ and UDMH combination are used. The hypergolic action of these two propellants in the combustion chamber produces hot gas which causes the reaction force. The simplified diagram of a bipropellant system is shown in Fig. 14.35.

14.7.3 Salient Design Aspects and Specifications for Actuation Systems

The actuation systems used in the launch vehicle is the innermost control loop of the navigation guidance and control system of the vehicle. The autopilot generally has a bandwidth of 0.6–0.8 Hz, and therefore the actuation control loop bandwidth should be at least 5–6 times of autopilot bandwidth to provide enough separation. This bandwidth is defined for 10 % of the total angular deflection amplitude of the servo system used. This defines the overall speed of the servo system. The maximum torque for the servo system is computed taking into account loads such as inertia of the engine, viscous friction, torque due to flexible joints for propellants and all other disturbance torques. Thus, the actuation torque T_A needed for the system is computed as:

Fig. 14.35 Typical bi propellant reaction control systems



$$T_A = J \ddot{\delta}_e + \beta \dot{\delta}_e + C_e \frac{\dot{\delta}_e}{|\dot{\delta}_e|} + K \delta_e + T_L \quad (14.114b)$$

where

J = Engine inertia

β = Viscous friction

C_e = Coulomb friction

K = Flexible joint restraint

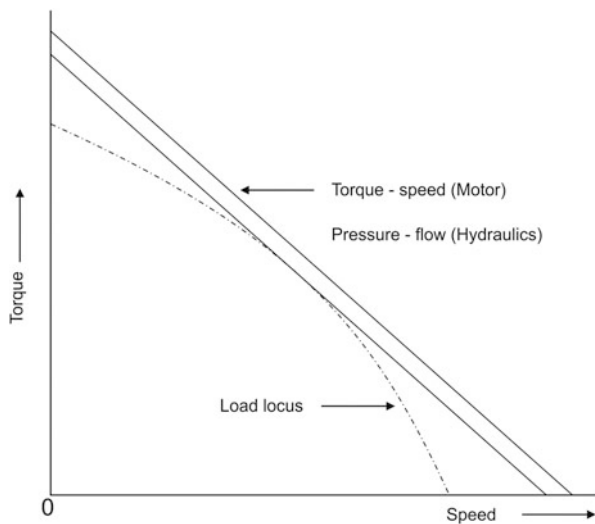
T_L = External torque

δ_e = Engine deflection

In actuation systems, the drive motor selection for an electro mechanical system or pressure and flow selection for an electro hydraulic system depend on the torque and speed requirements needed for the overall system. The torque-speed requirement for the servo is computed by generating a torque-speed plot known as load locus curve.

The torque-speed requirement is computed using the Eq. 14.114b for a sinusoidal deflection of 10 % amplitude of the total engine deflection at various initial angles of deflection. A typical load locus so generated is given in Fig. 14.36. The torque speed characteristic of the electric motor chosen or pressure flow characteristic of hydraulic system chosen should encompass the load locus plot with sufficient margin. This margin is necessary to account for many uncertainties on the system like unforeseen loads, performance variation at higher temperatures, etc.

Fig. 14.36 Load locus curve for actuator system



Depending on the selection of a suitable actuation system, various elements of the system are chosen to give the required performance. The major system specifications can be given as follows.

- Maximum engine deflection in degrees (\pm)
- Maximum slew rate in degrees/s
- System bandwidth; 10 % input amplitude in Hz
- Type of actuation system
- Position error (steady state) in %
- Period of operation in seconds
- Length of the actuator in mm
- Actuator strokes in mm (\pm)
- Envelope size
- Power requirement per actuator in watts
- Actuator mass in kg

It is also essential to specify the operating environment for the servo system in terms of vibration, shock, longitudinal acceleration and operating temperature (thermal environment)

The actuation systems in a launch vehicle are mission critical elements, because mostly they are prone to single point failures. Therefore its reliability should be very high. Wherever possible, suitable redundant systems are to be introduced. These systems are also subjected to exhaustive qualification tests at different stages of their preparation. The acceptance and qualification levels are to be defined carefully to ensure its performance under all operating environment conditions.

14.8 Integrated NGC System Validation

The NGC system in a vehicle is a complex combination of hardware and software elements wherein hardware consists of inertial sensors, associated electronics, onboard computers in which navigation, guidance, control and sequencing software resides, sequence execution relays, control actuators and its electronics. Software consists of navigation algorithm, guidance and autopilot law. Flawless performance of the NGC system under various conditions of flight environment is very vital for the successful mission of a launch vehicle. Therefore, the NGC hardware and software residing in onboard computers have to perform without any failures under all disturbances and vehicle environment. To ensure the above objectives, the NGC system has to be evaluated in detail by adopting systematic simulation techniques during the system development phase.

The navigation system consisting of sensors, associated electronics and its software are realized independently and tested extensively during the development phase. Similarly the guidance and autopilot software undergo exhaustive tests independently. On satisfactory performance, all the subsystems are integrated into NGC system. In order to improve the overall reliability of NGC system, invariably redundancy is introduced either as duplex or triplex chain depending on the overall requirement. Systematic validation procedure has to be followed at various phases of development using various test beds to evaluate the subsystem performance and integrated system performance in terms of intended functions, to identify the deficiencies in hardware, software or its interfaces and to implement the necessary corrections wherever needed to guarantee the successful flight.

14.8.1 Requirements and Simulation Test Beds

The major software elements of the integrated NGC system are:

- Navigation software which computes the instantaneous position, velocity and attitude of the vehicle with respect to a defined reference frame.
- Guidance algorithm and law generates the desired attitude angles to meet the defined target orbit.
- Digital autopilot algorithm and law generates the necessary control commands to achieve the desired attitudes.
- The vehicle sequencing issues commands as a function of flight time and also based on real time decision whenever the vehicle transits from one propulsive stage to another.

The major hardware elements are:

- Computer hardware wherein software elements reside
- Redundant computer systems
- Sensors
- Control power plants

The various requirements for the validation of integrated NGC system can be broadly defined as:

1. Ensuring the flawless flight performance of NGC system under the defined vehicle environment during the entire regime of flight
2. Establishing the robustness of the software and system under both nominal and abnormal flight conditions
3. Ensuring correct interfaces between various elements
4. Identifying the anomalous behavior of the software under extreme flight environment including certain failures
5. Evaluating the mission performance and stability of the vehicle with the actual control actuators including its nonlinearities under different flight conditions
6. Verifying the mission performance with actual inertial sensors under closed loop environments
7. Ensuring the end-to-end compatibility of the entire NGC hardware and software and signal flow for proper performance
8. Verifying the end-to-end sign checks with entire NGC chain in the loop
9. Checking the redundancy aspects wherever it is used and verifying the impact of failures

Ideally to validate the integrated NGC system in a ground test bed, one should use all the elements of NGC including sensors and actuators similar to the flight configuration. In order to generate sensor outputs as in flight, the inertial sensors are necessarily to be mounted on three axis angular motion simulator (AMS). Based on the vehicle attitude dynamics as computed by the simulation system, the AMS is commanded in three axes to simulate the vehicle pitch, yaw and roll motion, and the attitude sensors mounted on the AMS thus produce the corresponding outputs. As the AMS is commanded with the output of the vehicle dynamics, in order to simulate the realistic sensor output, the AMS system should have infinite bandwidth. But realistically, it is not possible and due to finite bandwidth limitations of AMS, there is a lag in sensor output relative to the one observed in flight. Also as number of validation simulations is large, it is difficult to bring in the actuators in all the simulations due to operational limitations. Additionally, if the same actuators are repeatedly used in all the simulations, the actuator performance can be degraded relative to the flight actuator performance and in this case, the results can lead to wrong conclusion. These limitations lead to simulations with a single actuator hardware. Therefore, in order to have comprehensive evaluation of NGC system, validation has to be carried out in different test beds in a progressive manner with specific objectives as given in Fig. 14.37.

The overall validation cycle for NGC need several steps as given below:

1. Algorithm validation
2. Code level evaluation
3. Subsystem level tests with both open and closed loop tests
4. Integrated processor level open loop tests
5. Onboard computer in loop (OILS) tests

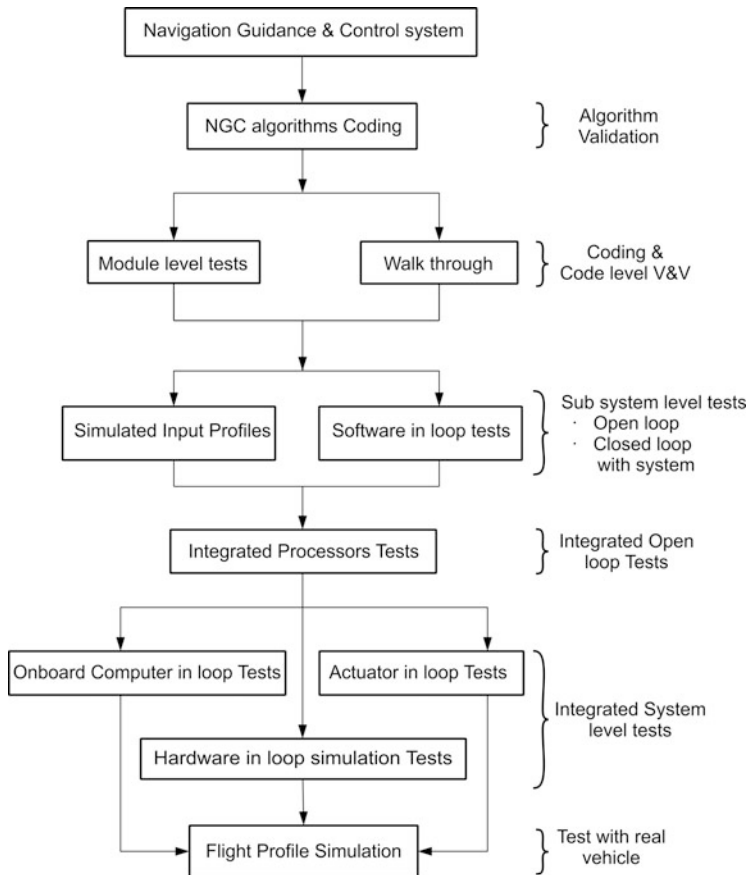


Fig. 14.37 Systematic validation procedure using various test beds

6. Actuators in loop tests (ALS)
7. Hardware in loop tests (HLS)
8. Tests with final integrated vehicle level

The algorithm validation, code level evaluation and subsystem level tests are to be carried out extensively during the design phase to ensure that each of the designed algorithm meets the overall requirements of mission. The integrated open loop processor tests are essential to carry out integrated mode testing of actual hardware with all onboard computers and actual flight software. From the digital simulation test bed, the open loop simulation profiles are generated and used in these tests essentially to verify the redundancy management aspects, error handling logics and several failure mode studies.

14.8.2 Integrated Validation Strategy

The closed loop evaluation of NGC system is to be carried out using three test beds namely: (a) onboard computer in loop tests, (b) actuator in loop tests and (c) hardware in loop tests. Figure 14.38 elaborates the NGC system validation methodology.

The various blocks shown inside the dotted line box in the figure is essentially a typical digital simulation test bed with detailed models on vehicle and subsystems, environment, gravity and vehicle dynamics. The NGC subsystems elements such as onboard algorithms, sensors and actuation, etc. are also modeled. The autopilot model has to include the gain schedules, control laws, filter characteristics, control dynamics of actuators and all other features. Guidance software includes open loop trajectory during atmospheric phase, closed loop guidance law and all other associated software. The navigation software comprises of navigation system simulator incorporating all features of the system including the sensor error compensation.

Digital simulation test bed has to be used extensively to evaluate the performance of the integrated navigation, guidance control and sequencing software by carrying out the following tests:

- System performance verification at various phases of flight to assess the tracking errors, flight loads, vehicle controllability at critical regions, control demand estimation, control impulse requirements, etc.
- Guidance performance studies, final mission dispersions under off nominal performance of the vehicles, guidance margin adequacy, etc.
- Vehicle failure mode studies and robustness estimation. These tests are the real indication of flight performance and it is necessary to identify all deficiencies and take necessary corrective actions by introducing the modifications wherever essential.

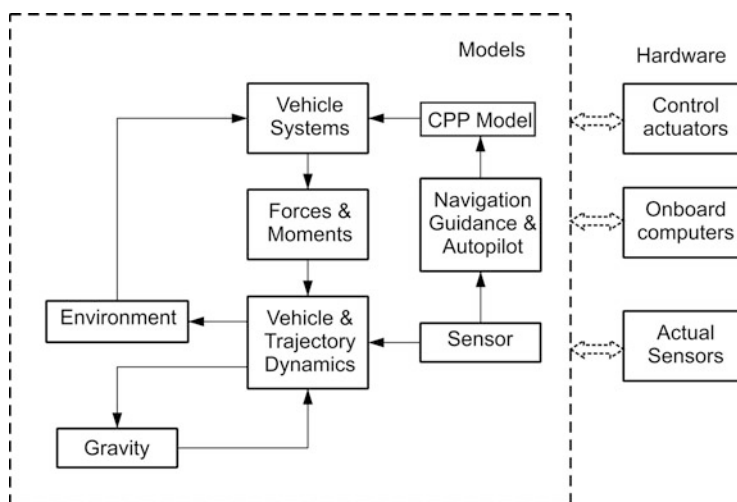


Fig. 14.38 NGC system validation methodology

Subsequent to completion of this simulation, the vehicle NGC hardware like onboard computers where the NGC algorithms are implemented, control actuators of all stages and the actual inertial sensors identified for the flight are to be progressively integrated with the simulation test bed as shown in Fig. 14.38. Once the hardware is interfaced with the system the corresponding software pertaining to these hardware, which were used earlier are disconnected.

14.8.3 Progressive Tests with NGC Hardware in the Loop

The first set of hardware to be interfaced with the all digital simulation test bed is the onboard computers in which onboard navigation, guidance and control software reside as in flight configuration. The vehicle systems, subsystems, vehicle dynamics, flight environment, inertial sensor dynamics and actuator dynamics are all modeled and reside in the simulation computer. The onboard computers are to be interfaced with simulation computer and also data acquisition computer appropriately. The main objectives of the tests are:

- (a) To evaluate the mission performance with flight software in the loop for different flight conditions namely
 - 1. Dispersion and disturbances within specified limits
 - 2. Dispersion beyond specified limits
 - 3. Very large disturbances which is termed as stress tests
- (b) To study the interactions with other systems and vehicle dynamics
- (c) To understand the mission implications under the subsystems failure conditions

Very extensive tests are needed in this test bed to ensure the expected mission performance under all combinations of flight disturbances throughout the duration of flight. This demands careful generation of test cases which encompasses all possible combinations of vehicle disturbances and their limits. The methodology for generation of such test cases is explained in the next section.

Subsequent to these tests the actual flight control actuators are to be interfaced with the system. These tests are essential to evaluate the mission performance and stability aspects of the vehicle by exercising all nonlinear behavior of the actuators. The specific areas which need attentions during these tests are vehicle loads, control forces, subsystem responses to disturbances, control capture analysis and vehicle stability particularly the control actuator slosh Interactions.

Integrating the actual sensors in the loop, termed as hardware-in-loop test, is the ultimate test for evaluating the integrated NGC system performance. Figure 14.39 illustrates various elements of test bed used in the progressive simulation of NGC system with onboard computers, actuators and sensors.

Drive commands for angular motion simulator (AMS) are issued from simulation computer as per the simulated vehicle attitude. The sensor output is used in the

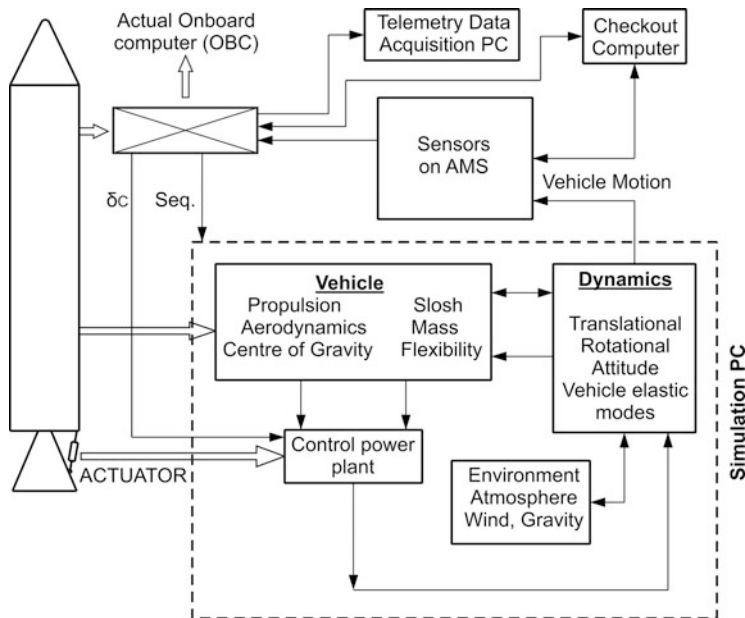


Fig. 14.39 Progressive simulation of NGC system with onboard hardware

onboard electronics packages mounted in AMS as in flight configuration. The output of onboard packages such as control command and sequencing are used in the simulation computer to simulate the vehicle responses, which in turn are used to drive the AMS. This test bed helps to ensure the end-to-end compatibility of entire NGC chain and also to verify the signal flow for satisfactory performance. Effect of sensor errors on the overall mission performance has to be assessed.

14.8.4 Criteria for Generation of Test Cases and Validate Results

The major objectives of NGC system validation in several test beds in a progressive manner are to verify the normal functioning of the system under nominal, dispersed and abnormal flight conditions and to evaluate the robustness of the system under the extreme environment. Therefore, the test cases are to be generated carefully to ensure that the hardware and software are tested for all combination of input parameters of the vehicle subsystems and also environmental disturbances

Typically the test cases should cover the nominal and all possible combination of dispersions for the parameters as per the details given below:

(a) Propulsion

1. Performance dispersions of the motors like chamber pressure, specific impulse, action time, mixture ratio, and propellant mass

2. Differential performance if more number of motors are used in a stage
 3. Tail off characteristics
 4. Thrust misalignment angles
- (b) Mass characteristics
1. Overall mass
 2. CG offset
- (c) Aerodynamics
3. Normal and side force coefficient
 4. Centre of pressure
- (d) Fluid slosh
1. Slosh characteristics
- (e) Winds
1. Measured and synthetic wind profiles
- (f) Separation disturbance

Different combinations of input parameters of all the above parameters are to be used for generation of test cases. The dispersion bands to be used should be not only within 3σ values but also extreme cases to the maximum possible extent depending on the parameters. The test cases generated should be aimed so that they exercise all possible logics embedded in on board software. The ultimate aim is to ensure that the tests carried out are comprehensive. The failure conditions are also to be defined properly so that they can be simulated during simulations and proper care has to be taken to avoid damage to any of the subsystems/system used in the simulation.

Bibliography

1. Vander Velde, W.E.: Space Vehicle Control Systems, Space Navigation, Guidance and Control, AGARDograph 105 (1966)
2. Newport, J.R.: Avionics Systems Design. CRC Press, Boca Raton (1994)
3. Etkin, B.: Dynamics of Flight. Wiley, New York (1959)
4. Collinson, R.P.G.: Introduction to Avionics. AIAA, Reston (1996)
5. Biezad, D.J.: Integrated Navigation and Guidance Systems. AIAA Education Series. AIAA, Reston (1999)
6. Cherry, G.W.: A General Explicit Optimizing Guidance Law for Rocket Propelled Space Flight", AIAA paper, 64-638 (August 1964)
7. Henry, M.C., Brand, R.L., Long, A.D., Cockwell, B.F., Thibodeau III, J.R.: Space Shuttle Ascent Guidance, Navigation and Control. J Astronaut Sci 27(1), 1-38 (1979)
8. Calise, A.J., Martin, S.K.L.: Optimal Guidance Law Development for an Advanced Launch System, NASA TR Issue, NASA CR 4667 (1995)
9. Sinha SK, Shrivastava S K., Bhat, M S, and Prabhu, K.S.: "Optimal Explicit Guidance for Three Dimensional Launch Trajectories", pp 115-123, Acta Astronautica, Vol-19 (1989)

10. Leung M.S.K., Anthony J. Calise.: "A Hybrid Approach to Near Optimal Launch Vehicle Guidance", AIAA-92-4304-CP (1992)
11. Vidyasagar. M.: Nonlinear Systems Analysis. Prentice Hall, Eaglewood Cliffs (1993)
12. Bryson, A. E.: Applied Linear Optimal Control. Cambridge University Press, Cambridge (2002)
13. Bruhn, E.F.: Analysis and Design of Flight Vehicle Structures. Tri-state offset Co., Cincinnati (1973)
14. Dukeman, G.A.: Atmospheric Ascent Guidance for Rocket Powered Launch Vehicle. AIAA guidance navigation and control conference and exhibit, Monterey, CA (2002)
15. Corban, J.E, Calise, A.J, Flandro, G.A.: Rapid near-optimal aerospace plane trajectory generation and guidance. *J. Guid. Contr. Dyn.* **14**(6), pp 1187–1188 (1991)
16. Gage, M.W.: FE Guidance and its Applications to the ELDO Launch Vehicle. Royal aircraft technical report – 68201 (1968)
17. Greensite A.L.: Analysis and Design of Space Vehicle Flight Control Systems. Spartan Books, New York (1970)
18. NASA space vehicle design criteria "Effects of Structural Flexibility on Launch Vehicle Control Systems", NASA TR, Issue, NASA-SP-8036 (1970)
19. Biezad, D.J.: Integrated Navigation and Guidance systems. AIAA Education series, Reston, VA (1999)
20. Peal, R.A.: Avionics Systems of the 21st Century. *Aerosp. Eng.* **12**(3), 22 (1992)
21. Wie, B.: Space Vehicle Dynamics and Control. AIAA Education Series. AIAA, Reston, VA (1998)
22. Hammond, W.E.: Space transportation: a systems approach to analysis and design. In: Przemieniecki, J. S. (eds.) AIAA Education Series. AIAA, Reston, VA (1999)
23. Britting, K.R.: Inertial Navigation Systems Analysis. Wiley Interscience, Somerset (1971)
24. Garner, D.: Control Theory Handbook, NASA TR, Issue, NASA TM X-53036 (1964)
25. Frosch, J.A., Valley, D.P.: Saturn AS-501/S-IC Flight Control System Design. *J. Spacecr.* **4**(8), 1003–1009 (1967)
26. Gupta, S.C., Suresh, B.N.: Development of navigation, guidance and control technology for Indian launch vehicles. *Sadhana* **12** (Part. 3) Publication of Indian Academy of Sciences, Bangalore (1988)
27. Haeussermann, W.: Description and Performance of the Saturn Launch Vehicle's Navigation, Guidance, and Control System, NASA TR issue, NASA TN D-5869 (1970)
28. Blakelock, J.H.: Automatic Control of Aircraft and Missiles, 2nd edn. Wiley, New York (1991)

Chapter 15

Re-entry Missions

Abstract After orbiting the spacecraft, in many cases the materials are to be brought back from space to Earth. It is also essential to bring back the humans safely from space after completion of the space exploration experiments. During the return of the vehicle from space, it re-enters the Earth's atmosphere with orbital speed and remains in the atmosphere for the entire duration of the mission till the vehicle is brought to rest at the specified location. During this regime, the vehicle travels with very high hypersonic speeds at relatively lower altitudes and this causes harsh environments to the vehicle along with different complex flight regimes. Design of such a vehicle which has to fly safely in the severe operating environment with highly varying flight operating regimes along with large dispersions in both flight and vehicle parameters and ensuring the safe landing at the specified location is quite complex. All the reentry space transportation systems are having a wide range of flight regimes with large dispersions in flight parameters, severe flight environments and different functional requirements. For the case of reentry missions, the aerothermal operating environment is entirely different for different missions and strongly depends on the trajectory of a particular reentry mission which makes the vehicle design as unique for the specified reentry mission. The reentry systems are truly interdisciplinary with strong coupling between various vehicle systems viz., aerodynamic configuration, thermal protection systems, structure and vehicle trajectory. Therefore, integrated systems approach is essential for the optimum reentry systems design. This chapter addresses the design guidelines, complexity of the flight environment and the design for reentry systems. The reentry dynamics and reentry vehicle configuration aspects are discussed. The aerothermodynamics aspects which involve aerodynamic design, structural design, thermal environment and thermal protection system design of reentry vehicles are included. The details of the thermal protection systems are presented. The salient aspects of the trajectory design, reentry guidance schemes and mission management are highlighted.

Keywords Reentry system • Flight environment • Reentry dynamics • Hypersonic aerothermodynamics • Thermal protection system • Reentry mission management • Guidance strategy and terminal area energy management

15.1 Introduction

The design aspects of STS to meet the requirements of ascent phase of the space missions have been extensively discussed in the previous chapters. These chapters essentially cover the system requirements, functional requirements and design of subsystems for an efficient, cost effective, robust and reliable STS to carry the specified payload from Earth and deliver it safely into the required orbit in space. The payloads for the ascent phase of STS are the satellites, materials or humans in orbits around Earth for various applications including space exploration as well as planetary probes for the space science and exploration missions.

After carrying out the intended experiments in orbit, in many cases the materials are to be brought back from space to Earth. It is also essential to bring back the humans safely from space after completion of the space exploration experiments. The return of space station crew members in case of emergency and recovery of space objects from orbit after completion of the space experiments are other essential requirements. The planetary probes sent for collecting the samples from the asteroids, planets and their moons have to be necessarily recovered back to retrieve the samples for experimentation. The instruments sent for the planetary exploration for carrying out science experiments in situ have to be brought back for further investigations.

The tasks of bringing the objects and materials from space to Earth safely can be achieved by any one of the options given below:

1. By using a module which is a part of the vehicle or payload of STS during its ascent mission.
2. By another small vehicle which is normally a glider, sent as a payload in ascent STS.
3. Or a major STS module which is used for launching satellites/humans into space itself is brought back to Earth.
4. To reduce the cost of launching materials into space, worldwide efforts are to develop an efficient and feasible reusable launch vehicle (RLV). Once the intended function during its ascent mission is completed, either separated stages or the entire vehicle as a whole is returned to launch site and prepared for the next mission after necessary refurbishment as in the case of conventional air transportation systems.

In all these cases, during the return of the vehicle from space, it re-enters the Earth's/planet's atmosphere with orbital speed and remains in the atmosphere for the entire duration of the mission till the vehicle is brought to rest at the specified location. During this regime, the vehicle travels with very high hypersonic speeds at relatively lower altitudes and this causes harsh environments to the vehicle along with different complex flight regimes. Design of such a vehicle which has to fly safely in the severe operating environment with highly varying flight operating regimes along with large dispersions in both flight and vehicle parameters and ensuring the safe landing at the specified location is a challenging task.

In the first option, where the module is used as part of the vehicle or payload of specific reentry mission, is to be designed with defined objectives. In these cases, robust designs of modules with the desired shape and appropriate thermal protection system to withstand the severe environment of reentry missions are feasible. Such designs are not expected to have additional features to cater to mission flexibility but still are being used worldwide. The disadvantages of this system are: (1) as the module is required to be transported to space by a separate ascent launcher, the module size and mass are constrained by the launch vehicle capabilities; (2) due to the simple shape, the operating regime of the module is limited; (3) as each module is designed and used for a specific purpose, there is no mission flexibility and (4) the modules are expendable and hence it has only one time use. It is essential to prepare a new module every time and therefore it is not cost effective.

In the second option of carrying a glider to the space by an expendable launch vehicle and using it in the reentry mission, the interfacing issues and the constraints with respect to the launch vehicle are to be carefully worked out. Since these vehicles are aerodynamically configured with good amount of lift, they provide a greater amount of mission flexibility. As this system can be recovered safely by the controlled reentry flight, it can be reused and thus becomes cost effective. However, the designs of such gliders are more complex than modules. But with the present day technologies, they are feasible and are being used.

For the case of third option, wherein the same STS is used for ascent and reentry missions, the subsystems designs have to meet the requirements of both phases. Even though system requirements are same; the functional and design requirements for ascent and reentry missions are entirely different and conflicting. Configuring such vehicles with aerodynamic lifting and control surfaces to meet the mission flexibility further complicates the design process. Considering the efficiency, cost effectiveness, reliability, reusability, the need to have frequent access to space, the higher performance and emerging space tourism, the design of such advanced STS systems has become quite attractive. Therefore this design is pursued by all major space-faring nations. However, certain critical technologies particularly in the area of material, thermal protection systems and advanced propulsion systems pose serious problems and they have to be mastered to realize and operationalize such vehicles.

In case of the interplanetary mission where it has to carry out in situ space science experiments, the experimental probes need to enter into the planetary atmosphere and land precisely at the designated location on the planetary surface. Such mission has to be planned by utilizing the aero assisted orbital transfers to reduce the propulsion requirements and by using the planetary atmosphere as aero braking device to reduce the orbit size. In all such missions, the design of space probes has to be robust to encounter the planetary atmospheric entry missions.

In summary, all the reentry space transportation systems are having a wide range of flight regimes with large dispersions in flight parameters, severe flight environments and different functional requirements. All of them have to be simultaneously satisfied to achieve the successful reentry missions. Unlike the expendable ascent STS, the reentry STS are not generic in nature. Even though complex and harsh, the

operating flight environments for various ascent missions are similar. Therefore, once a vehicle is designed for a mission, the same can be used for other missions also, depending on its capabilities to meet the mission objectives. For the case of reentry missions, the aerothermal operating environment is entirely different for different missions and strongly depends on the trajectory of a particular reentry mission which makes the vehicle design as unique for the specified reentry mission. The reentry systems are truly interdisciplinary with strong coupling between various vehicle systems viz., aerodynamic configuration, thermal protection systems, structure and vehicle trajectory. Therefore, integrated systems approach is essential for the optimum reentry systems design.

The process of designing reentry missions, complexity of the reentry flight environment and design guidelines of reentry systems is explained in the next section. The reentry dynamics and reentry vehicle configuration aspects are given in Sect. 15.3. The aerothermodynamics aspects which involve aerodynamic design, structural design, thermal environment and thermal protection system design of reentry vehicles are described in Sect. 15.4. Trajectory design and mission management play a major role in the reentry systems design and controlled reentry of the vehicle. These details are included in Sect. 15.5.

15.2 Operating Environment and Reentry System Design Guidelines

At the beginning of reentry mission, the vehicle possesses both kinetic and potential energies which are imparted to the vehicle by ascent phase propulsion systems. To bring the vehicle back to Earth at the designated location, the energy acquired by the vehicle during its ascent mission need to be completely dissipated. The ideal method of dissipating the energy would be to use braking rockets. In this case, theoretically, the braking rockets required have to be of the same size as that used during launch; i.e., this procedure, in essence, is nothing but a re-run of ascent mission, but in reverse direction and is prohibitively expensive. Instead, atmospheric drag encountered by the vehicle during its reentry mission is effectively utilized to dissipate the energy and bringing the vehicle back to a complete halt. This is simple, efficient and cost effective process of dissipating the energy of the reentry vehicle. The use of atmospheric drag force to dissipate the energy of reentry vehicles introduces two major challenges for the vehicle design as detailed below:

1. As the vehicle approaches Earth's atmosphere, its velocity is maximum and atmospheric density is minimum. Therefore, the initial drag force is not sufficient to dissipate the energy at the higher altitude and the vehicle penetrates the atmosphere very fast and reaches the dense atmosphere with velocity almost equal to the large magnitude reentry velocity. This causes a sharp increase in the aerodynamic loads including the drag force acting on the vehicle structure.

2. Vehicle reenters the atmosphere with very high kinetic energy due to speed almost equal to the orbital speed. During the process of energy dissipation, the kinetic energy of the vehicle is converted into thermal energy. As an example, for a return mission from low Earth orbit (LEO), the vehicle reenters the atmosphere with the velocity of about 8 km/s whereas for the return from lunar and interplanetary missions, the vehicle reenters the Earth atmosphere with the velocities of about 11 km/s and 16.4 km/s respectively. From aero thermodynamic point of view, these are the free stream hypersonic velocities of air particles with respect to the vehicle when it reenters the atmosphere. The strong normal shock generated by the hypersonic flow, standing in front of the vehicle, compresses and slows down the air particles and in this process, the internal energy of the air particles increases. In this energy conversion process, the aerodynamic drag force reduces the speed of the vehicle. Further the kinetic energy of air particles is dissipated and in turn the internal energy is increased. For the case of perfect gas, the internal energy increase is in the form of increasing the temperature of air particles i.e., the entire energy is converted into temperature rise of air particles between shock wave and front portion of the vehicle. This hot air bathes over the entire body of the vehicle behind the shock wave and through heat transfer mechanisms viz. convective and radiative transfer process, the thermal energy is transferred to the vehicle body. For the reentry from LEO, the heat transfer through convection of hot air flow process is crucial. For the case of reentry with higher velocity as in the case of lunar or interplanetary return missions, the temperature of hot air is sufficiently high, in addition to the convective heating process; the heat transfer to body through radiative process is also higher.

To emphasize the severity of thermal environment of the reentry vehicle, it may be noted that the water and carbon vaporize at the specific energy levels of about 2325 J/kg and at about 60,000 kJ/kg respectively, whereas the specific kinetic energy of reentry vehicles from LEO, lunar and interplanetary return missions at the time of reentry into atmosphere are about 30,000 kJ/kg, 60,000 kJ/kg and 136,000 kJ/kg, respectively. Therefore, if the entire kinetic energy is converted into thermal energy as in the case of perfect gas, the reentry vehicles would vaporize in the atmosphere itself. In reality, during atmospheric reentry, in addition to the temperature increase, the internal energy increase excites the vibration energy of the diatomic particles, dissociating the air molecules and converting into ions. Therefore, considerable amount of internal energy increase of air particles in the process of dissipation of kinetic energy is absorbed for the chemical reaction process which in turn limits the temperature increase of the air particles. As the temperature of the air particles increases, along with the heat transfer to the vehicle, some amount of heat is radiated to the atmosphere also. Therefore, in reality, while dissipating the kinetic energy of the vehicle, some portion of it only is transferred as thermal energy to the vehicle. However, as small fraction of a large quantity itself is quite substantial, the thermal environment to the vehicle during reentry is severe, and the vehicle needs to be protected against such a harsh environment.

An atmospheric reentry mission is successful only when the reentry vehicle survives the aerodynamic and heating loads. Therefore the overall objective of a reentry mission can be stated as “to bring safely the space vehicle from orbit to Earth and land precisely at a specified location”. To achieve this objective, it is essential to dissipate the kinetic energy in a controlled fashion so that this conversion along with the sharp increase in the structural loads is not disastrous to the vehicle. This complex task is carried out as follows:

1. Shaping of the reentry vehicle to reduce the thermal environment while meeting the mission requirements under the dispersed flight conditions.
2. Suitable thermal protection to reduce the severity of thermal environment to the vehicle structure.
3. Careful design of reentry mission trajectory so as to reduce the adverse environment during the entire mission. During actual mission, the feasible trajectory is to be designed within the reentry corridor, defined by heating, structural and controllability limits of the vehicle. It is also essential that it is planned in real time.
4. A precision guidance and control system has to steer the vehicle on the feasible trajectory to achieve the specified target conditions safely within the defined error margin.

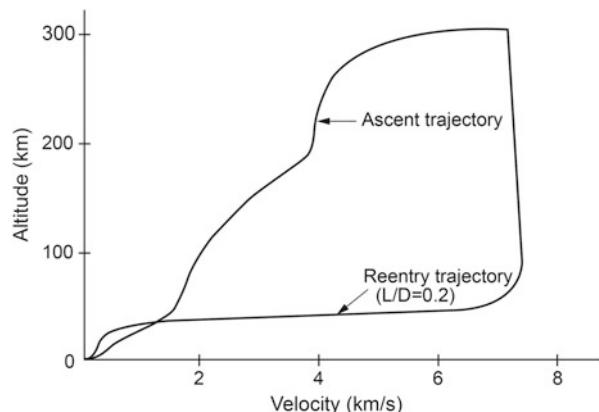
The first three refer to the robust design of reentry vehicle systems while the fourth one is to ensure successful execution of the reentry mission.

Complete in-depth analysis of hypersonic aero thermodynamic environment and design aspects of reentry systems are beyond the scope of this book. However, the complexity of hypersonic aero thermodynamic environment of a reentry mission, uniqueness of reentry system for a specified mission and the design and execution process are briefly given in this section. Highlights of design and reentry mission management aspects are given in subsequent sections.

15.2.1 Reentry Flight Environment

The most important input for the design of reentry vehicle is aero thermodynamic environment which defines the aerodynamic forces, moments and thermal loads on the vehicle during its hypersonic flight regime. This data is needed in addition to the conventional inputs used for designing other aerospace vehicles. Hypersonic environment experienced by the reentry vehicle is not just the extension of supersonic flows experienced by conventional ascent launch vehicle or other aerospace vehicles. The importance and criticality of hypersonic aero thermodynamic environment on a reentry vehicle as against that of ascent phase can be explained through the Space Shuttle Columbia (OV-102) disaster on February 1, 2003 [1]. During ascent phase flight of STS-107, a broken piece of foam protecting the external tank struck the left wing of the Columbia and caused a hair-line crack at its reinforced carbon-carbon leading edge. The aero thermodynamic environment of ascent phase

Fig. 15.1 Ascent and reentry trajectories



didn't cause any problem and STS-107 reached the orbit safely. However, during the reentry flight phase of OV-102, through this minor gap, the hot gases of hypersonic aero thermodynamic environment reached the inner part of the left wing, which finally led to the disaster of Columbia, OV-102.

The ascent phase trajectory of a typical space transportation system to a LEO mission of 300 km orbit and the return trajectory of a module with L/D of 0.2 from the same orbit to the surface of Earth are given in Fig. 15.1. The ascent vehicle quickly crosses the dense atmosphere in about 2 minutes and the vehicle velocity is of the order of only 2 km/s when it crosses the atmosphere. However, in case of return missions, the reentry vehicles fly with hypersonic velocities in the dense atmosphere regime almost for the entire duration of flight. The aero thermodynamic environments of ascent as well as reentry trajectories are compared in Fig. 15.2. The thermal environments for the ascent vehicles are not severe and the main design environment for the ascent phase vehicle is the high dynamic pressure regime which includes the transonic regime of flight also. In case of reentry vehicle, the entire flight duration happens only in the dense atmosphere and the kinetic energy dissipation causes severe thermal environment to the vehicle, viz. high heating rate and large total heat load to the vehicle. In addition to the severe thermal environment, reentry vehicles experience very complex flow phenomena as explained in Fig. 15.2 [2–4]. Depending on the various features, the reentry aero thermodynamic environment can be categorized into different flow fields, real gas effects with chemically reacting flows, as well as varying flow pattern over vehicles.

The regimes of the entire reentry flight from higher altitudes till the surface of the Earth can be divided based on the different flow characteristics. For a typical reentry vehicle, the flow regimes are given below [2–4]:

1. Free molecular flow regime (beyond altitude of 130 km)
2. Slip flow regime (altitude: 130–120 km)
3. Transition flow regime (altitude: 120–110 km)
4. Viscous merged flow regime (altitude: 110–75 km)
5. Continuum flow regime (altitude: 75–0 km)

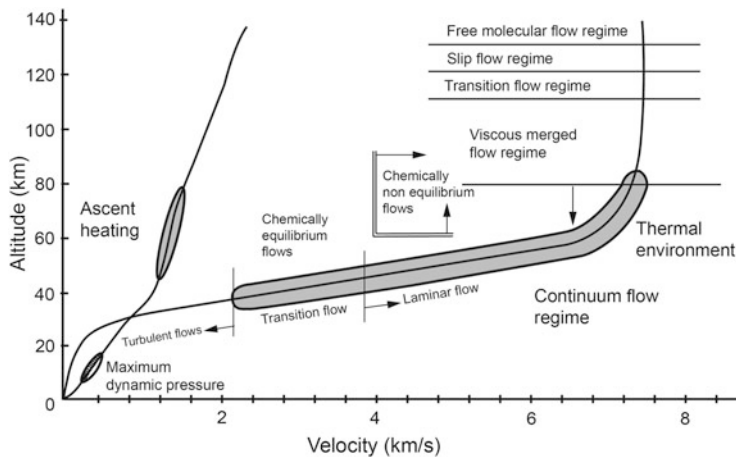


Fig. 15.2 Comparison of ascent and complex reentry flight environment

In the continuum flow regime, wherein the vehicle flies from 75 km till reaching surface of Earth, the flows are divided into hypersonic, supersonic, transonic and subsonic phases.

High temperature generated by the presence of strong shock waves during reentry causes chemical reactions. Therefore, the reentry vehicle encounters the characteristics of real gas effects with chemically reacting flows. The flow field can be categorized into chemically non-equilibrium flows and chemically equilibrium flows. Generally, for a typical reentry vehicle, chemically non-equilibrium flows occur beyond 70–60 km when Mach number is beyond 5 whereas below 40 km, it is considered as chemically equilibrium flows.

Another major feature of reentry environment is the boundary layer transition over the vehicle body. For a typical reentry vehicle, initially the flow over reentry vehicle is laminar upto the altitude of about 50 km, completely turbulent below 40 km whereas boundary layer transition occurs between 50 and 40 km.

In addition, the phenomenon such as viscous and inviscous interactions, separated flow, effects of surface catalycity and ablation on the aerodynamic parameters and thermal load distribution are also the characteristics of hypersonic reentry aero thermodynamic environment.

High temperature gas effects of aero thermodynamic environment change the flow field characteristics of a hypersonic reentry vehicle and strongly influence the aerodynamic pressure and shear forces acting on the surface of the vehicle as well as heat transfer rate to the vehicle. The unique feature of hypersonic aero thermodynamic environment for a reentry vehicle is that its characteristics depend mainly on the vehicle characteristics viz. size, shape, mass as well as the reentry trajectory of the vehicle. However, the distribution of pressure and thermal loads used for the vehicle design in terms of size, shape and mass depend on aero thermodynamic environment.

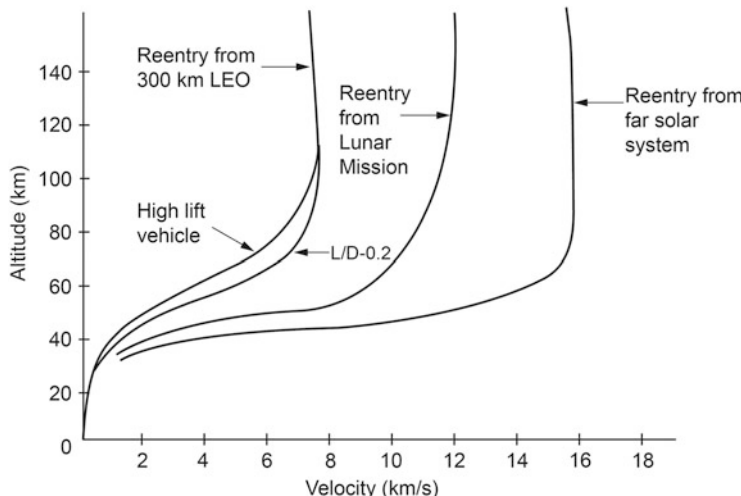


Fig. 15.3 Reentry trajectories of various return missions

All these characteristics depend on many factors like surface shape, size, surface roughness, chemical characteristics of vehicle surface material, local Reynold's number, Mach number, wall temperatures, air properties and its dispersions on a particular altitude. To predict these parameters at ground before flight is very difficult. It is also not feasible to characterize them in the test facilities due to the difficulty in simulating the real flight environment with detailed surface level characteristics of the vehicle used for reentry flight.

Reentry trajectories of typical return missions are given in Fig. 15.3. It can be seen that reentry trajectories of different missions are different and also for the same mission, different reentry vehicles follow different reentry trajectories. Once the reentry trajectories are different, aerothermal environments will also be different as explained in Fig. 15.2. Therefore, aero thermodynamic environment of each reentry mission is unique, and the relevant parameters evaluated from earlier reentry missions are not directly applicable for a new reentry vehicle/mission design process.

In addition, due to the large variations in the flow regimes from reentry till touchdown (hypersonic speed to zero), the aerodynamic coefficients vary to a large extent over the entire trajectory. These, along with variation of several orders of magnitudes of density, produce a very high level of nonlinearities in the aerodynamic characteristics of the vehicle.

In summary, during hypersonic aero thermodynamic environment, the thermal energy of the flow field around the vehicle influences the properties of air, which in turn affects the aerodynamic forces and moments as well as thermal environment to the vehicle. The vehicle configuration change due to the thermal energy passed on to the vehicle, alters the aerodynamic forces and moments. These forces and moments affect the vehicle trajectory, which in turn alter the aero thermodynamic environment. Therefore, there is very strong coupling between thermal and pressure

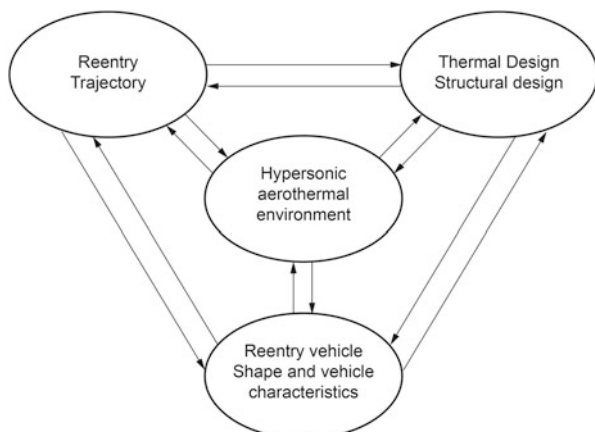
distributions, vehicle configuration and reentry trajectory. In addition prediction of these parameters a priori is not feasible, and variations of these parameters during flight with respect to prediction are invariably large. The strong coupling, the large variations in parameters during the entire flight regime and the large levels of uncertainties make the reentry vehicle design tasks very complex.

15.2.2 Reentry System Design Process

Each reentry mission is unique in nature and has strong coupling as explained earlier. It is to be noted that the aero thermodynamic environment is the major input for the reentry vehicle design and the environment depends on the vehicle characteristics as well as on the reentry trajectory. Thus the vehicle configuration, subsystem and trajectory designs cannot be decoupled and the integrated reentry system as given in Fig. 15.4 has to be considered to arrive at an optimum and robust reentry system design.

In general, typical reentry system requirement is to design a vehicle to bring a specified payload mass with specified volume safely from space and to precisely land at a specified location on the surface of the Earth. Typical reentry mission objectives are either reentry mission from LEO or return mission from lunar/ interplanetary mission. Requirements of entry to planetary atmosphere and aero-assisted orbital transfers are similar to that of reentry missions from space to the Earth. The major requirements for reentry systems are: (1) maximum safety, (2) minimum thermal environment, (3) minimum structural loads, (4) maximum performance, (5) minimum structural mass, thermal protection system mass and (6) minimum cost. In order to achieve the mission objectives under nominal as well as dispersed flight environments, the reentry system has to be configured and designed to provide mission flexibility, versatility, operability, reliability and

Fig. 15.4 Interactions of subsystems of reentry systems



compatibility with the flight environment. In addition, the system must be suitable for handling the emergent situations. In order to reduce the cost of multiple operations and maintainability, complete reusability is also another requirement.

Reentry system design involves

1. Reentry trajectory to meet the mission requirements while meeting the vehicle limitations
2. Aerodynamic configuration of the reentry vehicle, to meet the payload requirements while reducing the severity of aero thermodynamic environment
3. Structural design of reentry vehicle to ensure structural integrity during reentry flight
4. Thermal protection system design (TPS) to protect the primary load carrying vehicle structure
5. Usage of suitable materials for TPS
6. Intelligent mission management to successfully execute the reentry mission

Reentry trajectory has influence on the vehicle load and heat transfer rate to the vehicle. Shaping of the reentry trajectories with reduced reentry flight path angle at the instant of reentry interface ensures larger velocity reduction at higher altitude; thereby the vehicle enters the dense atmosphere with lower velocity. This process reduces the peak drag load acting on the vehicle along with reduced heat transfer rate to the vehicle. But, due to the lower flight path angle, the flight duration is more, which in turn increases the total heat load on the vehicle and therefore, design trade-off is required.

Aerodynamic configuration defines the drag coefficient and L/D of the vehicle. Blunt body with higher drag coefficient ensures the larger velocity reduction at higher altitude, thereby the peak drag load and heat rate are less. Another advantage is that the blunt body at the hypersonic flight produces very strong normal shock in front of the body. This process ensures that most of the thermal energy is used for heating, dissociating and ionizing the air particles downstream of the shock wave, thereby reducing the heat transferred to the vehicle.

The aerodynamic configuration of the vehicle, especially with higher L/D has the major influence on reducing the convective heat transfer to the vehicle as it ensures: (a) large velocity reduction at higher altitudes, (b) higher cross range capability of the vehicle, (c) ability to control the trajectory and (d) to meet the mission requirements even under dispersed flight environment.

To ensure the safety of the vehicle during reentry mission, the vehicle structure should be robust to withstand the aerothermal loads till it achieves the mission objectives. Generally, vehicle structural system is designed for the inertial, pressure and skin friction force distribution integrated loads due to the flow fields, whereas the thermal protection systems (TPS) are designed for protecting the primary load carrying structures. Protecting the reentry vehicle against aerothermal environment is a major task for the reentry system design. The aerothermal environment restricts the vehicle operating envelope and affects the TPS design which in turn affects the mass. The peak heat transfer rate and total heating load, which is the integral of heat rate over time, mapped over the vehicle surface are used for the design of TPS.

Three strategies viz. heat sink, ablative TPS and radiative TPS are being utilized for protecting the structures against harsh reentry aerothermal environment. The maximum heat transfer rate to the vehicle surface decides the TPS material selection whereas the total heat load decides thickness of the selected TPS material. Therefore, judicious choice of material along with integrated design process is required to reduce the mass of TPS and the mass of the vehicle structure.

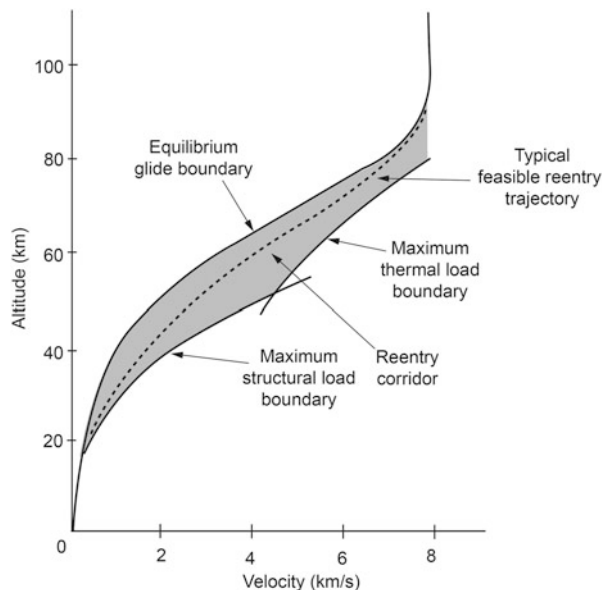
As the reentry environment restricts the flight operating envelope, intelligent flight management system has to be designed to ensure benign aero thermodynamic environment to the vehicle while meeting the mission requirements. The flight path angle at reentry interface has to be an optimum one. During the initial phase of reentry mission, the vehicle has to be flown at high angle of attack to create the maximum blunt body effects. In this case, most of the energy is used for heating the air in the shock layer and not the vehicle. At high angle of attack, flow is dominated by shocks and larger subsonic regime covers the windward side of the vehicle whereas large separated flow for the leeward side. After crossing the severe thermal environment, the vehicle has to be flown at an angle of attack which ensures that flow around the vehicle is supersonic excepting a small portion at the nose tip which experiences the subsonic flow. This strategy generally ensures an optimum aero thermodynamic flight environment to the reentry vehicle.

15.2.3 Reentry System Mission Management

In a reentry system design, it is essential to design a feasible trajectory and execute the same successfully through an intelligent reentry mission management during flight. At any instant of the flight, the thermal load, structural load, control system limitation, etc. define the lower limit on the vehicle operating altitude whereas the feasibility of achieving successful reentry defines the highest altitude limit. These limits can be mapped into the convenient work space viz. drag acceleration versus Mach number, altitude versus velocity etc. and the flyable reentry corridor is defined. Reentry corridor is unique for a reentry system and a typical one is given in Fig. 15.5.

In order to achieve the mission objectives successfully without violating any of the safety limits, the vehicle needs to fly within the specified reentry corridor under nominal and dispersed flight environments. Therefore, it is essential to design carefully the best possible trajectory within the reentry corridor which meets the above constraints even under the dispersed flight environments and still meet the mission objectives of reaching the defined target. During flight, an intelligent flight management system has to be employed in terms of commanding the vehicle to follow the defined trajectory even under the dispersed flight environment by modulating the necessary vehicle and trajectory system parameters. This ensures controlled dissipation of kinetic and potential energies, thus satisfying the thermal and structural loads within the limits and achieves the mission requirement.

Fig. 15.5 Reentry corridor and feasible trajectory of a typical reentry system



15.3 Reentry Dynamics and Reentry Vehicle Configurations

In order to bring the vehicle from orbit to Earth, initially a retro velocity of the order of 100 m/s is added to the vehicle. This reverse velocity reduces the orbital velocity of the vehicle, thus making the vehicle trajectory to become suborbital and vehicle travel towards Earth in an elliptic trajectory. The reentry mission from orbit to Earth consists of two major flight phases as shown in Fig. 15.6.

The first one is a Keplerian trajectory from orbit to reentry interface. The reentry interface is the atmospheric boundary, at which the drag force and deceleration are significant (0.01–0.1 g). This boundary depends on the reentry vehicle and types of initial orbits. However, for all practical purposes, the altitude of about 120 km can be considered as the reentry interface. For a typical reentry from 300 km LEO, the vehicle velocity at entry interface is about 8 km/s. The second phase is the atmospheric reentry phase, which extends from the reentry interface to the surface of Earth. This phase is the most crucial part of the mission and during the energy dissipation process, vehicle encounters high deceleration and thermal loads. Once all the energies are dissipated, vehicle follows approach and landing maneuver phase to land precisely at the designated location. From the atmospheric density variations with respect to altitude as given in Fig. 15.7, it is seen that atmospheric density is sufficiently large below the altitude of about 40 km. Therefore, if the vehicle with higher velocity penetrates deeper into the atmosphere below 40 km, it

Fig. 15.6 Reentry trajectory phases

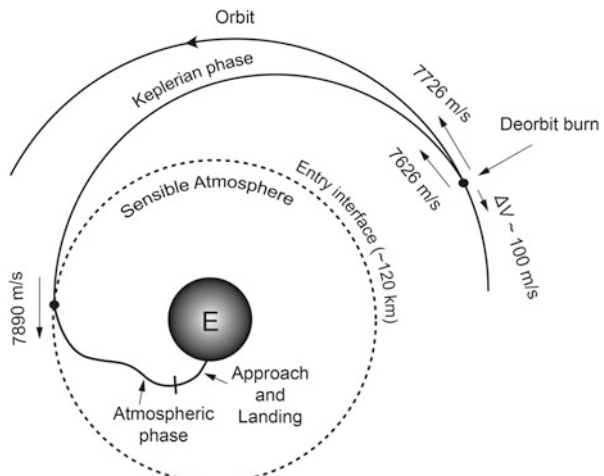
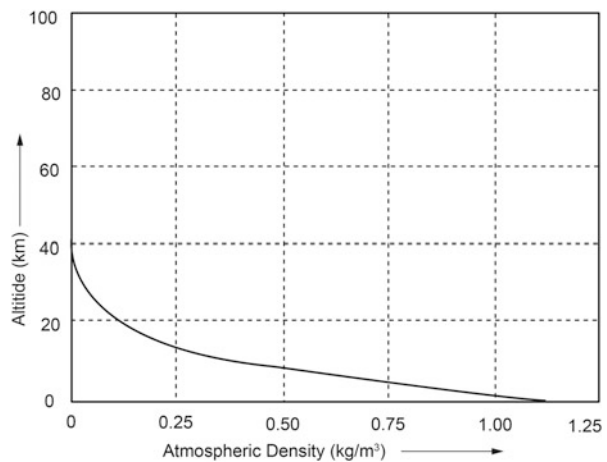


Fig. 15.7 Atmospheric density variation with respect to altitude

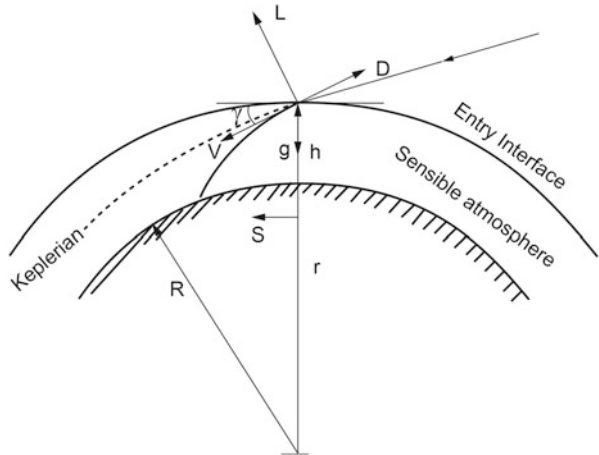


causes the deceleration and heat flux to be higher. Therefore, the reentry trajectory and vehicle configurations have to be designed such that maximum velocity is dissipated during the higher altitude itself.

15.3.1 Reentry Dynamics

To understand the atmospheric reentry dynamics from the reentry interface till reaching the surface of the Earth and associated problems, a simplified reentry

Fig. 15.8 Reentry trajectory dynamics parameters



dynamics with respect to the non-rotating spherical Earth is explained through two dimensional equations of motion in wind axes (Fig. 15.8) as given below:

$$\frac{dV}{dt} = -\frac{D}{m} + g \sin \gamma \quad (15.1)$$

$$V \frac{d\gamma}{dt} = -\frac{L}{m} + \left(g - \frac{V^2}{r} \right) \cos \gamma \quad (15.2)$$

$$\frac{dr}{dt} = -\frac{dh}{dt} = -V \sin \gamma \quad (15.3)$$

$$\frac{ds}{dt} = \left(\frac{R}{r} \right) V \cos \gamma \quad (15.4)$$

$$L = \frac{1}{2} \rho V^2 S C_L \quad (15.5)$$

$$D = \frac{1}{2} \rho V^2 S C_D \quad (15.6)$$

$$g = g_0 \left(\frac{R}{r} \right)^2 \quad (15.7)$$

where

V = Magnitude of relative velocity of the reentry vehicle

γ = Flight pathangle of relative velocity, measured positive below local horizontal

r = Radial distance of the vehicle from the centre of Earth

s = Down range distance

R = Radius of Earth

C_L = Lift force coefficient

C_D = Drag force coefficient

S = Reference area

L = Vehicle lift force

D = Vehicle drag force

g = Acceleration due to gravity at the instantaneous altitude

g_0 = Acceleration due to gravity at the surface of Earth

h = Altitude

m = Vehicle mass

ρ = Atmospheric density at the instantaneous altitude

The initial conditions for this reentry dynamics are:

$$\gamma = \gamma_e, r = r_e, V = V_e \quad (15.8)$$

Where γ_e , r_e , V_e are the values of γ , r , V at the reentry interface.

Although there is no closed form solution for these equations, use of appropriate assumptions can give analytical solutions which provide insight into the reentry dynamics.

15.3.2 Ballistic Bodies Reentry

Ballistic bodies are blunt bodies with zero lift, while having drag. Characteristics of these bodies are: (a) $L = 0$ and (b) $L/D = 0$. Analytical solutions for the ballistic bodies reentry trajectories can be obtained with the following assumptions:

1. Neglect the combined effects of gravity and centrifugal forces compared to the drag force
2. Flat Earth
3. $\gamma = \text{constant} = \gamma_e$
4. Exponential model for atmospheric density as given below:

Density ratio, σ is given by

$$\sigma = \frac{\rho}{\rho_0} \cong e^{-\beta h} \quad (15.9)$$

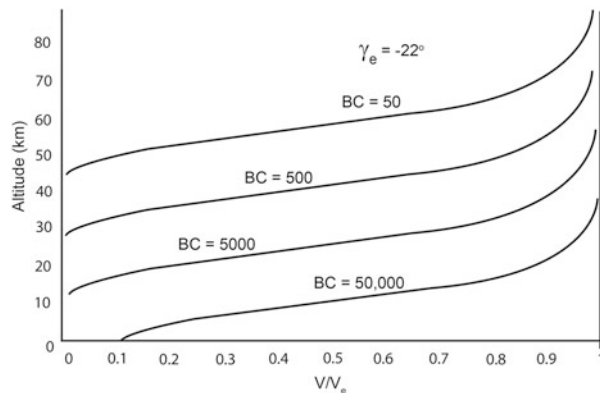
Where $1/\beta$ is the scale height and ρ_0 density of atmosphere at sea level.

1. Defining ballistic coefficient, (BC),

$$BC = \frac{W}{C_D S} = \frac{mg_0}{C_D S} \quad (15.10)$$

Then, from Eqs. (15.1), (15.2), (15.3), (15.4), (15.5), (15.6) and (15.7), the velocity of ballistic reentry trajectory is given as [5].

Fig. 15.9 Altitude vs velocity for ballistic entry



$$V = V_e e^{[B e^{(-\beta h)}]} \quad (15.11)$$

where

$$B = \frac{\rho_0 g_0}{2(BC)\beta \sin \gamma_e} \quad (15.12)$$

Using the Eq. (15.11), non-dimensionalized velocity as a function of altitude (h) for different ballistic coefficients for a typical reentry flight path angle is given in Fig. 15.9. It can be observed that as BC increases, the vehicle penetrates faster into the lower atmosphere with higher velocity. An increased reentry angle is also expected to have the same effect. Therefore, from this analysis, it can be concluded that the deceleration loads and heat loads on the vehicle will be more for the cases of:

1. Higher reentry interface flight path angle of reentry trajectory
2. Ballistic vehicles with higher ballistic coefficients

To assess the above parameters, the vehicle deceleration (D/m) and stagnation point heat flux (as given in Sect. 15.4) have been evaluated as parametric studies as given below:

The altitude profiles, deceleration and heat rate for reentry vehicles with different ballistic coefficients for a typical reentry angle are given in Fig. 15.10. It is seen that reduction in ballistic coefficient has a major impact on the heat rate and has a smaller effect on the deceleration loads. Therefore, vehicle configuration with reduced ballistic coefficient is preferable.

Reduced ballistic coefficient is achieved by the following methods:

1. Reduce the reentry vehicle mass
2. Increased drag coefficient with blunt bodies (C_D is more, S is more)

Therefore, blunt body designs with lower mass are preferable for reentry mission.

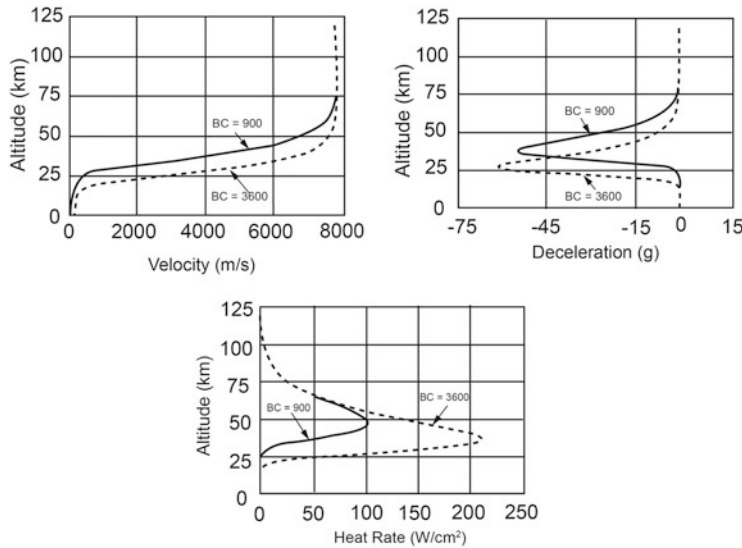


Fig. 15.10 Reentry trajectories and flight parameters for ballistic bodies with different ballistic coefficients for a typical flight path angle

It may be noted that successfully flown reentry vehicles such as Gemini, Apollo, Soyuz, Shenzhou and Space Recovery Experiment (SRE) are having blunt body configuration with reduced ballistic coefficients.

15.3.3 Influence of Reentry Flight Path Angle

For a typical reentry vehicle with the ballistic coefficient of 3600 kg/m^2 , reentry trajectory profiles, deceleration loads and heat rate values for different reentry angles have been evaluated and shown in Fig. 15.11.

It is seen that reduced flight path angle at reentry interface produces lower heat rate and less deceleration load on the vehicle. It is to be noted that, even though the reduced reentry flight path angle at reentry interface reduces the deceleration load and heat rate to a large extent, this shallow reentry flight trajectory duration increases considerably as given in Fig. 15.12. This increases the total heat load on the vehicle compared to the short and steeper reentry trajectory. Also, using the Eq. (15.4), it can be concluded that for the case of shallow reentry trajectory missions with uncontrolled trajectory management, the landing point dispersions

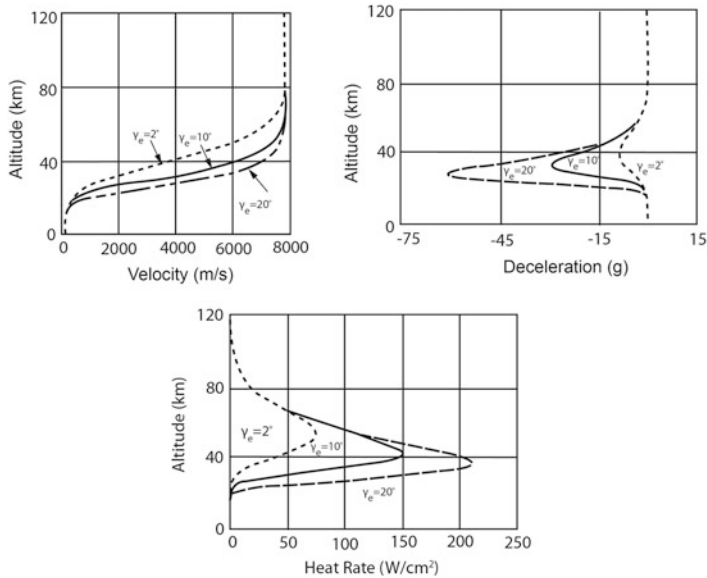


Fig. 15.11 Entry trajectories and flight parameters for various entry flight path angle for a typical ballistic body ($\text{BC} = 3600$)

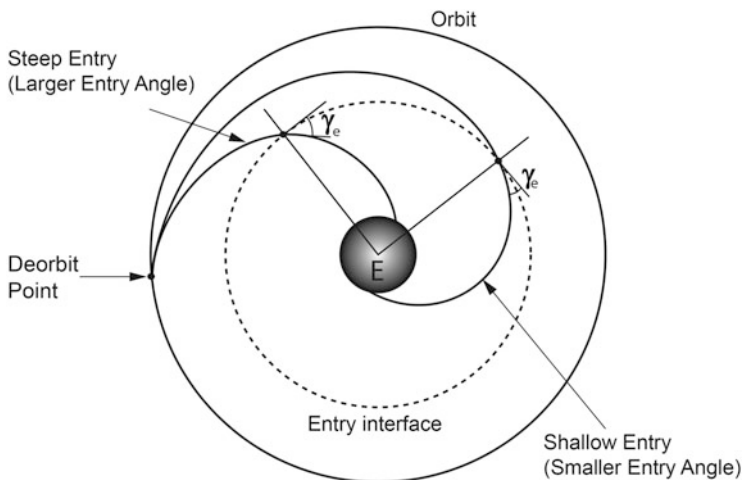


Fig. 15.12 Comparison between steeper and shallow reentry trajectories

are more compared to that of the sharp reentry trajectories. The characteristics of shallow and steep reentry trajectories are compared as given below:

Reentry trajectories	Deceleration load	Heat rate	Flight duration	Total heat load	Landing point dispersion of uncontrolled trajectories
Steep trajectory	More	More	Less	Less	Less
Shallow trajectory	Less	Less	More	More	More

From the table, it can be concluded that there has to be a design trade-off between various design and mission parameters. Therefore, depending on the mission requirement, proper reentry body shape, TPS material and thickness the reentry trajectory have to be judiciously selected.

15.3.4 Influence of Vehicle Lift on the Reentry System

Reentry missions executed by vehicles having lift are called lifting reentry trajectories. An important lifting reentry trajectory is the equilibrium glide, which is a shallow trajectory in which the gravitational force is balanced by the combination of lift and centrifugal forces, and therefore, $dy/dt = 0$ as per the Eq. (15.2). The small angle assumption for ($\sin \gamma \cong 0$, $\cos \gamma \cong 1$), and the equilibrium glide trajectory gives closed form solution for the lifting reentry trajectory. In actual case, there will be some dy/dt and hence these trajectories are called as pseudo equilibrium glide. Using the Eqs. (15.1, 15.2, 15.3, 15.4, 15.5, 15.6, and 15.7), the velocity along the lifting reentry trajectory is given as [5]

$$\frac{V^2}{g_0 R} = \frac{1}{1 + \left(\frac{R}{2}\right)(L/D) \left(\frac{C_D S}{W}\right) g_0 \rho_0 e^{-\beta h}} \quad (15.13)$$

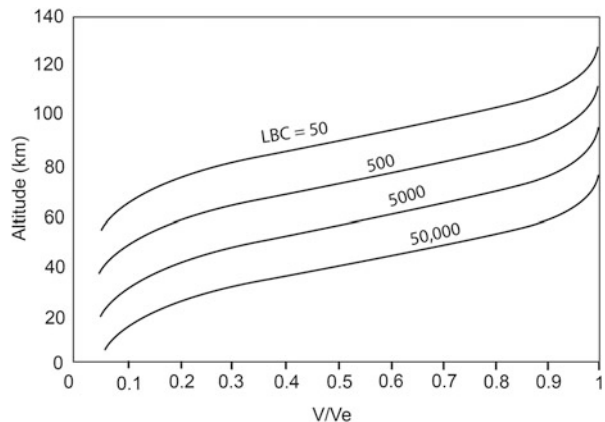
The non-dimensionalized velocity as a function of altitude for different lifting ballistic coefficients (LBC) as defined below

$$LBC = \frac{m}{C_D S (L/D)} = \frac{BC}{(L/D)} \quad (15.14)$$

is given in Fig. 15.13. It can be seen that adding lift, LBC is further reduced from BC.

Adding a lift to the reentry body ensures the body to be in upper atmosphere for more time and results into a gradual descent. More time spent in upper atmosphere dissipates more energy, while entering the dense atmosphere at lower altitude, the vehicle velocity reduces considerably, thereby reducing deceleration load as well as heat rate.

Fig. 15.13 Altitude vs velocity for lifting entry



The deceleration in terms of ‘g’ and the maximum deceleration are given by

$$\frac{a}{g_0} = \left(\frac{dV}{dt} \right) \left(\frac{1}{g_0} \right) = - \frac{\left[1 - \frac{V^2}{g_0 R} \right]}{(L/D)} \quad (15.15)$$

$$\left(\frac{a}{g_0} \right)_{\max} \approx \frac{-1}{(L/D)} \quad (15.16)$$

The trajectories, deceleration load and heat rate profiles of a typical ballistic body (BC of 360 kg/m^2) and with the addition of small (L/D) of 0.2 to the above body are given in Fig. 15.14. It is seen that the addition of small lift to a ballistic body considerably reduces the deceleration loads, while the improvement is seen in the heat rate also.

Because of this large reduction in the deceleration, generally the reentry vehicles are configured with lift. The trajectory control requirements, as explained in subsequent section, to achieve precise landing also require lifting entry.

At the same time, it is to be noted that blunt body with low ballistic coefficient is preferable from reentry dynamics point of view. The above ballistic body is generally configured with a small lateral center of gravity off-set to produce the required lift as shown in Fig. 15.15. Such bodies are called semi ballistic bodies. The addition of lift imposes further constraint. As the vehicle stays in atmosphere for more time, even though heat rate is less, the total heat load on the vehicle is large; therefore suitable thermal protection system has to be implemented.

15.3.5 Skipping Trajectory Reentry System

Although the equilibrium glide reentry trajectories are the most flat trajectory with the lowest deceleration load and heat rate, such glide trajectories are not possible

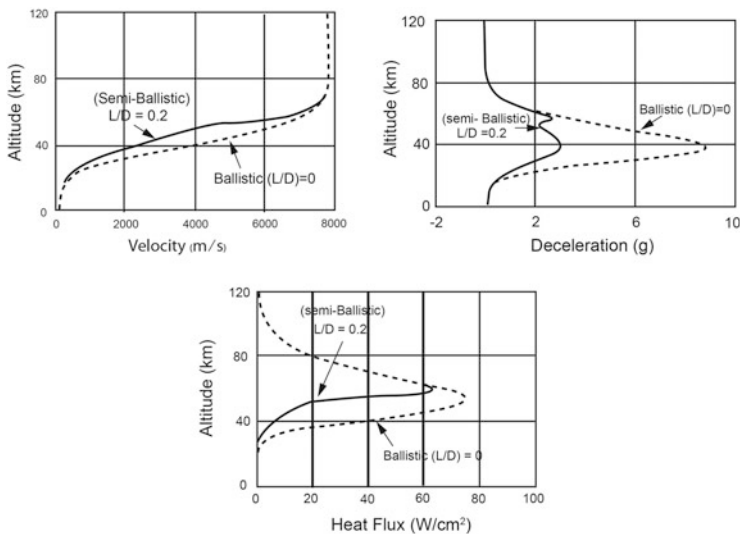
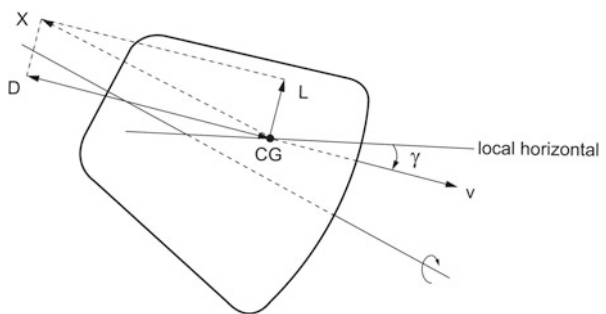


Fig. 15.14 Effect of adding lift to ballistic body on trajectory, deceleration load and heat rate

Fig. 15.15 Addition of lift through cg offset for ballistic body



always. If the flight path angle at reentry interface is less than a specified value and the vehicle has sufficient lift, after reaching certain level of dense atmosphere, the lift force will be more than the combination of gravity and centrifugal forces. In such cases, the flight path angle is above local horizontal and the vehicle altitude starts increasing. In this process, the vehicle skips out of atmosphere with reduced velocity. Once the altitude increases and the lift reduces, then the trajectory starts dipping. This process continues till the velocity reduces below certain value and then positive reentry takes place. This is called skipping reentry trajectories. In certain cases, after initial pull out, there may be velocity gain which is sufficient to make the vehicle skip out of the reentry process.

Reentry trajectories of a typical lifting reentry vehicle with different reentry interface flight path angles are given in Fig. 15.16. It is to be noted that for the specified reentry vehicle, a specified reentry interface flight path angle ensures

Fig. 15.16 Steep, shallow and skip reentry trajectory

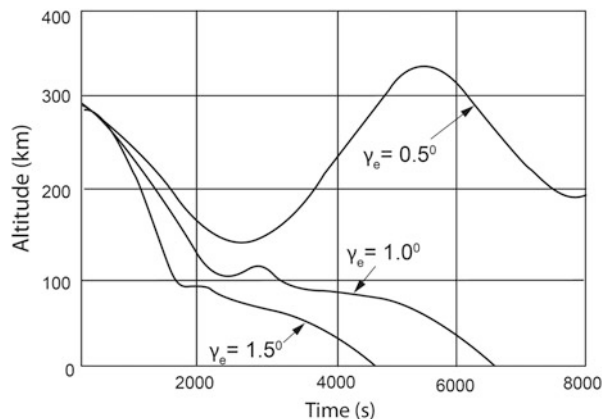
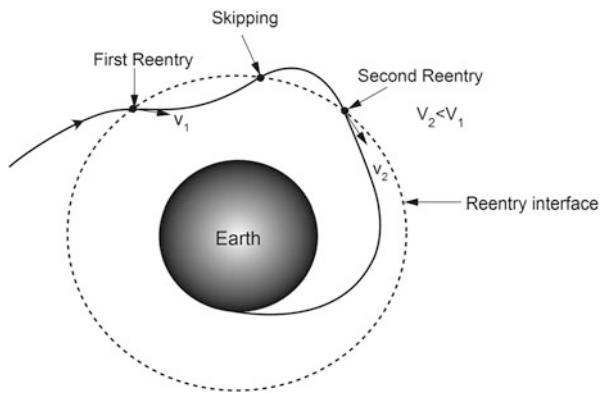


Fig. 15.17 Skipping reentry trajectories



positive reentry. Under such conditions, the increase in structural and thermal loads has to be considered suitably in the reentry vehicle design process.

In other words, the skipping trajectory process can be efficiently utilized for the case of reentry with super circular velocity (as in the case of lunar return mission, wherein the reentry velocity is about 11 km/s) [4]. For such missions, kinetic energy to be dissipated is twice that of reentry from LEO missions, which poses a major task of thermal management of the reentry vehicle. Instead, the flight path angle is designed such that, with higher velocity along with sufficient lift, the vehicle skips out of atmosphere with reduced velocity. In the second phase, vehicle reenters the atmosphere with reduced velocity and encounters the reentry mission till reaching the surface of Earth. This process is explained in Fig. 15.17. Since the velocity at reentry during the second phase is less, the kinetic energy to be dissipated in the atmospheric flight is less and therefore, thermal control of the vehicle is easily manageable.

Skipping reentry trajectory is also useful to land at a faraway location than the capability of the vehicle in the single reentry mode.

15.3.6 Range Capabilities and Reentry Foot-Print

It is essential to design the reentry system with down range and cross range capabilities to provide mission flexibility. To achieve the above objectives, the reentry vehicle must be capable of starting from a specified reentry interface location and land at various locations on the surface of Earth as per requirements. Under emergency situations, it should be able to start from different reentry locations with capability to land at the specified location on the Earth. To achieve these mission options, the reentry system has to be designed with maximum landing envelope of down range and cross range. Based on the capability of the reentry system, once specified point within the envelope is fixed, a trajectory control system has to be designed to meet the landing point even under dispersed flight environment and vehicle system parameters. The ranging capability of the reentry system is given in this section whereas the implication of this system on vehicle is explained in Sect. 15.5.

Integrating Eq. (15.15), the down range from reentry interface (velocity, V_e) to the touch down point for equilibrium glide trajectory can be written as [5]

$$s = -\left(\frac{R}{2}\right)\left(\frac{L}{D}\right)\ln\left[1 - \frac{V_e^2}{g_0 R}\right] \quad (15.17)$$

This is the total range in the direction of reentry velocity along the plane of motion (orbital plane). It can be seen that maximum down range can be achieved when the reentry vehicle flies with maximum (L/D) in the plane of motion. If the reentry vehicle is flying with a bank angle, σ with respect to the plane of motion, then there will be lateral force as given in Fig. 15.18.

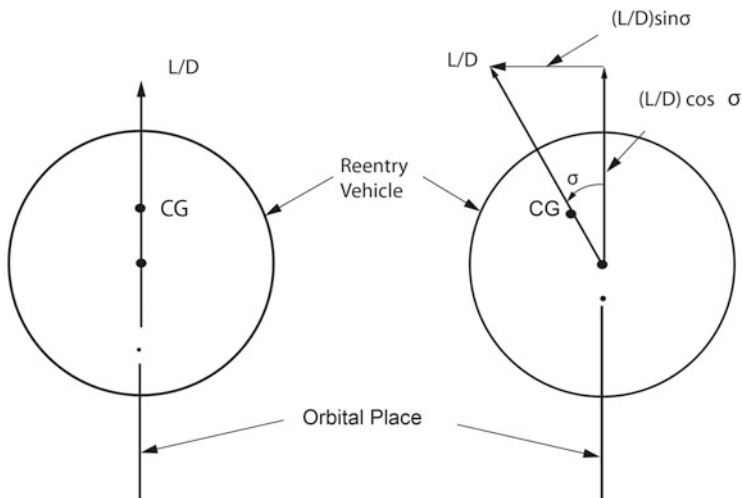
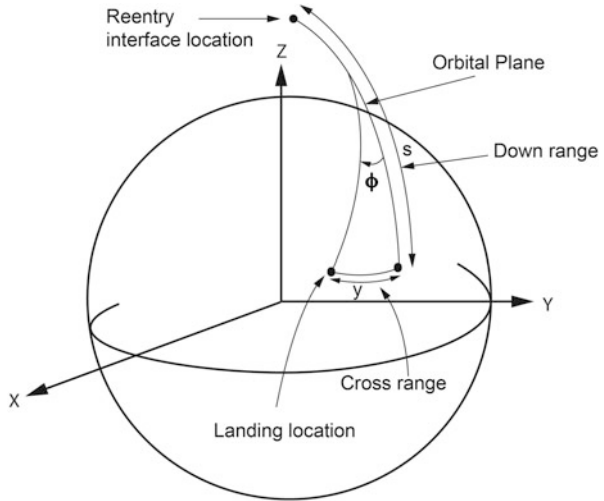


Fig. 15.18 Bank angle (σ) of reentry vehicle

Fig. 15.19 Down and cross ranges



The component of (L/D) along the orbital plane is given by

$$\left(\frac{L}{D}\right)_0 = \left(\frac{L}{D}\right) \cos \sigma \quad (15.18)$$

whereas the component of (L/D) along the lateral direction is given by

$$\left(\frac{L}{D}\right)_c = \left(\frac{L}{D}\right) \sin \sigma \quad (15.19)$$

The lateral force due to bank angle generates a cross range with respect to the orbital plane. However, due to the bank angle, the vertical component of (L/D) reduces, thereby reducing the down range, while there is an increase in the cross range as given in Fig. 15.19.

Maximum cross range achieved when the vehicle flies with an optimum bank angle in terms of (L/D) of the reentry vehicle is given by [4]

$$\sigma_{\text{opt}} \cong \cot^{-1} \left[1 + 0.106 \left(\frac{L}{D} \right)^2 \right]^{0.5} \quad (15.20)$$

and the maximum cross range is given by

$$Y_{\text{max}} \cong \left(\frac{R}{5.2} \right) \left(\frac{L}{D} \right)^2 \left[\frac{1}{\{1 + 0.106(L/D)^2\}^{0.5}} \right] \quad (15.21)$$

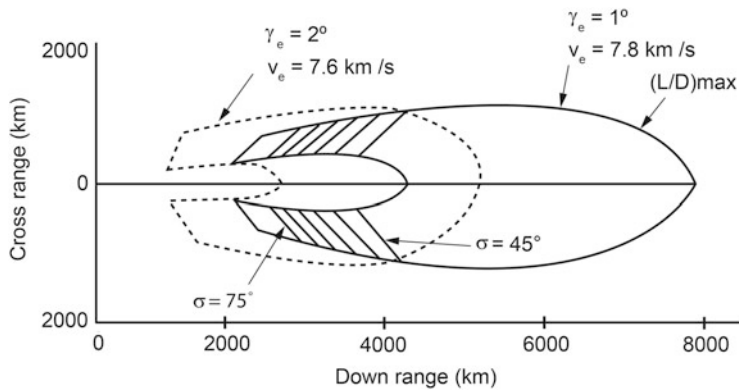


Fig. 15.20 Typical reentry foot-print

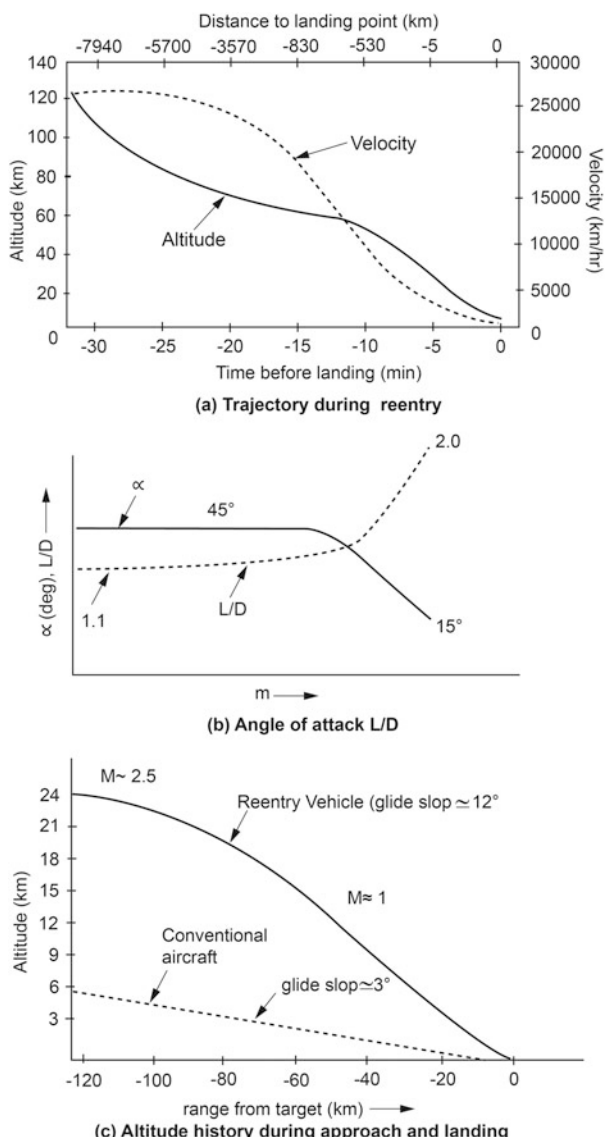
To achieve the cross range of $\pm\pi/2$, (i.e., 90° in both directions of the orbital plane), the (L/D) required is 3.5; however designing a vehicle to achieve hypersonic (L/D) of 3.5 is a difficult task.

The possible vehicle landing point boundary with down range and cross range from a specified reentry interface is called the ‘reentry foot-print’, which depends on the (L/D) of the vehicle, reentry interface velocity and flight path angle. Reentry foot-print of a typical lifting body reentry system is given in Fig. 15.20. In order to achieve maximum reentry mission flexibility, the foot-print of a reentry system has to be made as large as feasible.

15.3.7 Winged-Reentry Vehicles

As seen in the earlier sections, (L/D) plays a major role in the reentry system design, performance, mission flexibility and trajectory maneuverability. Increased (L/D) of a reentry vehicle significantly reduces the deceleration loads and heat rate; but of course with increased flight duration, which in turn increases the total heat load on the vehicle. Also, the increased (L/D) enlarges the foot-print capability with large down range and cross range which is a major mission flexibility. In addition, this provides better trajectory control features for the reentry vehicle. To achieve the reusability, the vehicle has to land precisely at a specified location like an aircraft. All these requirements need a higher (L/D) reentry vehicle. But semi-ballistic reentry bodies cannot provide a larger (L/D). Therefore, advanced reentry vehicles, especially Reusable Launch Vehicles (RLV), are configured with wings to provide the necessary (L/D). These vehicles land like an aircraft and are used for the next mission without much maintenance and refurbishing activities. Generally, the reentry vehicles fly with average flight path angle of about 1° during critical energy dissipation phase and cover the range of about 8000 km for the flight duration of about 30 minutes, whereas conventional aircraft takes about 9 h to cover this

Fig. 15.21 Reentry Trajectory of a Typical winged reentry vehicle.
(a) Trajectory during reentry. **(b)** Angle of attack L/D. **(c)** Altitude history during approach and landing



distance. At the end of reentry flight phase, when vehicle enters into approach and landing phase, vehicle has to land with steeper glide slope of about 12° that too without power. This requires large (L/D) during supersonic to subsonic speed range. Designing a winged-reentry vehicle which meets all the (L/D) requirements for hypersonic to subsonic flight range is a difficult task. Reentry trajectory of a typical winged-body reentry vehicle is given in Fig. 15.21.

Also, it is to be noted that the blunt body reentry is favorable from deceleration and heat rate point of view. Therefore, the winged-body vehicle design and mission execution are carried out as follows:

1. At the time of reentry, vehicle attitude is kept at a large angle of attack, to produce blunt body effects and at the same time have (L/D) of 0.8–1.2. This attitude is maintained during major energy dissipation phase.
2. After crossing the severe thermal environment, vehicle angle of attack is reduced to a lower value, which gives (L/D) of 1.5–2 at hypersonic speed and 2–5 at supersonic and subsonic speeds.

Implementation and execution aspects of the reentry mission management are explained in Sect. 15.5.

15.4 Aero Thermodynamic Environment and Reentry Vehicle Design Aspects

Aero thermodynamic environment is the major input for a reentry vehicle system design. Detailed analysis of the environment and vehicle design are beyond the scope of this book. However, the complexity of aero thermodynamic environment mentioned in Sect. 15.2 is briefly explained in this section, without getting into much detail. Also, the impact of these environments on the reentry vehicle design is also briefly outlined in this section.

15.4.1 Reentry Hypersonic Flow Environment

Different regimes of flow mentioned Sect. 15.2 are explained below [3]:

At the time of reentry, vehicle is in the free molecular flow regime, wherein the mean free path of the air molecules is more than characteristic length of the vehicle. In this regime of flight, the air molecules collide with the vehicle boundary and achieve the momentum of the vehicle after a single collision, i.e. the particles achieve the state of the vehicle boundary in the single collision. Subsequent to that, vehicle enters into the slip flow regime wherein the air molecules achieve the momentum of the vehicle after several collisions.

After coming out of the slip flow regime, before entering into viscous region, the vehicle passes through transition flow regime, wherein it is extremely difficult to characterize the aero thermodynamic aspects of the vehicle analytically. Subsequent to transition flow regime, vehicle enters into the viscous merged layer regime, wherein the viscous effects viz. formation of shock wave and boundary layer need to be considered as a single entity and not as a separated discontinuous phenomenon. This is due to the fact that in this regime, there is a strong coupling between

boundary layer and shock wave; boundary layer affects the boundary conditions of the shock wave while simultaneously the shock wave affects the boundary layer.

Further to this, the vehicle enters into the continuum flow regime, which extends till the vehicle reaches the surface of Earth. In this regime, shock wave and boundary layer can be considered as separate discontinuities. The continuum flow regime is further subdivided into hypersonic, supersonic, transonic and subsonic incompressible flow regimes, possibly defined in terms of Mach numbers.

Hypersonic flow can be defined in terms of free stream Mach number

$$M_{\infty} \equiv \frac{V_{\infty}}{a_{\infty}} \gg 1 \quad (15.22)$$

where

V_{∞} = free stream velocity

a_{∞} = speed of sound in free stream

wherein the kinetic energy of free stream air particles is very large compared to its internal energy. Also, for the hypersonic flows, the density ratios across the normal shock wave is very small,

$$\epsilon \equiv \frac{\rho_{\infty}}{\rho} \ll 1 \quad (15.23)$$

where

ρ_{∞} = free stream density

ρ = density downstream of shock wave

For the case of very small density ratios, the shock wave is very close to the body and therefore shock layer remains very thin. This is a characteristic of hypersonic flow. As $M_{\infty} \rightarrow \infty$, for a perfect gas, the density ratio as given in Eq. (15.23) can be written as

$$\epsilon = \frac{\gamma - 1}{\gamma + 1} \quad (15.24)$$

where γ is the ratio of specific heats

Thus, assuming perfect gas for air during reentry, the density ratio works out to be $\epsilon = 1/6$. But with real gas effects, the density ratio can go as low as $1/20$, which is realistically measured value. This is due to real gas effects. It is very difficult to simulate such a small dynamic ratios in ground wind tunnels to get reentry conditions to characterize the vehicle before flight. Therefore reentry vehicle design gets evolved only during flight. However, efforts are being made in the wind tunnels with different gases to simulate small density ratios.

Hypersonic flow cannot be considered as the extension of supersonic Mach numbers, and it has the following specific characteristics:

1. The shock waves of hypersonic flows lie very close to the vehicle body, causing very strong boundary layer-shock interactions.
2. Boundary layer thickness of hypersonic flight is about 10–100 times more than that of lower speeds. Therefore, in hypersonic flow, the effective body size is much bigger than that of lower speeds. This alters the effective shape of the body, which in turn affects the aerodynamic characteristics of the body.
3. High temperature effects on the flow field are predominant in the hypersonic flow, which alter the aerodynamic characteristics of the body.
4. The aerodynamic forces and moments are highly nonlinear.

15.4.2 Hypersonic Flow Over a Typical Reentry Vehicle

The features of flow field of a typical reentry vehicle during its hypersonic flight are given in Fig. 15.22 [3, 4]. The important feature of hypersonic flow field is the formation of a strong shock wave in front of the vehicle, of which significant portion, facing the flow experiences the characteristics of a normal shock. The free stream conditions of the flow are ρ_∞ (density), P_∞ (pressure), T_∞ (temperature) and V_∞ (velocity). As the flow passes through the normal shock in front of the body, the pressure (P), density (ρ) and temperature (T) of flow field downstream of the shock increase whereas the velocity (V) decreases. The flow then passes over the vehicle with different regions of flow field with varying speeds viz. subsonic, sonic and supersonic speeds. While the flow near the vehicle is within the boundary layer, wherein viscous effects are predominant, the remaining part is having the inviscid shock layer. At the corner point of the vehicle, the flow gets turned through Prandtl-Meyer expansion fan. Through the expansion fan, the flow expands to a lower value

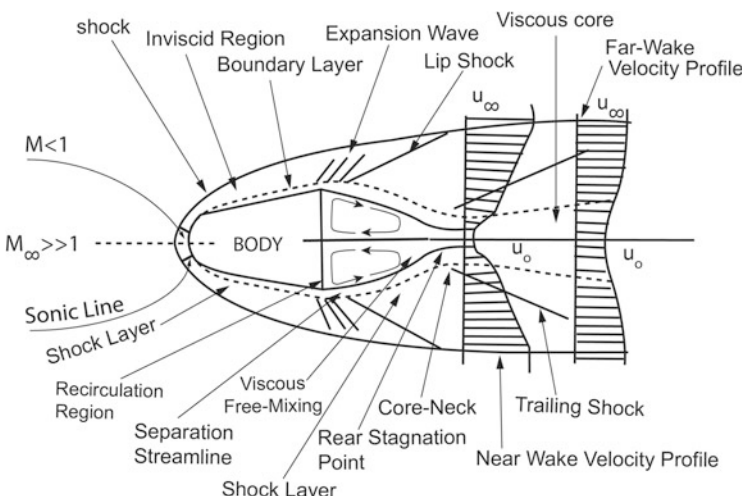


Fig. 15.22 Hypersonic flow features of a typical reentry blunt body

but still more than the free stream conditions. The flow leaving the body is called shear layer, which is mainly composed of boundary layer detached from the body. Between the shear layer and base of the vehicle, there is recirculation region. The shear layer converged at a point called rear stagnation point. At the convergence point, there is a trailing oblique shock and downstream of the shock, the shear layer develops into wake. The shear layer portion of the wake is called inner viscous core whereas the remaining portion up to oblique shock is called inviscid wake.

Boundary layer transition is an important feature in return mission. During orbital phase of reentry mission, the flow over the vehicle is laminar. During continuum flow regime, the viscous effects viz. skin friction and heat transfer are caused by the boundary layer. For the cases of shear stress of fluid motion which is comparable to the pressure responsible for fluid motion, the flow within the boundary layer is laminar, in which the particle motions are orderly. For the cases wherein the shear stresses are much less compared to that of pressure, then the flow within the boundary layer is turbulent (random). Effects of boundary layer are important irrespective of whether the flow within the layer is laminar or turbulent. But aerodynamics as well as thermal characteristics of the vehicle for these flows is different and it is difficult to predict and characterize these parameters during the transition zone.

15.4.3 Hypersonic Aerothermodynamics

One of the main features of reentry hypersonic aero thermodynamics is the real gas effect. In order to appreciate the real gas effects of aero thermodynamic environment of hypersonic flow [4], it is essential to know the following definitions:

A thermally perfect gas is the one that obeys the ideal gas equation,

$$P = \rho RT \quad (15.25)$$

where

P is pressure

ρ is density

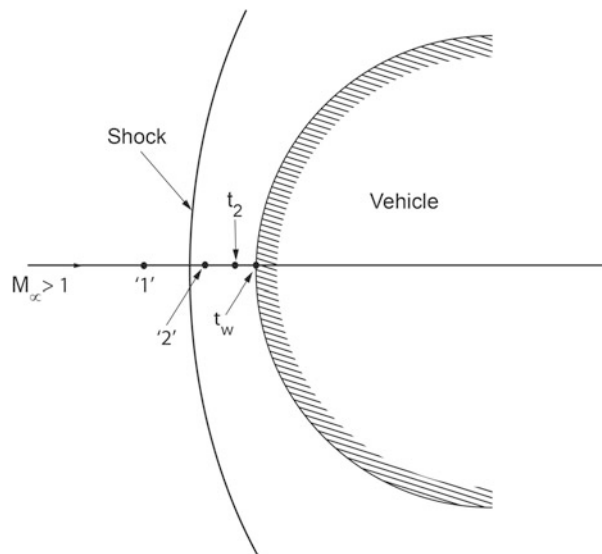
R is gas constant

T is temperature

According to compressible flow theory, this equation shows that internal energy and enthalpy depend only on temperature. A calorically perfect gas has constant values of specific heats, C_p and C_v , independent of temperature.

A perfect or ideal gas is the one which is both thermally and calorically perfect gas. Consider a blunt body as shown in Fig. 15.23. Due to hypersonic flow, there is a strong shock in front of the vehicle, and most portion of which is like a normal shock and there is temperature increase in the downstream of the normal shock. The high temperature gas effects are explained below:

Fig. 15.23 Nomenclature for definition of state



15.4.3.1 Caloric and Chemical Effects

Assuming perfect gas, [2]

$$\frac{T_2}{T_1} = \frac{[2\gamma M_1^2 - (\gamma - 1)][(\gamma - 1)M_1^2 + 2]}{(\gamma + 1)^2 M_1^2} \quad (15.26)$$

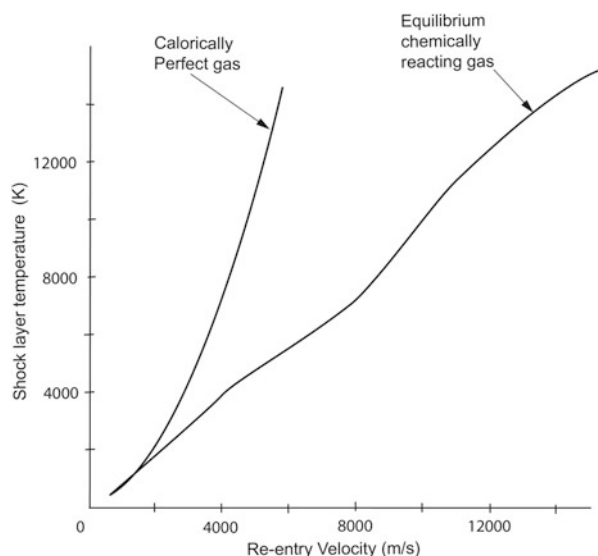
If one assumes that the flow deceleration is entropically downstream to the stagnation point outside the thermal boundary layer point (point t_2), then

$$\frac{T_{t_2}}{T_1} = \left(1 + \frac{\gamma - 1}{2} M_1^2 \right) \quad (15.27)$$

Assume a reentry vehicle enters the atmosphere with $M = 25$ at the altitude of 80 km, wherein the free stream temperature is about 166 K, then the stagnation temperature behind the shock is about 21,000 K, whereas the surface temperature of Sun itself is about 5800 K. But the temperatures measured by reentry vehicles are less, which obviously indicate there are real gas effects.

The composition of air downstream of normal shock differs greatly compared to the free stream air composition. This is due to the fact that, during kinetic energy dissipation process, the diatomic particles behind shock wave get vibrationally excited. They get dissociated and the resulting atoms and remaining molecules are partially ionized. Therefore, the remaining molecules downstream of normal shock cannot be assumed as calorically perfect gas. Within the boundary layer there is sufficient viscous dissipation, which also affects the stream chemistry and finally

Fig. 15.24 Post shock temperature of a reentry vehicle at $h = 52$ km and 1 atm



leads to chemically reacting boundary layer. In such situation, the specific heats C_p and C_v are not constant due to the chemical reaction, and therefore, $\gamma = C_p/C_v$ is also not constant and depends on temperature.

At elevated temperature, γ reduces and this phenomenon for air starts from temperature about 800 K. The reduction of γ at elevated temperature reduces the temperature of shock layer and the reduction depends on the amount of chemical reactions. As an example, shock layer temperature of a typical vehicle as a function of reentry velocity at a typical altitude is given in Fig. 15.24.

15.4.3.2 Aerodynamic Forces and Moments

As the ratio of specific heat is the isentropic exponent, change in γ significantly affects the rate of expansion or compression of the flow. Therefore, the pressure distribution over the vehicle changes significantly which in turn affects the aerodynamic forces and moments significantly.

15.4.3.3 Plasma Effects

At higher temperature, effect of ionization is important. Dissociation of oxygen in air at 1 atm pressure begins and ends at about temperature of 2000 K and 4000 K respectively and nitrogen between about 4000 K and 9000 K respectively. In the ionized flows, the free electrons absorb and reflect electromagnetic radiation especially in the radio frequency range of the communication system, which affects the link between ground and vehicle system during flight.

Aerodynamically also, partial-ionized flow characteristics are different from that of neutral flow, which in turn have impact on vehicle aerodynamic characteristics.

15.4.3.4 Viscous and Rarefaction Effects

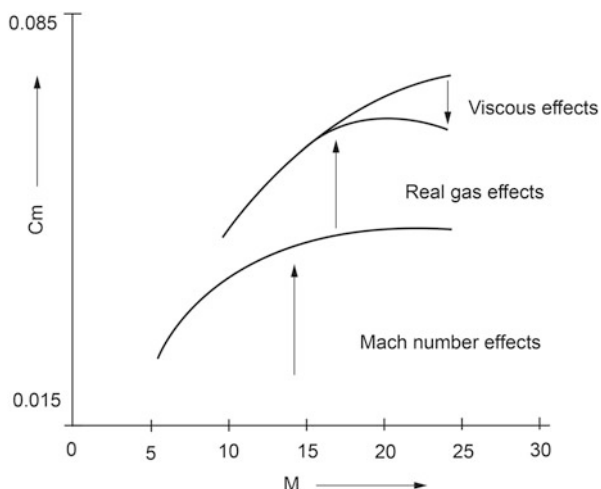
The vehicle encounters both rarefaction and viscous flows and their impacts are also different.

15.4.3.5 Chemically Non-equilibrium and Equilibrium Effects

In chemically reacting flow also, there are two types. At higher altitudes, wherein the density is lower, the collision between the air molecules is less and hence the dissociation process is also less. Therefore the flows are generally non-equilibrium. At lower altitudes, wherein the density of air is more, there are sufficient collisions between the air particles and the chemical phenomenon tends to achieve the equilibrium state. This lowers the ratio of specific heat than the free stream value. In actual environment, the thermodynamic state is in between frozen and complete equilibrium state.

All the above effects have significant impact on the aerodynamic characteristics of the reentry vehicle. Contribution of compressibility, real gas and viscous interaction effects on moment coefficient of a typical lifting reentry vehicle is given in Fig. 15.25. As the reentry vehicle flies through different regimes of flight, these effects also continually vary. It is to be noted that these effects cannot be accurately predicted at ground as it depend mainly on the real characteristics of the vehicle as well as the flight environment with dispersions in flight parameters. Therefore, it is essential to consider these aspects carefully in the reentry vehicle design process.

Fig. 15.25 Pitching moments contribution for a typical lifting reentry vehicle



15.4.4 Reentry Heating

The previous section explains the impact of aero thermodynamic environment on the aerodynamic forces and pressure loads on the vehicle. One of the most important aspects of the reentry vehicle design is the management of thermal loads acting on the vehicle. In hypersonic reentry flight environment, the normal shock in front of the vehicle compresses the air and temperature of air downstream of the shock and ahead of vehicle front portion increases considerably. Therefore, heat is transferred from high temperature air to vehicle through two heat transfer mechanisms as given below:

1. The hot air downstream of the shock flows over vehicle body and heat is transferred through convection.
2. If the temperature of air is sufficiently high, heat is transferred through radiation. Normally radiation heat transfer is important for reentry with speeds more than 10 km/s and may be significant at the lower speeds also.

The heat transfer rate at the vehicle surface depends on the free stream conditions, configuration of the vehicle and its orientation to the flow, difference between the hot air and vehicle surface and surface catalycity. Normally turbulent flow increases the heat rate in the aft body and delayed onset of turbulent flow reduces the heat rate.

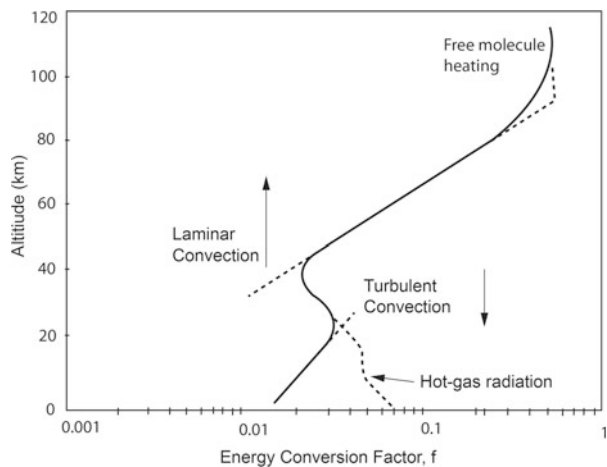
Two types of thermal loads act on the vehicle: total heat load and heat rate. Both these loads are important for the vehicle design. Due to the total heat load, temperature of the vehicle structural material increases. On higher temperature, mechanical properties of structural material reduce, which in turn limits the load carrying capacity of the structure. Regarding heat rate, either local or body average heat rate is important. For the cases of materials with non-zero coefficients of thermal expansion, the thermal gradient due to heat rate causes differential expansion, which in turn introduces mechanical stresses, in addition to the stress due to mechanical loads such as inertia and pressure loads.

Therefore, it is essential to design a suitable thermal protection system for reentry vehicles which transfers only a small percentage of the total thermal load to the vehicle structure.

15.4.4.1 Reentry Heat Loads [5]

Due to the real gas effects and vehicle configuration, only a fraction of thermal load is transferred to the vehicle. At high altitudes, in the free-molecular flow regime, almost entire thermal energy is transferred to the vehicle and the factor goes very close to 1. As the vehicle enters into continuum flow regime, the factor reduces as the flow over vehicle is laminar and the value reduces to as low as 0.01 around the altitude of 40–20 km. When the flow becomes turbulent, again the factor increases. Subsequent to that, in absence of radiative heat transfer, the factor again reduces. For the cases of radiative heat transfer at lower velocities, the factor further

Fig. 15.26 Variation of energy conversion factor for a typical entry vehicle



increases. This factor depends on the vehicle characteristics, reentry trajectory and flow characteristics. The above factors for a typical reentry system are given in Fig. 15.26 [5].

The actual heat rate transferred to the vehicle surface depends on this factor and on the rate of kinetic energy loss. The total heat load depends on the heat rate and duration of the heating.

The rate of change of kinetic energy into thermal energy is the product of drag and velocity. Assume total heat load is Q and instantaneous heat transfer rate to the surface is \dot{q} , where

$$\dot{q} = \frac{dQ}{dt} \quad (15.28)$$

Then,

$$\dot{q} \equiv \frac{dQ}{dt} = f D V = f \frac{\rho_0 \sigma C_D S V_\infty^3}{2} \quad (15.29)$$

$$\dot{q} \sim \sigma V_\infty^3 \quad (15.30)$$

where

σ is the density ratio, given by

$$\sigma = \frac{\rho_\infty}{\rho_0} \quad (15.31)$$

And ρ_∞ = free stream density

ρ_0 = density at sea level

The total heat load is,

$$Q = \int \dot{q} dt = \dot{q}_{ave} \Delta t \quad (15.32)$$

where

\dot{q}_{ave} = body average heat rate

Δt = reentry duration

Heat Loads on Ballistic Bodies

With the substitution of velocity profile expression given in Eq. (15.11) and with suitable substitution for the conversion factor, in terms of skin friction and heat transfer coefficients, integration of Eq. (15.29) gives the total heat [5]

$$Q \sim V_e^2 \sqrt{\frac{m}{C_D S} \left(\frac{1}{\sin \gamma_e} \right)} \quad (15.33)$$

i.e.,

$$Q \sim V_e^2 \sqrt{(BC) \left(\frac{1}{\sin \gamma_e} \right)} \quad (15.34)$$

The above equations show that the total heat load of a ballistic body increases with reentry velocity and ballistic coefficient. Increasing the flight path angle steepens the trajectory, reduces the flight duration, thereby qualitatively reducing the total load. Similarly, the maximum heat rate is given by [5]

$$\dot{q}_{max} \sim V^3 \sqrt{BC \sin \gamma_e} \quad (15.35)$$

The above equation shows that maximum heat rate increases with velocity, ballistic coefficient and reentry flight path angle.

Heat Loads on Lifting Reentry Bodies

The total heat load and maximum heat rate for lifting vehicles are given by [5]:

$$Q \sim V_e^2 \sqrt{\left(\frac{L}{D}\right)(BC) \left(\frac{1}{\sin \gamma_e} \right)} \quad (15.36)$$

and

$$\dot{q}_{\max} \sim V^3 \sqrt{\frac{(BC) \sin \gamma_e}{(L/D)}} \quad (15.37)$$

From the above expressions, one can make the following observations:

1. The thermal loads are more for vehicle reentering the atmosphere with higher velocity
2. Reduction in ballistic coefficient of the vehicle is preferable from heat load point of view
3. The reduction in the reentry interface flight path angle causes the reduction in the heat rate; but due to the extended duration of reentry flight, the total heat load is more
4. Adding lift to the vehicle reduces the heat rate, whereas the total heat load increases

Therefore, it is necessary to have trade-off to get optimum values for the total heat load, maximum heat rate, the optimum vehicle configuration and design.

15.4.4.2 Stagnation Point Heat Rate

The total heat load and body average heat rate are important for the reentry vehicle design process. The maximum local heat rate encountered by a vehicle is also very important input as that location needs maximum thermal protection. If the local after body hot spots due to the turbulence flow and shock-boundary layer interactions are removed, the maximum heat rate occurs at the stagnation point of a reentry vehicle. Generally the vehicle reenters the atmosphere as a blunt body and has a region of stagnation flow [2]. The detailed discussion on this topic is beyond the scope of this book and they can be referred through the relevant text books and technical papers. The relevant expressions being used are given here for reference.

Scott et al. [6, 2] model on engineering relation for the convective heat transfer rate to the stagnation point \dot{q}_t of a sphere is given by

$$\dot{q}_t = \frac{18300(\rho_\infty)^{0.5}}{\sqrt{R_N}} \left[\frac{V_\infty}{10^4} \right]^{3.05} \quad (15.38)$$

where

ρ_∞ = Free stream density in kg/m^3

V_∞ = Free stream velocity in m/s

R_N = Nose radius in m

Heat transfer rate, \dot{q}_t is in W/cm^2 . Since all reentry vehicles are flying as blunt bodies during maximum heating regime, the sphere assumption may not violate the reality. This model gives fairly good prediction as established through real flight

data. Also, it is established that this model consistently gives higher than measured values.

Delta et al. [7, 2] have developed another model for convective heat rate for flight application and is given by

$$\dot{q}_t = \frac{11030}{\sqrt{R_N}} \left(\frac{\rho_\infty}{\rho_0} \right)^{0.5} \left(\frac{V_\infty}{V_0} \right)^{3.15} \quad (15.39)$$

where

ρ_0 is sea level density in kg/m³

V_0 is circular orbital velocity at sea level (= 7950 m/s)

and \dot{q}_t is in W/cm²

When the vehicle flies at very high velocity, Martin [8, 2] model gives gas-to-surface radiation heat rate for reentry vehicles, given by

$$\dot{q}_r = 100 R_N \left(\frac{V_\infty}{10^4} \right)^{8.5} \left(\frac{\rho_\infty}{\rho_0} \right)^{1.6} \quad (15.40)$$

Suitable TPS system has to be implemented to protect the vehicle systems as against the severe stagnation point thermal load.

15.4.4.3 Thermal Protection Systems

Even though the minimum heat load of the total reentry heat environment is transferred to the vehicle, it is still higher with respect to the existing material capabilities. Therefore, the vehicle structure and various elements of the reentry vehicle must be protected during atmospheric reentry. Minimum mass of the vehicle is an important consideration while designing a suitable thermal protection system (TPS). Currently, three types of TPSs are being employed.

Heat Sink

This is a heat absorption method. In this method, the thermal energy transferred to the vehicle is absorbed in high thermal capacity material. The temperature of the heat sink material increases, whereas there is no transfer of the heat to the primary structure. The energy balance equation for this technique [5] is

$$Q = m C_v \Delta T \quad (15.41)$$

where Q is the total heat load transferred to the vehicle, C_v is the specific heat at constant volume for the selected TPS, ΔT is the allowable temperature of heat sink,

which must be below its melting point and m is the mass of the heat sink material. The choice of the material is important as it increases the mass of TPS. Copper and beryllium with a high thermal diffusivity, high thermal capacity and high density are the candidate materials. The main disadvantage of this method is the increased TPS mass.

Ablation TPS

This is also an absorption technique. The thermal energy transferred to the vehicle is used to sublime the ablative material and swept away in the flow field. The energy balance equation is

$$Q = h_v \Delta m \quad (15.42)$$

where h_v is heat of vaporization and Δm is the ablative mass loss by vaporization. The vaporization process of ablative material absorbs the heat at the surface. The gaseous products at the surface change the velocity and temperature profiles in the boundary layer which in turn reduces the incoming heat transfer (reduces conversion factor f). Here also the choice of material is important. Generally material with large heat of vaporization is required to reduce the mass of TPS. Graphite and phenolic compounds are typical materials for ablative TPS.

Ablation TPS is a most efficient system, but the disadvantages are: (1) change of vehicle shape during flight and associated aerodynamic characteristic change, and (2) reusability of the vehicle is limited.

Radiative TPS

This is a heat radiation technique. In this case, due to the incoming temperature, the surface of the TPS is allowed to become red hot which in turn radiates the heat back to the atmosphere. The increase in temperature of the TPS surface is allowed to a level such that radiative heat rate is equal to the incoming convective heat rate. The equilibrium equation is

$$\dot{q}_{\text{out}} = \dot{q}_{\text{in}} \cong \epsilon \sigma T_w^4 \quad (15.43)$$

where

ϵ = emissivity of the TPS surface

σ = Stefan-Boltzmann constant

T_w = TPS surface temperature, which is much larger than the gas temperature

Radiative TPS requires insulation between TPS and surface of vehicle primary structure. This can be overcome by usage of proper TPS materials. Refractive

(ceramic) materials with a high melting temperature, coated with a high emissivity substance are the choice.

Material selection and TPS design have to be such that while minimizing the TPS mass, the temperature transferred to the vehicle structure is within allowable limits of the vehicle primary structure and other associated elements.

15.5 Reentry Mission Management

15.5.1 System Requirement

Reentry system requirement is to bring back an identified payload from a specified location in space to Earth at a designated location within the specified accuracy. The requirements on the vehicle, design aspects of the vehicle and reentry trajectory are discussed in the previous sections. Once the vehicle and trajectory systems are designed and realized, to execute the mission successfully, an intelligent mission management system is required. Function of this system is to fly the vehicle safely through the harsh aerothermal environment and still meet the mission objectives. To carry out the task flawlessly under such adverse conditions, the mission management system has to provide ‘controlled dissipation’ of the combined kinetic and potential energy, the vehicle has at the time of reentry. The ‘controlled dissipation’ process ensures the restriction of both dynamic and heat loads on the vehicle, within the acceptable limits of vehicle design capability.

The ‘controlled dissipation’ requires a carefully designed trajectory, which is feasible within the reentry corridor, defined by heating loads, deceleration, dynamic pressure and controllability limits of the vehicle. The reentry mission management system has to ensure that the vehicle follows the feasible trajectory. Further, even though the trajectory is designed for nominal environment, the uncertainties in vehicle aerodynamics, mass characteristics, atmosphere variations, imperfect executions of deorbit maneuver and steering control commands during flight could deviate the trajectory. These deviations can violate the vehicle safety limits and also can affect the landing at the designated location. Therefore, a precision guidance and control system is needed to steer the vehicle on the trajectory, to achieve the specified terminal conditions within the specified error margin.

For a guidance and control system to be effective and to achieve the objective, it is necessary to get more accurate and realistic estimate of the trajectory and the missing critical parameters onboard in real time. This demands real time onboard estimation system, which contains navigation, guidance and control subsystems. Guidance is the only active element which acts as driver. The navigation provides input data to the guidance subsystem and the control subsystem executes the desired attitude generated by the guidance subsystem. It is the guidance element that processes the sensor information, generates the feasible trajectory, satisfying vehicle related constraints and decides appropriate attitudes to the control system to

follow the feasible trajectory. Therefore the design of a suitable guidance needs careful attention. Navigation and attitude control systems are generic in nature and similar to the ones followed for the aerospace vehicle. However, reentry guidance systems to execute orbital reentry trajectories are different from that of other systems.

15.5.2 Reentry Trajectory Guidance Strategy

Reentry trajectory of a typical winged-body reentry vehicle is given in Fig. 15.27. Depending on the trajectory characteristics, flight environment and the complexity of the guidance systems requirement, the reentry mission profile is broadly divided into four distinct flight phases: (1) Keplerian phase, (2) Reentry phase, (3) Terminal Area Energy Management (TAEM) phase and (4) Approach and landing phase.

When the vehicle leaves its orbit, it enters into Keplerian phase, in which the altitude decreases and the atmospheric density increases. The reentry phase of flight starts when the atmospheric density crosses a pre-determined threshold value. During reentry phase of the vehicle, almost all the energy is dissipated through aerodynamic drag and this phase extends from very high hypersonic Mach numbers to supersonic Mach numbers. The third phase is the TAEM phase, in which the trajectory dispersions accumulated in the previous phases are corrected, the energy level of the vehicle is decreased and the vehicle is placed at the approach/landing interface. Final phase is the approach/landing phase, wherein the vehicle is prepared and executed for automatic landing.

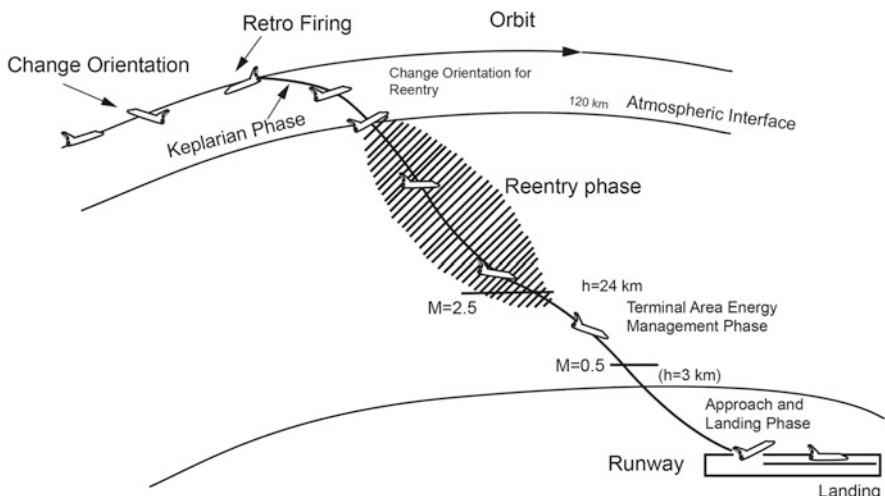


Fig. 15.27 Reentry trajectory phases of a typical winged reentry vehicle

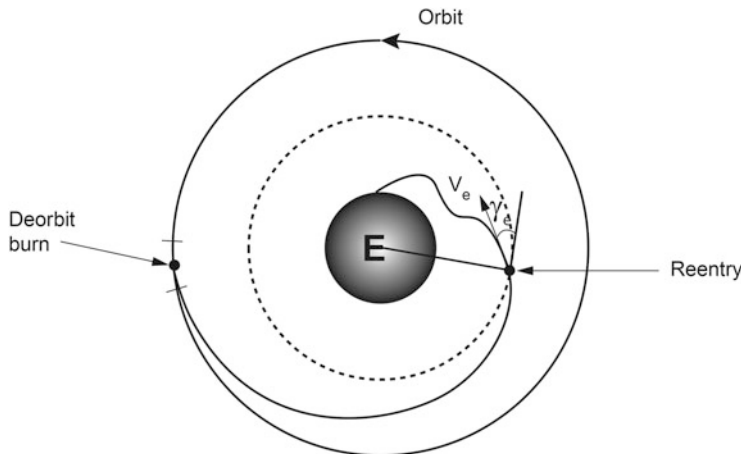


Fig. 15.28 Keplerian and reentry projection phases

During the Keplerian phase guidance, the deorbiting is carried out such that the perigee of the transferred orbit is just below the reentry interface. The magnitude and direction of the reverse velocity required for deorbiting the vehicle depend on the required reentry interface conditions viz. V_e and γ_e which ensures the vehicle reentry trajectory within the vehicle capability and reaches the landing site as given in Fig. 15.28. Guidance in this phase determines the time of initiation of the deorbiting maneuvers and the orientation and duration of the deorbiting maneuver. The guidance in this phase is similar to the ascent missions.

In comparison to the other three phases, the reentry phase guidance is more complex due to the following reasons:

The atmospheric flight of ascent phase of a typical space transportation system is only for a short duration of about 2 min. There is no trajectory control and no closed loop guidance system. The deviation created by the predefined trajectory of this phase is corrected in the long duration vacuum flight of the vehicle. The main force used in ascent phase to achieve the required energy is by the main propulsive systems, and the system function, performance and magnitude of propulsive forces are independent of vehicle state (except for a very weak interaction during about 1950s of flight during atmospheric flight phase). The vehicle attitude control during ascent phase is through a separate control system. Even in the case of achieving the control through gimbaling the main propulsion system, the impact of the same in terms of velocity reduction is minimal, which in anyway will be corrected by utilizing part of the guidance margin provided in the vehicle.

In contrast to the above features of ascent mission, the entire reentry flight phase is in the atmosphere that is very complex and harsh environment compared to the ascent phase atmospheric flight. The reentry atmospheric flight phase has wide range of parameters like environmental conditions, dynamic pressure, atmospheric parameters, Mach numbers (varying from 25 to 0) and angle of attack (varying from

50° to 0°) which introduce highly nonlinear aerodynamic characteristics. The main forces used to dissipate the energy of the vehicle are aerodynamic drag and lift, and these forces are dependent on the vehicle's current state of altitude and velocity. The direction of this force cannot be controlled without affecting its magnitude.

Since the aerodynamic forces are used to dissipate the vehicle energy, modulating these forces to control the trajectory violates the vehicle safety limits. Therefore, there is strong nonlinear coupling between trajectory control, energy dissipation process and the vehicle safety limits. Finally, due to the limitation on a priori prediction of the aerodynamic characteristics of the vehicle, the uncertainties of aerodynamic characteristics in flight are very large along with uncertainties of mass properties and environmental parameters. In addition, the situation is further aggravated by the narrow operating envelope, limited by the very narrow allowable reentry corridor.

The steering of the vehicle from the reentry interface state (defined by altitude, velocity, flight path angle, heading, latitude and longitude) to the specified terminal conditions at TDEM interface without violating path constraints under the severe environment is a complex task.

Before the reentry mission management, it is essential to define the control variables for carrying out the guidance function and the strategy of mission management (trajectory control) through these control variables.

15.5.2.1 Control Variables Selection

The energy dissipation during reentry flight is achieved through aerodynamic drag force and the trajectory depends mainly on the drag acceleration. Therefore, the trajectory modulation also has to be essentially achieved through drag force modulations.

One easy way is modulating drag force through angle of attack, α . For a specified vehicle, reentry is planned with a lower ballistic coefficient to reduce the thermal environment. This is achieved by increasing C_D and frontal area through large α . By modulating α , C_D characteristics change, ballistic coefficient changes, thereby violating the heat load constraint of the vehicle. Therefore, drag force modulation through α is not acceptable. Also, it is to be noted that in order to achieve the landing point within the required accuracy, it is essential that the reentry systems have both down range and cross range modulation capabilities. To achieve the above requirements as well as to widen the foot-print capability of the vehicle, the reentry system is provided with lifting feature. Therefore, (L/D) feature of reentry vehicle can also be used for trajectory regulation/control of the reentry vehicle.

The trajectory modulation using (L/D), any major modulation on α , alters the aerodynamic characteristics of the vehicle, which in turn violates many of the design limits of the vehicle. To get better control on the thermal loads, generally the vehicle follows a defined α profile. The α profile for a typical reentry vehicle mission is shown in Fig. 15.29. Therefore, a small modulation in α within a specified

Fig. 15.29 α -Profile pattern of a typical winged body reentry vehicle

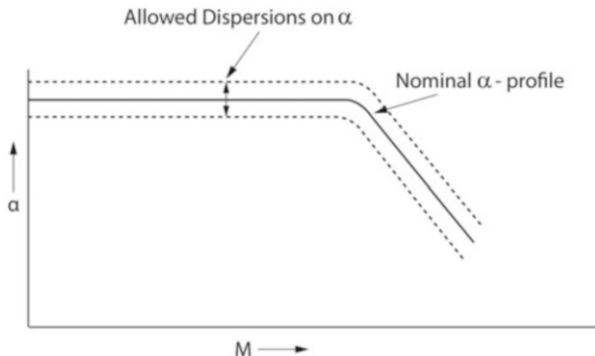
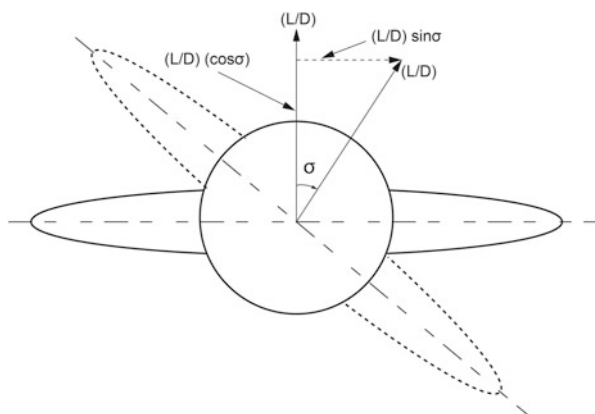


Fig. 15.30 Bank angle modulation for trajectory control of reentry vehicle

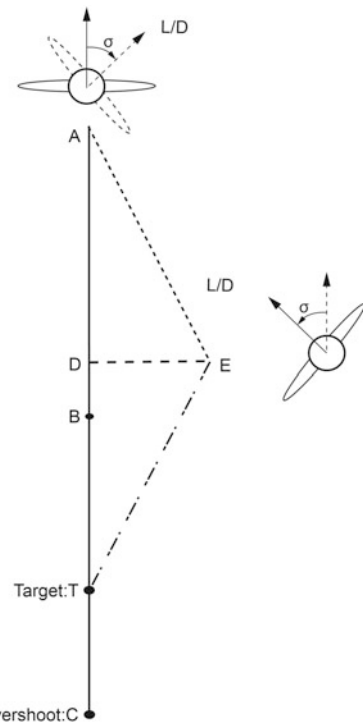


band is only permitted. Considering the above aspects, the main control parameter used for trajectory modulation is the vehicle bank angle, σ .

By modulating σ , the component of (L/D) in the plane of motion of the vehicle (along the down range plane) gets modulated as given in Fig. 15.30. This in turn modulates the altitude of the vehicle thereby modulating density, ρ . The change of ρ finally changes the drag force which in turn modulates the vehicle trajectory to meet the desired down range. In summary, it can be concluded that, even though α modulation has direct modulation effect on drag, to ensure vehicle safety limits, drag modulation is achieved through σ modulation. As this is achieved through altitude modulation, the response of the trajectory control system is very slow. Implication of this strategy is that it causes a lateral force as in Fig. 15.30 which in turn creates a cross range. The direction of bank angle can be reversed to nullify the undesired cross range. However, if the cross range is part of requirement, same would be achieved through the proper selection of σ .

As an example, consider a reentry flight with (L/D) more than the ground predicted value. The increase in (L/D) can be due to increased L or decreased D or

Fig. 15.31 Bank angle modulation to compensate trajectory over shoot in down range



both. Under such environments, the down range is more than the target as given in Fig. 15.31. The parameters in this figure are explained below: Reentry interface point is A and target point is T corresponding to the predicted (L/D). Due to the increased (L/D), vehicle reaches the point C with an overshoot of TC. Under those conditions, the guidance strategy finds a ‘ σ ’, which is function of violation ‘TC’. Due to increased σ , vertical component of (L/D) decreases which in turn reduces altitude. Subsequently density increases, and therefore drag force increases which causes the reduction of the down range. When the vehicle flies halfway through, instead of reaching the down range at B, with bank angle σ , the vehicle reaches the point E. This reduces the down range at that instant by BD and creates in addition a cross range DE. This cross range is not desirable. Therefore, at E, the guidance system generates the vehicle bank angle in the opposite direction, which at the end of mission, reaches the point T as shown in Fig. 15.31.

It is to be noted that the maximum down range possible by a reentry mission is by flying the vehicle with maximum (L/D). This is feasible by flying with $\sigma = 0$ throughout the reentry flight. Therefore, to have the ranging capabilities in both the directions, the nominal vehicle trajectory is generally designed with a nominal bank angle profile as given in Fig. 15.32 to meet a specified down range without any cross range.

During initial phase of reentry flight, the magnitude of lift/drag forces are less along with higher α . This in turn demands large value of σ to really effect a change in

Fig. 15.32 Typical nominal bank angle profile

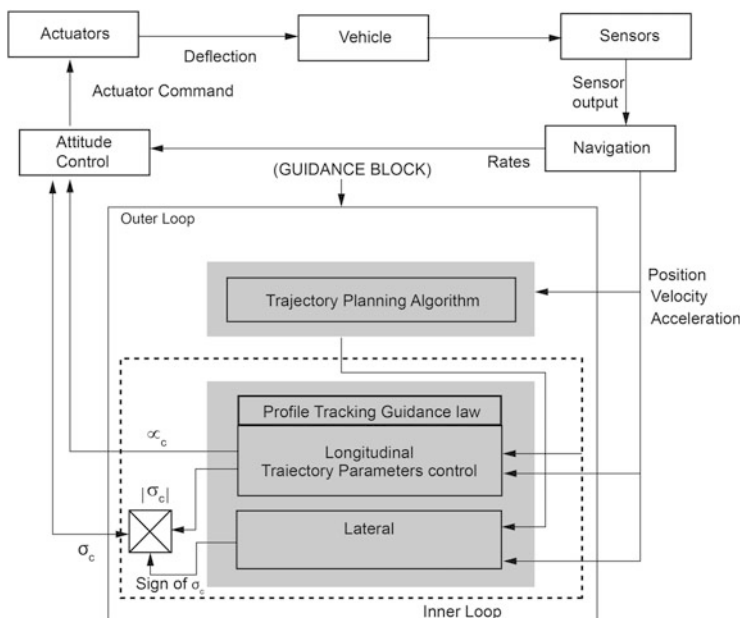
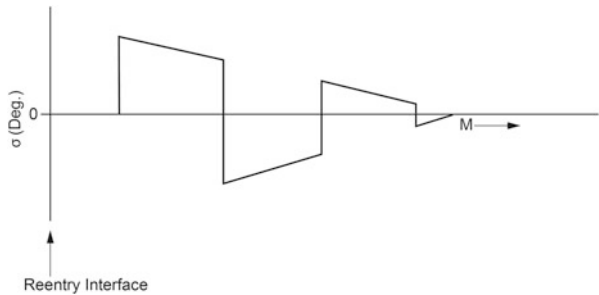


Fig. 15.33 Reentry guidance strategy

the trajectory. As the vehicle descents through the atmosphere the dynamic pressure is large and aerodynamic force levels are also larger. This along with reduced angle of attack flight makes larger sensitivity for σ to make the trajectory change.

But unlike the α profile, σ profile doesn't contain any constraint. Whatever is the guidance system demand it can be used for trajectory control, but within the capability of vehicle control and structural systems.

15.5.2.2 Guidance Functional Schematic and Guidance Strategy

The reentry guidance functional schematic is given in Fig. 15.33. In general, the reentry guidance strategy contains two components: (1) trajectory planning system

and (2) profile tracking guidance law. The trajectory planning system (outer loop) designs a feasible reference trajectory from a given state at reentry interface to a specified state at TAEM interface, satisfying path constraints. The profile tracking guidance law (inner loop) computes the angle of desired attack (α_c) and bank angle (σ_c) during reentry flight phase, in order to follow the reference trajectory. In most of the planning algorithms available in literature, the profile tracking algorithms compute α_c and magnitudes of σ_c to follow the longitudinal trajectory parameters viz. altitude, velocity, flight path angle and the corresponding down range. The lateral trajectory parameters viz. velocity heading and downrange are controlled by a series of bank angle reversals. The lateral trajectory guidance law computes the heading miss, which is defined as the angle between the current plane of motion and the plane formed by the current position vector and target vector. If the heading miss is beyond a defined dead band, the bank angle sign is reversed. Different values of dead bands are used at different phases of flight, thus the velocity heading and cross range dispersions are controlled within the specified values.

15.5.3 Reentry Guidance system

The flight proven classic Space Shuttle reentry guidance design [9, 10] is a benchmark for most of the advanced reentry guidance algorithms that are currently being reported in literatures. The summary of Space Shuttle reentry guidance algorithm and the advanced reentry guidance algorithm developments are briefly explained in the following subsections.

15.5.3.1 Summary of Reentry Guidance Concept

During most of the reentry flight phase, the vehicle flies in very low flight path angle. Assuming small angle approximation for γ ($\cos \gamma \cong 1$, $\sin \gamma \cong 0$), and the vehicle altitude during atmospheric flight phase is very small compared to radius of Earth, $R/r \sim 1$, then using the Eqs. (15.1) and (15.4), the down range can be written as

$$s = - \int \frac{V dV}{(D/m)} \quad (15.44)$$

Therefore, the range to be flown during reentry is a unique function of the drag acceleration profile maintained throughout the reentry flight. This reentry range is predictable using analytic techniques for simple geometric drag acceleration with respect to Earth-relative speed, provided flight path angle is near to zero. When the vehicle flies towards the end of reentry phase, where the flight path angle is not near zero, range predictions can be analytically computed for simple geometric drag

acceleration functions if the independent variable is changed from Earth – relative speed to energy.

Specific energy at any instant of flight is given as

$$E = gh + V^2/2 \quad (15.45)$$

Where g is the gravity acceleration at the altitude h , and the down range is given by [11]

$$s = - \int \frac{dE}{D} \quad (15.46)$$

Therefore, flight throughout the reentry corridor can be achieved by linking these geometric functions together in a series. The reentry guidance is designed on the principle of analytically defining a desired drag acceleration profile and generating desired attitude profile of the vehicle to achieve the desired drag acceleration profile. Thus the reentry guidance contains two main components: (1) planning of reference drag acceleration profile on ground before mission and (2) onboard computations which involve updating of reference profile to meet the range requirements and tracking control law which computes attitude commands to achieve the desired profile.

The drag acceleration profile is designed offline for the vehicle data to have a form that best fits within the reentry corridor. This also meets the mission requirement of achieving the range from the specified reentry point. During flight, the reentry range from the present position as given by the navigation system to the termination of reentry flight is predicted through the suitable analytical expressions using the stored drag acceleration profile. The magnitude of the stored drag acceleration profile is adjusted onboard, while retaining the basic profile shape, such that the predicted range and the range to the target are the same values. The updated drag acceleration profile is defined as the reference drag acceleration profile. A profile tracking control law computes guidance commands to fly the vehicle on this updated drag acceleration profile. This control law was developed using linearized analysis of the flight dynamics.

15.5.3.2 Reentry Corridor and Offline Computed Drag Acceleration Profile

To ensure safety of the vehicle and vehicle control capability during reentry flight, the reentry trajectory to be flown by the vehicle has to ensure that the heat rate, structural load acting on the vehicle and the hinge moment acting on the actuator are less than the corresponding allowable limits. To ensure maneuverability in terms of capability to change the trajectory slope, the vehicle should have the capability of flying in a trajectory below the limit specified by the equilibrium glide trajectory (rate of change of flight path angle = 0). These form path

constraints on the reentry trajectory generated by guidance system. The thermal constraint is generally expressed in terms of heat rate at stagnation point. The structural limit is defined in terms of structural load factor. In order to ensure that the required hinge moments of the actuators remain within the specified limit, the dynamic pressure level needs to be limited. These path constraints are expressed through the following inequality relations [11].

$$\left(\frac{L}{m}\right) \cos \sigma \leq \left[g - \left(\frac{V^2}{r}\right)\right] \cos \gamma \quad (15.47)$$

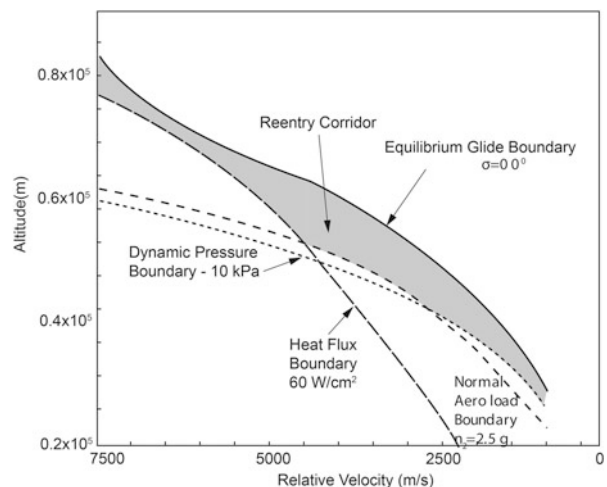
$$\dot{q}_t = \left(\frac{11030}{\sqrt{R_N}}\right) \left(\frac{\rho}{\rho_0}\right)^{0.5} \left(\frac{V}{V_{cir}}\right)^{3.15} \leq \dot{q}_{tmax} \quad (15.48)$$

$$n_z = \left(\frac{D}{m}\right) \left[1 + \left(\frac{L}{D}\right)^2\right]^{0.5} \leq n_{zmax} \quad (15.49)$$

$$q = \frac{1}{2} \rho V^2 \leq q_{max} \quad (15.50)$$

where \dot{q}_t is heat rate, n_z is aerodynamic normal acceleration, q is dynamic pressure and q_{tmax} , n_{zmax} and q_{max} are their maximum allowable values respectively. The other parameters used in the above expressions are: g is gravity acceleration, R_N is reference nose radius, ρ_0 is sea level density and V_{cir} is 7905 m/s. To achieve the mission objectives successfully under the complex reentry flight phase with dispersed conditions, the vehicle needs to fly within the reentry corridor defined by the above path constraints. At each velocity level, the upper limit of the vehicle altitude is decided by the equilibrium glide trajectory and lower limit of the altitude is decided by the thermal, structural and dynamic pressure constraints. The reentry corridor generated for a typical reentry vehicle is given in Fig. 15.34. The

Fig. 15.34 Reentry corridor altitude vs velocity



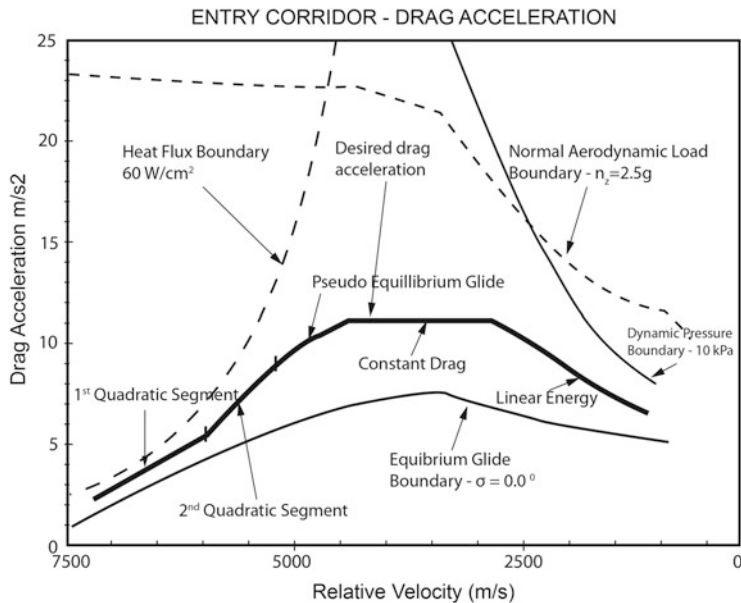


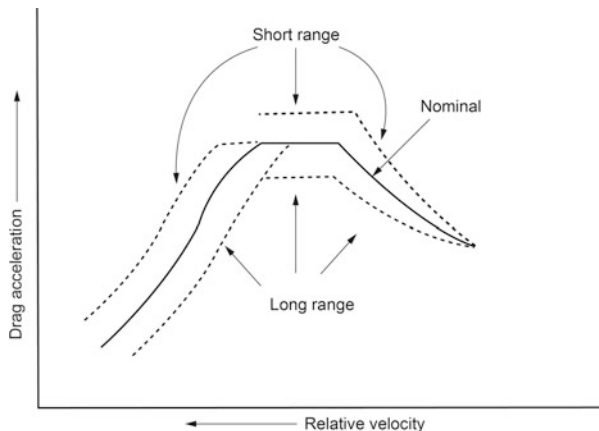
Fig. 15.35 Reentry corridor drag acceleration vs velocity

aerodynamic characteristics of typical vehicle are used for generating the reentry corridor. The constraints used for the generation of the reentry corridor are $q_t = 60 \text{ W/cm}^2$, $n_{\max} = 2.5 \text{ g}$, $q_{\max} = 10 \text{ kPa}$, which are typical of most reentry missions of a typical winged vehicle currently being flown. The reentry trajectory profile is mainly dictated by the drag acceleration. Therefore, it is convenient to represent the constraints, reentry corridor and allowable flight profile, in terms of drag acceleration with respect to the relative velocity. The reentry corridor given in Fig. 15.34 is represented in terms of drag acceleration – relative velocity in Fig. 15.35.

It is essential to define a drag acceleration profile within this reentry corridor which generates a feasible reentry trajectory. To obtain analytical solution onboard, the basic reference drag acceleration profile is converted into smaller and simple segments as given in Fig. 15.35

15.5.3.3 Adjustment of Drag Acceleration Profile Onboard to Achieve the Required Range

Using the initial conditions as estimated by the navigation system, the range is computed analytically by integrating the nominal stored drag acceleration profile. From the range-to-target computed using navigation data and the range predicted along the nominal profile to the termination of reentry flight, range errors are computed. The range errors are nulled by adjusting the magnitude of the stored

Fig. 15.36 Ranging

reference profile while retaining fundamental profile shape. Typical adjustments of magnitude of the profile during different flight regimes are shown in Fig. 15.36. The effect of this arrangement is to drive the trajectory back to nominal at the start of the next phase. Readers may refer [9, 10] to get more details.

15.5.3.4 Tracking Control Law [11]

Once desired drag acceleration profile is determined, a control law is required to compute vehicle attitude commands to control the vehicle to the desired acceleration profile. A control law based on linearized analysis of flight dynamics, which ensures damping of oscillatory type trajectory motion, is needed. Assuming bank angle modulation for trajectory control $(\delta C_D, \delta \dot{C}_D, \delta \ddot{C}_D) = 0$, a linear feedback function of the following form is needed to provide a means for achieving desirable dynamic response in controlling the vehicle to the reference profile.

$$\delta \left(\frac{L}{D} \right) = k_1 \delta D + k_2 \delta \dot{D} + k_3 \delta V \quad (15.51)$$

where

$$\delta D = D - D_0; \quad \delta \dot{D} = \dot{D} - \dot{D}_0; \quad \delta V = V - V_0 \quad (15.52)$$

$$\delta \left(\frac{L}{D} \right) = \left(\frac{L}{D} \right)_c - \left(\frac{L}{D} \right)_0 \quad (15.53)$$

and $D_0, \dot{D}_0, V_0, (L/D)_0$ are the desired values of drag acceleration, its rate, relative velocity and $(L/D), D, \dot{D}, V$ are the corresponding flight measured values and k_1, k_2, k_3 are gains. To avoid noisy data resulting from numerical differentiation to

obtain $\delta \dot{D}$, this feedback term is to be replaced with $\delta \dot{h}$, which can be determined from navigation data without differentiation. The errors in determining altitude rate induce a steady state drag acceleration standoff from the reference profile that is proportional to the error in the navigated altitude rate. Therefore, a feedback term proportional to the integral of δD is introduced to eliminate this steady state error. The resulting control law is given by

$$\left(\frac{L}{D}\right)_c = \left(\frac{L}{D}\right)_0 + f_1(D - D_0) + f_2(\dot{h} - \dot{h}_0) + f_3 \int (D - D_0) dt \quad (15.54)$$

where $(L/D)_c$ = commanded component of L/D in the plane formed by position and relative velocity vectors and f_1 , f_2 , f_3 are gains. $(L/D)_0$ from the desired drag acceleration profile D_0 and the gains are computed analytically. For details, readers may refer the expressions given in Ref. [10].

The commanded (L/D) can be achieved by angle of attack (α_c) or bank angle (σ_c) modulations or by combinations of the two. Generally, bank angle is chosen as the primary trajectory control parameter because the angle of attack is selected to minimize the aerodynamic heating environment while achieving the required cross range. This also minimizes the changes in the aerodynamic heating distributions over the vehicle because of the changes in the angle of attack. Therefore, bank angle is used to control both the total reentry range and cross range component of reentry range. The magnitude of the bank angle controls total range and the direction of the bank angle controls the vehicle heading relative to the path. When the vehicle heading relative to the desired path exceeds a predefined value, the bank angle direction is reversed to reduce the heading deviation. The trajectory response to σ_c modulation is relatively slow since this changes the flight path and thus achieves drag modulation capability through a long period change in atmospheric density. To minimize: (a) the effect of the bank reversal, (b) the resultant phugoid motion and (c) other transient effects such as density gradients, a short period drag control is essential. This is accomplished by modulating α_c , which changes the drag at much faster rate by changing the drag coefficient. At the same time, to maintain a desired angle of attack profile, the modulated angle of attack is driven back to the reference α_c schedule on a long-term basis. The trajectory control law to accomplish all these functions is given by commanded bank angle and angle of attack as given below:

$$\sigma_c = \cos^{-1} \left[\frac{(L/D)_c}{(L/D)} \right] + f_4(\alpha - \alpha_0) \quad (15.55)$$

$$\alpha_c = \alpha_0 + C_D(D_0 - D)/f_5 \quad (15.56)$$

where

$\frac{L}{D}$ = in-flight estimated (L/D) from navigation acceleration data

α_0 = desired angle of attack profile (predefined)

α = measured value of angle of attack

C_D = vehicle aerodynamic drag coefficient, measured onboard f_4, f_5 = gains

In the above computations, onboard measured values of drag acceleration and (L/D) are required. These parameters are estimated from the onboard measurements as given below [11]:

$$D = -\mathbf{a}_s \cdot \mathbf{i}_{vel} \quad (15.57)$$

$$L = [\mathbf{a}_s \cdot \mathbf{a}_s - D]^{0.5} \quad (15.58)$$

where

\mathbf{a}_s = acceleration vector measured onboard through inertial system

\mathbf{i}_{vel} = relative velocity vector

And D, L are the onboard measured drag and lift accelerations and (L/D), respectively. Measured (L/D) is computed using measured L and D .

15.5.3.5 Lateral Control Logic

Cross range is controlled by a series of bank reversals determined by an azimuth dead band error. The azimuth error is the angle between the plane formed by the vehicle position and velocity vector and the plane formed by vehicle position vector and a vector from the vehicle to the target point as given in Fig. 15.37 and explained below [11]:

$$\Delta_{miss} = \sin^{-1} \left[(\mathbf{i}_{per} \mathbf{i}_{TEF}) / \sin \sum \right] \quad (15.59)$$

Fig. 15.37 Heading angle definition

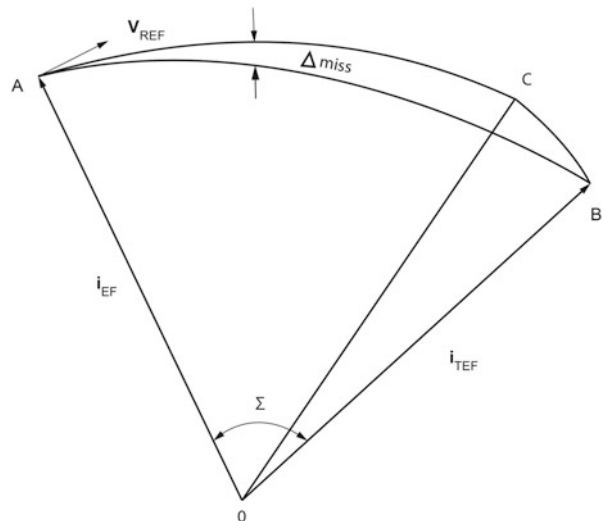


Fig. 15.38 Allowable tolerance for heading miss

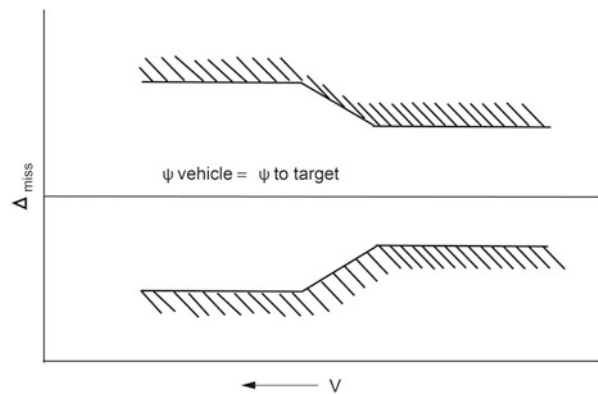
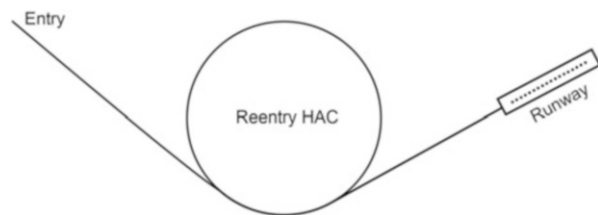


Fig. 15.39 Concept of reentry HAC



where the arc length \sum along the great circle containing instantaneous position and target vector is computed as

$$\sum = \cos^{-1}[(\mathbf{i}_{\text{EF}} \cdot \mathbf{i}_{\text{TEF}})] \quad (15.60)$$

where

\mathbf{i}_{per} = Unit vector normal to the plane of motion

\mathbf{i}_{TEF} = Unit vector along target

\mathbf{i}_{EF} = Unit vector along vehicle's instantaneous position

If the azimuth error is beyond the specified dead band, the bank angle sign is reversed. Depending upon the requirement and criticality of the phases, a profile of error band can be defined as given in Fig. 15.38.

In order to avoid populated area, reentry heading alignment cylinder (HAC) is used as given in Fig. 15.39. The HAC is an imaginary cylinder with the required radius fixed at required location. The reentry phase guidance target is on the HAC. Once the plane formed by position and velocity vectors touches the cylinder, vehicle will fly along the surface of the cylinder till the required conditions are met and exit the cylinder surface tangentially.

15.5.3.6 Advances in Reentry Guidance Law

To meet the requirements of new generation reentry vehicles, considering the new and emerging missions and the advancement in computing power, recent research is focused towards developing efficient and more advanced guidance algorithms particularly in the following specific areas.

Nonlinear control laws for tracking the reference trajectory parameters.

Advanced linear control system to track the reference profile, which is less sensitive to the reference mission.

Better schemes for updating the reference profiles onboard.

Generation of reference trajectory through onboard planning.

15.5.4 Terminal Area Energy Management (TAEM) Phase

As the vehicle flight safety is of prime importance, due to severe constraints, it is difficult to control the flight path to the required accuracy during the most disturbed reentry flight phase. The TAEM phase is used (a) to knock out the range errors during the reentry phase, (b) to manage the vehicle energy, (c) to place the vehicle with the specified targeted energy and (d) to position the vehicle for approach and landing. The role of guidance here is to generate steering commands to control total energy, dynamic pressure and altitude of the vehicle with respect to range. In addition, lateral position of the vehicle at the end of this phase should be aligned with the extension of the runway centerline.

The energy management phase consists of four flight phases as shown in Fig. 15.40 [12]. The S-turn range modulation phase aims at dissipating excessive energy that is carried over from the reentry phase. The whole trajectory length to approach and landing interface can be modulated by renewing the shape of lateral trajectory that consists of two circular arcs. On the HAC, the vehicle makes its heading alignment maneuver to the runway direction. The longitudinal acceleration command and speed brake deflection command are generated by using altitude, altitude rate, total energy and dynamic pressure. It is to reach and follow reference

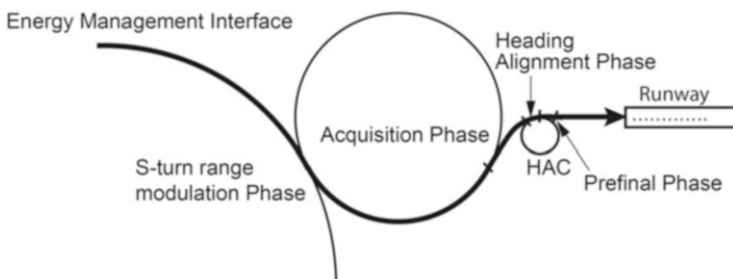


Fig. 15.40 Lateral flight trajectory of TEAM phase

altitude with respect to range to runway under the restriction of maximum and minimum dynamic pressure. The guidance algorithm in this phase is called direct energy feedback method. Reentry is over by this time.

As this phase is only to manage the dispersions of crucial reentry phase and also the guidance algorithm involved is generic in nature, the details are not included here and the relevant literatures may be referred for details.

15.5.5 Approach and Landing Phase

The guidance during this phase has to ensure the vehicle at the specified landing location within the allowable dispersion bands with the specified vertical velocity. The minimum vertical velocity is required to avoid bouncing. A natural trajectory to reach the nominal landing point is a straight line, corresponding to a constant flight path angle. The final velocity constraints require a flare before touchdown demanding a new flight path angle. Accordingly, four flight phases are defined as given in Fig. 15.41 [13–16].

The steep glide slope with flight path angle of about 20° , corresponds to a quasi equilibrium situation (aerodynamic force \approx gravity force). This phase is used for removing dispersions at transition, for maintaining a constant flight path angle and depends mainly on vehicle (L/D). A flare reduces the vertical velocity by linearly reducing the flight path angle from steep to shallow glide slope. If direct transfer from circular flare to shallow glide slope is done, acceleration discontinuity can occur. Hence an exponential flare segment is needed to dynamically smooth the transition to shallow glide slope. Shallow glide slope ($\sim 1.5^\circ$) flies with relatively small vertical velocity.

The guidance defines best trajectory to meet all the constraints and landing location and also to steer the vehicle along the trajectory. The commands α and σ are generated by h , \dot{h} , V lateral position to reduce the longitudinal and lateral

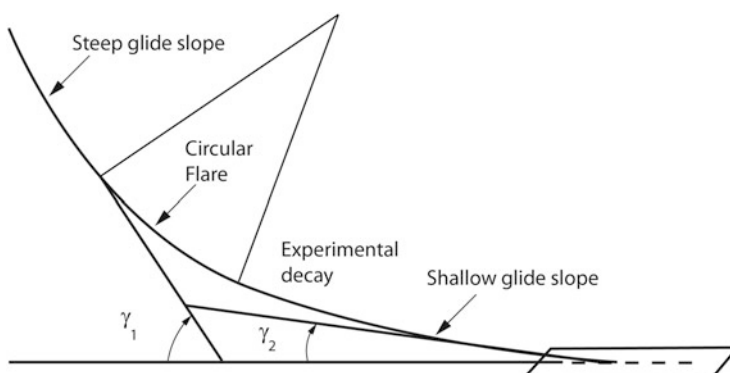


Fig. 15.41 Autolanding geometry and phases

errors with respect to reference trajectory. The speed brake deflection command is also used to reduce equivalent airspeed error. For further details, it is suggested to refer the suitable references given in this book.

Bibliography

1. Bertin, J.J., Cummings, R.M.: Critical Hypersonic Aerothermodynamics Phenomena. *Annu. Rev. Fluid Mech.*, **38** 129–157 (2006)
2. Bertin, J.J.: Hypersonic Aerothermodynamics. AIAA Educational Services, Washington, DC (1994)
3. Regan, F.J., Anandakrishnan, M.: Dynamics of Atmospheric Re-entry. AIAA Education Series, Washington, DC (1993)
4. Fletcher, D.G.: Fundamentals of Hypersonic Flow-Aerothermodynamics. Lecture Series on ‘Critical Technologies for Hypersonic Vehicle Development’, held at the Von Karman Institute, Rhode-St-Genise, Belgium, 10–14, May, 2004 and published in RTO-EN-AVT-116.
5. Hale, F.J.: Introduction to Space Flight. Prentice Hall, Englewood Cliffs (1994)
6. Scott, C.S., Ried, R.C., Maraia, R.J., Li, C.P., Derry, S.M.: An AOTV Aeroheating and Thermal Protection System Study. In: H.F. Nelson (ed.) Thermal design of Aero assisted Orbital Transfer Vehicles, Vol. 96 of Progress in Astronautics and Aeronautics, pt 198–229. AIAA, New York (1985)
7. Delta, R.W., Kamp, N.H., Riddel, F.R.: Addendum to Heat Transfer to Satellite Vehicles Reentering the Atmosphere. *Jet Propulsion* **27**(12), 1256–1257 (1957)
8. Martin, J.T.: Atmosphere Re-entry, An Introduction to Its Science and Engineering”. Prentice-Hall, Englewood Cliffs (1966)
9. Harpold, J.C., Graves, C.A.: Shuttle entry guidance. *J. Astronaut. Sci.* **27**(3), 239–268 (1979)
10. Harpold, J.C., Gavert, D.E.: Space shuttle entry guidance performance results. *J Guid. Control Dyn.* **6**(6), 442–447 (1983)
11. Sivan, K.: Generic Reentry Guidance Algorithms for Reusable Launch Vehicle Mission. Ph.D thesis, Department of Aerospace Engineering, Indian Institute of Technology, Bombay, India (December 2006).
12. Lzumi, T., Masoka, Y., Takatuka, H., Takano, J., Morito, T., Hara, Y., Ishimoto, S.: Flight control system of HOPE-X, AAS Paper No.AIAA-96-3403 (1996)
13. Naftel, C., Powel, R.W.: Guidance scheme for a Mach 3 staged gliding booster. *J. Spacecr. Rockets* **28**(5), 567–573 (1991)
14. Waigus, K.D., Dalton, C.: Approach and landing simulator for space shuttle orbiter touchdown conditions. *J. Spacecr. Rockets* **28**(8), 478–485 (1991)
15. Barton,G.H.: Autolanding trajectory design for the X-34. AIAA Paper No.AIAA-99-4161 Atmospheric Flight Mechanics Conference, Portland, OR (1999)
16. Matsumoto, S., Suzuki, H., Lzumi, T., Miyazawa, Y., Jwasaki, T.: Flight Data Analysis for the Integrated Navigation of ALFLEX (Automatic Landing Flight Experiment). AAS Paper No. AAS-97-464 (1997)
17. Hankey, W.L.: Re-Entry Aerodynamics. AIAA Education Series, Washington, DC (1988)
18. Hammond, W.E.: Space Transportation: A Systems Approach to Analysis and Design. AIAA Education Series, Washington, DC (1999)
19. Duncan, R.C.: Dynamics of Atmospheric Entry. McGraw-Hill Series, Missile and Space vehicles, McGraw-Hill, New York (1962)

Annexure A: Mathematical Modeling Aspects of Vehicle Dynamics

A.1 Propulsion Model

The detailed modeling aspects of propulsion discussed in Sect. 8.6.1 of Chap. 8 are presented here. Once the orientation of rocket motor with respect to body frame, cant angle, attachment misalignment and thrust misalignment angles are specified, the thrust and moment due to thrust along the body axes are computed as given below.

Let,

λ_{E_i} = Azimuthal location of the i^{th} motor with respect to the body frame (includes the azimuthal angle error also)

δ_{E1_i} = Attachment misalignment of i^{th} motor (normal to the core surface)

δ_{E2_i} = Attachment misalignment of i^{th} motor (tangential to the core surface)

δ_{E3_i} = Attachment misalignment of i^{th} motor (rotation about the longitudinal axis of the i^{th} motor)

Λ_{E_i} = Nozzle cant angle of i^{th} motor with respect to the longitudinal axis of the i^{th} motor (includes cant angle error also)

ϵ_{E1_i} = Nozzle misalignment of i^{th} motor (normal to the nozzle cant plane)

ϵ_{E2_i} = Nozzle misalignment of i^{th} motor (rotation about nozzle axis)

η_{E_i} = Azimuthal angle of i^{th} motor thrust with respect to the nozzle reference

ξ_{E_i} = Thrust misalignment angle of i^{th} motor with respect to the nozzle center line

η_{E_i} and ξ_{E_i} combinedly define thrust misalignment plane and thrust misalignment angle. They are defined with respect to nozzle. The sign convention for these angles is given in Figs. A.1, A.2 and A.3.

Let the location of the i^{th} motor thrust with respect to the body frame is defined as follows:

l_{t_i} = Distance of i^{th} motor thrust location with respect to the vehicle nose along longitudinal axis (Z_B – axis)

r_{t_i} = Radial distance between i^{th} motor thrust location and vehicle longitudinal axis

Fig. A.1 Orientation of ith motor with respect to the body frame

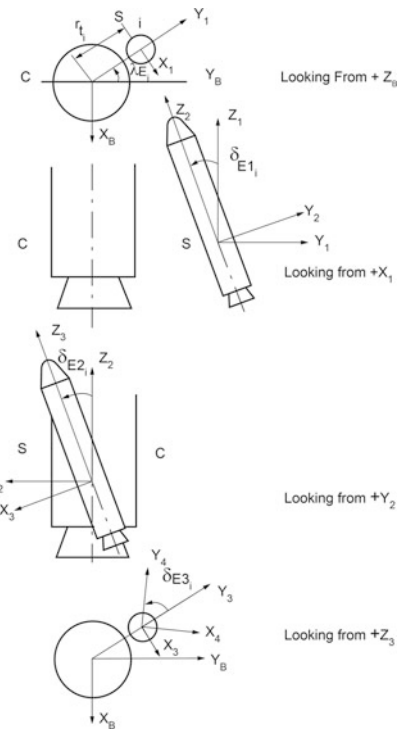


Fig. A.2 Orientation of ith motor nozzle with respect to its motor

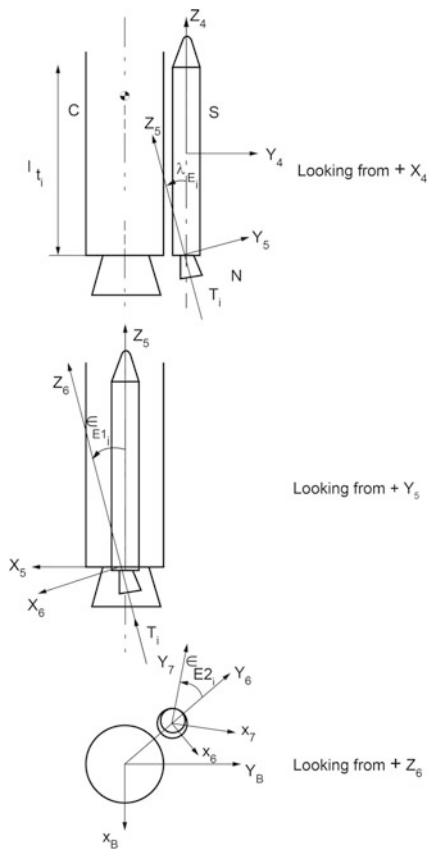
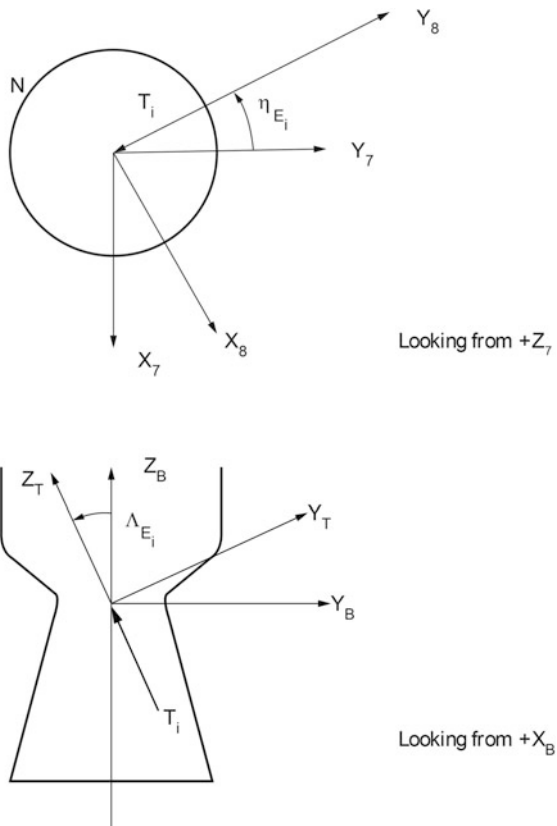


Fig. A.3 Thrust misalignment of i th motor with respect to its nozzle



NOTE:

C : CORE
S : STRAPON
N : NOZZLE

The unit vector along the thrust direction can be expressed in body frame using the transformation matrix generated from the following sequence of Euler angle rotations:

$$\lambda_{E_i} \rightarrow \delta_{E1_i} \rightarrow \delta_{E2_i} \rightarrow \delta_{E3_i} \rightarrow \Lambda_{E_i} \rightarrow \epsilon_{E1_i} \rightarrow \epsilon_{E2_i} \rightarrow \eta_{E_i} \rightarrow \xi_{E_i}$$

i.e.,

$$\begin{array}{ccc}
 X_B & Y_B & Z_B \\
 & \downarrow \lambda_{Ei} \\
 X_1 & Y_1 & Z_1 \\
 & \downarrow \delta_{E1_i} \\
 X_2 & Y_2 & Z_2 \\
 & \downarrow \delta_{E2_i} \\
 X_3 & Y_3 & Z_3 \\
 & \downarrow \delta_{E3_i} \\
 X_4 & Y_4 & Z_4 \\
 & \downarrow \Lambda_{Ei} \\
 X_5 & Y_5 & Z_5 \\
 & \downarrow \epsilon_{E1_i} \\
 X_6 & Y_6 & Z_6 \\
 & \downarrow \epsilon_{E2_i} \\
 X_7 & Y_7 & Z_7 \\
 & \downarrow \eta_{E_i} \\
 X_8 & Y_8 & Z_8 \\
 & \downarrow \xi_{E_i} \\
 X_T & Y_T & Z_T
 \end{array}$$

Hence,

$$\begin{aligned}
 \mathbf{r}_1 &= [BT_1]\mathbf{r}_B; & \mathbf{r}_2 &= [T_1 T_2]\mathbf{r}_1 \\
 \mathbf{r}_3 &= [T_2 T_3]\mathbf{r}_2; & \mathbf{r}_4 &= [T_3 T_4]\mathbf{r}_3 \\
 \mathbf{r}_5 &= [T_4 T_5]\mathbf{r}_4; & \mathbf{r}_6 &= [T_5 T_6]\mathbf{r}_5 \\
 \mathbf{r}_7 &= [T_6 T_7]\mathbf{r}_6; & \mathbf{r}_8 &= [T_7 T_8]\mathbf{r}_7 \\
 \mathbf{r}_{T_i} &= [T_8 T]\mathbf{r}_8
 \end{aligned} \tag{A.1}$$

where,

$$\begin{aligned}
 [BT_1] &= \begin{bmatrix} C_{\lambda_{E_i}} & S_{\lambda_{E_i}} & 0 \\ -S_{\lambda_{E_i}} & C_{\lambda_{E_i}} & 0 \\ 0 & 0 & 1 \end{bmatrix} \\
 [T_1 T_2] &= \begin{bmatrix} 1 & 0 & 0 \\ 0 & C_{\delta_{E1_i}} & S_{\delta_{E1_i}} \\ 0 & -S_{\delta_{E1_i}} & C_{\delta_{E1_i}} \end{bmatrix} \\
 [T_2 T_3] &= \begin{bmatrix} C_{\delta_{E2_i}} & 0 & -S_{\delta_{E2_i}} \\ 0 & 1 & 0 \\ S_{\delta_{E2_i}} & 0 & C_{\delta_{E2_i}} \end{bmatrix} \\
 [T_3 T_4] &= \begin{bmatrix} C_{\delta_{E3_i}} & S_{\delta_{E3_i}} & 0 \\ -S_{\delta_{E3_i}} & C_{\delta_{E3_i}} & 0 \\ 0 & 0 & 1 \end{bmatrix} \\
 [T_4 T_5] &= \begin{bmatrix} 1 & 0 & 0 \\ 0 & C_{\Lambda_{E_i}} & S_{\Lambda_{E_i}} \\ 0 & -S_{\Lambda_{E_i}} & C_{\Lambda_{E_i}} \end{bmatrix} \\
 [T_5 T_6] &= \begin{bmatrix} C_{\epsilon_{E1_i}} & 0 & -S_{\epsilon_{E1_i}} \\ 0 & 1 & 0 \\ S_{\epsilon_{E1_i}} & 0 & C_{\epsilon_{E1_i}} \end{bmatrix} \\
 [T_6 T_7] &= \begin{bmatrix} C_{\epsilon_{E2_i}} & S_{\epsilon_{E2_i}} & 0 \\ -S_{\epsilon_{E2_i}} & C_{\epsilon_{E2_i}} & 0 \\ 0 & 0 & 1 \end{bmatrix} \\
 [T_7 T_8] &= \begin{bmatrix} C_{\eta_{E_i}} & S_{\eta_{E_i}} & 0 \\ -S_{\eta_{E_i}} & C_{\eta_{E_i}} & 0 \\ 0 & 0 & 1 \end{bmatrix} \\
 [T_8 T] &= \begin{bmatrix} 1 & 0 & 0 \\ 0 & C_{\xi_{E_i}} & S_{\xi_{E_i}} \\ 0 & -S_{\xi_{E_i}} & C_{\xi_{E_i}} \end{bmatrix} \tag{A.2}
 \end{aligned}$$

and

r_B = A vector in body frame

r₁ = **r_B** expressed in X₁, Y₁, Z₁ frame

r₂ = **r₁** expressed in X₂, Y₂, Z₂ frame

- $\mathbf{r}_3 = \mathbf{r}_2$ expressed in X_3, Y_3, Z_3 frame
- $\mathbf{r}_4 = \mathbf{r}_3$ expressed in X_4, Y_4, Z_4 frame
- $\mathbf{r}_5 = \mathbf{r}_4$ expressed in X_5, Y_5, Z_5 frame
- $\mathbf{r}_6 = \mathbf{r}_5$ expressed in X_6, Y_6, Z_6 frame
- $\mathbf{r}_7 = \mathbf{r}_6$ expressed in X_7, Y_7, Z_7 frame
- $\mathbf{r}_8 = \mathbf{r}_7$ expressed in X_8, Y_8, Z_8 frame
- $\mathbf{r}_{T_i} = \mathbf{r}_8$ expressed in X_T, Y_T, Z_T frame

From (A.1), \mathbf{r}_B expressed in X_T, Y_T, Z_T frame is given as

$$\mathbf{r}_{T_i} = [TT_8][T_7T_8][T_6T_7][T_5T_6][T_4T_5][T_3T_4][T_2T_3][T_1T_2][BT_1]\mathbf{r}_B \quad (A.3)$$

i.e.,

$$\mathbf{r}_{T_i} = [BT]\mathbf{r}_B$$

Therefore,

$$\mathbf{r}_B = [BT]^{-1}\mathbf{r}_{T_i} \quad (A.4)$$

The unit vector along the i th motor thrust direction is expressed in $X_T Y_T Z_T$ frame as

$$\mathbf{u}_{T_i} = \begin{bmatrix} 0. \\ 0. \\ 1. \end{bmatrix}$$

\mathbf{u}_{T_i} is expressed in body frame as

$$\begin{aligned} \mathbf{u}_i &= [BT]^{-1}\mathbf{u}_{T_i} \\ \mathbf{u}_i &= \begin{bmatrix} BT_{31} \\ BT_{32} \\ BT_{33} \end{bmatrix} \end{aligned} \quad (A.5)$$

Hence, the net thrust of i th motor along the body axes is given by

$$\mathbf{F}_{TB_i} = T_i \mathbf{u}_i \quad (A.6)$$

Let,

\mathbf{r}_{TB_i} = vector representing i th motor thrust location with respect to body axes.

$$\mathbf{r}_{TB_i} = \begin{bmatrix} -r_{t_i} S_{\lambda_{E_i}} - X_{cg} \\ r_{t_i} C_{\lambda_{E_i}} - Y_{cg} \\ -(l_{t_i} - Z_{cg}) \end{bmatrix} \quad (A.7)$$

where, X_{cg} , Y_{cg} are the c.g. location with respect to body frame. Z_{cg} is longitudinal location of c.g. measured from vehicle nose and points towards base.

The moment due to thrust of the i th motor about the body axes is given by

$$\mathbf{M}_{TB_i} = \mathbf{r}_{TB_i} \times \mathbf{F}_{TB_i} \quad (A.8)$$

A.2 Aerodynamic Model

The components of the aerodynamic force and moment vectors are estimated in the body axis system. The aerodynamic force and moment coefficients C_λ , required for the computation of the force or moment are expressed in the form;

$$\begin{aligned} C_\lambda = & C_{\lambda_0} + C_{\lambda_\alpha} + C_{\lambda_\beta} \beta + C_{\lambda_{\dot{\alpha}}} \frac{\dot{\alpha} d}{2V_A} + C_{\lambda_{\dot{\beta}}} \frac{\dot{\beta} d}{2V_A} \\ & + C_{\lambda_p} \frac{pd}{2V_A} + C_{\lambda_q} \frac{qd}{2V_A} + C_{\lambda_r} \frac{rd}{2V_A} + (C_{\lambda_\delta} \delta + C_{\lambda_{\alpha\beta}} \alpha \beta) + \dots \end{aligned} \quad (A.9)$$

where

λ stands for X for the force along X_B axis

Y for the force along Y_B axis

Z for the force along Z_B axis

n for the moment about X_B axis

m for the moment about Y_B axis

l for the moment about Z_B axis

α = Angle of attack in pitch plane

β = Angle of attack in yaw plane

p, q, r = Vehicle rotational rates expressed in body frame

δ = Attachment misalignment of the strap-on motors (for definition, refer Sect. A.1)

C_{λ_α} = Represents the values of C_λ when $\alpha = \beta = 0$.

$$C_{\lambda_\alpha} \equiv \frac{\partial C_\lambda}{\partial \alpha}$$

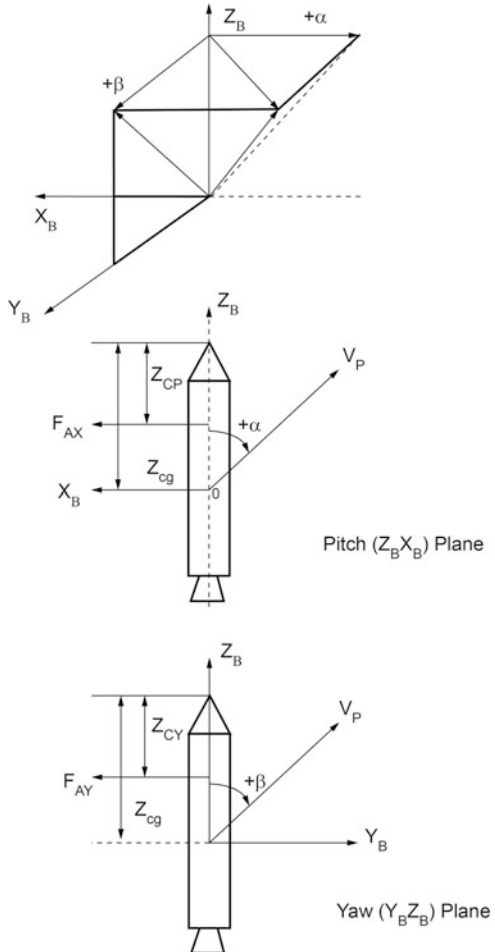
etc.

$$C_{\lambda_{\dot{\alpha}}} \equiv \frac{\partial C_\lambda}{\partial \left(\frac{\dot{\alpha} d}{2V_A} \right)}$$

etc.

The angles of attack in pitch plane and in yaw plane as defined in Fig. A.4 are computed as follows:

Fig. A.4 Definition for Aerodynamic angle of attack



The atmospheric relative velocity of the vehicle with respect to ECI frame, \mathbf{V}_{AI} is expressed in body frame as

$$\mathbf{V}_{AB} = \begin{bmatrix} u_A \\ v_A \\ w_A \end{bmatrix} = [\mathbf{IB}] \mathbf{V}_{AI} \quad (\text{A.10})$$

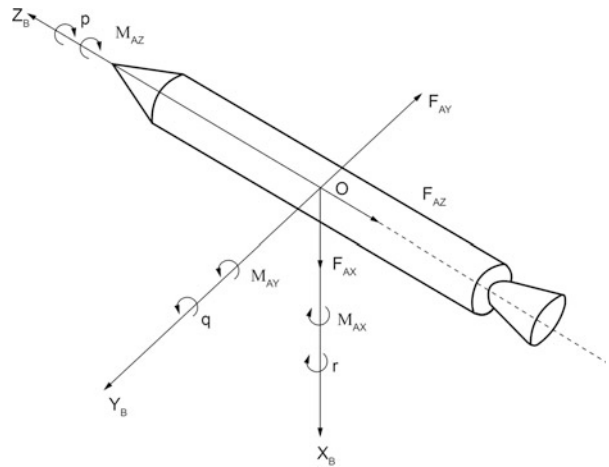
Then, the pitch angle of attack is given as

$$\alpha = \tan^{-1}(-u_A/w_A) \quad (\text{A.11})$$

and the yaw angle of attack is given as

$$\beta = \tan^{-1}(v_A/w_A) \quad (\text{A.12})$$

Fig. A.5 Aerodynamic force and moment



and the total angle of attack is

$$\alpha_T = \cos^{-1}(w_A/V_A) \quad (\text{A.13})$$

Using the general form of aerodynamic coefficients given by the Eq. (A.9), any order of aerodynamic model (simple or complex, including nonlinear and cross coupling term) may be incorporated depending on the requirements. Of the coefficients appearing in the general expression for C_λ , many vanish for the axi-symmetry of vehicle. Also, for large launch vehicles having little or no lifting surfaces, the damping derivatives are negligible.

By considering the sign convention for the body axes, body rates and the angles of attack, the aerodynamic force and moment coefficients as defined in Fig. A.5 is given below.

$$C_X = -C_{X_0} - C_{X_\alpha} \alpha - C_{X_\dot{\alpha}} \frac{\dot{\alpha}d}{2V_A} + C_{X_q} \frac{qd}{2V_A} \quad (\text{A.14})$$

$$C_Y = C_{Y_\beta} \beta + C_{Y_{\dot{\beta}}} \frac{\dot{\beta}d}{2V_A} + C_{Y_p} \frac{pd}{2V_A} - C_{Y_r} \frac{rd}{2V_A} \quad (\text{A.15})$$

$$C_Z = -C_{Z_0} - C_{Z_\alpha} \alpha - C_{Z_\dot{\alpha}} \frac{\dot{\alpha}d}{2V_A} + C_{Z_q} \frac{qd}{2V_A} \quad (\text{A.16})$$

$$C_n = -C_{n_\beta} \beta - C_{n_{\dot{\beta}}} \frac{\dot{\beta}d}{2V_A} - C_{n_p} \frac{pd}{2V_A} + C_{n_r} \frac{rd}{2V_A} \quad (\text{A.17})$$

$$C_m = -C_{m_0} - C_{m_\alpha} \alpha - C_{m_\dot{\alpha}} \frac{\dot{\alpha}d}{2V_A} + C_{m_q} \frac{qd}{2V_A} \quad (\text{A.18})$$

$$C_l = C_{l_\beta} \beta + C_{l_{\dot{\beta}}} \frac{\dot{\beta}d}{2V_A} + C_{l_p} \frac{pd}{2V_A} - C_{l_r} \frac{rd}{2V_A} - C_{l_\delta} \delta + C_{l_{\alpha\beta}} \alpha \beta \quad (\text{A.19})$$

Also, C_{m_α} and C_{n_β} can be computed as

$$C_{m_\alpha} = C_{Z_\alpha} \frac{(Z_{cg} - Z_{cp})}{d} \quad (A.20)$$

$$C_{n_\beta} = C_{Y_\beta} \frac{(Z_{cg} - Z_{cy})}{d} \quad (A.21)$$

where,

Z_{cp} = Center of pressure location in pitch plane on the longitudinal axis from vehicle nose

Z_{cy} = Center of pressure location in yaw plane on the longitudinal axis from vehicle nose (Fig. A.4)

The total aerodynamic force along the vehicle body axes (Fig. A.5) is given by

$$\mathbf{F}_{AB} = \begin{bmatrix} F_{AX} \\ F_{AY} \\ F_{AZ} \end{bmatrix} = QS \begin{bmatrix} C_X \\ C_Y \\ C_Z \end{bmatrix} \quad (A.22)$$

and the aerodynamic moment about the body axes is given by

$$\mathbf{M}_{AB} = \begin{bmatrix} M_{AX} \\ M_{AY} \\ M_{AZ} \end{bmatrix} = QSD \begin{bmatrix} C_n \\ C_m \\ C_l \end{bmatrix} \quad (A.23)$$

Where, the dynamic pressure Q is given by

$$Q = \frac{1}{2} \rho V_A^2 \quad (A.24)$$

S = Reference area

ρ = Atmospheric density

V_A = Atmospheric relative velocity

A.3 Jet Damping Model

For computing jet damping forces and moments, the nozzle axis of each motor is assumed to be parallel to the longitudinal axis of the vehicle (parallel to Z_B axis.)

Let,

l_{ei} = Distance of i th motor nozzle exit from vehicle nose (along the longitudinal axis)

r_{ei} = Radial distance between i th motor nozzle exit and vehicle longitudinal axis

Location of i th motor nozzle exit with respect to body frame, \mathbf{r}_{EBi} is given by

$$\mathbf{r}_{EB_i} = \begin{bmatrix} -r_{ei} S_{\Lambda_{E_i}} - X_{cg} \\ r_{ei} C_{\Lambda_{E_i}} - Y_{cg} \\ -(l_{ei} - Z_{cg}) \end{bmatrix} \quad (A.25)$$

Let

\dot{m}_i = Mass flow rate of i th motor

ω = Vehicle rotational velocity vector expressed in body frame

The jet damping force of i th motor along the body axes is

$$\mathbf{F}_{JB_i} = -\dot{m}_i \boldsymbol{\omega} \times \mathbf{r}_{EB_i} \quad (A.26)$$

The moment due to jet damping force of i th motor along bout the body axes is given by

$$\mathbf{M}_{JB_i} = \mathbf{r}_{EB_i} \times \mathbf{F}_{JB_i} \quad (A.27)$$

A.4 Slosh Model

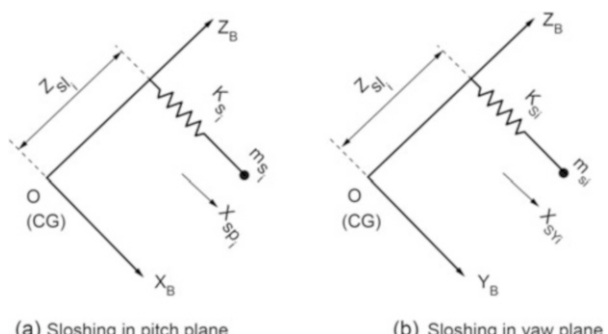
In this model, spring mass analogy has been used for simulating the liquid propellant sloshing in the tanks. Separate model is needed for pitch and yaw plane. Slosh masses in each tank are to be considered, and for each slosh mass sloshing in pitch and yaw planes are to be modeled separately. The forcing functions model for the slosh dynamics is the lateral acceleration at the slosh location, which comprises of translational and rotational acceleration. Since the lateral acceleration includes all the contributing factors including slosh effects, the system is totally coupled.

Spring mass analogy in pitch and yaw planes of i th slosh mass is given in Fig. A.6. The slosh related data for i th slosh mass are given as

m_{s_i} = i th slosh mass

\bar{f}_{s_i} = Frequency parameter for the i th slosh mass normalized with respect to longitudinal acceleration

Fig. A.6 Sloshing in pitch and yaw planes



$\begin{Bmatrix} X_{s_i} \\ Y_{s_i} \\ Z_{s_i} \end{Bmatrix}$ = Location of the ith slosh mass with respect to body reference frame

ζ_{sb_i} = Viscous damping for ith slosh mass

ζ_{svrt_i} = Vertical baffle damping for ith slosh mass

ζ_{sb_i} = Ring baffle damping for ith slosh mass, for unit pendulum angle (depends on the free surface motion)

Vehicle related data are given as

$\begin{Bmatrix} X_{cg} \\ Y_{cg} \\ Z_{cg} \end{Bmatrix}$ = Vehicle c.g. location of the with respect to body reference frame

$\boldsymbol{\omega} = \begin{bmatrix} r \\ q \\ p \end{bmatrix}$ = Vehicle body rate (yaw, pitch, roll) with respect to body frame

$\dot{\boldsymbol{\omega}} = \begin{bmatrix} \dot{r} \\ \dot{q} \\ \dot{p} \end{bmatrix}$ = Vehicle angular acceleration (yaw, pitch, roll)

Some derived parameters are given as

L_{s_i} = Equivalent slosh pendulum length

m_s = Total slosh mass

$$L_{s_i} = 1/\left(\bar{f}_{s_i}^2\right) \quad (\text{A.28})$$

$$m_s = \sum_{i=1}^{n_m} m_{s_i} \quad (\text{A.29})$$

where n_m is number of slosh masses.

The ith slosh mass location with respect to body frame is

$$X_{sl_i} = X_{s_i} - X_{cg} \quad (\text{A.30})$$

$$Y_{sl_i} = Y_{s_i} - Y_{cg} \quad (\text{A.31})$$

$$Z_{sl_i} = Z_{cg} - Z_{s_i} \quad (\text{A.32})$$

The lateral acceleration at the ith slosh mass location is given by

$$\mathbf{a}_{s_i} = \mathbf{a} + \dot{\boldsymbol{\omega}} \times \mathbf{r}_{s_i} + \boldsymbol{\omega} \times (\boldsymbol{\omega} \times \mathbf{r}_{s_i}) \quad (\text{A.33})$$

where

$\mathbf{a}_{s_i} = \begin{bmatrix} a_{xs_i} \\ a_{ys_i} \\ a_{zs_i} \end{bmatrix}$ = Acceleration at ith slosh mass location in body frame

$$\mathbf{a} = \begin{bmatrix} a_x \\ a_y \\ a_z \end{bmatrix} = \text{Acceleration of vehicle c.g. in body frame}$$

$$\mathbf{r}_{s_i} = \begin{bmatrix} X_{sl_i} \\ Y_{sl_i} \\ Z_{sl_i} \end{bmatrix} = \text{Slosh mass location}$$

From the Eq. A.33, the longitudinal component of acceleration can be derived as

$$a_{zs_i} = a_z + (\dot{r}Y_{sl_i} - \dot{q}X_{sl_i}) + p(rX_{sl_i} + qY_{sl_i}) - (r^2 + q^2)Z_{sl_i} \quad (\text{A.34})$$

Hence, the i th slosh mode undamped natural frequency can be expressed as

$$\omega_{s_i} = 2\pi\bar{f}_{s_i}\sqrt{a_{zs_i}} \quad (\text{A.35})$$

Let X_{sp_i} and X_{sy_i} are i th slosh mass movement in pitch and yaw planes respectively (the positive movements are given in Fig. A.6).

Then equivalent slosh pendulum angles in pitch and yaw planes are given as

$$\Gamma_{p_i} = \tan^{-1} \frac{X_{sp_i}}{L_{s_i}} \quad (\text{A.36})$$

$$\Gamma_{y_i} = \tan^{-1} \frac{Y_{sp_i}}{L_{s_i}} \quad (\text{A.37})$$

The slosh damping in pitch and yaw planes for i th slosh mass is given below:

$$\zeta_{sp_i} = \zeta_{svsi_i} + \zeta_{sverti_i} + \zeta_{bi} \sqrt{\Gamma_{p_i}} \quad (\text{A.38})$$

$$\zeta_{sy_i} = \zeta_{svsi_i} + \zeta_{sverti_i} + \zeta_{bi} \sqrt{\Gamma_{y_i}} \quad (\text{A.39})$$

The dynamics of i th slosh mass in pitch and yaw planes are given by

$$\ddot{X}_{sp_i} + 2\zeta_{sp_i}\omega_s \dot{X}_{sp_i} + \omega_{s_i}^2 X_{sp_i} = -a_{xs_i} \quad (\text{A.40})$$

$$\ddot{X}_{sy_i} + 2\zeta_{sy_i}\omega_s \dot{X}_{sy_i} + \omega_{s_i}^2 X_{sy_i} = -a_{ys_i} \quad (\text{A.41})$$

The forcing function in pitch and yaw plane are derived from the Eq. (A.33) as given below:

$$a_{xs_i} = a_x + (\dot{q}Z_{sl_i} - \dot{p}Y_{sl_i}) + [q(rY_{sl_i} - qX_{sl_i}) - (pX_{sl_i} - rX_{sl_i})] \quad (\text{A.42})$$

$$a_{ys_i} = a_y + (\dot{p}X_{sl_i} - \dot{r}Z_{sl_i}) + [p(qZ_{sl_i} - pY_{sl_i}) - r(rY_{sl_i} - qX_{sl_i})] \quad (\text{A.43})$$

The forces and moments due to i th slosh mass in body coordinate system are given by

$$F_{SX_i} = K_{si} X_{sp_i} \quad (A.44)$$

$$F_{SY_i} = K_{si} X_{sy_i} \quad (A.45)$$

$$F_{SZ_i} = 0 \quad (A.46)$$

$$M_{SX_i} = -(K_{si} Z_{sl_i} + C_{si}) X_{sy_i} \quad (A.47)$$

$$M_{SY_i} = (K_{si} Z_{sl_i} + C_{si}) X_{sp_i} \quad (A.48)$$

$$M_{SZ_i} = K_{si} X_{sy_i} X_{sl_i} - K_{si} X_{sp_i} Y_{sl_i} \quad (A.49)$$

where

K_{si} = Spring constant for i th slosh mass

C_{si} = Moment coefficient for i th slosh mass and these are given by the following expressions

$$K_{si} = \omega_{si}^2 m_{si} \quad (A.50)$$

$$C_{si} = K_{si} L_{si} \quad (A.51)$$

A.5 Mass Properties

1. Mass

Mass of the vehicle at any instant of flight is always computed from the remaining propellant mass and the remaining non-propulsive mass and mass of stage motors, heat shield, satellite, etc. as per the details given below:

n_s = Number of stages

n_{mi} = Number of motors of the i th stage

m_{sat} = Satellite mass

m_{hs} = Heat shield mass

m_{pj} = Propellant mass of j th motor of i th stage

m_{sij} = Structural mass of j th motor of i th stage

m_{cij} = Consumable mass of j th motor of i th stage

m_{ei} = Consumable mass of i th stage

The remaining propellant mass, consumed propellant mass, etc. of the motors of the burning stage areas given below:

m_{rpj} = Remaining propellant mass of j th motor

m_{cpj} = Consumed propellant of j th motor

m_{rcj} = Remaining portion of consumable mass of j th motor

m_{ccj} = Consumed portion of the consumable mass of j th motor

m_r = Remaining portion of the consumable mass of the stage

m_c = Remaining portion of the consumable mass of the stage

Let i th stage be the operating stage. Then the mass of the upper stage is computed as:

$$m_{us} = m_{sat} + \sum_{l=i+1}^{n_s} \left\{ \sum_{j=1}^{n_{mj}} (m_{pj} + m_{sj} + m_{cj}) + m_{el} \right\} \quad (A.52)$$

The mass of the vehicle during the burning of i th stage is given as:

$$m = m_{us} + \sum_{j=1}^{n_{mj}} (m_{rpj} + m_{rcj}) + m_r + \sum_{j=1}^{n_{mj}} (m_{sj}) + m_{hs} \quad (A.53)$$

The Eq. (A.53) is the general expression for the computation of mass. However, after the separation of the stage motors and heat shield, the Eq. (A.53) may have to be suitably modified. The remaining propellant mass, consumed propellant mass and mass flow rate of a stage are computed in different ways as given below:

(i) *Propellant Consumption History*

(a) *Input is consumed propellant mass history*

In this option, propellant consumption history of each motor is given as an input table. The propellant mass consumed by the j th motor at any instant, m_{cpj} , is calculated by table interpolation.

The remaining propellant mass of j th motor is given as

$$m_{rpj} = m_{pj} - m_{cpj} \quad (A.54)$$

The mass flow rate of j th motor is given as

$$\dot{m}_j = \left[(m_{rpj})_0 - (m_{rpj})_1 \right] / \Delta t \quad (A.55)$$

where $(m_{rpj})_0$ and $(m_{rpj})_1$ are the remaining propellant mass at the beginning and end of the cycle time Δt .

(b) *Input is remaining propellant mass*

In this case, remaining propellant mass history of each motor is to be given as an input table. The remaining propellant mass of j th motor at any instant, m_{cpj} , is calculated by table interpolation. The consumed propellant mass of j th motor is calculated as

$$m_{cpj} = m_{pj} - m_{rpj} \quad (A.56)$$

and the mass flow rate is calculated using the Eq. (A.55).

(c) *Input is the propellant flow rate*

In this option, propellant mass flow rate history of each motor is also given as an input table. The flow rate of jth motor \dot{m}_j at any instant is computed from the input table. The remaining propellant mass of the jth motor is calculated as

$$m_{rp_j} = (m_{rp_j})_0 - \dot{m}_j * \Delta t \quad (\text{A.57})$$

where

$(m_{rp_j})_0$ is the previous cycle remaining propellant mass of jth motor.

The consumed propellant mass of jth motor is calculated using the Eq. (A.56).

(d) *Propellant flow rate from vacuum thrust and specific impulse*

In this case, propellant flow rate of jth motor at any instant is computed as below

$$\dot{m}_1 = T_{v_j} / I_{sp_j} \quad (\text{A.58})$$

Let \dot{m}_0 be the value of \dot{m}_1 , at the previous cycle, then the flow rate of jth motor is given as

$$\dot{m}_j = (\dot{m}_0 + \dot{m}_1)/2 \quad (\text{A.59})$$

The computations for m_{rp_j} and m_{cp_j} are same as given in the previous section.

(ii) *Non-propulsive Mass Consumption Model*

(a) *Remaining part of consumable mass of motors*

This option is useful to simulate the consumable mass history of non-propulsive elements of the motors apart from the propellant consumption. Consumable mass history of each motor is to be given as an input table. The consumed part of the consumable mass of the jth motor at any instant m_{cc_j} is calculated by interpolation. The remaining part of consumable mass of jth motor is given by

$$\dot{m}_{rc_j} = m_{c_{ij}} - m_{cc_j} \quad (\text{A.60})$$

The mass flow rate of jth motor consumable mass is given by

$$\dot{m}_{c_j} = [(m_{rc_j})_0 - (m_{rc_j})_1]/\Delta t \quad (\text{A.61})$$

where $(m_{rc_j})_0$ and $(m_{rc_j})_1$ are the remaining part of consumable mass at the beginning and end of cycle time Δt .

(b) *Remaining part of consumable mass of the stage*

This option is useful to simulate the consumable mass history of the complete stage. For example, the secondary injection thrust vector control (SITVC) system fluid consumption can be simulated by this option. The consumption can be computed either from the input table or from the SITVC flow rate computed as part of subsystem dynamics. In case, the consumable mass history is given as an input table, the consumed part of the consumed mass of the stage at any instant, m_c , is calculated by interpolation. The remaining consumable mass of the stage is computed as

$$m_r = m_{e_i} - m_c \quad (\text{A.62})$$

The flow rate of the consumable mass of the stage is given as

$$\dot{m}_{e_i} = [(m_r)_0 - (m_r)_1] / \Delta t \quad (\text{A.63})$$

where $(m_r)_0$ and $(m_r)_1$ are the remaining consumable mass at the beginning and end of cycle time Δt .

2. Center of Gravity

The location of the center of gravity of the vehicle is given with respect to the body reference frame as shown in Fig. A.7.

X_{cg} = Center of gravity location along X_{BR} direction (Along positive yaw axis)

Y_{cg} = Center of gravity location along Y_{BR} direction (Along positive pitch axis)

Z_{cg} = Center of gravity location along Z_{BR} direction (Along longitudinal axis from nose)

The center of gravity location can be computed by the methods given below:

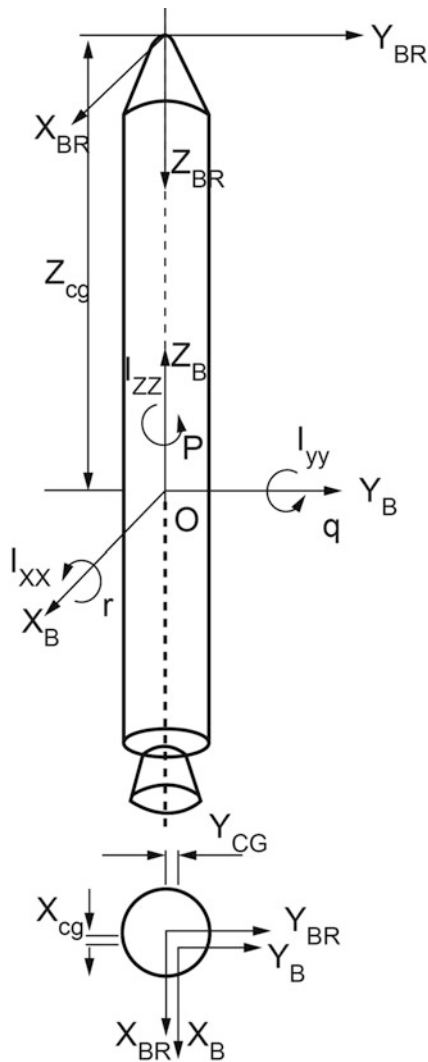
- (i) X_{cg} , Y_{cg} , Z_{cg} values computed by interpolation from the input tables. In order to get realistic modeling, the input may be given as functions of remaining propellant mass in each tank.
- (ii) Alternatively, vehicle c.g. location computed from the c. g. locations of the components (structural mass, propellant mass, heat shield, payload etc.).

3. Moments and Products of Inertia

The moments and products of inertia about the body axes (B-frame) are defined as integrals.

$$I_{XX} = \int (y^2 + z^2) dm; I_{XY} = \int xy dm$$

Fig. A.7 C.G and MI in body axis



$$I_{YY} = \int (x^2 + z^2) dm; I_{YZ} = \int yz dm$$

$$I_{ZZ} = \int (x^2 + y^2) dm; I_{ZX} = \int zx dm$$

where $[x \ y \ z]^T$ is location of the mass dm with respect to body frame.

The inertia matrix is given as

$$[\dot{I}] = \begin{bmatrix} I_{XX} & -I_{XY} & -I_{ZX} \\ -I_{XY} & I_{YY} & -I_{YZ} \\ -I_{ZX} & -I_{YZ} & I_{ZZ} \end{bmatrix} \quad (\text{A.64})$$

The rate of change of the inertia matrix is given as

$$[\ddot{I}] = [\dot{I}_{XX} - \dot{I}_{XY} - \dot{I}_{ZX} - \dot{I}_{XY}\dot{I}_{YY} - \dot{I}_{YZ} - \dot{I}_{ZX} - \dot{I}_{YZ}\dot{I}_{ZZ}] \quad (\text{A.65})$$

where

$$\begin{aligned} \dot{I}_{XX} &= [I_{XX_0} - I_{XX}] / \Delta t \\ \dot{I}_{YY} &= [I_{YY_0} - I_{YY}] / \Delta t \\ \dot{I}_{ZZ} &= [I_{ZZ_0} - I_{ZZ}] / \Delta t \\ \dot{I}_{XY} &= [I_{XY_0} - I_{XY}] / \Delta t \\ \dot{I}_{YZ} &= [I_{YZ_0} - I_{YZ}] / \Delta t \\ \dot{I}_{ZX} &= [I_{ZX_0} - I_{ZX}] / \Delta t \end{aligned} \quad (\text{A.66})$$

I_{XX_0} , I_{YY_0} , I_{ZZ_0} , I_{XY_0} , I_{YZ_0} , I_{ZX_0} are the moments and products of inertia at the previous cycle of integration.

In general, for launch vehicles, the products of inertia are small compared to the moments of inertia. Assuming I_{XY} , I_{YZ} , I_{ZX} are very small compared to I_{XX} , I_{YY} , I_{ZZ} , then the inverse of inertia matrix is computed as

$$[I]^{-1} = \frac{1}{\Delta} \begin{bmatrix} I_{YY}I_{ZZ} & -I_{XY}I_{ZZ} & -I_{ZX}I_{YY} \\ -I_{XY}I_{ZZ} & I_{XX}I_{ZZ} & -I_{YZ}I_{XX} \\ -I_{ZX}I_{YY} & -I_{YZ}I_{XX} & I_{XX}I_{YY} \end{bmatrix} \quad (\text{A.67})$$

where

$$\Delta = I_{XX}I_{YY}I_{ZZ} - (I_{XX}I_{YZ}^2 + I_{YY}I_{ZX}^2 + I_{ZZ}I_{XY}^2) \quad (\text{A.68})$$

If the body axes are assumed to be the principal axes of inertia, then $I_{XY} = I_{YZ} = I_{ZX} = 0$. In this case,

$$[I] = \begin{bmatrix} I_{XX} & 0 & 0 \\ 0 & I_{YY} & 0 \\ 0 & 0 & I_{ZZ} \end{bmatrix} \quad (\text{A.69})$$

$$[\dot{I}] = [\dot{I}_{XX} \ 0 \ 0 \ \dot{I}_{YY} \ 0 \ 0 \ \dot{I}_{ZZ}] \quad (\text{A.70})$$

and

$$[I]^{-1} = \begin{bmatrix} 1/I_{XX} & 0 & 0 \\ 0 & 1/I_{YY} & 0 \\ 0 & 0 & 1/I_{ZZ} \end{bmatrix} \quad (\text{A.71})$$

The moments and products of inertia can be computed in two ways.

1. $I_{XX}, I_{YY}, I_{ZZ}, I_{XY}, I_{YZ}, I_{ZX}$ values are computed from input tables by interpolation. In order to get the realistic variations of these parameters, the input table may be given as function of remaining propellant mass in each motor.
2. Alternatively, the moments and products of inertia of the complete vehicle can be computed from the moments and products of inertia of the components (structural mass, propellant mass, ullage, heat shield, satellite, etc.).

A.6 Control Power Plant Model

Based on the control commands, the control system hardware generates the required control forces. Two typical systems are explained.

1. Secondary Injection Thrust Vector Control (SITVC)

In this system, injectant fluid is stored in separate tank at high pressure. As per the requirement, these fluids are injected at the appropriate location in the nozzle. The fluids are vaporized and form a normal shock in the exhaust flow of the nozzle. This normal shock deflects the exhaust flow through nozzle which in turn generates a side force and this side force is used to control the vehicle. Typical system is given in Fig. A.8.

The side force varies based on the quantity of fluid injected into the nozzle depending on the valve opening, which is controlled by the pintle movement. Typical modeling of this system is given in Fig. A.9.

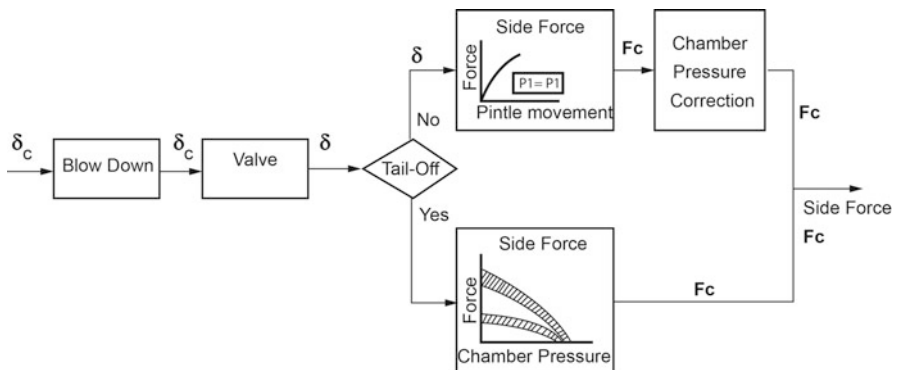
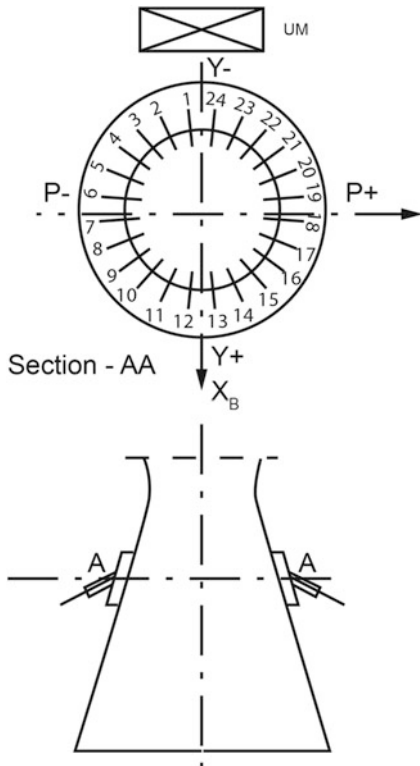
The force generated by this system is given by

$$\mathbf{F}_{CB} = \begin{bmatrix} F_{PC} \\ F_{YC} \\ 0 \end{bmatrix} \quad (\text{A.72})$$

and the location of the control force with respect to the body frame is given as

$$\mathbf{r}_c = \begin{bmatrix} x_c - X_{cg} \\ y_c - Y_{cg} \\ Z_{cg} - z_c \end{bmatrix} \quad (\text{A.73})$$

Hence, the control moment generated is given as

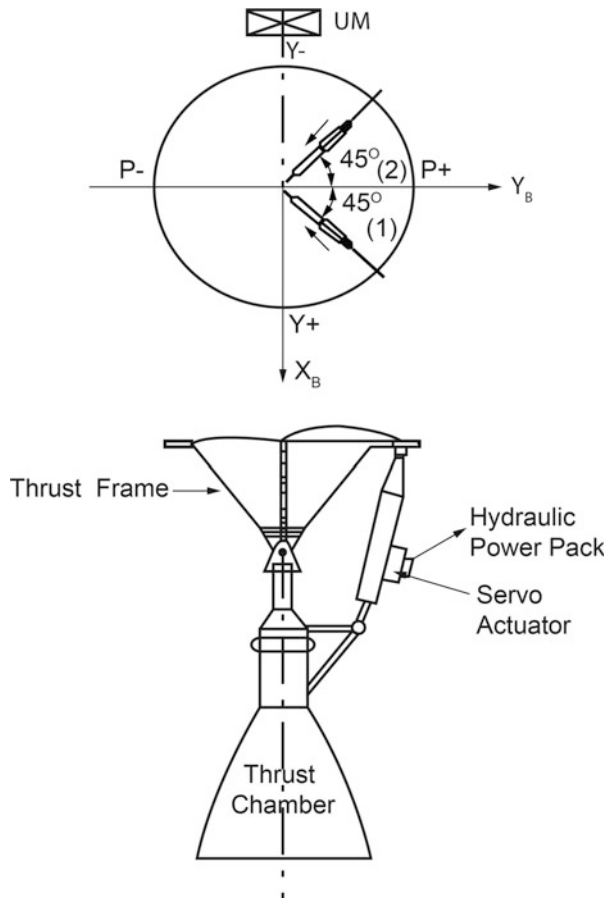
Fig. A.8 SITVC system**Fig. A.9** Typical modeling of SITVC system

$$\mathbf{M}_{CB} = \mathbf{r}_c \times \mathbf{F}_{CB} \quad (\text{A.74})$$

2. Engine Gimbal Control System

In this system, control command is issued to gimbal the total engine system and the deflected engine configuration is represented in Fig. A.10.

Fig. A.10 Engine gimbal control system



If the thrust of engine is T then the side force generated is given as

$$\mathbf{F}_{CB} = \begin{bmatrix} -T \sin \delta p \\ T \sin \delta y \\ 0 \end{bmatrix} \quad (\text{A.75})$$

where $\delta p, \delta y$ are the output of control power plant dynamics. The control moment generated is given by the Eq. (A.74).

Another important factor to be simulated is the engine inertia. When the engine is moving, its inertia along with lateral acceleration produces lateral force. The lateral acceleration acting on the engine is from vehicle lateral translational acceleration and lateral acceleration due to rotational acceleration of the vehicle along with the rotational acceleration of the engine about its gimbal point. The side force depends on thrust. During ignition and tail-off transients, for the same amount of engine deflection, the available control force reduces whereas the force coming

from inertia term remains same. At a particular level, inertia force becomes more than control and acts as disturbance. This phenomenon is called “Tail-wag-dog” (TWD) effect, which is of importance for engine gimbal control system, when the thrust levels are less. To simulate the vehicle response under this condition, the engine inertia contribution has to be simulated accordingly.

The engine inertia force is given by

$$\mathbf{F}_{EB} = \begin{bmatrix} -m_r \{ a_x - (l_r + l_c) \ddot{\theta} + l_r \ddot{\delta}_p \} \\ -m_r \{ a_y + (l_r + l_c) \ddot{\Psi} - l_r \ddot{\delta}_y \} \\ 0 \end{bmatrix} \quad (A.76)$$

The engine inertia moment is given by

$$\mathbf{M}_{EB} = \begin{bmatrix} l_r \ddot{\delta}_y - (I_r + m_r l_r l_c) \ddot{\Psi} - m_r l_r a_y \\ l_r \ddot{\delta}_p - (I_r + m_r l_r l_c) \ddot{\theta} + m_r l_r a_x \\ 0 \end{bmatrix} \quad (A.77)$$

where m_r is mass of the engine; l_r , distance from engine c.g. to gimbal point; l_c is the distance between gimbal point and vehicle c.g.; a_x , a_y are lateral acceleration at the vehicle c.g.; $\ddot{\theta}$, $\ddot{\Psi}$ are rotational acceleration; $\ddot{\delta}_p$, $\ddot{\delta}_y$ are the engine rotational acceleration.

Annexure B: Inertial Sensors

Chapter 14 discusses in detail the functional requirements, integrated design aspects using systems engineering approach and details of navigation system design. The inertial navigation system makes use of the property of inertial sensors mounted onboard the vehicle to carry out the navigation function. The measurements in this system are using gyros and accelerometers. While a gyroscope measures angular rates, the accelerometer measures the specific force and both the measurements are without any external references. Different types of gyros and accelerometers sensors used in launch vehicle navigation system are explained in the following sections.

B.1 Gyroscopes

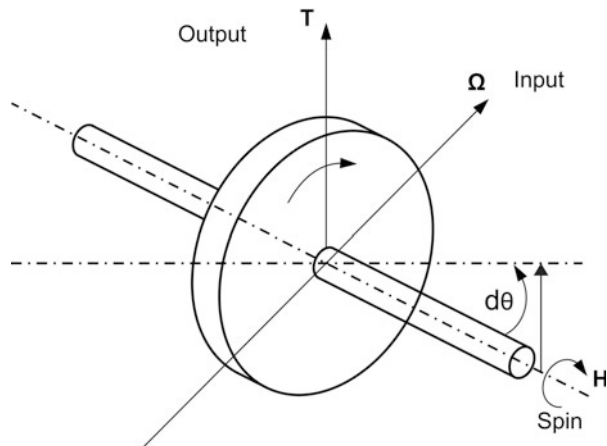
The spinning mass gyroscope basically consists of a spinning wheel with inertia J . The wheel spinning at an angular rate of ω produces high angular momentum. Because of the higher angular momentum generated by the spinning inertia it increases its resistance to external disturbance torques. Due to this, the gyro tends to retain its spin axis orientation fixed in inertial space. The angular momentum of the wheel is $\mathbf{H} = \mathbf{j}\omega$. The gyroscopic principle of a spinning body is given in Fig. B.1.

If a torque \mathbf{T} is applied along an axis which is perpendicular to spin axis, the spin axis precess about an axis which is perpendicular to both spin and torque axes. If the angle of precession is taken as $d\theta$ then change in angular momentum can be given as

$$d\mathbf{H} = \mathbf{H}d\theta \quad (\text{B.1})$$

As per Newton's law, the rate of change of angular momentum is

Fig. B.1 Gyroscopic principles of spinning body



$$\mathbf{T} = \frac{d\mathbf{H}}{dt} = \mathbf{H} \frac{d\theta}{dt} \quad (\text{B.2})$$

Assume Ω is the precession rate of spin axis, $(d\theta/dt) = \Omega$, then

$$\mathbf{T} = \boldsymbol{\Omega} \times \mathbf{H} \quad (\text{B.3})$$

From this equation, it is clear that in a gyro in which a spinning wheel with angular momentum \mathbf{H} experiences an external angular rate $\boldsymbol{\Omega}$ (input axis), it produces a torque \mathbf{T} (output axis) perpendicular to both spin and input axis. This torque is known as gyroscopic torque and is proportional to angular rate $\boldsymbol{\Omega}$ on the instrument. \mathbf{H} is a known constant. Therefore, measurement of the torque by suitable system gives the angular rate acting on gyros (in turn vehicle). This principle is used in gyros to measure the angular rate of the vehicle.

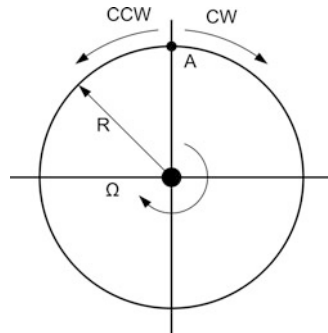
B.2 Different Types of Gyros

Rate gyro, rate integrating gyro, dry tuned gyro and free gyro functions are based on spinning rotor concept. The working principle and construction details of these gyros are beyond the scope of this book. The working principle of ring laser gyro and vibrating gyro are briefly given below.

1. Ring Laser Gyro

Ring laser gyro (RLG) which works on the principle of sagnac effect has been under development since 1960s. Since it has no moving parts, RLG is expected to have better reliability than that of spinning wheel gyros. The simple representation of classic Sagnac effect gyro is given in Fig. B.2.

Fig. B.2 Simple representation of classic Sagnac effect gyro



In a devise with a closed circular path as shown in Fig. B.2, if two oppositely directed beams enter at A in inertial space, they travel in opposite directions and take same time to reach 'A' in the absence of angular rate Ω . However if the devise is subjected to angular rate Ω in clockwise direction then the travel time for clockwise (cw) and counter clockwise (ccw) beams are different. The beam in cw takes longer time compared to that of ccw. Thus the angular rate on the devise causes the path difference between oppositely directed beams. This effect is termed as Sagnac effect. Since the velocity of light, c is constant, the transit time for the light travelling in two opposite directions can be given as:

Transit time of cw beam is

$$t_+ = \frac{2\pi r}{(c - R\Omega)} \quad (\text{B.4})$$

And that of ccw beam is

$$t_- = \frac{2\pi r}{(c + R\Omega)} \quad (\text{B.5})$$

This shows that there is path length difference, ΔL between cw, ccw beams due to the rotation of the device. The difference in transit time can be approximated as

$$\Delta t = \frac{4\pi R^2}{c^2} \Omega = \frac{4A}{c^2} \Omega \quad (\text{B.6})$$

where

$A = \text{Enclosed area traversed by beams} = \pi R^2$

$c = \text{Velocity of light}$

$\Omega = \text{Input angular rate}$

From the above, it can be seen that the measurement of Δt by suitable system provides the input rate (vehicle rate) as given below:

The path length difference ΔL is given as

$$\Delta L = c\Delta t = \frac{4A\Omega}{c} \quad (\text{B.7})$$

In laser gyro, the closed optical cavity consists of an integral number of wavelengths around the path length L . The closed path is used as a resonator (feedback path) for a self-tunable optical oscillator. When the cavity is of a ring laser oscillator configuration, the two oppositely directed waves have different frequencies. Clockwise travelling wave be of lower frequency f_2 with respect to nominal frequency f and the counter propagating wave have higher frequency f_1 . They interfere and form a standing wave of frequency, $\Delta f = f_1 - f_2$. Therefore,

$$\frac{\Delta L}{L} = \frac{\Delta f}{f} \quad (\text{B.8})$$

where

$L = m\lambda$; corresponds to normal frequency, f

L = total length of closed path

λ = beam wavelength

m = integer

Combining (B.7) with (B.8) one gets the fundamental RLG equation.

$$\Delta f = \frac{4A\Omega}{\lambda L} \quad (\text{B.9})$$

This frequency difference gives the measure of the angular rate of devise (vehicle). For further technical details of RLG, reader may go through appropriate references listed in the end.

2. Vibratory Gyros

The vibratory gyro's development started in 1980s. All MEMs gyros are based on vibratory principle. The basic principle of operation of a vibratory structure gyroscope is an understanding of the coriolis force. Vibrating cylinder and hemispherical resonating gyroscopes have the potential to use as inertial grade gyroscopes. The operating principle of a vibrating gyroscope is explained in Fig. B.3.

In all vibrating gyroscopes, a vibrating mechanical element suspended by springs to a frame is used to sense the angular rate. The proof mass is subjected to vibrating modes with prescribed amplitude and this mode is termed as primary mode. When the frame is subjected to rotation about an axis normal to the plane

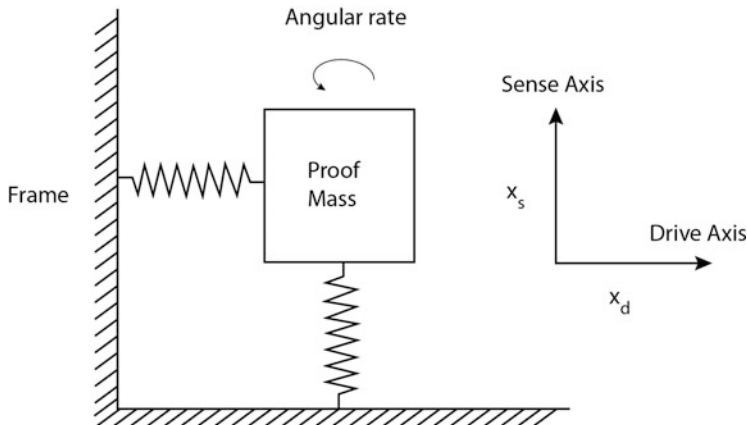


Fig. B.3 Operating principle of a vibratory gyroscope

containing drive and sense axis, the resulting coriolis force causes the proof mass to move in a direction orthogonal to both drive and rotation axes. The coriolis acceleration so generated is proportional to the product of drive velocity and the angular rate. This vibrating mode is referred as sense mode.

If the drive axis vibration is expressed as

$$X_d = X_{do} \cos(\omega_{dt}) \quad (\text{B.10})$$

where

$$X_{do} = \text{amplitude}$$

$$\omega_d = \text{frequency}$$

The Coriolis force F_c acting on the mass is

$$F_c = 2m\Omega\dot{X}_d \quad (\text{B.11})$$

The sensing motion has to be along the direction of Coriolis force and measure of the input rate. Hemispherical resonant gyro (HRG) is one of the coriolis vibration sensors which has achieved the inertial quality performance. In this gyro, the vibrating member is a thin-walled axi-symmetric shell made from fused quartz. This shell is made to vibrate at flexing mode of resonance at constant amplitude. When the vibrating shell is rotated about its sensitive axis, the coriolis force precess standing stress wave pattern and it is the measure of rotation rate.

B.3 Accelerometers

Figure B.4 demonstrates the principles of a simple accelerometer. When a vehicle accelerates, an accelerating force along the sensitive axis is applied to the body.

The proof mass when subjected to external force compresses the spring until the acceleration of the mass matches the acceleration of the body. The displacement of the mass with respect to the body is proportional to the acceleration applied to the body. It may be noted that the motion of the proof mass is in the opposite direction of the accelerating force and this is due to the inertia force which is equal and opposite of the accelerating force. With proper measurement of this displacement by a suitable pick-off, the acceleration can be obtained. It is to be noted that gravitational force acts on the proof mass directly and there is no relative motion of the mass with respect to the case. Hence the accelerometer senses only specific force, the non-gravitational acceleration and not the total acceleration. To get the true acceleration, the acceleration due to gravity which is a function of altitude must be calculated and gravity corrections are to be applied to the measured thrust acceleration.

The force balance equation for the open loop accelerometer given in Fig. B.4 can be written as

$$M \frac{d^2y}{dt^2} + C \frac{dy}{dt} + ky = Ma \quad (\text{B.12})$$

where

y is displacement of proof mass

M is the proof mass

C is damping coefficient

k is the spring constant

a is the acceleration of the proof mass

Under steady state condition, the derivatives become zero, therefore

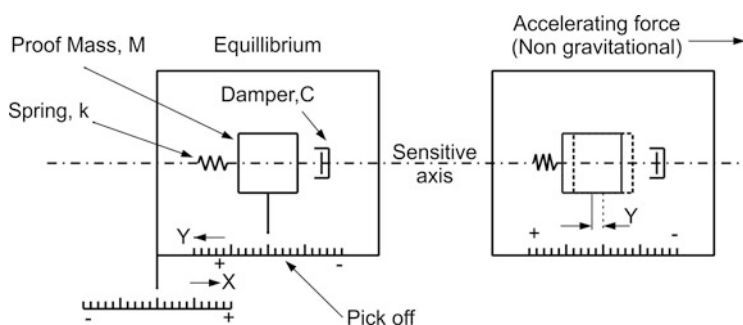


Fig. B.4 Principles of a simple accelerometer

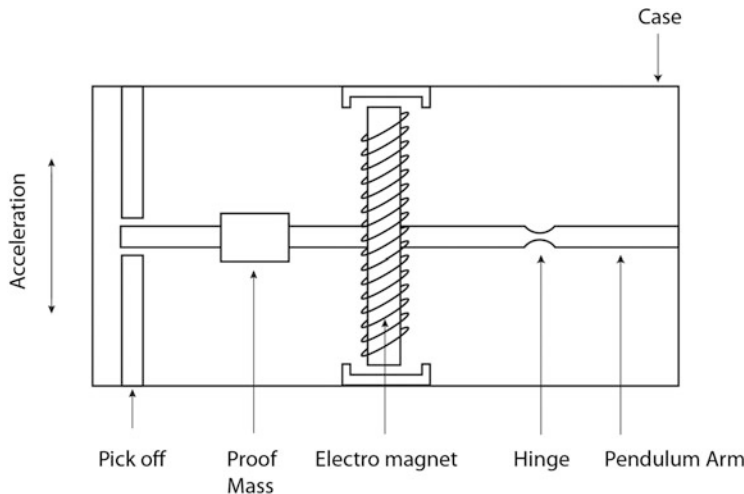


Fig. B.5 Force feedback pendulum accelerometer

$$Ma = ky \quad (\text{B.13})$$

This gives

$$a = \frac{k}{M}y \quad (\text{B.14})$$

One can deduce the damping ratio and natural frequency for this sensor as follows

$$\omega_n = \sqrt{(k/M)} \quad (\text{B.15})$$

$$\zeta = \frac{c}{2\sqrt{kM}} \quad (\text{B.16})$$

Practical accelerometers used in navigation systems are either pendulous or vibrating beam design. Pendulous designs have been there since a long time whereas the vibrating beam design was initiated in mid 1980s.

1. Pendulous Accelerometer

Precision accelerometers use closed loop force feedback pendulous accelerometer as shown in Fig. B.5. In this accelerometer, a proof mass is fixed to the body through a pendulous arm and a hinge. A torque used in the accelerometer maintains the pendulous arm at a constant position irrespective of the specific force applied to the body. The pick-off provided in the end always senses the displacement from the equilibrium and torque always adjusts the pendulum position to return to null. The force exerted by the torque is proportional to the applied specific force. This type of accelerometer is also called as torque to balance pendulous accelerometer and

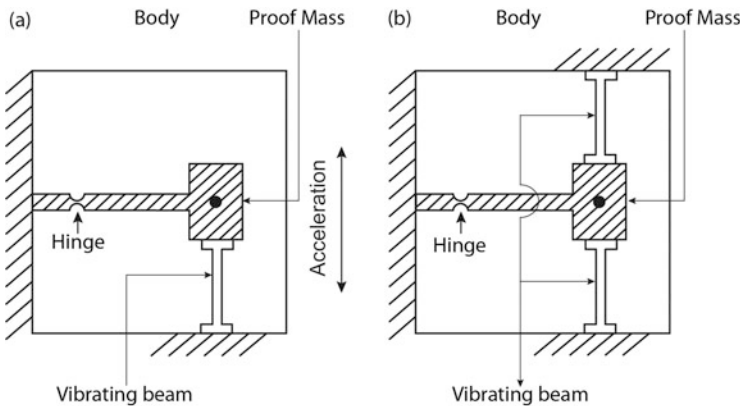


Fig. B.6 Vibratory beam accelerometer

needs a rebalance servo loop. In such accelerometers, the pick-off output is amplified, demodulated and used to generate the torque which brings back the mass to the null position.

2. Vibrating Beam Accelerometer

In a vibrating beam accelerometer, the proof mass and the pendulous arm are retained similar to pendulous accelerometer. Additionally a vibrating beam supports the proof mass along the sensitive axis as shown in Fig. B.6a. This vibrating beam known as resonating beam vibrates at its natural frequency when it is subjected to external force.

When a force is applied to the accelerometer along its sensitive axis, the beam is subjected to tension or compression depending on the direction of the force. The necessary electronics of the accelerometer drives the beam to vibrate at its resonant frequency. While the frequency of the beam increases when it is tensioned, it decreases when it is subjected to compression. Therefore direct measurement of the frequency of the vibrating beam gives the specific force applied along the sensitive axis. The piezoelectric crystalline quartz, which has high resonator Q factor, is the preferred material for the vibrating beam.

The performance of the accelerometer can be improved further by using a pair of vibrating beams arranged in push pull configuration as shown in Fig. B.6b. In this scheme, one resonator will be under tension while the other is under compression. The proof mass remains when and there is no change in the sensitive axis. If the accelerometer is subjected to acceleration fixed along the sensitive axis, the two beams will have different frequencies due to change in loading pattern for the beams. Therefore the specific force will be directly proportional to the differences of the two resonated frequencies. This mechanization supports to have either a single proof mass or two separate masses. While single proof mass offers the ease of fabrication and size reduction, the dual proof mass has the advantage of providing the mechanical isolation between the two resonators.

There are several types of accelerometers which are presently used in the inertial navigation systems and a few advanced sensors are being developed for aerospace applications. The discussion on these sensors is beyond the scope of this book.

Nomenclature

A

a	Semi-major axis of ellipse, Acceleration of the vehicle
\mathbf{a}_T	Acceleration vector
A	Sectional area of the vent hole
A_c	Chamber area at inlet to nozzle
A_e	Nozzle exit area
A_s	Frontal cross sectional area
A_{WH}	Wind speed in horizontal plane
A_{zl}	Launch azimuth
A_{ZW}	Wind azimuth
A_{ZWB}	Wind azimuth bias

B

b	Semi-minor axis of ellipse
---	----------------------------

C

C	Effective exhaust velocity
C^*	Characteristic exhaust velocity
C_l	Rolling moment coefficient
C_m	Pitching moment coefficient
C_n	Yawing moment coefficient
C_p	Pressure distribution on the surface of the vehicle
C_s	Speed of sound
C_A	Axial force coefficient acting along X-axis of vehicle
C_D	Coefficient of drag, Discharge coefficient of the vent holes
C_F	Force coefficient

C_L	Coefficient of Lift
C_N	Normal force coefficient acting along Z-axis of vehicle
C_S	Side force coefficient acting along Y-axis of vehicle
C_{A0}	Axial force coefficient for zero angle of attack
$C_{l\delta}$	Rolling moment coefficient slope due to the misalignment of strap-on motors and fins attachments, etc.
C_{l0}	Rolling moment coefficient for zero angle of attack
$C_{N\alpha}$	Normal force coefficient in pitch plane
$C_{S\beta}$	Normal force coefficient in yaw plane
$C_{\theta 0}$	Aerodynamic coefficient for zero angle of attack
$C_{\theta \alpha}$	Variation of aerodynamic coefficient with respect to pitch angle of attack
$C_{\theta \beta}$	Variation of aerodynamic coefficient with respect to yaw angle of attack

D

D	Atmospheric drag force
D_{ref}	Reference diameter

E

e	Eccentricity of conic section
\mathbf{e}	Quaternion parameter vector
$\dot{\mathbf{e}}$	Quaternion parameter rates
ξ	Specific mechanical energy (energy per unit mass of the spacecraft)
E	Total energy of the vehicle during coasting phase

F

\mathbf{f}	Specific force vector
f	Frequency of the wave
\mathbf{F}	Force acting on body
\mathbf{F}_A	Aerodynamic force vector
\mathbf{F}_{AB}	Aerodynamic force vector in body frame
\mathbf{F}_{AUB}	Auxiliary force vector in body frame
\mathbf{F}_{AF}	Aerodynamic force with fin
\mathbf{F}_{ANF}	Aerodynamic force without fin
\mathbf{F}_B	Total external force vector in ECI-frame
\mathbf{F}_{CB}	Control force vector in body frame
\mathbf{F}_{EB}	Engine inertia force vector along the body axis
\mathbf{F}_{JB}	Jet damping force vector in body frame
\mathbf{F}_{SB}	Slosh force vector in body frame
\mathbf{F}_{TB}	Thrust force vector in body frame
ΔF	Incremental aerodynamic force
ΔF_F	Incremental aerodynamic force due to fin

G

- g Acceleration due to gravity
 G Universal Gravitational constant
 \mathbf{G}_I Acceleration due to gravity vector in ECI frame

H

- h Instantaneous altitude of the vehicle
 \mathbf{H} Angular momentum vector of satellite orbit

I

- i Orbital inclination
 i_0 Orbital inclination as achieved by the launch vehicle
 i_f Inclination of the final orbit
 i_r Orbital inclination as demanded by the satellite
 I Total impulse of the motor
 I_{sp} Specific impulse of propellant
 I_{XX}
 I_{YY}
 I_{ZZ}
 I_{XY}
 I_{YZ}
 I_{ZX} Components of moments of inertia about the body axes
Components of products of inertia about the body axes

J

- J_1, J_2, J_3, J_4 Gravitational harmonics of the earth

K

- K_n Knudson number

L

- l_r Distance from engine CG to nozzle gimbal location
 l_c Distance between vehicle CG and gimbal location
 L Lift force

L_n Length of the nozzle

L_{ref} Reference length

M

m Instantaneous mass of the vehicle

\dot{m} Mass flow rate

m_i Initial mass

m_p Propellant mass

m_s Final mass of the spacecraft in the satellite specified orbit

M_0 Molecular weight

\mathbf{M}_{AB} Moment vector due to aerodynamic force

\mathbf{M}_B Total moment vector about body axes

\mathbf{M}_{CB} Moment vector due to control force

\mathbf{M}_{EB} Moment vector due to engine inertia force

\mathbf{M}_{JB} Moment vector due to jet damping force

\mathbf{M}_s Aerodynamic moment vector due to shear force

\mathbf{M}_{SB} Moment vector due to slosh force

\mathbf{M}_{TB} Moment vector due to thrust force

N

n Polytropic index

P

p, q, r Roll, Pitch, Yaw rates about X_B, Y_B, Z_B axes, respectively

p_c Period of a circular orbit

p_s Local pressure at the surface

p_∞ Free stream pressure

P Axial load

P_a Atmospheric pressure

P_c Chamber pressure

P_e Exit pressure at nozzle end

P_l Local aerodynamic pressure

P_{ref} Reference pressure of sound which human ear can hear

P_{steady} Steady pressure component

P_{total} Total pressure

P_t Pressure at throat

Q

Q	Dynamic pressure
$q(x)$	Dynamic pressure at station location x
q_∞	Free stream dynamic pressure
Q_R	Ratio of wind tunnel dynamic pressure and flight dynamic pressure

R

\mathbf{r}	Position vector of vehicle
$\dot{\mathbf{r}}$	Velocity of vehicle
$\ddot{\mathbf{r}}$	Acceleration of vehicle
r_0	Radial distance from the center of the Earth
r_a	Radial distance of apogee
r_c	Radial distance of the circular orbit
$\dot{\mathbf{r}}_I$	Velocity vector
r_p	Radial distance of perigee
r_{SL}	Radius of earth at launch site
R	Nose bluntness of PLF
R_e	Reynold's number
R_s	Radius of Earth at specified latitude
Δr	Change in altitude

S

S	Surface area
S_{ref}	Reference area

T

T	Trajectory time
t_b	Burn time of the stage
t_s	Shell thickness
T	Vehicle thrust
T_0	Initial time
T_c	Temperature in combustion chamber
T_{go}	Remaining burn time for the flight of a stage to meet target condition
T_i	Atmospheric thrust of i th motor
T_{vi}	Vacuum thrust of i th motor

U

$u(r)$	Potential energy per unit mass of the vehicle
\mathbf{u}	Unit vector
\mathbf{u}_I	Inertial velocity vector of the vehicle in ECI-frame

u_w, v_w, w_w	Vertical, zonal and meridional components of wind velocity in G-frame
U	Gravitational potential

V

v	Velocity vector of satellite
\dot{v}	Acceleration of satellite
v_a	Velocity vector of satellite at apoapsis
v_c	Velocity of the spacecraft in a circular orbit (circular velocity)
v_{esc}	Escape velocity of spacecraft
v_p	Velocity vector of satellite at periapsis
V	Vehicle velocity
V_a	Apogee velocity of the launch vehicle orbit
V_{AI}	Atmospheric relative velocity of the vehicle in ECI-frame
V_B	Inertial velocity vector in body frame
V_e	Exhaust velocity
V_f	Velocity of final orbit
V_i	Velocity vector of the vehicle in ECI frame
V_{id}	Ideal velocity needed from the vehicle
V_L	Linear velocity at launch site
V_0	Initial velocity of vehicle
V_i	Initial velocity of vehicle
V_{rot}	Rotational velocity component of Earth
V_r	Velocity of the vehicle with respect to rotational frame
V_R	Required velocity
V_G	Derivative of vector for velocity to be gained
V_{WG}	Wind velocity vector in G-frame
V_{WI}	Wind velocity vector in ECI-frame
$V(x)$	Wind velocity at station location x
V_θ	Present horizontal velocity
V_∞	Free stream velocity
ΔV	Total velocity imparted by the satellite to transfer from launch vehicle orbit to satellite specified orbit
ΔV_{drag}	Velocity loss due to drag
$V_{gravity}$	Velocity loss due to gravity
ΔV_{loss}	Total velocity loss during the flight
ΔV_{thrust}	Velocity due to thrust

X

X_{CG}	Center of gravity location along X_{BR} direction
X_{CP}	Distance from the center of pressure in pitch plane
X_{CP_F}	Center of pressure location with fin

$X_{CP_{NF}}$	Center of pressure location without fin
X_{CY}	Distance from the center of pressure in yaw plane

Z

Z_{cg}	Center of gravity location along Z_{BR} axis
----------	--

Special characters

α	Angle of attack in pitch plane
α_l	Local angle of attack due to the elastic deformation of the vehicle
α_t	Cone angle (total angle of attack)
β	Angle of attack in yaw plane
γ	Flight path angle (Angle measured from the local horizontal to the velocity vector)
δ_p, δ_y	Control deflections in pitch and yaw planes
ω	Rotational velocity vector in body frame
$\dot{\omega}$	Rotational acceleration in body frame
ϕ_{GC_L}	Geocentric latitude of launch point
ϕ_{GD_L}	Geodetic latitude of launch point
θ, ψ, ϕ	Vehicle pitch, yaw and roll Euler angles with respect to LPI frame
$\dot{\theta}, \dot{\psi}, \dot{\phi}$	Vehicle pitch, yaw and roll Euler angle rates with respect to LPI frame
θ_c, ψ_c	Steering commands
ϕ_t	Clock angle (aerodynamic roll angle)
μ	Earth's gravitational constant
μ_∞	Free stream viscosity
λ	Longitude
λ_L	Launch point longitude
Ω	Right ascension of ascending node
Ω_e	Earth rotation rate
v	True anomaly of the spacecraft
ρ	Atmospheric density
ρ_{sl}	Atmospheric density at sea level
ρ_c	Compartment inside density
ρ_0	Sea-level density
ρ_∞	Free stream density
ξ	Damping ratio
σ	Ratio of densities
$\dot{\Omega}$	Angular rate of spinning
ϵ	Area ratio